World Meteorological Organization
Global Ozone Research and Monitoring Project — Report No. 44

# Scientific Assessment of Ozone Depletion: 1998

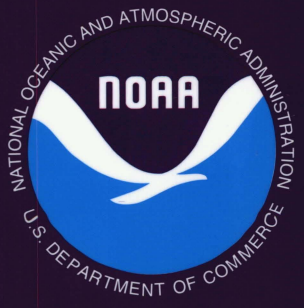


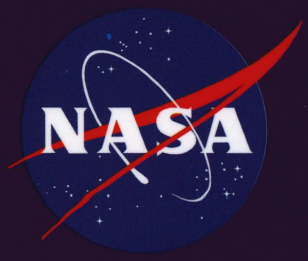


National Oceanic and Atmospheric Administration
National Aeronautics and Space Administration
United Nations Environment Programme
World Meteorological Organization
European Commission

**World Meteorological Organization**
**Global Ozone Observing System ($GO_3OS$)**
41 Avenue Giuseppe Motta
P.O. Box 2300
Geneva 2, CH 1211
Switzerland

**United Nations Environment Programme**
**United Nations Headquarters**
Ozone Secretariat
P.O. Box 30552
Nairobi
Kenya

**U.S. Department of Commerce**
**National Oceanic and Atmospheric Administration**
14th Street and Constitution Avenue NW
Herbert C. Hoover Building, Room 5128
Washington, D.C. 20230
USA

**National Aeronautics and Space Administration**
**Office of Earth Science**
NASA Headquarters
300 E Street SW
Washington, DC 20546-00001
USA

**European Commission**
**Directorate General XII - Science, Research and Development**
Rue de la Loi 200
B-1049 Bruxelles
Belgium

Published in February 1999.

ISBN: 92-807-1722-7

Requests for extra copies by scientific users should be directed to:

WORLD METEOROLOGICAL ORGANIZATION
Global Ozone Observing System ($GO_3OS$)
P.O. Box 2300
1211-Geneva-2, Switzerland

World Meteorological Organization
Global Ozone Research and Monitoring Project – Report No. 44

# SCIENTIFIC ASSESSMENT OF OZONE DEPLETION: 1998

National Oceanic and Atmospheric Administration
National Aeronautics and Space Administration
United Nations Environment Programme
World Meteorological Organization
European Commission

# List of International Authors, Contributors, and Reviewers

## Assessment Cochairs

Daniel L. Albritton, Pieter J. Aucamp, Gérard Mégie, and Robert T. Watson

## Chapter Lead Authors

1: Ronald G. Prinn and R. Zander
2: Michael J. Kurylo and José M. Rodríguez
3: Sophie Godin and Lamont R. Poole
4: Rumen D. Bojkov and Robert Hudson
5: Marie-Lise Chanin and V. Ramaswamy
6: Rolf Müller and Ross J. Salawitch
7: A.R. Ravishankara and Theodore G. Shepherd
8: Jos Lelieveld and Anne M. Thompson
9: Jay R. Herman and Richard L. McKenzie
10: Claire Granier and Keith P. Shine
11: Sasha Madronich and Guus J.M. Velders
12: David J. Hofmann and John A. Pyle

## Coordinating Editor

Christine A. Ennis

## Authors, Contributors, and Reviewers

| | | | |
|---|---|---|---|
| Alberto Adriani | Italy | C. Rocky Booth | US |
| Daniel L. Albritton | US | Stephan Borrmann | Germany |
| Georgios T. Amanatidis | Belgium | Byron Boville | US |
| James G. Anderson | US | Guy Brasseur | US |
| Meinrat O. Andreae | Germany | Christoph Brühl | Germany |
| James K. Angell | US | William H. Brune | US |
| Roger Atkinson | Australia | Neal Butchart | UK |
| Elliot L. Atlas | US | James H. Butler | US |
| Pieter J. Aucamp | South Africa | Pablo O. Canziani | Argentina |
| John Austin | UK | Daniel Cariolle | France |
| Linnea Avallone | US | Ken Carslaw | Germany |
| Dimitrios S. Balis | Greece | Edward Celarier | US |
| John Barnes | US | Marie-Lise Chanin | France |
| J. Barnett | UK | Martyn Chipperfield | UK |
| Darrel Baumgardner | US | H. Claude | Germany |
| Slimane Bekki | France | Cathy Clerbaux | France |
| Germar Bernhard | Germany | Michael Coffey | US |
| Richard Bevilacqua | US | Peter S. Connell | US |
| P.K. Bhartia | US | David B. Considine | US |
| Lane Bishop | US | R.A. Cox | UK |
| Donald R. Blake | US | Paul J. Crutzen | Germany |
| Mario Blumthaler | Austria | Derek M. Cunnold | US |
| Greg Bodeker | New Zealand | Martin Dameris | Germany |
| Barry A. Bodhaine | US | John S. Daniel | US |
| Rumen D. Bojkov | Switzerland | Christine David | France |

| | |
|---|---|
| Richard Derwent | UK |
| Terry Deshler | US |
| Roseanne D. Diab | South Africa |
| Susana Diaz | Argentina |
| Ed Dlugokencky | US |
| Guido Di Donfrancesco | Italy |
| Thomas Duafala | US |
| Dieter H. Ehhalt | Germany |
| James W. Elkins | US |
| Andreas Engel | Germany |
| Christine A. Ennis | US |
| David E. Etheridge | Australia |
| Simon J. Evans | UK |
| David W. Fahey | US |
| Vitali Fioletov | Canada |
| Jack Fishman | US |
| Eric L. Fleming | US |
| Lawrence E. Flynn | US |
| Piers M. de F. Forster | UK |
| J. Paul F. Fortuin | The Netherlands |
| Paul J. Fraser | Australia |
| Lucien Froidevaux | US |
| Michael Fromm | US |
| Jan Fuglestvedt | Norway |
| Dian J. Gaffen | US |
| Marvin A. Geller | US |
| Melvyn E. Gelman | US |
| Sophie Godin | France |
| Allen Goldstein | UK |
| George S. Golitsyn | Russia |
| Claire Granier | France/US |
| William B. Grant | US |
| Jens-Uwe Grooß | Germany |
| Robert Guicherit | The Netherlands |
| Michael R. Gunson | US |
| James Hansen | US |
| Jochen Harnisch | Germany |
| Neil R.P. Harris | UK |
| Dana E. Hartley | US |
| Fumio Hasebe | Japan |
| Alain Hauchecorne | France |
| Didier Hauglustaine | US |
| Peter Haynes | UK |
| Jay R. Herman | US |
| Mark Hervig | US |
| David J. Hofmann | US |
| Stacey M. Hollandsworth | US |
| James R. Holton | US |
| Øystein Hov | Norway |
| Robert Hudson | US |
| Drusilla Hufford | US |
| Dale F. Hurst | US |
| Abdel Moneim Ibrahim | Egypt |
| Mohammad I. Ilyas | Malaysia |
| Ivar S.A. Isaksen | Norway |
| Tomoyuki Ito | Japan |
| Charles H. Jackman | US |
| Daniel J. Jacob | US |
| Evgeny A. Jadin | Russia |
| Horst Jäger | Germany |
| Nicholas B. Jones | New Zealand |
| Rod Jones | UK |
| Jan-Eiof Jonson | Norway |
| Torben S. Jørgensen | Denmark |
| Kenneth W. Jucks | US |
| Igor Karol | Russia |
| David Karoly | Australia |
| Randy Kawa | US |
| Jack A. Kaye | US |
| Philippe Keckhut | France |
| Hennie Kelder | The Netherlands |
| James B. Kerr | Canada |
| Jhoon Kim | Republic of Korea |
| Douglas E. Kinnison | US |
| Volker Kirchhoff | Brazil |
| Dieter Kley | Germany |
| Malcolm K.W. Ko | US |
| Kunihiko Kodera | Japan |
| Yutaka Kondo | Japan |
| Yuri Koshelkov | Russia |
| Nickolay Krotkov | US |
| Janusz Krzyścin | Poland |
| Michael Kuhn | Germany |
| Michael J. Kurylo | US |
| Karin Labitzke | Germany |
| G.J. Labow | US |
| William A. Lahoz | UK |
| Murari Lal | India |
| Shyam Lal | India |
| Neils Larsen | Denmark |
| David J. Lary | UK |
| Yuan-Pern Lee | Taiwan |
| Franck Lefèvre | France |
| Jos Lelieveld | The Netherlands |
| Jacqueline Lenoble | France |
| Kirsti Leszczynski | Finland |

| | |
|---|---|
| Joel M. Levy | US |
| J.-J. Roger Lin | US |
| Jennifer A. Logan | US |
| Craig S. Long | US |
| Beiping Luo | China |
| E.V. Lysenko | Russia |
| Sasha Madronich | US |
| Emmanuel Mahieu | Belgium |
| Jerry D. Mahlman | US |
| Manfred Maiss | Germany |
| Gloria L. Manney | US |
| Andrew Matthews | New Zealand |
| Bernhard Mayer | Germany |
| M. Patrick McCormick | US |
| Archie McCulloch | UK |
| Mack McFarland | US |
| Danny McKenna | Germany |
| Richard L. McKenzie | New Zealand |
| Richard D. McPeters | US |
| Gérard Mégie | France |
| Pauline M. Midgley | Germany |
| Jana B. Milford | US |
| Alvin J. Miller | US |
| Forrest Mims | US |
| Philippe Mirabel | France |
| Masa Miyauchi | Japan |
| Mario J. Molina | US |
| Stephen A. Montzka | US |
| Gary A. Morris | US |
| Mike Mozurkewich | Canada |
| Rolf Müller | Germany |
| Gunnar Myhre | Norway |
| Hideaki Nakane | Japan |
| John Nash | UK |
| Patrick Neale | US |
| Gerald E. Nedoluha | US |
| Roland Neuber | Germany |
| Cynthia D. Nevison | US |
| Paul A. Newman | US |
| Ole J. Nielsen | Denmark |
| Paul C. Novelli | US |
| Alan O'Neill | US |
| Donal O'Sullivan | US |
| Samuel J. Oltmans | US |
| Michael Oppenheimer | US |
| David E. Oram | UK |
| John J. Orlando | US |
| Mary Osborn | US |
| Stuart A. Penkett | UK |
| Joyce Penner | US |
| Thomas Peter | Germany |
| Ruben Piacentini | Argentina |
| Michel Pirre | France |
| Giovanni Pitari | Italy |
| Alan Plumb | US |
| Jean-Pierre Pommereau | France |
| Lamont R. Poole | US |
| Bob Portmann | US |
| Gilles Poulet | France |
| Michael Prather | US |
| M. Margarita Préndez | Chile |
| Ronald G. Prinn | US |
| John A. Pyle | UK |
| V. Ramaswamy | US |
| William J. Randel | US |
| Lakshman Randeniya | Australia |
| A.R. Ravishankara | US |
| Claire E. Reeves | UK |
| George C. Reid | US |
| Wolfgang Renger | Germany |
| Markus Rex | Germany |
| Curtis P. Rinsland | US |
| Henning Rodhe | Sweden |
| José M. Rodríguez | US |
| Bjoerg Rognerud | Norway |
| Richard B. Rood | US |
| James M. Rosen | US |
| Michel Rossi | Switzerland |
| James M. Russell III | US |
| Keith R. Ryan | Australia |
| Ken G. Ryan | New Zealand |
| Nelson A. Sabogal | Kenya |
| Karen H. Sage | US |
| Ross J. Salawitch | US |
| Stan Sander | US |
| Eugenio Sanhueza | Venezuela |
| Michelle L. Santee | US |
| K.M. Sarma | Kenya |
| Sue M. Schauffler | US |
| Ulrich Schmidt | Germany |
| Ulrich Schumann | Germany |
| M. Daniel Schwarzkopf | US |
| Gunther Seckmeyer | Germany |
| Theodore G. Shepherd | Canada |
| Drew Shindell | US |
| Keith P. Shine | UK |

## AUTHORS, CONTRIBUTORS, AND REVIEWERS

| | |
|---|---|
| Masato Shiotani | Japan |
| Howard W. Sidebottom | Ireland |
| Peter G. Simmonds | UK |
| David E. Siskind | US |
| Harry Slaper | The Netherlands |
| James R. Slusser | US |
| Herman Smit | Germany |
| Sergei P. Smyshlyaev | Russia |
| Susan Solomon | US |
| Boris Soukharev | Russia |
| Johannes Stähelin | Switzerland |
| L. Paul Steele | Australia |
| Leopoldo Stefanutti | Italy |
| William R. Stockwell | Germany |
| Richard Stolarski | US |
| Frode Stordal | Norway |
| William T. Sturges | UK |
| B.H. Subbaraya | India |
| Michael E. Summers | US |
| Richard Swinbank | US |
| Petteri Taalas | Finland |
| Xiao-Yan Tang | China |
| Hubert Teyssèdre | France |
| Larry Thomason | US |
| Anne M. Thompson | US |
| Thayne M. Thompson | US |
| Brian Toon | US |
| Geoffrey C. Toon | US |
| Ralf Toumi | UK |
| Kleareti Tourpali | Greece |
| Michael Trainer | US |
| Jörg Trentmann | Germany |
| Adrian Tuck | US |
| Osamu Uchino | Japan |
| Jan C. van der Leun | The Netherlands |
| Karel Vanicek | Czech Republic |
| Guus J.M. Velders | The Netherlands |
| Guido Visconti | Italy |
| C. Michael Volk | Germany |
| Andreas Volz-Thomas | Germany |
| Peter von der Gathen | Germany |
| Ray H.J. Wang | US |
| Wei-Chyung Wang | US |
| Joe Waters | US |
| Robert T. Watson | US |
| Darryn Waugh | US |
| Debra K. Weisenstein | US |
| Ray F. Weiss | US |
| Paul O. Wennberg | US |
| James C. Wilson | US |
| Martin Wirth | Germany |
| Russell Wooldridge | US |
| Doug Worsnop | US |
| Donald J. Wuebbles | US |
| Youko Yokouchi | Japan |
| Vladimir Yushkov | Russia |
| Shari A. Yvon-Lewis | US |
| Ahmed Zand | Iran |
| R. Zander | Belgium |
| Christos Zerefos | Greece |
| Xiuji Zhou | China |
| Jerry Ziemke | US |

# TABLE OF CONTENTS

## SCIENTIFIC ASSESSMENT OF OZONE DEPLETION: 1998

**TABLE OF CONTENTS**

**TABLE OF CONTENTS**

## PART 4. PREDICTIONS OF FUTURE CHANGES

# PREFACE

The present document will be part of the information upon which the Parties to the United Nations Montreal Protocol will base their future decisions regarding protection of the stratospheric ozone layer.

Specifically, the Montreal Protocol on Substances that Deplete the Ozone Layer states (Article 6): ". . . the Parties shall assess the control measures . . . on the basis of available scientific, environmental, technical, and economic information." To provide the mechanisms whereby these assessments are conducted, the Protocol further states: ". . . the Parties shall convene appropriate panels of experts" and "the panels will report their conclusions . . . to the Parties."

Three assessment reports have been prepared during 1998 to be available to the Parties in advance of their meeting in 1999, at which they will consider the need to amend or adjust the Protocol. The two companion reports to the present scientific assessment focus on the environmental and health effects of ozone layer depletion and on the technological feasibilities and economic implications of various mitigation approaches.

The present report is the latest in a series of eight scientific assessments prepared by the world's leading experts in the atmospheric sciences and under the international auspices of the World Meteorological Organization (WMO) and/or the United Nations Environment Programme (UNEP). The present assessment is the fifth in the set that has been prepared directly as input to the Montreal Protocol process. The chronology of the scientific assessments on the understanding of ozone depletion and their relation to the international policy process is summarized as follows:

| Year | Policy Process | Scientific Assessment |
|---|---|---|
| 1981 | | *The Stratosphere 1981. Theory and Measurements.* WMO No. 11. |
| 1985 | Vienna Convention | *Atmospheric Ozone 1985.* Three volumes. WMO No. 16. |
| 1987 | Montreal Protocol | |
| 1988 | | *International Ozone Trends Panel Report 1988.* Two volumes. WMO No. 18. |
| 1989 | | *Scientific Assessment of Stratospheric Ozone: 1989.* Two volumes. WMO No. 20. |
| 1990 | London Adjustments and Amendment | |
| 1991 | | *Scientific Assessment of Ozone Depletion: 1991.* WMO No. 25. |
| 1992 | | *Methyl Bromide: Its Atmospheric Science, Technology, and Economics* (Assessment Supplement). UNEP (1992). |
| 1992 | Copenhagen Adjustments and Amendment | |
| 1994 | | *Scientific Assessment of Ozone Depletion: 1994.* WMO No. 37. |

| Year | Policy Process | Scientific Assessment |
|---|---|---|
| 1995 | Vienna Adjustment | |
| 1997 | Montreal Adjustments and Amendment | |
| 1998 | | *Scientific Assessment of Ozone Depletion: 1998.* WMO No. 44. |
| 1999 | 11th Meeting of the Parties (China) | |

The genesis of *Scientific Assessment of Ozone Depletion: 1998* occurred at the 7th Meeting of the Conference of the Parties to the Montreal Protocol in Vienna, Austria, in December 1995, at which the scope of the scientific needs of the Parties was defined. The formal planning of the present report was started in January 1997 by an *ad hoc* international steering group who crafted the outline and suggested scientists from the world community to serve as authors. The first drafts of the chapters were examined at a meeting that occurred on 12 - 14 November 1997 in Washington, D.C., at which the Lead Authors and a small number of international experts focused on the content of the draft chapter and the coordination among the chapters.

The second drafts of the chapters were reviewed by 124 scientists worldwide in a mail peer review. These comments were considered by the authors. At a Panel Review Meeting in Les Diablerets, Switzerland, held on 1 - 5 June 1998, the responses to these mail review comments were proposed by the authors and discussed by the 73 participants. Final changes to the chapters were decided upon there, and the Executive Summary contained herein was prepared by the participants.

The group also focused on updating a set of questions that are frequently asked about the ozone layer. Based upon the scientific understanding represented by the assessments, answers to these frequently asked questions were updated. These questions and answers are included in this report.

The final result of this two-year endeavor is the present assessment report. As the accompanying list indicates, the *Scientific Assessment of Ozone Depletion: 1998* is the product of 304 scientists from the developed and developing world[1] who contributed to its preparation and review (218 scientists prepared the report and 148 scientists participated in the peer review process).

What follows is a summary of their current understanding of the stratospheric ozone layer and its relation to humankind.

---

1 Participating were Argentina, Australia, Austria, Belgium, Brazil, Canada, Chile, Czech Republic, Denmark, Egypt, Finland, France, Germany, Greece, India, Iran, Ireland, Italy, Japan, Kenya, Malaysia, New Zealand, Norway, Poland, Russia, South Africa, Republic of Korea, Sweden, Switzerland, Taiwan, The Netherlands, The People's Republic of China, United Kingdom, United States of America, and Venezuela.

# EXECUTIVE SUMMARY

The 1987 Montreal Protocol on Substances that Deplete the Ozone Layer commemorated its 10th anniversary in September 1997. Among the provisions of the Protocol was the requirement that the Parties to the Protocol base their future decisions on the available scientific, environmental, technical, and economic information as assessed by the worldwide expert communities. The advances of the understanding in ozone science over this decade were assessed in 1988, 1989, 1991, and 1994. This information was input to the subsequent Amendments and Adjustments of the 1987 Protocol. The Assessment summarized here is the fifth in that series.

## Recent Major Scientific Findings and Observations

Since the *Scientific Assessment of Ozone Depletion: 1994*, significant advances have continued to be made in the understanding of the impact of human activities on the ozone layer, the influence of changes in chemical composition on the radiative balance of the Earth's climate, and, indeed, the coupling of the ozone layer and the climate system. Numerous laboratory investigations, atmospheric observations, and theoretical and modeling studies have produced several key ozone- and climate-related findings:

- **The total combined abundance of ozone-depleting compounds in the lower atmosphere peaked in about 1994 and is now slowly declining. Total chlorine is declining, but total bromine is still increasing.** As forecast in the 1994 Assessment, the long period of increasing total chlorine abundances – primarily from the chlorofluorocarbons (CFCs), carbon tetrachloride ($CCl_4$), and methyl chloroform ($CH_3CCl_3$) – has ended. The peak total tropospheric chlorine abundance was $3.7 \pm 0.1$ parts per billion (ppb) between mid-1992 and mid-1994. The declining abundance of total chlorine is due principally to reduced emissions of methyl chloroform. Chlorine from the major CFCs is still increasing slightly. The abundances of most of the halons continue to increase (for example, Halon-1211, almost 6% per year in 1996), but the rate has slowed in recent years. These halon increases are likely to be due to emissions in the 1990s from the halon "bank," largely in developed countries, and new production of halons in developing countries. The observed abundances of CFCs and chlorocarbons in the lower atmosphere are consistent with reported emissions.

- **The observed abundances of the substitutes for the CFCs are increasing.** The abundances of the hydrochlorofluorocarbons (HCFCs) and hydrofluorocarbons (HFCs) are increasing as a result of a continuation of earlier uses and of their use as substitutes for the CFCs. In 1996, the HCFCs contributed about 5% to the tropospheric chlorine from the long-lived gases. This addition from the substitutes offsets some of the decline in tropospheric chlorine associated with methyl chloroform, but is nevertheless about 10 times less than that from the total tropospheric chlorine growth rate throughout the 1980s. The atmospheric abundances of HCFC-141b and HCFC-142b calculated from reported emissions data are factors of 1.3 and 2, respectively, smaller than observations. Observed and calculated abundances agree for HCFC-22 and HFC-134a.

- **The combined abundance of stratospheric chlorine and bromine is expected to peak before the year 2000.** The delay in this peak in the stratosphere compared with the lower atmosphere reflects the average time required for surface emissions to reach the lower stratosphere. The observations of key chlorine compounds in the stratosphere up through the present show the expected slower rate of increase and show that the peak had not occurred at the time of the most recent observations that were analyzed for this Assessment.

- **The role of methyl bromide as an ozone-depleting compound is now considered to be less than was estimated in the 1994 Assessment, although significant uncertainties remain.** The current best estimate of the Ozone Depletion Potential (ODP) for methyl bromide ($CH_3Br$) is 0.4, compared with an ODP of 0.6 estimated in the previous Assessment. The change is due primarily to both an increase in the estimate of ocean removal processes and the identification of an uptake by soils, with a smaller contribution from the change in our estimate of the atmospheric removal rate. Recent research has shown that the science of atmospheric methyl bromide is complex and still not well understood. The current understanding of the sources and sinks of atmospheric methyl bromide is incomplete.

- **The rate of decline in stratospheric ozone at midlatitudes has slowed; hence, the projections of ozone loss made in the 1994 Assessment are larger than what has actually occurred.** Total column ozone decreased significantly at midlatitudes (25-60°) between 1979 and 1991, with estimated linear downward trends of 4.0, 1.8, and 3.8% per decade, respectively, for northern midlatitudes in winter/spring, northern midlatitudes in summer/fall, and southern midlatitudes year round. However, since 1991 the linear trend observed during the 1980s has not continued, but rather total column ozone has been almost constant at midlatitudes in both hemispheres since the recovery from the 1991 Mt. Pinatubo eruption. The observed total column ozone losses from 1979 to the period 1994-1997 are about 5.4, 2.8, and 5.0%, respectively, for northern midlatitudes in winter/spring, northern midlatitudes in summer/fall, and southern midlatitudes year round, rather than the values projected in the 1994 Assessment assuming a linear trend: 7.6, 3.4, and 7.2%, respectively. The understanding of how changes in stratospheric chlorine/bromine and aerosol loading affect ozone suggests some of the reasons for the unsuitability of using a linear extrapolation of the pre-1991 ozone trend to the present.

- **The link between the long-term build-up of chlorine and the decline of ozone in the upper stratosphere has been firmly established.** Model predictions based on the observed build-up of stratospheric chlorine in the upper stratosphere indicate a depletion of ozone that is in good quantitative agreement with the altitude and latitude dependence of the measured ozone decline during the past several decades, which peaks at about 7% per decade near 40 km at midlatitudes in both hemispheres.

- **The springtime Antarctic ozone hole continues unabated.** The extent of ozone depletion has remained essentially unchanged since the early 1990s. This behavior is expected given the near-complete destruction of ozone within the Antarctic lower stratosphere during springtime. The factors contributing to the continuing depletion are well understood.

- **The late-winter/spring ozone values in the Arctic were unusually low in 6 out of the last 9 years, the 6 being years that are characterized by unusually cold and protracted stratospheric winters.** The possibility of such depletions was predicted in the 1989 Assessment. Minimum Arctic vortex temperatures are near the threshold for large chlorine activation. Therefore, the year-to-year variability in temperature, which is driven by meteorology, leads to particularly large variability in ozone for current chlorine loading. As a result, it is not possible to forecast the behavior of Arctic ozone for a particular year. Elevated stratospheric halogen abundances over the next decade or so imply that the Arctic will continue to be vulnerable to large ozone losses.

- **The understanding of the relation between increasing surface UV-B radiation and decreasing column ozone has been further strengthened by ground-based observations, and newly developed satellite methods show promise for establishing global trends in UV radiation.** The inverse dependence of surface UV radiation and the overhead amount of ozone, which was demonstrated in earlier Assessments, has been further demonstrated and quantified by ground-based measurements under a wide range of atmospheric conditions. In addition, the influences of other variables, such as clouds, particles, and surface reflectivity, are better understood. These data have assisted the development of a satellite-based method to estimate global UV changes, taking into account the role of cloud cover. The satellite estimates for 1979-1992 indicate that the largest UV increases occur during spring at high latitudes in both hemispheres.

- **Stratospheric ozone losses have caused a cooling of the global lower stratosphere and global-average negative radiative forcing of the climate system.** The decadal temperature trends in the stratosphere have now been better quantified. Model simulations indicate that much of the observed downward trend in lower stratospheric temperatures (about 0.6°C per decade over 1979-1994) is attributed to the ozone loss in the lower stratosphere. A lower stratosphere that is cooler results in less infrared radiation reaching the surface/troposphere system. Radiative calculations, using extrapolations based on the ozone trends reported in the 1994 Assessment for reference, indicate that stratospheric ozone losses since 1980 may have offset about 30% of the positive forcing due to increases in the well-mixed greenhouse gases (i.e., carbon dioxide, methane, nitrous oxide, and the halocarbons) over the same time period. The climatic impact of the slowing of midlatitude ozone trends and the enhanced ozone loss in the Arctic has not yet been assessed.

- **Based on past emissions of ozone-depleting substances and a projection of the maximum allowances under the Montreal Protocol into the future, the maximum ozone depletion is estimated to lie within the current decade or the next two decades, but its identification and the evidence for the recovery of the ozone layer lie still further ahead.** The falloff of total chlorine and bromine abundances in the stratosphere in the next century will be much slower than the rate of increase observed in past decades, because of the slow rate at which natural processes remove these compounds from the stratosphere. The most vulnerable period for ozone depletion will be extended into the coming decades. However, extreme perturbations, such as natural events like volcanic eruptions, could enhance the loss from ozone-depleting chemicals. Detection of the beginning of the recovery of the ozone layer could be achievable early in the next century if decreasing chlorine and bromine abundances were the only factor. However, potential future increases or decreases in other gases important in ozone chemistry (such as nitrous oxide, methane, and water vapor) and climate change will influence the recovery of the ozone layer. When combined with the natural variability of the ozone layer, these factors imply that unambiguous detection of the beginning of the recovery of the ozone layer is expected to be well after the maximum stratospheric loading of ozone-depleting gases.

## Supporting Scientific Evidence and Related Issues

### Recent Halogen and Methane Changes

- Tropospheric abundances of total organic chlorine (Cl) contained in long- and short-lived halocarbons reached maximum values of 3.7 ± 0.1 parts per billion (ppb) between mid-1992 and mid-1994 and are beginning to decrease slowly in the global troposphere. The decline in the tropospheric abundance of methyl chloroform ($CH_3CCl_3$) (at a rate of about 40 to 42 parts per trillion (ppt) Cl $yr^{-1}$ in 1996) is the principal cause of the decrease and reversal in the Cl growth rate. At the same time, chlorine from the sum of the major CFCs grew at 7 ppt Cl $yr^{-1}$ (CFC-12, 9 ppt Cl $yr^{-1}$; CFC-11, -2 ppt Cl $yr^{-1}$; CFC-113, 0 ppt Cl $yr^{-1}$) and by 10 ppt Cl $yr^{-1}$ from the three major hydrochlorofluorocarbons (HCFCs) (HCFC-22, 5 ppt Cl $yr^{-1}$; HCFC-141b, 4 ppt Cl $yr^{-1}$; HCFC-142b, 1 ppt Cl $yr^{-1}$). The rate of decay of $CH_3CCl_3$ is expected to slow down to less than 10 ppt Cl $yr^{-1}$ by 2005. By that point its concentration should be so small that it will no longer be an important contributor to atmospheric organic chlorine.

- Space-based remote measurements of hydrogen chloride (HCl), hydrogen fluoride (HF), and total chlorine in the stratosphere, as well as column abundances of HCl, chlorine nitrate ($ClONO_2$), HF, and carbonyl difluoride ($COF_2$) from the ground, are consistent with the content and rate of change of the total organic chlorine and fluorine abundance of the troposphere. These observations provide evidence that the rate of increase of stratospheric chlorine loading has slowed in recent years.

- Growth in the tropospheric concentrations of HCFCs and hydrofluorocarbons (HFCs) has been observed as expected from continuation of previous uses and from their use as replacements for chlorofluorocarbons (CFCs). Emissions calculated by industry from sales and use data are in accordance with the current global abundances of HCFC-22 and HFC-134a. For HCFC-141b and -142b, the industry data underestimate the current global abundances by factors of approximately 1.3 and 2 respectively. No production and sales data are currently available for other HCFCs and HFCs being used as CFC alternatives.

- New studies suggest a major reduction in the magnitude of the estimated oceanic source of methyl chloride ($CH_3Cl$). As a result, the sum of known sources is inadequate to explain the observed atmospheric burden of $CH_3Cl$, thus requiring a larger contribution from other sources, either natural or anthropogenic.

- Tropospheric bromine loading continues to rise largely because of the ongoing growth of Halon-1211 (almost 6% $yr^{-1}$), Halon-2402 (2% $yr^{-1}$), and Halon-1301 (1% $yr^{-1}$). Possible causes are the large "banking" in developed countries of that compound during the 1980s and its subsequent use and release during the 1990s, and new production in developing countries. Continued increases of halons over the next few years could cause the abundance of equivalent chlorine to decline more slowly than predicted in the 1994 Assessment.

- Recent measurements and intercomparisons of calibration standards have confirmed that the average global mixing ratio of methyl bromide ($CH_3Br$) is between 9 and 10 ppt and that the interhemispheric ratio is $1.3 \pm 0.1$ (north/south). New estimates of methyl bromide losses yield magnitudes of 77 Gg $yr^{-1}$ (ranging from 37 to 133 Gg $yr^{-1}$) for ocean uptake; 42 Gg $yr^{-1}$ (ranging from 10 to 214 Gg $yr^{-1}$) for soil uptake; and 86 Gg $yr^{-1}$ (ranging from 65 to 107 Gg $yr^{-1}$) for removal by hydroxyl radical (OH), for a total removal rate of 205 Gg $yr^{-1}$ with a range of about 110 to 450 Gg $yr^{-1}$. The current best estimate of the lifetime of atmospheric $CH_3Br$, as calculated from losses within the atmosphere, to the ocean, and to soils, is 0.7 years, with a range of 0.4 to 0.9 years. The Ozone Depletion Potential (ODP) of methyl bromide is 0.4, with a range of 0.2 to 0.5.

- No new important sources of methyl bromide have been identified. The ocean now appears to be a net sink, with an estimated net flux from the atmosphere of -21 Gg $yr^{-1}$ (ranging from -3 to -32 Gg $yr^{-1}$). Estimates of ocean emissions of order 60 Gg $yr^{-1}$ can be directly deduced from the above estimates for uptake and net ocean flux. The total emission of $CH_3Br$ from identified sources is 122 Gg $yr^{-1}$, with a range of 43 to 244 Gg $yr^{-1}$. The best-quantified source is fumigation, with a magnitude of 41 Gg $yr^{-1}$ and a range of 28 to 64 Gg $yr^{-1}$. Other anthropogenic sources include biomass burning (20 Gg $yr^{-1}$, ranging from 10 to 40 Gg $yr^{-1}$) and leaded gasoline use (5 Gg $yr^{-1}$, ranging from negligible to 10 Gg $yr^{-1}$). Identified sources of $CH_3Br$ thus constitute only about 60% of identified sinks on a globally averaged basis. This disagreement is difficult to reconcile with estimated uncertainties in the source and sink terms. The short lifetime of methyl bromide, coupled with the inhomogeneity of its sources and sinks, complicates the interpretation of its global budget.

- Based on the most recent analysis of the methyl chloroform ($CH_3CCl_3$) observational record (including a refinement in calibration), the estimated atmospheric lifetimes (with respect to reactive removal by OH) of $CH_3CCl_3$, HCFCs, HFCs, and $CH_4$ have been reduced by about 15% since the 1994 Assessment. The 1995 assessment of the Intergovernmental Panel on Climate Change (IPCC) mostly reflected these revisions, with a slightly smaller correction factor of about 10%. For species whose chemical lifetime is shorter than 1 to 2 years, the use of a global-mean lifetime may not be appropriate.

- The atmospheric abundance of $CH_4$ continues to increase, but with a declining growth rate. The average growth rate between 1980 and 1992 of about 10 ppb $yr^{-1}$ can be compared with the 1996-1997 rate of approximately 3 to 4 ppb $yr^{-1}$. The current best estimate for the total atmospheric lifetime of methane has been lowered to $8.9 \pm 0.6$ years.

### Stratospheric Particles

- Observations and models have further confirmed that stratospheric sulfate aerosol (SSA) and polar stratospheric clouds (PSCs) play a key role in ozone loss chemistry through heterogeneous reactions that activate halogen species and deactivate nitrogen species.

- Observations have increased our knowledge of particle formation processes, the dispersal and decay of volcanic SSA, and particle climatology. They show that supercooled ternary solution (STS) droplets that form from SSA without a nucleation barrier are an important class of PSC particles. The formation processes of solid PSC particles that play a significant role in denitrification of the polar vortices remain uncertain. Recent studies suggest that mesoscale temperature fluctuations, especially over mountain ranges, may be important in PSC formation processes, particularly in the Arctic.

- The two most recent major volcanic eruptions, El Chichón (1982) and Mt. Pinatubo (1991), both temporarily increased SSA amounts by more than an order of magnitude.

- There is no clear trend in SSA abundances from 1979 to 1997, demonstrating that any anthropogenic contribution must be smaller than thought in the 1994 Assessment. SSA models including known tropospheric sulfur sources underpredict 1979 values, which were thought to represent the non-volcanic background, but it is not clear that this period was truly free of volcanic influence.

### Ozone in the Midlatitudes and Tropics

- As noted in the 1994 Assessment, Northern Hemisphere midlatitude column ozone decreased markedly in 1992-1993, following the large enhancement of stratospheric aerosol caused by the eruption of Mt. Pinatubo in 1991. Column ozone has now reached amounts higher than a linear extrapolation of the pre-Pinatubo trend would predict. Between 25 and 60°N, ozone abundances for 1994-1997 averaged about 4% below 1979 values, although with large variability, while extrapolation of the pre-1991 trend would predict current (1997) abundances about 5.5% below 1979 values. The corresponding winter/spring and summer/fall losses average about 5.4 and 2.8%, respectively, while a linear extrapolation would predict 7.6 and 3.4%, respectively. The average ozone abundances between 25 and 60°S are currently about 4% (satellite) or 5% (ground) below 1979 values, while the linear extrapolation would predict 7.2% (both satellite and ground).

- Our understanding of how changes in halogen and aerosol loading affect ozone suggests some of the reasons for the unsuitability of using a linear extrapolation of the pre-1991 ozone trend to the present. For example, observations of stratospheric HCl and $ClONO_2$ show a build-up of stratospheric chlorine in recent years consistent with halocarbon emissions, but slower than would have been predicted by the chlorine trends observed before 1992. In addition, enhanced stratospheric aerosol was also present throughout much of the decade of the 1980s due to earlier volcanic eruptions (e.g., El Chichón and Ruiz), likely enhancing the downward trend of ozone observed even before Pinatubo.

- There are no statistically significant trends in total ozone in the equatorial regions (20°S to 20°N).

- The amplitude of the annual cycle of ozone at middle to high latitudes has decreased by approximately 15% in the last decades because larger declines have occurred during the season of maximum ozone values.

- For northern midlatitudes, combined vertical profile ozone trends through 1996 are negative at all altitudes between 12 and 45 km and are statistically significant at the $2\sigma$ level. The downward trend is largest near 40 and 15 km (approximately 7% per decade) and is smallest at 30 km (2% per decade). The bulk of column ozone decline is between the tropopause and 25 km.

- The re-evaluation of the Stratospheric Aerosol and Gas Experiment (SAGE) I/II satellite data indicates that there are no significant interhemispheric differences in upper stratospheric trends through 1996. Agreement is good, within estimated uncertainties, between SAGE I/II and ozonesonde trends in the lower to middle stratosphere in northern midlatitudes.

- The total ozone and the vertical profile trends derived for the northern midlatitudes are consistent with each other over the periods studied.

- Most of the midlatitude column ozone decline during the last two decades arose because of depletion in the lower stratosphere. That region is influenced by local chemical ozone loss that is enhanced by volcanic aerosol, and by transport from other regions. The vertical, latitudinal, and seasonal characteristics of the depletion of midlatitude ozone are broadly consistent with the understanding that halogens are the primary cause. The expected low ozone amounts in the midlatitude lower stratosphere following the Mt. Pinatubo eruption further strengthened the connection between ozone destruction and anthropogenic chlorine.

- Models that represent processes affecting ozone are able to calculate variations in ozone abundances that are broadly consistent with the observed midlatitude column ozone trend as well as the response to volcanic enhancement of stratospheric sulfate aerosol. In particular, models reproduce the lower ozone abundances observed immediately following Mt. Pinatubo and the subsequent increases as the aerosol disappeared.

- Current two-dimensional (2-D) assessment models that allow for the observed build-up of stratospheric chlorine calculate reductions in ozone that are in good quantitative agreement with the altitude and latitude dependence of the measured decline in upper stratospheric ozone during the past several decades. This clearly confirms the hypothesis put forth in 1974 that release of CFCs to the atmosphere would lead to a significant reduction of upper stratospheric ozone, with the peak percentage decline occurring around 40 km.

- Comparison of recent observations and model results shows that the overall partitioning of reactive nitrogen and chlorine species is well understood for the upper stratosphere. The previously noted discrepancy for the chlorine monoxide/hydrogen chloride (ClO/HCl) ratio has been resolved based on new kinetic information. Balloonborne observations of OH and hydroperoxyl radicals ($HO_2$) agree well with theory, but satellite and ground-based observations of these species exhibit systematic differences compared with model calculations.

- An improved understanding of the relevant kinetic processes has resulted in a close balance between the calculated production and loss of ozone at 40 km (i.e., the long-standing difference between calculated and observed ozone abundance has been mostly resolved).

- Constituent measurements show that the tropics are relatively isolated from midlatitudes in the lower stratosphere. The extent of isolation affects the budgets (and lifetimes) of chemical species that affect ozone abundance.

### Ozone in High-Latitude Polar Regions

- The large ozone losses in the Southern Hemisphere polar region during spring continued unabated with approximately the same magnitude and areal extent as in the early 1990s. In Antarctica, the monthly total ozone in September and October has continued to be 40 to 55% below the pre-ozone-hole values of approximately 320 m-atm cm ("Dobson units"), with up to a 70% decrease for periods of a week or so. This depletion occurs primarily over the 12- to 20-km altitude range, with most of the ozone in this layer disappearing during early October. These ozone changes are consistent overall with our understanding of chemistry and dynamics.

- In the Arctic vortex, low column ozone values were observed in the late-winter/spring for 6 out of the last 9 years. Monthly mean values were about 100 m-atm cm below 1960-1970 averages, with shorter-period differences exceeding 200 m-atm cm (equivalent to about 20 to 45% of values found in the 1960s and early 1970s). Within the column, the largest ozone differences were observed in the lower stratosphere.

- Years with large seasonal ozone depletion in the late-winter/spring Arctic are characterized by specific meteorological conditions. These conditions are lower-than-normal late-winter Arctic temperatures, which lead to enhanced activated chlorine, and a more isolated vortex and weaker planetary-wave driving, which lead to less transport of ozone-rich air into the Arctic. Low temperatures, an isolated vortex, and reduced wave driving are coupled processes that occur in concert in the stratosphere. Chemical ozone losses have been identified within the Arctic vortex and are associated with activated chlorine augmented by bromine. The total seasonal chemical ozone losses within the vortex have been estimated to be approximately 100 m-atm cm.

- With the present high abundances of chlorine loading, late-winter/spring Arctic chemical ozone loss is particularly sensitive to meteorological conditions (temperature and vortex isolation) because minimum vortex temperatures are at a critical value in terms of activating chlorine. Winter vortex temperatures in the 1990s have been particularly low. In the absence of low temperatures and an isolated vortex, reduced chemical ozone loss would be expected. However, such a reduced ozone loss would not indicate chemical recovery. The Arctic will remain vulnerable to extreme seasonal loss as long as chlorine loading remains high.

- Chlorine activation in liquid particles in the lower stratosphere (both SSA and liquid PSCs) increases strongly with decreases in temperature and is at least as effective as that on solid particles. Thus, chlorine activation is to a first approximation controlled by temperature and water vapor pressure and only secondarily by particle composition.

- Rapid polar ozone loss requires enhanced chlorine monoxide in the presence of sunlight. Maintenance of elevated ClO in late-winter/spring is dependent upon temperature and requires either repeated heterogeneous processing or denitrification. Since the 1994 Assessment, new understanding has shown that cold liquid aerosol can maintain elevated ClO in non-denitrified air.

### Stratospheric Temperatures

- Radiosonde and satellite observations indicate a decadal cooling trend of the global, annual-mean lower stratosphere (approximately 16 to 21 km) since about 1980. Over the period 1979 to 1994, its amplitude is approximately 0.6°C per decade. At midlatitudes the trend is larger (approximately 0.75°C per decade) and broadly coherent among the various datasets with regard to the magnitude and statistical significance.

- Substantial cooling (approximately 3°C per decade) is observed in the polar lower stratosphere during late-winter/spring in both hemispheres. A decadal-scale cooling is evident in the Antarctic since the early 1980s and in the Arctic since the early 1990s. However, the dynamical variability is large in these regions, particularly in the Arctic, and this introduces difficulties in establishing the statistical significance of trends.

- The vertical profile of the annual-mean stratospheric temperature change observed in the Northern Hemisphere midlatitudes is robust for the 1979-1994 period within the different datasets. The trend consists of an approximately 0.75°C per decade cooling of the 15- to 35-km region, a slight reduction in the cooling at about 35 km, and increased cooling with height above 35 km (approximately 2°C per decade at 50 km).

- Model simulations based on known changes in the stratospheric concentrations of various radiatively active species indicate that the depletion of lower stratospheric ozone is the dominant radiative factor in the explanation of the observed global-mean lower stratospheric cooling trends for the period 1979-1990 (approximately 0.5°C per decade). The contribution to these trends from increases in well-mixed greenhouse gases is estimated to be less than one-fourth that due to ozone loss.

- Model simulations indicate that ozone depletion is an important causal factor in the latitude-month pattern of the decadal (1979-1990) lower stratospheric cooling. The simulated lower stratosphere in Northern and Southern Hemisphere midlatitudes and in the Antarctic springtime generally exhibit a statistically significant cooling trend over this period consistent with observations.

- In the middle and upper stratosphere, both the well-mixed greenhouse gases and ozone change contribute in an important manner to the cooling. However, the computed cooling due to these gases underestimates the observed decadal trend.

### Tropospheric Ozone

- Trends in tropospheric ozone since 1970 in the Northern Hemisphere show large regional differences, with increases in Europe and Japan, decreases in Canada, and only small changes in the United States. The trend in Europe since the mid-1980s has reduced to virtually zero (at two recording stations). In the Southern Hemisphere, small increases have now been observed in surface ozone.

- Recent field studies have shown that anthropogenic emissions of ozone precursors (nitrogen oxides, carbon monoxide, and hydrocarbons) lead to large-scale production of ozone, which, through long-range transport, influences the ozone concentration in large regions of the troposphere in both hemispheres. However, significant uncertainties remain in the budget of tropospheric ozone, its precursors, and the chemical and physical processes involved. Large spatial and temporal variability is observed in tropospheric ozone, resulting from important regional differences in the factors controlling its concentration.

- Important improvements in global chemical transport models (CTMs) have allowed better simulations of tropospheric ozone distributions and of ozone perturbations resulting from anthropogenic emissions.

- Considerable progress has been made in testing tropospheric photochemistry through field measurements. Our theoretical understanding of tropospheric OH is nevertheless incomplete, specifically in regard to sources of upper tropospheric OH and polluted conditions.

- Increases in air traffic and the resulting emissions could have impacts on atmospheric chemistry and cloud formation, with implications for the ozone layer and the climate system. The understanding of the effects of aircraft emissions are currently being assessed as part of the Intergovernmental Panel on Climate Change (IPCC) special report *Aviation and the Global Atmosphere: 1999*. Consequently, this topic is not included in the scope of the present Assessment.

### Changes in UV Radiation

- The inverse correlation between ozone column amounts and ultraviolet-B (UV-B) irradiance has been reconfirmed and firmly established by numerous ground-based measurements. The ground-based measurements have increased our understanding of additional effects such as albedo, altitude, clouds and aerosols, and geographic differences on UV irradiance at the Earth's surface.

- A controversy concerning anomalous UV-trend estimates from the Robertson-Berger (RB) meter network located in the continental United States. (1974-1985) has been explained in terms of poor calibration stability. The reanalysis of this U.S. RB-meter dataset shows that the errors are too large for determining UV-irradiance trends over that period.

- Increases in UV-B irradiance (e.g., 1989-1997; 1.5% $yr^{-1}$ at 300 nm, 0.8% $yr^{-1}$ at 305 nm) have been detected with a few ground-based spectroradiometers at midlatitudes (near 40°) and are consistent with expected changes from the decreasing amounts of ozone. Although these UV changes are consistent with those estimated from satellite data, the ground-based data records from suitably stable and calibrated instruments are not yet long enough to determine decadal trends. Local irradiance changes, not seen in the coarse-spatial-resolution satellite data, caused by pollution and aerosols have been detected in both UV-B (280 to 315 nm) and UV-A (315 to 400 nm).

- New satellite estimates of global (±65°) UV irradiance that now include cloud, surface reflectivity, and aerosol effects have been estimated from measured backscattered radiances from the Total Ozone Mapping Spectrometer (TOMS) using radiative transfer models. Climatological maps of UV irradiance can be produced from the daily data. In addition, the satellite data have been used to estimate zonally averaged global and seasonal trends in UV irradiance from 1979 to 1992. For this period, annual erythemal UV-irradiance decadal increases were estimated to be 3.7 ± 3% at 60°N and 3 ± 2.8% at 40°N. Larger decadal increases were observed in the Southern Hemisphere: 3.6 ± 2% at 40°S and 9 ± 6% at 60°S. No statistically significant trends were observed between ±30° latitude. Zonally averaged UV-A irradiances have not changed.

- Current zonal-average UV-irradiance trend estimations from satellite data that include cloud effects are nearly identical to clear-sky estimates. The currently estimated trends are slightly lower than the clear-sky trend estimates in the 1994 Assessment because of the new TOMS retrieval algorithm.

- Instrument intercomparison and newly developed calibration and database centers have improved the quality and availability of ground-based data.

### Changes in Climate Parameters

- Increased penetration of UV radiation to the troposphere as a result of stratospheric ozone depletion influences key photochemical processes in the troposphere. Model results suggest that a 1% decrease in global total ozone leads to a global increase of 0.7 to 1% in globally averaged tropospheric OH, which would affect the lifetimes of several climate-related gases.

- The global average radiative forcing due to changes in stratospheric ozone since the late 1970s, using extrapolations based on the ozone trends reported in the 1994 Assessment for reference, is estimated to be -0.2 ± 0.15 $Wm^{-2}$, which offsets about 30% of the forcing due to increases in other greenhouse gases over the same period. The climatic impact of the slowing of midlatitude trends and the enhanced ozone loss in the Arctic has not yet been assessed. Recovery of stratospheric ozone would reduce the offset to the radiative forcing of the other greenhouse gases. The ozone recovery will therefore lead to a more rapid increase in radiative forcing than would have occurred due to increases in other greenhouse gases alone.

- The global average radiative forcing due to increases in tropospheric ozone since preindustrial times is estimated to be +0.35 ± 0.15 $Wm^{-2}$, which is about 10 to 20% of the forcing due to long-lived greenhouse gases over the same period.

- Coupled ocean-atmosphere general circulation models (GCMs) have been used to calculate the impact of stratospheric ozone loss on the thermal structure of the atmosphere. The calculated altitude of the transition from tropospheric warming to stratospheric cooling due to increases in well-mixed greenhouse gases is in better agreement with observations when ozone depletion is taken into account.

- Radiative forcings and Global Warming Potentials (GWPs) are now available for an expanded set of gases. New categories include fluorinated organic molecules. The CFC-11 radiative forcing has been revised by +12% from the value used since IPCC (1990), primarily because of the use of an improved vertical profile of CFC-11 mixing ratio. This and other updates lead to GWPs relative to $CO_2$ that are typically 20% higher than those in IPCC (1995).

### Future Halogen Changes

- Large reductions in the production and atmospheric release of ozone-depleting substances (ODSs) have been achieved by international regulations (Montreal Protocol and its Amendments and Adjustments). Without such controls, and assuming a (conservative) 3% annual growth rate in production, ODSs would have led to an equivalent effective chlorine loading of around 17 ppb in 2050. The control measures of the original Montreal Protocol (1987) reduce this to approximately 9 ppb; the Amendments of London (1990) to about 4.6 ppb; and the Amendments of Copenhagen (1992) to approximately 2.2 ppb (but with stratospheric halogen loading increasing again in the second half of the 21st century). The Adjustments of Vienna (1995) and the Amendments of Montreal (1997) further reduce this to about 2.0 ppb (approximately the 1980 abundance) around the year 2050.

- Stratospheric halogen loading lags tropospheric loading by up to 6 years. Given that tropospheric halogen loading peaked around 1994 and assuming a scenario with a 3-yr lag time, the equivalent effective stratospheric chlorine loading is estimated to have peaked in 1997, at an abundance 1.7 times higher than in 1980. If annual ozone trends observed in the 1980s are attributed solely to these halogen increases, the peak ozone reductions in 1997, relative to 1980, are estimated to be about 5% at 45°N and 6% at 45°S. The corresponding increases in erythemally weighted UV radiation in 1997 are estimated to be 5% at 45°N and 8% at 45°S relative to the 1980 values.

### Recovery of the Ozone Layer

- In the absence of other changes, stratospheric ozone abundances should rise in the future as the halogen loading falls in response to regulation. However, the future behavior of ozone will also be affected by the changing atmospheric abundances of methane ($CH_4$), nitrous oxide ($N_2O$), water vapor ($H_2O$), sulfate aerosol, and changing climate. Thus, for a given halogen loading in the future, the atmospheric ozone abundance may not be the same as found in the past for that same halogen loading.

- Several two-dimensional models were used to look at the response of ozone to past and future changes in atmospheric composition. Future global ozone abundances are predicted to recover only slowly toward their 1980 values. The return toward 1980 ozone values in the models depends sensitively on the emission scenarios used. The $CH_4$ scenario used here has a lower growth rate than in previous assessments, which slows the modeled ozone recovery significantly. Understanding the methane trend is an important priority for understanding the future ozone recovery.

- Temperatures in the Arctic winter lower stratosphere are generally close to the threshold for substantial chlorine activation, making Arctic ozone particularly sensitive to small changes in temperature (e.g., cooling of the lower stratosphere by changes in greenhouse gases). Preliminary calculations with coupled chemistry/climate models suggest that recovery in the Arctic could be delayed by this cooling and, because of the large natural variability, recovery will be difficult to detect unambiguously until well into the next century.

- The detection of the onset of ozone recovery from halogen-induced depletion should be possible earlier in the Antarctic than in the Arctic or globally because there is less variability in the ozone loss in the Antarctic. Estimates of the timing of the detection of the onset of ozone recovery are uncertain. However, it is clear that unambiguous detection of the beginning of recovery will be delayed beyond the maximum loading of stratospheric halogens.

## Implications for Policy Formulation

The results from more than two decades of research have provided a progressively better understanding of the interaction of human activities and the chemistry and physics of the global atmosphere. New policy-relevant insights to the roles of trace atmospheric constituents have been conveyed to decision-makers through the international state-of-the-understanding assessment process. This information has served as a key input to policy decisions by governments, industry, and other organizations worldwide to limit the anthropogenic emissions of gases that cause environmental degradation: (1) the 1987 Montreal Protocol on ozone-depleting substances, and its subsequent Amendments and Adjustments, and (2) the 1997 Kyoto Protocol on substances that alter the radiative forcing of the climate system.

The research findings that are summarized above are of direct interest and significance as scientific input to governmental, industrial, and other policy decisions associated with the Montreal Protocol (ozone layer) and the Kyoto Protocol (climate change):

- **The Montreal Protocol is working.** Global observations have shown that the combined abundance of anthropogenic chlorine-containing and bromine-containing ozone-depleting substances in the lower atmosphere peaked in 1994 and has now started to decline. One measure of success of the Montreal Protocol and its subsequent Amendments and Adjustments is the forecast of "the world that was avoided" by the Protocol:

  - The abundance of ozone-depleting gases in 2050, the approximate time at which the ozone layer is now projected to recover to pre-1980 levels, would be at least 17 ppb of equivalent effective chlorine (this is based on the conservative assumption of a 3% per annum growth in ozone-depleting gases), which is about 5 times larger than today's value.

  - Ozone depletion would be at least 50% at midlatitudes in the Northern Hemisphere and 70% at midlatitudes in the Southern Hemisphere, about 10 times larger than today.

  - Surface UV-B radiation would at least double at midlatitudes in the Northern Hemisphere and quadruple at midlatitudes in the Southern Hemisphere compared with an unperturbed atmosphere. This compares to the current increases of 5% and 8% in the Northern and Southern Hemispheres, respectively, since 1980.

  Furthermore, all of the above impacts would have continued to grow in the years beyond 2050. It is important to note that, while the provisions of the original Montreal Protocol in 1987 would have lowered the above growth rates, recovery (i.e., an improving situation) would have been impossible without the Amendments and Adjustments (London, 1990; Copenhagen, 1992; and Vienna, 1995).

- **The ozone layer is currently in its most vulnerable state.** Total stratospheric loading of ozone-depleting substances is expected to maximize before the year 2000. All other things being equal, the current ozone losses (relative to the values observed in the 1970s) would be close to the maximum. These are:

  - about 6% at Northern Hemisphere midlatitudes in winter/spring;
  - about 3% at Northern Hemisphere midlatitudes in summer/fall;
  - about 5% at Southern Hemisphere midlatitudes on a year-round basis;
  - about 50% in the Antarctic spring; and
  - about 15% in the Arctic spring.

  Such changes in ozone are predicted to be accompanied by increases in surface erythemal radiation of 7, 4, 6, 130, and 22%, respectively, if other influences such as clouds remain constant. It should be noted that these values for ozone depletion at midlatitudes are nearly a factor of 2 lower than projected in 1994, primarily because the linear trend in ozone observed in the 1980s did not continue in the 1990s. However, springtime depletion of ozone in Antarctica continues unabated at the same levels as observed in the early 1990s, and large depletions of ozone have been observed in the Arctic in most years since 1990, which are characterized by unusually cold and protracted winters.

  Some natural and anthropogenic processes that do not in themselves cause ozone depletion can modulate the ozone loss from chlorine and bromine compounds, in some cases very strongly. For example, in coming decades midlatitude ozone depletion could be enhanced by major volcanic eruptions, and Arctic ozone depletion could be increased by cold polar temperatures, which in turn could be linked to greenhouse gases or to natural temperature fluctuations. On the other hand, increases in methane would tend to decrease chlorine-catalyzed ozone loss.

  The current vulnerability to ozone depletion over the next few decades is primarily due to past use and emissions of the long-lived ozone-depleting substances. The options to reduce this vulnerability over the next two decades are thus rather limited. The main drivers of ozone change could be natural and anthropogenic processes not related to chlorine and bromine compounds, but to which the ozone layer is sensitive because of the elevated abundances of ozone-depleting substances.

- **The ozone layer will slowly recover over the next 50 years.** The stratospheric abundance of halogenated ozone-depleting substances is expected to return to its pre-1980 (i.e., "unperturbed") level of 2 ppb chlorine equivalent by about 2050, assuming full compliance with the Montreal Protocol and its Amendments and Adjustments. The atmospheric abundances of global and Antarctic ozone will start to slowly recover within coming decades toward their pre-1980 levels once the stratospheric abundances of ozone-depleting (halogen) gases start to decrease. However, the future abundance of ozone will be controlled not only by the abundance of halogens, but also by the atmospheric abundances of methane, nitrous oxide, water vapor, and sulfate aerosols and by the Earth's climate. Therefore, for a given halogen loading in the future, atmospheric ozone abundance is unlikely to be the same as found in the past for the same halogen loading.

- **Few policy options are available to enhance the recovery of the ozone layer.** Relative to the current, but not yet ratified, control measures (Montreal, 1997), the equivalent effective chlorine loading above the 1980 level, integrated from now until the 1980 level is re-attained, could be decreased by:

  - 9% by eliminating global Halon-1211 emissions in the year 2000, thus requiring the complete elimination of all new production and destruction of all Halon-1211 in existing equipment;

  - 7% by eliminating global Halon-1301 emissions in the year 2000, thus requiring the complete elimination of all new production and destruction of all Halon-1301 in existing equipment;

- 5% by eliminating the global production of all HCFCs in the year 2004;
- 2.5% by eliminating the global production of all CFCs and carbon tetrachloride in the year 2004;
- 1.6% by reducing the cap on HCFC production in developed countries from 2.8% to 2.0% in the year 2000, by advancing the phase-out from the year 2030 to 2015, and by instituting more rapid intermediate reductions; and
- about 1% by eliminating the global production of methyl bromide beginning in 2004.

These policy actions would advance the date at which the abundance of effective chlorine returns to the 1980 value by 1-3 years. A complete and immediate global elimination of all emissions of ozone-depleting substances would result in the stratospheric halogen loading returning to the pre-1980 values by the year 2033. It should also be noted that if the currently allowed essential uses for metered dose inhalers are extended from the year 2000 to 2004, then the equivalent effective chlorine loading above the 1980 level would increase by 0.3%.

- **Failure to comply with the international agreements of the Montreal Protocol will affect the recovery of the ozone layer.** For example, illegal production of 20-40 ktonnes per year of CFC-12 and CFC-113 for the next 10-20 years would increase the equivalent effective chlorine loading above the 1980 abundance, integrated from now until the 1980 abundance is re-attained, by about 1-4% and delay the return to pre-1980 abundances by about a year.

- **The issues of ozone depletion and climate change are interconnected; hence, so are the Montreal and Kyoto Protocols.** Changes in ozone affect the Earth's climate, and changes in climate and meteorological conditions affect the ozone layer, because the ozone depletion and climate change phenomena share a number of common physical and chemical processes. Hence, decisions taken (or not taken) under one Protocol have an impact on the aims of the other Protocol. For example, decisions made under the Kyoto Protocol with respect to methane, nitrous oxide, and carbon dioxide will affect the rate of recovery of ozone, while decisions regarding controlling HFCs may affect decisions regarding the ability to phase out ozone-depleting substances.

# Frequently Asked Questions about Ozone

Ozone is very rare in our atmosphere, averaging about three molecules of ozone for every 10 million air molecules. In spite of this small amount, ozone plays vital roles in the atmosphere. This appendix to the Executive Summary of the *Scientific Assessment of Ozone Depletion: 1998* provides answers to some of the questions that are most frequently asked about ozone and the changes that have been occurring in recent years. These questions and answers are based on the information presented in this 1998 report, which was prepared by 304 scientists from 35 countries worldwide. Therefore, the information presented here represents the knowledge of a large group of experts from the international scientific community.

Ozone is mainly found in two regions of the Earth's atmosphere. Most ozone (about 90%) resides in a layer that begins between 8 and 18 kilometers (5 and 11 miles) above the Earth's surface and extends up to about 50 kilometers (30 miles). This region of the atmosphere is called the stratosphere. The ozone in this region is commonly known as the ozone layer. The remaining ozone is in the lower region of the atmosphere, which is commonly called the troposphere. The figure below shows an example of how ozone is distributed in the atmosphere.

The ozone molecules in these two regions are chemically identical, because they all consist of three oxygen atoms and have the chemical formula $O_3$. However, they have very different effects on humans and other living beings. Stratospheric ozone plays a beneficial role by absorbing most of the biologically damaging ultraviolet sunlight (called UV-B), allowing only a small amount to reach the Earth's surface. The absorption of ultraviolet radiation by ozone creates a source of heat, which actually forms the stratosphere itself (a region in which the temperature rises as one goes to higher altitudes). Ozone thus plays a key role in the temperature structure of the Earth's atmosphere. Without the filtering action of the ozone layer, more of the Sun's UV-B radiation would penetrate the atmosphere and would reach the Earth's surface. Many experimental studies of plants and animals and clinical studies of humans have shown the harmful effects of excessive exposure to UV-B radiation.

At the Earth's surface, ozone comes into direct contact with life-forms and displays its destructive side. Because ozone reacts strongly with other molecules, high levels of ozone are toxic to living systems. Several studies have documented the harmful effects of ozone on crop production, forest growth, and human health. The substantial negative effects of surface-level tropospheric ozone from this direct toxicity contrast with the benefits of the additional filtering of UV-B radiation that it provides.

The dual role of ozone leads to two separate environmental issues. There is concern about *increases* in ozone in the troposphere. Low-lying ozone is a key component of photochemical smog, a familiar problem in the atmosphere of many cities around the world. Higher

**Atmospheric Ozone**

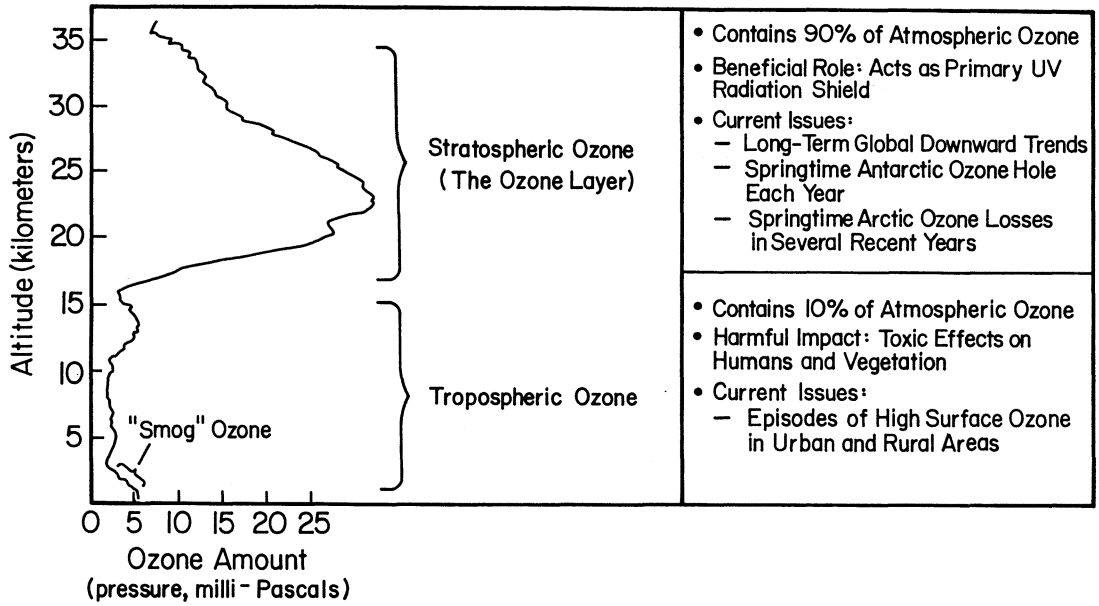

amounts of surface-level ozone are increasingly being observed in rural areas as well.

There is also widespread scientific and public interest and concern about *losses* of ozone in the stratosphere. Ground-based and satellite instruments have measured decreases in the amount of stratospheric ozone in our atmosphere. Over some parts of Antarctica, up to 60% of the total overhead amount of ozone (known as the column ozone) is depleted during Antarctic spring (September-November). This phenomenon is known as the Antarctic ozone hole. In the Arctic polar regions, similar processes occur that have also led to significant chemical depletion of the column ozone during late winter and spring in 6 out of the last 9 years. The ozone loss from January through late March has been typically 20-25%, and shorter-period losses have been higher, depending on the meteorological conditions encountered in the Arctic stratosphere. Smaller, but still significant, stratospheric ozone decreases have been seen at other, more-populated regions of the Earth. Increases in surface UV-B radiation have been observed in association with local decreases in stratospheric ozone, from both ground-based and satellite-borne instruments.

The scientific evidence, accumulated over more than two decades of study by the international research community, has shown that human-produced chemicals are responsible for the observed depletions of the ozone layer. The ozone-depleting compounds contain various combinations of the chemical elements chlorine, fluorine, bromine, carbon, and hydrogen and are often described by the general term halocarbons. The compounds that contain only chlorine, fluorine, and carbon are called chlorofluorocarbons, usually abbreviated as CFCs. CFCs, carbon tetrachloride, and methyl chloroform are important human-produced ozone-depleting gases that have been used in many applications including refrigeration, air conditioning, foam blowing, cleaning of electronics components, and as solvents. Another important group of human-produced halocarbons is the halons, which contain carbon, bromine, fluorine, and (in some cases) chlorine and have been mainly used as fire extinguishants. Governments have decided to eventually discontinue production of CFCs, halons, carbon tetrachloride, and methyl chloroform (except for a few special uses), and industry has developed more "ozone-friendly" substitutes.

Two responses are natural when a new problem has been identified: cure and prevention. When the problem is the destruction of the stratospheric ozone layer, the corresponding questions have been the following ones: Can we repair the damage already done? How can we prevent further destruction? Remedies have been investigated that could (1) remove CFCs selectively from the atmosphere, (2) intercept ozone-depleting chlorine before much depletion has taken place, or (3) replace the ozone lost in the stratosphere (perhaps by shipping the ozone from cities that have too much smog or by making new ozone). However, because ozone reacts strongly with other molecules, it is too unstable to be made elsewhere (e.g., in the smog of cities) and transported to the stratosphere. Considering the huge volume of the Earth's atmosphere and the magnitude of global stratospheric ozone depletion, the suggested remedies quickly become much too expensive, too energy consuming, impractical, and potentially damaging to the global environment.

Repair involves the internationally agreed-upon Montreal Protocol and its Amendments and Adjustments. This agreement regulates the production of CFCs and other ozone-depleting substances. Production of the most damaging ozone-depleting substances was eliminated, except for a few critical uses, by 1996 in developed countries and will be eliminated by 2010 in developing countries. As a result, the total concentration of chlorine in the lower atmosphere that can be carried to the stratosphere has peaked already. The concentrations in the stratosphere will likely peak by the end of this decade and then will start to decrease slowly as natural processes remove the ozone-depleting substances. All other things being equal, and with adherence to the international agreements, the ozone layer is expected to recover over the next 50 years or so.

# How Can Chlorofluorocarbons (CFCs) Get to the Stratosphere If They're Heavier than Air?

CFCs reach the stratosphere because the Earth's atmosphere is always in motion and mixes the chemicals added into it.

CFC molecules are indeed several times heavier than air. Nevertheless, thousands of measurements from balloons, aircraft, and satellites demonstrate that the CFCs are actually present in the stratosphere. This is because winds and other air motions mix the atmosphere to altitudes far above the top of the stratosphere much faster than molecules can settle according to their weight. Gases such as CFCs that do not dissolve in water and that are relatively unreactive in the lower atmosphere are mixed relatively quickly and therefore reach the stratosphere regardless of their weight.

Measured changes in the concentration of constituents versus altitude teach us more about the fate of compounds in the atmosphere. For example, the two gases carbon tetrafluoride ($CF_4$, produced mainly as a by-product of the manufacture of aluminum) and CFC-11 ($CCl_3F$, used in a variety of human activities) are both heavier than air.

Carbon tetrafluoride is completely unreactive at altitudes up to at least 50 kilometers in the atmosphere. Measurements show it to be nearly uniformly distributed throughout the atmosphere (as illustrated in the figure below, the abundance of $CF_4$ is nearly the same at all altitudes where measurements have been made). There have been measurements over the past two decades of several other completely unreactive gases, both lighter than air (neon) and heavier than air (argon and krypton), that show that they also mix upward through the stratosphere regardless of their weight.

CFC-11 is unreactive in the lower atmosphere (below about 15 kilometers) and is similarly uniformly mixed there, as shown in the figure. However, the abundance of CFC-11 decreases as the gas reaches higher altitudes, because it is broken down by high-energy solar ultraviolet radiation. Chlorine released from this breakdown of CFC-11 and other CFCs remains in the stratosphere for several years, where every chlorine atom destroys many thousands of molecules of ozone.

**Atmospheric Measurements of CFC-11 and $CF_4$**

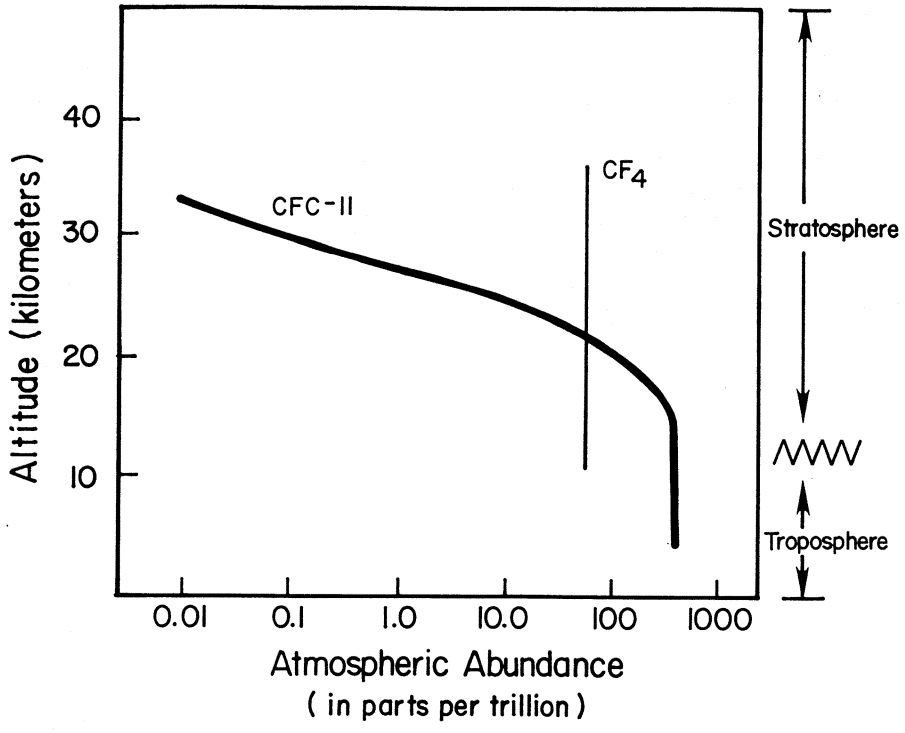

# What is the Evidence that Stratospheric Ozone is Destroyed by Chlorine and Bromine?

Numerous laboratory investigations and analyses of worldwide measurements made in the stratosphere have demonstrated that chlorine- and bromine-containing chemicals destroy ozone molecules.

Research studies in the laboratory show that chlorine (Cl) reacts very rapidly with ozone. They also show that the reactive chemical chlorine monoxide (ClO) formed in that reaction can undergo further processes that regenerate the original chlorine, allowing the sequence to be repeated very many times (a chain reaction). Similar reactions also take place between bromine and ozone.

But do these ozone-destroying reactions occur in the "real world"? All the accumulated scientific experience demonstrates that the same chemical reactions do take place in nature. Many other reactions (including those of other chemical species) are often also taking place simultaneously in the stratosphere. This makes the connections among the changes difficult to untangle. Nevertheless, whenever chlorine (or bromine) and ozone are found together in the stratosphere, the ozone-destroying reactions are taking place.

Sometimes a small number of chemical reactions are so dominant in the natural circumstance that the connections are almost as clear as in laboratory experiments. Such a situation occurs in the Antarctic stratosphere during the springtime formation of the ozone hole. Independent measurements made by instruments from the ground and from balloons, aircraft, and satellites have provided a detailed understanding of the chemical reactions in the Antarctic stratosphere. Large areas reach temperatures so low (less than -80°C, or -112°F) that stratospheric clouds form, which is a rare occurrence, except during the polar winters. These polar stratospheric clouds allow chemical reactions that transform chlorine species from forms that do *not* cause ozone depletion into forms that do cause ozone depletion. Among the latter is chlorine monoxide, which initiates ozone destruction in the presence of sunlight. The amount of reactive chlorine in such regions is therefore much higher than that observed in the middle latitudes, which leads to much faster chemical ozone destruction. The chemical reactions occurring in the presence of these clouds are now well understood from studies under laboratory conditions that mimic those found naturally in the atmosphere.

Scientists have repeatedly observed a large number of chemical species over Antarctica since 1986. Among the chemicals measured were ozone and chlorine monoxide, which is the reactive chemical identified in the laboratory as one of the participants in the ozone-destroying chain reactions. The satellite maps shown in the figure below relate the accumulation of chlorine monoxide observed over Antarctica and the subsequent ozone depletion that occurs rapidly in a few days over very similar areas.

Similar reactions involving chlorine and bromine have also been shown to occur during winter and spring in the Arctic polar regions, which leads to some chemical depletion of ozone in that region. Because the Arctic is not usually as persistently cold as the Antarctic, fewer stratospheric clouds form, and therefore there is less ozone depletion in the Arctic, which is the subject of a later question.

**Chlorine Monoxide and the Antarctic Ozone Hole: Late August 1996**

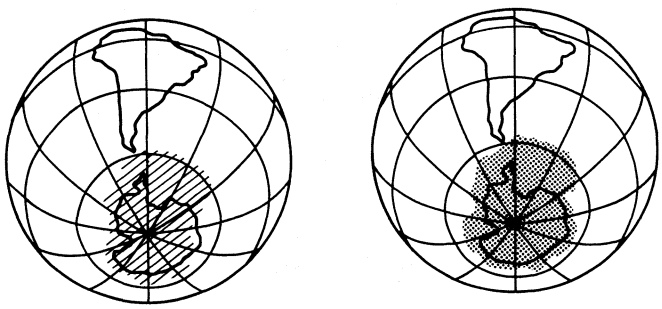

Region of
High Chlorine Monoxide (ClO)

Region of
Low Ozone ($O_3$)

# Does Most of the Chlorine in the Stratosphere Come from Human or Natural Sources?

Most of the chlorine in the stratosphere is there as a result of human activities, as the figure below illustrates.

Many compounds containing chlorine are released at the ground. Those that dissolve in water cannot reach stratospheric altitudes in significant amounts because they are "washed out" of the atmosphere in rain or snow. For example, large quantities of chlorine are released from evaporated ocean spray as sea salt (sodium chloride) particles. However, because sea salt dissolves in water, this chlorine is taken up quickly in clouds or in ice, snow, or rain droplets and does not reach the stratosphere. Another ground-level source of chlorine is from its use in swimming pools and as household bleach. When released, this chlorine is rapidly converted to forms that dissolve in water and therefore are removed from the lower atmosphere. Such chlorine never reaches the stratosphere in significant amounts. Volcanoes can emit large quantities of hydrogen chloride, but this gas is rapidly converted to hydrochloric acid, which dissolves in rain water, ice, and snow and does not reach the stratosphere. Even in explosive volcanic plumes that rise high in the atmosphere, nearly all of the hydrogen chloride is removed by precipitation before reaching stratospheric altitudes. Finally, although the exhaust from the Space Shuttle and from some rockets does inject some chlorine directly into the stratosphere, the quantities are very small (less than 1% of the annual input from halocarbons in the present stratosphere).

In contrast, the major ozone-depleting human-produced halocarbons — such as chlorofluorocarbons (CFCs) and carbon tetrachloride ($CCl_4$) — do not dissolve in water, do not react with snow or other natural surfaces, and are not broken down chemically in the lower atmosphere. Therefore, these and other human-produced substances containing chlorine do reach the stratosphere.

Several pieces of evidence combine to establish human-produced halocarbons as the primary source of stratospheric chlorine. First, measurements have shown that the chlorinated species that rise to the stratosphere are primarily manufactured compounds [mainly CFCs, carbon tetrachloride, methyl chloroform, and the hydrochlorofluorocarbon (HCFC) substitutes for CFCs], together with small amounts of hydrochloric acid (HCl) and methyl chloride ($CH_3Cl$), which are partly natural in origin. Second, researchers have measured nearly all known gases containing chlorine in the stratosphere. They have found that the emissions of the human-produced halocarbons, plus the much smaller contribution from natural sources, could account for all of the stratospheric chlorine. Third, the *increase* in total stratospheric chlorine measured between 1980 and 1998 corresponds to the known increases in concentrations of human-produced halocarbons during that time.

**Primary Sources of Chlorine Entering the Stratosphere in the Early 1990s**

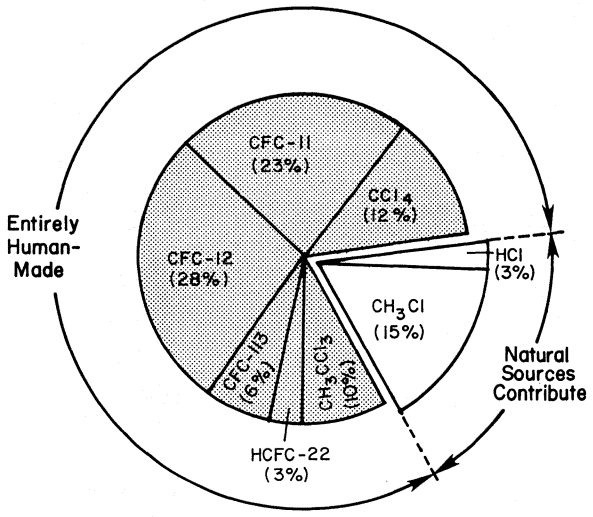

# Can Natural Changes Such As the Sun's Output and Volcanic Eruptions Be Responsible for the Observed Changes in Ozone?

Although there are natural forces that cause fluctuations in ozone amounts, there is no evidence that natural changes are contributing significantly to the observed long-term trend of decreasing ozone.

The formation of stratospheric ozone is initiated by ultraviolet (UV) light coming from the Sun. As a result, the Sun's output affects the rate at which ozone is produced. The Sun's energy release (both as UV light and as charged particles such as electrons and protons) does vary, especially over the well-known 11-year sunspot cycle. Observations over several solar cycles (since the 1960s) show that total global ozone levels vary by 1-2% from the maximum to the minimum of a typical cycle. However, changes in the Sun's output cannot be responsible for the observed long-term changes in ozone, because the ozone downward trends are much larger than 1-2%. As the figure below shows, since 1978 the Sun's energy output has gone through maximum values in about 1980 and 1991 and minimum values in about 1985 and 1996. It is now increasing again toward its next maximum around the year 2002. However, the trend in ozone was downward throughout that time. The ozone trends presented in this and previous international scientific assessments have been obtained by evaluating the long-term changes in ozone after accounting for the solar influence (as has been done in the figure below).

Major, explosive volcanic eruptions can inject material directly into the ozone layer. Observations and model calculations show that volcanic particles cannot on their own deplete ozone. It is only the interaction of human-produced chlorine with particle surfaces that enhances ozone depletion in today's atmosphere.

Specifically, laboratory measurements and observations in the atmosphere have shown that chemical reactions on and within the surface of volcanic particles injected into the lower stratosphere lead to enhanced ozone destruction by increasing the concentration of chemically active forms of chlorine that arise from the human-produced compounds like the chlorofluorocarbons (CFCs). The eruptions of Mt. Agung (1963), Mt. Fuego (1974), El Chichón (1982), and particularly Mt. Pinatubo (1991) are examples. The eruption of Mt. Pinatubo resulted in a 30- to 40-fold increase in the total surface area of particles available for enhancing chemical reactions. The effect of such natural events on the ozone layer is then dependent on the concentration of chlorine-containing molecules and particles available in the stratosphere, in a manner similar to polar stratospheric clouds. Because the particles are removed from the stratosphere in 2 to 5 years, the effect on ozone is only temporary, and such episodes cannot account for observed long-term changes. Observations and calculations indicate that the record-low ozone levels observed in 1992-1993 reflect the importance of the relatively large number of particles produced by the Mt. Pinatubo eruption, coupled with the relatively higher amount of human-produced stratospheric chlorine in the 1990s compared to that at times of earlier volcanic eruptions.

**Global Ozone Trend, Major Volcanic Eruptions, and Solar Cycles**

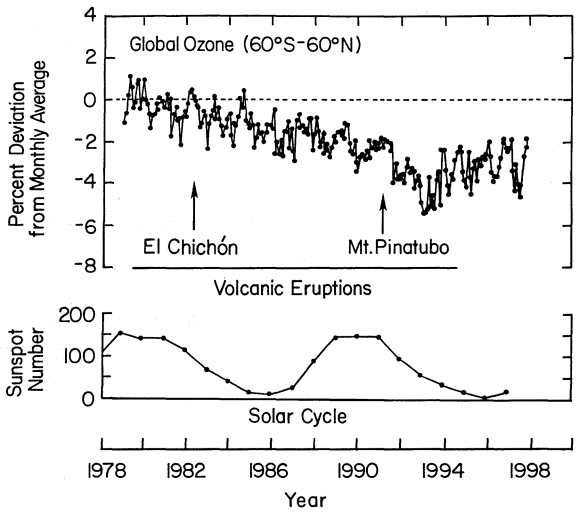

# When Did the Antarctic Ozone Hole First Appear?

The springtime Antarctic ozone hole is a new phenomenon that appeared in the early 1980s.

The observed average amount of ozone during September, October, and November over the British Antarctic Survey station at Halley, Antarctica, first revealed notable decreases in the early 1980s, compared with the preceding data obtained starting in 1957. The ozone hole is formed each year when there is a sharp decline (currently up to 60%) in the total ozone over most of Antarctica for a period of about three months (September-November) during spring in the Southern Hemisphere. Late-summer (January-March) ozone amounts show no such sharp decline in the 1980s and 1990s. Observations from three other stations in Antarctica and from satellite-based instruments reveal similar decreases in springtime amounts of ozone overhead. Balloonborne ozone instruments show dramatic changes in the way ozone is distributed with altitude. As the figure below from the Syowa site shows, almost all of the ozone is now depleted at some altitudes as the ozone hole forms each springtime, compared to the normal ozone profile that existed before 1980. As explained in an earlier question (page *xxx*), the ozone hole has been shown to result from destruction of stratospheric ozone by gases containing chlorine and bromine, whose sources are mainly human-produced halocarbon gases.

Before the stratosphere was affected by human-produced chlorine and bromine, the naturally occurring springtime ozone levels over Antarctica were about 30-40% lower than springtime ozone levels over the Arctic. This natural difference between Antarctic and Arctic conditions was first observed in the late 1950s by Dobson. It stems from the exceptionally cold temperatures and different winter wind patterns within the Antarctic stratosphere as compared with the Arctic. This is not at all the same phenomenon as the marked downward trend in ozone over Antarctica in recent years.

Changes in stratospheric meteorology cannot explain the ozone hole. Measurements show that wintertime Antarctic stratospheric temperatures of past decades had not changed prior to the development of the ozone hole each September. Ground, aircraft, and satellite measurements have provided, in contrast, clear evidence of the importance of the chemistry of chlorine and bromine originating from human-made compounds in depleting Antarctic ozone in recent years.

**Springtime Depletion of the Ozone Layer over Syowa, Antarctica**

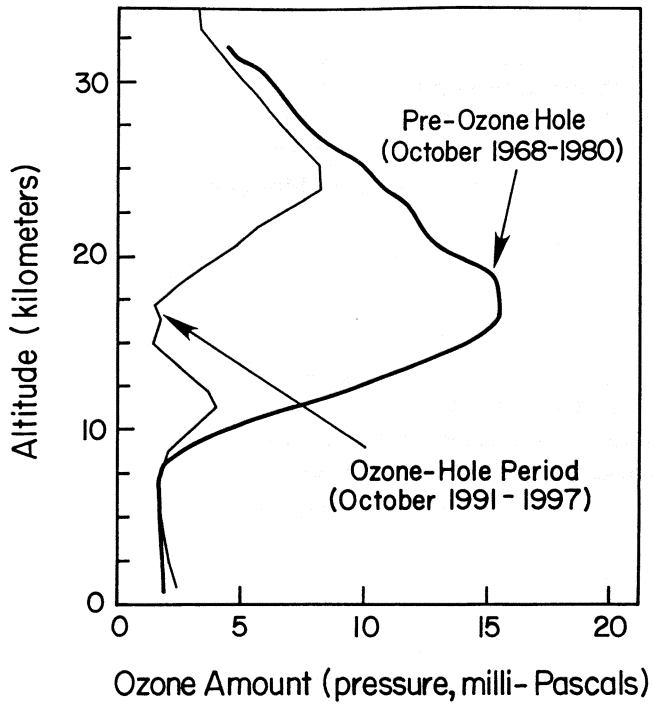

# Why Has an Ozone Hole Appeared over Antarctica When CFCs and Halons Are Released Mainly in the Northern Hemisphere?

The Earth's atmosphere is continuously stirred over the globe by winds. As a result, ozone-depleting gases get mixed throughout the atmosphere, including Antarctica, regardless of where they are emitted. The special meteorological conditions in Antarctica cause these gases to be more effective there in depleting ozone compared to anywhere else.

Human emissions of chlorofluorocarbons (CFCs) and halons (bromine-containing gases) have occurred mainly in the Northern Hemisphere. About 90% have been released in the latitudes corresponding to Europe, Russia, Japan, and North America. Gases such as CFCs and halons, which are insoluble in water and relatively unreactive, are mixed within a year or two throughout the lower atmosphere. The CFCs and halons in this well-mixed air rise from the lower atmosphere into the stratosphere mainly in tropical latitudes. Winds then move this air poleward—both north and south—from the tropics, so that air throughout the global stratosphere contains nearly equal amounts of chlorine and bromine.

In the Southern Hemisphere, the South Pole is part of a very large land mass (Antarctica) that is completely surrounded by ocean. This symmetry is reflected in the meteorological conditions that allow the formation in winter of a very cold region in the stratosphere over the Antarctic continent, isolated by a band of strong winds circulating around the edge of that region. The very low stratospheric temperatures lead to the formation of clouds (polar stratospheric clouds) that are responsible for chemical changes that promote production of chemically active chlorine and bromine. This chlorine and bromine activation then leads to rapid ozone loss when sunlight returns to Antarctica in September and October of each year, which then results in the Antarctic ozone hole. As the figure below depicts, the magnitude of the ozone loss has generally grown through the 1980s as the amount of human-produced ozone-depleting compounds has grown in the atmosphere.

Similar conditions do not exist over the Arctic. The wintertime temperatures in the Arctic stratosphere are not persistently low for as many weeks as over Antarctica, which results in correspondingly less ozone depletion in the Arctic (see the next question).

**Schematic of the Growth of the Antarctic Ozone Hole**

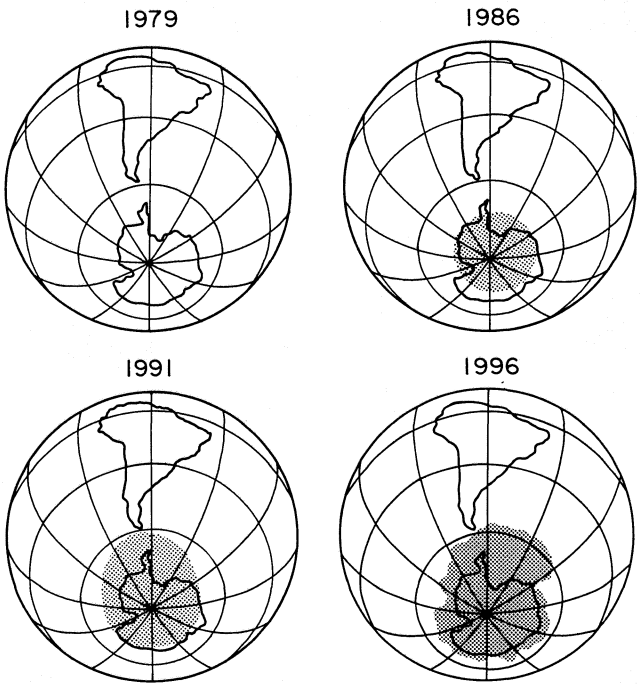

# Is There an Ozone Hole over the Arctic?

Significant reductions in ozone content in the stratosphere above the Arctic have been observed during the late winter and early spring (January-March) in 6 of the last 9 years. However, these reductions, typically 20-25%, are much smaller than those observed currently each spring over the Antarctic (the ozone hole).

The difference between ozone content in the two polar regions (see figure below) is caused by dissimilar weather patterns. The Antarctic continent is a very large land mass surrounded by oceans. This symmetrical condition produces very low stratospheric temperatures within a meteorologically isolated region, the so-called polar vortex, which extends from about 65°S to the pole. The cold temperatures lead in turn to the formation of clouds, known as polar stratospheric clouds. These clouds provide surfaces that promote production of forms of chlorine and bromine that are chemically active and can rapidly destroy ozone. The conditions that maintain elevated levels of chemically active chlorine and bromine persist into September and October in Antarctica, when sunlight returns over the region to initiate ozone depletion.

The winter meteorological conditions in the Northern Hemisphere, just like in the Southern Hemisphere, lead to the formation of an isolated region bounded by strong winds, in which the temperature is also cold enough for polar stratospheric clouds to form. However, the geographic symmetry about the North Pole is less than about the South Pole. As a result, large-scale weather systems disturb the wind flow, making it less stable over the Arctic region than over the Antarctic continent. These disturbances prevent the temperature in the Arctic stratosphere from being as cold as in the Antarctic stratosphere, and fewer polar stratospheric clouds are therefore formed. Nevertheless, chemically active chlorine and bromine compounds are also formed over the Arctic, as they are over Antarctica, from reactions at the surface of the clouds. But the cold conditions rarely persist into March, when sufficient sunlight is available to initiate large ozone depletion.

In recent years, there has been a string of unusually cold winters in the Arctic, compared with those in the preceding 30 years. The cold and persistent conditions have led to enhanced ozone depletion, because the atmospheric concentrations of ozone-depleting gases have also been relatively large during these years. However, the cause of the observed change in meteorological conditions is not yet understood. Such conditions might persist over the coming years, further enhancing ozone depletion. But it is also possible that, in the next few years, they could revert to conditions characteristic of a decade ago. In the latter case, chemical ozone depletion in the Arctic would be expected to diminish.

Therefore, although there has been significant ozone depletion in the Arctic in recent years, it is difficult to predict what may lie ahead, because the future climate of the Arctic stratosphere cannot be predicted with confidence.

**A Schematic of the Ozone over the Arctic and Antarctica in 1996**

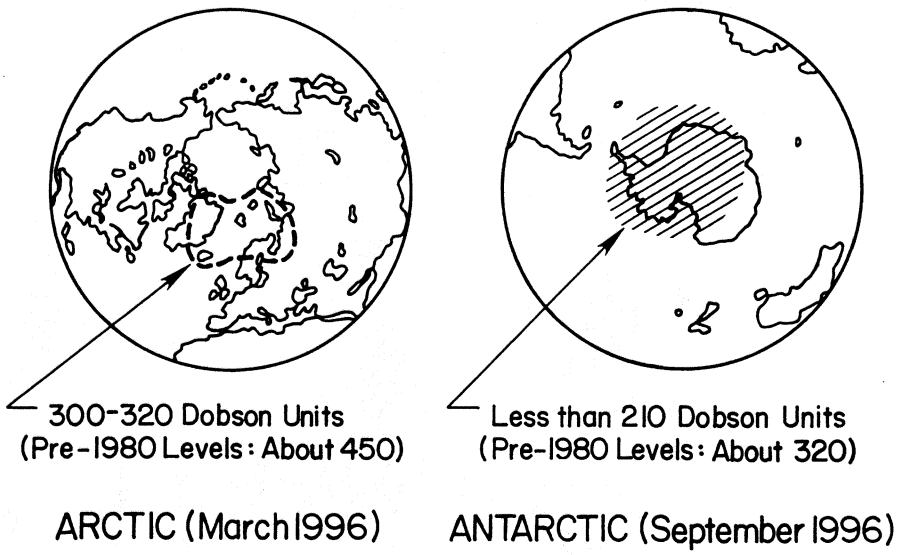

# Is the Depletion of the Ozone Layer Leading to an Increase in Ground-Level Ultraviolet Radiation?

The depletion of the ozone layer leads, on the average, to an increase in ground-level ultraviolet radiation, because ozone is an effective absorber of ultraviolet radiation.

The Sun emits radiation over a wide range of energies, with about 2% in the form of high-energy, ultraviolet (UV) radiation. Some of this UV radiation (UV-B) is especially effective in causing damage to living beings, for example, sunburn, skin cancer, and eye damage to humans. The amount of solar UV radiation received at any particular location on the Earth's surface depends upon the position of the Sun above the horizon, the amount of ozone in the atmosphere, and local cloudiness and pollution. Scientists agree that, in the absence of changes in clouds or pollution, decreases in atmospheric ozone lead to increases in ground-level UV radiation.

The largest decreases in ozone during the past 15 years have been observed over Antarctica, especially during each September and October when the ozone hole forms. During the last several years, simultaneous measurements of UV radiation and total ozone have been made at several Antarctic stations. In the late spring, the biologically damaging ultraviolet radiation in parts of the Antarctic continent can exceed that in San Diego, California, where the Sun is much higher above the horizon.

In areas or the world where smaller ozone depletion has been observed, UV-B increases are more difficult to detect. In particular, detection of trends in UV-B radiation associated with ozone decreases can be further complicated by changes in cloudiness, by local pollution, and by difficulties in keeping the detection instrument in precisely the same operating condition over many years. Prior to the late 1980s, instruments with the necessary accuracy and stability for measurement of small long-term trends in ground-level UV-B were not available. Therefore, the data from urban locations with older, less-specialized instruments provide much less reliable information, especially since simultaneous measurements of changes in cloudiness or local pollution are not available. When high-quality measurements have been made in other areas far from major cities and their associated air pollution, decreases in ozone have regularly been accompanied by increases in UV-B. This is shown in the figure below, where clear-sky measurements performed at six different stations demonstrate that ozone decreases lead to increased UV-B radiation at the surface in amounts that are in good agreement with that expected from calculations (the "model" curve).

**Increases in Erythemal (Sunburning) Ultraviolet Radiation Due to Ozone Decreases**

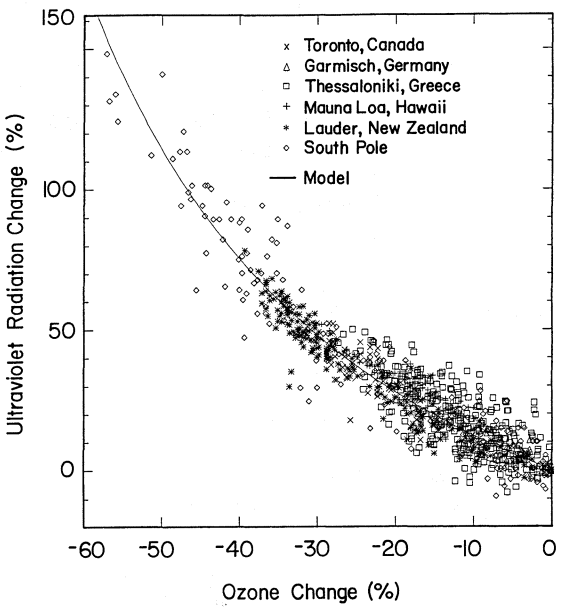

# Does Ozone Depletion Cause Climate Change?

Ozone depletion and climate change are linked in a number of ways, but ozone depletion is not a major cause of climate change.

Atmospheric ozone has two effects on the temperature balance of the Earth. It absorbs solar ultraviolet radiation, which heats the stratosphere. It also absorbs infrared radiation emitted by the Earth's surface, effectively trapping heat in the troposphere. Therefore, the climate impact of changes in ozone concentrations varies with the altitude at which these ozone changes occur. The major ozone losses that have been observed in the lower stratosphere due to the human-produced chlorine- and bromine-containing gases have a cooling effect on the Earth's surface. On the other hand, the ozone increases that are estimated to have occurred in the troposphere because of surface-pollution gases have a warming effect on the Earth's surface, thereby contributing to the "greenhouse" effect.

In comparison to the effects of changes in other atmospheric gases, the effects of both of these ozone changes are difficult to calculate accurately. In the figure below, the upper ranges of possible effects from the ozone changes are indicated by the open bars, and the lower ranges are indicated by the solid bars.

As shown in the figure, the increase in carbon dioxide is the major contributor to climate change. Carbon dioxide concentrations are increasing in the atmosphere primarily as the result of the burning of coal, oil, and natural gas for energy and transportation. The atmospheric abundance of carbon dioxide is currently about 30% above what it was 150 years ago. The relative impacts on climate of various other "greenhouse" gases are also shown on the figure.

There is an additional factor that indirectly links ozone depletion to climate change; namely, many of the same gases that are causing ozone depletion are also contributing to climate change. These gases, such as the chlorofluorocarbons (CFCs), are greenhouse gases, absorbing some of the infrared radiation emitted by the Earth's surface, thereby effectively heating the Earth's surface.

Conversely, changes in the climate of the Earth could affect the behavior of the ozone layer, because ozone is influenced by changes in the meteorological conditions and by changes in the atmospheric composition that could result from climate change. The major issue is that the stratosphere will most probably cool in response to climate change, therefore preserving over a longer time period the conditions that promote chlorine-caused ozone depletion in the lower stratosphere, particularly in polar regions. At present, the amplitude and extent of such a cooling, and therefore the delay in the recovery of the ozone layer, still have to be assessed.

**Relative Importance of the Changes in the Abundance of Various Gases in the Atmosphere**

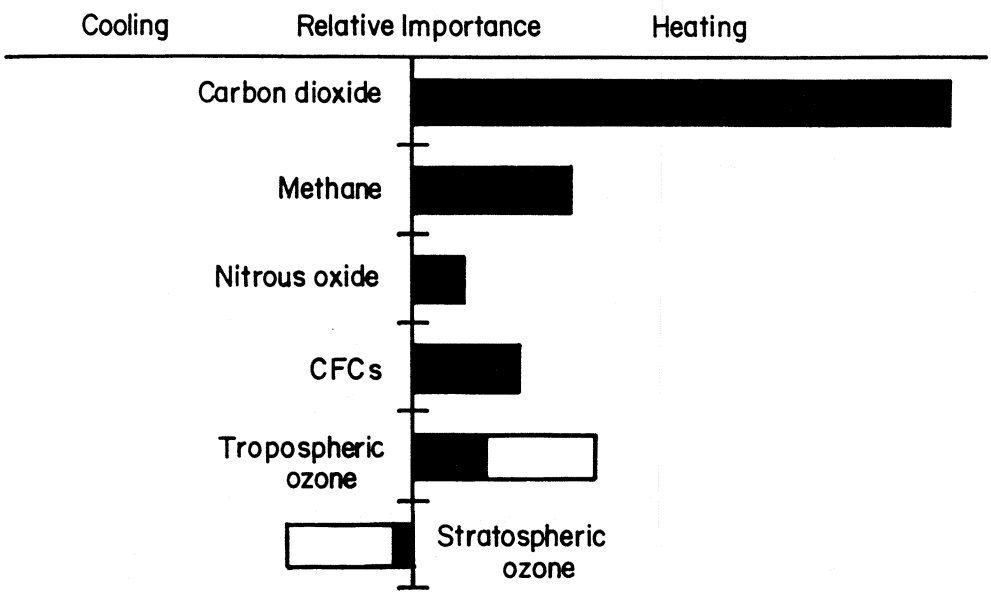

# How Severe Is the Ozone Depletion Now?

Stratospheric ozone depletion, caused by increasing concentrations of human-produced chemicals, has increased since the 1980s. The springtime loss in Antarctica is the largest depletion. Currently, in nonpolar regions, the ozone layer has been depleted up to several percent compared with that of two decades ago.

As the figure below indicates, the magnitude of ozone depletion varies between the regions of the Earth. For example, there has been little or no ozone depletion in the tropics (about 20 degrees north and south of the equator). The magnitude of the depletion also depends on the season. From 1979 to 1997, the observed losses in the amount of ozone overhead have totaled about 5-6% for northern midlatitudes in winter and spring, about 3% for northern midlatitudes in summer and fall, and about 5% year round for southern midlatitudes. Since the early 1980s, the ozone hole has formed over Antarctica during every Southern Hemisphere spring (September to November), in which up to 60% of the total ozone is depleted. Since the early 1990s, ozone depletion has also been observed over the Arctic, with the ozone loss from January through late March typically being 20-25% in most of the recent years. All of these decreases are larger than known long-term natural variations.

The large increase in atmospheric concentrations of human-made chlorine and bromine compounds is responsible for the formation of the Antarctic ozone hole. Furthermore, the overwhelming weight of evidence indicates that those same compounds also play a major role in the ozone depletion in the Arctic and at midlatitudes.

In addition to these long-term changes, transient effects have also been observed in the stratospheric ozone layer following major volcanic eruptions such as Mt. Pinatubo in 1991. During 1992 and 1993, ozone in many locations dropped to record low values. For example, springtime depletions exceeded 20% in some populated northern midlatitude regions, and the levels in the Antarctic ozone hole fell to the lowest values ever recorded. These unusually large, but short-term, ozone decreases of 1992 and 1993 are believed to be related in part to the large amounts of volcanic particles injected into stratosphere, which temporarily increased the ozone depletion caused by human-produced chlorine and bromine compounds, much as polar stratospheric clouds increase these chemicals' effect on ozone depletion in polar regions. Because these particles settle out of the stratosphere within a few years, the ozone concentrations have largely returned to the depleted levels consistent with the downward trend observed before the Mt. Pinatubo eruption. Should a similar eruption occur in the coming decade, ozone losses of the same magnitude might be expected, because the chlorine levels in the stratosphere will still be high.

**Schematic of the North-to-South Ozone Depletion: 1979-1997**

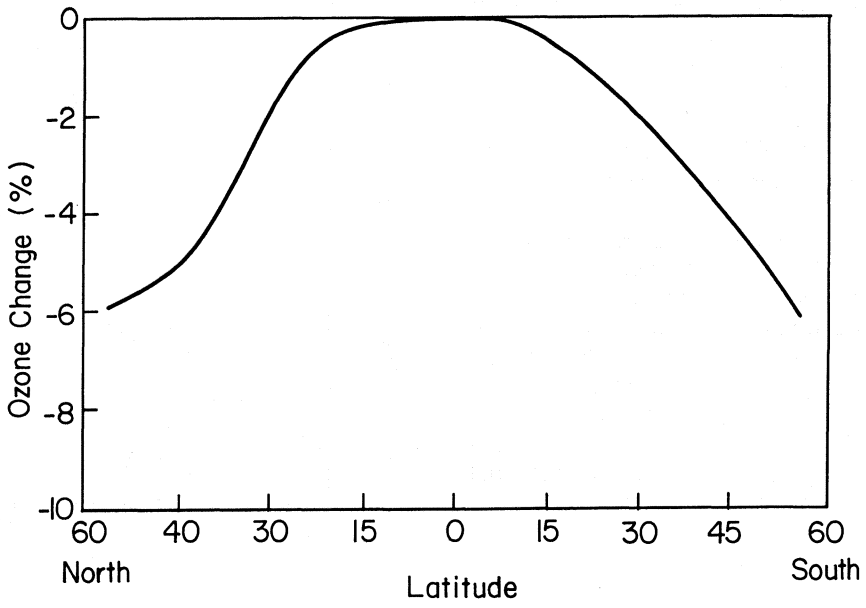

# Is the Ozone Layer Expected to Recover? If So, When?

The ozone depletion caused by human-produced chlorine and bromine compounds is expected to gradually disappear by about the middle of the 21st century as these compounds are slowly removed from the stratosphere by natural processes. This environmental achievement is due to the landmark international agreement to control the production and use of ozone-depleting substances. Full compliance would be required to achieve this expected recovery.

In 1987, the recognition of the potential for chlorine and bromine to destroy stratospheric ozone led to the Montreal Protocol on Substances that Deplete the Ozone Layer, as part of the 1985 Vienna Convention for the Protection of the Ozone Layer, to reduce the global production of ozone-depleting substances. Subsequently, global observations of significant ozone depletion have prompted amendments to strengthen the treaty. The 1990 London Amendment calls for a ban on the production of the most damaging ozone-depleting substances by 2000 in developed countries and 2010 in developing countries. The 1992 Copenhagen Amendment changed the date of the ban to 1996 in developed countries. Further restrictions on ozone-depleting substances have been agreed upon in Vienna (1995) and Montreal (1997).

The figure on the right shows past and projected stratospheric abundances of chlorine and bromine without the Protocol, under the Protocol's original provisions, and under its subsequent agreements. Without the Montreal Protocol and its Amendments, continuing use of chlorofluorocarbons (CFCs) and other ozone-depleting substances would have increased the stratospheric abundances of chlorine and bromine tenfold by the mid-2050s compared with the 1980 amounts. Such high chlorine and bromine abundances would have caused very large ozone losses, which would have been far larger than the depletion observed at present.

In contrast, under the current international agreements that are now reducing the human-caused emissions of ozone-depleting gases, the net tropospheric concentrations of chlorine- and bromine-containing compounds started to decrease in 1995. Because 3 to 6 years are required for the mixing from the troposphere to the stratosphere, the stratospheric abundances of chlorine are starting to reach a constant level and will slowly decline thereafter. With full compliance, the international agreements will eventually eliminate most of the emissions of the major ozone-depleting gases. All other things being constant, the ozone layer would be expected to return to a normal state during the middle of the next century. This slow recovery, as compared with the relatively rapid onset of the ozone depletion due to CFC and bromine-containing halon emissions, is related primarily to the time required for natural processes to eliminate the CFCs and halons from the atmosphere. Most of the CFCs and halons have atmospheric residence times of about 50 to several hundred years.

However, the future state of the ozone layer depends on more factors than just the stratospheric concentrations of human-produced chlorine and bromine. It will also be affected to some extent by the changing atmospheric abundances of several other human-influenced constituents, such as methane, nitrous oxide, and sulfate particles, as well as by the changing climate of the Earth. As a result, the ozone layer is unlikely to be identical to the ozone layer that existed prior to the 1980s. Nevertheless, the discovery and characterization of the issue of ozone depletion from chlorine and bromine compounds and a full global compliance with the international regulations on their emissions will have eliminated what would have been, as the figure illustrates, a major deterioration of the Earth's protective ultraviolet shield.

**Effect of the International Agreements on Ozone-Depleting Stratospheric Chlorine/Bromine**

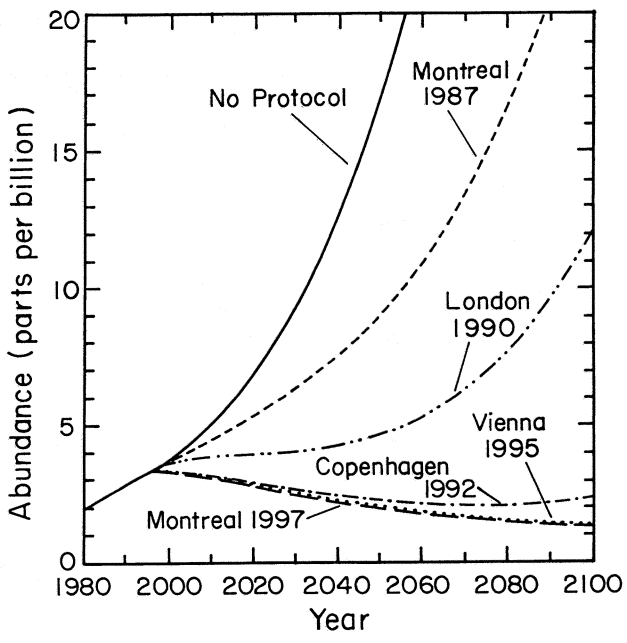

# PART 1

## Halocarbon, Ozone, and Temperature Changes

### Chapter 1
Long-Lived Ozone-Related Compounds

### Chapter 2
Short-Lived Ozone-Related Compounds

### Chapter 3
Global Distributions and Changes in Stratospheric Particles

### Chapter 4
Ozone Variability and Trends

### Chapter 5
Trends in Stratospheric Temperatures

# CHAPTER 1

# Long-Lived Ozone-Related Compounds

**Lead Authors:**
R.G. Prinn
R. Zander

**Coauthors:**
D.M. Cunnold
J.W. Elkins
A. Engel
P.J. Fraser
M.R. Gunson
M.K.W. Ko
E. Mahieu
P.M. Midgley
J.M. Russell III
C.M. Volk
R.F. Weiss

**Contributors:**
D.R. Blake
J.H. Butler
D.W. Fahey
J. Harnisch
D. Hartley
D.F. Hurst
N.B. Jones
M. Maiss
A. McCulloch
S.A. Montzka
D.E. Oram
S.A. Penkett
C.P. Rinsland
R.J. Salawitch
S.M. Schauffler
U. Schmidt
P.G. Simmonds
T.M. Thompson
G.C. Toon

# CHAPTER 1

## LONG-LIVED OZONE-RELATED COMPOUNDS

### Contents

## SCIENTIFIC SUMMARY

Since the previous Assessment (WMO, 1995), significant progress has been achieved in determining and understanding the distributions of long-lived ozone-related gases in both the troposphere and stratosphere. In this chapter, we deal primarily with long-lived halocarbons (chlorofluorocarbons (CFCs), halons, perfluorinated and perchlorinated compounds) and other significant long-lived non-halocarbon species.

- Tropospheric measurements show that:

  (a) International "compliance" with the Montreal Protocol and its Amendments has resulted in the amounts of most CFCs and chlorocarbons in the atmosphere being equal to or lower than amounts that are consistent with the Protocol's provisions regarding production and emission.

  (b) The total amount of organic chlorine ($CCl_y$) contained in long- and short-lived chlorocarbons reached maximum values of $3.7 \pm 0.1$ parts per billion (ppb) between mid-1992 and mid-1994 and is beginning to decrease slowly in the global troposphere. This slowing down and reversal in the growth rate resulted primarily from reduced emissions of methyl chloroform ($CH_3CCl_3$).

  (c) Despite significant reduction in the emission of halons, the total amount of organic bromine in the troposphere continues to rise, largely because of the ongoing growth of Halon-1211 ($CBrClF_2$). Possible causes are releases during the 1990s from the large halon "bank" that accumulated in developed countries during the 1980s and from increased production of Halon-1211 in developing countries. The recent observations of Halon-1211 concentrations are higher and growing faster than concentrations calculated from emissions derived from industry and United Nations Environment Programme (UNEP) data. Halon increases over the next few years could delay the time of the currently expected total organic bromine maximum in the troposphere.

  (d) The amount of nitrous oxide ($N_2O$) in the troposphere continues to increase at 0.2 to 0.3% per year. As concluded in previous assessments, this trend indicates that the global sources exceed the sinks by approximately 30%. The imbalance appears to be caused by anthropogenic sources whose relative strengths remain uncertain.

- Stratospheric measurements reflect the tropospheric chlorocarbon changes with a time delay ranging from 3 to 6 years, depending on latitude and altitude. Assuming the maximum delay, the peak in chlorine loading in the middle stratosphere (and consequently chlorine-catalyzed ozone loss) is expected to be reached around the year 2000. The impact of organic bromine is not going to significantly alter the time of maximum ozone depletion.

  Specifically:

  (a) Space-based measurements of hydrogen chloride (HCl) near the stratopause and of total chlorine throughout the stratosphere are consistent with the amount and rate of change of total $CCl_y$ in the troposphere. The rate of increase of stratospheric chlorine has slowed in recent years.

  (b) The rate of increase of the total amount of inorganic chlorine ($Cl_y$) in the atmosphere obtained by combining HCl and chlorine nitrate ($ClONO_2$) ground-based measurements and a model-computed chlorine monoxide (ClO) background has slowed significantly, from about 3.7% per year in 1991 to 1992 to about 1.8% per year in 1995 to 1996.

(c) The long-term remote monitoring of hydrogen fluoride (HF) near 55 km altitude from space and of total column amounts of HF and carbonyl fluoride ($COF_2$) from the ground, along with the HCl trends, have confirmed that CFC and chlorocarbon compounds included in the Montreal Protocol have been the principal sources of both inorganic fluorine and $Cl_y$ in the stratosphere.

(d) Volcanoes have not contributed significantly in recent decades to the total amount of chlorine in the stratosphere.

- Industrial production, sales data, and end-use modeling indicate that global emissions of the long-lived CFCs (-11, -12, -113, -114, and -115), carbon tetrachloride ($CCl_4$), and Halon-1211 and -1301 ($CBrF_3$) are all in decline. For CFC-12 ($CCl_2F_2$) and Halon-1211, the emissions still exceed their atmospheric removal rates; hence, their concentrations are still increasing.

- Estimations using global tropospheric measurements and atmospheric chemical models show that:

  (a) The CFCs whose emissions are accurately known appear to have atmospheric lifetimes consistent with destruction in the stratosphere being their principal removal mechanism.

  (b) CFC and chlorocarbon emissions inferred from atmospheric observations are consistent, approximately, with independent estimates of emissions based on industrial production and sales data. CFC-113 ($CCl_2FCClF_2$) is an exception: emissions based on atmospheric observations are significantly lower than those calculated by industry.

  (c) While $CCl_4$ in the atmosphere is declining at approximately 0.8% per year, the interhemispheric difference is effectively constant, indicating that there are still significant Northern Hemispheric (NH) emissions. Atmospheric measurements and estimates of developed countries' emissions indicate that developing countries have dominated world releases of $CCl_4$ after 1991. A recent investigation of stratospheric $CCl_4$ observations and some three-dimensional (3-D) model studies suggest that its lifetime is closer to 35 years, instead of the previously reported 42 years; if this shorter lifetime is correct, then larger emissions are indicated, presumably from developing countries.

  (d) Perfluorocarbons (PFCs) and sulfur hexafluoride ($SF_6$) continue to increase in the background atmosphere. They are not ozone depleters but are of potential concern because they are strong absorbers of infrared radiation on a per-molecule basis and, once released, they persist in the atmosphere for millennia.

- Simultaneous determinations of the stratospheric mixing ratio of a species and the age of the air can be used together with tropospheric measurements to estimate steady-state atmospheric lifetimes for species that lack tropospheric sinks. In general, the lifetimes obtained in this way are consistent with the model-derived lifetime ranges and lifetimes based on tropospheric measurements. However, the recommended reference lifetimes for CFC-11 ($CCl_3F$) and $CCl_4$ are approximately 45 and 35 years, respectively, which are shorter than the previously recommended estimates (50 and 42 years, respectively); some recent 3-D models also support these changes. Recommended reference lifetimes for major ozone-depleting source gases discussed in this chapter and also in Chapter 2 are summarized in Table 1-1.

**Table 1-1. Summary of current (WMO, 1998) and previous (WMO, 1995) reference and observed steady-state lifetimes for several ozone-related source species.** Lifetime is defined as the total amount of a compound in the atmosphere divided either by its total rate of removal or by its rate of destruction by tropospheric OH alone (values in parentheses). Additional information on calculated ranges for different models and lifetime-related uncertainties can be found in Tables 1-3, 1-4, 1-5, 1-6, and in Chapter 2 (Tables 2-2, 2-4, and 2-6).

| Industrial Name | Chemical Formula | Lifetime, WMO (1998)[a] (years) | Lifetime, Observed Range (years) | Lifetime, WMO (1995) (years) |
|---|---|---|---|---|
| Nitrous oxide | $N_2O$ | 120 | 75 to 173[d] | 120 |
| CFC-11 | $CCl_3F$ | 45[f] | 29 to 76[e] | 50 |
| CFC-12 | $CCl_2F_2$ | 100 | 77 to 185[e] | 102 |
| CFC-113 | $CCl_2FCClF_2$ | 85 | 54 to 143[d] | 85 |
| Carbon tetrachloride | $CCl_4$ | 35[f] | 21 to 43[d] | 42 |
| H-1211 | $CBrClF_2$ | 11[f] | 10 to 31[d] | 20 |
| H-1301 | $CBrF_3$ | 65 | 60 to 65[g] | 65 |
| Methyl chloroform | $CH_3CCl_3$ | 4.8 (5.7) | 4.5 to 5.1[b] | 5.4 |
| HCFC-22 | $CHClF_2$ | 11.8 (12.3) | 7.0 to 14.4[c] | 13.3 |
| HCFC-141b | $CH_3CCl_2F$ | 9.2 (10.4) | (h) | 9.4 |
| HCFC-142b | $CH_3CClF_2$ | 18.5 (19.5) | (h) | 19.5 |
| HFC-134a | $CH_2FCF_3$ | 13.6 (14.1) | (h) | 14 |
| HFC-23 | $CHF_3$ | 243 (255) | (h) | 250 |
| Methyl chloride | $CH_3Cl$ | ~1.3 (1.3) | (h) | 1.5 |
| Methyl bromide | $CH_3Br$ | 0.7 (1.8) | (h) | 1.3 |
| Methane | $CH_4$ | 8.9[i] (9.3) | (h) | 10 |

[a] The numbers in parentheses represent lifetimes for removal by tropospheric OH scaled to the total atmospheric lifetime of $CH_3CCl_3$ (4.8 years) derived by Prinn *et al.* (1995), and adopting $CH_3CCl_3$ lifetimes for ocean removal of 85 years and stratospheric removal of 45 years (Kaye *et al.*, 1994). Adopting a shorter stratospheric removal time of 37 years (Prinn *et al.*, 1995; see also Volk *et al.*, 1997) yields a lifetime for $CH_3CCl_3$ removal by tropospheric OH of 5.9 years which is within the uncertainty limits of the above (WMO, 1998) reference value.

[b] Prinn *et al.*, 1995.

[c] Miller *et al.*, 1998.

[d] Volk *et al.*, 1997. Note that this analysis gives only stratospheric lifetimes. Additional loss of H-1211 in the troposphere (see Section 1.4.4) reduces its lifetime to 11 years. When considering recently updated emissions of H-1211 (see Figure 1-11) and observations, the Butler *et al.* (1998) lifetime evaluation approach leads to an H-1211 lifetime of 10 years.

[e] For CFC-11, combined range of Volk *et al.* (1997) and updated values from Cunnold *et al.* (1997); for CFC-12, range covered by the central estimates of Volk *et al.* (1997) and updated central estimates from Cunnold *et al.* (1997).

[f] WMO 1998 CFC-11, H-1211, and $CCl_4$ lifetimes are lower than WMO (1995) values to take account of recent estimates based on stratospheric observations and models. Note that some calculations in later chapters were carried out before these WMO (1998) values were finalized and therefore used WMO (1995) values instead.

[g] Butler *et al.*, 1998.

[h] Not available or not applicable.

[i] Lifetime as calculated by Prinn *et al.* (1995). The adjustment time for $CH_4$ recovery would be somewhat longer due to $CH_4$ feedback on CO and OH (WMO, 1995).

## 1.1 INTRODUCTION

A wide range of long- and short-lived trace gases play very significant roles in the atmosphere. These roles include production of nitrogen, chlorine, bromine, and hydrogen free radicals that control catalytic ozone destruction in the stratosphere, and perturbations of the atmospheric infrared (IR) radiative budget that can force climatic change.

These gases are conveniently divided into two classes depending on whether their atmospheric chemical destruction occurs predominantly (or exclusively) in the stratosphere, or predominantly in the troposphere; the former are generally longer-lived than the latter. In this chapter, we focus primarily on those long-lived gases for which stratospheric processes govern their chemical removal. In Chapter 2, gases with major tropospheric sinks (including reaction with hydroxyl free radicals) are discussed. We emphasize, however, that these two classes of gases share many common factors in both their life cycles and effects. Hence these two chapters are closely linked and not merely complementary.

The number of measurements of the atmospheric concentrations of long-lived gases has increased significantly since the previous Assessment (WMO, 1995), at which time a complementary comprehensive review of measurements and lifetimes of the halogenated source gases was also produced (Kaye *et al.*, 1994). Since then, important new remote sensing and in situ sampling datasets have been obtained. In addition to the continuation of ground-based sampling by global networks of stations around the globe that have provided measurements of the temporal evolution of gases in the troposphere, there have been ground-, aircraft-, balloon-, and space-based instruments that have provided complementary views of the total column abundances and vertical distributions of the gaseous sources and sinks of ozone-depleting catalysts on a near-global scale.

Substantial progress in the understanding of the precision and accuracy of measurement techniques has recently resulted from the implementation of intercomparison and independent absolute calibration activities to achieve better accuracy and internal and long-term consistency among a number of databases reported on or referred to in this chapter. A successful example of such activities is the independent development of calibrations in the two major ground-based in situ networks, Advanced Global Atmospheric Gases Experiment (AGAGE) (Prinn *et al.*, 1998) and National Oceanic and Atmospheric Administration-Climate Monitoring and Diagnostics Laboratory (NOAA/CMDL) (Elkins *et al.*, 1998), and the intercomparisons of these and other calibrations in the Nitrous Oxide and Halocarbons Intercomparison Experiment (NOHALICE) (Fraser *et al.*, 1996; Oram *et al.*, 1996; Cunnold *et al.*, 1997; Miller *et al.*, 1998). The general aim of NOHALICE is to compare the trace gas standards (for nitrous oxide ($N_2O$), chlorofluorocarbons (CFCs), hydrochlorofluorocarbons (HCFCs), hydrofluorocarbons (HFCs), halons, perfluorocarbons (PFCs), and other halocarbon species) used in various laboratories around the world making long-term, background measurements of these chemicals. This activity enables datasets for individual species obtained from participating laboratories to be ultimately combined, on a common calibration scale, for subsequent analysis and interpretation. Typical performances achieved within NOHALICE are provided in Section 1.2.1.

Important developments for the upper atmosphere include the Network for the Detection of Stratospheric Change (NDSC), which is a ground-based, long-term, international measuring network specifically designed to make worldwide observations through which changes in the physical and chemical state of the stratosphere can be determined and understood (Kurylo and Solomon, 1990). This dual objective requires high-precision, state-of-the-art measurements of ozone as well as a broad range of chemical species and dynamical tracers that influence ozone chemistry. These measurement requirements have been achieved by properly selecting a suite of primary NDSC instruments (lidars, ultraviolet (UV)-visible spectrometers, Fourier transform infrared (FTIR) instruments, microwave radiometers, balloon sondes, etc.) and establishing documented procedures for instrument- and retrieval algorithm intercomparisons, as well as protocols for archiving "NDSC-quality" data (for additional information, visit the World Wide Web site http://climon.wwb.noaa.gov).

A large amount of information on the vertical distribution of atmospheric compounds has been further acquired since the 1994 Assessment (WMO, 1995) during airplane- and balloon-campaigns, as well as space-based missions, among which the Upper Atmospheric Research Satellite (UARS) (Reber *et al.*, 1993) and the Atmospheric Trace Molecule Spectroscopy (ATMOS) experiment (Kaye and Miller, 1996; Gunson *et al.*, 1996) have provided substantial data of relevance to this

chapter. Assessments of space-based data using nearly coincident measurements with airplane- and balloon-based instruments have contributed to measurement quality control and estimation of accuracy; relevant examples are described later in this chapter.

In the following three sections of this chapter we address primarily the current status of the concentrations, long-term trends, and global halogen loading budgets of halogens based on measurements performed since the 1994 Assessment and, finally, we summarize the recent findings about atmospheric lifetimes for a number of them.

Concentrations of long-lived gases and their trends are discussed for five subclasses, namely, CFCs, chlorobromocarbons including halons, fluorinated compounds ($SF_6$, $CF_4$, etc.), perchlorinated compounds ($CCl_4$), and significant miscellaneous species ($N_2O$, HF, HCl, etc.). In each case, measured behavior in both the troposphere and stratosphere are addressed. Also reviewed is information on the preindustrial abundances of these compounds where available and relevant. The contributions of this ensemble of chemicals to the global budgets of chlorine, bromine, and fluorine are fundamental to quantification of the magnitude and trend of ozone depletion induced by them. These budgets can be elucidated by judicious use of tropospheric and stratospheric observations, reported emissions from industrial and other anthropogenic activity, and fitting of model simulations to observations (by trial and error or preferably optimally).

Deduction of the atmospheric lifetime, defined as the atmospheric content divided by the atmospheric removal rate of the gas, is fundamental to testing chemical theory and to ranking the contributions of each gas to ozone depletion. We discuss lifetime determinations based on three complementary approaches: modeling using laboratory measurements of rate constants and absorption cross sections, estimates using stratospheric and tropospheric measurements, and inverse methods, which optimally fit model simulations to tropospheric measurements. The last approach uses industrial estimates of emissions.

In this chapter, we further seek answers to several key scientific questions. Are observed trends for various gases consistent with expectations based on reported emissions, and are the latter complying with the Montreal Protocol? Has the total atmospheric chlorine and bromine contained in these chemicals peaked? Are tropospheric and stratospheric trends consistent? Are measured concentrations and temporal variations consistent with estimates of industrial emissions and chemical theory? Finally, what are the lifetimes of these gases and what are the major sources of uncertainty in their estimation?

Ground-based stations cited in the chapter, along with their geographic coordinates, are listed in the Appendix of this chapter. Unless otherwise stated, the terms "concentrations," "abundances," "loadings," "mixing ratios," and "volume mixing ratios" refer to concentrations as dry air mole fractions. Acronyms and all species, generally referred to by their chemical formulae, are defined in the appendices of this Assessment report.

## 1.2 CONCENTRATION MEASUREMENTS AND TRENDS

This section updates the review of abundances and trends of CFCs, halons, carbon tetrachloride ($CCl_4$), PFCs, $SF_6$, $N_2O$, and other relevant species compiled by Sanhueza *et al.* (1995) in WMO (1995). Table 1-2 lists the 1992, 1995, and 1996 concentrations and recent growth rates for these long-lived trace gases, as well as for the species from Chapter 2, that make significant contributions to tropospheric budgets of chlorine, bromine, and fluorine.

### 1.2.1 Data Calibration and Intercomparisons

During the past decade, a variety of measurement techniques has been used in various programs to assess the current and past chemical composition of the atmosphere. This has required independent calibration and intercomparison activities to improve absolute accuracy and achieve long-term consistency amongst the respective datasets.

Air samples, collected at clean-air sites, have been used to compare absolute calibrations of $N_2O$ and halocarbon measurements made at a number of international laboratories since the late 1970s (Rasmussen, 1978; Fraser, 1980). Such activities have been expanded significantly by the establishment of the Nitrous Oxide and Halocarbons Intercomparison Experiment (NOHALICE), an International Global Atmospheric Chemistry (IGAC) Project activity. Two types of intercomparison experiments have been conducted within the NOHALICE framework. The first involves the circulation of a common background air sample among participating laboratories for trace gas

**Table 1-2. Global tropospheric concentrations and trends for CFCs, halons, chlorocarbons, HCFCs, HFCs, PFCs, $SF_6$, and $N_2O$.** The 1992 data from the previous (1994) Assessment (Sanhueza *et al.*, 1995) are shown in parentheses. The 1992 data not in parentheses are from this current Assessment. Note the large change in the $CCl_4$ and $CH_3CCl_3$ concentrations for 1992, due to the adoption of new calibration scales in AGAGE ($CH_3CCl_3$, Prinn *et al.*, 1995; $CCl_4$, Simmonds *et al.*, 1998) and smaller changes in the NOAA/CMDL calibration scales for $CCl_2F_2$ and $CCl_4$ (Elkins *et al.*, 1998). The growth rates are the average increase over the period 1995-1996 or from the most recent available data. The relevant references are given in the text.

| Species | Industrial Name | Concentration (ppt) 1992 | 1995 | 1996 | Growth ppt $yr^{-1}$ | Growth % $yr^{-1}$ | Laboratory [d] | Method |
|---|---|---|---|---|---|---|---|---|
| **CFCs** | | | | | | | | |
| $CCl_2F_2$ | CFC-12 | (503) 504 | 524.6 | 529.7 | 5.1±0.5 | 1.0 | AGAGE | in situ |
| | | 505 | 526.7 | 530.4 | 3.7±0.2 | 0.7 | NOAA/CMDL | in situ |
| $CCl_3F$ | CFC-11 | (268) 263 | 264.3 | 263.6 | -0.7±0.3 | -0.3 | AGAGE | in situ |
| | | 271 | 271.4 | 270.7 | -0.7±0.2 | -0.3 | NOAA/CMDL | in situ |
| $CClF_3$ | CFC-13 | 4 | | | 0.2 | 5 | MPAE | flask, NH |
| $CCl_2FCClF_2$ | CFC-113 | (82) 80 | 83.0 | 83.0 | 0.0±0.2 | 0.0 | AGAGE | in situ |
| | | 81 | 84.0 | 84.0 | 0.1±0.1 | 0.1 | NOAA/CMDL | flask |
| $CClF_2CClF_2$ | CFC-114 | (20) 15 | | | 1.2 | 8 | MPAE, UCI, UT | flask, NH |
| $CClF_2CF_3$ | CFC-115 | 5 | | | 0.4 | 8 | MPAE, NCAR | flask, NH |
| **Halons** | | | | | | | | |
| $CBrClF_2$ | H-1211 | (2.5) 2.7 | 3.22 | 3.40 | 0.18±0.03 | 5.4 | NOAA/CMDL | flask |
| | | 2.9 | 3.55 | 3.82 | 0.27±0.02 | 7.3 | UEA | flask, SH |
| $CBrF_3$ | H-1301 | (2.0) 1.9 | 2.27 | 2.29 | 0.02±0.03 | 0.9 | NOAA/CMDL | flask |
| | | 1.7 | 1.96 | 2.02 | 0.06±0.04 | 3.0 | UEA | flask, SH |
| $CBr_2F_2$ | H-1202 | 0.02 | 0.031 | 0.037 | 0.006±0.001 | 18 | UEA | flask, SH |
| $CBrF_2CBrF_2$ | H-2402 | | 0.47 | 0.48 | 0.01±0.01 | 1.9 | NOAA/CMDL | flask |
| | | 0.36 | 0.41 | 0.42 | 0.01±0.01 | 2.4 | UEA | flask, SH |
| **Chlorocarbons** | | | | | | | | |
| $CH_3Cl$ | | (600) | | 550 | | | Chapter 2 | |
| $CCl_4$ | | (132) 103 | 100.8 | 99.7 | -1.1±0.3 | -1.1 | AGAGE | in situ |
| | | 106 | 104.1 | 103.2 | -0.9±0.1 | -0.9 | NOAA/CMDL | in situ |
| $CH_3CCl_3$ | | (160) 127 | 102.5 | 88.7 | -13.2 | -14 | AGAGE | in situ |
| | | | 110 | 97 | -14 | -14 | NOAA/CMDL | in situ |
| $COCl_2$ | | | | 20 | | | Chapter 2 | |
| **Bromocarbons**[a] | | | | | | | | |
| $CH_3Br$ | | (11) | | 9-11 | | | Chapter 2 | |
| $CH_2Br_2$ | | | | 0.6-1.0 | | | Chapter 2 | |
| $CHBr_3$ | | | | 0.2-0.6 | | | Chapter 2 | |
| $CH_2BrCl$ | | | | 0.1-0.2 | | | Chapter 2 | |
| $CHBrCl_2$ | | | | 0.1-0.2 | | | Chapter 2 | |
| $CHBr_2Cl$ | | | | 0.1 | | | Chapter 2 | |
| $CH_2BrCH_2Br$ | | | | 0.1 | | | Chapter 2 | |

**Table 1-2, continued.**

| Species | Industrial Name | Concentration (ppt) 1992 | 1995 | 1996 | Growth ppt yr$^{-1}$ | Growth % yr$^{-1}$ | Laboratory [d] | Method |
|---|---|---|---|---|---|---|---|---|
| **HCFCs** | | | | | | | | |
| $CHClF_2$ | HCFC-22 | (102) 102 | 117 | 122 | 5.0 | 4.2 | NOAA/CMDL | flask |
| | | | 119 | 125 | 5.7 | 4.5 | AGAGE | flask |
| $CH_3CCl_2F$ | HCFC-141b | (0.3) | 3.5 | 5.4 | 1.9 | 43 | NOAA/CMDL | flask |
| | | 0.13 | | | | | UEA | flask, SH |
| $CH_3CClF_2$ | HCFC-142b | (3.5) 3.1 | 6.6 | 7.6 | 1.1 | 15 | NOAA/CMDL | flask |
| | | 1.9 | | | | | UEA | flask, SH |
| **HFCs** | | | | | | | | |
| $CHF_3$ | HFC-23 | 9.0 | 10.7 | | 0.55 | 5.1 | UEA | flask, SH |
| $CH_2FCF_3$ | HFC-134a | | 1.6 | 3.0 | 1.4 | 59 | NOAA/CMDL | flask |
| | | 0.03 | 0.7 | | 0.64 | 91 | UEA | flask, SH |
| **PFCs** | | | | | | | | |
| $CF_4$ | PFC-14 | (70) 72 | 75 | | 1.00±0.05 | 1.3 | MPAE | flask, NH |
| | | | 74 | | 1.1±0.4 | 1.5 | ATMOS | FTIR, NH |
| $CF_3CF_3$ | PFC-116 | (4) 2.4 | 2.6 | | 0.084±0.005 | 3.2 | MPAE | flask, NH |
| **Others** | | | | | | | | |
| $SF_6$ | | | 3.5 | 3.7 | 0.24±0.01 | 6.9 | NOAA/CMDL | flask |
| | | (2-3) 2.7 | 3.4 | 3.7 | 0.27 | 7.2 | UH | flask |
| | | | 4.0 | 4.2 | 0.2 | 4.8 | ULg | FTIR, NH |
| $N_2O$ [b] | | (310) 308 | 310.0 | 311.1 | 1.0±0.3 | 0.3 | AGAGE | in situ |
| | | 309.9 | 311.6 | 312.4 | 0.8±0.3 | 0.3 | NOAA/CMDL | in situ |
| Total Cl [c] | | | | 3580 | -25 | -0.7 | | |
| Br | | | | 20.2 | 0.23 | 1.1 | | |
| F | | | | 2370 | 44 | 1.8 | | |

[a] For most bromocarbon concentrations listed, refer to Table 2-7 to assess local variability.
[b] $N_2O$ concentrations and growth rates are in parts per billion (ppb) and ppb yr$^{-1}$.
[c] Add about 100 ppt for source species not considered here (e.g., $CH_2Cl_2$, $CHCl_3$, $CCl_2CCl_2$, etc.) discussed in Chapter 2.
[d] Advanced Global Atmospheric Gases Experiment (AGAGE); Atmospheric Trace Molecule Spectroscopy (ATMOS); Max-Planck-Institute for Aeronomy (MPAE); National Center for Atmospheric Research (NCAR); National Oceanic and Atmospheric Administration/Climate Monitoring and Diagnostics Laboratory (NOAA/CMDL); University of California at Irvine (UCI); University of East Anglia (UEA); University of Heidelberg (UH); University of Liège (ULg); University of Tokyo (UT); Chapter 2 entries refer to Chapter 2 of the current Assessment (WMO, 1998).

analyses, thus achieving a direct comparison, via the same air sample, between these laboratories. The second involves sending air samples from the same clean air location, collected at the same time or close together, to various laboratories for trace gas analyses. The resulting data are compared, thus achieving an indirect comparison between laboratories. Laboratories that have participated in one or both types of NOHALICE intercomparisons are from Australia (Commonwealth Scientific and Industrial Research Organisation (CSIRO)), Germany (University of Heidelberg), Japan (University of Tokyo), South Africa (Department of Scientific and Industrial Research (DSIR)), United Kingdom (University of Bristol, University of East Anglia (UEA)) and United States (National Center for Atmospheric Research (NCAR), NOAA/CMDL, Oregon Graduate Institute (OGI), University of California at Irvine (UCI), Scripps Institution of Oceanography (SIO)-AGAGE, and United

States Geological Survey (USGS)). Species that have been compared by one or both intercomparison methods include $N_2O$; CFC-11, -12, and -113 ($CCl_3F$, $CCl_2F_2$, and $CCl_2FCClF_2$); HCFC-22, -141b, and -142b ($CHClF_2$, $CH_3CCl_2F$, $CH_3CClF_2$); HFC-134a ($CH_2FCF_3$); Halon-1211, -1301, and -2402 ($CBrClF_2$, $CBrF_3$, and $CBrF_2CBrF_2$); methyl chloroform ($CH_3CCl_3$); $CCl_4$; methyl chloride ($CH_3Cl$); methyl bromide ($CH_3Br$); and $SF_6$.

Comparisons have been published for $CCl_2FCClF_2$ (NOAA/CMDL, OGI, SIO-AGAGE, U. Tokyo); $CH_3CCl_2F$, $CH_3CClF_2$, and $CH_2FCF_3$ (NOAA/CMDL, UEA); $CHClF_2$ (NOAA/CMDL, SIO-AGAGE); $CBrClF_2$, $CBrF_3$, and $CBrF_2CBrF_2$ (NOAA/CMDL, UEA). A summary of the comparability between participating laboratories in NOHALICE for various species is shown in Table 1-3.

Most routine measurements of the stratospheric distribution of CFCs and other long-lived species have been performed by whole air sampling with subsequent gas chromatographic analysis (e.g., Kaye *et al.*, 1994). More recently, however, in situ measurements using automated gas chromatographic methods have become available for both aircraft (e.g., the Airborne Chromatograph for Atmospheric Trace Species-IV (ACATS-IV) (Elkins *et al.*, 1996b; Bujok *et al.*, 1998)) and balloonborne platforms (e.g., the Lightweight Airborne Chromatograph Experiment (LACE) (F.L. Moore, NOAA/CMDL, U.S., personal communication, 1998)) that are able to measure with time resolutions of one to a few minutes, depending on the target gas. These instruments provide a much larger dataset than that obtained with whole air samplers (WAS) and avoid sample degradation. Intercomparisons between these diverse techniques and measurements have resulted in a better understanding of calibration issues and improvements in accuracy (e.g., Chang *et al.*, 1996a,b; Sen *et al.*, 1998).

Remote sensing investigations, which derive atmospheric composition information from spectral absorption or emission features, rely upon spectroscopic parameters determined in the laboratory to invert these features into concentrations. The uncertainty of the reported concentrations reflects the accuracy with which these spectroscopic parameters have been obtained. The most recently updated line parameters compilation has been described by Rothman *et al.* (1998), and Abrams *et al.* (1996a) have evaluated the precision and accuracy with which concentrations of some 30 key atmospheric constituents can be derived from IR space-based solar occultation observations.

Two space-based experiments have provided substantial data for this chapter, namely the Halogen Occultation Experiment (HALOE) on the UARS satellite (Russell *et al.*, 1993) and Atmospheric Trace Molecule Spectroscopy (ATMOS) on shuttles (Gunson *et al.*, 1996). Besides having their individual datasets intercompared, these experiments were involved in intercomparison and validation tests based on independent measurements provided by ground-, airplane-, and balloon-based instruments (a description of the evaluation of the UARS data has been reported in a special issue of *Journal of Geophysical Research*, Vol. 101, No. D6, pp. 9539-10476, 1996). On that basis, Russell *et al.* (1996a,b) reported intercomparison exercises indicating that HALOE concentration measurements of HCl and HF throughout the middle atmosphere could be retrieved with an accuracy of 5 to

**Table 1-3. The differences between participating laboratories in NOHALICE for measurements of $N_2O$ and various halocarbon species.** The number of participating laboratories is given in parentheses after each species (Oram *et al.*, 1995, 1996; Fraser *et al.*, 1996, 1998; Miller *et al.*, 1998; Geller *et al.*, 1997; P. Fraser, CSIRO, Australia, personal communication of unpublished NOHALICE data, 1998).

| Species | Differences (%) between laboratories |
|---|---|
| $N_2O$ (3), $CCl_2F_2$ (4), $CHClF_2$ (2), $CH_3Cl$ (2), $SF_6$ (2) | ≤ 1 |
| $CCl_2FCClF_2$ (4), $CCl_4$ (3), $CH_3CCl_2F$ (2) | 3 to 6 |
| $CCl_3F$ (4), $CBrClF_2$ (2), $CBrF_3$ (2), $CBrF_2CBrF_2$ (2), $CH_3Br$ (2) | 8 to 10 |
| $CH_3CCl_3$ (3), $CH_3CClF_2$ (2), $CH_2FCF_3$ (2) | 20 to 35 |

10%. ATMOS was a core part of the 1992, 1993, and 1994 Space Shuttle-based Atmospheric Laboratory for Applications and Science (ATLAS) missions (Kaye and Miller, 1996). Assessments were made of absolute accuracy and efficiency of retrieval methods, based on simultaneous measurements of identical parameters and on intercomparisons of collocated measurements by UARS experiments, including HALOE and the Cryogenic Limb Array Etalon Spectrometer (CLAES) (Nightingale *et al.*, 1996). During the 1994 ATLAS-3 mission, a series of ATMOS measurements were near-coincident with a flight of the NASA ER-2 high-altitude aircraft at northern midlatitudes as part of the Airborne Southern Hemisphere Ozone Experiment/Measurements for Assessing the Effects of Stratospheric Aircraft (ASHOE/MAESA) campaign. The intercomparisons of volume mixing ratio profiles for a number of tracers of atmospheric transport (Chang *et al.*, 1996a) and halogenated gases (Chang *et al.*, 1996b) showed good agreement between the ER-2 in situ and ATMOS remote measurements, with the exception of $CCl_4$ (15% differences) and carbon monoxide (CO) (up to 25% differences in the lower stratosphere).

To provide independent calibration and validation measurements for space-based measurements, the NDSC has established specific activities to ensure data quality. These include intercomparison campaigns among instruments that can be brought to a common site and, if this is not feasible, regular side-by-side exercises using portable instruments that travel to the various stations of the network are organized. Details on the NDSC composition, organization, and activities can be found on the worldwide web (http://climon.wwb.noaa.gov), while geophysical data verified according to the data quality protocols are archived at the NOAA/NDSC Data Center, Washington, D.C., U.S.

### 1.2.2 Chlorofluorocarbons (CFCs)

Figure 1-1 shows the $CCl_3F$, $CCl_2F_2$, and $CCl_2FCClF_2$ mole fractions from the late 1970s through to the mid-1990s from surface sites of the ALE/GAGE/AGAGE (Prinn *et al.*, 1998) and NOAA/CMDL (Elkins *et al.*, 1998) networks. Tropospheric $CCl_3F$, $CCl_2F_2$, and $CCl_2FCClF_2$ growth rates, as observed in the NOAA/CMDL global flask air sampling and in situ networks (Figure 1-1), have continued to decline. Global $CCl_2F_2$ growth rates in 1995 to 1996 were approximately 4 parts per trillion (ppt) $yr^{-1}$ (Table 1-2), having slowed down by more than two-thirds since the late 1980s. For $CCl_2FCClF_2$ and $CCl_3F$, tropospheric growth rates in 1995 to 1996 were near zero or in decline (0.1 and -0.7 ppt $yr^{-1}$, respectively (Thompson *et al.*, 1994; Montzka *et al.*, 1996; Elkins *et al.*, 1996a, 1998).

In situ observations from the Atmospheric Lifetime Experiment-Global Atmospheric Gases Experiment (ALE-GAGE)-AGAGE global network (Figure 1-1) showed that global levels of $CCl_3F$ reached a maximum in 1993 (approximately 265 ppt) and started to decay in 1994, while $CCl_2F_2$ continued to increase throughout the 1990s, but at growth rates clearly slowing down. These observations have been interpreted using a global two-dimensional (2-D) transport model and show that global emissions of $CCl_3F$ and $CCl_2F_2$ since 1993 were lower than estimated by industry and have decreased faster than expected under the Montreal Protocol (Cunnold *et al.*, 1997; see also Figure 1-12). $CCl_2FCClF_2$ abundances stopped growing by 1996 and remained static at about 83 ppt (Prinn *et al.*, 1998). The global release estimates by industry consistently exceed those deduced from atmospheric measurements by approximately 10% from 1980 to 1993. This difference suggests that up to 10% of past production of $CCl_2FCClF_2$ might not yet have been released (Fraser *et al.*, 1996). The global mean in situ 1996 data (Table 1-2) for $CCl_3F$, $CCl_2F_2$, and $CCl_2FCClF_2$ show AGAGE concentrations lower than NOAA/CMDL by 2.7, 0.1, and 1.2%, respectively.

Observations of $CCl_3F$, $CCl_2F_2$, and $CCl_2FCClF_2$ in Japan and Antarctica by the University of Tokyo (UT) from flask air samples gave average 1996 concentrations of 266, 531, and 81 ppt, respectively (Makide *et al.*, 1987, 1994; Y. Makide, University of Tokyo, Japan, personal communication of unpublished data, 1998). The UT global data for CFCs agree to within 1 to 3% with AGAGE and NOAA/CMDL data from similar latitude sites (Table 1-2). The UT data show small, negative trends (1995-1996) for all three CFCs on Hokkaido (Japan), and small, positive trends in Antarctica, that are not inconsistent with the regional trends observed in the AGAGE and NOAA/CMDL global networks. The same laboratory (UT) reported an average 1992 CFC-114 ($CClF_2CClF_2$) concentration and growth rate of 13.5 ppt and 0.6 ppt $yr^{-1}$, respectively (Chen *et al.*, 1994). The UCI global flask sampling program (Rowland *et al.*, 1994) gave average 1995 concentrations for $CCl_3F$, $CCl_2F_2$, and $CCl_2FCClF_2$ of 266, 518, and 84 ppt, respectively (O.W. Wingenter, University of California

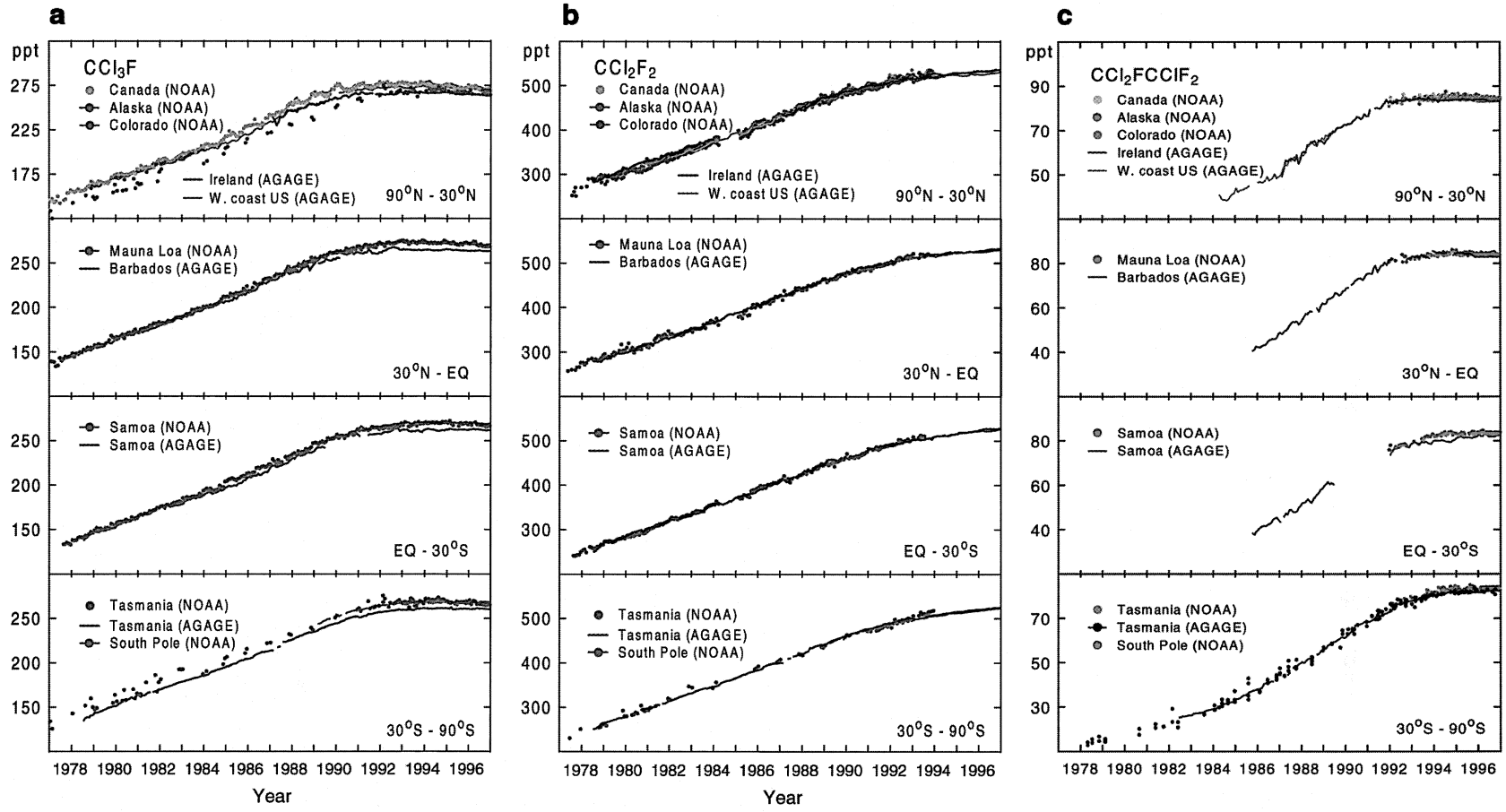


**Figure 1-1.** Monthly mean background data (in situ and flask) for $CCl_3F$, $CCl_2F_2$, and $CCl_2FCClF_2$ from the ALE/GAGE/AGAGE (Prinn *et al.*, 1998) and NOAA/CMDL (Elkins *et al.*, 1998) global networks.

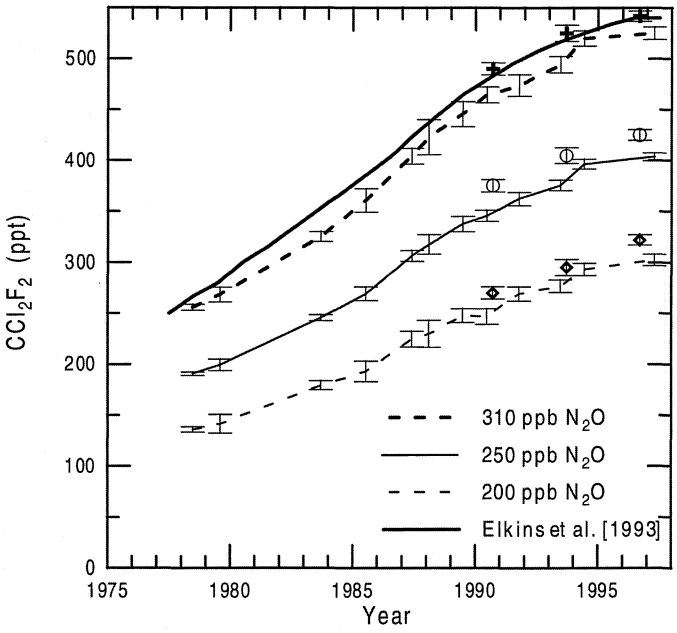


**Figure 1-2.** Temporal trend of $CCl_2F_2$ (CFC-12) mole fraction derived from balloonborne whole air sampling for different $N_2O$ levels of the stratosphere, i.e., 310 ppb $N_2O$ (in the lowermost stratosphere), 250 ppb $N_2O$ (about 19 km at midlatitudes) and 200 ppb $N_2O$ (about 21.5 km) (Engel *et al.*, 1998). The values are corrected for an assumed tropospheric $N_2O$ increase of about 0.2% $yr^{-1}$. The crosses, circles, and diamonds indicate $CCl_2F_2$ concentrations measured remotely with the MkIV FTIR balloon instrument (Sen *et al.*, 1996). The top solid black line refers to globally averaged tropospheric $CCl_2F_2$ measurements from the NOAA/CMDL network (Elkins *et al.*, 1998).

at Irvine, United States, personal comunication of unpublished data archived at UCI, 1998), in good agreement (within 2%) with the NOAA/CMDL and AGAGE data.

Extensive, aircraft-based air sampling campaigns were conducted in the NW Pacific (Pacific Exploratory Mission (PEM)-West A, September-October, 1991) and NE Atlantic (Atlantic Stratocumulus Transition Experiment/Marine Aerosol and Gas Exchange (ASTEX/MAGE), June 1992) regions. Average free tropospheric values for $CCl_3F$, $CCl_2F_2$, and $CCl_2FCClF_2$ of 274, 509, and 88 ppt, respectively (NW Pacific) and 267, 512, and 83 ppt, respectively (NE Atlantic) were obtained and a free tropospheric value of 15 ppt was observed for $CClF_2CClF_2$ (Blake *et al.*, 1996a,b). Concentrations of $CCl_3F$, $CCl_2F_2$, $CCl_2FCClF_2$, CFC-114 ($CClF_2CClF_2$), and CFC-115 ($CClF_2CF_3$) at the tropical tropopause in 1992 averaged 264, 494, 75, 16, and 4 ppt (Daniel *et al.*, 1996). A late 1980s/early 1990s Northern Hemisphere (NH) growth rate of 0.4 ppt $yr^{-1}$ for $CClF_2CF_3$ has been derived from NCAR data (Daniel *et al.*, 1996).

Tropospheric and stratospheric abundance data for several CFCs have been derived from balloonborne cryogenic air samplers flown at 17.5°N, 44°N, and 62°N from 1977 to 1993 (Max-Planck-Institute for Aeronomy (MPAE), Germany) (Fabian *et al.*, 1996). Free troposphere abundances of $CClF_3$, $CClF_2CClF_2$, and $CClF_2CF_3$ (4, 15, and 5 ppt respectively) and growth rates (5, 8, and 8% $yr^{-1}$ respectively) for 1990 have been derived from this dataset.

Vertical profiles of ozone-depleting substances (ODSs) extending into the stratosphere are important in assessing the relative contribution an individual ODS makes to total ozone depletion. Stratospheric measurements of ODSs up to 1990 were reviewed by Fraser *et al.* (1994). More recently, a large number of ODSs have been measured using whole air samples collected on balloon (Fabian *et al.*, 1994, 1996; Schmidt *et al.*, 1994; Lee *et al.*, 1995; Engel *et al.*, 1997, 1998; Patra *et al.*, 1997) and aircraft flights (Schauffler *et al.*, 1993; Woodbridge *et al.*, 1995; Daniel *et al.*, 1996). Stratospheric measurements of ODSs using in situ gas chromatography have been reported by Elkins *et al.* (1996b), Volk *et al.* (1997), and Wamsley *et al.* (1998). Sen *et al.* (1996) have reported mixing ratio profiles of $CCl_2F_2$, $CCl_3F$, and $CCl_2FCClF_2$ from a balloon flight over New Mexico (34°N, 104°W) during September 1993. The latter data provide mixing ratio profiles extending from 5 to 38 km, thus encompassing the entire free troposphere and most of the stratospheric layers of importance for these species.

Very few stratospheric datasets span a time frame that is sufficient for the investigation of stratospheric trends. The latter are different from those observed in the troposphere, due to the time lag associated with the exchange of air between the troposphere and the

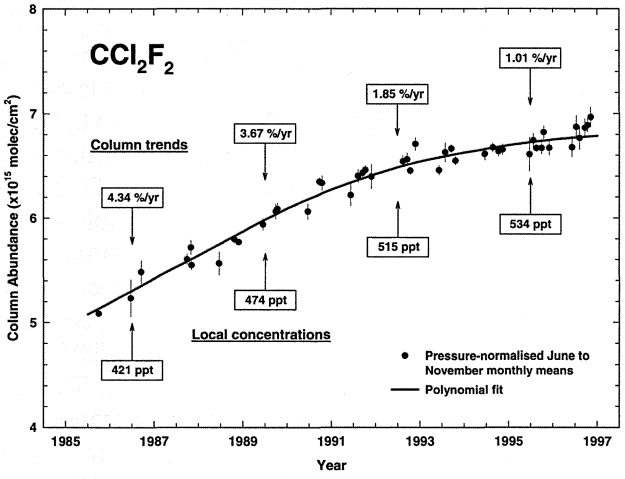


**Figure 1-3.** The evolution of the column amount of $CCl_2F_2$ above the Jungfraujoch from 1985 to 1996, based on June to November monthly mean vertical column abundances. Column trends (% yr$^{-1}$) and local volume mixing ratios (ppt) are indicated for 1986, 1989, 1992, and 1995 (Zander *et al.*, 1994a; updated with unpublished data). The continuous line is a 6$^{th}$ order polynomial fit to the data points.

stratosphere (the so-called "age" of stratospheric air; see Chapter 7) and due to the strong vertical gradients above the tropopause for many compounds that are destroyed in the stratosphere. These gradients differ with season and latitude and show significant short-term variations related to stratospheric dynamics, which can mask the long-term trends. One way of eliminating the short-term variations from the individual species data is to use another trace gas (e.g., $N_2O$) with similar behavior and no (or only a very small, well-defined) tropospheric increase as a reference substance. Based on this method, Engel *et al.* (1998) have derived stratospheric trends of $CCl_2F_2$ (Figure 1-2) that are calibrated relative to the NOAA/CMDL standard. The small tropospheric trend of $N_2O$ was taken into account by using 1993 as the base year with an approximately 310-ppb tropospheric mixing ratio for $N_2O$, and then assuming a trend of 0.2% forward and backward for all levels. In the lowermost stratosphere they reproduce the observed $CCl_2F_2$ tropospheric trends quite well, with an average increase rate of 18.5 ± 1.8 ppt yr$^{-1}$ for the time period 1978 to 1990. At higher altitudes (i.e., lower $N_2O$ levels) the absolute rates of increase were smaller due to photodissociation. For the time period from 1990 to 1997, a significant slowing down of the increase in the mixing ratio of $CCl_2F_2$ was observed in the lowermost stratospheric level, with an increase rate of only 11.9 ± 4.2 ppt yr$^{-1}$. Because of the larger difference in lifetime versus $N_2O$, this method gave less satisfactory results for $CCl_3F$, where a larger scatter in the correlations was observed. When compared with the global surface means from the NOAA/CMDL network (Elkins *et al.*, 1998), the differences in the observed $CCl_2F_2$ stratospheric trend (Figure 1-2) can be attributed to a time lag of about one year for tropospheric air to reach the lowermost stratosphere, in agreement with a time lag of about 0.8 years determined by Volk *et al.* (1997). The error bars represent the 1-sigma statistical uncertainty of the derived $CCl_2F_2$ mixing ratio based on the fit between $N_2O$ and $CCl_2F_2$. The sets of crosses, circles and diamonds in Figure 1-2 represent $CCl_2F_2$ mixing ratios measured remotely by balloon at the 310, 250, and 200 ppb reference $N_2O$ concentration levels on 27 September 1990, 25 September 1993, and 28 September 1996 (Sen *et al.*, 1996). While these data are biased high with respect to the in situ measurements (4 to 5%, which is commensurate with the accuracy of both techniques), they are in excellent agreement with the ground-based concentrations of $CCl_2F_2$ displayed in Figure 1-1.

The total atmospheric loadings and long-term changes of various halogenated compounds can be determined by regular spectrometric observations from the ground. Figure 1-3 shows the evolution of the vertical column abundance of $CCl_2F_2$ as retrieved from IR solar observations performed at the International Scientific Station of the Jungfraujoch (ISSJ, Switzerland) from the mid-1980s to 1996 (Zander *et al.* (1994a); R. Zander, University of Liège, Belgium, personal communication of unpublished data, 1998). The monthly mean $CCl_2F_2$ column data (June to November only, to avoid significant variability during winter and spring) show rates of increase and local volume mixing ratios (assuming a standard distribution profile derived from in situ balloon soundings at northern midlatitudes) that compare very well with those displayed in Figure 1-1. The significant slowing down of the rate of increase of the $CCl_2F_2$ column

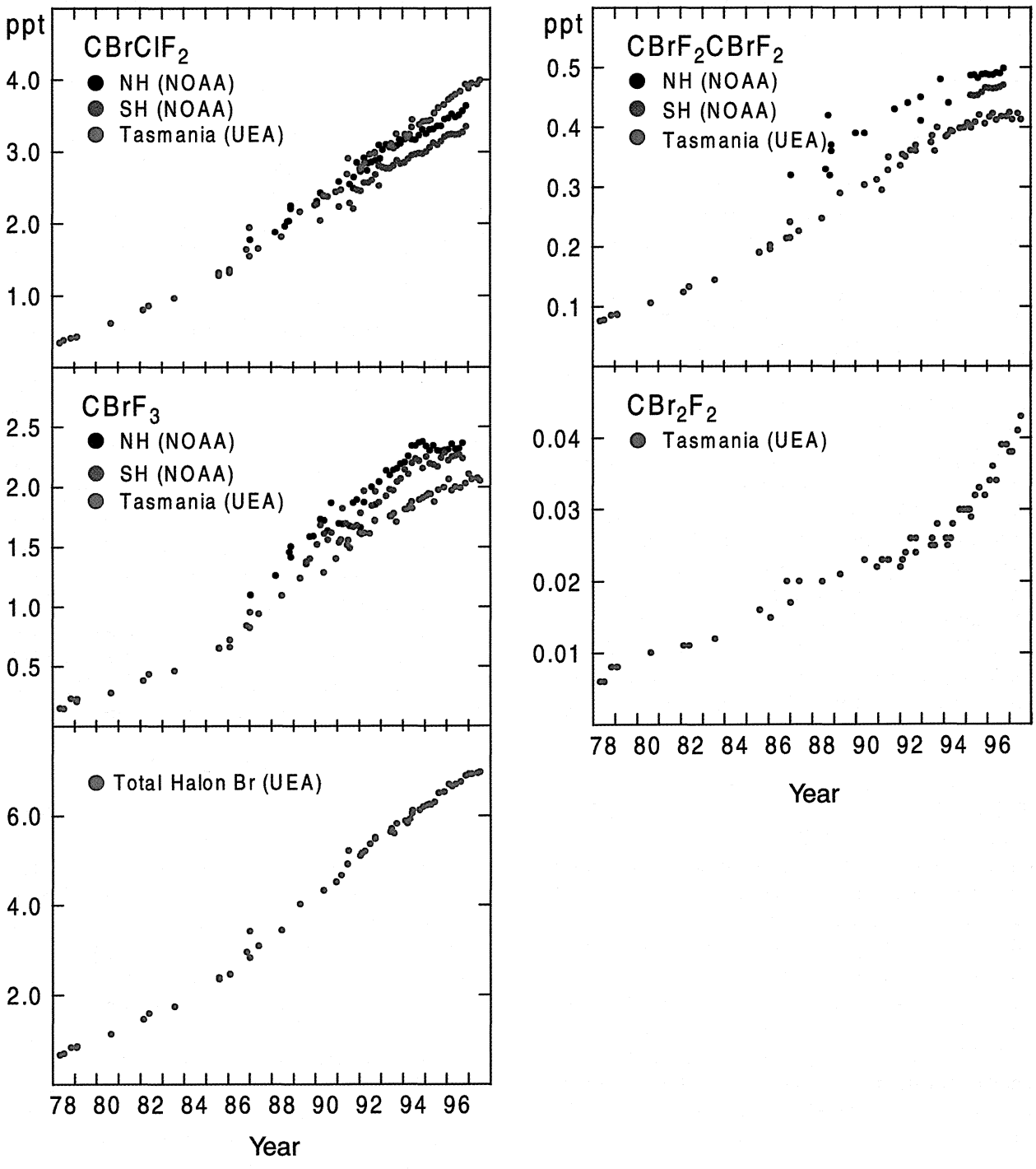


**Figure 1-4.** Measurements of $CBrClF_2$, $CBrF_3$, $CBrF_2CBrF_2$, $CBr_2F_2$, and total halon bromine made at UEA on air from the CSIRO Cape Grim air archive (SORG, 1996; Fraser *et al.*, 1998) and at NOAA/CMDL ($CBrClF_2$, $CBrF_3$, and $CBrF_2CBrF_2$) on air samples collected from their global flask sampling network (Montzka *et al.*, 1996; Butler *et al.*, 1998).

above ISSJ is a further manifestation of the reduction in the emissions of $CCl_2F_2$ as imposed by the Montreal Protocol and its Amendments and Adjustments (see Figure 1-11).

### 1.2.3 Halons

The presence of bromine in the atmosphere has been given increased attention during recent years because of its high efficiency in destroying ozone and its continued atmospheric accumulation. The bromine-bearing source gases (halons) considered in this section are the long-lived $CBrClF_2$, $CBrF_3$, and Halon-2402 ($CBrF_2CBrF_2$), and the relatively short-lived Halon-1202 ($CBr_2F_2$).

Throughout the 1990s, data from the NOAA/CMDL flask network showed that global abundances of $CBrClF_2$ and $CBrF_3$ continued to increase, with $CBrF_3$ exhibiting a marked slowing in its growth rate in recent years (Thompson *et al.*, 1994; Montzka *et al.*, 1996; Elkins *et al.*, 1996a; Wamsley *et al.*, 1998). During 1996 the tropospheric abundances of $CBrClF_2$, $CBrF_3$, and $CBrF_2CBrF_2$ were 3.4, 2.3, and 0.48 ppt, respectively, with their 1995 to 1996 mole fractions growing at 0.18, 0.06, and 0.01 ppt $yr^{-1}$, respectively (Figure 1-4; Butler *et al.*, 1998). Large amounts of $CBrF_3$ and $CBrClF_2$ are stored in fixed and portable fire fighting systems and emissions of these species could continue for decades, based on estimates of their current release rates (Butler *et al.*, 1998).

Measured tropospheric volume mixing ratios of $CBrClF_2$, $CBrF_3$, $CBrF_2CBrF_2$, and $CBr_2F_2$ made at UEA on air from the CSIRO Cape Grim air archive (Langenfelds *et al.*, 1996) show large increases between 1978 and 1996. The 1996 concentrations for these species averaged 3.8, 2.0, 0.42, and 0.04 ppt, respectively, and the 1995-1996 growth rates were 0.27, 0.06, 0.01, and 0.006 ppt $yr^{-1}$, respectively. Total bromine in halons has increased by a factor of 10 since the late 1970s (Figure 1-4). While the growth rates of $CBrF_3$ and $CBrF_2CBrF_2$ are slowing, $CBrClF_2$ continues to accumulate at a quasi-steady rate, and the $CBr_2F_2$ growth rate is accelerating (SORG 1996; Fraser *et al.*, 1998). Based on a 2-D model calculation, global emissions of both $CBr_2F_2$ and $CBrF_2CBrF_2$ averaged about 0.7 to 0.8 Gg in 1997 (Fraser *et al.*, 1998). NOAA/CMDL and UEA halon data agree to within 10 to 15% for $CBrClF_2$, $CBrF_3$, and $CBrF_2CBrF_2$ (Table 1-2).

During the ASTEX/MAGE aircraft-based campaign over the NE Atlantic (30°N to 40°N, June 1992) region, average free tropospheric (2 to 3.5 km) values for $CBrClF_2$ and $CBrF_3$ of 3.0 and 2.1 ppt, respectively, were found (Blake *et al.*, 1996b), in good agreement with the NH NOAA/CMDL data (Figure 1-4). Aircraft measurements at the tropical tropopause and in the NH troposphere during 1996 were also in good agreement with the NOAA/CMDL measurements and trends (Schauffler *et al.*, 1998a,b). NH (17.5°N, 44°N, and 69°N) upper tropospheric $CBrClF_2$ and $CBrF_3$ abundances (2 ppt and 1.7 ppt, respectively) and growth rates (3% $yr^{-1}$ and 8% $yr^{-1}$, respectively) for 1990 have been derived from air samples collected by balloon between 1977 and 1993 (Fabian *et al.*, 1996). These data are consistent with the abundances and trends reported in Table 1-2.

Measurements of halons have been performed in the upper troposphere and lower stratosphere both by in situ gas chromatograph (GC) ($CBrClF_2$) and by whole air sampling techniques with subsequent GC analysis ($CBrF_3$, $CBrF_2CBrF_2$) (Wamsley *et al.*, 1998, and references therein). Significant correlations between the volume mixing ratios of each of these halon species and $CCl_3F$ are observed. In stratospheric air masses approximately 6 years old, Wamsley *et al.* (1998) calculated that 98% of the organic bromine was converted into inorganic bromine ($Br_y$), while Daniel *et al.* (1996) found somewhat less efficient conversion (90%) in air masses of average age between 5 and 6 years.

### 1.2.4 Carbon Tetrachloride ($CCl_4$)

In the 1994 Assessment, Sanhueza *et al.* (1995) reported $CCl_4$ values in the GAGE (OGI) calibration scale (Simmonds *et al.*, 1988) that were about 20% higher than the new AGAGE (SIO) values reported here (Simmonds *et al.*, 1998). Data from a number of laboratories, from direct and indirect comparisons of standards, showed a wide range (25%) of $CCl_4$ values (Fraser *et al.*, 1994), with the GAGE data being at the extreme high end of the range (the reasons for the high GAGE $CCl_4$ calibration are unknown). With the introduction of the AGAGE calibration scale, there has been a significant improvement in the agreement between laboratories reporting $CCl_4$ data, i.e., three laboratories making background $CCl_4$ observations (SIO-AGAGE, NOAA/CMDL, UT) now agree to ± 3% (P. Fraser, CSIRO, Australia, personal communication of NOHALICE unpublished data, 1998).

NOAA/CMDL and ALE/GAGE/AGAGE $CCl_4$ data are shown in Figure 1-5. In situ observations from the global ALE/GAGE/AGAGE network show that

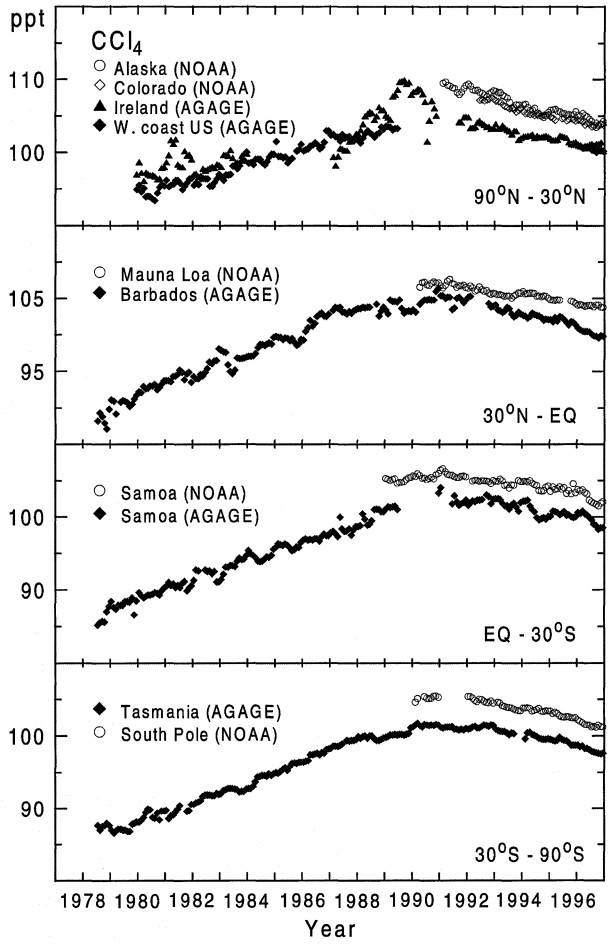


**Figure 1-5.** Monthly mean background data (in situ) for $CCl_4$ mole fractions (ppt) from the NOAA/CMDL (Elkins *et al.*, 1996a; Montzka *et al.*, 1996; Elkins *et al.*, 1998) and ALE/GAGE/AGAGE (Simmonds *et al.*, 1998) global networks.

atmospheric concentrations of $CCl_4$ reached a maximum in 1989-1990 (104 ppt) and have been decreasing by, on average, 0.7 ppt $yr^{-1}$ throughout the 1990s, declining to 100 ppt in 1996 (Simmonds *et al.*, 1998). Data from the NOAA/CMDL in situ observational network show that atmospheric abundances of $CCl_4$ declined steadily throughout the 1990s (-0.9 ppt $yr^{-1}$) and were 103 ppt in 1996 (Montzka *et al.*, 1996; Elkins *et al.*, 1996b; Elkins *et al.*, 1998).

During the ASTEX/MAGE aircraft-based campaign conducted over the NE Atlantic region (30°N to 40°N, June 1992), an average lower tropospheric (2 to 3.5 km) volume mixing ratio of 110 ppt for $CCl_4$ was measured by Blake *et al.* (1996b), which is similar (3 to 6% higher) to results from ground-based sampling at northern midlatitudes. Other measurements on air samples obtained via aircraft averaged 109 ppt in the northern midlatitudes during January to March 1992 (Daniel *et al.*, 1996).

Lower stratospheric $CCl_4$ mixing ratios derived from ATMOS/ATLAS-3 observations in November 1994 at northern latitudes are similar to the tropospheric $CCl_4$ values reported above. $CCl_4$ measurements obtained from an airborne GC during the ASHOE/MAESA campaign appear consistently lower than the ATMOS/ATLAS-3 measurements by some 15% (Chang *et al.*, 1996b; Elkins *et al.*, 1996b).

### 1.2.5 Perfluorocarbons (PFCs) and Sulfur Hexafluoride ($SF_6$)

PFCs and $SF_6$ do not contribute to ozone depletion; however, they are very strong IR absorbers on a per-molecule basis and are very useful atmospheric tracers. Because of its long lifetime and monotonic growth in the atmosphere, $SF_6$, like carbon dioxide ($CO_2$), has been used to estimate the mean age of a parcel of stratospheric air at the time of entry into the stratosphere (see Chapter 7). Harnisch *et al.* (1996a) have reconstructed tropospheric trends of the two very long-lived trace gases PFC-14 ($CF_4$) and PFC-116 ($CF_3CF_3$) from stratospheric vertical profiles by dating the air samples based on the measured $SF_6$ mixing ratio (see Figure 1-6). NH tropospheric $CF_4$ and $CF_3CF_3$ abundances of 75 ppt and 2.6 ppt were obtained for the year 1995. From 1982 to 1995, the derived mean rates of increase for $CF_4$ and $CF_3CF_3$ were $1.00 \pm 0.05$ ppt $yr^{-1}$ and $0.084 \pm 0.005$ ppt $yr^{-1}$, respectively, corresponding to accumulation rates of $14.6 \pm 0.5$ Gg $yr^{-1}$ and $1.9 \pm 0.15$ Gg $yr^{-1}$, respectively.

From ATMOS solar occultation measurements at northern sub-tropical and midlatitudes during the ATLAS-3 shuttle mission of November 1994, Zander *et al.* (1996c) derived nearly constant volume mixing ratios of $CF_4$ throughout the stratosphere ($74 \pm 3$ ppt). By comparing this value to the mean $CF_4$ volume mixing ratio of $63 \pm 4$ ppt measured during the ATMOS/Spacelab-3 mission (spring 1985), they derived an average annual increase for $CF_4$ of $1.6 \pm 0.6\%$ $yr^{-1}$ or 1.1 ppt $yr^{-1}$ over the 9.5 years separating the two missions.

Atmospheric $SF_6$ data in the 1990s have been inferred from NH and Southern Hemispheric (SH) oceanic surface water $SF_6$ concentrations, assuming surface ocean-air equilibrium. When combined with other data from the 1970s and 1980s, it can be deduced

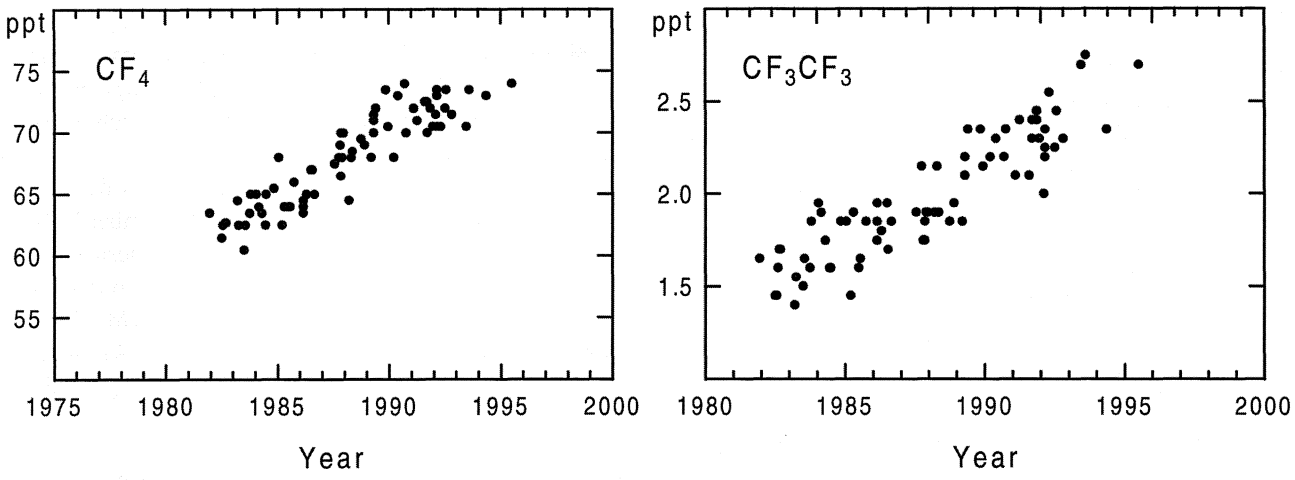


**Figure 1-6.** NH tropospheric $CF_4$ and $CF_3CF_3$ concentrations derived from $SF_6$-dated stratospheric air (Harnisch *et al.*, 1996a).

that atmospheric $SF_6$ grew exponentially in the atmosphere through the 1970s (about 30% $yr^{-1}$) and linearly (0.16 ppt $yr^{-1}$) through the 1980s and 1990s, reaching 3 ppt in 1994 (Law *et al.*, 1994).

Direct measurements of $SF_6$ in the global background atmosphere have been reported recently, including data obtained by analysis of the Cape Grim air archive (1978 to 1994). The global mean tropospheric abundance and growth rate in late 1994 were 3.3 ppt and 0.23 ppt $yr^{-1}$ (6.9% $yr^{-1}$) (Maiss *et al.*, 1996). Data from the NOAA/CMDL flask sampling network show that the global average abundance of $SF_6$ in 1995 was 3.4 ppt, growing at 0.23 ppt $yr^{-1}$ or 6.8% $yr^{-1}$ (Elkins *et al.*, 1996a). By mid-1996 the $SF_6$ global background abundance reached 3.6 ppt and the global growth rate was 0.24 ppt $yr^{-1}$ (6.7% $yr^{-1}$) (Geller *et al.*, 1997). Laboratory intercomparisons have shown that the NOAA/CMDL $SF_6$ calibration scale is 1% lower than the University of Heidelberg scale (Maiss *et al.*, 1996; Geller *et al.*, 1997). The NOAA/CMDL and the University of Heidelberg $SF_6$ data are shown in Figure 1-7.

By adopting an $SF_6$ mixing ratio profile of the "no loss" type (Ko *et al.*, 1993), $SF_6$ concentrations at the altitude of the ISSJ of 2.0, 3.1, and 4.4 ppt were found in 1988, 1992, and 1997, respectively, growing exponentially at 8.3 ± 0.5% $yr^{-1}$ (Mahieu *et al.*, 1996). Compared with the surface mixing ratios measured at various NH sites (see Figure 1-7), the Jungfraujoch remote IR data are higher by 8 to 10%. A similar bias (5%) was reported by Chang *et al.* (1996b), when comparing measurements of $SF_6$ (November 1994) from the Space Shuttle-based ATMOS-FTIR and the ACATS-GC onboard the NASA ER-2 high-altitude aircraft. These differences are within the accuracy currently achievable for $SF_6$ analysis by remote sensing in the IR (Abrams *et al.*, 1996a).

Based on the comparison of $SF_6$ mixing ratio profiles measured in the lower stratosphere by ATMOS during spring 1985 and fall 1994, Rinsland *et al.* (1996a) derived an increase of 8.0 ± 0.7% $yr^{-1}$, in good agreement with the increases cited above. Furthermore, a comparison of the 1985 ATMOS measurements of $SF_6$ with those made during a balloon flight in September 1993 (Sen *et al.*, 1996) indicates an $SF_6$ growth rate of 8.1 ± 0.7% $yr^{-1}$ in the 18- to 24-km region. These are in very good agreement with the early 1990 $SF_6$ rate of increase of 8.3% $yr^{-1}$ reported by Maiss and Levin (1994).

### 1.2.6 Nitrous Oxide ($N_2O$)

$N_2O$ is the major source of stratospheric $NO_x$, which is involved in catalytic ozone destruction (see Chapters 6 and 7). Long-term changes in $N_2O$ sources, primarily anaerobic processes in the soils and oceans, and secondarily industrial activity, will therefore impact the ozone layer.

Global average $N_2O$ concentrations have increased steadily in the troposphere from an estimated 275 ppb in preindustrial times (Machida *et al.*, 1995; Battle *et al.*, 1996) to 299 ppb by 1976 and 311 to 312 ppb by 1996 (Elkins *et al.*, 1998; Prinn *et al.*, 1990, 1998). The mean trend was +0.25% $yr^{-1}$ during the 1980s, with substantial

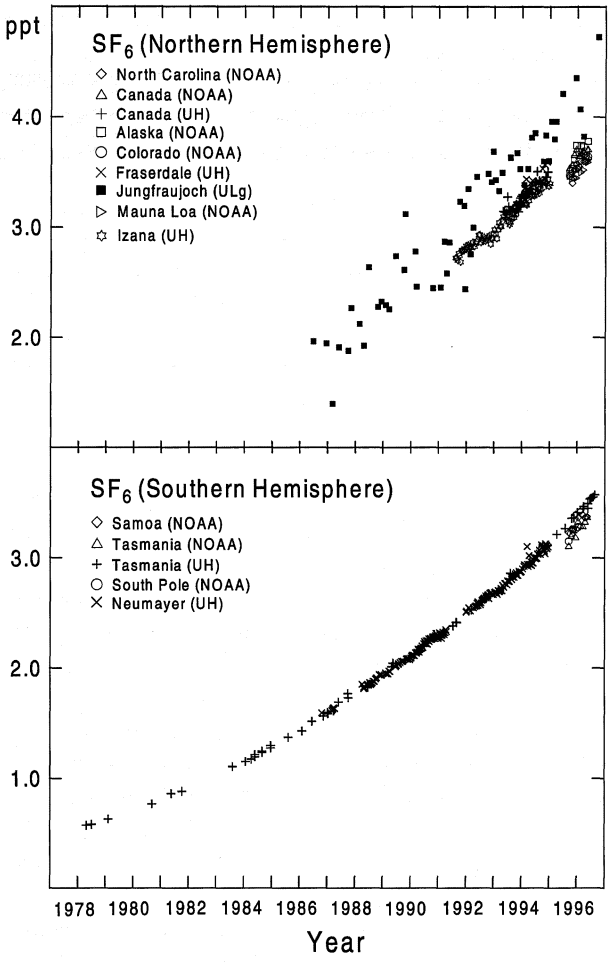


**Figure 1-7.** Global $SF_6$ data measured in the Cape Grim air archive (UH) (Maiss *et al.*, 1996) and in the global flask network of NOAA/CMDL (Geller *et al.*, 1997). Spectroscopic data from ISSJ (Jungfraujoch, ULg) are shown by filled squares in the upper frame (Mahieu *et al.*, 1996).

year-to-year variations. More recently, the growth rate of $N_2O$ decreased from about 1 ppb $yr^{-1}$ in 1991 to 0.5 ppb $yr^{-1}$ in 1993. The cause of this decrease is unknown, but global reductions in the use of nitrogenous fertilizer, post-Pinatubo temperature reductions and their effect on soil $N_2O$ production and reduced tropical oceanic upwelling of $N_2O$-rich waters have been suggested (Thompson *et al.*, 1994). Another possibility is that the trend was influenced by stratospheric circulation changes induced by volcanic aerosols from Mt. Pinatubo (Schauffler and Daniel, 1994). By 1995, the growth rate had increased again to 0.6 ppb $yr^{-1}$ (Elkins *et al.*, 1996a).

In situ $N_2O$ data from the ALE/GAGE/AGAGE network (1979-1996) and NOAA/CMDL flask and in situ $N_2O$ data (1978-1996) are shown in Figure 1-8 (Prinn *et al.*, 1990, 1998; Elkins *et al.*, 1996a, 1998). In general the NOAA/CMDL data are higher than the ALE/GAGE/AGAGE data by 1 to 2 ppb, except in the mid- to- late-1980s, when $N_2O$ observations from both networks were similar for similar latitudes. The GAGE $N_2O$ data at Cape Grim, Tasmania, appear to have unresolved calibration problems during the 1980s (P. Fraser, CSIRO, Australia, personal communication of unpublished data, 1998), which may apply to the entire GAGE network during this period.

Vertical column abundances of $N_2O$, monitored remotely above the ISSJ by IR solar observations, show a long-term trend of $0.36 \pm 0.06\%$ $yr^{-1}$ for the period 1984 to 1992 (Zander *et al.*, 1994b). This trend reduced slightly, when evaluated over the 1984 to 1996 period, to $0.33 \pm 0.04\%$ $yr^{-1}$. This latter value is higher than the mean increase (0.25% $yr^{-1}$) derived from ground-based in situ measurements. This may be due to a rise of the tropopause by about 150 m during the 12-year period of ISSJ measurements. Such a rise can result from either warming of the troposphere and/or cooling of the lower stratosphere. The magnitude of the rise required to reconcile the column and ground-based increases of $N_2O$ is similar to the rise that is deduced from long-term series of ozone and temperature measurements at Hohenpeissenberg, Germany (Claude and Steinbrecht, 1996; Steinbrecht *et al.*, 1998).

In the 1994 Assessment, Sanhueza *et al.* (1995) estimated the annual global $N_2O$ source to be 6 to 19 Tg (N) $yr^{-1}$ and the sinks plus atmospheric accumulation to be 12 to 22 Tg (N) $yr^{-1}$. A more recent international assessment of $N_2O$ sources and sinks was carried out for the Intergovernmental Panel on Climate Change (IPCC) (Prather *et al.*, 1995). The global $N_2O$ source was estimated to be 10 to 17 Tg (N) $yr^{-1}$, of which 4 to 8 Tg (N) $yr^{-1}$ was of anthropogenic origin, and total sinks plus atmospheric accumulation were 13 to 20 Tg (N) $yr^{-1}$. Bouwman *et al.* (1995) estimated a similar global $N_2O$ source of 11 to 17 Tg (N) $yr^{-1}$. They identified several sources not considered in the IPCC budget, including $N_2O$ formation from atmospheric ammonia ($NH_3$) oxidation, and $N_2O$ emissions from soil waters and from soil N deposited from the atmosphere. At least 40% of sources evaluated by Bouwman *et al.* (1995) were subject to anthropogenic influence. Recently there have been

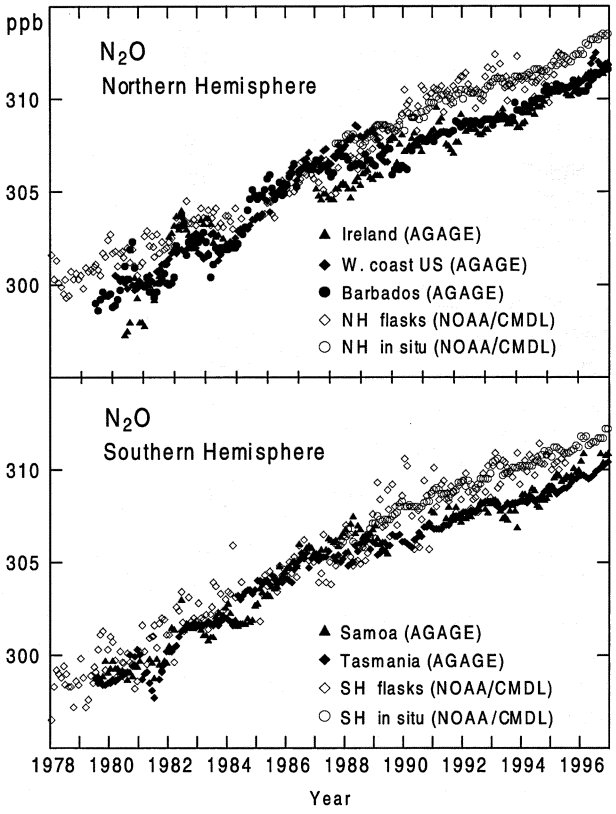


**Figure 1-8.** Monthly mean $N_2O$ data from the ALE/GAGE/AGAGE (in situ) and NOAA/CMDL (flask and in situ) global networks (Prinn *et al.*, 1990, 1998; Elkins *et al.*, 1996a, 1998).

upward revisions in the strength of various agricultural sources (Berges and Crutzen, 1996; Nevison and Holland, 1997; Mosier and Kroeze, 1998). With these revisions, the central value of the total sources (16 Tg (N) $yr^{-1}$) (Mosier and Kroeze, 1998) now matches the estimates of the total of atmospheric removal (12 Tg (N) $yr^{-1}$) and atmospheric increase (4 Tg (N) $yr^{-1}$). $N_2O$ emissions from agricultural systems worldwide have increased from 3.4 Tg (N) $yr^{-1}$ in 1960 to 6.2 Tg (N) $yr^{-1}$ in 1994, a growth rate of 1 to 2% $yr^{-1}$ (Mosier and Kroeze, 1998).

Isotopic studies (Kim and Craig, 1993; Johnston *et al.*, 1995; Rahn and Whalen, 1997), and a previously (perhaps wrongly) implied imbalance between $N_2O$ sources and sinks, have led to suggestions of a significant stratospheric source of $N_2O$ (Prasad, 1994; McElroy and Jones, 1996; Prasad *et al.*, 1997), possibly as large as 25% of the biological $N_2O$ source (Prasad, 1997). However, recently, Yung and Miller (1997) have been able to explain the stratospheric isotopic behavior of $N_2O$ without invoking stratospheric $N_2O$ sources. The ocean could also be a source of isotopically enriched $N_2O$ (Yoshinari *et al.*, 1997).

### 1.2.7 Regional Studies

The abundance and trend data on long-lived trace gases discussed above have been selected to be representative of large (hemispheric to global) space scales. However long-term or large-scale regional studies of trace gases can also provide useful information on regional trends and on regional emissions.

Estimates of the recently declining emissions of $CCl_3F$, $CCl_2F_2$, $CCl_2FCClF_2$, $CH_3CCl_3$, and $CCl_4$ from Europe have been made using selected in situ AGAGE data from Ireland (Simmonds *et al.*, 1993, 1996). From 1987 to 1994, emissions of the CFCs from Europe fell by a factor of 5, $CH_3CCl_3$ by a factor of 2, and $CCl_4$ by a factor of 4. The European source of $N_2O$ (1 to 2 Tg (N) $yr^{-1}$) does not appear to exhibit a trend.

In situ AGAGE $N_2O$ observations from Cape Grim, Tasmania, have been used to estimate SE Australian fluxes of $N_2O$ from 1985 to 1993, which exhibit a significant dependence on rainfall (Wilson *et al.*, 1997).

Trends of $CCl_3F$, $CCl_2F_2$, $CCl_2FCClF_2$, $CCl_4$, and $SF_6$ (-0.8, 5.4, 1.8, -1.4, and 0.25 ppt $yr^{-1}$ respectively), which are in good agreement with recent trends of remote background mixing ratios in the NH, have been deduced from in situ NOAA/CMDL data collected on a tall tower (610 m) in North Carolina, U.S., (Hurst *et al.*, 1997).

An $SF_6$ longitudinal transect has been obtained along the 9000-km Trans-Siberian railway. The data show the eastward dilution of the European-sourced $SF_6$ emission plume and local Russian $SF_6$ sources (Crutzen *et al.*, 1998).

### 1.2.8 Hydrogen Fluoride (HF) and Hydrogen Chloride (HCl)

HF is the ultimate inorganic sink for stratospheric fluorine atoms resulting from the photodissociation of fluorinated organic source gases transported into the stratosphere. The detection of atmospheric HF in the mid-1970s and subsequent rapid growth of HF over the last two decades are consistent with its production resulting from the decomposition of anthropogenic CFCs. As no significant natural sources of HF in or to the

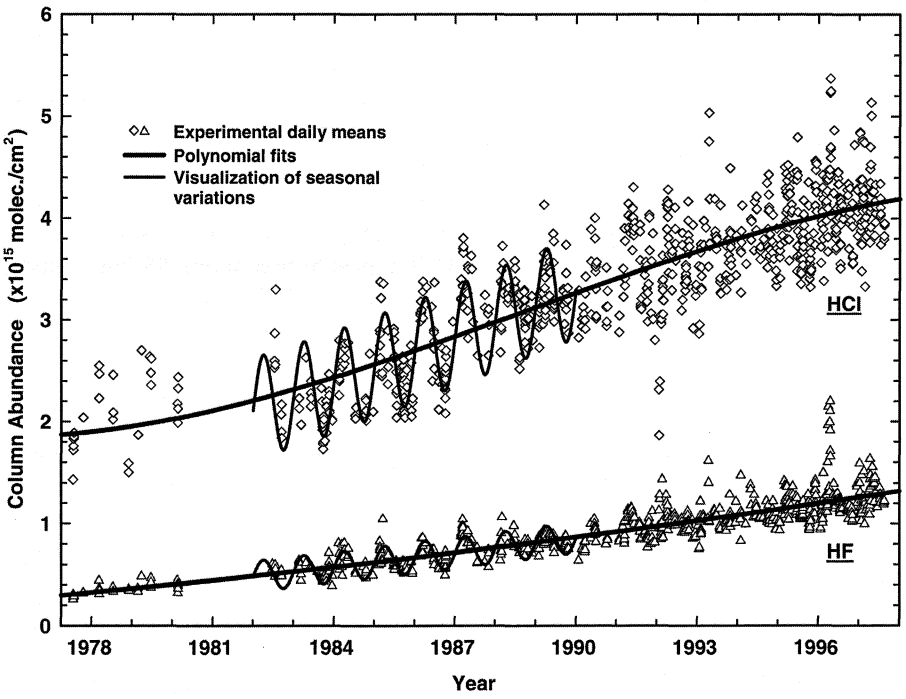


**Figure 1-9.** Evolution of the daily mean column abundances of HF and HCl above the Jungfraujoch during the last two decades (Zander *et al.*, 1998). Overall fits to the data are shown by solid lines. The sinusoidals (drawn only over a limited period for clarity) reflect observed seasonal variations in both columns. Significant short-term variability is observed during the winter-spring period, primarily associated with intrusions of high-latitude air masses.

atmosphere have been identified, the HF loading is an indicator of the total abundance and mix of CFCs, HCFCs, and HFCs in the atmosphere and its exceptional stability in the stratosphere makes it an excellent tracer of latitudinal and vertical transport and dynamics (Chipperfield *et al.*, 1997). In addition to HF, carbonyl fluoride ($COF_2$) and chlorofluorocarbonyl (COClF) are important for inorganic fluorine budget evaluations.

On a global basis, HCl is the major reservoir for inorganic stratospheric chlorine resulting from the breakdown of chlorinated organics.

Analyses of IR solar observations at the ISSJ since 1977 indicate a steady increase in the HF vertical column abundance above this northern midlatitude NDSC site (see Figure 1-9) from $0.29 \times 10^{15}$ molecules $cm^{-2}$ in 1977 to $1.22 \times 10^{15}$ molecules $cm^{-2}$ in 1997; this amounts to an exponential increase of 7.2% $yr^{-1}$, or a mean HF burden increase of $0.47 \times 10^{14}$ molecules $cm^{-2}$ $yr^{-1}$. The steady HF column increase above ISSJ contrasts with the slowing down of the HCl column growth rate from $(1.9 \pm 0.2) \times 10^{14}$ molecules $cm^{-2}$ $yr^{-1}$ between 1984 and 1989 to $(1.0 \pm 0.2) \times 10^{14}$ molecules $cm^{-2}$ $yr^{-1}$ from mid-1991 to mid-1996 (Zander *et al.*, 1998). These changes result from the recent reduction of CFC releases as set out in the Montreal Protocol and related Amendments, and subsequent CFC replacements by HCFCs and HFCs. A recently published record of stratospheric column measurements of HCl above Kitt Peak National Solar Observatory (KPNSO) (Wallace and Livingstone, 1997) is consistent with an increase of $0.74 \times 10^{14}$ molec $cm^{-2}$ $yr^{-1}$ over the 1971 to 1997 period, with some indication of a slowing down during the latter years.

Since the previous Assessment (WMO, 1995), some space-based experiments have added significantly to the quantification and understanding of the chlorine and fluorine loading in the stratosphere. Among these is the ATMOS FTIR experiment flown aboard the Space Shuttle in 1985, 1992, 1993, and 1994 (Gunson *et al.*, 1996) as part of the ATLAS program (Kaye and Miller, 1996). From the first and last ATMOS deployments, it was found that the concentration of HCl in the upper stratosphere (above 1 mbar) increased from a mean 2.5

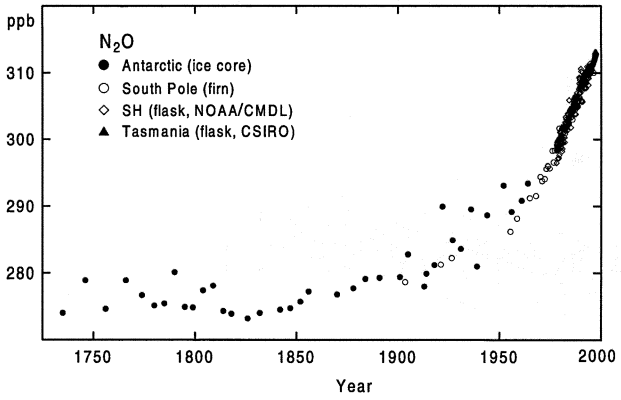


**Figure 1-10.** Mole fractions of $N_2O$ (ppb) for the past 250 years inferred from firn air (blue) (Battle *et al.*, 1996), air in Antarctic ice (red) (Machida *et al.*, 1995), in flask samples collected at SH sites and measured by NOAA/CMDL (purple) (Elkins *et al.*, 1996a) and in flasks collected at Cape Grim, Tasmania and measured by CSIRO (green) (Langenfelds *et al.*, 1996; Steele *et al.*, 1996).

± 0.1 ppb in April to May 1985, to a mean 3.5 ± 0.2 ppb in November 1994; this 9.5-year change corresponds to an annual growth rate of HCl equal to 3.5% $yr^{-1}$, or a mole fraction increase of 105 ppt $yr^{-1}$ (Zander *et al.*, 1992; 1996b).

Over that same 9.5-year period, the ATMOS measurements indicate that the upper stratospheric HF concentration increased by almost a factor of 2, from a mean 0.76 ± 0.08 ppb to 1.50 ± 0.15 ppb, corresponding to a growth rate of 7.2% $yr^{-1}$ or 78 ppt $yr^{-1}$ (Zander *et al.*, 1992; Abrams *et al.*, 1996b). From a global time series of satellite (UARS/HALOE) observations of HCl and HF in the stratosphere between October 1991 and April 1995, Russell *et al.* (1996c) found increases near 55 km of 102 ± 6 and 72 ± 2 ppt $yr^{-1}$, respectively. While the ATMOS and HALOE trends are in good agreement, the HALOE HCl and HF concentrations tend to be lower throughout the stratosphere than those obtained by ATMOS (Russell *et al.*, 1996a,b; Liu *et al.*, 1996; Achard *et al.*, 1997). However, a revision of the HALOE databases for HCl and HF has significantly improved this situation (J.M. Russell III, Hampton University, U.S., personal communication, 1998; also, http://haloedata.larc.nasa.gov/HALOE/home.html)). Based on these revised data, Considine *et al.* (1997) analyzed monthly average concentrations of HF above 55 km altitude over the 50°N to 50°S latitude band and found that the rate of increase of HF in the lower mesosphere has definitely slowed down, in a manner consistent with the tropospheric loadings and trends of $CCl_3F$ and $CCl_2F_2$ in the early 1990s (Montzka *et al.*, 1996; Cunnold *et al.*, 1997). A similar analysis scheme has been applied to the revised HALOE HCl time series of the past years (Considine *et al.*, 1998); it also indicates a definite slowdown of the HCl concentration above 55 km altitude, in a manner consistent with the decreasing rate of tropospheric chlorine (Cl) loading reported by Montzka *et al.* (1996).

### 1.2.9 Preindustrial Atmospheric Abundances

While increases of the atmospheric abundance of $CF_4$ and $CF_3CF_3$ in recent decades can be attributed to the electrolytic production of aluminum, ice core studies indicate that there is an additional source of $CF_4$ predating aluminum production (Harnisch *et al.*, 1996a,b). Both ice core and air archive studies indicate that the preindustrial atmospheric background level was about 40 ppt (Harnisch *et al.*, 1996b). Natural fluorites and granites are found to exhibit mass contents of up to $10^{-9}$ of $CF_4$, $SF_6$, and $CClF_3$ and, due to weathering and crustal metamorphism, 100 to 5000 kg of these substances are naturally released annually from the Earth's crust into the atmosphere (Harnisch and Eisenhauer, 1998). From extrapolated crustal abundances of these gases and their atmospheric lifetimes, Harnisch and Eisenhauer (1998) concluded that natural atmospheric background levels of about 40 ppt $CF_4$, less than 0.05 ppt of $SF_6$, and less than 0.005 ppt of $CClF_3$ can be expected from this source.

A precise record of atmospheric $N_2O$ levels throughout this century has been obtained from air trapped in Antarctic glacial firn. Firn air ages are determined from correlation of the $CO_2$ mole fractions in the firn samples with the atmospheric $CO_2$ history as determined by Etheridge *et al.* (1996). Because $CO_2$ and $N_2O$ are assumed to have the same diffusivities in firn, $CO_2$ ages also apply to $N_2O$. In the early 1900s, $N_2O$ levels were about 280 ppb (see Figure 1-10). During the first half of this century the atmospheric mole fraction grew at (0.06 ± 0.01)% $yr^{-1}$, reaching about 290 ppb by the early 1960s. Thereafter $N_2O$ increased more rapidly at (0.22 ± 0.02)% $yr^{-1}$ to contemporary SH values of around 310 ppb (Machida *et al.*, 1995; Elkins *et al.*, 1996a; Battle *et al.*, 1996).

In the preindustrial period (i.e., before significant release of industrial halocarbons, including CFCs, occurred), chlorine-containing gases (such as methyl

chloride) were emitted to the atmosphere from natural processes. Assuming that the preindustrial HCl levels can be related to non-CFC organochlorine releases and that all HF originates from CFCs, correlation plots of simultaneously measured HCl and HF column abundances during the 1970s and 1980s indicate that the preindustrial HCl column abundances, corresponding to zero HF abundances, were $(0.90 \pm 0.15) \times 10^{15}$ molecules $cm^{-2}$ above the KPNSO (Rinsland *et al.*, 1991; Wallace and Livingstone, 1991, 1997) and $(0.70 \pm 0.10) \times 10^{15}$ molecules $cm^{-2}$ above ISSJ (Zander *et al.*, 1996d). The relative difference results from KPNSO being located at 2.06 km and ISSJ at 3.58 km, indicating that most of that HCl resided in the troposphere.

## 1.3 THE BUDGETS OF CHLORINE, BROMINE, AND FLUORINE

### 1.3.1 Background

Organic compounds containing bromine, chlorine, fluorine, and iodine are released at the Earth's surface, mix rapidly, and are exchanged between hemispheres in the troposphere. Whereas most of these compounds originate predominantly from human activities, natural biological and chemical processes can also contribute to the total organic budget (WMO, 1995). Some of these organics (e.g., $CH_3CCl_3$, $CH_3Br$, $CH_3Cl$, HFCs, HCFCs) that contain hydrogen are destroyed by reaction with the hydroxyl radical (OH) in the troposphere. For these compounds (see Chapter 2), their atmospheric lifetimes and their effect on stratospheric ozone depletion are reduced compared to similar compounds (i.e., CFCs and halons) that are fully halogenated. Transport time scales are important in describing when stratospheric ozone losses can be expected to occur and can be estimated from observations of long-lived trace gases (like $CO_2$ (Boering *et al.*, 1996), $SF_6$ (Elkins *et al.*, 1996b), and CFC-115 (Daniel *et al.*, 1996)) and from atmospheric models (Mahowald *et al.*, 1997; Hartley *et al.*, 1994). Mixing within a hemisphere occurs in the troposphere on time scales of a few weeks to three months, whereas exchange between hemispheres occurs between 1.1 and 1.7 years (Levin and Hesshaimer, 1996; Geller *et al.*, 1997). The halocarbons also are transported into the stratosphere, where photolysis and reaction with OH lead to the formation of inorganic species of bromine, chlorine, and fluorine. Mixing between the troposphere and the lower and middle stratosphere, where most of the ozone depletion occurs, takes place within 1 to 3 years in the tropics and between 3 to 6.5 years at midlatitudes and in the polar regions at altitudes of 21 km and below (Elkins *et al.*, 1996b; Harnisch *et al.*, 1996a; Waugh *et al.*, 1997; Volk *et al.*, 1997; Wamsley *et al.*, 1998). Mean ages of an air parcel deduced from observations of $SF_6$ over different latitudes and altitudes from October through November 1994 demonstrate these mixing times (Volk *et al.*, 1997; Wamsley *et al.*, 1998). The inorganic species can form compounds that either react with stratospheric ozone (reactive species) or do not react (nonreactive species, also called reservoirs). Volcanic eruptions inject inorganic chlorine ($Cl_y$) into the atmosphere, primarily in the form of HCl; however, most of it is rained out in the troposphere and very little reaches the stratosphere (Tabazadeh and Turco, 1993; Russell *et al.*, 1996c; Zander *et al.*, 1996a; Coffey 1996). Under normal stratospheric conditions, oxides of nitrogen, primarily NO and $NO_2$, can temporarily tie up both bromine and chlorine atoms in nonreactive reservoirs such as bromine nitrate ($BrONO_2$) and chlorine nitrate ($ClONO_2$), but these atoms can be freed efficiently in the presence of sulfate aerosols and polar stratospheric clouds, leading to enhanced local ozone depletion. So far, inorganic fluorine and iodine have not contributed to any appreciable ozone depletion, the former because of the stability of its ultimate sink, HF (Stolarski and Rundel, 1975), and the latter because of its low concentration in the atmosphere (Wennberg *et al.*, 1997).

### 1.3.2 Anthropogenic Sources of Atmospheric Chlorine, Bromine, and Fluorine

Worldwide emissions of halocarbons have changed dramatically in recent years. With the implementation of the Montreal Protocol on Substances that Deplete the Ozone Layer and its Amendments, production in developed countries ceased by the end of 1993 for halons and by the end of 1995 for CFCs, $CCl_4$, and $CH_3CCl_3$ (see Chapter 2), apart from a comparatively small amount for essential uses and an allowance to supply the needs of developing countries, which have a ten-year grace period. The evidence from production statistics is that compliance with the Montreal Protocol is proceeding either on or ahead of schedule and CFC production in the major industrialized nations is now below the level of the early 1960s (AFEAS, 1998; UNEP, 1997).

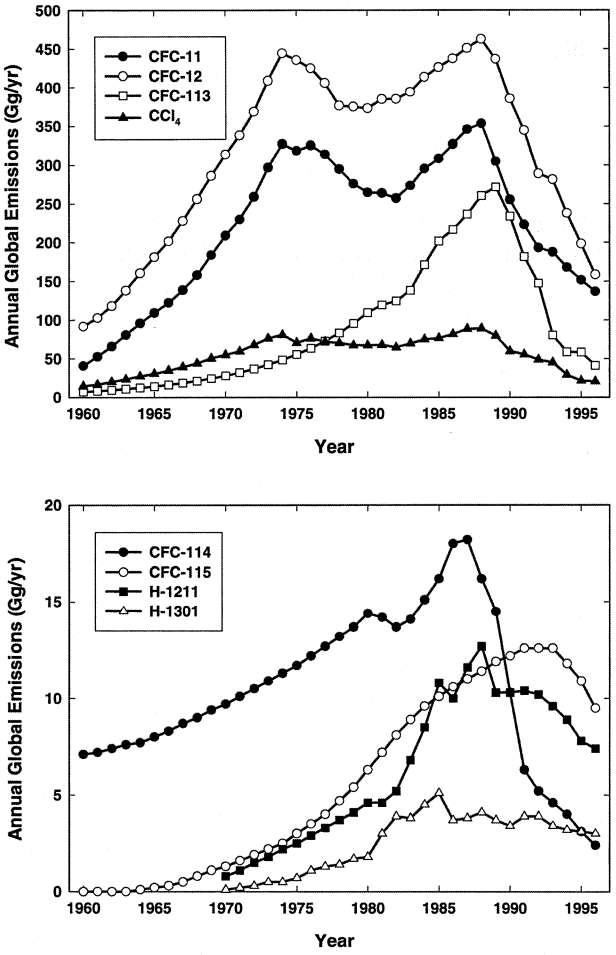


**Figure 1-11.** Annual global emissions (in Gg $yr^{-1}$) of long-lived halocarbons estimated by industry from audited production, sales, and other data (AFEAS, 1998; Fisher *et al.*, 1994; McCulloch, 1992; Fraser *et al.*, 1998; updated by P. Midgley, personal communication).

Emissions of the controlled substances continue from the permitted, comparatively small use in developing countries and also, more significantly, from the slow release of halocarbons held in existing equipment and plastic foams. Nevertheless, worldwide emissions of halocarbons have declined dramatically in recent years (see Figure 1-11). Although illegal imports of CFCs, estimated to be some 10 Gg, may be affecting the market for CFC alternatives in developed countries, their effect on CFC emissions and chlorine loading is estimated to be significantly less, by about a factor of 10, than that from legal use (SORG, 1996).

### 1.3.2.1 CFCs

The most detailed compilation of the annual production and sales of individual CFCs in recent years is the industrial survey issued by the Alternative Fluorocarbons Environmental Acceptability Study (AFEAS). The survey participants, located in Europe, North America, and Japan, together with their subsidiaries elsewhere in the world, provide essentially complete global coverage for the early years of production. Subsequently, production not reported by AFEAS began elsewhere, primarily in India, China, and Russia. It has been estimated, however, that AFEAS inventories cover over 90% of the global production until the mid-1980s, and still about 80% of the much-diminished global total for the major products (CFC-11 and -12) as late as 1993 (Fisher *et al.*, 1994; UNEP, 1997). Currently, production in the industrialized nations has been phased out except for the minor amount permitted for essential internal uses and CFCs exported to supply the needs of developing countries. The Montreal Protocol permits up to 15% of base year 1986 production, amounting to some 160 Gg of combined CFCs, for this export market. Consequently, production reported to AFEAS now represents a much smaller fraction of the global total, around 60% from 1994 to 1995.

The databases compiled by UNEP provide a detailed geographical breakdown with potentially complete global coverage, but it takes a long time for all national returns to come in. UNEP publishes totals of aggregated CFC production on an Ozone Depletion Potential-weighted basis with no sales breakdown. In order to get global emission numbers for individual compounds, it is necessary to combine these two UNEP datasets and this has been done to calculate the global emissions shown in Figure 1-11 (Fisher *et al.*, 1994; McCulloch *et al.*, 1994; Fraser *et al.*, 1998; P.M. Midgley, M & D Consulting, Germany, personal communication, 1998).

Industrial sales of CFCs have declined rapidly in recent years; surveys of the world's major producers show that sales in 1995 were 32 Gg, 83 Gg, and 23 Gg, respectively, for the major products CFC-11, -12, and -113. These were less than 10% of the amounts reported in the years of peak production for CFC-11 and -113, and less than 20% for CFC-12 (AFEAS, 1998). Calculated emissions of CFC-113 are also less than 10% of the peak year (1989) for this compound; its main application as a solvent results in its rapid emission

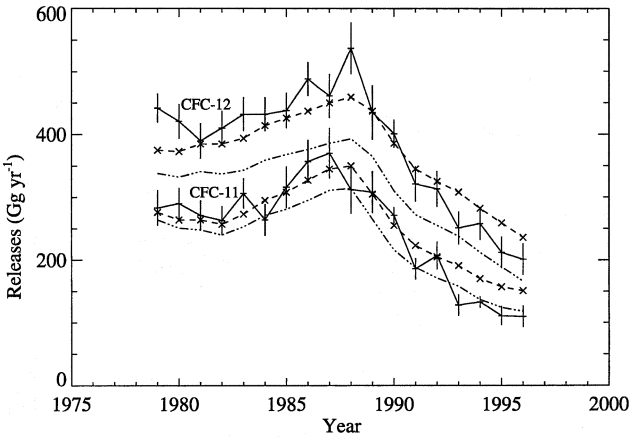


**Figure 1-12.** Global yearly releases of CFC-11 and CFC-12 (Gg $yr^{-1}$) estimated from the ALE/GAGE/AGAGE measurements assuming lifetimes of 50 and 110 years, respectively (solid lines and plus symbols; Cunnold *et al.*, 1997). Also shown are industry estimated emissions from reporting companies only (3 dots and dash line) and world releases including reporting and nonreporting companies (dashed lines joining crosses) estimated by Cunnold *et al.* (1997).

(Fisher and Midgley, 1993). The principal uses of CFC-11 and -12, namely, foam blowing, refrigeration, and air conditioning, all involve delays between CFC use and its release to the atmosphere (Fisher and Midgley, 1994). A large fraction of emissions comes from the bank of previously used CFCs held in equipment and foams. Therefore, the reductions in calculated emissions lag behind those in reported sales, being less in 1995 than 40% of the peak year (1974) for CFC-11 and 45% for CFC-12. Total consumption of CFCs in developing countries operating under Article 5 of the Montreal Protocol was about 170 Gg in 1994 (UNEP, 1997). It has been estimated that about half of these requirements were met by production in the developing countries themselves and the rest by material exported from developed countries (UNEP, 1994). Consumption in developing countries will be phased out by 2010.

Modeled atmospheric mixing ratios for CFC-11 and CFC-12 from emission estimates by industry tend to overestimate the recent mixing ratios and trends from both the NOAA/CMDL and AGAGE global networks (Elkins *et al.*, 1993; Cunnold *et al.*, 1994, 1997; Montzka *et al.*, 1996). As an example, Figure 1-12 reproduces the comparison between the global yearly releases estimated from the ALE/GAGE/AGAGE measurements and estimates from industry using reporting companies and world releases versus time. The inconsistency during the last years (Cunnold *et al.*, 1997) cannot be explained by errors in lifetimes (e.g., by using the WMO (1998) values recommended in Table 1-1) because atmospheric data show the growth rate declining more rapidly in recent times. Possible reasons may be changing emission factors for various uses, overestimates of the banked reservoir, or inaccurate estimates of emissions for nonreporting companies. In Figure 1-12, the nonreporting company emissions have been held constant in recent years, primarily because of lack of other information. One interpretation of the results is that nonreporting company emissions have dropped in recent years.

### 1.3.2.2 Halons

The production of Halon-1211 and -1301 peaked in 1988 and ceased in the developed world at the end of 1993 under the provisions of the Montreal Protocol. Production is known to occur in developing countries (e.g., China, India, Korea) and is permitted until 2002. However, large quantities of these gases, which are used as specialized fire extinguishing agents, are stored (banked) in equipment and emissions come predominantly from this bank. Using a combination of audited industry data and national data reported to the UNEP, estimates have been made of the annual emissions of Halon-1211 and -1301 (McCulloch, 1992; UNEP, 1997). To illustrate the size and growth of the bank, production of Halon-1211 in 1988 was 20 Gg, emissions were about 13 Gg, but the bank was 49 Gg and grew by 1994-1996 to an estimated 60 Gg. The equivalent figures for Halon-1301 were 8 Gg for 1988 production, 4 Gg for 1988 emissions, 60 Gg for the 1988 bank, and 70 Gg for the 1994-1996 bank (A. McCulloch, ICI Chemicals and Polymers Limited, U.K., personal communication, 1998; SORG, 1996).

Measured abundances of Halon-1211 and -1301 (Butler *et al.*, 1998) are lower than those derived from estimates of emissions by factors of about 0.75 and 0.97, respectively (see Figure 1-13). A simulation adjusting the atmospheric lifetime of Halon-1211 from 20 to 10 years produces a good fit between emission estimates (see Figure 1-11; also Fraser *et al.*, 1998) and measurements prior to 1993. This lower lifetime estimate

is consistent with photolysis results calculated in the troposphere and stratosphere (see Section 1.4.4), but inconsistent with the observed interhemispheric ratio of Halon-1211 (Butler *et al.*, 1998). The cause of the discrepancy between emissions and measurements of Halon-1211 is not fully understood at this time.

For Halon-2402, which was manufactured almost exclusively in eastern Europe, reports to UNEP show production of about 4 Gg in 1986, falling to less than 10% of this total in 1994 to 1995 (UNEP, 1997). On the other hand, not much is known about the production of Halon-1202, which is used as a fire extinguishing agent only in military transport aircraft and is not covered by UNEP reports (SORG, 1996).

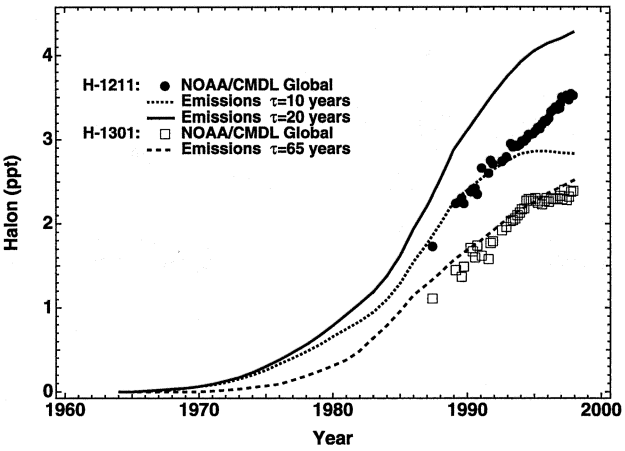


**Figure 1-13.** Atmospheric history of Halon-1211 and -1301 from NOAA/CMDL measurements and modeled emissions. Global average concentrations for Halon-1211 and -1301 are shown as filled circles and gray open squares, respectively. Lines are emission-based predictions (Figure 1-11; Fraser *et al.*, 1998), using atmospheric lifetimes given in the previous WMO Assessment (Solomon *et al.* in WMO, 1995), i.e., 20 years for Halon-1211 (solid black line) and 65 years for Halon-1301 (dashed gray line). The black dotted line represents concentration predictions for Halon-1211, based on an atmospheric lifetime of 10 years. Note the elevated mixing ratios for observed Halon-1211 since the mid-1990s compared to the latter predictions; if both the 10-year lifetime and the emissions from developed countries are correct, then these elevations would be the result of unreported emissions from developing countries and/or some unaccounted release from the large bank of Halon-1211 in developed countries. If the lifetime of Halon-1211 is significantly larger than 10 years, then emission estimates for all years are suspect. Data and model predictions are from Butler *et al.* (1998), updated for a lifetime of 10 years.

### 1.3.2.3 Carbon Tetrachloride ($CCl_4$)

Emissions of $CCl_4$ into the atmosphere, which arise during its use as a chemical feedstock for CFC-11 and -12, and during the manufacture of $CCl_4$ itself, have decreased roughly in proportion to the decline in CFC production. Neither the quantities of $CCl_4$ produced nor the losses are recorded specifically but analysis of the UNEP data in combination with the AFEAS reports on CFC production can be used to derive $CCl_4$ emissions. These had declined to about 20 Gg $yr^{-1}$ by 1995 (A. McCulloch, ICI Chemicals and Polymers Limited, U.K., personal communication, 1998). The minor uses of $CCl_4$ as a process agent are also controlled under the Montreal Protocol and give rise to much lower emission totals (UNEP, 1995). Using an atmospheric lifetime for $CCl_4$ of $42 \pm 12$ years, Simmonds *et al.* (1998) found that ALE/GAGE/AGAGE atmospheric measurements and industry estimates were consistent if nonreporting countries are dominating world releases after a sharp drop in production in 1991 by reporting countries. However if the lifetime of $CCl_4$ is 35 years as recommended in Table 1-1, then the industrial emission scenario provided in Simmonds *et al.* (1998) underestimates emissions by about 17%.

### 1.3.2.4 Other Compounds

Estimated industrial emissions of the shorter lived organic compounds like $CH_3CCl_3$, selected HCFCs, and HFCs are presented in Chapter 2. While there are currently no available yearly emissions from industry for compounds composed mainly of fluorine (i.e., $CF_4$, $C_2F_6$, ...), atmospheric measurements and simple atmospheric models can provide important confirmation of estimates of emissions. As an example, Geller *et al.* (1997) use global measurements of $SF_6$ from the NOAA/CMDL Cooperative Network and selected ocean cruises, and from Maiss *et al.* (1996), together with a simple two-box atmospheric model to calculate emissions for 1996 of $5.9 \pm 0.2$ Gg $SF_6$ $yr^{-1}$. This value is in agreement with estimates of industrial emissions made by Ko *et al.* (1993). Industrial production values (S&PS, 1997) are consistent with atmospheric observations (after

accounting for banking) since 1972 and are estimated at 7.6 Gg $yr^{-1}$ in 1996 (Maiss and Brenninkmeijer, 1998). From the Geller *et al.* (1997) global emission rate for 1996, it appears that a large fraction (approximately 80%) of $SF_6$ produced each year is released from the stored bank and recent production into the atmosphere.

From the observed increase rates of the mixing ratios of atmospheric $CF_4$ and $C_2F_6$, annual global emissions of 15 to 18 Gg of $CF_4$ (Harnisch *et al.*, 1996a) and $1.9 \pm 0.15$ Gg of $C_2F_6$ (Harnisch *et al.*, 1996a) have been inferred for 1994. Similarly, Zander *et al.* (1996c) estimated the amount of $CF_4$ injected into the atmosphere at $18 \pm 7$ Gg during 1994 based on the rate of increase determined from ATMOS observations in 1985 and 1994. Using data from an extensive survey on emissions carried out by the International Primary Aluminium Institute (IPAI) between 1990 and 1993 (IPAI, 1996), annual emissions of 12 to 17 Gg of $CF_4$ and 1 to 2 Gg of $C_2F_6$ can be calculated. Atmospheric accumulation and reported emissions thus agree reasonably well.

### 1.3.3 Chlorine Budget Estimates

#### 1.3.3.1 Distribution of Organic Chlorine ($CCl_y$)

Total $CCl_y$ in the atmosphere is defined as the sum of the chlorine atoms bound in all organic chlorine-bearing source gases released to the atmosphere. This includes both natural and anthropogenic as well as short- and long-lived compounds. Based on the dominant Cl-bearing organic species, $CCl_y$ can be evaluated according to

$$\begin{aligned} CCl_y = {} & 3[CCl_3F] + 2[CCl_2F_2] + 3[CCl_2FCClF_2] \\ & + 3[CH_3CCl_3] + 4[CCl_4] + [CH_3Cl] \\ & + [CHClF_2] + [\text{minor contributors}] \end{aligned} \quad (1\text{-}1)$$

where brackets indicate concentrations as dry mole fractions. Multipliers before the brackets indicate the number of chlorine atoms per molecule. Minor contributors (e.g., $CClF_3$, $CH_2Cl_2$, CFC-114, CFC-114a, CFC-115, $CHCl_3$, $C_2Cl_4$, HCFC-141b, HCFC-142b, H-1211), which account for approximately 100 ppt (less than 3% of the total under all current circumstances), are neglected here.

None of the monitoring networks measures all species making up $CCl_y$, but two of them measure different but significant fractions, $CCl_y$*, of the total $CCl_y$ on a global basis. The ALE/GAGE/AGAGE network has estimated global $CCl_y$* from CFC-11, -12, and -113, $CH_3CCl_3$, and $CCl_4$ measurements since 1978, which is labeled as $(CCl_y^*)_a$ in Figure 1-14a (gray dotted line). Recently, ALE/GAGE/AGAGE has begun measuring HCFC-22 at SIO and Cape Grim, Tasmania, along with making measurements from archived flask samples containing air from Cape Grim. Including HCFC-22 global means generated from this dataset with a 2-D model, ALE/GAGE/AGAGE estimates the peak $CCl_y$* at approximately 2950 ppt at some time between mid-1992 and mid-1994 (Figure 1-14a, gray solid line). Similar global estimates of the two different $CCl_y$* sums (i.e., without and with HCFC-22) using NOAA/CMDL data are reproduced in Figure 1-14a as black dotted and solid lines, respectively. The offsets in $CCl_y$* from the two networks represent small calibration differences. Tropospheric measurements of total $CCl_y$ (Montzka *et al.*, 1996) from the NOAA/CMDL flask network (including both flask and in situ measurements for the CFCs, $CH_3CCl_3$, $CCl_4$, HCFC-141b, HCFC-142b, and Halon-1211) also show that the peak in $CCl_y$* occurred sometime between mid-1992 and mid-1994 (Figure 1-14b) and was decreasing at a rate of $25 \pm 5$ ppt $yr^{-1}$ by mid-1995 (Montzka *et al.*, 1996). In both of these studies, explicit measurements of methyl chloride ($CH_3Cl$) were not available for consideration. Because the presence of $CH_3Cl$ in the atmosphere is believed to mostly result from natural processes (see Chapter 2), it was assumed that the $CH_3Cl$ mixing ratio has remained constant during recent years; this assumption is supported by Khalil and Rasmussen (1998). When augmenting the data from Figure 1-14 with contributions from $CH_3Cl$ and other minor species, it is estimated that the global peak $CCl_y$ (as defined in Equation 1) occurred between mid-1992 and mid-1994, at a level equal to $3700 \pm 100$ ppt. The subsequent $CCl_y$ decline was primarily the result of the decrease observed in mixing ratios of $CH_3CCl_3$ (Prinn *et al.*, 1995; Montzka *et al.*, 1996). Similar results for $CCl_y$ have been obtained from the AGAGE measurements (Cunnold *et al.*, 1997).

One recent example of the detailed $CCl_y$ determination in the stratosphere is based on measurements from the ATMOS instrument during the ATLAS-3 Space Shuttle mission in November 1994 (Zander *et al.*, 1996b). The source gases involved were CFC-11, CFC-12, HCFC-22, $CCl_4$, and $CH_3Cl$, all measured by ATMOS, complemented by $CH_3CCl_3$ and CFC-113 derived from gas chromatographic analyses of flasks collected on a balloon platform, over southern France, one month before the ATLAS-3 mission; they are consistent with earlier stratospheric profile

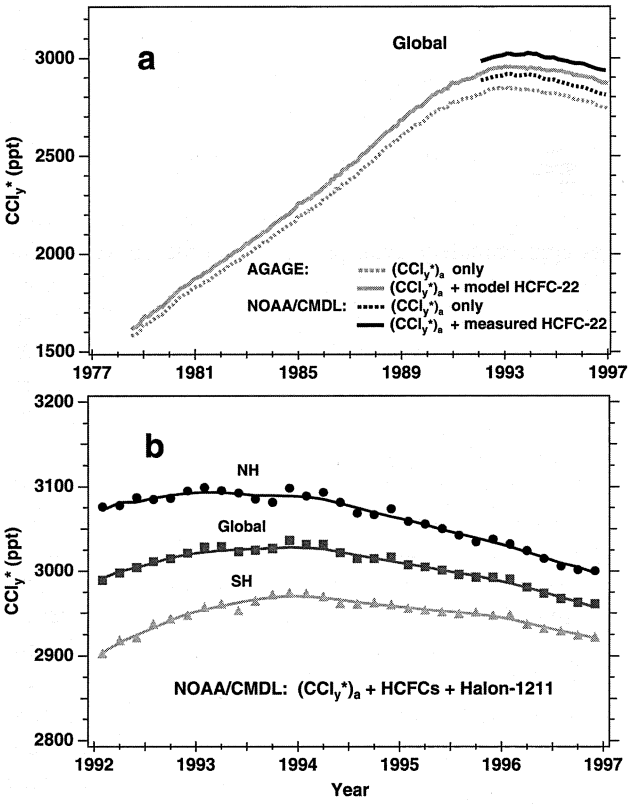


**Figure 1-14.** (a) Different global mean estimates of tropospheric $CCl_y$* from the ALE/GAGE/AGAGE and NOAA/CMDL networks. Dotted lines represent measured global means labeled $(CCl_y^*)_a$ from the principal chlorocarbons CFC-11, -12, and -113, $CH_3CCl_3$, and $CCl_4$. Solid lines include HCFC-22 global mixing ratios. ALE/GAGE/AGAGE updated data available from Prinn *et al.* (1998). (b) Tropospheric $CCl_y$* estimated on a bimonthly basis for the Northern Hemisphere (circles, NH), Southern Hemisphere (triangles, SH), and global (squares) from the halocarbons measured by the NOAA/CMDL flask network since early 1992 (updated from Montzka *et al.* (1996) in Elkins *et al.* (1998)). For total $CCl_y$ as per Equation (1-1), add about 650 ppt to each line for the unmeasured species $CH_3Cl$ and the relatively minor contributors listed in the text. Curves through data points represent a non-parametric least-squares fit, where the fractional weighting factor is 30% (Cleveland and Devlin 1988).

determinations (e.g., Zander *et al.*, 1992) and with tropospheric concentrations for the individual compounds involved.

### 1.3.3.2 Distribution of Inorganic Chlorine ($Cl_y$)

$CCl_y$ compounds (see Equation (1-1)) mix into the stratosphere and are broken apart by photolysis and reaction with OH and $O(^1D)$, producing $Cl_y$ bound in reactive and reservoir gases. The dominant species of reactive (with ozone) $Cl_y$ are: chlorine monoxide (ClO) and its dimer ClOOCl, hypochlorous acid (HOCl), and chlorofluorocarbonyl (COClF). The dominant reservoir species of $Cl_y$ are $ClONO_2$ and HCl. Total $Cl_y$, which includes the carbonyl compound COClF, is equal to the sum of both reactive and nonreactive forms, i.e.,

$$Cl_y = [Cl] + 2[Cl_2] + [OClO] + [ClO] + 2[ClOOCl] + [HOCl] + [COClF] + [HCl] + [ClONO_2] + [ClONO] + [BrCl] \quad (1\text{-}2)$$

As a logical complement to the $CCl_y$ evaluation discussed in Section 1.3.3.1, Zander *et al.* (1996b) combined the ATMOS/ATLAS-3 measurements of the inorganic species HCl and $ClONO_2$ with mixing ratios of: (i) ClO obtained by the Millimeterwave Atmospheric Sounder (MAS) during ATLAS-3, (ii) HOCl obtained with the MkIV FTIR spectrometer during a balloon flight in September 1993 near 32°N, scaled by a 3% increase per year to represent the HOCl loading at the time of the ATLAS mission, and (iii) COClF calculated by an atmospheric chemistry model.

The total chlorine $Cl_{TOT}$ at the time of entry into the stratosphere, which includes the sum of $CCl_y$ and $Cl_y$, is defined as

$$Cl_{TOT}(entry) = [CCl_y] + [Cl_y] \quad (1\text{-}3)$$

The resulting mean $Cl_{TOT}$ between 16.5 and 50 km altitude was $3.53 \pm 0.1$ ppb (1 standard deviation) during the ATLAS-3 mission; its observed partitioning, for the latitudinal zone 35°N to 49°N, is displayed in Figure 1-15. It should be noted here that, within the measurement uncertainties of typically ±5%, $Cl_{TOT}$ is equal to $Cl_y$ above 40 km altitude, as only trace amounts of Cl-bearing source gases persist at such heights. A difference of about 6% in $Cl_{TOT}$ between the lower and upper stratospheric layers can be explained by invoking the lag time to mix $Cl_{TOT}$ between these two levels (Zander *et al.*, 1996b).

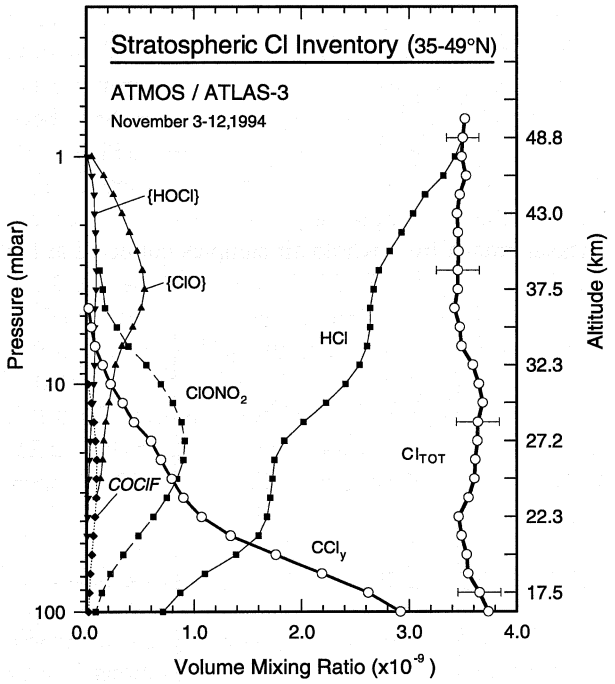


**Figure 1-15.** Mean vertical volume mixing ratio profiles of individual dominant species of $Cl_y$, $CCl_y$, and total chlorine ($Cl_{TOT}$) derived from the ATMOS/ATLAS-3 mission of November 1994 (Zander *et al.*, 1996b). $Cl_{TOT}$ is the sum of $CCl_y$, HCl, $ClONO_2$, ClO, HOCl, and COClF.

### 1.3.3.3 Consistency and Trends of $Cl_y$ and $CCl_y$

There is overall approximate consistency in chlorine atom inventories for the source, sink, and reservoir species. The resulting $Cl_{TOT}$ is preserved throughout the stratosphere and is consistent with chlorine loading monitored at the ground, when accounting for a troposphere-to-middle-stratosphere mixing time of about five years (Zander *et al.*, 1996b; Chang *et al.*, 1996b).

In addition, after accounting for transport lags, the trends of $Cl_y$ observed from ground- and space-based platforms are consistent with measurements of $CCl_y$ in the troposphere. HCl and $ClONO_2$, which are the largest and longest-lived reservoirs of $Cl_y$, should show growth rates commensurate with total $CCl_y$ trends in the troposphere, after accounting for the troposphere-stratosphere mixing time. Thus, a comparison of both forms of chlorine is possible under the assumption that this mixing time is known, i.e., 3 to 6.5 years depending on latitude and altitude (Russell *et al.*, 1996c; Volk *et al.*, 1997; Harnisch, 1996). The column abundances above ISSJ of HCl from 1985 to 1995 (Zander *et al.*, 1996a) and of $ClONO_2$ from 1986 to 1994 (Rinsland *et al.*, 1996b) showed mean trends of $3.9 \pm 0.2\%$ $yr^{-1}$ and $4.0 \pm 0.7\%$ $yr^{-1}$, respectively. By combining these updated observational databases over the current overlapping period (Figure 1-16) and adding a ClO background loading derived from model calculations, it is found that the rate of increase of (HCl + $ClONO_2$ + ClO) was equal to $3.7 \pm 0.3\%$ $yr^{-1}$ from 1991 to 1993 and $1.8 \pm 0.3\%$ $yr^{-1}$ from 1995 to 1997. The former value is comparable with the mean stratospheric $3.3 \pm 0.2\%$ $yr^{-1}$ trend of $Cl_{TOT}$ measured by ATMOS over the spring 1985 to fall 1994 time period (Zander *et al.*, 1996b), and all are consistent with the growth of $CCl_y$ that prevailed during the mid- and late 1980s, i.e., between 3 and 4% $yr^{-1}$ (WMO, 1990, 1992). The $ClONO_2$ columns derived above the ISSJ are commensurate with those derived by Reisinger *et al.* (1994) over Lauder (45.0°S) between September 1990 and August 1994, but the latter show no statistically significant trend (i.e., $1.3 \pm 2\%$ $yr^{-1}$) over that four-year period.

An additional and independent confirmation of the consistency between total $Cl_y$ and total $CCl_y$ comes from the UARS HALOE experiment (Russell *et al.*, 1993). From a global series of HCl volume mixing ratios measured near 55 km altitude from October 1991 to April 1995 (see Section 1.2.8), and model evaluations of Cl-bearing compounds not fully converted into HCl, Russell *et al.* (1996c) derived a $Cl_y$ rate of increase equal to $(108 \pm 7)$ ppt $yr^{-1}$, which translates into a trend of $(3.7 \pm 0.3)\%$ $yr^{-1}$ referred to mid-1993, in good agreement with the above reported $Cl_y$ increases. From comparisons with tropospheric Cl-bearing source gas inventories and model calculations, Russell *et al.* (1996c) concluded that all but a few percent (3 to 7%) of observed stratospheric chlorine amounts can be accounted for by known anthropogenic and natural tropospheric emissions, the former dominating the latter.

Recent in situ measurements of $CCl_y$ from ACATS-IV (Elkins *et al.*, 1996b), $CCl_y$ from whole air samples (Daniel *et al.*, 1996), HCl from Aircraft Laser Infrared Absorption Spectrometer (ALIAS) (Webster *et al.*, 1994, 1998), and ClO and $ClONO_2$ from a new $Cl_y$ instrument, aboard the NASA ER-2 aircraft during the Photochemistry of Ozone Loss in Arctic Region in Summer (POLARIS) mission from Fairbanks, Alaska, show that calculated $Cl_y$ from ($Cl_{TOT}$ -$CCl_y$) agrees with observed $Cl_y$ at most altitudes within the experimental errors of

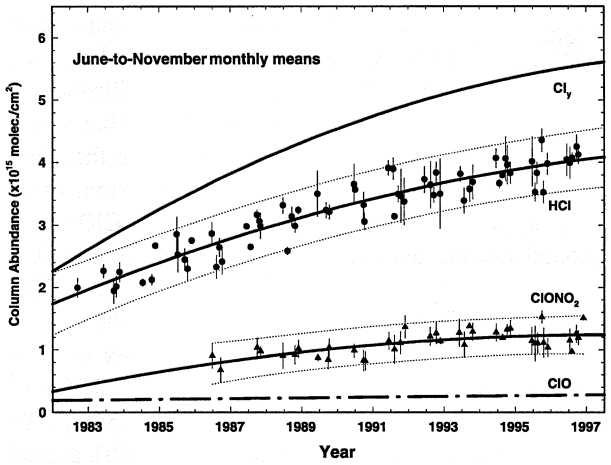


**Figure 1-16.** Evolution of the total inorganic $Cl_y$ loading, based on HCl and $ClONO_2$ monthly mean vertical column abundance determinations above the Jungfraujoch and a background ClO amount derived from model calculations. The observational databases are extensions of those reported by Zander *et al.* (1996a) for HCl and by Rinsland *et al.* (1996b) for $ClONO_2$. Only measurements made between June and November are included, to avoid significant column variability during winter and spring periods.

the measurements (Sen *et al.*, 1998).

The conclusion that can be made from the data discussed above is that there remains little doubt that the bulk of chlorine atoms in today's stratosphere and its temporal evolution are primarily associated with the release of anthropogenic chlorine-bearing gases at the Earth's surface.

## 1.3.4 Bromine Budget Estimates

### 1.3.4.1 Trends of Organic Bromine

Six gases contribute predominantly to the organic bromine budget in the troposphere, i.e., methyl-bromide ($CH_3Br$), bromochloromethane ($CH_2BrCl$), dibromomethane ($CH_2Br_2$), and Halon-1211, -1301, and -2402. The total organic bromine mixing ratio, $CBr_y$, using only these dominant species, is defined as:

$$CBr_y = [CH_3Br] + [CH_2BrCl] + 2[CH_2Br_2] + [CBrClF_2] + [CBrF_3] + 2[CBrF_2CBrF_2] \quad (1\text{-}4)$$

where brackets indicate dry mixing ratios and multipliers before the brackets indicate the numbers of bromine atoms per molecule. Concentration measurements and rates of increase for the long-lived halons have been reviewed in Section 1.2.3 and summarized in Figure 1-4. The other shorter-lived compounds of Equation (1-4) are dealt with in Chapter 2. Total organic bromine measurements from whole air samples collected at the tropical tropopause in 1996 averaged 17.4 ± 0.9 ppt (Schauffler *et al.*, 1998a); methyl bromide accounted for 55% of the total organic bromine, Halon-1301 for 13.6%, Halon-1211 for 19.8%, Halon-2402 for 5.1%, $CH_2Br_2$ for 5.7%, $CH_2BrCl$ for 0.7%, and $CHBrCl_2$ for 0.1%. The resulting $CBr_y$ shows a growth rate of about 2.2% per year, all from the halons (Butler *et al.*, 1998; Wamsley *et al.*, 1998).

### 1.3.4.2 Organic Bromine in the Stratosphere

The correlation of the concentrations of organic bromine species with CFC-11 concentrations is very reproducible when normalized for the atmospheric growth of the species (Wamsley *et al.*, 1998). This normalization is required to compare datasets from different locations and times. The results from a number of aircraft and balloon measurements, and two-dimensional (2-D) model calculations (Weisenstein *et al.*, 1996) are consistent with each other (Figure 1-17). Additional aircraft measurements from whole air samples collected in 1996 (Schauffler *et al.*, 1998b) show consistent correlations with previous 1991 to 1992 measurements from whole air samples (Avallone and Prather, 1997). The correlation between two species with stratospheric mixing ratios that are represented by a stratospheric loss rate ($1/\tau$) can be described by a power law relationship with a power coefficient equal to the ratios of the loss rates of the two species (Wamsley *et al.*, 1998). The correlations between the brominated species and CFC-11 are adequately described by a simple power law,

$$[X]/[X]_o = ([CFC\text{-}11]/[CFC\text{-}11]_o)^{1/d} \quad (1\text{-}5)$$

where the mixing ratio of each brominated species is represented by [X], the subscript, o, designates the mid-October 1994 volume mixing ratio at the tropopause, and ($1/d$) is the power coefficient. Wamsley *et al.* (1998) were able to calculate $CBr_y$ for each bromine species in Equation (1-4) using the measured values of Halon-1211

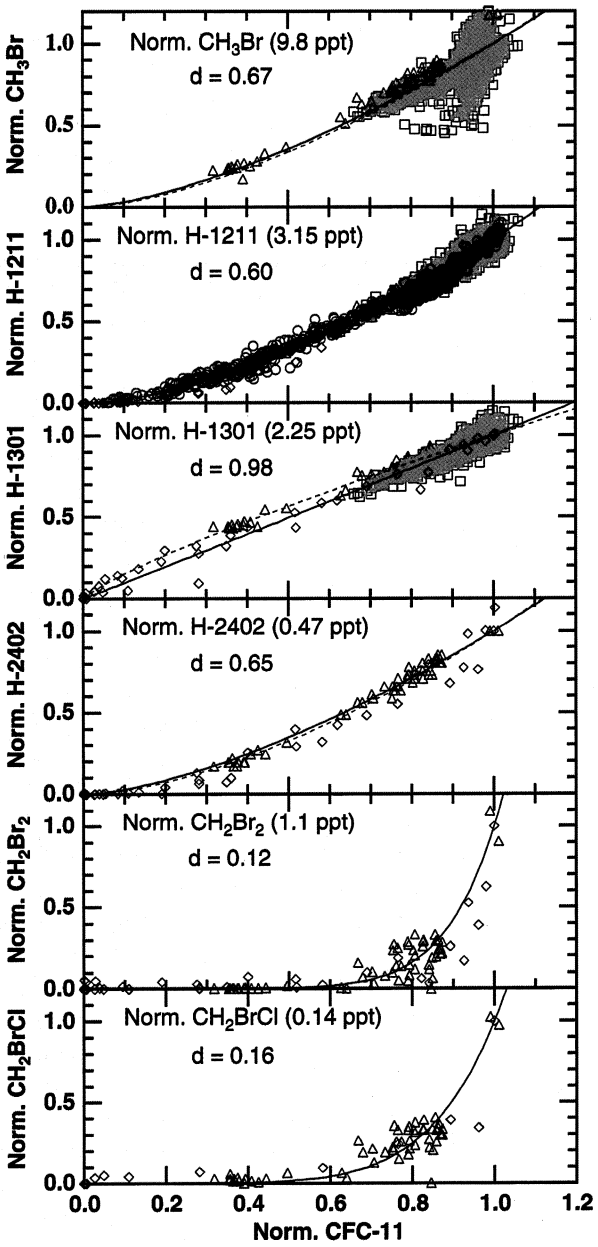


**Figure 1-17.** Normalization datasets and resulting correlations for the six organic bromine species versus CFC-11 included in the calculation of organic bromine from Wamsley *et al.* (1998). The solid curves are the best fits to the data using Equation (1-5). The October 1994 surface mixing ratio for each molecule is given in parentheses. ACATS-IV data are shown in black circles (Elkins *et al.*, 1996b), National Center for Atmospheric Research (NCAR) data in blue triangles (Schauffler *et al.*, 1993), University of East Anglia (UEA) data in green diamonds, and University of California-Irvine in red squares (Blake *et al.*, 1992). The dashed curves are fits to the Atmospheric and Environmental Research, Inc. (AER) model results (Weisenstein *et al.*, 1996) matched for season and location with the NCAR data. The value of *d* for the modeled Halon-1211 correlation is 0.60, which makes it difficult to distinguish from the measured correlation (0.53).

and CFC-11 during the ASHOE/MAESA campaign of 1994, and the correlations of the unmeasured species with CFC-11 (Figure 1-17). Adding up the individual components from Equation (1-4), it is found that the correlation between $CBr_y$ and CFC-11 is very good in the stratosphere (Figure 1-18a). The solid curve is the best fit to the correlation using Equation (1-5) with $d$ = 0.58. The effective stratospheric lifetime of $CBr_y$ in today's atmosphere is estimated to be approximately one half that of CFC-11.

### 1.3.4.3 Inorganic Bromine ($Br_y$) in the Stratosphere

Measurements of $Br_y$ species in the stratosphere are extremely difficult because of their low volume mixing ratios and high reactivity to surfaces. Total $Br_y$ is composed of the following:

$$Br_y = [Br] + [BrO] + 2[Br_2] + [BrONO] + [BrCl] + [BrONO_2] + [HOBr] + [HBr] \quad (1\text{-}6)$$

where the factor before the bracket indicates the number of bromine atoms per molecule and the brackets indicate the dry volume mixing ratio of the compound. A recent study (Lary, 1996) found that the lifetimes of $Br_2$, BrONO, BrCl, $BrONO_2$, and HOBr are less than one day in sunlight at 20 km altitude. For typical midlatitude conditions, model calculations show that the volume mixing ratio of $Br_y$ is about 2 times the value of BrO (Salawitch *et al.*, 1994).

$Br_y$ can be calculated indirectly using the total organic bromine, $CBr_y$ from Equation (1-4), and the observed tropospheric trends for total bromine ($Br_{TOT}$) at the time of entry into the stratosphere at the tropical tropopause, from the relation

$$Br_{TOT}(entry) = [Br_y] + [CBr_y] \quad (1\text{-}7)$$

and solving for $Br_y$ (Daniel *et al.*, 1996).

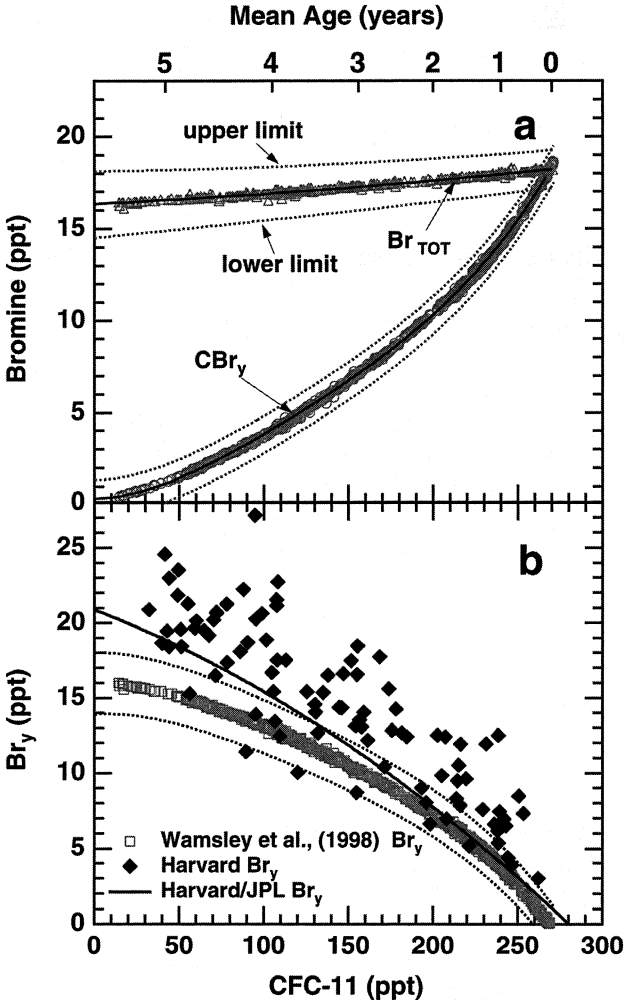


**Figure 1-18.** (a) Calculated results for $Br_{TOT}$ (triangles) as a function of CFC-11, using the age of the air mass from $SF_6$ observations, reported trends for the atmospheric halons (Butler *et al.*, 1998), and the sum of all organic bromine compounds, $CBr_y$ (circles) for each observation during ASHOE/MAESA (Wamsley *et al.*, 1998). (b) Calculated mixing ratios of $Br_y$ as a function of CFC-11, using the Wamsley *et al.* (1998) $Br_y$ estimates from (a), and an earlier result labeled Harvard/JPL $Br_y$, derived from AASE II measurements (Salawitch *et al.*, 1994). The diamonds represent Harvard $Br_y$ calculated using in situ BrO measurements during ASHOE/MAESA and $Br_y$ partitioning from a photochemical model. The dashed curves represent upper and lower limits within one-standard-deviation windows including all measurement uncertainties for bromine estimates by Wamsley *et al.* (1998).

During the ASHOE/MAESA mission in 1994, concurrent measurements were made of Halon-1211 by NOAA/CMDL and BrO by Harvard (Wamsley *et al.*, 1998). From these measurements, $Br_y$ was calculated using the indirect organic bromine method (Wamsley *et al.* (1998) $Br_y$ in Figure 1-18b) and an indirect $Br_y$ method based on BrO and other species measurements (Harvard $Br_y$ in Figure 1-18b). A fit to earlier organic bromine measurements by the whole air sampler (WAS) instrument during AASE II in 1992 is included for comparison (Harvard/Jet Propulsion Laboratory (JPL) $Br_y$ in Figure 1-18b; Salawitch *et al.*, 1994). The value of the Harvard $Br_y$ in the oldest air parcels (lowest CFC-11) is 20 (+11, -9.8) ppt. This value is higher than the Wamsley *et al.* (1998) $Br_y$, but within the experimental errors of each approach. The differences between the two methods could be explained if $Br_y$ from the troposphere is transported to the stratosphere, as suggested by Ko *et al.* (1997), or if there is some missing compound in the calculation of organic bromine ($CBr_y$ as per Equation (1-4)), or if the $Br_y$ partitioning is in error (Wamsley *et al.*, 1998). Lower values of BrO (by 30%) were measured using the same BrO instrument discussed in Wamsley *et al.* (1998) but were based on an earlier airborne mission in 1991 to 1992 and a different instrument calibration (Avallone *et al.*, 1995). If these lower values of BrO are correct, then the calculated $Br_y$ would be in better agreement with the Wamsley *et al.* (1998) $Br_y$ estimates in Figure 1-18b. The Harvard/JPL $Br_y$ calculated by Salawitch *et al.* (1994) did not include a later calibration scale change of the WAS results (Daniel *et al.*, 1996), which would improve the agreement between the Wamsley *et al.* (1998) $Br_y$ and the Harvard/JPL $Br_y$. If the lower Wamsley *et al.* (1998) $Br_y$ mixing ratios are confirmed, then there could be 20% less calculated BrO abundance and consequently, 20% less calculated ozone loss resulting from bromine chemistry in old air, relative to previous estimates.

### 1.3.5 Total Equivalent Chlorine Evaluation

Although amounts of organic Cl in the troposphere have started declining, Br from halons is still increasing. In order to estimate how the future abundance of stratospheric ozone will respond to these changes, the trends for both Cl- and Br-containing compounds must be considered. This is especially true, despite the low concentrations observed for atmospheric Br, because on a per-atom basis, Br has an inordinately large influence upon stratospheric ozone concentrations when compared

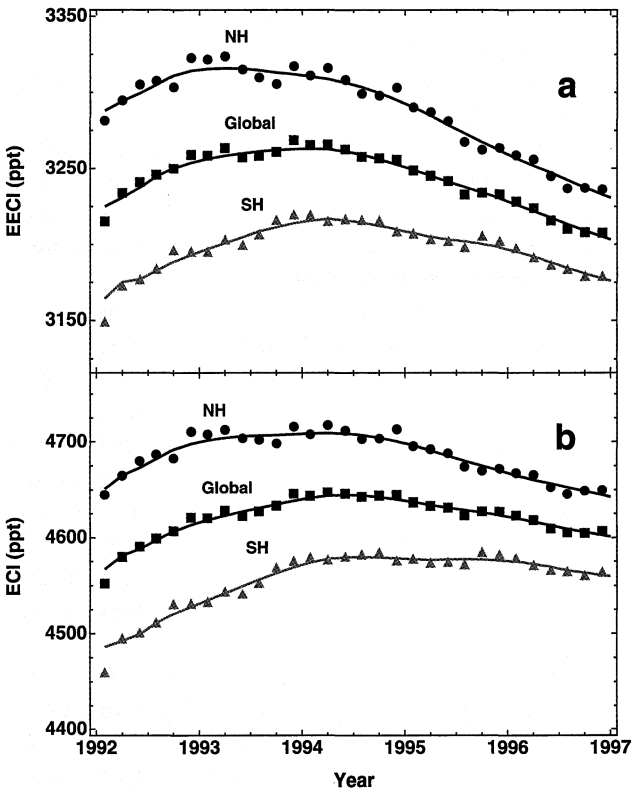


**Figure 1-19.** Amounts of Cl and Br in the NH (circles), SH (triangles) and global (squares) troposphere, expressed as effective equivalent chlorine (EECl; frame a) and as equivalent chlorine (ECl; frame b) that are predicted to be released (at some future time) from the halocarbons shown in Figure 1-14b, as inorganic halogen, respectively in the lower midlatitude stratosphere (EECl) and in the springtime, polar stratospheric vortex (ECl). Both EECl and ECl are calculated using $\alpha = 60$. Curves through data points represent a nonparametric least-squares fit where the fractional weighting factor is 30% (Cleveland and Devlin, 1988). Predictions are updates from Montzka *et al.* (1996), with all data available in Elkins *et al.* (1998).

to Cl. The relative impact of bromine compared to chlorine at destroying stratospheric ozone is characterized by a parameter called $\alpha$ (e.g., Solomon *et al.*, 1992). Whereas bromine atoms may be about 40 times more effective than chlorine atoms in destroying stratospheric ozone in the polar vortex, they may be as much as 100 times more efficient in the lower midlatitude stratosphere (Daniel *et al.*, 1995; Montzka *et al.*, 1996). The values of $\alpha$ remain highly uncertain, and a mean value of approximately 60 is being adopted when dealing with globally averaged ozone losses (see Section 11.4.1 of Chapter 11). By weighting tropospheric mixing ratios according to their relative decomposition rates for individual compounds within the different regions, it is possible to use tropospheric measurements to predict how mixing ratios of inorganic halogens will affect stratospheric ozone in the future. Estimates of the future abundances of reactive halogen compounds for the lower midlatitude stratosphere (effective equivalent chlorine, EECl) and for the springtime polar stratosphere (equivalent chlorine, ECl) are made with halogen release rates for each region and $\alpha = 60$ (Figure 1-19). Note that EECl is similar to the equivalent effective stratospheric chlorine (EESC) described in Chapter 11, but does not explicitly include a delay of three years for transport from the troposphere to the stratosphere (Daniel *et al.*, 1995). Compounds not measured but included in Figure 1-19, such as $CH_3Cl$, $CH_3Br$, $CClF_3$, $CH_2Cl_2$, CFC-114 and -115, $CHCl_3$ and $CCl_2CCl_2$, contribute about 990 ppt to EECl and about 1300 ppt to ECl. After these inclusions, the estimate for ECl (Figure 1-19b) is an upper limit for the amount of reactive halogen available to participate in the ozone-depleting reactions in the polar regions. The mean global tropospheric burden of organic halogen that will become inorganic halogen in the future midlatitude stratosphere reached a maximum between 1993 and 1994 and was declining afterwards at $-22 \pm 2$ ppt EECl $yr^{-1}$ (updated from Montzka *et al.* (1996), with $\alpha = 60$). By comparison, the tropospheric burden of halogen predicted in the future polar stratosphere peaked in late 1993 and early 1994, and was decreasing afterwards at $-18 \pm 3$ ppt ECl $yr^{-1}$ (updated from Montzka *et al.* (1996), with $\alpha = 60$). The small growth rate of $CH_3Br$ and the contribution from the unaccounted species are not expected to significantly change these results.

### 1.3.6 Fluorine Budget Estimates

Measurements of atmospheric fluorine, which does not affect stratospheric ozone, provide us with an independent check on the anthropogenic contribution to stratospheric chlorine loading by CFCs, because CFCs are also the predominant sources of inorganic fluorine-bearing compounds in the stratosphere. Total inorganic fluorine ($F_y$), which includes the carbonyl compounds $COF_2$ and COClF, is defined as:

$$F_y = [HF] + 2[COF_2] + [COClF] \qquad (1\text{-}8)$$

HF and $COF_2$ contribute 98% of the total $F_y$ column (Zander *et al.*, 1992) and 92% or more of the $F_y$ vertical profile when considering altitude distributions (Sen *et al.*, 1996). The combination of vertical column abundance measurements of HF and $COF_2$ (Mélen *et al.*, 1998) made at the ISSJ between 1985 and 1997, indicates that $F_y$ increased at a mean rate of $4.8 \pm 0.3\%$ $yr^{-1}$ for the period 1985 to 1997 (Zander *et al.*, 1996a). Recent space-based investigations of the inorganic fluorine budget of the stratosphere have been made with ATMOS and HALOE. While the ATMOS measurements of HF and $COF_2$ in 1985 and 1992 led to stratospheric $F_y$ rates of change equal to $73 \pm 5$ ppt $yr^{-1}$ (Zander *et al.*, 1994c; Gunson *et al.*, 1994), surrogates of $F_y$ deduced from HF measurements by HALOE near the stratopause were $85 \pm 2$ ppt $yr^{-1}$ for the period November 1991 to April 1995 (Russell *et al.*, 1996c). These values are commensurate with the tropospheric organic fluorine ($CF_y$) rates of change measured during the 1980s, i.e., $75 \pm 13$ ppt $yr^{-1}$, which result primarily from changes in CFC releases. Including the results for chlorine (Section 1.3.3.3), this agreement between the two total fluorine estimates strengthens the conclusion that the CFCs are responsible for most of the stratospheric loading of both inorganic fluorine and chlorine, as well as for the ozone depletion by the latter.

The midlatitude fluorine abundance reported for September 1993 by Sen *et al.* (1996) indicates a steady decrease of total fluorine with increasing altitude, from a tropospheric value of about 1.82 ppb to 1.48 ppb at 38 km altitude. The latter value, made up entirely of the reservoir species, is commensurate with tropospheric concentrations of fluorine reported in the late 1980s, with time-dependent 2-D model predictions (1.45 ppb), and with the fluorine budget derived from the ATMOS/ATLAS-1 Space Shuttle flight in 1992 (Zander *et al.*, 1994c).

### 1.3.7 Budgets Based on Model Assimilations

As discussed later, the observed mole fractions can be used to constrain sources and sinks (Section 1.4.3). Deduction of emissions is possible using a global chemical transport model in which sources are adjusted using optimal inverse methods until a satisfactory fit to observed concentrations is obtained (Prinn and Hartley, 1995; Hartley and Prinn, 1993).

These methods have been applied to determine global emissions of $CCl_3F$, $CCl_2F_2$, $CCl_4$, and $CCl_2FCClF_2$ for comparison with industry estimates (Cunnold *et al.*, 1997; Simmonds *et al.*, 1998; Fraser *et al.*, 1996). Considering the uncertainty in industry estimates introduced by end-use and nonreporting-company uncertainties, the agreement between the inverse and industry estimates is satisfactory for $CCl_3F$ and $CCl_2F_2$ but not for $CCl_2FCClF_2$. Possible reasons for the latter discrepancy are discussed in Fraser *et al.* (1996).

Inverse methods have also been applied to determine regional emissions (Hartley and Prinn, 1993; Hartley *et al.*, 1994, 1996; Haas-Laursen *et al.*, 1996; Mulquiney *et al.*, 1998). From studies of $CCl_3F$, whose regional emissions are quite well known, it is apparent that transport processes predicted in climate models are not accurate enough to be used in the estimation of regional emissions. Climate models, for example, do not simulate the El Niño-Southern Oscillation (ENSO), which clearly affects SH trace gas concentrations (Prinn *et al.*, 1992; Elkins *et al.*, 1993). The use of transport models based on observed winds shows promise but there are still significant discrepancies between industry and inverse-method estimates of regional $CCl_3F$ emissions (Mahowald *et al.*, 1997). These discrepancies could result from inadequate treatment of transport or from insufficient spatial density in the current observing networks (Hartley *et al.*, 1996).

## 1.4 LIFETIMES

### 1.4.1 Introduction

This section examines the lifetimes of species discussed in this chapter. The atmospheric abundance of a trace gas that is released at the Earth's surface and removed by photochemical reactions in the atmosphere is governed by the equation

$$\frac{dB(t)}{dt} = E(t) - \int L n \, dV \qquad (1\text{-}9)$$

where $B(t)$ is the burden defined by $\int n \, dV$; $n(x,y,z,t)$ is the local number density of the gas; $E(t) = \int E(x, y, z = 0, t) \, dx dy$ is the emission rate at the surface; the in situ removal rate is given by $Ln$ where $L(x,y,z,t)$ is the loss frequency; $t$ is the time coordinate; $dV = dx dy dz$; $x$, $y$, $z$ are the Cartesian coordinates along the longitudinal, latitudinal, and vertical directions, respectively; and the integral is over the whole atmosphere. The loss frequency could be generalized to include washout and deposition at the ground. In this chapter, we will limit our discussion to in situ photochemical removal.

Equation (1-9) can be written in the form

$$\frac{dB(t)}{dt} = E(t) - \frac{B(t)}{\tau(t)} \qquad (1\text{-}10)$$

where $\tau(t)$ is the instantaneous lifetime defined by the atmospheric burden divided by the atmospheric removal rate:

$$\tau(t) = \frac{\int n \, dV}{\int L n \, dV} \qquad (1\text{-}11)$$

For trace gases with lifetimes of a few years or longer, it is more appropriate to look at the annually averaged versions of Equations (1-10) and (1-11), which are denoted by adding brackets < > around the relevant variables and replacing $t$ by $T$, where $T$ represents time variations on the interannual time scale.

The lifetime $<\tau>(T)$ can be computed from the annually averaged Equation (1-11) using the distributions of $L$ and $n$ determined either from observations or model computation. One advantage for model computation is that one can compute lifetimes for species that are not yet emitted to the atmosphere. This will be the subject for Section 1.4.2.1. Alternatively, for species whose burden is proportional to the surface concentrations, the annually averaged Equation (1-10) can be used to derive $<\tau>(T)$ from the time series of observed surface concentrations and known emission rates using statistical techniques without referring to specific details about $L$ and $n$. This method of deriving lifetime will be discussed in Section 1.4.3.

## 1.4.2 Lifetimes from Stratospheric Distributions and Stratospheric Removal Rates

Here we discuss the determination of lifetimes using $L$ and $n$ either from model calculations or observations. It is useful to distinguish between instantaneous lifetimes and steady-state lifetimes. Instantaneous lifetimes correspond to the values from the annually averaged Equation (1-10) where values of $n$ and $L$ in the current atmosphere are used. Steady-state lifetimes correspond to the special situation where the species is in steady state and $\frac{d<B>(T)}{dT}$ is zero. The instantaneous lifetime can be different from the steady-state lifetime as it depends on the emission history of the gas and the changes in the chemical composition of the atmosphere. Current estimates indicate that there is a delay of about 2 to 4 years in transporting material from the troposphere to the lower/middle stratosphere (see Chapter 8, WMO, 1992; Schmidt and Khedim, 1991; Pollock *et al.*, 1992; Woodbridge *et al.*, 1995; Daniel *et al.*, 1996; Boering *et al.*, 1996; Volk *et al.*, 1997). For a species whose burden is increasing (decreasing) with time, the concentration in the stratospheric sink region is systematically smaller (larger) than would be obtained at steady-state, when the emission is balanced by stratospheric removal. Thus, the instantaneous lifetime of the species is longer (shorter) than the steady-state lifetime if the burden is increasing (decreasing) with time.

### 1.4.2.1 Lifetimes from Model-Calculated Stratospheric Distribution and Stratospheric Removal

#### *Model Results*

A numerical model simulating transport and removal of trace gases can be used to compute $L$ and $n$. These simulations require the use of appropriate boundary conditions. The boundary values could be constant in time to simulate a steady state, or they can be time-dependent to simulate the temporal evolution in the atmosphere. For either case, model-calculated $L$ and $n$ for any particular species can be used in Equation (1-10) to calculate $<\tau>(T)$. If a time-dependent boundary condition is used in the calculation, this lifetime is the instantaneous lifetime. A steady-state lifetime can be obtained from Equation (1-10) where $n$ is the steady-

**Table 1-4. Model-calculated steady-state lifetimes in years.**

| Species | AER[a] | GSFC[a] | CSIRO[a] | Harvard 2-D[a] | LLNL[a] | SUNY -SPB[a] | UNIVAQ 2-D[a] | LaRC 3-D[a] | GISS-UCI 3-D[b] | MIT 3-D[c] |
|---|---|---|---|---|---|---|---|---|---|---|
| $N_2O$ | 109 | 130 | 117 | 122 | 106 | 125 | 122 | 175 | 113 | 124 |
| $CCl_3F$ (CFC-11) | 47 | 61 | 53 | 68 | 49 | 49 | 44 | 57 | 35 | 42 |
| $CCl_2F_2$ (CFC-12) | 92 | 111 | 100 | 106 | 92 | 107 | 105 | 149 | 90 | 107 |
| $CCl_2FCClF_2$ (CFC-113) | 77 | 101 | 83 | 55 | 81 | 87 | 81 | - | 70 | 79 |
| $CCl_4$ | 41 | 53 | 46 | 64 | 42 | 39 | 36 | 42 | 28 | 30 |
| $CBrClF_2$ (H-1211) | 16[d] | 12[e] | 36[f] | - | - | - | 21[f] | 29[f] | 21 | - |
| $CBrF_3$ (H-1301) | 63 | 78 | 69 | - | - | - | 61 | 93 | 52 | - |

[a] Results are taken from the Model and Measurement Workshop II (M&M II) (Park *et al.*, 1998). The models and the contact persons are as follows: AER - Atmospheric and Environmental Research, Inc., U.S., Malcolm Ko; GSFC - NASA Goddard Space Flight Center, U.S., Charles Jackman; CSIRO - Commonwealth Scientific and Industrial Research Organisation (CSIRO) Telecommunications and Industrial Physics, Australia, Keith Ryan; Harvard 2-D - Harvard University, U.S., Hans Schneider; LLNL - Lawrence Livermore National Laboratory, U.S., Doug Kinnison; SUNY-SPB - State University of New York at Stony Brook, U.S., Marvin Geller; UNIVAQ 2-D - University of L'Aquila, Italy, Giovanni Pitari; LaRC 3-D - NASA Langley Research Center, U.S., William Grose. LaRC is the only 3-D model that participated in M&M II.

[b] Results given are for steady-state lifetimes from Avallone and Prather (1997). The values should be close to the atmospheric lifetimes except for Halon-1211.

[c] Results for MIT model from Table 5-2 of Kaye *et al.* (1994). MIT model described in Golombek and Prinn (1993) and references therein.

[d] Calculated using cross section from Burkholder *et al.* (1991).

[e] Calculated using cross section from DeMore *et al.* (1987).

[f] Calculated using the Halon-1211 cross section from DeMore *et al.* (1997) that did not give any recommendation beyond 288 nm.

state distribution calculated assuming $E$ is constant in time and $L$ is calculated assuming fixed (time invariant) boundary conditions for all trace gases.

Table 1-4 gives the calculated steady-state lifetimes from several models. The differences in the lifetimes can be attributed to differences in both photochemistry and transport in the models. Equation (1-11) states that $1/\langle\tau\rangle$ is the average of $L$ weighted by $n$. The species distribution is determined by the local balance between transport and $L$. The removal rate, $L$, also depends on transport because transport can affect the calculated ozone in the model that drives the photolysis rates. Thus, to resolve the difference, one would have to compare the model-computed ozone with the observed ozone. Next, we discuss how observations can be used to resolve some of these differences.

### *Reducing Uncertainties by Comparison with Observations*

For the purpose of validating the model-calculated lifetimes, we use comparisons of $L$ and $n$ in the lower stratosphere where the product $Ln$ contributes to the bulk of the integrated removal rate.

Several components that enter into the model calculation of photolysis rates contribute to the uncertainties in the computed lifetime. The photolysis rate ($J$) of a species is the sum of the product of the local solar flux, absorption cross section, and quantum yield of the species at each wavelength. The solar flux at a particular location in the atmosphere is determined by attenuation of the solar flux by the overhead $O_2$ and $O_3$ columns. The unattenuated solar flux, $F$, is uncertain by

about 5% and varies as a function of wavelength with cyclical solar activity. It is difficult to use in situ measurements of local solar UV flux to validate $F$ because small uncertainties in the $O_2$ and $O_3$ columns can translate into large changes in $J$ for large optical depth. Further coordination with the measurement programs such as those reported in Herman and Mentall (1982), Anderson and Hall (1986), and McElroy (1995) is needed for future validation. Uncertainties in the absorption cross section and quantum yield of the species will also translate into uncertainties for the calculated photolysis rate. However, because all models used the same photolysis rates (DeMore *et al.*, 1997), it would not explain the spread in the model results shown in Table 1-4. Finally, questions can be raised about the algorithms that are used in the models to compute the photolysis rates. Many of the models have participated in an intercomparison of the photolysis rates in 1995. In that exercise, the algorithm for computing $J$ was tested by comparing the computed $J$ in the models to that computed by a detailed radiative transfer code. Many models have modified their algorithms to get good agreement. For some models that participated in the intercomparison exercise (Atmospheric and Environmental Research, Inc. (AER), Goddard Space Flight Center (GSFC), Lawrence Livermore National Laboratory (LLNL)), it is reasonably certain that any difference in photolysis rate is due to differences in the ozone distribution computed by each model.

Transport is uncertain because both the strength of the resolved circulation (vertical and horizontal winds) and the magnitude of the eddy diffusion (vertical and horizontal) are uncertain. Model transport can be tested by comparing model-computed distributions of long-lived tracers such as $N_2O$ and CFCs with observations. However, this is complicated by the uncertainties in the removal rates of these gases. An alternative is to use a photochemically inert tracer such as the radioactive tracer $^{14}C$, which is produced from galactic cosmic rays and nuclear explosions (Johnston, 1989; Shia *et al.*, 1989; Kinnison *et al.*, 1994). Unfortunately, this test is not sensitive to the transport parameters in the lower stratosphere. A more fundamental issue in the comparison of model results (which represent climatological mean conditions) with observations involves the large variabilities in the observed concentrations at any location caused by the short-term vertical and horizontal displacements of air during passages of synoptic-scale disturbances. Thus, one can never be certain whether any particular measurement is representative of the climatological mean condition at that location. Several techniques have been developed to facilitate model-observation comparisons. Some studies (e.g., Schoeberl *et al.*, 1989; Lait *et al.*, 1990) showed that observations taken at different locations and times can be compared more readily if they are collated using potential temperature and potential vorticity instead of altitude and latitude. Hartmann *et al.* (1989) pointed out that if one displays the observed species concentrations against the concentration of $N_2O$ of the same air mass in a correlation diagram, the results from different locations show an almost linear correlation with $N_2O$. This feature can be exploited as discussed in the next section.

In addition, it is possible to extract information from observations to compare with transport parameters for the lower stratosphere in 2-D models. Several studies (Minschwaner *et al.*, 1996; Volk *et al.*, 1996; Schoeberl *et al.*, 1997) derived a replacement time constant of 10 to 18 months for air in the lower tropical stratosphere from mixing of midlatitude air. Shia *et al.* (1998) showed that this can be related to the value of the horizontal diffusion coefficient $K_{yy}$ used in the model and that a $K_{yy}$ value of $7 \times 10^4$ m$^2$ sec$^{-1}$ is appropriate for the tropical lower stratosphere. The observed ratio of $NO_y/O_3$ (Fahey *et al.*, 1996) also provides a constraint for the combination of advection and eddy mixing in the lower stratosphere. Weisenstein *et al.* (1996) showed that a value for $K_{yy}$ of $3 \times 10^4$ m$^2$ sec$^{-1}$ in the tropics best reproduces the results in the AER model. However, the interpretation is made more difficult because of the uncertainties in the $NO_2$ and ozone budgets in the upper troposphere. In the AER model, steady-state lifetimes calculated using the smaller $K_{yy}$ ($3 \times 10^4$ m$^2$ sec$^{-1}$) are about 10% shorter than the values given in Table 1-4 (calculated using $7 \times 10^4$ m$^2$ sec$^{-1}$). Other methods for validating the combined effects of advection and eddy mixing include comparing the model-computed age of air (Hall and Plumb, 1994) with that derived from observation of $SF_6$ (Volk *et al.*, 1997). Given these uncertainties, it is difficult to use direct comparison of $n$ and $L$ from model and observation to constrain the model-calculated lifetime to better than 30%.

### 1.4.2.2 Instantaneous Lifetime from Observations

Johnston *et al.* (1979) used concentrations of $N_2O$ from balloon profiles along with model-calculated $L$ to estimate the lifetime of $N_2O$. Ko *et al.* (1991) used satellite-measured concentrations from Stratospheric and Mesospheric Sounder (SAMS) in their analysis and demonstrated that using the observed $N_2O$ distributions from different years could cause a change of about 15% in calculated lifetime. Recent satellite measurement programs have provided more data to construct $n(x,y,z,t)$ for ozone and certain species. The distributions ($n(x,y,z,t)$) for these species can be used along with photochemical loss rates ($L(x,y,z,t)$) computed using the observed distribution of ozone to compute the lifetimes for these gases via Equation (1-11). Minschwaner *et al.* (1998) used observed concentrations of CFC-12 and $N_2O$ in the stratosphere from the Cryogenic Limb Array Etalon Spectrometer (CLAES) instrument on the Upper Atmosphere Research Satellite (UARS) to determine the global destruction rates and instantaneous lifetimes for these gases. Photolysis rates are calculated using the unattenuated solar UV irradiances measured from the Solar Stellar Irradiance Comparison Experiment (SOLSTICE) instrument on UARS and a line-by-line model of absorption in the Schumann-Runge bands. The computed instantaneous lifetimes based on the observed concentrations between March 1992 and January 1993 are 114 ± 22 years for CFC-12 and 118 ± 25 years for $N_2O$. The uncertainties are estimates based on the standard deviation of the CLAES measurements in the midtropical stratosphere, uncertainties in the solar flux measurements and atmospheric transmission, and uncertainties in absorption cross sections of CFC-12 and $N_2O$. The instantaneous lifetimes can be used to obtain a steady-state lifetime by assuming a mean age of air in the tropical midstratosphere, and a growth rate for the gas. After adjusting for the growth rate, Minschwaner *et al.* (1998) reported estimates for the steady-state lifetimes of 103 ± 25 years for CFC-12 and 117 ± 26 years for $N_2O$.

As a modeling exercise for the "Models and Measurements Workshop II" (Park *et al.*, 1998) monthly averaged fields for $N_2O$, CFC-12, and ozone were constructed from the UARS data and the GSFC model output. Five groups participated in computing the lifetimes using these fields. The range for the computed lifetimes is typically 10% above and below the mean among the five models. This suggests that different ways of calculating photolysis rates and mapping of data into the model grid introduce an uncertainty of this magnitude in lifetimes.

### 1.4.2.3 Stratospheric Lifetimes from Observed Tracer Correlations and Tropospheric Growth Rate

The theoretical work of Plumb and Ko (1992) provides an independent method for the semiempirical derivation of tracer lifetimes from stratospheric observations without the need to accurately describe stratospheric transport or chemistry. These authors investigated a conceptual "global mixing" model of the stratosphere, in which horizontal mixing everywhere dominates vertical advection. In this case mixing ratios of sufficiently long-lived tracers are globally homogenized along the same quasi-horizontal mixing surfaces such that their surfaces of constant mixing ratio coincide. This implies that the stratospheric abundances of two sufficiently long-lived tracers are uniquely correlated with each other, even as they fluctuate in time and space. Plumb and Ko (1992) also showed that in the "global mixing" model, stratospheric transport can be described by a one-dimensional flux-gradient relation. If the mixing ratios of two long-lived tracers, $\sigma_1$ and $\sigma_2$, are in steady state, then the slope of their correlation in the lowermost stratosphere (below the regions where chemical sinks act) equals the ratio of their stratospheric removal rates and thus

$$\frac{\tau_1}{\tau_2} \cong \frac{d\sigma_2}{d\sigma_1}\frac{B_1}{B_2} \qquad (1\text{-}12)$$

where $B_i$ is the total atmospheric burden for species $i$ (as defined in Section 1.4.1), and $\tau_i$ is its steady-state stratospheric lifetime, equal to the steady-state atmospheric lifetime for species without tropospheric sinks. Studies have demonstrated that Equation (1-12) is valid for model-generated lifetimes and slopes of the correlation diagrams from a 2-D model (Plumb and Ko, 1992) and a 3-D model (Avallone and Prather, 1997).

Recent research has shown that the simple "global mixing" picture is violated in the tropics where horizontal mixing is not fast compared to vertical advection (Volk *et al.*, 1996; Hall and Waugh, 1997; Schoeberl *et al.*, 1997). As a consequence, stratospheric tracer interrelations are observed to differ between the tropics and midlatitudes (Volk *et al.*, 1996) or between the two hemispheres (Keim *et al.*, 1997). Plumb (1996) investigated the implications of a "tropical pipe" model, i.e., completely excluding horizontal mixing into the tropical region, and concluded that Equation (1-12) still applies provided that (i) the two tracers are tightly correlated in each hemisphere in the extratropical lower stratosphere, (ii) the interhemispheric difference of the extratropical correlation slope is small, and (iii) the correlation slope in Equation (1-12) is evaluated at the extratropical tropopause and from data taken during the winter half year that dominates net transport. Volk *et al.* (1997) argued that the same conclusions apply in the more realistic case of slow horizontal mixing into the tropics. An analysis of a comprehensive set of tracer observations from the 1994 ASHOE/MAESA ER-2 campaign shows that the above conditions for Equation (1-12) are indeed met (Volk *et al.*, 1997).

Volk *et al.* (1997) showed that, under the same conditions, steady-state stratospheric lifetimes may be derived from the gradient of the steady-state tracer mixing ratio, $\sigma_i$, with respect to the mean age of stratospheric air (Hall and Plumb, 1994), $\Gamma$, in the measured air parcels:

$$\frac{B_i}{\tau_i} = -\frac{d\sigma_i}{d\Gamma} N_u \qquad (1\text{-}13)$$

where $B_i$ is again the atmospheric burden of the respective species, $N_u$ is the total number of molecules above the tropopause, and the gradient with respect to age, $d\sigma_i/d\Gamma$, needs to be evaluated exactly at the extratropical tropopause.

The variable $\tau_i$ in Equations (1-12) and (1-13) corresponds to a steady-state lifetime only when the tracers are in steady state in the atmosphere. Thus, they cannot be easily used to obtain steady-state lifetimes of species that are not in steady state in the present-day atmosphere. If the tropospheric concentration of the species is changing with time, part of the tracer gradient at the tropopause is due to accumulation in the stratosphere and $1/\tau_i$ in either equation has to be replaced with $\tau_i^{-1} + B_u'/B_i$ where $\tau_i$ is the instantaneous lifetime and $B_u'$ is the total accumulation rate of $i$ above the tropopause, a quantity not easily assessed unless tropospheric growth has been linear for a long time and is accurately known. Volk *et al.* (1997) proposed an alternative method of accounting for tropospheric growth and non-steady-state mixing ratios, $\chi_i$, to obtain steady-state lifetimes. In the method, one deduces the correction factors $C_i$ for each species using the following information:

- the tracer gradient with respect to age at the tropopause, observed $d\chi_i/d\Gamma$;
- the time series of tropospheric mixing ratios of the respective species during a 5-year period prior to the stratospheric observations; and
- estimates of the width of the stratospheric age spectrum (Hall and Plumb, 1994) from 3-D transport models.

The steady-state gradient, $d\sigma_i/d\Gamma$, defined as (observed $d\chi_i/d\Gamma$) $\cdot$ $C_i$ is used in Equation (1-13) to obtain the steady-state lifetime. Volk *et al.* (1997) also showed that corrected steady-state correlation slopes defined as

$$\frac{d\sigma_i}{d\sigma_{CFC-11}} = \frac{d\chi_i}{d\chi_{CFC-11}} \frac{C_i}{C_{CFC-11}} \qquad (1\text{-}14)$$

can be used in Equation (1-12) to derive steady-state lifetimes based on a given CFC-11 lifetime (CFC-11 is best suited as a reference tracer as its lifetime is known most accurately from the method discussed in Section 1.4.3).

Table 1-5 shows steady-state stratospheric lifetimes derived from ASHOE/MAESA observations by Volk *et al.* (1997). The stratospheric lifetimes listed in Table 1-5 equal atmospheric lifetimes with the exception of Halon-1211, because the other species are removed predominantly in the stratosphere. Results shown are obtained using two approaches: via Equation (1-12) using the corrected correlations of tracers with CFC-11 and an assumed CFC-11 lifetime of 45 ± 7 years; and via Equation (1-13) whereby the age of stratospheric air was calculated from in situ observations of $SF_6$. The correction factors ($C_i$) for tropospheric growth and non-steady state $\chi$ are also given. Note that these correction factors are time dependent and valid only for October 1994.

**Table 1-5. Stratospheric steady-state lifetimes (from Volk *et al.*, 1997).**

| Species | Observed $d\chi_i/d\Gamma$ from ASHOE/MAESA (ppt $yr^{-1}$, ±%) | Steady-state lifetime based on corrected gradient with respect to age (years ± years) | $d\chi_i/d\chi_{CFC\text{-}11}$ observed correlation slope relative to CFC-11 from ASHOE/MAESA (ppt/ppt, ± %) | Steady-state lifetime based on corrected correlation slope and $\tau_{CFC\text{-}11} = 45$ ± 7 years (years ± years) | Correction factor for tropospheric growth $C_i$ |
|---|---|---|---|---|---|
| $N_2O$ | -13,000 ± 38% | 124 ± 49 | 436 ± 11% | 122 ± 22 | 0.97 ± 0.02 |
| $CCl_3F$ (CFC-11) | -33.5 ± 28% | 41 ± 12 | | (45 ± 7) | 0.96 ± 0.02 |
| $CCl_2F_2$ (CFC-12) | -43.8 ± 25% | 77 ± 26 | 1.29 ± 7% | 87 ± 17 | 0.77 ± 0.07 |
| $CCl_2FCClF_2$ (CFC-113) | -7.3 ± 22% | 89 ± 35 | 0.212 ± 20% | 100 ± 32 | 0.65 ± 0.12 |
| $CCl_4$ | -15.9 ± 32% | 32 ± 11 | 0.515 ± 3.6% | 32 ± 6 | 1.03 ± 0.02 |
| $CBrClF_2$ (H-1211) | -0.84 ± 31% | 20 ± 9 | 0.0237 ± 7% | 24 ± 6 | 0.90 ± 0.10 |

Besides the uncertainty of the growth correction in the case of rapidly growing species, the main limitation of these methods lies in the determination of the correlation slope at the tropopause. The ASHOE/MAESA observations show that most correlations exhibit significant curvature toward the tropopause, presumably due to tropospheric growth and/or changes in the tracer fluxes across the tropical/midlatitude boundary. Highly resolved measurements in the vicinity of the tropopause are thus required to accurately measure the slope at the tropopause. With the data presently available, lifetimes based on the correlation with CFC-11 can be constrained to within about 20% (cf. Table 1-5), assuming that the lifetime of CFC-11 is known to within 15%.

### 1.4.3 Lifetimes Estimated from Global Tropospheric Measurements of Trace Gases

The observed mole fraction ($\chi$) of a species at a given time and location can be expressed as a line integral of the Lagrangian form of the continuity equation over a back-trajectory in space (or, equivalently, time). The integrand includes the net chemical production ($Y$) of the species, defined as the difference between true chemical production and true chemical loss. Determination of $Y$ is a classical inverse problem (Prinn and Hartley, 1995). It requires accurate definition of initial conditions and atmospheric circulation, and with these, an estimate of $Y$ produces an estimate ($\chi_e$) of the mole fraction. Let $E$ be the vector of errors (random with zero mean and uncorrelated in time) in the observable $\chi$ at a network of observing stations. Hence the difference between observed and estimated mole fractions is

$$\chi - \chi_e = E - \Delta\chi_e \qquad (1\text{-}15)$$

where $\Delta\chi_e$ is the vector of errors in $\chi_e$ caused by the error ($\Delta Y$) in the previous estimate of $Y$. Now $Y$ is formally a continuous function of space and time, but can be approximated by appropriate regional averages contained in a vector. The quasi-linear relation between the vector $\Delta\chi_e$ and the vector of $\Delta Y$ values is computed in a global chemical transport model to provide a so-called "partial derivative matrix."

Fundamentally, we can only determine the net production ($Y$) from the measurements. Hence, to interpret, say, surface measurements in terms of surface emissions as discussed in Section 1.3.7, we need to know the true chemical destruction rates (or equivalently, lifetimes). Alternatively, if we wish to determine lifetimes we must be given the surface emissions. To solve the inverse problem (i.e., determine the vector of $Y$ values given the observed time series of $\chi$ values at each station), it is common to use an optimal linear recursive least squares filter of the Kalman-type (Gelb, 1974; Cunnold and Prinn, 1991; Prinn and Hartley, 1995). This approach enables inclusion of measurement errors, $E$, and an objective estimate of the uncertainty in

**Table 1-6. Equilibrium atmospheric lifetimes (years) estimated from ALE/GAGE/AGAGE measurements.** The tabulated values are based on the trend and inventory estimates; the values are similar to those reported in Cunnold *et al.* (1997) but they are for a slightly different time period.

| Species | Inverse Lifetime (years$^{-1}$) | Lifetime (years) | Observation Period Utilized |
|---|---|---|---|
| $CCl_3F$ (CFC-11) | 0.019 ± 0.0059 | 52 (-12, +24) | July 1978 - June 1993 |
| $CCl_2F_2$ (CFC-12) | 0.0054 ± 0.0041 | 185 (-80, +584) | July 1978 - June 1993 |

estimated $Y$ values (related to the variance in the time series of corrections $\Delta Y$ made to the previous estimates of $Y$). In this way, the atmospheric lifetimes of long-lived gases, for which the atmospheric releases are well-quantified, may be estimated from the atmospheric inventory of these gases and from long-term trends in the atmospheric concentrations over periods of five or more years. Estimates of the lifetimes of $CCl_3F$ and $CCl_2F_2$ (Cunnold *et al.*, 1994) and $CH_3CCl_3$ (Prinn *et al.*, 1995) have thus been reported.

The inventory estimates of the lifetimes for the CFCs have been obtained by comparing measured concentrations (from the ALE/GAGE/AGAGE) against predicted values. Differences between measured and predicted values are minimized over a specified time period (e.g., 1978 to 1993) and in essence, the lifetimes by the inventory technique represent average estimates over the period. During times when CFCs are increasing in the atmosphere, the stratospheric content lags behind the tropospheric content because of the several-year time lag associated with the time for CFCs released at the ground to reach the stratosphere. The atmospheric lifetime is therefore time-dependent; consequently the lifetimes reported here refer to an equilibrium period (similar to that for $CCl_3F$ currently) when the releases at the surface exactly equal the global losses in the stratosphere. The uncertainties in the lifetime estimates by the inventory technique for the CFCs consist of absolute calibration uncertainties of approximately 1%, uncertainties in the representativeness of four or five ground-based sites, combined with the use of a 2-D model to infer the atmospheric content (approximately 3%) (Cunnold *et al.*, 1994) and uncertainties in release. Although the historical record of production figures for companies that report to AFEAS is believed to be very accurate (approximately 1%), uncertainties of approximately 3% in the annual release figures are associated with estimates of the time lag between production and release (Fisher and Midgley, 1994). Moreover, the production and release uncertainties were larger for the nonreporting companies such as those in Russia, China, and India. This situation has improved with the availability of UNEP data.

Atmospheric lifetimes are also estimated from the trends in the measured concentrations. The ability of the ALE/GAGE/AGAGE network to maintain a constant calibration over the 17-year period is most important for this estimation. This has been validated by comparisons against recent measurements of archived air samples from the entire 17-year period. The release uncertainties described in the previous paragraph dominate the uncertainties in the lifetime estimates from the trend technique.

The lifetimes of $CCl_3F$ and $CCl_2F_2$ are given in Table 1-6. Lifetime estimates by the inventory technique from any sub-period within this 15-year period are similar. There is some tendency for the trend lifetime estimate to change with time but the change is well within the stated error bars. Because of the long lifetimes, the estimates are equally as sensitive to the uncertainties in release in the early 1970s as they are to the releases in 1992. Starting from 1992, the chemical industry has no longer attempted to include estimates of releases by non-reporting countries in their estimates of world production and release. Moreover, both industry practices and atmospheric observations suggest that there could have been changes in the delay between production and release of the CFCs since 1992 (Cunnold *et al.*, 1997). Therefore the lifetime estimates are based on the mid-1978 to mid-1993 period only.

The ALE/GAGE/AGAGE measurements of $CCl_2FCClF_2$ should have provided good estimates of its

**Table 1-7. Comparison of reference steady-state lifetimes from WMO (1995) with model-calculated ranges and lifetimes derived from observations.** All lifetimes are in years.

| Species | Reference Lifetimes from WMO [1995] [a] | Model Range [b] | Volk $SF_6$ [c] | Volk CFC-11 [d] | Minschwaner UARS [g] | AGAGE [e] |
|---|---|---|---|---|---|---|
| $N_2O$ | 120 | 106-175 | 124 ± 49 | 135 ± 16 | 117 ± 26 | |
| $CCl_3F$ (CFC-11) | 50 | 35-68 | 41 ± 12 | 50[d] | | 52 (40-76) |
| $CCl_2F_2$ (CFC-12) | 102 | 90-149 | 77 ± 26 | 96 ± 12 | 103 ± 25 | 185 (105-769) |
| $CCl_2FCClF_2$ (CFC-113) | 85 | 55-101 | 89 ± 35 | 112 ± 31 | | |
| $CCl_4$ | 42 | 28-64 | 32 ± 11 | 36 ± 4 | | |
| $CBrClF_2$ (H-1211) | 20 | 12-36 | 20 ± 9[f] | 26 ± 5[f] | | |
| $CBrF_3$ (H-1301) | 65 | 61-93 | | | | |

[a] From Table 13-1, WMO (1995).
[b] From Table 1-4.
[c] Derived steady-state stratospheric lifetimes based on gradient with age derived from $SF_6$ data; from Volk *et al.* (1997).
[d] Derived steady-state stratospheric lifetimes based on gradient with CFC-11 and an adopted lifetime of 50 years for CFC-11; from WMO (1995). Compare to values based on 45 years from Table 1-5.
[e] From Table 1-6. The range is calculated using the uncertainty in the inverse lifetime given in the table.
[f] Because Halon-1211 is dissociated by photolysis in the longwave, there is significant removal in the troposphere so that the stratospheric lifetimes should not be compared directly to the global lifetime. See text for further discussion.
[g] Steady-state lifetime from Minschwaner *et al.* (1998) derived using UARS observations, assumed mean age, and tropospheric growth rates.

lifetime using procedures similar to those used for $CCl_3F$ and $CCl_2F_2$. Unfortunately the emissions inferred from the atmospheric measurements are approximately 10% smaller than the estimates by industry (Fraser *et al.*, 1996). This difference is similar in magnitude to the estimates of the emissions by the nonreporting companies (AFEAS, 1998). This disagreement results in lifetime estimates of approximately 26 years by the inventory technique and greater than 100 years by the trend technique (Fraser *et al.*, 1996). This spread has narrowed somewhat with the addition of two more years of measurements but the lifetime estimates currently only indicate that the results are not inconsistent with stratospheric photodissociation being the only sink for $CCl_2FCClF_2$.

### 1.4.4 Reference Steady-State Lifetimes

The previous Assessment report (WMO, 1995) gave a set of reference steady-state lifetimes for use in calculations of the Ozone Depletion Potentials (ODPs) and Global Warming Potentials (GWPs) of the species. The same reference lifetimes were also used as response times in halogen loading calculations. These values (from Table 13-1 of WMO (1995)) are listed in Table 1-7. Given the new information in this chapter, particularly the new formalism (Volk *et al.*, 1997) that enables us to derive steady-state lifetimes from stratospheric measurements, we conclude that the WMO (1995) reference lifetimes for some gases need revision.

With the exception of CFC-11, the WMO (1995) reference lifetimes for the species listed are the mean

values from model results of several groups reported in Kaye *et al.* (1994). This method is clearly unsatisfactory in the present context because there are no well-established criteria on which model results listed in Table 1-4 should be included in taking the average. It is more useful to examine how the model-computed lifetimes have changed as the models have evolved. As discussed in Section 1.4.2.3, several 2-D models have modified the transport parameters in the models to simulate the effect of a tropical barrier. Results from the AER model show that restricting the mixing through the barrier leads to shorter calculated lifetimes (Shia *et al.*, 1998). A second observation is that the lifetimes for CFC-11 and $CCl_4$ from two of the three 3-D models are much shorter than those calculated by the 2-D models (see Table 1-4). It could be argued that lifetimes calculated by 3-D models may be more realistic because they have a more direct (i.e., 3-D) representation of the transport processes in the atmosphere. However, more work is needed to assure that the vertical resolution in such models is sufficient to resolve the scale heights of the species with short local lifetimes.

The Volk *et al.* (1997) formalism provides, for the first time, a way to obtain steady-state stratospheric lifetimes from observations. With the exception of Halon-1211, the species listed in Table 1-7 have very little removal in the troposphere. As a result, the derived stratospheric lifetimes can be compared directly to atmospheric lifetimes. As is evident in Table 1-7, the derived lifetimes for CFC-11, $CCl_4$, and CFC-12 are in the shorter end of the model range, and shorter than the WMO (1995) reference lifetimes. It is also interesting to note that the derived shorter lifetimes are in better agreement with the lifetimes calculated by two of the three 3-D models in Table 1-4. The large uncertainties in the derived lifetimes given in column 4 of Table 1-7 arise from the uncertainty in the $SF_6$ measurement from the 1994 ASHOE/MAESA campaign. The uncertainty has been reduced in subsequent flights. The lifetimes relative to CFC-11 derived by Volk *et al.* (1997) have much smaller uncertainties because $d\sigma_i/d\sigma_{CFC\text{-}11}$ can be determined more accurately. When referenced to a CFC-11 lifetime of either 45 years (Table 1-5, column 5) or 50 years (Table 1-7, column 5), with the exception of $CCl_4$ and Halon-1211, these derived lifetimes agree within their uncertainties with the WMO (1995) reference lifetimes.

Because CFC-11 is used as the reference gas in the definition of the Ozone Depletion Potential, extra care was used in selecting its WMO (1995) reference value, basing it on observations as well as model calculations. The WMO (1995) value of 50 years is in good agreement with the central estimate of the lifetime from ALE/GAGE/AGAGE measurements (Cunnold *et al.*, 1997), but not with the central estimate of 41 years by Volk *et al.* (1997). The derived lifetime range for CFC-11 using the Volk *et al.* (1997) method (29 to 53 years) just includes the value of 50 years. However, a new reference value between 41 and 50 years would lie well within the ranges of both the Cunnold *et al.* (1997) and Volk *et al.* (1997) estimates.

Butler *et al.* (1998) showed that the observed burden of Halon-1211 is inconsistent with the emissions if one uses the H-1211 reference lifetime of 20 years. Because of disagreement between the measurements of Gillotay and Simon (1989) and Burkholder *et al.* (1991) for the absorption cross sections for wavelengths longer than 288 nm, the Jet Propulsion Laboratory Data Evaluation Panel did not give any recommended values for these wavelengths (DeMore *et al.*, 1997). Burkholder *et al.* (1991) estimated the partial lifetime due to photolysis in the long-wavelength region to be about 20 years. If one combines this with the derived stratospheric lifetime of 24 years (Table 1-5, column 5), the atmospheric lifetime should be about 11 years. The WMO (1995) reference lifetime of 20 years was again obtained by averaging the model results from Kaye *et al.* (1994). It is likely that some models ignored the longwave photolysis in their calculations and biased the average toward the longer lifetimes.

Based on the above discussion, we recommend new reference lifetimes for three gases. The new reference lifetime for CFC-11 of 45 years lies between the central estimates of Volk *et al.* (1997) and Cunnold *et al.* (1997) (Tables 1-5 and 1-6), provides the same estimated $CCl_4$ lifetime by the two Volk *et al.* (1997) methods (Table 1-5), and gives an estimate of the atmospheric lifetime for H-1211 of 11 years, in better agreement with observations of its atmospheric burden (Butler *et al.*, 1998). The new reference lifetime for $CCl_4$ of 35 years lies just above the central estimates of Volk *et al.* (1997), but at the low end of the model range (Table 1-4). We have also rounded the reference lifetime of CFC-12 to 100 years, to better reflect its uncertainty. These new reference lifetimes were reported earlier in Table 1-1 of the scientific summary of this chapter. Note that some calculations in later chapters were carried out before these WMO 1998 values were finalized and hence

used WMO 1995 values instead. While a more comprehensive analysis is required, adoption of the above CFC-11, Halon-1211, and $CCl_4$ lifetimes as reference values is an appropriate response to knowledge gained since the WMO (1995) Assessment.

## REFERENCES


Abrams, M.C., A.Y. Chang, M.R. Gunson, M.M. Abbas, A. Goldman, F.W. Irion, H.A. Michelsen, M.J. Newchurch, C.P. Rinsland, G.P. Stiller, and R. Zander, On the assessment and uncertainty of atmospheric trace gas burden measurements with high-resolution infrared solar occultation spectra from space by the ATMOS experiment, *Geophys. Res. Lett.*, *23*, 2337-2340, 1996a.

Abrams, M.C., G.L. Manney, M.R. Gunson, M.M. Abbas, A.Y. Chang, A. Goldman, F.W. Irion, H.A. Michelsen, M.J. Newchurch, C.P. Rinsland, R.J. Salawitch, G.P. Stiller, and R. Zander, ATMOS/ATLAS-3 observations of long-lived tracers and descent in the Antarctic vortex in November 1994, *Geophys. Res. Lett.*, *23*, 2345-2348, 1996b.

Achard, V., M. De Mazière, C. Camy-Peyret, F. Karcher, and C. Lippens, Spaceborne measurements of the upper stratospheric HCl vertical distribution in early 1992 and the trend in total stratospheric chlorine since 1985, *J. Geophys. Res.*, *102*, 8985-8990, 1997.

AFEAS (Alternative Fluorocarbons Environmental Acceptability Study), *Production, Sales and Atmospheric Release of Fluorocarbons through 1996*, edited by P.M. Midgley and K.D. Smythe, AFEAS Science and Policy Services, Inc., Washington, D.C., 1998.

Anderson, G.P, and L.A. Hall, Stratospheric determination of $O_2$ cross sections and photodissociation rate coefficients: 1991-215 nm, *J. Geophys. Res.*, *91*, 14509-14514, 1986.

Avallone, L.M., D.W. Toohey, S.M. Schauffler, W.H. Pollock, L.E. Heidt, and E.L. Atlas, In situ measurements of BrO during AASE II, *Geophys. Res. Lett.*, *22*, 831-834, 1995.

Avallone, L.M., and M.J. Prather, Tracer-tracer correlations: Three-dimensional model simulation and comparison to observations, *J. Geophys. Res.*, *102*, 19233-19246, 1997.

Battle, M., M. Bender, T. Sowers, P.P. Tans, J.H. Butler, J.W. Elkins, T. Conway, N. Zhang, P. Lang, and A.D. Clarke, Atmospheric gas concentrations over the past century measured in air from firn at the South Pole, *Nature*, *383*, 231-235, 1996.

Berges, M.G.M., and P.J. Crutzen, Estimates of global $N_2O$ emissions from cattle, pig and chicken manure, including a discussion of $CH_4$ emissions, *J. Atmos. Chem.*, *24*, 241-269, 1996.

Blake, D.R., D.F. Hurst, T.W. Smith, Jr., W.J. Whipple, T.-Y. Chen, N.J. Blake, and F.S. Rowland, Summertime measurements of nonmethane hydrocarbons in the Arctic and sub-Arctic during the 1988 Arctic Boundary Layer experiment (ABLE 3A), *J. Geophys. Res.*, *97*, 16559-16588, 1992.

Blake, D.R., T.-Y. Chen, T.W Smith, Jr., C.J.-L. Wang, O.W. Wingenter, N.J. Blake, and F.S. Rowland, Three-dimensional distribution of nonmethane hydrocarbons and halocarbons over the northwestern Pacific during the 1991 Pacific Exploratory Mission (PEM-West A), *J. Geophys. Res.*, *101*, 1763-1778, 1996a.

Blake, D.R., N.J. Blake, T.W. Smith, Jr., O.W. Wingenter, and F.S. Rowland, Nonmethane hydrocarbon and halocarbon distributions during Atlantic Stratocumulus Transition Experiment/Marine Aerosol and Gas Exchange, June 1992, *J. Geophys. Res.*, *101*, 4501-4514, 1996b.

Boering, K.A., S.C. Wofsy, B.C. Daube, H.R. Schneider, M. Loewenstein, J.R. Podolske, and T.J. Conway, Stratospheric mean ages and transport rates from the observation of carbon dioxide and nitrous oxide, *Science*, *274*, 1340-1343, 1996.

Bouwman, A.F., K.W. Van der Hoek, and J.G.J. Olivier, Uncertainties in the global source distribution of nitrous oxide, *J. Geophys. Res.*, *100*, 2785-2800, 1995.

Bujok, O., V. Tan, E. Klein, R. Bauer, D.S. McKenna, A. Engel, and U. Schmidt, In-situ measurements of long-lived tracers in the tropopause region: A novel automated airborne gas chromatograph, in *Atmospheric Ozone: Proceedings of the XVIII Quadrennial Ozone Symposium*, 12-21 September 1996, L'Aquila, Italy, edited by R.D. Bojkov and G. Visconti, pp. 477-480, Parco Scientifico e Technologico d'Abruzzo, L'Aquila, Italy, 1998.

Burkholder, J.B., R.R. Wilson, T. Gierczak, R. Talukdar, S.A. McKeen, J.J. Orlando, G.L. Vaghjiani, and A.R. Ravishankara, Atmospheric fate of $CF_3Br$, $CF_2Br_2$, $CF_2ClBr$, and $CF_2BrCF_2Br$, *J. Geophys. Res.*, *96*, 5025-5043, 1991.

Butler, J.H., S.A. Montzka, A.D. Clarke, J.M. Lobert, and J.W. Elkins, Growth and distribution of halons in the atmosphere, *J. Geophys. Res.*, *103*, 1503-1511, 1998.

Chang, A.Y., R.J. Salawitch, H.A. Michelsen, M.R. Gunson, M.C. Abrams, R. Zander, C.P. Rinsland, M. Loewenstein, J.R. Podolske, M.H. Proffitt, J.J. Margitan, D.W. Fahey, R.-S. Gao, K.K. Kelly, J.W. Elkins, C.R. Webster, R.D. May, K.R. Chan, M.M. Abbas, A. Goldman, F.W. Irion, G.L. Manney, M.J. Newchurch, and G.P. Stiller, A comparison of measurements from ATMOS and instruments aboard the ER-2 aircraft: Tracers of atmospheric transport, *Geophys. Res. Lett.*, *23*, 2389-2392, 1996a.

Chang, A.Y., R.J. Salawitch, H.A. Michelsen, M.R. Gunson, M.C. Abrams, R. Zander, C.P. Rinsland, J.W. Elkins, G.S. Dutton, C.M. Volk, C.R. Webster, R.D. May, D.W. Fahey, R.-S. Gao, M. Loewenstein, J.R. Podolske, R.M. Stimpfle, D.W. Kohn, M.H. Proffitt, J.J. Margitan, K.R. Chan, M.M. Abbas, A. Goldman, F.W. Irion, G.L. Manney, M.J. Newchurch, and G.P. Stiller, A comparison of measurements from ATMOS and instruments aboard the ER-2 aircraft: Halogenated gases, *Geophys. Res. Lett.*, *23*, 2393-2396, 1996b.

Chen, L., Y. Makide, and T. Tominaga, Determination of 1,2-dichlorotetrafluoroethane (CFC-114) concentration in the atmosphere, *Chem. Lett.*, 571-574, 1994.

Chipperfield, M.P., M. Burton, W. Bell, C.P. Walsh, T. Blumenstock, M.T. Coffey, J.W. Hannigan, W.G. Mankin, B. Galle, J. Mellqvist, E. Mahieu, R. Zander, J. Notholt, B. Sen, and G.C. Toon, On the use of HF as a reference for the comparison of stratospheric observations and models, *J. Geophys. Res.*, *102*, 12901-12919, 1997.

Claude, H., and W. Steinbrecht, Ozone and temperature changes in the Hohenpeissenberg time series, *Proceedings of the 3rd European Workshop on Polar Stratospheric Ozone*, edited by J.A. Pyle, N.R.P. Harris, and G.T. Amanatidis, pp. 502-505, 1996.

Cleveland, W.S., and S.J. Devlin, Locally-weighted regression: An approach to regression analysis by local fitting, *J. Amer. Stat. Assoc.*, *83*, 596-610, 1988.

Coffey, M.T., Observations of the impact of volcanic activity on stratospheric chemistry, *J. Geophys. Res.*, *101*, 6767-6780, 1996.

Considine, D.G., L.E. Deaver, E.E. Remsberg, and J.M. Russell III, HALOE observations of a slowdown in the rate of increase of HF in the lower mesosphere, *Geophys. Res. Lett.*, *24*, 3217-3220, 1997.

Considine, D.G., L.E. Deaver, E.E. Remsberg, and J.M. Russell III, Analysis of near-global trends and variability in HALOE HCl and HF data in the middle atmosphere, *J. Geophys. Res.*, submitted, 1998.

Crutzen, P.J., N.F. Elansky, M. Hahn, G.S. Golitsyn, C.A.M. Brenninkmeijer, D.H. Scharffe, I.B. Berlikov, M. Maiss, P. Bergamaschi, T. Röckmann, A.M. Grisenko, and V.M. Sevostyanov, Trace gas measurements between Moscow and Vladivostok using the Trans-Siberian Railroad, *J. Atmos. Chem.*, *29*, 179-194, 1998.

Cunnold, D.M., and R.G. Prinn, Comment on 'Tropospheric OH in a 3D chemical tracer model: An assessment based on observations of $CH_3CCl_3$' by Spivakovsky *et al.*, *J. Geophys. Res.*, *96*, 17391-17393, 1991.

Cunnold, D.M., P.J. Fraser, R.F. Weiss, R.G. Prinn, P.G. Simmonds, B.R. Miller, F.N. Alyea, and A.J. Crawford, Global trends and annual releases of $CFCl_3$ and $CF_2Cl_2$ estimated from ALE/GAGE measurements from July 1978 to June 1991, *J. Geophys. Res.*, *99*, 1107-1126, 1994.

Cunnold, D.M., R.F. Weiss, R.G. Prinn, D. Hartley, P.G. Simmonds, P.J. Fraser, B. Miller, F.N. Alyea, and L. Porter, GAGE/AGAGE measurements indicating reductions in global emissions of $CCl_3F$ and $CCl_2F_2$ in 1992-1994, *J. Geophys. Res.*, *102*, 1259-1269, 1997.

Daniel, J.S., S. Solomon, and D.L. Albritton, On the evaluation of halocarbon radiative forcing and global warming potentials, *J. Geophys. Res.*, *100*, 1271-1285, 1995.

Daniel, J.S., S.M. Schauffler, W.H. Pollock, S. Solomon, A. Weaver, L.E. Heidt, R.R. Garcia, E.L. Atlas, and J.F. Vedder, On the age of stratospheric air and inorganic chlorine and bromine release, *J. Geophys. Res.*, *101*, 16757-16770, 1996.

DeMore, W.B., D.M. Golden, R.F. Hampson, C.J. Howard, M.J. Kurylo, M.J. Molina, A.R. Ravishankara, and S.P. Sander, *Chemical Kinetics and Photochemical Data for Use in Stratospheric Modeling*, Data Evaluation No. 8, JPL Publication 87-41, Jet Propulsion Laboratory, Pasadena, Calif., 1987.

DeMore, W.B., D.M. Golden, R.F. Hampson, M.J. Kurylo, C.J. Howard, A.R. Ravishankara, C.E. Kolb, and M.J. Molina, *Chemical Kinetics and Photochemical Data for Use in Stratospheric Modeling*, Evaluation No. 12, JPL Publication 97-4, Jet Propulsion Laboratory, Pasadena, Calif., 1997.

Elkins, J.W., T.M. Thompson, T.H. Swanson, J.H. Butler, B.D. Hall, S.O. Cummings, D.A. Fisher, and A.G. Raffo, Decrease in the growth rates of atmospheric chlorofluorocarbons 11 and 12, *Nature*, *364*, 780-783, 1993.

Elkins, J.W., J.H. Butler, T.M. Thompson, S.A. Montzka, R.C. Myers, J.M. Lobert, S.A. Yvon, P.R. Wamsley, F.L. Moore, J.M. Gilligan, D.F. Hurst, A.D. Clarke, T.H. Swanson, C.M. Volk, L.T. Lock, L.S. Geller, G.S. Dutton, R.M. Dunn, M.F. Dicorleto, T.J. Baring, and A.H. Hayden, 5. Nitrous Oxide and Halocompounds, in *Climate Monitoring and Diagnostics Laboratory—No. 23, Summary Report 1994-1995*, edited by D.J. Hofmann and R.M. Rosson, U.S. Department of Commerce, NOAA/ERL, Boulder, Colo., 1996a.

Elkins, J.W., D.W. Fahey, J.M. Gilligan, G.S. Dutton, T.J. Baring, C.M. Volk, R.E. Dunn, R.C. Myers, S.A. Montzka, P.R. Wamsley, A.H. Hayden, J.H. Butler, T.M. Thompson, T.H. Swanson, E.J. Dlugokencky, P.C. Novelli, D.F. Hurst, J.M. Lobert, S.J. Ciciora, R.J. McLaughlin, T.L. Thompson, R.H. Winkler, P.J. Fraser, L.P. Steele, and M.P. Lucarelli, Airborne gas chromatograph for in situ measurements of long-lived species in the upper troposphere and lower stratosphere, *Geophys. Res. Lett.*, *23*, 347-350, 1996b.

Elkins, J.W., J.H. Butler, D.F. Hurst, S.A. Montzka, F.L. Moore, and T.M. Thompson, Nitrous Oxide and Halocompounds Group/Climate Monitoring and Diagnostics Laboratory (NOAH/CMDL) web site (http://www.cmdl.noaa.gov/noah/), Boulder, CO, updated data available on anonymous ftp site (file://ftp.cmdl.noaa.gov/noah/), 1998.

Engel, A., U. Schmidt, and R.A. Stachnik, Partitioning between chlorine reservoir species deduced from observations in the Arctic winter stratosphere, *J. Atmos. Chem.*, *27*, 107-126, 1997.

Engel, A., U. Schmidt, and D.S. McKenna, Stratospheric trends of CFC-12 over the past two decades: Recent observational evidence of declining growth rates, *Geophys. Res. Lett.*, *25*, 3319-3322, 1998.

Etheridge, D.M., L.P. Steele, R.L. Langenfelds, R.J. Francey, and J.-M. Barnola, Natural and anthropogenic changes in atmospheric $CO_2$ over the last 1000 years from air in Antarctic ice and firn, *J. Geophys. Res.*, *101*, 4115-4128, 1996.

Fabian, P., R. Borchers, and K. Kourtidis, Bromine-containing source gases during EASOE, *Geophys. Res. Lett.*, *21*, 1219-1222, 1994.

Fabian, P., R. Borchers, R. Leifer, B.H. Subbaraya, S. Lal, and M. Boy, Global stratospheric distribution of halocarbons, *Atmos. Environ.*, *30*, 1787-1796, 1996.

Fahey, D.W., S.G. Donnelly, E.R. Keim, R.-S. Gao, R.C. Wamsley, L.A. Del Negro, E.L. Woodbridge, M.H. Proffitt, K.H. Rosenlof, M.K.W. Ko, D.K. Weisenstein, C.J. Scott, C. Nevison, S. Solomon, and K.R. Chan, In situ observations of $NO_y$, $O_3$, and the $NO_y/O_3$ ratio in the lower stratosphere, *Geophys. Res. Lett.*, *23*, 1653-1656, 1996.

Fisher, D.A., and P.M. Midgley, The production and release to the atmosphere of CFCs 113, 114 and 115, *Atmos. Environ.*, *27A*, 271-276, 1993.

Fisher, D.A., and P.M. Midgley, Uncertainties in the calculation of atmospheric releases of chlorofluorocarbons, *J. Geophys. Res.*, *99*, 16643-16650, 1994.

Fisher, D.A., T. Duafala, P.M. Midgley, and C. Niemi, Production and emission of CFCs, halons, and related molecules, Chapter 2 in *Report on Concentrations, Lifetimes, and Trends of CFCs, Halons, and Related Species*, NASA Reference Publication 1339, edited by J.A. Kaye, S.A. Penkett, and F.M. Ormond, National Aeronautics and Space Administration,Washington, D.C., 1994.

Fraser, P., Baseline atmospheric halocarbon measurements: An interlaboratory calibration comparison, *WMO Special Environmental Report No. 14*, WMO No. 549, 1980.

Fraser, P., M. Gunson, S. Penkett, F.S. Rowland, U. Schmidt, and R.F. Weiss, Measurements, Chapter 1 in *Report on Concentrations, Lifetimes, and Trends of CFCs, Halons, and Related Species*, NASA Reference Publication 1339, edited by J.A. Kaye, S.A. Penkett, and F.M. Ormond, National Aeronautics and Space Administration, Washington, D.C., 1994.

Fraser, P., D. Cunnold, F. Alyea, R. Weiss, R. Prinn, P. Simmonds, B. Miller, and R. Langenfelds, Lifetime and emission estimates of 1,1,2-trichlorotrifluoroethane (CFC-113) from daily global background observations June 1982-June 1994, *J. Geophys. Res.*, *101*, 12585-12599, 1996.

Fraser, P.J., D.E. Oram, C.E. Reeves, S.A. Penkett, and A. McCulloch, Southern Hemispheric halon trends (1978-1998) and global halon emissions, *J. Geophys. Res.*, submitted, 1998.

Gelb, A., *Applied Optimal Estimation*, 364 pp., MIT Press, Cambridge, Mass., 1974.

Geller, L.S., J.W. Elkins, J.M. Lobert, A.D. Clarke, D.F. Hurst, J.H. Butler, and R.C. Myers, Tropospheric $SF_6$: Observed latitudinal distribution and trends, derived emissions and interhemispheric exchange time, *Geophys. Res. Lett.*, *24*, 675-678, 1997.

Gillotay, D., and P.C. Simon, Ultraviolet absorption spectrum of trifluoro-bromo-methane, difluoro-dibromo-methane and difluoro-bromo-chloro-methane in the vapor phase, *J. Atmos. Chem.*, *8*, 41-62, 1989.

Golombek, A., and R.G. Prinn, A global three-dimensional model of the stratospheric sulfuric acid layer, *J. Atmos. Chem.*, *16*, 179-200, 1993.

Gunson, M.R., M.C. Abrams, L.L. Lowes, E. Mahieu, R. Zander, C.P. Rinsland, M.K.W. Ko, N.D. Sze, and D.K. Weisenstein, Increase in levels of stratospheric chlorine and fluorine loading between 1985 and 1992, *Geophys. Res. Lett.*, *20*, 2223-2226, 1994.

Gunson, M.R., M.M. Abbas, M.C. Abrams, M. Allen, L.R. Brown, T.L. Brown, A.Y. Chang, A. Goldman, F.W. Irion, L.L. Lowes, E. Mahieu, G.L. Manney, H.A. Michelsen, M.J. Newchurch, C.P. Rinsland, R.J. Salawitch, G.P. Stiller, G.C. Toon, Y.L. Yung, and R. Zander, The Atmospheric Trace Molecule Spectroscopy (ATMOS) experiment: Deployment on the ATLAS Space Shuttle missions, *Geophys. Res. Lett.*, *23*, 2333-2336, 1996.

Haas-Laursen, D., D.E. Hartley, and R.G. Prinn, Optimizing an inverse method to deduce time varying emissions of trace gases, *J. Geophys. Res.*, *101*, 22823-22831, 1996.

Hall, T.M., and R.A. Plumb, Age as a diagnostic of stratospheric transport, *J. Geophys. Res.*, *99*, 1059-1070, 1994.

Hall, T.M., and D.W. Waugh, Tracer transport in the tropical stratosphere due to vertical diffusion and horizontal mixing, *Geophys. Res. Lett.*, *24*, 1383-1386, 1997.

Harnisch, J., Emission scenarios for $CF_4$ and $C_2F_6$ based on reconstructed atmospheric concentrations, *Proceedings of workshop on 'Successful Partnership to Reduce PFC Emissions from Primary Aluminium Production,'* United States Environmental Protection Agency, Washington, D.C., 1996.

Harnisch, J., and A. Eisenhauer, Natural $CF_4$ and $SF_6$ on Earth, *Geophys. Res. Lett.*, *25*, 2401-2404, 1998.

Harnisch, J., R. Borchers, P. Fabian, and M. Maiss, Tropospheric trends for $CF_4$ and $C_2F_6$ since 1982 derived from $SF_6$ dated stratospheric air, *Geophys. Res. Lett.*, *23*, 1099-1102, 1996a.

Harnisch, J., R. Borchers, P. Fabian, H.W. Gaggeler, and U. Schotterer, Effect of natural tetrafluoromethane, *Nature*, *384*, 32, 1996b.

Hartley, D.E., and R.G. Prinn, On the feasibility of determining surface emissions of trace gases using an inverse method in a three-dimensional chemical transport model, *J. Geophys. Res.*, *98*, 5183-5198, 1993.

Hartley, D.E., D.L. Williamson, P.J. Rasch, and R.G. Prinn, Examination of tracer transport in the NCAR CCM2 by comparison of $CCl_3F$ simulations with ALE/GAGE observations, *J. Geophys. Res.*, *99*, 12885-12896, 1994.

Hartley, D.E., T. Kindler, D.C. Cunnold, and R.G. Prinn, Evaluating chemical transport models: Comparison of effects of different CFC-11 emission scenarios, *J. Geophys. Res.*, *101*, 14381-14385, 1996.

Hartmann, D.L., K.R. Chan, B.L. Gary, M.R. Schoeberl, P.A. Newman, R.L. Martin, M. Loewenstein, J.R. Podolske, and S.E. Strahan, Potential vorticity and mixing in the south polar vortex during spring, *J. Geophys. Res.*, *94*, 11625-11640, 1989.

Herman, J.R., and J.E. Mentall, $O_2$ absorption cross sections (187-225 nm) from stratospheric solar flux measurements, *J. Geophys. Res.*, *87*, 8967-8975, 1982.

Hurst, D.F., P.S. Bakwin, R.C. Myers, and J.W. Elkins, Behavior of trace gas mixing ratios on a very tall tower in North Carolina, *J. Geophys. Res.*, *102*, 8825-8835, 1997.

IPAI (International Primary Aluminum Institute), *Anode Effect and PFC Emission Survey: 1990-1993*, IPAI, London, 1996.

Johnston, H.S., Evaluation of excess carbon-14 and strontium-90 data for suitability to test two-dimensional stratospheric models, *J. Geophys. Res.*, *94*, 18485-18493, 1989.

Johnston, H.S., O. Serang, and J. Podolske, Instantaneous global nitrous oxide photochemical rates, *J. Geophys. Res.*, *84*, 5077-5082, 1979.

Johnston, J.C., S.S. Cliff, and M.H. Thiemens, Measurements of multioxygen isotopic ($\delta^{18}O$ and $\delta^{17}O$) fractionation factors in the stratospheric sink reactions of nitrous oxide, *J. Geophys. Res.*, *100*, 16801-16804, 1995.

Kaye, J.A., and T.L. Miller, The ATLAS series of Shuttle missions, *Geophys. Res. Lett.*, *23*, 2285-2288, 1996.

Kaye, J.A., S. Penkett, and F.M. Ormond (eds.), *Report on Concentrations, Lifetimes and Trends of CFCs, Halons, and Related Species*, NASA Reference Publication 1339, NASA Office of Mission to Planet Earth, 247 pp., National Aeronautics and Space Administration, Washington, D.C., 1994.

Keim, E.R., M. Loewenstein, J.R. Podolske, D.W. Fahey, R.S. Gao, E.L. Woodbridge, R.C. Wamsley, S.G. Donnelly, L.A. Del Negro, C.D. Nevison, S. Solomon, K.H. Rosenlof, C.J. Scott, M.K.W. Ko, D. Weisenstein, and K.R. Chan, Measurements of $NO_y$-$N_2O$ correlation in the lower stratosphere: Latitudinal and seasonal changes and model comparisons, *J. Geophys. Res.*, *102*, 13193-13212, 1997.

Khalil, M.A.K., and R.A. Rasmussen, Atmospheric methyl chloride, *Atmos. Environ.*, in press, 1998.

Kim, K.-R., and H. Craig, Nitrogen-15 and oxygen-18 characteristics of nitrous oxide: A global perspective, *Science*, *262*, 1855-1857, 1993.

Kinnison, D.E., H.S. Johnston, and D.J. Wuebbles, Model study of atmospheric transport using carbon 14 and strontium 90 as inert tracers, *J. Geophys. Res.*, *99*, 20647-20664, 1994.

Ko, M.K.W., N.D. Sze, and D.K. Weisenstein, Use of satellite data to constrain the model-calculated atmospheric lifetime for $N_2O$: Implications for other trace gases, *J. Geophys. Res.*, *96*, 7547-7552, 1991.

Ko, M.K.W., N.D. Sze, W.-C. Wang, G. Shia, A. Goldman, F.J. Murcray, D.G. Murcray, and C.P. Rinsland, Atmospheric sulfur hexafluoride: Sources, sinks, and greenhouse warming, *J. Geophys. Res.*, *98*, 10499-10507, 1993.

Ko, M.K.W., N.D. Sze, C.J. Scott, and D.K. Weisenstein, On the relation between stratospheric chlorine/bromine loading and short-lived tropospheric source gases, *J. Geophys. Res.*, *102*, 25507-25517, 1997.

Kurylo, M.J., and S. Solomon, *Network for the Detection of Stratospheric Change: A Status and Implementation Report*, issued by NASA Upper Atmosphere Research Program and NOAA Climate and Global Change Program, NASA Headquarters, Washington, D.C., 1990.

Lait, L.R., M.R. Schoeberl, P.A. Newman, M.H. Proffitt, M. Loewenstein, J.R. Podolske, S.E. Strahan, K.R. Chan, B. Gary, J.J. Margitan, E. Browell, M.P. McCormick, and A. Torres, Reconstruction of $O_3$ and $N_2O$ fields from ER-2, DC-8 and balloon observations, *Geophys. Res. Lett.*, *17*, 521-524, 1990.

Langenfelds, R., P. Fraser, R. Francey, P. Steele, L. Porter, and C. Allison, The Cape Grim air archive: The first seventeen years, 1978-1995, in *Baseline Atmospheric Program (Australia) 1994-95*, edited by A.L. Dick, R.J. Francey, and N. Derek, Bureau of Meteorology and CSIRO Division of Atmospheric Research, Melbourne, Australia, 1996.

Lary, D.J., Gas phase atmospheric bromine photochemistry, *J. Geophys. Res.*, *101*, 1505-1516, 1996.

Law, C.S., A.J. Watson, and M.I. Liddicoat, Automated vacuum analysis of sulfur hexafluoride in seawater: Derivation of the atmospheric trend (1970-1993) and potential as a transient tracer, *Marine Chem.*, *48*, 57-69, 1994.

Lee, J.M., W.T. Sturges, S.A. Penkett, D.E. Oram, U. Schmidt, A. Engel, and R. Bauer, Observed stratospheric profiles and stratospheric lifetimes of HCFC 141b and HCFC 142b, *Geophys. Res. Lett.*, *22*, 1369-1372, 1995.

Levin, I., and V. Hesshaimer, Refining of atmospheric transport model entries by the globally observed passive tracer distributions of $^{85}Kr$ and sulfur hexafluoride, *J. Geophys. Res.*, *101*, 16745-16755, 1996.

Liu, X., F.J. Murcray, D.G. Murcray, and J.M. Russell III, Comparison of HF and HCl vertical profiles from ground-based high-resolution infrared solar spectra with Halogen Occultation Experiment observations, *J. Geophys. Res.*, *101*, 10175-10181, 1996.

Machida, T., T. Nakazawa, Y. Fujii, S. Aoki, and O. Watanabe, Increase in the atmospheric nitrous oxide concentration during the last 250 years, *Geophys. Res. Lett*, *22*, 2921-2924, 1995.

Mahieu, E., R. Zander, M.R. Gunson, G.C. Toon, C.P. Rinsland, and P. Demoulin, Evaluation of the lifetime of $SF_6$ in the Earth's atmosphere, based on ATMOS and Jungfraujoch IR solar observations, *Proceedings of the Atmospheric Spectroscopy Applications Workshop*, *ASA-Reims 96*, Reims 4-6 September 1996, edited by A. Barbe, J.M. Flaud, M. Jacon, M.F. Mérienne, and L. Rothman, UFR Sciences Exactes et Naturelles, BP 1039-51687, Reims, 1996.

Mahowald, N.M., R.G. Prinn, and P.J. Rasch, Deducing $CCl_3F$ emissions using an inverse method and chemical transport models with assimilated winds, *J. Geophys. Res.*, *102*, 28153-28168, 1997.

Maiss, M., and I. Levin, Global increase of $SF_6$ observed in the atmosphere, *Geophys. Res. Lett.*, *21*, 569-572, 1994.

Maiss, M., and C.A.M. Brenninkmeijer, Atmospheric $SF_6$, trends, sources, and prospects, *Environ. Sci. Technol.*, *32*, 3077-3086, 1998.

Maiss, M., L.P. Steele, R.J. Francey, P.J. Fraser, R.L. Langenfelds, N.B.A. Trivett, and I. Levin, Sulfur hexafluoride—a powerful new atmospheric tracer, *Atmos. Environ.*, *30*, 1621-1629, 1996.

Makide, Y., A. Yokohata, Y. Kubo, and T. Tominaga, Atmospheric concentrations of halocarbons in Japan in 1979-1986, *Bull. Chem. Soc. Japan*, *60*, 571-574, 1987.

Makide, Y., L. Chen, and T. Tominaga, Accurate measurements and changing trends of atmospheric concentrations of CFC-11, CFC-12, CFC-113, CFC-114, $CH_3CCl_3$, $CCl_4$, Halon-1301 and Halon-1211, *Proceedings of the International Symposium on Global Cycles of Atmospheric Greenhouse Gases*, Sendai, Japan, 7-10 March 1994.

McCulloch, A., Global production and emissions of bromochlorodifluoromethane and bromotrifluoromethane (Halons -1211 and -1301), *Atmos. Environ.*, *26A*, 1325-1329, 1992.

McCulloch, A., P.M. Midgley, and D.A. Fisher, Distribution of emissions of chlorofluorocarbons (CFCs) 11, 12, 113, 114 and 115 among reporting and non-reporting countries in 1986, *Atmos. Environ.*, *28*, 2567-2582, 1994.

McElroy, C.T., A spectroradiometer for the measurement of direct and scattered solar irradiance from on-board the NASA ER-2 high-altitude research aircraft, *Geophys. Res. Lett.*, *22*, 1361-1364, 1995.

McElroy, M.B., and D.B.A. Jones, Evidence for an additional source of atmospheric $N_2O$, *Global Biogeochem. Cycles*, *10*, 651-659, 1996.

Mélen, F., E. Mahieu, R. Zander, C.P. Rinsland, P. Demoulin, G. Roland, L. Delbouille, and C. Servais, Vertical column abundances of $COF_2$ above the Jungfraujoch station, derived from ground-based infrared solar observations, *J. Atmos. Chem.*, *29*, 119-134, 1998.

Miller, B.R., J. Huang, R.F. Weiss, R.G. Prinn, and P.J. Fraser, Atmospheric trend and lifetime of chlorodifluoromethane (HCFC-22) and the global tropospheric OH concentration, *J. Geophys. Res.*, *103*, 13237-13248, 1998.

Minschwaner, K., A.E. Dessler, J.W. Elkins, C.M. Volk, D.W. Fahey, M. Loewenstein, J.R. Podolske, A.E. Roche, and K.R. Chan, Bulk properties of isentropic mixing into the tropics in the lower stratosphere, *J. Geophys. Res.*, *101*, 9433-9439, 1996.

Minschwaner, K., R.W. Carter, and B.P. Briegleb, Infrared radiative forcing and atmospheric lifetimes of trace species based on observations from UARS, *J. Geophys. Res.*, submitted, 1998.

Montzka, S.A., J.H. Butler, R.C. Myers, T.M. Thompson, T.H. Swanson, A.D. Clarke, L.T. Lock, and J.W. Elkins, Decline in the tropospheric abundance of halogen from halocarbons: Implications for stratospheric ozone depletion, *Science*, *272*, 1318-1322, 1996.

Mosier, A., and C. Kroeze, A new approach to estimate emissions of nitrous oxide from agriculture and its implications to the global $N_2O$ budget, *IGBP Global Change Newsletter*, *No. 34*, 8-13 June 1998.

Mulquiney, J.E., J.A. Taylor, A.J. Jakeman, J.P. Norton, and R.G. Prinn, A new inverse method for trace gas flux estimation: 2, Application to tropospheric $CFCl_3$ fluxes, *J. Geophys. Res.*, *103*, 1429-1442, 1998.

Nevison, C.D., and E.A. Holland, A re-examination of the impact of anthropogenically fixed nitrogen on atmospheric $N_2O$ and the stratospheric $O_3$ layer, *J. Geophys. Res.*, *102*, 25519-25536, 1997.

Nightingale, R.W., A.E. Roche, J.B. Kumer, J.L. Mergenthaler, J.C. Gille, S.T. Massie, P.L. Bailey, D.P. Edwards, M.R. Gunson, G.C. Toon, B. Sen, J.-F. Blavier, and P.S. Connell, Global $CF_2Cl_2$ measurements by UARS cryogenic limb array etalon spectrometer: Validation by correlative data and a model, *J. Geophys. Res.*, *101*, 9711-9736, 1996.

Oram, D.E., C.E. Reeves, S.A. Penkett, and P.J. Fraser, Measurements of HCFC-142b and HCFC-141b in the Cape Grim air archive: 1978-1993, *Geophys. Res. Lett.*, *22*, 2741-2744, 1995.

Oram, D.E., C.E. Reeves, W.T. Sturges, S.A. Penkett, P.J. Fraser, and R.L. Langenfelds, Recent tropospheric growth rates and distribution of HFC-134a ($CF_3CH_2F$), *Geophys. Res. Lett.*, *23*, 1949-1952, 1996.

Park, J., M.K.W. Ko, R.A. Plumb, and C. Jackman (eds.), *Report of the 1998 Models and Measurements Workshop II*, NASA Reference Publication, National Aeronautics and Space Administration, Washington, D.C., in press, 1998.

Patra, P.K., S. Lal, B.H. Subbaraya, C.H. Jackman, and P. Rajaratnam, Observed vertical profile of sulfur hexafluoride ($SF_6$) and its atmospheric implications, *J. Geophys. Res.*, *102*, 8855-8859, 1997.

Plumb, R.A., A 'tropical pipe' model of stratospheric transport, *J. Geophys. Res.*, *101*, 3957-3972, 1996.

Plumb, R.A., and M.K.W. Ko, Interrelationships between mixing ratios of long-lived stratospheric constituents, *J. Geophys. Res.*, *97*, 10145-10156, 1992.

Pollock, W.H., L.E. Heidt, R.A. Lueb, J.F. Vedder, M.J. Mills, and S. Solomon, On the age of stratospheric air and ozone depletion potentials in polar regions, *J. Geophys. Res.*, *97*, 12993-12999, 1992.

Prasad, S.S., Natural atmospheric sources and sinks of nitrous oxide: 1, An evaluation based on 10 laboratory experiments, *J. Geophys. Res.*, *99*, 5285-5294, 1994.

Prasad, S.S., Potential atmospheric sources and sinks of nitrous oxide: 2, Possibilities from excited $O_2$, 'embryonic' $O_3$, and optically pumped excited $O_3$, *J. Geophys. Res.*, *102*, 21527-21536, 1997.

Prasad, S.S., E.C. Zipf, and X. Zhao, Potential atmospheric sources and sinks of nitrous oxide: 3, Consistency with the observed distributions of the mixing ratios, *J. Geophys. Res.*, *102*, 21537-21541, 1997.

Prather, M., R. Derwent, D. Ehhalt, P. Fraser, E. Sanhueza, and X. Zhou, Other trace gases and atmospheric chemistry, Chapter 2 in *Climate Change 1994: Radiative Forcing of Climate Change and An Evaluation of the IPCC IS92 Emission Scenarios*, edited by J.T. Houghton, L.G. Meira Filho, J. Bruce, H. Lee, B.A. Callander, N. Harris, A. Kattenberg, and K. Maskell, Cambridge University Press, Cambridge, U.K., 1995.

Prinn, R.G., and D.E. Hartley, Inverse methods in atmospheric chemistry, in *Progress and Problems in Atmospheric Chemistry*, edited by J. Barker, pp. 172-197, World Sci. Publ., Singapore, 1995.

Prinn, R.G., D.M. Cunnold, R. Rasmussen, P.G. Simmonds, F.N. Alyea, A.J. Crawford, P.J. Fraser, and R.D. Rosen, Atmospheric emissions and trends of nitrous oxide deduced from 10 years of ALE/GAGE data, *J. Geophys. Res.*, *95*, 18369-18385, 1990.

Prinn, R.G., D.M. Cunnold, P.G. Simmonds, F.N. Alyea, R. Boldi, A.J. Crawford, P.J. Fraser, D. Gutzler, D.E. Hartley, R.D. Rosen, and R. Rasmussen, Global average concentration and trend for hydroxyl radicals deduced from ALE/GAGE trichloroethane (methyl chloroform) data for 1978-1990, *J. Geophys. Res.*, *97*, 2445-2461, 1992.

Prinn, R.G., R.F. Weiss, B.R. Miller, J. Huang, F.N. Alyea, D.M. Cunnold, P.J. Fraser, D.E. Hartley, and P.G. Simmonds, Atmospheric trends and lifetimes of $CH_3CCl_3$ and global OH concentrations, *Science*, *269*, 187-192, 1995.

Prinn, R.G., R.F. Weiss, P.J. Fraser, P.G. Simmonds, F.N. Alyea, and D.M. Cunnold, The ALE/GAGE/AGAGE database, *DOE-CDIAC World Data Center* (E-mail to: cpd@ornl.gov), Dataset No. DB-1001, 1998.

Rahn, T., and M. Whalen, Stable isotope enrichment in stratospheric nitrous oxide, *Science*, *278*, 1776-1778, 1997.

Rasmussen, R., Interlaboratory comparison of fluorocarbon measurements, *Atmos. Environ.*, *12*, 2505-2508, 1978.

Reber, C.A., C.E. Trevathan, R.J. McNeal, and M.R. Luther, The Upper Atmosphere Research Satellite, *J. Geophys. Res.*, *98*, 10643-10647, 1993.

Reisinger, A.R., N.B. Jones, W.A. Matthews, and C.P. Rinsland, Southern Hemisphere ground-based measurements of carbonyl fluoride ($COF_2$) and hydrogen fluoride (HF): Partitioning between fluorine reservoir species, *Geophys. Res. Lett.*, *21*, 797-800, 1994.

Rinsland, C.P., J.S. Levine, A. Goldman, N.D. Sze, M.K.W. Ko, and D.W. Johnson, Infrared measurements of HF and HCl total column abundances above Kitt Peak, 1977-1990: Seasonal cycles, long-term increases, and comparison with model calculations, *J. Geophys. Res.*, *96*, 15523-15540, 1991.

Rinsland, C.P., E. Mahieu, R. Zander, M.R. Gunson, R.J. Salawitch, A.Y. Chang, A. Goldman, M.C. Abrams, M.M. Abbas, M.J. Newchurch, and F.W. Irion, Trends of OCS, HCN, $SF_6$, $CHClF_2$ (HCFC-22) in the lower stratosphere from 1985 and 1994 Atmospheric Trace Molecule Spectroscopy experiment measurements near 30°N latitude, *Geophys. Res. Lett.*, *23*, 2349-2352, 1996a.

Rinsland, C.P., R. Zander, P. Demoulin, and E. Mahieu, $ClONO_2$ total vertical column abundances above the Jungfraujoch Station, 1986-1994: Long-term trend and winter-spring enhancements, *J. Geophys. Res.*, *101*, 3891-3899, 1996b.

Rothman, L.S., C.P. Rinsland, A. Goldman, S.T. Massie, D.P. Edwards, J.-M. Flaud, A. Perrin, V. Dana, J.-Y. Mandin, J. Schroeder, A. McCann, R.R. Gamache, R.B. Wattson, K. Yoshino, K. Chance, K. Jucks, L.R. Brown, V. Nemtchinov, and P. Varanasi, The HITRAN molecular spectroscopic database and HAWKS (HITRAN atmospheric workstation): 1996 edition, *J. Quant. Spectrosc. Radiat. Transfer*, submitted, 1998.

Rowland, F.S., C.J.-L. Wang, and D.R. Blake, Reduction in the rates of growth of global atmospheric concentrations for $CCl_3F$ (CFC-11) and $CCl_2F_2$ (CFC-12) during 1988-1993, *Proceedings of the International Symposium on Global Cycles of Atmospheric Greenhouse Gases*, Sendai, Japan, 7-10 March 1994.

Russell, J.M. III, L.L. Gordley, J.H. Park, S.R. Drayson, D.H. Hesketh, R.J. Cicerone, A.F. Tuck, J.E. Frederick, J.E. Harries, and P.J. Crutzen, The Halogen Occultation Experiment, *J. Geophys. Res.*, *98*, 10777-10797, 1993.

Russell, J.M. III, L.E. Deaver, M. Luo, J.H. Park, L.L. Gordley, A.F. Tuck, G.C. Toon, M.R. Gunson, W.A. Traub, D.G. Johnson, K.W. Jucks, D.G. Murcray, R. Zander, I. Nolt, and C.R. Webster, Validation of hydrogen chloride measurements made by HALOE from the UARS platform, *J. Geophys. Res.*, *101*, 10151-10162, 1996a.

Russell, J.M. III, L.E. Deaver, M. Luo, R.J. Cicerone, J.H. Park, L.L. Gordley, G.C. Toon, M.R. Gunson, W.A. Traub, D.G. Johnson, K.W. Jucks, R. Zander, and I. Nolt, Validation of hydrogen fluoride measurements made by the HALOE Experiment from the UARS platform, *J. Geophys. Res.*, *101*, 10163-10174, 1996b.

Russell, J.M. III, M. Luo, R.J. Cicerone, and L.E. Deaver, Satellite confirmation of the dominance of chlorofluorocarbons in the global stratospheric chlorine budget, *Nature*, *379*, 526-529, 1996c.

S&PS (Science & Policy Services, Inc.), *Sales of Sulfur Hexafluoride ($SF_6$) by End-Use Applications*, Science & Policy Services, Inc., Washington, D.C., 1997.

Salawitch, R.J., S.C. Wofsy, P.O. Wennberg, R.C. Cohen, J.G. Anderson, D.W. Fahey, R.S. Gao, E.R. Keim, E.L. Woodbridge, R.M. Stimpfle, J.P. Koplow, D.W. Kohn, C.R. Webster, R.D. May, L. Pfister, E.W. Gottlieb, H.A. Michelsen, G.K. Yue, J.C. Wilson, C.A. Brock, H.H. Jonsson, J.E. Dye, D. Baumgardner, M.H. Proffitt, M. Loewenstein, J.R. Podolske, J.W. Elkins, G.S. Dutton, E.J. Hintsa, A.E. Dessler, E.M. Weinstock, K.K. Kelly, K.A. Boering, B.C. Daube, K.R. Chan, and S.W. Bowen, The distribution of hydrogen, nitrogen, and chlorine radicals: Implications for changes in $O_3$ due to emission of $NO_y$ from supersonic aircraft, *Geophys. Res. Lett.*, *21*, 2547-2550, 1994.

Sanhueza, E., P.J. Fraser, and R.J. Zander, Source gases: Trends and budgets, Chapter 2 in *Scientific Assessment of Ozone Depletion: 1994*, Global Ozone Research and Monitoring Project—Report No. 37, World Meterological Organization, Geneva, 1995.

Schauffler, S.M., and J.S. Daniel, On the effects of stratospheric circulation changes on trace gas trends, *J. Geophys. Res.*, *99*, 25747-25754, 1994.

Schauffler, S.M., L.E. Heidt, W.H. Pollock, T.M. Gilpin, J.F. Vedder, S. Solomon, R.A. Lueb, and E.L. Atlas, Measurements of halogenated organic compounds near the tropical tropopause, *Geophys. Res. Lett.*, *20*, 2567-2570, 1993.

Schauffler, S.M., E.L. Atlas, F. Flocke, R.A. Lueb, V. Stroud, and W. Travnicek, Measurements of bromine containing organic compounds at the tropical tropopause, *Geophys. Res. Lett.*, *25*, 317-320, 1998a.

Schauffler, S.M., E.L. Atlas, F. Flocke, R.A. Lueb, J.M. Lee, V. Stroud, and W. Travnicek, Distributions of brominated organic compounds in the troposphere and lower stratosphere, *J. Geophys. Res.*, in press, 1998b.

Schmidt, U., and A. Khedim, In situ measurements of carbon dioxide in the Arctic vortex and at mid-latitudes: An indicator for the 'age' of stratospheric air, *Geophys. Res. Lett.*, *18*, 763-766, 1991.

Schmidt, U., R. Bauer, A. Engel, R. Borchers, and J. Lee, The variation of available chlorine, $Cl_y$, in the Arctic polar vortex during EASOE, *Geophys. Res. Lett.*, *21*, 1215-1218, 1994.

Schoeberl, M.R., L.R. Lait, P.A. Newman, R.L. Martin, M.H. Proffitt, D.L. Hartmann, M. Loewenstein, J. Podolske, S.E. Strahan, J. Anderson, K.R. Chan, and B. Gary, Reconstruction of the constituent distribution and trends in the Antarctic polar vortex from ER-2 flight observations, *J. Geophys. Res.*, *94*, 16815-16845, 1989.

Schoeberl, M.R., A.E. Roche, J.M. Russell III, D. Ortland, P.B. Hays, and J.W. Waters, An estimation of the dynamical isolation of the tropical lower stratosphere using UARS wind and trace gas observations of the quasi-biennial oscillation, *Geophys. Res. Lett.*, *24*, 53-56, 1997.

Sen, B., G.C. Toon, J.-F. Blavier, E.L. Fleming, and C.H. Jackman, Balloon-borne observations of mid-latitude fluorine abundance, *J. Geophys. Res.*, *101*, 9045-9054, 1996.

Sen, B., G.B. Osterman, R.J. Salawitch, G.C. Toon, J.J. Margitan, J.-F. Blavier, A.Y. Chang, R.D. May, C.R. Webster, R.M. Stimpfle, P.B. Voss, J.G. Anderson, G.P. Boone, K.K. Perkins, R.C. Cohen, L.C. Koch, J.W. Elkins, G.S. Dutton, E.L. Atlas, S.M. Schauffler, and M. Loewenstein, The budget and partitioning of stratospheric chlorine during POLARIS, *J. Geophys. Res.*, submitted, 1998.

Shia, R.-L., Y.L. Yung, M. Allen, R.W. Zurek, and D. Crisp, Sensitivity study of advection and diffusion coefficients in a two-dimensional stratospheric model using excess carbon 14 data, *J. Geophys. Res.*, *94*, 18467-18484, 1989.

Shia, R.-L., M.K.W. Ko, D.K. Weisenstein, C. Scott, and J. Rodriguez, Transport between the tropical and mid-latitude lower stratosphere: Implication for ozone response to HSCT emissions, *J. Geophys. Res.*, in press, 1998.

Simmonds, P.G., D.M. Cunnold, F.N. Alyea, C.A. Cardelino, A.J. Crawford, R.G. Prinn, P.J. Fraser, R.A. Rasmussen, and R.D. Rosen, Carbon tetrachloride lifetimes and emissions determined from daily global measurements during 1978-1985, *J. Atmos. Chem.*, *7*, 35-58, 1988.

Simmonds, P., D. Cunnold, G. Dollard, T. Davies, A. McCulloch, and R. Derwent, Evidence of the phase-out of CFC use in Europe over the period 1987-1990, *Atmos. Environ.*, *27A*, 1397-1407, 1993.

Simmonds, P., R. Derwent, A. McCulloch, S. O'Doherty, and A. Gaudry, Long-term trends in concentrations of halocarbons and radiatively active trace gases in Atlantic and European air masses monitored at Mace Head, Ireland from 1987-1994, *Atmos. Environ.*, *30*, 4041-4063, 1996.

Simmonds, P.G., D.M. Cunnold, R.F. Weiss, R.G. Prinn, P.J. Fraser, A. McCulloch, F.N. Alyea, and S. O'Doherty, Global trends and emission estimates of $CCl_4$ from in situ background observations from July 1978 to June 1996, *J. Geophys. Res.*, *103*, 16017-16027, 1998.

Solomon, S., M. Mills, L.E. Heidt, W.H. Pollock, and A.F. Tuck, On the evaluation of ozone depletion potentials, *J. Geophys. Res.*, *97*, 825-842, 1992.

Solomon, S., D. Wuebbles, I. Isaksen, J. Kiehl, M. Lal, P. Simon, and N.-D. Sze, Ozone depletion potentials, global warming potentials, and future chlorine/bromine loading, Chapter 13 in *Scientific Assessment of Ozone Depletion: 1994*, Global Ozone Research and Monitoring Project—Report No. 37, World Meterological Organization, Geneva, 1995.

SORG (U.K. Stratospheric Ozone Review Group), *Stratospheric Ozone 1996*, U.K. Department of the Environment, DOE Reference Number: 96DPL0021, October 1996.

Steele, P., R. Langenfelds, M. Lucarelli, P. Fraser, L. Cooper, D. Spencer, S. Chea, and K. Broadhurst, Atmospheric methane, carbon dioxide, carbon monoxide, hydrogen and nitrous oxide from Cape Grim flask air samples analyzed by gas chromatography, in *Baseline Atmospheric Program (Australia) 1994-95*, edited by A.L. Dick, R.J. Francey, and N. Derek, Bureau of Meteorology and CSIRO Division of Atmospheric Research, Melbourne, Australia, 1996.

Steinbrecht, W., H. Claude, U. Köhler, and K.P. Hoinka, Correlations between tropopause height and total ozone: Implications for long-term changes, *J. Geophys. Res.*, *103*, 19183-19192, 1998.

Stolarski, R.S., and R.D. Rundel, Fluorine photochemistry in the stratosphere, *Geophys. Res. Lett.*, *2*, 443-444, 1975.

Tabazadeh, A., and R.P. Turco, Stratospheric chlorine injection by volcanic eruptions—HCl scavenging and implications for ozone, *Science*, *260*, 1082-1086, 1993.

Thompson, T.M., J.W. Elkins, J.H. Butler, S.A. Montzka, R.C. Myers, T.H. Swanson, T.J. Baring, A.D. Clarke, G.S. Dutton, A.H. Hayden, J.M. Lobert, J.M. Gilligan, and C.M. Volk, 5. Nitrous Oxide and Halocarbons Division, in *Climate Monitoring and Diagnostics Laboratory—No. 22 Summary Report 1993*, edited by J.T. Peterson and R.M. Rosson, pp. 72-91, U.S. Department of Commerce, NOAA/ERL, Boulder, Colo., 1994.

UNEP (United Nations Environment Programme), UNEP/OzL.Pro/WG.1/11/5, 19 December 1994, Meeting the Needs of Article 5 Parties for Controlled Substances during the Grace and Phase-Out Periods: An Update, Nairobi, 1994.

UNEP (United Nations Environment Programme), Montreal Protocol on Substances that Deplete the Ozone Layer, Supplement to the 1994 Assessment, Part 2. Reporting of the Technology and Economic Assessment Panel, Nairobi, March, 1995.

UNEP (United Nations Environment Programme), UNEP/OzL.Pro.9/3, 26 June 97 (The Reporting of Data by the Parties to the Montreal Protocol on Substances that Deplete the Ozone Layer), UNEP, Nairobi, 1997.

Volk, C.M., J.W. Elkins, D.W. Fahey, R.J. Salawitch, G.S. Dutton, J.M. Gilligan, M.H. Proffitt, M. Loewenstein, J.R. Podolske, K. Minschwaner, J.J. Margitan, and K.R. Chan, Quantifying transport between the tropical and mid-latitude lower stratosphere, *Science*, *272*, 1763-1768, 1996.

Volk, C.M., J.W. Elkins, D.W. Fahey, G.S. Dutton, J.M. Gilligan, M. Loewenstein, J.R. Podolske, K.R. Chan, and M.R. Gunson, Evaluation of source gas lifetimes from stratospheric observations, *J. Geophys. Res.*, *102*, 25543-25564, 1997.

Wallace, L., and W. Livingstone, Spectroscopic observations of atmospheric trace gases over Kitt Peak: 3, Long-term trends of hydrogen chloride and hydrogen fluoride from 1978 to 1990, *J. Geophys. Res.*, *96*, 15513-15521, 1991.

Wallace, L., and W. Livingstone, A twenty-five year record of stratospheric hydrogen chloride, *Geophys. Res. Lett.*, *24*, 2363-2366, 1997.

Wamsley, P.R., J.W. Elkins, D.W. Fahey, G.S. Dutton, C.M. Volk, R.C. Myers, S.A. Montzka, J.H. Butler, A.D. Clarke, P.J. Fraser, L.P. Steele, M.P. Lucarelli, E.L. Atlas, S.M. Schauffler, D.R. Blake, F.S. Rowland, W.T. Sturges, J.M. Lee, S.A. Penkett, A. Engel, R.M. Stimpfle, K.R. Chan, D.K. Weisenstein, M.K.W. Ko, and R.J. Salawitch, Distribution of Halon-1211 in the upper troposphere and lower stratosphere and the 1994 total bromine budget, *J. Geophys. Res.*, *103*, 1513-1526, 1998.

Waugh, D.W., T.M. Hall, W.J. Randel, P.J. Rasch, B.A. Boville, K.A. Boering, S.C. Wofsy, B.C. Daube, J.W. Elkins, D.W. Fahey, G.S. Dutton, C.M. Volk, and P.F. Vohralik, Three-dimensional simulations of long-lived tracers using winds from MACCM2, *J. Geophys. Res.*, *102*, 21493-21513, 1997.

Webster, C.R., R.D. May, C.A. Trimble, R.G. Chave, and J. Kendall, Aircraft Laser Infrared Absorption Spectrometer (ALIAS) for in situ stratospheric measurements of HCl, $N_2O$, $CH_4$, $NO_2$, and $HNO_3$, *Appl. Opt.*, *33*, 454-472, 1994.

Webster, C.R., R.D. May, H.A. Michelsen, D.C. Scott, J.C. Wilson, H.H. Jonsson, C.A. Brock, J.D. Dye, D. Baumgardner, R.M. Stimpfle, J.P. Koplov, J.J. Margitan, M.H. Proffitt, L. Jaeglé, R.L. Herman, H. Hu, G.L. Flesch, and M. Loewenstein, Evaluation of HCl concentrations in the lower stratosphere from 1991 to 1996 following the eruption of Mt. Pinatubo, *Geophys. Res. Lett.*, in press, 1998.

Weisenstein, D.K., M.K.W. Ko, N.D. Sze, and J.M. Rodriguez, Potential impact of $SO_2$ emissions from stratospheric aircraft on ozone, *Geophys. Res. Lett.*, *23*, 161-164, 1996.

Wennberg, P.O., J.W. Brault, T.F. Hanisco, R.J. Salawitch, and G.H. Mount, The atmospheric column abundance of IO: Implications for stratospheric ozone, *J. Geophys. Res.*, *102*, 8887-8898, 1997.

Wilson, S.R., A.L. Dick, P.J. Fraser, and S. Whittlestone, Nitrous oxide flux estimates for south-eastern Australia, *J. Atmos. Chem.*, *26*, 169-188, 1997.

WMO (World Meteorological Organization), *Report of the International Ozone Trends Panel 1988*, Global Ozone Research and Monitoring Project—Report No. 18, Geneva, 1990.

WMO (World Meteorological Organization), *Scientific Assessment of Ozone Depletion: 1991*, Global Ozone Research and Monitoring Project—Report No. 25, Geneva, 1992.

WMO (World Meteorological Organization), *Scientific Assessment of Ozone Depletion: 1994*, Global Ozone Research and Monitoring Project—Report No. 37, Geneva, 1995.

WMO (World Meteorological Organization), *Scientific Assessment of Ozone Depletion: 1998*, Global Ozone Research and Monitoring Project—Report No. 44, Geneva, in press, 1998.

Woodbridge, E.L., J.W. Elkins, D.W. Fahey, L.E. Heidt, S. Solomon, T.J. Baring, T.M. Gilpin, W.H. Pollock, S.M. Schauffler, E.L. Atlas, M. Loewenstein, J.R. Podolske, C.R. Webster, R.D. May, J.M. Gilligan, S.A. Montzka, K.A. Boering, and R.J. Salawitch, Estimate of total organic and inorganic chlorine in the lower stratosphere from in situ and flask measurements during AASE II, *J. Geophys. Res.*, *100*, 3057-3064, 1995.

Yoshinari, T., M.A. Altabet, S.W.A. Naqvi, L. Codispoti, A. Jayakumar, M. Kuhland, and A. Devol, Nitrogen and oxygen isotopic composition of $N_2O$ from suboxic waters of the eastern tropical north Pacific and the Arabian Sea—Measurements by continuous-flow isotope-ratio monitoring, *Marine Chem.*, *56*, 253-264, 1997.

Yung, Y.L., and C.E. Miller, Isotopic fractionation of stratospheric nitrous oxide, *Science*, *278*, 1778-1780, 1997.

Zander, R., M.R. Gunson, C.B. Farmer, C.P. Rinsland, F.W. Irion, and E. Mahieu, The 1985 chlorine and fluorine inventories in the stratosphere based on ATMOS observations at 30° North latitude, *J. Atmos. Chem.*, *15*, 171-186, 1992.

Zander, R., P. Demoulin, and E. Mahieu, Monitoring of the atmospheric burdens of $CH_4$, $N_2O$, CO, $CHClF_2$ and $CF_2Cl_2$ above central Europe during the last decade, *Environ. Monitoring and Assessment*, *31*, 203-209, 1994a.

Zander, R., D.H. Ehhalt, C.P. Rinsland, U. Schmidt, E. Mahieu, J. Rudolph, P. Demoulin, G. Roland, L. Delbouille, and A.J. Sauval, Secular trend and seasonal variability of the column abundance of $N_2O$ above the Jungfraujoch station determined from IR solar spectra, *J. Geophys. Res.*, *99*, 16745-16756, 1994b.

Zander, R., C.P. Rinsland, E. Mahieu, M.R. Gunson, C.B. Farmer, M.C. Abrams, and M.K.W. Ko, Increase of carbonyl fluoride ($COF_2$) in the stratosphere and its contribution to the 1992 budget of inorganic fluorine in the upper stratosphere, *J. Geophys. Res.*, *99*, 16737-16744, 1994c.

Zander, R., E. Mahieu, F. Mélen, P. Demoulin, G. Roland, L. Delbouille, and C. Servais, Stratospheric changes monitored above the Jungfraujoch: The budgets of inorganic chlorine and fluorine since 1985, *Proceedings of the 3rd Europ. Workshop on Polar Stratospheric Ozone*, edited by J.A. Pyle, N.R.P. Harris, and G.T. Amanatidis, pp. 239-243, European Commission Air Pollution Report 56, 1996a.

Zander, R., E. Mahieu, M.R. Gunson, M.C. Abrams, A.Y. Chang, M. Abbas, C. Aellig, A. Engel, A. Goldman, F.W. Irion, N. Kämpfer, H.A. Michelsen, M.J. Newchurch, C.P. Rinsland, R.J. Salawitch, G.P. Stiller, and G.C. Toon, The 1994 northern midlatitude budget of stratospheric chlorine derived from ATMOS/ATLAS-3 observations, *Geophys. Res. Lett.*, *23*, 2357-2360, 1996b.

Zander, R., S. Solomon, E. Mahieu, A. Goldman, C.P. Rinsland, M.R. Gunson, M.C. Abrams, A.Y. Chang, R.J. Salawitch, H.A. Michelsen, M.J. Newchurch, and G.P. Stiller, Increase of stratopheric carbon tetrafluoride ($CF_4$) based on ATMOS observations from space, *Geophys. Res. Lett.*, *23*, 2353-2356, 1996c.

Zander, R., E. Mahieu, P. Demoulin, and G. Roland, The pre-CFCs background of HCl above the Jungfraujoch station, *Proceedings of the 3rd Europ. Workshop on Polar Stratospheric Ozone*, edited by J.A. Pyle, N.R.P. Harris, and G.T. Amanatidis, pp. 244-248, European Commission Air Pollution Report 56, 1996d.

Zander, R., P. Demoulin, E. Mahieu, L. Delbouille, G. Roland, F. Mélen, C. Servais, M. De Mazière, and M. Van Roozendael, An overview of NDSC-related activities at the Jungfraujoch through high-resolution infrared solar observations, in *Atmospheric Ozone: Proceedings of the XVIII Quadrennial Ozone Symposium*, 12-21 September 1996, L'Aquila, Italy, edited by R.D. Bojkov and and G. Visconti, pp. 1005-1008, Pacro Scientifico e Technologico D'Abruzzo, L'Aquila, Italy, 1998.

# Appendix

## Ground-Based Stations and Their Geographic Coordinates

| Station | Latitude | Longitude | Elevation (m) | Network(s) [1] |
|---|---|---|---|---|
| Adrigole, Ireland | 52°N | 10°W | 50 | AGAGE |
| Alert, North West Territories, Canada | 82.45°N | 62.52°W | 210 | CMDL, UH |
| Cape Grim, Tasmania, Australia | 40.41°S | 144.64°E | 94 | AGAGE, CMDL |
| Cape Kumukahi, Hawaii, U.S. | 19.52°N | 154.82°W | 3 | CMDL |
| Cape Meares, Oregon, U.S. | 45.48°N | 123.97°W | 10 | AGAGE |
| Fraserdale, Canada | 49.88°N | 81.57°N | 210 | UH |
| Izana, Tenerife | 28.33°N | 16.48°W | 2376 | UH |
| Jungfraujoch, Switzerland | 46.5°N | 8.0°E | 3580 | NDSC |
| Kitt Peak, Arizona, U.S. | 31.9°N | 111.6°W | 2090 | NDSC |
| Lauder, New Zealand | 45.0°S | 169.7°E | 370 | NDSC |
| Mace Head, Ireland | 53.33°N | 9.90°W | 16 | AGAGE |
| Mauna Loa, Hawaii, U.S. | 19.54°N | 155.58°W | 3397 | CMDL, NDSC |
| Neumayer, Antarctica | 71.6°S | 8.3°W | 16 | UH |
| Niwot Ridge, Colorado, U.S. | 40.04°N | 105.54°W | 3013 | CMDL |
| Ragged Point, Barbados | 13.17°N | 59.02°W | 34 | AGAGE |
| Scripps Pier, California, U.S. | 32.83°N | 117.27°W | 14 | AGAGE |
| South Pole, Antarctica | 89.98°S | 102.00°E | 2841 | CMDL |
| Table Mountain, California, U.S. | 34.4°N | 117.7°W | 2258 | NDSC |
| Trinidad Head, California, U.S. | 41.05°N | 124.15°W | 109 | AGAGE |
| Tuluila, American Samoa | 14.23°S | 170.56°W | 77 | CMDL, AGAGE |
| WITN tower, North Carolina, U.S. | 35.37°N | 77.39°W | 9 | CMDL |

[1] Advanced Global Atmospheric Gases Experiment (AGAGE); NOAA Climate Monitoring and Diagnostics Laboratory (CMDL); Network for the Detection of Stratospheric Change (NDSC); University of Heidelberg (UH).

# CHAPTER 2

# Short-Lived Ozone-Related Compounds

**Lead Authors:**
M.J. Kurylo
J.M. Rodríguez

**Coauthors:**
M.O. Andreae
E.L. Atlas
D.R. Blake
J.H. Butler
S. Lal
D.J. Lary
P.M. Midgley
S.A. Montzka
P.C. Novelli
C.E. Reeves
P.G. Simmonds
L.P. Steele
W.T. Sturges
R.F. Weiss
Y. Yokouchi

**Contributors:**
D.M. Cunnold
E.J. Dlugokencky
J.W. Elkins
D.M. Etheridge
P.J. Fraser
D.E. Hartley
M.K.W. Ko
S. Madronich
E. Mahieu
W.A. Matthews
A. McCulloch
D.E. Oram
J.J. Orlando
S.A. Penkett
S.M. Schauffler
S.A. Yvon-Lewis

# CHAPTER 2

## SHORT-LIVED OZONE-RELATED COMPOUNDS

### Contents

## SHORT-LIVED COMPOUNDS

### Methyl Bromide ($CH_3Br$)

- Recent measurements and intercomparison of calibration standards have confirmed that the average global mixing ratio of $CH_3Br$ lies between 9 and 10 ppt, and that the interhemispheric ratio is $1.3 \pm 0.1$ (North/South), decreasing seasonally by as much as 0.2. Available data are not sufficient to determine the magnitude of $CH_3Br$ trends since 1992.

- The amplitude of the seasonal behavior of $CH_3Br$ shows wide geographical variability. The lack of an appreciable seasonal variation in the Southern Hemisphere (SH) suggests the existence of seasonality in other processes (sources or sinks) that offsets the signal for chemical removal by OH.

- Additional laboratory and shipboard measurements carried out since the 1994 Assessment (WMO, 1995) have changed our understanding of the ocean's role in the $CH_3Br$ global budget. The ocean now appears to be a net sink, with an estimated net flux across the surface of about -21 Gg $yr^{-1}$, ranging from -3 to -32 Gg $yr^{-1}$. There is some evidence of seasonality in the saturation of $CH_3Br$ at high latitudes, which suggests a close interplay between aquatic sources and sinks of $CH_3Br$ and which further complicates narrowing the uncertainty in the global net flux across the ocean surface.

- New laboratory and field measurements and calculations utilizing global climatological data have increased the estimated total removal rates of $CH_3Br$. The magnitude of ocean uptake is -77 Gg $yr^{-1}$, with a range of -37 to -133 Gg $yr^{-1}$. Chemical removal in the ocean accounts for 70% of this estimate, with a newly identified biological ocean sink contributing the remaining 30%. Two different studies suggest a significant soil sink for $CH_3Br$. Although measured deposition velocities in similar soil types are consistent with each other, extrapolation to a global soil sink for $CH_3Br$ yield estimates that differ widely due to utilization of different global soil type inventories. The best estimate for the soil sink for $CH_3Br$ is -42 Gg $yr^{-1}$, with a range of -10 to -214 Gg $yr^{-1}$. Removal by atmospheric OH has been increased by 15% over the value in the 1994 Assessment (WMO, 1995) due to the impact of the recalibration of the $CH_3CCl_3$ data. The current estimate for OH removal is -86 Gg $yr^{-1}$, ranging from -65 to -107 Gg $yr^{-1}$. Thus the total removal rate of $CH_3Br$ is -205 Gg $yr^{-1}$, with a range of -454 to -112 Gg $yr^{-1}$.

- No new important sources of $CH_3Br$ have been identified. The total emission of $CH_3Br$ from identified sources is 122 Gg $yr^{-1}$, with a range of 43 to 244 Gg $yr^{-1}$. The best-quantified source is fumigation, with a magnitude of 41 Gg $yr^{-1}$ and a range of 28 to 64 Gg $yr^{-1}$. Other anthropogenic sources include biomass burning (20 Gg $yr^{-1}$, ranging from 10 to 40 Gg $yr^{-1}$) and leaded gasoline use (5 Gg $yr^{-1}$, ranging from 0 to 10 Gg $yr^{-1}$). Estimates of ocean emissions of order 60 Gg $yr^{-1}$ can be directly deduced from the above estimates for ocean uptake and net ocean flux.

- The budget of atmospheric $CH_3Br$, calculated from our current understanding of sources and sinks, does not balance. Identified sinks (about 200 Gg $yr^{-1}$) outweigh identified sources (about 120 Gg $yr^{-1}$). The range in the imbalance is -315 to +36 Gg $yr^{-1}$, obtained by combining estimated ranges for each of the sources and sinks. Because these ranges do not represent a statistical uncertainty, we cannot ascribe a probability to obtaining a balanced budget. Still, uncertainties in sources and sinks cannot easily explain the discrepancy.

- The current best estimate of the lifetime of atmospheric $CH_3Br$, calculated from losses within the atmosphere, to the ocean, and to soils, is 0.7 (0.4 to 0.9) years, contrasted with 1.3 (0.8 to 1.7) years given in the 1994 Assessment (WMO, 1995). The range is estimated by calculating the separate impacts of uncertainties in each of the sinks. The change from the 1994 Assessment is due primarily to both an increase in the ocean sink and the identification of a soil uptake, with a smaller contribution from the increase in the atmospheric removal rate. The Ozone Depletion Potential (ODP) for $CH_3Br$, calculated using the above lifetime and a bromine (Br)

efficiency factor of 58, is 0.4, with a range of 0.2 to 0.5. The ODP range is again calculated by considering the separate impacts of uncertainties in each of the parameters used for the ODP estimate. The bromine efficiency factor of 58 is greater than the value of 48 given in the 1994 Assessment due to improvements in our knowledge of stratospheric bromine chemistry.

### Other Brominated Compounds

- Measurements of shorter-lived organic Br compounds ($CH_2Br_2$, $CHBr_3$, $CH_2BrCl$, $CHBrCl_2$, $CHBr_2Cl$, and $C_2H_4Br_2$) indicate that these chemicals contribute 5 to 10 ppt Br to the tropospheric organic Br burden. However, such measurements have not been part of long-term monitoring programs and the data are sporadic in time and location, with a bias toward coastal and oceanic regions. Variable concentrations of these compounds (ranging from 1.0 to 1.7 ppt ) have been reported at the tropical tropopause, but the paucity of data and the high variability make it difficult to quantify their contribution to reactive Br in the lower stratosphere.

### Methane ($CH_4$) and Carbon Monoxide (CO)

- The current best estimate for the total atmospheric lifetime of $CH_4$ is $8.9 \pm 0.6$ years. The lifetime decrease since the 1994 Assessment (WMO, 1995) reflects the impact of the $CH_3CCl_3$ recalibration.

- The burden of atmospheric $CH_4$ continues to increase, but the rate of growth is declining. A growth rate of about 3 to 4 ppb $yr^{-1}$ was reported for the 1996 to 1997 period, contrasting with an average increase rate of about 10 ppb $yr^{-1}$ in the late 1980s. Apart from the anomalously low growth period after the 1991 eruption of Mt. Pinatubo, the above growth rate is the lowest since the mid-1940s. These lower growth rates are in contrast with the commonly used scenarios of future $CH_4$ emissions.

- Ground-based networks for carbon monoxide (CO) monitoring continue to expand, with many laboratories beginning new CO-monitoring programs. A recent intercomparison of measurements showed that large differences still exist between groups, which may be related to the calibration scales used in the analyses.

- The long-term increase in CO observed in the Northern Hemisphere (NH) until the mid- to late 1980s reversed at that time, with a steady average decrease of 2% $yr^{-1}$ since 1990. This decrease continues today. No significant long-term trend in the SH has been deduced from measurements made over the past 20 years. However, periods of sharp decline in 1992 to 1993 and again in 1995 have yielded the lowest SH mixing ratios in the past two decades.

**Table 2-1. Summary of current (WMO, 1998) and previous (WMO, 1995) reference and observed steady-state lifetimes for several ozone-related source species.** Lifetime is defined as the total amount of a compound in the atmosphere divided by its total rate of removal (or by its rate of destruction by tropospheric OH alone; values in parentheses). Additional information on calculated ranges for different models and lifetime-related uncertainties can be found in Chapter 1 (Tables 1-3, 1-4, 1-5, 1-6) and in Tables 2-2, 2-4, and 2-6 of this chapter.

| Industrial Name | Chemical Formula | Lifetime, WMO (1998)[a] (years) | Lifetime, Observed Range (years) | Lifetime, WMO (1995) (years) |
|---|---|---|---|---|
| Nitrous oxide | $N_2O$ | 120 | 75 to 173[d] | 120 |
| CFC-11 | $CCl_3F$ | 45[f] | 29 to 76[e] | 50 |
| CFC-12 | $CCl_2F_2$ | 100 | 77 to 185[e] | 102 |
| CFC-113 | $CCl_2FCClF_2$ | 85 | 54 to 143[d] | 85 |
| Carbon tetrachloride | $CCl_4$ | 35[f] | 21 to 43[d] | 42 |
| H-1211 | $CBrClF_2$ | 11[f] | 10 to 31[d] | 20 |
| H-1301 | $CBrF_3$ | 65 | 60 to 65[g] | 65 |
| Methyl chloroform | $CH_3CCl_3$ | 4.8 (5.7) | 4.5 to 5.1[b] | 5.4 |
| HCFC-22 | $CHClF_2$ | 11.8 (12.3) | 7.0 to 14.4[c] | 13.3 |
| HCFC-141b | $CH_3CCl_2F$ | 9.2 (10.4) | (h) | 9.4 |
| HCFC-142b | $CH_3CClF_2$ | 18.5 (19.5) | (h) | 19.5 |
| HFC-134a | $CH_2FCF_3$ | 13.6 (14.1) | (h) | 14 |
| HFC-23 | $CHF_3$ | 243 (255) | (h) | 250 |
| Methyl chloride | $CH_3Cl$ | ~1.3 (1.3) | (h) | 1.5 |
| Methyl bromide | $CH_3Br$ | 0.7 (1.8) | (h) | 1.3 |
| Methane | $CH_4$ | 8.9[i] (9.3) | (h) | 10 |

[a] The numbers in parentheses represent lifetimes for removal by tropospheric OH scaled to the total atmospheric lifetime of $CH_3CCl_3$ (4.8 years) derived by Prinn *et al.* (1995), and adopting $CH_3CCl_3$ lifetimes for ocean removal of 85 years and stratospheric removal of 45 years (Kaye *et al.*, 1994). Adopting a shorter stratospheric removal time of 37 years (Prinn *et al.*, 1995; see also Volk *et al.*, 1997) yields a lifetime for $CH_3CCl_3$ removal by tropospheric OH of 5.9 years, which is within the uncertainty limits of the above (WMO, 1998) reference value.

[b] Prinn *et al.*, 1995.

[c] Miller *et al.*, 1998.

[d] Volk *et al.*, 1997. Note that this analysis gives only stratospheric lifetimes. Additional loss of H-1211 in the troposphere (see Section 1.4.4) reduces its lifetime to 11 years. When considering recently updated emissions of H-1211 (see Figure 1-11) and observations, the Butler *et al.* (1998) lifetime evaluation approach leads to an H-1211 lifetime of 10 years.

[e] For CFC-11, combined range of Volk *et al.* (1997) and updated values from Cunnold *et al.* (1997); for CFC-12, range covered by the central estimates of Volk *et al.* (1997) and updated central estimates from Cunnold *et al.* (1997).

[f] WMO (1998) CFC-11, H-1211, and $CCl_4$ lifetimes are lower than WMO (1995) values to take account of recent estimates based on stratospheric observations and models. Note that some calculations in later chapters of this 1998 Assessment were carried out before these WMO (1998) values were finalized and therefore used WMO (1995) values instead.

[g] Butler *et al.*, 1998.

[h] Not available or not applicable.

[i] Lifetime as calculated by Prinn *et al.* (1995). The adjustment time for $CH_4$ recovery would be somewhat longer due to $CH_4$ feedback on CO and OH (WMO, 1995).

## 2.1 INTRODUCTION

As indicated in past ozone assessments, knowledge of the distributions, trends, sources, and sinks of a wide range of atmospheric trace gases is required for understanding the present-day distribution of stratospheric ozone and to predict its future behavior in response to natural and anthropogenic forcings. These gases may also play a role in the forcing of climate change by altering the infrared radiative budget of the atmosphere. Such source gases are emitted as a result of naturally occurring processes or as a result of human activity and have lifetimes ranging from days to centuries. Chapter 1 of this Assessment focuses on "long-lived" source gases whose atmospheric photochemical destruction occurs predominantly (if not exclusively) in the stratosphere, and which thus tend to have lifetimes on the order of many years. The present chapter deals with the "short-lived" subset of ozone-related source gases that undergo significant chemical destruction in the troposphere, occurring primarily via reaction with tropospheric hydroxyl radicals (OH) or (as in the case of some iodine-containing compounds) via photolysis at wavelengths longer than 300 nanometers (nm). The lifetimes of these species tend to be shorter, ranging from days to several years. However, to keep the discussion together for all gases primarily destroyed through reaction with OH, the much longer-lived HFC-23 ($CHF_3$) also is included in this chapter. The present and future budgets of the source gases within this combined suite strongly influence the chemical composition of the Earth's atmosphere and determine the atmospheric concentrations of free radicals, which define the magnitude of stratospheric ozone destruction. In particular, the combined data reviewed in Chapters 1 and 2 determine the loadings of stratospheric bromine (Br) and chlorine (Cl), which have played and continue to play a major role in the decreasing trends of stratospheric ozone.

In the following four sections of this chapter the measurements, distributions, sources, sinks, observed trends, and lifetimes of several subclasses of the short-lived source gases are reviewed. These subclasses include fluorinated and chlorinated compounds (the hydrochlorofluorocarbons (HCFCs), hydrofluorocarbons (HFCs), other proposed chlorofluorocarbon (CFC) substitutes); methyl chloroform ($CH_3CCl_3$); brominated compounds (with a principal emphasis on methyl bromide ($CH_3Br$)); other halocarbons (such as the chlorinated methanes and ethylenes as well as alkyl iodides); and other ozone-related compounds (methane ($CH_4$) and carbon monoxide (CO)). This information is used together with similar data for the long-lived source gases to determine the global halogen budgets that are given in Chapter 1. As in Chapter 1, we present model-calculated atmospheric lifetimes based on photochemical and kinetic data provided by laboratory studies. Whenever available, we also present lifetimes derived by inverse methods, in which atmospheric measurements are fit by model simulations that employ industrial emission estimates.

## 2.2 FLUORINATED AND CHLORINATED COMPOUNDS

### 2.2.1 Hydrochlorofluorocarbons (HCFCs) and Hydrofluorocarbons (HFCs)

#### 2.2.1.1 Sources

***Production of HCFCs and HFCs***

Worldwide emissions of halocarbons have changed dramatically in recent years (Figure 2-1 and Figure 1-11 of Chapter 1) with the coming into force of the Montreal Protocol and its Amendments. The consumption (consumption = production + imports - exports) and most production of CFCs and $CH_3CCl_3$ were phased out in developed countries at the end of 1995. Exceptions include feedstock use and an allowance to supply the needs of developing countries whose own phase-out schedule begins with a freeze in 1999 and culminates in phase-out in 2010. This phase-out has stimulated a market for replacement products such as halocarbon alternatives and hydrocarbons, and alternative technologies such as aqueous cleaning systems. Conservation by means of improved design, recovery, and recycling has played a major role in reducing CFC emissions (UNEP, 1995). For certain applications, principally the servicing of existing refrigeration and air-conditioning equipment, the use of compounds with properties similar to those of the CFCs, such as HCFCs and HFCs, has been necessary in order to achieve the rapid phase-out of CFCs while permitting existing equipment to be operated for its useful economic life. However, because of their potential to deplete ozone, HCFCs are controlled under the Montreal Protocol as "transitional substances," with a cap on consumption and

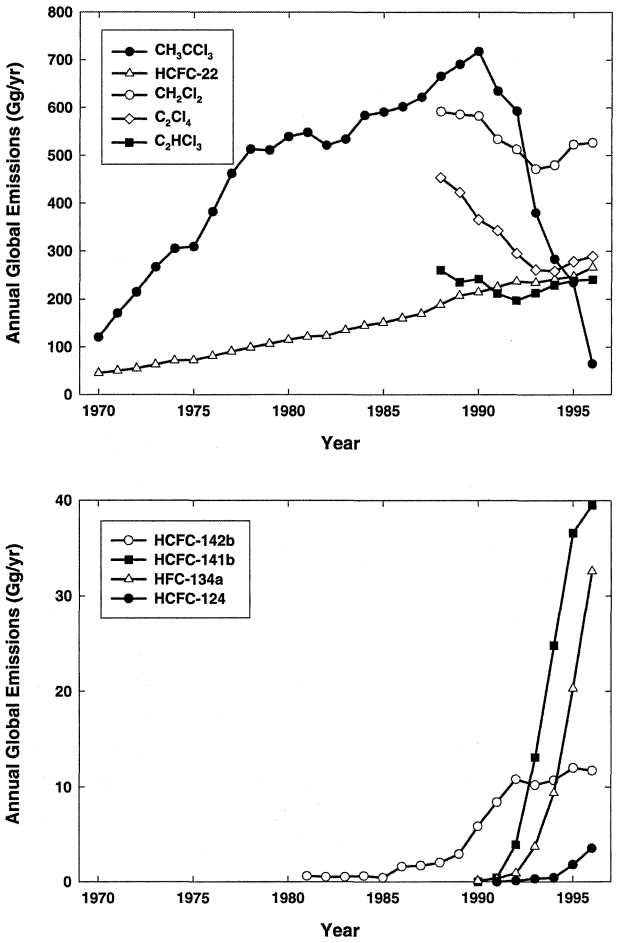


**Figure 2-1.** Annual global emissions of short-lived halocarbons (kt $yr^{-1}$, Gg $yr^{-1}$) estimated by industry from audited production, sales, and other data (AFEAS, 1998; Fisher *et al.*, 1994; Midgley and McCulloch, 1995; McCulloch and Midgley, 1996; and Midgley *et al.*, 1998). Note: There are no surveyed data for $CH_2Cl_2$, $C_2Cl_4$, and $C_2HCl_3$ prior to 1988.

a 2030 phase-out date in developed countries, and a cap on consumption and a 2040 phase-out date in developing countries.

HCFCs and HFCs are exclusively of industrial origin and their principal uses are in refrigeration and air conditioning (HCFC-22 ($CHClF_2$), HFC-134a ($CH_2FCF_3$)) and as foam-blowing agents (HCFC-142b ($CH_3CClF^2$), HCFC-141b ($CH_3CCl_2F$)). The range of minor applications of HCFCs and HFCs includes propellants in medical and other aerosols, sterilants, and cleaning solvents. Certain HCFCs, notably HCFC-22 and HCFC-142b, are used as chemical feedstocks. That fraction of their production is captively converted and is not emitted to the atmosphere. HFC-23 is emitted into the atmosphere as a byproduct during the manufacture of HCFC-22.

The production and sales of HCFCs and HFCs for emissive uses are surveyed annually by the Alternative Fluorocarbons Environmental Acceptability Study (AFEAS). AFEAS participants include all of the world's major producers, located in Europe, North America, and Japan, and their subsidiaries, giving virtually complete global coverage for HFCs and for most HCFCs (AFEAS, 1998). However, there is some evidence for additional HCFC-22 production, amounting to up to 10% of the total reported in the AFEAS survey (Midgley and Fisher, 1993; Fisher *et al.*, 1994; UNEP, 1997). The data presented in Figure 2-1 are annual global emission totals derived from industry reports and other data.

Production of HCFC-22 from companies reporting to AFEAS has increased steadily since the 1970s (AFEAS, 1998). The late 1980s were a period of faster growth in sales as HCFC-22 replaced CFCs in refrigeration. Approximately 95% of reported sales were made in the Northern Hemisphere (NH) through the period 1970 to date. Sales into dispersive uses in 1996 were 270 Gg, an almost fivefold increase since 1970 (AFEAS, 1998).

Industrial production of HCFC-141b and HCFC-142b increased markedly in the late 1980s and early 1990s as these HCFCs found use as replacements for CFCs and chlorinated solvents. Although production of HCFC-142b, initially mainly for feedstock use, began earlier than that of HCFC-141b, by 1996 the amount of HCFC-141b sold into dispersive uses was 3 times as much as HCFC-142b. Sales figures for that year were 121 Gg for HCFC-141b and 38 Gg for HCFC-142b, and indicate that more than 99% of sales of these compounds were in the NH (AFEAS, 1998). Sales of HCFC-142b in the last three years of reported data (1994 through 1996) have remained virtually constant.

Data have recently been reported on the production and sales of HCFC-124 ($CF_3CHClF$). Sales into dispersive uses in 1996 amounted to 4 Gg, again with over 99% in the NH (AFEAS, 1998).

The only HFC for which surveyed data has been reported by AFEAS is HFC-134a. Industrial sales of this "chlorine-free" refrigerant increased from zero in 1990 to 84 Gg in 1996 (AFEAS, 1998). The rapid growth in production and emission of HFC-134a and HCFC-

141b (and HCFC-124) is typical of newly introduced, industrial products and will gradually slow over a period of years to decades (McCulloch, 1994; Prather *et al.*, 1996).

Although demand for other HCFCs and HFCs such as HCFC-123 ($CF_3CHCl_2$), HFC-125 ($CHF_2CF_3$), HFC-143a ($CH_3CF_3$), and HFC-152a ($CH_3CHF_2$) have also increased lately as alternatives to CFCs in some applications, there are no production and sales data available at present.

***Estimates of Emissions to the Atmosphere***

The production and sales data reported by industry are used to generate annual emission estimates for each compound. This process, which has been extensively described (see, e.g., Midgley and Fisher, 1993; Fisher and Midgley, 1994; Midgley and McCulloch, 1995), involves the development of release algorithms based on the pattern of use and time scale of release from the various applications of each compound. This process is relatively straightforward for compounds with a single, well-defined use with immediate emissions, such as the solvent use of $CH_3CCl_3$, $CH_2Cl_2$, $C_2Cl_4$, and $C_2HCl_3$. It becomes less so for applications with longer and ill-defined delays between use of the compound and its emission to the atmosphere. This is particularly critical for the release of blowing agents from closed cell foams, where a complex, multi-stage pattern of release takes place over decades. Thus emission estimates for compounds such as HCFC-142b and HCFC-141b have greater uncertainties principally because of difficulties in defining release from foams. Emissions of HCFCs, HFCs, and selected solvents estimated from global production data are given in Figure 2-1.

### 2.2.1.2 Sinks

Because they contain at least one carbon-hydrogen bond, HCFCs and HFCs react with OH. This oxidation occurs predominantly in the troposphere, where scavenging of water-soluble oxidation products prevents most of the reactive halogen carried by these trace gases from being transmitted to the stratosphere. Lifetimes with respect to oxidation by OH for most HCFCs are longer than several years (see Table 2-2), thereby permitting significant amounts of these compounds to reach the stratosphere (Lee *et al.*, 1995; Zander *et al.*, 1996). Once in the stratosphere, the propensity for a compound to degrade via photodissociation or chemical oxidation at stratospheric temperatures determines its contribution to the reactive halogen burden of the stratosphere.

**Table 2-2. Calculated lifetimes.**

| | $\tau_{OH}$ [a] (years) | $\tau_{strat}$ [a] (years) | $\tau_{atmos}$ [b] (years) |
|---|---|---|---|
| $CH_3CCl_3$ | 5.7[c] | 45 | 4.8 |
| HCFC-22 | 12.3 | 306 | 11.8 |
| HFC-134a | 14.1 | 377 | 13.6 |
| HCFC-141b | 10.4 | 81 | 9.2 |
| HCFC-142b | 19.5 | 372 | 18.5 |
| HFC-23 | 255 | 5310 | 243 |

[a] $\tau_{OH}$ and $\tau_{strat}$ are defined as the total atmospheric burden divided by the integrated loss due to reaction with OH in the troposphere and to reactive and photolytic losses in the stratosphere, respectively. Values of $\tau_{OH}$ were calculated using the scaling procedure suggested by Prather and Spivakovsky (1990) with the global OH concentration constrained by $CH_3CCl_3$ measurements. Values of $\tau_{strat}$ were calculated using the AER 2-D model.

[b] $$\frac{1}{\tau_{atmos}} = \frac{1}{\tau_{OH}} + \frac{1}{\tau_{strat}} + \frac{1}{\tau_{ocean}}$$
where $\tau_{ocean}$ = 85 yr for $CH_3CCl_3$. Table entries for other compounds assumed that there is no ocean uptake.

[c] The 5.7-yr value of $\tau_{OH}$ for $CH_3CCl_3$ was derived using the 4.8-yr value of $\tau_{atmos}$ based on observations (Prinn *et al.*, 1995) together with a value of $\tau_{strat}$ of 45 yr and $\tau_{ocean}$ of 85 yr. Other values for $\tau_{OH}$ in this table are based on this 5.7-yr value. Prinn *et al.* (1995) used $\tau_{strat}$ = 37 yr to calculate a slightly higher value of $\tau_{OH}$ = 5.9 yr.

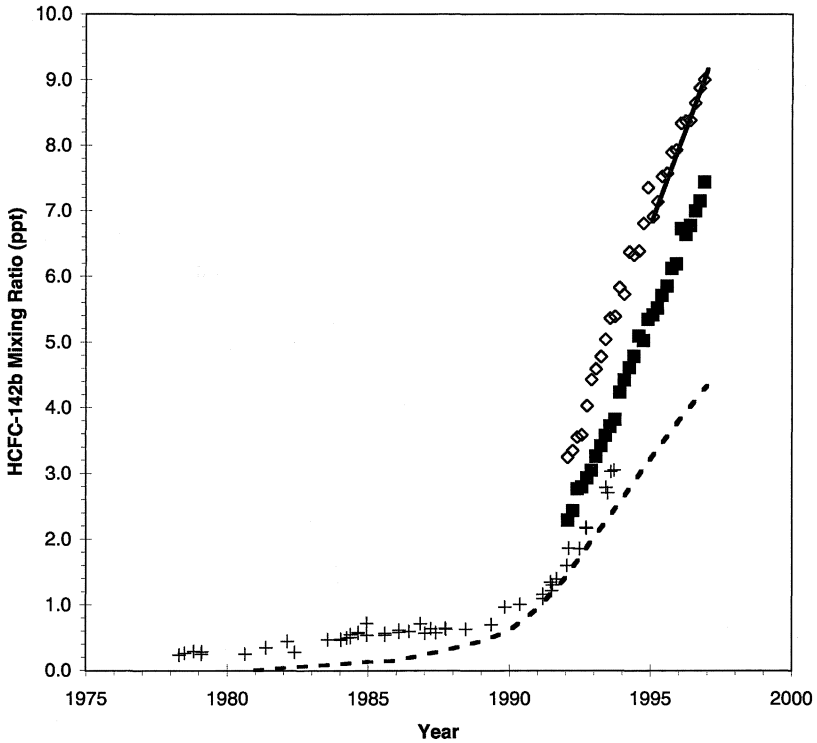


**Figure 2-4.** Ground-based measurements of HCFC-142b. NH means (flask sampling at four remote sites; open diamonds) and SH means (flask sampling at three remote sites, filled squares) (Montzka *et al.*, 1994, 1996a) are displayed along with results from the analysis of the Cape Grim (Tasmania) Air Archive (CGAA; plus symbols) (Oram *et al.*, 1995), and 6-hour measurements made at Mace Head, Ireland (smoothed to a solid line) (Simmonds *et al.*, 1998a). Also displayed are global-mean surface mixing ratios calculated from estimates of global emission (AFEAS, 1998) and a lifetime of 18.5 yr (dashed line) (Table 2-1).

Exchanges of real-air samples and standards between the National Oceanic and Atmospheric Administration Climate Monitoring and Diagnostics Laboratory (NOAA/CMDL) and the Scripps Institution of Oceanography (SIO) reveal agreement to within 1% between these two laboratories for measurements of HCFC-22 (Miller *et al.*, 1998), suggesting improved calibration over earlier studies (Rasmussen *et al.*, 1980; Chen *et al.*, 1994) where significantly higher values were reported (see also Chapter 1 in Kaye *et al.*, 1994).

From a series of vertical column abundance measurements at the Lauder site (New Zealand; 45.0°S, 169.7°W, 370 m above sea level (asl)), Sherlock *et al.* (1997) derived an exponential rate of increase for HCFC-22 of $7.5 \pm 0.3\%$ yr$^{-1}$ over the period 1985 to 1994. This SH trend compares well with those reported for NH sites in the 1994 Assessment: 7.0% yr$^{-1}$ at Kitt Peak, Arizona (31.9°N, 111.6°W, 2090 m asl) from 1980 to 1992 (Zander *et al.*, 1994a); 7.0% yr$^{-1}$ at the Jungfraujoch, Switzerland (46.5°N, 8.0° E, 3580 m asl) from 1986 to 1992 (Zander *et al.*, 1994a); and 6.7% yr$^{-1}$ at Table Mountain, California (34.4°N, 117.7°W, 2258 m asl) from 1985 to 1990 (Irion *et al.*, 1994) (Figure 2-3). More recent measurements at the Jungfraujoch return an exponential rate of increase of $5.9 \pm 0.2\%$ yr$^{-1}$ for the entire period from 1986 to mid-1997. This rate is significantly lower than the $7.0 \pm 0.3\%$ yr$^{-1}$ trend derived over the shorter 1986 to 1992 time interval (Zander *et al.*, 1994a) and suggests that the growth rates derived from remote column measurements during the 1980s and early 1990s have not been sustained during recent years. This is also suggested by the 1992 to 1996 ground-based flask-sampling studies discussed earlier in this section.

Based upon the global OH burden estimated from the analysis of measurements of $CH_3CCl_3$, Prinn *et al.* (1995) calculate a global atmospheric lifetime for HCFC-22 of $11.5 \pm 0.7$ yr. The lifetime of 11.8 yr given in Table 2-2 (calculated using the scaling procedure

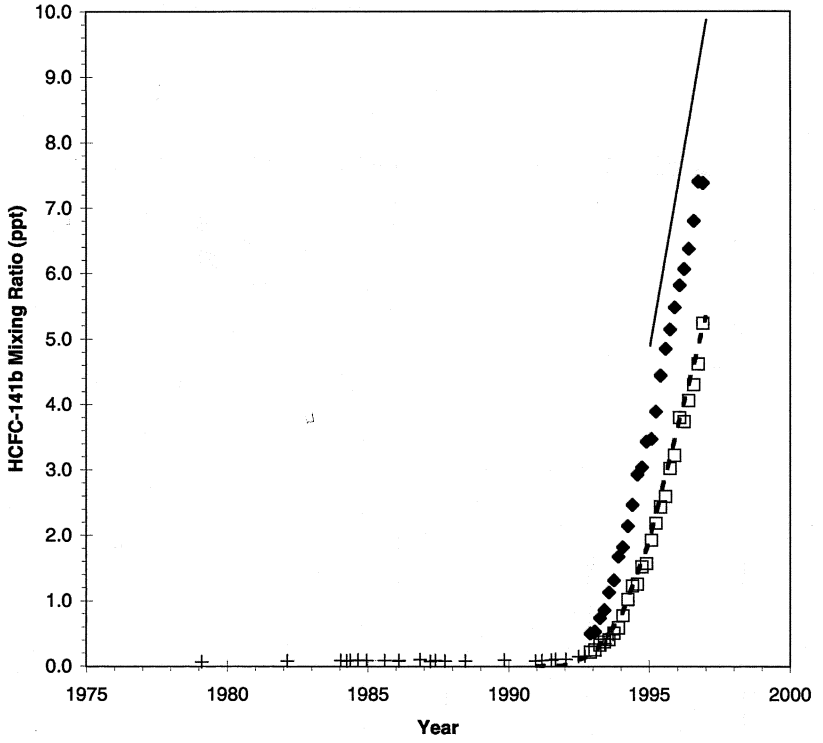


**Figure 2-5.** Ground-based measurements of HCFC-141b. NH means (flask sampling at four remote sites; filled diamonds) and SH means (flask sampling at three remote sites, open squares) (Montzka *et al.*, 1994, 1996a) are displayed along with results from the analysis of the Cape Grim (Tasmania) Air Archive (CGAA; plus symbols) (Oram *et al.*, 1995), and 6-hour measurements made at Mace Head, Ireland (smoothed to a solid line) (Simmonds *et al.*, 1998a). Also displayed are global-mean surface mixing ratios calculated from estimates of global emission (AFEAS, 1998) and a lifetime of 9.2 yr (dashed line) (Table 2-1).

described by Prather and Spivakovsky, 1990) is in good agreement with this value. Although lifetimes estimated from a budget analysis (comparison of measurements with emission estimates) do not differ significantly from 11.5 yr (Montzka *et al.*, 1993; Miller *et al.*, 1998), they have a larger uncertainty associated with them owing to the greater uncertainty in emissions estimated for HCFC-22 compared to $CH_3CCl_3$ (Midgley and Fisher, 1993).

### *HCFC-141b ($CH_3CCl_2F$) and HCFC-142b ($CH_3CClF_2$)*

Observations of HCFC-141b and HCFC-142b reveal background tropospheric mixing ratios that are presently below 10 ppt but increasing rapidly on a relative basis since the early 1990s, and much higher amounts are observed in the NH when compared to the SH (Montzka *et al.*, 1994, 1996a; Oram *et al.*, 1995; Schauffler *et al.*, 1995; Simmonds *et al.*, 1998a; Shirai and Makide, 1998) (Figures 2-4, 2-5, and 2-6).

Data from a global ground-based flask sampling network indicate that the mean global tropospheric mixing ratio of HCFC-141b increased from 0.7 ppt in mid-1993 to 3.5 ppt in mid-1995; the rate of increase in mid-1995 was estimated at 1.9 ppt $yr^{-1}$ (Montzka *et al.*, 1994, 1996a). From flask samples collected in the marine boundary layer of the eastern Pacific Ocean in April of 1993, mixing ratios for HCFC-141b of 0.83 ± 0.23 ppt in the NH and 0.28 ± 0.07 ppt in the SH were measured (Schauffler *et al.*, 1995). They also noted an increase in the midlatitude NH from 0.26 ppt in March 1992 to 1.41 ppt in September 1993. Similarly significant increases have been noted from in situ sampling and analysis of air at Mace Head, Ireland (Simmonds *et al.*, 1998a). In this study, a mean increase of 2.49 ppt $yr^{-1}$ was noted for the period October 1994 through March 1997. The atmospheric mixing ratio reported at this site in January 1996 (the midpoint of the time series) was 7.38 ppt. A mean increase of 63 ± 9% $yr^{-1}$ for HCFC-141b was

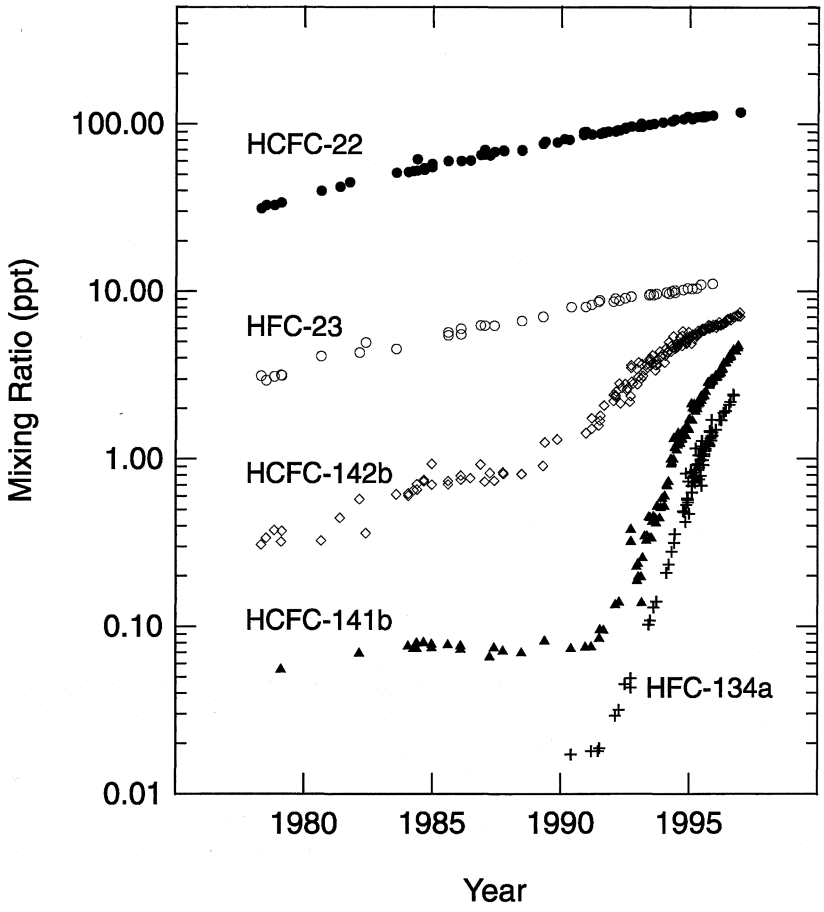


**Figure 2-6.** Ground-based measurements from Cape Grim, Tasmania, of HCFC-22 (filled circles) (Miller *et al.*, 1998), HFC-23 (open circles) (Oram *et al.*, 1998), HCFC-142b (open diamonds) (Montzka *et al.*, 1994, 1996a; Oram *et al.*, 1995), HCFC-141b (filled triangles) (Montzka *et al.*, 1994, 1996a; Oram *et al.*, 1995), and HFC-134a (plus symbols) (Montzka *et al.*, 1996a,b; Oram *et al.*, 1996) from the Cape Grim (Tasmania) Air Archive (CGAA) and ongoing sampling programs. For HCFCs -142b and -141b and HFC-134a, the data of Oram *et al.* (1995, 1996) have been scaled in this figure to the NOAA calibration scale.

calculated from measurements at Hokkaido, Japan, and Syowa Station, Antarctica, for the period from July 1995 to January 1997. The mean from these two stations was 5.7 ± 0.6 ppt in January 1997 (Shirai and Makide, 1998).

The mean global tropospheric mixing ratio of HCFC-142b increased from 4.3 ppt in mid-1993 to 6.6 ppt in mid-1995; the rate of increase has been fairly constant over the period 1992 to 1996 at 1.1 ppt $yr^{-1}$ (Montzka *et al.*, 1994, 1996a; Elkins *et al.*, 1996). For the 30-month period preceding March 1997, Simmonds *et al.* (1998a) measured a mean increase of 1.16 ppt $yr^{-1}$ at Mace Head, Ireland. They also report a January 1996 mixing ratio (the midpoint of the time series) of 8.0 ppt. Slightly larger increases of 1.6 ± 0.1 ppt $yr^{-1}$ were determined from measurements made at Hokkaido, Japan, and Syowa Station, Antarctica (Shirai and Makide, 1998). The mean mixing ratio from these two sites was 10.4 ± 1.1 ppt in January 1997.

Data from archived air samples collected at Tasmania also reveal large increases for HCFC-141b and HCFC-142b since 1978 (Oram *et al.*, 1995). For both HCFCs, small amounts (0.08 ppt for HCFC-141b in the 1980s, and 0.2 to 0.3 ppt for HCFC-142b in the early 1980s) were detected in the period before surveys report significant emissions from industrial production (AFEAS, 1998). Analysis of a smaller air archive dating back to 1987 from the NH (Elkins *et al.*, 1996) shows data supporting the observations of Oram *et al.* (1995) from Tasmania. More recently, large increases have been observed in the archive from Tasmania: in the period from 1992 to September 1993, mixing ratios of HCFC-141b increased from 0.08 ± 0.01 ppt to 0.46 ± 0.05 ppt. Similarly, between 1978 and 1993 the abundance of HCFC-142b increased from 0.20 ± 0.02 to 3.0 ± 0.3 ppt (Oram *et al.*, 1995).

The consistency observed by four independent laboratories reporting measurements for HCFC-141b is on the order of ± 5% (Montzka *et al.*, 1994; Schauffler *et al.*, 1995; Oram *et al.*, 1995; Simmonds *et al.*, 1998a). For HCFC-142b, consistency within 5% is observed

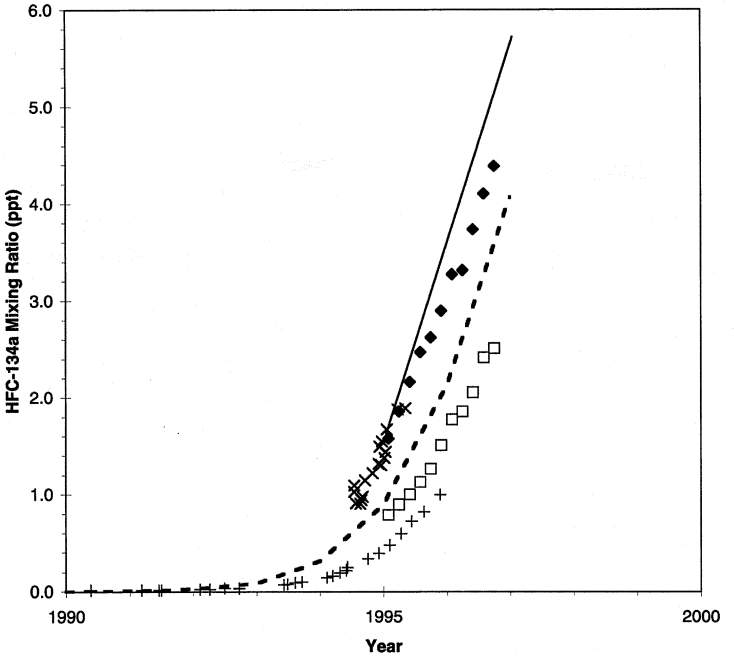


**Figure 2-7.** Ground-based measurements of HFC-134a. NH means (flask sampling at four remote sites; filled diamonds) and SH means (flask sampling at three remote sites, open squares) (Montzka *et al.*, 1994, 1996a) are displayed along with results from the analysis of the Cape Grim (Tasmania) Air Archive (CGAA; plus symbols) and Mace Head, Ireland (crosses) (Oram *et al.*, 1995), and 6-hour measurements made at Mace Head, Ireland (smoothed to the solid line) (Simmonds *et al.*, 1998a). Also displayed are global mean surface mixing ratios calculated from estimates of global emission (AFEAS, 1998) and a lifetime of 13.6 yr (dashed line) (Table 2-1).

between NOAA/CMDL and the University of Bristol (Simmonds *et al.*, 1998a); however, results reported by the University of East Anglia (UEA) (Oram *et al.*, 1995) are approximately 30% lower.

Despite these calibration uncertainties, preliminary estimates of emission (AFEAS, 1998) for both HCFC-141b and HCFC-142b lead to an underestimation of the amount observed in the atmosphere. Between 1990 and 1995, mixing ratios deduced from these emissions appear to underestimate the atmospheric burden of HCFC-142b by a consistent factor of between 1.6 and about 2 (Montzka *et al.*, 1994; Oram *et al.*, 1995; Simmonds *et al.*, 1998a; Shirai and Makide, 1998). For HCFC-141b, the discrepancy between observed mixing ratios and those calculated from emission estimates has decreased from a factor of about 2.0 in early 1993 to approximately 1.3 at the end of 1995 (Elkins *et al.*, 1996; Simmonds *et al.*, 1998a). For both compounds, these differences cannot be reconciled by simply adjusting estimates of global lifetime for these compounds. Depending on the specific use of a chemical, the delay between production and release into the atmosphere can vary considerably. Hence the atmospheric abundances calculated from industrial emission estimates are highly sensitive to the use-model employed.

Measurements of these two HCFCs have also been made from samples collected in the stratosphere (Lee *et al.*, 1995). Observed relationships to nitrous oxide ($N_2O$) allowed for an estimate of the stratospheric chemical lifetime for HCFC-141b of 68 ± 11 years and a lower limit for HCFC-142b of 138 years (referenced to a chemical lifetime for $N_2O$ of 110 years). These values are consistent with those estimated from models (Table 2-2).

### *HFC-134a ($CH_2FCF_3$)*

Atmospheric measurements of HFC-134a indicate non-detectable levels before 1989-1990 in both hemispheres (<0.01 to 0.05 ppt) and large relative increases since that time (Figures 2-6 and 2-7) (Montzka

*et al.*, 1996b; Oram *et al.*, 1996). Analyses of samples in the Cape Grim (Tasmania) Air Archive (CGAA) revealed no detectable HFC-134a (<0.01 ppt) until May of 1990. Between 1992 and mid-1995, the concentration at Cape Grim increased exponentially at approximately 200% $yr^{-1}$ (i.e., by a factor of 3) (Oram *et al.*, 1996). Also noted in this study was an increase of 1.24 ± 0.11 ppt $yr^{-1}$ between July 1994 and May 1995 at Mace Head, Ireland. Slightly higher increases of 2.05 ppt $yr^{-1}$ were noted at Mace Head for a later period in a separate study (October 1994 to March 1997; Simmonds *et al.*, 1998a), consistent with accelerated emissions growth for this compound. These authors also report a mixing ratio at the midpoint of the time series (January 1996) of 3.67 ppt. Furthermore, mixing ratios calculated from industry emission estimates are in reasonable agreement with observed concentrations (Simmonds *et al.*, 1998a). A mean increase of 83 ± 6% $yr^{-1}$ for HFC-134a was calculated from measurements at Hokkaido, Japan, and Syowa Station, Antarctica, for the period from July 1994 to January 1997. The mean from these two stations was determined to be 5.9 ± 1.2 ppt in January 1997 (Shirai and Makide, 1998).

From samples collected at multiple sites in both hemispheres, a global tropospheric mean mixing ratio of 1.6 ppt was estimated for mid-1995, and mixing ratios in the NH were 2 times those observed in the SH (Montzka *et al.*, 1996a,b). Analyses of archived samples from the NH show increases above detection (0.05 ppt) in the period between 1989 and 1990. The rate of global increase was estimated for mid-1995 at 1.2 ppt $yr^{-1}$.

Mixing ratios reported by these three groups span a range of approximately 30%. However, results from a limited exchange of synthetic air samples, and from a comparison between ambient air measurements from Mace Head and Barrow, Alaska, suggest that the agreement between NOAA/CMDL and the University of Bristol is within 5% (Simmonds *et al.*, 1998a).

### *HFC-23 ($CHF_3$)*

HFC-23 is produced primarily as a byproduct during the manufacture of HCFC-22 via the over-fluorination of chloroform ($CHCl_3$). Until recently, it was used as a starting material in the production of H-1301 ($CBrF_3$); however, such use has dropped to near zero in developed countries as a result of the phase-out of halon manufacture under the Montreal Protocol. Some limited use continues in plasma etching processes, as a low-temperature refrigerant, and as a fire suppressant. Measurements made on the CGAA indicate that the HFC-23 mixing ratio has risen from approximately 2 ppt in 1978 to nearly 11 ppt by the end of 1995 (Oram *et al.*, 1998). As an expected result of its aforementioned source, HFC-23 exhibited long-term, near-linear growth through the 1980s and 1990s, similar to that of HCFC-22, with an abundance consistently about 10% of that of HCFC-22 (see Figure 2-6). This figure collectively shows data from the CGAA and ongoing sampling programs for HCFC-22, -141b, and -142b, and HFC-23 and -134a from Cape Grim, Tasmania.

#### 2.2.1.4 Trifluoroacetic Acid (TFA, $CF_3C(O)OH$)

Atmospheric breakdown of HFC-134a and certain other compounds containing a $-CF_3$ group, such as HCFC-123 and HCFC-124, will produce trifluoroacetyl halides ($CF_3COCl$ or $CF_3COF$) that dissolve in water to give trifluoroacetic acid (TFA). Thus, TFA would then be present in rain or seawater. Reports suggest that growth is inhibited in certain plants following exposure to TFA at concentrations several thousands of times greater than expected in rain and snow from atmospheric oxidation of HCFCs and HFCs (Boutonnet *et al.*, 1998). TFA has already been detected at low levels in surface water, rain and tropospheric air samples (Frank *et al.*, 1996; Frank and Jordan, 1998; Zehavi and Seiber, 1996). The source of TFA in today's environment is uncertain but the breakdown of HCFCs and HFCs can only explain a tiny fraction of the observed levels because of the small quantities of these precursor compounds that have been produced and released to date (Kotamarthi *et al.*, 1998).

#### 2.2.1.5 Total Cl from HCFCs

A summary of our best estimates for concentrations and trends of HCFC/HFCs is given in Table 2-3. As can be seen for the most recent measurement period, tropospheric Cl in HCFCs was increasing by about 11 ppt $yr^{-1}$ and accounted for an equivalent of about 5% of the Cl present in long-lived anthropogenic trace gases in 1996. Of this 11-ppt $yr^{-1}$ increase, approximately 6 ppt $yr^{-1}$ is due to HCFC-22, associated primarily with a continuation of previous uses. The remainder is due to HCFC-141b and -142b, associated with their use as replacements for CFCs. This growth rate in tropospheric

Cl due to HCFCs can be contrasted to the current 40 to 42 ppt $yr^{-1}$ decline in tropospheric Cl associated with the decreasing atmospheric burden of $CH_3CCl_3$ (see Section 2.2.3.3). It also is considerably lower than the total tropospheric Cl growth rate throughout the 1980s, which exceeded 100 ppt $yr^{-1}$.

### 2.2.2 Other Proposed CFC Substitutes

As noted in Section 2.2.1.1, production and sales of other HCFCs and HFCs have increased lately. Preliminary measurements now indicate very low levels of HCFC-123 and -124 and HFC-143a and -152a in the atmosphere. In addition to HCFCs and HFCs, perfluorocarbons and fluorinated ethers have been proposed as alternatives to CFCs, but they have not gone beyond the development stage to that of having significant emissions. Moreover, some have deliberately been chosen because they have such short atmospheric lifetimes that there is negligible flux of halogen to the stratosphere and their general environmental impact is reduced.

**Table 2-3. Mixing ratios and trends for short-lived halocarbons at the Earth's surface.** Mixing ratios are given as parts per trillion (ppt). Unless otherwise indicated, growth rates are estimated as the mean rate of change over the two years 1995 to 1996 and are in units of ppt $yr^{-1}$.

| Compound | Mixing Ratio, Mid-1995 (ppt) | Mixing Ratio, Mid-1996 (ppt) | Growth (ppt $yr^{-1}$) | Technique | Site | Reference |
|---|---|---|---|---|---|---|
| $CH_3CCl_3$ | 110 | 97 | -14 | CMDL/in situ | Global | (a) |
| | 102.5 | 88.7 | -13.2 | AGAGE/in situ | Global | (b) |
| $CHClF_2$ | 117 | 122 | 5.0 | CMDL/flasks | Global | (a, c) |
| (HCFC-22) | 110.8 | 116.7 | 6.0 | AGAGE/flasks | 40°S | (d) |
| | 126.9 | 132.4 | 5.5 | AGAGE/flasks | 32°N | (d) |
| $CH_3CCl_2F$ | 3.5 | 5.4 | 1.9 | CMDL/flasks | Global | (a, e) |
| (HCFC-141b) | ——— 7.4 ——— | | 2.5 | Univ. Bristol/in situ | 53°N | (f) |
| $CH_3CClF_2$ | 6.6 | 7.6 | 1.1 | CMDL/flasks | Global | (a, e) |
| (HCFC-142b) | ——— 8.0 ——— | | 1.2 | Univ. Bristol/in situ | 53°N | (f) |
| $CH_2FCF_3$ | 1.6 | 3.0 | 1.4 | CMDL/flasks | Global | (a, g) |
| (HFC-134a) | 0.7 | | 0.64 | UEA/flasks | 40°S | (h) |
| | ——— 3.7 ——— | | 2.1 | Univ. Bristol/in situ | 53°N | (f) |
| $CHF_3$ (HFC-23) | 10.7 | | 0.55 | UEA/flasks | 40°S | (i) |

[a] Montzka *et al.* (1996a), updated by Elkins *et al.* (1998); mean global estimate from measurements at five remote surface sites.
[b] Prinn *et al.* (1995; 1998); mean global estimate from measurements at five remote surface sites.
[c] Montzka *et al.* (1993), updated by Elkins *et al.* (1998); growth estimated as mean change over the period 1992 through 1996; mean global estimate from samples collected at seven remote surface sites.
[d] Miller *et al.* (1998); growth estimated for mid-1996.
[e] Montzka *et al.* (1994), updated by Elkins *et al.* (1998); mean global estimate from samples collected at seven remote surface sites.
[f] Simmonds *et al.* (1998a); mean growth rate reported over the period between October 1994 and March 1997; mixing ratio reported was estimated for January 1996.
[g] Montzka *et al.* (1996b), updated by Elkins *et al.* (1998); mean global estimate from samples collected at seven remote surface sites.
[h] Oram *et al.* (1996); growth rate estimated from data through 1995 only.
[i] Oram *et al.* (1998).

## 2.2.3 Methyl Chloroform ($CH_3CCl_3$)

### 2.2.3.1 Sources

$CH_3CCl_3$ is used primarily as a cleaning solvent. It is also used as a chemical feedstock, but that fraction of its production is not emitted into the atmosphere. Industrial sales of $CH_3CCl_3$ have declined rapidly in recent years; surveys of the world's major producers show that sales were 220 Gg in 1995, less than one-third of the amount reported for 1990, the year of peak production (Midgley and McCulloch, 1995; Midgley *et al.*, 1998). In 1996 there was no new production for sales into emissive uses in the developed world. Total consumption of $CH_3CCl_3$ in developing countries operating under Article 5 of the Montreal Protocol was approximately 30 Gg in 1994 (UNEP, 1997). It has been estimated that these requirements were mostly met by material exported from developed countries and that production capacity in developing countries lies well below this figure (Midgley and McCulloch, 1995). Consumption in developing countries is frozen in 2003 and phased out in 2005.

Emission estimates are most accurate for solvents such as $CH_3CCl_3$, because release from solvent uses is immediate. Estimated global emissions of $CH_3CCl_3$ are shown in Figure 2-1.

### 2.2.3.2 Sinks

$CH_3CCl_3$ is destroyed primarily through its reaction with OH in the troposphere. Measurements of the atmospheric burden and distribution of $CH_3CCl_3$ have been used to indirectly determine global average OH concentrations by different estimation techniques. These estimation techniques incorporate model calculations and inverse methods. In the hypothetical situation in which emission and loss rates for a compound are known, it is straightforward to calculate the concentration of that gas over time with an atmospheric model (e.g., Hartley *et al.*, 1994). However, for gases oxidized primarily by OH, the results of such calculations are affected by uncertainties in modeling the global OH burden. For these gases, loss rates are determined by inverting the calculation: estimates of emission and atmospheric observations are reconciled with an appropriate loss rate. These inverse methods are used to find an OH field that optimally "fits" the known emissions and the observations of the gas. This has been the focus of recent studies using inverse methods with $CH_3CCl_3$ observations and emissions (Prinn *et al.*, 1995).

Three different inverse methods are common in atmospheric modeling. The "trend" method generates an optimal fit of OH based upon estimated emissions and the observed trend of the gas. This method is insensitive to the absolute accuracy of the measurement calibration. The other common techniques are sensitive to the calibration accuracy. They include finding an OH field that optimally fits atmospheric observations given estimates of emission (the content method), and finding an OH field that optimally fits the measured concentrations at different latitudes relative to the global average (the gradient method). Thus, using all three methods gives a measure of consistency. The latest estimates of OH are consistent in all three methods (Prinn *et al.*, 1995), yielding a tropospheric-average OH concentration of $(9.7 \pm 0.6) \times 10^5$ cm$^{-3}$. When combined with the smaller stratospheric and oceanic sinks, these estimates correspond to a total atmospheric lifetime of $4.8 \pm 0.3$ years for $CH_3CCl_3$.

Emission estimates and measurements of HCFCs and HFCs also can allow for independent estimates of OH (e.g., Miller *et al.*, 1998). The ability of this approach to constrain estimates for the global OH burden will likely vary depending upon the accuracy and precision of emission estimates and measurements, and the lifetime of the gas relative to its period of use.

### 2.2.3.3 Recent Trends

Data for $CH_3CCl_3$ from two ground-based global sampling networks have been updated since the 1994 Assessment (WMO, 1995) (Prinn *et al.*, 1995, 1998; Montzka *et al.*, 1996a; Elkins *et al.*, 1998). In both studies, significant declines in the global tropospheric abundance of $CH_3CCl_3$ were noted (Figure 2-8, Table 2-3). Whereas the mixing ratio of this gas increased before 1991, it decreased after 1991 and the rate of decline was between 13 and 14 ppt yr$^{-1}$ by mid-1996. Similar declines have been noted at Mace Head, Ireland (Simmonds *et al.*, 1996), and at a less remote site in the eastern United States (Hurst *et al.*, 1997). For example, mixing ratios at Mace Head have declined from a peak maximum of 153 ppt in 1990 to 93 ppt in 1996, or less than observed when measurements were first made in 1978 (Derwent *et al.*, 1998). Hurst *et al.* (1998) observed a 72% decrease in the atmospheric variability of $CH_3CCl_3$ during 1995 through 1997 at a tall (610-m) transmission

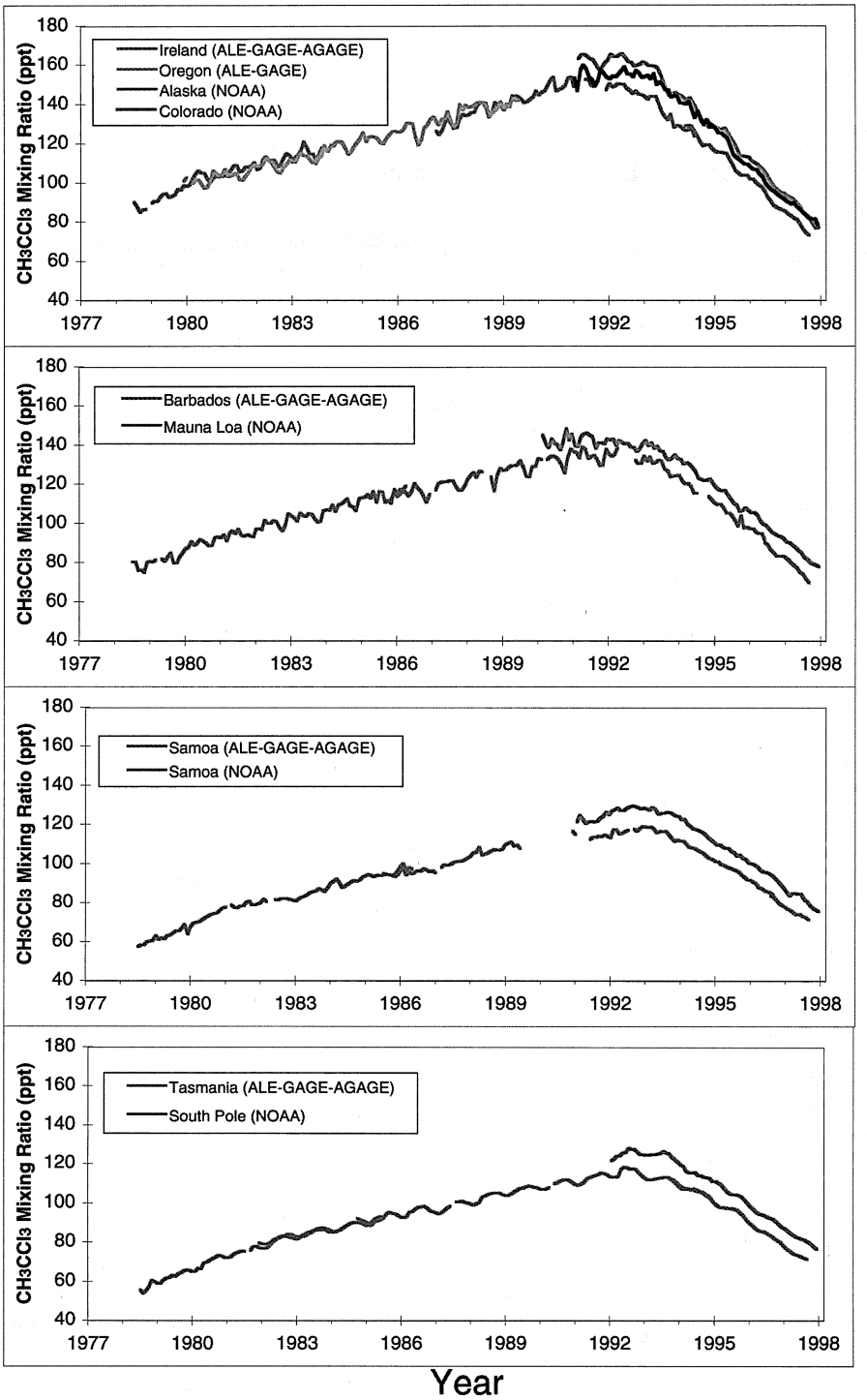


**Figure 2-8.** Monthly mean $CH_3CCl_3$ mixing ratios from the NOAA/CMDL (Montzka *et al.*, 1996a; Elkins *et al.*, 1998) and ALE/GAGE/AGAGE (Prinn *et al.*, 1995, 1998) global sampling networks. The Advanced Global Atmospheric Gas Experiment (AGAGE) is the successor to GAGE, which in turn was successor to the Atmospheric Lifetime Experiment (ALE).

tower in eastern North Carolina, U.S. (35°21'N, 77°23'W, 505 m), which they attribute to reductions in emissions.

The decline in mixing ratio for this gas and the changes observed in its global tropospheric distribution are consistent with reduced NH emissions (Midgley and McCulloch, 1995; Bakwin *et al.*, 1997) and a global lifetime of 4.8 ± 0.3 years (Prinn *et al.*, 1995). This lifetime estimate is lower than in previous assessments owing to new gas calibration procedures incorporated by the Advanced Global Atmospheric Gas Experiment (AGAGE) program (Prinn *et al.*, 1995). With this improvement, good consistency is now observed between estimates of lifetime based on techniques that are calibration-dependent and those that are calibration-independent. This was not true for earlier, longer estimates of $CH_3CCl_3$ lifetime (Bloomfield *et al.*, 1994). Despite these revisions, measurements of $CH_3CCl_3$ from two independent global sampling networks (AGAGE and NOAA/CMDL) still disagree by about 10%; estimates of the global burden at the Earth's surface in mid-1996 from these networks range from 89 ppt (Prinn *et al.*, 1995, 1998) to 97 ppt (Montzka *et al.*, 1996a; Elkins *et al.*, 1998) (Table 2-3).

Volk *et al.* (1997) estimate a stratospheric lifetime (i.e., total burdened stratospheric loss) for $CH_3CCl_3$ at 34 ± 7 years based on a CFC-11 lifetime of 45 years and measured mixing ratios above the tropopause. Model calculations suggest a stratospheric lifetime for $CH_3CCl_3$ of 45 years (Table 2-2) (Kaye *et al.*, 1994). Such differences reflect the sensitivity of the stratospheric lifetime calculated for compounds removed by OH to the altitude at which the tropopause is placed.

### 2.2.4 Methyl Chloride ($CH_3Cl$)

The most abundant halocarbon in the atmosphere is $CH_3Cl$. Numerous results of ambient samples collected during various measurement campaigns have been published during the past 20 years and range in mole fraction from 300 to 1100 ppt. In previous assessments the average global mixing ratio was reported as approximately 600 ppt. Recent results from shipboard and airborne programs suggest a north/south gradient (Koppmann *et al.*, 1993; Moore *et al.*, 1996b), seasonality, and tropospheric vertical structure (Blake *et al.*, 1997). Use of these and other archived data gives a global average $CH_3Cl$ mixing ratio of 550 ± 30 ppt. In contrast Khalil (1998) and Khalil and Rasmussen (1998a) report consistently higher values (global average of 597 ppt). This suggests that there may exist unresolved calibration issues. Khalil and Rasmussen (1998a) also show evidence for a slight decrease (by about 4%) in global $CH_3Cl$ levels between 1981 and 1997 at the Cape Meares, Oregon, site. No other studies have indicated temporal changes, and future determination of possible trends will need to address the aforementioned calibration issues.

The main known sources of $CH_3Cl$ are from biomass burning (Crutzen *et al.*, 1979), emission from ocean surface waters (Singh *et al.*, 1983), and wood-rotting fungi (Watling and Harper, 1998). A considerable amount of new information is available with respect to the marine production of $CH_3Cl$, suggesting a much lower source strength than had been previously assumed (Moore *et al.*, 1996b). Extrapolation from measurements in the northwest Atlantic and Pacific Oceans suggests emission of $CH_3Cl$ at lower latitudes from warmer waters (0.4 to 0.6 Tg $yr^{-1}$), but uptake at higher latitudes by colder waters (0.1 to 0.3 Tg $yr^{-1}$), yielding a global net oceanic source strength of 0.2 to 0.4 Tg $yr^{-1}$. Based on these estimates, the net oceanic emission would only account for some 7 to 13% of the sources needed to balance the calculated sink (discussed below as being about 3 Tg $yr^{-1}$).

Rudolph *et al.* (1995) estimated that biomass burning emissions may represent up to half of the $CH_3Cl$ emissions, whereas Graedel and Keene (1995) have suggested that natural sources dominate over biomass burning and anthropogenic emissions. The most recent estimates of $CH_3Cl$ emissions from biomass burning are approximately 1.0 ± 0.3 Tg $yr^{-1}$ (Andreae *et al.*, 1996; N.J. Blake *et al.*, 1996), with substantial uncertainties still persisting due to the lack of data from tropical forest fires. Wood-rotting fungi appear to be a potentially significant global source of $CH_3Cl$. Watling and Harper (1998) estimate a global emission of 0.16 Tg $yr^{-1}$ from fungal species of the *Hymenochaetaceae*. They suggest that actual emissions could be as much as an order of magnitude greater if fungal uptake of chloride from soil and leaf litter also occurs. Production from non-Hymenochaetaceous fungi has yet to be studied in detail. Given the recent downward revision of the marine source and the small size of the industrial emissions (0.2 to 0.4 Tg $yr^{-1}$), primarily from waste incineration (Graedel and Keene, 1995), biomass burning may be the single largest source of atmospheric $CH_3Cl$, followed by ocean emissions and fungal production.

**Table 2-4. Lifetimes for miscellaneous halocarbons [a].**

| Compound | Lifetime | Major Removal Process |
|---|---|---|
| $CH_3Cl$ | 1.3 years | OH reaction |
| $CH_2Cl_2$ | 5 to 6 months [b] | OH reaction |
| $CHCl_3$ | ~6 months | OH reaction |
| $C_2HCl_3$ | ~1 week | OH reaction |
| $C_2Cl_4$ | 3 to 4 months | OH reaction |
| $COCl_2$ | 70 days [c] | Wet Deposition |
| $CH_3I$ | 4 days at surface<br>1.5 days at 10 km [c] | Photolysis |
| $C_2H_5I$ | Similar to $CH_3I$ [c] | Photolysis |
| $CH_2ClI$ | ~100 minutes [c] | Photolysis |
| $CH_2I_2$ | 2.5 minutes [c] | Photolysis |
| $CH_3CHICH_3$ | ~16 hours [c] | Photolysis |
| $CH_3CH_2CH_2I$ | ~1 day [c] | Photolysis |
| $CF_3I$ | 1 day [d] | Photolysis |

[a] Unless otherwise stated, lifetimes are calculated from the reaction rates with OH (De More *et al.*, 1997), assuming an OH concentration of $9.7 \times 10^5$ $cm^{-3}$ (Prinn *et al.*, 1995), using an average temperature of 277 K (Prather and Spivakovsky, 1990).
[b] Kindler *et al.*, 1995.
[c] Roehl *et al.*, 1997.
[d] Rattigan *et al.*, 1997.

The main removal process for $CH_3Cl$ is reaction with OH. Based on an average OH concentration of $9.7 \times 10^5 cm^{-3}$ (Prinn *et al.*, 1995), $CH_3Cl$ has an atmospheric lifetime of approximately 1.3 years (see Table 2-4). This estimate does not include other unquantified potential losses, such as attack by Cl atoms, as hypothesized by Keene *et al.* (1996), or uptake by soils as observed by Khalil (1998). Transport to the stratosphere accounts for approximately 1% of $CH_3Cl$ removal (Graedel and Crutzen, 1993). Given an average global mixing ratio of 550 ppt, a global burden of 4.3 Tg is calculated which, in conjunction with the estimated lifetime, implies a global turnover rate of about 3 Tg $yr^{-1}$.

It should be noted that the sum of quantified sources given above (biomass burning, marine emissions, fungal production, and industrial emissions) is only 1.2 to 2.5 Tg $yr^{-1}$, well short of the rate at which $CH_3Cl$ is oxidized by OH. This inconsistency between the sources and sinks of $CH_3Cl$ is very similar to the budget imbalance noted for $CH_3Br$ in Section 2.3.1.5. It is possible that terrestrial emissions are important. Higher concentrations have indeed been observed over land (Khalil and Rasmussen, 1998a). The possibility of in situ production, such as the oxidation of dimethyl sulfide by Cl atoms (Langer *et al.*, 1996), has also been suggested.

### 2.2.5 Methylene Chloride ($CH_2Cl_2$)

$CH_2Cl_2$ is present in the atmosphere due to a variety of applications in industrial and consumer products ranging from food processing to paint stripping. McCulloch and Midgley (1996; updated by P.M. Midgley, M & D Consulting, Germany, private communication, 1998) estimate global emissions from audited sales data at 592 Gg and 527 Gg for 1988 and 1996, respectively (Figure 2-1), with over 90% of sales in the NH. The 1995 NH usage was 486 Gg, whereas usage in the SH was 37 Gg. NH and SH values of 40 to 50 ppt and 15 to 20 ppt, respectively, were obtained during a northern and southern Atlantic cruise and a northern and southern Pacific cruise (Koppmann *et al.*, 1993; Atlas *et al.*, 1993). Elkins *et al.* (1996) observed similar results from several NH and SH ground-based sites. The main removal process for $CH_2Cl_2$ is by reaction with OH. Assuming an average global OH concentration of $9.7 \times 10^5 cm^{-3}$ yields an atmospheric lifetime of 5 to 6 months for $CH_2Cl_2$. Elkins *et al.* (1996) report seasonal variations in both hemispheres (six months out of phase), with maximum NH concentrations during winter. Graedel and Keene (1995) estimate that about 2% of $CH_2Cl_2$ emissions reach the stratosphere. Measurements of $CH_2Cl_2$ near the tropical tropopause in 1992 averaged $14.9 \pm 1.1$ ppt (Schauffler *et al.*, 1993). No long-term measurement data have been reported for $CH_2Cl_2$ but, with fairly flat sales figures since 1991, no temporal trend is expected.

### 2.2.6 Chloroform ($CHCl_3$)

$CHCl_3$ emissions arise from a variety of anthropogenic activities including coal combustion, waste incineration, and industrial processes. Emissions may occur during the deliberate production and use of the material or when it is present as a significant byproduct of an industrial process such as from paper-making or waste-water treatment. There are no audited production data for $CHCl_3$ because of multiple sources, some of which are hard to quantify. According to a recent detailed

study (Aucott *et al.*, 1998) industrial emissions are much lower than previously thought (Khalil and Rasmussen, 1983), totaling about 60 Gg $yr^{-1}$, of which pulp and paper manufacture contributed about 30 Gg $yr^{-1}$, and wastewater treatment about 20 Gg $yr^{-1}$. It also has been suggested that termites could be a significant source of $CHCl_3$, 3 to 30 Gg $yr^{-1}$ (Khalil *et al.*, 1990). Frank and Frank (1990) and Hoekstra and De Leer (1993) have demonstrated production of $CHCl_3$ from soils, and Hoekstra *et al.* (1998) have shown production by fungi. An ocean source of around 0.36 Gg $yr^{-1}$ was estimated by Khalil and Rasmussen (1983), but this number has not been updated recently. No significant $CHCl_3$ emissions were observed during NASA's 1992 Transport and Atmospheric Chemistry near the Equator-Atlantic (TRACE-A) biomass burning study conducted in Africa and South America (N.J. Blake *et al.*, 1996).

A seasonal cycle in phase with $CH_2Cl_2$, tetrachloroethene ($C_2Cl_4$), and $CH_3Cl$ is reported for $CHCl_3$ using three years of remote-site flask data (Elkins *et al.*, 1996). Elkins *et al.* (1996) reported a NH concentration range of 10 to 15 ppt whereas the SH was 5 to 7 pptv. Similar results were obtained on a cruise in the tropical Pacific (Atlas *et al.*, 1993). Khalil and Rasmussen (1998b) report NH concentrations of about 12 to 38 ppt at coastal sites, and 10 to 15 ppt in the SH, again suggesting calibration differences between groups. Concentrations at remote inland sites were higher again, up to 50 ppt. The NH scatter is significantly greater for $CHCl_3$ than for the other gases mentioned, supporting the suggestion that $CHCl_3$ has multiple uncoupled sources. Khalil and Rasmussen (1998b) found no significant long-term trend over 9 years at six different sites, although there were substantial year-to-year variations. Kindler *et al.* (1995) estimate that about 2% of $CHCl_3$ emissions are destroyed in the stratosphere. Measurements of $CHCl_3$ near the tropical tropopause in 1992 averaged $3.1 \pm 0.7$ ppt (Schauffler *et al.*, 1993).

The main removal process is reaction with OH. Assuming an average OH concentration of $9.7 \times 10^5$ $cm^{-3}$ yields an atmospheric lifetime for $CHCl_3$ of approximately 6 months (Table 2-4). If we exclude the ocean source and use the recent estimates of anthropogenic (i.e., industrial) emissions, the source total is inconsistent (i.e., too small) with a lifetime for $CHCl_3$ slightly longer than that for $CH_2Cl_2$ and atmospheric concentrations approximately one-third those of $CH_2Cl_2$. Inclusion of a large estimate for either the ocean or soil source (Khalil and Rasmussen, 1983) shifts this source/burden inconsistency in the direction of too high a total source strength. More accurate quantification of these sources is clearly required.

### 2.2.7 Trichloroethene ($C_2HCl_3$)

The major source of $C_2HCl_3$ is from industrial usage as a degreasing agent. McCulloch and Midgley (1996; updated by P.M. Midgley, M & D Consulting, Germany, private communication, 1998) report global emissions estimated from audited sales for 1988 and 1996 of 260 Gg and 240 Gg (Figure 2-1). All but about 2% of the sales are in the NH. The main removal process is with OH. Assuming an average OH concentration of $9.7 \times 10^5$ $cm^{-3}$, the atmospheric lifetime for $C_2HCl_3$ is about 1 week (Table 2-4). From weekly samples collected at Alert, Canada, between early 1992 and mid-1994, Yokouchi *et al.* (1996) report winter/summer NH concentration ratios of approximately 60, with winter peak concentrations of 6 to 8 ppt. This illustrates the very short atmospheric lifetime of $C_2HCl_3$ and also why $C_2HCl_3$ itself is unlikely to impact stratospheric Cl levels.

### 2.2.8 Tetrachloroethene ($C_2Cl_4$)

$C_2Cl_4$ is mainly used for dry cleaning and as a metal degreasing solvent. Emissions of 580 kt estimated for 1984 by Class and Ballschmiter (1987) are significantly greater than global emissions derived from audited production figures for the years 1993 to 1996 of 261 Gg, 258 Gg, 278 Gg, and 289 Gg, respectively (Figure 2-1) (McCulloch and Midgley, 1996; updated by P.M. Midgley, M & D Consulting, Germany, private communication, 1998). There are no published results of long-term background measurements for $C_2Cl_4$, but comparison of recent results with data published in the early 1980s suggests that the atmospheric burden has measurably decreased during the last decade (Koppmann *et al.*, 1993; Wang *et al.*, 1995).

McCulloch and Midgley (1996; updated by P.M. Midgley, M & D Consulting, Germany, private communication, 1998) calculate that in the last few years SH usage has increased. However, 93% of 1995 industrial $C_2Cl_4$ usage was still in the NH. Thus, remote $C_2Cl_4$ concentrations are substantially higher in the NH (Atlas *et al.*, 1993; Koppmann *et al.*, 1993; Weidmann *et al.*, 1994; Wang *et al.*, 1995; Elkins *et al.*, 1996). The main $C_2Cl_4$ removal process is reaction with OH. Its atmospheric lifetime, assuming an average OH

concentration of $9.7 \times 10^5$ $cm^{-3}$, is approximately 3 to 4 months (Table 2-4). Wang *et al.* (1995), Yokouchi *et al.* (1996), and Elkins *et al.* (1996) report significant seasonal variations in surface-level background concentrations. Blake *et al.* (1997) discuss seasonal differences in the $C_2Cl_4$ vertical distribution. The current background-surface NH mixing ratio varies from about 15 ppt in winter to 5 ppt during summer. Samples collected at Cape Grim, Tasmania, exhibit seasonality 6 months out of phase with the NH, with concentrations ranging from about 1.5 to 0.7 ppt (Elkins *et al.*, 1996). Kindler *et al.* (1995) estimate stratospheric loss of $C_2Cl_4$ at approximately 1% of its anthropogenic emissions.

### 2.2.9 Phosgene ($COCl_2$)

$COCl_2$, which is not directly anthropogenically emitted to the troposphere, is a product of the breakdown of $C_2HCl_3$, $C_2Cl_4$, $CHCl_3$, and $CH_3CCl_3$. Its atmospheric mixing ratio is in the range of 10 to 60 ppt, with an average of about 20 ppt. The main removal process is wet deposition. Kindler *et al.* (1995) estimate a lifetime of 70 days, mostly due to hydrolysis in cloud water. These authors also estimate that $COCl_2$ transports about 10% as much Cl to the stratosphere as did $CH_3CCl_3$ when its NH concentration was approximately 150 ppt.

### 2.2.10 Other Chlorocarbons

There are isolated reports of measurement of other chlorocarbons in the atmosphere. Dichloroethane ($C_2H_4Cl_2$) was reported by Class and Ballschmiter (1987) in Atlantic air at concentrations of 10 to 30 ppt. Dichloroethane has a lifetime of about 1 month and an estimated global flux of about 0.7 Tg $yr^{-1}$ (Khalil, 1998). Tetrachloroethane ($C_2H_2Cl_4$), hexachlorobutadiene ($C_4Cl_6$), and vinyledene chloride ($C_2H_2Cl_2$) have all been observed at sub-ppt levels in marine or Arctic air (Class and Ballschmiter, 1986a,b, 1987; Atlas *et al.*, 1993; Yokouchi *et al.*, 1996). All are believed to be of anthropogenic origin. The mixed chlorobromomethanes are described elsewhere (Section 2.3.2).

### 2.2.11 Contributions to the Total Cl Budget

Although the longer-lived gases are generally the ones that come to mind when we think of stratospheric ozone depletion, collectively, the "other halocarbons" play a significant role. In 1998 $CH_3Cl$, at a mixing ratio of 550 ± 30 ppt, is the most abundant chlorocarbon in the atmosphere. Using measured tropical upper troposphere mixing ratios for $CH_2Cl_2$ (15 ppt × 2 Cl molec.$^{-1}$) and $CHCl_3$ (3 ppt × 3 Cl molec.$^{-1}$), $C_2Cl_4$ (5 ppt × 4 Cl molec.$^{-1}$) estimated from a comparison of industrial source strength and lifetime with $CH_2Cl_2$, and $COCl_2$ (20 ppt × 2 Cl molec.$^{-1}$) estimated for the lower stratosphere, these gases deliver 100 ± 20 ppt Cl to the stratosphere. Thus, the complete inventory of "other halocarbons" contributes approximately 650 ± 50 ppt Cl to the stratosphere (or about 20% of the total organic Cl as reported in Chapter 1, Table 1-2).

## 2.3 BROMINATED COMPOUNDS

### 2.3.1 Methyl Bromide ($CH_3Br$)

Atmospheric $CH_3Br$ is derived from both natural and anthropogenic sources. Once in the atmosphere, it is removed by atmospheric, terrestrial, and oceanic processes. Our understanding of the sources and sinks of this gas has improved since publication of the 1994 Assessment (Chapter 10 in WMO, 1995), but the overall picture is not yet resolved. A current summary of the estimated source and sink strengths is given in Table 2-5. The lifetime of $CH_3Br$ in the atmosphere is shorter than that given in the 1994 Assessment, owing to the inclusion of new findings about its sinks. Uncertainties in the magnitude of specific processes have been reduced and new sinks have been identified since the 1994 Assessment. Nevertheless, uncertainties in our estimates of specific sources and sinks are still large. Based on our current understanding, the budget remains out of balance.

#### 2.3.1.1 Distribution and Trends

Measurements of the spatial distribution and trends of $CH_3Br$ place important constraints on the distribution and magnitude of its sources and sinks. An analysis of the implications of these constraints would be best carried out by sensitivity studies in a global model that can accurately represent its short lifetime and the inhomogeneity of its sources and sinks. Although some initial efforts have been carried out in this area with three-dimensional (3-D) models (e.g., Lee *et al.*, 1998) no complete modeling study exists that incorporates all the existing constraints. This is a reflection of the increasing complexity of the processes controlling $CH_3Br$. We review in this section the state of $CH_3Br$ measurements

## Table 2-5. Summary of the estimated source and sink strengths of $CH_3Br$ (Gg $yr^{-1}$).

| Source or Sink Type | Source or Sink Best Estimate (Gg $yr^{-1}$) | Source or Sink Range (Gg $yr^{-1}$) |
|---|---|---|
| Sources | | |
| Fumigation [a] - soils [b] | 26.5 | 16 to 48 |
| Fumigation [a] - durables [c] | 6.6 | 4.8 to 8.4 |
| Fumigation [a] - perishables [d] | 5.7 | 5.4 to 6.0 |
| Fumigation [a] - structure [e] | 2 | 2 to 2 |
| Gasoline [f] | 5 | 0 to 10 |
| Ocean [g] | 56 | 5 to 130 [h] |
| Biomass burning [i] | 20 | 10 to 40 |
| *Subtotal* | *122* | *43 to 244* |
| Sinks | | |
| Ocean [g] | -77 | -133 to -37 [h] |
| Reactions (OH and hν) | -86 | -107 to -65 |
| Soils [j] | -42 | -214 to -10 |
| *Subtotal* | *-205* | *-454 to -112* [h] |
| TOTAL | -83 | -315 to 36 [h] |

[a] Based on 1992 production data (MBGC, 1994).

[b] Assumes a mean 50% emission factor. Individual studies (Chapter 10 in WMO, 1995) indicate a range of 30 to 90% for the emission factors. These extremes have been adopted for the global uncertainty.

[c] Assumes 51 to 88% emission factor.

[d] Assumes 85 to 95% emission factor.

[e] Assumes 100% emission factor.

[f] Based on Chen *et al.* (1998), Baker *et al.* (1998a), and Hao (1986). These estimates are for emissions today, although in the past, when use of leaded gasoline was predominant in global consumption, this value could have been much higher (Thomas *et al.*, 1997).

[g] The ocean uptake is from Yvon-Lewis and Butler (1997); low and high estimates are obtained by considering the full possible range in the physical parameters utilized in the uptake calculation (Yvon and Butler, 1996). The ocean source and range is obtained from:

Source = Net Flux - Sink

where Net Flux = -21 (-3 to -32) Gg $yr^{-1}$ (Lobert *et al.*, 1997; Groszko and Moore, 1998).

[h] This table is constructed to demonstrate the balance or imbalance in the $CH_3Br$ budget, yet also to keep all sources and sinks separate. The ocean is both a source and a sink for $CH_3Br$ and the numbers are arranged in the table in such a way as to obtain maximum and minimum values for the source and sink subtotals simply by adding columns. For determining the range for the total budget, there is a constraint that the oceanic net flux equals -21 (-3 to -32) Gg $yr^{-1}$, which is based upon measurements of the surface saturation of $CH_3Br$ (e.g., Lobert *et al.*, 1995, 1996, 1997; Butler *et al.*, 1995; Moore and Webb, 1996; Groszko and Moore, 1998). Oceanic sources and sinks must always add up to a value within this range. Thus, it is not possible to combine a very large oceanic sink with a very small oceanic source in evaluating the budget. However, the range for the atmospheric lifetime is calculated (e.g., based upon sinks) by separately adding up all of the large values within the sink ranges and all of the small values within the sink ranges and dividing each total into the atmospheric burden which, for a tropospheric mean of 10 ppt, is 146 Gg. For sinks, this yields a possible lifetime range of 0.32 to 1.3 years.

[i] Andreae *et al.*, 1996; N.J. Blake *et al.*, 1996.

[j] Full range encompasses data of Shorter *et al.* (1995) and Serca *et al.* (1998). The "best estimate" used here is that given in Shorter *et al.* (1995).

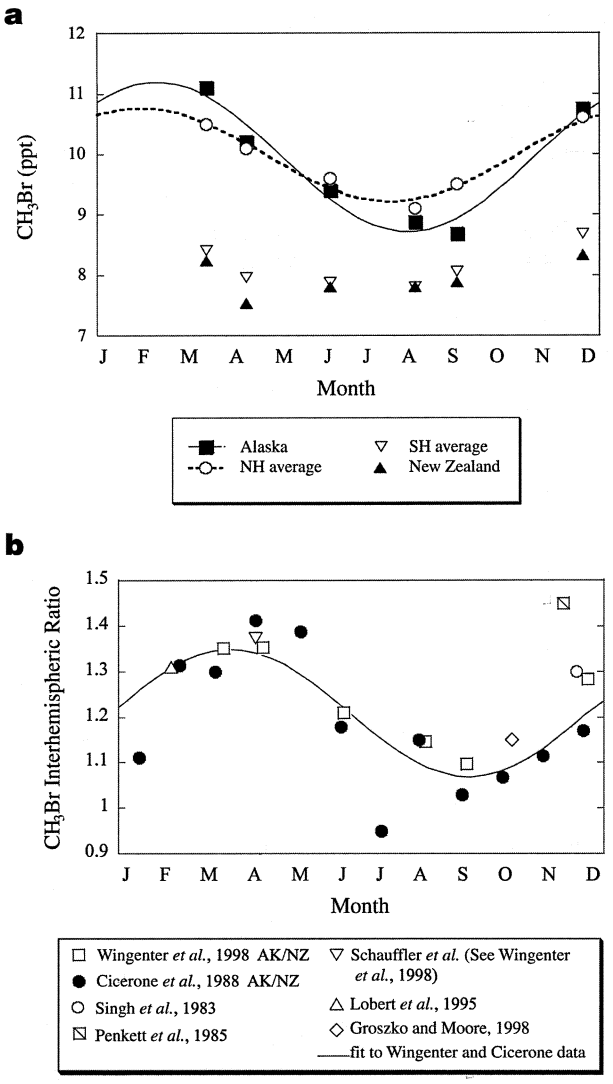


**Figure 2-9.** (a) Seasonal $CH_3Br$ mole fractions in the NH, SH, Alaska, and New Zealand. (b) Seasonal variations in the $CH_3Br$ interhemispheric ratio (NH/SH). The curve was fit to Cicerone *et al.* (1988) and Wingenter *et al.* (1998) data only, which are ratios of data from Alaska and New Zealand. Data points from Singh *et al.* (1983), Penkett *et al.* (1985), Lobert *et al.* (1995), Groszko and Moore (1998), and Schauffler *et al.* (as cited in Wingenter *et al.*, 1998) are ratios of estimated hemispheric averages.

that provide these constraints. Whenever possible, the implications of these measurements are discussed.

In recent years there has been a considerable increase in the number and scope of programs to measure the distribution and trends of atmospheric $CH_3Br$. The techniques being used are generally reporting comparable results (Lobert *et al.*, 1995a,b; 1996; Schauffler *et al.*, 1998a,b), but there remains a need for improved propagation and intercomparison of calibration standards among the laboratories engaged in these measurements so that the data can be combined for interpretive studies. Recent measurements and intercalibrations suggest that the current mean global, background tropospheric dry air mole-fraction of $CH_3Br$ is between 9 and 10 ppt (Schauffler *et al.*, 1998a,b; Lobert *et al.*, 1995a,b; N.J. Blake *et al.*, 1996). From calculations that account for the vertical distribution of $CH_3Br$ (e.g., Yvon and Butler, 1996), a tropospheric mixing ratio of 10 ppt corresponds to an atmospheric burden of 146 Gg.

The interhemispheric gradient of $CH_3Br$ is of interest as a tool in diagnosing the geographical distribution of the sources and sinks of this compound. Because data from a range of different oceanic environments indicate that the oceans collectively constitute a net sink for tropospheric $CH_3Br$ (see below), sources needed to balance the budget would need to be probably of terrestrial origin. The NH is thus expected to have higher mean concentrations than the SH, even without an anthropogenic component. To the extent that seasonal amplitudes and annual mean values apparently vary within each hemisphere (see below), these differences must be taken into account in quantifying the mean hemispheric abundances (Figure 2-9) (Wingenter *et al.*, 1998). The recent data generally support the 1994 Assessment (Chapter 10 in WMO, 1995) that the mean NH/SH surface concentration ratio is $1.3 \pm 0.1$ (Lobert *et al.*, 1995b, 1996; Groszko and Moore, 1998; Schauffler *et al.*, 1998b). In one study, consideration of the seasonal variability of $CH_3Br$ yielded an equal-area, seasonally weighted average of $1.21 \pm 0.03$ (Wingenter *et al.*, 1998).

In the 1994 Assessment (WMO, 1995), only one study of the stratospheric vertical distribution of $CH_3Br$ was available (Lal *et al.*, 1994), along with limited data on tropospheric vertical distributions that have now been published (D.R. Blake *et al.*, 1996; N.J. Blake *et al.*, 1996). Since then, a number of studies of stratospheric $CH_3Br$ in the tropics, at midlatitudes, and at high latitudes

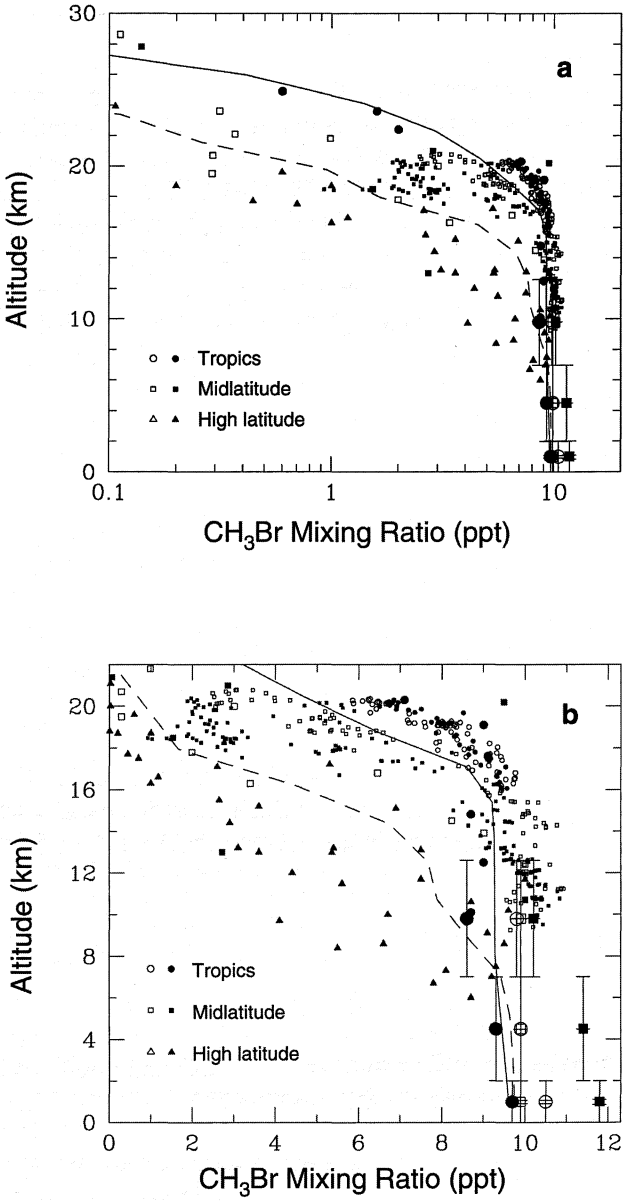


**Figure 2-10.** (a) Vertical profiles of $CH_3Br$ measured at various latitudes during winter (filled symbols) and summer (open symbols) using different techniques (big symbols - Blake *et al.*, 1997; small symbols - Schauffler *et al.*, 1998a; medium symbols - Lal *et al.*, 1994, Kourtidis *et al.*, 1998). Some of the data are normalized to 10 ppt at the tropospheric level. Measurements are compared with the NASA Goddard Space Flight Center 2-D model (Jackman *et al.*, 1996) results; continuous line is for 15°N and dotted line is for 65°N. (b) Data shown on linear scale for greater clarity.

have been conducted (Figure 2-10). These studies together show tropospheric levels of $CH_3Br$ penetrating vertically to as deep as 20 km in the tropics and as shallow as 10 km at high latitudes. Once in the stratosphere, $CH_3Br$ decreases rapidly with height, suggesting that it is a significant source of free stratospheric Br. There is considerable variability of $CH_3Br$ in the stratosphere, particularly around the Arctic vortex, where $CH_3Br$ drops to below detection limits. Summertime vertical profiles in the tropical troposphere over the Atlantic Ocean do not appear to decline with increasing height, but during the winter, when flow from Asia is greatest and vertical convection is at a minimum, a vertical decrease of up to 1.5 ppt has been observed from the boundary layer to 10 to 12 km (Blake *et al.*, 1997). These same authors also show that the $CH_3Br$ seasonal variations tend to decay in amplitude with increasing altitude in the troposphere. The midlatitude profiles in the lower stratosphere decrease faster in January than in July, presumably due to enhanced downward transport in the winter (Schauffler *et al.*, 1998b). Measurements of $CH_3Br$ at the tropical tropopause in 1996 averaged 9.5 ± 0.4 ppt and represented 55% of the observed total organic Br (Schauffler *et al.*, 1998a).

The amplitude of the seasonal variation in tropospheric $CH_3Br$ abundance appears to vary widely, even within the same hemisphere. Stations located at high northern latitudes tend to show the greatest seasonal variations in background $CH_3Br$ (Wingenter *et al.*, 1998) of ± ~15%, which are roughly in phase with the variations in $CH_3CCl_3$ (Prinn *et al.*, 1995) and suggest the influence of OH seasonal variations. Such seasonal variations in $CH_3Br$ at high NH latitudes (e.g., Pt. Barrow, Alaska; Mace Head, Ireland) are much larger than they are at SH midlatitudes (Cape Grim, Tasmania). This is not consistent with patterns observed for other gases, such as $CH_3CCl_3$ or $C_2Cl_4$, with mixing ratios controlled primarily by tropospheric OH and for which seasonal variations are roughly in phase at these sites (Prinn *et al.*, 1995). This suggests that factors in addition to tropospheric OH are involved in controlling variability of $CH_3Br$; these additional factors may be sources or sinks present in one or both hemispheres (Simmonds *et al.*, 1998b).

Although tropospheric vertical profiles (e.g., Blake *et al.*, 1997; Schauffler *et al.*, 1998a) (see Figure 2-11) can be used to place lower limits on the lifetimes of some gases, this may not be the case for $CH_3Br$. If the tropospheric chemical lifetime of a gas is short with

respect to vertical mixing in the free troposphere, and the gas is emitted primarily at the surface (i.e., the bottom of the troposphere), then one would expect to see lower amounts in the upper troposphere. However, once emitted, the tropospheric chemical lifetime of $CH_3Br$ due to removal by OH is about 1.7 years. This lifetime is sufficiently long to prevent the development of a large negative vertical gradient. The only apparent lowering of $CH_3Br$ is near the tropopause, where there is some exchange with the lower stratosphere. A positive or negative vertical gradient might be expected near the surface for a gas such as $CH_3Br$, which has potentially large surface sources or sinks in some regions. It is thus possible that temporary vertical gradients of $CH_3Br$ could appear at some locations that represent primarily sources or primarily sinks, but this would depend heavily on local mixing and would not place a significant constraint on the large-scale atmospheric lifetime of this gas.

The search for temporal trends in tropospheric $CH_3Br$ has received special attention during the past few years because of its importance with respect to assessing the magnitude of anthropogenic releases relative to the natural sources. Unfortunately, from this perspective the period of greatest interest is not the present, when anthropogenic releases are believed to be relatively constant (see below and Chapter 10 in WMO, 1995), but rather the decades of the 1960s through the 1980s, when agricultural fumigation and leaded gasoline usage were undergoing the greatest changes. The only time series measurements from the critical period are those of Khalil *et al.* (1993) dating from 1978 in the NH and from 1983 globally. These show a significant mean, latitudinally weighted global rate of increase of 0.15 ± 0.08 (90% confidence limit) ppt $yr^{-1}$ between 1983 and 1992. Available data are not sufficient at this point to determine the magnitude of $CH_3Br$ trends since 1992.

### 2.3.1.2 Anthropogenic Sources of Atmospheric $CH_3Br$

#### *Automobile Emissions*

Two estimates of $CH_3Br$ emissions by automobiles were mentioned in the 1994 Assessment (WMO, 1995), one that represented emissions of 9 to 22 Gg $yr^{-1}$ and one that represented emissions of 0.5 to 1.5 Gg $yr^{-1}$. The high estimate was based upon a study by Baumann and Heumann (1989) and the low estimate was from unpublished calculations. Since then, Thomas *et al.* (1997) estimated the global use of Br in gasoline since 1945, noting a peak production in 1970 of 160 Gg of Br, which subsequently has declined to near 30 Gg in 1995. This study suggested that $CH_3Br$ emissions from leaded gasoline could have fallen from about 17 ± 5 to 7.6 ± 2 Gg $yr^{-1}$ between 1984 and 1992. Two other papers (Chen *et al.*, 1998; Baker *et al.*, 1998a), along with the findings of Hao (1986), suggest that global $CH_3Br$ emissions from automobiles today probably are below 5 Gg $yr^{-1}$ (Table 2-5) and may be insignificant. Although there is still a large degree of uncertainty involved in making these estimates, none of the recent studies tends to support high emissions from automobiles today.

#### *Fumigation*

Emissions from the use of $CH_3Br$ as a fumigant for durables, perishables, and structures historically have been considered to be a large fraction of the amount applied. Emissions from fumigation of soils, which represents the heaviest use of $CH_3Br$ (approximately 80%), are more difficult to quantify. The 1994 Assessment noted that there was a wide range of possibilities for the fraction of $CH_3Br$ emitted (Chapter 10 in WMO, 1995). Since then, a number of studies have shown that standard polyethylene tarps do little to retard the emission of $CH_3Br$ to the atmosphere and provide little information to change the estimate of about 50% for globally averaged emissions to the boundary layer (Yagi *et al.*, 1995; Yates *et al.*, 1996a,b,c, 1997; Majewski *et al.*, 1995). Specific agricultural practices and processes could reduce emissions in the future. Wang *et al.* (1997a,b) have demonstrated the efficacy of high-barrier films in reducing $CH_3Br$ emissions from fumigated soils, and Yates *et al.* (1998) noted that shallow injections could still be conducted with a low loss rate to the atmosphere (about 1%), if a high-barrier film (HBF) is used for a period of 10 to 15 days.

Removal of $CH_3Br$ within soils following fumigation is likely both microbially mediated and abiotic (Miller *et al.*, 1997; Oremland *et al.*, 1994). It also has been suggested recently that $CH_3Br$ can be removed from a plume originating from a fumigated field by interaction with soils during dispersal throughout the boundary layer (Woodrow *et al.*, 1997). However, not enough is known about the global impact of these effects to improve the estimates given in the 1994 WMO Assessment.

*Biomass Burning*

Biomass burning was first suggested as a source for atmospheric $CH_3Br$ by Manö and Andreae (1994). From a rather limited study, the authors reported a possible range of 10 to 50 Gg $yr^{-1}$ for global emissions from this source. Although the mean of 30 Gg $yr^{-1}$ was used in earlier estimates of this flux, it was later revised to 20 Gg $yr^{-1}$ based upon additional studies of savanna fires by Andreae *et al.* (1996) and of savanna and Brazilian agricultural areas by N.J. Blake *et al.* (1996). The consistency of emissions and emission ratios for the various fires suggests a slightly narrower range for the global mean than that of Manö and Andreae (1994), perhaps 10 to 40 Gg $yr^{-1}$. The remaining uncertainty is to a large extent due to the scarcity of data from tropical forest burning, one of the largest sources of pyrogenic emissions. The few fires investigated showed highly diverse emission ratios and represent only a small fraction of the burning practices and deforestation regions.

### 2.3.1.3 Surface Interactions

*Ocean*

The ocean is both a source and a sink of $CH_3Br$. Observations of surface saturations and calculations of degradation rates indicate that $CH_3Br$ is produced and destroyed simultaneously everywhere in the ocean. The complexities of the interactions between ocean and atmosphere require an understanding of ocean production, ocean consumption, and net flux. The relationships among these processes have been discussed by Butler (1994), Penkett *et al.* (Chapter 10 in WMO, 1995), and Butler and Rodríguez (1996). We summarize our understanding of the different processes, in particular how the magnitudes of sources and sinks are determined, with a view to evaluating their relative uncertainties. Details of the calculations and measurements supporting the current estimates are discussed.

The magnitude of the ocean uptake is determined by the atmosphere-to-ocean transfer of $CH_3Br$, followed by degradation in the ocean waters by chemical and biological processes. Given a parameterization of air-sea gas exchange, ocean uptake and degradation by inorganic processes can be calculated from a knowledge of the winds near the ocean surface, the sea surface temperature, and laboratory measurements of $CH_3Br$ solubility, diffusivity, hydrolysis, and nucleophilic substitution in seawater. Uncertainties in diffusivity, solubility, and chemical degradation have been reduced significantly since the 1994 Assessment (WMO, 1995) (DeBruyn and Saltzman 1997a,b; Jeffers and Wolfe 1996b; King and Saltzman, 1997). Based on chemical loss alone, Yvon and Butler (1996) estimated a partial ocean lifetime of 2.7 (2.4 to 6.5) years. This estimate is more constrained than the value of 3.7 (1.3 to 14) years for this partial lifetime used in the 1994 Assessment (Butler, 1994). The reduction in the uncertainty of the partial oceanic lifetime was achieved by taking into account the seasonal and spatial covariance among ocean surface and boundary layer parameters using a 2-D database of sea surface temperature, salinity, and surface wind speed, and assuming an interhemispheric ratio of 1.3 (Yvon and Butler, 1996). We must emphasize that the above estimates do not depend on the new measurements of super- or undersaturation discussed below, but only on the physical and chemical state of the ocean mixed layer and air-sea interface.

Shipboard measurements are used to obtain the net flux across the sea surface. A negative flux is deduced from an undersaturation of the surface waters, indicating that the ocean uptake is larger than ocean emission of $CH_3Br$. Knowledge of the physical and chemical conditions at a specific location enables calculation of the expected ocean undersaturation, in the absence of biological processes. However two measurement campaigns in the Labrador Sea (Moore and Webb, 1996) and the Southern Ocean (Lobert *et al.*, 1997) showed that the cold high-latitude waters in both hemispheres were significantly more undersaturated than expected. Because chemical removal is slow in the cold waters, some other process must be removing $CH_3Br$ in order to sustain the observed undersaturations (-35%). Work by King and Saltzman (1997) showed that bacteria in warmer waters could remove $CH_3Br$ at almost twice the rate of chemical processes alone. Biological degradation of aquatic $CH_3Br$ in fresh water and in salt water also has been found by Goodwin *et al.* (1997) and Connell *et al.* (1997). Yvon-Lewis and Butler (1997) used the recent in situ measurements and biological degradation data to update their estimate of the ocean uptake to -77 Gg $yr^{-1}$, yielding a partial lifetime of atmospheric $CH_3Br$ with respect to oceanic loss of 1.9 (1.1 to 3.9) years due to both chemical and biological degradation. Thus, their assessment of biological degradation to a global scale reduces the estimated partial lifetime due to oceanic removal by 30%.

As discussed by Butler (1994), by Butler and Rodríguez (1996), and in Chapter 10 of WMO (1995),

the ocean uptake discussed above (which determines the partial ocean lifetime) is not the same as the globally extrapolated net flux across the ocean surface. The latter determines whether the ocean is a net source or sink of $CH_3Br$ to the troposphere. Since the 1994 Assessment (WMO, 1995), which stated that the ocean was a net source of atmospheric $CH_3Br$, studies in the Pacific (Lobert *et al.*, 1995b; Groszko and Moore, 1998), the Atlantic (Butler *et al.*, 1995; Lobert *et al.*, 1996), the Labrador Sea (Moore and Webb, 1996), and the Southern Ocean (Lobert *et al.*, 1997) showed that much of the ocean was a net sink for atmospheric $CH_3Br$. These studies tighten constraints upon the estimate of the global net flux of $CH_3Br$. The latest estimates indicate that the ocean today is a net sink for atmospheric $CH_3Br$. Lobert *et al.* (1997) derived a net flux of -21 (-11 to -32) Gg $yr^{-1}$ from data collected on two extensive cruises and one regional cruise; Groszko and Moore (1998) derived a net flux of -10 (-3 to -13) Gg $yr^{-1}$ with data combined from one extensive and one regional expedition. The uncertainties quoted arise from uncertainties in the physical parameters used in the derivation of ocean uptake for regions sampled. Uncertainties due to extrapolation of measurements to the global ocean are more difficult to quantify, and this should be kept in mind in assessing the uncertainties in the $CH_3Br$ budget. However, changes in this net flux are separate from the estimated partial oceanic lifetime. Because the Lobert *et al.* (1997) estimate includes data that are based upon broader spatial and temporal coverage than those of Groszko and Moore (1998), we have kept the "best estimate" of -21 Gg $yr^{-1}$ given by Lobert *et al.* (1997) for budget and lifetime calculations in Table 2-5 (footnote h), but have extended the possible range to include that given by Groszko and Moore (1998). These extrapolations are based primarily on sampling of diverse regions of the oceans (i.e., coastal upwelling, equatorial, high latitude) and do not assume any correlation with indicators of biological activity.

Two models using apparent correlations of productivity with temperature and chlorophyll indicated that there might be a net source of atmospheric $CH_3Br$ in sub-polar and polar waters and that this source could outweigh the sink in the remainder of the ocean (Anbar *et al.*, 1996; Pilinis *et al.*, 1996). However, the measurements in the cold waters of the Labrador Sea and the Southern Ocean indicated that these regions were also a net sink during a time of year when they were expected to be a net source. From these studies, it is clear that one cannot depend upon a simple relationship between $CH_3Br$ and chlorophyll or temperature for predicting net $CH_3Br$ production or net $CH_3Br$ fluxes from the ocean. Recently, Baker *et al.* (1998b) found a seasonal cycle in the saturation of $CH_3Br$ in the coastal waters of the North Sea, with supersaturation occurring between June and September, when a particular type of phytoplankton was present (see below), and undersaturation for the rest of the year. Furthermore Baker *et al.* (1998b) also observed the northeast Atlantic open ocean to be supersaturated during a cruise in September, when there was again evidence for the presence of these phytoplankton. This confirms that the relationship between $CH_3Br$ and chlorophyll is not simple but also depends on the type of species present, which are both spatially and temporally variable. Further studies of this seasonal behavior are needed to place additional constraints on global estimates of the net flux.

Given the oceanic net $CH_3Br$ flux of -21 Gg $yr^{-1}$ (extrapolated from measurements, with a possible range of -3 to -32 Gg $yr^{-1}$) (Lobert *et al.*, 1997) and the calculated oceanic uptake of -77 Gg $yr^{-1}$ (with an estimated range of -37 to -133 Gg $yr^{-1}$) (Yvon-Lewis and Butler, 1997), emission from the ocean is estimated at 56 Gg $yr^{-1}$ (with an estimated range of 5 to 130 Gg $yr^{-1}$). We emphasize that the ocean source and its uncertainty range are calculated from the net flux and ocean sink. Oceanic sources and sinks must always add up to a value within the -3 to -32 Gg $yr^{-1}$ range currently estimated for the net ocean flux. Thus, it is not possible to combine a very large oceanic source with a very small oceanic sink in evaluating the budget.

Until recently, little information on the production of $CH_3Br$ by marine organisms was available. Scarratt and Moore (1996) and Saemundsdóttir and Matrai (1998) have found in laboratory studies that numerous species of marine phytoplankton produce $CH_3Br$, at rates that vary by almost a factor of 20 (1.7 to 30 picograms $CH_3Br$ per day per microgram of chlorophyll *a*). However, only the highest observed rates of production by these organisms begin to support observed field concentrations. Baker *et al.* (1998b) have observed $CH_3Br$ concentrations in the North Sea, a coastal environment, to be higher when the spring and summer bloom of phytoplankton is dominated by the prymnesiophyte *Phaeocystis*. Coastal waters are often supersaturated in $CH_3Br$ (e.g., Lobert *et al.*, 1995b, 1996; Butler *et al.*, 1995; Sturges *et al.*, 1993). Baker *et al.* (1998b) also observed, in the open ocean of the northeast Atlantic, a strong correlation between

$CH_3Br$ and the pigment hexanoyloxyfucoxanthin, which indicates the presence of prymnesiophytes.

In summary, data from five field investigations suggest that the oceans as a whole can be considered as a net sink for atmospheric $CH_3Br$, sustained by a balance between aquatic production and degradation. As noted by Anbar *et al.* (1996), changes in water temperature, and, for that matter, anything affecting the community composition of marine organisms, could alter this picture. Production by phytoplankton and degradation by bacteria have been observed, but this does not rule out the possibility of production by bacteria or production or degradation by zooplankton. There even may be some degradation by certain species of phytoplankton.

### *Soils*

Whereas microbial losses in the soil during fumigation can be thought of as reducing a source of $CH_3Br$, the loss of ambient levels of $CH_3Br$ to soils must be treated as a global sink and built in to computations of the $CH_3Br$ atmospheric lifetime. The study of Shorter *et al.* (1995) estimated a partial lifetime of 3.4 years for soil uptake of $CH_3Br$. This study was not included in the 1994 Assessment (WMO, 1995), and the calculated lifetime of atmospheric $CH_3Br$ (1.3 years) included only oceanic and atmospheric sinks. With the addition of the Shorter *et al.* (1995) results, this calculation yielded an atmospheric lifetime of 0.8 yr (0.7 yr, now, with the biological oceanic sink included). Unfortunately, the large uncertainties of the Shorter *et al.* (1995) estimate ($42 \pm 32$ Gg $yr^{-1}$) make this a difficult sink to quantify with much confidence. Additional studies are needed to narrow this range.

Serca *et al.* (1998) have carried out measurements similar to those of Shorter *et al.* (1995). Although the deposition velocities measured are of a similar magnitude, they estimate an even larger global soil sink of $143.4 \pm 70.2$ Gg $yr^{-1}$. The higher estimate is primarily due to their using a different global inventory for soil types. With an atmospheric abundance of 146 Gg, such values would reduce the estimated partial lifetime of $CH_3Br$ due to soil uptake to 1.0 (0.7 to 2.0) years, but adoption of such large soil uptake rates would increase even further the imbalance between sources and sinks. Other findings by Miller *et al.* (1997) and Woodrow *et al.* (1997), both done mainly with regard to fumigation levels, also qualitatively support the presence of a natural soil sink for atmospheric $CH_3Br$.

### *Plants*

No solid evidence of a plant sink for $CH_3Br$ was presented in the 1994 Assessment (Chapter 10 in WMO, 1995). Recently, however, Jeffers and Wolfe (1996a, 1998) have shown that leaves, roots, and stems of many plants remove $CH_3Br$ from air. The measurements were made on plant parts in enclosed, 20-ml vials at predominantly nmol $mol^{-1}$ to µmol $mol^{-1}$ (parts per billion-parts per million (ppb-ppm)) levels of $CH_3Br$, but the observed loss rates, ranging from 0.96 to 150 $h^{-1}$ $cm^{-2}$, were linear with concentration. Current calculations suggest that these rates, applied to the global atmosphere, may be small relative to the atmospheric, oceanic, and soil sinks. Additional studies conducted at ambient levels of $CH_3Br$ with whole plants and plants in natural systems are needed.

The possibility of plants being a source of atmospheric $CH_3Br$ exists, but no published studies to date have focused on $CH_3Br$ fluxes from plants at ambient levels. Some studies have shown that methyl iodide ($CH_3I$) is emitted at high rates from rice plants (Muramatsu and Yoshida, 1995) and others have shown that $CH_3Br$, $CH_3I$, and $CH_3Cl$ are emitted from the leaf disks of many plants (e.g., Saini *et al.*, 1995).

## 2.3.1.4 Atmospheric Sinks

The one significant change in our estimate of the magnitude of this dominant removal process since the 1994 Assessment (WMO, 1995) is the recomputation of the mean tropospheric amount of OH, owing to a change in the AGAGE calibration scale for $CH_3CCl_3$ (Prinn *et al.*, 1995). This effectively raised the estimated mean concentration of tropospheric OH by about 15%, which correspondingly increased the calculated removal rate of $CH_3Br$ by in situ atmospheric reaction and decreased the calculated $CH_3Br$ atmospheric lifetime. The best estimate for the partial lifetime of atmospheric $CH_3Br$ with respect to in situ reactions is now 1.7 years (±25%) (Yvon-Lewis and Butler, 1997). No new information has evolved regarding photolytic loss of $CH_3Br$, which remains small with a lifetime on the order of 35 years.

We note that the calculation of the atmospheric lifetime of $CH_3Br$ is carried out by global two-dimensional models that assume that the $CH_3Br$ distribution is uniform enough that the scaling of lifetimes with that of $CH_3CCl_3$ (Prinn *et al.*, 1995) is a good approximation. Because recent studies have

suggested a shorter lifetime for $CH_3Br$ than given in the 1994 Assessment (WMO, 1995), this assumption should be reconsidered to determine whether use of three-dimensional models is required.

#### 2.3.1.5 Summary Budget, Lifetime, and Ozone Depletion Potentials (ODPs)

Because the observed growth rate of atmospheric $CH_3Br$ has been near zero in recent years, a balanced budget requires that the source and sink strengths are equal. However, current best estimates for those sources and sinks that have been studied differ, with the sinks being 83 Gg $yr^{-1}$ larger than the sources (Table 2-5) [1]. There are still large uncertainties in the estimates of the individual flux strengths, which allow the possibility of a balanced budget. In particular uncertainties exist in the net flux across the ocean surface and even more in the estimated soil sink, because both of these are extrapolated from measurements at specific sites. It is pertinent to ask what changes in ocean and soil sink estimates would be necessary to balance the $CH_3Br$ budget. Examination of Table 2-5 indicates that one way to achieve such a balance would require both negligible soil sinks and a change in the estimated ocean net flux from -21 Gg $yr^{-1}$ to +20 Gg $yr^{-1}$. Although regions of ocean supersaturation have been observed in various ocean cruises, it is difficult to envision an unsampled ocean "hot spot" of $CH_3Br$ production that would change the global flux estimates by this amount. At the same time, several studies have found evidence of soil sinks, and again it is unreasonable to completely neglect them.

Thus, the data given in Table 2-5 suggest that there is an unaccounted source of atmospheric $CH_3Br$. Similar inconsistencies between the sources, sinks, and global atmospheric burden of $CH_3Cl$ are discussed in Section 2.2.4. The relationship between these two compounds has not been sufficiently studied.

The current best estimate of the lifetime of atmospheric $CH_3Br$ is 0.7 years and, considering uncertainties in the estimates of the individual sink processes, ranges from 0.32 to 1.3 years (Table 2-5, footnote h). It should be noted that the lowest value in this range would require sources far in excess of (i.e., 310 Gg $yr^{-1}$ greater than) current estimates (Table 2-5). If current estimates for $CH_3Br$ sources in Table 2-5, together with the global atmospheric burden, were used to estimate the atmospheric lifetime, we would obtain a value of 1.2 (0.8 to 3.0) years. A recent study (Colman *et al.*, 1998) has compared the variance of $CH_3Br$ measurements taken from aircraft to those of $CH_3Cl$ and other species. Utilizing a relationship between variance and atmospheric residence time first proposed by Junge (1963), these investigators have estimated a lifetime of about 0.7 to 0.8 years, consistent with the estimates utilizing the sinks in Table 2-5.

The values in Table 2-5 indicate that roughly 50% of the accounted $CH_3Br$ sources arise from anthropogenic activity (defined as both fumigation and biomass burning). Specifically, about 30% of the accounted $CH_3Br$ sources are due to fumigation. On the other hand, the magnitude of the total anthropogenic sources is 30% of the magnitude of the total estimated sinks, with fumigation practices being 20%. Consideration of the uncertainties in the $CH_3Br$ budget introduces uncertainties of at least a factor of 2 in the above fractions.

The steady-state Ozone Depletion Potential (ODP) of $CH_3Br$ was discussed in the previous 1994 Assessment (Chapter 10 in WMO, 1995). An approximate expression for the steady-state ODP is given by (Solomon and Albritton, 1992):

$$ODP_{CH_3Br} \approx \left[\frac{1}{3}\frac{MW_{CFC-11}\tau_{CH_3Br}}{MW_{CH_3Br}\tau_{CFC-11}}\beta\right]\left[\left\langle\frac{F_{CH_3Br}(z)}{F_{CFC-11}(z)}\alpha\right\rangle\right]$$

$$ODP_{CH_3Br} \approx [BLP]\,[BEF] \qquad (2\text{-}1)$$

where $MW_{CH_3Br}$ and $MW_{CFC-11}$ denote the molecular weights of $CH_3Br$ and CFC-11, respectively; $F_{CH_3Br}(z)/F_{CFC-11}(z)$ represents the Br release from $CH_3Br$ relative to the Cl release from CFC-11 in the stratosphere; $\alpha$ denotes the efficiency of the released Br in catalytic removal of ozone, relative to Cl; $\beta$ is the decrease in the mixing ratio of $CH_3Br$ at the tropical tropopause, relative to the mixing ratio at the Earth's surface; $\langle\ \rangle$ denotes

[1] The ranges in the values given in Tables 2-5 and 2-6 should not be interpreted as indicating a probability distribution of the parameters discussed, since the methodology used in deriving some of these ranges is not amenable to a statistical interpretation. For example, there are only a few studies of the percent of soil fumigation released to the boundary layer, or of the soil sink, and the maxima and minima of available estimates have been adopted.

spatial averaging of the quantity with the appropriate weighting; and 1/3 is the ratio of the number of halogen atoms in $CH_3Br$ relative to those in CFC-11. The time constants $\tau_{CFC\text{-}11}$ and $\tau_{CH_3Br}$, relating the change in atmosphere burden to a change in emissions at steady state, are equal to the total atmospheric lifetimes. The terms in brackets are the so-called Bromine Loading Potential (BLP) and Bromine Efficiency Factor (BEF). The value of the BLP depends on tropospheric surface removal processes, whereas the value of the BEF is determined by the chemistry of $CH_3Br$ and inorganic Cl in the stratosphere.

Evaluation of the BEF requires use of a model incorporating both stratospheric transport and chemistry. Changes in recommended reaction rates for Br species have been documented in the latest NASA/Jet Propulsion Laboratory (JPL) review (DeMore *et al.*, 1997). Inclusion of the new recommended rates in 2-D models has increased the calculated BEF from a recommended value of 48 in the 1994 Assessment (WMO, 1995) to 58 in this Assessment (Ko *et al.*, 1998; Wuebbles *et al.*, 1998). These changes arise mostly from incorporation of fast hydrolysis rates for $BrONO_2$ in sulfate aerosols, and new absorption cross sections for hypobromous acid (HOBr).

The 1994 Assessment considered uncertainties in stratospheric Br partitioning due to possible production of hydrogen bromide (HBr) from reaction of bromine monoxide (BrO) with hydroperoxyl radicals ($HO_2$). Two groups have recently reported observations of stratospheric HBr using far infrared emission. Johnson *et al.* (1995) derived an average HBr mixing ratio of 2.8 ± 0.8 ppt in the altitude range 22 to 34 km based on seven balloon flights between 1988 and 1994 around 34°N. Carlotti *et al.* (1995) reported HBr observations of 1.15 ± 0.46 ppt between 20 and 36.5 km at 34°N in May 1993. Nolt *et al.* (1997) reported measurements from May 1994 showing an average HBr mixing ratio of 1.31 ± 0.39 ppt between 20 and 36.5 km. These observations of about 1 to 2 ppt of HBr are larger than model predictions that consider HBr production due only to reactions of Br with $HO_2$ and formaldehyde.

The HBr observations have prompted suggestions that the reaction between BrO and $HO_2$ may have a minor channel producing HBr. Larichev *et al.* (1995) reported an upper limit for this channel of 1.5% from the non-observation of ozone as a product of this reaction, whereas Mellouki *et al.* (1994) studied the reverse reaction and predicted that the upper limit for the yield is in fact less than 0.01%. A branching ratio of 0.6% would be required to match the observations, according to the model study of Ko *et al.* (1998). Chipperfield *et al.* (1997) and Chartrand and McConnell (1998) have considered whether an HBr production channel in the reaction between BrO + OH could resolve the HBr discrepancy. The only reported study of this reaction is by Bogan *et al.* (1996), who did not measure the reaction branching ratio. A branching ratio of 1.3% would be required to match the measured HBr from the balloon studies (Ko *et al.*, 1998).

Using a lifetime of 0.7 years and a value of 58 for the BEF, a steady-state ODP of 0.4 is calculated. Equation (2-1) is also useful to determine the impact of uncertainties in various parameters on the calculated ODP. Table 2-6 shows the range of ODP values resulting from our incomplete knowledge of various parameters.

### 2.3.2 Other Brominated Compounds

The abundance and composition of organic Br in the troposphere can be quite variable. In contrast to the more stable halons or $CH_3Br$, there are a number of organic Br compounds that exhibit a large range in concentration and have a significant impact on the budget of atmospheric Br. The presence of a pool of reactive organic Br species may lead to significant effects on atmospheric oxidation processes. For example, there has been compelling evidence of significant tropospheric ozone depletion in the Arctic marine boundary layer due to reactive Br chemistry, and organic Br precursors have been suggested as the source of reactive Br (Barrie *et al.*, 1988; Hausmann and Platt, 1994). In the stratosphere, the impact of reactive Br on catalytic ozone loss has been examined and found to be significant, but the role of short-lived organic Br in the upper troposphere and lower stratosphere is not yet well defined (see Ko *et al.*, 1997).

In addition to $CH_3Br$ and halons, the major compounds that contribute to total organic Br in the atmosphere are dibromomethane ($CH_2Br_2$), bromoform ($CHBr_3$), mixed bromochloromethanes ($CH_2BrCl$, $CHBrCl_2$, $CHBr_2Cl$), and ethylene dibromide ($C_2H_4Br_2$). Minor amounts of ethyl bromide ($C_2H_5Br$) and halothane ($CF_3CHBrCl$) have also been reported, but these are not considered here.

### 2.3.2.1 Measurements, Distributions, and Trends

*Surface Measurements*

Measurements of shorter-lived organic Br compounds (i.e., organic Br compounds other than $CH_3Br$ and the halons) in the atmosphere have been made on samples from a number of surface sites (Table 2-7). These sites have been concentrated either in polar regions or in marine and coastal areas. Because of different analytical techniques applied, few studies report simultaneous measurements of all the organic Br species relevant to this discussion. Still, a reasonably consistent picture of the atmospheric concentrations of different organic Br compounds can be obtained from the existing dataset. From these data, the relative abundance of shorter-lived organic Br species in the boundary layer is typically $CHBr_3 > CH_2Br_2 > CHBr_2Cl \approx CHBrCl_2 \approx CH_2BrCl > C_2H_4Br_2$, though it should be kept in mind that these measurements are often made near biogenic source regions. Average values of 5 to 10 ppt (as Br) from these gases correspond to 30 to 50% of the Br contribution from $CH_3Br$ and the halons. There are no published data on ambient levels of these trace gases in urban or midcontinental regions.

Latitudinal surveys have shown increased levels of shorter-lived organic Br compounds over biologically productive marine waters. Both coastal and equatorial upwelling areas are associated with the highest levels of reactive organic Br. Typically, strong correlations are observed between atmospheric concentrations of $CHBr_3$,

**Table 2-6. Summary of the range in the calculated steady-state ODP for $CH_3Br$.** Each row illustrates the impact of uncertainties in a given parameter by keeping other parameters fixed to their best estimates and by using Equation (2-1) to propagate the uncertainty in the parameter examined. We have assumed a value of 1.0 for β (the decrease in the mixing ratio of $CH_3Br$ at the tropical tropopause, relative to the mixing ratio at the Earth's surface).

| Parameter | Value | Range | $\tau_{CH_3Br}$ | BLP | BEF [a] | ODP |
|---|---|---|---|---|---|---|
| $\tau_{atmos}$ [b] (yrs) | 1.7 ± 25% | 1.3 to 2.1 | 0.62 to 0.77 | 0.0060 to 0.0073 | 58 | 0.35 to 0.42 |
| $\tau_{ocean}$ [c] (yrs) | 1.9 | 1.1 to 3.9 | 0.56 to 0.88 | 0.0053 to 0.0083 | 58 | 0.31 to 0.48 |
| $\tau_{soil}$ [d] (yrs) | 3.4 | 6.8 to 14.6 | 0.39 to 0.84 | 0.0037 to 0.0080 | 58 | 0.22 to 0.46 |
| $\tau_{CFC\text{-}11}$ [e] (yrs) | 50 ± 10% | 55 to 45 | 0.71 | 0.0061 to 0.0075 | 58 | 0.35 to 0.44 |
| $F_{CH_3Br}/F_{CFC\text{-}11}$ [f] | 1.12 ± 5% | 0.92 to 1.24 | 0.71 | 0.0067 | 49.2 to 66.6 | 0.33 to 0.45 |
| Branching ratio of 0.006 for $BrO + HO_2 \rightarrow HBr + O_3$ | | | 0.71 | 0.0067 | 52 | 0.35 |
| Branching ratio of 0.013 for $BrO + OH \rightarrow HBr + O_2$ | | | 0.71 | 0.0067 | 56 | 0.37 |

[a] We have used a bromine efficiency factor (BEF) of 58 as presented by Ko *et al.* (1998). This is derived from the AER 2-D model and was calculated using the DeMore *et al.* (1997) recommendations. Other models may give different values. We note that, in general, the model-calculated BEF is a convolution of the ratio of F factors and α, and the expression in Equation (2-1) is only approximate. Equation (2-1) is used to estimate the uncertainty in BEF induced by the uncertainty in the ratio of F factors derived from observations.

[b] An overall ±25% uncertainty is assumed based on ±10% uncertainty in the reaction rate with OH (DeMore *et al.*, 1997), a ±20% uncertainty in the scaling with the $CH_3CCl_3$ lifetime, and a ±30% uncertainty in the stratospheric loss rate.

[c] Lifetime and range as quoted in Yvon-Lewis and Butler (1997).

[d] Shorter *et al.*, 1995; Serca *et al.*, 1998.

[e] Chapter 5 in Kaye *et al.*, 1994.

[f] Schauffler *et al.*, 1998b.

**Table 2-7. Measurements of short-lived (reactive) organic Br compounds in the atmosphere.** Concentrations are given in ppt.

| Location | Concentration (ppt) | | | | | | |
|---|---|---|---|---|---|---|---|
| | $CH_2Br_2$ | $CH_2BrCl$ | $CHBrCl_2$ | $CHBr_2Cl$ | $CHBr_3$ | $C_2H_4Br_2$ | Ref. |
| Continental/Coastal (Surface) | | | | | | | |
| Alert, NWT, 82°N | | | | 0.13 | 1.7 | 0.2 | 4,5 |
| Alert, NWT, 82°N, before polar sunrise | 0.8 | | | 0.3 | 2.6 | | 8 |
| Alert, NWT, 82°N, after polar sunrise | 0.8 | 0.22 | 0.26 | 0.2 | 1.6 | | 8 |
| Alert, NWT, 82°N, winter | | 0.15 | | 0.3 | 3.0 | | 9 |
| Alert, NWT, 82°N, summer | | 0.14 | | 0.14 | 0.84 | | 9 |
| Spitzbergen, 79°N | 0.45 | | 0.12 | 0.33 | 0.45 | | 11 |
| Barrow, AK, 71°N | 1.9 | 0.5 | 0.6 | 0.3 | 2.3 | 0.1 | 17 |
| Barrow, AK, 71°N | | | | | ≈6 | | 12* |
| Marine/Coastal (Surface) | | | | | | | |
| Pacific, 19°N, Hawaii | | | | | ≈3 | | 12* |
| Pacific, 19°N, Hawaii | | | | 0.25 | 3.4 | 0.4 | 4 |
| Pacific, 10°S to 15°N | 1.8 | | | 0.24 | 1.8 | | 3 |
| Pacific, 30 to 40°N | | | | 0.17 | 0.89 | | 4 |
| W. Pacific, 40°S to 40°N | 0.87 | | | | 1.04 | | 7 |
| W. Pacific, 40°S to 40°N | 0.59 | | | | 0.63 | | 7 |
| Tropical Pacific (< 500 m) | 1.01 | | 0.16 | 0.17 | 1.55 | | 16 |
| SE Asia, marine, 0 to 30°N | 0.77 | | | | 1.2 | | 7 |
| N. Atlantic | 2.7 | | | | 0.85 | | 13 |
| NE Atlantic | 3.4 | | 0.6 | 0.5 | 6.6 | | 10 |
| S. Atlantic | 1.6 | | | | 0.88 | | 13 |
| SE Atlantic | 1.2 | | 0.4 | 0.3 | 1 | | 10 |
| Antarctic, 64°S | 3.7 | | 3.8 | | 6.3 | | 6 |
| Free Troposphere | | | | | | | |
| Mauna Loa, HI, 3.4 km | | | | 0.13 | 0.20 | 0.06 | 4 |
| Mauna Loa, HI, 3.4 km: | | | | | | | |
| Autumn | 0.78 | 0.13 | 0.19 | 0.10 | 0.33 | | 14 |
| Winter | 0.86 | 0.18 | 0.21 | 0.14 | 0.61 | | 14 |
| Spring | 0.86 | 0.20 | 0.21 | 0.10 | 0.30 | | 14 |
| Summer | 0.67 | 0.14 | 0.15 | 0.07 | 0.22 | | 14 |
| Atlantic, above inversion | 1.2 | | 0.2 | 0.1 | 0.6 | | 10 |
| Tropical tropopause | 0.5 - 0.72 | 0.12 | 0.02 | | | | 1,18 |
| Tropical tropopause | 0.7 | | | | | | 2 |
| Arctic tropopause, 68°N | 0 - 0.84 | | | | | | 2 |
| Midlatitude | 1.1 | 0.14 | | | | | 15 |
| Midlatitude | 0.76 | 0.16 | 0.07 | 0.07 | 0.32 | | 16 |
| Tropical Pacific, 4 to 6 km | 0.80 | | 0.10 | 0.09 | 0.44 | | 16 |
| Tropical Pacific, > 10 km | 0.76 | | 0.07 | 0.07 | 0.32 | | 16 |

* Data taken from graph.

References:
[1]Schauffler *et al.*, 1993; [2]Kourtidis *et al.*, 1996; [3]Atlas *et al.*, 1993; [4]Atlas *et al.*, 1992; [5]Bottenheim *et al.*, 1990; [6]Reifenhaüser and Heumann, 1992; [7]Yokouchi *et al.*, 1997; [8]Yokouchi *et al.*, 1994; [9]Yokouchi *et al.*, 1996; [10]Class and Ballschmiter, 1986b; [11]Schall and Heumann, 1993; [12]Cicerone *et al.*, 1988; [13]Penkett *et al.*, 1985; [14]Atlas and Ridley, 1996; [15]Wamsley *et al.*, 1998; [16]Schauffler *et al.*, 1998b; [17]Sturges, 1993; [18]Schauffler *et al.*, 1998a.

$CH_2Br_2$, and the bromochloromethanes associated with source regions (e.g., Atlas *et al.*, 1993; Yokouchi *et al.*, 1996).

Few studies have sufficient temporal coverage to examine a seasonal trend in reactive organic Br. One study (Cicerone *et al.*, 1988) reported a strong seasonal cycle in bromoform at Barrow, Alaska; a smaller magnitude seasonal cycle was observed at Cape Kumakahi, a surface coastal site on the island of Hawaii. The Arctic trend for bromoform and other bromocarbons was also seen at Alert, NWT, by Yokouchi *et al.* (1996). A winter/summer concentration ratio of 3.6, 2.1, and 1.1 was observed for $CHBr_3$, $CHBr_2Cl$, and $CH_2BrCl$, respectively. A one-year study at the Mauna Loa Observatory also revealed a seasonal cycle in atmospheric bromocarbon concentration (Atlas and Ridley, 1996). Interestingly, the seasonality observed at this site in the Pacific free troposphere was similar to that observed in the Arctic. Winter/summer concentration ratios of 2.8, 2.0, 1.4, and 1.3 were observed at Mauna Loa for $CHBr_3$, $CHBr_2Cl$, $CHBrCl_2$, and $CH_2BrCl$, respectively. The seasonality in shorter-lived organic Br at these sites represents differences resulting from source and transport variations and seasonality in loss processes (see below). No long-term temporal trends are evident from examination of the available datasets.

### *Airborne/Free Troposphere Measurements*

Relatively few studies of the distributions of shorter-lived organic Br compounds in the free troposphere or into the stratosphere have been reported. Some ground-based measurements from island sites can be representative of the marine free troposphere. The measurements at Mauna Loa Observatory showed significantly lower mixing ratios of bromocarbons at the observatory site at 3.4 km compared to measurements near the island coastline. Similar island-based measurements at Tenerife (Class *et al.*, 1986; Class and Ballschmiter, 1988) also demonstrate a significant decline in bromocarbon concentrations above the marine inversion layer.

In the tropical and South Pacific atmosphere, highest mixing ratios of shorter-lived organic brominated compounds are observed in the marine boundary layer, with smaller concentrations aloft (Figure 2-11). A secondary maximum in the 6- to 8-km range may be due to convective redistribution of species. On average, 40% of the shorter-lived organic Br compounds measured in the boundary layer is still present at altitudes between 10 and 12 km. At the highest altitudes sampled, $CH_2Br_2$ is the most abundant of these compounds and, in total, organic Br compounds other than $CH_3Br$ contribute about 15% to the total load of organic Br in the upper Pacific troposphere.

An unresolved issue concerning the impact of shorter-lived organic Br species on stratospheric ozone is related to their input into the upper troposphere and lower stratosphere, where they are converted to reactive inorganic forms of Br. Schauffler *et al.* (1993) and Kourtidis *et al.* (1996) report concentrations of $CH_2Br_2$ of about 0.7 ppt at the tropical tropopause. These measurements are consistent with the tropospheric dataset from the Pacific Exploratory Mission (PEM) Tropics (Schauffler *et al.*, 1998b). Tropopause concentrations of $CH_2Br_2$ were reported to be more variable in the Arctic region. A rapid decrease in $CH_2Br_2$ and $CH_2BrCl$ above the tropopause has been reported (Wamsley *et al.*, 1998; Kourtidis *et al.*, 1996; Schauffler *et al.*, 1998b). Wamsley *et al.* (1998) related the concentrations of brominated organic compounds to CFC-11 and report an approximately 50% reduction in the concentration of $CH_2Br_2$ and $CH_2BrCl$ relative to a 10% reduction in CFC-11. Thus, the conversion of shorter-lived organic Br compounds to reactive inorganic species is most significant in the tropopause region and the lower stratosphere.

The role of bromoform in the tropopause region is undetermined. Schauffler *et al.* (1998b) report a decrease in mixing ratios between 10 and 15 km at NH mid-latitudes of about 90% for $CHBr_3$ and about 40% for $CH_2Br_2$. These data suggest that $CHBr_3$ is more rapidly depleted in the lower stratosphere compared to $CH_2Br_2$, as may be expected from their respective photochemical loss rates. However, the available data are insufficient to estimate the rate and magnitude of reactive organic Br input to the lower stratosphere. Current data (see Table 2-7) indicate the presence of $\leq$2 ppt Br from shorter-lived organic Br compounds at the tropopause and hence place an upper limit on the amount of Br entering the tropical stratosphere. However, the potential variability in these compounds is high and the appropriate altitude range is undersampled with respect to the reactive organic species. Data are not available yet to assess how episodic convection of surface air rich in bromoform and other bromocarbons can impact chemistry in the tropopause region. It is generally assumed that all Br released in the troposphere is removed by wet scavenging; however, this assumption has not been tested by model calculations.

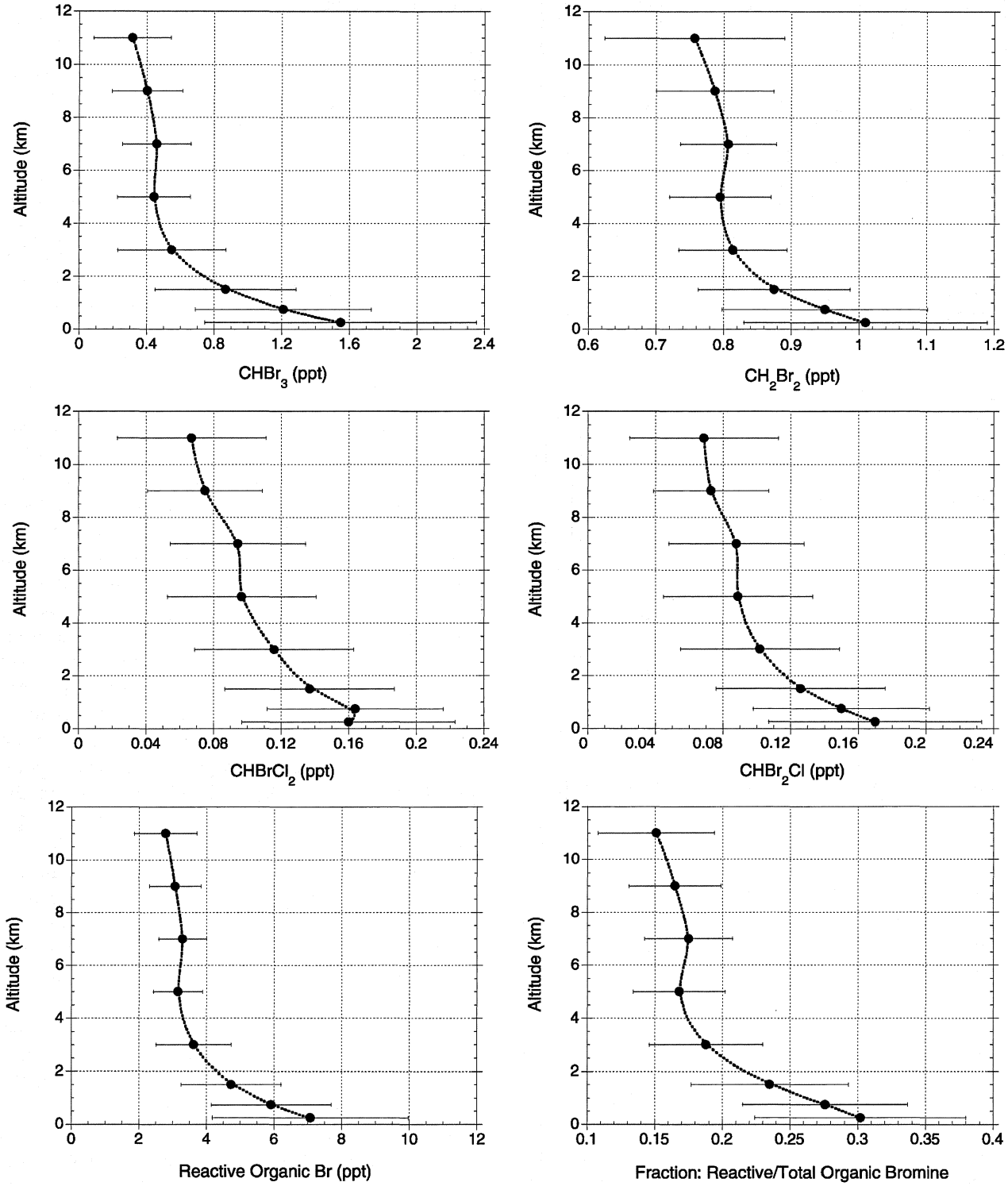


**Figure 2-11.** Vertical profiles of individual reactive organic Br gases, total reactive organic Br, and fraction of reactive/total organic Br over the Pacific Ocean (adapted from Schauffler *et al.*, 1998b). Mean and standard deviation are plotted.

### 2.3.2.2 Sources and Sinks/Lifetimes

*Sources*

Reactive organic Br compounds have both natural and anthropogenic sources. The anthropogenic source of bromoform and bromochloromethanes is primarily related to treatment and disinfection of drinking water and cooling waters. In addition to the trihalomethanes, several brominated acids and acetonitriles are produced in the treatment process. Gschwend *et al.* (1985) estimated a production rate of organic Br compounds from water chlorination of 0.6 Gg Br $yr^{-1}$ from seawater and 4 Gg $yr^{-1}$ from freshwater treatment. Emission of ethylene dibromide (EDB) from gasoline additives and fumigation has been significant in past decades, but there are fewer emissions today due to increased regulation of the compound. Consistent with the reduced emission, current atmospheric measurements suggest low (> 0.05 ppt) levels of EDB in the ambient atmosphere.

Natural production of reactive organic Br compounds from algal sources has been clearly demonstrated. To date, a wide range of species of macroalgae and microalgae, from temperate as well as polar regions, has been examined for organohalogen production, and analysis of algal tissues has revealed a complex suite of different organohalogen compounds (McConnell and Fenical, 1977). The relative release rates of individual organic Br compounds from different algal species can vary, and a wide variety of halocarbons can be formed, but most often bromoform is the major compound measured. There have been suggestions, too, that bromochloromethanes can be formed from chloride ion substitution of bromoform in seawater (Class and Ballschmiter, 1988), but laboratory studies indicate a clear primary source of bromochloromethanes from algae. The mechanism of bromoform production in algae has been linked to a pathway involving bromoperoxidase enzyme (Moore *et al.*, 1996a).

The magnitude of the natural organic Br source is difficult to assess. Studies of halocarbon production in laboratory systems have shown that production is species specific and apparently is quite variable within samples of the same species. Also, procedures for reporting and estimating production rates vary between different investigators. Finally, some estimate must be made of the fraction of organic Br compounds produced by algae which undergoes air-sea exchange. Sturges *et al.* (1992) estimate that the combined annual production of organic Br from Antarctic and Arctic ice algae is in the range of 10 to 150 Gg Br. This can be contrasted to estimates of 0.08 to 36 Gg Br $yr^{-1}$ from macroalgae (Gschwend *et al.*, 1985; Schall *et al.*, 1994). These estimates do not include the potentially large open-ocean source associated with algal production associated with equatorial upwelling. The industrial source of bromoform and bromochloromethanes is considerably less than these estimates (4.6 Gg). Overall, algal production of reactive organic Br compounds is the same order of magnitude as that estimated for halon and $CH_3Br$ emission (see Chapter 1 and Section 2.3).

*Sinks/Lifetimes*

The reactive organic Br compounds discussed here have photochemical sinks from photolysis and OH and Cl oxidation. Rate constants for the OH reactions, which constitute the most important tropospheric oxidative loss processes, are summarized in Table 2-8. Using these rate constants and measured photolysis cross sections, an approximate photochemical lifetime has been estimated (Table 2-9). These calculations indicate that photolytic loss is most important for bromoform, oxidation by OH controls the lifetimes of $CH_2BrCl$ and $CH_2Br_2$, and both OH oxidation and photolysis are significant for $CHBrCl_2$ and $CHBr_2Cl$. The lifetimes calculated here can be used to provide another estimate of the surface flux of reactive organic Br compounds. Assuming a total atmospheric loss rate based on OH reaction and photolysis (Table 2-9) and a global average concentration for $CHBr_3$ and $CH_2Br_2$ of 0.4 and 0.8 ppt, respectively, and 0.1 ppt for $CH_2BrCl$, $CHBrCl_2$, and $CHBr_2Cl$ (see Table 2-7), we approximate fluxes of slightly greater than 270 Gg $yr^{-1}$ of Br from these reactive organic species. We note that this calculation necessarily provides only a rough estimate of the Br flux because of the uncertainty in the spatial and seasonal distributions of reactive organic Br compounds. A more comprehensive model is required to more accurately assess the global flux of reactive organic Br compounds. Still, the estimated fluxes may not be inconsistent with emission estimates from algal production reported above, and reinforce the idea that approximately 50 to 65% of the flux of all organic Br is related to natural emission of short-lived bromocarbon gases. This provides another upper bound for the flux of Br delivered to the stratosphere.

**Table 2-8. Rate constants for OH reactions with short-lived organic Br compounds.**

| Compound | OH Rate Constant ($cm^3$ $molec^{-1}$ $s^{-1}$) | | |
|---|---|---|---|
| | $k(T)$ | $k(298)$ | Ref. |
| $CH_2BrCl$ | $2.3 \times 10^{-12} \exp(-930/T)$ | $1.0 \times 10^{-13}$ | 1 |
| $CH_2Br_2$ | $2.4 \times 10^{-12} \exp(-900/T)$ | $1.2 \times 10^{-13}$ | 1 |
| $CHBrCl_2$ | - | $1.2 \times 10^{-13}$ | 2 |
| $CHBr_2Cl$ | - | $1.2 \times 10^{-13}$ | est'd |
| $CHBr_3$ | $1.6 \times 10^{-12} \exp(-710/T)$ | $1.5 \times 10^{-13}$ | 1 |

[1] DeMore *et al.*, 1997.
[2] Bilde *et al.*, 1998.

**Table 2-9. Approximate tropospheric lifetimes and fluxes.**

| Compound | Lifetime | | [X] (ppt Br)† | Flux (Gg Br $yr^{-1}$) |
|---|---|---|---|---|
| | OH Reaction* | Photolysis** | | |
| $CH_2BrCl$ | 150 days | 15000 days | 0.1 | 2.9 |
| $CH_2Br_2$ | 130 days | 5000 days | 1.6 | 53.7 |
| $CHBrCl_2$ | (120) days†† | 222 days | 0.1 | 5.5 |
| $CHBr_2Cl$ | (120) days†† | 161 days | 0.2 | 12.4 |
| $CHBr_3$ | 100 days | 36 days | 1.2 | 196.5 |

* Lifetimes calculated for $T = 275$ K, [OH] = $1 \times 10^6$ molecule $cm^{-3}$.
** Photolysis lifetimes based on globally and seasonally averaged J-value estimated for 5 km.
† Estimated global average mixing ratio as ppt-Br.
†† T-dependence of OH rate is estimated.

## 2.4 IODINATED COMPOUNDS

For iodine, the efficiency for ozone removal is much larger per molecule than that of Cl or even Br. This is due to the fact that essentially all of inorganic iodine is expected to be in the active form $IO_x$, and the rate-limiting reactions for catalytic removal (i.e., reactions of IO with $HO_2$, ClO, and BrO) are faster than the corresponding Cl and Br reactions. Iodine chemistry has recently been invoked to help understand lower stratospheric and upper tropospheric ozone levels. Modeling results reported by Solomon *et al.* (1994) suggested that IO reactions could be playing an important causal role in the decadal trends in ozone currently observed (see Section 7.6.2). Davis *et al.* (1996) report model results that indicate that under certain conditions, iodine chemistry could significantly impact the rate of destruction of upper tropospheric ozone.

### 2.4.1 Methyl Iodide ($CH_3I$)

The main source of methyl iodide ($CH_3I$) is thought to be oceanic (Chameides and Davis, 1980), with some impact from biomass burning (Andreae *et al.*, 1996; N.J. Blake *et al.*, 1996). Work by Happell and Wallace (1996) and Moore and Zafiriou (1994) suggests that photochemical processes dominate marine $CH_3I$ production and that the ocean is most likely a sink at high latitudes and during winter, and a source only at low latitudes and during summer. Blake *et al.* (1997) discuss latitudinal and vertical profiles obtained during two Pacific-region airborne missions flown in the summer of 1991 and winter of 1994. They report that, during summer, marine boundary layer mixing ratios in the 0.5- to 1.0-ppt range were observed in the northern Pacific, whereas in the winter this range was encountered only in or near the tropics. Marine hot spots exceeding

1 ppt occurred during both seasons. During the 1992 Polar Sunrise Experiment, Yokouchi *et al.* (1996) observed wintertime $CH_3I$ values of 1 to 1.5 ppt, whereas the springtime concentrations were in the 0.6- to 0.3-ppt range. Blake *et al.* (1998) report seasonal changes in $CH_3I$ concentrations near Tasmania. The $CH_3I$ levels increased as summer approached, the opposite of what Yokouchi *et al.* (1996) observed. Davis *et al.* (1996) report $CH_3I$ concentrations obtained during a summer 1991 airborne mission; a significant amount of their Asian Pacific study area was under the influence of rapid vertical transport resulting from numerous typhoons. They report $CH_3I$ mixing ratios in excess of 1 ppt at altitudes of 12 km. They also indicate that some typhoons had cloud tops at altitudes greater than 18 km and likely transported significant amounts of marine boundary layer air into the lower stratosphere. Although $CH_3I$ mixing ratios in coastal waters can be quite elevated (Oram and Penkett (1994) reported 43 ppt), generally over the open ocean the concentrations range between 0.1 and 2 ppt (Atlas *et al.*, 1993; Yokouchi *et al.*, 1996, 1997; D.R. Blake *et al.*, 1996; Blake *et al.*, 1997, 1998).

Wennberg *et al.* (1997) studied the IO absorption observed in high-resolution, high-airmass solar spectra taken at the Kitt Peak National Solar Observatory, Arizona. Their results suggest that the total stratospheric iodine mixing ratio is 0.2 (+0.3, -0.2) ppt, thus limiting its contribution to ozone depletion in the lower stratosphere. This is consistent with reported upper tropospheric $CH_3I$ mixing ratios of 0.05 to 0.2 ppt (Blake *et al.*, 1997) and with upper limits of 0.1 to 0.2 ppt in the 15- to 20-km region (Pundt *et al.*, 1997). The only significant removal process for $CH_3I$ is photolysis. Roehl *et al.* (1997) report the ultraviolet absorption spectra of a number of alkyl halides. They calculate that the surface photolysis rate constant at a solar zenith angle of 40° for $CH_3I$ is approximately 4 days and decreases to about 1.5 days at 10 km. No $CH_3I$ trend studies have been published.

### 2.4.2 Ethyl Iodide ($C_2H_5I$) and Other Iodocarbons

Atmospheric data are scarce for iodocarbons other than $CH_3I$. During a western Pacific cruise, Yokouchi *et al.* (1997) observed ethyl iodide ($C_2H_5I$) at mixing ratios of 0 to 0.3 ppt. During the same time $CH_3I$ was in the 0.4- to 2-ppt range. The photolysis rate for ethyl iodide is slightly faster than that of $CH_3I$ (Roehl *et al.*, 1997). Thus, ethyl iodide has a slightly shorter photolytic lifetime than $CH_3I$ (Table 2-4). Additional surface and airborne studies are needed in order to determine if ethyl iodide emissions at some locations are large enough for it to play a role in upper tropospheric/lower stratospheric ozone chemistry.

A number of shorter-lived iodocarbons have been observed. Chloroiodomethane ($CH_2ClI$) has a typical photolytic lifetime of about two hours (Table 2-4). Yokouchi *et al.* (1996) observed an annual cycle in chloroiodomethane in the Arctic, with peak levels of 0.05 ppt during winter and undetectable levels (< 0.005 ppt) in summer. Schall and Heumann (1993) reported 0.07 ppt (ranging from less than 0.004 to 0.18 ppt) of chloroiodomethane during September in Spitzbergen. Undetectable levels were reported by Yokouchi *et al.* (1997) during the western Pacific cruise mentioned above. Other reported iodocarbons include diiodomethane ($CH_2I_2$), isopropyl iodide ($CH_3CHICH_3$), and n-propyl iodide ($CH_3CH_2CH_2I$), with concentrations ranging from tenths to several ppt (Schall and Heumann, 1993). All have photolytic lifetimes less than ethyl iodide, with diiodomethane having a lifetime on the order of minutes (Table 2-4). All of the above organoiodine compounds are believed to be of natural origin. One human-made iodocarbon, $CF_3I$, has been developed as a potential halon replacement (Solomon *et al.*, 1994). It has a lifetime of about 1 day (Table 2-4). There are no known reports of its occurrence in the atmosphere.

## 2.5 OTHER OZONE-RELATED COMPOUNDS

In this section we discuss the atmospheric budgets of methane ($CH_4$) and carbon monoxide (CO). $CH_4$ plays an important role both as a greenhouse gas and a reactive tropospheric and stratospheric chemical species. In the troposphere, $CH_4$ is a source of OH radicals produced via its reaction with excited oxygen atoms, $O(^1D)$, and also is an OH sink. In the stratosphere, $CH_4$ controls the abundance of Cl atoms by converting them to HCl. CO also plays an important chemical role in the troposphere by converting OH radicals into $HO_2$.

### 2.5.1 Methane ($CH_4$)

#### 2.5.1.1 Recent Trends

The burden of atmospheric $CH_4$ continues to increase, but the rate of growth of this burden is declining (Dlugokencky *et al.*, 1994a; Matsueda *et al.*, 1996). Recent measurements indicate growth rates of about 3

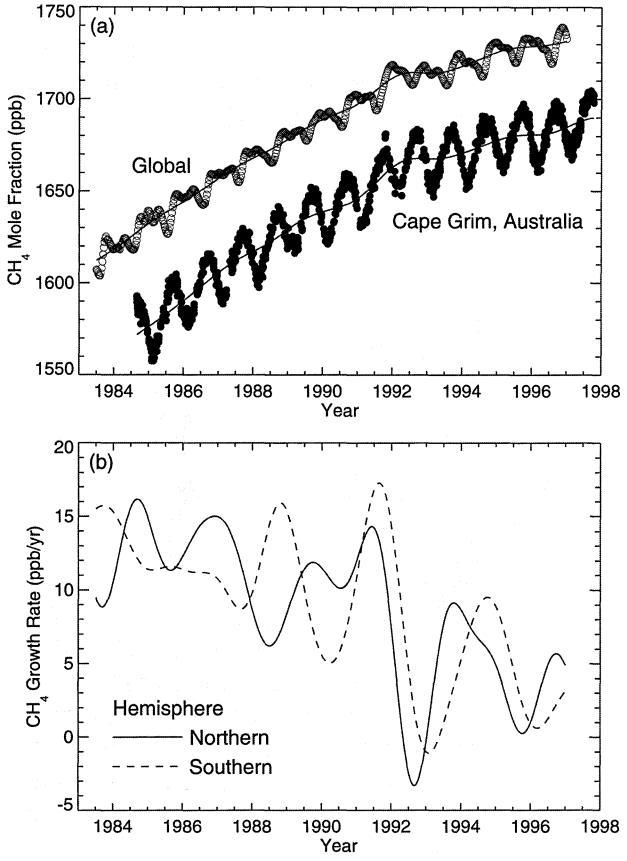


**Figure 2-12.** (a) Globally averaged $CH_4$ mole fractions (open symbols). The averages are determined by smoothing the measurements from the NOAA/CMDL cooperative air sampling network in time and latitude (see Dlugokencky *et al.*, 1994a, 1998, for details). Also shown are atmospheric $CH_4$ mole fractions determined from discrete samples collected at Cape Grim, Tasmania, after selection for baseline conditions (closed symbols) (Steele *et al.*, 1996). In both cases, the solid line represents the long-term trend. (b) Instantaneous growth rate curves determined from zonal averages for NH (solid line) and SH (dashed line) (Dlugokencky *et al.*, 1994a, 1998).

to 4 ppb $yr^{-1}$ in the 1996 to 1997 period (Dlugokencky *et al.*, 1998; Steele *et al.*, 1996) (see Figures 2-12 and 2-13). Apart from the anomalously low growth rates during 1992/93 (Dlugokencky *et al.*, 1994b, 1996), the growth rate of $CH_4$ is now at its lowest value since the 1940s (Figure 2-14), as indicated by the recent analysis by Etheridge *et al.* (1998). In their analysis, $CH_4$ data from three Antarctic ice cores, Antarctic firn air, the Cape Grim (Tasmania) Air Archive (CGAA) dating back to 1978 (Langenfelds *et al.*, 1996a), and direct atmospheric measurements since 1984 have been combined to present a very high time resolution record of atmospheric $CH_4$ from 1000 AD to the present. An analysis of the NOAA/CMDL global $CH_4$ dataset by Dlugokencky *et al.* (1998) suggests that the observed decrease in the growth rate of $CH_4$ over the period of their data (1984 to 1996) is consistent with an approach to steady state, where both the total global source of $CH_4$ and the average OH concentration have stayed nearly constant over this period. They conclude that "Unless the global $CH_4$ budget changes, the globally averaged $CH_4$ mole fraction will slowly increase to about 1800 ppb, and the contribution of $CH_4$ to the greenhouse effect will not increase significantly above its current level." It would seem to be appropriate that the large body of observational evidence now showing declining growth rates of $CH_4$ since the early 1980s be reflected in the range of emission scenarios being used in model simulations of climate over the next century.

Further analysis of the period of low $CH_4$ growth in 1992/93 has been reported by Dlugokencky *et al.* (1996). They show that following the eruption of Mt. Pinatubo in June 1991, there were sudden temporary increases in the growth rates of both $CH_4$ and CO in the tropics and high southern latitudes. Calculations made with a radiative-transfer model showed that ultraviolet (UV) actinic flux in the 290- to 330-nm wavelength region was attenuated by about 12% immediately after the eruption due to absorption by $SO_2$ and scatterintg by sulfate aerosols. Dlugokencky *et al.* (1996) suggest that decreased UV penetration into the troposphere led to a decrease in OH and subsequent increases in the growth rates of both $CH_4$ and CO. The enhanced growth rates during late 1991 and early 1992 were then followed by very low growth rates in 1992/93. It has been suggested that these low growth rates were due to the cooler temperatures following the Mt. Pinatubo eruption causing lower $CH_4$ emissions from NH wetlands (Hogan and Harriss, 1994). It also has been suggested that volcanic aerosols injected into the lower tropical stratosphere from Mt. Pinatubo induced changes in stratospheric circulation that impacted tropospheric $CH_4$ trends (Schauffler and Daniel, 1994). The features described above also have been observed in vertical column abundance measurements of $CH_4$ at the Jungfraujoch station between the mid-1980s and April 1997. That database indicates mean

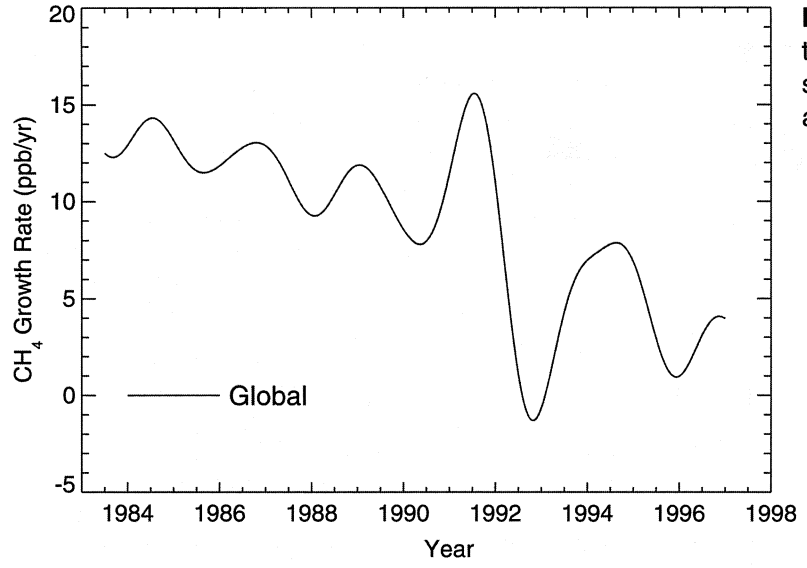


**Figure 2-13.** Growth rate calculated as the derivative of the long-term trend line shown for the NOAA/CMDL global $CH_4$ averages in Figure 2-12.

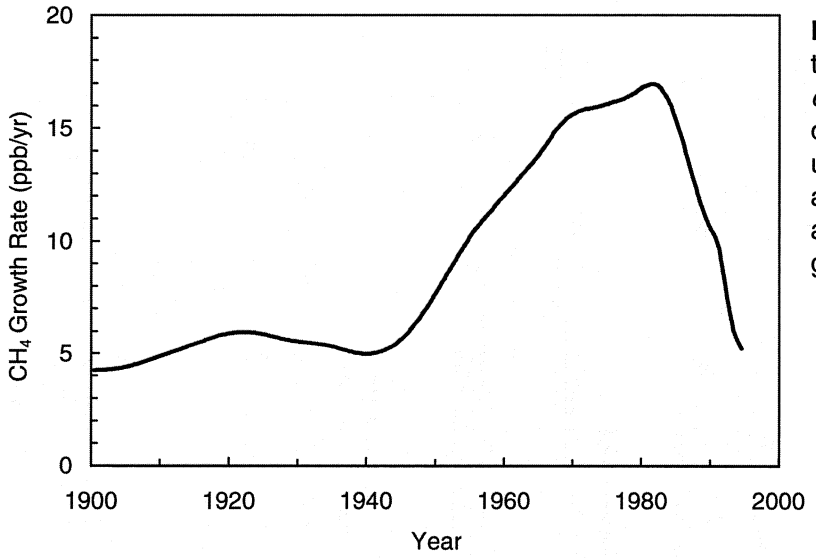


**Figure 2-14.** Global $CH_4$ growth rate for the period 1900 to 1995 from Etheridge *et al.* (1998). It was calculated as the derivative of a curve fitted to $CH_4$ measurements from Antarctic ice cores, Antarctic firn air, and Cape Grim air, after an adjustment of the measurements to global values.

rates of increase prior to and after January 1991 equal to 0.73% $yr^{-1}$ and 0.44% $yr^{-1}$, respectively (Zander *et al.*, 1997).

Paleo records of atmospheric $CH_4$ have been recently updated and improved. A high-resolution record over the Holocene (the last 11,500 years) derived from both Antarctic and Greenland ice cores has been presented by Chappellaz *et al.* (1997). They find an average interpolar difference of 44 ± 7 ppb, compared with a present-day interpolar difference of 143 ± 1 ppb derived from the NOAA/CMDL global data (Dlugokencky *et al.*, 1994a). The variations in the interpolar difference over the Holocene are interpreted with a three-box model of the atmosphere to indicate variations with time in the magnitudes of tropical and high-northern-latitude sources of $CH_4$. Using very high time resolution ice cores from Antarctica, Etheridge *et al.* (1998) have determined the global average $CH_4$ mixing ratio during the late preindustrial Holocene (1000 to 1800 AD) to be 695 ppb, with variations around this value of up to 40 ppb. These variations are strongly correlated with indicators of climate variation and serve to emphasize that it is inappropriate to represent the preindustrial level of atmospheric $CH_4$ by a single value.

**Table 2-10. Global budget of $CH_4$.**

| Source or Sink | Magnitude (Tg $yr^{-1}$) | | |
|---|---|---|---|
| | WMO (1995) | Fung *et al.* (1991) [a] | Hein *et al.* (1997)[b] |
| Sources | | | |
| Wetlands | 110 | 115 | 237 |
| Termites | 20 | 20 | - |
| Ocean | 10 | 10 | - |
| Freshwater | 5 | | - |
| Hydrates | 10 | 5 | - |
| Energy-related | 100 | 75 | 97 |
| Sewage treatment | 25 | - | - |
| Landfills | 30 | 40 | 35 |
| Animal waste | 25 | 80 | 90 |
| Ruminants | 80 | | |
| Biomass burning | 40 | 55 | 40 |
| Rice paddies | 60 | 100 | 88 |
| **Total Sources** | 515 | 500 | 587 |
| Sinks | | | |
| Soils | 30 | 10 | - |
| Reaction with OH | 445 | 450 | 489 |
| Removal in stratosphere | 40 | | 46 |
| **Total Sinks** | 515 | 460 | 535 |

[a] Scenario preferred by Fung *et al.* (1991) as a fit to a 1984 to 1987 database.
[b] Fit to a 1991 to 1993 database.

A notable development over recent years has been the increase in the number and range of aircraft-based observations of $CH_4$. Vertical profiles of $CH_4$ from the surface to an altitude of about 8 km near Cape Grim, Tasmania (41°S), have been measured approximately monthly since 1991 (Langenfelds *et al.*, 1996b). These data sometimes show strong average vertical gradients (about 20 ppb higher at 8 km than at the surface), particularly during the austral summer (Pak *et al.*, 1996), and possibly are signatures of biomass burning plumes from Africa and South America. Similar vertical gradients were observed by Bartlett *et al.* (1996) during research flights over the south Atlantic Ocean during September to October 1992.

Airborne measurements of $CH_4$ over western Siberia in August 1994 showed highly elevated levels near oil production sites or pipelines, suggesting leakage of natural gas (Tohjima *et al.*, 1996). Regular measurements of atmospheric $CH_4$ are being made from a Boeing 747 commercial airliner flying between Japan and Australia (Matsueda and Inoue, 1996). Another important method for obtaining information on trace gas budgets, including that of $CH_4$, has been recently described (Crutzen *et al.*, 1998). By making measurements from a laboratory wagon traveling along the Trans-Siberian railroad, these investigators have demonstrated an elegant way of collecting such data from the vast continental area of Russia, a region for which there has been relatively little data in the past, and which is needed to supplement the largely marine boundary layer datasets available to now.

### 2.5.1.2 Sources and Sinks

Current knowledge on the sources and sinks of $CH_4$ has been summarized and discussed in previous assessments (WMO, 1995; IPCC, 1995). Recently revised budgets of atmospheric $CH_4$ are broadly similar to those

published previously (Hein *et al.*, 1997). Most individual $CH_4$ source terms continue to have relatively large uncertainties. Using an inverse modeling approach, Hein *et al.* (1997) found that the average uncertainty of the magnitudes of $CH_4$ sources could be reduced by at least one-third using the present observational network. Table 2-10 shows the "best" estimates for the magnitude of the different sources and sinks for $CH_4$, as given in WMO (1995), compared to the values derived and preferred by Fung *et al.* (1991) and Hein *et al.* (1997) using inverse modeling methods. Differences in estimates reflect the sensitivity of inverse methods to the assumed geographical distribution of sources and sinks, and the inclusion of specific minor processes. Further reductions in the uncertainties almost certainly will require additional observations near source regions.

Improvements in the knowledge of the $CH_4$ budget have come from a more accurate estimation of the lifetime of $CH_4$ due to removal by OH (Prinn *et al.*, 1995). The new total atmospheric lifetime value of $8.9 \pm 0.6$ years is lower than the previous estimate of 10.0 years and is based upon a new calibration scale for $CH_3CCl_3$ measurements and a good knowledge of the respective reaction rate constants with OH. The adjustment time for $CH_4$ recovery would be somewhat longer due to $CH_4$ feedback on CO and OH (see Chapter 2 in WMO, 1995).

The question of whether Cl atoms significantly influence the oxidizing capacity of the atmosphere is addressed by studies of tetrachloroethylene ($C_2Cl_4$). This chemical is known to react about 300 times faster with Cl atoms than with OH. Analyses of $C_2Cl_4$ measurement data in the context of a global 2-D atmospheric model indicate that Cl atoms are likely to enhance $CH_4$ oxidation by less than 2% (Singh *et al.*, 1996; Rudolph *et al.*, 1996).

## 2.5.2 Carbon Monoxide (CO)

### 2.5.2.1 Atmospheric Distributions

#### *Surface Measurements*

Over the past several years the number of CO monitoring sites in both the background and regionally polluted troposphere have continued to increase. The NOAA/CMDL cooperative air sampling network established new sites chosen to study regions impacted by pollution in the United States, Europe, Africa, and Asia. These non-background sites typically show greater winter mixing ratios than background sites at similar latitude, whereas levels in summertime are often similar (Novelli *et al.*, 1998a). In the background atmosphere, measurements of CO in air collected at several sites on Antarctica now extend the global network from 82°N to 90°S. Background CO mixing ratios range from a high of 200 to 225 ppb in winter in the high northern latitudes to a low of 40 to 50 ppb during summer in the high southern latitudes. The WMO has proceeded with the Global Atmospheric Watch (GAW) program, which has established Global Environmental Facilities (GEF) to provide continuous or semi-continuous monitoring of CO at six locations (China, Indonesia, Brazil, Argentina, Algeria, Kenya) (WMO, 1995). Measurements of CO are currently made at the GAW/GEF sites in Argentina and China; grab samples from these sites are collected for analysis at CMDL to provide comparison of the datasets. Samples of air are also collected by the Commonwealth Scientific and Industrial Research Organisation (CSIRO) at the WMO site in Indonesia for trace-gas analysis.

In the background atmosphere, spatial distributions of CO in the marine boundary layer (MBL) have become better defined. CO is well mixed in the high latitudes of both hemispheres, with times series from widely separated sites nearly indistinguishable. Time series from the tropics and extratropics show both greater short-term and interannual variations, which is attributed to their proximity to surface sources. CO mixing ratios in the MBL continue to decline, with values in the high SH now often reaching seasonal minimums below 40 ppb (Novelli *et al.*, 1998a). Issues of calibration and the consistency of measurements between laboratories remain a concern. Data from different laboratories should not be combined until measurements are compared. A recent intercomparison of standards as part of the Measurement of Air Pollution from Satellite (MAPS) validation revealed that differences up to 50% may still exist between laboratories (Novelli *et al.*, 1998b).

#### *Middle and Upper Troposphere*

Compared to the boundary layer, less is known about the distributions and seasonal cycles of CO in the middle and upper troposphere. Long-term measurements of the vertical profiles of trace gases above Carr, Colorado (Bakwin *et al.*, 1994), and Cape Grim, Tasmania (Pak *et al.*, 1996), have helped define differences in CO between the surface and middle troposphere in the two hemispheres. At Carr, CO tends to decrease with altitude, often with clearly defined layers of higher CO and other carbon gases such as carbon

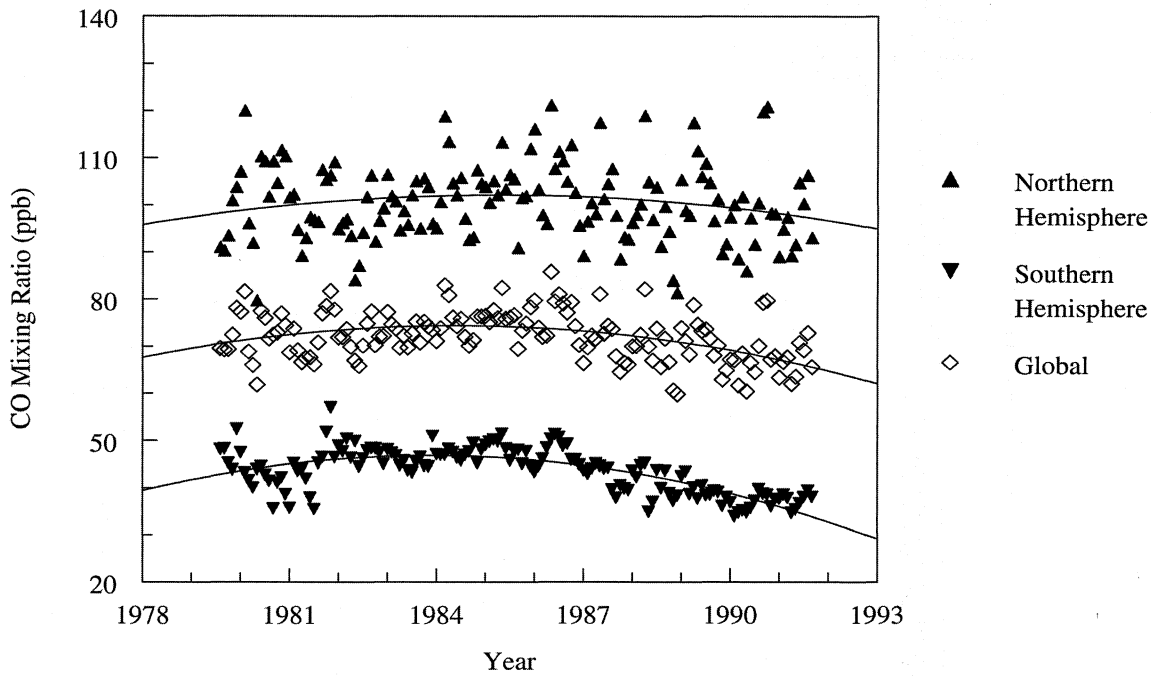


**Figure 2-15.** Zonally averaged, deseasonalized CO mixing ratios (from six sites 70°N to 90°S). Estimated average trends (ppb $yr^{-1}$) between 1981 and 1986: global = 0.9 ± 0.4, NH = 0.8 ± 0.7, SH = 1.0 ± .4; between 1986 and 1992: global = -1.8 ± 0.5, NH = -1.3 ± 0.9, SH = -2.3 ± 0.3. Reprinted with permission from *Nature*. (Khalil, M. A. K., and R. A. Rasmussen, Figure 1b, Trends from Table 1, *Nature, 370*, pp. 639-640, copyright 1994, MacMillan Magazines Limited.)

dioxide ($CO_2$) and $CH_4$. At Cape Grim, CO typically increases with altitude all year long, with a strong seasonal maximum in spring. Such measurements show that significant amounts of CO, produced at the surface by biomass burning, are transported above the boundary layer into the middle troposphere. Thus, the networks that measure CO in the planetary boundary layer see only a part of the annual cycle of this gas. Additional locations of vertical profiles are planned under the Measurement Of Pollution In The Troposphere (MOPITT) validation. Regular measurements from a commercial jet between Japan and Australia show strong seasonal cycles in both hemispheres, with surprisingly strong CO enhancement in the southern extratropics between 9 and 12 km during the spring (Matseuda *et al.*, 1998).

Measurements of CO from space have advanced. The MAPS Space Shuttle instrument has a maximum CO signal at approximately 300 mb. MAPS was flown for 10-day missions during April and October, 1994, during which time nearly global distributions were determined. Modifications to the instrument and data retrieval procedures indicated that the large bias error in the earlier flights was reduced to about 10% (Reichle *et al.*, 1990, 1998). MAPS showed very high levels of CO over the tropical south Atlantic, southern Africa and Indochina, which likely reflected transport of emissions from surface fires into the middle troposphere (Newell *et al.*, 1998). Scheduled for launch as part of the EOS/ MTPE AM-1 (Earth Observing System - Mission to Planet Earth *ante meridian* equatorial crossing) satellite, MOPITT promises to define global tropospheric CO averaged mixing ratios at three to four altitude ranges, extending from the surface to 15 km (Drummond, 1992). An extensive validation program will include in situ measurements of CO vertical profiles from aircraft and vertical column abundances from ground-based solar observations.

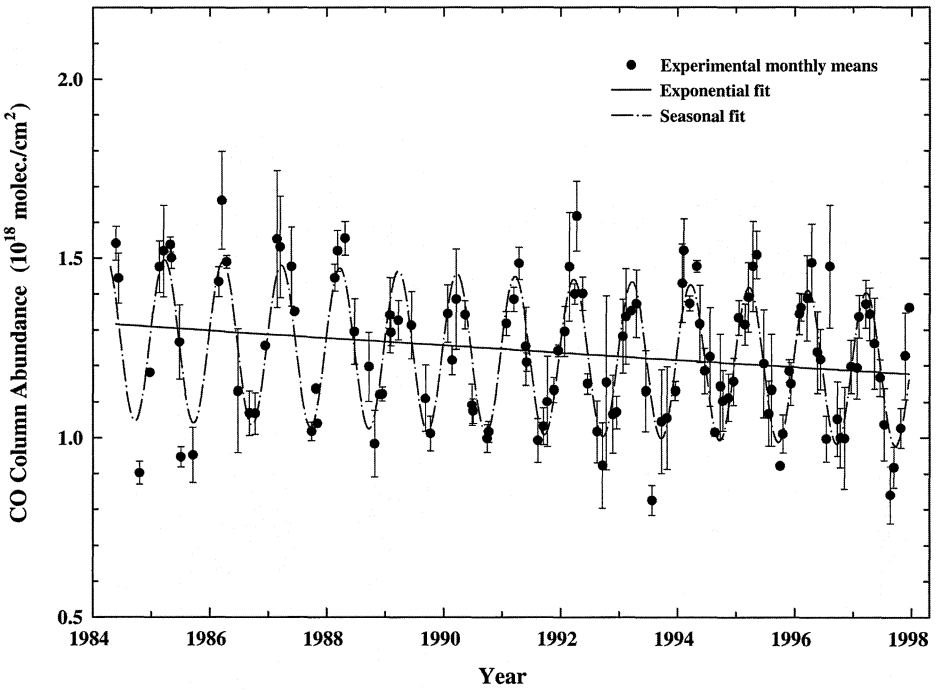


**Figure 2-16.** Vertical column abundances of CO monitored above the Jungfraujoch. The monthly means shown are adapted from the daily data given in Mahieu *et al.* (1997), with the data extended through the end of 1997. Both the seasonal and exponential fits to the data are shown. The trend derived from an [exponential + sine] fit is -0.53 ± 0.18% yr$^{-1}$, whereas an exponential fit alone (shown by the solid line) yields -0.82 ± 0.34% yr$^{-1}$.

#### 2.5.2.2 Trends

CO mixing ratios at sites around the world show considerable interannual variation. Whereas this may be attributed in part to variations in transport (Allen *et al.*, 1996), the average global changes represent changes in sources and sinks. Although the evaluation of long-term trends in CO are limited by the available measurements, comparisons of solar spectra determined during 1950 to 1951 above Switzerland to measurements made in the mid-1980s at the same site suggested a linear rate of increase of column CO of slightly less than 1% yr$^{-1}$ (Zander *et al.*, 1989). Time series determined at six sites, three in the NH and three in the SH, indicated a similar rate of increase in the early to mid-1980s (Khalil and Rasmussen, 1988). CO measurements in Greenland ice cores suggest that there has been an increase in the high NH since 1850, whereas samples from Antarctica show no trend (Haan *et al.*, 1996). Monitoring of CO at Cape Point, South Africa, since 1979 have shown periods of CO increase and decrease, with no significant trend discernible.

This trend of increasing CO appears to have reversed in the late 1980s (Figure 2-15). Since then, CO is reported to have decreased at surface sites in both hemispheres (Khalil and Rasmussen, 1994; Novelli *et al.*, 1994). A decrease in CO is also evident in the atmospheric column above Europe (Figure 2-16) (Zander *et al.*, 1994b; Mahieu *et al.*, 1997). The NOAA/CMDL record shows a sharp global decrease during late 1991 through mid-1993 (Novelli *et al.*, 1998a). After a short period of increased growth rate in the second half of 1991 (see Section 2.5.1.1 for analogous discussion of $CH_4$), CO decreased rapidly. This decline has been attributed, in part, to an increase in tropospheric OH resulting from a decrease in stratospheric ozone following the Mt. Pinatubo eruption (Granier *et al.*, 1996). Particularly low levels of biomass burning in 1992 may also have contributed to the CO decrease. Comparison of recent time series determined in the SH by different laboratories

**Table 2-11. Global budget of CO.** (Adapted from IPCC (1995) except where noted.)

| Sources | Magnitude (Tg $yr^{-1}$) | Sinks | Magnitude (Tg $yr^{-1}$) |
|---|---|---|---|
| Fossil fuels and industry | 300 to 500 | Reaction w/ OH[a] | 1400 to 3000 |
| Biomass burning | 300 to 700 | Removal in the stratosphere | ~100 |
| $CH_4$ oxidation | 400 to 800 | Soil uptake[b] | 100 to 600 |
| NMHC oxidation | 200 to 600 | | |
| Oceans | 20 to 200 | | |
| Vegetation[c] | 20 to 200 | | |
| **Total Sources** | 1240 to 3000 | **Total Sinks** | 1600 to 3700 |

[a] Reflects increased estimates of the atmospheric concentration of OH (Prinn *et al.*, 1995).
[b] Lower end of range includes recent results of Sanhueza *et al.* (1998) and Potter *et al.* (1996).
[c] Badr and Probert, 1994.

shows significant differences. Time series from Cape Grim, Tasmania, determined by NOAA/CMDL and CSIRO show similar features, but of different magnitudes. Both records show declines in CO from late 1991 to mid-1993, though the NOAA/CMDL time series shows a sharper decrease. This change is not evident in the Cape Point record (Scheel *et al.*, 1996). At Cape Grim, partial (NOAA/CMDL) to full (CSIRO) recovery in CO occurred during 1993 to 1995 (Novelli *et al.*, 1998a; Steele *et al.*, 1996).

The consistency and breadth of CO measurements have improved in recent years. However, given the considerable interannual variability in CO as well as unresolved differences in measurements, predictions of future long-term trends remain uncertain.

### 2.5.2.3 The Global Budget

There continue to be considerable uncertainties in the CO budget. Although fossil fuel combustion, biomass burning, and the oxidation of $CH_4$ are considered the major sources, the range of emissions still remains large (Table 2-11). The source of CO from the oxidation of nonmethane hydrocarbons (NMHC) has been reduced based upon evidence that on average, one, rather than three, CO are produced from the oxidation of isoprene (Jacob and Wofsy, 1990). No new studies have narrowed the uncertainty on the CO + OH reaction rate constant (±30%) which, combined with the error associated with global concentrations of OH derived from $CH_3CCl_3$ analysis, provide a range of estimates of the global sink between 1400 to 2600 Tg $yr^{-1}$. Additional uncertainty in the sink comes from the magnitude of soil uptake.

The most significant sources and sinks of CO have been identified; however, the budget is limited by a lack of emission data and the unavailability of atmospheric distributions for many areas. More measurements and statistical emission data are needed to constrain the CO budget. Trends in emissions can be used in chemical models to examine the effects on atmospheric composition. The measured isotopic partitioning of carbon in CO (Manning *et al.*, 1997) provides additional constraints that could reduce budget uncertainties. However, at present the limited geographical extent of the isotopic data makes global extrapolations using such an analysis difficult.

## REFERENCES

AFEAS (Alternative Fluorocarbons Environmental Acceptability Study), *Production, Sales and Atmospheric Release of Fluorocarbons through 1996*, AFEAS Science and Policy Services, Inc., Washington, D.C., 1998.

Allen, D.J., P. Kasibhatla, A.M. Thompson, R.B. Rood, B.G. Doddridge, K.E. Pickering, R.D. Hudson, and S.-J. Lin, Transport-induced interannual variability of carbon monoxide determined using a chemistry and transport model, *J. Geophys. Res.*, *101*, 28655-28669, 1996.

Anbar, A.D., Y.L. Yung, and F.P. Chavez, Methyl bromide: Ocean sources, ocean sinks, and climate sensitivity, *Global Biogeochem. Cycles*, *10*, 175-190, 1996.

Andreae, M.O., E. Atlas, C.W. Harris, G. Helas, A. de Kock, R. Koppmann, W. Maenhaut, S. Manö, W.H. Pollock, J. Rudolph, D. Scharffe, G. Schebeske, and M. Welling, Methyl halide emissions from savanna fires in southern Africa, *J. Geophys. Res.*, *101*, 23603-23614, 1996.

Atlas, E., and B.A. Ridley, The Mauna Loa Photochemistry Experiment, *J. Geophys. Res.*, *101*, 14531-14541, 1996.

Atlas, E., S.M. Schauffler, J.T. Merrill, C.J. Hahn, B. Ridley, J. Walega, J. Greenberg, L. Heidt, and P. Zimmerman, Alkyl nitrate and selected halocarbon measurements at Mauna Loa Observatory, Hawaii, *J. Geophys. Res.*, *97*, 10331-10348, 1992.

Atlas, E., W. Pollock, J. Greenberg, L. Heidt, and A.M. Thompson, Alkyl nitrates, nonmethane hydrocarbons, and halocarbon gases over the equatorial Pacific Ocean during SAGA 3, *J. Geophys. Res.*, *98*, 16933-16947, 1993.

Aucott, M.L., T.E. Graedel, G. Kleiman, A. McCulloch, P.M. Midgley, and Y.-F. Lee, Anthropogenic emissions of trichloromethane (chloroform) and chlorodifluoromethane (HCFC-22): The reactive chlorine emissions inventory, *J. Geophys. Res.*, submitted, 1998.

Badr, O., and S.D. Probert, Sources of atmospheric carbon monoxide, *Appl. Energy*, *49*, 145-195, 1994.

Baker, J.M., C.E. Reeves, S.A. Penkett, L.M. Cardenas, and P.D. Nightingale, An estimate of the global emissions of methyl bromide from automobile exhausts, *Geophys. Res. Lett.*, *25*, 2405-2408, 1998a.

Baker, J.M., C.E. Reeves, P.D. Nightingale, S.A. Penkett, S.W. Gibb, and A.D. Hatton, Biological production of methyl bromide in the coastal waters of the North Sea and open ocean of the Northeast Atlantic, *Mar. Chem.*, in press, 1998b.

Bakwin, P.S., T.J. Conway, E.J. Dlugokencky, D.W. Guenther, D. Kitzis, P.M. Lang, K.A. Masarie, P.C. Novelli, K.W. Thoning, P.P. Tans, and L.S. Waterman, Report of the Carbon Cycle Division, in *Climate Monitoring and Diagnostics Laboratory — No. 22 Summary Report 1993*, edited by J.T. Peterson and R.M. Rosson, pp. 18-30, NOAA Environmental Research Laboratories, Boulder, 1994.

Bakwin, P.S., D.F. Hurst, P.P. Tans, and J.W. Elkins, Anthropogenic sources of halocarbons, sulfur hexafluoride, carbon monoxide, and methane in the southeastern United States, *J. Geophys. Res.*, *102*, 15915-15925, 1997.

Barrie, L.A., J.W. Bottenheim, R.C. Schnell, P.J. Crutzen, and R.A. Rasmussen, Ozone destruction and photochemical reactions at polar sunrise in the lower Arctic atmosphere, *Nature*, *334*, 138-141, 1988.

Bartlett, K.B., G.W. Sachse, J.E. Collins, Jr., and R.C. Harriss, Methane in the tropical South Atlantic: Sources and distribution during the late dry season, *J. Geophys. Res.*, *101*, 24139-24150, 1996.

Baumann, H., and K.G. Heumann, Analysis of organobromine compounds and HBr in motor car exhaust gases with a GC/microwave plasma system, *Fresenius Z. Anal. Chem.*, *333*, 186-192, 1989.

Bilde, M., T.J. Wallinton, C. Ferronato, J.J. Orlando, G.S. Tyndall, E. Estupiñan, and S. Haberkorn, Atmospheric chemistry of $CH_2BrCl$, $CHBrCl_2$, $CHBr_2Cl$, $CF_3CHBrCl$, and $CBr_2Cl_2$, *J. Phys. Chem.*, *102*, 1976-1986, 1998.

Blake, D.R., N.J. Blake, T.W. Smith, Jr., O.W. Wingenter, and F.S. Rowland, Nonmethane hydrocarbon and halocarbon distributions during Atlantic Stratocumulus Transition Experiment/Marine Aerosol and Gas Exchange, June 1992, *J. Geophys. Res.*, *101*, 4501-4514, 1996.

Blake, N.J., D.R. Blake, B.C. Sive, T.-Y. Chen, F.S. Rowland, J.E. Collins, Jr., G.W. Sachse, and B.E. Anderson, Biomass burning emissions and vertical distribution of atmospheric methyl halides and other reduced carbon gases in the south Atlantic region, *J. Geophys. Res.*, *101*, 24151-24164, 1996.

Blake, N.J., D.R. Blake, T.-Y. Chen, J.E. Collins, Jr., G.W. Sachse, B.E. Anderson, and F.S. Rowland, Distribution and seasonality of selected hydrocarbons and halocarbons over the Western Pacific basin during PEM-West A and PEM-West B, *J. Geophys. Res.*, *102*, 28315-28331, 1997.

Blake, N.J., D.R. Blake, O.W. Wingenter, B.C. Sive, C.H. Kang, D.C. Thornton, A.R. Bandy, E. Atlas, F. Flocke, J.M.Harris, and F.S. Rowland, Aircraft measurements of the latitudinal, vertical, and seasonal variations of NMHCs, methyl nitrate, methyl halides and DMS during ACE-1, *J. Geophys. Res.*, submitted, 1998.

Bloomfield, P., M. Heimann, M. Prather, and R. Prinn, Inferred lifetimes, Chapter 3 in *Report on Concentrations, Lifetimes, and Trends of CFCs, Halons, and Related Species*, edited by J.A. Kaye, S.A. Penkett, and F.M. Ormond, NASA Reference Publication 1339, National Aeronautics and Space Administration, Washington, D.C., 1994.

Bogan, D.J., R.P. Thorne, F.L. Nesbitt, and L.J. Stief, Experimental 300 K measurement of the rate constant of the reaction OH + BrO → products, *J. Phys. Chem.*, *100*, 14383-14389, 1996.

Bottenheim, J.W., L.A. Barrie, E. Atlas, L.E. Heidt, H. Wiki, R.A. Rasmussen, and P.B. Shepson, Depletion of lower tropospheric ozone during Arctic spring: The Polar Sunrise Experiment, 1988, *J. Geophys. Res.*, *95*, 18555-18568, 1990.

Boutonnet, J.-C., P. Bingham, D. Calamari, C. de Rooij, J. Franklin, T. Kawano, J.-M. Libre, A. McCulloch, G. Malinverno, M. Odom, G.M. Rusch, K. Smythe, I. Sobolev, R. Thompson, and J. Tiedje, Environmental risk assessment of trifluoroacetic acid, *Hum. Ecol. Risk Assess.*, in press, 1998.

Butler, J.H., The potential role of the ocean in regulating atmospheric $CH_3Br$, *Geophys. Res. Lett.*, *21*, 185-188, 1994.

Butler, J.H., Methyl bromide under scrutiny, *Nature*, *376*, 469-470, 1995.

Butler, J.H., Scientific uncertainties in the budget of atmospheric methyl bromide, *Atmos. Environ.*, *30*, R1-R3, 1996.

Butler, J.H., and J.M. Rodríguez, Methyl bromide in the atmosphere, Chapter 2 in *The Methyl Bromide Issue*, edited by C. Bell, N. Price, and B. Chakrabarti, pp. 27-90, John Wiley and Sons, Ltd., London, 1996.

Butler, J.H., J.W. Elkins, T.M. Thompson, B.D. Hall, T.H. Swanson, and V. Koropalov, Oceanic consumption of $CH_3CCl_3$: Implications for tropospheric OH, *J. Geophys. Res.*, *96*, 22347-22355, 1991.

Butler, J.H., J.M. Lobert, S.A. Yvon, and L.S. Geller, The distribution and cycling of halogenated trace gases between atmosphere and ocean, in *The Expedition Antarktis XII of RV "Polarstern" in 1994/95, Reports of Legs ANT XII/1 and 2*, edited by G. Kattner and K. Fütterer, pp. 27-40, Alfred Wegener Institute for Polar and Marine Research, Bremerhaven, Germany, 1995.

Butler, J.H., S.A. Montzka, A.D. Clarke, J.M. Lobert, and J.W. Elkins, Growth and distribution of halons in the atmosphere, *J. Geophys. Res.*, *103*, 1503-1511, 1998.

Carlotti, M., P.A.R. Ade, B. Carli, P. Ciarpallini, U. Cortesi, M.J. Griffin, G. Lepri, F. Mencaraglia, A.G. Murray, I.G. Nolt, J.H. Park, and J.V. Radostitz, Measurement of stratospheric HBr using high resolution far infrared spectroscopy, *Geophys. Res. Lett.*, *22*, 3207-3210, 1995.

Chameides, W.L., and D.D. Davis, Iodine: Its possible role in tropospheric photochemistry, *J. Geophys. Res.*, *85*, 7383-7398, 1980.

Chappellaz, J., T. Blunier, S. Kints, A. Dallenbach, J.-M. Barnola, J. Schwander, D. Raynaud, and B. Stauffer, Changes in the atmospheric $CH_4$ gradient between Greenland and Antarctica during the Holocene, *J. Geophys. Res.*, *102*, 15987-15997, 1997.

Chartrand, D.J., and J.C. McConnell, Evidence for HBr reduction due to minor channel branching at mid-latitudes, *Geophys. Res. Lett.*, *25*, 55-58, 1998.

Chen, L., Y. Makide, and T. Tominaga, Distribution and trend of chlorodifluoromethane (HCFC-22) in the atmosphere, *Chem. Lett.*, (12), 2423-2426, 1994.

Chen, T.-Y., D.R. Blake, and F.S. Rowland, Estimation of global vehicular methyl bromide emission: Extrapolation from a case study in Santiago, Chile, *Geophys. Res. Lett.*, submitted, 1998.

Chipperfield, M.P., D.E. Shallcross, and D.J. Lary, A model study of the potential role of the reaction BrO+OH in the production of stratospheric HBr, *Geophys. Res. Lett.*, *24*, 3025-3028, 1997.

Cicerone, R.J., L.E. Heidt, and W.H. Pollock, Measurements of atmospheric methyl bromide and bromoform, *J. Geophys. Res.*, *93*, 3745-3749, 1988.

Class, T., and K. Ballschmiter, Chemistry of organic traces in air V: Determination of halogenated C1-C2 hydrocarbons in clean marine air and ambient continental air and rain by high resolution gas chromatography using different stationary phases, *Fresenius Z. Anal. Chem.*, *325*, 1-7, 1986a.

Class, T., and K. Ballschmiter, Chemistry of organic traces in air VI: Distribution of chlorinated C1-C4 hydrocarbons in air over the northern and southern Atlantic Ocean, *Chemosphere*, *15*, 413-427, 1986b.

Class, T., and K. Ballschmiter, Atmospheric halocarbons: Global budget estimations of tetrachloride, 1,2-dichloroethane, 1,1,1,2-dichloroethane, hexachloroethane and hexachlorobutadiene, *Fresenius Z. Anal. Chem.*, *327*, 198-204, 1987.

Class, T., and K. Ballschmiter, Chemistry of organic traces in air VIII: Sources and distribution of bromo- and bromochloromethanes in marine air and surface waters of the Atlantic Ocean, *J. Atmos. Chem.*, *15*, 429-436, 1988.

Class, T., R. Kohnle, and K. Ballschmiter, Chemistry of organic traces in air VII: Bromo- and bromochloromethanes in air over the Atlantic Ocean, *Chemosphere*, *15*, 429-436, 1986.

Colman, J.J., D.R. Blake, and F.S. Rowland, The atmospheric residence time of $CH_3Br$ estimated from the Junge spatial variability relationship, *Science*, in press, 1998.

Connell, T.L., S.B. Joye, L.G. Miller, and R.S. Oremland, Bacterial oxidation of methyl bromide in Mono Lake, California, *Environ. Sci. Technol.*, *31*, 1489-1495, 1997.

Crutzen, P.J., L.E. Heidt, J.P. Krasnec, W.H. Pollock, and W. Seiler, Biomass burning as a source of atmospheric trace gases CO, $H_2$, $N_2O$, $CH_3Cl$, and COS, *Nature*, *282*, 253-256, 1979.

Crutzen, P.J., N.F. Elansky, M. Hahn, G.S. Golitsyn, C.A.M. Brenninkmeijer, D.H. Scharffe, I.B. Belikov, M. Maiss, P. Bergamaschi, T. Röckmann, A.M. Grisenko, and V.M. Sevostyanov, Trace gas measurements between Moscow and Vladivostok using the Trans-Siberian Railroad, *J. Atmos. Chem.*, *29*, 179-194, 1998.

Cunnold, D.M., R.F. Weiss, R.G. Prinn, D. Hartley, P.G. Simmonds, P.J. Fraser, B. Miller, F.N. Alyea, and L. Porter, GAGE/AGAGE measurements indicating reductions in global emissions of $CCl_3F$ and $CCl_2F_2$ in 1992-1994, *J. Geophys. Res.*, *102*, 1259-1269, 1997.

Davis, D., J. Crawford, S. Liu, S. McKeen, A. Bandy, D. Thornton, F. Rowland, and D. Blake, Potential impact of iodine on tropospheric levels of ozone and other critical oxidants, *J. Geophys. Res.*, *101*, 2135-2147, 1996.

DeBruyn, W.J., and E.S. Saltzman, Diffusivity of methyl bromide in water, *Mar. Chem.*, *57*, 55-59, 1997a.

DeBruyn, W.J., and E.S. Saltzman, The solubility of methyl bromide in pure water, 35% sodium chloride and seawater, *Mar. Chem.*, *56*, 51-57, 1997b.

DeMore, W.B., S.P. Sander, D.M. Golden, R.F. Hampson, M.J. Kurylo, C.J. Howard, A.R. Ravishankara, C.E. Kolb, and M.J. Molina, *Chemical Kinetics and Photochemical Data for Use in Stratospheric Modeling, Evaluation Number 12*, JPL Publication 97-4, NASA Jet Propulsion Laboratory, Pasadena, Calif., 1997.

Derwent, R.G., P.G. Simmonds, S. O'Doherty, and D.B. Ryall, The impact of the Montreal Protocol on halocarbon concentrations in Northern Hemisphere baseline and European air masses at Mace Head, Ireland over a ten year period from 1987-1996, *Atmos. Environ.*, *32*, 3689-3702, 1998.

Dlugokencky, E.J., L.P. Steele, P.M. Lang, and K.A. Masarie, The growth rate and distribution of atmospheric methane, *J. Geophys. Res.*, *99*, 17021-17043, 1994a.

Dlugokencky, E.J., K.A. Masarie, P.M. Lang, P.P. Tans, L.P. Steele, and E.G. Nisbet, A dramatic decrease in the growth rate of atmospheric methane in the Northern Hemisphere during 1992, *Geophys. Res. Lett.*, *21*, 45-48, 1994b.

Dlugokencky, E.J., E.G. Dutton, P.C. Novelli, P.P. Tans, K.A. Masarie, K.O. Lantz, and S. Madronich, Changes in $CH_4$ and CO growth rates after the eruption of Mt. Pinatubo and their link with changes in tropical tropospheric UV flux, *Geophys. Res. Lett.*, *23*, 2761-2764, 1996.

Dlugokencky, E.J., K.A. Masarie, P.M. Lang, and P.P. Tans, Continuing decline in the growth rate of atmospheric methane, *Nature*, *393*, 447-450, 1998.

Drummond, J.R., Measurement Of Pollution In The Troposphere (MOPITT), in *The Use of EOS for Studies of Atmospheric Physics*, edited by J. Gille and G. Visconti, pp. 77-101, North Holland, 1992.

Elkins, J.W., J.H. Butler, T.M. Thompson, S.A. Montzka, R.C. Myers, J.M. Lobert, S. Yvon, P.R. Wamsley, F.L. Moore, J.M. Gilligan, D.F. Hurst, A.D. Clarke, T.H. Swanson, C.M. Volk, L.T. Lock, L.S. Geller, G.S. Dutton, R.M. Dunn, M.F. Dicorelto, T.J. Baring, and A.H. Hayden, Nitrous oxide and halocompounds, Chapter 5 in *Climate Monitoring and Diagnostics Laboratory No. 23 — Summary Report 1994-1995*, edited by D.J. Hofmann, J.T. Peterson, and R.M. Rosson, pp. 84-111, U.S. Dept. of Commerce, Boulder, 1996.

King, D.B., and E.S. Saltzman, Removal of methyl bromide in coastal seawater: Chemical and biological rates, *J. Geophys. Res.*, *102*, 18715-18721, 1997.

Ko, M.K.W., N.D. Sze, C.J. Scott, and D.K. Weisenstein, On the relation between stratospheric chlorine/bromine loading and short-lived tropospheric source gases, *J. Geophys. Res.*, *102*, 25507-25517, 1997.

Ko, M.K.W., N.D. Sze, C. Scott, J.M. Rodríguez, D. Weisenstein, and S.P. Sanders, The ozone depletion potential of $CH_3Br$, *J. Geophys. Res.*, in press, 1998.

Koppmann, R., F.J. Johnen, C. Plass-Dulmer, and J. Rudolph, Distribution of methylchloride, dichloromethane, trichloroethene and tetrachloroethene over the North and South Atlantic, *J. Geophys. Res.*, *98*, 20517-20526, 1993.

Kotamarthi, V.R., J.M. Rodríguez, M.K.W. Ko, T.K. Tromp, N.D. Sze, and M.J. Prather, Trifluoroacetic acid from degradation of HCFCs and HFCs: A three-dimensional modeling study, *J. Geophys. Res.*, *103*, 5747-5758, 1998.

Kourtidis, K., R. Borchers, and P. Fabian, Dibromomethane ($CH_2Br_2$) measurements at the upper troposphere and lower stratosphere, *Geophys. Res. Lett.*, *23*, 2581-2583, 1996.

Kourtidis, K., R. Borchers, and P. Fabian, Vertical distribution of methyl bromide in the stratosphere, *Geophys. Res. Lett.*, *25*, 505-508, 1998.

Lal, S., R. Borchers, P. Fabian, P.K. Patra, and B.H. Subbaraya, Vertical distribution of methyl bromide over Hyderabad, India, *Tellus*, *46B*, 373-377, 1994.

Langenfelds, R.L., P.J. Fraser, R.J. Francey, L.P. Steele, L.W. Porter, and C.E. Allison, The Cape Grim Air Archive: The first seventeen years, 1978-1995, in *Baseline Atmospheric Program Australia 1994-95*, edited by R.J. Francey, A.L. Dick, and N. Derek, pp. 53-70, Bureau of Meteorology and CSIRO Division of Atmospheric Research, Melbourne, Australia, 1996a.

Langenfelds, R.L., R.J. Francey, L.P. Steele, P.J. Fraser, S.A. Coram, M.R. Hayes, D.J. Beardsmore, M.P. Lucarelli, and F.R. de Silva, Improved vertical sampling of the trace gas composition of the troposphere above Cape Grim since 1991, in *Baseline Atmospheric Program Australia 1993*, edited by R.J. Francey, A.L. Dick, and N. Derek, pp. 46-57, Bureau of Meteorology and CSIRO Division of Atmospheric Research, Melbourne, Australia, 1996b.

Langer, S., B.T. McGovney, B.J. Finlayson-Pitts, and R.M. Moore, The dimethyl sulfide reaction with atomic chlorine and its implications for the budget of methyl chloride, *Geophys. Res. Lett.*, *13*, 1661-1664, 1996.

Larichev, M., F. Maguin, G. LeBras, and G. Poulet, Kinetics and mechanism of the $BrO+HO_2$ reaction, *J. Phys. Chem.*, *99*, 15911-15918, 1995.

Lee, J.M., W.T. Sturges, S.A. Penkett, D.E. Oram, U. Schmidt, A. Engel, and R. Bauer, Observed stratospheric profiles and stratospheric lifetimes of HCFC-141b and HCFC-142b, *Geophys. Res. Lett.*, *22*, 1369-1372, 1995.

Lee, J.M., S.C. Doney, G.P. Brasseur, and J.-F. Müller, A global 3-D coupled atmosphere-ocean model of methyl bromide, *J. Geophys. Res.*, submitted, 1998.

Lobert, J.M., J.H. Butler, T.J. Baring, R.C. Myers, S.A. Montzka, and J.W. Elkins, *OAXTC 92: Ocean/Atmosphere Exchange of Trace Compounds 1992*, National Oceanic and Atmospheric Administration, Tech. Memo. ERL CMDL-9, Boulder, Colo. 1995a.

Lobert, J.M., J.H. Butler, S.A. Montzka, L.S. Geller, R.C. Myers, and J.W. Elkins, A net sink for atmospheric $CH_3Br$ in the east Pacific Ocean, *Science*, *267*, 1002-1005, 1995b.

Lobert, J.M., J.H. Butler, L.S. Geller, S.A. Yvon, S.A. Montzka, R.C. Myers, A.D. Clarke, and J.W. Elkins, *BLAST 94: Bromine Latitudinal Air/Sea Transect, 1994, Report on Oceanic Measurements of Methyl Bromide and Other Compounds*, National Oceanic and Atmospheric Administration, Environmental Research Laboratories, Boulder, Colo. 1996.

Lobert, J.M., S.A. Yvon-Lewis, J.H. Butler, S.A. Montzka, and R.C. Myers, Undersaturation of $CH_3Br$ in the Southern Ocean, *Geophys. Res. Lett.*, *24*, 171-172, 1997.

Mahieu, E., R. Zander, L. Delbouille, P. Demoulin, G. Roland, and C. Servais, Observed trends in total vertical column abundances of atmospheric gases from IR solar spectra recorded at the Jungfraujoch, *J. Atmos. Chem.*, *28*, 227-243, 1997.

Majewski, M.S., M.M. McChesney, J.E. Woodrow, J.H. Pruger, and J.N. Seiber, Aerodynamic measurements of methyl bromide volatilization from tarped and nontarped fields, *J. Environ. Qual.*, *24*, 742-752, 1995.

Manning, M.R., C.A.M. Brenninkmeijer, and W. Allan, Atmospheric carbon monoxide budget of the Southern Hemisphere: Implications of $^{13}C/^{12}C$ measurements, *J. Geophys. Res.*, *102*, 10673-10682, 1997.

Manö, S., and M.O. Andreae, Emission of methyl bromide from biomass burning, *Science*, *263*, 1255-1258, 1994.

Matsueda, H., and H.Y. Inoue, Measurements of atmospheric $CO_2$ and $CH_4$ using a commercial airliner from 1993 to 1994, *Atmos. Environ.*, *30*, 1647-1655, 1996.

Matsueda, H., H.Y. Inoue, M. Ishii, and Y. Nogi, Atmospheric methane over the North Pacific from 1987 to 1993, *Geochem. J.*, *30*, 1-15, 1996.

Matsueda, H., H.Y. Inoue, Y. Sawa, Y. Tsutsumi, and M. Ishii, Carbon monoxide in the upper troposphere over the western Pacific between 1993 and 1996, *J. Geophys. Res.*, in press, 1998.

MBGC (Methyl Bromide Global Coalition), *Methyl Bromide Annual Production and Sales for the Years 1984-1992*, Grant Thornton, Washington, D.C., 1994.

McConnell, O., and W. Fenical, Halogen chemistry of the red alga Asparagopsis, *Phytochemistry*, *16*, 367-374, 1977.

McCulloch, A., Sources of hydrochlorofluorocarbons, hydrofluorocarbons and fluorocarbons and their potential emissions during the next 25 years, *Environ. Mon. Assess.*, *31*, 167-174, 1994.

McCulloch, A., and P.M. Midgley, The production and global distribution of emissions of trichloroethene, tetrachloroethene and dichloromethane over the period 1988-1992, *Atmos. Environ.*, *30*, 601-608, 1996.

Mellouki, A., R.K. Talukdar, and C.J. Howard, Kinetics of the reactions of HBr with $O_3$ and $HO_2$: The yield of HBr from $HO_2$ + BrO, *J. Geophys. Res.*, *99*, 22949-22954, 1994.

Midgley, P.M., and D.A. Fisher, The production and release to the atmosphere of chlorodifluoromethane (HCFC-22), *Atmos. Environ.*, *27A*, 2215-2223, 1993.

Midgley, P.M., and A. McCulloch, The production and global distribution of emissions to the atmosphere of 1,1,1-trichloroethane (methyl chloroform), *Atmos. Environ.*, *29*, 1601-1608, 1995.

Midgley, P.M., and A. McCulloch, Production, sales, and emissions of halocarbons from industrial sources, in *The Handbook of Environmental Chemistry: Reactive Halogen Compounds in the Atmosphere*, edited by P. Fabian and O.N. Singh, Springer-Verlag, Heidelberg, Germany, in press, 1998.

Midgley, P.M., A. McCulloch, and P.G. Simmonds, The phase-out of methyl chloroform and the decline in tropospheric chlorine, in *Proceedings of EUROTRAC-2 Symposium '98: Transport and Chemical Transformation in the Troposphere*, edited by P.M. Borrell and P. Borrell, WITpress, Southampton, in press, 1998.

Miller, B.R., R.F. Weiss, R.G. Prinn, J. Huang, and P.J. Fraser, Atmospheric trend and lifetime of chlorodifluoromethane (HCFC-22) and the global tropospheric OH concentration, *J. Geophys. Res.*, in press, 1998.

Miller, L.G., T.L. Connell, J.R. Guidetti, and R.S. Oremland, Bacterial oxidation of methyl bromide in fumigated agricultural soils, *Appl. Environ. Microbiol.*, *63*, 4346-4354, 1997.

Montzka, S.A., R.C. Myers, J.H. Butler, J.W. Elkins, and S.O. Cummings, Global tropospheric distribution and calibration scale of HCFC-22, *Geophys Res. Lett.*, *20*, 703-706, 1993.

Montzka, S.A., R.C. Myers, J.H. Butler, and J.W. Elkins, Early trends in the global tropospheric distribution of hydrofluorocarbon-141b and -142b, *Geophys. Res. Lett.*, *21*, 2483-2486, 1994.

Montzka, S.A., J.H. Butler, R.C. Myers, T.M. Thompson, T.H. Swanson, S.D. Clarke, L.T. Lock, and J.W. Elkins, Decline in the tropospheric abundance of halogen from halocarbons: Implications for stratospheric ozone depletion, *Science*, *272*, 1318-1322, 1996a.

Montzka, S.A., R.C. Myers, J.H. Butler, J.W. Elkins, L.T. Lock, A.D. Clarke, and A.H. Goldstein, Observations of HFC-134a in the remote troposphere, *Geophys. Res. Lett.*, *23*, 169-172, 1996b.

Moore, R.M., and M. Webb, The relationship between methyl bromide and chlorophyll a in high-latitude ocean waters, *Geophys. Res. Lett.*, *23*, 2951-2954, 1996.

Moore, R.M., and O.C. Zafiriou, Photochemical production of methyl iodide seawater, *J. Geophys. Res.*, *99*, 16415-16420, 1994.

Serca, D., A. Günther, L. Klinger, D. Helmig, D. Hereid, and P. Zimmerman, Methyl bromide deposition to soils, *Atmos. Environ.*, *32*, 1581-1586, 1998.

Sherlock, V. J., N.B. Jones, W.A. Matthews, F.J. Murcray, R.D. Blatherwick, D.G. Murcray, A. Goldman, C.P. Rinsland, C. Bernardo, and D.W.T. Griffith, Increase in the vertical column abundance of HCFC-22 ($CHClF_2$) above Lauder, New Zealand, between 1985 and 1994, *J. Geophys. Res.*, *102*, 8861-8865, 1997.

Shirai, T., and Y. Makide, Rapidly increasing concentrations of CFC alternatives (HFC-134a, HCFC-141b, and HCFC-142b) in the atmosphere as observed in Hokkaido and Antarctica, *Chem. Lett.*, *4*, 357-358, 1998.

Shorter, J.H., C.E. Kolb, P.M. Crill, R.A. Kerwin, R.W. Talbot, M.E. Hines, and R.C. Harriss, Rapid degradation of atmospheric methyl bromide in soils, *Nature*, *377*, 717-719, 1995.

Simmonds, P.G., R.G. Derwent, A. McCulloch, S. O'Doherty, and A. Gaudry, Long-term trends in concentrations of halocarbons and radiatively active trace gases in Atlantic and European air masses monitored at Mace Head, Ireland from 1987-1994, *Atmos. Environ.*, *30*, 4041-4063, 1996.

Simmonds, P.G., S. O'Doherty, J. Huang, R. Prinn, R.G. Derwent, D. Ryall, G. Nickless, and D. Cunnold, Calculated trends and the atmospheric abundance of 1,1,1,2-tetrafluoroethane, 1,1-dichloro-1-fluoroethane, and 1-chloro-1,1,-difluoroethane using automated in-situ gas chromatography-mass spectrometry measurements recorded at Mace Head, Ireland, from October 1994 to March 1997, *J. Geophys. Res.*, *103*, 16029-16037, 1998a.

Simmonds, P.G., R.G. Derwent, M. Bassford, S. O'Doherty, C. Jensen, D. Ryall, and G. Nickless, Measurements of methyl bromide at Mace Head, Ireland: Implications for the budget of methyl bromide, *J. Geophys. Res.*, submitted, 1998b.

Singh, H.B., L.J. Salas, and R.E. Stiles, Methyl halides in and over the eastern Pacific (40°N-32°S), *J. Geophys. Res.*, *88*, 3684-3690, 1983.

Singh, H.B., A.N. Thakur, Y.E. Chen, and M. Kanakidou, Tetrachloroethylene as an indicator of low Cl atom concentrations in the troposphere, *Geophys. Res. Lett.*, *23*, 1529-1532, 1996.

Solomon, S., and D.L. Albritton, Time-dependent ozone depletion potentials for short- and long-term forecasts, *Nature*, *357*, 33-37, 1992.

Solomon, S., R.R. Garcia, and A.R. Ravishankara, On the role of iodine in ozone depletion, *J. Geophys. Res.*, *99*, 20491-20499, 1994.

Steele, L.P., R.L. Langenfelds, M.P. Lucarelli, P.J. Fraser, L.N. Cooper, D.A. Spencer, S. Chea, and K. Broadhurst, Atmospheric methane, carbon dioxide, carbon monoxide, hydrogen, and nitrous oxide from Cape Grim flask air samples analysed by gas chromatography, in *Baseline Atmospheric Program Australia 1994-95*, edited by R.J. Francey, R.J., A.L. Dick, and N. Derek, pp. 107-110, Bureau of Meteorology and CSIRO Division of Atmospheric Research, Melbourne, Australia, 1996.

Sturges, W.T., Halocarbons in the Arctic and Antarctic atmosphere, in *The Tropospheric Chemistry of Ozone in the Polar Regions*, edited by H. Niki and K.H. Becker, pp. 117-130, Springer-Verlag, Berlin, 1993.

Sturges, W.T., G.F. Cota, and P.T. Buckley, Bromoform emission from Arctic ice algae, *Nature*, *358*, 660-662, 1992.

Sturges, W.T., C.W. Sullivan, R.C. Schnell, L.E. Heidt, and W.H. Pollock, Bromoalkane production by Antarctic ice algae, *Tellus*, *45B*, 120-126, 1993.

Thomas, V.M., J.A. Bedford, and R.J. Cicerone, Bromine emissions from leaded gasoline, *Geophys. Res. Lett.*, *24*, 1371-1374, 1997.

Tohjima, Y., S. Maksyutov, T. Machida, and G. Inoue, Airborne measurements of atmospheric methane over oil fields in western Siberia, *Geophys. Res. Lett.*, *23*, 1621-1624, 1996.

UNEP (United Nations Environment Programme), *Montreal Protocol on Substances that Deplete the Ozone Layer: Reporting of the Technology and Economic Assessment Panel*, March, 1995.

UNEP (United Nations Environment Programme), *Production and Consumption of Ozone Depleting Substances 1986-1995*, Ozone Secretariat, Nairobi, Kenya, 1997.

Volk, C.M., J.W. Elkins, D.W. Fahey, G.S. Dutton, J.M. Gilligan, M. Loewenstein, J.R. Podolske, K.R. Chan, and M.R. Gunson, Evaluation of source gas lifetimes from stratospheric observations, *J. Geophys. Res.*, *102*, 25543-25564, 1997.

Wamsley, P.R., J.W. Elkins, D.W. Fahey, G.S. Dutton, C.M. Volk, R.C. Myers, S.A. Montzka, J.H. Butler, A.D. Clarke, P.J. Fraser, L.P. Steele, M.P. Lucarelli, E.L. Atlas, S.M.Schauffler, D.R. Blake, F.S. Rowland, W.T. Sturges, J.M. Lee, S.A. Penkett, A. Engel, R.M. Stimpfle, K.R. Chan, D.K. Weisenstein, M.K.W. Ko, and R.J. Salawitch, Distribution of Halon-1211 in the upper troposphere and lower stratosphere and the 1994 total bromine budget, *J. Geophys. Res.*, *103*, 1513-1526, 1998.

Wang, C.J.-L., D.R. Blake, and F.S. Rowland, Seasonal variations in the atmospheric distribution of a reactive chlorine compound, tetrachloroethene ($CCl_2 = CCl_2$), *Geophys. Res. Lett.*, *9*, 1097-1100, 1995.

Wang, D., S.R. Yates, F.F. Ernst, J. Gan, F. Gao, and O.J. Becker, Methyl bromide emission reduction with field management practices, *Environ. Sci. Technol.*, *31*, 3017-3022, 1997a.

Wang, D., S.R. Yates, F.F. Ernst, J. Gan, and W.A. Jury, Reducing methyl bromide emission with high-barrier film and reduced dosage, *Environ. Sci. Technol.*, *31*, 3686-3691, 1997b.

Watling, R., and D.B. Harper, Chloromethane production by wood-rotting fungi and an estimate of the global flux to the atmosphere, *Mycolog. Res.*, in press, 1998.

Weidmann, T.O., B. Guthner, T.J. Class, and K. Ballschmiter, Global distribution of tetrachloroethene in the troposphere: Measurements and modeling, *Environ. Sci. Technol.*, *28*, 2321-2329, 1994.

Wennberg, P.O., J.W. Brault, T.F. Hanisco, R.J. Salawitch, and G.H. Mount, The atmospheric column abundance of IO: Implications for stratospheric ozone, *J. Geophys. Res.*, *102*, 8887-8898, 1997.

Wingenter, O.W., C.J.-L. Wang, D.R. Blake, and F.S. Rowland, Seasonal variations of tropospheric methyl bromide concentrations: Constraints on anthropogenic input, *Geophys. Res. Lett.*, in press, 1998.

WMO (World Meteorological Organization), *Scientific Assessment of Ozone Depletion: 1994*, Global Ozone Research and Monitoring Project—Report No. 37, Geneva, 1995.

Woodrow, J.E., J.S. LeNoir, and J.S. Seiber, Soil as a terrestrial sink for methyl bromide fumigant: Preliminary results, *Chemosphere*, *35*, 2543-2551, 1997.

Wuebbles, D.J., A.K. Jain, K.O. Patten, and P.S. Connell, Evaulation of ozone depletion potentials for chlorobromomethane ($CH_2ClBr$) and 1-bromopropane ($CH_2BrCH_2CH_3$), *Atmos. Environ.*, *32*, 107-113, 1998.

Yagi, K., J. Williams, N.-Y. Wang, and R.J. Cicerone, Atmospheric methyl bromide ($CH_3Br$) from agricultural soil fumigations, *Science*, *267*, 1979-1981, 1995.

Yates, S.R., F.F. Ernst, J. Gan, F. Gao, and M.V. Yates, Methyl bromide emissions from a covered field: II, Volatilization, *J. Environ. Qual.*, *25*, 192-202, 1996a.

Yates, S.R., J. Gan, F.F. Ernst, A. Mutziger, and M.V. Yates, Methyl bromide emissions from a covered field: I, Experimental conditions and degradation in soil, *J. Environ. Qual.*, *25*, 184-192, 1996b.

Yates, S.R., J. Gan, F.F. Ernst, and D. Wang, Methyl bromide emissions from a covered field: III, Correcting chamber flux for temperature, *J. Environ. Qual.*, *25*, 892-898, 1996c.

Yates, S.R., J. Gan, D. Wang, and F.F. Ernst, Methyl bromide emissions from agricultural fields: Bare-soil deep injection, *Environ. Sci. Technol.*, *31*, 1136-1143, 1997.

Yates, S.R., D. Wang, J. Gan, F.F. Ernst, and W.A. Jury, Minimizing methyl bromide emissions from soil fumigation, *Geophys. Res. Lett.*, *25*, 1633-1636, 1998.

Yokouchi, Y., H. Akimoto, L.A. Barrie, J.W. Bottenheim, K. Anlauf, and B.T. Jobson, Serial gas chromatographic/mass spectrometric measurements of some volatile organic compounds in the Arctic atmosphere during the 1992 Polar Sunrise Experiment, *J. Geophys. Res.*, *99*, 25379-25389, 1994.

Yokouchi, Y., L.A. Barrie, D. Toom, and H. Akimoto, The seasonal variation of selected natural and anthropogenic halocarbons in the Arctic troposphere, *Atmos. Environ.*, *30*, 1723-1727, 1996.

Yokouchi, Y., H. Mukai, H. Yamamoto, A. Otsuki, C. Saitoh, and Y. Nojiri, Distribution of methyl iodide, ethyl iodide, bromoform, and dibromoethane over the ocean (east and southeast Asian seas and the western Pacific), *J. Geophys. Res.*, *102*, 8805-8809, 1997.

## SCIENTIFIC SUMMARY

Much progress has been made recently in our understanding of the two major classes of stratospheric particles: stratospheric sulfate aerosol (SSA), and polar stratospheric clouds (PSCs). Thermodynamic models have provided a clearer picture of particle behavior at low temperatures, while a richer and longer measurement suite has increased our knowledge of particle formation processes, the dispersal and decay of volcanic SSA, and particle climatology.

- There is no clear trend in background SSA from 1979 to 1997. SSA levels in late 1997 were below those observed before the 1991 Mt. Pinatubo eruption and are likely still decreasing. Hence, any anthropogenic contribution to the SSA layer must be smaller than previously estimated from observed changes from 1979 to 1989. Peak aerosol scattering ratios in 1997 were about 40% greater than those observed during 1979, but due to uncertainties and natural variability in the measurements, this difference must be viewed with caution at present.

- It is not clear that the 1979 minimum SSA period was truly free of volcanic influence. Recent model calculations of SSA production from known tropospheric sulfur sources significantly underestimate the 1979 observations. Other non-volcanic sources are thought to be insignificant.

- Post-volcanic SSA decay varies with time, space, and aerosol property. The $e^{-1}$ decay time for column backscatter following the eruption of Mt. Pinatubo was about 1 year until 1994, and nearly twice as long (1.8 years) from 1994 to 1997. Derived surface areas decayed back to pre-Pinatubo levels in about 3.5 years at 25 km and about 5 years at 15 km. Surface area decayed 20-30% more slowly than backscatter or mass.

- PSC observations are still divided into two broad classes: Type 1 PSCs, containing nitric acid ($HNO_3$) as a major component, that form at temperatures above the water ($H_2O$) ice point; and Type 2 PSCs, containing predominantly $H_2O$ ice particles. Most of the observations of Type 1 PSCs can be subclassified as Type 1b liquid particles or Type 1a solid particles. Other types of particles have been proposed to explain some specific observations.

- It is now generally accepted that Type 1b PSCs are supercooled ternary solution (STS) droplets that form from SSA without a nucleation barrier. Type 1a PSC particles are generally interpreted as solid nitric acid trihydrate (NAT), but understanding of the phase transition mechanisms leading to their formation is still poor. Better understanding of Type 1a PSCs is needed because solid particles play a significant role in denitrification.

- Many of the Type 1b PSC observations occurred during ongoing fast synoptic cooling events, shortly after the air parcels experienced cold temperatures. Type 1a PSCs, in contrast, have been observed when synoptic temperatures were below the NAT existence temperature for several days. It now appears that theoretical models of Type 1a PSC formation may require knowledge of the air parcel thermal history.

- Mesoscale temperature fluctuations, especially over mountain ranges where such fluctuations can reach 20 K peak-to-peak, are important in PSC formation processes, particularly in the Arctic. The integral effect of such phenomena on polar ozone depletion is still unclear.

- Increases in source gases and cooling of the lower stratosphere from ozone depletion and increasing greenhouse gases favor increased formation and persistence of PSCs. However, an upward trend in PSC occurrence is not discernible in the present satellite data record due to the relatively short length of the record as well as the large variability in cloud sightings from year to year.

in the absence of a nucleation barrier, accompanied by a sharp increase in particle volume and an almost complete removal of $HNO_3$ from the gas phase. In contrast, the liquid phase, even at 193 K is still mainly $H_2SO_4$/$H_2O$. However, at lower temperatures between 193 K and 190 K, increasing solubilities enable a strong, coupled uptake of gas-phase $HNO_3$ and $H_2O$. This uptake transforms the solution within this interval from quasi-binary $H_2SO_4/H_2O$ into quasi-binary $HNO_3/H_2O$ with about 40% $HNO_3$ by weight and less than 3% $H_2SO_4$ by weight. The liquid volume grows by a factor of 10, as was observed during the flight of the National Aeronautics and Space Administration (NASA) Earth Resources-2 (ER-2) aircraft on 24 January 1989 (Dye *et al.*, 1992) (data points in Figure 3-1a). As the temperature drops further toward $T_{ice}$, the remaining $HNO_3$ is readily taken up, and the droplets grow to a total volume higher than that of NAT in equilibrium. Figure 3-1c also shows the uptake of other species that are of primary importance for heterogeneous chemistry. Type 1b clouds are highly efficient processors of halogen species (see Chapter 7). Because some field observations of Type 1 PSCs cannot be explained in terms of NAT or STS clouds in equilibrium, other metastable phases in equilibrium (Tabazadeh *et al.*, 1995) or highly nonequilibrium particles (Meilinger *et al.*, 1995; Peter, 1997) have been proposed as explanations. STS droplets or other metastable particles would not coexist for long with NAT particles because NAT particles would be expected to grow slowly at the expense of the other particles due to lower NAT saturation vapor pressures.

#### 3.1.2.3 Type 2 PSCs

It is now fairly well established that Type 2 PSCs are primarily water ice particles. Laboratory experiments (Koop *et al.*, 1995) suggest that ice nucleates inside liquid Type 1 PSC particles or on the surface of solid Type 1 PSC particles once the temperature falls to 2-4 K below $T_{ice}$. The reason for this rather well-constrained relationship between temperature and ice nucleation is the onset of strong uptake of $H_2O$ by binary or ternary solutions at these temperatures, leading to highly diluted, water-like droplets that must freeze. A supercooling of about 4 K below $T_{ice}$ has recently also been observed (Carslaw *et al.*, 1998) during the formation of mountain-wave-induced Type 2 clouds (see Sections 3.4.3 and 7.4.1).

Once formed, ice particles develop further according to well-known thermodynamics. However, despite the close coupling between temperature and ice formation, the remaining uncertainty in supercooling is still a critical issue. Whether ice formation begins at 2 K or at 4 K of supercooling determines the extent of ice cloud occurrence, particularly in the Arctic, and is also likely to influence the particle number density in individual clouds and, thus, their optical and chemical properties. This is similar to open issues in our understanding of cirrus cloud formation in the upper troposphere.

After ice nucleation from liquid ternary solution droplets, the fate of the acidic components ($HNO_3$, $H_2SO_4$) is not well known. In some particles they might freeze as NAT and SAT (Koop *et al.*, 1995, 1997), while in others some of the $HNO_3$ might partition back into the gas phase and the remaining acid might stay as a liquid coating on the ice particle (Carslaw *et al.*, 1998). Furthermore, it is not clear whether soluble species such as $HNO_3$ could be trapped within the ice matrix or to what extent such species might lead to a solid coating of ice particles, influencing their microphysical properties (see Chapter 7).

### 3.1.3 Particle Source Gases

#### 3.1.3.1 Sulfur

The predominant source of SSA in the stratosphere is strong, sulfur-rich volcanic eruptions, which are by nature highly intermittent and unpredictable. The average flux of volcanic sulfur (S) to the stratosphere over the last 200 years has been estimated to be around 1 Tg $yr^{-1}$ S, with lower and upper bounds of 0.3 and 3 Tg $yr^{-1}$ (Pyle *et al.*, 1996). A minimum flux of 0.5-1 Tg $yr^{-1}$ S for the past 9000 years has been derived from ice core sulfate data. There have been two large sulfur-rich eruptions in the last two decades: El Chichón in 1982 (3.5 Tg S) and Mt. Pinatubo in 1991 (9 Tg S).

OCS oxidation is believed to be the major nonvolcanic source of stratospheric sulfur (Crutzen, 1976). Recent estimates of this source range from 0.03 Tg $yr^{-1}$ S (Chin and Davis, 1995) to 0.049 Tg $yr^{-1}$ S (Weisenstein *et al.*, 1997). Although most OCS sources are natural, there are some indications that anthropogenic emissions of OCS may be substantial, and possibly increasing (Khalil and Rasmussen, 1984; Zander *et al.*, 1988; Hofmann, 1990a). However, historical data on industrial releases suggest that anthropogenic emissions of OCS and its precursor carbon disulfide ($CS_2$) have been relatively constant over the 1977-1992 period (Chin and Davis, 1993). Furthermore, no statistically significant

trend in lower stratospheric OCS was inferred from spaceborne observations made in 1985 and 1994 (Rinsland *et al.*, 1996).

Other surface sources of sulfur are approximately 3 orders of magnitude larger than the OCS source. Although most reduced sulfur gases other than OCS are rapidly oxidized to $SO_2$ and therefore are not expected to reach the stratosphere in large amounts, 2-D model calculations suggest that the stratospheric aerosol loading may be strongly influenced by upper tropospheric sulfur (Weisenstein *et al.*, 1997). However, large uncertainties are associated with tropospheric sulfur chemistry, tropospheric removal, vertical transport of short-lived species (Langner and Rodhe, 1991), and stratospheric-tropospheric exchange (Holton *et al.*, 1995). Such uncertainties reduce the level of confidence in model assessments of the impact of the massive surface emissions of short-lived sulfur ($CS_2$, dimethyl sulfide (DMS), hydrogen sulfide ($H_2S$), $SO_2$) on the stratosphere.

#### 3.1.3.2 Nitric Acid

Nitrous oxide ($N_2O$) is the principal precursor of stratospheric reactive nitrogen ($NO_y$) and hence of $HNO_3$. Anthropogenic emissions of $N_2O$ stem primarily from agricultural sources and are about half as large as natural emissions. The rate of $NO_y$ production from $N_2O$ oxidation is approximately 0.5-1 Tg $yr^{-1}$ N (Kasibhatla *et al.*, 1991; WMO, 1995; Vitt and Jackman, 1996). $N_2O$ concentrations are increasing at a rate of about 0.25% $yr^{-1}$ (WMO, 1995; IPCC, 1996). Lightning may also be another significant, though uncertain, source of nitrogen in the tropical lower stratosphere (Kotamarthi *et al.*, 1994).

#### 3.1.3.3 Water Vapor

The main sources of $H_2O$ to the stratosphere are thought to be injection through the tropical tropopause and in situ production from methane ($CH_4$) oxidation (Harries *et al.*, 1996). Stratospheric-tropospheric exchange at middle and high latitudes might also be important. Direct evidence of the link between the tropical $H_2O$ distribution and the annual cycle in tropopause temperature has been provided by satellite data (Mote *et al.*, 1995, 1996). The average $H_2O$ mixing ratio of air entering the stratosphere inferred from satellite, aircraft, and balloon data ranges from 3.2 to 4.2 parts per million (ppm) (Dessler *et al.*, 1994; Abbas *et al.*, 1996; Engel *et al.*, 1996; Mote *et al.*, 1996; Remsberg *et al.*, 1996). Because, to first order, two molecules of $H_2O$ can be formed from one of $CH_4$, the quantity $H_2O + 2CH_4$ is approximately conserved over the lower and middle stratosphere at a value of 6.7 to 7.6 ppm, as shown by satellite and aircraft observations. Tropospheric $CH_4$ has been increasing at an average rate of 0.6% $yr^{-1}$ over the last 10 years (IPCC, 1996). Because production of $H_2O$ by $CH_4$ oxidation is relatively small in the lower stratosphere, any $H_2O$ trend there should be substantially smaller than the $CH_4$ trend.

A statistically significant upward trend in $H_2O$ concentration has been detected at altitudes from 16 to 26 km at northern midlatitudes from balloonborne hygrometer measurements carried out from 1981 to 1994 (Oltmans and Hofmann, 1995). The maximum trend was found to be 0.8% $yr^{-1}$ at 18-20 km. This finding is corroborated by an apparent increase in $H_2O + 2\ CH_4$ derived from a variety of measurements made since 1975 (Engel *et al.*, 1996). However, the $H_2O$ trend seems to be larger than the trend expected from the oxidation of increased $CH_4$ alone (Oltmans and Hofmann, 1995; Engel *et al.*, 1996). Nedoluha *et al.* (1998) also reported an upward trend in $H_2O$ in the stratosphere based on Halogen Occultation Experiment (HALOE) and ground-based millimeter-wave spectrometer data.

## 3.2 INSTRUMENTS

### 3.2.1 Measurement Principles

Instruments to measure SSA can be broadly divided into two categories, those that provide ensemble measurements and those that provide individual particle measurements. Ensemble measurements detect the signature of a population of particles at one instant and include passive extinction measurements, such as from the sunphotometer (Volz and Goody, 1962), and active scattering measurements, such as lidar (Fiocco and Grams, 1964). Individual measurements include those that use optical scattering to count and size single particles (Rosen, 1964; Baumgardner *et al.*, 1992) and those that use impaction to collect particles that can then be counted, sized, and chemically analyzed (Bigg, 1975; Farlow *et al.*, 1979). The range of instruments available allows for a variety of measurement platforms. Ensemble measurements are usually conducted on the ground for high temporal and vertical resolution, or from satellites for global coverage. Single-particle measurements are usually conducted using aircraft for high vertical and

horizontal resolution, or balloons for high vertical resolution and accessibility to regions of the stratosphere above aircraft altitudes.

### 3.2.2 Contemporary Data Records

Regular measurements using ground-based lidar began in the early 1970s, and some of these records extend to the present (Jäger, 1991; Osborn *et al.*, 1995; Barnes and Hofmann, 1997). Lidars provide high-vertical-resolution measurements of particle backscatter, and often depolarization ratio as well, at one or more wavelengths. Lidar sites now range in latitude from 90°S to 79°N, with a number of sites in the low to midlatitudes, and a few stations in the subtropics. Sunphotometer measurements began in the 1950s and extend to the present. Aerosol optical depth is usually measured at several wavelengths and can then be used to infer column size distributions. Long-term ground-based measurements are available from polar (Herber *et al.*, 1993) and tropical regions (Russell *et al.*, 1993a), and sunphotometers have been deployed on aircraft as well (Russell *et al.*, 1993b).

Aerosol extinction measurements from spaceborne platforms began in 1975 (Pepin *et al.*, 1977). These became routine with the launch of the autonomous limb-viewing optical extinction instruments, Stratospheric Aerosol Measurement (SAM) II and SAGE, in 1979 (McCormick *et al.*, 1979). The near-global, multi-wavelength measurements from SAGE and its successor SAGE II cover the periods 1979-1981 and 1984 to the present, respectively. The single-wavelength record from SAM II, whose spatial coverage was limited to high latitudes, extends continuously from 1978 to 1991, with intermittent data thereafter until late 1993. Satellite extinction measurements were expanded in 1991 with the launch of the Upper Atmosphere Research Satellite (UARS), carrying HALOE, which measures infrared limb extinction, and CLAES (Cryogenic Limb Array Etalon Spectrometer) and ISAMS (Improved Stratospheric and Mesospheric Sounder), which measure infrared limb emission (see *Geophysical Research Letters, Vol. 20*, No. 12, 1993). The lifetimes of CLAES and ISAMS were limited to less than two years, but HALOE is still operational. High-resolution middle-infrared measurements of extinction by Mt. Pinatubo SSA were made by the Atmospheric Trace Molecule Spectroscopy (ATMOS) instrument during a March-April 1992 Space Shuttle mission (Rinsland *et al.*, 1994). High-latitude solar occultation aerosol measurements were also made from 1993-1996 by the Polar Ozone and Aerosol Measurement (POAM) II instrument on the French SPOT (Satellite Pour l'Observation de la Terre) 3 satellite (Glaccum *et al.*, 1996). More recently there are new infrared extinction measurements available from ILAS (Improved Limb Atmospheric Spectrometer) on the Japanese ADEOS (Advanced Earth Observing Satellite) platform from August 1996 to June 1997. The nadir-viewing AVHRR (Advanced Very High Resolution Radiometer) satellite instruments measure the reflected solar radiance and infer aerosol optical thickness (Griggs, 1983). These observations have a fine horizontal resolution over oceans for tracking dense volcanic clouds but cannot provide any vertical resolution (Stowe *et al.*, 1992).

Individual particle measurements are obtained in situ with aerosol spectrometers. Spectrometers deployed on aircraft include ones with sampling volumes external to the instrument ($0.15\ \mu m < r < 10\ \mu m$) (Baumgardner *et al.*, 1992) and those with internal sampling volumes ($0.03\ \mu m < r < 1.0\ \mu m$) (Jonsson *et al.*, 1995). Particle counters carried on balloons require internal sampling volumes ($0.15\ \mu m < r < 10\ \mu m$) (Hofmann *et al.*, 1975; Hofmann and Deshler, 1991). In situ sampling is also done using impaction devices on aircraft (Pueschel *et al.*, 1989; Sheridan *et al.*, 1994) and on balloons (Sheridan *et al.*, 1992). The physical samples collected by the impaction devices are returned to the laboratory for analysis. Regular stratospheric aerosol measurements using aerosol counters carried on balloon platforms have continued since the 1970s (Hofmann, 1990a; Deshler *et al.*, 1997). Aerosol impactors carried on balloons are employed much less frequently (Bigg, 1975; Sheridan *et al.*, 1992). Stratospheric aerosol measurements using aircraft-borne aerosol spectrometers began with the investigations of polar ozone loss in 1987 and 1989 (Dye *et al.*, 1990a; Wilson *et al.*, 1992) and have continued through the eruption of Mt. Pinatubo (Jonsson *et al.*, 1996). Aerosol impactors on aircraft have been used since the late 1970s (Farlow *et al.*, 1979; Goodman *et al.*, 1994). In number concentration, a large fraction of aerosol has sizes below the minimum sizes detectable with optical instruments. To measure the concentration of these CN, diffusion chambers are placed ahead of optical counters to grow all available particles to optically detectable sizes prior to counting (Rosen and Hofmann, 1977; Wilson *et al.*, 1983). Although CN counters do not discriminate particles according to size,

laboratory tests indicate they are sensitive to particles with $r > 0.01$ μm at stratospheric pressures (Wilson *et al.*, 1983). The first regular sampling of stratospheric CN began in the mid-1970s from balloons and in the 1980s from aircraft. A balloonborne backscattersonde combines in situ methods with an ensemble measurement (Rosen and Kjome, 1991). These instruments have been used in the 1990s for regular midlatitude measurements (Rosen *et al.*, 1994a) and for seasonal Arctic measurements (Larsen *et al.*, 1997).

### 3.2.3 Derivation of Particle Characteristics

For many applications the directly measured particle properties, i.e., extinction, scattering, number, or size, are not the quantities required. In particular, heterogeneous chemical reaction rates may be a function of aerosol surface area or volume, depending on the ratio of the molecular diffusion coefficient to the molecular loss rate coefficient (Hanson *et al.*, 1994). For example, the reaction of chlorine nitrate ($ClONO_2$) with hydrochloric acid (HCl) dissolved in SSA seems to depend on aerosol volume, whereas the hydrolysis of dinitrogen pentoxide ($N_2O_5$) on SSA is fast enough that only aerosol surface area is important. At cold temperatures, particle phase is also important, because the effective uptake coefficient is smaller on solid hydrates than on liquid particles at the same temperature (Ravishankara and Hanson, 1996; Borrmann *et al.*, 1997b). Phase is also important when considering particle growth rates, because STS droplets can be quite a bit smaller than solid $HNO_3$ hydrate particles.

#### 3.2.3.1 Surface Area and Volume

Aerosol surface area and volume concentrations can be obtained from individual particle measurements either by directly integrating the measured discrete size distribution (Dye *et al.*, 1992; Pueschel *et al.*, 1992; Wilson *et al.*, 1993; Goodman *et al.*, 1994; Jonsson *et al.*, 1995) or by fitting measured particle number concentrations with an analytic size distribution function and integrating (Deshler *et al.*, 1993). The uncertainties of 30-50% estimated for surface area and volume obtained in this way arise from Poisson counting statistics at low concentrations, and from sizing errors. The sizing errors (10-20%) arise primarily from uncertainties in particle refractive index, from inhomogeneities in particle illumination, and from spectral broadening (Baumgardner *et al.*, 1992). Discrete size distributions measured simultaneously by several individual particle measurement techniques have been compared and found to agree favorably when differences in sampling technique are accounted for (Pueschel *et al.*, 1992).

Because the wavelength dependence of extinction is related to particle size (Ångström, 1908), in situ individual and remote ensemble particle measurements can be compared using Mie scattering theory. One approach is to compare satellite extinction measurements to extinctions calculated using discrete and fitted size distributions derived from particle counter data (Wilson *et al.*, 1992; Jonsson *et al.*, 1995; Hervig *et al.*, 1996). The opposite approach is to derive particle size information by inverting multi-wavelength extinction, scattering, or emission data. Twomey (1974) and Capps *et al.* (1982) concluded that extinction measurements at a few wavelengths cannot be expected to yield detailed information about the particle size distribution, but can be used to reliably estimate moments of the distribution. The inversion of multi-wavelength extinction/scattering measurements is complex, and a number of techniques have been tried (Grainger *et al.*, 1995; Yue *et al.*, 1995; Anderson and Saxena, 1996). For estimating surface area or volume using four-wavelength SAGE II extinction data, Thomason and Poole (1993) found that principal component analysis (Twomey, 1977) worked well. Uncertainties in volume and surface area estimated in this way were shown to be ~30%. Other recent estimates of surface area and volume have been made using multi-wavelength lidar data (e.g., Del Guasta *et al.*, 1994; Stein *et al.*, 1994; Gobbi, 1995; Wandinger *et al.*, 1995) and HALOE infrared extinction measurements (Hervig *et al.*, 1997). These estimates were made using empirical relationships established from Mie scattering calculations performed with a large set of observed size distributions. Uncertainties on these surface area estimates are around 30% as well.

Figure 3-2 shows comparisons of surface area and volume estimated from in situ optical particle counter data over Laramie, Wyoming (41°N), and from relevant SAGE II and HALOE satellite extinction measurements (Thomason *et al.*, 1997a; Hervig *et al.*, 1998). These comparisons show differences of roughly 50%, with the satellite estimates typically greater than the particle counter data. Another study of closure among various measurement approaches (Russell *et al.*, 1996) showed that during the 2 years following the Mt. Pinatubo eruption, the area-weighted, or effective, particle radius de-

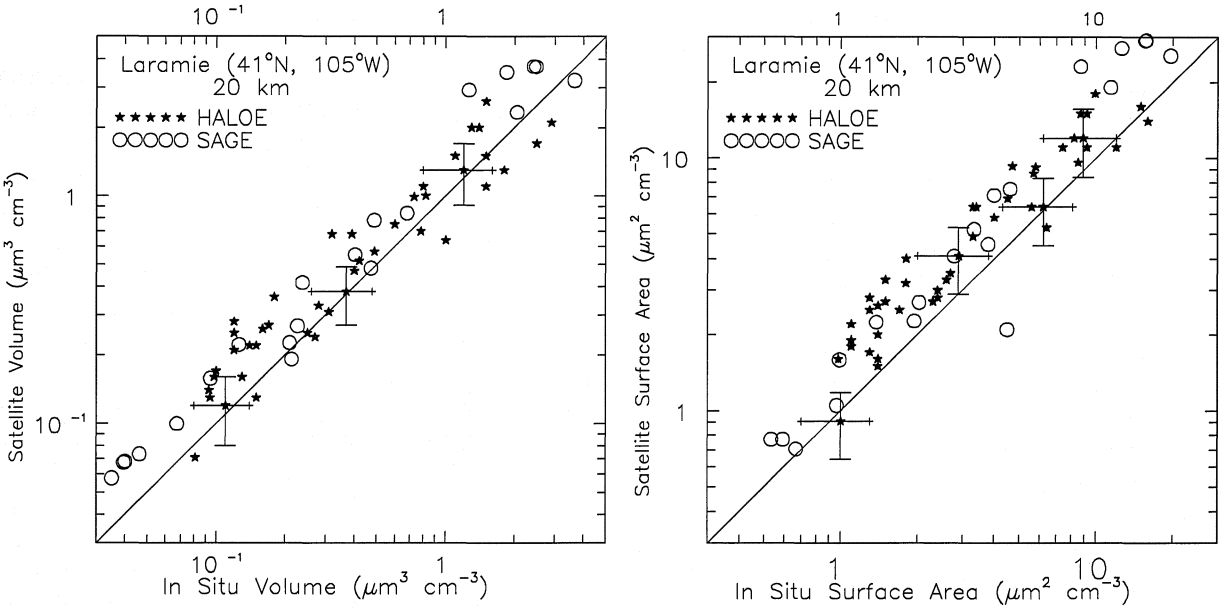


**Figure 3-2.** Volumes and surface areas inferred from satellite measurements of visible (SAGE II) and infrared (HALOE) extinction compared with balloonborne optical particle counter measurements over Laramie, Wyoming (41°N). The SAGE data are monthly medians over the 35°-45°N latitude band, while the HALOE data are chosen within a time and distance window as described in Hervig *et al.* (1997). A one-to-one agreement line and error bars of 30% are included for reference.

termined by sunphotometers, satellite instruments, airborne wire impactors, and balloonborne particle counters agreed to within roughly 25%.

#### 3.2.3.2 Phase

Information on particle phase has been obtained to date primarily from active optical scattering measurements using polarized light. Lidar is the most common instrument with this capability, although some backscattersondes have this capability as well. Linearly polarized light is transmitted, and the returned signal is measured in both the parallel-polarized and cross-polarized channels. Depolarization from an ensemble of scatterers in excess of that expected from the molecular atmosphere is an indication that non-spherical particles are present. The standard value for molecular depolarization is 1.4% (Young, 1980), although some systems with narrowband interference filters use a limit of 0.5% (Shibata *et al.*, 1997). Depolarizing aerosol may consist of a mixture of solid and liquid particles, or of solid particles with a variety of forms. Because of size-dependent polarization properties for fixed particle shape (Mischenko and Sassen, 1998), it is difficult to quantify depolarization as a measure of the non-sphericity of the scattering particles, although some attempts have been made (Flesia *et al.*, 1994; Carslaw *et al.*, 1998). Browell *et al.* (1990) were the first to report that PSCs above the frost point could be separated into two classes based on depolarization. Stefanutti *et al.* (1991) and Adriani *et al.* (1995) made similar observations in the Antarctic. Observations of depolarized signals from Mt. Pinatubo volcanic aerosol were made in the Antarctic (Gobbi and Adriani, 1993), in northern midlatitudes (Vaughan *et al.*, 1994), and in the Arctic (Toon *et al.*, 1993; Godin *et al.*, 1994; Rosen *et al.*, 1994b). The measurements by Toon *et al.* were above the Mt. Pinatubo ash layer and those by Rosen *et al.* were obtained in January 1993 after most of the volcanic ash should have been removed from the stratosphere. These observations might therefore indicate the presence of solid $H_2SO_4/H_2O$ particles (see Section 3.4 and Chapter 7).

#### 3.2.3.3 Composition

The composition of SSA was first assessed using impactors to physically collect the aerosol, which could then be sized and chemically analyzed (Junge *et al.*, 1961;

Bigg, 1975). Other early methods used heaters positioned ahead of aerosol counters to evaporate the aerosol (Rosen, 1971). Determining the temperature at which the majority of aerosol evaporated to sizes below the counter limits allowed the $H_2SO_4$-$H_2O$ composition to be estimated (Hofmann and Rosen, 1983). Both of these techniques have been used for recent measurements of Mt. Pinatubo aerosol (Sheridan *et al.*, 1992; Deshler *et al.*, 1993; Goodman *et al.*, 1994; Sheridan *et al.*, 1994) and of aerosol in the polar regions (Pueschel *et al.*, 1989; Goodman *et al.*, 1997), and to determine the volatile fraction of tropical CN (Brock *et al.*, 1995) and CN in aircraft plumes (Hofmann and Rosen, 1978; Fahey *et al.*, 1995). An alternate technique using ion mass spectrometry to analyze vaporized particles in situ and comparing the resultant $H_2SO_4$ concentrations with correlative in situ aerosol concentrations has been recently applied (Arnold *et al.*, 1998). Measurements at temperatures above 200 K are all consistent and indicate that SSA are predominantly droplets of highly concentrated $H_2SO_4$. Analyses of spaceborne infrared extinction and limb emission data on aerosols also show consistency with a concentrated $H_2SO_4$ composition (Rinsland *et al.*, 1994; Massie *et al.*, 1996).

As mentioned in Sections 3.1.2.2 and 3.1.2.3, there are still uncertainties with regard to the exact composition of PSCs. Recent approaches to determining the composition of these particles include the use of multiangle aerosol scattering devices (Baumgardner *et al.*, 1996) and comparison of nearly coincident lidar and in situ measurements (Adriani *et al.*, 1995). These methods have both been shown to be consistent when applied to the well-known SSA, and some initial results are available for Antarctic PSC measurements.

## 3.3 SSA OBSERVATIONS

Direct measurements of SSA were first made in 1957 by Junge *et al.* (1961) using balloonborne impactors. The SSA layer is often called the Junge layer in recognition of these measurements. However, the existence of the layer was suggested some 50 years earlier from twilight observations (Gruner and Kleinert, 1927). As discussed previously, systematic measurements of SSA have been made from a variety of platforms since the early 1970s.

### 3.3.1 Volcanic Aerosol

All the contemporary data records clearly illustrate the strong perturbations to SSA levels caused by sulfur-rich volcanic eruptions (Hofmann, 1990a; Jäger, 1991; Chazette *et al.*, 1995; Osborn *et al.*, 1995; Uchino *et al.*, 1995; Thomason *et al.*, 1997b). Sulfur gases in the eruption plumes are oxidized to $H_2SO_4$, which then condenses into SSA within about 2 months of an eruption. Historical records spanning the last 100 years or more suggest that the most recent 30-year period can be characterized as a relatively active volcanic period. Primarily through the use of historical pyrheliometric data, Stothers (1996) showed that eight major eruptions occurred during the past century. Four of these occurred between 1880 and 1910 (Krakatau, an unidentified eruption, Santa Maria, and Katmai) and four occurred since 1960 (Agung, Fernandina, El Chichón, and Mt. Pinatubo). Between 1910 and 1960, the stratosphere was almost undisturbed by volcanic activity. Junge's measurements of the SSA layer came at the end of this period, but the contemporary long-term records did not begin until after the start of the current volcanically active period. In terms of impact on the stratosphere, the two largest eruptions in the last 100 years were Krakatau first, and then Mt. Pinatubo (Stothers, 1996). Analyses of ice cores from Greenland permit an even longer view (Hammer *et al.*, 1980), which indicates that global volcanism has an approximate 80-year periodicity. The mid-twentieth century lull in volcanism may be the most recent manifestation of this periodicity.

#### 3.3.1.1 Dispersal of Volcanic Aerosol

The two most recent major eruptions have occurred in the tropics: El Chichón (17°N, April 1982) and Mt. Pinatubo (15°N, June 1991). However, since they occurred in different seasons and at different phases in the vertical structure of the quasi-biennial oscillation (QBO), the dispersal and decay of aerosol from the eruptions were different. A notable feature of low-latitude eruptions is the accumulation of aerosol in a tropical stratospheric reservoir (Trepte and Hitchman, 1992). This reservoir has an abrupt, narrow boundary on the winter hemisphere side and a broad boundary on the summer hemisphere side, as noted following the Mt. Pinatubo eruption (Grant *et al.*, 1996; Lambert *et al.*, 1997). Above about 20 km, detrainment of material from the tropical reservoir is related to planetary wave activity. Thus, aerosol is preferentially transported into the winter hemi-

sphere. When QBO easterly winds overlie the equator, the aerosol reservoir remains relatively isolated from midlatitudes because the penetration of planetary waves into the tropics is inhibited, and removal of aerosols from the tropics occurs on a smaller scale along the periphery of the reservoir and just above the tropopause. Such was the case immediately following eruption of both El Chichón and Mt. Pinatubo (Trepte *et al.*, 1993). When QBO westerly winds are prevalent over the tropics, planetary waves can propagate deeper into the tropics and more easily transport aerosol poleward from the tropical reservoir. A large increase in aerosol loading from the El Chichón eruption was observed in the Northern Hemisphere during the autumn of 1982 after the equatorial stratosphere had made the transition to the westerly phase of the QBO (Pollack *et al.*, 1983).

The secondary circulation in the tropics associated with the QBO also has a strong influence on the dispersal of aerosols to higher latitudes (e.g., Plumb and Bell, 1982). In the westerly phase, there is equatorward flow above the shear layer, which leads to descent and a poleward spreading of conserved tracers below it. The descent of the QBO westerly shear in mid-1982 probably enhanced the transport of El Chichón aerosols into the Northern Hemisphere later that year (Hitchman *et al.*, 1994). The secondary circulation is reversed during the easterly QBO phase, so that aerosols tend to be lofted over the equator, as manifested by enhanced upward transport of Mt. Pinatubo aerosol over the equator during the last half of 1991.

Even though both El Chichón and Mt. Pinatubo are at approximately the same latitude, there was a distinct difference within the tropics in the movement of aerosols from these eruptions. In the case of El Chichón, most aerosols remained in the Northern Hemisphere (Pollack *et al.*, 1983; Stothers, 1996) whereas for Mt. Pinatubo, aerosols were rapidly transported south of the equator (Rosen *et al.*, 1994a; Godin *et al.*, 1996; Deshler *et al.*, 1997). Mt. Pinatubo simulations by Young *et al.* (1994) and Fairlie (1995) showed that meridional circulation resulting from aerosol-induced local heating caused the initial southward movement of SSA across the equator. However, significant aerosol heating was also noted after the eruption of El Chichón, even though no large-scale cross-equatorial drift of SSA was observed. Trepte *et al.* (1993) noted that strong QBO easterly winds above about 21 km over the equator might have inhibited transport into the Southern Hemisphere immediately after the eruption of El Chichón. In contrast, Mt. Pinatubo erupted when the easterly phase of the QBO was just descending through 25 km, and the absence of strong easterlies may have allowed significant amounts of material to be transported across the equator at lower altitudes.

A history of the dispersal of Mt. Pinatubo aerosol as measured by Northern Hemisphere ground-based lidars is shown in Figure 3-3 for the first 2 years following the eruption. The progression of SSA northward can be followed, and its intermittent nature in the first 6 months is obvious. The conservative nature of the volcanic aerosol between 6 and 9 months following eruption of Mt. Pinatubo has been illustrated by Borrmann *et al.* (1995), indicating that microphysical and vertical mixing processes were nearly completed by that time. This is apparent in the lidar data in Figure 3-3. The top of the aerosol layer is near 25 km, with the peak loading in the 16-22 km region. The altitude of the layer top and that of peak loading both decrease toward higher latitudes. Wintertime subsidence is clearly apparent in the northernmost measurements. A global view from SAGE II of the evolution of aerosol surface area from Mt. Pinatubo at two altitudes is shown in Figure 3-4. The relatively quiescent 6 years between eruption of El Chichón and Mt. Pinatubo are apparent, and within this period at 20 km the eruptions of Ruiz (in 1985) and Kelut (in 1990) can be seen. Ruiz erupted in the middle of the westerly phase of the QBO, which is favorable for the spread of material poleward in both hemispheres. Kelut erupted when strong easterlies were present at 20 km, and thus aerosol would be inhibited from crossing the equatorial region, leading to a preferential dispersal of the aerosol southward (Hitchman *et al.*, 1994). At 25 km the tropical stratospheric reservoir (20°S-20°N) is clearly evident (Trepte and Hitchman, 1992). The strength of the tropical barrier is illustrated by the confinement of the highest surface areas in the tropics even though Mt. Pinatubo was at the edge of the northern boundary. The preferential transport of aerosol to the winter hemisphere is also evident in Figure 3-4. The data indicate some hemispheric differences in the midlatitudes after 1994, as do balloonborne measurements (Deshler *et al.*, 1997).

#### 3.3.1.2 Decay of Volcanic Aerosol

The decay of stratospheric volcanic aerosol proceeds at fairly well-defined rates. An exponential ($e^{-1}$) decay time of $1 \pm 0.2$ years generally characterizes the

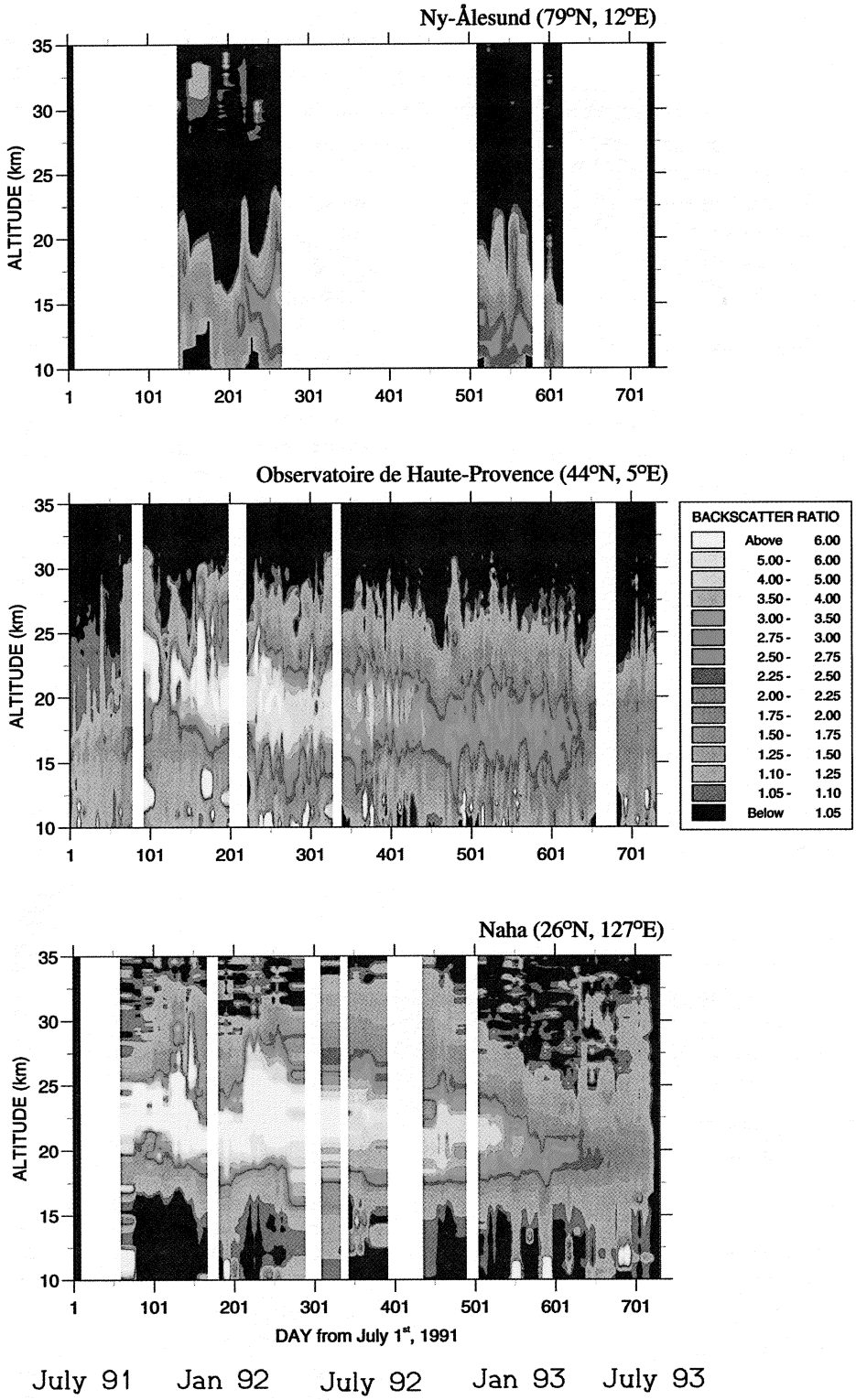


**Figure 3-3.** Time-height profiles of backscatter ratio from lidar measurements at Ny-Ålesund (79°N), Observatoire de Haute Provence, France (44°N), and Naha, Japan (26°N).

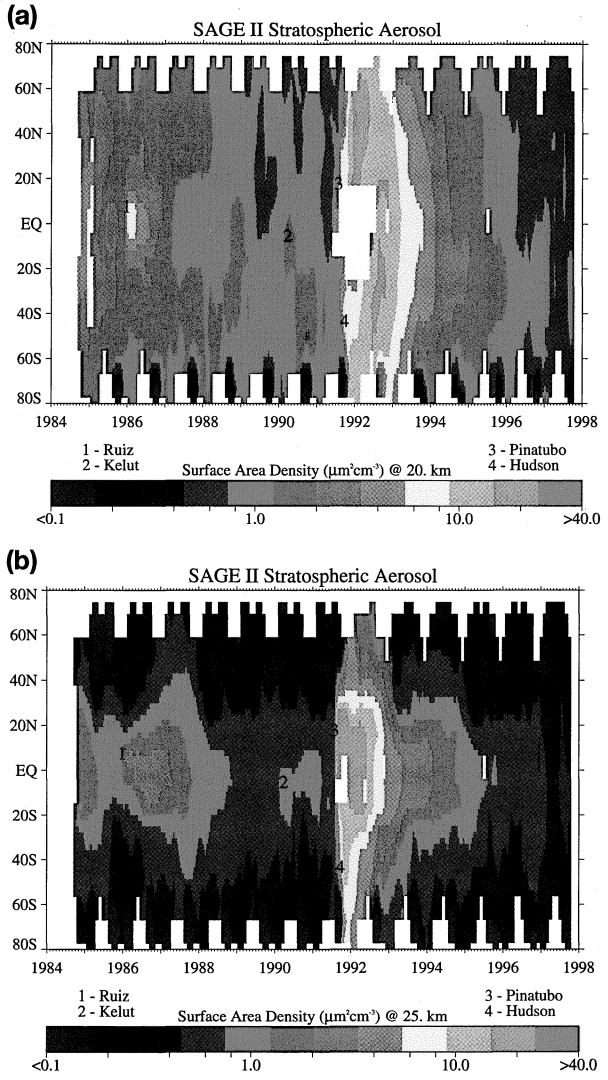


**Figure 3-4.** SAGE II aerosol surface area density as a function of time and latitude at altitudes of (a) 20 and (b) 25 km. White regions indicate no data are available. The latitude and time of significant volcanic events are noted. (Adapted from Thomason *et al.*, 1997a.)

behavior of any of several aerosol measurements during the first 3 years following the Mt. Pinatubo eruption: peak backscatter, peak mass, column backscatter, and column mass (Rosen *et al.*, 1994a; Jäger *et al.*, 1996; Barnes and Hofmann, 1997; Deshler *et al.*, 1997). The decay of the peak parameters is smoother than the decay of columnar quantities because the latter are more influenced by air mass transport, fluctuations in tropopause height, and stratospheric-tropospheric exchange (Rosen *et al.*, 1994a). The peak parameters reflect primarily sedimentation, are much less influenced by global- and synoptic-scale circulation after the initial mixing period, and are not influenced by fluctuations in tropopause height. Column backscatter measurements by Kent and Hansen (1998) show an $e^{-1}$ time from September 1994 to December 1997 that was more than double (1.8 years) that observed during the immediate post-Pinatubo period (0.8 year). The decay of aerosol surface area at three altitudes in the northern midlatitudes following eruption of Mt. Pinatubo is shown in Figure 3-5. The nature of the decay curves and the time required to reach pre-eruption conditions are different at the three altitudes. At 25 km, there is a clear QBO signature, and average surface areas reached pre-Pinatubo values by early 1995, some 3.5 years after the eruption. The decay at 20 km is considerably smoother, but it took an additional year (until early 1996) to reach pre-eruption conditions. The record at 15 km is quite different, clearly showing seasonal changes, namely, increases in winter/spring and decreases in summer/fall. At this altitude, pre-Pinatubo surface areas were not reached until mid- to late 1996, more than 5 years after the eruption. The decay of aerosol surface area is on the order of 20-30% slower than the decay of backscatter or mass (Rosen *et al.*, 1994a; Jonsson *et al.*, 1996; Deshler *et al.*, 1997). Chazette *et al.* (1995) found the decay of integrated backscatter between 15 and 20 km to be on the order of 25% longer after Mt. Pinatubo than after El Chichón eruption. They attributed this slower decay to the higher lofting of particles following eruption of Mt. Pinatubo. Russell *et al.* (1996) showed that the stratospheric aerosol effective radius increased from 0.15 μm prior to the Mt. Pinatubo eruption, to a maximum near 0.55 μm one year later, then decreased to 0.45 μm by spring 1993. The effective radius continued to decrease to a value of <0.2 μm by fall 1994 in the midlatitudes of both hemispheres and has remained between 0.15 and 0.2 μm since then (Deshler *et al.*, 1997).

Number size distributions at 20 km for the first five springs following Mt. Pinatubo eruption are shown in Figure 3-6 and are compared with a pre-Pinatubo measurement, when the data were well represented by a unimodal lognormal distribution. After the eruption the data are represented with a bimodal lognormal distribution. The two modes of the distribution were initially quite narrow, and the median radius in the small-particle mode ($r_1$) increased by a factor of 2. In the next 3 years $r_1$ decreased, and the width ($\sigma_1$) in the first mode in-

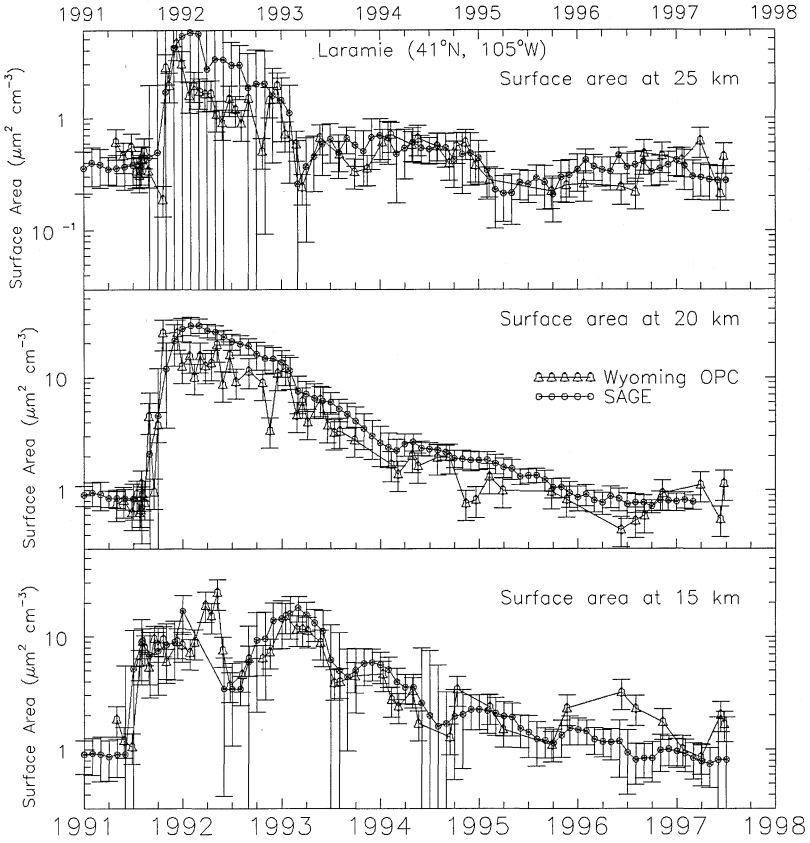


**Figure 3-5.** History of the evolution of aerosol surface area at 25, 20, and 15 km following the Mt. Pinatubo eruption. Surface areas estimated from balloonborne in situ optical particle counter (OPC) measurements above Laramie (41°N) and from SAGE II data in the 35°-45°N latitude band are shown. The error bars on the in situ data represent an uncertainty of 30%. The SAGE II error bars represent the standard deviation about the zonal median. (Adapted from Thomason *et al.*, 1997a.)

creased. The particle concentrations ($N_1$, $N_2$) and surface areas ($A_1$, $A_2$) shown for the springs of 1992 and 1993 compare favorably with ER-2 measurements by Jonsson *et al.* (1996). The second (large-particle) mode is well defined throughout the 5 years shown in Figure 3-6, preserving a quite similar shape. The primary change in the second mode is in the number concentration ($N_2$), which decreased steadily by about a factor of 5 per year. The second mode had almost disappeared by spring of 1997.

Quite similar decay rates have been observed for SSA from the El Chichón and Mt. Pinatubo eruptions (Rosen *et al.*, 1994a; Chazette *et al.*, 1995; Barnes and Hofmann, 1997), and from the decay at different latitudes for Mt. Pinatubo aerosol (Jayaraman *et al.*, 1995; Jäger *et al.*, 1996). These decay rates are also similar to that observed for the removal of strontium from the stratosphere (Fabian *et al.*, 1968). These similarities reflect the fact that the removal of SSA, once it is dispersed meridionally, is controlled by relatively steady and robust processes, such as gravitational settling and stratospheric-tropospheric exchange. The maximum stratospheric-tropospheric exchange of tracers is in the Northern Hemisphere spring (Holton *et al.*, 1995), which may explain the clear signature of a surface area minimum at 15 km in Figure 3-5 during that season each year. The temporal and vertical resolution required to capture stratospheric-tropospheric exchange processes in detail is provided by lidar, and several such studies have pointed out the influence of volcanic SSA on the upper troposphere (Menzies and Tratt, 1995; Sassen *et* al., 1995; Post *et al.*, 1996).

### 3.3.2 Background Aerosol

Since the discovery of the SSA layer in 1957 (Junge *et al.*, 1961) there has been much speculation about the stability of the layer and the source of the $H_2SO_4$ that is the primary component of the aerosol. The measurements by Junge *et al.* were made at the end of a lengthy period free of volcanic eruptions (Stothers, 1996), but were not extensive enough to establish a baseline. There are four periods in the modern (post-1970) measurement era when the influence of volcanic eruptions has been at a minimum: 1974, 1979, 1989 to early 1991, and the present (1998). Many studies have focused on these data

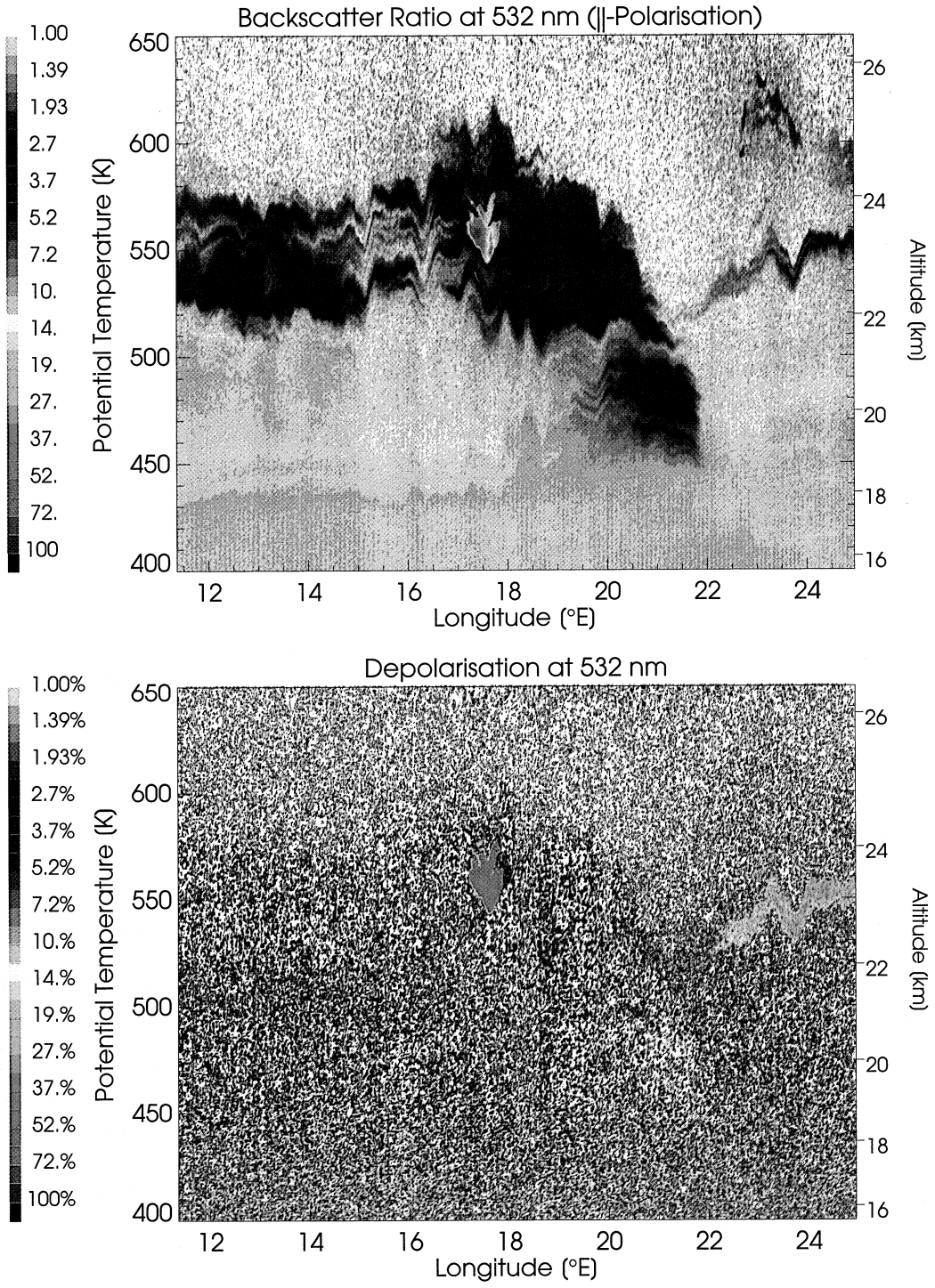


**Figure 3-13.** Altitude/longitude plot of airborne lidar observations from the German Transall aircraft on 15 January 1995 over the Norwegian mountains west of Kiruna, showing 0.532-μm aerosol backscatter ratio (upper panel) and depolarization (lower panel). The wind direction was from west to east (left to right in the figure). (Adapted from Carslaw *et al.*, 1998.)

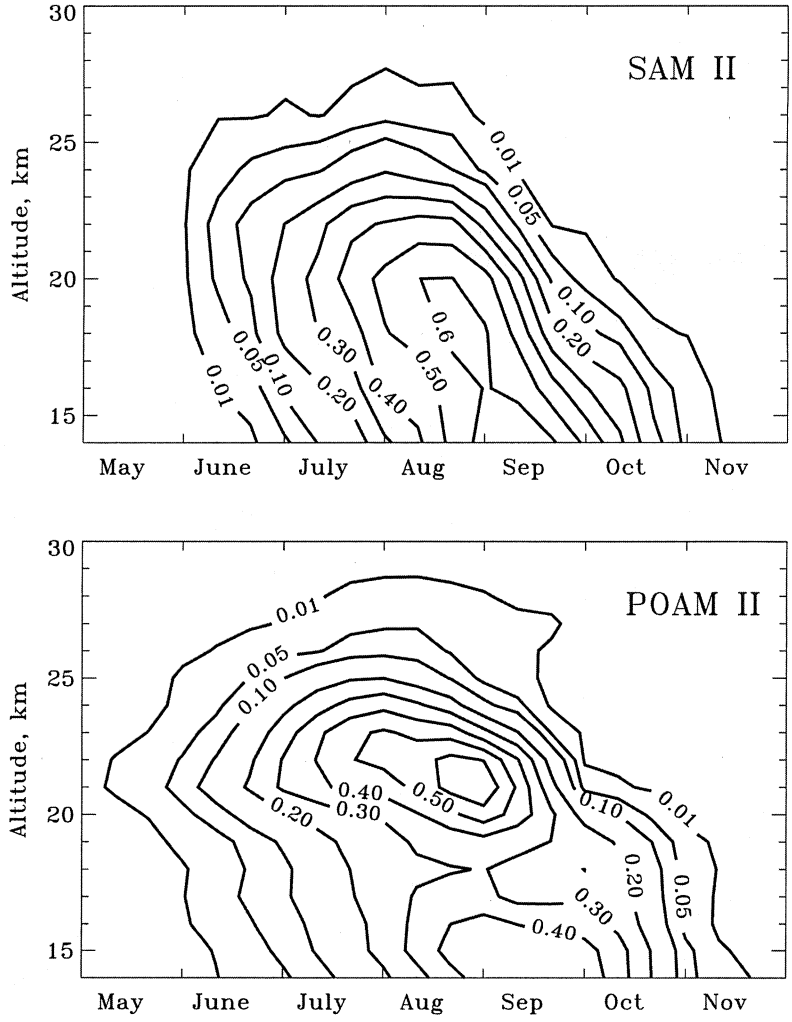


**Figure 3-14.** Zonally averaged PSC sighting probabilities for the Antarctic from measurements by SAM II for 1979-1989 (upper panel) and POAM II for 1994-1996 (lower panel). (Adapted from Poole and Pitts, 1994; and Fromm *et al.*, 1997.)

### 3.4.4.2 PSC Climatology

A PSC climatology was developed from more than 10 years of measurements by the Stratospheric Aerosol Measurement (SAM) II satellite instrument (Poole and Pitts, 1994). The frequency of occurrence of Antarctic PSCs observed by CLAES in 1992 generally agreed with this climatology (Mergenthaler *et al.*, 1997). PSC observations in both hemispheres were also made more recently (October 1993-November 1996) by POAM II (Fromm *et al.*, 1997). Figure 3-14 shows SAM II and POAM II zonally averaged PSC sighting probabilities for the Antarctic. Both datasets show Antarctic PSCs forming from mid-May until early November, with sighting probability increasing throughout the winter to a peak of about 60% in mid to late August. There is a downward trend in the altitude of peak sighting probability related to the seasonal descent of the altitude of coldest temperature, a feature also noted in lidar measurements (David *et al.*, 1998). SAM II and POAM II Arctic PSC sighting probabilities (not shown) differ in an absolute sense, primarily because of the difference in latitude sampling of the two instruments. However, the Arctic data records are qualitatively similar, showing that PSCs occur there much less frequently and over a shorter time period (from early December to mid March) than in the Antarctic (Poole and Pitts, 1994).

Poole and Pitts (1994) noted that PSC existence temperatures inferred from SAM II data were nearly constant throughout the winter season in the Arctic, whereas a gradual lowering of existence temperatures was inferred over Antarctica from June through September, indicating a systematic removal of $HNO_3$ and $H_2O$ by denitrification and dehydration in that region. The

existence temperatures in the early winter season in both hemispheres were close to the expected NAT equilibrium temperatures. On the other hand, gas-phase $HNO_3$ measurements by the Microwave Limb Sounder (MLS) instrument (Santee *et al.*, 1998) show early-winter $HNO_3$ condensation beginning at roughly 3 K below $T_{NAT}$. This indicates that STS PSC particles were formed initially. Later in the season, $HNO_3$ concentrations approached the equilibrium levels for NAD (or NAT).

#### 3.4.4.3 Effects of Volcanic Loading on PSC Formation

Large concentrations of volcanic SSA were observed to influence PSC formation in the years following the 1991 Mt. Pinatubo eruption. Antarctic measurements by Deshler *et al.* (1994b) showed that PSCs formed in the volcanic layer had numerous small particles ($r <$ 0.5 μm) and essentially no particles with $r > 2$ μm, and that surface areas increased by a factor of 4 to 6 relative to the surrounding SSA. At altitudes above the volcanic layer, particles with $r \approx$ 2-3 μm were observed, as had been the usual case in Antarctica prior to the eruption. Lidar observations show that most of the PSCs formed near the peak in SSA backscatter and at lower altitudes in the first years after eruption of Mt. Pinatubo. The larger volcanic aerosol loading apparently led to increased Type 1b PSC formation at higher temperatures, compared to pre-volcanic conditions (David *et al.*, 1998). Satellite measurements also show a more pronounced $HNO_3$ uptake in STS droplets at higher temperatures under the enhanced aerosol loading from Mt. Pinatubo (Santee *et al.*, 1998). Both of these findings are in good agreement with the equilibrium STS model calculations of Carslaw *et al.* (1994).

## 3.5 OUTSTANDING ISSUES IN STRATOSPHERIC PARTICLES

One outstanding issue that must be resolved is the quantification of the non-volcanic background SSA level, which cannot be determined from the current data record because of the influence of volcanoes. Understanding of this background level is required to assess the validity of models of SSA production, to allow detection of possible future anthropogenic trends, and to determine the partitioning of ozone destruction amongst the chlorine, hydrogen, and nitrogen radical families (Wennberg *et al.*, 1994). Except for this issue, there is a general consistency of SSA observations with dynamical and microphysical modeling results.

In contrast, the interpretation of PSC observations still suffers from many unknowns and uncertainties with relevance to stratospheric chemistry (see Chapter 7). Recent progress in understanding PSCs came with the recognition that some of these clouds are liquid and do not require any kind of phase transition during their growth. While there is overwhelming evidence for the existence of solid particles in the stratosphere, our understanding of the mechanisms of phase transitions leading to the formation of solid PSC particles is still very poor. Solid particle formation could be crucial for the heterogeneous chemical reactions occurring on PSCs because the solid $HNO_3$ hydrates can exist under warmer conditions than STS clouds. Furthermore, solidification of a few particles by some highly selective mechanism appears to be a necessary prerequisite for the denitrification of the polar vortices, which may lead to enhanced polar ozone destruction. For the modeling of Type 1a PSC formation, knowledge of the particle size distribution and phase at one particular point in time may not be sufficient, but rather the full thermal history of the air parcel containing the cloud particles may be required. There is a need for quasi-Lagrangian in situ measurements to follow particle evolution and to observe freezing events themselves.

Another outstanding issue is the effect that increases in source gases coupled with decreasing stratospheric temperatures may have on stratospheric particles. There are reports of an upward trend in $H_2O$, and Chapter 5 presents clear evidence of a long-term cooling in the lower stratosphere. An increase in $HNO_3$ in the lower stratosphere might also be expected because there is an upward trend in tropospheric $N_2O$. Both the surface area and heterogeneous reactivity of SSA should increase under these conditions. Surface area increases should be small, but there may be larger increases in heterogeneous reactivity (see Chapter 7).

More significant changes may occur in the properties and heterogeneous reactivity of Type 1b PSCs. For example, Figure 3-1 illustrates that particle surface area increases by 5-18% per 0.1 K temperature decrease in the interval between 192 and 191 K, around the STS threshold temperature. This could be of particular significance in the Arctic, where PSCs often form in limited synoptic-scale cold-temperature areas. The STS threshold temperature is also shifted upward by approximately 1 K per 1 ppm increase in $H_2O$ in the lower strato-

sphere. An example of this sensitivity is shown by HALOE data late in the 1993 Antarctic spring, where there was enhanced PSC development due to an intrusion of $H_2O$ from lower latitudes (Hervig *et al.*, 1997). However, no trend in PSCs is discernible in the present satellite PSC data record because of the relatively short record length and the large interannual variability in the number of clouds observed.

It also should be noted that current models used for assessment calculations are limited in the accuracy to which they can represent PSC processes. For example, only large-scale PSC events can be reproduced in global models because of the models' relatively coarse resolution. Furthermore, most models include relatively simple microphysical assumptions or parameterizations, whereas field observations show that PSCs exhibit very complex and variable behavior. 2-D models inherently cannot represent the fact that PSC formation is not zonally symmetric, particularly in the Arctic, as shown by SAM II and POAM II data. Some progress has been made in this area (Considine *et al.*, 1994), whereby PSC formation is modeled using statistical temperature fluctuations about the zonal mean values, hence producing more PSCs than would occur using zonal average temperatures. Even a 3-D formulation has limitations in capturing small-scale phenomena such as gravity or mountain waves, where rapid temperature fluctuations may result in nonequilibrium microphysical processes that could be important in forming solid PSC particles, especially in the Arctic. The integral role of such phenomena in ozone depletion is unclear.

## REFERENCES


Abbas, M.M., H.A. Michelsen, M.R. Gunson, M.C. Abrams, M.J. Newchurch, R.J. Salawitch, A.Y. Chang, A. Goldman, F.W. Irion, G.L. Manney, E.J. Moyer, R. Nagaraju, C.P. Rinsland, G.P. Stiller, and R. Zander, Seasonal-variations of water-vapor in the lower stratosphere inferred from ATMOS/ATLAS-3 measurements of $H_2O$ and $CH_4$, *Geophys. Res. Lett.*, *23*, 2401-2404, 1996.

Adriani, A., T. Deshler, G.P. Gobbi, B.J. Johnson, and G. Di Donfrancesco, Polar stratospheric clouds over McMurdo, Antarctica, during the spring 1991: Lidar and particle counter measurements, *Geophys. Res. Lett.*, *19*, 1755-1758, 1992.

Adriani, A., T. Deshler, G. Di Donfrancesco, and G.P. Gobbi, Polar stratospheric clouds and volcanic aerosol during spring 1992 over McMurdo Station, Antarctica: Lidar and particle counter comparisons, *J. Geophys. Res.*, *100*, 25877-25897, 1995.

Anderson, J., and V.K. Saxena, Temporal changes of Mount Pinatubo aerosol characteristics over northern midlatitudes derived from SAGE II extinction measurements, *J. Geophys. Res.*, *101*, 19455-19463, 1996.

Ångström, A., On the atmospheric transmission of sun radiation and on dust in the air, *Geogr. Ann.*, *11*, 156-166, 1908.

Anthony, S.E., R.T. Tisdale, R.S. Disselkamp, M.A. Tolbert, and J.C. Wilson, FTIR studies of low-temperature sulfuric-acid aerosols, *Geophys. Res. Lett.*, *22*, 1105-1108, 1995.

Arnold, F., J. Curtius, S. Spreng, and T. Deshler, Stratospheric aerosol sulfuric acid: First direct in situ measurements using a novel balloon-based mass spectrometer apparatus, *J. Atmos. Chem.*, *30*, 3-10, 1998.

Ayers, G.P., R.W. Gillett, and J.L. Gras, On the vapor pressure of sulfuric acid, *Geophys. Res. Lett.*, *7*, 433-436, 1980.

Barnes, J.E., and D.J. Hofmann, Lidar measurements of stratospheric aerosol over Mauna Loa Observatory, *Geophys. Res. Lett.*, *24*, 1923-1926, 1997.

Baumgardner, D., J.E. Dye, B.W. Gandrud, and R.G. Knollenberg, Interpretation of measurements made by the forward scattering spectrometer probe (FSSP-300) during the airborne Arctic stratospheric expedition, *J. Geophys. Res.*, *97*, 8035-8046, 1992.

Baumgardner, D., J.E. Dye, B. Gandrud, K. Barr, K. Kelly, and K.R. Chan, Refractive indices of aerosols in the upper troposphere and lower stratosphere, *Geophys. Res. Lett.*, *23*, 749-752, 1996.

Bekki, S., On the possible role of aircraft-generated soot in middle latitude ozone depletion, *J. Geophys. Res.*, *100*, 7195-7202, 1995.

Bekki, S., and J.A. Pyle, Two-dimensional assessment of the impact of aircraft sulphur emissions on the stratospheric sulphate aerosol layer, *J. Geophys. Res.*, *97*, 15839-15847, 1992.

Bekki, S., M.P. Chipperfield, J.A. Pyle, J.J. Remedios, S.E. Smith, R.G. Grainger, A. Lambert, J.B. Kumer, and J.L. Mergenthaler, Coupled aerosol-chemical modeling of UARS $HNO_3$ and $N_2O_5$ measurements in the arctic upper stratosphere, *J. Geophys. Res.*, *102*, 8977-8984, 1997.

Beyer, K.D., S.W. Seago, H.Y. Chang, and M.J. Molina, Composition and freezing of aqueous $H_2SO_4$/ $HNO_3$ solutions under polar stratospheric conditions, *Geophys. Res. Lett.*, *21*, 871-874, 1994.

Beyerle, G., R. Neuber, O. Schrems, F. Wittrock, and B. Knudsen, Multiwavelength lidar measurements of stratospheric aerosols above Spitsbergen during winter 1992/93, *Geophys. Res. Lett.*, *21*, 57-60, 1994.

Beyerle, G., B. Luo, R. Neuber, T. Peter, and I.S. McDermid, Temperature dependence of ternary solution particle volumes as observed by lidar in the Arctic stratosphere during 1992/93, *J. Geophys. Res.*, *102*, 3603-3609, 1997.

Biermann, U.M., T. Presper, T. Koop, J. Mößinger, P.J. Crutzen, and T. Peter, The unsuitability of meteoritic and other nuclei for polar stratospheric cloud freezing, *Geophys. Res. Lett.*, *23*, 1693-1696, 1996.

Bigg, E.K., Stratospheric particles, *J. Atmos. Sci.*, *32*, 910-917, 1975.

Blake, D.F., and K. Kato, Latitudinal distribution of black carbon soot in the upper troposphere and lower stratosphere, *J. Geophys. Res.*, *100*, 7195-7202, 1995.

Borrmann, S., J.E. Dye, D. Baumgardner, M.H. Proffitt, J.J. Margitan, J.C. Wilson, H.H. Jonsson, C.A. Brock, M. Loewenstein, J.R. Podolske, and G.V. Ferry, Aerosols as dynamical tracers in the lower stratosphere: Ozone versus aerosol correlation after the Mount Pinatubo eruption, *J. Geophys. Res.*, *100*, 11147-11156, 1995.

Borrmann, S., S. Solomon, J.E. Dye, and B. Luo, The potential of cirrus clouds for heterogeneous chlorine activation, *Geophys. Res. Lett.*, *23*, 2133-2136, 1996.

Borrmann, S., S. Solomon, L. Avallone, D. Toohey, and D. Baumgardner, On the occurrence of ClO in cirrus clouds and volcanic aerosol in the tropopause region, *Geophys. Res. Lett.*, *24*, 2011-2014, 1997a.

Borrmann, S., S. Solomon, J.E. Dye, D. Baumgardner, K.K. Kelly, and K.R. Chan, Heterogeneous reactions on stratospheric background aerosols, volcanic sulfuric acid droplets, and type I polar stratospheric clouds: Effects of temperature fluctuations and differences in particle phase, *J. Geophys. Res.*, *102*, 3639-3648, 1997b.

Brock, C.A., P. Hamill, J.C. Wilson, H.H. Jonsson, and K.R. Chan, Particle formation in the upper tropical troposphere: A source of nuclei for the stratospheric aerosol, *Science*, *270*, 1650-1653, 1995.

Browell, E.V., C.F. Butler, S. Ismail, P.A. Robinette, A.F. Carter, N.S. Higdon, O.B. Toon, M.R. Schoeberl, and A.F. Tuck, Airborne lidar observations in the wintertime Arctic stratosphere: Polar stratospheric clouds, *Geophys. Res. Lett.*, *17*, 385-388, 1990.

Capps, C.D., R.L. Henning, and G.M. Hess, Analytic inversion of remote sensing data, *Appl. Opt.*, *21*, 3581-3587, 1982.

Carslaw, K.S., B.P. Luo, S.L. Clegg, T. Peter, P. Brimblecombe, and P.J. Crutzen, Stratospheric aerosol growth and $HNO_3$ gas phase depletion from coupled $HNO_3$ and water uptake by liquid particles, *Geophys. Res. Lett.*, *21*, 2479-2482, 1994.

Carslaw, K.S., S.L. Clegg, and P. Brimblecombe, A thermodynamic model of the system HCl-$HNO_3$-$H_2SO_4$-$H_2O$ including solubilities of HBr, from <200 K to 328 K, *J. Phys. Chem.*, *99*, 11557-11574, 1995.

Carslaw, K.S., T. Peter, and S.L. Clegg, Modeling the composition of liquid stratospheric aerosols, *Rev. Geophys.*, *35*, 125-154, 1997.

Carslaw, K.S., M. Wirth, A. Tsias, B.P. Luo, A. Dörnbrack, M. Leutbecher, H. Volkert, W. Renger, J.T. Bacmeister, and T. Peter, Particle processes and chemistry in remotely observed mountain polar stratospheric clouds, *J. Geophys. Res.*, *103*, 5785-5796, 1998.

Chazette, P., C. David, J. Lefrere, S. Godin, J. Pelon, and G. Mégie, Comparative lidar study of the optical, geometrical, and dynamical properties of stratospheric post-volcanic aerosols, following the eruptions of El Chichón and Mount Pinatubo, *J. Geophys. Res.*, *101*, 23195-23207, 1995.

Chin, M., and D.D. Davis, Global sources and sinks of OCS and $CS_2$ and their distributions, *Global Biogeochem. Cycles*, *7*, 321-337, 1993.

Chin, M., and D.D. Davis, A reanalysis of carbonyl sulfide as a source of stratospheric background sulfur aerosol, *J. Geophys. Res.*, *100*, 8993-9005, 1995.

Considine, D.B., A.R. Douglass, and C.H. Jackman, Effects of a polar stratospheric cloud parameterization on ozone depletion due to stratospheric aircraft in a two-dimensional model, *J. Geophys. Res.*, *99*, 18879-18894, 1994.

Crutzen, P.J., The possible importance of CSO for the sulfate layer of the stratosphere, *Geophys. Res. Lett.*, *3*, 73-76, 1976.

David, C., S. Godin, G. Mégie, Y. Emery, and C. Flesia, Physical state and composition of polar stratospheric clouds inferred from airborne lidar measurements during SESAME, *J. Atmos. Chem.*, *27*, 1-16, 1997.

David, C., S. Bekki, S. Godin, G. Mégie, and M.P. Chipperfield, Polar stratospheric clouds climatology over Dumont d'Urville between 1989 and 1993 and the influence of volcanic aerosols on their formation, *J. Geophys. Res.*, *103*, 22163-22180, 1998.

Del Guasta, M., M. Morandi, L. Stefanutti, B. Stein, and J.P. Wolf, Derivation of Mount Pinatubo stratospheric aerosol mean size distribution by means of a multiwavelength lidar, *Appl. Opt.*, *33*, 5690-5697, 1994.

Del Negro, L.A., D.W. Fahey, S.G. Donnelly, R.S. Gao, E.R. Keim, R.C. Wamsley, E.L. Woodbridge, J.E. Dye, D. Baumgardner, B.W. Gandrud, J.C. Wilson, H.H. Jonsson, M. Loewenstein, J.R. Podolske, C.R. Webster, R.D. May, D.R. Worsnop, A. Tabazadeh, M.A. Tolbert, K.K. Kelly, and K.R. Chan, Evaluating the role of NAT, NAD, and liquid $H_2SO_4/H_2O/HNO_3$ solutions in Antarctic polar stratospheric cloud aerosol: Observations and implications, *J. Geophys. Res.*, *102*, 13255-13282, 1997.

Deshler, T., and S.J. Oltmans, Vertical profiles of volcanic aerosol and polar stratospheric clouds above Kiruna, Sweden: Winters 1993 and 1995, *J. Atmos. Chem.*, *30*, 11-23, 1998.

Deshler, T., A. Adriani, D.J. Hofmann, and G.P. Gobbi, Evidence for denitrification in the 1990 Antarctic spring stratosphere: II, Lidar and aerosol measurements, *Geophys. Res. Lett.*, *18*, 1999-2002, 1991.

Deshler, T., D.J. Hofmann, B.J. Johnson, and W.R. Rozier, Balloon-borne measurements of Pinatubo aerosol size distribution and volatility at Laramie, Wyoming during the summer of 1991, *Geophys. Res. Lett.*, *19*, 199-202, 1992.

Deshler, T., B.J. Johnson, and W.R. Rozier, Balloonborne measurements of Pinatubo aerosol during 1991 and 1992 at 41°N, vertical profiles, size distribution, and volatility, *Geophys. Res. Lett.*, *20*, 1435-1438, 1993.

Deshler, T., B.J. Johnson, and W.R. Rozier, Changes in the character of polar stratospheric clouds over Antarctica in 1992 due to the Pinatubo volcanic aerosol, *Geophys. Res. Lett.*, *21*, 273-276, 1994a.

Deshler, T., T. Peter, R. Müller, and P.J. Crutzen, The lifetime of leewave-induced ice particles in the Arctic stratosphere: I, Balloonborne observations, *Geophys. Res. Lett.*, *21*, 1327-1330, 1994b.

Deshler, T., G.B. Liley, G. Bodeker, W.A. Matthews, and D.J. Hofmann, Stratospheric aerosol following Pinatubo: Comparison of the north and south midlatitudes using in situ measurements, *Adv. Space Res.*, *20*, 2057-2061, 1997.

Dessler, A.E., E.M. Weinstock, E.J. Hintsa, J.G. Anderson, C.R. Webster, R.D. May, J.W. Elkins, and G.S. Dutton, An examination of the total hydrogen budget of the lower stratosphere, *Geophys. Res. Lett.*, *21*, 2563-2566, 1994.

Drdla, K., A. Tabazadeh, R.P. Turco, M.Z. Jacobson, J.E. Dye, C. Twohy, and D. Baumgardner, Analysis of the physical state of one Arctic polar stratospheric cloud based on observations, *Geophys. Res. Lett.*, *21*, 2475-2478, 1994.

Dye, J.E., B.W. Gandrud, D. Baumgardner, and L. Sanford, A survey of particle measurements in the Arctic from the forward scattering spectrometer probe model 300, *Geophys. Res. Lett.*, *17*, 409-412, 1990a.

Dye, J.E., B.W. Gandrud, D. Baumgardner, K.R. Chan, G.V. Ferry, M. Loewenstein, K.K. Kelly, and J.C. Wilson, Observed particle evolution in the polar stratospheric cloud of January 24, 1989, *Geophys. Res. Lett.*, *17*, 413-416, 1990b.

Dye, J.E., D. Baumgardner, B.W. Gandrud, S.R. Kawa, K.K. Kelly, M. Loewenstein, G.V. Ferry, K.R. Chan, and B.L. Gary, Particle size distribution in Arctic polar stratospheric clouds, growth and freezing of sulfuric acid droplets, and implications for cloud formation, *J. Geophys. Res.*, *97*, 8015-8034, 1992.

Dye, J.E., D. Baumgardner, B.W. Gandrud, K. Drdla, K. Barr, D.W. Fahey, L.A. Del Negro, A. Tabazadeh, H.H. Jonsson, J.C. Wilson, M. Loewenstein, J.R. Podolske, and K.R. Chan, In-situ observations of an Antarctic polar stratospheric cloud: Similarities with Arctic observations, *Geophys. Res. Lett.*, *23*, 1913-1916, 1996.

Engel, A., C. Schiller, U. Schmidt, R. Borchers, H. Ovarlez, and J. Ovarlez, The total hydrogen budget in the arctic winter stratosphere during the European Arctic Stratospheric Ozone Experiment, *J. Geophys. Res.*, *101*, 14495-14503, 1996.

Fabian, P., W.F. Libby, and C.E. Palmer, Stratospheric residence time and interhemispheric mixing of strontium 90 from fallout in rain, *J. Geophys. Res.*, *73*, 3611-3616, 1968.

Fahey, D.W., K.K. Kelly, G.V. Ferry, L.R. Poole, J.C. Wilson, D.M. Murphy, M. Loewenstein, and K.R. Chan, In situ measurements of total reactive nitrogen, total water, and aerosol in a polar stratospheric cloud in the Antarctic, *J. Geophys. Res.*, *94*, 11299-11315, 1989.

Fahey, D.W., E.R. Keim, K.A. Boering, C.A. Brock, J.C. Wilson, S. Anthony, T.F. Hanisco, P.O. Wennberg, R.C. Miake-Lye, R.J. Salawitch, N. Louisnard, E.L. Woodbridge, R.S. Gao, S.G. Donnelly, R.C. Wamsley, L.A. Del Negro, B.C. Daube, S.C. Wofsy, C.R. Webster, R.D. May, K.K. Kelly, M. Loewenstein, J.R. Podolske, and K.R. Chan, Emission measurements of the Concorde supersonic aircraft in the lower stratosphere, *Science*, *270*, 70-74, 1995.

Fairlie, T.D., Three-dimensional transport simulations of the dispersal of volcanic aerosol from Mount Pinatubo, *Quart. J. Roy. Meteorol. Soc.*, *121*, 1943-1980, 1995.

Farlow, N.H., G.V. Ferry, H.Y. Lem, and D.M. Haynes, Latitudinal variations of stratospheric aerosols, *J. Geophys. Res.*, *84*, 733-743, 1979.

Ferry, G.V., E. Neish, M. Schultz, and R.F. Pueschel, Concentrations and size distributions of Antarctic stratospheric aerosols, *J. Geophys Res.*, *94*, 16459-16474, 1989.

Fiocco, G., and G. Grams, Observation of aerosol layer of 20 km by optical radar, *J. Atmos. Sci.*, *21*, 323-324, 1964.

Flesia, C., A. Mugnai, Y. Emery, S. Godin, L. de Schoulepnikoff, and V. Mitev, Interpretation of lidar depolarization measurements of the Pinatubo stratospheric aerosol layer during EASOE, *Geophys. Res. Lett.*, *21*, 1443-1446, 1994.

Fromm, M.D., R.M. Bevilacqua, E.P. Shettle, J. Hornstein, J.D. Lumpe, S.T. Massie, and K.H. Fricke, Observations of Antarctic polar stratospheric clouds by POAM II: 1994-1996, *J. Geophys. Res.*, *102*, 23659-23672, 1997.

Gable, C.M., H.F. Betz, and S.H. Maron, Phase equilibria of the system sulfur trioxide-water, *J. Amer. Chem. Soc.*, *72*, 1445-1448, 1950.

Gandrud, B.W., J.E. Dye, D. Baumgardner, G.V. Ferry, M. Loewenstein, K.R. Chan, B. Gary, and K.K. Kelly, The January 30, 1989 Arctic polar stratospheric cloud (PSC) event: Evidence for a mechanism of dehydration, *Geophys. Res. Lett.*, *17*, 457-459, 1990.

Glaccum, W., R.L. Lucke, R.M. Bevilacqua, E.P. Shettle, J.S. Hornstein, D.T. Chen, J.D. Lumpe, S.S. Krigman, D.J. Debrestian, M.D. Fromm, F. Dalaudier, E. Chassefière, C. Deniel, C.E. Randall, D.W. Rusch, J.J. Olivero, C. Brogniez, J. Lenoble, and R. Kremer, The Polar Ozone and Aerosol Measurement (POAM II) instrument, *J. Geophys. Res.*, *101*, 14479-14787, 1996.

Gobbi, G.P., Lidar estimation of stratospheric aerosol properties: Surface, volume, and extinction to backscatter ratio, *J. Geophys. Res.*, *100*, 11219-11235, 1995.

Gobbi, G.P., and A. Adriani, Mechanisms of formation of stratospheric clouds observed during the Antarctic late winter of 1992, *Geophys. Res. Lett.*, *20*, 1427-1430, 1993.

Godin, S., G. Mégie, C. David, D. Haner, C. Flesia, and Y. Emery, Airborne lidar observation of mountain-wave-induced polar stratospheric clouds during EASOE, *Geophys. Res. Lett.*, *21*, 1335-1338, 1994.

Godin, S., C. David, and M. Guirlet, Evolution of the Mt. Pinatubo volcanic cloud and analysis of its effect on the ozone amount as observed from ground-based measurements performed in northern and southern latitudes, in *The Mount Pinatubo Eruption: Effects on the Atmosphere and Climate*, NATO ASI Series, Series I Global Environmental Change, Vol. 42, edited by G. Fiocco, D. Fua, and G. Visconti, Springer-Verlag, Berlin, 1996.

Goodman, J., O.B. Toon, R.F. Pueschel, K.G. Snetsinger, and S. Verma, Antarctic stratospheric ice crystals, *J. Geophys. Res.*, *94*, 16449-16457, 1989.

Goodman, J., K.G. Snetsinger, R.F. Pueschel, and S. Verma, Decay of Mount Pinatubo volcanic perturbation, *Geophys. Res. Lett.*, *21*, 1129-1132, 1994.

Goodman, J., S. Verma, R.F. Pueschel, P. Hamill, G.V. Ferry, and D. Webster, New evidence of size and composition of polar stratospheric cloud particles, *Geophys. Res. Lett.*, *24*, 615-618, 1997.

Grainger, R.G., A. Lambert, C.D. Rodgers, F.W. Taylor, and T. Deshler, Stratospheric aerosol effective radius, surface area, and volume estimated from infrared measurements, *J. Geophys. Res.*, *100*, 16507-16518, 1995.

Grant, W.B., E.V. Browell, C.S. Long, L.L. Stowe, R.G. Grainger, and A. Lambert, Use of volcanic aerosols to study the tropical stratospheric reservoir, *J. Geophys. Res.*, *101*, 3973-3988, 1996.

Griggs, M., Satellite measurements of tropospheric aerosols, *Adv. Space Res.*, *2*, 109-118, 1983.

Gruner, P., and H. Kleinert, Die dammerungerscheinen, *Probl. Kosm. Phys.*, *10*, 1-113, 1927.

Hammer, C.U., H.B. Clausen, and W. Dansgaard, Greenland ice sheet evidence of postglacial volcanism and its climatic impact, *Nature*, *288*, 230-235, 1980.

Hanson, D.R., and K. Mauersberger, Laboratory studies of the nitric acid trihydrate: Implication for the south polar stratosphere, *Geophys. Res. Lett.*, *15*, 855-858, 1988.

Hanson, D.R., A.R. Ravishankara, and S. Solomon, Heterogeneous reactions in sulfuric acid aerosols: A framework for model calculations, *J. Geophys. Res.*, *99*, 3615-3629, 1994.

Harries, J.E., J.M. Russell III, A.F. Tuck, L.L. Gordley, P. Purcell, K. Stone, R.M. Bevilacqua, M. Gunson, G. Nedoluha, and W.A. Traub, Validation of measurements of water vapor from the Halogen Occultation Experiment (HALOE), *J. Geophys. Res.*, *101*, 10205-10216, 1996.

Herber, A., L.W. Thomason, V.F. Radinov, and U. Leiter, Comparison of trends in the tropospheric and stratospheric aerosol optical depths in the Antarctic, *J. Geophys. Res.*, *98*, 18441-18447, 1993.

Hervig, M.E., J.M. Russell III, L.L. Gordley, J.H. Park, S.R. Drayson, and T. Deshler, Validation of aerosol measurements from the Halogen Occulation Experiment, *J. Geophys. Res.*, *101*, 10267-10275, 1996.

Hervig, M.E., K.S. Carslaw, T. Peter, T. Deshler, L.L. Gordley, G. Redaelli, U. Biermann, and J.M. Russell III, Polar stratospheric clouds due to vapor enhancement: HALOE observations of the Antarctic vortex in 1993, *J. Geophys. Res.*, *102*, 28185-28193, 1997.

Hervig, M.E., T. Deshler, and J.M. Russell III, Aerosol size distributions obtained from HALOE spectral extinction measurements, *J. Geophys. Res.*, *103*, 1573-1583, 1998.

Hitchman, M.H., M. McKay, and C.R. Trepte, A climatology of stratospheric aerosol, *J. Geophys. Res.*, *99*, 20689-20700, 1994.

Hofmann, D.J., Increase in the stratospheric background sulfuric acid aerosol mass in the past 10 years, *Science*, *248*, 996-1000, 1990a.

Hofmann, D.J., Measurement of the condensation nuclei profile to 31 km in the Arctic in January 1989 and comparisons with Antarctic measurements, *Geophys. Res. Lett.*, *17*, 357-360, 1990b.

Hofmann, D.J., Stratospheric cloud micro-layers and small-scale temperature variations in the Arctic in 1989, *Geophys. Res. Lett.*, *17*, 369-372, 1990c.

Hofmann, D.J., Aircraft sulphur emissions, *Nature*, *349*, 659, 1991.

Hofmann, D.J., and T. Deshler, Comparison of stratospheric clouds in the Antarctic and the Arctic, *Geophys. Res. Lett.*, *16*, 1429-1432, 1989.

Hofmann, D.J., and T. Deshler, Balloonborne measurements of polar stratospheric clouds and ozone at -93°C in the Arctic in February 1990, *Geophys. Res. Lett.*, *17*, 2185-2188, 1990.

Hofmann, D.J., and T. Deshler, Stratospheric cloud observations during formation of the Antarctic ozone hole in 1989, *J. Geophys. Res.*, *96*, 2897-2912, 1991.

Hofmann, D.J., and J.M. Rosen, Balloon observations of a particle layer injected by a stratospheric aircraft at 23 km, *Geophys. Res. Lett.*, *5*, 511-514, 1978.

Hofmann, D.J., and J.M. Rosen, Balloon-borne observations of stratospheric aerosol and condensation nuclei during the year following the Mt. St. Helens eruption, *J. Geophys. Res.*, *87*, 11039-11061, 1982.

Hofmann, D.J., and J.M. Rosen, Stratospheric sulfuric acid fraction and mass estimate for the 1982 volcanic eruption of El Chichón, *Geophys. Res. Lett.*, *4*, 313-316, 1983.

Hofmann, D.J., J.M. Rosen, T.J. Pepin, and R.G. Pinnick, Stratospheric aerosol measurements: I, Time variations at northern midlatitudes, *J. Atmos. Sci.*, *32*, 1446-1456, 1975.

Hofmann, D.J., J.M. Rosen, and W. Gringel, Delayed production of sulfuric acid condensation nuclei in the polar stratosphere from El Chichón volcanic vapors, *J. Geophys. Res.*, *90*, 2341-2354, 1985.

Hofmann, D.J., J.M. Rosen, and J.W. Harder, Aerosol measurements in the winter/spring Antarctic stratosphere: 1, Correlative measurements with ozone, *J. Geophys. Res.*, *93*, 665-676, 1988.

Hofmann, D.J., T. Deshler, F. Arnold, and H. Schlager, Balloon observations of nitric acid aerosol formation in the Arctic stratosphere: II, Aerosol, *Geophys. Res. Lett.*, *17*, 1279-1282, 1990.

Holton, J.R., P.H. Haynes, M.E. McIntyre, A.R. Douglass, R.B. Rood, and L. Pfister, Stratosphere-troposphere exchange, *Rev. Geophys.*, *33*, 403-439, 1995.

Höpfner, M., C.E. Blom, T. Blumenstock, H. Fischer, and T. Gulde, Evidence of the removal of gaseous $HNO_3$ inside the Arctic polar vortex in January 1992, *Geophys. Res. Lett.*, *22*, 149-152, 1996.

IPCC (Intergovernmental Panel on Climate Change), *Climate Change 1995*: *The Science of Climate Change*, edited by J.T Houghton, L.G. Meira Filho, J. Bruce, H. Lee, B.A. Callander, E. Haites, N.R.P. Harris, and K. Maskell, Cambridge University Press, Cambridge, U.K., 1996.

IPCC (Intergovernmental Panel on Climate Change), *Aviation and the Global Atmosphere: A Special Report of IPCC Working Groups I and III*, edited by J.T. Houghton, D. Lister, J. Penner, M. McFarland, D. Griggs, and D. Dokken, Cambridge University Press, Cambridge, U.K., 1999 (in preparation).

Iraci, L.T., A.M. Middlebrook, and M.A. Tolbert, Laboratory studies of the formation of polar stratospheric clouds: Nitric acid condensation on thin sulfuric acid films, *J. Geophys. Res.*, *100*, 20969-20977, 1995.

Iwasaka, Y., T. Hirasawa, and H. Fukunishi, Lidar measurements on the Antarctic stratospheric aerosol layer: I, Winter enhancement, *J. Geomagn. Geoelectr.*, *37*, 1087-1095, 1985.

Jackman, C.H., D.B. Considine, and E.L. Fleming, Space Shuttle's impact on the stratosphere: An update, *J. Geophys. Res.*, *101*, 12523-12529, 1996.

Jäger, H., Stratospheric aerosols: Observations, trends, and effects, *J. Aerosol Sci.*, *22*, suppl. 1, S517-S520, 1991.

Jäger, H., O. Uchino, T. Nagai, T. Fujimoto, V. Freudenthaler, and F. Homburg, Ground-based remote sensing of the decay of the Pinatubo eruption cloud at three Northern Hemisphere sites, *Geophys. Res. Lett.*, *23*, 607-610, 1996.

Jayaraman, A., S. Ramachandran, Y.B. Acharya, and B.H. Subbaraya, Pinatubo volcanic aerosol layer decay observed at Ahmedabad (23°N), India, using neodymium:yttrium/aluminum/garnet backscatter lidar, *J. Geophys. Res.*, *100*, 23209-23214, 1995.

Jones, A.E., S. Bekki, and J.A. Pyle, On the stratospheric impact of launching the Ariane 5 rocket, *J. Geophys. Res.*, *100*, 20969-20977, 1995.

Jonsson, H.H., J.C. Wilson, C.A. Brock, R.G. Knollenberg, R. Newton, J.E. Dye, D. Baumgardner, S. Borrmann, G.V. Ferry, R. Pueschel, D.C. Woods, and M.C. Pitts, Performance of a focused cavity aerosol spectrometer for measurements in the stratosphere of particle size in the 0.06-2.0 μm diameter range, *J. Atmos. Oceanic Technol.*, *12*, 115-129, 1995.

Jonsson, H.H., J.C. Wilson, C.A. Brock, J.E. Dye, G.V. Ferry, and K.R. Chan, Evolution of the stratospheric aerosol in the Northern Hemisphere following the June 1991 volcanic eruption of Mount Pinatubo: Role of tropospheric-stratospheric exchange and transport, *J. Geophys. Res.*, *101*, 1553-1570, 1996.

Junge, C.E., C.W. Changnon, and J.E. Manson, Stratospheric aerosols, *J. Meteorol.*, *18*, 81-108, 1961.

Kasibhatla, P.S., H. Levy, W.J. Moxim, and W.L. Chameides, The relative impact of stratospheric photochemical production on tropospheric $NO_y$ levels: A model study, *J. Geophys. Res.*, *96*, 18631-18646, 1991.

Kent, G.S., and G.M. Hansen, Multiwavelength lidar observations of the decay phase of the stratospheric aerosol layer produced by the eruption of Mount Pinatubo in June 1991, *Appl. Opt.*, *37*, 3861-3872, 1998.

Khalil, M.A.K., and R.A. Rasmussen, Global sources, lifetimes and mass balances of carbonyl sulfide (OCS) and carbon-disulfide ($CS_2$) in the Earth's atmosphere, *Atmos. Environ.*, *18*, 1805-1813, 1984.

Koop, T., U.M. Biermann, W. Raber, B.P. Luo, P.J. Crutzen, and T. Peter, Do stratospheric aerosol droplets freeze above the ice frost point? *Geophys. Res. Lett.*, *22*, 917-920, 1995.

Koop, T., B.P. Luo, U.M. Biermann, P.J. Crutzen, and T. Peter, Freezing of $HNO_3/H_2SO_4/H_2O$ solutions at stratospheric temperatures: Nucleation statistics and experiments, *J. Phys. Chem. A*, *101*, 1117-1133, 1997.

Kotamarthi, V.R., M. Ko, D.K. Weisenstein, J.M. Rodriguez, and N.D. Sze, Effect of lightning on the concentration of odd nitrogen species in the lower stratosphere: An update, *J. Geophys. Res.*, *99*, 8167-8173, 1994.

Lambert, A., R.G. Grainger, C.D. Rodgers, F.W. Taylor, J.L. Mergenthaler, J.B. Kumer, and S.T. Massie, Global evolution of the Mt. Pinatubo volcanic aerosols observed by the infrared limb-sounding instruments CLAES and ISAMS on the Upper Atmospheric Research Satellite, *J. Geophys. Res.*, *102*, 1495-1512, 1997.

Langner, J., and H. Rodhe, A global three-dimensional model of the tropospheric sulfur cycle, *J. Atmos. Chem.*, *13*, 225-263, 1991.

Larsen, N., J.M. Rosen, N.T. Kjome, and B. Knudsen, Deliquescence and freezing of stratospheric aerosol observed by balloonborne backscattersondes, *Geophys. Res. Lett.*, *22*, 1233-1236, 1995.

Larsen, N., B.M. Knudsen, J.M. Rosen, N.T. Kjome, and E. Kyrö, Balloonborne backscatter observations of type 1 PSC formation: Inference about physical state from trajectory analysis, *Geophys. Res. Lett.*, *23*, 1091-1094, 1996.

Larsen, N., B.M. Knudsen, J.M. Rosen, N.T. Kjome, R. Neuber, and E. Kyrö, Temperature histories in liquid and solid polar stratospheric cloud formation, *J. Geophys. Res.*, *102*, 23505-23517, 1997.

Luo, B.P., T. Peter, and P.J. Crutzen, Freezing of stratospheric aerosol droplets, *Geophys. Res. Lett.*, *21*, 1447-1450, 1994.

Luo, B.P., K.S. Carslaw, T. Peter, and S.L. Clegg, Vapor-pressures of $H_2SO_4/HNO_3/HCl/HBr/H_2O$ solutions to low stratospheric temperatures, *Geophys. Res. Lett.*, *22*, 247-250, 1995.

Luo, B., U.K. Krieger, and T. Peter, Densities and refractive indices of $H_2SO_4/HNO_3/H_2O$ solutions to stratospheric temperatures, *Geophys. Res. Lett.*, *23*, 3707-3710, 1996.

MacKenzie, A.R., M. Kulmala, A. Laaksonen, and T. Vesala, On the theories of Type I polar stratospheric cloud formation, *J. Geophys. Res.*, *100*, 11275-11288, 1995.

Massie, S.T., J.C. Gille, D.P. Edwards, P.L. Bailey, L.V. Lyjak, C.A. Craig, C.P. Cavanaugh, J.L. Mergenthaler, A.E. Roche, J.B. Kumer, A. Lambert, R.G. Grainger, C.D. Rodgers, F.W. Taylor, J.M. Russell III, J.H. Park, T. Deshler, M.E. Hervig, E.F. Fishbein, J.W. Waters, and W.A. Lahoz, Validation studies using multiwavelength Cryogenic Limb Array Etalon Spectrometer (CLAES) observations of stratospheric aerosol, *J. Geophys. Res.*, *101*, 9757-9773, 1996.

Massie, S.T., J.E. Dye, D. Baumgardner, W.J. Randel, F. Wu, X. Tie, L. Pan, F. Figarol, G.P. Brasseur, M.L. Santee, W.G. Read, R.G. Grainger, A. Lambert, J.L. Mergenthaler, and A. Tabazadeh, Simultaneous observations of polar stratospheric clouds and $HNO_3$ over Scandinavia in January 1992, *Geophys. Res. Lett.*, *24*, 595-598, 1997.

McCormick, M.P., P. Hamill, T.J. Pepin, W.P. Chu, T.J. Swissler, and L.R. McMaster, Satellite studies of the stratospheric aerosol, *Bull. Amer. Meteorol. Soc.*, *60*, 1038-1046, 1979.

McCormick, M.P., H.M. Steele, P. Hamill, W.P. Chu, and T.J. Swissler, Polar stratospheric cloud sightings by SAM II, *J. Atmos. Sci.*, *39*, 1387-1397, 1982.

McCormick, M.P., G.S. Kent, W.H. Hunt, M.T. Osborn, L.R. Poole, and M.C. Pitts, Arctic polar stratospheric cloud observations by airborne lidar, *Geophys. Res. Lett.*, *17*, 381-384, 1990.

Meilinger, S.K., T. Koop, B.P. Luo, T. Huthwelker, K.S. Carslaw, U. Krieger, P.J. Crutzen, and T. Peter, Size-dependent stratospheric droplet composition in leewave temperature fluctuations and their potential role in PSC freezing, *Geophys. Res. Lett.*, *22*, 3031-3034, 1995.

Menzies, R.T., and D.M. Tratt, Evidence of seasonally dependent stratosphere troposphere exchange and purging of lower stratospheric aerosol from a multiyear lidar data set, *J. Geophys. Res.*, *100*, 3139-3148, 1995.

Sassen, K., D.O'C. Starr, G.G. Mace, M.R. Poellot, S.H. Melfi, W.L. Eberhard, J.D. Spinhirne, E.W. Eloranta, D.E. Hagen, and J. Hallett, The 5-6 December 1991 FIRE IFO II jet stream cirrus case study: Possible influences of volcanic aerosols, *J. Atmos. Sci.*, *52*, 97-123, 1995.

Schlager, H., F. Arnold, D.J. Hofmann, and T. Deshler, Balloon observations of nitric acid aerosol formation in the Arctic stratosphere: I, Gaseous nitric acid, *Geophys. Res. Lett.*, *17*, 1275-1278, 1990.

Sheridan, P.J., R.C. Schnell, D.J. Hofmann, and T. Deshler, Electron microscope studies of Mt. Pinatubo aerosol layers over Laramie, Wyoming during summer 1991, *Geophys. Res. Lett.*, *19*, 203-206, 1992.

Sheridan, P.J., C.A. Brock, and J.C. Wilson, Aerosol particles in the upper troposphere and lower stratosphere: Elemental composition and morphology of individual particles in northern midlatitudes, *Geophys. Res. Lett.*, *21*, 2587-2590, 1994.

Shibata, T., Y. Iwasaka, M. Fujiwara, M. Hayashi, M. Nagatani, K. Shiraishi, J. Adachi, T. Sakai, K. Susumu, and Y. Nakura, Polar stratospheric clouds observed by lidar over Spitsbergen in the winter 1994/95: Liquid particles and vertical "sandwich" structure, *J. Geophys. Res.*, *102*, 10829-10840, 1997.

Solomon, S., S. Borrmann, R.R. Garcia, R. Portmann, L. Thomason, L.R. Poole, D. Winker, and M.P. McCormick, Heterogeneous chlorine chemistry in the tropopause region, *J. Geophys. Res.*, *102*, 21411-21429, 1997.

Stanford, J.L., and J.S. Davis, A century of stratospheric cloud reports: 1870-1972, *Bull. Amer. Meteorol. Soc.*, *55*, 213-219, 1974.

Stebel, K., O. Schrems, R. Neuber, G. Beyrle, J. Biele, I. Beninga, H. Schütt, and P. von der Gathen, Polar stratospheric clouds above Spitsbergen, in *Atmospheric Ozone: Proceedings of the XVIII Quadrennial Ozone Symposium*, edited by R.D. Bojkov and G. Visconti, pp. 607-610, Parco Scientifico e Technologico d'Abruzzo, L'Aquila, Italy, 1998.

Steele, H.M., and P. Hamill, Effects of temperature and humidity on the growth and optical properties of sulfuric acid-water droplets in the stratosphere, *J. Aerosol Sci.*, *12*, 517-528, 1981.

Stefanutti, L., M. Morandi, M. Del Guasta, S. Godin, G. Mégie, J. Brechet, and J. Piquard, Polar stratospheric cloud observations over the Antarctic continent at Dumont d'Urville, *J. Geophys. Res.*, *96*, 12975-12987, 1991.

Stefanutti, L., M. Morandi, M. Del Guasta, S. Godin, and C. David, Unusual PSCs observed by lidar in Antarctica, *Geophys. Res. Lett.*, *22*, 2377-2380, 1995.

Stein, B., M. Del Guasta, J. Kolenda, M. Morandi, P. Rairous, L. Stefanutti, J.P. Wolf, and L. Wöste, Stratospheric aerosol size distributions from multispectral lidar measurements at Sodankylä during EASOE, *Geophys. Res. Lett.*, *21*, 1311-1314, 1994.

Stein, B., F. Immler, B. Mielke, P. Rairoux, C. Wedekind, L. Wöste, M. del Guasta, M. Morandi, L. Stefanutti, F. Masci, V. Rizi, R. Matthey, V. Mitev, M. Douard, J.P. Wolf, and E. Kyrö, Microlayers of solid particles observed by lidar at Sodankylä during SESAME, in *Polar Stratospheric Ozone 1995*, Air Pollution Research Report 56, edited by J.A. Pyle, N.R.P. Harris, and G.T. Amanatidis, pp. 132-135, European Commission, 1995.

Stothers, R.B., Major optical depth perturbations to the stratosphere from volcanic eruptions: Pyrheliometric period, 1881-1960, *J. Geophys. Res.*, *101*, 3901-3920, 1996.

Stowe, L.L., R.M. Carey, and P.P. Pellegrino, Monitoring the Mt. Pinatubo aerosol layer with NOAA/11 AVHRR data, *Geophys. Res. Lett.*, *19*, 159-162, 1992.

Tabazadeh, A., and O.B. Toon, The presence of $HNO_3$/$H_2O$ solid phases in the stratosphere inferred from ER-2 data, *J. Geophys. Res.*, *101*, 9071-9078, 1996.

Tabazadeh, A., R.P. Turco, and M.Z. Jacobson, A model for studying the composition and chemical effects of stratospheric aerosols, *J. Geophys. Res.*, *99*, 12897-12914, 1994.

Tabazadeh, A., O.B. Toon, and P. Hamill, Freezing behavior of stratospheric sulfate aerosols inferred from trajectory studies, *Geophys. Res. Lett.*, *22*, 1725-1725, 1995.

Tabazadeh, A., O.B. Toon, B.L. Gary, J.T. Bacmeister, and M.R. Schoeberl, Observational constraints on the formation of Type 1a polar stratospheric clouds, *Geophys. Res. Lett.*, *23*, 2109-2112, 1996.

Taylor, F.W., A. Lambert, R.G. Grainger, C.D. Rodgers, and J.J. Remedios, Properties of Northern Hemisphere stratospheric clouds and volcanic aerosol in 1991/92 from UARS/ISAMS satellite measurements, *J. Atmos. Sci.*, *51*, 3019-3026, 1994.

Thomason, L.W., and L.R. Poole, Use of stratospheric aerosol properties as diagnostics of Antarctic vortex processes, J. *Geophys. Res.*, *98*, 23003-23012, 1993.

Thomason, L.W., L.R. Poole, and T. Deshler, A global climatology of stratospheric aerosol surface area density deduced from Stratospheric Aerosol and Gas Experiment II measurements: 1984-1994, *J. Geophys. Res.*, *102*, 8967-8976, 1997a.

Thomason, L.W., G.S. Kent, C.R. Trepte, and L.R. Poole, A comparison of the stratospheric aerosol background periods of 1979 and 1989-1991, *J. Geophys. Res.*, *102*, 3611-3616, 1997b.

Tie, X.X., G.P. Brasseur, B. Briegleb, and C. Granier, 2-dimensional simulation of Pinatubo aerosol and its effect on stratospheric ozone, *J. Geophys. Res.*, *99*, 20545-20562, 1994.

Toon, O.B., and M.A. Tolbert, Spectroscopic evidence against nitric acid trihydrate in polar stratospheric clouds, *Nature*, *375*, 218-221, 1995.

Toon, O.B., E.V. Browell, S. Kinne, and J. Jordan, An analysis of lidar observations of polar stratospheric clouds, *Geophys. Res. Lett.*, *17*, 393-396, 1990.

Toon, O., E. Browell, B. Gary, L. Lait, J. Livingston, P. Newman, R. Pueschel, P. Russell, M. Schoeberl, G. Toon, W. Traub, F.P.J. Valero, H. Selkirk, and J. Jordan, Heterogeneous reaction probabilities, solubilities, and the physical state of cold volcanic aerosols, *Science*, *261*, 1136-1140, 1993.

Trepte, C.R., and M.H. Hitchman, Tropical stratospheric circulation deduced from satellite aerosol data, *Nature*, *355*, 626-628, 1992.

Trepte, C.R., R.E. Veiga, and M.P. McCormick, The poleward dispersal of Mount Pinatubo volcanic aerosol, *J. Geophys. Res.*, *98*, 18563-18573, 1993.

Turco, R.P., P. Hamill, O.B. Toon, R.C. Whitten, and C.S. Kiang, A one-dimensional model describing aerosol formation and evolution in the stratosphere: I, Physical processes and mathematical analogs, *J. Atmos. Sci.*, *36*, 699-717, 1979.

Turco, R.P., R.C. Whitten, and O.B. Toon, Stratospheric aerosols: Observations and theory, *Rev. Geophys. Space Phys.*, *20*, 233-279, 1982.

Turco, R.P., O.B. Toon, and P. Hamill, Heterogeneous physicochemisty of the polar ozone hole, *J. Geophys. Res.*, *94*, 16493-16510, 1989.

Twomey, S.A., Information content in remote sensing, *Appl. Opt.*, *13*, 942-945, 1974.

Twomey, S.A., *Introduction to the Mathematics of Inversion in Remote Sensing and Indirect Measurements*, 243 pp., Elsevier Science, New York, 1977.

Uchino, O., T. Nagai, T. Fujimoto, W.A. Matthews, and J. Orange, Extensive lidar observations of the Pinatubo aerosol layers at Tsukuba (36.1°N), Naha (26.2°N), Japan, and Lauder (45.0°S), New Zealand, *Geophys. Res. Lett.*, *22*, 57-60, 1995.

Vaughan, G., D.P. Wareing, S.B. Jones, L. Thomas, and N. Larsen, Lidar measurements of Mt. Pinatubo aerosols at Aberystwyth from August 1991 through March 1992, *Geophys. Res. Lett.*, *21*, 1315-1318, 1994.

Vitt, F.M., and C.H. Jackman, A comparison of sources of odd-nitrogen production from 1974 through 1993 in the Earth's middle atmosphere as calculated using a 2-dimensional model, *J. Geophys. Res.*, *101*, 6729-6739, 1996.

Volkert, H., and D. Intes, Orographically forced stratospheric waves over northern Scandinavia, *Geophys. Res. Lett.*, *19*, 1205-1208, 1992.

Volz, F.E., and R.M. Goody, The intensity of the twilight and upper atmospheric dust, *J. Atmos. Sci.*, *19*, 385-406, 1962.

Wandinger, U., A. Ansmann, J. Reichadt, and T. Deshler, Determination of stratospheric aerosol microphysical properties from independent extinction and backscattering measurements with a Raman lidar, *Appl. Opt.*, *34*, 8315, 1995.

Wang, P.H., P. Minnis, M.P. McCormick, and G.S. Kent, A 6-year climatology of cloud occurrence frequency from Stratospheric Aerosol and Gas Experiment II observations (1985-1991), *J. Geophys. Res.*, *101*, 29407-29429, 1996.

Wedekind, C., F. Immler, B. Mielke, P. Rairoux, B. Stein, L. Wöste, M. Del Guasta, M. Morandi, L. Stefanutti, F. Masci, V. Rizi, R. Matthey, V. Mitev, M. Douard, J.P. Wolf, and E. Kyrö, Polar stratospheric cloud measurements by multispectral lidar in Sodankylä in winter 1994/95, in *Advances in Atmospheric Remote Sensing with Lidar*, edited by A. Ansmann, R. Neuber, P. Rairoux, and U. Wandinger, pp. 513-516, Springer-Verlag, Berlin, 1997.

Weisenstein, D.K., G.K. Yue, M.K.W. Ko, N.-D. Sze, J.M. Rodriguez, and C.J. Scott, A two-dimensional model of sulfur species and aerosols, *J. Geophys. Res.*, *102*, 13019-13035, 1997.

Wennberg, P.O., R.C. Cohen, R.M. Stimpfle, J.P. Koplow, J.G. Anderson, R.J. Salawitch, D.W. Fahey, E.L. Woodbridge, E.R. Keim, R.S. Gao, C.R. Webster, R.D. May, D.W. Toohey, L.M. Avallone, M.H. Proffitt, M. Loewenstein, J.R. Podolske, K.R. Chan, and S.C. Wofsy, Removal of stratospheric $O_3$ by radicals: In situ measurements of OH, $HO_2$, NO, $NO_2$, ClO, and BrO, *Science*, *266*, 398-404, 1994.

Wilson, J.C., J.H. Hyun, and E.D. Blackshear, The function and response of an improved stratospheric condensation nuclei counter, *J. Geophys. Res.*, *88*, 6781-6785, 1983.

Wilson, J.C., M. Loewenstein, D.W. Fahey, B. Gary, S.D. Smith, K.K. Kelly, G.V. Ferry, and K.R. Chan, Observations of condensation nuclei in the Airborne Antarctic Ozone Experiment: Implications for new particle formation and polar stratospheric cloud formation, *J. Geophys. Res.*, *94*, 16437-16448, 1989.

Wilson, J.C., M.R. Stoltzenburg, W.E. Clark, M. Loewenstein, G.V. Ferry, K.R. Chan, and K.K. Kelly, Stratospheric sulfate aerosol in and near the Northern Hemisphere polar vortex: The morphology of the sulfate layer, multimodal size distributions, and the effect of denitrification, *J. Geophys. Res.*, *97*, 7997-8013, 1992.

Wilson, J.C., H.H. Jonsson, C.A. Brock, D.W. Toohey, L.M. Avallone, D. Baumgardner, J.E. Dye, L.R. Poole, D.C. Woods, R.J. DeCoursey, M. Osborn, M.C. Pitts, K.K. Kelly, K.R. Chan, G.V. Ferry, M. Loewenstein, J.R. Podolske, and A. Weaver, In situ observations of aerosol and chlorine monoxide after the 1991 eruption of Mount Pinatubo: Effect of reactions on sulfate aerosol, *Science*, *261*, 1140-1143, 1993.

WMO (World Meteorological Organization), *Scientific Assessment of Ozone Depletion: 1994*, Global Ozone Research and Monitoring Project—Report No. 37, Geneva, 1995.

Wofsy S.C., R.J. Salawitch, J.H. Yatteau, M.B. McElroy, B.W. Gandrud, J.E. Dye, and D. Baumgardner, Condensation of $HNO_3$ on falling ice particles: Mechanisms for denitrification of the polar stratosphere, *Geophys. Res. Lett.*, *17*, 449-460, 1990.

Young, A.T., Revised depolarization corrections for atmospheric extinction, *Appl. Opt.*, *19*, 3427-3428, 1980.

Young, R.E., H. Houben, and O.B. Toon, Radiatively forced dispersion of the Mt. Pinatubo volcanic cloud and induced temperature perturbations in the stratosphere during the first few months following the eruption, *Geophys. Res. Lett.*, *21*, 369-372, 1994.

Yue, G.K., L.W. Thomason, L.R. Poole, P.H. Wang, D. Baumgardner, and J.E. Dye, Aerosol surface areas deduced from early 1993 SAGE II data and comparisons with stratospheric photochemistry, aerosols, and Dynamics Expedition measurements, *Geophys. Res. Lett.*, *22*, 2933-2936, 1995.

Zander, R., C.P. Rinsland, C.B. Farmer, J. Namkung, R.H. Norton, and J.M. Russell III, Concentrations of carbonyl sulfide and hydrogen cyanide in the free upper troposphere and lower stratosphere deduced from ATMOS/Spacelab 3 infrared solar occultation spectra, *J. Geophys. Res.*, *93*, 1669-1678, 1988.

Zhang, R., P.J. Wooldridge, J.P.D. Abbatt, and M.J. Molina, Physical chemistry of the $H_2SO_4/H_2O$ binary system at low temperatures: Stratospheric implications, *J. Phys. Chem.*, *97*, 7351-7358, 1993.

Zhang, R.Y., M.T. Leu, and M.J. Molina, Formation of polar stratospheric clouds on preactivated background aerosols, *Geophys. Res. Lett.*, *23*, 1669-1672, 1996.

Zhao, J., O.B. Toon, and R.P. Turco, Origin of condensation nuclei in the springtime polar stratosphere, *J. Geophys. Res.*, *100*, 5215-5227, 1995.

Zolensky, M.E., D.S. McKay, and L.A. Kaczor, A tenfold increase in the abundance of large solid particles in the stratosphere, as measured over the period 1976-1984, *J. Geophys. Res.*, *94*, 1047-1056, 1989.

# CHAPTER 4

# Ozone Variability and Trends

**Lead Authors:**
R.D. Bojkov
R.D. Hudson

**Coauthors:**
L. Bishop
V. Fioletov
J.M. Russell III
R.S. Stolarski
O. Uchino
C.S. Zerefos

**Contributors:**
R. Atkinson
D.S. Balis
P.K. Bhartia
H. Claude
L. Flynn
R. Guicherit
F. Hasebe
G. Labow
J.A. Logan
R.D. McPeters
A.J. Miller
R. Müller
R. Piacenti
W.J. Randel
H. Smit
B.H. Subbaraya
K. Tourpali
P. von der Gathen
A. Zand
Members of the SPARC/IOC Profile Trends Panel

# CHAPTER 4

## OZONE VARIABILITY AND TRENDS

### Contents

## SCIENTIFIC SUMMARY

### Non-Polar Ozone

#### Total Column Ozone

- The 1994 Assessment noted large negative trends in midlatitude total ozone in the 1980s, with an additional marked decrease in Northern Hemisphere midlatitude ozone following the large enhancement of stratospheric aerosol caused by the eruption of Mt. Pinatubo in 1991. By 1994, the transient effect on total ozone of the Mt. Pinatubo aerosols had largely disappeared. Since 1994, non-polar total ozone, while variable, has not shown an overall negative trend, and total ozone levels are now at a higher level than would be predicted by a linear extrapolation of the pre-Pinatubo trend. Extrapolation of the pre-Pinatubo trend of -2.9%/decade in Northern Hemisphere midlatitudes (25°-60°) would predict an ozone depletion relative to 1979 of -5.5% at the end of 1997, whereas instead the deviations have averaged about -4% in the last 2 or 3 years. Seasonally, the corresponding winter/spring (December-May) and summer/fall (June-November) changes averaged about -5.5% and -2.8%, respectively, whereas a linear extrapolation of the pre-Pinatubo trend would predict -7.6% and -3.4%, respectively. In the Southern Hemisphere (25°-60°), trend extrapolation would predict -7.2% depletion at the end of 1997, whereas the smoothed data indicate a 1997 value of about -4% (satellite) or -5% (ground).

- As shown in Table 4-1, trends in total ozone from January 1979 updated through the end of 1997 exhibit the now-familiar pattern of negative trends with the following features:

  1. Trends in both hemispheres in mid and high latitudes in all seasons are negative, large, and statistically significant.

  2. Trends in the equatorial regions (20°S to 20°N) are statistically nonsignificant.

**Table 4-1. Total ozone trends in percent per decade and uncertainties (two standard errors) from Total Ozone Mapping Spectrometer (TOMS) data*.**

| Latitudes | | Trend (%/decade) | | |
|---|---|---|---|---|
| | | Annual | Dec-May[1] | Jun-Nov[2] |
| North | 50°–65° | –3.7 ± 1.6 | –4.4 ± 2.6 | –2.8 ± 1.3 |
| North | 30°–50° | –2.8 ± 1.7 | –3.8 ± 2.4 | –1.7 ± 1.3 |
| Equatorial | 20°–20° | –0.5 ± 1.3 | –0.3 ± 1.6 | –0.7 ± 1.3 |
| South | 30°–50° | –1.9 ± 1.3 | –2.4 ± 1.2 | –1.4 ± 1.9 |
| South | 50°–65° | –4.4 ± 1.8 | –3.4 ± 1.6 | –5.2 ± 2.6 |

* Values in table are averages from Total Ozone Mapping Spectrometer (TOMS) trends in Table 4-5. Ground-based trends are shown in Table 4-4 for somewhat different latitude bands.

1 North winter/spring and south summer/fall.

2 North summer/fall and south winter/spring.

## OZONE TRENDS

- In the middle and high latitudes, the overall ozone amount has declined during all months of the year, and the amplitude of the annual cycle for stations has decreased by about 15% mainly as a result of a decline in the maximum. In the Northern Hemisphere, the trends are much larger (more negative) in the winter and spring seasons (December-January-February, March-April-May) about -3 to -6%/decade, than in summer and fall (June-July-August, September-October-November), about -1 to -3%/decade.

- Regional trends in total ozone show some systematic differences among continental-scale regions at the same latitudes, e.g., Siberia, Europe, and North America. The longitudinal trend calculations using gridded data from TOMS show the strongest negative trends over Siberia in spring and large negative trends over Europe in winter and spring. North America shows relatively smaller trends in winter/spring.

- Total ozone levels at 60°N-60°S were at their lowest in 1993 in the aftermath of the Mt. Pinatubo eruption. Since that time, ground-based ozone values have remained fairly constant, whereas the Earth Probe (EP)-TOMS record, which began in 1996, shows global ozone to be about 2% higher. This discrepancy, which is not seen in the northern midlatitudes (the region where we have most confidence in the observational record) has not been resolved.

- New scientific understanding shows that quasi-decadal ozone oscillations have been induced by major volcanic eruptions in the past 20 years. The confounding influences of solar and volcanic effects on ozone time-series analyses could affect the interpretation of recent changes.

### Vertical Ozone Distribution

- Based on the Stratospheric Aerosol and Gas Experiment (SAGE I/II) Version 5.96 data, there is no significant inter-hemispheric difference in upper stratospheric trends for data extended through 1996.

- Combined trends and uncertainties (including both statistical and systemic errors) have been estimated from all available measurement systems. This was done only for the northern midlatitudes. The combined trends are negative at all altitudes between 10 and 50 km and are statistically significant at the 2-sigma level. The combined trend has two local maxima, $-7.4 \pm 2.0\%$/decade at 40 km and $-7.6 \pm 4.6\%$/decade at 15 km. The smallest trend deduced, $-2.0 \pm 1.8\%$/decade, occurred at 30 km. This combined trend, representing the results from all the independent data sources, is an indicator of the robustness of the trend results.

- Statistically significant trends of -6 to -8%/decade have been found at 40-50 km altitude for the midlatitudes. There is good agreement between SAGE I/II and Umkehr. The Solar Backscatter Ultraviolet (SBUV/SBUV2) spectrometer combined record shows less-negative trends. There is a factor of 2 seasonal variation in the trends, with the maximum value in winter.

- Trends in the column amount of ozone above 20 km deduced from SAGE I/II are much less than the column trends deduced from TOMS. However, the TOMS-SAGE differences are consistent with the sonde trends below 20 km. There is also a consistent seasonal variation for the satellite and sonde data.

- There is good agreement between SAGE I/II trends and sonde trends over the altitude region from 15 to 27 km at northern latitudes for the time period 1980 to 1996. This is a significant improvement compared with previous comparisons due principally to the revision of the SAGE dataset. The agreement in the derived trends from SAGE II-only and the sondes is excellent for the period 1984-1996.

- Both sonde and SAGE data show that most of the column ozone loss at midlatitudes occurs between 10 and 25 km altitude, with peak loss between 15 and 20 km. The seasonal variation of the trend occurs primarily between 10 and 20 km, with largest trends in winter and spring.

## Polar Ozone

### Arctic Ozone

- In the Arctic vortex, extremely low ozone values were deduced in late-winter/spring (a loss of about 100 Dobson units (DU; m-atm cm) with extremes exceeding ~200 DU below the 1964-1976 averages) in 6 out of the last 9 years. They are comparable with the values recorded (episodically) in the areas adjacent to the vortex. The ozone deficiencies are observed mostly in the layer a few kilometers above the tropopause.

- In the spring seasons of 1993, 1995, 1996, and 1997, the difference in total ozone from the pre-1976 level was comparable with differences observed in the austral spring.

### Antarctic Ozone

- The large ozone losses continued at high latitudes in the Southern Hemisphere. The trends from 1979 in winter (June-July-August) are up to -6%/decade, and especially, in spring (September-October-November), up to -10%/decade, due to the influence of the Antarctic ozone hole. Trends in the summer months are smaller (-2 to -5%).

- Since the last Assessment, the monthly total ozone in September and October in Antarctica continued at a level of 40 to 55% below the pre-ozone-hole values, with up to a 70% decrease for periods of a week or so.

- At maximum expansion, the size of the ozone hole (defined as the area containing ozone values less than 220 DU) was nearly the same as during the early 1990s ($>20 \times 10^6$ km$^2$).

- In the lower stratosphere, between 12 and 20 km, over the September-November period, the monthly-mean ozone content was, on the average, between 60 and 90% below the pre-ozone-hole values and at times nearly completely destroyed.

## 4.1 INTRODUCTION

Several techniques, both satellite and ground based, have been developed to measure ozone in the atmosphere; some detect the absorption and emission of solar and atmospheric radiation, and others use chemical titration. While it has been relatively easy to measure total column ozone at a particular time and place, it has not proved easy to detect changes in total column ozone or the profile of a few percent over periods exceeding a decade. To do this one must know how the absolute calibration of the instrument (or instruments) and any information (a priori, viewing geometry, etc.) used in the retrieval algorithms change with time. One way of verifying that the drifts in these quantities are properly understood is by comparing the trends obtained by independent instruments. Thus, for example, the reason that one has confidence in the total ozone trends is that data from the satellite-based Nimbus-7 Total Ozone Mapping Spectrometer (TOMS) and the ground-based Dobson network both give the same trend within their assigned errors.

In Section 4.2 the sources of the data used in this Assessment are discussed. Detailed descriptions of many of the major techniques and instruments can be found in two reports. The report of the International Ozone Trends Panel (WMO, 1990a) contains descriptions of the instruments used in the total ozone studies. Since the 1994 Assessment (WMO, 1995), scientists from the World Climate Research Programme (WCRP) project on Stratospheric Processes and their Role in Climate (SPARC) and the International Ozone Commission (IOC) have performed a similar study of the trends in the vertical distribution of ozone (WMO, 1998). The reader is referred to those documents for details of the instruments and the associated algorithms.

The various sources of the variability in the ozone fields are discussed in Section 4.3. It is this variability that often sets the upper limit on the ability to make estimates of the long-term trends. Section 4.4 gives an account of the statistical methods used in estimating ozone trends, including a comparison of the different techniques that are currently used. Sections 4.5 and 4.6 describe the long-term changes in total ozone and vertical profiles, respectively. The data used in this analysis extend to December 1997 for the total ozone and to January 1997 for the ozone profiles.

## 4.2 DATA SOURCES

### 4.2.1 Total Ozone

#### 4.2.1.1 Ground-Based Total Ozone Measurements

Three types of ground-based total ozone instruments have been used in this Assessment: the Dobson spectrophotometer, the Brewer spectrophotometer, and the filter ozonometer. The error in the most accurate direct-sun ozone observations by the Dobson spectrophotometer for a well-calibrated and operated instrument is about 1% ($1\sigma$) (Basher, 1995). For zenith sky measurements it is about 3%. The potential long-term stability of the Dobson instrument is about $\pm 0.5\%$ ($1\sigma$) for annual means (WMO, 1980). Details on Dobson instrument accuracy and error sources can be found in a number of publications (e.g., WMO, 1990a, 1992, 1993). More than 90 Dobson stations are operated continuously. These are periodically calibrated against the World Primary Standard Dobson no. 83. WMO traveling standard lamp tests show that more than 75% of the Dobson instruments differ with the standard lamp by less than $\pm 1.5\%$ (Basher, 1995).

The Brewer spectrophotometers demonstrate performances similar to those of the Dobson instruments (Kerr *et al.*, 1988). Most Brewer instruments are calibrated by the traveling standard, with the traveling standard itself calibrated against the Brewer reference "triad" in Toronto (Kerr *et al.*, 1998). Observed long-term trends between the different Brewer instruments of the triad, with Toronto Dobson instrument no. 77 and TOMS, do not exceed 1%/decade (Kerr *et al.*, 1998).

The M-83 filter ozonometer and its later modification, the M-124, have been used for total ozone observations, mostly in the former USSR, since the early 1960s. The filter ozonometer data have recently been reevaluated (Bojkov *et al.*, 1994). Data prior to the modernization of the M-83 instruments in 1972 were found to be largely unreliable. The filter instruments tend to be less accurate than the Dobson and Brewer spectrophotometers. Unlike the Dobson and Brewer stations, filter instrument stations have used several different instruments over their period of operation. Typically, the former-USSR network filter instruments were replaced every 2-3 years. The errors reported by the

instrument developers for well-calibrated and maintained filter instruments (M-124) are about 3% for direct sun and 5% for zenith sky observations (Gustin *et al.*, 1985). The reevaluated dataset is consistent with these numbers. More than 40 stations using filter instruments had long enough records for use in this Assessment.

All ground-based total ozone data deposited in the World Ozone and Ultraviolet Data Centre (WOUDC) were examined for possible inclusion in this Assessment, but for a variety of reasons a number were rejected. In general, the quality criteria as defined by Bojkov *et al.* (1995b) were used and are summarized here. First, only records starting before 1984 and having data after 1992 were considered sufficiently long for meaningful analyses. Second, a minimum of 10 days of data was required for a monthly mean to be included. Exceptions were made only for Buenos Aires for a few years in the 1970s and for Nairobi. In these cases the limit was decreased to 6 days if distributed evenly throughout the month. Third, some data records show large variations and deviations against nearby stations and satellite overpasses that could not be explained in terms of any natural phenomena and for which calibration data were not available. For a few stations it was obvious that the data were in error, but information on their correction or reevaluation was lacking (e.g., Casablanca, Manila). These data were not used. For this Assessment, the period of analysis was selected as January 1964 to December 1997, because before 1964 a sufficiently dense network was operating only in Europe, Japan, Australia, and North America.

The necessity for data reevaluation has been described before (e.g., Bojkov *et al.*, 1990), and the recommended procedures (WMO, 1993) for data reevaluation have been followed. For 34 stations from Brazil, Germany, Japan, United Kingdom, United States, and other countries the records were reevaluated by the national operating agencies (Angreji, 1989; Lapworth 1991; Lehmann *et al.*, 1992; Komhyr *et al.*, 1994; Kohler and Claude, 1998; Sahai *et al.*, 1998; Staehelin *et al.*, 1998a) and the reevaluated data submitted to the WOUDC. The present Assessment is based on the dataset currently available from the WOUDC. However, in some cases, some additional considerations have been applied:

- Data from three Indian stations were used, but only those starting from 1975, coinciding with their participation with their national standard Dobson in the World Meteorological Organization (WMO) intercomparison in Belsk (1974).
- Dobson instrument no. 97 operated at Buenos Aires before the calibration in March 1977 had readings 5.4% too low, and these data were not corrected or redeposited with the WOUDC. Based on this calibration, all data before March 1977 were increased by 5.4%.
- The Macquarie Island record was verified and revised back to 1979 (Lehmann *et al.*, 1992) and these data were used in the analysis. Lehmann *et al.* (1992) also show some problems with the data in the early 1980s, and for the period 1979-1986 a provisionally reevaluated dataset (WMO, 1990a) was used.
- Major problems with the Brisbane record in the early 1980s have been reported by Bojkov (1986). Provisionally reevaluated data prior to May 1985, as shown in WMO (1996), were used for Brisbane.
- Following a recommendation from the Japan Meteorological Agency (T. Ito, Japan Meteorological Agency, Japan, personal communication, 1998), the data for Kagoshima from November 1963 to July 1967 and January 1970 to March 1987 data have been increased by 9 Dobson units (DU; m-atm cm).
- On the basis of an instrument intercomparison in Arosa, in 1995, and comparisons with nearby stations and satellite data, all Sestola data from 1981-1994 have been reduced by 2%.
- Based on a few calibrations of the Nairobi Dobson instrument, the zenith sky data were not used, and the direct sun data prior to 1 May 1995 were increased by 2.6%.
- To obtain a longer record, data from nearby stations were combined for two cases. The record from the New Zealand station at Invercargill was added to the Lauder record up to 1985 with a small (1-2%) correction for the annual cycle. Also, the earlier Bracknell data were incorporated in the record of the U.K. station at Camborne.

The main dataset used in the present analysis is composed of monthly means of total ozone from 44 Dobson stations, some of which (Edmonton, Goose Bay, Churchill, Kodaikanal) were equipped with Brewer instruments during the last 10 years. The differences between Dobson and Brewer data for overlapping periods are within ±1%. Brewer data were also used to fill short gaps in Dobson records at Hohenpeissenberg and Vigna Di Valle. (The stations and their latitude, data availabil-

ity, and seasonal and annual trends since 1979 are listed in Table 4-4.) Data from 21 ground-based stations north of 60°N were used for calculating Arctic trends, and from four Dobson stations south of 60°S for Antarctic trends. All total ozone data used in this Assessment are based on the Bass-Paur absorption coefficients.

#### 4.2.1.2 Satellite Total Ozone Measurements

***Total Ozone Mapping Spectrometer (TOMS)***

Data from three TOMS instruments were considered in this Assessment: Nimbus-7, Meteor-3, and Earth Probe (EP). The Nimbus-7 spacecraft operated from October 1978 to May 1993. Meteor-3 TOMS was in operation from August 1991 to December 1994. EP TOMS was launched in August 1996 and, at the time of the writing of this report, is still operating. All TOMS data were processed with the Version 7 TOMS algorithm. Nimbus-7 TOMS total ozone has an absolute error of ±3%, a random error of ±2% (1σ), and the uncertainty in the drift for 14 years is ±1.5% (though somewhat higher at higher latitudes) (McPeters *et al.*, 1996). For Meteor-3 TOMS these numbers are ±3%, ±3%, and ±1% for 3 years, respectively (Herman *et al.*, 1996).

Nimbus-7 TOMS data were used for the period November 1978 through April 1993, and Meteor-3 data for May 1993 until October 1994. The Meteor-3 data have gaps due to high solar zenith angle conditions because of the precessing orbit. During periods when the solar zenith angle is greater than 80°, the data are considered unreliable and were not used in this Assessment. Preliminary Earth Probe data from August 1996 to March 1998 were used. Following the recommendation by McPeters and Labow (1996), only TOMS data taken at solar zenith angles less than 80° were used.

***Solar Backscatter Ultraviolet (SBUV), SBUV/2, BUV***

The SBUV instrument on board the Nimbus-7 spacecraft and the SBUV/2 instruments on board the National Oceanic and Atmospheric Administration (NOAA) spacecraft NOAA-9, NOAA-11, and NOAA-14 measure both total ozone and the vertical distributions of ozone (reported as ozone profiles in DU for 12 Umkehr layers (~5 km thick each), although the actual vertical resolution is poorer). The uncertainties are: absolute error, 3%; random error, 2%; and time-dependent drift error, 3% (Fleig *et al.*, 1990). The SBUV data are available from November 1978 to May 1990. The data after February 1987 are affected by an out-of-synchronization condition and have been corrected by a "scene-stabilization" method described by Gleason and McPeters (1995).

The NOAA-11 SBUV/2 data are available from January 1989 to October 1994, with decreasing coverage of the Southern Hemisphere over the instrument lifetime due to precession of the NOAA-11 equator crossing times. The NOAA-11 SBUV/2 data have recently been reprocessed using updated calibrations and instrument behavior characterizations and an algorithm change to correct for grating position errors in the latter part of the record to produce the Version 6.1.2 dataset. The NOAA-11 absolute calibration was adjusted to match the Shuttle SBUV (SSBUV) calibration (Hilsenrath *et al.*, 1993), while the time-dependent calibration was maintained using an onboard calibration lamp system and verified through comparisons with SSBUV measurements. NOAA-9 SBUV/2 data have also been reprocessed with an adjustment to SSBUV and an updated calibration. Version 6.1.2 data are available for April 1985 to December 1996. The precession of the NOAA-9 orbit led to a period of poor viewing conditions from 1989 to 1992 (e.g., Fioletov *et al.*, 1998b).

All datasets have been processed with the Version 6 Backscatter Ultraviolet (BUV) algorithm described in Chapter 1 of the SPARC/IOC report (WMO, 1998) and Bhartia *et al.* (1996). Nimbus-7 SBUV data were used from November 1978 through December 1988, and NOAA-11 SBUV/2 data were used from January 1989 through January 1994. The NOAA-9 data for February 1994 to December 1996 were used. The NOAA-14 data have not been used in this Assessment.

The BUV instrument was launched on the Nimbus-4 satellite in April 1970. The satellite was placed in a sun-synchronous orbit with a near-noon local crossing time. The instrument was similar in design to the SBUV instruments (Heath *et al.*, 1975). The Nimbus-4 satellite had a series of power array failures that limited the instrument's data coverage. The first and most serious power failure occurred in May 1972, causing the data coverage to be sporadic throughout the rest of the mission (May 1977). Details on the BUV instrument and algorithm can be found in Dave and Mateer (1967), Heath *et al.* (1973), and Krueger *et al.* (1973).

and 60°N. The 1994 Assessment (WMO, 1995) showed some significant differences between SAGE- and ozonesonde-derived trends in the lower stratosphere, with SAGE trends being larger. These differences were a major focus of the SPARC/IOC study (WMO, 1998). The validity of SAGE measurements for altitude ($Z$) ≤ 25 km was carefully scrutinized due to possible errors in the data caused, for example, by high aerosol loading resulting from volcanic eruptions (e.g., Mt. Pinatubo) or by ice crystal absorption due to high cirrus clouds (Cunnold *et al.*, 1996).

During the pre-satellite period, before 1978/1979, ozonesonde and Umkehr/Dobson measurements provided the only datasets for study of ozone change in any altitude region. Therefore, it is important to characterize the quality of the sonde and Umkehr time series during that period (i.e., 1965-1979). There are indications from the SPARC/IOC study (WMO, 1998) that in the tropopause region up to 17-20 km, ozonesonde results are more reliable than satellite measurements. That study used the newest, latest, and revised versions of the different ozone ground-based, in situ, and satellite datasets available before the end of June 1997. Those data were either linked to or stored on a dedicated temporary database. Once the report is released in the fall of 1998, all the data will be made publicly available at the SPARC/Ozone Trend Assessment World Wide Web site, and additionally the sonde data will be placed in the WOUDC in Toronto.

#### 4.2.2.2 Data Limitations for Use in Trend Determinations

The upper altitude limit for applying SAGE II data to determine trends is on the order of 50 km, based on noise in SAGE II and intercomparisons with HALOE data. The lower limit is less determinate, most likely because of atmospheric variability at low altitudes and aerosol effects both in SAGE II measurements and the data used for comparisons. In most instances, the differences in trends between SAGE II and correlative data start to increase below about 20 km and they become much more variable, thus limiting the lower altitude at which derived trends can be validated. This is not to say that trends from the different measurement systems are invalid in this range, but only that for the systems used in the intercomparisons, a less definitive statement can be made about trend validity. The low-altitude problems represent one of the most serious limitations for using the data because they affect the region that is most in need of improved understanding. Even though great attempts were made to reduce or eliminate aerosol effects in the latest SAGE II algorithm (Version 5.96), it is clear that the effects remain and are prominent.

Various screening approaches for the SAGE II data were evaluated by the SPARC/IOC study team, including eliminating values based on the aerosol extinction value, eliminating values based on the magnitude of the SAGE II error bars for ozone, or eliminating specific time periods. The latter approach was chosen and the time and altitude screening guide is included in Table 2-2 of the report (WMO, 1998).

There are some obvious sunrise-sunset differences in the SAGE II data that are important only above approximately 45 km. The data show a difference of ~10% between sunrise and sunset ozone values at 1 mb (sunset higher). This is not physical and is much greater, for example, than the difference between HALOE sunrise-sunset values, which is approximately 2%. There is no reason to prefer SAGE II sunrise measurements over sunset (or vice versa). The SPARC/IOC study recommends combining sunrise and sunset for doing trend studies, but because the reason for the sunrise-sunset differences is unknown, the error bars for derived trends will be increased above 45 km.

Another possible limitation is the effect of any SAGE I/II data offsets. While some evidence exists from Hohenpeissenberg, Payerne, and Uccle ozonesonde-SAGE comparisons to suggest that SAGE I and SAGE II overlapping measurements are inconsistent, the results are not statistically significant. It is known, however, that there is a latitude-dependent altitude registration difference between the two datasets that should be corrected before combining them. The correction scheme developed by Wang *et al.* (1996) was adopted as a satisfactory correction, leading to approximately a 300-m adjustment. The uncertainty in this correction for each latitude is about 100 m. Below 20-km altitude, the simple upward shift of the SAGE I profiles may be incorrect because of the large Rayleigh scattering contribution to the 0.6-nm extinction at these altitudes. A rigorous inversion of the SAGE I data to correct the altitude registration problem would be preferable. It is recommended that if the SAGE I data are used for trend calculations at altitudes below 20 km, they be used with caution. More intercomparisons and further study are needed to draw

firm conclusions about the offset, its errors, and any latitudinal dependence in the uncertainties.

The SBUV measurement system is believed to provide good information over layers 5 to 9 (25 km to 45 km). The upper altitude limit is driven by the coarse vertical resolution of the SBUV (~8 km) coupled with the declining ozone levels with increasing altitude. The lower limit is a result of reduced sensitivity due to poor vertical resolution, declining ozone values, and low information content below the ozone peak. The Umkehr has similar limitations (layers 4 to 8, or 20 km to 40 km) for comparable reasons. The ozonesonde measurements are generally limited to an upper altitude of about 27 km due to pump correction errors and sensing solution changes. Also, both the Brewer-Mast (BM) and electrochemical concentration cell (ECC) sondes are affected by the presence of sulfur dioxide ($SO_2$) in the atmosphere, and when this is enhanced by a volcanic event, for example, there could be false short-term changes in measured ozone as the $SO_2$ layer decays. There are still important differences observed between results from different sounding stations using the same type of ozonesonde, and this is believed to be due to differences in the preparation and correction procedures applied at the various launch sites. Although much progress has been made to improve the quality and homogeneity of the ozonesonde data since the last Assessment (WMO, 1995), there is still an urgent need to investigate and intercompare the instrumental performance of the different sonde types as well as a need to revise and agree on procedures for preparation and data processing. Until this happens and methods are uniformly applied, the differences will persist.

#### 4.2.2.3 INTERCOMPARISONS

Coincidence criteria used for all comparisons shown are ±2° latitude, ±12.5° longitude, and 2 days time, unless otherwise noted. It was found, however, when validating the Nimbus-7 Limb Infrared Monitor of the Stratosphere (LIMS) data, that even 3 hours could make an important difference in the temperature agreement; but because SAGE II uses the solar occultation experiment approach, the number of coincidence opportunities are limited, requiring adoption of the criteria used. When comparisons are done against SAGE II, SAGE II is usually the reference for calculating percentages. Also unless otherwise noted, the error bars shown are the 2 standard error mean bars (or 2 sem), calculated by dividing twice the standard deviation by the square root of the number of samples used in the comparison.

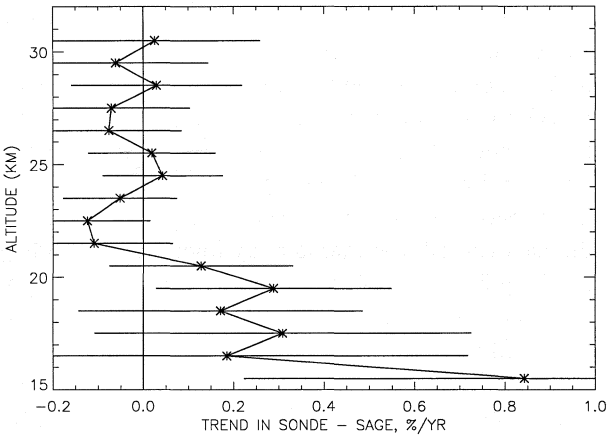


**Figure 4-2.** The altitude dependence of the trend in the sonde-SAGE II differences for the combined coincidences of the eight sonde sites. (From WMO, 1998.)

#### *SAGE Versus Ozonesondes*

The drift of SAGE II versus the sondes was determined by developing a single combined time series, at each altitude, of the coincident differences between the sondes and SAGE II for eight sounding sites ranging from 36°N to 52°N (Hohenpeissenberg, Payerne, Uccle, Boulder, Goose Bay, Sapporo, Edmonton, and Toronto) and then finding the slope of a least-squares straight-line fit through the points. Because each point in the time series is a difference between the sonde and SAGE II data, latitudinal, annual and semiannual oscillation, the quasi-biennial oscillation (QBO), and other effects are inconsequential to first order because the differencing would tend to cancel them out. If there is no drift in one measurement system relative to the other, the differences will remain constant with time. Measurements from the eight stations were combined to reduce geophysical and sampling noise caused by the fairly loose coincidence criteria used. The result is shown in Figure 4-2.

Note that a statistically significant indicated drift at the $2\sigma$ level occurs at 19.5 km and it is only 0.28%/yr. Above about 20 km, the differences are on the order of -0.1%/yr and below 20 km, in the mean they are about 0.25%/yr, except at 15.5 km where the difference is 0.85%/yr.

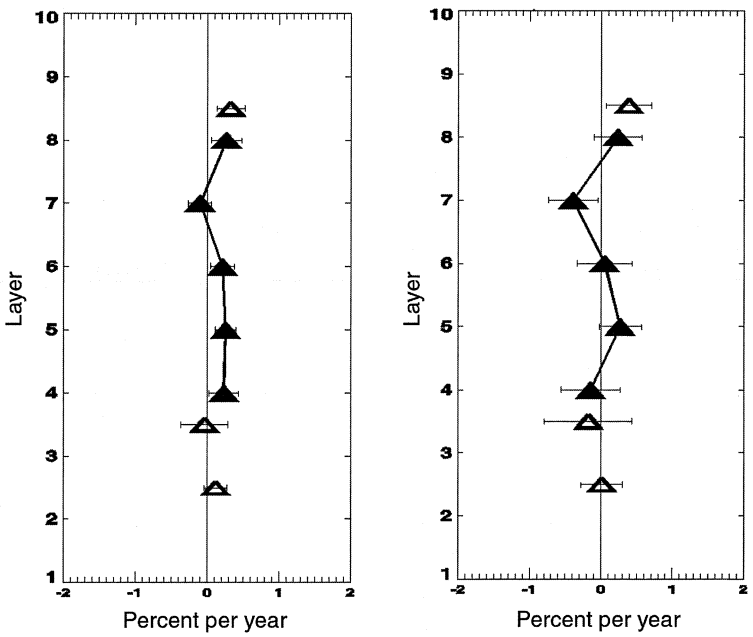


**Figure 4-3.** Hemispheric average regression slopes (% per year) of the layer-ozone time series of Umkehr-SAGE coincident-pair differences for the northern midlatitudes (left panel) and the southern midlatitudes (right panel). All error bars shown are ±2 standard errors of the mean. Panels show the variance-weighted average slopes ±95% confidence intervals associated with the variance-weighted means of the coincident-pair differences. The disconnected open triangles represent layers 2 through 10 plotted at layer 2.5, layers 2+3+4 plotted at layer 3.5, and layers 8+9+10 plotted at layer 8.5. The solid triangles represent individual levels. All Umkehr observations are individually corrected for aerosol interferences by using the Mateer and DeLuisi (1992) aerosol correction factors. (Modified from a figure in WMO, 1998.)

### *SAGE Versus Lidar*

In most cases, the lidar-SAGE difference time series show generally no trend significant at the two sigma standard error confidence level. Due to the higher variability of ozone at altitudes below 20 km, the standard deviation is higher in this range and the trend of the difference can be larger than 1% $yr^{-1}$. At 17.5 km, the only record exceeding 100 coincidences (Hohenpeissenberg) shows a nonsignificant trend of (0.5 ± 0.6)% $yr^{-1}$. The trends are also higher above 40 km, due to the decrease in the signal-to-noise ratio of the lidar measurements. In these regions, the trends can exceed 1% $yr^{-1}$. The average trend for the records exceeding 100 coincidences in the range 40-50 km is (0.6 ± 1.4)% $yr^{-1}$. Over the 20-35 km interval, the trend does not exceed (0.5 ± 1)% $yr^{-1}$. On average in this range, values of about 0.3% $yr^{-1}$ with standard errors not exceeding 0.4% are found.

### *SAGE Versus Umkehr*

Average regression slopes and 95% confidence intervals of the SAGE-Umkehr coincident-pair-difference time series for the northern and southern midlatitudes (NML, SML) are shown versus altitude in Figure 4-3. The largest discrepancy between Umkehr and SAGE regression slopes occurs in layers 8 and 9, where the slope of the coincident-pair differences is (0.3 ± 0.2)%/yr, significantly different from zero at the 95% confidence level. In all other layers and layer combinations, the absolute slope of the differences is less than or equal to (0.2 ± 0.2)%/yr. The southern midlatitude averages show marginally significant discrepancies between Umkehr and SAGE only in layers 7 and $8^{+}$. The vertical structure of the Umkehr-SAGE differences in the variance-weighted SML averages is similar to the NML results. Primarily due to the smaller sample size,

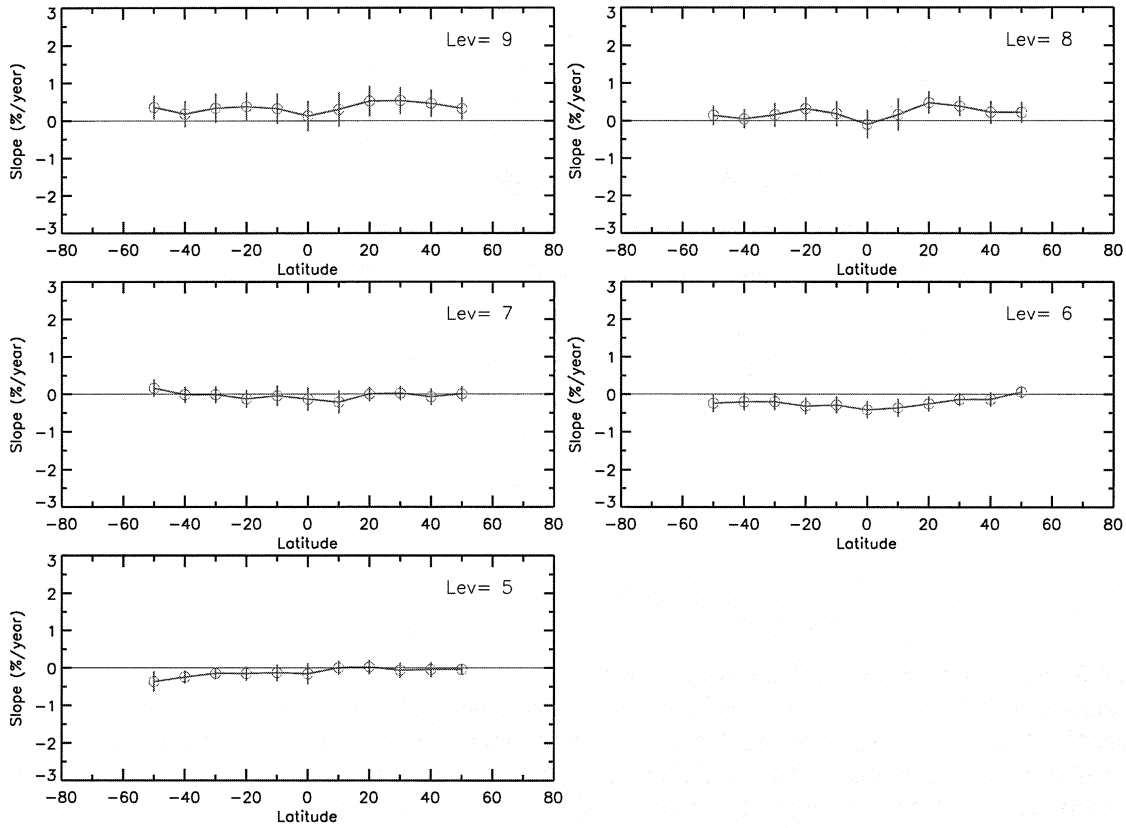


**Figure 4-4.** Linear slopes of the differences (SBUV-SAGE) between SAGE and coincident SBUV ozone observations from 1979 to 1990 expressed as a percentage of the SAGE Umkehr layer. Mean values were binned by month and placed in 10°-wide latitude bins. Error bars are twice the standard errors of the differences in slopes. (From WMO, 1998.)

the uncertainties in the SML are somewhat larger (~0.3%/yr) than the uncertainties in the NML averages. Overall Umkehr-SAGE drift rates relative to each other are verified in a statistically significant sense to be no worse than ±0.2%/yr in the NML and ±0.3%/yr in the SML.

### *SAGE Versus SBUV*

A comparison of the linear slopes of the coincident-pair differences between SBUV and combined SAGE I/II measurements is shown in Figure 4-4. SAGE data possess a more positive slope in layers 5 and 6 and a less positive slope in layers 8 and 9. The most significant difference is $(+0.4 \pm 0.2)\%\ yr^{-1}$ in layer 9. However because of the offsetting differences in layers 5 to 7, it is concluded that overall there is no evidence of a drift in the SAGE (and overall SBUV) calibration of greater than $0.2\%\ yr^{-1}$, based on comparisons over the period 1979-1990. This is perhaps the longest period over which comparisons can be made between coincident ozone measurements obtained by essentially two separate instruments. It is likely to provide the strongest constraint possible on the absence of a drift in the SAGE ozone calibration. Additional details of SBUV-SAGE comparisons are provided in the SPARC report (WMO, 1998).

### *SAGE II Versus HALOE*

Because SAGE II and HALOE (Russell *et al.*, 1993) are both solar occultation experiments, there are not enough coincidences to examine the trends of coincident differences. Instead, the entire data records for each experiment were used and the linear slopes of each experiment were compared. Down to 30 km, the

**Table 4-3. Seasonal mean ozone values and the standard deviation (in ppbv) of the mean in the mid-troposphere (4.5-5.5 km height) at the Observatoire de Haute Provence (OHP).** The number of profiles is denoted by *n*.

| | ECC Measurements 1991-1995 | | Lidar Measurements 1990-1995 | |
|---|---|---|---|---|
| Time | mean $O_3$ | *n* | mean $O_3$ | *n* |
| November–February | 49.0 ± 0.8 | 66 | 47.2 ± 1.2 | 96 |
| March | 53.5 ± 2.7 | 18 | 53.8 ± 2.7 | 23 |
| April–June | 65.2 ± 1.5 | 52 | 63.2 ± 2.3 | 56 |
| July–September | 63.0 ± 1.5 | 54 | 60.7 ± 1.8 | 74 |
| October | 53.1 ± 2.1 | 52 | 55.2 ± 3.0 | 14 |
| All | 54.3 ± 0.6 | 207 | 53.8 ± 1.2 | 263 |

differences in the annual change (i.e., the indicated drift rate) are ≤0.5% at all latitudes except 55°S, where they are ~1%. This is also true for 25 km at many latitudes, but there are two latitude bands, i.e., 15°N and 55°S, where the differences are 1.5 to 2% $yr^{-1}$. At 20 km, the differences are on the order of 2 to 4% $yr^{-1}$. When latitudinal averages of the indicated drift rates at a given altitude are taken, the mean indicated drift rate for the 60°S to 60°N range and for 50 km down to 25 km, while not statistically significant, are less than 0.2% $yr^{-1}$ at all altitudes except 30 km, where the value is (0.4 ± 0.25)% $yr^{-1}$. At 20 km, the latitudinally averaged differences are barely significant at the (1.4 ± 1.2)% $yr^{-1}$ level. Below 20 km, the differences are large, and no useful results are obtained in the tropics because of poor sampling.

### *SAGE II Versus MLS and HALOE*

Because MLS uses limb emission, there are many coincidences with SAGE II and, at different times, with HALOE. Therefore, MLS can be used as a transfer standard to, in effect, examine the linear slopes of coincident differences, i.e., the indicated drift rates between MLS and SAGE II or MLS and HALOE. The overlap period is less than 6 years (and is only half this at altitudes below 40 mb because of the prescribed time filtering of SAGE II data to remove aerosol effects). SAGE II slopes equal or exceed MLS slopes in the latitudinal mean at all levels from 1 to 46 mb, but there is no recognizable pattern in the differences and only at 22 mb is the difference barely significant at the 95% confidence level. The mean of the indicated drift rates between 1 and 46 mb is (-0.4 ± 0.8)%/yr. SAGE ozone slopes can be related to HALOE ozone slopes based on a comparison of slopes in coincident HALOE and MLS measurements. The only significant MLS-HALOE slope difference at the 95% confidence level between 1 and 22 mb occurs at 22 mb, where the HALOE slope is 0.9% $yr^{-1}$ less than the MLS slope. The differences in the 1 to 22 mb region are latitude and altitude dependent and average (-0.1 ± 0.8)%/yr. It is concluded that HALOE, MLS, and SAGE II do not drift relative to each other by more than 0.5%/yr, which is within the measurement uncertainties.

### *SAGE II Versus Ozonesonde*

The SPARC/IOC study (WMO, 1998) carried out an extensive analysis of the three different types of ozonesondes in use today (electrochemical concentration cell (ECC), Brewer-Mast (BM), and the Japanese KC68/79) including evaluation of the Joint Ozone Sonde Intercomparison Experiment (JOSIE) laboratory intercomparison study and field intercomparisons. Comparisons of ozonesondes in the stratosphere with other ozone-profiling techniques show consistent results, with agreement of about ±(3-5)% at altitudes between the tropopause and 28 km. The precision of the different sonde types is better than ±3%. Above 27 km the results are not consistent due to instrumental uncertainties (e.g., pump corrections and sensing solution changes) and caution must be used, at least for the non-ECC types of sondes, when applying the data for long-term trend determinations.

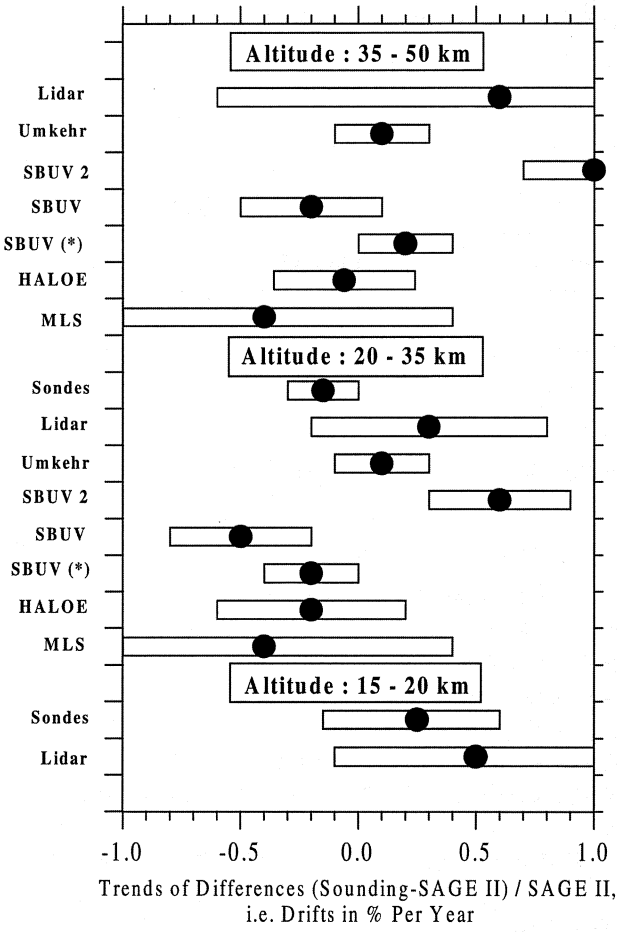


**Figure 4-5.** Trends of differences (i.e., drifts) between ozone measurements made by various ozone profiling instruments and SAGE II, in percent per year [(Sounding-SAGE II)/SAGE II]. Trends of ozonesondes, lidar, and Umkehr differences are presented as averages for eight northern midlatitude sounding stations. Trends of satellite differences are presented as global means. The average differences are indicated by the dots, and the bars represent the 99% confidence interval of the drift estimation. The entries for SBUV are for SBUV/SAGE II comparison; entries for SBUV* are for SBUV/combined SAGE I and SAGE II comparison. (From WMO, 1998.)

In general, ECC sondes provide more consistent results than the other two types of sondes. The precision of the ECC sonde is better than ±(5-10)% and shows a small positive bias of about 3%. BM and KC79 sondes are less precise, ±(10-20)%, but there are no indications of any bias larger than ±5%. It appears that large relative changes in accuracy between BM sondes and ECC sondes may have occurred between 1970 and 1991. A recent study done by Ancellet and Beekmann (1997), however, shows some encouraging results for future long-term tropospheric observations. These authors evaluated the ozone-profiling capability of the ECC sonde by performing comparisons with routine lidar measurements made at the Observatoire de Haute Provence (OHP) during the 1990-1995 period.

The seasonal means of mid-tropospheric ozone (4.4-4.5 km altitude) obtained by the ECC sonde and lidar are summarized in Table 4-3. ECC values are not corrected by total ozone normalization. Both datasets show excellent agreement in the annual mean (54.3 ppbv for ECC, 53.8 ppbv for lidar) and in seasonal variations in the mid-troposphere. Differences in particular periods are generally in the range of 2 ppbv (5%). For 15 simultaneous ECC versus lidar profiles, the mean of the differences observed between 4 and 7 km was 2.5 ± 1.8 ppbv (4 ± 3%). Although there is a dearth of comparative studies to evaluate the performance of ozonesondes in the troposphere, this present study under regular field operations together with the studies under controlled laboratory conditions show that there is sufficient confidence in the performance of the ECC sondes to use them for future tropospheric trend assessment studies.

#### 4.2.2.4 Summary

The regression slopes for time series of coincident differences between SAGE II and other measurements, for individual stations or latitudes, are summarized in Figure 4-5. Values range from ~(-0.3 ± 0.15)% $yr^{-1}$ to ~(0.5 ± 0.7)% $yr^{-1}$ (sondes, lidar, Umkehr, HALOE) for altitudes between 20 km and 35 km and ~(-0.5 ± 0.5)% $yr^{-1}$ to ~(1 ± 1)% $yr^{-1}$ for altitudes between 35 and 50 km. Only two systems (sondes and lidar) provide useful trend comparison data for the altitude range between 15 and 20 km. The best-matched SAGE-sonde agreement was obtained when the eight midlatitude sonde stations covering from 36°N to 52°N were combined into a single time series to calculate the regression slope of the differences. No statistically significant differences were

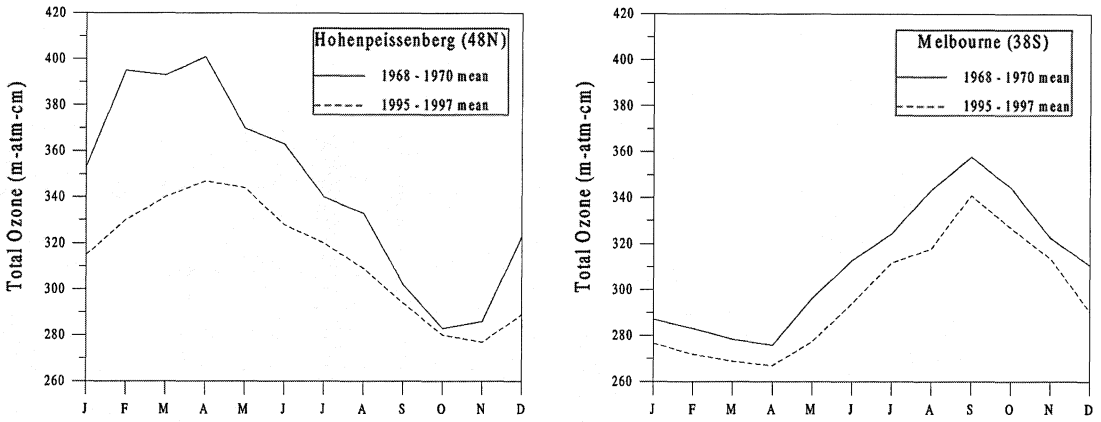


**Figure 4-6.** Changes in the annual cycle as seen at Hohenpeissenberg (48°N) and Melbourne (38°S).

obtained for the combined time series, but the mean difference was ~0.25% with an error of from ±(0.3 to 0.4)%/yr above ~15 km altitude. This represents a significant improvement in SAGE versus sonde agreement since the 1994 Assessment report (WMO, 1995).

Examination of latitudinally averaged trends of differences (i.e., global trends) shows negative drifts of (-0.06 to -0.4%) ± ~0.6%/yr for comparisons of SBUV, HALOE, and MLS with SAGE II (i.e., the SAGE II trend is larger than other measurements). These differences, although statistically insignificant, give a slight indication of a SAGE II drift with time (the SAGE II trend is larger). SBUV/2 differences with SAGE II are of opposite sign to SBUV, HALOE, and MLS, but this is most likely due to algorithm effects brought on by a drifting orbit. Globally averaged analyses of the longest satellite time series, SBUV compared with the composite time series of SAGE I/II (1979 to 1997), show agreement to (-0.2 to 0.2)% ± 0.2%/yr in the altitude region between 20 and 50 km. All of these results show a remarkable degree of consistency and add confidence to the use of SAGE II and other satellite data in calculating long-term ozone trends.

Ozonesonde studies show good consistency throughout the stratosphere for the three ozonesonde types currently in use, and they generally agree to within about 3 to 5% from the tropopause to about 28 km. Recent analyses of a 5-year record of ozonesonde and lidar soundings in the troposphere give an encouraging indication of the ability of the sondes and the lidars to provide useful data for assessing long-term tropospheric ozone trends.

## 4.3 OZONE NATURAL VARIABILITY

The natural variability of atmospheric ozone occurs in a broad spectrum of time scales, ranging from day to day, month to month, interseasonal to interannual, and decadal. Atmospheric circulation, chemistry, and radiative processes all play important roles in the variability of ozone, as described in the previous assessments (e.g., WMO, 1990a, 1995). Natural fluctuations in total ozone include subsynoptic- and synoptic-scale variations, semiannual and annual variations, and those variations associated with the quasi-biennial oscillation (QBO), regional El Niño/La Niña effects, volcanic effects, and the solar activity cycle. The amplitude of synoptic-scale variations can be about 30% of the monthly mean over middle and polar latitudes, while the peak-to-peak amplitude of the annual cycle ranges from less than 6% in the equatorial and tropical belts to about 30% at 60°N or 60°S latitude. The amplitude of the QBO ranges from 4% to about 7-8%, and the solar activity amplitude is between 1 and 2% in the total ozone and up to 5-7% in the upper stratospheric ozone. The large transient El Niño/La Niña events produce localized regional fluctuations of up to about 5%. Large volcanic eruptions reaching the stratosphere could cause significant temporary changes that range from 2% at low latitudes up to 5% over high latitudes in winter.

### 4.3.1 Short-Term Variations

Subsynoptic and synoptic fluctuations in ozone amounts of about 10% in the tropics, increasing to ~30% over middle and high latitudes, are known from the

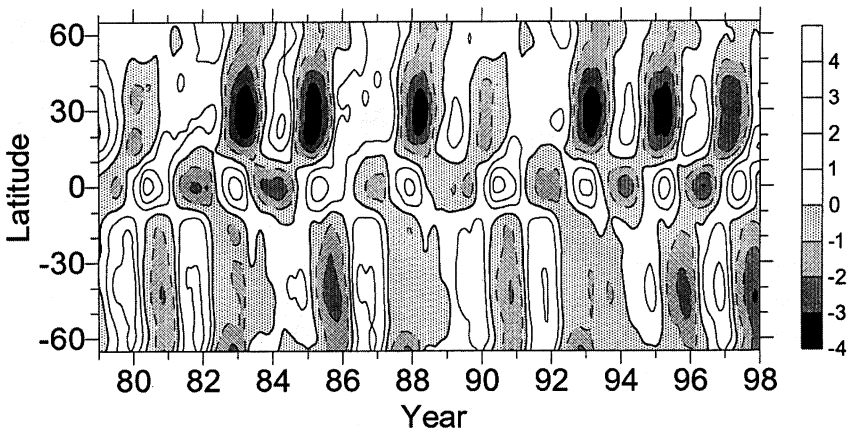


**Figure 4-7.** Time-latitude cross section of the amplitude of the QBO (in %) of the zonal-mean total ozone. (Updated from Zerefos *et al.*, 1994.)

pioneering work of Dobson *et al.* (1946) and Meetham (1937) and from more recent studies (e.g., WMO, 1995; Atkinson, 1997). Springtime tropopause folding events are accompanied by intrusion of stratospheric ozone air in the troposphere. During such events total column ozone increases by 10% or more for a day or two. In the polar winter/spring, during stratospheric warming events, large ozone increases exceeding 100-130 DU for a few days are observed.

### 4.3.2 Longer Term Variations

#### 4.3.2.1 The Annual Cycle

Total ozone in the polar and middle latitudes reaches its annual maximum in the winter/spring months and its minimum in the fall months. The annual peak-to-trough differences were, respectively, ~180 and ~145 DU in the pre-1976 period. Comparing these numbers with those of the most recent years (1985-1997) strongly affected by the ozone decline, it is clear that not only has the annual average ozone in the middle and polar latitudes declined by 4-7% (up to 20% over Antarctica), but also changes have occurred in the annual course. The annual peak-to-trough differences decreased by 15-20% from those of the 1964-1976 period. The changes in the annual cycle are caused mainly by the decline of the total ozone during the period of the ozone maximum (e.g., late winter/spring). An illustration of this change is shown on Figure 4-6 based on data from Hohenpeissenberg (48°N) and Melbourne (38°S).

For the global ozone annual cycle, the existence of a double maximum in the pre-ozone-hole years, related to the seasonal spring maxima in northern and southern mid and polar latitudes, is well pronounced. The ozone decline in the last two decades, particularly over Antarctica, has resulted in nearly complete disappearance of the secondary maximum of the global total ozone in September-October (e.g., Bojkov *et al.*, 1995a).

#### 4.3.2.2 The QBO

The QBO signal in total ozone is in phase with equatorial zonal winds within ~10°N to ~10°S, changing phase as one moves poleward. The amplitude of QBO zonal ozone anomalies is 2-4% of the long-term mean (see Figure 4-7); this is smaller than at individual stations, where it can be up to 7-8%. The effect of the QBO over middle and high latitudes is more pronounced if the transition from easterlies to westerlies happens just prior to the winter/spring season in each hemisphere. In general, during the westerly phase of the QBO the negative ozone anomalies are more pronounced over the middle and polar latitudes than the positive anomalies during the easterly phase (e.g., Bojkov, 1987; Zerefos *et al.*, 1992; Randel and Cobb, 1994; Yang and Tung, 1995; Hollandsworth *et al.*, 1995a).

The vertical profile of ozone associated with the QBO signal has been analyzed by a number of recent studies, using either SAGE II data (e.g., Hasebe, 1994; Randel and Wu, 1996) or long-term ozonesonde records over the European and Canadian regions (e.g., Bojkov and Fioletov, 1998). The analyses of the vertical structure of the QBO (Hasebe, 1994; Randel and Wu, 1996) indicate that there are two cells over the tropics and middle latitudes with peak amplitudes between 20 and

minor effects on total ozone trends. The SPARC/IOC Report (WMO, 1998, Chapter 3) contains a discussion of the statistical and ancillary variable issues involved, and presents the results of an intercomparison study in which 10 researchers (or research teams) used their standard statistical models to derive ozone trends on three test datasets. Section 4.4.3 summarizes the findings.

The typical necessary or desirable terms in the statistical model include the following:

- *Seasonal means:* Some form of seasonality in ozone mean level must be accounted for; for example, with a monthly trend model it is common to fit monthly means, although sometimes a sum of seasonal harmonic terms is used, often with fewer than the 12 degrees of freedom used with monthly means. With weekly data, harmonic seasonal terms are the norm.
- *Seasonal trends:* We now know that ozone trends vary by season and that this must be allowed for by use of seasonal trend terms such as monthly or seasonal trends (sometimes also incorporated as harmonics). Figure 4-9 shows for Northern Hemisphere Dobson stations the monthly dependence of ozone jointly with the monthly dependence of ozone trends calculated from the model used for Table 4-4 in Section 4.5.1. The largest trends in ozone occur at the times of the highest ozone, in the winter-spring.
- *Ancillary variables:* Other variables are known to affect ozone levels; accounting for them can reduce noise levels, thereby improving trend detection capability, and in some cases can remove bias. An example of the latter would be accounting for a solar effect when the trend period does not cover several solar cycles. The most common ancillary variables accounted for are the solar effect (the 10.7-cm radio flux or the sunspot number are used as proxies) or the quasi-biennial oscillation (QBO) in equatorial stratospheric winds. Failure to account for the QBO, especially in the tropics, can aggravate autoregression in the residuals from the regression and lead to larger uncertainty (standard errors) in the trends.
- *Autoregression:* Even when all of the above effects are taken into account, monthly ozone residuals remain correlated with the previous month's residuals, especially when noise levels are lower, such as for total ozone or zonal means; this effect is known as autocorrelation. This is usually accounted for by permitting the residual series, $N_t$, to depend on its previous values, often as an order-1 autoregressive (AR(1)) series, $N_t = \phi \cdot N_{t-1} + e_t$, where the $e_t$ series is uncorrelated (Box *et al.*, 1994; Bojkov *et al.*, 1990). Allowing for this in the regression model does not usually change the calculated trends by much, but it increases the reported standard errors to reflect an increased uncertainty in the trend estimate. Some authors use ordinary least-squares techniques for the regression estimates but obtain the standard errors of the trend estimates through bootstrap or jackknife (resampling) techniques; these techniques have been found to lead to standard errors similar to those of methods using autoregressive models.
- *Seasonal weighting:* Ozone is more variable in winter/spring and many researchers take this into account by statistical weighting of the observations according to some estimate of seasonal variance, for example, using the reciprocals of the monthly variances of the residuals from the fit. Although this has little effect on the calculated trends themselves, it increases the uncertainty estimates of the winter/spring trends while decreasing those of the summer/fall trends.
- *Dynamical variables:* Several authors (e.g., Ziemke *et al.*, 1997; Wege and Claude, 1997) have investigated

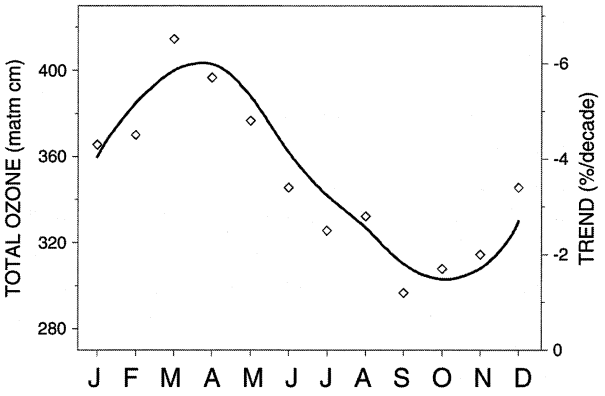


**Figure 4-9.** The seasonal dependence of total ozone levels (solid line) and total ozone trends (symbols) for January 1979 to December 1997 over Dobson stations in the band 35°-60°N (average of station trends). (From Bojkov *et al.*, 1995a, and updated by the authors.)

the effects of dynamical/meteorological variables on ozone and on ozone time trends. These dynamical variables can be associated with a substantial fraction of the variance in ozone. Nevertheless, use of these variables in regression models where the primary purpose is to estimate ozone time trends leads to difficulties in interpretation of the resulting trends in ozone. As an example, long-term changes in ozone will themselves lead to changes in stratospheric temperatures; regression of ozone on both time and temperature will lead to ozone time trends (usually of lesser magnitude), trends which do not represent changes in ozone due to any particular external influence. Dynamical variables are not included in any of the trend regression models considered in this chapter.

- *Standard errors for seasonal trends:* Proper calculation of the trend standard errors for seasonal trends when monthly trends are fitted, or for a year-round trend when monthly or seasonal trends are fitted, requires use of the covariance matrix of the trend estimates. This is particularly important when the autoregression coefficient is large, because then, for example, the January trend is highly correlated with the February and December trends, and the December-January-February average trend will have larger uncertainty than one would calculate if it were assumed that these trends had statistically independent errors.
- *Model variations:* A number of model variations have been considered, usually for purposes of more detailed analysis of ancillary variables. For example, possible seasonal effects of solar or QBO variations or in the autoregression coefficient have been considered, either in magnitude or time lag. These variations typically have little effect on reported ozone time trends, although inflation of the standard errors can occur if the model is seriously over-parameterized.

The above model aspects are discussed in more detail in the SPARC/IOC trends report (WMO, 1998), and specific features of the models of 10 research groups are tabulated. Intercomparison results on three test datasets for these groups are summarized in Section 4.4.3 below.

The total ozone trend results in Section 4.5 are calculated from statistical models identical (or nearly so) to those used in the last Assessment (WMO, 1995). This model is described in more detail in Section 4.4.2. The ozone vertical profile trends in Section 4.6 were calculated by a variety of researchers, depending on instrument system; the SPARC/IOC report (WMO, 1998) contains the details of these statistical models.

### 4.4.2 Total Ozone Trend Statistical Model

This section describes the core statistical model used in deriving the total ozone trends in Section 4.5 (see Bojkov *et al.*, 1990). Let $y_t$ represent monthly total ozone values for a particular series, for example, a Dobson station or a TOMS zonal mean. The statistical model for $y_t$ is of the form

$$y_t = (\text{Monthly mean}) + (\text{Monthly trend}) + (\text{Solar effect}) + (\text{QBO effect}) + \text{Noise}$$

or more precisely,

$$y_t = \sum_{i=1}^{12} \mu_i I_{i;t} + \sum_{i=1}^{12} \beta_i I_{i;t} R_t + \gamma_1 Z_{1;t} + \gamma_2 Z_{2;t} + N_t \qquad (4\text{-}1)$$

with the following definitions:

$\mu_i$ = Ozone mean in month $i$, $i = 1 \ldots 12$.
$I_{i;t}$ = Indicator series for month $i$ of the year, i.e., 1 if the month corresponds to month $i$ of the year, and 0 otherwise.
$\beta_i$ = Trend in Dobson units/yr in month $i$ of the year.
$R_t$ = Linear ramp function measuring years from the first month of the series; equal to $(t - t_o)/12$. For series beginning before 1970, it is often taken to be a ramp function equal to zero for $t < t_o$, where $t_o$ corresponds to 12/69, and then $(t - t_o)/12$ for $t \geq t_o$.
$Z_{1;t}$ = Solar 10.7-cm flux series, with $\gamma_1$ the associated coefficient.
$Z_{2;t}$ = QBO 50-mb wind series lagged some appropriate number of months (latitude dependent), with $\gamma_2$ the associated coefficient (TOMS analyses). These terms are sometimes represented as two terms (50-mb and 30-mb winds) (Dobson analyses).
$N_t$ = Residual noise series.

The residual noise series $N_t$ is modeled as an autoregressive AR(1) series, with weights inversely proportional to the monthly residual variances.

### 4.4.3 SPARC/IOC Statistical Model Intercomparison

As part of the SPARC/IOC trends report (WMO, 1998), an intercomparison of trend models was done, in which each research group was asked to analyze the same three datasets. The purpose of the exercise was to determine to what extent the differences in the statistical trend models commonly in use would affect ozone trend estimates and their uncertainties (standard errors). The three datasets used were (a) Nimbus-7 TOMS 40°-50°N zonal-mean ozone from November 1978-April 1993; (b) Uccle sondes monthly-mean ozone at 13 km from January 1969-December 1996; (c) SAGE I and II monthly-mean ozone at 40.5 km, 35°-45°N, from February 1979-December 1996. The test sets differed in the amount of missing data, with the TOMS dataset having a complete series, and at the other extreme, the SAGE combination dataset having serious missing-data issues with a monthly pattern that caused some researchers to obtain somewhat different results when calculating seasonal trends.

The following are the main conclusions of the model intercomparison (taken from the SPARC/IOC report), which are also illustrated in Figure 4-10 (also from the SPARC/IOC report); this is the comparison for the SAGE I/II test data, in which inter-researcher differences were the most extreme. For the test data (TOMS) with no missing monthly values, all researchers obtained similar results for trends. There were variations in standard errors, however, that were large enough to give some concern, as they affect the statistical significance of the trends. For example, long-term total ozone trends from SBUV near the equator border on statistical significance (WMO, 1995). Lack of proper calculation of standard errors in such a situation may result in non-significant trends being declared statistically significant, or vice versa.

For the test datasets with missing values, particularly the SAGE set with large numbers of missing values in a strong pattern form, some researchers' results deviated substantially from the average, with respect to both trend estimate and, especially, standard error. Some researchers feel that in such situations, it is better to fit a simpler model to maintain stability; for example, by fitting seasonal trends directly or by use of reduced numbers of harmonic terms for the seasonal trends and possibly also the seasonal cycle.

Based on these intercomparisons, there seems reason to suggest that researchers provide good documentation for the features of their statistical model. Particularly, when any patterns of missing data exist that have strong time-dependent features, the methods of handling the missing data should be discussed in detail.

## 4.5 LONG-TERM CHANGES IN TOTAL OZONE

### 4.5.1 Global, Latitudinal, and Longitudinal Trends

The last Assessment (WMO, 1995) reported trend results for total ozone for observations through February 1994 for ground-based stations and through 5/94 for satellite (SBUV + SBUV/2) instruments. This section updates those trends through 12/97 for ground-based stations and satellite data (TOMS). Additional TOMS data through 6/98 (indicated by different symbols) are included in the time series plots of total ozone in order to show the most recent data; however, these months are not included in the trend calculations, in order that the ground-based and satellite data time periods be identical.

Prior Assessments (WMO, 1992, 1995) have documented substantial declines in mid- to high-latitude total ozone amounts, while indicating little if any change over equatorial latitudes. Percentage changes have been found to be higher in the winter/spring seasons than in the summer/fall seasons; the larger percentage changes follow the higher levels of ozone in the winter/spring seasons (see Figure 4-9). Figure 4-11 shows contour plots of mean ozone by month and latitude for a baseline period (1964-1976) compared to recent years. The left panels show mean ozone from ground-based stations for the period 1964-1976 (upper panel) and 1985-1997 (lower panel). The right panels show satellite data, using BUV data 1970-1972 in the upper panel with Nimbus-7 TOMS (1985-1993) and Earth Probe TOMS (1996-1997) data in the lower. Ground and satellite data are in good agreement, with ozone field differences within ±2% except over the polar regions. The decline between the two periods in southern midlatitudes is 6.1%, with monthly contributions of more than 10% coming from September-November (ozone-hole months). Over northern latitudes the decline is 3.5%, with monthly contributions of more than 5.5% coming from December-April.

The most recent available data indicate a lessening of the large negative trends in total ozone seen in the 1980s and early 1990s. Figure 4-12 shows monthly deviations from (non-polar) total ozone (area weighted,

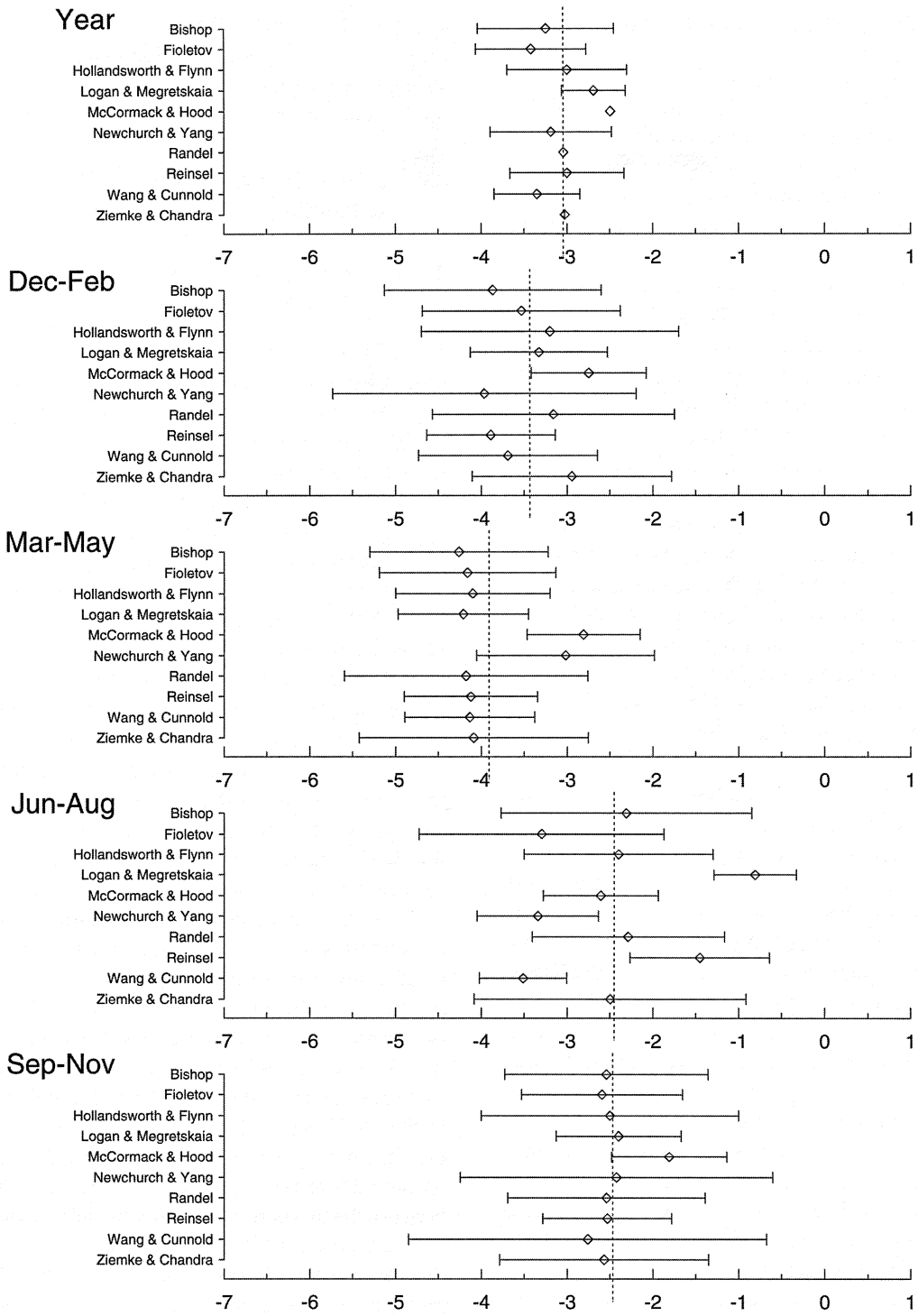


**Figure 4-10.** Ozone trend estimates by researchers for SPARC/IOC Test Set 3, SAGE I/II 40.5-km ozone at 35˚-45˚N for February 1979-December 1996. Trends are in $10^9$ $cm^{-3}$/yr. Uncertainty intervals are one standard error. Year-round trends (average over all months) were calculated where possible if not given directly by the researcher, but in some cases not enough information was given to calculate the corresponding standard error. The vertical dotted line is the mean of all researchers' trend estimates. (From WMO, 1998.)

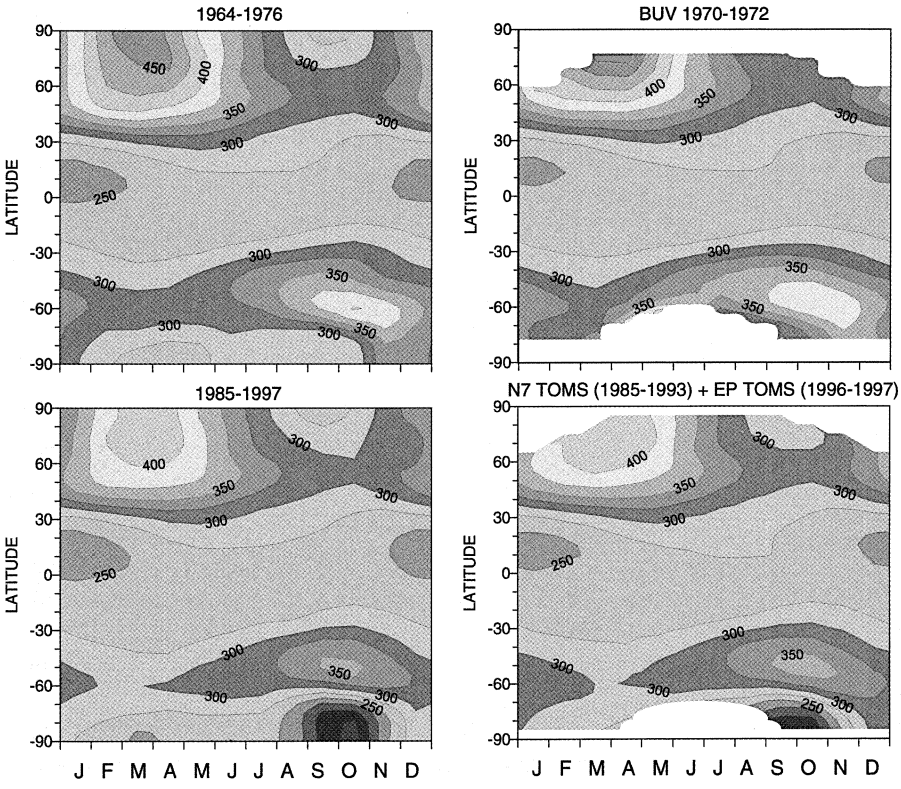


**Figure 4-11.** Contour plots of levels of total ozone by latitude and month. Left plots: Ground-based data for the periods 1964-1976 (upper panel) and 1985-1997 (lower panel). Right plots: Satellite data for the periods 1970-1972 (BUV, upper panel) and 1985-1997 (Nimbus-7 and Earth Probe TOMS, lower panel).

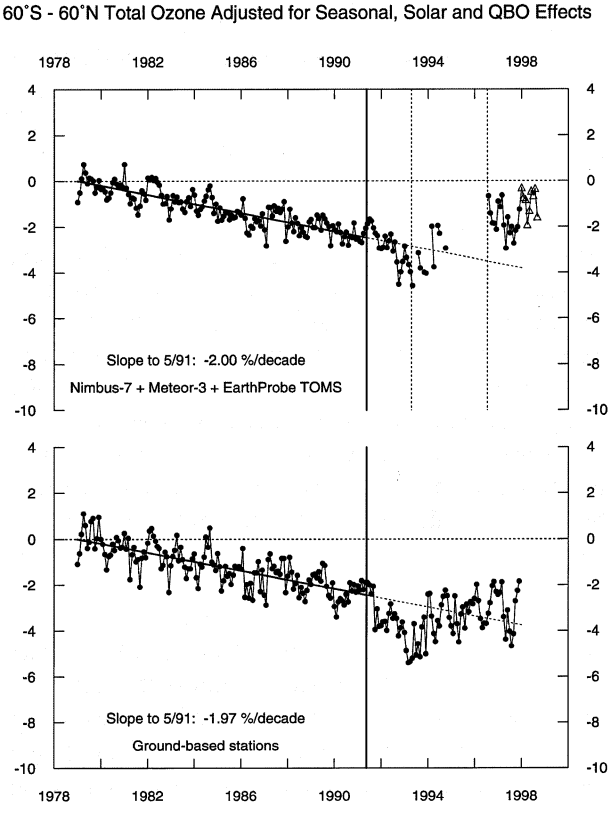


**Figure 4-12.** Deviations in total ozone, area weighted over 60°S-60°N. A seasonal trend model, including solar and QBO effects, was fit to ozone over the period 1/79 to 5/91. Deviations represent ozone adjusted for baseline monthly means (1/79 intercepts), solar and QBO effects, and seasonal differences in the trend, while the year-round average trend is not removed; then deviations are expressed in percentage of baseline monthly mean. The upper panel shows TOMS deviations and the lower panel represents a ground-based series constructed from average ozone at stations in 5° latitude zones. Trend models are fit independently to TOMS and ground-based ozone. The solid straight line represents the least squares fit to the deviations up to 5/91, and is extended as a dotted line through 12/97. The bold vertical line is at the time of the Mt. Pinatubo eruption, 5/91. Dotted vertical lines represent switches from one TOMS satellite to another. Open triangles distinguish TOMS data for the months 1/98 through 6/98.

60°S-60°N) over time for two instrument systems: (a) Nimbus-7 (11/78-4/93) + Meteor-3 (5/93-10/94) + Earth Probe (8/96-9/98) TOMS; and (b) ground-based stations (1/64-12/97). For this figure, no further adjustments were made over the most recently revised data for any possible calibration differences between different satellites (see Section 4.2 for discussion of the instrument data quality). The deviations shown in Figure 4-12, obtained from monthly total ozone using a least-squares fit of the data up to 5/91, are adjusted for seasonal cycle (1/79 monthly intercepts), solar and QBO effects, and monthly differences in the trend while leaving in the average trend, and are expressed as a percentage of the 1/79 monthly intercepts. Satellite and ground-based data are fit separately, but have nearly identical trends of about -2%/decade up to 5/91.

Both data systems show the same features. There is a strong, nearly linear, decrease in total ozone throughout the 1980s, followed by a sudden decrease in 1992-1993 due to effects of the Mt. Pinatubo eruption. There is a recovery from the Mt. Pinatubo effect in 1994, and subsequent total ozone levels (through 9/98 for Earth Probe TOMS) show no evidence of further decreases. It must be kept in mind that the 1996-1998 Earth Probe data are considered preliminary, but current overpass intercomparisons with the ground-based network indicate only about a 1%-level difference (Earth Probe higher) and perhaps 0 to 0.5% difference between Earth Probe TOMS and Nimbus-7 TOMS (Earth Probe higher). The ground-based data in the post-1994 period are slightly lower than the Earth Probe TOMS data, even if one were to consider that the Earth Probe data might be biased high relative to Nimbus-7 TOMS by perhaps 0.5%. However, it should be noted that the ground-based stations are very scarce in the tropics and Southern Hemisphere; the ground-based series in Figure 4-12 is constructed from average ozone for stations in 5° latitude zones, and for a few zones in the Southern Hemisphere, the zonal average had to be interpolated from adjacent zones.

One reason why the pre-Pinatubo trend does not extrapolate well to the present time is that a reduction in the slope of the downward trend in total ozone is to be expected from the leveling off of the stratospheric equivalent chlorine loading. Figure 4-13 shows a plot of the equivalent effective stratospheric chlorine (EESC) from Chapter 11 (A1 scenario) on the expanded time scale of 11/78-6/98, indicating a flattening of the equivalent chlorine concentration over the years 1995-1998, so that the

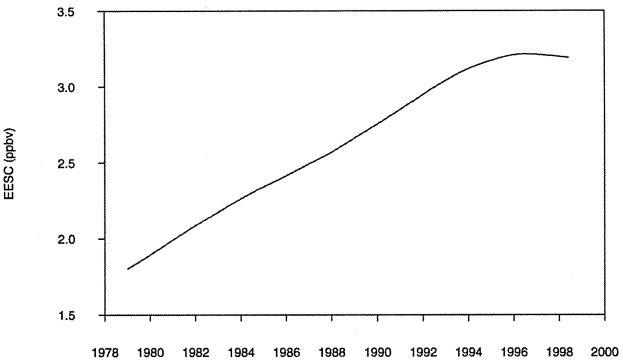


**Figure 4-13.** Equivalent effective stratospheric chlorine (scenario A1) from Chapter 11, on an expanded time scale of 1/79 to 6/98.

pre-Pinatubo trend in chlorine loading has not been maintained. Furthermore, enhanced stratospheric aerosols were present throughout much of the decade of the 1980s due to earlier volcanic eruptions, likely enhancing the downward trend in ozone observed before the eruption of Mt. Pinatubo. It is also possible that long-term variations such as the solar effect are not represented well enough in the statistical model and may account for some of the leveling off. Figure 4-14 shows the 25°N-60°N deviations when the seasonal, solar, and QBO effects are adjusted for by the linear regression, and Figure 4-15 for the same latitude range, but where the seasonal effect only is adjusted for. The long-term ozone variations are larger on Figure 4-15 than on Figure 4-14 because the solar effect is not removed, and as a result the recent data do not appear to show as much of a significant deviation from the long-term trend; furthermore, the recent data are for a solar minimum, and adjustment for the solar effect in Figure 4-14 results in a relative raising of the data compared to Figure 4-15. It seems likely that even if the recent decline of the 1980s midlatitude trends is primarily due to a leveling of the stratospheric equivalent chlorine concentration, it may be several more years before we can make this attribution. It should also be noted that this reduction of downward trend should *not* be interpreted as a recovery of ozone (see Chapter 12).

Figure 4-14 shows the consistency of the TOMS and ground-based records where the ground-based data are plentiful. Though much more variable than the near-global data, the satellite and ground-based Northern Hemisphere data show nearly identical deviations on a month-to-month basis. Again, there is a leveling of the

**Table 4-4. Total ozone trend estimates for individual stations and regions.** Seasonal and annual trend estimates by station/region are shown for the period January 1979 through December 1997. The first and the last months of observations are shown if they are different from January 1964 and December 1997 (read 68-08 as August 1968). For regions, an approximate mean latitude is indicated. For stations marked by the asterisk see discussion in Section 4.2. For all other stations the data available from the World Ozone Data Centre were used. The June-August Antarctic trend is based on a very limited number of moon observations and is not reliable.

| | | Year-Month | | Trend (%/decade ±2σ) | | | | |
|---|---|---|---|---|---|---|---|---|
| Station/Region | Latitude | First | Last | Dec–Feb | Mar–May | Jun–Aug | Sep–Nov | Year |
| | | | | *Individual Stations* | | | | |
| St. Petersburg | 60.0°N | 68-08 | | -7.4 ±4.0 | -6.6 ±2.7 | -4.1 ±1.9 | -3.7 ±2.2 | -5.6 ±1.7 |
| Churchill | 58.8°N | 64-12 | | -6.2 ±4.1 | -4.0 ±2.4 | -4.5 ±1.8 | -4.2 ±2.9 | -4.8 ±1.6 |
| Edmonton | 53.6°N | | | -3.0 ±3.1 | -5.5 ±2.4 | -4.2 ±2.0 | -2.2 ±2.5 | -3.8 ±1.5 |
| Goose Bay | 53.3°N | | | -3.0 ±3.6 | -3.8 ±3.1 | -4.3 ±2.3 | -3.0 ±2.5 | -3.5 ±1.8 |
| Potsdam | 52.4°N | | | -4.1 ±3.7 | -6.6 ±3.0 | -2.3 ±2.1 | -1.6 ±2.4 | -3.8 ±1.7 |
| Belsk | 51.8°N | | | -6.0 ±3.4 | -5.6 ±2.6 | -3.1 ±1.9 | -1.1 ±2.2 | -4.1 ±1.6 |
| Bracknell/Camborne | 51.4°N | | | -3.6 ±3.6 | -7.0 ±2.7 | -3.2 ±1.7 | -1.2 ±2.6 | -4.0 ±1.5 |
| Uccle | 50.8°N | 71-07 | | -4.9 ±3.4 | -7.8 ±2.7 | -2.2 ±1.7 | -1.8 ±2.5 | -4.4 ±1.5 |
| Hradec Kralove | 50.2°N | | | -5.2 ±3.4 | -6.3 ±2.3 | -3.9 ±1.7 | -1.0 ±2.0 | -4.3 ±1.4 |
| Hohenpeissenberg | 47.8°N | 68-05 | | -6.0 ±3.3 | -7.2 ±3.1 | -2.8 ±1.6 | -1.4 ±2.2 | -4.6 ±1.6 |
| Caribou | 46.9°N | | | -3.4 ±3.4 | -4.4 ±2.5 | -3.0 ±1.6 | -2.2 ±2.3 | -3.3 ±1.5 |
| Bismarck | 46.8°N | | | -2.0 ±2.5 | -4.6 ±2.3 | -2.0 ±1.4 | -2.0 ±1.7 | -2.7 ±1.2 |
| Arosa | 46.8°N | | | -4.4 ±2.8 | -5.9 ±2.6 | -1.7 ±1.4 | -0.8 ±1.9 | -3.4 ±1.4 |
| Sestola* | 44.2°N | 76-11 | | -4.1 ±3.7 | -7.4 ±3.3 | -3.5 ±1.9 | -1.7 ±2.4 | -4.4 ±1.7 |
| Haute Province | 43.9°N | 83-09 | | -4.7 ±5.4 | -9.2 ±4.0 | -1.7 ±3.0 | -0.4 ±2.7 | -4.4 ±2.3 |
| Toronto* | 43.8°N | | | -2.8 ±3.1 | -4.2 ±2.4 | -2.4 ±1.6 | -0.3 ±2.3 | -2.5 ±1.4 |
| Sapporo | 43.1°N | | | -5.5 ±2.4 | -5.1 ±2.3 | -4.0 ±2.1 | -2.7 ±1.8 | -4.5 ±1.4 |
| Vigna Di Valle | 42.1°N | | 97-02 | -7.8 ±3.1 | -7.6 ±3.6 | -3.7 ±2.2 | -3.4 ±2.3 | -5.8 ±1.8 |
| Boulder | 40.0°N | | | -2.1 ±2.3 | -5.9 ±2.5 | -2.8 ±1.3 | -1.4 ±1.7 | -3.2 ±1.2 |
| Xianghe | 39.8°N | 79-01 | | -2.7 ±2.1 | -3.9 ±2.4 | -1.3 ±1.9 | -0.2 ±1.7 | -2.1 ±1.3 |
| Lisbon | 38.8°N | 67-08 | | -0.7 ±2.4 | -5.9 ±2.2 | -2.9 ±1.6 | -0.7 ±1.8 | -2.7 ±1.1 |
| Wallops Island | 37.9°N | 67-06 | | -3.9 ±3.1 | -5.0 ±2.6 | -2.9 ±1.6 | -1.5 ±2.0 | -3.4 ±1.4 |
| Nashville | 36.3°N | | | -3.2 ±2.7 | -4.8 ±3.0 | -2.4 ±1.8 | -1.3 ±2.1 | -3.0 ±1.5 |
| Tateno | 36.1°N | | | -2.3 ±2.8 | -1.9 ±2.4 | -1.3 ±1.7 | 0.1 ±1.6 | -1.4 ±1.3 |
| Kagoshima* | 31.6°N | | | -2.1 ±2.4 | -1.7 ±2.0 | -0.7 ±1.6 | 1.0 ±1.6 | -0.9 ±1.2 |
| Quetta | 30.2°N | 69-08 | | -4.3 ±2.4 | -2.8 ±2.9 | -1.5 ±2.2 | -0.9 ±1.9 | -2.4 ±1.8 |
| Cairo | 30.1°N | 74-11 | | -1.6 ±2.6 | -2.3 ±2.3 | -1.9 ±1.2 | -1.3 ±1.3 | -1.8 ±1.2 |
| New Delhi | 28.6°N | 75-01 | | -1.9 ±2.1 | -1.4 ±2.3 | -0.3 ±1.9 | 0.5 ±1.3 | -0.8 ±1.4 |
| Naha | 26.2°N | 74-04 | | -1.4 ±2.2 | -1.4 ±1.9 | 0.2 ±1.3 | 0.5 ±1.4 | -0.5 ±1.1 |
| Varanasi | 25.5°N | 75-01 | 97-08 | -2.8 ±2.2 | -2.8 ±2.0 | -2.8 ±1.3 | -2.0 ±1.4 | -2.6 ±1.1 |
| Kunming | 25.0°N | 80-01 | | -0.5 ±2.3 | -1.0 ±2.3 | 0.7 ±1.6 | -0.4 ±1.4 | -0.3 ±1.2 |
| Mauna Loa | 19.5°N | | | -1.5 ±2.4 | -2.2 ±2.1 | 0.0 ±1.6 | 0.2 ±1.4 | -0.9 ±1.3 |
| Kodaikanal | 10.2°N | 76-08 | | 0.6 ±1.7 | -1.0 ±1.5 | -1.8 ±1.8 | -1.5 ±1.7 | -1.0 ±1.1 |
| Singapore | 1.3°N | 79-02 | | 1.2 ±1.6 | 1.1 ±1.7 | -0.4 ±1.9 | 0.0 ±1.6 | 0.4 ±1.3 |
| Nairobi* | 4.7°S | 84-04 | | -1.2 ±2.5 | 0.9 ±2.1 | -1.4 ±2.3 | -0.8 ±2.4 | -0.6 ±1.4 |
| Natal | 5.8°S | 78-12 | | 0.8 ±1.6 | 1.4 ±1.7 | -1.4 ±1.5 | -0.3 ±1.5 | 0.1 ±1.1 |
| Samoa | 14.3°S | 76-01 | | -1.6 ±1.4 | -1.6 ±1.3 | -1.8 ±1.8 | -1.0 ±1.7 | -1.5 ±1.1 |

**Table 4-4, continued.**

| Station/Region | Latitude | Year-Month First | Year-Month Last | Trend (%/decade ±2σ) Dec–Feb | Mar–May | Jun–Aug | Sep–Nov | Year |
|---|---|---|---|---|---|---|---|---|
| Cachoeira-Paulista | 22.7°S | 74-05 | | -1.4 ±1.7 | -1.5 ±1.7 | -3.4 ±2.1 | -2.0 ±1.6 | -2.1 ±1.2 |
| Brisbane* | 27.5°S | | | -1.3 ±1.4 | -2.2 ±1.3 | -2.1 ±1.7 | -1.6 ±1.4 | -1.8 ±0.9 |
| Perth | 32.0°S | 69-03 | | -1.6 ±1.4 | -1.5 ±1.5 | -1.9 ±1.9 | -1.9 ±1.4 | -1.7 ±0.9 |
| Buenos Aires* | 34.6°S | 65-10 | | -0.9 ±2.0 | -1.3 ±1.8 | -3.4 ±2.1 | -0.7 ±2.2 | -1.6 ±1.3 |
| Melbourne | 38.0°S | | | -2.1 ±1.3 | -2.5 ±1.2 | -3.4 ±1.6 | -1.9 ±1.4 | -2.5 ±0.8 |
| Lauder/Invercargill | 45.0°S | 70-07 | | -4.0 ±2.1 | -3.1 ±1.7 | -2.5 ±2.5 | -2.7 ±2.1 | -3.0 ±1.3 |
| Macquarie Island* | 54.5°S | | | -4.6 ±2.2 | -1.9 ±2.3 | -4.3 ±2.8 | -2.9 ±3.0 | -3.4 ±1.7 |
| | | | | *Regions* | | | | |
| Arctic | 65°N | | | -7.9 ±2.7 | -7.7 ±2.6 | -2.5 ±1.5 | -3.6 ±1.4 | -5.7 ±1.6 |
| Western Siberia | 56°N | 73-01 | | -5.0 ±3.0 | -7.2 ±3.1 | -2.1 ±1.6 | -2.7 ±1.7 | -4.5 ±1.5 |
| Eastern Siberia & Far East | 53°N | 73-01 | | -5.7 ±2.5 | -7.1 ±2.7 | -3.2 ±2.1 | -3.8 ±1.9 | -5.1 ±1.6 |
| European USSR | 52°N | 73-01 | | -5.0 ±2.9 | -5.3 ±2.6 | -2.3 ±1.3 | -1.1 ±1.6 | -3.6 ±1.3 |
| Dobson Europe | 49°N | | | -5.2 ±2.8 | -6.6 ±2.4 | -3.0 ±1.5 | -1.4 ±1.9 | -4.3 ±1.4 |
| North America | 46°N | | | -3.6 ±2.0 | -4.8 ±1.9 | -3.3 ±1.2 | -2.2 ±1.3 | -3.5 ±1.1 |
| Central Asia | 42°N | 73-01 | | -3.3 ±2.2 | -3.3 ±2.5 | -2.1 ±1.8 | -1.1 ±1.6 | -2.5 ±1.4 |
| Australia & New Zealand | 39°S | | | -2.7 ±1.1 | -2.4 ±1.0 | -3.1 ±1.4 | -2.3 ±1.6 | -2.6 ±0.9 |
| Antarctica | 75°S | | | -6.3 ±1.9 | -2.4 ±3.2 | -6.5 ±4.3 | -20 ±4.0 | -8.9 ±2.0 |

winter, the estimated trend ending 1993 is 2.6% stronger than the trend ending 1997. In contrast with the Northern Hemisphere, in the Southern Hemisphere the effect of the 1993 anomaly seems negligible. Figure 4-16 indicates a much lower impact at that time in the Southern Hemisphere than in the Northern Hemisphere (Figure 4-14). Moreover, southern midlatitude trends tend to actually slow down. The trend estimates ending in 1990 and 1991 were more negative than trends finishing in the years after.

A puzzling result was shown in the last Assessment (WMO, 1995, Tables 1-2 and 1-3), where for the period of 1979-1994 the June-August trend over southern midlatitudes (30-55°S) was estimated at (-3.6 ± 1.7)%/decade from ground-based data and (-7.5 ± 2.5)%/decade for the SBUV-SBUV/2 record; i.e., SBUV data show almost twice the decline (Fioletov *et al.*, 1998b). It is especially strange, because direct comparisons of the ground-based and SBUV data show only 1-2% differences, and there are no such large discrepancies in trends in the Northern Hemisphere (WMO, 1995). The SBUV-SBUV/2 trend reported in WMO (1995) at 55°S for June-August (-10.7%/decade) is much stronger than the ozone trends during the corresponding winter months in northern middle and polar latitudes and comparable with the sub-Antarctic trend (-13.6% at 65°S) during "ozone hole" months (September-November). Hollandsworth *et al.* (1995b) found that due to the NOAA-11 orbit some of the data in the Southern Hemisphere are missing, and these gaps should be accounted for when interpreting the trend results. The statistical model used in their paper was less sensitive to errors and gaps in data than the model used by WMO (1995), and the estimated trends were closer to trends for the Dobson data (about 8%/decade in June-August at 60°S).

For a possible explanation of the difference between Dobson and SBUV-SBUV/2 total ozone trends one should look at the combination of SBUV-SBUV/2 instrument and/or algorithm errors for high zenith angles (>83°) and specific features of the orbit of the NOAA-11 satellite, on which the SBUV/2 instrument was operated in 1989-1994 as discussed by Fioletov *et al.* (1998a).

**Table 4-7. Total ozone trends over different time intervals for 35-60°N and 35-60°S latitudinal belts (% per decade).** Trends were calculated as averages of individual station trends.

| | 1/70*-12/97 | 1/79-12/91 | 1/79-12/92 | 1/79-12/93 | 1/79-12/94 | 1/79-12/95 | 1/79-12/96 | 1/79-12/97 | 1/79-12/97 without 1992, 1993 |
|---|---|---|---|---|---|---|---|---|---|
| | | | | *35°-60°N* | | | | | |
| DJF | -3.1 | -4.2 | -5.6 | -6.7 | -5.2 | -4.9 | -4.4 | -4.1 | -3.1 |
| MAM | -3.2 | -4.3 | -5.2 | -6.5 | -6.0 | -6.0 | -5.7 | -5.7 | -5.0 |
| JJA | -1.6 | -1.8 | -2.8 | -3.3 | -3.4 | -3.4 | -3.3 | -2.9 | -2.5 |
| SON | -1.2 | -0.4 | -1.7 | -1.5 | -1.5 | -1.5 | -1.7 | -1.6 | -1.3 |
| Year | -2.3 | -2.8 | -3.9 | -4.7 | -4.2 | -4.1 | -3.9 | -3.7 | -3.1 |
| | | | | *35°-60°S* | | | | | |
| DJF | -2.8 | -5.6 | -5.0 | -4.5 | -3.8 | -3.3 | -3.0 | -2.9 | -2.8 |
| MAM | -2.3 | -3.5 | -3.2 | -2.9 | -2.9 | -2.3 | -2.3 | -2.2 | -2.2 |
| JJA | -3.1 | -5.0 | -4.7 | -4.2 | -4.0 | -3.5 | -3.1 | -3.4 | -3.3 |
| SON | -2.2 | -3.7 | -3.3 | -3.2 | -2.5 | -2.1 | -1.6 | -2.0 | -1.8 |
| Year | -2.6 | -4.4 | -4.1 | -3.7 | -3.3 | -2.8 | -2.5 | -2.6 | -2.5 |

* Data from January 1964.

spring in the early 1990s (e.g., Müller *et al.*, 1997a,b, 1998; Bojkov *et al.*, 1998a; Goutail and Pommereau, 1997). These major ozone losses are related not only to the increasing chlorine loading in the stratosphere but also to the unusually low stratospheric winter/spring temperatures (e.g., see Pawson and Naujokat (1997); Chapter 5 of this Assessment).

Although negative deviations exceeding 150 DU were common for days and sometimes weeks in the northern middle and polar latitudes during most of the springs in the 1990s, ozone hole values of below 220 DU were not observed (except as one-day events in the winter/springs of the 1990s). This is related to the very high background spring-season ozone (~420-450 DU) in the 1960s and early 1970s. Compared with the Antarctic mean values of earlier decades, the winter/spring averages in the northern latitudes were always 100 to 130 DU higher (e.g., Bojkov, 1986, 1988; Stolarski *et al.*, 1997).

#### 4.5.2.1 Trends and Variability

The ozone decline in the Northern mid and polar latitudes can be assessed from the calculated ozone trends in the previous section (4.5.1). In percent per decade the decline in the Arctic region is more than 2 times stronger during the winter/spring (-7.8) than during the fall (-3.6) or the summer (-3.5). In the upper midlatitudes (50°-65°N) on the average the trends in the winter/spring are -4.4 and in summer/fall -2.8% %/decade. However, from Table 4-5 and Figure 4-19 it is clear that there are substantial regional differences. The spring trends over Siberia are stronger than -7%, and over Europe close to -7%, but over North America they are only about -5%/decade. Summer trends are much more uniform (about -3%/decade).

Figure 4-20 shows the seasonal (December-January-February-March) area-averaged total ozone departures from the pre-1976 mean values between 45 and 65° N over three continental-size regions. In general the winter/spring departures are negative, exceeding the $2\sigma$ levels, at least over two of the regions for the past 10 years except in 1991 and 1994. Depending on the position of the polar vortex and its expansion south of 65°N, the February-March negative ozone deviations have extreme values over Siberia of -21% in 1996, -17% in 1995, and -14% in 1993. A number of recent studies (e.g., Hood and Zaff, 1995; McCormack and Hood, 1997; Peters and Entzian, 1998) show that close to half of the longitudinal differences in the ozone trends are probably related to decadal variations in the structure of the quasi-stationary planetary (Rossby) waves. It should be recalled that Stolarski *et al.* (1992) already have demon-

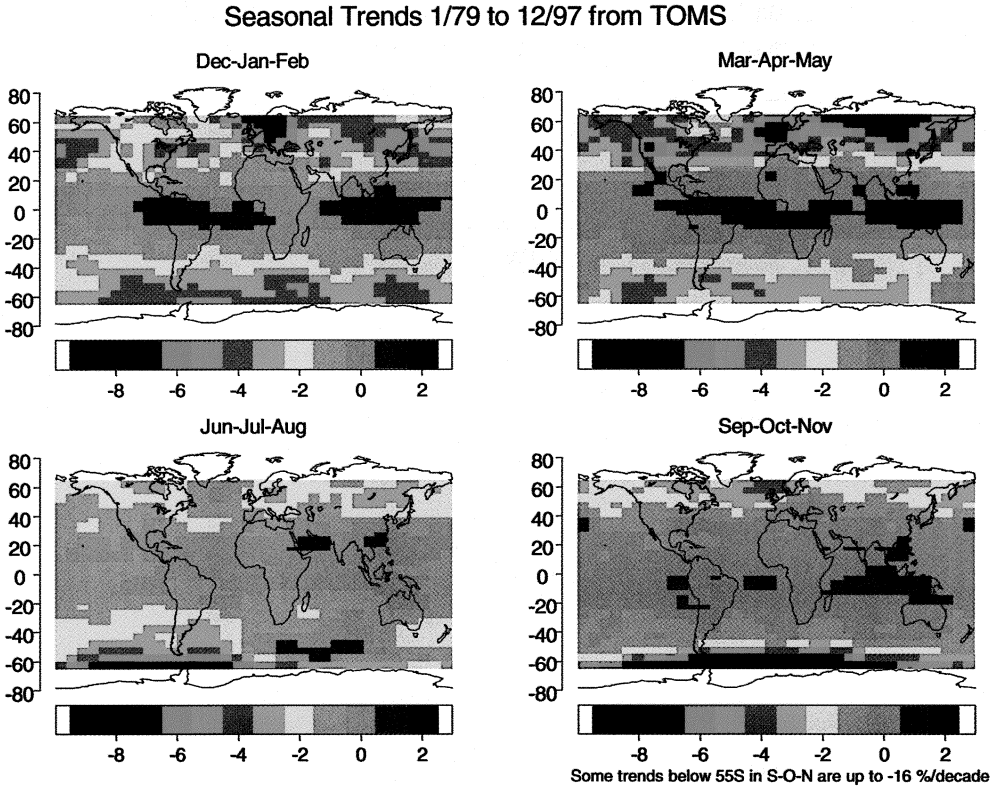


**Figure 4-19.** TOMS trends in percent per decade (Nimbus-7 + Meteor-3 + Earth Probe) over the period 1/79-12/97 in 5° latitude × 10° longitude blocks (latitudes 65°S-65°N).

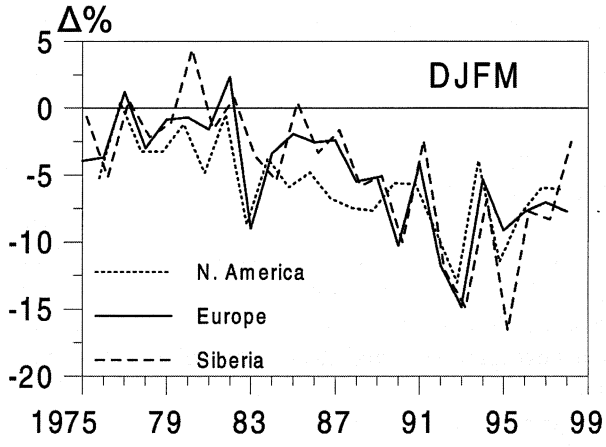


**Figure 4-20.** Area-averaged (45°N-65°N) total ozone departures (in %) from the long-term pre-1976 averages over Europe, North America, and Siberia, for the winter/spring (DJFM) seasons, 1975-1998, calculated from ground-based total ozone measurements. The 2-sigma deviation of the natural seasonal variability in the pre-1976 period was less than 6%.

strated the existence of significant longitudinal differences in the ozone trends, which are also seen on Figure 4-20. The regional fluctuations are mostly related to the specifics of the stratospheric circulation and temperature conditions, as discussed for example by Bekoryukov *et al.* (1997); Bojkov *et al.* (1998b); Hood *et al.* (1997); and others.

The major contributions to the winter/spring seasonal negative deviations are during February and March, when the height of the sun above the horizon is rapidly increasing. The mean total ozone departures from the long-term averages for February-March 1992-1997 over the Northern Hemisphere are plotted in Figure 4-21. Over this 2-month-long period, deviations larger than -12% (in excess of $2\sigma$) dominate, with highest deviations stronger than -20% (i.e., $>3\sigma$) for the Arctic and most of Siberia. A measure of the unusually strong decline observed during the 1990s over the polar and midlatitudes is provided by the frequency of days with ozone values deviating below the long-term mean by more than $2\sigma$ during the winter/spring season, as discussed by Bojkov *et al.* (1998b) and in WMO (1997).

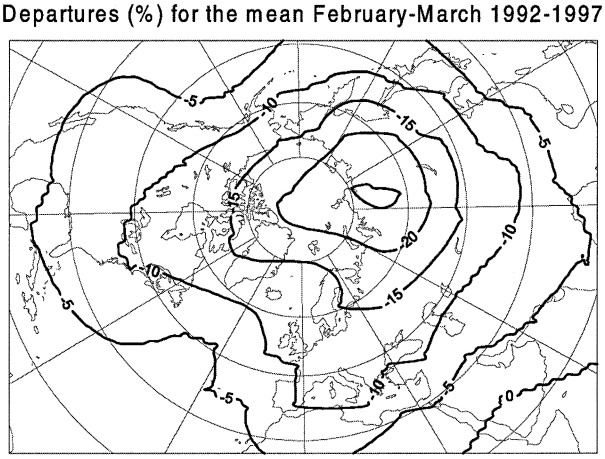


**Figure 4-21.** Mean February-March 1992-1997 total ozone departures (%) from the long-term average in the Northern Hemisphere. (Updated from Bojkov *et al.*, 1998b.)

Except for the 1990/91, 1993/94, and 1997/98 seasons, all other winter/springs in the 1990s have days with deviations 6 to 10 times their pre-1976 averages. The bulk of the winter/spring ozone deficiency within the Arctic polar vortex appears mostly in the lower stratosphere, similar to the ozone depletion during the austral spring in Antarctica (see also Section 4.5.3 and Chapter 7).

#### 4.5.2.2 Estimating the Ozone Mass Deficiency

One approach to detecting the lower stratospheric ozone loss is the Match analysis (von der Gathen *et al.*, 1995; Rex *et al.*, 1997). The ozone loss rates in an ensemble of air parcels were determined from ozonesonde data obtained by a coordinated launch strategy. Through statistical analysis, ozone loss rates in winter and early spring, inside the vortex, could be determined as a function of time and altitude, and ultimately estimates of the loss in column ozone were made. For the winter/spring of 1994/95, a chemical ozone loss of 127 DU in the Arctic vortex was calculated. (See also Chapter 7.)

Manney *et al.* (1997) and Goutail and Pommereau (1997) estimated the chemical ozone loss in the lower stratosphere based on MLS and Système d'Analyse par Observation Zénithale (SAOZ) observations. The cumulative depletion in the vortex based on six SAOZ stations was estimated to reach 30-40% in 1993, 1995, and 1996 and 25-30% in 1997 for the winter/spring season. These numbers are only slightly different from the estimates of the ozone-mass deficiencies given below. Tsvetkova *et al.* (1997), using ozone soundings at Yakutsk, estimated that the ozone loss rate in the 13-19 km layer during the spring of 1995 reached 0.4%/day of the total ozone amount. A different approach is to consider the correlation between a chemically inert tracer and ozone in the Arctic vortex over winter and spring to determine changes in ozone concentrations due to diabatic descent (Müller *et al.*, 1996, 1997a,b, 1998). Using this technique, Müller *et al.* (1997a,b, 1998) estimated that the average ozone loss in the lower stratosphere (12-21 km) during the winter/springs of 1992 through 1996 ranged between 102 DU in 1994 to 140 DU in 1996.

In order to get precise information on the overall ozone changes over the Northern mid and polar latitudes, Bojkov *et al.* (1998a) carried out a comparison of the long-term pre-1976 total ozone field, with data for each day from 1 January to 15 April for 1979-1998. The spread of the polar stratospheric vortex was determined through potential vorticity analysis on the 475-K potential temperature surface for each day for the last 10 years (1989-1998) and compared with the gridded ozone-change analysis. All calculations were carried out for the entire sunlit surface poleward of 35°N.

Figure 4-22 presents the ozone mass deficiency ($O_3$MD) poleward from 35°N within the -10% and -15% contours and corresponding areas for the 1 January-15 April period. These two contours were selected in order to explore the morphology of negative ozone deviations, which generally exceed the natural variability (~2$\sigma$ and 3$\sigma$, respectively). It shows substantial interannual variability and a clear increase of $O_3$MD, especially during 1993 and 1995. In those 2 years the integrated $O_3$MD within the -10% ozone-deviations contour exceeded 12000 Mt over an integrated surface of $\sim 8000 \times 10^6$ km$^2$ for 105 days. The seasonally integrated average $O_3$MD for the 1990s is ~7800 Mt, which is nearly 3 times larger than the average (~2800 Mt ) in the years up to the mid-1980s. It should be noted that the contributions to the overall $O_3$MD (for 35°N) from regions with even stronger deficiencies (-15% contour) also increased from ~55% up to the mid-1980s to an average of ~70% in the 1990s, with the highest values exceeding 75% in 1993, 1995, 1996, and 1997.

The overall increase of ozone deficiency within the -10% contours is not a result of any redistribution (an increase of ozone) within the +10% contours in the middle and polar latitudes of the Northern Hemisphere.

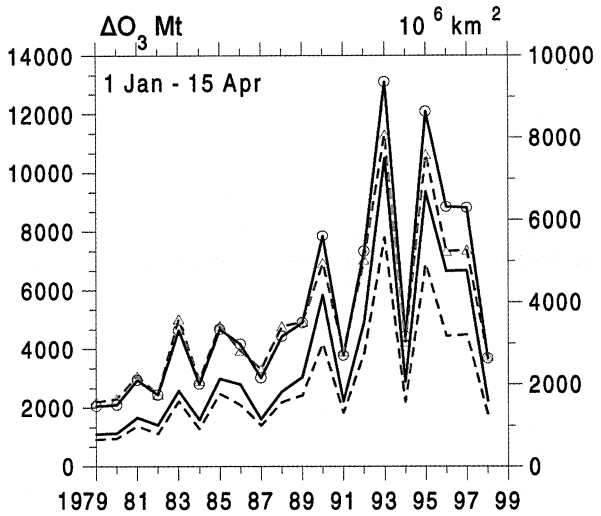


**Figure 4-22.** Ozone mass deficiency integrated over the period 1 January to 15 April, expressed in Mt, inside the -10% contour (continuous line with circles) and the -15% contour (continuous line alone), poleward from 35°N, 1979-1998. The dashed lines show, for each year, the surface area of the -10% contour (with triangles) together with the -15% contour (dashed lines alone) expressed in $10^6$ km$^2$.

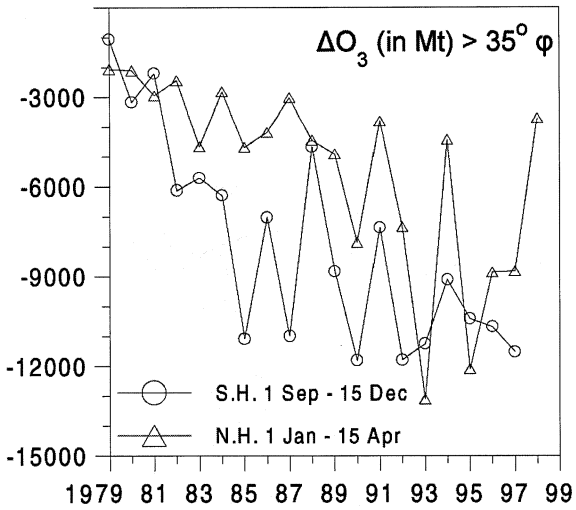


**Figure 4-23.** Ozone mass deficiency (in Mt) integrated over 105 days, inside the -10% contour: (1) north of 35°N, over the period 1 January to 15 April (diamonds), and (2) south of 35°S over the period 1 September to 15 December (circles), for 1979-1998.

The fraction of the -10% contour area from the entire area poleward from 35°N has grown from less than 20% in the early-1980s to ~50% for the 1990s, with the highest values (>70%) in 1993 and 1995. At the same time the area covered by positive deviation >+10% has declined from ~10% in the early 1980s to a negligible ~3% in the 1990s.

#### 4.5.2.3 Comparisons with $O_3$MD in the Southern Hemisphere

Figure 4-23 shows the $O_3$MD (in Mt) within the -10% contours integrated over equal 105-day-long periods poleward from 35°N and 35°S. The periods of 1 January to 15 April and 1 September to 15 December are when major ozone declines have occurred, in the respective north and south polar regions. During the 1980s the average of the 105-day integrated $O_3$MD was ~6000 Mt over the southern latitudes versus ~3500 Mt over the northern latitudes (the latter $O_3$MD was ~42% smaller). During the 1990s, however, in the northern latitudes, a substantial increase in $O_3$MD was observed, up to an average of ~7800 Mt vs. ~10500 Mt over the southern latitudes (the northern $O_3$MD was now only 26% smaller). Furthermore, in two particular seasons (1993 and 1995), the overall $O_3$MD in the northern latitudes >35°N exceeded the $O_3$MD over the corresponding southern latitudes.

The differences between the two hemispheres are better understood if one looks at two specific latitudinal belts. During the 1990s over the middle latitudes from 35° to 50° the average $O_3$MD was ~2700 Mt over the northern and only ~1650 Mt over the same southern latitudes. Over the upper middle and polar latitudes, >60°, the average $O_3$MD was ~5900 Mt over the southern and only ~3100 Mt over the northern region. This shows that, although for the entire region poleward from 35°, on a molecule-per-molecule basis, the $O_3$MD over the Southern Hemisphere exceeds the $O_3$MD over the Northern Hemisphere, this difference is due to the severe ozone deficiency over Antarctica. However, over the southern middle latitudes the $O_3$MD is much less (~39%) than over the northern 35°-50° belt.

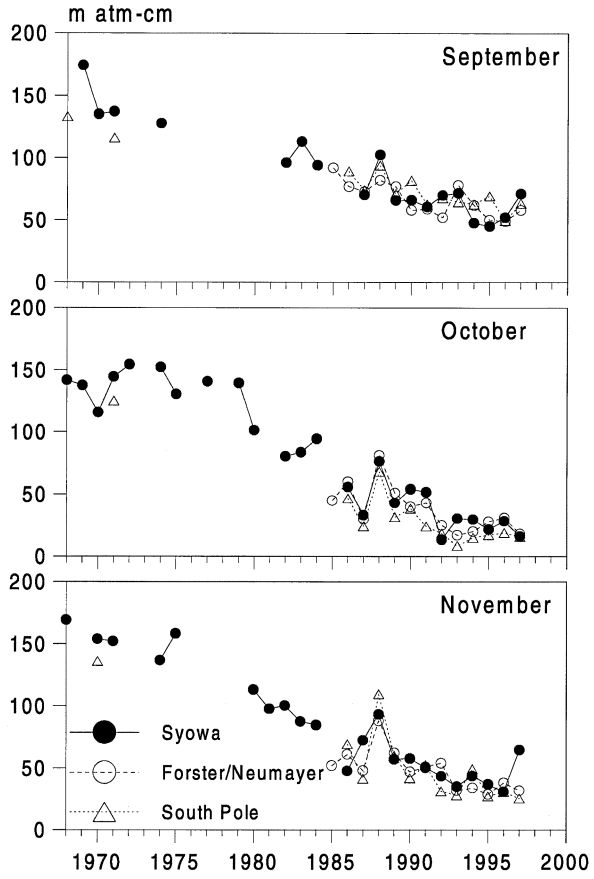


**Figure 4-27.** Change of the ozone content in the 12-20 km layer in September-October-November plotted with data from Syowa by the Japan Meteorological Agency (1968-1997), from South Pole by NOAA (1968, 1970, 1971, and 1986-1997), and from Forster-Neumayer by Alfred Wegener Institute (1984-1997), showing the drastic decline of the ozone in the lower stratosphere during the last years.

negative ozone trends for each layer since the end of the 1970s. The ozone at 100 hPa (~16 km) and 70 hPa (~18 km) has been almost completely depleted for the entire month of October since 1992 (Uchino *et al.*, 1998). Similar findings for the ozone changes over the South Pole are presented by Hofmann *et al.* (1997).

Figure 4-29 summarizes the observed change of ozone and temperature over Antarctica using the entire Syowa ozonesonde record since 1968. The coincidence in location of the region of severe ozone decline with the region of major temperature decline can be clearly seen. The largest values of the temperature change seem to lag, by about 2 weeks, the occurrence of the maximum ozone decline. The ozone decline over the southern polar latitudes started to be especially strong in the second half of the 1980s. Despite the year-to-year variations, the ozone decline seems to have reached its highest values during most of the 1990s. One indirect confirmation of this is that the fraction of the -10% contour area from the entire surface area poleward from 35°S has grown from about 20% in 1979-1984 to an average of above 50% for the 1990s, or it has increased by ~2.5 times. At the same time the area covered by positive ozone deviations >+10% has actually declined to less than 5% of the surface area poleward from 35°S during the 1990s.

## 4.6 LONG-TERM CHANGES IN VERTICAL PROFILES

A general theme of WMO (1998) is a focus on the revised SAGE data, as this is the only long-term dataset that provides global measurements in the lower stratosphere. Three time periods, 1970-1996, 1980-1996, and 1984-1996, are of interest (the SPARC/IOC report was put in final form during mid-1997 and used data only through the end of 1996). The first time period covers the entire length of the available record from the ground-based observations. The second period encompasses the period of satellite records and, in addition, avoids the problem of merging the Brewer-Mast sonde data with the ECC sonde data at the Canadian stations. Finally, the last period is that for which SAGE II data are available, thus avoiding the issue of treating the gap in the SAGE I to SAGE II data and possible lower-stratospheric altitude registration errors in the SAGE I data.

### 4.6.1 Upper Stratosphere

Upper stratospheric time series from three measurement systems have been analyzed. These are the SAGE, Umkehr, and SBUV. Figure 4-30 shows time series at 40 km for northern midlatitudes from each of these systems. All three show a general decline over this period, with a more rapid decline between 1980 and 1984 followed by a relatively flat period between 1984 and 1991. The Umkehr and SAGE systems then show a more rapid decrease after 1991. The SBUV system does not show this last decrease, which has been traced to an apparent drift in the NOAA-11 SBUV/2 instrument with time (WMO, 1998). When the upper stratospheric data

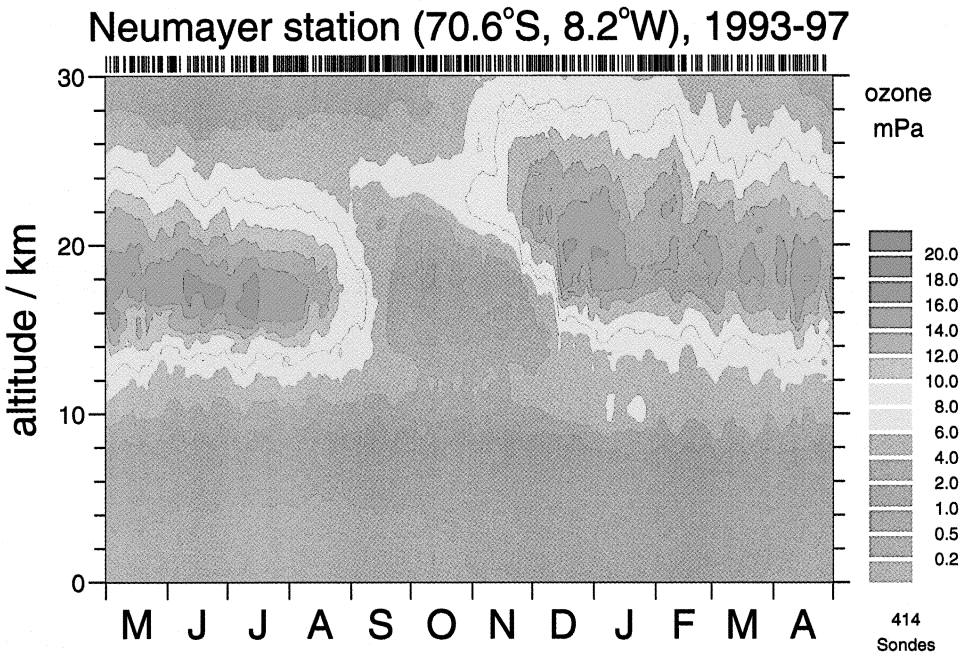


**Figure 4-28.** Average annual cross section of the ozone partial pressure over Neumayer (70°S) for the period 1993-1997, demonstrating the steep decline with the appearance of the sun in August and nearly complete disappearance of the ozone in the lower stratosphere in September-October. Short vertical lines at the top of the panel denote occurrences of sonde launches.

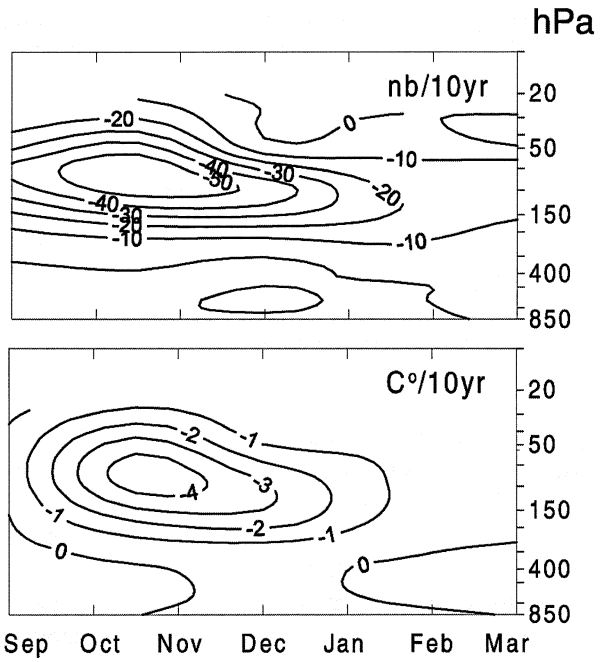


**Figure 4-29.** Annual vertical cross section of the ozone and temperature trends over Syowa (1968-1997). All stratospheric-level trends are significant at the two-sigma level.

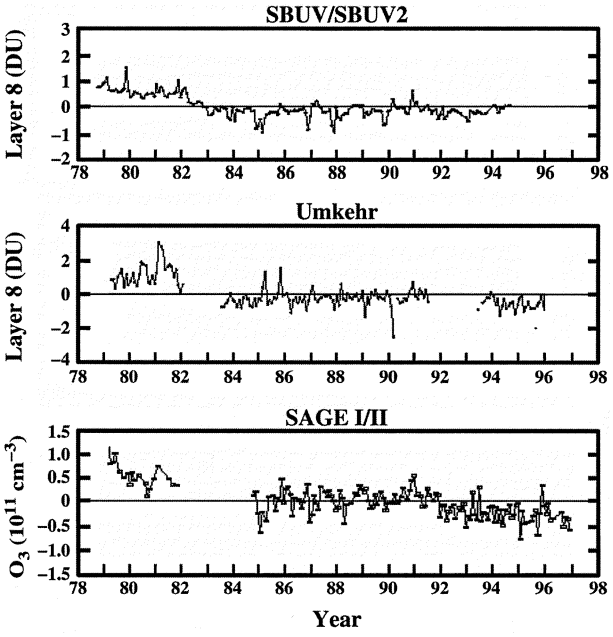


**Figure 4-30.** Monthly time series (deseasonalized) for layer 8 from the Umkehr and SBUV datasets compared with a similar series at 40 km from the SAGE dataset. (From WMO, 1998.)

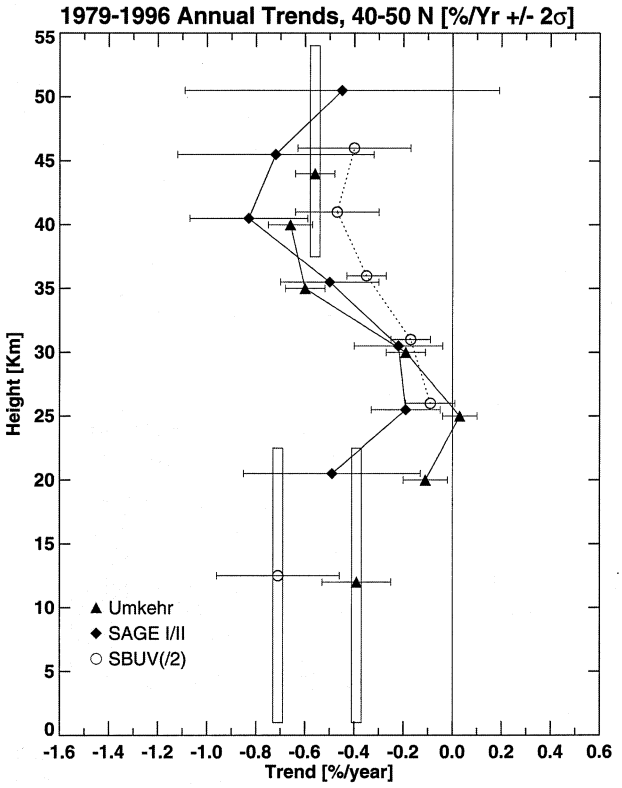


**Figure 4-31.** Ozone trends (%/yr) for 40-50°N over the period 1979-1996 calculated from the following measurement systems: three Dobson/Umkehr stations (Boulder, Haute Provence, and Belsk) reported at individual layers 4 through 8 (triangles), layers 1+2+3+4 (plotted as a vertical bar from ~1 to 22 km with a triangle), and layers 8+9+10 (plotted as a vertical bar from ~37 to 54 km with a triangle); SAGE I/II average sunrise and sunset observations (diamonds) reported at individual layers 4-10; SBUV (/2) (circles) reported at individual layers 5 through 9 and layer 1+2+3+4. All error bars are 95% confidence intervals of the trend. SAGE I/II error bars represent SAGE I altitude-correction uncertainties, SAGE II sunrise/sunset trend difference uncertainties, and statistical uncertainties. Umkehr and SBUV(/2) error bars represent only statistical uncertainty. Small vertical offsets are for clarity only (e.g., all values plotted near 30 km represent layer-6 results). (From WMO, 1998.)

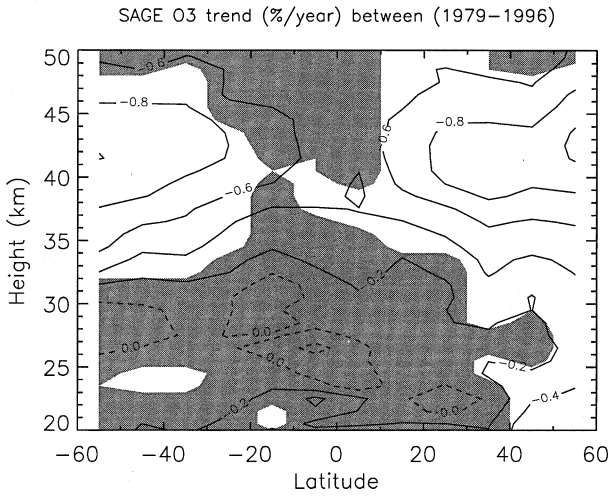


**Figure 4-32.** Ozone trends calculated from SAGE I/II observations from 1979 to 1996 expressed in %/year of the midpoint of the time series (1987). Results are contoured from calculations done in 5° latitude bands and 1-km altitude intervals. Contours differ by 0.2%/year with the dashed contours indicating zero or positive trend. The shaded area indicates where the trends do not differ from zero within 95% confidence limits. The estimate of uncertainty contains terms due to the SAGE I reference height correction and the SAGE II sunrise-sunset trend differences. (From WMO, 1998.)

are fit to a standard statistical model, negative trends are found throughout the region, with statistically significant peak values of -5 to -8%/decade at 40-45 km altitude (Figure 4-31). There is good agreement between SAGE I/II and Umkehr. The SBUV-SBUV/2 combined record shows less negative trends principally because of the lack of decline in that record after 1991. Because of the potential drift problems with the present version (6.1.2) of the NOAA-11 SBUV2 data, less confidence should be placed on the trends from the combined SBUV-SBUV/2 record.

Figure 4-32 shows the annual-average trend over the time period of 1979 through 1996 from SAGE I/II as a function of altitude and latitude. The peak negative trend is strongest at high latitudes, with a maximum negative trend of nearly 1%/yr occurring between 40 and 45 km altitude. The maximum negative trend in the equatorial region is a little less than 0.6%/yr. There is no significant interhemispheric difference in upper stratospheric trends. This contrasts with earlier results based

on SBUV (WMO, 1995). The earlier SBUV asymmetry was not statistically significant and has mostly disappeared with the extension of the dataset. The trend in layer 8 (around 40-km altitude or near the peak trend value) exhibits a seasonal variation with a maximum negative trend in both hemispheres during late winter (Figure 4-33). The seasonal variation in the trend in each hemisphere is nearly a factor of 2, ranging from -0.6%/yr to more than -1%/yr. The equatorial trend is not statistically significant except for the period from about April through July.

### 4.6.2 Lower Stratosphere

Previous evaluations have demonstrated that significant trends also occur in the lower stratosphere (altitudes between about 10 and 30 km). As we will see below, a second peak occurs in the percentage trend in the lower stratosphere. Because of the higher ozone density in the lower stratosphere, this second peak is responsible for most of the trend observed in the column amount of ozone. The primary trend instruments in this region are sondes (ground up to 27 km) and SAGE (SAGE I from 20 km up and SAGE II from 15 km up).

Two groups, Logan and Megretskaia (LM, Harvard University) and Tiao *et al.* (University of Chicago), carried out analyses of the sonde data. They used different methods to screen the sonde data and arrived at somewhat different trend results, which will be shown below. Tiao *et al.* used a more stringent selection criterion for the so-called "correction factor" deduced for a sonde measurement. After applying this more-stringent criterion, Tiao *et al.* then used uncorrected data. Logan and Megretskaia allowed more data to pass the screening by adopting a less stringent criterion for correction factors, and then used the corrected data. This resulted in a time

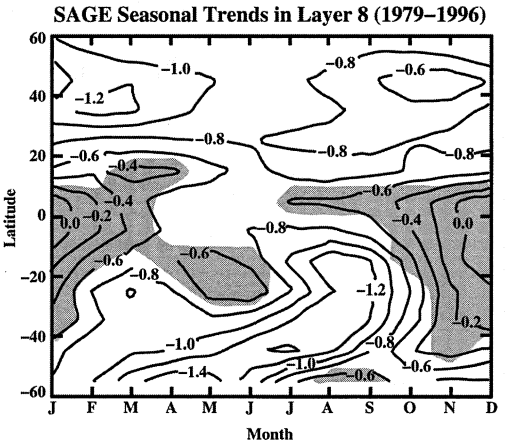


**Figure 4-33.** Seasonal variation of ozone trends in layer 8 (in %/year) calculated from SAGE I/II (1979-1996) for latitudes 55°S to 55°N. Non-shaded areas indicate 95% confidence intervals that include SAGE I altitude correction, SAGE II sunrise-sunset trend differences, and statistical uncertainties. (From WMO, 1998.)

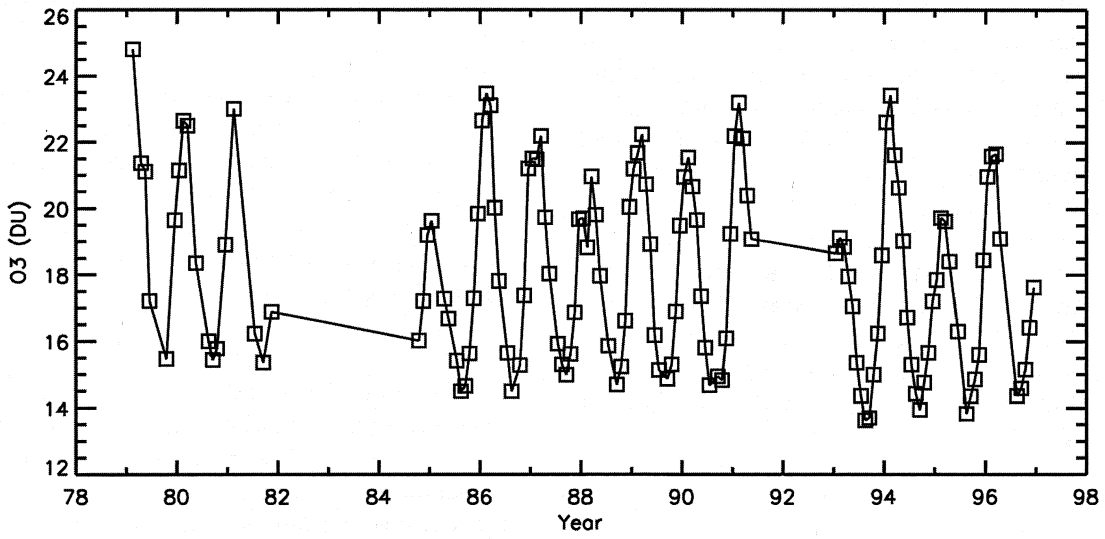


**Figure 4-34.** SAGE I/II monthly mean ozone measurements between 45°N and 50°N integrated from 20 to 21 km altitude in Dobson units. (From WMO, 1998.)

series with significantly more data points. The results of the two analyses are in agreement on major points but do have some important differences, some of which will be shown below.

Figure 4-34 shows a time series from the SAGE I/II measurements integrated between 40 and 45°N latitudes and 20 and 21 km altitudes. The series is dominated by seasonal cycles, but a trend can also be seen in the data. A problem pointed out in previous Assessments (e.g., WMO, 1995) is the disagreement between trends derived from sondes and SAGE in the lower stratosphere. With the reanalyzed sonde data and the new version of SAGE data, this disagreement no longer exists. Figure 4-35 shows the average ozonesonde trend derived from seven stations at northern midlatitudes compared with those derived from SAGE for the zonal mean between 45 and 50°N latitudes as a function of altitude. The comparison now shows excellent agreement.

Figure 4-36 shows the trends derived from nine separate stations as a function of altitude. The analyses of both LM and Tiao *et al.* are shown. While the details of the two analyses are different, both reach the conclusion that the trends are negative over the region of the lower stratosphere at all stations. The trends near 100 mb (~17 km) range from about -3%/decade to -10%/decade and are statistically significant at all stations. The trends decrease at higher altitudes and are near zero at 20 mb. The trends in the troposphere are much more widely varying from station to station (see Chapter 8 for a discussion of tropospheric ozone trends).

Figure 4-37 shows the combined calculated trends for the time period from 1970 through 1996 from eight sonde stations as a function of altitude for four seasons. The results from both the LM and Tiao *et al.* analyses are shown. Both indicate that the trends are not a function of season above about 70 mb and in the troposphere. The seasonal dependence of ozone trends appears to be confined to the region between about 10 and 20 km altitude. The two analyses get a somewhat different seasonality in the 10-20 km region. When the stations are divided up by region, some interesting differences appear. In Figure 4-38, the trends calculated by LM for 1970-1996 are shown for the four seasons for three combined European stations and three combined Canadian stations. The Canadian stations show a seasonal variation that is quite different from that seen at the European stations and extends over a larger altitude range.

The trends shown for the lower stratosphere thus

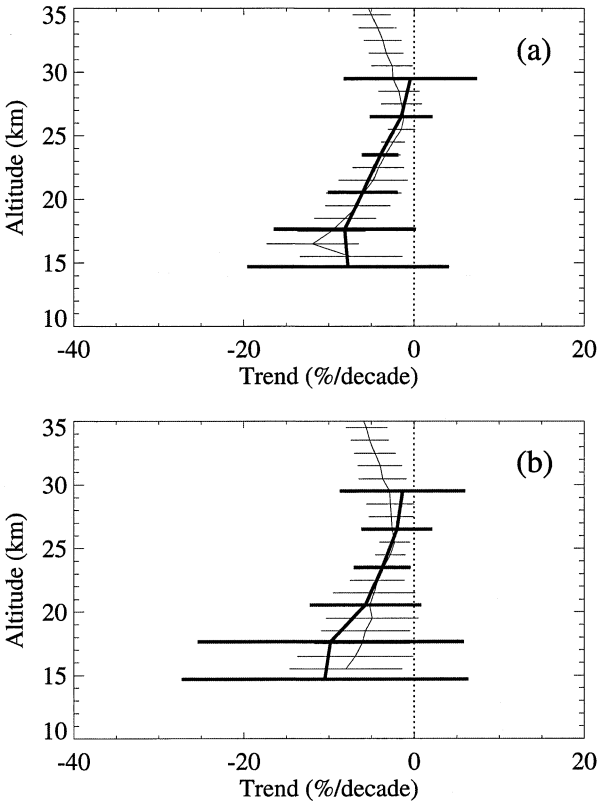


**Figure 4-35.** Average ozonesonde trends for Uccle, Hohenpeissenberg, Payerne, Edmonton, Goose Bay, Boulder, and Sapporo (40-53°N) for the time periods (a) 1980-1996 and (b) 1984-1996, in percent/decade (darker lines). These are compared to (a) trends for SAGE I/II and (b) trends for SAGE II alone for 45-50°N (lighter lines). The SAGE trends were analyzed at 1-km intervals, and the ozonesonde trends have been expressed as a function of altitude using the 1976 standard, midlatitude atmosphere. The 2-sigma error bars are given. (From WMO, 1998.)

far have been for the time period starting in 1970. The SAGE data begin in 1979 with SAGE I and resume again in 1984 with SAGE II. The SPARC/IOC report showed calculations of the trend from sondes over the time period of 1970-1996 compared with those for 1980-1996 (see also Chapter 8 of this report). Only minor differences were seen in the stratosphere. We can use the SAGE measurements to give us a global picture of the trends since 1979. These trends, which extend from 20-km altitude upward, were shown in Figure 4-32. For the

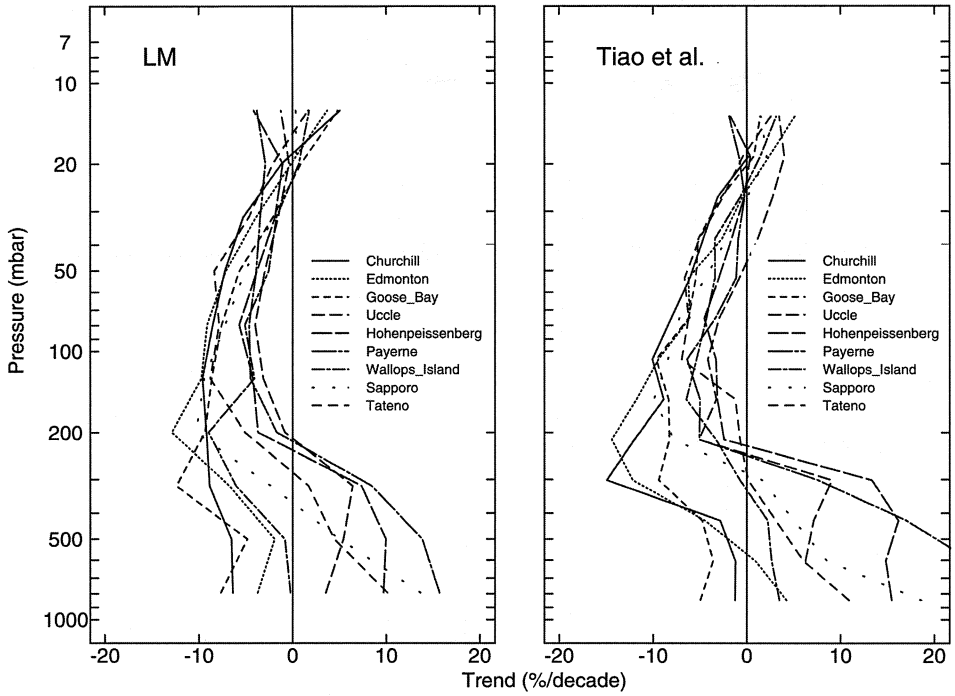


**Figure 4-36.** Annual ozone trends for individual sonde stations located between 59°N and 36°N for the period 1970-1996: LM results (left), and Tiao *et al.* results (right). (Modified from a figure in WMO, 1998.)

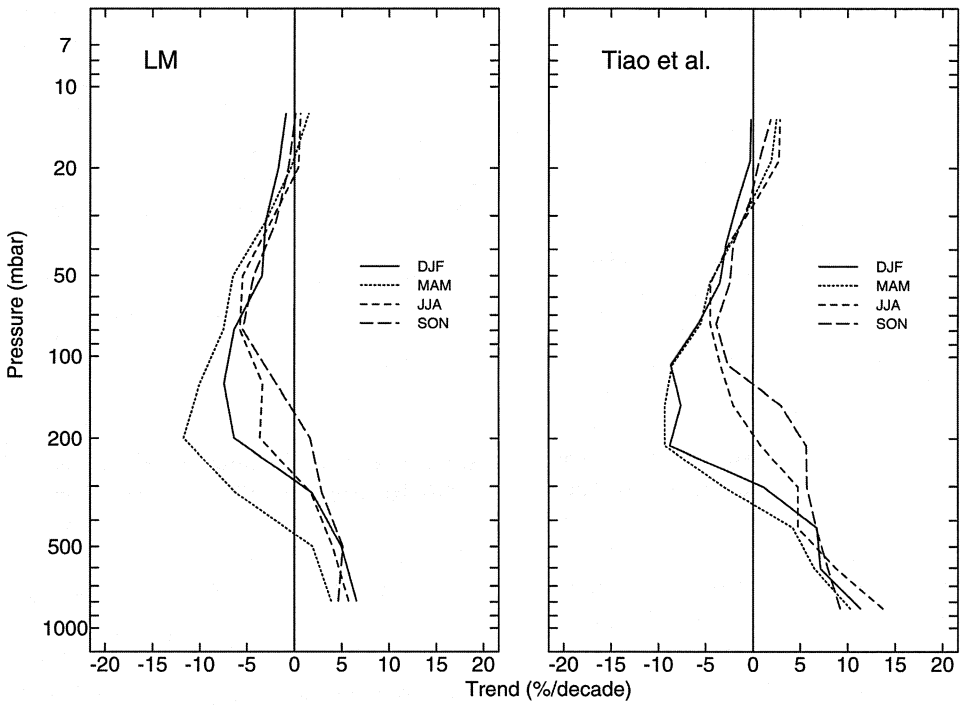


**Figure 4-37.** Seasonal-mean profiles of ozone trends for eight sonde stations located between 59°N and 36°N: LM results (left), and Tiao *et al.* results (right). (Modified from a figure in WMO, 1998.)

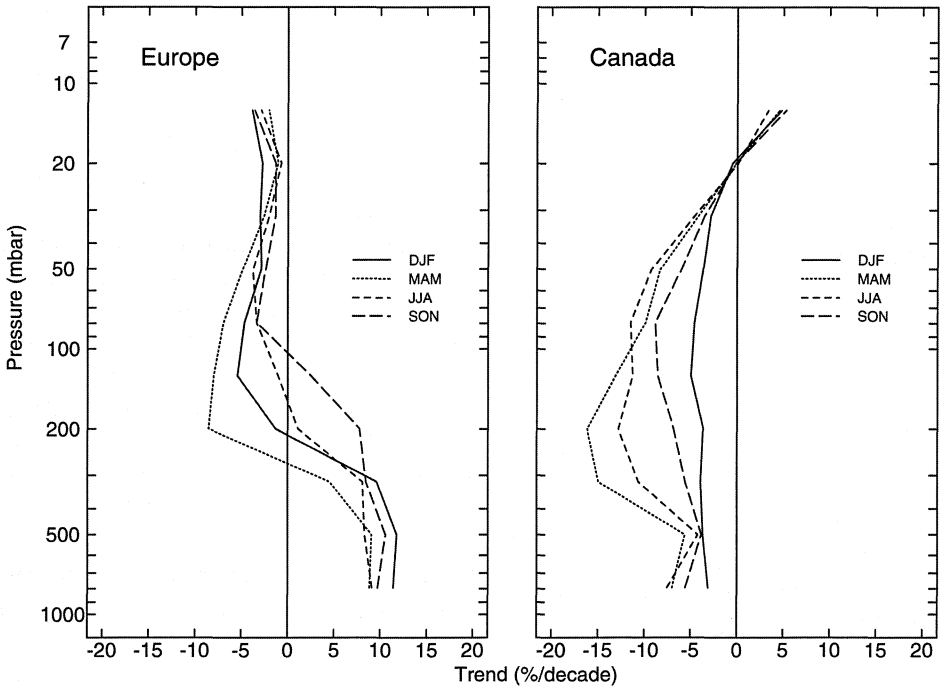


**Figure 4-38.** Seasonal mean profiles of ozone trend for three European stations, 48-51°N (left) and three Canadian stations, 53-59°N (right); LM results. (Modified from a figure in WMO, 1998.)

shorter time period from 1984 through 1996 where SAGE II data are available, the record can be extended down to 15 km. The resulting annually averaged trend is shown in Figure 4-39 as a function of altitude and latitude. The northern midlatitude negative peak in the trend, previously shown in Figure 4-32, is apparent. At southern midlatitudes, no such peak in the negative trend is seen, and the trends are in fact slightly positive. Note that between 15 and 20 km altitude, the trends shown are mostly statistically not different from zero. This is because of the shortness of the record, the variability of ozone, and the sampling frequency.

### 4.6.3 Combined Trends

The SPARC/IOC (WMO, 1998) report made a first attempt at combining the trends and uncertainties (including both statistical and systematic) estimated from all available measurement systems. This was done only for northern midlatitudes, where sufficient measurements from multiple systems are available. The calculations are all for the trend since 1979. The combination of the trends was done by using the following prescription. First, trends and statistical uncertainties were determined for each instrument or station. Then instrumental uncertainties were estimated for each instrument. These were limited to those uncertainties that would result in potential drift errors in the data. Thus, cross section errors were not counted in this estimate because they would be constant in time. Next, the statistical and instrumental errors were combined by taking the root sum of their squares.

The trends for the sonde stations were then averaged by taking a weighted mean of their results at each altitude. The weighting factor was one over the square of the combined estimated standard error. The uncertainty in the averaged trend over all of the stations was determined in two ways. One was to combine the uncertainties deduced from each sonde station. The other was to calculate the standard error of the mean for the individually determined trends. This second method gave the largest estimate of uncertainty for 20 km and below and was used in all subsequent calculations.

Trends as a function of altitude were derived for each of the four measurement systems and their uncertainties were estimated according to the above description. These were then combined into a single trend as a function of altitude by using a weighted mean of the individual trends and a weighted mean of the individual

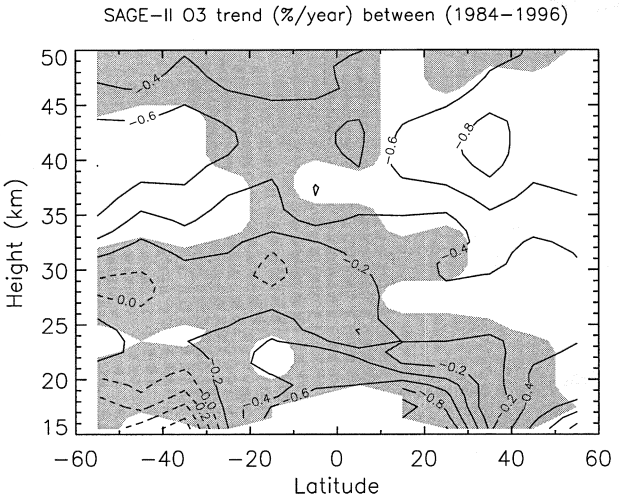


**Figure 4-39.** Annual trends for SAGE II only for the time period 1984 to 1996. (From WMO, 1998.) The shaded area indicates where the trends do not differ from zero within 95% confidence limits.

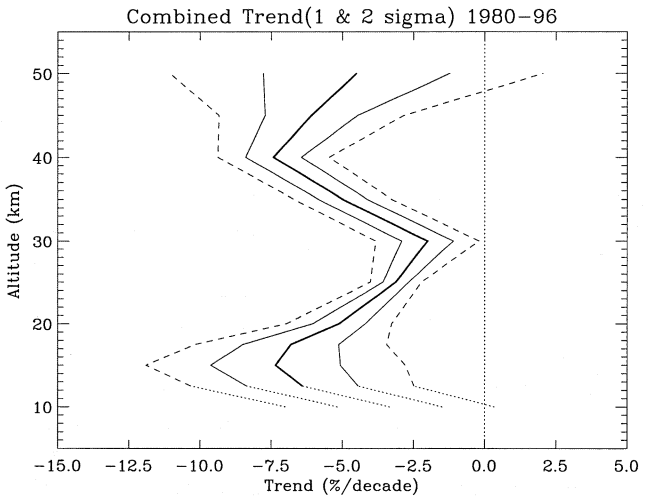


**Figure 4-40.** Estimate of the mean trend using all four measurement systems at northern midlatitudes (heavy solid line). Combined uncertainties are also shown as 1 sigma (light solid line) and 2 sigma (dashed line). Combined trends and uncertainties are extended down to 10 km as shown by the light dotted lines. The results below 15 km are a mixture of tropospheric and stratospheric trends and the exact numbers should be viewed with caution. Combined trends have not been extended lower into the troposphere because the small sample of sonde stations have an additional unquantified uncertainty concerning their representativeness of mean trends. (From WMO, 1998.)

uncertainties at each altitude where more than one system made measurements. This procedure results in a single trend estimate as a function of altitude for the northern midlatitude data. The trend estimate is weighted at each altitude toward the result from the system that had the smallest combined statistical and instrumental drift uncertainties. The result is shown in Figure 4-40.

The estimated trend for the upper stratosphere peaks at (-7.4 ± 2.0)%/decade at 40 km. This result is dominated by the SAGE data which have the smallest estimated uncertainty. At 20 km, the trend is from the combined SAGE, sonde, and Umkehr results. Below 20 km, the trend estimate comes from sondes alone. The lower stratospheric trend shows a maximum negative value of (-7.3 ± 4.6)%/decade at 15 km. The minimum trend between these peaks is (-2.0 ± 1.8)%/decade at 30 km, which is just statistically significant at the 95% confidence level. Thus, at northern midlatitudes, a statistically significant negative trend is found at all altitudes between 12 and 45 km.

### 4.6.4 Consistency between Total Ozone and Vertical Profile Trends

It is clear from the preceding sections that our ozone trend assessment capabilities have increased in recent years. One particular concern highlighted by WMO (1995) was the disagreement found between the TOMS-based total ozone trends and vertically integrated profile trends derived from sonde and SAGE I and II data. This now appears to have been largely resolved.

In WMO (1998), column ozone trends derived from TOMS data were compared to the integrated ozone profile trends derived from SAGE I/II and from ozonesonde data, in order to determine the consistency between the independent results. Figure 4-41 (a direct reproduction of Figure 3.49 in WMO (1998)) shows the first results of this analysis. Figure 4-41 (top) shows the TOMS column ozone trends as a function of latitude and season. The data show negative trends in NH midlatitudes during late-winter/spring; the March-April values of about -24 DU/decade correspond to percentage changes of about -6%/decade. There are smaller magnitude midlatitude trends in the SH (about -10 DU/decade) and no significant trends in the tropics. The trends in column ozone over 20-55 km derived from SAGE I/II data are shown in Figure 4-41 (middle panel). Significant negative trends of order -4 to -8 DU/decade are observed in NH midlatitudes throughout most of the year (with a maximum in April-May near 50°N) and in

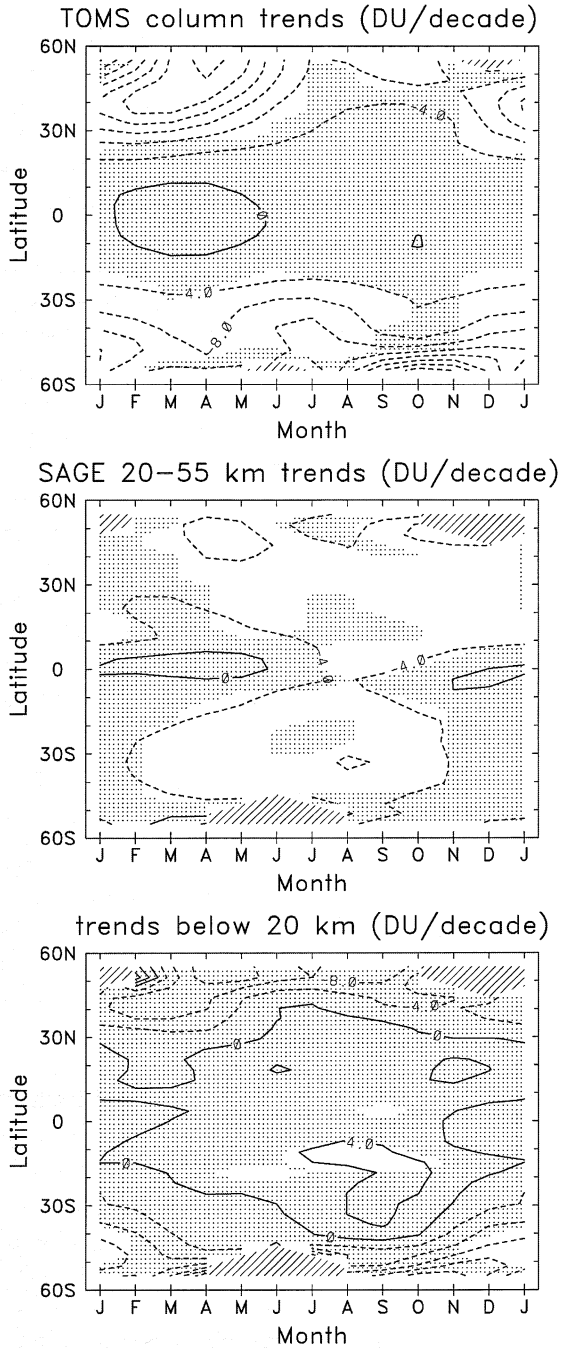


**Figure 4-41.** Top panel: Seasonal and latitudinal variation of trends in column ozone from TOMS. Middle panel: Seasonal and latitudinal variation of trends in column integral of SAGE from 20 to 55 km. Bottom panel: Seasonal and latitudinal variations of trends in TOMS minus SAGE (i.e., column ozone below 20 km). The contour interval for all panels is 4 DU/decade. Statistically insignificant 2σ trends are shaded. (From WMO, 1998.)

SH midlatitudes during winter. Significant trends are not observed near the equator. Comparison with the much larger TOMS trends in NH spring midlatitudes suggests that a majority of these column trends occur at altitudes below 20 km. Figure 4-41 (bottom) shows trends in the difference between the TOMS column ozone data and the SAGE I/II data integrated from 20 to 55 km. This corresponds to trends in the column below 20 km (i.e., the difference between the top and middle frames of Figure 4-41). Negative trends are observed poleward of 40° in each hemisphere; there are relative maxima in NH spring and in SH summer. Small positive trends are seen in the tropics (~30°N-30°S); because of the small background (seasonal) values in the tropics below 20 km, these latter trends equate to a relatively high percentage (~5-10%/decade).

## REFERENCES

Ancellet, G., and M. Beekmann, Evidence for changes in the ozone concentration in the free troposphere over southern France from 1976-1995, *Atmos. Environ.*, *31*, 2835-2851, 1997.

Angell, J.K., Estimated impacts of Agung, El Chichón, and Pinatubo volcanic eruptions on global and regional total ozone after adjustment for the QBO, *Geophys. Res. Lett.*, *24*, 647-650, 1997.

Angreji, P.D., Reevaluation of total ozone measurements with Dobson spectrophotometer at Mt. Abu/ Ahmedabad during 1951-1985, *Scientific Rep. ISRO-PRL-SR-34-89*, Indian Space Research Organization, Bangalore, 1989.

Atkinson, R.J., and R.A. Plumb, Three-dimensional ozone transport during ozone hole break-up in December 1987, *J. Geophys. Res.*, *102*, 1451-1466, 1997.

Basher, R.E., *Survey of WMO-Sponsored Dobson Spectrophotometer Intercomparisons*, World Meteorological Organization Global Ozone Research and Monitoring Project—Report No. 19, Geneva, 1995.

Bekoryukov, V.I., I.V. Bugaeva, G.R. Zakharov, B.M. Kiryushov, G.M. Kruchenitskii, and D.A. Tarasenko, Influence of atmospheric centres of action on total ozone in Siberia, *Meteorol. Gidrol.*, *No. 7*, 33-39, 1997.

Bhartia, P.K., R.D. McPeters, C.L. Mateer, L.E. Flynn, and C. Wellemeyer, Algorithm for the estimation of vertical ozone profiles from the backscattered ultraviolet technique, *J. Geophys. Res.*, *101*, 18793-18806, 1996.

Bojkov, R.D., The 1979-85 ozone decline in the Antarctic as reflected in ground based observations, *Geophys. Res. Lett.*, *13*, 1236-1239, 1986.

Bojkov, R.D., The 1983 and 1985 anomalies in ozone distribution in perspective, *Mon. Wea. Rev.*, *115*, 2187-2201, 1987.

Bojkov, R.D., Ozone variations in the northern polar region, *Meteorol. Atmos. Phys.*, *38*, 117-130, 1988.

Bojkov, R.D., and V. Fioletov, Changes of the lower stratospheric ozone over Europe and Canada, *J. Geophys. Res.*, *102*, 1337-1347, 1997.

Bojkov, R.D., and V. Fioletov, Latitudinal and regional total ozone trends from quality controlled ground-based data, in *Atmospheric Ozone: Proceedings of the XVIII Quadrennial Ozone Symposium*, L'Aquila, Italy, 12-21 September 1996, edited by R.D. Bojkov and G. Visconti, pp. 13-16, Parco Scientifico e Technologico d'Abruzzo, L'Aquila, Italy, 1998.

Bojkov, R.D., C. Mateer, and A. Hanson, Comparison of ground-based and Total Ozone Mapping Spectrometer measurements used in assessing the performance of the global ozone observing system, *J. Geophys. Res.*, *93*, 9525-9533, 1988.

Bojkov, R.D., L. Bishop, W.J. Hill, G.C. Reinsel, and G.C. Tiao, A statistical trend analysis of revised Dobson total ozone data over the Northern Hemisphere, *J. Geophys. Res.*, *95*, 9785-9807, 1990.

Bojkov, R.D., C.S. Zerefos, D.S. Balis, I.C. Ziomas, and A.F. Bais, Record low total ozone during northern winters of 1992 and 1993, *Geophys. Res. Lett.*, *20*, 1351-1354, 1993.

Bojkov, R.D., V.E. Fioletov, and A.M. Shalamjansky, Total ozone changes over Eurasia since 1973 based on reevaluated filter ozonometer data, *J. Geophys. Res.*, *99*, 22985-22999, 1994.

Bojkov, R.D., V.E. Fioletov, D.S. Balis, C.S. Zerefos, T.V. Kadygrova, and A.M. Shalamjansky, Further ozone decline during the Northern Hemisphere winter-spring of 1994-1995 and the new record low ozone over Siberia, *Geophys. Res. Lett.*, *22*, 2729-2732, 1995a.

Bojkov, R.D., L. Bishop, and V.E. Fioletov, Total ozone trends from quality controlled ground-based data (1964-1994), *J. Geophys. Res.*, *100*, 25867-25876, 1995b.

Bojkov, R.D., D.S. Balis, C.S. Zerefos, K. Tourpali, M. Tzortziou, and T.V. Kadygrova, An update of ozone changes in the Northern Hemisphere through April 1997, in *Report on the Fourth European Symposium on Stratospheric Ozone Research*, Schliersee, Bavaria, September 1997, pp.185-189, 1997.

Bojkov, R.D., D.S. Balis, and C.S. Zerefos, Characteristics of the ozone decline in the northern polar and middle latitudes during the winter-spring, *Meteorol. Atmos. Phys.*, in press, 1998a.

Bojkov, R.D., D.S. Balis, C.S. Zerefos, and K. Tourpali, Northern Hemisphere winter-spring ozone changes in 1990-1996, in *Atmospheric Ozone: Proceedings of the XVIII Quadrennial Ozone Symposium*, L'Aquila, Italy, 12-21 September 1996, edited by R.D. Bojkov and G. Visconti, pp. 251-254, Parco Scientifico e Technologico d'Abruzzo, L'Aquila, Italy, 1998b.

Box, G.E.P., G.M. Jenkins, and G.C. Reinsel, *Time Series Analysis: Forecasting and Control*, 3rd ed., Prentice Hall, Englewood Cliffs, N.J., 1994.

Brasseur, G.P., The response of the middle atmosphere to long-term and short-term solar variability: A two dimensional model, *J. Geophys. Res.*, *98*, 23079-23090, 1993.

Brasseur, G., and C. Granier, Mount Pinatubo aerosols, chlorofluocarbons, and ozone depletion, *Science*, *257*, 1239-1242, 1992.

Chandra, S., and R.D. McPeters, The solar cycle variation of ozone in the stratosphere inferred from Nimbus 7 and NOAA 11 satellites, *J. Geophys. Res.*, *99*, 20665-20671, 1994.

Chernikov, A.A., Yu.A. Borisov, A.M. Zvyagintsev, G.M. Kruchenitskii, S.P. Perov, N.S. Sidorenkov, and O.V. Stasyuk, The 1997-1998 El Niño influence on the Earth's ozone layer, *Meteorol. Gidrol.*, *No. 3*, 104-110, 1998.

Chesters, D., and A.C. Neuendorffer, Comparison between TOMS, TOVS and Dobson observations: Satellite and surface view of total column ozone, *Paleogeogr. Paleoclimatol. Paleoecol.*, *90*, 61-73, 1991.

Chubachi S., Annual variation of total ozone at Syowa Station, Antarctica, *J. Geophys. Res.*, *107*, 1349-1354, 1997.

Cunnold, D.M., H. Wang, W. Chu, and L. Froidevaux, Comparisons between SAGE II and MLS ozone measurements and aliasing of SAGE II ozone trends in the lower stratosphere, *J. Geophys. Res.*, *101*, 10061-10075, 1996.

Dave, J.V., and C.L. Mateer, A preliminary study on the possibility of estimating total atmospheric ozone from satellite measurements, *J. Atmos. Sci.*, *24*, 414-427, 1967.

Dobson, G.M.B., A.W. Brewer, and B.M. Cwilong, Meteorology of the lower stratosphere, *Proc. Roy. Meteorol. Soc. London*, *A185*, 144-175, 1946.

Donovan, D.P., J.C. Bird, J.A. Whiteway, T.J. Duck, S.R. Pal, and A.I. Carwell, Lidar observations of stratospheric ozone and aerosol above the Canadian high Arctic during the 1994-95 winter, *Geophys. Res. Lett.*, *22*, 3489-3492, 1995.

Dorokhov, V.M., and T.E. Potapova, Variation of total ozone and $NO_2$ at polar latitudes in eastern sector of the Arctic, in *Atmospheric Ozone: Proceedings of the XVIII Quadrennial Ozone Symposium*, L'Aquila, Italy, 12-21 September 1996, edited by R.D. Bojkov and G. Visconti, pp. 201-204, Parco Scientifico e Technologico d'Abruzzo, L'Aquila, Italy, 1998.

Fioletov, V.E., J.B. Kerr, E.W. Hare, G. Labow, and R. McPeters, An assessment of the world ground-based total ozone network performance from the comparison with satellite data, *J. Geophys. Res.*, submitted, 1998a.

Fioletov, V.E., R.D. Bojkov, P.K. Bhartia, R. McPeters, A.J. Miller, and W. Planet, Total ozone trends derived from Solar Backscatter Ultraviolet (SBUV) and SBUV/2 measurements, in *Atmospheric Ozone: Proceedings of the XVIII Quadrennial Ozone Symposium*, L'Aquila, Italy, 12-21 September 1996, edited by R.D. Bojkov and G. Visconti, pp. 37-40, Parco Scientifico e Technologico d'Abruzzo, L'Aquila, Italy, 1998b.

Fleig, A.J., R.D. McPeters, P.K. Bhartia, B.M. Schlesinger, R.P. Cebula, K.R. Klenk, S.L. Taylor, and D.F. Heath, *Nimbus 7 Solar Backscatter Ultraviolet (SBUV) Ozone Products User's Guide*, NASA Ref. Publ. 1234, National Aeronautics and Space Administration, Washington, D.C., 1990.

Gernandt, H., A. Herber, P. von der Gathen, M. Rex, A. Rinke, S. Wessel, and S. Kaneto, Variability of ozone and aerosols in the polar stratosphere, *Mem. Natl. Inst. Polar Res.*, *Spec. Issue*, *51*, 189-215, 1996.

Gernandt, H., P. von der Gathen, A. Herber, and S. Kaneto, Interannual ozone changes in the lower and middle stratosphere above the Antarctic in spring, in *Atmospheric Ozone: Proceedings of the XVIII Quadrennial Ozone Symposium*, L'Aquila, Italy, 12-21 September 1996, edited by R.D. Bojkov and G. Visconti, pp. 205-208, Parco Scientifico e Technologico d'Abruzzo, L'Aquila, Italy, 1998.

Gleason, J.F., and R.D. McPeters, Corrections to the Nimbus 7 Solar Backscatter Ultraviolet data on the "nonsync" period (February 1987 to June 1990), *J. Geophys. Res.*, *100*, 16873-16877, 1995.

Gleason, J.F., P.K. Bhartia, J.R. Herman, R. McPeters, P. Newman, R.S. Stolarski, L. Flynn, G. Labow, D. Larko, C. Seftor, C. Wellemeyer, W.D. Komhyr, A.J. Miller, and W. Planet, Record low global ozone in 1992, *Science*, *260*, 523-526, 1993.

Goutail, F., and J.P. Pommereau, Ozone loss: The northern polar picture, in *Report on the Fourth European Symposium on Stratospheric Ozone Research*, Schliersee, Bavaria, September 1997, pp. 273-276, 1997.

Goutail, F.J., J.P. Pommereau, F. Lefévre, E. Kyrö, M. Rummukainen, P. Ericksen, S.B. Andersen, B.-A. Kaastad-Hoiskar, G. Breathen, V. Dorokhov, and V. Khattatov, Total ozone reduction in the Arctic vortex during the winters of 1995/96 and 1996/97, in *Report on the Fourth European Symposium on Stratospheric Ozone Research*, Schliersee, Bavaria, September 1997, pp. 277-280, 1997.

Gustin, G.P., S.A. Sokolenko, B.G. Dudko, and V.V. Lagutina, Ozonometer M-124 (in Russian), *Tr. Glav. Geofiz. Obs.*, *499*, 60-67, 1985.

Hansen, G., T. Svenoe, M.P. Chipperfield, A. Dahlback, and U.P. Hoppe, Evidence of substantial ozone depletion in winter 1995/96 over northern Norway, *Geophys. Res. Lett.*, *24*, 799-802, 1997.

Harris, N.R.P., G. Ancellet, L. Bishop, D.J. Hofmann, J.B. Kerr, R.D. McPeters, M. Prendez, W.J. Randel, J. Staehelin, B.H. Subbaraya, A. Volz-Thomas, J. Zawodny, and C.S. Zerefos, Trends in stratospheric and free tropospheric ozone, *J. Geophys. Res.*, *102*, 1571-1590, 1997.

Hasebe, F., Quasi-biennial oscillations of ozone and diabatic circulation in the equatorial stratosphere, *J. Atmos. Sci.*, *51*, 729-745, 1994.

Heath, D.F., C.L. Mateer, and A.J. Krueger, The Nimbus-4 backscatter ultraviolet atmospheric ozone experiment, *Pure Appl. Geophys.*, *106-108*, 1238-1253, 1973.

Heath, D.F., A.J. Krueger, H.A. Roeder, and B.D. Henderson, The Solar Backscatter Ultraviolet and Total Ozone Mapping Spectrometer (SBUV/TOMS) for Nimbus G, *Opt. Eng.*, *14*, 323-331, 1975.

Herman, J.R., P.K. Bhartia, A.J. Krueger, R.D. McPeters, C.G. Wellemeyer, C.J. Seftor, G. Jaross, B. Schlesinger, O. Torres, G. Labow, W. Byerly, S.L. Taylor, T. Swissler, R.P. Cebula, and X. Gu, *Meteor 3 Total Ozone Mapping Spectrometer (TOMS) Data Protocol User's Guide*, NASA Ref. Publ. 1393, 1996.

Hilsenrath, E., D.E. Williams, R.T. Caffrey, R.P. Cebula, and S.J. Hynes, Calibration and radiometric stability of the Shuttle Solar Backscatter Ultraviolet (SSBUV) experiment, *Metrologia*, *30*, 243-248, 1993.

Hofmann, D.J., and T. Deshler, Evidence from balloon measurements for chemical depletion of stratospheric ozone in the Arctic winter of 1989-90, *Nature*, *349*, 300-305, 1991.

Hofmann, D.J., and S. Solomon, Ozone destruction through heterogeneous chemistry following the eruption of El Chichón, *J. Geophys. Res.*, *94*, 5029-5041, 1989.

Hofmann, D.J., S.J. Oltmans, J.M. Harris, B.J. Johnson, and J.A. Lathrop, Ten years of ozonesonde measurements at the South Pole: Implications for recovery of spring time Antarctic ozone, *J. Geophys. Res.*, *102*, 8931-8943, 1997.

Hollandsworth, S.M., K.P. Bowman, and R.D. McPeters, Observational study of the quasi-biennial oscillation in ozone, *J. Geophys. Res.*, *100*, 7347-7361, 1995a.

Hollandsworth, S.M., R.D. McPeters, L.E. Flynn, W. Planet, A.J. Miller, and C. Chandra, Ozone trends deduced from combined Nimbus 7 SBUV and NOAA 11 SBUV/2 data, *Geophys. Res. Lett.*, *22*, 905-908, 1995b.

Hood, L.L., The solar cycle variation of total ozone: Dynamical forcing in the lower stratosphere, *J. Geophys. Res.*, *102*, 1355-1369, 1997.

Hood, L.L., and D.A. Zaff, Lower stratospheric stationary waves and the longitude dependence of ozone trends in winter, *J. Geophys. Res.*, *100*, 25791-25800, 1995.

Hood, L.L., J.P. McCormack, and K. Labitzke, An investigation of dynamical contributions to midlatitude ozone trends in winter, *J. Geophys. Res.*, *102*, 13079-13093, 1997.

Jackman, C.H., E.L. Fleming, S. Chandra, D.B. Considine, and J.E. Rosenfield, Past, present, and future modelled ozone trends with comparisons to observed trends, *J. Geophys. Res.*, *101*, 28753-28767, 1996.

Jones, A.E., and J.D. Shanklin, Continued decline of total ozone over Halley, Antarctica, since 1985, *Nature*, *376*, 409-411, 1995.

Kayano, M.T., Principal modes of the total ozone on the Southern Oscillation timescale and related temperature variations, *J. Geophys. Res.*, *102*, 25797-25806, 1997.

Kerr, J.B., I.A. Asbridge, and W.F.J. Evans, Intercomparison of total ozone measured by the Brewer and Dobson spectrophotometers at Toronto, *J. Geophys. Res.*, *93*, 11129-11140, 1988.

Kerr, J.B., C.T. McElroy, and D.W. Wardle, The Brewer instrument calibration centre 1984-1996, in *Atmospheric Ozone: Proceedings of the XVIII Quadrennial Ozone Symposium*, L'Aquila, Italy, 12-21 September 1996, edited by R.D. Bojkov and G. Visconti, pp. 915-918, Parco Scientifico e Technologico d'Abruzzo, L'Aquila, Italy, 1998.

Knudsen, B.M., N. Larsen, I.S. Mikkelsen, J.-J. Morcrette, G.O. Braathen, E. Kyrö, H. Fast, H. Gernandt, H. Kanzawa, H. Nakane, V. Dorokhov, V. Yushkov, G. Hansen, M. Gil, and R.J. Shearman, Ozone depletion in and below the Arctic vortex for 1997, *Geophys. Res. Lett.*, *25*, 627-630, 1998.

Köhler, U., and H. Claude, Homogenized ozone record at Hohenpeissenberg, in *Atmospheric Ozone: Proceedings of the XVIII Quadrennial Ozone Symposium*, L'Aquila, Italy, 12-21 September 1996, edited by R.D. Bojkov and G. Visconti, pp. 57-60, Parco Scientifico e Technologico d'Abruzzo, L'Aquila, Italy, 1998.

Koike, M., Y. Kondo, M. Hayashi, Y. Iwasake, P.A. Newman, M. Helten, and P. Aimedieu, Depletion of Arctic ozone in the winter 1990, *Geophys. Res. Lett.*, *18*, 791-794, 1991.

Staehelin, J., A. Renaud, J. Bader, R. McPeters, P. Viatte, B. Hoeffer, V. Bugnion, M. Giroud, and H. Schill, Total ozone series at Arosa (Switzerland): Homogenization and data comparison, *J. Geophys. Res.*, *103*, 5827-5841, 1998a.

Staehelin, J., R. Kegel, and N.R.P. Harris, Trend analysis of the homogenized ozone series of Arosa (Switzerland), 1926-1996, *J. Geophys. Res.*, *103*, 8389-8399, 1998b.

Stolarski, R., R.D. Bojkov, L. Bishop, C. Zerefos, J. Staehelin, and J. Zawodny, Measured trends in stratospheric ozone, *Science*, *256*, 343-349, 1992.

Stolarski, R.S., G.J. Labow, and R.D. McPeters, Springtime Antarctic total ozone measurements in the early 1970's from the BUV instrument on Nimbus 4, *Geophys. Res. Lett.*, *24*, 591-594, 1997.

Trepte, C.R., and M.H. Hitchman, Tropical stratospheric circulation deduced from satellite aerosol data, *Nature*, *355*, 626-628, 1992.

Tsvetkova, N.D., V.A. Yushkov, V.M. Dorokhov, and I.G. Zaitsev, Some results of measurements of vertical ozone distribution over Yakutsk during the 1995-96 winter/spring season, *Meteorol. Gidrol.*, *9*, 45-51, 1997.

Uchino, O., R.D. Bojkov, D.S. Balis, K. Akagi, M. Hayashi, and R. Kajiwara, Essential characteristics of the Antarctic ozone decline, *Geophys. Res. Lett.*, submitted, 1998.

von der Gathen, P., M. Rex, N.R.P. Harris, D. Lucic, G.M. Knudsen, G.O. Braathen, H. De Backer, R. Fabian, H. Fast, M. Gil, E. Kyrö, I.S. Mikkelsen, M. Rummukainen, J. Stähelin, and C. Varotsos, Observational evidence for chemical ozone depletion over the Arctic in winter 1991-92, *Nature*, *375*, 131-134, 1995.

Wallace, J.M., and D.S. Gutzler, Teleconnections in the geopotential height field during the north hemisphere winter, *Mon. Wea. Rev.*, *109*, 784-812, 1981.

Wang, H.J., D.M. Cunnold, and X. Bao, A critical analysis of SAGE ozone trends, *J. Geophys. Res.*, *101*, 12495-12514, 1996.

Wege, K., and H. Claude, Über Zusammenhänge zwischen stratosphärischem Ozon und meteorologischen Parametern mit Folgerungen für die Zeiträume nach den Ausbrüchen von Chichón und Pinatubo, *Meteorol. Z.*, *6*, 73-87, 1997.

WMO (World Meteorological Organization), *Report of the Meeting of Experts on Assessment of Performance Characteristics of Various Ozone Observing Systems*, Boulder, Colo., U.S., 28 July-2 August, 1980, Global Ozone Research and Monitoring Project—Report No. 9, Geneva, 1980.

WMO (World Meteorological Organization), *Report of the International Ozone Trends Panel: 1988*, Global Ozone Research and Monitoring Project—Report No. 18, Geneva, 1990a.

WMO (World Meteorological Organization), *Scientific Assessment of Stratospheric Ozone: 1989*, Global Ozone Research and Monitoring Project—Report No. 20, Geneva, 1990b.

WMO (World Meteorological Organization), *Scientific Assessment of Ozone Depletion: 1991*, Global Ozone Research and Monitoring Project—Report No. 25, Geneva, 1992.

WMO (World Meteorological Organization), *Handbook for Ozone Data Reevaluation*, Global Ozone Research and Monitoring Project—Report No. 29, Geneva, 1993.

WMO (World Meteorological Organization), *Scientific Assessment of Ozone Depletion: 1994*, Global Ozone Research and Monitoring Project—Report No. 37, Geneva, 1995.

WMO (World Meteorological Organization), *Atlas of GO3OS Total Ozone Maps for the Northern Hemisphere Winter-Spring of 1993-1994 and 1994-1995*, Global Ozone Research and Monitoring Project—Report No. 38, edited by R.D. Bojkov, and C.S. Zerefos, Geneva, 1996.

WMO (World Meteorological Organization), *Atlas of GO3OS Total Ozone Maps for the Northern Hemisphere Winter-Spring of 1995-1996, 1996-1997*, Global Ozone Research and Monitoring Project—Report No. 39, edited by R.D. Bojkov and C.S. Zerefos, Geneva, 1997.

WMO (World Meteorological Organization), *SPARC/IOC/GAW Assessment of Trends in the Vertical Distribution of Ozone*, edited by N. Harris, R. Hudson, and C. Phillips, SPARC Report No. 1, World Meteorological Organization Global Ozone Research and Monitoring Project—Report No. 43, Geneva, 1998.

Yang, H., and K.K. Tung, On the phase propagation of extratropical ozone quasi-biennial oscillation in observational data, *J. Geophys. Res.*, *100*, 9091-9100, 1995.

Yushkov, V., V. Dorokhov, V. Khattatov, A. Lukyanov, I. Zaitcev, N. Zvetkova, H. Nakane, H. Akiyoshi, and T. Ogawa, Evidence of ozone depletion over Yakutsk, Eastern Siberia, in 1995, in *Atmospheric Ozone: Proceedings of the XVIII Quadrennial Ozone Symposium*, L'Aquila, Italy, 12-21 September 1996, edited by R.D. Bojkov and G. Visconti, pp. 241-244, Parco Scientifico e Technologico d'Abruzzo, L'Aquila, Italy, 1998.

Zerefos, C.S., A.F. Bais, T.C. Ziomas, and R.D. Bojkov, On the relative importance of quasi-biennial oscillation and El Niño/Southern Oscillation in the revised Dobson total ozone records, *J. Geophys. Res.*, *97*, 10135-10144, 1992.

Zerefos, C.S., K. Tourpali, and A.F. Bais, Further studies on possible volcanic signal to the ozone layer, *J. Geophys. Res.*, *99*, 25741-25746, 1994.

Zerefos, C.S., K. Tourpali, and A.F. Bais, Recent volcanic signals in the ozone layer, in *The Mount Pinatubo Eruption: Effect on the Atmosphere and Climate*, NATO ASI Series I, Vol. 142, edited by G. Fiocco, D. Fua, and G. Visconti, pp. 211-216, Springer-Verlag, Berlin, 1996.

Zerefos, C.S., K. Tourpali, B.R. Bojkov, D.S. Balis, B. Rognerud, and I.S.A. Isaksen, Solar activity-total column ozone relationships: Observations and model studies with heterogeneous chemistry, *J. Geophys. Res.*, *102*, 1561-1569, 1997.

Zerefos, C.S., K. Tourpali, I.S.A. Isaksen, B. Rognerud, B.R. Bojkov, and C.J.E. Schuurmans, The solar output and total ozone, in *Atmospheric Ozone: Proceedings of the XVIII Quadrennial Ozone Symposium*, L'Aquila, Italy, 12-21 September 1996, edited by R.D. Bojkov and G. Visconti, pp. 279-282, Parco Scientifico e Technologico d'Abruzzo, L'Aquila, Italy, 1998.

Ziemke, J.R., S. Chandra, R.D. McPeters, and P.A. Newman, Dynamical proxies of column ozone with applications to global trend models, *J. Geophys. Res.*, *102*, 6117-6129, 1997.

# CHAPTER 5

## TRENDS IN STRATOSPHERIC TEMPERATURES

### Contents

## Model Results and Model-Observation Comparisons

- Model simulations based on the known changes in the stratospheric concentrations of various radiatively active species indicate that the depletion of lower stratospheric ozone is the dominant factor in the explanation of the observed global-mean lower stratospheric cooling trend (~0.5-0.6 K/decade) for the period 1979-1990. The contribution to this trend from increases in well-mixed greenhouse gases is estimated to be less than one-fourth that due to ozone loss.

- Model simulations indicate that ozone depletion is an important causal factor in the latitude-month pattern of the decadal (1979-1990) lower stratospheric cooling. The simulated lower stratosphere in Northern and Southern Hemisphere midlatitudes, and in the Antarctic springtime, generally exhibits a statistically significant cooling trend over this period, consistent with observations.

- The Fixed Dynamical Heating (FDH; equivalently, the pure radiative response) calculations yield a mid- to high-latitude annual-mean cooling that is approximately consistent with a GCM's radiative-dynamical response (Figure 5B); however, changes in circulation simulated by the GCM cause an additional cooling in the tropics, besides affecting the meridional pattern of the temperature decrease.

- FDH model results indicate that both well-mixed greenhouse gases and ozone changes are important contributors to the cooling in the middle and upper stratosphere; however, the computed upper stratospheric cooling is smaller than the observed decadal trend. Increased water vapor in the lower to upper stratosphere domain could also be an important contributor to the cooling; however, decadal-scale global stratospheric water vapor trends have not yet been determined.

- Model simulations of the response to the observed global lower stratospheric ozone loss in mid to high latitudes suggest a radiative-dynamical feedback leading to a warming of the middle and upper stratospheric regions, especially during springtime; however, while the modeled warming is large and can be statistically significant during the Antarctic spring, it is not statistically significant during the Arctic spring. Antarctic radiosonde observations indicate a statistically significant warming trend in spring at ~30 hPa (24 km) and extending possibly to even higher altitudes; this region lies above a domain of strong cooling that is approximately collocated with the altitude of the observed ozone depletion.

- There is little evidence to suggest that tropospheric climate changes (e.g., induced by greenhouse gas increases in the troposphere) and sea surface temperature variations have been dominant factors in the global-mean stratospheric temperature trend over the 1979-1994 period. The effect of potential shifts in atmospheric circulation patterns upon the decadal trends in global stratospheric temperatures remains to be determined.

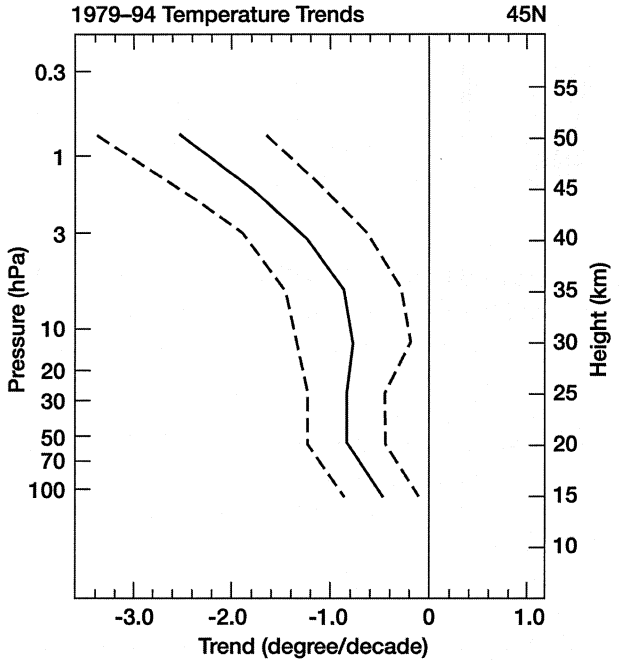


**Figure 5A.** Summary figure illustrating the overall mean vertical profile of temperature trend (K/decade) over the 1979-1994 period in the stratosphere at 45°N, as compiled using radiosonde, satellite, and analyzed datasets (Section 5.2.3.3). The vertical profile of the averaged trend estimate was computed as a weighted mean of the individual system trends shown in Figure 5-9, with the weighting being inversely proportional to the individual uncertainty. The solid line indicates the weighted trend estimate while the dashed lines denote the uncertainty at the 2-sigma level (note: Table 5-6 lists the numerical values of the trends and the uncertainty at the one-sigma level). (Figure assembled for this chapter in cooperation with the SPARC-Stratospheric Temperature Trends Assessment project.)

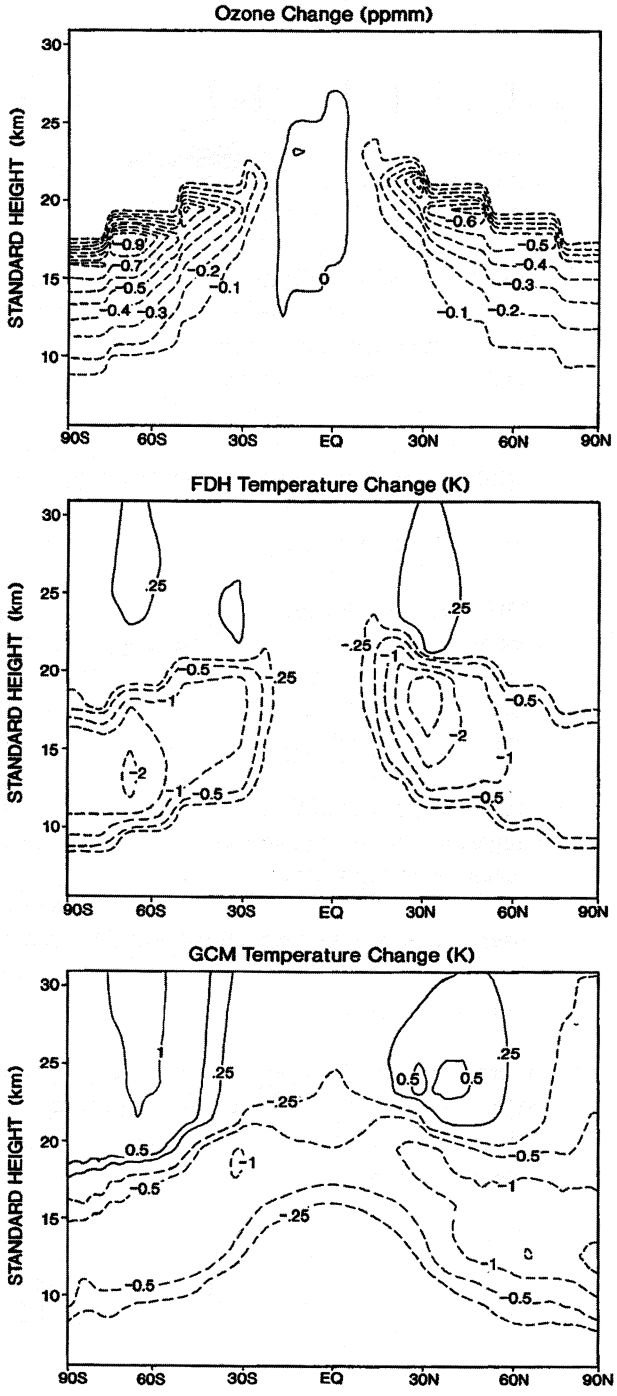


**Figure 5B.** Top panel: Idealized, annual-mean stratospheric ozone loss profile, based on Total Ozone Mapping Spectrometer (TOMS) and Stratospheric Aerosol and Gas Experiment (SAGE) satellite-observed ozone trends. Middle panel: Corresponding temperature change, as obtained using a Fixed Dynamical Heating (FDH) model, which illustrates the pure radiative response, and (bottom panel) a general circulation model (GCM), which illustrates the radiative-dynamical response (Section 5.3.3.1). (Adapted from Ramaswamy *et al.*, 1992, 1996).

## 5.1 INTRODUCTION

For at least a decade now, the investigation of trends in stratospheric temperatures has been recognized by the World Meteorological Organization (WMO) to be an integral part of the ozone trends report. A comprehensive international scientific assessment of stratospheric temperature changes was undertaken in WMO (1990a). Analyses of the then-available datasets (rocketsonde, radiosonde, and satellite records) over the period 1979/80 to 1985/86 indicated that the observed temperature trend was inconsistent with the then-apparent ozone losses inferred from Solar Backscatter Ultraviolet (SBUV) spectrometer data, but consistent with Stratospheric Aerosol and Gas Experiment (SAGE) ozone changes. The largest cooling in the observed datasets was in the upper stratosphere, while the lower stratosphere had experienced no significant cooling except in the tropics and Antarctica. It is interesting to note that the period analyzed by WMO (1990a) was one when severe ozone losses were just beginning to be recognized in the Antarctic springtime lower stratosphere. It was also a period from sunspot maximum to sunspot minimum. Standard interactive photochemical-radiation models then available that incorporated trace-gas changes (including ozone) were found to yield a cooling in the upper/middle stratosphere that was broadly consistent with the available observations but under-predicted the observed cooling in the lower stratosphere. A warming due to the El Chichón volcanic eruption (1982-1983) was also reported, with simple models using imposed aerosol inputs reproducing the observed transient warming.

Since the time of the 1988 WMO Assessment (WMO, 1990a), there has been an ever-growing impetus for observational and model investigations of stratospheric temperature trends (WMO, 1990b, 1992, 1995). This has occurred owing to the secular increases in greenhouse gases and the now well-documented global and seasonal losses of stratospheric ozone, both of which have a substantial impact on the stratospheric radiative-dynamical equilibrium. The availability of various temperature observations and the ever-increasing length of the data record have also been encouraging factors. In addition, models have progressively acquired the capability to perform more realistic simulations of the stratosphere. This has provided a motivation for comparing model results with observations, and thereby the search for causal explanation(s) of the observed trends. The developments seen in modeling underscore the significance of the interactions between radiation, dynamics, and chemistry in the interpretation of linkages between changes in trace species and temperature trends. Temperature changes are also instrumental in the microphysical-chemical processes of importance in the stratosphere (see Chapter 7).

The assessment of stratospheric temperature trends is now regarded as a high priority in climate change research inasmuch as it has been shown to be a key entity in the detection and attribution of the observed vertical profile of temperature changes in the Earth's atmosphere (Hansen *et al.*, 1995; Santer *et al.*, 1996; Tett *et al.*, 1996). Indeed, the subject of trends in stratospheric temperatures is of crucial importance to the Intergovernmental Panel on Climate Change assessment (IPCC, 1996) and constitutes a significant scientific input into policy decisions.

We summarize here the principal results concerning stratospheric temperature trends from the previous WMO ozone assessments. In general, the successive assessments since the WMO (1986) and WMO (1990a) reports have traced the evolution of the state of the science on both the observation and model simulation fronts. On the observational side, WMO has reported on available temperature trends from various kinds of instruments: radiosonde, rocketsonde, satellite, and lidar. On the modeling side, since the 1986 report, WMO has reported on model investigations that illustrate the role of greenhouse gases and aerosols in the thermal structure of the stratosphere, and the effects due to changes in their concentrations upon stratospheric temperature trends. The 1989 Assessment (WMO, 1990b) began to recognize, from observational and modeling standpoints, the substantial lower stratospheric cooling occurring during springtime in the Antarctic as a consequence of the large ozone depletion. The low- and middle-latitude lower stratosphere were inferred to have a cooling of less than 0.4 K/decade over the prior 20 years. The upper stratosphere was estimated to have cooled by $1.5 \pm 1$ K between 1979/80 and 1985/86.

The 1991 Assessment (WMO, 1992) reported that, based on radiosonde analyses, a global-mean lower stratospheric cooling of ~0.3 K had occurred over the previous 2-3 decades. Model calculations indicated that the observed ozone losses had the potential to yield substantial cooling of the global lower stratosphere. At

44°N during summer, an observed cooling of the upper stratosphere (~1 K/decade at ~35 km) and mesosphere (~4 K/decade) was also reported. However, in general, for assessment purposes, the global stratospheric temperature record and understanding of temperature changes were found to be not as sound as those related to ozone changes.

The 1994 Assessment (WMO, 1995) discussed the observational and modeling efforts through 1994, focusing entirely on trends in lower stratospheric temperatures. That Assessment concluded, based on radiosonde and satellite microwave observations, that there were short-term variations superposed on the long-term trends. A contributing factor to the former was stratospheric aerosol increases following the El Chichón and Mt. Pinatubo volcanic eruptions, which resulted in an increase of the global stratospheric temperature. These transient warmings posed a complication when analyzing the long-term trends and inferring their causes. The long-term trends from the radiosonde and satellite data indicated a cooling of 0.25 to 0.4 K/decade since the late 1970s, with suggestions of an acceleration of the cooling during the 1980s. The global cooling of the lower stratosphere suggested by the observations was reproduced reasonably well by models considering the observed decreases of ozone in the lower stratosphere. For altitudes above the lower stratosphere, a clear conclusion concerning trends could not be made. The 1991 and 1994 Assessments (WMO, 1992, 1995) laid the basis for the conclusion that the observed trends in the lower stratosphere during the 1980s were largely attributable to halocarbon-induced ozone losses.

This 1998 Assessment extends the evaluations of the earlier ones by focusing on the decadal-scale lower to upper stratospheric temperature trends arising out of observational (Section 5.2) and model simulation (Section 5.3) analyses. The temperature observations considered span at least 10 years; the period considered for evaluation is typically at least 15 years. The trend estimates discussed here include (i) a long-term period that spans two decades or more, (ii) the period since 1979 and extending to either 1994 or the present (i.e., up to 1998), and (iii) the period extending from 1979 to about the early 1990s. The last-mentioned period is that for which several model simulations have been compared with observations. In Section 5.4, we use the results from Sections 5.2 and 5.3 to investigate the extent to which the observed temperature trends can be attributed to changes in the concentrations of radiatively active species.

## 5.2 OBSERVATIONS

### 5.2.1 Data

The types of observational data available for investigation into stratospheric temperature trends are diverse. They differ in type of measurement, length of time period, and space-time sampling. There have been several investigations of trends that have considered varying time spans with the different available datasets, as will be discussed shortly. In recent years, the World Climate Research Programme's SPARC-STTA (Stratospheric Processes and their Role in Climate-Stratospheric Temperature Trends Assessment) group has initiated a project to bring together various datasets covering the period 1966-1994 and to intercompare the resulting global stratospheric temperature trends. The authors and contributors of this current WMO/UNEP 1998 Assessment chapter largely constitute the working group of the SPARC-STTA. The data and trends obtained by this group are used in some of the intercomparisons reported here. The chapter prepared for the current WMO/UNEP Assessment will serve as an input to the ongoing SPARC investigation of stratospheric temperature trends.

SPARC-STTA chose two different time periods to examine the trends, based on the availability of the data, viz., 1979-1994 and 1966-1994. The former period coincides with the period when severe global ozone losses have been detected and also coincides with the period of global satellite observations. The second period is a longer one for which radiosonde (and a few rocketsonde) datasets are available.

The updated datasets made available to and employed by the SPARC-STTA for the analyses are shown (with the exception of rocketsonde datasets) in Table 5-1 along with their respective latitudes, altitudes, and periods of coverage. Additionally, independent of the STTA activity, some investigations (Dunkerton *et al.*, 1998; Keckhut *et al.*, 1998; Komuro, 1989; Golitsyn *et al.*, 1996; Kokin and Lysenko, 1994; Lysenko *et al.*, 1997) have analyzed trends from rocketsonde observations made at a few geographical locations and over specific time periods (see Table 5-2). We utilize these datasets in some of the presentations to follow. It is convenient to group the currently known datasets in the following manner:

- *Ground-based instruments*: radiosonde, rocketsonde, and lidar

**Table 5-1. Zonal temperature time series made available to and considered by SPARC-STTA.** For the MSU and Nash satellite data, the approximate peak levels "sensed" are listed. References to earlier versions of the datasets are also listed. See Section 5.2.1 for details.

| Dataset | Period | Latitude Coverage | Averaging | Levels (hPa) |
|---|---|---|---|---|
| | | **Radiosonde Datasets** | | |
| Angell | 1958-1994 | 8 bands | 3-monthly | 100-50 |
| (Angell, 1988) | | 4 bands | 3-monthly | 50, 30, 20, 10 |
| Oort | 1958-1989 | 85°S-85°N | monthly | 100, 50 |
| (Oort and Liu, 1993) | | | | |
| Russia | 1959-1994 | 70°N, 80°N | monthly | 100 |
| (Koshelkov and Zakharov, 1998) | 1961-1994 | 70°N, 80°N | monthly | 50 |
| UK RAOB (or RAOB) | 1961-1994 | 87.5°S-87.5°N | monthly | 100, 50, 30, 20 |
| (Parker and Cox, 1995) | | | | |
| Berlin | 1965-1994 | 10-90°N | monthly | 100, 50, 30 |
| (Labitzke and van Loon, 1994) | | | | |
| | | **Lidar Dataset** | | |
| Lidar | 1979-1994 | 44°N, 6°E | monthly | 10, 5, 2, 1, 0.4 |
| (Hauchecorne *et al.*, 1991) | | (Haute Provence) | | |
| | | **Satellite Datasets** | | |
| MSU | 1979-1994 | 85°S-85°N | monthly | 90 |
| (Spencer and Christy, 1993) | | | | |
| Nash | 1979-1994 | 75°S-75°N | monthly | 50, 20, 15, 6, 5, 2, 1.5, 0.5 |
| (Nash and Forrester, 1986) | | | | |
| | | **Analyzed Datasets** | | |
| CPC | 1979-1994 | 85°S-85°N | monthly | 70, 50, 30, 10, 5, 2, 1 |
| (Gelman *et al.*, 1994) | 1964-1978 | 20°N-85°N | monthly | 50, 30, 10 |
| Reanal | 1979-1994 | 85°S-85°N | monthly | 100, 70, 50, 30, 10 |
| (Kalnay *et al.*, 1996) | | | | |
| GSFC | 1979-1994 | 90°S-90°N | monthly | 100, 70, 50, 30, 20 |
| (Schubert *et al.*, 1993) | | | | |
| UKMO/SSUANAL | 1979-1994 | 90°S-90°N | monthly | 50, 20, 10, 5, 2, 1 |
| (Bailey *et al.*, 1993) | | | | |

- *Satellite instruments*: microwave and infrared sounders

- *Analyses*: employing data from one or both of the above instrument types, without/with a numerical model

The datasets indicated in Table 5-1 are a collection of monthly-mean, zonal-mean temperature time series. All but one of these datasets cover the years 1979-1994, and some extend farther back in time. The pressure-altitude levels of the datasets vary, but overall they cover the range 100 to 0.4 hPa (approximately 16-55 km). Most datasets provide temperatures at specific pressure levels, but some provide data as mean temperatures representative of various pressure layers. The instrumental records from radiosondes, rocketsondes, lidar, and satellite (Microwave Sounding Unit (MSU) and Stratospheric Sounding Unit (SSU)) are virtually independent of each other. General characteristics of the different datasets are discussed below (see also WMO, 1990a,b).

#### 5.2.1.1 Radiosonde Datasets

Radiosonde data are available dating back to approximately the early 1940s. Although the sonde data do not cover the entire globe, there have been several well-documented efforts to use varied techniques in order to obtain the temperatures over the entire Northern Hemisphere or the global domains. The sonde data cover primarily the lower stratospheric region (approximately, pressures greater than 10 hPa). The geographical coverage is quite reasonable in the Northern Hemisphere (particularly midlatitudes) but is poor in the extremely high latitudes and tropics, and is seriously deficient in the Southern Hemisphere (Oort and Liu, 1993).

As was the case at the time of the 1988 Assessment, two organizations monitor trends and variations in lower stratospheric temperatures using radiosonde data alone. The "Berlin" group (e.g., Labitzke and van Loon, 1995) prepares daily hand-drawn stratospheric maps based on synoptic analyses of radiosonde data at 100, 50, 30, and, in some months, 10 hPa, beginning from 1964. The Berlin monthly dataset examined by SPARC-STTA is derived from these daily analyses. The National Oceanic and Atmospheric Administration (NOAA) Air Resources Laboratory (e.g., Angell, 1988) uses daily radiosonde soundings to calculate seasonal layer-mean "virtual temperature" anomalies from long-term means, and uses these to determine trends since 1958 in the 850-300, 300-100, and 100-50 hPa layers (lower stratosphere). (Virtual temperature is the temperature of dry air having the same pressure and density as the actual moist air. Virtual temperature always exceeds temperature, but the difference is negligible in the stratosphere (Elliott *et al.*, 1994).) The layer-mean virtual temperatures are determined from the geopotential heights of the layer endpoints. The Berlin analyses are of the Northern Hemisphere stratosphere and troposphere and are based on all available radiosonde data, whereas the Air Resources Laboratory monitors trends at 63 stations in eight zonal bands covering the globe. Additionally, Angell (1991b) also monitors stratospheric temperature, particularly its response to volcanic eruptions, at four levels between 20 km (50 hPa) and 31 km (10 hPa) using a network of 12 stations ranging from 8°S to 55°N. The "Angell" data used here represent a subset.

Extensive analyses of radiosonde temperature data by the NOAA Geophysical Fluid Dynamics Laboratory (GFDL) (Oort and Liu, 1993) and the U.K. Meteorological Office's (UKMO) Hadley Centre for Climate Prediction and Research (Parker *et al.*, 1997) have also been used for quantifying stratospheric trends. The GFDL database consists of gridded global objective analyses based on monthly means derived from daily soundings for the period 1958-1989 for the tropospheric levels and the 100-, 70-, 50-, and 30-hPa levels in the lower stratosphere. Layer-mean trends for the 100-50 hPa layer are based on temperature data at the 100-, 70-, and 50-hPa levels. A subset of this dataset, labeled "Oort," is used here. The UKMO gridded dataset (RAwinsonde OBservations, denoted as "RAOB" or "UK RAOB") for 1958-1996 is based on monthly mean (CLIMAT TEMP) station reports, adjusted (using MSU Channel 4 data, discussed below, as a reference) to remove some time-varying biases since 1979 for stations in Australia and New Zealand, and interpolated in some data-void regions. The "Russia" set consists of data from the high northern latitudes (70 and 80°N; Koshelkov and Zakharov, 1998). Thus, the Angell, Berlin, Oort, Russia, and RAOB datasets used by SPARC-STTA are compilations of data from various radiosonde stations, grouped, interpolated, and/or averaged in various ways to obtain monthly-mean and latitude-mean, pressure-level or vertical-average temperatures.

**Table 5-2. Rocketsonde locations and periods of coverage utilized for the present Assessment.** (Based on Dunkerton *et al.*, 1998; Golitsyn *et al.*, 1996; Keckhut *et al.*, 1998; Kokin and Lysenko, 1994; Lysenko *et al.*, 1997; and Komuro, 1989 (updated).)

| Station | Latitude, Longitude (degrees) | Period |
|---|---|---|
| Heiss Island | 81N, 58E | 1964-1994 |
| Volgograd | 49N, 44E | 1965-1994 |
| Balkhash | 47N, 75E | 1973-1992 |
| Ryori | 39N, 141.5E | 1970-present |
| Wallops Island | 37.5N, 76W | 1965-1990 |
| Point Mugu | 34N, 119W | 1965-1991 |
| Cape Kennedy | 28N, 80W | 1965-1993 |
| Barking Sands | 22N, 160W | 1969-1991 |
| Antigua | 17N, 61W | 1969-1991 |
| Thumba | 08N, 77E | 1971-1993 |
| Kwajalein | 09N, 167E | 1969-1990 |
| Ascension Island | 08S, 14W | 1965-1993 |
| Molodezhnaya | 68S, 46E | 1969-1994 |

#### 5.2.1.2 Rocketsonde and Lidar Datasets

Rocketsonde and lidar data cover the altitude range from about the middle stratosphere into the upper stratosphere and mesosphere. Rocketsonde data are available through the early 1990s from some locations, but the activity appears to be virtually terminated except in Japan (see Table 5-2). The lidar measurement, just like the rocketsonde measurement, has a fine vertical resolution. Lidar measurements of stratospheric temperatures are available since 1979 from the Haute Provence Observatory (OHP) in southern France (44°N, 6°E). Specifically, the "lidar" (Table 5-1) temperatures observed at altitudes of 30 to 90 km are obtained from two lidar stations, with data interpolated to pressure levels (Keckhut *et al.*, 1995). Several other lidar sites have initiated operations and could potentially contribute in future temperature trends assessments.

#### 5.2.1.3 MSU and SSU Satellite Datasets

Satellite instruments of interest have become available since ~1979 (Table 5-1). These fall into two categories: those that remotely sense in the microwave wavelengths (Spencer and Christy, 1993) and those that remotely sense in the thermal infrared wavelengths (Nash and Forrester, 1986). The "MSU" Channel 4 dataset derives from the lower stratosphere channel (~150-50 hPa) of the Microwave Sounding Unit on NOAA polar-orbiting operational satellites (Figure 5-1, left panel). The "Nash" dataset consists of brightness temperatures from observed (25, 26, and 27) and derived (47X, 36X, 35X, 26X, and 15X) channels of the Stratospheric Sounding Unit (SSU) instrument on these same satellites (Figure 5-1). The SSU data used in this report are extensions (J. Nash, UKMO, UK, personal communication, 1997) of earlier works (e.g., Nash and Forrester, 1986) and have been provided to SPARC and WMO for temperature trends assessment purposes. One complication with satellite data is the fact that there are discontinuities in the time series owing to the measurements being made by different satellites monitoring the stratosphere since 1979. Adjustments have been made in the Nash channel data provided to compensate for radiometric differences, tidal differences between spacecraft, long-term drift in the local time of measurements, and spectroscopic drift in Channels 26 and 27. Adjustments have also been made to MSU data (e.g., Christy *et al.*, 1995).

An important attribute of the satellite instruments is their global coverage. However, in contrast to the ground-based instruments, e.g., radiosondes, which perform measurements at specific pressure levels, the available satellite sensors have response functions that sense the signal from a wide range in altitude. The nadir

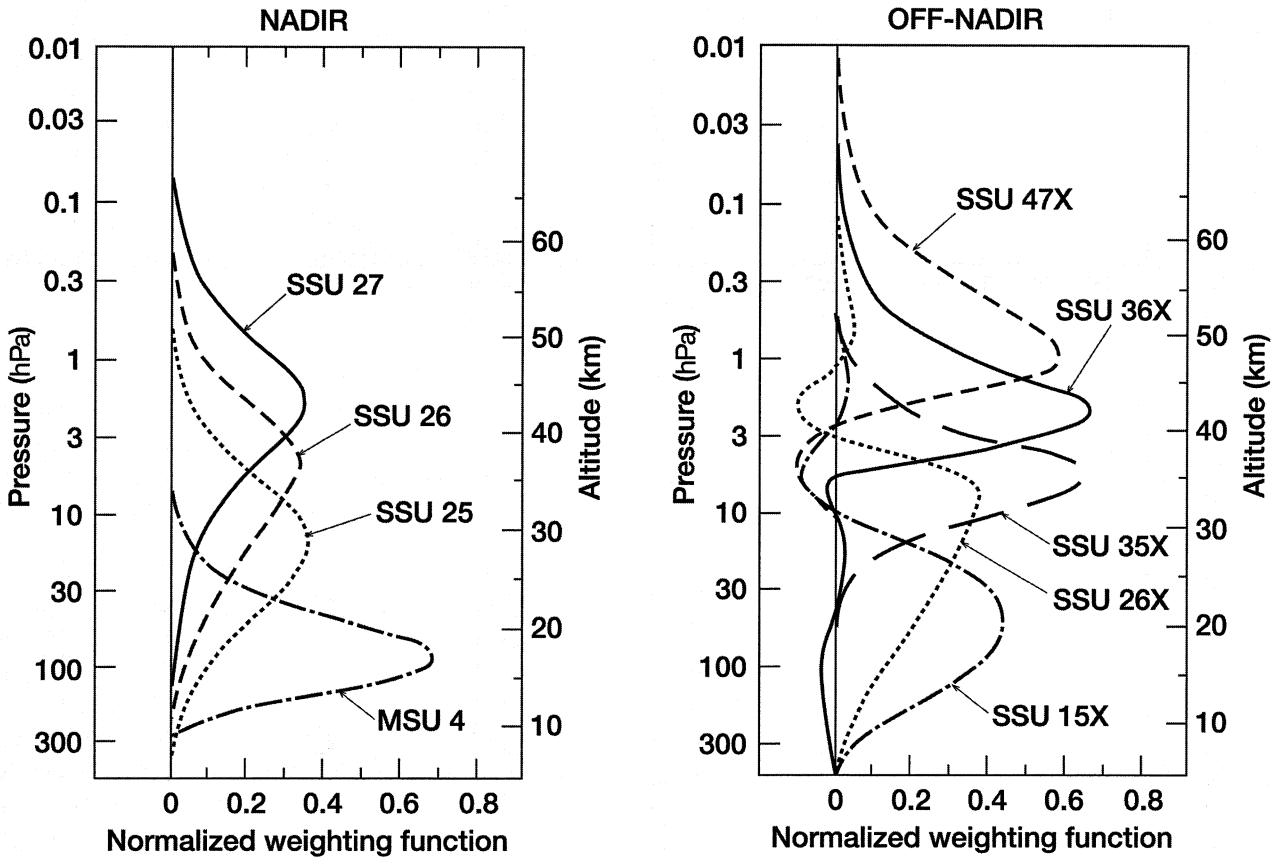


**Figure 5-1.** Altitude range of the signals "sensed" by the various thermal infrared channels of the Stratospheric Sounding Unit instrument (SSU) and by Channel 4 of the Microwave Sounding Unit (MSU). Nadir (left panel) and off-nadir (right panel) channel weighting functions.

satellite instruments "sense" the emission originating from a layer of the atmosphere approximately 10-15 km thick. Figure 5-1 illustrates the weighting function for the MSU and SSU channels analyzed here, exhibiting the thick-layer nature of the measurements. For example, the emission for microwave MSU Channel 4 comes from the ~12-22 km layer, while, for the thermal infrared SSU Channel 15X, it is from the ~12-28 km layer. In Table 5-1, a nominal center pressure of each satellite channel has been designated, but it is emphasized that the preponderance of energy comes from a vertical layer, ~8-12 km thick, centered around the concerned pressure level, as indicated in Figure 5-1. A perspective into the global-mean anomalies of temperature at various stratospheric altitudes between 1979 and 1995 (deviations with respect to the mean over this period), as derived from different SSU channels, can be obtained from Figure 5-2. The MSU record was discussed in WMO (1995).

#### 5.2.1.4 Analyzed Datasets

A number of datasets involve some kind of analyses of the observations. They employ one or more types of observed data, together with the use of some mathematical technique and/or a general circulation assimilation model, to construct the global time series of the temperatures. They are, in essence, more of a derived dataset than the satellite- or the ground-based ones. The "CPC" analyses (from the Climate Prediction Center, formerly Climate Analysis Center) and "UKMO/SSUANAL" stratospheric analyses (Table 5-1) do not involve any numerical atmospheric circulation model. The CPC Northern Hemisphere 70-, 50-, 30- and 10-hPa analyses use radiosonde data. Both the CPC and UKMO/SSUANAL analyses (see also Swinbank and O'Neill, 1994) use Television and InfraRed Observational Satellite (TIROS) Operational Vertical Sounder (TOVS) temperatures, which incorporate data

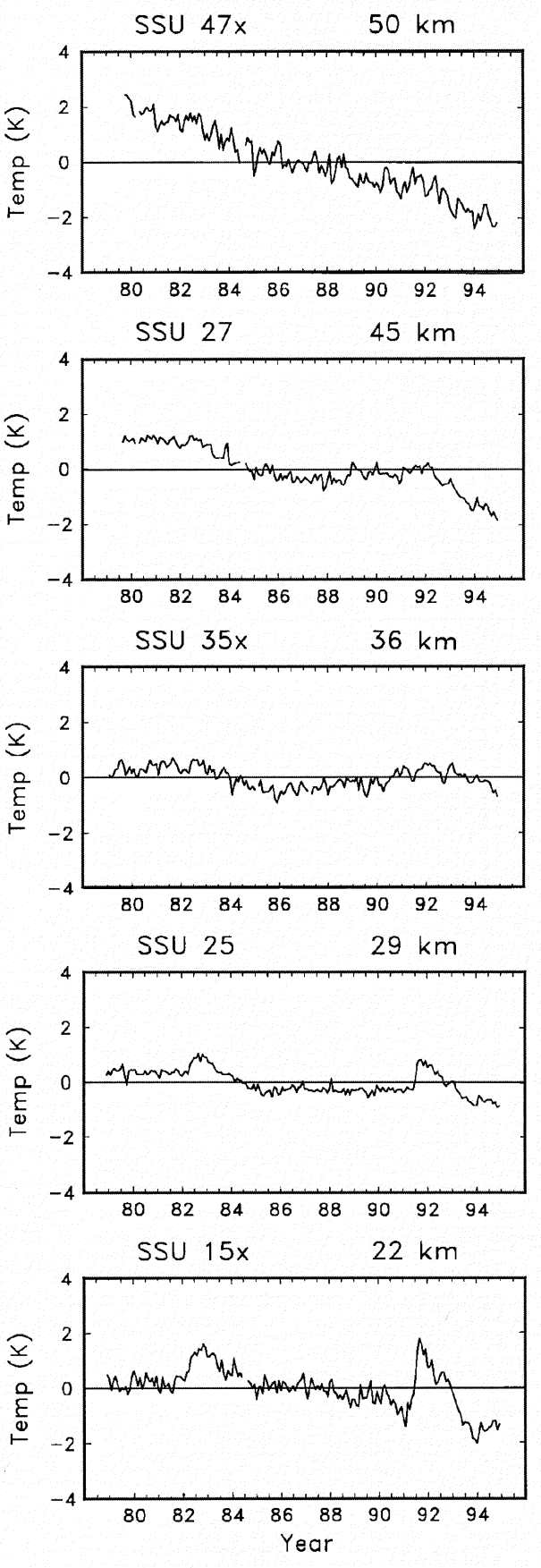


**Figure 5-2.** Time series of global temperature anomalies from the overlap-adjusted SSU data. These data measure the thermal structure over thick layers (thickness ~10-15 km) of the stratosphere; the label of each panel indicates the approximate altitude of the weighting function maximum. (Figure assembled for this chapter in cooperation with the SPARC-Stratospheric Temperature Trends Assessment project.)

from the SSU, High-Resolution Infrared Sounder (HIRS-2), and MSU on the NOAA polar-orbiting satellites. Adjustments based on rocketsonde data (Finger *et al.*, 1993) have been applied to the CPC 5-, 2-, and 1-hPa temperatures for the SPARC dataset. (However, both the CPC data above 10-hPa altitude and the UKMO/SSUANAL datasets may be limited in scope for trend studies, as they have not yet been adjusted for some of the known problems associated with SSU satellite retrievals from many different satellites (see Section 5.2.5.2); hence, they are not considered in this chapter.)

The "Reanal" (viz., the U.S. National Centers for Environmental Prediction (NCEP) reanalyzed) and the "GSFC" (Goddard Space Flight Center, National Aeronautics and Space Administration (NASA)) datasets are derived using numerical atmospheric general circulation models (GCMs) as part of the respective data assimilation systems. These analysis projects provide synoptic meteorological data extending over many years using an unchanged assimilation system. In general, analyzed datasets are dependent on the quality of the data sources, such that a spurious trend in a data source could be inadvertently incorporated in the assimilation. Also, analyses do not necessarily account for longer-term calibration-related problems in the data. Further, the analyzed datasets may not contain adjustments for satellite data discontinuities (Santer *et al.*, 1998).

### 5.2.2 Summary of Various Radiosonde-Based Investigations of Trends

Radiosonde data show a cooling of the lower stratosphere over the past several decades. Table 5-3 summarizes published temperature trend estimates by various investigators, including those mentioned in Section 5.2.1. The data periods and the analysis techniques vary, as do the levels and layers analyzed. No attempt is made here to critically evaluate these diverse estimation techniques. The reported trends have

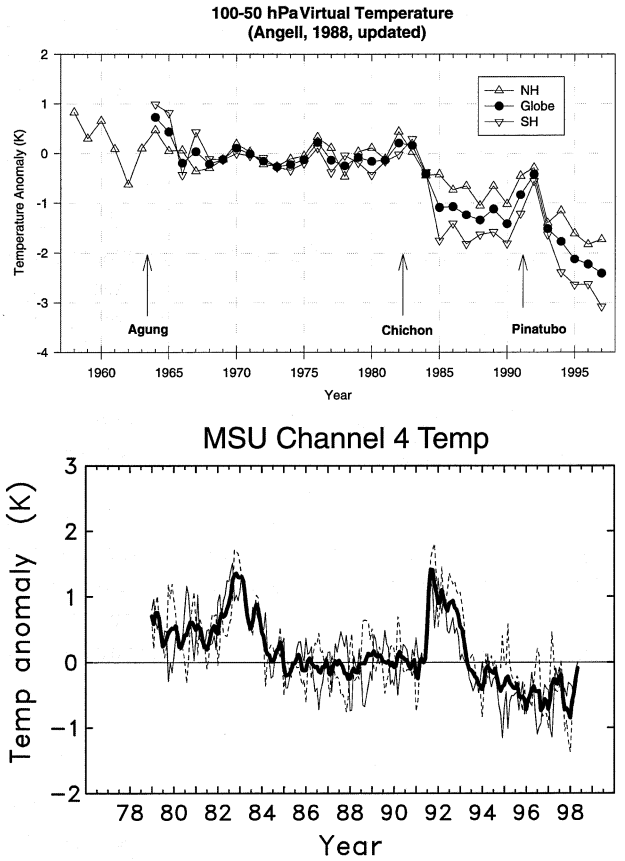


**Figure 5-3.** Top panel: Global and hemispheric averages of annual anomalies of 100-50 hPa layer-mean virtual temperature, from 63 radiosonde stations (Angell, 1988, updated; Halpert and Bell, 1997). Bottom panel: Same as top panel, except from MSU Channel 4 (see Section 5.1 for stratospheric altitudes "sensed"); the thick, solid line denotes global-mean, the thin, solid line denotes the Northern Hemisphere mean, and the dashed line denotes the Southern Hemisphere mean. (Updated from Randel and Cobb, 1994.)

all been converted to units of degrees Kelvin per decade. Overall, the trends, based on areal averages and all seasons, are negative and range from zero to several tenths of a degree per decade. The few studies with global coverage show more cooling of the Southern Hemisphere (SH) lower stratosphere than the Northern Hemisphere (NH). Large trends evaluated for the decade of the 1980s emphasize the period of ozone loss. Positive trends have been found at a few individual stations in the tropics by Reid *et al.* (1989) for the period 1966-1982, possibly due to the influence of El Chichón volcano effects. (It may be noted that Labitzke and van Loon (1995) find positive trends (not listed in Table 5-3) at high and low latitudes for the month of January.)

The sensitivity of trend estimates to the period of record considered is evident from the time series of global or hemispheric mean lower stratospheric temperature anomalies (Angell, 1988; Oort and Liu, 1993; Parker *et al.*, 1997). These data (Figure 5-3 (top); Angell, 1988, updated; Halpert and Bell, 1997) show relatively high temperatures (particularly in the Southern Hemisphere) during the early 1960s, fairly steady temperatures till about 1981, and relatively low temperatures since about 1984, with episodic warmings associated with prominent volcanic eruptions. Figure 5-3 (bottom) shows the global temperature anomalies from the MSU satellite. The evolution of the anomalies is qualitatively similar to the radiosonde anomalies (Christy, 1995), including the warming in the wake of the El Chichón and Mt. Pinatubo eruptions (WMO, 1995), followed by a cooling to somewhat below the pre-eruption levels. The long-term cooling tendency of the global stratosphere is discernible in both datasets, although the satellite data exhibit less interhemispheric difference.

The Berlin analysis (Figure 5-4) shows that the radiosonde temperature time series for the 30-hPa region at the northern pole in July acquires a distinct downward trend when the 1955-1997 period is considered, in contrast to the behavior for the 1955-1977 period. The trend estimates are seen to depend on the end years chosen. The summertime temperature decreases in the high northern latitudes have been more substantial and significant when the decade of 1980s and after are considered; note that this does not necessarily imply a sharp downward trend for the other months.

A few studies have examined radiosonde observations of extreme temperatures in the lower stratosphere. At Sodankylä, Finland, Taalas and Kyrö (1994) found an increase in the frequency of occurrence of temperatures below 195 K at 50 hPa during 1965-1992. At both 50 and 30 hPa over the Northern Hemisphere (10-90°N), Pawson and Naujokat (1997) found a decrease in the minimum and an increase in the maximum daily wintertime temperatures during 1965-1996. They also found an increase in the area with temperatures less than 195 K and suggested that extremely low temperatures appear to have occurred more frequently over the past 15 years.

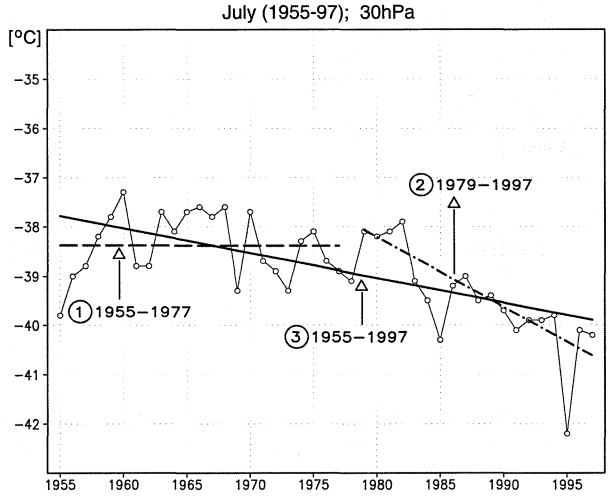


**Figure 5-4.** Time series of July 30-hPa temperatures for 1955-1997 at high northern latitude (80°N). Trends over the 1955-1977, 1979-1997, and 1955-1997 time periods are -0.01, -1.41, and -0.5 K/decade, respectively. Of these, only the 1979-1997 trend is statistically significant. (Updated from Labitzke and van Loon, 1995.)

### 5.2.3 Zonal, Annual-Mean Trends

#### 5.2.3.1 Trends Determination

There is a wide range in the numerical methods used in the literature to derive trends and their significance. Most studies are based on linear regression analyses, although details of the mathematical models and particularly aspects of the standard error estimates are different. Differences in details of the models include the method of fitting seasonal variability, the number and types of dynamical proxies included, and the method used to account for serial autocorrelation of meteorological data (e.g., the multiple linear regression analysis (MLRA) model of Keckhut *et al.* (1995) and the model used by Randel and Cobb, 1994).

The SPARC-STTA group calculated the temperature trends (K/decade) from each of the datasets using autoregressive time-series analyses (maximum likelihood estimation method; e.g., Efron, 1982). The methodology consists of fitting the time series of monthly-mean values at each latitude with a constant and six variables (annual sine, annual cosine, semiannual sine, semiannual cosine, solar cycle, and linear trend). The derived trend and standard error are the products of this computation. The t-test for significance at the 95% confidence level is met if the absolute value of the trend divided by the standard error estimate exceeds 2. The results from the statistical technique used by SPARC-STTA have been intercompared with other methods employed in the literature (A.J. Miller, NOAA, U.S., personal communication, 1998) and found to yield similar trend estimates. It is cautioned, however, that the estimates of the statistical uncertainties could be more sensitive to details of the method than the trend results themselves, especially if the time series has lots of missing data.

An important caveat to the interpretation of the significance of the datasets is that the time series analyzed below, in some instances, is only 15 years long or, in the case of the lengthier rocketsonde and radiosonde records, up to ~30 years long. In this context, it must be noted that the low-frequency variability in the stratosphere, especially at specific locations, is yet to be fully ascertained and, as such, could have a bearing on the robustness of the derived trend values.

#### 5.2.3.2 Trends at 50 and 100 hPa

Figure 5-5 illustrates the decadal trends for the different datasets over the 1979-1994 period. For the non-satellite datasets, the trends at 50 and 100 hPa are illustrated in panels (a) and (b), respectively; panel (c) illustrates the satellite-derived trends. The latitudes where the trends are statistically significant for the different datasets are listed in Table 5-4. (The Oort data (Oort and Liu, 1993), which have been used widely (e.g., Hansen *et al.*, 1995; Santer *et al.*, 1996), are not included in this plot owing to the fact that they span a shorter period of time (1979-1989) than the other datasets.) In the case of the MSU and Nash (SSU 15X) satellite data, the trend illustrated in panel (c) is indicative of a response function that spans a wide range in altitude (Figure 5-1); e.g., for MSU, about half of the signal originates from the upper troposphere at the low latitudes. Because of this, caution must be exercised in comparing the magnitudes of the non-satellite trends in Figure 5-5 panels (a) and (b) with those for the satellite in panel (c). This aspect could explain, in part, the lesser cooling obtained by the satellites relative to radiosondes in the tropical regions; however, this argument is contingent upon the trends in the tropical upper troposphere (not investigated in this report). The MSU data indicate less cooling than Nash in the tropics. One reason for this

**Table 5-5. Latitude bands where the 1966-1994 observed 50-hPa temperature trends from various data sources (see Table 5-1 and Figure 5-6) are statistically significant at the 2-sigma level.** SH and NH denote Southern and Northern Hemisphere, respectively. A dash denotes either no data or no statistically significant latitude belt in that hemisphere.

| 50-hPa Dataset | Latitude Band | |
|---|---|---|
| | SH | NH |
| Berlin | - | 20-70°N |
| CPC | - | 10-20°N; 50-60°N |
| Angell | - | 10, 20, 50°N |
| RAOB | 37.5-32.5°S; 22.5-17.5°S | 17.5°N; 32.5°N; 42.5-72.5°N |
| Oort | 84-56°S; 30-28°S; 24-22°S; 18-16°S | 20-30°N; 34°N; 40°N; 46°N; 52-68°N |
| Russia | - | 70°N |

considered (note that the Berlin radiosonde time series for July, Figure 5-4, exhibits a similar feature). The cooling trend in the 30-60°N belt is about 0.3 K/decade. The strong cooling trend in the Oort data in the high southern latitudes is consistent with Oort and Liu (1993), Parker *et al.* (1997), and the Angell data (D. Gaffen, NOAA, U.S., personal communication, 1998). Regions of statistically significant trends in the datasets are listed in Table 5-5. In the Southern Hemisphere, the two global radiosonde datasets indicate a significant cooling over broad belts in the low and midlatitudes, with the Oort data exhibiting this feature at even the higher latitudes. The Oort global-mean trend is -0.33 K/decade over the 1966-1989 period. In the Northern Hemisphere, again, the midlatitude regions stand out in terms of the significance of the estimated trends. Latitudes as low as 10-20° exhibit significant trends over the longer period considered.

#### 5.2.3.3 Vertical Profiles

Figure 5-7 shows the vertical and latitudinal structure of the zonal, annual-mean temperature trend as obtained from the SSU and MSU satellite measurements. The plot is constructed by considering 5-km-thick levels from linear combinations of the weighting functions of the different channels (Figure 5-1). Figure 5-7 shows panels with and without the inclusion of the volcanic periods (i.e., the "no-volcano" calculations omit 2 years of data following the El Chichón and Mt. Pinatubo eruptions; see Figure 5-2). The omission of the volcano-induced warming period (particularly that due to Mt. Pinatubo near the end of the record) yields an enhanced cooling trend in the lower stratosphere. The vertical profile of the temperature trend in the middle and upper stratosphere between ~60°N and ~60°S shows a strong cooling, particularly in the upper stratosphere (up to 3 K/decade). Cooling at these latitudes in large portions of the middle and upper stratosphere is seen to be statistically significant.

We next focus on 45°N latitude. At this latitude, lidar records from the Haute Provence Observatory (OHP) are available, which afford a high vertical resolution above 30 km, relative to the other instrumental data available. Figure 5-8 displays the annual-mean trend profile for 1979-1998 updated from Keckhut *et al.* (1995) and shows a cooling of ~1-3 K/decade over the entire altitude range 35-70 km, but with statistical significance obtained only around 60 km. The vertical gradient in the profile of cooling between 40 and 50 km differs somewhat from the 1979-1990 summer trend reported in the 1991 WMO Assessment (WMO, 1992, Figure 2-20).

Figure 5-9 compares the vertical pattern of the temperature trend at 45°N obtained from different datasets for the 1979-1994 period. There is a broad agreement in the cooling at the lower stratospheric altitudes, reiterating results in Figure 5-5. The vertical patterns of the trends from the various data are also in qualitative agreement, except for the lidar data (which,

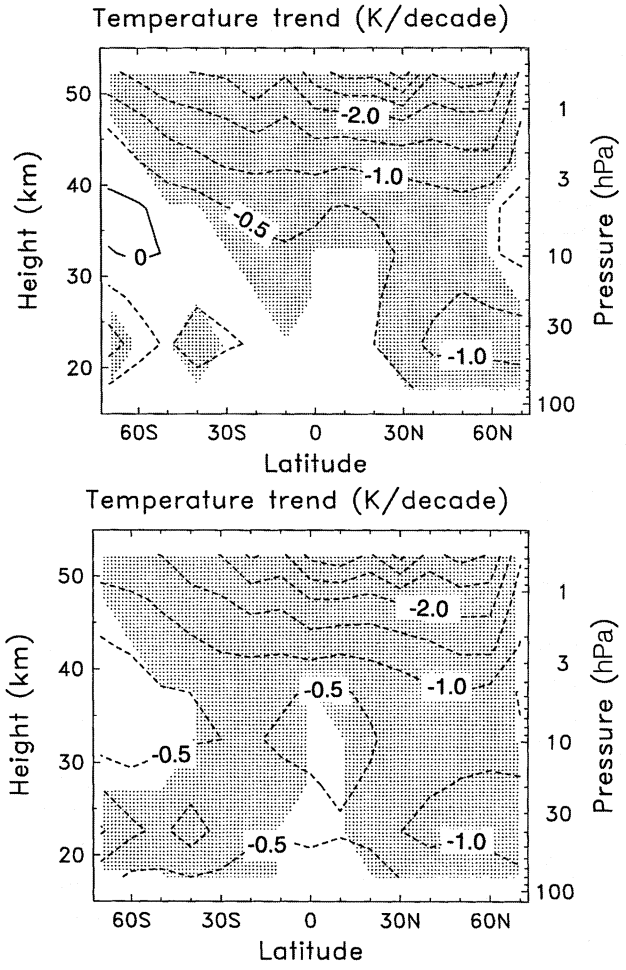


**Figure 5-7.** Zonal, annual-mean decadal temperature trends versus altitude for the 1979-1994 period, as obtained from the satellite (including MSU and SSU channels) retrievals, with volcanic periods included (top) and with volcanic periods omitted (bottom). Shaded area denotes significance at the 2-sigma level. (Figure assembled for this chapter in cooperation with the SPARC-Stratospheric Temperature Trends Assessment project.)

in any case, are not statistically significant over that height range). Note that the lidar trend for the 1979-1998 period (Figure 5-8) exhibits better agreement with the satellite trend than that in Figure 5-9c, indicating a sensitivity of the decadal trend to the end year considered. Generally speaking, there is an approximately uniform cooling of about 0.8 K/decade between ~50 and 5 hPa (~20-35 km), followed by increasing cooling with height (e.g., ~2.5 K/decade at 1 hPa (~50 km)). The analyzed datasets (Table 5-1), examined here for pressures > 10 hPa, are in approximate agreement with the instrument-based data. Figure 5A (see this chapter's Scientific Summary) illustrates the overall mean vertical profile of the trend and uncertainty at 45°N, taking into account all of the datasets and accounting for the uncertainties of the individual measurements (see also Table 5-6 for numerical values of the trend estimates and the uncertainty at the one-sigma level). The vertical profile of cooling, and especially the large upper stratospheric cooling, are consistent with the global plots in WMO (1990a, e.g., Figure 6.17; 1990b, e.g., Figure 2.4-5) constructed from shorter data records.

#### 5.2.3.4 Rocket Data and Trends Comparisons

Substantial portions of the three available rocket datasets (comprising data from U.S., Russian, and Japanese rocketsondes; see Table 5-2) have been either reanalyzed or updated since the review by Chanin (1993). Golitsyn *et al.* (1996) and Lysenko *et al.* (1997) updated the data from five different locations over the period 1964-1990 or 1964-1995. Golitsyn *et al.* (1996) conclude a statistically significant cooling from 25 to 75 km, except around 45 km (Figure 5-10a). Lysenko *et al.* (1997)

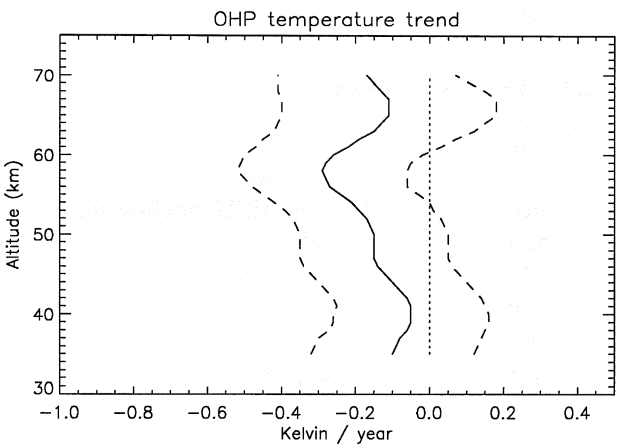


**Figure 5-8.** Annual-mean trend (K/yr) from the all-seasons lidar record at Haute Provence, France (44°N, 6°E), over the period 1979-1998. The 2-sigma uncertainties are also indicated. (Updated from Keckhut *et al.*, 1995.)

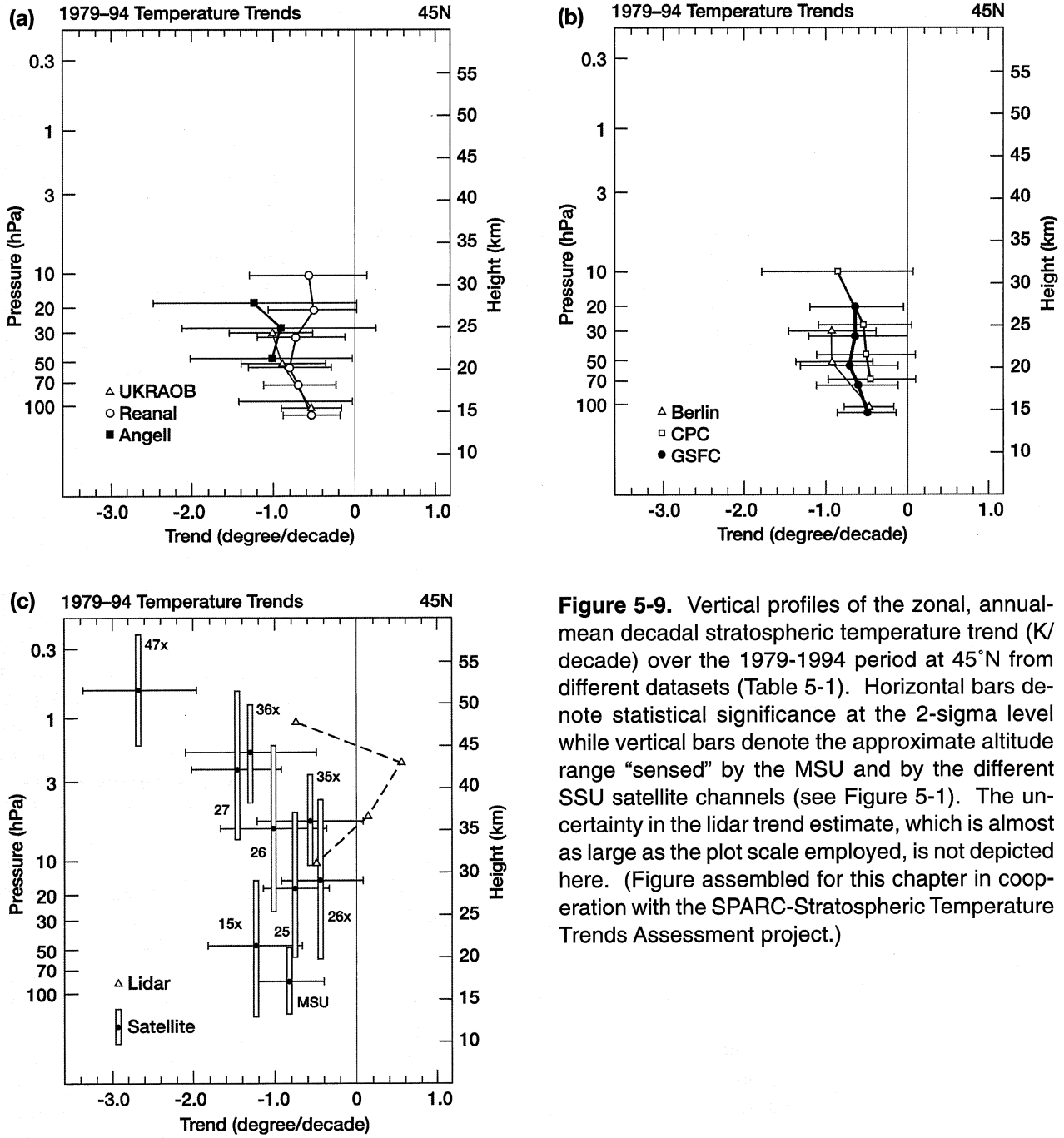


**Figure 5-9.** Vertical profiles of the zonal, annual-mean decadal stratospheric temperature trend (K/decade) over the 1979-1994 period at 45°N from different datasets (Table 5-1). Horizontal bars denote statistical significance at the 2-sigma level while vertical bars denote the approximate altitude range "sensed" by the MSU and by the different SSU satellite channels (see Figure 5-1). The uncertainty in the lidar trend estimate, which is almost as large as the plot scale employed, is not depicted here. (Figure assembled for this chapter in cooperation with the SPARC-Stratospheric Temperature Trends Assessment project.)

obtain a similar vertical profile of the trend for the individual rocketsonde sites (Figure 5-10b). They find a significant negative trend in the mesosphere particularly at the midlatitude sites.

Out of the 22 stations of the U.S. network, nine have provided data for more than 20 years. Some series have noticeable gaps that prevent them from being used for trend determination. Independently, two groups have revisited the data: Keckhut *et al.* (1998) selected six low-latitude sites (8°S-28°N), and Dunkerton *et al.* (1998) selected five out of six of the low-latitude sites plus Wallops Islands (37°N). Both accounted for spurious jumps in the data by applying correction techniques.

Keckhut *et al.* (1998) found a significant cooling

**Table 5-6. Weighted trend estimates and uncertainty at the 1-sigma level computed from the individual system estimates shown in Figure 5-9.** The weighted trend estimates and the uncertainty at the 2-sigma level are illustrated in Figure 5A.

| Altitude (km) | Trend (K/decade) | Uncertainty (1-sigma level) |
|---|---|---|
| 15 | -0.49 | 0.18 |
| 20 | -0.84 | 0.18 |
| 25 | -0.86 | 0.20 |
| 30 | -0.80 | 0.29 |
| 35 | -0.88 | 0.30 |
| 40 | -1.23 | 0.33 |
| 45 | -1.81 | 0.37 |
| 50 | -2.55 | 0.40 |

between 1969 and 1993 of about 1-3 K/decade between 20 and 60 km (Figure 5-11a). A similar result is seen in the data available since 1970 from the single and still operational Japanese rocket station (Figure 5-11b, updated from Komuro, 1989). Dunkerton *et al.* (1998), using data from 1962 to 1991, infer a downward trend of -1.7 K/decade for the altitude range 29-55 km; they also obtain a solar-induced variation of ~1 K in amplitude. It should be noted that the amplitude of the lower-mesosphere cooling observed in the middle and high latitudes from the Russian rockets (between 3 and 10 K/decade) is somewhat larger than from the U.S. dataset. Nevertheless, all four rocketsonde analyses shown in Figures 5-10 and 5-11, together with the lidar trend at 44°N (Figure 5-8), are consistent in yielding trends of ~1-2 K/decade between about 30 and 50 km.

Figure 5-12 compares the vertical profiles of trends over the 1979-1994 period from various datasets at

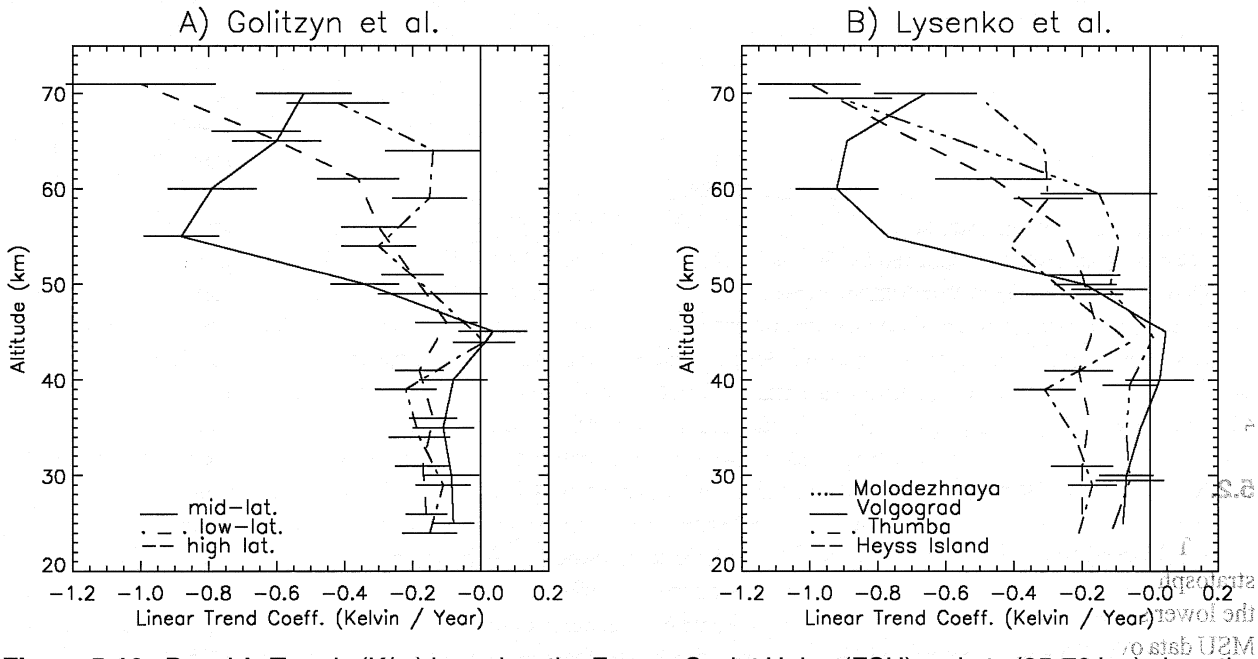


**Figure 5-10.** Panel A: Trends (K/yr) based on the Former Soviet Union (FSU) rockets (25-70 km) since the mid-1960s (see Table 5-2). (Adapted from Golitsyn *et al.*, 1996.) Panel B: Trends (K/yr) at specific sites based on the same FSU rocket dataset. (Adapted from Lysenko *et al.*, 1997.)

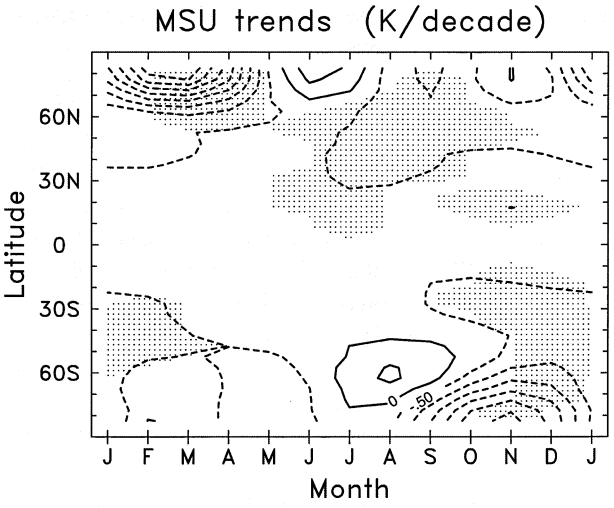


**Figure 5-13.** Latitude-time section of trends in MSU Channel 4 temperature over January 1979-May 1998. Dashed lines indicate cooling trends. The contour interval is 0.5 K/decade, and shading indicates the trends are significant at the 5% level. (Updated from Randel and Cobb, 1994.)

the model's systematic error. Naujokat and Pawson (1996) also noted the relatively cold 1994/95 and 1995/96 northern polar winters. The 1990s-averaged temperature in March is lower than that for the 1980s. Manney *et al.* (1996) suggest that an unusual circulation pattern (low planetary wave forcing and an intense polar vortex) was primarily responsible for this feature. In particular, March 1997 was very cold, about 18 K below the 1980-1989 decadal average. Indeed, the monthly-mean 30-hPa temperature over the pole in March 1997 may have been one of the coldest years since 1966 ("Monthly Report on Climate System, 1997" by Japan Meteorological Agency). Newman *et al.* (1997) indicate that this coincided with the occurrence of the lowest total ozone amount in the Northern Hemisphere for this season. The extreme low temperatures in March 1997 appear to be associated with record-low planetary wave activity (Coy *et al.*, 1997). There are suggestions that the observed Arctic polar stratospheric conditions in recent years may be linked to changes in tropospheric circulation (see Chapter 12). It is not certain whether these are secular trends or whether they are the consequence of a decadal-scale variability in the climate system. With regard to the frequency of major sudden stratospheric warmings, Labitzke and van Loon (1992) note that, before 1992, the largest lapse of time between two major warmings was about 4 years. In comparison, no major warming appears to have occurred between 1991 and 1997, i.e., over seven winters. This is broadly consistent with the sense of the temperature trend in the 1990s up to 1997.

In the Antarctic, analyses of long-term records of radiosonde data continue to reveal substantial cooling trends in spring, further endorsing the early study of Newman and Randel (1988). This cooling trend is closely linked to springtime ozone depletion (Angell, 1986; Chubachi, 1986; Trenberth and Olson, 1989; Jones and Shanklin, 1995; Butchart and Austin, 1996). This springtime cooling is an obviously large feature of the MSU temperature trends shown in Figure 5-13. Figure 5-14 (bottom) shows the time series of 100-hPa temperatures in November over Halley Bay, derived from radiosonde data, together with time series from the NCEP reanalysis interpolated to Halley Bay. Both these records reveal a decadal-scale change in temperature beginning in about the early 1980s, together with significant year-to-year variability (see also Chapter 4). The timing of the change in the Antarctic may be compared with that at 80°N (March) around 1990, as illustrated in the top panel of Figure 5-14. It is notable that temperatures in NH springtime polar regions indicate a strong cooling in recent years and an enhancement above natural variability (also, compare Figure 5-13 with Figure 8-11 of WMO, 1995) that is reminiscent of that observed in the Antarctic about a decade ago.

The structure of the decadal-scale temperature change over Antarctica as a function of altitude and month is shown in Figure 5-15, calculated as the difference in decade means (1986-1995 minus 1970-1979), and averaged over seven radiosonde stations (Randel and Wu, 1998). These data show a significant cooling (of ~6 K) in the lower stratosphere in spring (October-December). Significant cooling persists through austral summer (March), while no significant temperature changes are found during winter. These data also show a statistically significant warming trend (3 K or more) at the uppermost data level (30 hPa; 24 km) during spring.

Kokin and Lysenko (1994) have analyzed the seasonal trends in the middle and upper stratosphere from their data for five rocketsonde stations for the 1972-1990 period. Generally, the cooling is evident almost throughout the year at all sites, but there are exceptions. Figure 5-16 indicates a significant positive trend during spring above Molodezhnaya (at ~35 km) and during

winter above Volgograd and Balkhash (at ~40 km). The warming feature for Molodezhnaya is consistent with the springtime warming inferred for lower altitudes in the Antarctic by Randel (1988), and with that shown in Figure 5-15. The warming is located above a domain of cooling in both Figures 5-15 and 5-16. It is interesting that such an effect also takes place during the northern winter over the Volgograd and Balkhash locations.

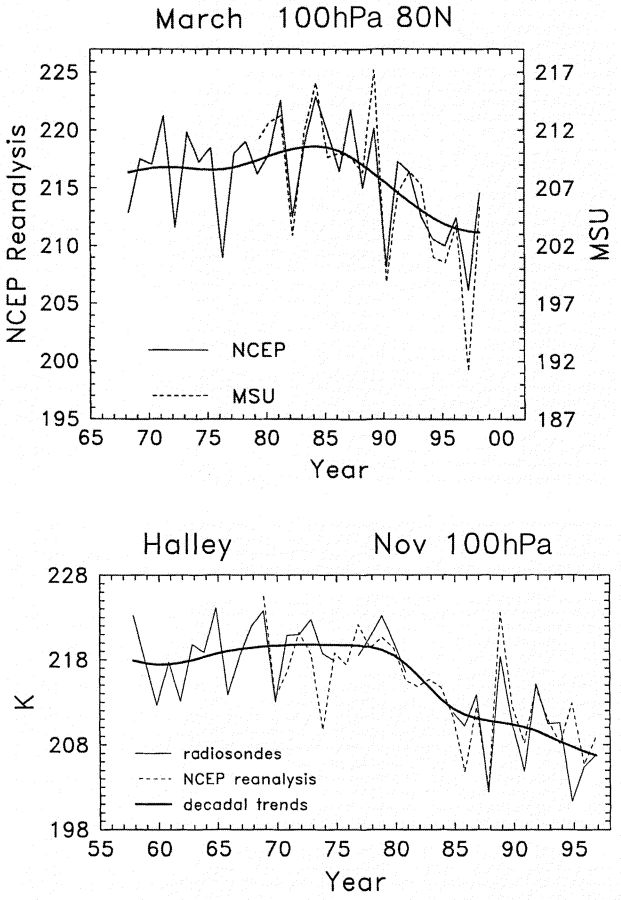


**Figure 5-14.** Top panel: Time series of 100-hPa zonal-mean temperatures at 80°N in March from NCEP reanalyses (solid lines), together with data from MSU. The smooth curve through the reanalysis data indicates the decadal-scale variation. Bottom panel: Time series of 100-hPa temperature in November at Halley Bay, Antarctica, from radiosonde data (solid lines) and NCEP reanalyses (dashed lines). The smooth curve through radiosonde data indicates the decadal-scale variation. (Randel and Wu, 1998.)

### 5.2.5 Uncertainties in Trends Estimated from Observations

Determining stratospheric temperature trends from long-term observations is complicated by the presence of additional, non-trend variability in the data. Two types of phenomena contribute to the uncertainty in trend estimates. The first is true atmospheric variability that is not trend-like in nature. Major sources of such variability include the (quasi-) periodic signals associated with the annual cycle, the quasi-biennial oscillation (QBO), the solar cycle, and the El Niño-Southern Oscillation (ENSO). In addition, stratospheric temperatures vary in response to episodic injections of volcanic aerosols. To first approximation, these atmospheric phenomena have negligible effects on the long-term temperature trend because they are periodic or of relatively short duration. Nevertheless, because current data records are only a few decades long, at most, these phenomena may appear to enhance or reduce an underlying trend. At a minimum, the additional temperature variability associated with these signals reduces the statistical confidence with which long-term trends can be identified. Whereas periodic signals can be removed, the effects of sporadic events are more difficult to model and remove. Furthermore, there may be long-term trends in these cycles and forcings that confound the analysis. A second source of uncertainty is due to spurious signals in the time series that are the result of changes in methods of observation rather than changes in the atmosphere. The problem of detecting

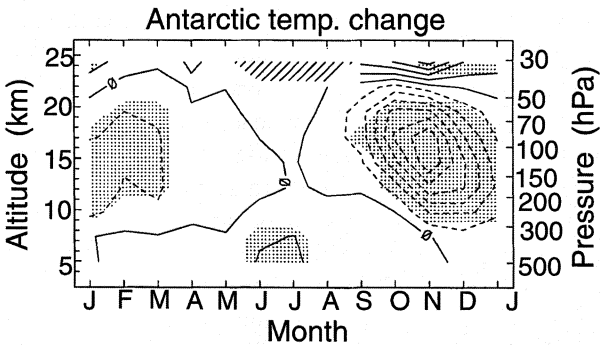


**Figure 5-15.** Altitude-time section of temperature differences over Antarctica, 1986-1995 minus 1970-1979, derived from an average of seven radiosonde stations. Dashed lines indicate cooling trends. The contour interval is 1 K. Shading denotes that the temperature differences are significantly different from natural variability. (Randel and Wu, 1998.)

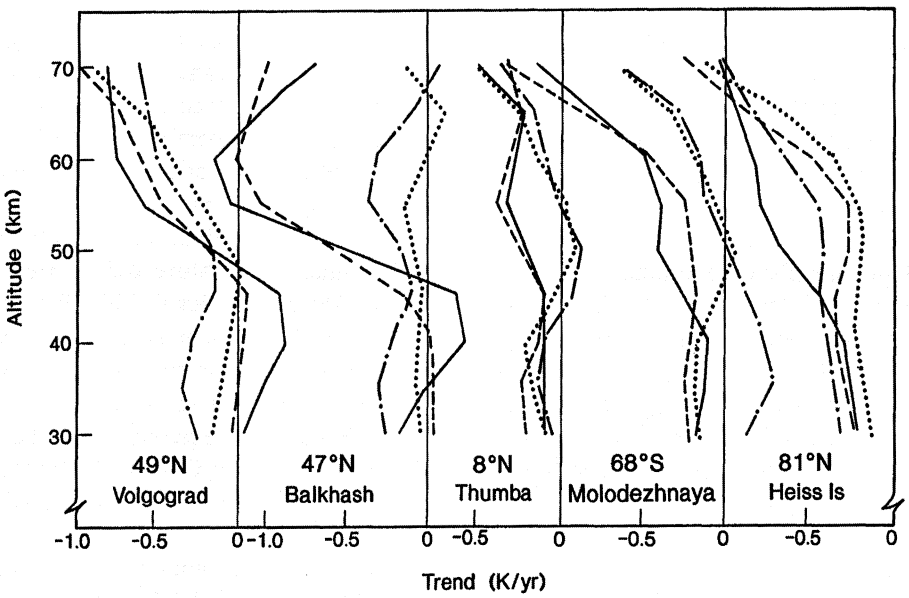


**Figure 5-16.** Seasonal rocketsonde trends (in K/yr), using Former Soviet Union rocket data from 1972 to 1990 at five sites (see Table 5-2), for winter (solid line), spring (dot-dash line), summer (dotted line), and autumn (dashed line). (Adapted from Kokin and Lysenko, 1994.)

temperature trends in the presence of changes in the bias characteristics of the observations is receiving increased attention (Christy, 1995; Santer *et al.*, 1998). It seems likely that over the next few years, better methods will be employed to quantify and reduce the uncertainty in stratospheric temperature trend estimates attributable to these spurious signals.

#### 5.2.5.1 Uncertainties Associated with Radiosonde Data

Although most radiosonde analyses show cooling of the lower stratosphere in recent decades, it is important to recognize that they all rely on subsets of the same basic dataset, the global observing system upper-air network. This network is fundamentally a meteorological one, not a climate monitoring network, not a reference network for satellite observations, and not a network for detection of stratospheric change. When the radiosonde data are used for temperature trends analyses, any difficulties that plague the radiosonde network will also affect the analyses that use those data.

Karl *et al.* (1995) and Christy (1995) have reviewed some of the problems associated with using radiosonde data for the detection of atmospheric temperature trends. These fall into two categories: the uneven spatial distribution of the observations, and temporal discontinuities in station records.

The radiosonde network is predominantly a Northern Hemisphere, midlatitude land network. About half the stations are in the 30-60°N latitude band, and less than 20% are in the Southern Hemisphere (Oort and Liu, 1993). Moreover, the uneven distribution of stations is worse for stratospheric data than for lower tropospheric data, because low-latitude and Southern Hemisphere soundings have a higher probability of taking only one observation daily (other stations make two, and many formerly made four) and because the soundings more often terminate at lower altitudes (Oort and Liu, 1993). Estimates of layer-mean trends, and comparisons of trends at different levels, are less meaningful when data at the top of the layer are fewer than at the bottom.

For trend detection, the temporal homogeneity of the data is the key. As discussed by Parker (1985), Gaffen (1994), Finger *et al.* (1993), and Parker and Cox (1995), numerous changes in operational methods have led to discontinuities in the bias characteristics of upper-air temperature observations, which are particularly severe in the lower stratosphere (Gaffen, 1994). Because radiosondes are essentially expendable probes (although some are recovered and reconditioned), changing methods is much easier than, for example, in surface observations at fixed locations. Effects on data have been shown for changes in instrument manufacturer and replacement of old models with newer ones from the same

manufacturer (Parker, 1985; Gaffen, 1994), changes in time of observation (Elliott and Gaffen, 1991; Zhai and Eskridge, 1996), changes in the lag characteristics of the temperature sensors (Parker, 1985; Huovila and Tuominen, 1990), and even changes in the length of the suspension cord connecting the radiosonde balloon with the instrument package (Suzuki and Asahi, 1978; Gaffen, 1994) and in balloon type (Parker and Cox, 1995).

Daytime stratospheric temperature data in the early years of radiosonde operations were particularly affected by errors due to solar radiation, and substantial changes in both data correction methods (e.g., Scrase, 1956; Teweles and Finger, 1960) and instrument design have been made to address the problem. In general, the result has been a reduction in a high bias over time, leading to an artificial "cooling" in the data (Gaffen, 1994). The example in Figure 5-17, monthly-mean 100-hPa temperatures at Tahiti, shows that a 1976 change from one model of the French Mesural radiosonde to another, each with different temperature sensors, was associated with an artificial temperature drop of several degrees. Given estimated temperature trends on the order of tenths of a degree Kelvin per decade, such inhomogeneities introduce substantial uncertainty regarding the magnitude of the trends in the lower stratosphere. Furthermore, Luers (1990) has demonstrated that daytime radiosonde temperature errors can exceed 1 K at altitudes above 20 km (50 hPa) and that the magnitude of the error is a strong function of the temperature and radiative environment, which suggests that, as the atmosphere changes, so will the nature of the measurement errors.

A few investigators have attempted to adjust radiosonde temperature time series to account for "change-points," or level shifts like the one illustrated in Figure 5-17. Miller *et al.* (1992), using data from 1970-1986, made adjustments to lower stratospheric data at four of 62 stations in Angell's (1988) network on the basis of a statistical regression model that includes a level shift term. However, Gaffen (1994) concluded that, over a longer period, many more of the Angell stations showed data inhomogeneities. Parker *et al.* (1997) have made adjustments to temperature data from Australia and New Zealand for the period 1979-1995 by using MSU data as a reference time series, and station histories (Gaffen, 1994) to identify potential change-points. The adjustments (of earlier data relative to 1995 data) ranged from 0 to -3.3 K and reduced the estimated zonal-mean temperature change between the periods 1965-1974 and 1987-1996 at about 30°S (30 hPa) from -2.5 K/decade to about -1.25 K/decade (Parker et al., 1997).

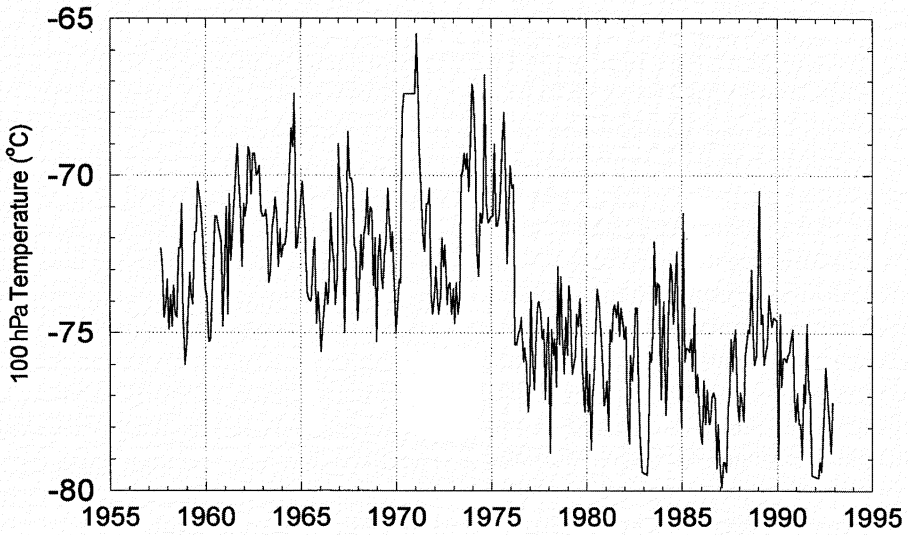


**Figure 5-17.** Monthly-mean 100-hPa raw temperatures measured by radiosondes at Tahiti. Several instrument changes occurred during this data period, but the 1976 change from the Mesural FMO 1943B, with a bimetal temperature sensor, to the Mesural FMO 1944C, with a thermistor, had the most obvious effect on the time series. (Gaffen, 1996; see also Gaffen, 1994.)

short-term phenomenon is the large build-up of stratospheric aerosols following volcanic eruptions (see Chapter 3). The SAGE extinction data and other satellite data (e.g., McCormick *et al.*, 1995) reveal a notable increase in stratospheric aerosol concentrations for 1-2 years following volcanic eruptions. Over the past two decades, such transient enhancements have come about due to volcanic eruptions of different intensities. Data from earlier ground-based observations reveal other episodes of volcanic loading of the stratosphere dating back to the 1960s. It is well understood that aerosols injected into the lower stratosphere by major volcanic eruptions result in a warming of this region of the atmosphere owing to enhanced absorption of solar radiation and the upwelling terrestrial infrared radiation (Pollack and Ackerman, 1983; WMO, 1990a; Labitzke and McCormick, 1992).

Three volcanoes stand out in particular since the 1960s, the period when widespread and routine radiosonde observations began. The three volcanoes of particular importance for climate variations have been Agung (Bali, Indonesia, 1963), El Chichón (Mexico, 1982), and Mt. Pinatubo (Philippines, 1991). In each one of these three cases, well-documented instrumental records indicate that the temperatures increased and stayed elevated until the aerosol concentrations were depleted completely (WMO, 1990a, 1995). All three eruptions produced somewhat similar warming characteristics (Angell, 1993), viz., a warming of the lower stratosphere (~15-25 km) centered in the tropics (~30°N-30°S), with a magnitude of 1-2 K (up to 3 K for Mt. Pinatubo). The warming diminishes in time, but anomalies are observed for approximately 2 years following each eruption (Figures 5-2 (SSU 15X) and 5-3). Because the volcanic effects are episodic and clearly identifiable, their direct effect on calculation of trends is minimal (the volcanic time periods simply need to be omitted prior to trend calculation), except as they possibly overlap with other potentially causal phenomena such as the solar cycle.

The magnitude and evolution of the transient warming agree reasonably well between the radiosonde and satellite datasets (Labitzke and McCormick, 1992; Christy and Drouilhet, 1994; Randel and Cobb, 1994; Figure 5-3). Relative to the analyses in WMO (1995), the temperature of the global-mean lower stratosphere has become progressively colder in both the satellite and radiosonde time series (Figures 5-2 (bottom panel) and 5-3).

In the upper stratosphere and mesospheric regions, an indirect effect could be expected from the change of circulation and/or the upwelling flux arising from the lower stratospheric heating. Such an indirect effect appears to have been observed after the Mt. Pinatubo eruption in the OHP lidar data. A cooling of 1.5 K in the upper stratosphere and a warming of 5 K at 60-80 km were detected (Keckhut *et al.*, 1995). Thus, a trend analysis for these regions also requires the omission or correction of post-volcanic eruption data (e.g., such a correction was applied to the data plotted in Figure 5-8 by adding a term proportional to the aerosol optical thickness in the analysis technique).

### 5.2.6.2 Solar Cycle

The 11-year modulation of the ultraviolet (UV) solar flux, which is now well documented, is expected to, through photochemistry, influence stratospheric ozone and therefore stratospheric temperature. A number of investigators have attempted to identify a signature of the 11-year solar cycle in the temperature dataset. The solar proxy used in most studies is the 10.7-cm radio flux, which spans the longest period, even though more realistic proxies would be the He I line, Mg II line, or UV irradiance. However, several analyses using these different proxies justify the choice of the 10.7-cm flux (Donnelly *et al.*, 1986; Keckhut *et al.*, 1995).

Satellite data provide a global view of the signature due to solar variations, but the time series is relatively short. The overlap-adjusted SSU and MSU datasets (spanning 1979-1995) exhibit a coherent temperature variation approximately in phase with the solar cycle. Figure 5-19 shows the vertical-latitudinal structure of the solar signal (derived via regression onto the 10.7-cm solar flux time series) using the overlap-adjusted MSU and SSU data. Even though the dataset is limited to 17 years, this shows a statistically significant solar component of order 0.5-1 K throughout most of the low-latitude (30°N-30°S) stratosphere, with a maximum near 40 km. The spatial patterns show maxima in the tropics, with an approximate symmetry about the equator. A small solar response is observed in these data at the high latitudes. The 0.5-1 K solar signal seen in the Nash data is in reasonable agreement with results from the longer records of radiosondes/rocketsondes discussed below. At northern midlatitudes, the satellite-derived signature, which is not statistically significant, goes from slightly positive at ~17 km to slightly negative at ~25 km, with a

null value at 45-50 km. This is similar to the OHP lidar record (Keckhut *et al.*, 1995) and to the Volgograd rocket record (Kokin *et al.*, 1990). At high latitudes, although the satellite data uncertainty is large, there is a hint of a large positive response in the mesosphere, as is observed in the Heiss Island rocket data (Kokin *et al.*, 1990).

The longest time series are provided by radiosondes and rockets; even then, they barely cover at best four solar cycles. There is, thus, in general, some difficulty in establishing a firm relationship with the 11-year solar cycle. Labitzke and van Loon (1989) and van Loon and Labitzke (1990) use the Berlin meteorological analyses, beginning in 1964 and spanning the NH lower stratosphere, to isolate coherent temperature cycles in the subtropics in phase with the solar cycle. Labitzke and van Loon (1997) update their previous analysis and find a correlation of 0.7 with the 30-hPa geopotential height (which can be taken to imply a similar correlation with layer-mean temperature below this level). The maximum correlation occurs over the west Pacific near China. Using the NCEP reanalyzed global dataset, van Loon and Labitzke (1998) show a similar solar signal manifest in the Southern Hemisphere, with higher correlations in the tropical regions.

Angell (1991b) has used radiosonde and rocketsonde data to deduce tropical and NH midlatitude solar cycle variations of approximately 0.4 and 0.8 K in the lower and upper stratosphere, respectively (changes per 100 units of 10.7-cm solar flux, or approximately solar maximum minus solar minimum values). Dunkerton and Baldwin (1992) isolate a weak solar cycle in CPC temperatures in the NH winter lower stratosphere, using data from 1964-1991 (these analyses are based primarily on radiosonde data). Isolation of a solar cycle signal in CPC upper stratospheric temperature data beginning in 1979 is somewhat problematic, due to the spurious discontinuities introduced by satellite changes (see Figure 5-18; Section 5.2.5.2). This suggests that the solar cycle variations derived from these data (e.g., Kodera and Yamazaki, 1990; Hood *et al.*, 1993) should be treated with caution.

In their rocket data analysis, Dunkerton *et al.* (1998) found a 1.1-K response to the solar cycle for the integrated altitude range of 29-55 km (Figure 5-20). Kokin *et al.* (1990), Angell (1991b), and Mohanakumar (1995), using rocket data, and Keckhut *et al.* (1995), using lidar data, infer a clear solar signature in the mesosphere of +4 to 10 K per 100 units of 10.7-cm flux.

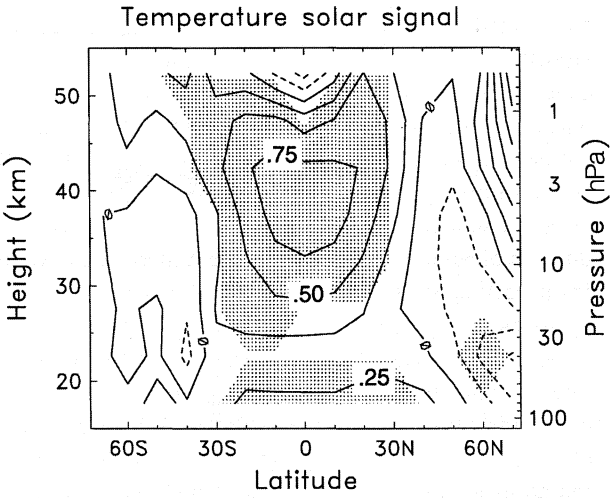


**Figure 5-19.** Latitude-altitude structure of the solar cycle signal in the satellite temperature (K) dataset, derived from regression analyses. Shaded areas show 95% confidence intervals for the regression estimates. (Figure assembled for this chapter in cooperation with the SPARC-Stratospheric Temperature Trends Assessment project.)

On the other hand, the results obtained in the upper stratosphere and around the stratopause are different in both amplitude and sign for the different sites, and are also variable with season.

From the records, it thus appears that the solar cycle signature in stratospheric temperatures need not be uniform and identical all over the globe and at all altitudes. This has been manifest in Labitzke and van Loon (1997) on the horizontal scale, as well as on the vertical scale in Chanin and Keckhut (1991) and may be attributable to the role of planetary waves. An additional point to note is that the solar-induced temperature changes need not occur at the same latitudes as any changes in ozone.

In the lower stratosphere, the effect of solar variations is found to have a relatively small effect on trend calculations for time series longer than 15 years such as those analyzed here. Regression estimates of trends neglecting a solar cycle term change by only ~10% (this sensitivity was determined by testing several of the time series analyzed here). Elsewhere in the stratosphere, the amplitude of the solar cycle signature has the potential to introduce a bias in trend estimates (especially if the number of cycles involved in the time series is small). The determination of the amplitude and structure of the

## 5.3.3 Stratospheric Ozone

### 5.3.3.1 Lower Stratosphere

Over the past decade or so, much of the work on stratospheric temperature trends has focused on the effects due to lower stratospheric ozone change, following the realization of the large ozone loss trends in this region, as well as the accumulating evidence for substantial temperature changes in this region (WMO, 1990b, 1992, 1995). In particular, the large Antarctic springtime ozone losses were the first to be examined for their potential temperature effects. Subsequently, investigations have been extended to examine the changes initiated by ozone depletion in the global lower stratosphere.

As a general demonstration of the sensitivity of the global lower stratosphere to changes in ozone, Figure 5-25 shows the change in lower stratospheric and tropospheric temperatures when the entire ozone in the 70-250 hPa region is removed. Temperature decreases of up to about 4 K are obtained. Note that the region in the vicinity of the tropopause is most substantially affected, consistent with the known radiative sensitivity and large radiative damping time of this region (Fels, 1982; Kiehl and Solomon, 1986). A warming is seen above the cooling, which is in part due to more upwelling thermal infrared radiation reaching this region in the absence of ozone in the 70-250 hPa layer, and in part due to dynamical changes; these will be elaborated upon later in this section.

With regard to actual decadal trends, Miller *et al.* (1992) estimated a cooling of the lower stratosphere by about 0.3 K/decade over the 1970-1986 period, based on radiosonde observations. By performing a calculation of temperature changes using observed ozone trends, they inferred a substantial role due to ozone losses in the observed temperature trend. Because ozone changes vary greatly with latitude, there is a need to proceed beyond global means and perform model calculations that resolve the latitudinal variations. Locally, the stratosphere is not in radiative equilibrium, and the temperature is determined by both radiative and dynamical processes. However, by considering the stratosphere to be in a local radiative-dynamical equilibrium, with the dynamical heating rates fixed over some specific time scale (e.g., season), the FDH concept in effect has been extended to derive the local columnar temperature changes. Shine (1986) demonstrated that a large cooling would occur in

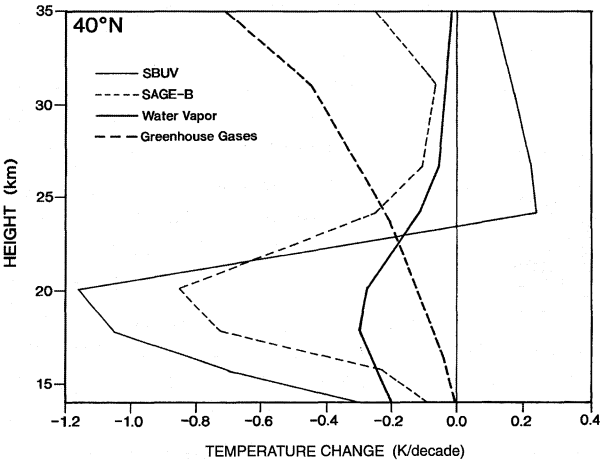


**Figure 5-23.** Vertical profile (~15-35 km) of the FDH-computed annually averaged temperature change during the 1980s at 40°N due to changes in the concentrations of various stratospheric species. "Greenhouse gases" denotes well-mixed greenhouse gases; the "SBUV" ozone refers to a calculation that considers the column loss using SBUV satellite trends; the "SAGE-B" calculation uses the vertical profile of ozone change observed by the SAGE satellite; "water vapor" refers to the decadal change in water vapor reported by Oltmans and Hofmann (1995). (Adapted from Forster and Shine, 1997.)

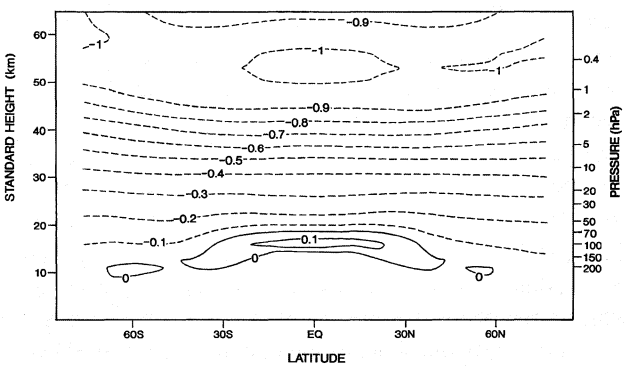


**Figure 5-24.** Vertical profile of the zonal, annual-mean temperature change from the lower to upper stratosphere resulting from the 1979-1990 changes in the well-mixed greenhouse gases. (The results are from the FDH model used in Ramaswamy *et al.*, 1992.)

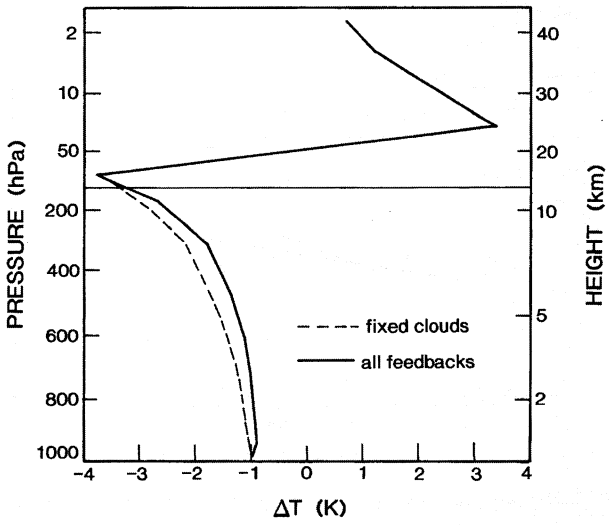


**Figure 5-25.** GCM-computed temperature change in the atmosphere due to a total loss of ozone between 70 and 250 hPa. Results are shown for the case with fixed clouds (dashed line), and with consideration of all feedbacks including cloud feedback effects (solid line). (Adapted from Hansen *et al.*, 1997a.)

the Antarctic winter/spring lower stratosphere owing to the ozone hole.

McCormack and Hood (1994) presented the first attempt to match the observed seasonal and latitudinal variation of lower stratospheric temperature with that predicted by an FDH model using imposed ozone changes based on observations. The resemblance between the size and pattern of the model temperature changes (with peak changes in the winter/spring of northern midlatitudes and spring of southern high latitudes) and MSU satellite observations (Randel and Cobb, 1994) was found to be encouraging. As discussed below, this work has been taken further by using GCMs, which strengthens the model-observation comparisons.

One particular item of interest in the case of FDH calculations (e.g., McCormack and Hood, 1994) is that the peak cooling in the Antarctic springtime tends to occur about one month earlier than in the observations. This occurs because the standard FDH approximation does not account for the time period during which the perturbation in the constituent (in this case ozone) persists. In the Antarctic springtime, typical radiative time scales are in excess of a month and yet the time scale of the most marked ozone change is only one month. Hence, the atmosphere does not have time to fully equilibrate to the ozone-induced radiative perturbation (Shine, 1986). The standard FDH approximation does not account for this and assumes that the temperature adjustment occurs essentially instantaneously. Figure 5-26, from Forster *et al.* (1997), shows the temperature change at 80°S and 18.5 km using seasonally varying ozone changes in the context of the standard FDH approach, and a modified FDH approach (termed the Seasonally Evolving FDH (SEFDH)) that accounts for the time scale of the perturbation. The SEFDH result is obtained by time-marching the radiation calculations through the seasons. As can be seen, the maximum cooling in the FDH occurs earlier in the austral spring and is significantly larger than the SEFDH-derived maximum cooling. Also notable is that the FDH model does not retain a "memory" of perturbations at other times of year. An ozone loss only in October would have no effect on temperatures at other times of year. The SEFDH model does retain a memory of the radiative perturbations, and the increased cooling that persists from late spring to late summer in the SEFDH calculations is because the model temperatures have not yet recovered from the large loss of ozone in the springtime.

Early GCM works investigating the effects of ozone depletion did so assuming uniform stratospheric ozone losses, with a view toward diagnosing in a simple manner the radiative-dynamical response of the stratosphere (e.g., Fels *et al.*, 1980; Kiehl and Boville, 1988). Although the depletion profiles employed did not quite represent those observed subsequently in the lower stratosphere, these studies have provided insights on the mechanism of the stratospheric response to ozone changes there. Recently, Christiansen *et al.* (1997) have further examined the nature of the stratospheric response to different types of idealized ozone perturbations.

With the steady build-up of knowledge since the early to middle 1980s about the spatial and temporal distribution of ozone losses in the lower stratosphere, GCM experiments of two types have been carried out to determine the resulting temperature changes in the stratosphere. One type of investigation concerns attempts to simulate the interactive radiative-chemistry-dynamical changes due to ozone losses in the Antarctic polar region during springtime; e.g., Cariolle *et al.* (1990) and Prather *et al.* (1990) found a substantial lower stratospheric cooling during the duration of the ozone hole. Mahlman

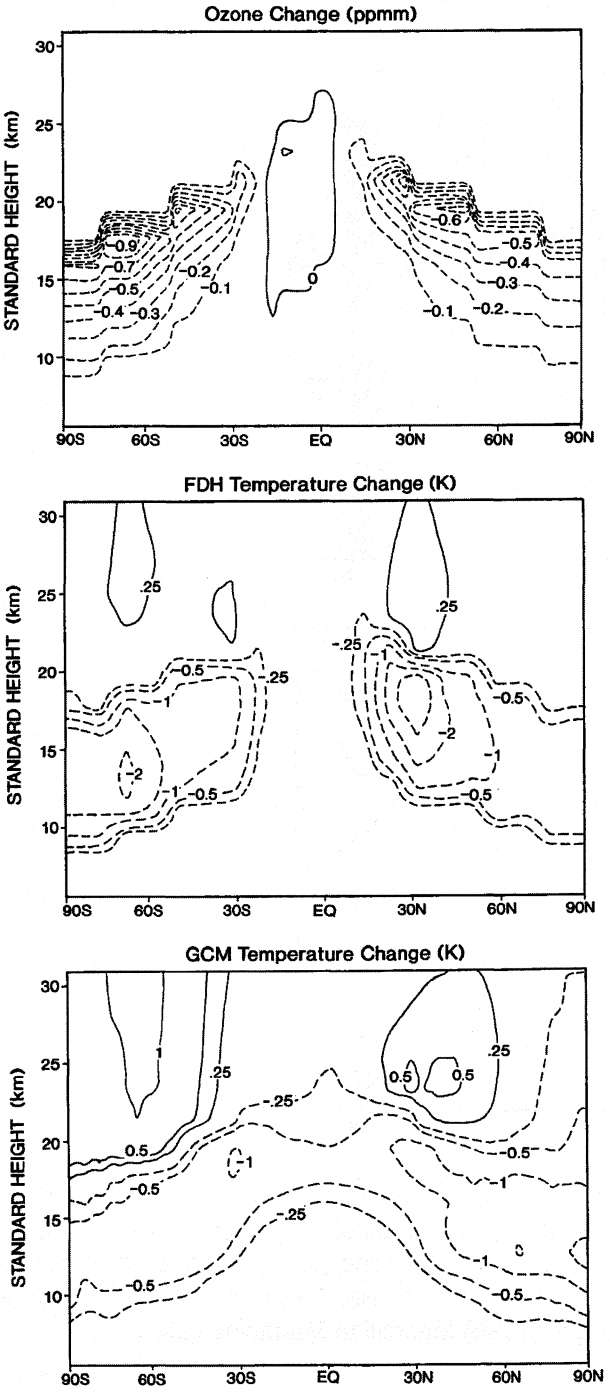


**Figure 5-28.** Idealized, annual-mean stratospheric ozone loss profile based on TOMS and SAGE satellite-observed ozone trends (top panel), and the corresponding temperature changes, as obtained using a FDH model (middle panel) and GCM (bottom panel). (Adapted from the model simulations of Ramaswamy *et al.*, 1992, 1996).

month pattern of cooling with observations bears a fair resemblance to the FDH-based study of McCormack and Hood (1994). In the midlatitudes, both panels illustrate a cooling from ~January to October in the Northern Hemisphere and from ~September to July in the Southern Hemisphere. The cooling in the midlatitudes of the Northern Hemisphere from ~December to July, and in the Southern Hemisphere from ~December to May, are statistically significant in both model and observation. Comparing Figure 5-29 with Figure 5-13, it is apparent that the observed space-time domain of statistically significant cooling is also dependent on the end year chosen for the analysis. Near the poles, both the simulation and observation exhibit a relatively large magnitude of cooling during winter and spring. The simulated cooling in the Antarctic is highly significant during the austral spring (period of the ozone hole), consistent with observation. The springtime cooling in the Arctic does not show a high significance owing to a large dynamical variability there. The simulated cooling in the tropics, which arises as a result of changes in circulation and is absent in FDH, is not significant for most of the year owing to small temperature changes there. There exist some quantitative differences between the simulated and observed trends. In addition, there is less variability in the model compared to observations.

In general, the observed ozone losses introduce a nonuniform space-time cooling. This is in contrast to well-mixed greenhouse gas effects that tend to yield a more uniform lower stratospheric cooling with season (not shown). Thus, the observed seasonal trend (Figure 5-29b), which exhibits a spatial dependence, is unlikely to be due solely to increases in well-mixed greenhouse gases. Note that, in the context of the GCM results, it is not possible to associate specific seasonal cooling at any location with the corresponding seasonal ozone loss.

Some models that have been principally used to study tropospheric climate changes due to greenhouse gases (e.g., IPCC, 1996) have also considered the lower stratospheric ozone depletion. However, as noted earlier, several of these climate models have a poor vertical resolution in the stratosphere that affects the accuracy of the calculated temperature changes. Nevertheless, the cooling predicted by these models using observed ozone loss in the lower stratosphere is generally consistent with the observed global-mean cooling trend, typically 0.5 K/decade.

Model calculations illustrate that, in addition to lower stratospheric ozone change, tropospheric ozone

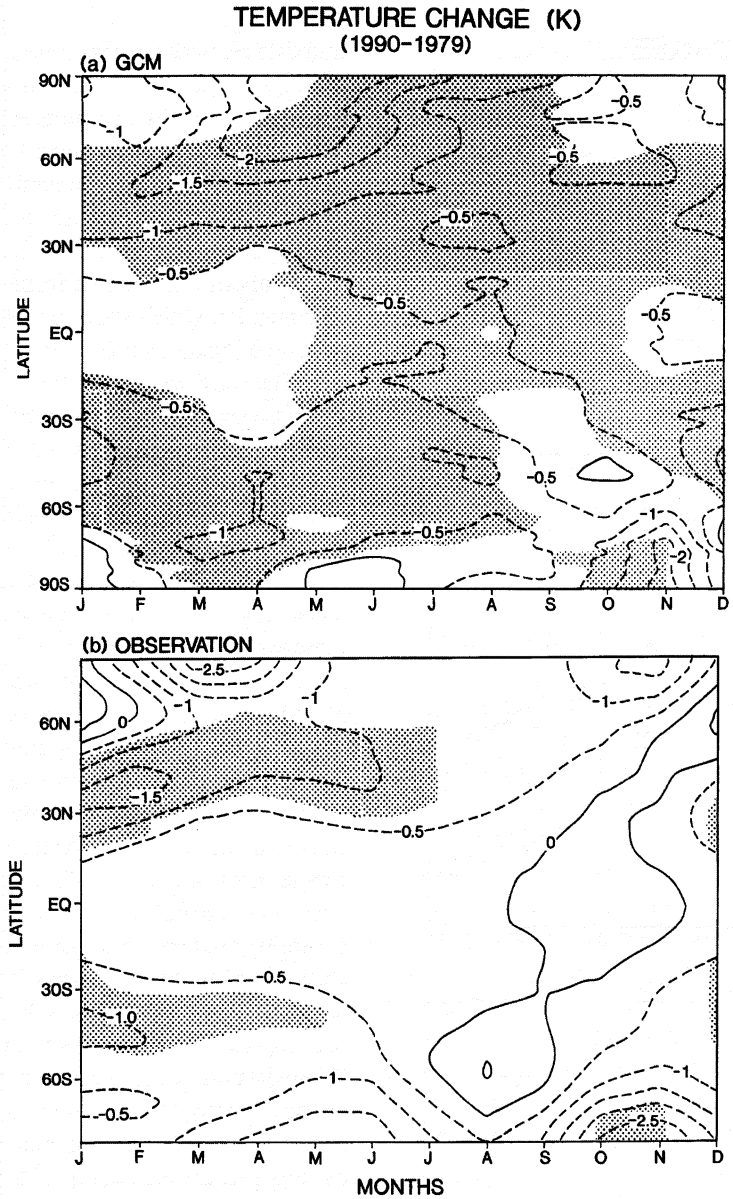


**Figure 5-29.** Zonally-averaged, monthly-mean, lower stratospheric temperature change for ~1979-1991: (a) as simulated by the general circulation model (90°S to 90°N) due to the observed global ozone depletion, and (b) as inferred (Randel and Cobb, 1994) from satellite observations (82.5°S to 82.5°N). Shaded areas show statistical significance at the 95% confidence level. (Reprinted by permission from *Nature* (Ramaswamy *et al.*, *Nature*, *382*, 616-618, 1996) Copyright (1996) Macmillan Magazines Ltd.).

change could also have a smaller but non-negligible effect on stratospheric temperatures (Ramaswamy and Bowen, 1994). Since preindustrial times, tropospheric ozone may have increased by ~50% or more in some regions in the Northern Hemisphere (IPCC, 1995; Berntsen *et al.*, 1997). As a result, this may have contributed to a substantial cooling tendency in the lower stratosphere in specific regions.

In a diagnostic study, Fortuin and Kelder (1996) discuss relationships between ozone and temperature changes by analyzing concurrent measurements of these two quantities made at eight stations over the past two decades. They find that both vertical displacement and radiative adjustment to trace gas concentrations need to be considered in order to explain the observed ozone and temperature variations at the various locations.

### 5.3.4 Aerosols

As stated in Section 5.2.6.1, major volcanic eruptions result in temporary increases of stratospheric aerosol concentrations which, in turn, cause transient warmings of the lower stratosphere (WMO, 1990a, 1992). One-dimensional radiative-convective, two-dimensional, and three-dimensional models have all been used to estimate the effects on stratospheric temperatures (e.g., Hansen *et al.*, 1978, 1997b; Harshvardhan, 1979; Pitari *et al.*, 1987). An important research outcome in recent years has been the fact that simulations of the climatic effect of the Mt. Pinatubo eruption (Hansen *et al.*, 1993, 1997b) reproduce the observed lower stratospheric warming (refer to Section 5.2.6.1; Christy, 1995; Randel *et al.*, 1995; Angell, 1997; also Figures 5-2 (bottom panel) and 5-3), the peak and its duration, remarkably well (IPCC, 1995). Although temporary, the volcanic aerosol-induced lower stratospheric warming is in the opposite sense of the cooling due to ozone depletion and the cooling due to the combined well-mixed greenhouse gas increases (Figures 5-23, 5-24, and 5-27).

Rind *et al.* (1992) investigated the role of volcanic effects on the stratosphere in GCM experiments with and without sea surface temperature changes. Their results show that, in response to the volcanic injections, the lower stratosphere warmed, while the upper stratosphere cooled and the mesosphere warmed at middle and high latitudes. These responses are similar qualitatively to the OHP lidar observations. The occurrence of mesospheric warming is indirectly supported by a decrease in the occurrence of noctilucent clouds in the summer of 1992 (Zalcik, 1993).

Several 2-D radiative-dynamical-photochemical models (Brasseur and Granier, 1992; Tie *et al.*, 1994; Rosenfield *et al.*, 1997), with different degrees of complexity in the representation of physical and chemical processes, have been deployed to study the temperature, circulation, and ozone changes due to the increase in stratospheric aerosol concentrations following the Mt. Pinatubo volcanic eruption. Additionally, Eluszkiewicz *et al.* (1997) have used Upper Atmosphere Research Satellite (UARS) measurements to investigate the stratospheric heating rate sensitivity and the resulting residual circulation. These studies indicate a warming of the tropical lower stratosphere that is approximately consistent with observations. This heating is found to be sensitive to the presence of tropospheric clouds and to the aerosol vertical extinction profiles, which corroborates the sensitivity results of WMO (1990a). The perturbed heating in the tropics results in an upwelling and an altered circulation, a feature seen in model simulations and diagnosed from observations. Thus, the transient volcanic aerosol-induced warming has the potential to alter atmospheric dynamics and could thereby affect the surface-troposphere system (Hansen *et al.*, 1997b). Ozone depletions are obtained by the 2-D model as a result of the heterogeneous processes involving aerosols, changes in photolysis rates, and changes in the meridional circulation (Tie *et al.*, 1994). The ozone loss at high latitudes yields a cooling there (Rosenfield *et al.*, 1997), which could have contributed to the prolonged duration of the colder-than-normal temperatures in the Arctic region (Section 5.2.4; Figures 5-4 and 5-14 (top)).

Although both the El Chichón and Mt. Pinatubo eruptions have resulted in a large transient warming, these are estimated to have only a small direct effect on the decadal temperature trends in the lower stratosphere, with even smaller effects higher up. However, an indirect effect through aerosol-induced, chemically catalyzed ozone loss, and the subsequent ozone radiative feedback, can yield an enhanced global cooling trend (Solomon *et al.*, 1996). Figures 5-2 (bottom panel) and 5-3 illustrate the colder global-mean lower stratospheric temperatures now than in the pre-Pinatubo period (see also Chapter 7). Thus, the volcanic events could have had an important bearing on the lower stratospheric temperature trend observed over the decade of the 1980s and early 1990s.

Ramaswamy and Bowen (1994) show that changes in tropospheric aerosols can affect lower stratospheric temperatures. While the tropospheric aerosols assumed in that study acted to oppose the greenhouse warming in the troposphere, they enhanced the cooling in the stratosphere by reducing the upwelling thermal infrared radiation coming from a cooler troposphere. It should be noted that there is considerable uncertainty in the distribution and optical properties of aerosols; in addition, they may have a substantial effect on the optical properties of clouds (see IPCC, 1995, 1996), which would also affect the upwelling longwave flux from the troposphere. Thus, it is not possible as yet to be quantitative about the present-day tropospheric aerosols' effect on stratospheric temperatures.

### 5.3.5 Water Vapor

Stratospheric water vapor is an important radiatively active constituent, and it is expected to increase in concentration due to increased methane oxidation. It could also be influenced by changes in tropospheric water vapor concentration and changes in the transport of water vapor across the tropopause. Oltmans and Hofmann (1995) reported significant trends of 0.5%/yr in water vapor over Boulder, Colorado, from balloonsonde observations between 1981 and 1994. It is not clear whether these changes are occurring at other locations and, more important, on a global scale. Forster and Shine (1997) have used a FDH model to calculate the possible impact of these changes. At 40°N and between 15 and 20 km, the cooling due to water vapor changes exceeds 0.2 K/decade (Figure 5-23). This is much larger than the effect of changes in the well-mixed greenhouse gases at the same altitude (typically 0.1 K/decade; Figures 5-23 and 5-24); depending on the vertical profile of ozone loss adopted, the water vapor change causes a cooling of about 20-30% of the effect of the ozone change. Recent observational analyses (Nedoluha *et al.*, 1998) suggest an increase in $H_2O$ of 1-2% or more per year (between 1991 and 1996) in the middle and upper stratosphere and mesosphere. If sustained for a decade, the heating rate change would be about 0.05 K/day. Combining this with a radiative damping time of ~10 days (Fels, 1982; Kiehl and Solomon, 1986) would yield a cooling of 0.5 K/decade at 50 km. This value would be about half of that for the well-mixed greenhouse gases (Section 5.3.2; Figure 5-24), and could exceed that due to ozone change at that altitude (Section 5.3.3.2).

### 5.3.6 Other (Solar Cycle, QBO)

All the above constituent changes are essentially ones that have taken place in the stratosphere itself. External changes, such as changes in the incoming solar radiation, reflected solar radiation from the troposphere, and emitted thermal infrared radiation, can also impact stratospheric temperatures.

Changes in the output of the Sun can clearly influence the amount of UV and visible radiation absorbed by the stratosphere. In the absence of changes in ozone, WMO (1990a) radiative-convective model calculations showed that, over the course of a solar cycle, the temperature at the stratopause can vary by about 1 K, but by 20 km, the changes are less than 0.1 K. If planetary wave propagation plays a role in the way the solar cycle influences the stratosphere, as observations appear to indicate, then model simulations need to adequately account for these dynamical processes. Several numerical model simulations (Garcia *et al.*, 1984; Brasseur, 1993; Fleming *et al.* 1995; McCormack and Hood, 1996) indicate that the maximum of the solar effect should be situated at the stratopause at all latitudes, with a value of about 1.5-2 K/cycle in the tropics. Figure 5-31 illustrates results from two models for the equatorial latitudes and compares them with rocket and satellite (see also Figure 5-19) observations. The models yield amplitudes of ~2 K at the tropical stratopause. The modeled temperature change is roughly consistent with observations, although the maximum at the stratopause is not manifest in the satellite data; the same models are less successful when compared with observations at middle and high latitudes. In fact, any potential dynamical effects associated with the observed solar cycle signature (Section 5.2.6.2) are likely not being captured adequately by interactive radiative-chemical-dynamical models as yet.

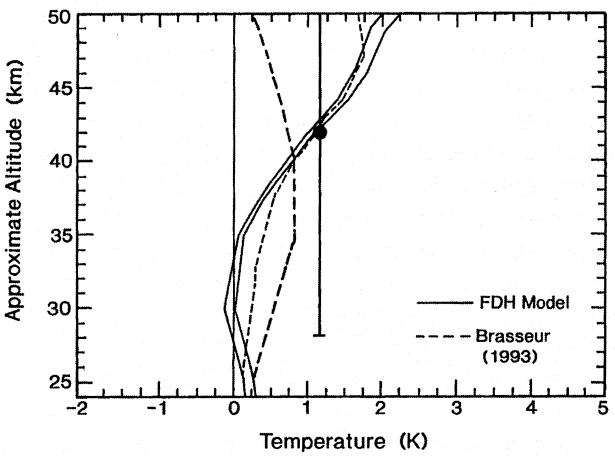


**Figure 5-31.** Comparison of low-latitude (5°N) temperature response due to solar cycle variation, as computed by two models (Brasseur, 1993; McCormack and Hood, 1996), with SSU satellite observations (thick, dashed line), and rocket data (Dunkerton *et al.*, 1998) for the altitude range ~28-55 km (vertical bar). McCormack and Hood (1996) performed two FDH calculations using the range of the observed ozone values; their model results (solid curves) are quite similar to the result of Brasseur, 1993 (thin dashed curve). (Adapted from McCormack and Hood, 1996.)

Indeed, the effect of tropospheric climate change due to changes in trace gases and aerosols, equator-to-pole tropospheric temperature gradient, waves propagating into the stratosphere, and the ensuing effects on the radiative-dynamical-chemical stratospheric equilibrium are not well understood in a quantitative manner. For example, different GCMs suggest a substantially different manner of changes in the characteristics of the planetary wave activity due to increase of $CO_2$, which would, in turn, impact the radiative-dynamical interactions and the magnitude of stratospheric temperature changes (Fels *et al.*, 1980; Fels, 1985; Rind *et al.*, 1990; Mahlman *et al.*, 1992; Graf *et al.*, 1995; Shindell *et al.*, 1998; Rind *et al.*, 1998).

### 5.4.2 Middle and Upper Stratosphere

Unlike the case for the lower stratosphere, the trends estimated from the different observational platforms for the middle and upper stratosphere are not as robust. The satellite, lidar, and rocket data, although having a consistency of pattern above ~50 hPa (e.g., Figures 5-9 and 5-12), do not exhibit the same degree of coherency that exists with respect to both magnitude and statistical significance for the different datasets of the lower stratosphere (Figures 5-5 and 5-6).

In the middle and upper stratosphere, model results suggest that the increases in the well-mixed greenhouse gases and changes in ozone will contribute to temperature changes. Figure 5-24 shows the zonal, annual-mean temperature trend due to the well-mixed greenhouse gas increases in the 1980s. The overall picture in the annual mean is one of cooling from the lower to the upper stratosphere (see also Figure 5-23). This cooling in the middle stratosphere due to the well-mixed gases can be expected to be enhanced in FDH calculations that also consider ozone losses in the middle stratosphere; the latter is estimated to yield about a 0.3 K/decade cooling using the SAGE depletion for the 1980s period (Section 5.3.3.2). The computed vertical profile bears a qualitative similarity to the observations (e.g., Figures 5-7 and 5-9) with regard to the cooling of the entire stratosphere. This reaffirms the secular cooling trend due to greenhouse gas increases inferred for the stratosphere from shorter records (WMO, 1990a,b).

However, at altitudes above the lower stratosphere, there are major quantitative differences between the modeled and observed cooling. The FDH simulated cooling increases with height when only the well-mixed gases are considered (Figure 5-24), whereas the observations indicate a rather uniform trend between 20 and 35 km (with perhaps even a slight reduction at ~30-35 km; see Figure 5A and Figures 5-7 to 5-12). It must be noted here that the GCM's simulation of the effects due to ozone loss involve a dynamical change (not evident in FDH) that causes some warming above the location of the cooling in the lower stratosphere (Section 5.3.3.1 and Figure 5-28). This GCM-simulated warming, which may not be statistically significant, occurs mainly in winter/spring and is qualitatively consistent with observations during that season (Figures 5-15 and 5-16). Consideration of this warming could retard somewhat the rapid increase of the well-mixed greenhouse gas-induced cooling with height seen in Figure 5-24 (e.g., above 25 km) and enable a full radiative-dynamical (i.e., GCM) computation to become more consistent with observations than the FDH results.

Additionally, the magnitude of the modeled cooling in the upper stratosphere is less than that observed; e.g., at ~45 km, the modeled cooling is about 1 K/decade due to the well-mixed greenhouse gases and about 0.3 K/decade due to ozone, while the observed cooling is greater than 1.5 K/decade (e.g., at 45 km in Figure 5A). Some of this bias could be due to water vapor, whose decadal trend in the 1980s globally is not known. Recent satellite data suggest an upward trend over the past 5 years, which would add to the cooling trend computed for the upper stratosphere (Section 5.3.5) and reduce the present discrepancy.

The vertical and latitudinal magnitude of the cooling, and likewise the location of the warming region above the cooling in the lower stratosphere, are very sensitive to the vertical profile of ozone depletion imposed in the model. The models invariably locate the cooling at exactly the region of the imposed ozone loss, with a warming immediately above it at the higher latitudes. Thus, any shift of the altitude extent of ozone depletion in the model has the potential to shift the peak cooling, and thus alter the vertical profile of the computed cooling trend. In turn, this affects the quantitative inferences about the consistency between computed and observed temperature trends in the middle and upper stratosphere.

### 5.4.3 Upper Troposphere

The cooling of the lower stratosphere in response to ozone losses there also leads to a cooling below the ozone loss region in the global upper troposphere (~10-14 km), in part due to reduced infrared emission from the stratosphere (Ramanathan and Dickinson, 1979). The cooling of the lower stratosphere also impacts the forcing of the troposphere (WMO, 1992, 1995; Chapter 10). Specifically, an ozone-induced cooling of the lower stratosphere implies a reduction in the longwave radiative emission from the stratosphere into the troposphere. This leads to a negative radiative forcing of the surface-troposphere system (Hansen *et al.*, 1997a). In general, GCMs simulating the effects of stratospheric ozone loss indicate a cooling of the upper troposphere (see Figures 5-25, 5-27, and 5-28).

All modeling efforts that have considered appropriate changes in trace gases yield a cooling of the tropopause region (e.g., Hansen *et al.*, 1995; see also Figure 5-27; Vinnikov *et al.*, 1996; Santer *et al.*, 1996; Hansen *et al.*, 1997a). Here, again, the lower stratospheric ozone depletion effects dominate over all other gases including $CO_2$. Further, the vertical profile of changes in ozone critically determines the profile of the temperature change in the upper troposphere.

A difficulty arises in comparing simulated upper tropospheric temperature changes due to ozone losses with observations over the past decade, as the "signal" from models (see Figures 5-27, and 5-28) is quite small, less so than that in the lower stratosphere (say, at 50 hPa or ~20 km). It may be noted that the modeled upper tropospheric changes, even for as a large a forcing as a doubling of $CO_2$, are generally small compared with those in the lower troposphere or higher in the stratosphere (Vinnikov *et al.*, 1996). It is difficult at present to interpret the small change in the upper tropospheric temperatures inferred from observations in terms of a change originating primarily from the stratosphere (e.g., lower stratospheric ozone loss) or one arising in the troposphere (e.g., tropospheric ozone chemistry). Further, the halocarbon-induced depletion of ozone in the lower stratosphere can also be expected to affect upper tropospheric ozone through a downward transport of the anomalies, thereby contributing to a cooling of the upper troposphere.

In general, the temperature changes near the tropopause have the potential to affect the water vapor distribution and cloudiness, especially cirrus clouds, which in turn can cause feedback effects in the climate system. One example available from observations of the effects in the upper troposphere due to a stratospheric perturbation concerns the aftermath of the Mt. Pinatubo eruption. Lidar and other observations (Sassen *et al.*, 1995) suggest that the aerosols from this volcanic eruption affected cirrus (ice) cloud formations near the tropopause.

The interactions between trace species' changes and the associated chemistry, microphysics, radiation, and dynamics remain to be more thoroughly explored, both from modeling and observational perspectives, taking into account the three-dimensional nature of the problem (Holton *et al.*, 1995). Meteorological parameters such as tropopause location (Schubert and Munteanu, 1988; Hoinka *et al.*, 1998a), temperature, and geopotential height (Ohring and Muench, 1960; Spankuch and Schulz, 1995) tend to be highly correlated to total ozone. They can, therefore, be expected to exhibit changes owing to trends in ozone. At this time, such changes are not well documented (Section 5.2.7). There is growing evidence of a connection between variability and trends in the stratosphere with those in the troposphere (e.g., Kodera *et al.*, 1990; Kitoh *et al.*, 1996; Perlwitz and Graf, 1995). As noted earlier, Thompson and Wallace (1998) show a connection between the trend in winter-mean NH surface temperature and pressure and the trend in polar vortex strength. Such linkages inferred from observations emphasize that the radiative-chemical-dynamical interactions, which couple the stratospheric and tropospheric processes, need to be fully accounted for in order to attribute the observed temperature variations and trends to well-defined mechanisms that include changes in trace species.

## REFERENCES

Angell, J.K., The close relation between Antarctic total-ozone depletion and cooling of the Antarctic low stratosphere, *Geophys. Res. Lett.*, *13*, 1240-1243, 1986.

Angell, J.K., Variations and trends in tropospheric and stratospheric global temperatures, *J. Clim.*, *1*, 1296-1313, 1988.

Angell, J.K., Changes in tropospheric and stratospheric global temperatures, 1958-1988, in *Greenhouse-Gas-Induced Climatic Change: A Critical Appraisal of Simulations and Observations*, edited by M. E. Schlesinger, pp. 231-247, Elsevier, Amsterdam, 1991a.

Angell, J.K., Stratospheric temperature change as a function of height and sunspot number during 1972-89 based on rocketsonde and radiosonde data, *J. Clim.*, *4*, 1170-1180, 1991b.

Angell, J.K., Comparisons of stratospheric warming following Agung, El Chichón, and Pinatubo volcanic eruptions, *Geophys. Res. Lett.*, *20*, 715-718, 1993.

Angell, J.K., Stratospheric warming due to Agung, El Chichón, and Pinatubo taking into account the quasi-biennial oscillation, *J. Geophys. Res.*, *102*, 9479-9485, 1997.

Austin, J., N. Butchart, and K.P. Shine, Probability of an Arctic ozone hole in a doubled $CO_2$ climate, *Nature*, *360*, 221-225, 1992.

Bailey, M.J., A. O'Neill, and V.D. Pope, Stratospheric analyses produced by the United Kingdom Meteorological Office, *J. Appl. Meteorol.*, *32*, 1472-1483, 1993.

Balachandran, N.K., and D. Rind, Modeling the effects of solar variability and the QBO on the troposphere/stratosphere system: Part I, The middle atmosphere, *J. Clim.*, *8*, 2058-2079, 1995.

Baldwin, M.P., and T.J. Dunkerton, Biennial, quasi-biennial, and decadal oscillations of potential vorticity in the northern stratosphere, *J. Geophys. Res.*, *103*, 3919-3928, 1998a.

Baldwin, M.P., and T.J. Dunkerton, Quasi-biennial modulation of the southern hemisphere stratospheric polar vortex, *Geophys. Res. Lett.*, in press, 1998b.

Baldwin, M.P., X. Cheng, and T.J. Dunkerton, Observed correlation between winter-mean tropospheric and stratospheric anomalies, *Geophys. Res. Lett.*, *21*, 1141-1144, 1994.

Berntsen, T., I.S.A. Isaksen, G. Myrhe, J.S. Fuglestvedt, F. Stordal, T.A. Larsen, R.S. Freckleton, and K.P. Shine, Effects of anthropogenic emissions on tropospheric ozone and its radiative forcing, *J. Geophys. Res.*, *102*, 28101-28126, 1997.

Bojkov, R., and V.E. Fioletov, Estimating the global ozone characteristics during the last 30 years, *J. Geophys. Res.*, *100*, 16537-16551, 1995.

Bojkov, R., and V.E. Fioletov, Changes of the lower stratospheric ozone over Europe and Canada, *J. Geophys. Res.*, *102*, 1337-1347, 1997.

Brasseur, G., The response of the middle atmosphere to long-term and short-term solar variability: A two-dimensional model, *J. Geophys. Res.*, *98*, 23079-23090, 1993.

Brasseur, G., and C. Granier, Mt. Pinatubo aerosols, chlorofluorocarbons and ozone depletion, *Science*, *258*, 1239-1242, 1992.

Brühl, C., and P. Crutzen, Scenarios of possible changes in atmospheric temperatures and ozone concentrations due to man's activities, estimated with a one-dimensional coupled photochemical climate model, *Clim. Dyn.*, *2*, 173-203, 1988.

Butchart, N., and J. Austin, On the relationship between the quasi-biennial oscillation, total chlorine and the severity of the Antarctic ozone hole, *Quart. J. Roy. Meteorol. Soc.*, *122*, 183-217, 1996.

Cariolle, D., A. Lasserre-Bigorry, J.-F. Royer, and J.F. Geleyn, A GCM simulation of the springtime Antarctic decrease and its impact on midlatitudes, *J. Geophys. Res.*, *95*, 1883-1898, 1990.

Chanin, M.-L., Long term trend in the middle atmosphere temperature, in *The Role of the Stratosphere in Global Change*, NATO ASI Series I, Vol. 8, edited by M.-L. Chanin, pp. 301-317, Springer-Verlag, Berlin, 1993.

Chanin, M.-L., and P. Keckhut, Influence on the middle atmosphere of the 27-day and 11-year solar cycles: Radiative and/or dynamical forcing? *J. Geomagn. Geoelectr.*, *43*, 647-655, 1991.

Chipperfield, M.P., and J.A. Pyle, Two-dimensional modelling of the Antarctic lower stratosphere, *Geophys. Res. Lett.*, *15*, 875-878, 1988.

Christiansen, B., A. Guldberg, A.W. Hansen, and L.P. Riishojgaard, On the response of a three-dimensional general circulation model to imposed changes in the ozone distribution, *J. Geophys. Res.*, *102*, 13051-13077, 1997.

Christy, J.R., Temperature above the surface layer, *Clim. Change*, *31*, 455-474, 1995.

Christy, J.R., and S.J. Drouilhet, Variability in daily, zonal-mean lower stratospheric temperatures, *J. Clim.*, *7*, 106-120, 1994.

Christy, J.R., R.W. Spencer, and R.T. McNider, Reducing noise in the daily MSU lower tropospheric temperature dataset, *J. Clim.*, *8*, 888-896, 1995.

Chubachi, S., On the cooling of stratospheric temperatures at Syowa, Antarctica, *Geophys. Res. Lett.*, *13*, 1221-1223, 1986.

Coy, L., E.R. Nash, and P.A. Newman, Meteorology of the polar vortex: Spring 1997, *Geophys. Res. Lett.*, *24*, 2693-2696, 1997.

Cunnold, D.M., H. Wang, W. Chu, and L. Froidevaux, Comparisons between SAGE II and MLS ozone measurements and aliasing of SAGE II ozone trends in the lower stratosphere, *J. Geophy. Res.*, *101*, 10061-10075, 1996a.

Cunnold, D.M., L. Froidevaux, J. Russell, B. Connor, and A. Roche, An overview of UARS ozone validation based primarily on intercomparisons among UARS and SAGE II measurements, *J. Geophy. Res.*, *101*, 10335-10350, 1996b.

Donnelly, R.F., H.E. Hinterreger, and D.F. Heath, Temporal variation of solar EUV, UV, and 10830-Å radiations, *J. Geophy. Res.*, *91*, 5567-5578, 1986.

Dunkerton, T.J., and M.P. Baldwin, Modes of interannual variability in the stratosphere, *Geophys. Res. Lett.*, *19*, 49-52, 1992.

Dunkerton T.J., and D.P. Delisi, Climatology of the equatorial lower stratosphere: An observational study, *J. Atmos. Sci.*, *42*, 376-396, 1985.

Dunkerton, T., D. Delisi, and M. Baldwin, Examination of middle atmosphere cooling trend in historical rocketsonde data, *Geophys. Res. Lett.*, submitted, 1998.

Efron, B., *The Jackknife, The Bootstrap, and Other Resampling Plans*, 92 pp., Society for Industrial and Applied Mathematics (SIAM), Philadelphia, Pa., 1982.

Elliott, W.P., and D.J. Gaffen, On the utility of radiosonde humidity archives for climate studies, *Bull. Amer. Meteorol. Soc.*, *72*, 1507-1520, 1991.

Elliott, W.P., D.J. Gaffen, J.D. Kahl, and J.K. Angell, The effect of moisture on layer thicknesses used to monitor global temperatures, *J. Clim.*, *7*, 304-308, 1994.

Eluszkiewicz, J., D. Crisp, R.G. Grainger, A. Lambert, A.E. Roche, J. B. Kumer, and J.L. Mergenthaler, Sensitivity of the residual circulation diagnosed from UARS data to the uncertainties in the input fields and to the inclusion of aerosols, *J. Atmos. Sci.*, *54*, 1739-1757, 1997.

Fels, S.B., A parameterization of scale-dependent radiative damping rates in the middle atmosphere, *J. Atmos. Sci.*, *39*, 1141-1152, 1982.

Fels, S.B., Radiative-dynamical interactions in the middle atmosphere, *Adv. Geophys.*, *28A*, 277-300, 1985.

Fels, S.B., and L.D. Kaplan, A test of the role of longwave radiative transfer in a general circulation model, *J. Atmos. Sci.*, *33*, 779-789, 1975.

Fels, S.B., J.D. Mahlman, M.D. Schwarzkopf, and R.W. Sinclair, Stratospheric sensitivity to perturbations in ozone and carbon dioxide: Radiative and dynamical response, *J. Atmos. Sci.*, *37*, 2265-2297, 1980.

Finger, F.G., M.E. Gelman, J.D. Wild, M.-L. Chanin, A. Hauchecorne, and A.J. Miller, Evaluation of NMC upper-stratospheric temperature analyses using rocketsonde and lidar data, *Bull. Amer. Meteorol. Soc.*, *74*, 789-799, 1993.

Fleming, E., S. Chandra, C.H. Jackman, D.B. Considine, and A.R. Douglass, The middle atmosphere response to short and long term solar UV variations: Analysis of observations and 2D model results, *J. Atmos. Terr. Phys.*, *57*, 333-365, 1995.

Folland, C.K., D.M.H. Sexton, D.J. Karoly, C.E. Johnson, D.P. Rowell, and D.E. Parker, Influence of anthropogenic and oceanic forcing on recent climate change, *Geophys. Res. Lett.*, *25*, 353-356, 1998.

Forster, P., and K.P. Shine, Radiative forcing and temperature trends from stratospheric ozone changes, *J. Geophys. Res.*, *102*, 10841-10855, 1997.

Forster, P., R.S. Freckleton, and K.P. Shine, On aspects of the concept of radiative forcing, *Clim. Dyn.*, *13*, 547-560, 1997.

Fortuin, J.P.F., and H. Kelder, Possible links between ozone and temperature profiles, *Geophys. Res. Lett.*, *23*, 1517-1520, 1996.

Gaffen, D.J., Temporal inhomogeneities in radiosonde temperature records, *J. Geophys. Res.*, *99*, 3667-3676, 1994.

Gaffen, D.J., *A Digitized Metadata Set of Global Upper-Air Station Histories*, NOAA Tech. Memo. ERL-ARL 211, 38 pp., National Oceanic and Atmospheric Administration, Silver Spring, Md., 1996.

Garcia, R.R., S. Solomon, R.G. Roble, and D.W. Rusch, A numerical study of the response of the middle atmosphere to the 11-year solar cycle, *Planet. Space Sci.*, *32*, 411-423, 1984.

Gelman, M.E., A.J. Miller, K.W. Johnson, and R.M. Nagatani, Detection of long-term trends in global stratospheric temperature from NMC analyses derived from NOAA satellite data, *Adv. Space Res.*, *6*, 17-26, 1986.

Gelman, M.E., A.J. Miller, R.M. Nagatani, and H.D. Bowman III, Use of UARS data in the NOAA stratospheric monitoring program, *Adv. Space Res.*, *14*, 21-31, 1994.

Gille, S.T., A. Hauchecorne, and M.-L. Chanin, Semidiurnal and diurnal tide effects in the middle atmosphere as seen by Rayleigh lidar, *J. Geophys. Res.*, 96, 7579-7587, 1991.

Golitsyn, G.S., A.I. Semenov, N.N. Shefov, L.M. Fishkova, E.V. Lysenko, and S.P. Perov, Long-term temperature trends in the middle and upper atmosphere, *Geophys. Res. Lett.*, *23*, 1741-1744, 1996.

Goody, R.M., and Y.L. Yung, *Atmospheric Radiation*, pp. 388-425, Oxford University Press, Oxford, U.K., 1989.

Graf, H.-F., J. Perlwitz, I. Kirchner, and I. Schult, Recent northern winter climate trends, ozone changes and increased greenhouse gas forcing, *Contrib. Atmos. Phys.*, *68*, 233-248, 1995.

Graham, N.E., Simulation of recent global temperature trends, *Science*, *267*, 666-671, 1995.

Haigh, J., The impact of solar variability on climate, *Science*, *272*, 981-984, 1996.

Haigh, J., A GCM study of climate change in response to the 11-year solar cycle, *Quart. J. Roy. Meteorol. Soc.*, in press, 1998.

Halpert, M.S., and G.D. Bell, Climate assessment for 1996, *Bull. Amer. Meteorol. Soc.*, *78*, S1-S49, 1997.

Hamilton, K., R.J. Wilson, J.D. Mahlman, and L.J. Umscheid, Climatology of the GFDL SKYHI troposphere-stratosphere-mesosphere general circulation model, *J. Atmos. Sci.*, *52*, 5-43, 1995.

Hansen, J., and H. Wilson, Commentary on the significance of global temperature records, *Clim. Change*, *25*, 185-191, 1993.

Hansen, J.E., W.-C. Wang, and A.A. Lacis, Mt. Agung provides test of a global climate perturbation, *Science*, *199*, 1065-1068, 1978.

Hansen, J., A. Lacis, R. Ruedy, M. Sato, and H. Wilson, How sensitive is the world's climate? *Natl. Geogr. Res. Explor.*, *9*, 142-158, 1993.

Hansen, J.E., H. Wilson, M. Sato, R. Ruedy, K. Shah, and E. Hansen, Satellite and surface temperature data at odds? *Clim. Change*, *30*, 103-117, 1995.

Hansen, J.E., M. Sato, and R. Ruedy, Radiative forcing and climate response, *J. Geophys. Res.*, *102*, 6831-6864, 1997a.

Hansen, J., M. Sato, R. Ruedy, A. Lacis, K. Asamoah, K. Beckford, S. Borenstein, E. Brown, B. Cairns, B. Carlson, B. Curran, S. de Castro, L. Druyan, P. Etwarrow, T. Ferede, M. Fox, D. Gaffen, J. Glascoe, H. Gordon, S. Hollandsworth, X. Jiang, C. Johnson, N. Lawrence, J. Lean, J. Lerner, K. Lo, J. Logan, A. Luckett, M.P. McCormick, R. McPeters, R. Miller, P. Minnis, I. Ramberan, G. Russell, P. Russell, P. Stone, I. Tegen, S. Thomas, L. Thomason, A. Thompson, J. Wilder, R. Willson, and J. Zawodny, Forcings and chaos in interannual to decadal climate change, *J. Geophys. Res.*, *102*, 25679-25720, 1997b.

Harshvardhan, Perturbation of the zonal radiation balance by a stratospheric aerosol layer, *J. Atmos. Sci.*, *36*, 1274-1285, 1979.

Hauchecorne, A., M.-L. Chanin, and P. Keckhut, Climatology and trends of the middle atmospheric temperature (33-87 km) as seen by Rayleigh lidar over the south of France, *J. Geophys. Res.*, *96*, 15297-15309, 1991.

Hoinka, K.P., Statistics of the global tropopause, *Mon. Wea. Rev.*, in press, 1998a.

Hoinka, K.P., Temperature, humidity and wind at the global tropopause, *Mon. Wea. Rev.*, submitted, 1998b.

Holton, J.R., and H.-C. Tan, The influence of the equatorial quasi-biennial oscillation on the global circulation at 50 mb, *J. Atmos. Sci.*, *37*, 2200-2208, 1980.

Holton, J.R., and H.-C. Tan, The quasi-biennial oscillation in the Northern Hemisphere lower stratosphere, *J. Meteorol. Soc. Japan*, *60*, 140-148, 1982.

Holton, J.R., P.H. Haynes, M.E. McIntyre, A.R. Douglass, R.B. Rood, and L. Pfister, Stratosphere-troposphere exchange, *Rev. Geophys.*, *33*, 403-439, 1995.

Hood, L.L., J. L. Jirikowic, and J.P. McCormack, Quasi-decadal variability of the stratosphere: Influence of long-term solar ultraviolet variations, *J. Atmos. Sci.*, *50*, 3941-3958, 1993.

Huovila, S., and A. Tuominen, *On the Influence of Radiosonde Lag Error on Upper-Air Climatological Data in Finland 1951-1988*, Meteorological Publications, No. 14, 29 pp., Finnish Meteorological Institute, Helsinki, 1990.

IPCC (Intergovernmental Panel on Climate Change), *Climate Change 1994: Radiative Forcing of Climate Change and An Evaluation of the IPCC IS92 Emission Scenarios*, edited by J.T. Houghton, L.G. Meira Filho, J. Bruce, H. Lee, B.A. Callander, E. Haites, N. Harris, and K. Maskell, 339 pp., Cambridge University Press, Cambridge, U.K., 1995.

IPCC (Intergovernmental Panel on Climate Change), *Climate Change 1995: The Science of Climate Change*, edited by J.T. Houghton, L.G. Meira Filho, B.A. Callander, N. Harris, A. Kattenberg, and K. Maskell, 572 pp., Cambridge University Press, Cambridge, U.K., 1996.

Jones, A.E., and J.D. Shanklin, Continued decline of total ozone over Halley, Antarctica, since 1985, *Nature*, *376*, 409-411, 1995.

Jones, P.D., Recent warming in global temperature series, *Geophys. Res. Lett.*, *21*, 1149-1152, 1994.

Kalnay, E., M. Kanamitsu, R. Kistler, W. Collins, D. Deaven, L. Gandin, M. Iredell, S. Saha, G. White, J. Woollen, Y. Zhu, M. Chelliah, W. Ebisuzaki, W. Higgins, J. Janowiak, K.C. Mo, C. Ropelewski, J. Wang, A. Leetmaa, R. Reynolds, R. Jenne, and D. Joseph, The NCEP/NCAR 40-year reanalysis project, *Bull. Amer. Meteorol. Soc.*, *77*, 437-471, 1996.

Karl, T.R., V.E. Derr, D.R. Easterling, C.K. Folland, D.J. Hofmann, S. Levitus, N. Nicholls, D.E. Parker, and G.W. Withee, Critical issues for long-term climate monitoring, *Clim. Change*, *31*, 185-221, 1995.

Keckhut, P., A. Hauchecorne, and M.-L. Chanin, Midlatitude long-term variability of the middle atmosphere: Trends and cyclic and episodic changes, *J. Geophys. Res.*, *100*, 18887-18897, 1995.

Keckhut, P., M.E. Gelman, J.D. Wild, F. Tissot, A.J. Miller, A. Hauchecorne, M.-L. Chanin, E.F. Fishbein, J. Gille, J.M. Russell III, and F.W. Taylor, Semidiurnal and diurnal temperature tides (30-55 km): Climatology and effect on UARS lidar data comparisons, *J. Geophys. Res.*, *101*, 10299-10310, 1996.

Keckhut P., F.J. Schmidlin, A. Hauchecorne, and M.-L. Chanin, Trend estimates from rocketsondes at low latitude station (8S-34N), taking into account instrumental changes and natural variability, *J. Atmos. Solar-Terr. Phys.*, in press, 1998.

Kiehl, J.T., and B.A. Boville, The radiative-dynamical response of a stratospheric-tropospheric general circulation model to changes in ozone, *J. Atmos. Sci.*, *45*, 1798-1817, 1988.

Kiehl, J.T., and S. Solomon, On the radiative balance of the stratosphere, *J. Atmos. Sci.*, *43*, 1525-1534, 1986.

Kiehl, J.T., B.A. Boville, and B.P. Briegleb, Response of a general circulation model to a prescribed Antarctic ozone hole, *Nature*, *332*, 501-504, 1988.

Kitoh, A., H. Koide, K. Kodera, S. Yukimoto, and A. Noda, Interannual variability in the stratospheric-tropospheric circulation in a coupled ocean-atmosphere GCM, *Geophys. Res. Lett.*, *23*, 543-546, 1996.

Kodera, K., and K. Yamazaki, Long-term variation of upper stratospheric circulation in the Northern Hemisphere in December, *J. Meteorol. Soc. Japan*, *68*, 101-105, 1990.

Kodera, K., K. Yamazaki, M. Chiba, and K. Shibata, Downward propagation of upper stratospheric mean zonal wind perturbation to the troposphere, *Geophys. Res. Lett.*, *17*, 1263-1266, 1990.

Kokin, G.A., and E.V. Lysenko, On temperature trends of the atmosphere from rocket and radiosonde data, *J. Atmos. Terr. Phys.*, *56*, 1035-1044, 1994.

Kokin, G.A., E.V. Lysenko, and S.K. Rozenfeld, Temperature changes in the stratosphere and mesosphere in 1964-1988 based on rocket sounding data, *Izv. Atmos. Oceanic Phys.*, *26*, 518-523, 1990.

Komuro, H., Long-term cooling in the stratosphere observed by aerological rockets at Ryori, Japan, *J. Meteorol. Soc. Japan*, *67*, 1081-1082, 1989.

Koshelkov, Yu P., and G.R. Zakharov, On temperature trends in the Arctic lower stratosphere, *Meteorol. Gidrol.*, in press, 1998.

Labitzke, K., and M.P. McCormick, Stratospheric temperature increases due to Pinatubo aerosols, *Geophys. Res. Lett.*, *19*, 207-210, 1992.

Labitzke, K., and H. van Loon, Association between the 11-year solar cycle, the QBO and the atmosphere: Part I, The troposphere and stratosphere in the northern hemisphere in winter, *J. Atmos. Terr. Phys.*, *50*, 197-206, 1988.

Labitzke, K., and H. van Loon, The 11-year solar cycle in the stratosphere in the northern summer, *Ann. Geophys.*, *7*, 595-598, 1989.

Labitzke, K., and H. van Loon, On the association between the QBO and the extratropical stratosphere, *J. Atmos. Terr. Phys.*, *54*, 1453-1463, 1992.

Labitzke, K., and H. van Loon, Trends of temperature and geopotential height between 100 and 10 hPa in the Northern Hemisphere, *J. Meteorol. Soc. Japan*, *72*, 643-652, 1994.

Labitzke, K., and H. van Loon, A note on the distribution of trends below 10hPa: The extratropical northern hemisphere, *J. Meteorol. Soc. Japan*, *73*, 883-889, 1995.

Labitzke, K., and H. van Loon, The signal of the 11-year sunspot cycle in the upper troposphere-lower stratosphere, *Space Sci. Rev.*, *80*, 393-410, 1997.

Lacis, A.A., D.J. Wuebbles, and J.A. Logan, Radiative forcing of climate by changes in the vertical distribution of ozone, *J. Geophys. Res.*, *95*, 9971-9981, 1990.

Lait, L.R., M.R. Schoeberl, and P.A. Newman, Quasi-biennial modulation of Antarctic ozone depletion, *J. Geophys. Res.*, *94*, 11559-11571, 1989.

Luers, J.K., Estimating the temperature error of the radiosonde rod thermistor under different environments, *J. Atmos. Oceanic Technol.*, *7*, 882-895, 1990.

Lysenko, E.V., G. Nelidova, and A. Prostova, Changes in the stratospheric and mesospheric thermal conditions during the last 3 decades: 1, The evolution of a temperature trend, *Izv. Atmos. Oceanic Phys.*, *33*, 218-225, 1997.

Mahlman, J.D., A looming Arctic ozone hole? *Nature*, *360*, 209, 1992.

Mahlman, J.D., J.P. Pinto, and L.J. Umscheid, Transport, radiative, and dynamical effects of the Antarctic ozone hole: A GFDL "SKYHI" model experiment, *J. Atmos. Sci.*, *51*, 489-508, 1994.

Manabe, S., and R.T. Wetherald, Thermal equilibrium of the atmosphere with a given distribution of relative humidity, *J. Atmos. Sci.*, *24*, 241-259, 1967.

Manney, G.L., R. Swinbank, S.T. Massie, M.E. Gelman, A.J. Miller, R. Nagatani, A. O'Neill, and R.W. Zurek, Comparison of U.K. Meteorological Office and U.S. National Meteorological Center stratospheric analyses during northern and southern winter, *J. Geophys. Res.*, *101*, 10311-10334, 1996.

McCormack, J.P., and L.L. Hood, Relationship between ozone and temperature trends in the lower stratosphere: Latitude and seasonal dependencies, *Geophys. Res. Lett.*, *21*, 1615-1618, 1994.

McCormack, J.P., and L.L. Hood, Apparent solar cycle variations of upper stratospheric ozone and temperature: Latitudinal and seasonal dependencies, *J. Geophys. Res.*, *101*, 20933-20944, 1996.

McCormick, M.P., L.W. Thomason, and C.R. Trepte, Atmospheric effects of the Mt. Pinatubo eruption, *Nature*, *373*, 399-404, 1995.

Miller, A.J., R.M. Nagatani, G.C. Tiao, X.F. Niu, G.C. Reinsel, D. Wuebbles, and K. Grant, Comparisons of observed ozone and temperature trends in the lower stratosphere, *Geophys. Res. Lett.*, *19*, 929-932, 1992.

Mohanakumar, K., Solar activity forcing of the middle atmosphere, *Ann. Geophys.*, *13*, 879-885, 1995.

Nash, J., and G.F. Forrester, Long-term monitoring of stratospheric temperature trends using radiance measurements obtained by the TIROS-N series of NOAA spacecraft, *Adv. Space Res.*, *6*, 37-44, 1986.

Naujokat, B., An update of the observed quasi-biennial oscillation of the stratospheric winds over the tropics, *J. Atmos. Sci.*, *43*, 1873-1877, 1986.

Naujokat, B., and S. Pawson, The cold stratospheric winters 1994/95 and 1995/96, *Geophys. Res. Lett.*, *23*, 3703-3706, 1996.

Nedoluha, G.E., R.M. Bevilacqua, R.M. Gomez, D.E. Siskind, and B.C. Hicks, Increases in middle atmospheric water vapor as observed by the Halogen Occultation Experiment and the ground-based water vapor millimeter-wave spectrometer from 1991 to 1997, *J. Geophys. Res.*, *103*, 3531-3543, 1998.

Newman, P.A., and W.J. Randel, Coherent, ozone-dynamical changes during the Southern Hemisphere spring, 1979-1986, *J. Geophys. Res.*, *93*, 12585-12606, 1988.

Newman, P., J. Gleason, R.D. McPeters, and R. Stolarski, Anomalously low ozone over the Arctic, *Geophys. Res. Lett.*, *24*, 2689-2692, 1997.

Ohring, G., and H.S. Muench, Relationship between ozone and meteorological parameters in the lower stratosphere, *J. Meteorol.*, *17*, 195-206, 1960.

Oltmans, S., and D. Hofmann, Increase in lower stratospheric water vapor at midlatitude northern hemisphere, *Nature*, *374*, 146-149, 1995.

Oort, A.H., and H. Liu, Upper-air temperature trends over the globe, 1956-1989, *J. Clim.*, *6*, 292-307, 1993.

Pan, Y.H., and A.H. Oort, Global climate variations connected with sea surface temperature anomalies in the eastern equatorial Pacific Ocean for the 1958-1973 period, *Mon. Wea. Rev.*, *111*, 1244-1258, 1983.

Parker, D.E., On the detection of temperature changes induced by increasing atmospheric carbon dioxide, *Quart. J. Roy. Meteorol. Soc.*, *111*, 587-601, 1985.

Parker, D.E., and D.I. Cox, Towards a consistent global climatological rawindsonde data-base, *Intl. J. Climatol.*, *15*, 473-496, 1995.

Parker, D.E., M. Gordon, D.P.N. Cullum, D.M.H. Sexton, C.K. Folland, and N. Rayner, A new global gridded radiosonde temperature data base and recalculated temperature trends, *Geophys. Res. Lett.*, *24*, 1499-1502, 1997.

Pawson, S., and B. Naujokat, Trends in daily wintertime temperatures in the northern stratosphere, *Geophys. Res. Lett.*, *24*, 575-578, 1997.

Perlwitz, J., and H.F. Graf, The statistical connection between tropospheric and stratospheric circulation of the northern hemisphere in winter, *J. Clim.*, *8*, 2281-2295, 1995.

Pinnock, S., M.D. Hurley, K.P. Shine, T.J. Wallington, and T.J. Smyth, Radiative forcing by hydrochlorofluorocarbons and hydrofluorocarbons, *J. Geophys. Res.*, *100*, 23227-23238, 1995.

Pitari, G., M. Verdecchia, and G. Visconti, A transformed Eulerian model to study possible effects of the El Chichón eruption on stratospheric circulation, *J. Geophys. Res.*, *92*, 10961-10975, 1987.

Pollack, J., and T. Ackerman, Possible effects of the El Chichón cloud on the radiation budget of the northern tropics, *Geophys. Res. Lett.*, *10*, 1057-1060, 1983.

Prather, M.J., M.M. Garcia, R. Suozzo, and D. Rind, Global impact of the Antarctic ozone hole: Dynamical dilution with a three-dimensional chemical transport model, *J. Geophys. Res.*, *95*, 3449-3471, 1990.

Ramanathan, V., The role of ocean-atmosphere interactions in the $CO_2$ climate problem, *J. Atmos. Sci.*, *38*, 918-930, 1981.

Ramanathan, V., and R.E. Dickinson, The role of stratospheric ozone in the zonal and seasonal radiative energy balance of the Earth-troposphere system, *J. Atmos. Sci.*, *36*, 1084-1104, 1979.

Ramanathan, V., R.J. Cicerone, H.B. Singh, and J.T. Kiehl, Trace gas trends and their potential role in climate change, *J. Geophys. Res.*, *90*, 5547-5566, 1985.

Ramaswamy, V., and M.M. Bowen, Effect of changes in radiatively active species upon the lower stratospheric temperatures, *J. Geophys. Res.*, *99*, 18909-18921, 1994.

Ramaswamy, V., M.D. Schwarzkopf, and K.P. Shine, Radiative forcing of climate from halocarbon-induced global stratospheric ozone loss, *Nature*, *355*, 810-812, 1992.

Ramaswamy, V., M.D. Schwarzkopf, and W. Randel, Fingerprint of ozone depletion in the spatial and temporal pattern of recent lower-stratospheric cooling, *Nature*, *382*, 616-618, 1996.

Randel, W.J., The anomalous circulation in the Southern Hemisphere stratosphere during spring 1987, *Geophys. Res. Lett.*, *15*, 911-914, 1988.

Randel, W.J., and J.B. Cobb, Coherent variations of monthly mean total ozone and lower stratospheric temperature, *J. Geophys. Res.*, *99*, 5433-5447, 1994.

Randel, W.J., and F. Wu, Cooling of the Arctic and Antarctic polar stratospheres due to ozone depletion, *J. Clim.*, in press, 1998.

Randel, W.J., F. Wu, J.M. Russell III, J.W. Waters, and L. Froidevaux, Ozone and temperature changes in the stratosphere following the eruption of Mt. Pinatubo, *J. Geophys. Res.*, *100*, 16753-16764, 1995.

Randel, W.J., F. Wu, R. Swinbank, J. Nash, and A. O'Neill, Global QBO circulation derived from UKMO stratospheric analyses, *J. Atmos. Sci.*, in press, 1998.

Reid, G.C., Seasonal and interannual temperature variations in the tropical stratosphere, *J. Geophys. Res.*, *99*, 18923-18932, 1994.

Reid, G.C., K.S. Gage, and J.R. McAfee, The thermal response of the tropical atmosphere to variations in equatorial Pacific sea surface temperature, *J. Geophys. Res.*, *94*, 14705-14716, 1989.

Rind, D., R. Suozzo, N. Balachandran, and M. Prather, Climate change and the middle atmosphere: Part I, The doubled $CO_2$ climate, *J. Atmos. Sci.*, *4*, 475-494, 1990.

# CHAPTER 6

# Upper Stratospheric Processes

**Lead Authors:**
R. Müller
R.J. Salawitch

**Coauthors:**
P.J. Crutzen
W.A. Lahoz
G.L. Manney
R. Toumi

**Contributors:**
D.B. Considine
S.J. Evans
J.-U. Grooß
C.H. Jackman
K.W. Jucks
D.E. Kinnison
A.J. Miller
G.A. Morris
G.E. Nedoluha
C.D. Nevison
W.J. Randel
A.R. Ravishankara
J.M. Russell III
K.H. Sage
M.L. Santee
D.E. Siskind
M.E. Summers
J. Trentmann
R.H.J. Wang
J.R. Ziemke

# CHAPTER 6

## UPPER STRATOSPHERIC PROCESSES

### Contents

## SCIENTIFIC SUMMARY

Since the previous Assessment (WMO, 1995), an improved understanding of upper stratospheric processes has been gained through numerous atmospheric observations that have better defined long-term changes in ozone and better constrained our understanding of reactive hydrogen, nitrogen, and chlorine gases. The original hypothesis put forth in 1974 that a release of industrial chlorofluorocarbons (CFCs) to the atmosphere would lead to a significant reduction of upper stratospheric ozone, with the peak percentage decline occurring around 40 km, is now clearly confirmed.

- The global distributions calculated by current two-dimensional "assessment models" of the long-lived source gases (e.g., $H_2O$, methane ($CH_4$), nitrous oxide ($N_2O$), CFCs) of the radicals that catalyze ozone loss compare well with global observations. Consequently, the simplified representations of dynamics used by these models have proved to be useful for studies of the observed changes in upper stratospheric ozone ($O_3$) during the past several decades.

- Several independent recent studies show increases in upper stratospheric $H_2O$ of about 55 to 150 parts per billion by volume (ppbv) per year from 1992 to 1996/1997, which cannot be explained by a concurrently observed downward trend in upper stratospheric $CH_4$ (about 15 ppbv/year). Should this rise in $H_2O$ continue to occur, it could have important long-term radiative and photochemical consequences. However, changes in $H_2O$ do not contribute a large fraction to the observed decline in upper stratospheric ozone over the last decades.

- Balloonborne observations of hydroxyl radicals (OH) and hydroperoxyl radicals ($HO_2$) near 40 km agree with calculated concentrations to within ±20%. Ground-based column observations of OH, which have a substantial contribution from the mesosphere, exhibit larger discrepancies with models. Satellite observations of OH near 50 km are considerably less than calculated using standard photochemical kinetics. These discrepancies are unlikely to have a substantial effect on calculated trends of upper stratospheric ozone.

- Comparisons of recent observations and model calculations show that the overall partitioning of reactive nitrogen and chlorine species is well understood. The previously noted discrepancy for the chlorine monoxide/hydrogen chloride ratio (ClO/HCl) has been resolved, provided allowance is made for production of HCl from a minor channel of the ClO + OH reaction, which is consistent with a recent laboratory study.

- Measurements of the total stratospheric chlorine loading demonstrate that long-lived organic chlorine compounds (mainly CFCs) released by anthropogenic activity are the dominant source of ClO, the chlorine compound that depletes $O_3$. The observed increases in upper stratospheric hydrogen chloride (HCl) and hydrogen fluoride (HF) are in excellent agreement with the rise of the chlorine and fluorine content of their organic source gases in the troposphere.

- An improved understanding of the relevant kinetic processes has resulted in close balance between the calculated production and loss of $O_3$ at 40 km (i.e., the long-standing difference between calculated and observed ozone abundance, the so-called "ozone deficit problem," has been resolved at this altitude). Although there are remaining uncertainties regarding a possible ozone deficit at higher altitudes, the severity of this problem has been substantially reduced throughout the upper stratosphere.

- Several independent long-term datasets show a decline of the concentration of $O_3$ that peaks around 40 km altitude at a value of 7.4 ± 1.0%/decade. Photochemical model simulations likewise reveal a long-term decline of ozone throughout the upper stratosphere that is driven by the accumulation of anthropogenic chlorine. There is good quantitative agreement between the observed and simulated meridional and vertical structure of the long-term reductions in upper stratospheric ozone.

## 6.1 INTRODUCTION

Ozone depletion in the upper stratosphere, predicted more than two decades ago (Molina and Rowland, 1974; Crutzen, 1974), is now clearly observed. In addition to this predicted change, loss of ozone is observed also at lower altitudes (Figure 6-1; see also Chapter 4). The vertical distribution of stratospheric ozone decline has a distinct minimum around 30 km; the focus of this chapter is on the changes in ozone above this altitude. The causes of changes in ozone below 30 km are discussed in Chapter 7.

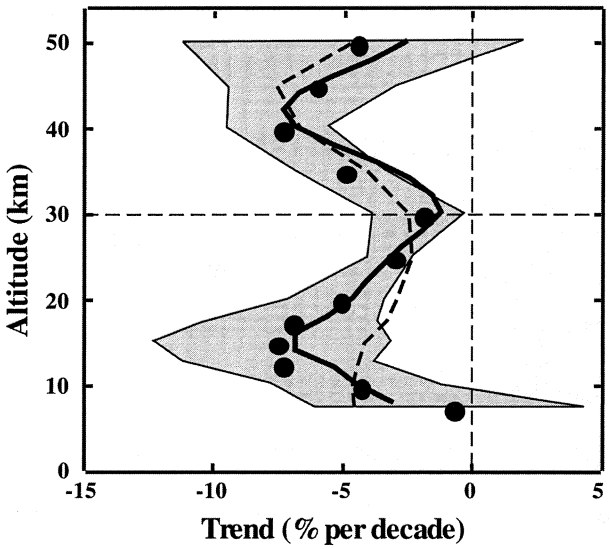


**Figure 6-1.** Stratospheric ozone decline in % per decade (filled circles) and uncertainties (at the 2σ level; gray area) for northern midlatitudes from the Stratospheric Processes and Their Role in Climate-International Ozone Commission (SPARC-IOC) Assessment of trends (1980-1996) in the vertical distribution of ozone (Stolarski and Randel, 1998). The lines are 2-D model calculations of the ozone trend due to catalytic destruction by halogen radicals: solid line from Solomon *et al.* (1998) and dashed line, a recent calculation using the model of Jackman *et al.* (1996). There is a statistically significant negative trend at all altitudes, except at the lowest and the highest altitudes (see Chapter 4). The minimum ozone depletion occurs around 30 km. The causes of ozone changes above this altitude are discussed in this chapter; those in the region below are discussed in Chapter 7.

Ozone ($O_3$) in the upper stratosphere, although originally thought to be most vulnerable to catalytic destruction by chlorine radicals ($ClO_x$) (Molina and Rowland, 1974; Crutzen, 1974), has attracted comparably little scientific attention since the discovery of extreme ozone losses due to perturbed halogen chemistry in the lower stratosphere in Antarctica (WMO, 1995; see also Chapter 7). However, about 15% of the ozone column resides in the upper stratosphere (above about 30 km) and ozone loss in this region affects global stratospheric temperatures and therefore may impact the radiative balance of the stratosphere (see Chapter 10).

The abundance of stratospheric ozone is governed by photochemical production (mostly the photolysis of $O_2$), destruction by catalytic cycles involving hydrogen ($HO_x$), nitrogen ($NO_x$), and halogen ($ClO_x$, $BrO_x$) radicals, as well as transport processes. In the upper stratosphere (between about 30 and 50 km), with the exception of the winter high latitudes (poleward of about 45°N), photochemical reactions are sufficiently fast that the concentrations of ozone are solely determined by a local balance of photochemical production and loss; i.e., ozone is in photochemical steady state. However, the abundances of gases such as methane ($CH_4$), $H_2O$, chlorofluorocarbons (CFCs), and nitrous oxide ($N_2O$) that act as radical precursors are affected by transport because these gases are longer lived than $O_3$. Transport thus has a significant indirect influence on ozone.

Stratospheric ozone is produced by photolysis of molecular oxygen ($O_2$) at wavelengths below 242 nm, with the subsequent reaction of the photolysis product oxygen atoms (O) with $O_2$ to form ozone. It is common for the sum $[O_3] + [O]$ to be referred to as odd oxygen, or $O_x$, because the sum of these compounds varies slowly during the day. The concentrations of $O_3$ and O adjust rapidly to photochemical steady state via the reactions $O_3 + h\nu \rightarrow O + O_2$ and $O + O_2 + M \rightarrow O_3 + M$. Throughout the altitude range of interest, $O_3$ constitutes the vast majority of total $O_x$, and thus a change in the abundance of $O_x$ will for convenience be referred to as change in $O_3$. Owing to the large abundance of ground-state atomic oxygen $O(^3P)$ in the upper stratosphere compared with concentrations present at lower altitudes, ozone loss in this region is dominated by cycles whose rate-limiting step involves reaction with $O(^3P)$. In addition to the Chapman reaction, $O + O_3 \rightarrow 2O_2$, the most important loss cycles for ozone in the upper stratosphere are catalytic cycles involving $NO_x$ radicals

$$\begin{aligned} NO_2 + O &\rightarrow NO + O_2 \\ NO + O_3 &\rightarrow NO_2 + O_2 \\ \text{Net: } O + O_3 &\rightarrow 2\,O_2 \end{aligned} \qquad (6\text{-}1)$$

chlorine radicals

$$\begin{aligned} ClO + O &\rightarrow Cl + O_2 \\ Cl + O_3 &\rightarrow ClO + O_2 \\ \text{Net: } O + O_3 &\rightarrow 2\,O_2 \end{aligned} \qquad (6\text{-}2)$$

and hydrogen radicals

$$\begin{aligned} OH + O &\rightarrow H + O_2 \\ H + O_3 &\rightarrow OH + O_2 \\ \text{Net: } O + O_3 &\rightarrow 2\,O_2 \end{aligned} \qquad (6\text{-}3)$$

$$\begin{aligned} OH + O &\rightarrow H + O_2 \\ H + O_2 + M &\rightarrow HO_2 + M \\ HO_2 + O &\rightarrow OH + O_2 \\ \text{Net: } O + O &\rightarrow O_2 \end{aligned} \qquad (6\text{-}4)$$

$$\begin{aligned} HO_2 + O &\rightarrow OH + O_2 \\ OH + O_3 &\rightarrow HO_2 + O_2 \\ \text{Net: } O + O_3 &\rightarrow 2\,O_2 \end{aligned} \qquad (6\text{-}5)$$

Owing to the strong increase of $O(^3P)$ with altitude, the rates of these cycles increase substantially between 25 and 40 km (Figure 6-2). Loss of $O_3$ by the cycle limited by the reaction BrO + O occurs at a much slower rate (~1% of the total loss at 30 km, smaller contributions at highter altitudes) than loss by the cycles given above, and is not considered here. Loss of $O_3$ through cycles limited by reactions such as ClO + ClO, ClO + BrO, ClO + $HO_2$, and BrO + $HO_2$ is important only for altitudes below ~25 km because each of these cycles involves reactions including $O_3$, but not $O(^3P)$. Consequently, these cycles are considered in Chapter 7, but not here.

The relative importance of the various loss cycles varies with altitude (Figure 6-2). Above the 42 to 45 km altitude region, loss of ozone is dominated by catalytic cycles involving hydrogen radicals, whereas for lower altitudes, $NO_x$-catalyzed loss of ozone is most important. The importance of the chlorine-catalyzed ozone loss cycle peaks at about 40 km where, at present atmospheric chlorine abundances, it is comparable to loss of ozone by the hydrogen and nitrogen catalytic cycles.

Sections 6.2 and 6.3 review our understanding of the dynamical and chemical processes in the upper stratosphere that maintain the distribution of the major

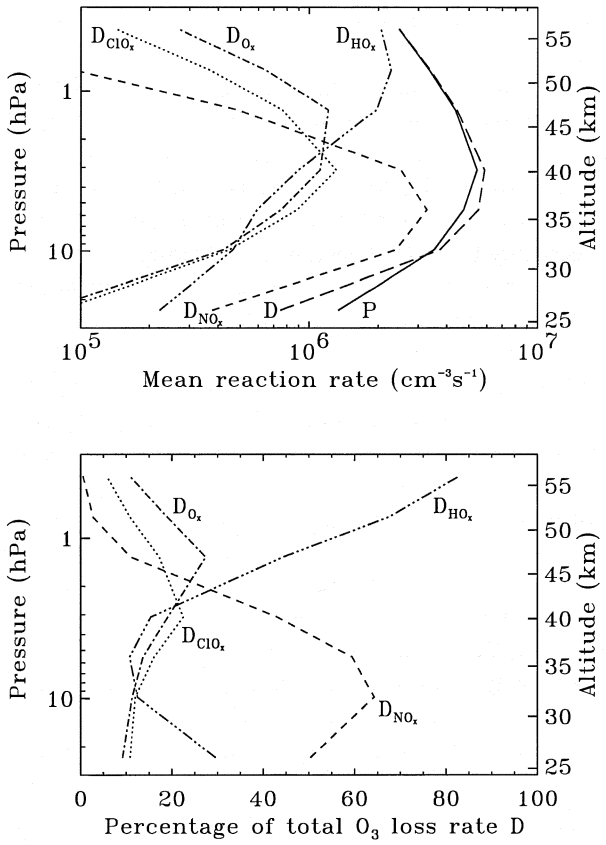


**Figure 6-2.** The vertical distribution of the total $O_x$ production (P) and destruction rate (D). Also shown are the individual contributions by the $HO_x$ ($D_{HO_x}$), $ClO_x$ ($D_{ClO_x}$), and $NO_x$ ($D_{NO_x}$) cycles as well as the Chapman loss cycle ($D_{O_x}$). The top panel shows absolute values and the bottom panel shows relative values. Calculations are for conditions of strongest photochemical control on stratospheric chemistry (January 1994, 23°S). Adapted from Crutzen *et al.* (1995); updated to current kinetic parameters (DeMore *et al.*, 1997; Lipson *et al.*, 1997) and using Version 18 HALOE data.

radical precursors, which determine the concentration of the radicals that regulate ozone and that also lead to the observed decline in ozone. Although, owing to the absence of heterogeneous chemical processes, the chemistry in the middle and upper stratosphere appears to be less complicated than in the lower stratosphere, uncertainties still exist in the quantitative understanding of the ozone budget. The fact that models underpredict the observed abundance of ozone in the upper

stratosphere, a long-standing issue commonly referred to as the "ozone deficit" problem (WMO, 1995; see also Section 6.4.1 below), is still not completely resolved. Uncertainties remain in particular for altitudes above 45 km, where the $O_x$ loss cycles are mostly controlled by $HO_x$ chemistry. Here, the rates of several key radical reactions are known only to within relatively large uncertainty limits (see Section 6.3.1 below).

In spite of known deficiencies, calculations using two-dimensional (2-D) models have heretofore been the only means to simulate long-term trends of ozone (WMO, 1995). Both observations of the ozone vertical distribution and model results indicate a downward trend in the ozone concentrations above 30 km (Section 6.4). However, while the signature of both the altitude distribution and the latitudinal variation of the ozone trend were in reasonable agreement between model results and observations, past model calculations tended to overpredict the observed negative trend in ozone (e.g., WMO, 1995; Jackman *et al.*, 1996). This problem has been largely resolved in recent model calculations (Figure 6-1; see in particular Section 6.4.4 below).

Strong evidence has accumulated during the past two decades that the decline of ozone in the upper stratosphere is linked with increased levels of chlorine (e.g., Hilsenrath *et al.*, 1992; WMO, 1995; see also Section 6.5 below). Therefore, as only a slow decline of the stratospheric chlorine loading is predicted over the coming decades (see Chapter 11), the problem of stratospheric ozone loss is expected to persist in the foreseeable future. Nonetheless, because of the direct correspondence between the chlorine burden and loss of ozone in the upper stratosphere (see below), it is conceivable that the "recovery" of ozone due to the declining burden of anthropogenic halogens will first become apparent for the upper stratosphere (Chapter 12).

## 6.2 TRANSPORT PROCESSES IN THE UPPER STRATOSPHERE

The distributions throughout the stratosphere of long-lived compounds such as $H_2O$, $CH_4$, $N_2O$, and CFCs are controlled by transport. Because decomposition of these compounds supplies the hydrogen, nitrogen, and chlorine radicals involved in catalytic cycles that remove $O_3$, these cycles thus depend indirectly on transport processes in the upper stratosphere. As the chemical reactions are temperature dependent, dynamical processes that affect the temperatures in the upper stratosphere are also relevant to $O_3$ changes in this region. Dynamical and transport processes also play a more direct role in the regulation of $O_3$ between 30 and 40 km in the extratropics, where chemical time scales are longer than at higher altitudes and thus closer to transport time scales.

As discussed in more detail in Chapter 7 (Section 7.3), the Brewer-Dobson circulation (ascent across the tropical tropopause, poleward motion in the stratosphere, descent into the extratropical troposphere in both hemispheres) accounts for the gross features of the annual mean stratospheric meridional circulation. The equinoctial circulation in the upper stratosphere resembles the Brewer-Dobson circulation; the solstice circulation comprises rising motion above 30 km in summer high latitudes, summer pole to winter pole flow in the upper stratosphere and mesosphere, and strong descent in winter middle and high latitudes (e.g., Andrews *et al.*, 1987). This global mass circulation is driven primarily by wave motions in the extratropical stratosphere (e.g., Holton *et al.*, 1995; Chapter 7), with both planetary-scale and gravity waves playing a role. Mesospheric gravity wave drag plays a strong role in determining the temperature structure and circulation of the middle and upper stratosphere (down to below 30 km), with largest effects during southern winter and early northern winter, when planetary wave driving is relatively weak (e.g., Garcia and Boville, 1994). In winter, the polar vortex dominates the extratropical circulation throughout the stratosphere, and planetary-scale waves associated with variability of the polar vortex result in a region of strong quasi-horizontal mixing and weak tracer gradients between regions of strong tracer gradients associated with the polar vortex boundary (e.g., McIntyre and Palmer, 1984) and the sub-tropical transport barrier (e.g., Plumb, 1996; Chapter 7). Trajectory modeling studies (Sutton *et al.*, 1994; Schoeberl and Newman, 1995; Manney *et al.*, 1998) have shown that generation of filaments in the midlatitude region of strong mixing is common in the middle and upper stratosphere as well as in the lower stratosphere (Chapter 7); Schoeberl and Newman (1995) applied their filamentation calculations to quantification of this mixing in Northern Hemisphere winter, showing most rapid mixing to be associated with large planetary-scale wave amplitudes. Recent tracer data from satellites (e.g., the Upper Atmosphere Research Satellite (UARS)) with hemispheric or global and year-round coverage, and other observations (e.g., Atmospheric Trace Molecule Spectroscopy (ATMOS))

with vertical profile information through the upper stratosphere, confirm that the above picture gives a reasonably good description of the largest scale features of observed distributions of $N_2O$ (Figure 6-3), $CH_4$ (Figure 6-4), $H_2O$, hydrogen fluoride (HF), and CFCs (e.g., Randel *et al.*, 1993, 1994, 1998a; Ruth *et al.*, 1994; Luo *et al.*, 1995; Nightingale *et al.*, 1996; Michelsen *et al.*, 1998). A useful, although not directly observable, measure of transport in the meridional plane is the age of stratospheric air (e.g., Hall and Plumb, 1994; Chapter 7); the mean age of air typically shows a pattern similar to that of a long-lived tracer, with the oldest air (possibly as old as 10-12 years) residing in the polar upper stratosphere (see Figure 7-8). The air in the midlatitude stratosphere has a mean age of about 5-6 years (e.g., Harnisch *et al.*, 1996; Waugh *et al.*, 1997; Bacmeister *et al.*, 1998; see also Chapter 7). Models (including general circulation models, chemical transport models, and 2-D models) can reproduce the main ingredients of the meridional distribution of long-lived tracers and the age-of-air spectrum (e.g., Randel *et al.*, 1994; Waugh *et al.*, 1997; Bacmeister *et al.*, 1998), although details such as quantitative determinations of age vary widely between models (e.g., Hall and Waugh, 1997; Waugh *et al.*, 1997; Bacmeister *et al.*, 1998).

Seasonal variations in the tropics are dominated by a semi-annual oscillation (SAO) above about 35 km and a quasi-biennial oscillation (QBO) below about 35 km. Theories regarding the QBO and its influence on the lower stratosphere and total $O_3$ are discussed in Chapter 7; it is recognized to be driven by wave momentum

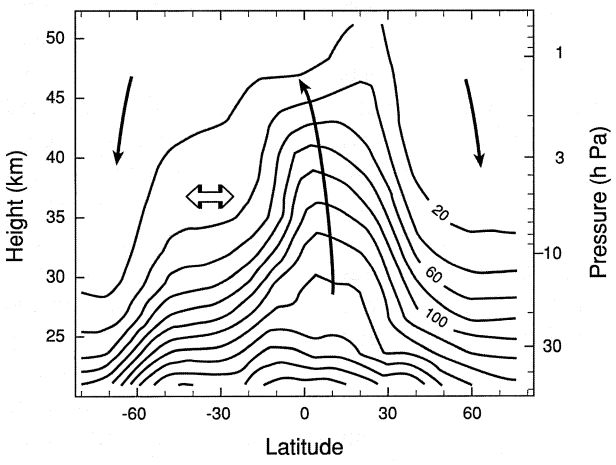


**Figure 6-3.** Longitudinally averaged structure of $N_2O$ mixing ratios (in ppbv) during 1-20 September 1992 measured by the Cryogenic Limb Array Etalon Spectrometer (CLAES) instrument on the Upper Atmosphere Research Satellite (UARS). Heavy solid lines denote the mean stratospheric circulation in the latitude-height plane, and the horizontal arrows denote the location of quasi-horizontal mixing by planetary waves. Adapted from Randel *et al.* (1993).

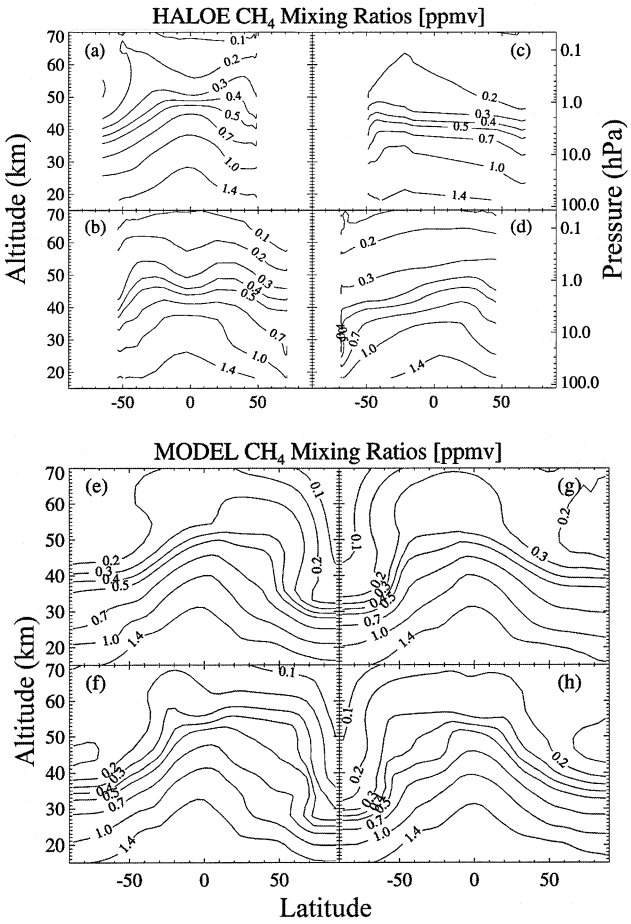


**Figure 6-4.** Comparison of zonal mean $CH_4$ mixing ratios as observed by the Halogen Occulation Experiment (HALOE) (panels a-d) and calculated using a two-dimensional model that includes interactive temperatures and transport circulation, but uses climatological ozone for the radiation calculations (panels e-h). Fields are shown for (a) and (e) NH winter solstice, (b) and (f) NH vernal equinox, (c) and (g) NH summer solstice, and (d) and (h) NH autumnal equinox. Adapted from Summers *et al.* (1997b).

transport, which involves planetary-scale equatorial waves, intermediate inertia-gravity waves, and mesoscale gravity waves (Dunkerton, 1997). Several momentum sources are thought to contribute to generation of the SAO (e.g., Sassi and Garcia, 1997, and references therein), including forcing of westerly accelerations via momentum deposition by Kelvin and gravity waves propagating into the upper stratosphere and forcing of easterly accelerations by planetary waves. Both QBO and SAO drive meridional transport circulations that affect the distribution of long-lived tracers (Gray and Pyle, 1986), as discussed below. Filtering of upward-propagating waves by the QBO modulates the SAO, so that transport in the upper stratosphere is influenced by both the QBO and the SAO. Dunkerton and Delisi (1997) also show evidence that descending westerly phases of the SAO are strongly influenced by the underlying QBO.

That the QBO strongly influences long-lived tracer distributions in the equatorial upper stratosphere (Gray and Pyle, 1986) has been verified in several recent studies (e.g., Ruth *et al.*, 1997; Kennaugh *et al.*, 1997; Luo *et al.*, 1997b; Randel *et al.*, 1998a; Jones *et al.*, 1998); a QBO signal has also been seen in HCl, HF, nitrogen dioxide ($NO_2$), and $O_3$ in the middle stratosphere (Zawodny and McCormick, 1991; Luo *et al.*, 1997b). Evidence of the SAO appears in satellite observations of temperature and $O_3$ (Ray *et al.*, 1994), as well as long-lived tracer distributions (Carr *et al.*, 1995; Ruth *et al.*, 1997; Randel *et al.*, 1998a). Modulation of the position and intensity of subtropical tracer gradients (sharpening gradients during QBO easterlies) in the middle stratosphere is associated with the QBO (Hitchman *et al.*, 1994; Randel *et al.*, 1998a; Jones *et al.*, 1998). The QBO modulation of $NO_2$ is caused by transport-induced variations in $NO_y$, and indirectly causes the QBO in $O_3$ above 30 km through chemical effects (Chipperfield *et al.*, 1994; Jones *et al.*, 1998). A double peak in long-lived tracer distributions seen below the equatorial stratopause near equinox (e.g., Ruth *et al.*, 1994, 1997; Luo *et al.*, 1995; Eluszkiewicz *et al.*, 1996; Randel *et al.*, 1998a) is associated with the SAO. During westerly SAO acceleration, there is induced descent near the equator and ascent in the subtropics below the level of maximum forcing, and ascent near the equator and descent in the subtropics above this level; for an easterly acceleration, the induced circulation has the opposite sense (Gray and Pyle, 1986; Kennaugh *et al.*, 1997). However, recent evidence (Randel *et al.*, 1998a) suggests that this induced circulation may not be the determining factor in producing the double peak. Recent model studies show a double peak when QBO winds are westerly, but a single peak in the summer hemisphere when QBO winds are easterly (Kennaugh *et al.*, 1997), in agreement with satellite observations of $CH_4$ (Ruth *et al.*, 1997; Randel *et al.*, 1998a).

The dominant feature of the extratropical stratospheric circulation in winter is a cold westerly polar vortex extending throughout the depth of the stratosphere. The wave-driven mass circulation and associated radiative cooling result in strong descent in and around the polar vortex, with mesospheric air descending through the middle stratosphere (Fisher *et al.*, 1993; Abrams *et al.*, 1996a,b; Aellig *et al.*, 1996a). Inter-hemispheric differences in the intensity, variability, and persistence of the polar vortex in the middle and upper stratosphere and the impact of these differences on long-lived tracer distributions are elucidated in recent studies (e.g., Lahoz *et al.*, 1994, 1996; Manney *et al.*, 1994a, 1995b; Considine *et al.*, 1998) (see Chapter 7 for related studies of the lower stratosphere). Northern winter is characterized by strong planetary-scale variability, with a strong persistent anticyclone typically occurring near the dateline (e.g., Harvey and Hitchman, 1996), large interannual variability, and frequent occurrence of stratospheric sudden warmings. The largest effects of sudden warmings are in the middle and upper stratosphere, where "major" warmings (e.g., Andrews *et al.*, 1987) result in a temporary transition to zonal mean easterlies at and above 10 hPa (about 30 km), zonal mean temperatures that increase toward the pole, and may result in a temporary or permanent breakdown of the upper stratospheric vortex. The flow in the southern winter upper stratosphere is characterized by an intense polar vortex with weak planetary-scale variability represented by one or more eastward-traveling anticyclones, with a transition in late winter/early spring to a circulation with a weakened upper stratospheric vortex and a quasi-stationary anticyclone (e.g., Lahoz *et al.*, 1996). This Southern Hemisphere spring flow regime shares many of the characteristics of the Northern Hemisphere winter flow regime (Lahoz *et al.*, 1994, 1996). The northern vortex typically breaks down in the upper stratosphere at about the time of the spring equinox; the southern upper stratospheric vortex persists for 1 to 2 months longer (e.g., Manney *et al.*, 1994a). Although many studies have focused on the lower stratosphere (Chapter 7), several recent studies based on

trajectory modeling (Fisher *et al.*, 1993; Manney *et al.*, 1994a; Eluszkiewicz *et al.*, 1995) and observations of long-lived tracers (Manney *et al.*, 1994b, 1995b; Lahoz *et al.*, 1994, 1996; Abrams *et al.*, 1996a,b; Aellig *et al.*, 1996a; Michelsen *et al.*, 1998) have refined our understanding of transport, interhemispheric differences in transport, and the impact of these processes on the distribution of long-lived tracers in the upper stratosphere. The interhemispheric differences in large-scale variability described above are associated with hemispheric asymmetries in the global mass circulation; such asymmetries are predicted in calculations based on observed fields (e.g., Rosenlof, 1995; Appenzeller *et al.*, 1996; Eluszkiewicz *et al.*, 1996; Coy and Swinbank, 1997) and confirmed by observations of hemispheric asymmetries in long-lived tracer distributions (e.g., Rosenlof *et al.*, 1997; Morrey and Harwood, 1998; Considine *et al.*, 1998).

The region between approximately 25 and 35 km represents a transition region between dynamical (in the absence of heterogeneous chemistry in the polar vortex; see Chapter 7) control of $O_3$ in the lower stratosphere and photochemical control in the upper stratosphere (e.g., Hartmann and Garcia, 1979). Recent studies using UARS Microwave Limb Sounder (MLS) ozone data (Allen *et al.*, 1997) confirm that the response of $O_3$ to planetary-scale waves in winter is consistent with Hartmann and Garcia's model wherein the $O_3$ distribution below about 30 km is determined primarily by transport by time-varying wave motions and above about 50 km is determined by temperature variations associated with wave motions through temperature-dependent photochemistry, with both processes playing a role in the region between. Luo *et al.* (1997a) showed that transport of $O_3$ and other gases by summertime planetary waves at 30-40 km could take place on time scales comparable to or shorter than their chemical relaxation times. Manney *et al.* (1998) showed that many small vertical-scale $O_3$ variations seen in lidar observations at altitudes up to about 40 km can be explained by advection of filaments of air with varying $O_3$ concentrations, verifying the importance of transport in determining the details of the $O_3$ distribution in the middle stratosphere. The common phenomenon of low ozone pockets forming in the anticyclone between 30 and 45 km (Manney *et al.*, 1995a) is another example of the interplay between transport and chemistry in the transition region. Long-lived tracer observations show that air from low latitudes is drawn into the anticyclone and confined there for days to weeks; $O_3$ mixing ratios in this air decrease rapidly as it becomes confined in the anticyclone (Manney *et al.*, 1995a). Nair *et al.* (1998) and Morris *et al.* (1998) confirmed that the isolation of this air results in relaxation (via known chemical processes) to $O_3$ concentrations much lower than those prevailing in midlatitudes outside the anticyclone where air experiences strong mixing. In contrast to the above examples, Douglass *et al.* (1997) showed a chemical transport model simulation where, near 40 km, tropical to midlatitude distributions of long-lived tracers were not well simulated but, because $O_3$ lifetimes are very short in the tropics and sub-tropics at this altitude, reasonably good agreement was obtained between model and observed $O_3$. The above examples illustrate that the degree to which transport at altitudes in the transition region influences ozone chemistry varies widely depending on location, season, and dynamical conditions.

To date, the vast majority of assessment studies relevant to the upper stratosphere have been done using two-dimensional models (see Chapter 12) in which many of the processes discussed above cannot be explicitly represented. Realistic zonal mean temperature distributions and transport in such models are highly dependent on parameterizations of gravity waves and planetary-scale waves. Bacmeister *et al.* (1995) and Summers *et al.* (1997b), for example, discuss the adjustment of these parameters to obtain realistic distributions of long-lived tracers and zonal mean temperatures. Such tuning of 2-D models is greatly assisted by improved understanding of processes being parameterized, as detailed above, as well as by the availability of global observations of long-lived tracers for all seasons from satellite instruments such as those on UARS. As shown in Figure 6-4, good agreement can be obtained between satellite-observed long-lived tracer fields and those obtained from 2-D models, including representation of strong tracer gradients in the subtropics and along the polar night jet, a region of very weak tracer gradients in midlatitudes, a signature of strong descent in the polar vortex, and separation of relationships between long-lived tracers in tropics and extratropics (e.g., Bacmeister *et al.*, 1995; Luo *et al.*, 1995; Jackman *et al.*, 1996; Nightingale *et al.*, 1996; Summers *et al.*, 1997b; Rosenfield *et al.*, 1997). Considine *et al.* (1998) simulated interhemispheric differences in high latitude $CH_4$ and $N_2O$, and Summers *et al.* (1997b) were able to simulate interhemispheric differences in both stratospheric and mesospheric $H_2O$. These asymmetries may

impact the distribution of chlorine and hydrogen radicals, and thus both the upper stratospheric $O_3$ concentrations and decadal trends (Section 6.4.4). Two-dimensional models typically fail to capture, or else underestimate, the double-peaked structure in long-lived tracers in the equatorial upper stratosphere (see Figure 6-4), a problem related to deficiencies in their ability to model the SAO and QBO (e.g., Summers *et al.*, 1997b).

Although most 2-D models capture the general features of the upper stratospheric circulation mentioned above, a number of different approaches to parameterizing planetary-scale and gravity waves are used in various models, and there is considerable model-to-model variability in details of temperature structure, tracer-tracer relationships, age spectra, and the shapes of tracer isopleths (Park *et al.*, 1998). In addition, many 2-D models used for assessment are further simplified by using transport circulations based on a specified climatology of zonal mean temperatures, so that the circulation and chemistry are not interactive (Jackman *et al.*, 1996; Chapter 12); significant differences can result in otherwise similar models that are run with interactive versus non-interactive chemistry, radiation, and dynamics (Considine *et al.*, 1998; Chapter 12). For multi-year simulations, a single annual cycle of the circulation and temperature is typically repeated for the duration of the simulation, making it impossible to represent interannual variability, trends in long-lived gases or temperatures, or multi-year oscillations such as the QBO. Thus, although 2-D models can be adjusted to give adequate representations of contemporary temperature and tracer fields, possible effects on simulations of ozone change due to interannual variability, long-term temperature and source gas trends, and QBO cycles have not as yet been thoroughly evaluated. Despite these obvious deficiencies in the representation of transport processes in current assessment models, these models can give reasonable representations of many of the large-scale features of the distribution of long-lived source gases; such simplified assessment models have been quite successful in reproducing observed trends in ozone in the upper stratosphere (Section 6.4).

## 6.3 PHOTOCHEMISTRY OF THE UPPER STRATOSPHERE

### 6.3.1 Hydrogen Species

The role of hydrogen radicals in regulating the abundance of stratospheric $O_3$ was first described by Bates and Nicolet (1950). In the upper stratosphere, hydrogen radicals ($HO_x$) are produced by the reactions of excited-state atomic oxygen ($O(^1D)$) with $H_2O$ and with $CH_4$. Loss of $HO_x$ occurs primarily by the reaction $HO_2 + OH$, with important contributions from the $OH + HNO_3$ reaction below ~35 km. Hydrogen radicals catalyze loss of ozone in the upper stratosphere by the catalytic cycles (6-3), (6-4), and (6-5) (see Section 6.1).

#### Hydrogen Source Gases

Global distributions of $H_2O$ (Harries *et al.*, 1996) and $CH_4$ (Park *et al.*, 1996) measured by the Halogen Occultation Experiment (HALOE) instrument aboard UARS have been reproduced fairly well by a three-dimensional (3-D) general circulation model (GCM) (Mote, 1995). The observed shapes of tracer isopleths, bowing in the tropics and flattening at midlatitudes, are consistent with calculated isopleths. Similarly, 2-D models provide an adequate representation of observed $CH_4$ and $H_2O$ fields (see Section 6.2). Abbas *et al.* (1996a) have shown that vertical profiles of $H_2O$ and $CH_4$ measured by the ATMOS instrument are consistent with production of $H_2O$ from oxidation of $CH_4$ as well as the general features of the profile for molecular hydrogen ($H_2$) calculated by 2-D models. These studies suggest good overall understanding of the distributions of $H_2O$ and $CH_4$ in the upper stratosphere.

Current issues of importance regarding the budget of upper stratospheric hydrogen are long-term trends of $H_2O$ and $CH_4$. Evans *et al.* (1998), Nedoluha *et al.* (1998a), and Randel *et al.* (1998b) reported an upward trend of 55 to 150 ppbv/year in the volume mixing ratio of upper stratospheric $H_2O$ based on analyses of HALOE data obtained between altitudes of 30 to 60 km during the years 1992 to 1996/1997 (Figure 6-5). The time series for upper stratospheric $H_2O$ exhibits nonlinear variations due to numerous forcings, such as quasi-biennial and seasonal variations in stratospheric winds (e.g., Evans *et al.*, 1998). The $H_2O$ mixing ratio increase between 1992 and 1996 measured by HALOE is not monotonic with time and appears to have leveled off during 1997 (Randel *et al.*, 1998b). Consequently, the computed $H_2O$ trend is sensitive to the statistical technique used to extract the linear component from the nonlinear signal, to the time period of the data record, and also to the range of latitudes and altitudes under consideration (Evans *et al.*, 1998; Nedoluha *et al.*, 1998a; Randel *et al.*, 1998b). Evans *et al.* (1998) (data obtained between 1992 and 1996, inclusive) and Nedoluha *et al.* (1998a) (data

upper stratospheric $HO_x$ has been guided by the numerous atmospheric observations described below, as well as the recognition that a larger quantum yield of $O(^1D)$ from photolysis of $O_3$ (Michelsen *et al.*, 1994; DeMore *et al.*, 1997; Ravishankara *et al.*, 1998, and references therein) leads to an increase in calculated concentrations of $O(^1D)$ and OH of ~12% and ~6%, respectively, at 30 km (Michelsen *et al.*, 1994), with larger effects at lower altitudes.

An analysis of balloonborne observations of radicals and precursors obtained with a far-infrared Fourier transform spectrometer (FIRS-2) that detects atmospheric thermal emission in a limb-viewing geometry revealed generally good agreement (differences less than 10%) between theory and observation of OH between 25 and 36 km (Chance *et al.*, 1996). The largest discrepancy occurred near 38 km, where measured OH exceeded model estimates by ~20%. Osterman *et al.* (1997) and Pickett and Peterson (1996) reached similar conclusions based on analyses of near-simultaneous profiles of OH obtained by the Far Infrared Limb Observing Spectrometer (FILOS) and $HO_2$ measured by the Submillimeter Limb Sounder (SLS), $O_3$ measured by an in situ UV photometer, and $H_2O$, $CH_4$, and $NO_y$ detected by the MkIV Fourier transform spectrometer. The measured profile for OH extended to 40 km altitude and was shown to agree with model values to better than 5%. Theory and observation of $HO_2$ agreed to better than 10% below 40 km. However, observed values of $HO_2$ exceeded model values by 20 to 30% between 40 and 50 km, although the discrepancy was within the uncertainty of measurement. A similar conclusion of ~20% excess $HO_2$ relative to standard models for altitudes near 38 km was reached by Chance *et al.* (1996) based on earlier FIRS-2 observations. Osterman *et al.* (1997) and Jucks *et al.* (1996) have shown that rates for removal of $O_3$ by the $HO_x$ catalytic cycles inferred from simultaneous measurements of profiles of OH and $HO_2$ obtained by the FILOS, SLS, and FIRS-2 instruments between 30 and 50 km agree with theoretical removal rates to within the uncertainties of the atmospheric observations and laboratory measurements of the relevant kinetic rate constants.

Summers *et al.* (1997a), in contrast to the above studies, have concluded that a serious deficiency exists in our understanding of the processes that regulate $HO_x$ in the upper stratosphere based on their analysis of observations of OH and $O_3$ obtained by the Middle Atmosphere High Resolution Spectrograph Investigation (MAHRSI) (Conway *et al.*, 1996) and the Cryogenic Infrared Spectrometers and Telescopes for the Atmosphere (CRISTA) shuttle-borne instruments, and near-simultaneous profiles of $H_2O$ and $CH_4$ obtained by HALOE. Concentrations of OH observed by MAHRSI were found to be 30 to 40% lower than calculated values near 50 km (Figure 6-6). Summers *et al.* (1997a) outlined two scenarios that would lead to good agreement between theory and observation of OH: either a 50% reduction in the rate of $O + HO_2 \rightarrow OH + O_2$ (based on an earlier suggestion by Clancy *et al.* (1994) from a study of ground-based microwave observations of $HO_2$ and $O_3$), or a 20% reduction in the rate of $O + HO_2$ and a 30% increase in the rate of $OH + HO_2 \rightarrow H_2O + O_2$. Both scenarios predict lower concentrations of $HO_2$ in the upper stratosphere relative to standard model values, an important consequence that cannot yet be tested by shuttle and spaceborne instruments. Additionally, both

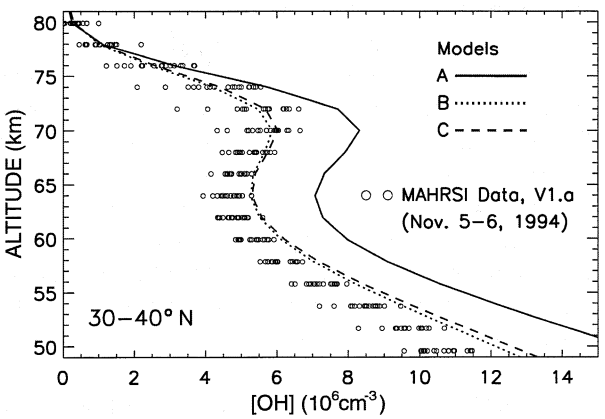


**Figure 6-6.** Concentration profiles of OH (open circles) retrieved by the Middle Atmosphere High Resolution Spectrograph Investigation (MAHRSI) instrument from 18 orbits of observations during 5 and 6 November 1994 between 30° and 40°N. The photochemical model results (lines, as indicated) at the appropriate local solar times were convolved with the MAHRSI weighting functions. Results are shown for three models. Model A used rate constants and cross sections from DeMore *et al.* (1994); model B used a 50% reduction for the rate constant of $O + HO_2 \rightarrow OH + O_2$; and model C used a 20% reduction for the rate constant of $O + HO_2 \rightarrow OH + O_2$ and a 30% increase for the rate constant of $OH + HO_2 \rightarrow H_2O + O_2$. Adapted from Summers *et al.* (1997a).

scenarios lead to a decrease in the removal rate of $O_3$ by catalytic cycles involving $HO_x$ in the upper stratosphere because of the reduction in the rate of $O + HO_2$ (the rate-limiting step of the most important $HO_x$ cycle) and the decrease in the concentration of $HO_2$. The shuttle-borne measurements of OH (Summers *et al.*, 1997a) reach only to altitudes as low as 50 km and the balloonborne profiles (Pickett and Peterson, 1996; Chance *et al.*, 1996) typically extend upward to 40 km, limiting direct comparison of observations obtained by the two techniques. However, the MAHRSI retrievals are currently being extended downward to 45 km altitude and the balloonborne observations have been extended upward to 50 km (Jucks *et al.*, 1998), allowing for direct comparisons in the future.

Jucks *et al.* (1998) have recently presented FIRS-2 balloonborne measurements of OH and $HO_2$ to 50 km altitude (Figure 6-7). The profiles of OH reported by Jucks *et al.* (1998) were within 5% of model values between 30 and 50 km. However, observed concentrations of $HO_2$ exceeded calculated values by 20% between altitudes of 40 and 50 km. Observations of the $[OH]/[HO_2]$ ratio place constraints on the rates of $O + HO_2$ and $O + OH$, the reactions that control the partitioning of $HO_x$ in the upper stratosphere. Jucks *et al.* (1998) concluded their observations of OH and $HO_2$ were best described by a model using rate constants for $O + HO_2$ and $OH + HO_2$ that are 25% slower than recommended values, adjustments consistent with the uncertainties for both reactions (DeMore *et al.*, 1997). The implications for catalytic removal of $O_3$ by $HO_x$ were determined to be minor, however, because the decrease for the rate of $O + HO_2$ was offset by higher-than-expected concentrations of $HO_2$. The observations of Jucks *et al.* (1998) and Summers *et al.* (1997a) appear to point to a significant difference in the concentration of upper stratospheric OH measured by the two spectrometers.

Observations of the abundance of $HO_2$ in the uppermost stratosphere and mesosphere obtained at Kitt Peak, Arizona, United States (31°N), using microwave line-emission spectrometry exceeded model estimates by 25 to 45% (Clancy *et al.*, 1994; Sandor and Clancy, 1998). Agreement between theory and observation of $HO_2$ was obtained allowing for a 40% reduction in the rate of $O + HO_2$ (Sandor and Clancy, 1998). Because Clancy *et al.* (1994) and Sandor and Clancy (1998) do not obtain data below 50 km, the implications of these observations for the upper stratosphere are unclear.

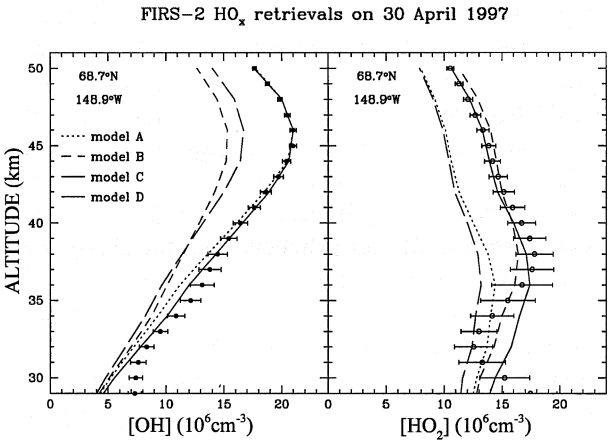


**Figure 6-7.** Concentration profiles of OH and $HO_2$ measured during mid-morning by FIRS-2 on 30 April 1997 near Fairbanks, Alaska (65°N). Photochemical model results (lines, as indicated) are for the appropriate local solar time, constrained by FIRS-2 measurements of $O_3$, $H_2O$, and $CH_4$. Overhead $O_3$ was constrained by a near-coincident profile measured by the ILAS instrument on ADEOS. Results are shown for four models. Models A, B, and C are the same as described by Summers *et al.* (1997a) (see caption for Figure 6-6), except that standard kinetic parameters originated from DeMore *et al.* (1997). Model D, which provides a good simulation of measured OH and $HO_2$, is the same as model A except that the rates of both $O + HO_2 \rightarrow OH + O_2$ and $OH + HO_2 \rightarrow H_2O + O_2$ were reduced by 25%. Adapted from Jucks *et al.* (1998).

However, mesospheric observations provide a strong test of the link between $HO_x$ chemistry and $O_3$, because nitrogen and chlorine radicals do not contribute significantly to loss of mesospheric $O_3$. The reductions for the rate constant of $O + HO_2$ (which exceed the reported uncertainties of the laboratory measurements) proposed by Summers *et al.* (1997a) and Sandor and Clancy (1998) would, in the absence of any other kinetic changes, resolve the long-standing ozone deficit problem in the lower mesosphere and also have important implications for the balance between production and loss of upper stratospheric $O_3$. However, this kinetic change alone leads to a poorer simulation of the observed diurnal variation of ozone in the upper stratosphere and mesosphere (Connor *et al.*, 1994) than found using standard kinetic parameters (Siskind *et al.*, 1995).

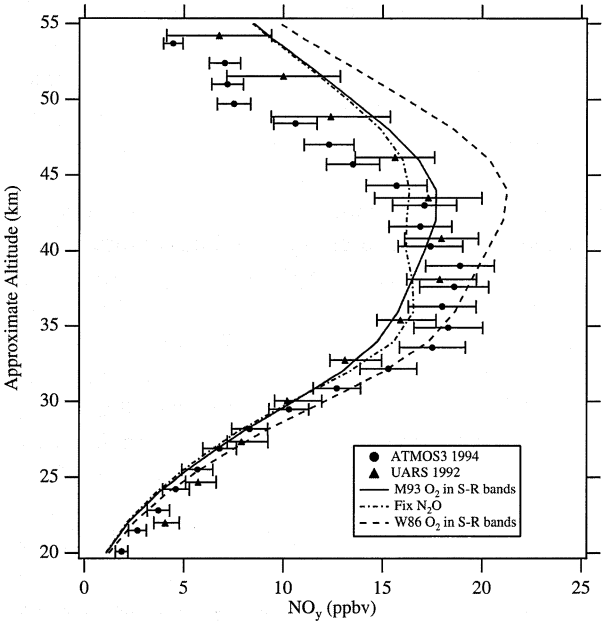


**Figure 6-9.** Volume mixing ratio profiles of $NO_y$ measured in November at 24°N by ATMOS (circles) and UARS (triangles) compared to profiles calculated by the Garcia and Solomon 2-D model (Nevison *et al.*, 1997, and references therein) using the Minschwaner *et al.* (1993) formulation for $O_2$ photolysis in the Schumann-Runge bands (solid line), a fixed $N_2O$ profile specified from CLAES observations (long dashed line), and the WMO (1986) formulation for $O_2$ photolysis in the Schumann-Runge bands (short dashed line). All calculations used the Minschwaner and Siskind (1993) formulation for the photolysis rate of nitric oxide (NO) and other kinetic parameters from DeMore *et al.* (1994). Adapted from Nevison *et al.* (1997).

instruments aboard UARS as well as ATMOS (Figure 6-9). Nevison *et al.* (1997) stated that this result was relatively insensitive to assumptions concerning transport because of the short photochemical lifetime of $NO_y$ in the upper stratosphere. They suggested an increase in the photochemical sink for $NO_y$ was necessary to resolve the discrepancy and noted this could be accommodated by an increase in either the photolysis rate of NO or the N + NO rate constant, or a decrease in the N + $O_2$ rate constant. Each of these rates is subject to considerable uncertainty.

Descent during polar winter of $NO_y$ produced by auroral processes in the thermosphere has been thought to be an additional source of upper stratospheric $NO_y$. Recent HALOE and ATMOS observations have confirmed that such a source most likely does exist (Callis *et al.*, 1996; Rinsland *et al.*, 1996; Siskind and Russell, 1996). However, an analysis of HALOE observations of $NO_x$ has suggested models may overestimate the magnitude of this source (Siskind *et al.*, 1997). An analysis of Improved Stratospheric and Mesospheric Sounder (ISAMS) data indicates mesospheric $NO_y$ formed during particular precipitating electron events affects upper stratospheric $NO_2$ to latitudes as low as 30° to 40° in both hemispheres (Callis and Lambeth, 1998). It is unclear whether this process has an appreciable effect on the overall budget of stratospheric $NO_y$ (Callis and Lambeth, 1998).

Theory and observation of $NO_y$ appear to be in reasonably good agreement between 25 and 40 km (Nevison *et al.*, 1997; Kondo *et al.*, 1996), the altitude range where photochemical loss of $O_3$ is dominated by the nitrogen oxide cycle (e.g., Jucks *et al.*, 1996; Osterman *et al.*, 1997; see also Figure 6-2). The discrepancy at higher altitudes noted by Nevison *et al.* (1997) is unlikely to have a profound effect on calculated values of $O_3$ because of the relatively minor role of the $NO_x$ cycle above 40 km.

### Nitrogen Partitioning

Recent satellite and balloonborne observations have allowed for stringent tests of our understanding of the partitioning of the $NO_y$ family of gases. Accurate knowledge and use of observed profiles of $O_3$, and aerosol surface area at lower altitudes, are essential for proper interpretation of these observations (e.g., Morris *et al.*, 1997). Sen *et al.* (1998) examined concentration profiles of NO, $NO_2$, $HNO_3$, $HNO_4$, $N_2O_5$, and $ClONO_2$ obtained at sunset between 20 and 39 km by the MkIV Fourier transform interferometer using solar occultation. They showed good agreement between measured profiles of the $NO_y$ gases and calculated concentrations, with the only serious disagreement being the tendency of the observed $[NO_2]/[NO]$ and $[NO_2]/[HNO_3]$ ratios to exceed calculated values for altitudes below 30 km (Figure 6-10). They stated that these discrepancies could largely be explained by the use of recent laboratory measurements of the pressure broadened half-widths of $NO_2$ lines near 2900 $cm^{-1}$ as well as a 15% increase in the rate constant of $NO + O_3 \rightarrow NO_2 + O_2$ at temperatures near 220 K that would be consistent with existing laboratory measurements at low temperature.

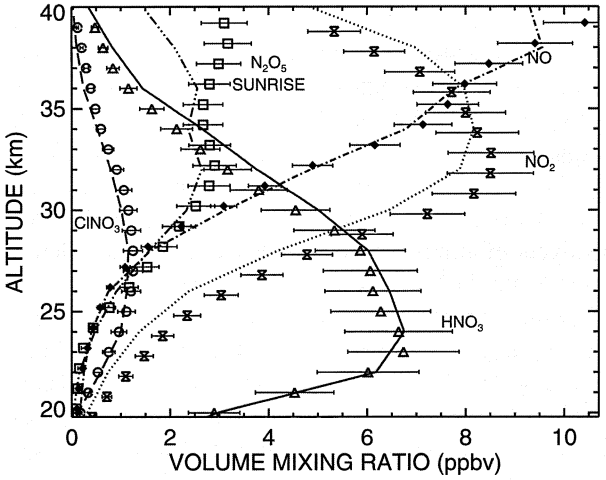


**Figure 6-10.** Volume mixing ratio profiles of NO, $NO_2$, $HNO_3$, and $ClONO_2$ measured at sunset and of $N_2O_5$ measured at sunrise by the MkIV balloonborne FTIR instrument at 35°N on 25 September 1993 (symbols, as indicated) compared to calculated profiles assuming photochemical steady state over a 24-hour period (lines, as indicated). Model profiles were constrained by values for $NO_y$, $Cl_y$, $O_3$, $H_2O$, $CH_4$, etc., from MkIV, and aerosol surface area from SAGE II, and are shown for the appropriate solar times. Calculations used kinetic parameters from DeMore *et al.* (1994) except for the Michelsen *et al.* (1994) formulation for the quantum yield of $O(^1D)$. Adapted from Sen *et al.* (1998).

Modeling studies of $NO_x$ partitioning have been affected by recent revisions to the rate constant of the $OH + NO_2 + M \rightarrow HNO_3 + M$ reaction. Donahue *et al.* (1997) reported that, at room temperature, the rate constant for the reaction $OH + NO_2 + M$ is about 20% lower than the previously recommended rate constant (DeMore *et al.*, 1994). In contrast, for temperatures and pressures typical of the upper stratosphere, the DeMore *et al.* (1997) recommendation for the rate constant of $OH + NO_2 + M$ is larger than the rate constant given by DeMore *et al.* (1994). Use of the DeMore *et al.* (1997) rate constant leads to lower values of the $[NO_x]/[NO_y]$ ratio near 30 km compared to models based on the DeMore *et al.* (1994) value, resulting in poorer agreement with the observed $NO_x/NO_y$ ratio (Sen *et al.*, 1998).

Morris *et al.* (1997) examined the ratio of $NO_x/NO_y$ between 20 and 35 km based on observations by the HALOE and Cryogenic Limb Array Etalon Spectrometer (CLAES) instruments aboard UARS and calculations using the Goddard photochemical model constrained by observed $O_3$ and aerosol surface area. They concluded the measured $[NO_x]/[NO_y]$ ratio was systematically higher than the model at all altitudes between ~22 to ~35 km, with the largest disparity between ~26 and 31 km. The disparity was found to decrease with altitude above ~31 km (Figure 6-11). Similar conclusions regarding the tendency of the $[NO_x]/[NO_y]$ ratio to exceed theory between 20 and 30 km were reached by Rinsland *et al.* (1996), Kondo *et al.* (1997), Lary *et al.* (1997), and Sen *et al.* (1998). For altitudes above 30 km, theory and observation of the $[NO_x]/[NO_y]$ ratio have been shown to be in good agreement by many studies (Rinsland *et al.*, 1996; Kondo *et al.*, 1997; Lary *et al.*, 1997; Morris *et al.*, 1997; Sen *et al.*, 1998). The observed upper stratospheric ratio of $[NO_2]/[NO]$ is also simulated reasonably well (Sen *et al.*, 1998). Consequently, these measurements indicate that the catalytic removal of $O_3$ by the $NO_x$ cycle in the upper stratosphere proceeds at a rate consistent with theory (Jucks *et al.*, 1996; Osterman *et al.*, 1997).

Further evidence of a strong fundamental understanding of the processes that partition $NO_y$ gases was shown by two studies that examined the relation between $NO_x$ and $N_2O_5$. Nevison *et al.* (1996) showed that sunset/sunrise ratios for $NO_x$ measured by HALOE are consistent with the calculated diurnal variation of $N_2O_5$. Sen *et al.* (1998) similarly concluded that the measured variation of concentrations of $N_2O_5$ and $NO_x$ between sunrise and sunset agreed well with model simulations and exhibited the expected ~2:1 stoichiometry at all altitudes between 22 and 35 km. These studies have important implications also for the lower stratosphere, because the hydrolysis of $N_2O_5$ on sulfate aerosols is an important sink for $NO_x$ below 30 km.

The most notable exception to the numerous studies showing relatively good understanding of the partitioning of $NO_y$ gases in the upper stratosphere is the study of Kawa *et al.* (1995) that focused on CLAES and ISAMS measurements of $N_2O_5$ and $HNO_3$ at high altitude. An analysis of these observations using the Goddard 3-D model indicated the occurrence of an unknown process that converts $N_2O_5$ to $HNO_3$ above ~35 km in polar regions during winter. Kawa *et al.* (1995) suggested heterogeneous conversion on hydrated ion clusters as a possible explanation for the observations. Bekki *et al.* (1997) suggested that the observed partitioning may be caused in part by enhanced

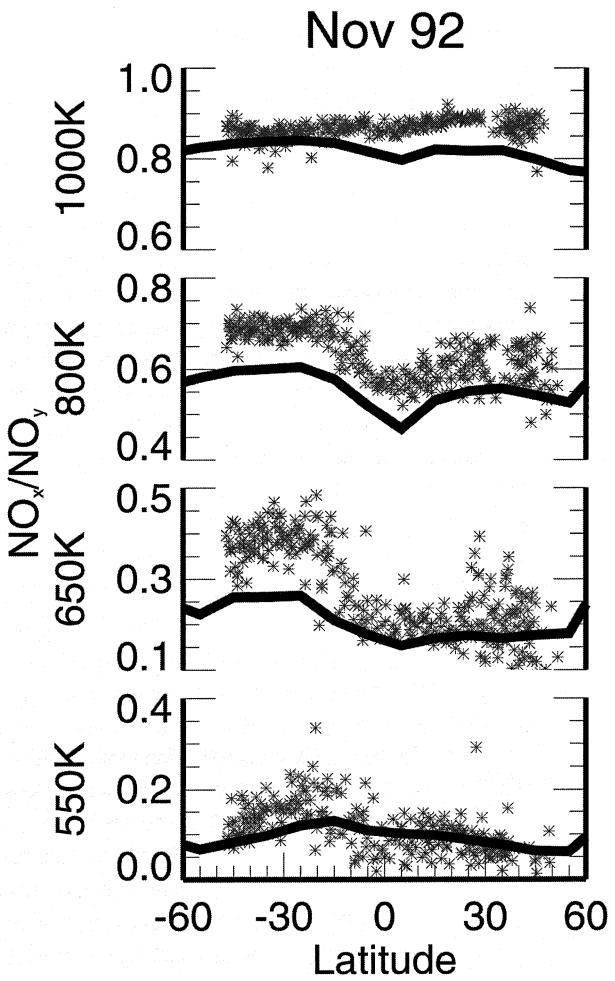


**Figure 6-11.** The $NO_x/NO_y$ ratio at four potential temperature levels (550, 650, 800, and 1000 K that correspond to approximately 22, 26, 31, and 35 km, respectively) for November 1992 based on a trajectory mapped analysis of UARS data (asterisks) compared to calculated values from the Goddard 2-D model (solid line), constrained by distributions of temperature, $O_3$, $H_2O$, $N_2O$, and $CH_4$ from UARS instruments and aerosol surface area from SAGE II. Kinetic parameters from DeMore *et al.* (1994). Adapted from Morris *et al.* (1997).

concentrations of small sulfate aerosol particles. Although this problem bears further investigation, it is important to note that the anomalous ratios of $[N_2O_5]/[HNO_3]$ are confined to high latitudes. Ratios observed for the midlatitude upper stratosphere agree well with theory (Kawa *et al.*, 1995).

Catalytic removal of $O_3$ by the $NO_x$ cycle in the upper stratosphere has been shown to proceed at a rate consistent with theory *provided the distribution of* $NO_y$ *is known accurately* (e.g., Jucks *et al.*, 1996; Osterman *et al.*, 1997). However, few studies have focused on quantitative comparisons of calculated and observed $NO_y$ in the upper stratosphere. The substantial variability in the concentration of $NO_y$ between 30 and 50 km exhibited by 2-D model simulations underscores the need for further investigations (Park *et al.*, 1998). A wealth of existing balloon (Kondo *et al.*, 1996; Oelhaf *et al.*, 1996; Sen *et al.*, 1998), ATMOS (Rinsland *et al.*, 1996), and UARS (Gordley *et al.*, 1996) observations of $NO_y$ in the upper stratosphere are available to better quantify our understanding of the seasonal and altitude distribution of $NO_y$. Instruments on each of these platforms also measure the concentration of $N_2O$; correlation diagrams of $NO_y$ (sink) versus $N_2O$ (source) provide a stringent test of our understanding of processes that regulate $NO_y$. Nevison *et al.* (1997) have pointed out possible deficiencies in our understanding of upper stratospheric $NO_y$ that should be addressed by future studies.

### 6.3.3 Chlorine Species

Catalytic removal of ozone by chlorinated compounds derived from industrial chlorofluorocarbons (CFCs) was first suggested by Molina and Rowland (1974). Chlorine monoxide (ClO) participates in numerous catalytic cycles that lead to removal of ozone in the lower stratosphere. In the upper stratosphere, however, the cycle limited by the reaction $ClO + O \rightarrow Cl + O_2$ is the only significant halogen-related loss process. Organic chlorine gases such as CFCs and $CCl_4$ are extraordinarily inert in the troposphere, demonstrated by observations of nearly uniform volume mixing ratios for these compounds in the lower atmosphere (Montzka *et al.*, 1996). These gases decompose in the stratosphere due to increased levels of ultraviolet radiation as well as much higher concentrations of OH and $O(^1D)$. Inorganic chlorine species ($Cl_y$) are produced in the stratosphere following photolysis and reaction of the organic source species. Because HCl and sodium chloride (NaCl) are highly water soluble, they are effectively scavenged in the troposphere, and air entering the stratosphere does not normally contain significant concentrations of either compound. Removal of $Cl_y$ from the stratosphere occurs by transport to the troposphere, where HCl is removed by precipitation.

### The Chlorine Budget

The global distribution of $CCl_2F_2$ (CFC-12) was observed for six seasons (January 1992 to May 1993) by the CLAES instrument aboard UARS (Nightingale *et al.*, 1996). The observations indicate features such as upward bowing of isopleths in the tropics and minimum values in the polar regions consistent with progressively faster removal of CFC-12 at higher altitudes. The overall patterns and morphology of the CLAES observations of CFC-12 are simulated well by the Lawrence Livermore National Laboratory (LLNL) 2-D model and are also consistent with profiles of CFC-12 measured by ATMOS, MkIV, and a whole-air sampler (Nightingale *et al.*, 1996; see also Section 6.2).

Our understanding of the budget of chlorinated compounds can be tested in a simpler and more precise manner than for the hydrogen and nitrogen families of gases owing to the long lifetime of $Cl_y$ at all levels in the stratosphere and the fact that the entire chlorine content of the organic source molecules is converted directly to $Cl_y$ gases. In contrast, only a fraction of $N_2O$ is converted to $NO_y$, and this fraction varies with altitude, latitude, and season. The sum of the total organic and inorganic chlorine content should be nearly uniform throughout the stratosphere, with slight variations due to the ensemble age of air parcels that reflects the changing tropospheric burden of organic chlorine. Zander *et al.* (1996) constructed profiles of the total organic chlorine content ($CCl_y$) of the midlatitude stratosphere during November 1994 from ATMOS and balloon measurements of the eight most important chlorinated source gases. The profile of $CCl_y$ was compared to measurements of HCl and $ClONO_2$ obtained by ATMOS, ClO from the shuttle-borne Millimeter-wave Atmospheric Sounder (MAS), and HOCl from the MkIV interferometer (Figure 6-12). The total chlorine burden of the stratosphere, defined as $Cl_{TOT} = [CCl_y] + [HCl] + [ClONO_2] + [ClO] + [HOCl] + [COClF]$, was shown to be nearly constant with altitude at a value of ~3.5 ppbv.

The stratospheric chlorine loading derived by Zander *et al.* (1996) for 1994 is similar to the tropospheric organic chlorine content that prevailed in 1989-1990 (Kaye *et al.*, 1994). Observations of $CO_2$, $SF_6$, and HF have demonstrated that upper stratospheric air at midlatitudes is about 5-6 years old (Harnisch *et al.*, 1996; Russell *et al.*, 1996; Sen *et al.*, 1996; see also Chapter 7 and Section 6.2), accounting for the ~6-year lag in the chlorine loading of the upper stratosphere relative to the surface. The only organic source gas with a significant natural source is $CH_3Cl$, which contributes about 0.55 ppbv to the organic chlorine content of the troposphere (Kaye *et al.*, 1994; Chapter 2). The observations of Zander *et al.* (1996) provide strong scientific evidence that the bulk of stratospheric inorganic chlorine is derived

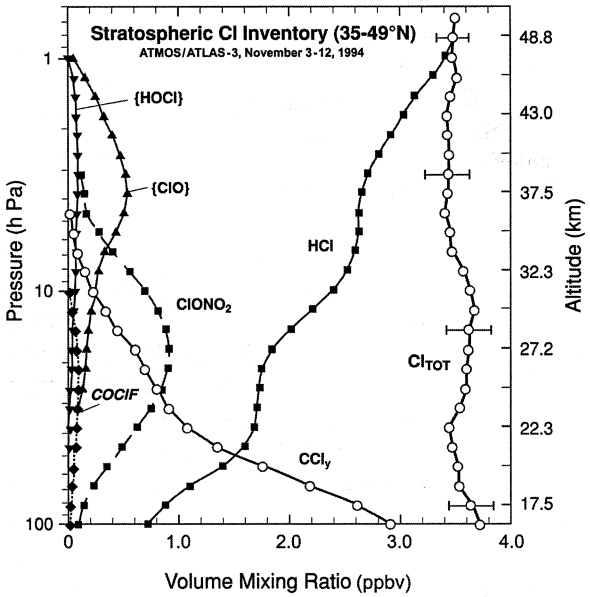


**Figure 6-12.** Profiles of $CCl_y$ (total chlorine content of organic source gases) for the Northern Hemisphere midlatitude region based on ATMOS measurements during November 1994 (the Atmospheric Laboratory for Applications and Science-3 (ATLAS-3) mission) of $CCl_3F$, $CCl_2F_2$, $CHClF_2$, and $CH_3Cl$ as well as in situ measurements of $CH_3CCl_3$ and $C_2Cl_3F_3$ obtained by the Research Center Jülich cryogenic whole-air sampler during a balloon flight in October 1994. Profiles of HCl and $ClONO_2$ were obtained by ATMOS during the same mission. The braces denote gases whose mixing ratio profile was measured by an instrument other than ATMOS. The profile for ClO was measured by the MAS experiment on the same ATLAS-3 Space Shuttle payload (Aellig *et al.*, 1996b) and the profile for HOCl was measured by the MkIV FTIR during September 1993 at 32°N. The profile for chlorofluorocarbonyl (COClF) originates from a model calculation (Zander *et al.*, 1996). $Cl_{TOT}$ represents a summation of concentrations of $CCl_y$, HCl, $ClONO_2$, ClO, HOCl, and COClF. Adapted from Zander *et al.* (1996).

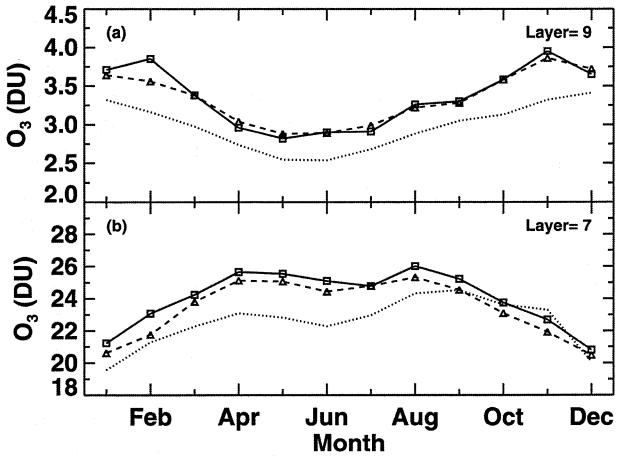


**Figure 6-18.** Seasonal cycle of the ozone amount in Umkehr layer 9 (1-2 hPa, ~48-42 km, top panel) and 7 (4-8 hPa, ~38-33 km, bottom panel). Each point is a monthly mean value; latitude region is between 35°N and 45°N. The squares and solid lines indicate SAGE II values (Version 5.96); the triangles and dashed lines, SBUV(2). Shown are average monthly mean values using all SAGE and SBUV data between October 1984 and October 1994. (Adapted from Wang *et al.*, 1996). Dotted line shows results from the Max Planck Institute for Chemistry (MPIC) model (see Chapter 12) for 1990, including the reaction ClO + OH → HCl + $O_2$.

altitude range, the seasonal variation of ozone is controlled by the temperature variation of the relevant ozone destruction rates; i.e., ozone destruction rates are most rapid when temperatures are warmest during summer (Perliski *et al.*, 1989). For Umkehr layer 7 (38-33 km) outside the tropics, in contrast, concentrations of ozone during winter are about 20% lower than maximum concentrations that occur during summer (Figure 6-18). For these altitudes, the seasonal variation is strongly influenced by the variation of the odd-oxygen production rates, which peak during summer (Perliski *et al.*, 1989). The seasonal behavior of upper stratospheric ozone is reasonably well reproduced by current 2-D models (e.g., Figure 6-18). Chandra *et al.* (1993) showed that the agreement in the amplitude of the seasonal cycle of upper stratospheric ozone between model simulations and Solar Backscatter Ultraviolet (SBUV) spectrometer observations was improved if models allowed for production of HCl from a minor channel of the reaction ClO + OH.

### 6.4.3 Solar Effects on Ozone

Stratospheric $O_3$ is produced by the photolysis of $O_2$ at ultraviolet wavelengths (Section 6.3.5). The solar ultraviolet flux has been observed to vary as a consequence of the 27-day period of solar rotation and the 11-year variation in the frequency of solar sunspots and faculae, commonly referred to as the 11-year solar cycle. Spaceborne measurements obtained by instruments aboard UARS have led to accurate definitions of the amplitude of the variation of solar irradiance, as a function of wavelength, for both the 27-day solar rotation (e.g., London *et al.*, 1993) and 11-year solar cycle (e.g., Lean *et al.*, 1997). These measurements have been used in a number of model studies described below.

The effects of the 27-day solar rotation on stratospheric $O_3$ are small, with an amplitude of 0.2 to 0.3% variation (Hood and Cantrell, 1988). Chen *et al.* (1997) have shown that the observed amplitude and phase of this variation of stratospheric $O_3$ is simulated well using a model that allows for feedbacks between temperature and $O_3$ (the temperature response in the middle atmosphere is largely determined by the solar-induced variation of $O_3$). Neglecting the observed solar-induced temperature variation worsens the agreement between measured and calculated changes in $O_3$ (Chen *et al.*, 1997). The small variations of $O_3$ over the 27-day period of solar rotation have no direct consequences for long-term changes in stratospheric $O_3$. However, these studies provide increased confidence in our quantitative understanding of the sensitivity of $O_3$ to changes in solar flux and temperature, which is relevant for understanding decadal reductions in upper stratospheric $O_3$ (see Sections 6.4.4 and 6.5).

Significant variations in upper stratospheric $O_3$ occur over the 11-year solar cycle. Chandra and McPeters (1994) reported changes of 5 to 7%, with $O_3$ peaking during solar maximum due primarily to the 7 to 8% increase in solar irradiance near 200 nm. McCormack and Hood (1996) have conducted a detailed analysis of the latitude, altitude, and seasonal dependence of the variations of upper stratospheric $O_3$ and temperature over the 11-year solar cycle based on 15 years of satellite data. They found that the largest variations of $O_3$ occur between 42 and 47 km, with peak values of 5.9 ± 1.2% near 40°S and 4.6 ± 1.0% near 40°N.

The amplitude of the solar-induced response of $O_3$ between 40 and 50 km is larger than found by models,

whereas the observed variation in $O_3$ between 30 and 40 km is smaller than calculated (McCormack and Hood, 1996). The three models described in that study have various means of accounting for $O_3$-temperature feedbacks. Best agreement with the observed change in $O_3$ near 40 km is found by the model of Fleming *et al.* (1995), the only model constrained by the observed temperature variation. It must be noted, however, that the observed variations in temperature, especially at higher latitudes in the altitude regime between 35 and 40 km, are not simulated particularly well by a radiative model constrained by observed variations in solar irradiance and $O_3$ (McCormack and Hood, 1996). This has led McCormack and Hood (1996) to suggest that changes in dynamical heating of the stratosphere over the 11-year solar cycle, perhaps related to solar-induced changes in the mean meridional circulation, may contribute to the observed temperature response at higher latitudes. The recent study of Siskind *et al.* (1998) has established the need to consider variations in $CH_4$ (which may also be affected by the mean circulation and which regulates the partitioning of ClO relative to HCl in the upper stratosphere) as well in studies of the response of upper stratospheric $O_3$ to the 11-year solar cycle.

It has been clearly established that upper stratospheric $O_3$ varies with an amplitude of 5 to 7% over the 11-year solar cycle. While models are able to simulate the general response of $O_3$, the lack of precise quantitative agreement between theory and observation requires further study. The satellite record for profiles of upper stratospheric $O_3$ currently covers slightly less than two full solar-cycles, so continued observation will be important for gaining a better understanding of this problem.

Because the amplitude of the response of upper stratospheric $O_3$ to the 11-year solar cycle is comparable to the magnitude of the expected decrease in $O_3$ due to the build-up of anthropogenic chlorine during a 10-year time period, it is important that this process be considered when studying long-term trends of $O_3$. The signature of the 11-year solar cycle is straightforward to identify in a long time series of $O_3$ observations (e.g., Chandra and McPeters, 1994; Miller *et al.*, 1997). Typically, the 11-year solar cycle is accounted for when estimating long-term trends of stratospheric $O_3$ by using statistical analyses based on a proxy for the variation in solar ultraviolet irradiance (e.g., Miller *et al.*, 1997; Stolarski and Randel, 1998), often provided by the long-term space-based measurement of the chromospheric MgII absorption line at 280 nm (e.g., DeLand and Cebula, 1993). The estimates for the long-term trends of stratospheric $O_3$ described in Section 6.4.4 and Section 6.5 have been found by accounting for this effect. Reconstructions of the variation of solar ultraviolet irradiance over the time period from 1980 to 1996 (e.g., Figure 20 of Lean *et al.*, 1997) show that the maximum and minimum irradiances over the past two solar cycles repeat in a similar fashion, demonstrating that the observed decline in upper stratospheric $O_3$ over this period was not driven by changes in solar irradiance. Other solar-related processes, such as production of $NO_x$ and $HO_x$ by solar proton events, can have significant effects on polar upper stratospheric $O_3$ over short time periods but are unimportant when considering long-term trends of $O_3$ (Jackman *et al.*, 1996).

### 6.4.4 Ozone Trends

A significant decline of upper stratospheric ozone has been identified between the years 1979 to 1991 (i.e., before the eruption of Mt. Pinatubo) from analysis of satellite, Umkehr, and lidar measurements of ozone profiles for both the Northern and Southern Hemisphere midlatitudes (e.g., WMO, 1995; Claude *et al.*, 1994; Hollandsworth *et al.*, 1995; Wang *et al.*, 1996; Harris *et al.*, 1997; Miller *et al.*, 1997; see also Chapter 4). Comparisons of the trends derived from different instruments for the Northern Hemisphere midlatitudes in the 1980s (Miller *et al.*, 1997) agree relatively well and show a statistically significant decline, increasing from about 2.5% per decade at 30 km to about 7.5% per decade at 40 to 45 km (Figure 6-19). Because most of the stratospheric ozone column resides in the lower stratosphere, total ozone measurements (e.g., from TOMS or Dobson instruments) are not useful for the detection of changes in upper stratospheric ozone.

Consideration of a longer time series of Stratospheric Aerosol and Gas Experiment (SAGE), SBUV, and Umkehr measurements, from 1980 to 1996, yields very similar estimates of the long-term decline in upper stratospheric ozone (Figure 6-19; Chapter 4; see also Stolarski and Randel, 1998). Generally, the confidence intervals are somewhat smaller because of the longer time period. These findings are confirmed by an analysis of a 9-year time series of midlatitude lidar observations (Steinbrecht *et al.*, 1998). The quantitative similarity of the observed trends from several independent measurement systems provides confidence that a true atmospheric phenomenon has been observed.

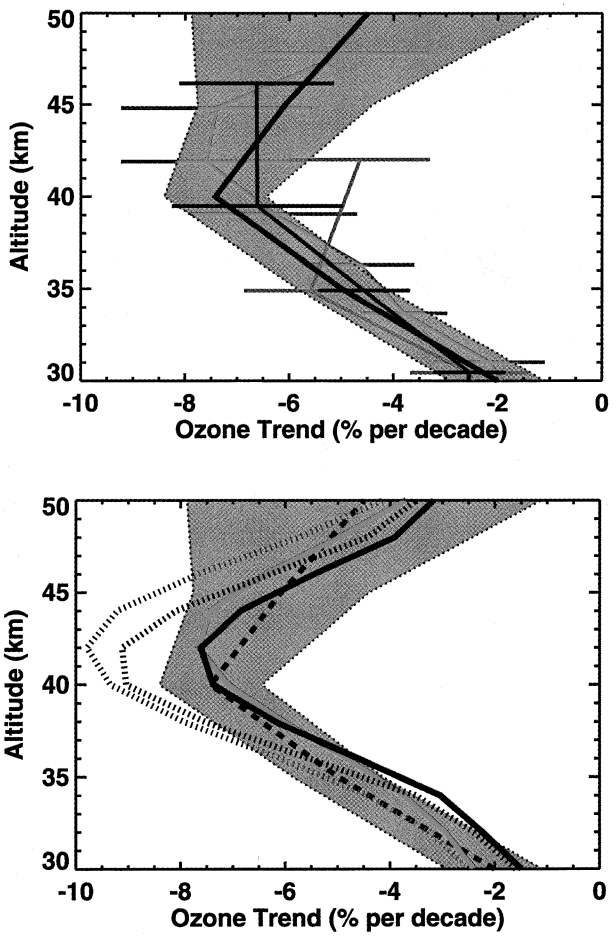


**Figure 6-19.** Ozone trends for the Northern Hemisphere midlatitudes (30°N-50°N). Top panel: trends derived from SBUV (1979-1991, blue line), from Umkehr (1968-1991, green line), and from SAGE (1979-1990, red line) observations, in %/decade (adapted from Miller *et al.*, 1997). The combined trend (black line) of all three measurement systems for the period 1980-1996 (adapted from Stolarski and Randel, 1998) is also shown with an estimate of the trend uncertainty (gray shaded area). Bottom panel: the combined trend (black dashed line) of all three measurement systems for the period 1980 to 1996 compared to ozone trends (likewise for 30°N-50°N) calculated by the Goddard Space Flight Center (GSFC) (red lines) and the Lawrence Livermore National Laboratory (LLNL) (blue lines) two-dimensional models, for scenario A (see Chapter 12) for the period 1979 to 1995, in %/decade. Both the standard scenario (solid lines) and results neglecting reaction $ClO + OH \rightarrow HCl + O_2$ (stippled lines) are shown.

Recent calculations of the long-term changes in ozone found using 2-D models are in reasonable agreement with the latitude and altitude characteristics of the observed trends in upper stratospheric ozone (e.g., Jackman *et al.*, 1996; Considine *et al.*, 1998), but the calculated trends are somewhat larger than those derived from observations. However, these models also tend to overestimate ClO (Chandra *et al.*, 1995; Jackman *et al.*, 1996), leading to an overestimate of the ozone loss rate due to the chlorine catalytic cycle (6-2).

As discussed in Section 6.3.3, allowing for production of HCl from a minor (~6%) channel of the reaction ClO + OH (Lipson *et al.*, 1997) leads to good agreement between calculated and observed ClO (e.g., Stachnik *et al.*, 1992) and consequently results in a reduction of the calculated long-term trend of $O_3$ at 40 km. Calculated trends for Northern Hemisphere midlatitudes from current 2-D models that include the HCl channel are now in *good quantitative agreement* with observations (solid lines in Figure 6-19). If the HCl channel is neglected, the observed trends are overestimated (stippled lines in Figure 6-19).

The meridional pattern of the observed ozone decline (Figure 6-20) shows that trends are significantly different from zero in the upper stratosphere at all latitudes outside the tropics. The largest negative trend remains at about 40 to 45 km in this global view; however, the declines in ozone are larger for higher latitudes than for the lower latitudes (Figure 6-20). A larger trend at high latitudes is consistent with the fact that the "oldest" stratospheric air resides in this region (Section 6.2). An older age of air enhances the efficiency of the ozone-depleting chlorine cycle in two ways. As air ages, a larger fraction of total available chlorine is converted to the inorganic forms that react with $O_3$. Second, and more importantly, older air is characterized by smaller abundances of $CH_4$ (Figure 6-4), leading to a shift in the partitioning of $Cl_y$ species towards Cl and ClO, and away from HCl, thus enhancing the ozone loss rates (Solomon and Garcia, 1984). In the past, interhemispheric differences (i.e., larger trends in the Southern Hemisphere) were reported for upper stratospheric ozone trends (WMO, 1995; Hollandsworth *et al.*, 1995; Harris *et al.*, 1997). However, in the most recent evaluation of upper stratospheric ozone measurements (Stolarski and Randel, 1998; see also Figure 6-20), there is no longer evidence for this difference.

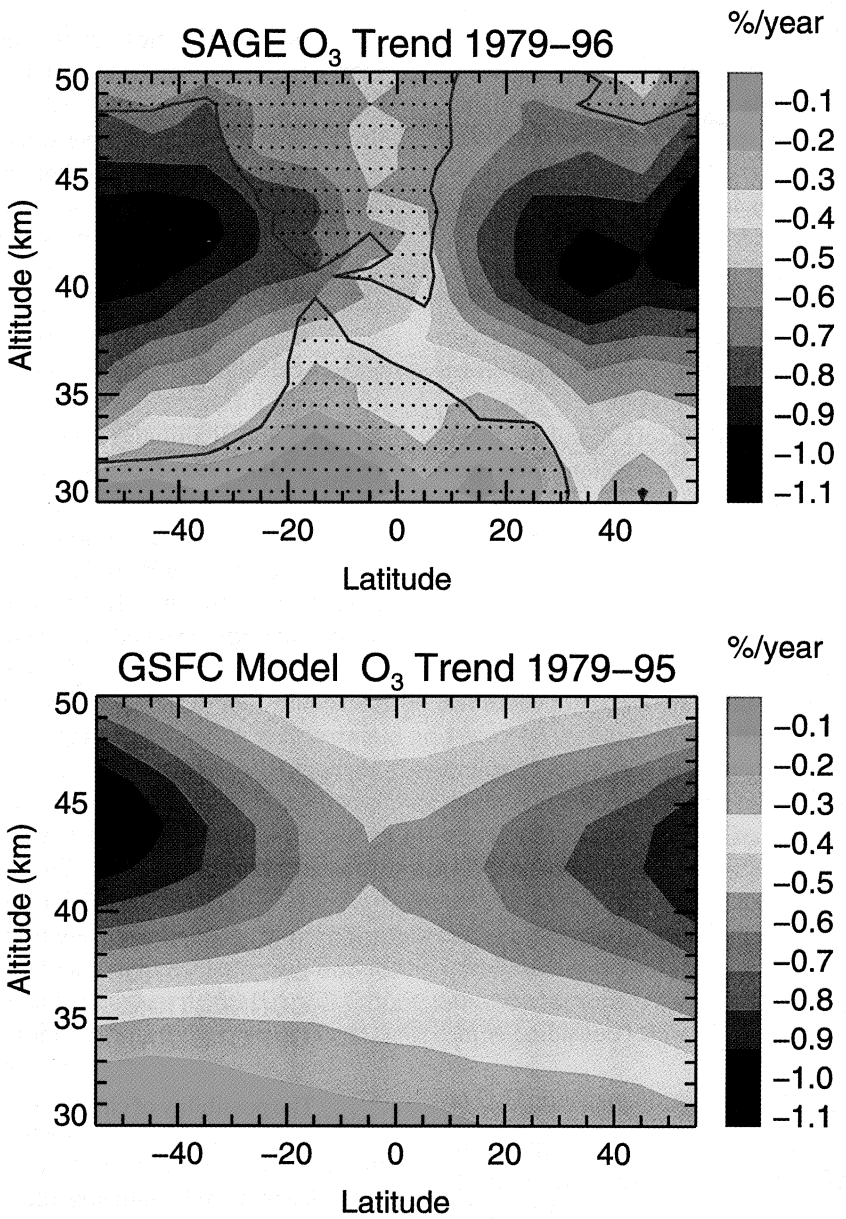


**Figure 6-20.** The meridional and vertical structure of stratospheric ozone trends. Top panel: Ozone trends derived from SAGE I/II observations from 1979 to 1996 expressed in %/year of the midpoint of the time series (1987). Results are contoured from calculations done in 5° latitude bands and 1-km altitude intervals. The stippled areas inside the gray contour lines indicate regions where the trends do not differ from zero, within 95% confidence limits. The estimate of uncertainty contains terms due to the SAGE I reference height correction and the SAGE II sunrise/sunset trend differences (adapted from Stolarski and Randel, 1998). Bottom panel: Ozone trends calculated by the GSFC two-dimensional model, for the standard scenario including the reaction channel ClO + OH → HCl + $O_2$ (scenario A, see Chapter 12), for the period 1979 to 1995 (in %/year).

Through a more precise knowledge of the relevant chemical kinetics, datasets with improved long-term calibration and internal consistency, as well as refined photochemical and dynamical models, there is now good quantitative agreement between observed and calculated long-term reductions of $O_3$ between 30 and 50 km altitude (Section 6.4.4).

The relation of the observed decline of upper stratospheric ozone and the increase of the stratospheric chlorine loading is depicted schematically in Figure 6-21. A significant reduction in the concentration of ozone was observed during the 1980s and 1990s, with the largest losses reaching 7.4 ± 1.0%/decade at 40 km altitude (Figure 6-21, panel b). A similar pattern of the decline in upper stratospheric $O_3$ due to the build-up of industrially derived chlorine was predicted by the earliest modeling efforts (Figure 6-21, panel a). These calculations were based on a projected increase of $Cl_y$ to a level of 5.3 ppbv, a value never reached in the contemporary stratosphere.

Photochemical model calculations using the most recent set of the relevant kinetic parameters (DeMore *et al.*, 1997; Lipson *et al.*, 1997) show that a substantial fraction of the loss of $O_3$ in today's upper stratosphere occurs by the ClO + O cycle, peaking at a value of ~30% of the overall ozone loss rate at an altitude of 40 km (Figure 6-21, panel d, and Figure 6-2). Current models have been shown to reproduce accurately the observed concentrations of the hydrogen, nitrogen, and chlorine gases that regulate photochemical removal of $O_3$ (Section 6.3).

Allowing in a photochemical model for the growth of upper stratospheric $Cl_y$ (at 55 km) from a value of 2 ppbv in 1980 to 3.6 ppbv in 1996, and keeping everything else unchanged, leads to a calculated increase in the overall $O_3$ loss rate very similar in shape and magnitude to the observed decline in $O_3$ (Figure 6-21, panel c, solid line). Allowing in addition for the decrease in upper stratospheric temperature observed during the past 16 years (Chapter 5) results in a slightly lower estimate for the increase in the overall $O_3$ loss rate (Figure 6-21, panel c, dashed line) mainly because of the temperature dependencies of the rate-limiting reactions for $O_3$ removal. Both the observed reduction in $O_3$ as well as the calculated increase in the $O_3$ loss rate peak at a value of ~7 to 8% per decade at about 40 km altitude. More sophisticated models, allowing for radiative, dynamical, and chemical feedbacks associated with the increased burden of stratospheric chlorine, lead to calculated reductions in upper stratospheric $O_3$ that also agree very closely with the observed depletion (e.g., Figures 6-19 and 6-20; see also Chapter 12).

A decrease in the concentration of stratospheric chlorine is expected because of the Montreal Protocol and its subsequent Amendments. Indeed, the tropospheric burden of ozone-depleting chlorine compounds has reached its maximum between mid-1992 and mid-1994 and is beginning to decline slowly (Montzka *et al.*, 1996; see also Chapter 1). Near 40 km altitude there is a direct and strong correspondence between the concentration of ClO and loss of $O_3$, less variability and shorter lifetimes of $O_3$ than in lower regions of the atmosphere, and little direct effect of transport or small changes in temperature on the concentration of $O_3$. Therefore, it is conceivable that the "recovery" of $O_3$ due to the decreasing burden of stratospheric chlorine will first become apparent at 40 km (Chapter 12). Future observations of the upper stratosphere will likely be directed toward detecting the expected recovery of upper stratospheric ozone.

## REFERENCES

Abbas, M.M., M.R. Gunson, M.J. Newchurch, H.A. Michelsen, R.J. Salawitch, M. Allen, M.C. Abrams, A.Y. Chang, A. Goldman, F.W. Irion, E.J. Moyer, R. Nagaraju, C.P. Rinsland, G.P. Stiller, and R. Zander, The hydrogen budget of the stratosphere inferred from ATMOS measurements of $H_2O$ and $CH_4$, *Geophys. Res. Lett.*, *23*, 2405-2408, 1996a.

Abbas, M.M., H.A. Michelsen, M.R. Gunson, M.C. Abrams, M.J. Newchurch, R.J. Salawitch, A.Y. Chang, A. Goldman, F.W. Irion, G.L. Manney, E.J. Moyer, R. Nagaraju, C.P. Rinsland, G.P. Stiller, and R. Zander, Seasonal variations of water vapor in the lower stratosphere inferred from ATMOS/ATLAS-3 measurements of $H_2O$ and $CH_4$, *Geophys. Res. Lett.*, *23*, 2401-2404, 1996b.

Abrams, M.C., G.L.Manney, M.R. Gunson, M.M. Abbas, A.Y. Chang, A. Goldman, F.W. Irion, H.A. Michelsen, M.J. Newchurch, C.P. Rinsland, R.J. Salawitch, G.P. Stiller, and R. Zander, ATMOS/ATLAS-3 observations of long-lived tracers and descent in the Antarctic vortex in November 1994, *Geophys. Res. Lett.*, *23*, 2345-2348, 1996a.

Abrams, M.C., G.L. Manney, M.R. Gunson, M.M. Abbas, A.Y. Chang, A. Goldman, F.W. Irion, H.A. Michelsen, M.J. Newchurch, C.P. Rinsland, R.J. Salawitch, G.P. Stiller, and R. Zander, Trace gas transport in the Arctic vortex inferred from ATMOS ATLAS-2 observations during April 1993, *Geophys. Res. Lett.*, *23*, 2341-2344, 1996b.

Aellig, C.P., J. Bacmeister, R.M. Bevilacqua, M. Daehler, D. Kriebel, T. Pauls, D. Siskind, N. Kämpfer, J. Langen, G. Hartmann, A. Berg, J.H. Park, and J.M. Russell III, Space-borne $H_2O$ observations in the Arctic stratosphere and mesosphere in the spring of 1992, *Geophys. Res. Lett.*, *23*, 2325-2328, 1996a.

Aellig, C.P., N. Kämpfer, C. Rudin, R.M. Bevilacqua, W. Degenhardt, P. Hartogh, C. Jarchow, K. Künzi, J.J. Olivero, C. Croskey, J.W. Waters, and H.A. Michelsen, Latitudinal distribution of upper stratospheric ClO as derived from space borne microwave spectroscopy, *Geophys. Res. Lett.*, *23*, 2321-2324, 1996b.

Allen, D.R., J.L. Stanford, L.S. Elson, E.F. Fishbein, L. Froidevaux, and J.W. Waters, The 4-day wave as observed from the Upper Atmosphere Research Satellite Microwave Limb Sounder, *J. Atmos. Sci.*, *54*, 420-434, 1997.

Allen, M., and M.L. Delitsky, Inferring the abundances of ClO and $HO_2$ from Spacelab 3 Atmospheric Trace Molecule Spectroscopy observations, *J. Geophys. Res.*, *96*, 2913-2919, 1991.

Allen, M., and J.E. Frederick, Effective photodissociation cross sections for molecular oxygen and nitric oxide in the Schumann-Runge bands, *J. Atmos. Sci.*, *39*, 2066-2075, 1982.

Amoruso, A., L. Crescentini, M.S. Cola, and G. Fiocco, Oxygen absorption cross-section in the Herzberg continuum, *J. Quant. Spectrosc. Radiat. Transfer*, *56*, 145-152, 1996.

Anderson, G.P., and L.A. Hall, Attenuation of solar irradiance in the stratosphere: Spectrometer measurements between 191 and 207 nm, *J. Geophys. Res.*, *88*, 6801-6806, 1983.

Andrews, D.G., J.R. Holton, and C.B. Leovy, *Middle Atmosphere Dynamics*, Academic Press, London, U.K., 1987.

Appenzeller, C., J.R. Holton, and K.H. Rosenlof, Seasonal variation of mass transport across the tropopause, *J. Geophys. Res.*, *101*, 15071-15078, 1996.

Bacmeister, J.T., M.R. Schoeberl, M.E. Summers, J.R. Rosenfield, and X. Zhu, Descent of long-lived trace gases in the winter polar vortex, *J. Geophys. Res.*, *100*, 11669-11684, 1995.

Bacmeister, J.T., D.E. Siskind, M.E. Summers, and S.D. Eckermann, Age of air in a zonally averaged two-dimensional model, *J. Geophys. Res.*, *103*, 11263-11288, 1998.

Bates, D.R., and M. Nicolet, The photochemistry of atmospheric water vapor, *J. Geophys. Res.*, *55*, 301-327, 1950.

Bekki, S., M.P. Chipperfield, J.A. Pyle, J.J. Remedios, S.E. Smith, R.G. Grainger, A. Lambert, J.B. Kumer, and J.L. Mergenthaler, Coupled aerosol-chemical modeling of UARS $HNO_3$ and $N_2O_5$ measurements in the Arctic upper stratosphere, *J. Geophys. Res.*, *102*, 8977-8994, 1997.

Blindauer, C., V. Rozanov, and J.P. Burrows, Actinic flux and photolysis frequency comparison computations using the model PHOTOGT, *J. Atmos. Chem.*, *24*, 1-21, 1996.

Burnett, C.R., and E.B. Burnett, The regime of decreased OH vertical column abundances at Fritz Peak Observatory, CO: 1991-1995, *Geophys. Res. Lett.*, *23*, 1925-1927, 1996.

Callis, L.B., and J.D. Lambeth, $NO_y$ formed by precipitating electron events in 1991 and 1992: Descent into the stratosphere as observed by ISAMS, *Geophys. Res. Lett.*, *25*, 1875-1878, 1998.

Callis, L.B., D.N. Baker, M. Natarajan, J.B. Blake, R.A. Mewaldt, R.S. Selesnick, and J.R. Cummings, A 2D model simulation of downward transport of $NO_y$ into the stratosphere: Effects on the 1994 austral spring $O_3$ and $NO_y$, *Geophys. Res. Lett.*, *23*, 1905-1908, 1996.

Carr, E.S., R.S. Harwood, P.W. Mote, G.E. Peckham, R.A. Suttie, W.A. Lahoz, A. O'Neill, L. Froidevaux, R.F. Jarnot, W.G. Read, J.W. Waters, and R. Swinbank, Tropical stratospheric water vapor measured by the Microwave Limb Sounder (MLS), *Geophys. Res. Lett.*, *22*, 691-694, 1995.

Chance, K., W.A. Traub, D.G. Johnson, K.W. Jucks, P. Ciarpallini, R.A. Stachnik, R.J. Salawitch, and H.A. Michelsen, Simultaneous measurements of stratospheric $HO_x$, $NO_x$, and $Cl_x$: Comparison with a photochemical model, *J. Geophys. Res.*, *101*, 9031-9043, 1996.

Chandra, S., and R.D. McPeters, The solar cycle variation of ozone in the stratosphere inferred from Nimbus 7 and NOAA 11 satellites, *J. Geophys. Res.*, *99*, 20665-20671, 1994.

Chandra, S., C.H. Jackman, A.R. Douglass, E.L. Fleming, and D.B. Considine, Chlorine catalyzed destruction of ozone: Implications for ozone variability in the upper stratosphere, *Geophys. Res. Lett.*, *20*, 351-354, 1993.

Chandra, S., C.H. Jackman, and E.L. Fleming, Recent trends in ozone in the upper stratosphere: Implications for chlorine chemistry, *Geophys. Res. Lett.*, *22*, 843-846, 1995.

Chen, L., J. London, and G. Brasseur, Middle atmospheric ozone and temperature responses to solar irradiance variations over 27-day periods, *J. Geophys. Res.*, *102*, 29957-29979, 1997.

Chipperfield, M.P., L.J. Gray, J.S. Kinnersley, and J. Zawodny, A two-dimensional model study of the QBO signal in SAGE II $NO_2$ and $O_3$, *Geophys. Res. Lett.*, *21*, 589-592, 1994.

Clancy, R.T., B.J. Sandor, D.W. Rusch, and D.O. Muhleman, Microwave observations and modeling of $O_3$, $H_2O$, and $HO_2$ in the mesosphere, *J. Geophys. Res.*, *99*, 5465-5473, 1994.

Claude, H., F. Schönenborn, W. Steinbrecht, and W. Vandersee, New evidence for ozone depletion in the upper stratosphere, *Geophys. Res. Lett.*, *21*, 2409-2412, 1994.

Coffey, M.T., Observations of the impact of volcanic activity on stratospheric chemistry, *J. Geophys. Res.*, *101*, 6767-6780, 1996.

Connor, B.J., D.E. Siskind, J.J. Tsou, A. Parrish, and E.E. Remsberg, Ground-based microwave observations of ozone in the upper stratosphere and mesosphere, *J. Geophys. Res.*, *99*, 16757-16770, 1994.

Considine, D.B., A.E. Dessler, C.H. Jackman, J.E. Rosenfield, P.E. Meade, M.R. Schoeberl, A.E. Roche, and J.W. Waters, Interhemispheric asymmetry in the 1 mbar $O_3$ trend: An analysis using an interactive zonal mean model and UARS data, *J. Geophys. Res.*, *103*, 1607-1618, 1998.

Considine, G.D., L. Deaver, E.E. Remsberg, and J.M. Russell III, HALOE observations of a slowdown in the rate of increase of HF in the lower mesosphere, *Geophys. Res. Lett.*, *24*, 3217-3220, 1997.

Conway, R.R., M.H. Stevens, J.G. Cardon, S.E. Zasadil, C.M. Brown, J.S. Morrill, and G.H. Mount, Satellite measurements of hydroxyl in the mesosphere, *Geophys. Res. Lett.*, *23*, 2093-2096, 1996.

Coy, L., and R. Swinbank, Characteristics of stratospheric winds and temperatures produced by data assimilation, *J. Geophys. Res.*, *102*, 25763-25781, 1997.

Crutzen, P.J., The influence of nitrogen oxides on the atmospheric ozone content, *Quart. J. Roy. Meteorol. Soc.*, *96*, 320-325, 1970.

Crutzen, P.J., Estimates of possible future ozone reductions from continued use of fluorochloro-methanes ($CF_2Cl_2$, $CFCl_3$), *Geophys. Res. Lett.*, *1*, 205-208, 1974.

Crutzen, P.J., Mesospheric mysteries, *Science*, *277*, 1951-1952, 1997.

Crutzen, P.J., and U. Schmailzl, Chemical budgets of the stratosphere, *Planet. Space Sci.*, *31*, 1009-1032, 1983.

Crutzen, P.J., J.-U. Grooß, C. Brühl, R. Müller, and J.M. Russell III, A reevaluation of the ozone budget with HALOE UARS data: No evidence for the ozone deficit, *Science*, *268*, 705-708, 1995.

Dahlback, A., and K. Stamnes, A new spherical model for computing the radiation field available for photolysis and heating at twilight, *Planet. Space Sci.*, *39*, 671-683, 1991.

DeLand, M.T., and R.P. Cebula, Composite Mg II solar activity index for solar cycles 21 and 22, *J. Geophys. Res.*, *98*, 12809-12823, 1993.

DeMore, W.B., S.P. Sander, D.M. Golden, R.F. Hampson, M.J. Kurylo, C.J. Howard, A.R. Ravishankara, C.E. Kolb, and M.J. Molina, *Chemical Kinetics and Photochemical Data for Use in Stratospheric Modeling, Evaluation No. 11*, JPL Publ. 94-26, Jet Propulsion Laboratory, Pasadena, Calif., 1994.

DeMore, W.B., S.P. Sander, D.M. Golden, R.F. Hampson, M.J. Kurylo, C.J. Howard, A.R. Ravishankara, C.E. Kolb, and M.J. Molina, *Chemical Kinetics and Photochemical Data for Use in Stratospheric Modeling, Evaluation No. 12*, JPL Publ. 97-4, Jet Propulsion Laboratory, Pasadena, Calif., 1997.

Dessler, A.E., E.M. Weinstock, E.J. Hintsa, J.G. Anderson, C.R. Webster, R.D. May, J.W. Elkins, and G.S. Dutton, An examination of the total hydrogen budget of the lower stratosphere, *Geophys. Res. Lett.*, *21*, 2563-2566, 1994.

Dessler, A.E., D.B. Considine, G.A. Morris, M.R. Schoeberl, J.M. Russell III, A.E. Roche, J.B. Kumer, J.L. Mergenthaler, J.W. Waters, J.C. Gille, and G.K. Yue, Correlated observations of HCl and $ClONO_2$ from UARS and implications for stratospheric chlorine partitioning, *Geophys. Res. Lett.*, *22*, 1721-1724, 1995.

Dessler, A.E., S.R. Kawa, A.R. Douglass, D.B. Considine, J.B. Kumer, A.E. Roche, J.L. Mergenthaler, J.W. Waters, J.M. Russell III, and J.C. Gille, A test of the partitioning between ClO and $ClONO_2$ using simultaneous UARS measurements of ClO, $NO_2$, and $ClONO_2$, *J. Geophys. Res.*, *101*, 12515-12521, 1996.

Donahue, N.M., M.K. Dubey, R. Mohrschladt, K.L. Demerjian, and J.G. Anderson, High-pressure flow study of the reactions $OH + NO_x \rightarrow HONO_x$: Errors in the falloff region, *J. Geophys. Res.*, *102*, 6159-6168, 1997.

Douglass, A.R., R.B. Rood, S.R. Kawa, and D.J. Allen, A three-dimensional simulation of the evolution of the middle latitude winter ozone in the middle stratosphere, *J. Geophys. Res.*, *102*, 19217-19232, 1997.

Dunkerton, T.J., The role of gravity waves in the quasi-biennial oscillation, *J. Geophys. Res.*, *102*, 26053-26076, 1997.

Dunkerton, T.J., and D.P. Delisi, Interaction of the quasi-biennial oscillation and stratopause semiannual oscillation, *J. Geophys. Res.*, *102*, 26107-26116, 1997.

Eckman, R.S., W.L. Grose, R.E. Turner, W.T. Blackshear, J.M. Russell III, L. Froidevaux, J.W. Waters, J.B. Kumer, and A.E. Roche, Stratospheric trace constituents simulated by a three-dimensional general circulation model: Comparison with UARS data, *J. Geophys. Res.*, *100*, 13951-13966, 1995.

Eluszkiewicz, J., and M. Allen, A global analysis of the ozone deficit in the upper stratosphere and lower mesosphere, *J. Geophys. Res.*, *98*, 1069-1082, 1993.

Eluszkiewicz, J., R.A. Plumb, and N. Nakamura, Dynamics of wintertime stratospheric transport in the Geophysical Fluid Dynamics Laboratory SKYHI general circulation model, *J. Geophys. Res.*, *100*, 20883-20900, 1995.

Eluszkiewicz, J., D. Crisp, R. Zurek, L. Elson, E. Fishbein, L. Froidevaux, J. Waters, R.G. Grainger, A. Lambert, R. Harwood, and G. Peckham, Residual circulation in the stratosphere and lower mesosphere as diagnosed from Microwave Limb Sounder data, *J. Atmos. Sci.*, *53*, 217-240, 1996.

Engel, A., C. Schiller, U. Schmidt, R. Borchers, H. Ovarlez, and J. Ovarlez, The total hydrogen budget in the Arctic winter stratosphere during the European Arctic Stratospheric Ozone Experiment, *J. Geophys. Res.*, *101*, 14495-14503, 1996.

Evans, S.J., R. Toumi, J.E. Harries, M.P. Chipperfield, and J.M. Russell III, Trends in stratospheric humidity and the sensitivity of ozone to these trends, *J. Geophys. Res.*, *103*, 8715-8725, 1998.

Fleming, E.L., S. Chandra, C.H. Jackman, D.B. Considine, and A.R. Douglass, The middle atmospheric response to short and long term solar UV variations: An analysis of observations and 2D model results, *J. Atmos. Terr. Phys.*, *57*, 333-365, 1995.

Fisher, M., A. O'Neill, and R. Sutton, Rapid descent of mesospheric air into the stratospheric polar vortex, *Geophys. Res. Lett.*, *20*, 1267-1270, 1993.

Frank, L.A., and J.B. Sigwarth, Atmospheric holes and small comets, *Rev. Geophys.*, *31*, 1-28, 1993.

Frank, L.A., and J.B. Sigwarth, Transient decreases of Earth's far-ultraviolet dayglow, *Geophys. Res. Lett.*, *24*, 2423-2426, 1997.

Froidevaux, L., M. Allen, and Y.L. Yung, A critical analysis of ClO and $O_3$ in the mid-latitude stratosphere, *J. Geophys. Res.*, *90*, 12999-13029, 1985.

Garcia, R.R., and B.A. Boville, "Downward control" of the mean meridional circulation and temperature distribution of the polar winter stratosphere, *J. Atmos. Sci.*, *51*, 2238-2245, 1994.

Gordley, L.L., J.M. Russell III, L.J. Mickely, J.E. Frederick, J.H. Park, K.A. Stone, G.M. Beaver, J.M. McInerney, L.E. Deaver, G.C. Toon, F.J. Murcray, R.D. Blatherwick, M.R. Gunson, J.P.D. Abbatt, R.L. Mauldin III, G.H. Mount, B. Sen, and J.-F. Blavier, Validation of nitric oxide and nitrogen dioxide measurements made by the Halogen Occultation Experiment for UARS platform, *J. Geophys. Res.*, *101*, 10241-10266, 1996.

Gray, L.J., and J.A. Pyle, The semi-annual oscillation and equatorial tracer distributions, *Quart. J. Roy. Meteorol. Soc.*, *112*, 387-407, 1986.

Grooß, J.-U., R. Müller, G. Becker, D.S. McKenna, and P.J. Crutzen, The upper stratospheric ozone budget: An update of calculations based on HALOE data, *J. Atmos. Chem.*, submitted, 1998.

Gunson, M.R., C.B. Farmer, R.H. Norton, R. Zander, C.P. Rinsland, J.H. Shaw, and B.-C. Gao, Measurements of $CH_4$, $N_2O$, CO, $H_2O$, and $O_3$ in the middle atmosphere by the Atmospheric Trace Molecule Spectroscopy experiment on Spacelab 3, *J. Geophys. Res.*, *95*, 13867-13882, 1990.

Gunson, M.R., M.C. Abrams, L.L. Lowes, E. Mahieu, R. Zander, C.P. Rinsland, M.K.W. Ko, N.D. Sze, and D.K. Weisenstein, Increase in levels of stratospheric chlorine and fluorine loading between 1985 and 1992, *Geophys. Res. Lett.*, *21*, 2223-2226, 1994.

Gunson, M.R., M.M. Abbas, M.C. Abrams, M. Allen, L.R. Brown, T.L. Brown, A.Y. Chang, A. Goldman, F.W. Irion, L.L. Lowes, E. Mahieu, G.L. Manney, H.A. Michelsen, M.J. Newchurch, C.P. Rinsland, R.J. Salawitch, G.P. Stiller, G.C. Toon, Y.L. Yung, and R. Zander, The Atmospheric Trace Molecule Spectroscopy (ATMOS) experiment: Deployment on the ATLAS Space Shuttle missions, *Geophys. Res. Lett.*, *23*, 2333-2336, 1996.

Hall, T.M., and R.A. Plumb, Age as a diagnostic of stratospheric transport, *J. Geophys. Res.*, *99*, 1059-1070, 1994.

Hall, T.M., and D.W. Waugh, Timescales for the stratospheric circulation derived from tracers, *J. Geophys. Res.*, *102*, 8991-9001, 1997.

Hannegan, B., S. Olsen, M. Prather, X. Zhu, D. Rind, and J. Lerner, The dry stratosphere: A limit on cometary water influx, *Geophys. Res. Lett.*, *25*, 1649-1652, 1998.

Harnisch, J., R. Borchers, P. Fabian, and M. Maiss, Tropospheric trends for $CF_4$ and $C_2F_6$ since 1982 derived from $SF_6$ dated stratospheric air, *Geophys. Res. Lett.*, *23*, 1099-1102, 1996.

Harries, J.E., J.M. Russell III, A.F. Tuck, L.L. Gordley, P. Purcell, K. Stone, R.M. Bevilacqua, M.R. Gunson, G. Nedoluha, and W.A. Traub, Validation of measurements of water vapor from the Halogen Occultation Experiment (HALOE), *J. Geophys. Res.*, *101*, 10205-10216, 1996.

Harris, N.R.P., G. Ancellet, L. Bishop, D.J. Hofmann, J.B. Kerr, R.D. McPeters, M. Prendez, W.J. Randel, J. Staehelin, B.H. Subbaraya, A. Volz-Thomas, J. Zawodny, and C.S. Zerefos, Trends in stratospheric and free tropospheric ozone, *J. Geophys. Res.*, *102*, 1571-1590, 1997.

Hartmann, D.L., and R.R. Garcia, A mechanistic model of ozone transport by planetary waves in the stratosphere, *J. Atmos. Sci.*, *36*, 350-364, 1979.

Harvey, V.L., and M.H. Hitchman, A climatology of the Aleutian High, *J. Atmos. Sci.*, *53*, 2088-2101, 1996.

Hernandez, R., R. Toumi, and D.C. Clary, State-selected vibrational-relaxation rates for highly vibrationally excited oxygen molecules, *J. Chem. Phys.*, *102*, 9544-9556, 1995.

Hilsenrath, E., R.P. Cebula, and C.H. Jackman, Ozone depletion in the upper stratosphere estimated from satellite and Space Shuttle data, *Nature*, *358*, 131-133, 1992.

Hitchman, M.H., M. McKay, and C.R. Trepte, A climatology of stratospheric aerosol, *J. Geophys. Res.*, *99*, 20689-20700, 1994.

Hollandsworth, S.M., R.D. McPeters, L.E. Flynn, W. Planet, A.J. Miller, and S. Chandra, Ozone trends deduced from combined Nimbus 7 SBUV and NOAA 11 SBUV/2 data, *Geophys. Res. Lett.*, *22*, 905-908, 1995.

Holton, J.R., P.H. Haynes, M.E. McIntyre, A.R. Douglass, R.B. Rood, and L. Pfister, Stratosphere-troposphere exchange, *Rev. Geophys.*, *33*, 403-439, 1995.

Hood, L.L., and S. Cantrell, Stratospheric ozone and temperature responses to short term solar ultraviolet variations: Reproducibility of low-latitude response measurements, *Ann. Geophys.*, *6*, 525-530, 1988.

Iwagami, N., S. Inomata, I. Murata, and T. Ogawa, Doppler detection of hydroxyl column abundance in the middle atmosphere, *J. Atmos. Chem.*, *20*, 1-15, 1995.

Iwagami, N., S. Inomata, and T. Ogawa, Doppler detection of hydroxyl column abundance in the middle atmosphere: 2. Measurement for three years and a comparison with a 1D model, *J. Atmos. Chem.*, *29*, 195-216, 1998.

Jackman, C.H., R.S. Stolarski, and J.A. Kaye, Two-dimensional monthly average ozone balance from Limb Infrared Monitor of the Stratosphere and Stratospheric and Mesospheric Sounder data, *J. Geophys. Res.*, *91*, 1103-1116, 1986.

Jackman, C.H., E.L. Fleming, S. Chandra, D.B. Considine, and J.E. Rosenfield, Past, present, and future modeled ozone trends with comparisons to observed trends, *J. Geophys. Res.*, *101*, 28753-28767, 1996.

Johnston, J.C., S.S. Cliff, and M.H. Thiemens, Measurement of multioxygen isotopic ($\delta^{18}O$ and $\delta^{17}O$) fractionation factors in the stratospheric sink reactions of nitrous oxide, *J. Geophys. Res.*, *100*, 16801-16804, 1995.

Jones, D.B.A., H.R. Schneider, and M.B. McElroy, Effects of the quasi-biennial oscillation on the zonally averaged transport of tracers, *J. Geophys. Res.*, *103*, 11235-11249, 1998.

Jucks, K.W., D.G. Johnson, K.V. Chance, W.A. Traub, R.J. Salawitch, and R.A. Stachnik, Ozone production and loss rate measurements in the middle stratosphere, *J. Geophys. Res.*, *101*, 28785-28792, 1996.

Jucks, K.W., D.G. Johnson, K.V. Chance, W.A. Traub, J.J. Margitan, G.B. Osterman, R.J. Salawitch, and Y. Sasano, Observations of OH, $HO_2$, $H_2O$, and $O_3$ in the upper stratosphere: Implications for $HO_x$ photochemistry, *Geophys. Res. Lett.*, *25*, 3935-3938, 1998.

Kawa, S.R., J.B. Kumer, A.R. Douglass, A.E. Roche, S.E. Smith, F.W. Taylor, and D.J. Allen, Missing chemistry of reactive nitrogen in the upper stratospheric polar winter, *Geophys. Res. Lett.*, *22*, 2629-2632, 1995.

Kaye, J.A., S. Penkett, and F.M. Ormond (eds.), *Report on Concentrations, Lifetimes, and Trends of CFCs, Halons, and Related Species*, NASA Reference Publication 1339, NASA Office of Mission to Planet Earth, 247 pp., National Aeronautics and Space Administration, Washington, D.C., 1994.

Kennaugh, R., S. Ruth, and L.J. Gray, Modeling quasi-biennial variability in the semiannual double peak, *J. Geophys. Res.*, *102*, 16169-16187, 1997.

Khosravi, R., G.P. Brasseur, A.K. Smith, D.W. Rusch, J.W. Waters, and J.M. Russell III, Significant reduction in the stratospheric ozone deficit using three-dimensional model constrained with UARS data, *J. Geophys. Res.*, *103*, 16203-16219, 1998.

Kim, K.R., and H. Craig, Nitrogen-15 and oxygen-18 characteristics of nitrous oxide: A global perspective, *Science*, *262*, 1855-1857, 1993.

Kondo, Y., U. Schmidt, T. Sugita, A. Engel, M. Koike, P. Aimedieu, M.R. Gunson, and J. Rodriguez, $NO_y$ correlation with $N_2O$ and $CH_4$ in the midlatitude stratosphere, *Geophys. Res. Lett.*, *23*, 2369-2372, 1996.

Kondo, Y., T. Sugita, R.J. Salawitch, M. Koike, and T. Deshler, Effect of Pinatubo aerosols on stratospheric NO, *J. Geophys. Res.*, *102*, 1205-1213, 1997.

Koppers, G.A.A., and D.P. Murtagh, Model studies of the influence of $O_2$ photodissociation parameterizations in the Schumann-Runge bands on ozone related photolysis in the upper atmosphere, *Ann. Geophys.*, *14*, 68-79, 1996.

Lahoz, W.A., A. O'Neill, E.S. Carr, R.S. Harwood, L. Froidevaux, W.G. Read, J.W. Waters, J.B. Kumer, J.L. Mergenthaler, A.E. Roche, G.E. Peckham, and R. Swinbank, Three-dimensional evolution of water vapor distributions in the Northern Hemisphere stratosphere as observed by the MLS, *J. Atmos. Sci.*, *51*, 2914-2930, 1994.

Lahoz, W.A., A. O'Neill, A. Heaps, V.D. Pope, R. Swinbank, R.S. Harwood, L. Froidevaux, W.G. Read, J.W. Waters, and G.E. Peckham, Vortex dynamics and the evolution of water vapour in the stratosphere of the southern hemisphere, *Quart. J. Roy. Meteorol. Soc.*, *122*, 423-450, 1996.

Lary, D.J., A.M. Lee, R. Toumi, M.J. Newchurch, M. Pirre, and J.B. Renard, Carbon aerosols and atmospheric photochemistry, *J. Geophys. Res.*, *102*, 3671-3682, 1997.

Lean, J.L., G.J. Rottman, H.L. Kyle, T.N. Woods, J.R. Hickey, and L.C. Puga, Detection and parameterization of variations in solar mid- and near-ultraviolet radiation (200-400 nm), *J. Geophys. Res.*, *102*, 29939-29956, 1997.

Lipson, J.B., M.J. Elrod, T.W. Beiderhase, L.T. Molina, and M.J. Molina, Temperature dependence of the rate constant and branching ratio for the OH + ClO reaction, *J. Chem. Soc., Faraday Trans.*, *93*, 2665-2673, 1997.

London, J., G.J. Rottman, T.N. Woods, and F. Wu, Time variations of solar UV irradiance as measured by the SOLSTICE (UARS) instrument, *Geophys. Res. Lett.*, *20*, 1315-1318, 1993.

Luo, M., R.J. Cicerone, and J.M. Russell III, Analysis of Halogen Occultation Experiment HF versus $CH_4$ correlation plots: Chemistry and transport implications, *J. Geophys. Res.*, *100*, 13927-13937, 1995.

Luo, M., J.H. Park, K.M. Lee, J.M. Russell III, and C. Brühl, An analysis of HALOE observations in summer high latitudes using airmass trajectory and photochemical model calculations, *J. Geophys. Res.*, *102*, 16145-16156, 1997a.

Luo, M., J.M. Russell III, and T.Y.W. Huang, Halogen Occultation Experiment observations of the quasi-biennial oscillation and the effects of Pinatubo aerosols in the tropical stratosphere, *J. Geophys. Res.*, *102*, 19187-19198, 1997b.

Manney, G.L., R.W. Zurek, A. O'Neill, and R. Swinbank, On the motion of air through the stratospheric polar vortex, *J. Atmos. Sci.*, *51*, 2973-2994, 1994a.

Manney, G.L., R.W. Zurek, A. O'Neill, R. Swinbank, J.B. Kumer, J.L. Mergenthaler, and A.E. Roche, Stratospheric warmings during February and March 1993, *Geophys. Res. Lett.*, *21*, 813-816, 1994b.

Manney, G.L., L. Froidevaux, J.W. Waters, R.W. Zurek, J.C. Gille, J.B. Kumer, J.L. Mergenthaler, A.E. Roche, A. O'Neill, and R. Swinbank, Formation of low-ozone pockets in the middle stratospheric anticyclone during winter. *J. Geophys*, *Res.*, *100*, 13939-13950, 1995a.

Manney, G.L., R.W. Zurek, W.A. Lahoz, R.S. Harwood, J.C. Gille, J.B. Kumer, J.L. Mergenthaler, A.E. Roche, A. O'Neill, R. Swinbank, and J.W. Waters, Lagrangian transport calculations using UARS data: Part I, Passive tracers, *J. Atmos. Sci.*, *52*, 3049-3068, 1995b.

Manney, G.L., J.C. Bird, D.P. Donovan, T.J. Duck, J.A. Whiteway, S.R. Pal, and A.I. Carswell, Modeling ozone laminae in ground-based arctic wintertime observations using trajectory calculations and satellite data, *J. Geophys. Res.*, *103*, 5797-5814, 1998.

McCormack, J.P., and L.L. Hood, Apparent solar cycle variations of upper stratospheric ozone and temperature: Latitude and seasonal dependences, *J. Geophys. Res.*, *101*, 20933-20944, 1996.

McElroy, M.B., and D.B.A. Jones, Evidence for an additional source of atmospheric $N_2O$, *Global Biogeochem. Cycles*, *10*, 651-659, 1996.

McElroy, M.B., and R.J. Salawitch, Changing composition of the global stratosphere, *Science*, *243*, 763-770, 1989.

McIntyre, M.E., and T.N. Palmer, The "surf zone" in the stratosphere, *J. Atmos. Terr. Phys.*, *46*, 825-849, 1984.

Michelsen, H.A., R.J. Salawitch, P.O. Wennberg, and J.G. Anderson, Production of $O(^1D)$ from photolysis of $O_3$, *Geophys. Res. Lett.*, *21*, 2227-2230, 1994.

Michelsen, H.A., R.J. Salawitch, M.R. Gunson, C. Aellig, N. Kämpfer, M.M. Abbas, M.C. Abrams, T.L. Brown, A.Y. Chang, A. Goldman, F.W. Irion, M.J. Newchurch, C.P. Rinsland, G.P. Stiller, and R. Zander, Stratospheric chlorine partitioning: Constraints from shuttle-borne measurements of [HCl], [$ClNO_3$], and [ClO], *Geophys. Res. Lett.*, *23*, 2361-2364, 1996.

Michelsen, H.A., G.L. Manney, M.R. Gunson, C.P. Rinsland, and R. Zander, Correlations of stratospheric abundances of $CH_4$ and $N_2O$ derived from ATMOS measurements, *Geophys. Res. Lett.*, *25*, 2777-2780, 1998.

Miller, A.J., L.E. Flynn, S.M. Hollandsworth, J.J. DeLuisi, I.V. Petropavlovskikh, G.C. Tiao, G.C. Reinsel, D.J. Wuebbles, J. Kerr, R.M. Nagatani, L. Bishop, and C.H. Jackman, Information content of Umkehr and solar backscattered ultraviolet (SBUV) 2 satellite data for ozone trends and solar responses in the stratosphere, *J. Geophys. Res.*, *102*, 19257-19263, 1997.

Miller, R.L., A.G. Suits, P.L. Houston, R. Toumi, J.A. Mack, and A.M. Wodtke, The ozone deficit problem: $O_2(X,v \geq 26) + O(^3P)$ from 226-nm ozone photodissociation, *Science*, *265*, 1831-1838, 1994.

Minschwaner, K., and D.E. Siskind, A new calculation of nitric oxide photolysis in the stratosphere, mesosphere, and lower thermosphere, *J. Geophys. Res.*, *98*, 20401-20412, 1993.

Minschwaner, K., G.P. Anderson, L.A. Hall, and K.Yoshino, Polynominal coefficients for calculating $O_2$ Schumann-Runge cross sections at 0.5 $cm^{-1}$ resolution, *J. Geophys. Res.*, *97*, 10103-10108, 1992.

Minschwaner, K., R.J. Salawitch, and M.B. McElroy, Absorption of solar radiation by $O_2$: Implications for $O_3$ and lifetimes of $N_2O$, $CFCl_3$, and $CF_2Cl_2$, *J. Geophys. Res.*, *98*, 10543-10561, 1993.

Molina, M.J., and F.S. Rowland, Stratospheric sink for chlorofluoromethanes: Chlorine atom catalysed destruction of ozone, *Nature*, *249*, 810-812, 1974.

Montzka, S.A., J.H. Butler, R.C. Meyers, T.M. Thompson, T.H. Swanson, A.D. Clarke, L.T. Lock, and J.W. Elkins, Decline in the tropospheric abundance of halogen from halocarbons: Implications for stratospheric ozone depletion, *Science*, *272*, 1318-1322, 1996.

Morrey, M.W., and R.S. Harwood, Interhemispheric differences in stratospheric water vapour during late winter, in version 4 MLS measurements, *Geophys. Res. Lett.*, *25*, 147-150, 1998.

Morris, G.A., D.B. Considine, A.E. Dessler, S.R. Kawa, J. Kumer, J. Mergenthaler, A. Roche, and J.M. Russell III, Nitrogen partitioning in the middle stratosphere as observed by the Upper Atmosphere Research Satellite, *J. Geophys. Res.*, *102*, 8955-8965, 1997.

Morris, G.A., S.R. Kawa, A.R. Douglass, M.R. Schoeberl, L. Froidevaux, and J.W. Waters, Low-ozone pockets explained, *J. Geophys. Res.*, *103*, 3599-3610, 1998.

Mosier, A., C. Kroeze, C. Nevison, O. Oenema, S. Seitzinger, and O. van Cleemput, Closing the global atmospheric $N_2O$ budget: Nitrous oxide emissions through the agricultural nitrogen cycle, *Nutr. Cyc. Agroecosyst.*, *52*, 225-248, 1998.

Mote, P.W., The annual cycle of stratospheric water vapor in a general circulation model, *J. Geophys. Res.*, *100*, 7363-7379, 1995.

Mote, P.W., K.H. Rosenlof, M.E. McIntyre, E.S. Carr, J.C. Gille, J.R. Holton, J.S. Kinnersley, H.C. Pumphrey, J.M. Russell III, and J.W. Waters, An atmospheric tape recorder: The imprint of tropical tropopause temperatures on stratospheric water vapor, *J. Geophys. Res.*, *101*, 3989-4006, 1996.

Nair, H., M. Allen, L. Froidevaux, and R.W. Zurek, Localized rapid ozone loss in the northern winter stratosphere: An analysis of UARS observations, *J. Geophys. Res.*, *103*, 1555-1571, 1998.

Natarajan, M., and L.B. Callis, Stratospheric photochemical studies with Atmospheric Trace Molecule Spectroscopy (ATMOS) measurements, *J. Geophys. Res.*, *96*, 9361-9370, 1991.

Nedoluha, G.E., D.E. Siskind, J.T. Bacmeister, R.M. Bevilacqua, and J.M. Russell III, Changes in upper stratospheric $CH_4$ and $NO_2$ as measured by HALOE and implications for changes in transport, *Geophys. Res. Lett.*, *25*, 987-990, 1998a.

Nedoluha, G.E., R.M. Bevilacqua, R.M. Gomez, D.E. Siskind, B.C. Hicks, J.M. Russell III, and B.J. Connor, Increases in middle atmospheric water vapor as observed by the Halogen Occultation Experiment and the ground-based Water Vapor Millimeter-wave Spectrometer from 1991 to 1997, *J. Geophys. Res.*, *103*, 3531-3543, 1998b.

Nevison, C.D., and E.A. Holland, A reexamination of the impact of anthropogenically fixed nitrogen on atmospheric $N_2O$ and the stratospheric $O_3$ layer, *J. Geophys. Res.*, *102*, 25519-25536, 1997.

Nevison, C.D., S. Solomon, and J.M. Russell III, Nighttime formation of $N_2O_5$ inferred from the Halogen Occultation Experiment sunset/sunrise $NO_x$ ratios, *J. Geophys. Res.*, *101*, 6741-6748, 1996.

Nevison, C.D., S. Solomon, and R.R. Garcia, Model overestimates of $NO_y$ in the upper stratosphere, *Geophys. Res. Lett.*, *24*, 803-806, 1997.

Nightingale, R.W., A.E. Roche, J.B. Kumer, J.L. Mergenthaler, J.C. Gille, S.T. Massie, P.L. Bailey, D.P. Edwards, M.R. Gunson, G.C. Toon, B. Sen, J.-F. Blavier, and P.S. Connell, Global $CF_2Cl_2$ measurements by UARS cryogenic limb array etalon spectrometer: Validation by correlative data and a model, *J. Geophys. Res.*, *101*, 9711-9736, 1996.

Oelhaf, H., G. Wetzel, T. von Clarmann, M. Schmidt, J.B. Renard, M. Pirre, E. Lateltin, P. Aimedieu, C. Phillips, F. Goutail, J.-P. Pommereau, Y. Kondo, T. Sugita, H. Nakajima, M. Koike, W.J. Williams, F.J. Murcray, P. Sullivan, A. Engel, U. Schmidt, and A.M. Lee, Correlative balloon measurements of the vertical distribution of $N_2O$, NO, $NO_2$, $NO_3$, $HNO_3$, $N_2O_5$, $ClONO_2$ and total reactive $NO_y$ inside the polar vortex during SESAME, in *Polar Stratospheric Ozone, Proceedings of the Third European Workshop*, 18 to 22 September 1995, edited by J.A. Pyle, N.R.P. Harris, and G.T. Amanatidis, pp. 187-192, European Commission, Luxembourg, 1996.

Oltmans, S.J., and D.J. Hofmann, Increase in lower-stratospheric water vapour at a mid-latitude Northern Hemisphere site from 1981 to 1994, *Nature*, *374*, 146-149, 1995.

Osterman, G.B., R.J. Salawitch, B. Sen, G.C Toon, R.A. Stachnik, H.M. Pickett, J.J. Margitan, and D.B. Peterson, Balloon-borne measurements of stratospheric radicals and their precursors: Implications for the production and loss of ozone, *Geophys. Res. Lett.*, *24*, 1107-1110, 1997.

Park, J.H., J.M. Russell III, L.L. Gordley, S.R. Drayson, D.C. Benner, J.M. McInerney, M.R. Gunson, G.C. Toon, B. Sen, J.-F. Blavier, C.R. Webster, E.C. Zipf, P. Erdman, U. Schmidt, and C. Schiller, Validation of Halogen Occultation Experiment $CH_4$ measurements from the UARS, *J. Geophys. Res.*, *101*, 10183-10203, 1996.

Park, J., M.K.W. Ko, R.A. Plumb, and C. Jackman (eds.), *Report of the 1998 Models and Measurements Workshop II*, NASA Reference Publication, National Aeronautics and Space Administration, Washington, D.C., in press, 1998.

Parks, G., Brittnacher, M., L.J. Chen, R. Elsen, M. McCarthy, G. Germany, and J. Spann, Does the UVI on Polar detect cosmic snowballs? *Geophys. Res. Lett.*, *24*, 3109-3112, 1997.

Perliski, L.M., S. Solomon, and J. London, On the interpretation of seasonal variations of stratospheric ozone, *Planet. Space Sci.*, *37*, 1527-1538, 1989.

Peter, R., Stratospheric and mesospheric latitudinal water vapor distributions obtained by an airborne millimeter-wave spectrometer, *J. Geophys. Res.*, *103*, 16275-16290, 1998.

Pickett, H.M., and D.B. Peterson, Comparison of measured stratospheric OH with prediction, *J. Geophys. Res.*, *101*, 16789-16796, 1996.

Plumb, R.A., A "tropical pipe" model of stratospheric transport, *J. Geophys. Res.*, *101*, 3957-3972, 1996.

Plumb, R.A., and M.K.W. Ko, Interrelationships between mixing ratios of long-lived stratospheric constituents, *J. Geophys. Res.*, *97*, 10145-10156, 1992.

Prasad, S.S., Natural atmospheric sources and sinks of nitrous oxide: 1, An evaluation based on 10 laboratory experiments, *J. Geophys. Res.*, *99*, 5285-5294, 1994.

Prasad, S.S., Potential atmospheric sources and sinks of nitrous oxide: 2, Possibilities from excited $O_2$, "embryonic" $O_3$, and optically pumped excited $O_3$, *J. Geophys. Res.*, *102*, 21527-21536, 1997.

Prather, M.J., and E.E. Remsberg (eds.), *The Atmospheric Effects of Stratospheric Aircraft: Report of the 1992 Models and Measurements Workshop*, NASA Reference Publication 1292, Vol. I-III, National Aeronautics and Space Administration, Washington, D.C., 1993.

Prather, M., R. Derwent, D. Ehhalt, P. Fraser, E. Sanhueza, and X. Zhou, Other trace gases and atmospheric chemistry, Chapter 2 in *Climate Change 1994: Radiative Forcing of Climate Change and an Evaluation of the IPCC IS92 Emission Scenarios*, edited by J.T. Houghton, L.G. Meira Filho, J. Bruce, H. Lee, B.A. Callander, E. Haites, N. Harris, and K. Maskell, Intergovernmental Panel on Climate Change, Cambridge University Press, Cambridge, U.K., 1995.

Rahn, T., and M. Whalen, Stable isotope enrichment in stratospheric nitrous oxide, *Science*, *278*, 1776-1778, 1997.

Randel, W.J., J.C. Gille, A.E. Roche, J.B. Kumer, J.L. Mergenthaler, J.W. Waters, E.F. Fishbein, and W.A. Lahoz, Stratospheric transport from the tropics to middle latitudes by planetary-wave mixing, *Nature*, *365*, 533-535, 1993.

Randel, W.J., B.A. Boville, J.C. Gille, P.L. Bailey, S.T. Massie, J.B. Kumer, J.L. Mergenthaler, and A.E. Roche, Simulation of stratospheric $N_2O$ in the NCAR CCM2: Comparison with CLAES data and global budget analyses, *J. Atmos. Sci.*, *51*, 2834-2845, 1994.

Randel, W.J., F. Wu, J.M. Russell III, A. Roche, and J.W. Waters, Seasonal cycles and QBO variations in stratospheric $CH_4$ and $H_2O$ observed in UARS HALOE data, *J. Atmos. Sci.*, *55*, 163-185, 1998a.

Randel, W.J., F. Wu, J.M. Russell III, J.W. Waters, and M.L. Santee, Space-time patterns of trends in stratospheric constituents derived from UARS measurements, *J. Geophys. Res.*, in press, 1998b.

Randeniya, L.K., P.F. Vohralik, I.C. Plumb, and K.R. Ryan, Heterogeneous $BrONO_2$ hydrolysis: Effect on $NO_2$ columns and ozone at high latitudes in summer, *J. Geophys. Res.*, *102*, 23543-23557, 1997.

Ravishankara, A.R., G. Hancock, M. Kawasaki, and Y. Matsumi, Photochemistry of ozone: Surprises and recent lessons, *Science*, *280*, 60-61, 1998.

Ray, E.A., J.R. Holton, E.F. Fishbein, L. Froidevaux, and J.W. Waters, The tropical semiannual oscillation in temperature and ozone as observed by the MLS, *J. Atmos. Sci.*, *51*, 3045-3052, 1994.

Rinsland, C.P., M.R. Gunson, R.J. Salawitch, H.A. Michelsen, R. Zander, M.J. Newchurch, M.M. Abbas, M.C. Abrams, G.L. Manney, A.Y. Chang, F.W. Irion, A. Goldman, and E. Mahieu, ATMOS/ATLAS-3 measurements of stratospheric chlorine and reactive nitrogen partitioning inside and outside the November 1994 Antarctic vortex, *Geophys. Res. Lett.*, *23*, 2365-2368, 1996.

Rizk, B., and A.J. Dessler, Small comets: Naked-eye visibility, *Geophys. Res. Lett.*, *24*, 3121-3124, 1997.

Rogaski, C.A., J.M. Price, J.A. Mack, and A.M. Wodtke, Laboratory evidence for a possible non-LTE mechanism of stratospheric ozone formation, *Geophys. Res. Lett.*, *20*, 2885-2888, 1993.

Rogaski, C.A., J.A. Mack, and A.M. Wodtke, State-to-state rate constants for relaxation of highly vibrationally excited $O_2$ and implications for its atmospheric fate, *Faraday Discuss. Chem. Soc.*, *100*, 229-251, 1995.

Rosenfield, J.E., D.B. Considine, P.E. Meade, J.T. Bacmeister, C.H. Jackman, and M.R. Schoeberl, Stratospheric effects of Mount Pinatubo aerosol studied with a coupled two-dimensional model, *J. Geophys. Res.*, *102*, 3649-3670, 1997.

Rosenlof, K.H., Seasonal cycle of the residual mean meridional circulation in the stratosphere, *J. Geophys. Res.*, *100*, 5173-5191, 1995.

Rosenlof, K.H., A.F. Tuck, K.K. Kelly, J.M. Russell III, and M.P. McCormick, Hemispheric asymmetries in water vapor and inferences about transport in the lower stratosphere, *J. Geophys. Res.*, *102*, 13213-13234, 1997.

Russell, J.M. III, M. Luo, R.J. Cicerone, and L.E. Deaver, Satellite confirmation of the dominance of chlorofluorocarbons in the global stratospheric chlorine budget, *Nature*, *379*, 526-529, 1996.

Ruth, S.L., J.J. Remedios, B.N. Lawrence, and F.W. Taylor, Measurements of $N_2O$ by the UARS Improved Stratospheric and Mesospheric Sounder during the early northern winter 1991/92, *J. Atmos. Sci.*, *51*, 2818-2833, 1994.

Ruth, S.L., R. Kennaugh, L.J. Gray, and J.M. Russell III, Seasonal, semiannual, and interannual variability seen in measurements of methane made by the UARS Halogen Occultation Experiment, *J. Geophys. Res.*, *102*, 16189-16199, 1997.

Sandor, B.J., and R.T. Clancy, Mesospheric $HO_x$ chemistry from diurnal microwave observations of $HO_2$, $O_3$, and $H_2O$, *J. Geophys. Res.*, *103*, 13337-13351, 1998.

Sassi, F., and R.R. Garcia, The role of equatorial waves forced by convection in the tropical semiannual oscillation, *J. Atmos. Sci.*, *54*, 1925-1942, 1997.

Schoeberl, M.R., and P.A. Newman, A multiple-level trajectory analysis of vortex filaments, *J. Geophys. Res.*, *100*, 25801-25815, 1995.

Sen, B., G.C. Toon, J.-F. Blavier, E.L. Fleming, and C.H. Jackman, Balloon-borne observations of mid-latitude fluorine abundance, *J. Geophys. Res.*, *101*, 9045-9054, 1996.

Sen, B., G.C. Toon, G.B. Osterman, J.-F. Blavier, J.J. Margitan, R.J. Salawitch, and G.K. Yue, Measurements of reactive nitrogen in the stratosphere, *J. Geophys. Res.*, *103*, 3571-3585, 1998.

Siskind, D.E., and J.M. Russell III, Coupling between middle and upper atmospheric NO: Constraints from HALOE observations, *Geophys. Res. Lett.*, 23, 137-140, 1996.

Siskind, D.E., and M.E. Summers, Implications of enhanced mesospheric water vapor observed by HALOE, *Geophys. Res. Lett.*, *25*, 2133-2136, 1998.

Siskind, D.E., K. Minschwaner, and R.S. Eckman, Photodissociation of $O_2$ and $H_2O$ in the middle atmosphere: Comparison of numerical methods and impact on model $O_3$ and OH, *Geophys. Res. Lett.*, 21, 863-866, 1994.

Siskind, D.E., B.J. Connor, R.S. Eckman, E.E. Remsberg, J.J. Tsou, and A. Parrish, An intercomparison of model ozone deficits in the upper stratosphere and mesosphere from two data sets, *J. Geophys. Res.*, *100*, 11191-11202, 1995.

Siskind, D.E., J.T. Bacmeister, M.E. Summers, and J.M. Russell III, Two-dimensional model calculations of nitric oxide transport in the middle atmosphere and comparison with Halogen Occultation Experiment data, *J. Geophys. Res.*, *102*, 3527-3545, 1997.

Siskind, D.E., L. Froidevaux, J.M. Russell III, and J. Lean, Implications of upper stratospheric trace constituent changes observed by HALOE for $O_3$ and ClO from 1992 to 1995, *Geophys. Res. Lett.*, *25*, 3513-3516, 1998.

Solomon, S., and R.R. Garcia, On the distributions of long-lived tracers and chlorine species in the middle atmosphere, *J. Geophys. Res.*, *89*, 11633-11644, 1984.

Solomon, S., R.W. Portmann, R.R. Gracia, W. Randel, F. Wu, R. Nagatani, J. Gleason, L. Thomason, L.R. Poole, and M.P. McCormick, Ozone depletion at mid-latitudes: Coupling of volcanic aerosols and temperature variability to anthropogenic chlorine, *Geophys. Res. Lett.*, *25*, 1871-1874, 1998.

Stachnik, R.A., J.C. Hardy, J.A. Tarsala, J.W. Waters, and N.R. Erickson, Submillimeter heterodyne measurements of stratospheric ClO, HCl, and $HO_2$: First results, *Geophys. Res. Lett.*, *19*, 1931-1934, 1992.

Steinbrecht, W., H. Claude, and F. Schönenborn, Nine years of lidar measurements at Hohenpeissenberg: Validation and results, in *Atmospheric Ozone: Proceedings of the XVIII Quadrennial Ozone Symposium*, L'Aquila, Italy, 12-21 September 1996, edited by R.D. Bojkov and G. Visconti, pp. 171-174, Parco Scientifico e Technologico d'Abruzzo, L'Aquila, Italy, 1998.

Stolarski, R.S. (ed.), *1995 Scientific Assessment of the Atmospheric Effects of Stratospheric Aircraft*, NASA Reference Publication 1381, National Aeronautics and Space Administration, Washington, D.C., 1995.

Stolarski, R.S., and R.J. Cicerone, Stratospheric chlorine: A possible sink for ozone, *Can. J. Chem.*, *52*, 1610-1615, 1974.

Stolarski, R.S., and W. Randel, Ozone change as a function of altitude, Chapter 3 in *Assessment of Trends in the Vertical Distribution of Ozone*, edited by N. Harris, R. Hudson, and C. Phillips, Stratospheric Processes and their Role in Climate (SPARC) Report No. 1, World Meteorological Organization Ozone Research and Monitoring Project–Report No. 43, Verrières le Buisson, France, 1998.

Summers, M.E., R.R. Conway, D.E. Siskind, M.H. Stevens, D. Offermann, M. Riese, P. Preusse, D.F. Strobel, and J.M. Russell III, Implications of satellite OH observations for middle atmospheric $H_2O$ and ozone, *Science*, *277*, 1967-1970, 1997a.

Summers, M.E., D.E. Siskind, J.T. Bacmeister, R.R. Conway, S.E. Zasadil, and D.F. Strobel, Seasonal variation of middle atmospheric $CH_4$ and $H_2O$ with a new chemical-dynamical model, *J. Geophys. Res.*, *102*, 3503-3526, 1997b.

Sutton, R.T., H. MacLean, R. Swinbank, A. O'Neill, and F.W. Taylor, High-resolution stratospheric tracer fields estimated from satellite observations using Lagrangian trajectory calculations, *J. Atmos. Sci.*, *51*, 2995-3005, 1994.

Tabazadeh, A., and R.P. Turco, Stratospheric chlorine injection by volcanic eruptions: HCl scavenging and implications for ozone, *Science*, *260*, 1082-1086, 1993.

Toumi, R., and S. Bekki, The importance of the reactions between OH and ClO for stratospheric ozone, *Geophys. Res. Lett.*, *20*, 2447-2450, 1993.

Toumi, R., P.L. Houston, and A.M. Wodtke, Reactive $O_2(X,v \geq 26)$ as a source of stratospheric $O_3$, *J. Chem. Phys.*, *104*, 775-776, 1996.

Wang, H.J., D.M. Cunnold, and X. Bao, A critical analysis of Stratospheric Aerosol and Gas Experiment ozone trends, *J. Geophys. Res.*, *101*, 12495-12514, 1996.

Watson, R.T., H. Rodhe, H. Oeschger, and U. Siegenthaler, Greenhouse gases and aerosols, Chapter 1 in *Climate Change: The IPCC Scientific Assessment*, edited by J.T. Houghton, G.J. Jenkins, and J.J. Ephraums, Intergovernmental Panel on Climate Change, Cambridge University Press, Cambridge, U.K., 1990.

Waugh, D.W., T.M. Hall, W.J. Randel, P.J. Rasch, B.A. Boville, K.A. Boering, S.C. Wofsy, B.C. Daube, J.W. Elkins, D.W. Fahey, G.S. Dutton, C.M. Volk, and P.F. Vohralik, Three-dimensional simulations of long-lived tracers using winds from MACCM2, *J. Geophys. Res.*, *102*, 21493-21513, 1997.

WMO (World Meteorological Organization), *Atmospheric Ozone 1985: Assessment of Our Understanding of the Processes Controlling Its Present Distribution and Change*, World Meteorological Organization Global Ozone Research and Monitoring Project—Report No. 16, Geneva, 1986.

WMO (World Meteorological Organization), *Scientific Assessment of Ozone Depletion: 1994*, World Meteorological Organization Global Ozone Research and Monitoring Project—Report No. 37, Geneva, 1995.

Wood, S.W., D.J. Keep, C.R. Burnett, and E.B. Burnett, Column abundance measurements of atmospheric hydroxyl at 45°S, *Geophys. Res. Lett.*, *21*, 1607-1610, 1994.

Woods, D.C., R.L. Chuan, and W.I. Rose, Halite particles injected into the stratosphere by the 1982 El Chichón eruption, *Science*, *230*, 170-172, 1985.

Yung, Y.L., and C.E. Miller, Isotopic fractionation of stratospheric nitrous oxide, *Science*, *278*, 1778-1780, 1997.

Zander, R., E. Mahieu, M.R. Gunson, M.C. Abrams, A.Y. Chang, M.M. Abbas, C. Aellig, A. Engel, A. Goldman, F.W. Irion, N. Kämpfer, H.A. Michelsen, M.J. Newchurch, C.P. Rinsland, R.J. Salawitch, G.P. Stiller, and G.C. Toon, The 1994 northern midlatitude budget of stratospheric chlorine derived from ATMOS/ATLAS-3 observations, *Geophys. Res. Lett.*, *23*, 2357-2360, 1996.

Zawodny, J.M., and M.P. McCormick, Stratospheric Aerosol and Gas Experiment II measurements of the quasi-biennial oscillation of ozone and nitrogen dioxide, *J. Geophys. Res.*, *96*, 9371-9377, 1991.

# CHAPTER 7

# Lower Stratospheric Processes

**Lead Authors:**
A.R. Ravishankara
T.G. Shepherd

**Coauthors:**
M.P. Chipperfield
P.H. Haynes
S.R. Kawa
T. Peter
R.A. Plumb
R.W. Portmann
W.J. Randel
D.W. Waugh
D.R. Worsnop

**Contributors:**
S. Borrmann
B.A. Boville
K.S. Carslaw
R.L. Jones
M. Mozurkewich
R. Müller
D. O'Sullivan
G. Poulet
M. Rossi
S.P. Sander

# CHAPTER 7

## LOWER STRATOSPHERIC PROCESSES

### Contents

## SCIENTIFIC SUMMARY

Chemical, microphysical, radiative-dynamical, and transport processes all play important roles in determining ozone abundance in the lower stratosphere. Since the last Assessment (WMO, 1995), there have been significant advances in our understanding of these processes and of the way in which they couple together to produce the observed distribution of ozone, and changes in this distribution.

### Current understanding of lower stratospheric ozone depletion

- The large ozone losses during spring over Antarctica continue unabated, with approximately the same magnitude and areal extent as in the early 1990s. The near-constant extent of seasonal column ozone losses from year to year reflects the near-complete destruction of ozone within the Antarctic lower stratosphere during springtime, and is consistent with our understanding of polar processes.

- Low abundances of late-winter/spring column ozone have been recorded both inside and outside the Arctic vortex in six of the last nine years. Observations show those years to be characterized by specific meteorological conditions: lower-than-normal late-winter/spring Arctic temperatures, which lead to enhanced activated chlorine; and a more isolated vortex and weaker planetary-wave driving, which lead to less transport of ozone-rich air into the Arctic. Under these meteorological conditions, both chemistry and dynamics act to reduce the seasonal levels of column ozone.

- During these years of low late-winter/spring column ozone, high abundances of active chlorine have been observed inside the Arctic vortex, and chemical ozone losses inside the vortex have been unambiguously identified. These chemical losses are associated with activated chlorine augmented by bromine. The total seasonal chemical ozone losses within the vortex have been estimated to be approximately 100 milli-atm cm (Dobson units), although this magnitude is subject to considerable uncertainty.

- Low polar temperatures, an isolated vortex, and reduced wave driving are coupled processes that occur in concert in the stratosphere; but their intensity and duration are highly variable. With the present high chlorine loading and winter/spring temperatures close to the threshold for significant chlorine activation, late-winter/spring Arctic chemical ozone loss is particularly sensitive to meteorological conditions (temperature and vortex isolation). Thus, it is not possible to predict the year-to-year variations.

- The decadal trend in springtime Arctic depletion during the 1990s is reminiscent of the early years of the Antarctic ozone hole. However, while the decadal trend in the Antarctic during the late 1970s and 1980s was driven by the trend in chlorine loading, the decadal trend in the Arctic during the 1990s has been driven by a decadal change in late-winter/spring meteorological conditions in the presence of already high chlorine loading. Thus, a reduced chemical ozone loss in the coming years would not necessarily indicate chemical recovery. The Arctic will remain vulnerable to extreme seasonal loss as long as chlorine loading remains high.

- The major contribution to the midlatitude column ozone decline during the last two decades has come from decreases in the lower stratosphere. This region is influenced by local chemical ozone loss, enhanced by volcanic aerosol, and by transport from other regions. The vertical, latitudinal, and seasonal characteristics of the decadal depletion of midlatitude ozone are broadly consistent with the understanding that halogens are the primary cause. The expected low ozone amounts in the midlatitude lower stratosphere following the Mt. Pinatubo eruption, and the progressively smaller decreases in the following years as the volcanic aerosol loading decreased, further strengthened the connection between ozone destruction and anthropogenic chlorine. (In the absence of chlorine, an increase in sulfate loading is expected to increase ozone abundance.)

- The apparent leveling-off in midlatitude column ozone losses since the last Assessment is consistent with recovery from the large losses following the Mt. Pinatubo eruption as the volcanic aerosol loading slowly declined. Recent modeling studies have shown that it takes several years for the chemical effects of a volcanic eruption to disappear. Indeed, the trend in midlatitude ozone depletion during the 1980s (prior to Mt. Pinatubo) is now understood to have been exacerbated by volcanic influences during that decade.

## Processes

- Chlorine activation in or on liquid particles in the lower stratosphere (both stratospheric sulfate aerosol (SSA) and supercooled ternary solutions (STS)) increases strongly with decreases in temperature. The rate coefficients are at least as large as those on solid polar stratospheric clouds (PSCs) close to nitric acid trihydrate (NAT) equilibrium temperatures. Thus, chlorine activation is to a first approximation controlled by temperature and water vapor pressure, and only secondarily by the phase of the condensed matter.

- Rapid polar ozone loss requires elevated chlorine monoxide (ClO) in the presence of sunlight. Maintenance of elevated ClO in late-winter/spring was previously thought to require denitrification. Since the last Assessment, new understanding has shown that cold liquid aerosol and/or repeated heterogeneous processing can also maintain elevated ClO in non-denitrified air.

- Some rate coefficients and photochemical parameters have been revised since the last Assessment. Although the impact of these findings has not yet been fully evaluated, our understanding of the lower stratosphere is not expected to change significantly. The lower measured rate coefficients for the reactions of iodine monoxide (IO) radicals mean that iodine may not contribute very significantly to the observed ozone depletion in the lower stratosphere.

- One of the most important new heterogeneous reactions identified since the last Assessment is the hydrolysis of bromine nitrate ($BrONO_2$), which serves to enhance odd hydrogen radicals ($HO_x$) and suppress nitrogen oxides ($NO_x$) and thereby plays a significant role in the midlatitude ozone chemistry.

- An individual stratospheric air parcel is made up of molecules that have spent differing amounts of time in the stratosphere. To calculate the composition of a given air parcel, one therefore needs to know the distribution of such times. The distribution varies as a function of height and latitude of the parcel. Different two-dimensional (2-D) and three-dimensional (3-D) model calculations of the distributions vary greatly and are generally inconsistent with measurements.

- The balance between radiation and dynamics controls upwelling and temperature in the tropics, and hence the amount of water vapor entering the stratosphere. This represents a potentially important mechanism by which stratospheric ozone depletion could be altered by changes in climate. The nature of this radiative-dynamical control is better understood since the last Assessment, although some important details remain unresolved.

- Constituent measurements show that the tropics are relatively isolated from midlatitudes, in some ways analogous to the wintertime polar vortex. The extent of isolation affects the budgets (and lifetimes) of chemical species. Simplified models that represent this dynamical feature (e.g., a leaky tropical pipe model) have been used to provide rough estimates of mixing time scales.

- Small-scale chemical tracer structure in the lower stratosphere, manifested as filaments or laminae, can arise from stirring by the large-scale flow. The importance of this process has been demonstrated since the last Assessment through transport calculations supported by in situ measurements. There have been significant advances in our understanding and quantification of this process, which affects mixing time scales in the lower stratosphere.

- Observations together with process-based modeling suggest that mesoscale PSC formation can activate chlorine in lee wave clouds. It is estimated that ozone can be destroyed downstream of such clouds for many days. Mesoscale chemical structure due to filamentation may also systematically impact rates of reactions (e.g., chlorine deactivation or ozone loss) on a larger spatial scale. However, the contribution of these two phenomena to midlatitude or polar ozone changes is yet to be quantified.

### Quantification and prediction of ozone changes

- Field measurements of the abundances of free radical catalysts involved in lower stratospheric ozone loss are consistent with model calculations and have enabled calculation of ozone loss rates in certain parts of the lower stratosphere. For example, it is now known that $HO_x$ is the dominant catalytic ozone destroyer in the midlatitude stratosphere below ~20 km. However, observations in the lowest part of the extratropical stratosphere within a few km above the tropopause remain very limited.

- Two-dimensional models, despite their shortcomings, are useful for characterizing radiative/chemical effects in the present climate system. They are able to calculate variations in total ozone amounts that are broadly consistent with the observed midlatitude column ozone trend. In particular, the models reproduce the lower ozone amounts observed immediately following Mt. Pinatubo and the subsequent increases as the aerosol disappeared.

- The major hindrance for future prognosis of ozone levels in the Arctic is the limited ability of models to predict the dynamics (hence temperatures and transport), due to the inherent chaotic variability of the atmospheric circulation on interannual and decadal time scales.

- Dynamical forcing of the stratosphere by gravity-wave drag is now believed to be a more important effect than was previously realized. Most gravity-wave drag parameterizations remain crude. This represents a significant obstacle for general circulation modeling and prediction of stratospheric climate change.

**Table 7-1. Changes in the data on gas phase reactions that affect stratospheric ozone chemistry.** Minor changes in some of the other reactions are not listed. In most cases, the data obtained after the 1994 Assessment are listed in DeMore *et al.* (1997).

| Reaction | Information for 1994 Assessment (WMO, 1995) | Update | Impact | Reference |
|---|---|---|---|---|
| $OH + ClO \rightarrow HO_2 + Cl$ or $\rightarrow HCl + O_2$ | HCl yield = 0. | ~5% HCl yield. | Reduces the impact of chlorine. | Lipson *et al.* (1997). |
| $ClO + ClO + M \rightarrow Cl_2O_2 + M$ | 10 to 60% uncertainty in rate constant. | No new data. Reanalysis reduced uncertainty to <30%. | Better definition of ozone loss rates. | Nickolaisen *et al.* (1994). |
| $ClO + BrO \rightarrow$ products | Uncertain to ~30%. | No change. | Contribution of this reaction still uncertain. | DeMore *et al.* (1997). |
| $ClOOCl + h\nu \rightarrow$ products | Limited information on products. Cross sections uncertain. | Quantum yields measured at 248 & 308 nm. | Assumption of Cl atom production OK. Photolysis rate still uncertain. | DeMore *et al.* (1997). |
| $HO_2 + BrO \rightarrow$ products | Not well defined. | Many studies. Defined to better than 50%. | Role of bromine-catalyzed ozone loss in midlatitudes better defined. | Cronkhite *et al.* (1998), Elrod *et al.* (1996), Larichev *et al.* (1995), and Li *et al.* (1997). |
| $HOBr + h\nu \rightarrow$ products | Inconsistent data on cross sections. | New band of HOBr discovered. Cross sections a little better defined. | HOBr photolysis rate will not determine the rate of $O_3$ loss. Helps explain the early morning OH. | DeMore *et al.* (1997), Ingham *et al.* (1998), and Deters *et al.* (1996). |
| $OH + BrO \rightarrow$ products | No information. | Fast reaction. Products unknown. | Small yield of HBr will help explain observations. | DeMore *et al.* (1997). |
| $BrO + O \rightarrow$ products | | Better defined. | Little impact. | DeMore *et al.* (1997). |
| $BrO + O_3 \rightarrow$ products | | Lower upper limit. | Makes this reaction unimportant. | Rowley *et al.* (1996). |
| $ClONO_2 + h\nu \rightarrow$ products | Possibility of pressure dependence in photolysis. | Pressure dependence of photolysis rate, if it exists, is small. Products are Cl and $NO_3$. | The pressure dependence of photolysis rate is not responsible for measured $ClONO_2$ to HCl ratio. | Moore *et al.* (1995), Tyndall *et al.* (1997), Yokelson *et al.* (1997), and Nickolaisen *et al.* (1996). |
| $BrONO_2 + h\nu \rightarrow$ products | Cross section measured by only one group at 298 K only. | Cross sections known as function of temperature. Quantum yields measured. Photolysis rate not pressure dependent. | Role of bromine better defined. | Harwood *et al.* (1998), Burkholder *et al.* (1995), and Deters *et al.* (1998). |
| $IO + ClO \rightarrow$ products<br>$IO + BrO \rightarrow$ products | Rate coefficients unknown. | Rate coefficients defined and some information on product yields available. | The role of iodine is better quantified. | DeMore *et al.* (1997). |
| $O_3 + h\nu \rightarrow O(^1D) + O_2$ | | Production of $O(^1D)$ at long wavelengths and lower T. | $HO_x$ production rate is enhanced. Full impact not yet assessed. | Ball *et al.* (1997), Silvente *et al.* (1997), Takahashi *et al.* (1996), and Talukdar *et al.* (1998). |

## 7.2.2 Microphysics

*Nitric acid-containing PSCs can exist 2-6 K above the frost point. The surface area of PSCs critically depends on their type. Particles of different composition and phase can coexist, but may not necessarily be in thermodynamic equilibrium with each other or with the gas phase. In particular there is evidence that solid PSCs, e.g., nitric acid trihydrate (NAT) clouds, often do not grow to their equilibrium sizes (Type-1a). In the absence of solid PSCs, gaseous nitric acid is taken up by solution droplets when temperatures fall to within 2-3 K of the frost point. The resulting ternary solution droplets form liquid PSCs (Type-1b) with a surface area typically 10-fold higher than background aerosols. While the thermodynamics and non-reactive kinetics of liquid PSCs are understood, the conditions that lead to the formation of solid PSCs are still highly uncertain. The role of solid particles in ozone depletion through sedimentary redistribution of $NO_y$ and water ($H_2O$) and through direct chemical processing of halogen species cannot yet be quantified.*

The size, phase, growth, and evaporation of stratospheric aerosol are fully governed by the highly temperature-dependent partitioning of nitric acid ($HNO_3$), sulfuric acid ($H_2SO_4$), and $H_2O$ and not by other species, such as those involved in chemical processing or nucleation (e.g., freezing). Despite the expected simplicity of such a ternary system, the composition and the phase of wintertime stratospheric particles are unclear.

The strong supercooling of supercooled ternary solutions (STS) leads to overall rates of chemical processing that vary continuously in going from sulfuric acid aerosols to PSCs (see Section 7.2.3). Due to increasing solubilities of reactants, the chemical processing increases very rapidly with decreasing temperature. Activation of chlorine occurs in a day or so around the NAT equilibrium temperature. This continuous but rapid activation was confused previously with a threshold process.

Currently, it is uncertain when gas-to-solid, liquid-to-solid, and solid-to-solid phase transitions (deposition-nucleation, freezing, and incongruent melting, respectively) occur. As long as these processes are poorly understood, the relevance of solid PSCs in chemical processing and sedimentary redistribution of $HNO_3$ and $H_2O$ remains unclear. This impedes a proper analysis of current ozone loss and prohibits accurate prognosis of future ozone levels.

### Thermodynamics of Solid and Liquid Stratospheric Particles

As noted in Chapter 3, under typical Arctic conditions, quasi-binary $H_2SO_4/H_2O$ solution droplets turn into quasi-binary $HNO_3/H_2O$ droplets upon cooling from 193 to 190 K. Under these conditions, species such as hydrogen chloride (HCl), hypochlorous acid (HOCl), and hydrogen bromide (HBr) can also take part in multiphase reactions in/on the liquid particles because of their increased solubility at low temperatures (see Figure 3-1 and Section 7.2.3). Other temperature-dependent contributions, such as liquid phase diffusion coefficients, second-order reaction rate coefficients, or the increase in surface area due to $HNO_3/H_2O$ uptake, are of relatively minor importance (Peter, 1997; Ravishankara and Hanson, 1996). Solubilities at very low temperatures have been mostly derived from thermodynamic models rather than direct experimental vapor pressure data but are believed to be robust (Carslaw *et al.*, 1997).

The thermodynamic stability of hydrates of nitric and sulfuric acid and their complex interactions are summarized in Figure 7-1. Under typical stratospheric conditions, nitric acid hydrates (NAX = NAT, nitric acid dihydrate (NAD), or nitric acid pentahydrate (NAP)) may coexist either with a liquid or with hydrates containing the $H_2SO_4$ of the background aerosol droplet. On the other hand, sulfuric acid hydrates (SAX = sulfuric acid tetrahydrate (SAT) or sulfuric acid hemihexahydrate (SAH)) or the mixed hydrate (MIX) in general cannot coexist with $HNO_3$-containing liquids, because they deliquesce below a certain temperature (e.g., at 191 K for SAT in Figure 7-1). As Koop and Carslaw (1996) noted, deliquescence leads to a "reset mechanism" of frozen $H_2SO_4$ aerosols back to the liquid state, provided NAT does not nucleate on these particles before the deliquescence temperature is reached.

### Are PSCs Solids, Liquids, or Both?

The only solid unambiguously known to be formed under stratospheric conditions is ice, which nucleates a few degrees below the frost point (see, for example, Carslaw *et al.*, 1997). Originally, PSCs were suggested to form upon freezing of the sulfate aerosols and condensation of $HNO_3$ and $H_2O$ onto it (Poole and McCormick, 1988), as indicated by the SAT-NAX-ice path in Figure 7-1. However, laboratory studies indicate

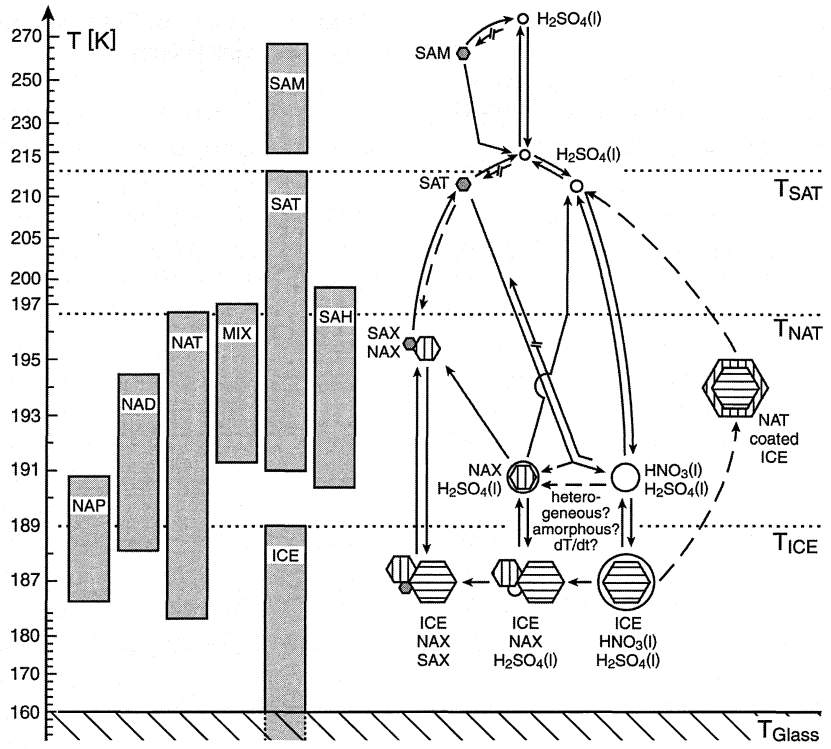


**Figure 7-1.** Stability regions of $HNO_3$ and $H_2SO_4$ hydrates and water ice (left) and phase transitions among these solids and with ternary solutions (right) for the following conditions: 50 hPa, 5 ppmv $H_2O$, and 10 ppbv $HNO_3$. Horizontal lines mark equilibrium temperatures for SAT, NAT, and ice. Solid arrows: kinetically allowed transitions. Crossed arrows: kinetically hindered. Particles in thermodynamic equilibrium are connected by solid arrows, in nonequilibrium by dashed arrows. Abbreviations for crystalline phases: NAX is generic name for nitric acid hydrates, NAT = $HNO_3 \cdot 3H_2O$, NAD = $HNO_3 \cdot 2H_2O$, NAP = $HNO_3 \cdot 5H_2O$; SAX is generic name for sulfuric acid hydrates, SAT = $H_2SO_4 \cdot 4H_2O$, SAH = $H_2SO_4 \cdot 6.5H_2O$, SAM = $H_2SO_4 \cdot H_2O$; MIX = $H_2SO_4 \cdot HNO_3 \cdot 5H_2O$, ICE = water ice. (l) marks aqueous liquids. Adapted from Peter (1997) after Koop *et al.* (1997b).

that precipitation of SAT from binary or ternary solutions ($H_2SO_4$ ($l$) $\rightarrow$ SAT) is kinetically unfavorable down to temperatures below the frost point (Carslaw *et al.*, 1997; Martin *et al.*, 1998), and that even ice crystals in STS are probably not suited for heterogeneous nucleation of acidic hydrates (Koop *et al.*, 1995; Koop *et al.*, 1997a). On the other hand, deposition nucleation (gas-to-solid) on ice without liquid intermediates sets in at moderate supersaturations (Hanson, 1992) and was suggested as a mechanism for NAT formation (Carslaw *et al.*, 1997).

Temperatures do not often drop below the frost point in the Arctic (at least on large scales). The need for such low temperatures could be circumvented if $HNO_3$ hydrates nucleated on $H_2SO_4$ hydrates, thereby avoiding their deliquescence. There are conflicting data on whether NAT can nucleate on SAT (dashed line from SAT to NAX in Figure 7-1) due to a pre-conditioning of the SAT (Iraci *et al.*, 1998; Zhang *et al.*, 1996). A differentiation between deliquescence or pre-activation, which is difficult to obtain from presently available observations (Larsen *et al.*, 1997) or laboratory investigations (Iraci *et al.*, 1998), is necessary to determine the evolution of the physical state of PSC particles. It has been suggested that solids could form above the frost point via crystallization of amorphous solids upon warming (Tabazadeh and Toon, 1996) or the freezing of highly nonequilibrium liquid states (Tsias *et al.*, 1997) (see dashed horizontal arrow in Figure 7-1).

It was thought that solid particles (ice, NAT, and other hydrates of $HNO_3$ and $H_2SO_4$) would nucleate close

to the NAT equilibrium temperature, leading to abrupt changes in surface area and chemical processing rates (WMO, 1995). Modeling and laboratory work have since revealed that PSCs could consist of supercooled ternary (liquid) solution (STS) droplets (Carslaw *et al.*, 1994; Tabazadeh *et al.*, 1994) and have led to the identification of Type-1b PSCs as liquid aerosol. Thus, PSCs can be solids or liquids. However, the circumstances that lead to solid PSCs remain unclear.

### Non-Reactive Uptake Kinetics

Particles and the gas phase can be out of equilibrium due to gas diffusion and partial pressure limitations. Growth/evaporation times depend on particle size and the saturation ratio (i.e., the difference between the vapor pressure and partial pressure of the condensing species). Therefore, the growth/evaporation of $HNO_3$-containing particles, such as NAT and STS particles, are much slower than that of ice particles. For 1-μm particles, typical growth times (or lifetimes) vary from less than one minute for ice (Toon *et al.*, 1989b) to more than one day for NAT (Peter *et al.*, 1994). Diffusion resistances may also lead to highly nonequilibrium compositions in growing/evaporating STS clouds, with small droplets acquiring $HNO_3$ concentrations well above the maximum equilibrium value (Meilinger *et al.*, 1995). The extent of deviation from equilibrium depends on the time rate of temperature change. Cooling/heating rates of 100 K/h, for example in mountain-induced gravity waves (lee waves; see Section 7.4.1.1) can lead to droplets with negligible $H_2SO_4$ concentrations and about 60 wt% $HNO_3$ (Tsias *et al.*, 1997). It is likely that NAD nucleates (Disselkamp *et al.*, 1996) in these wave-induced highly nonequilibrium solution droplets, which may subsequently convert into NAT.

Solid particles, which are few in number but can grow to large sizes, often take long times to grow. For example, from lidar measurements, Toon *et al.* (1990) concluded that Type-1a particles have radii on the order of 1 μm or larger, but that possibly only a part of the available $HNO_3$ condensed. This might be due to long growth/evaporation times, which are supported by balloon and aircraft-borne in situ observations that have frequently found nonequilibrium conditions. In Chapter 3 of this Assessment, Figure 3-12 shows particle counter measurements made on board the ER-2 in the Arctic. Each point in that figure corresponds to a size-resolved measurement. Particles in panel 1 (bottom left panel corresponding to the encircled 1 in the main panel) show a log-normal distribution shifted with respect to the background, most likely indicating STS droplets. In contrast, panel 2 shows a large particle mode with small number density but radii of about 1 μm immersed in a small particle mode representative of a background distribution. Most likely, the large mode consists of an $HNO_3$ hydrate and the small mode of liquid $H_2SO_4/H_2O$ droplets (with very small amounts of dissolved $HNO_3$). If the hydrate was NAT and had grown to its full equilibrium size, point (2) in the main panel of Figure 3-12 would lie on the NAT curve (dotted). At their small number density, however, it would take roughly a day for these particles to deplete the gas phase. Because air parcels in the Arctic rarely remain cold for such long periods, clouds with fully condensed large solid particles are rarely observed there.

Tabazadeh *et al.* (1995) and Tabazadeh and Toon (1996) have interpreted the flight observations in Figure 3-12 as the manifestation of a new thermodynamic phase rather than an indication of nonequilibrium particle distributions. By eliminating particles with radii larger than 2 μm from the particle counter measurements and constraining the evaluation to a certain time window, they obtained the more compact volume-temperature relationship shown in the insert in Figure 3-12. They argued that this relationship could represent a glass-like amorphous phase, as trajectory analyses indicate crystallization of the particles upon warming. However, the only laboratory investigation bearing directly on this issue suggests that crystal embryos in binary or ternary solutions show no growth impedance at stratospheric temperatures (Koop *et al.*, 1997a), thereby not supporting an amorphous high-viscosity state.

### Microphysical Aspects of Sedimentary Redistribution

Sedimentary redistribution of $HNO_3$ (also called denitrification and renitrification) and $H_2O$ (dehydration and rehydration) has been observed in the Antarctic (WMO, 1995) and, to a lesser extent, in the Arctic (Arnold *et al.*, 1998; Fahey *et al.*, 1990; Hübler *et al.*, 1990). Sedimentation rates depend critically on particle size. To sediment down by 5 km, representative of the observed redistributions, it takes 7 months to a week for 1 to 5 μm particles, respectively (Müller and Peter, 1992). For a particle number density of 10 $cm^{-3}$, NAT particles would reach radii of about 0.3 μm and ice particles of

about 1.6 μm, if all the $HNO_3$ and $H_2O$, respectively, in a lower stratospheric air parcel condensed. Such small particles obviously do not allow for significant sedimentary redistribution and a very small number of particles must grow to large sizes via some highly selective nucleation mechanism.

In the Arctic, matters are complicated because planetary waves make the air parcels go through temperature oscillations with a period of about 5 days and 15-30 K peak-to-peak amplitude. This warms the air well above the NAT evaporation temperature. Therefore, sedimentary redistribution could occur in many successive steps, possibly enhanced by mesoscale temperature fluctuations in mountain waves (Section 7.4.1.1). Another possibility is that $HNO_3$ coats an ice particle (Wofsy *et al.*, 1990; Peter *et al.*, 1994); see rightmost path in Figure 7-1. If particles grow to radii above 10 μm, sedimentation could proceed in a single step, which is unlikely for NAT. Goodman *et al.* (1997) found ice particles containing small amounts of $HNO_3$ with radii between 6 and 8 μm in the Antarctic stratosphere at temperatures 2-4 K above the frost point. They observed increases in the $HNO_3$ fraction with decreasing particle size and concluded that the ice might be protected by a NAT coating. In conclusion, redistribution of $HNO_3$ requires a selective nucleation mechanism whose nature is still uncertain and does not necessarily require significant dehydration.

### 7.2.3 Reactions on Condensed Matter

*The rates of the major stratospheric multiphase reactions in liquid aerosol are known to about a factor of 2. The rates of reactions on solids are very uncertain; inclusion of more detailed kinetic formulations in models requires improved laboratory data and analysis. $Cl_y$ activation rates vary with various stratospheric parameters as follows: a factor of 2 in heterogeneous processing rate corresponds to a factor of 2 in aerosol surface area; a change in T of 2-4 K; a factor of 2 to 4 change in HCl vapor pressure; or a 20% change in water vapor pressure (the latter corresponding to about 2 km in altitude). Within that uncertainty, the role of liquid aerosol from measurements of the partitioning of reactive families ($NO_x$ and $Cl_y$) is reasonably well understood at mid and high latitudes, particularly at low aerosol loading. Uncertainties remain at high aerosol loading and for coldest conditions (where solid particles may be important).*

Five reactions that take place in liquid droplets as well as on solid surfaces are routinely included in stratospheric models:

$$N_2O_5 + H_2O \rightarrow 2\ HNO_3 \qquad (7\text{-}1)$$

$$ClONO_2 + H_2O \rightarrow HOCl + HNO_3 \qquad (7\text{-}2)$$

$$ClONO_2 + HCl \rightarrow Cl_2 + HNO_3 \qquad (7\text{-}3)$$

$$HOCl + HCl \rightarrow Cl_2 + H_2O \qquad (7\text{-}4)$$

$$BrONO_2 + H_2O \rightarrow HOBr + HNO_3 \qquad (7\text{-}5)$$

In addition, the reaction of hypobromous acid (HOBr) with HCl is included in a few models:

$$HOBr + HCl \rightarrow BrCl + H_2O \qquad (7\text{-}6)$$

Reaction (7-1) on sulfate aerosol controls the relative weighting of $NO_x$ (where $NO_x \equiv NO + NO_2$) and $HO_x$ ozone loss cycles by converting $NO_x$ to $HNO_3$. At colder temperatures (T < 200K), reactions (7-2 to 7-4) shift $Cl_y$ speciation toward $ClO_x$ and $NO_x$ to $HNO_3$, enhancing Cl-induced ozone loss. The activation of $Cl_y$ via reactions (7-2 to 7-4) increases strongly with decrease in temperature. $Br_y$ reactions (7-5 and 7-6) are now believed to impact $ClO_x$ and $HO_x$ levels. Other reactions between species of different radical families ($N_2O_5$ + HCl and $BrONO_2$ + HCl, for example) are not currently included routinely in models.

Laboratory measurements of reactive uptake coefficients and physico-chemical parameters involved in these coefficients on many solids and liquids have been evaluated (Atkinson *et al.*, 1997; DeMore *et al.*, 1997). Overall, there is good agreement for reactions with condensed $H_2O$ (7-1, 7-2, and 7-5), especially on liquids. However, laboratory results for reactions of two gas phase species on or in condensed matter, e.g., reactions (7-3), (7-4), and (7-6), are still uncertain, especially on solid surfaces. Understanding of chemical mechanisms in terms of fundamental physico-chemical parameters is required to reduce uncertainties and apply kinetic formulations to all stratospheric conditions (see for example, Kolb *et al.*, 1995).

There has been much progress in understanding the mechanism of liquid phase reactivity, exemplified by the formulations of reactions (7-2) and (7-3) by Hanson *et al.* (1994). Figure 7-2 shows $ClONO_2$

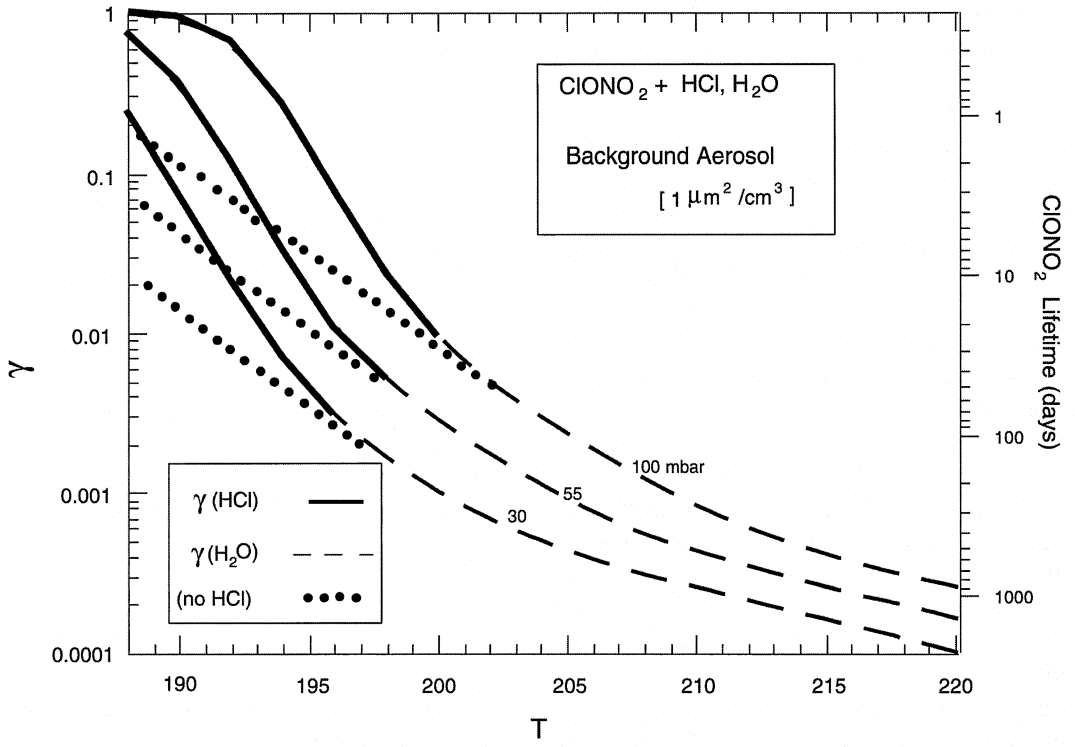


**Figure 7-2.** Reactivity of $ClONO_2$ with $H_2O$ and HCl (reactions (7-2) and (7-3)) as a function of stratospheric temperature ($T$). $ClONO_2$ processing lifetime on right axis is derived from reactive uptake coefficient ($\gamma$) on left axis, assuming background aerosol (ignoring PSC condensation below 195 K). Stratospheric pressures of 30, 55, and 100 mbar correspond roughly to 24, 20, and 16 km altitude, respectively. The steep rise in $\gamma$ below 195-200 K reflects increasing $H_2O$ and HCl condensation into the sulfuric acid solution. The corresponding shift from reaction with $H_2O$ (dashed line) to faster reaction with HCl (solid line) defines cold (polar) $Cl_y$ processing. The dotted line shows $H_2O$ reaction in absence of HCl. Curves come from updated formulation of the Henry's law solubility ($H$) and the rate coefficient ($k$) for reaction (7-2), derived from analysis of all experimental results (Robinson *et al.*, 1997). For reaction (7-3), $H$ for HCl was taken from Carslaw *et al.* (1995) and $k$ was derived from Hanson and Ravishankara (1994). Also included is a detailed formulation of the liquid phase diffusion coefficient ($D_l$) in $H_2SO_4/H_2O$ solution (Hanson and Ravishankara, 1993; Klassen *et al.*, 1998; Williams and Long, 1995). Adapted from Ravishankara and Hanson (1996) and Robinson *et al.* (1997).

reactivity on sulfuric acid/water mixtures under lower stratospheric conditions. The rate of $Cl_y$ processing shows a steep temperature dependence, largely due to condensation or dissolution of reactants ($H_2O$ and HCl) at cold temperatures (see Chapter 3). Rates of multiphase processing depend on Henry's law solubility (H), liquid phase diffusion coefficient ($D_l$), and rate coefficients ($k$) for the reaction in the liquid. Figure 7-2 uses an updated kinetic formulation (Robinson *et al.*, 1997) that refines previous work (Hanson *et al.*, 1994) by more comprehensively treating $H$, $D_l$, and $k$ in variable aerosol acid composition. This is particularly important for predicting variability with altitude, because the relationship between acid composition and stratospheric temperature ($T$) depends on absolute water vapor density, and because $D_l$ and $k$ determine how processing rates vary with the size of the particle.

The sharp increase in the $ClONO_2$ processing rate as $T$ gets close to 200 K is largely from reaction (7-3) in liquid aerosols. Reaction (7-2) is now identified to be acid-catalyzed (Robinson *et al.*, 1997) and is consistent with recent observation of protonated HOCl at high acid

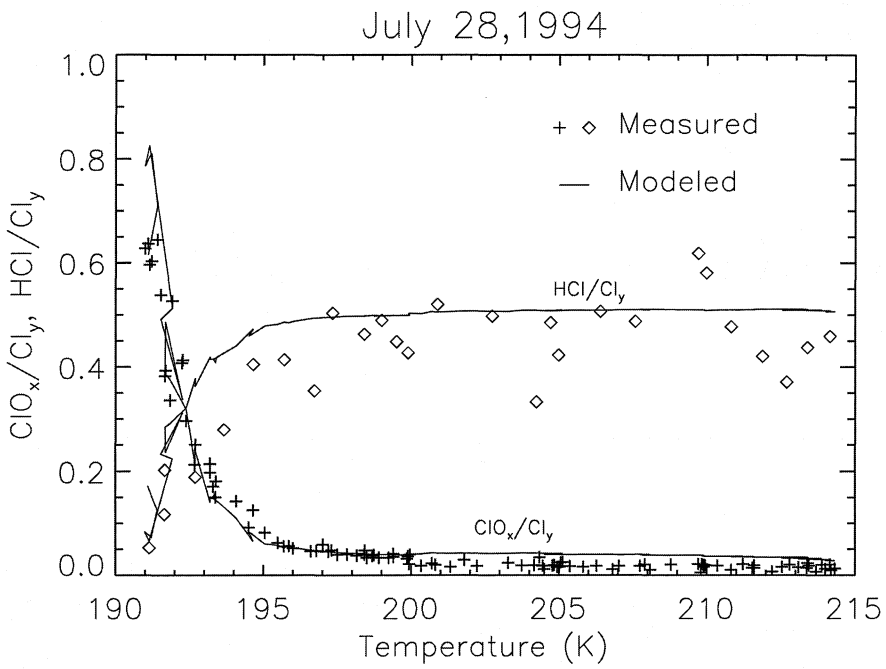


**Figure 7-3.** Measurements of $ClO_x/Cl_y$ and $HCl/Cl_y$ from the flight of 28 July 1994 near the southern vortex plotted versus temperature. On this day the measured temperature was the minimum of the previous 10 days for all trajectories originating south of 57°S. (Adapted from Kawa *et al.*, 1997.)

concentration (Hanson and Lovejoy, 1996; Donaldson *et al.*, 1997). Although reaction (7-3) dominates the Cl activation process, these faster rates for reactions (7-2) and (7-4) for T < 200K alter the $HCl/ClONO_2$ partitioning, particularly at low HCl levels (Carslaw and Peter, 1997). Reaction (7-6) is also potentially important (Abbatt, 1994). Reaction (7-5) remains fast even at lower $H_2O$ concentrations and, hence, at higher wt% (i.e., temperatures well above 200 K in the stratosphere) (Hanson *et al.*, 1996). Therefore, it is important in the lower stratosphere during all seasons and over a wide range of altitudes.

In contrast to reaction (7-2), the rate of $N_2O_5$ hydrolysis (reaction 7-1) is virtually independent of water activity. While a constant value of 0.1 for the reactive uptake coefficient ($\gamma$) represents results for background stratospheric aerosol conditions, the detailed mechanism is likely more complex (Robinson *et al.*, 1997). There are uncertainties in the rate of reaction (7-1) in STS (Hanson, 1997a; Zhang *et al.*, 1995). Reaction (7-1) is reported to be slower in warmer aerosols (Hu and Abbatt, 1997).

Parameterizations of chemical mechanisms in liquids, including estimation of surface reactivity (Hanson, 1997b) and the reacto-diffusive length for aerosol-size-dependent processing (Hanson and Lovejoy, 1995; Lovejoy and Hanson, 1995), are known well enough to quantify the rates of reactions (7-1)-(7-6) within a factor of 2 under various stratospheric conditions. The cal-culated processing rates are consistent with many field observations of $HNO_3$ and chlorine species, including Arctic ER-2 (Webster *et al.*, 1994) and balloon measurements (Oelhaf *et al.*, 1994; von Clarmann *et al.*, 1997) and global satellite measurements (Müller *et al.*, 1996; Roche *et al.*, 1994; Santee *et al.*, 1995). A recent example is plotted in Figure 7-3, showing sharp temperature-dependent shifts in $Cl_y$ partitioning measured from the ER-2 in the Southern Hemisphere (Kawa *et al.*, 1997) that match the predicted rates for reactions (7-2)-(7-4) on liquid aerosols (see Figure 7-2). Likewise, analyses of field observations of midlatitude $NO_x/NO_y$ ratios confirm the importance of $N_2O_5$ hydrolysis (reaction 7-1) on liquid sulfate aerosol in the lower stratosphere. This includes ER-2 (Gao *et al.*, 1997), balloon (Kondo *et al.*, 1997; Sen *et al.*, 1998), and UARS satellite (Morris *et al.*, 1997) observations. There are examples of models underpredicting $NO_x$ levels, such as sunrise measurements at high southern

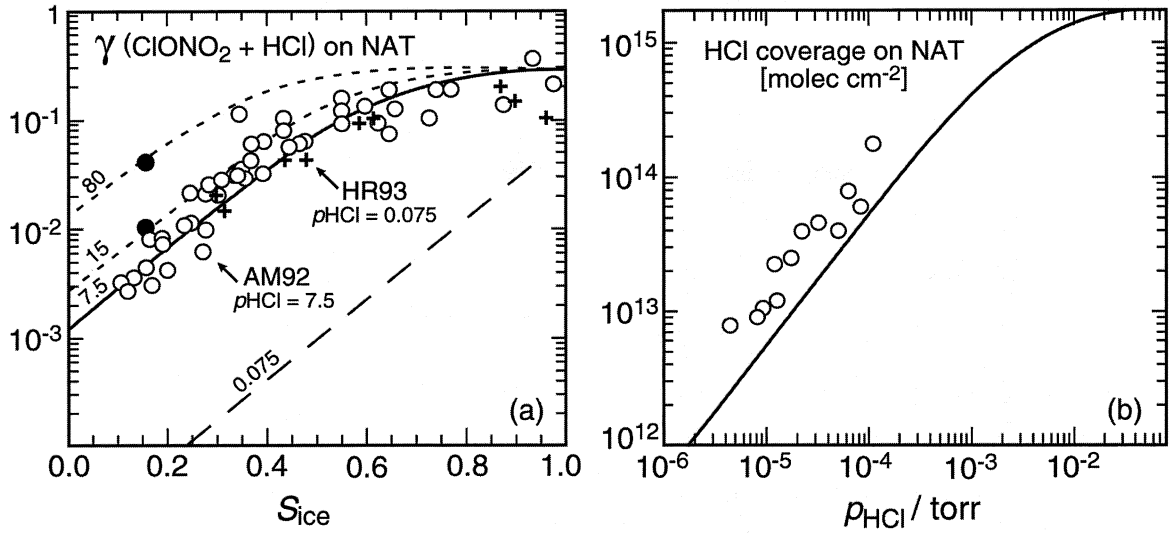


**Figure 7-4.** Left panel: Measured (from the data of Abbatt and Molina (1992) and from Hanson and Ravishankara (1993); see Carslaw and Peter (1997) for details) and calculated (by Carslaw and Peter) reactive uptake coefficients ($\gamma$) on NAT. Depending on the assumed surface coverage of HCl on NAT ($S_{ice}$), the calculated reactive uptake coefficients can be different by factors of 50 to 100 (see text). Right panel: Surface coverage of HCl on NAT as a function of the partial pressure of HCl measured by various investigators (see Carslaw and Peter (1997) for details). Adapted from Figure 2 of Carslaw and Peter (1997).

latitudes from ATMOS (Newchurch *et al.*, 1996; Rinsland *et al.*, 1996a), perhaps indicative of incomplete heterogeneous or gas phase chemistry.

On solid particles, characteristic of some PSCs or cirrus clouds in the lower stratosphere, uncertainties in reaction mechanisms are greater. $Cl_y$ activation rates on solids are similar to those in liquids; in fact, when solid formation thresholds are included, temperature-dependent reactivity on solids is virtually indistinguishable from that on liquids shown in Figure 7-2 (Ravishankara and Hanson, 1996). Rate measurements on a variety of surfaces (NAT, NAD, SAT, ice) indicate $Cl_y$ reactivity is somewhat slower than on liquids, with dependencies on relative humidity giving effective negative temperature dependencies (Ravishankara and Hanson, 1996).

Much of the uncertainty in reactivity on solids is associated with lack of knowledge of surface densities of reactants (Carslaw and Peter, 1997; Henson *et al.*, 1996), for which there are no good thermodynamic models, in contrast to gas condensation in liquids (see Section 7.2.2 and Figure 3-1). Uncertainties in fundamental quantities, such as surface area of solids prepared in the laboratory (e.g., see discussion of ice structure in Kolb *et al.*, 1995), lead to contradictory data and interpretation concerning surface coverage of HCl and other gases (Chu *et al.*, 1993; Hanson and Ravishankara, 1992; Oppliger *et al.*, 1997). For example, a reinterpretation of reaction (7-3) on NAT surfaces (Carslaw *et al.*, 1997) is shown in Figure 7-4. Extrapolation of data obtained at higher HCl concentration by assuming a linear variation in surface coverage with HCl partial pressure and a rate of reaction that is proportional to HCl surface coverage gives an effective rate of reaction (7-3) that is 100 times slower than that measured at lower concentrations. However, it is not known if the surface coverage increases linearly with HCl partial pressure and if the rate of reaction of $ClONO_2$ on the surface increases linearly with HCl surface coverage. Some experiments clearly show that the rate of reaction (7-3) is nearly independent of HCl partial pressure (Hanson and Ravishankara, 1992). If reaction (7-3) on NAT were as slow as that shown in Figure 7-4, and if a significant fraction of the surface area is due to NAT, solid PSC formation would slow $Cl_y$ activation (Carslaw and Peter, 1997).

Kinetic formulations on solid phases still require coupled models of chemical mechanisms and surface

morphology. For example, though protonation of HOCl adsorbed in ice matrices has been observed (see, e.g., Banham *et al.,* 1995), such behavior is not quantified as with Henry's law solubility for liquids. Despite much discussion, there is little quantitative knowledge on the existence and role of quasi-liquid like layers (see Ravishankara (1997) and references therein), for example on ice in the presence of condensable vapors such as HCl and $HNO_3$. A recent example involves laboratory results indicating that at stratospheric concentrations of a few parts per billion by volume (ppbv), $HNO_3$ will completely coat ice (Abbatt, 1997; Zondlo *et al.*, 1997). Formulation of generalized mechanisms of surface coverage and reactivity that might include such $HNO_3$ surface coverage requires more information before quantitative application to stratospheric models will be feasible (Carslaw and Peter, 1997).

Other heterogeneous reaction pathways have been discussed in the literature. These include solubility and reactivity of formaldehyde ($CH_2O$) in acid solution (Iraci and Tolbert (1997) and references therein), solubility and reactivity of nitrous acid (HONO) in sulfuric acid (DeMore *et al.*, 1997; Seisel and Rossi, 1997; Longfellow *et al.*, 1998; and references therein), and formation of peroxy nitric acid (Zhang *et al.*, 1997). Recent studies have also reported fast rates for HOBr, $BrONO_2$, and HCl reacting on ice (Allanic *et al.*, 1997), but they are unlikely to be very important in the stratosphere. However, none of these studies appears to indicate a significant perturbation of stratospheric photochemistry, though the mechanisms still need better characterization to quantify their relevance in the stratosphere. For example, despite much interest, a heterogeneous pathway for reduction of $HNO_3$ has not been demonstrated (Chatfield, 1994). Another example is the potential reactivity of carbonaceous soot particles (Rogaski *et al.*, 1997; Wyslouzil *et al.*, 1994). Modeling studies have suggested significant effects of reactions on carbonaceous aerosol (Bekki, 1997; Lary *et al.*, 1997). It seems very unlikely that a particle that is reactive enough to reduce an oxidized species such as $HNO_3$ will remain reactive in an oxidizing stratosphere. Further, it is unlikely that such a particle will not be covered with condensables such as sulfuric acid and water. If the soot particle is destroyed in the reaction, in view of the low stratospheric density of soot particles, it is unlikely that they will lead to significant non-local effects in the stratosphere.

## 7.3 RADIATIVE-DYNAMICAL AND TRANSPORT PROCESSES

### 7.3.1 Large-Scale Temperature and Wind Distribution

*The dynamical and radiative processes controlling the structure of the temperature and wind distribution in the lower stratosphere and its seasonal evolution are, broadly speaking, well understood. There remain some uncertainties over what balance of processes determines tropical temperature distributions and, by implication, tropical upwelling. The current troposphere-stratosphere general circulation models quantitatively differ from observations because there is still an insufficient understanding of how all these processes interact to determine the stratospheric climate (see Section 7.5.3). Small changes, or small uncertainties, in temperatures in the high latitudes and tropics will imply large changes, or large uncertainties, in chemical distributions.*

Significant coupling exists between radiation, dynamics, and ozone abundance in the lower stratosphere. Temperatures affect photochemistry and the distribution of condensed matter. Ozone in turn affects temperatures through both longwave and shortwave radiative processes. Because of the Earth's rotation there is a strong constraint between temperatures and winds, particularly in the extratropics, which has direct implications for transport.

The lower boundary of the stratosphere, the tropopause, is generally characterized by a change in static stability, from relatively high values in the stratosphere to relatively low values in the troposphere. This definition has limitations, as discussed by Holton *et al.* (1995) for example, but is a useful starting point. The height of the tropopause varies from about 15 km in the tropics to about 7 km at high latitudes. The tropical tropopause, which corresponds roughly to an isentropic surface, appears to be consistent with formation by radiative-convective adjustment, with the height of the tropopause set by the top of the region of moist convection. The extratropical tropopause, on the other hand, slopes across a number of isentropic surfaces and is more plausibly formed through the action of baroclinic eddies (Holton *et al.* (1995) and references therein). These different formation mechanisms, and the strong latitudinal variation of the height of the tropopause, have implications for chemistry and transport in the lowest part of the stratosphere (see Section 7.3.4.1).

The temperature field in the stratosphere arises from a balance between radiative and dynamical heating (or cooling). Dynamical heating is caused by vertical (diabatic) motion, which occurs partly in response to the annually varying distribution of solar radiation. However, a substantial part of the vertical motion occurs in response to forces arising from the breaking and dissipation of Rossby waves and gravity waves (e.g., Andrews *et al.*, 1987). In the extratropical stratosphere, the wave-induced forces are almost exclusively westward and act to drive air poleward, thus producing a meridional Brewer-Dobson circulation that is generally rising at low latitudes and sinking at high latitudes. The Brewer-Dobson circulation transports ozone poleward and downward from its photochemical production region into the extratropical lower stratosphere. It follows that variations in ozone transport are likely to be associated with variations in dynamical heating, with less transport corresponding to colder temperatures. This correlation is indeed seen in observations (e.g., Randel and Cobb, 1994).

The mechanism by which the meridional circulation is driven by breaking waves was termed the "extratropical pump" by Holton *et al.* (1995). However, extratropical wave driving cannot adequately explain the location of the tropical upwelling, which occurs throughout the year and maximizes on the summer side of the equator. This cannot be accomplished by "pumping" from the winter hemisphere alone, which would require air to cross angular momentum surfaces within the tropics. Plumb and Eluszkiewicz (1998) have suggested that forces within the tropics may be needed.

The extratropical lower stratosphere exhibits a strong seasonal cycle in temperatures, with coldest temperatures in winter. Although this is what one would expect from radiative considerations, the role of wave-driven vertical motion in modifying the temperature field is apparent from differences in the seasonal cycle between the hemispheres. The greater longitudinal asymmetry in surface conditions of the Northern Hemisphere, which is communicated up into the stratosphere by wave propagation, means that wave driving is stronger there. Since wave driving acts to increase temperatures in the extratropical lower stratosphere, the NH winter polar vortex is warmer (and hence also weaker) than the SH vortex. Indeed the NH vortex is often highly disturbed by strong dynamical events, called sudden warmings. These events tend to break up the vortex by early spring. In the SH, in contrast, the lower stratospheric vortex usually persists as a coherent dynamical entity, with correspondingly cold temperatures, at least until mid to late spring. The stronger dynamical activity in the NH extratropical stratosphere leads to greater interannual variability of temperatures and circulation. This inherently limits predictability and attribution of ozone depletion (see Section 7.6.1).

The contrast between the NH and SH winter vortices illustrates the particularly strong effect of dynamical forcing on wintertime polar temperatures and vortex stability. Because polar ozone chemistry exhibits strong sensitivity to these meteorological conditions (see Section 7.6.1), this points to a mechanism by which long-term changes in dynamical forcing, associated with climate change, could affect stratospheric ozone — quite apart from changes in ozone transport that would also result from a change in dynamical forcing. That such a mechanism is potentially significant is illustrated by the climate simulation results of Shindell *et al.* (1998b), who find an altered dynamical forcing resulting from greenhouse-gas-induced climate change, which leads to a colder, more isolated Arctic vortex and hence a delayed ozone recovery (see Chapter 12).

The effects of dynamical forcing on stratospheric temperatures tend to cancel out in the global mean at any given altitude. This is because downwelling (and dynamical heating) in the extratropics must, by mass conservation, be compensated by upwelling (and dynamical cooling) in the tropics. It follows that global-mean temperatures are largely insensitive to dynamical variability compared to mean temperatures defined over the tropics or extratropics alone (Figure 7-5). Long-term changes in global-mean stratospheric temperatures, such as those in Figure 7-5, must therefore be associated with changes in radiative forcing; conversely, long-term changes in dynamical forcing should be manifested as compensating changes, of opposite sign, in tropical and extratropical temperatures.

The tropical lower stratosphere represents a local temperature minimum, a combined effect of deep tropical tropospheric convection and dynamical cooling associated with stratospheric upwelling (the ascending branch of the Brewer-Dobson circulation). Upwelling rates within the tropics have been estimated from diabatic circulation calculations based on satellite measurements (e.g., Rosenlof, 1995; Eluszkiewicz *et al.*, 1996) and indicate a large seasonal variation with the value during NH winter ($0.4 \times 10^{-3}$ m s$^{-1}$) being around 2 to 3 times that in NH summer ($0.15 - 0.2 \times 10^{-3}$ m s$^{-1}$). There are

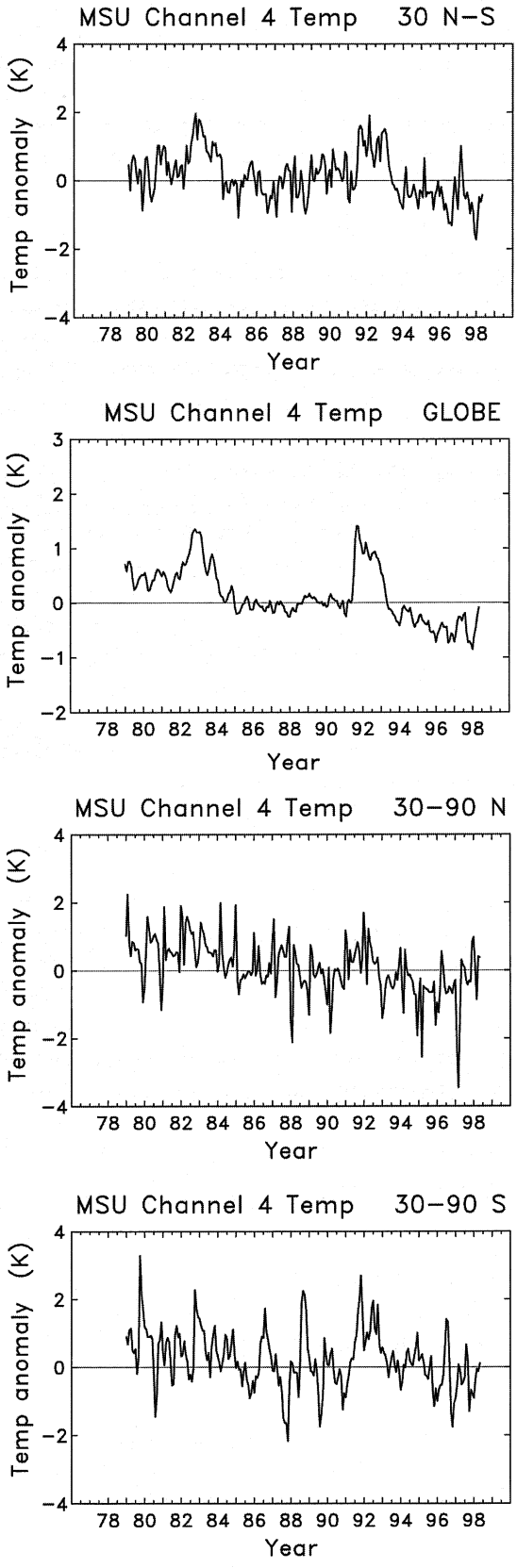


**Figure 7-5.** Time series of lower stratospheric temperatures measured by Microwave Sounding Unit (MSU) Channel 4, from which the annual cycle has been removed. Panel 1: tropical lower stratosphere. Panel 2: the same, but for globally averaged temperatures. The smaller variation in panel 2 shows the strong compensation between temperature variations in the tropics and extratropics, which variations are therefore presumably associated with the diabatic circulation (i.e., with dynamics). Exceptions are the strong signals from 1982 to 1984 and from 1991 to 1994, which are plausibly driven by heating effects associated with El Chichón and Mt. Pinatubo aerosol, and the long-term cooling, which has been attributed to decadal ozone depletion (see Chapter 5). Panels 3 and 4 are the lower stratospheric temperatures for northern and southern extratropics.

large uncertainties in the derived values, particularly near the tropical tropopause, although independent tracer observations (see Section 7.3.3.1) imply an upwelling rate in this region that is generally consistent with these values. The strength and seasonal cycle of this upwelling have important implications for understanding stratospheric water vapor (see Section 7.3.4.2).

Consistent with this seasonal cycle in tropical upwelling, tropical temperatures exhibit a weak but nonetheless clearly identifiable seasonal cycle, with coldest temperatures during NH winter. Early explanations for this cycle appealed to the seasonal cycle in tropospheric convection. It has recently been suggested by Yulaeva *et al.* (1994) that the seasonal cycle may be due instead to the seasonal cycle in extratropical wave driving, which is larger in the NH winter than in the SH winter for reasons stated earlier. Part of the evidence used by Yulaeva *et al.* (1994) is the observed compensation between tropical and extratropical temperatures. Recent studies (Holton *et al.*, 1995; Plumb and Eluszkiewicz, 1998) suggest that wave driving at subtropical or lower latitudes, perhaps together with the annual cycle of thermal forcing, is needed to account for the observed annual cycle in tropical temperatures.

The dominant component of interannual variability in tropical lower stratospheric temperatures is the quasi-biennial oscillation (QBO). It has long been recognized that the QBO is driven by wave momentum transport, but it remains unclear exactly which waves are involved

(see, e.g., Dunkerton, 1997). The role of Rossby waves has been particularly uncertain, though recent direct wind (Ortland, 1997) and constituent observations (O'Sullivan and Chen, 1996) have shown clear evidence of stratospheric Rossby waves radiating into the tropics when the QBO phase is westerly. In addition to the QBO, the observed interannual variability in extratropical wave driving might also, on the basis of the arguments of Yulaeva *et al.* (1994), be expected to affect interannual variability of tropical lower stratospheric temperatures. Certainly the extratropical compensation observed in the seasonal cycle is also seen in the interannual variation, suggesting that dynamical mechanisms account for much of this variation (Figure 7-5).

The influence of the QBO extends globally, particularly into the winter hemisphere. In general, the winter polar vortex is observed to be stronger and temperatures colder, with fewer sudden warmings in the NH, when the phase of the QBO in the lower stratosphere is westerly (Holton and Tan, 1980). As noted by Holton and Tan, this is plausibly due to the effect of tropical winds on the location of extratropical Rossby wave driving; when the tropical winds are westerly the wave driving occurs closer to the equator, and reduces descent (and therefore dynamical heating) over the pole. A recent study with the Geophysical Fluid Dynamics Laboratory (GFDL) "SKYHI" general circulation model, using an imposed forcing to create a QBO, reproduced this tropical-extratropical coupling and produced an extratropical QBO in NH winter in good agreement with observations (Hamilton, 1998).

The QBO is clearly evident in column ozone data, both in the tropics and extratropics (Bowman, 1989). The vertical structure in the tropics shows two cells, with a change of sign near 28 km altitude (Hasebe, 1994; Randel and Wu, 1996). Below 28 km, it appears that ozone is behaving as a tracer, so the QBO signal is a direct response to the QBO in tropical circulation; above 28 km, model studies indicate the link to be chemical, ozone at these altitudes responding to QBO transport of reactive nitrogen (Chipperfield *et al.*, 1994b). The extratropical QBO signal in (column) ozone is oppositely phased to the tropical signal, indicating that it is not caused by transport of the tropical ozone anomaly. Also, the midlatitude ozone QBO is seasonally synchronized (maximum in winter). The QBO effect on the location of extratropical wave driving mentioned above suggests the possibility of increased ozone transport by the Brewer-Dobson circulation during easterly QBO winters (e.g., Tung and Yang, 1994; Hess and O'Sullivan, 1995). However, a recent study by Jones *et al.* (1998) suggests that wave-drag feedbacks are not needed, since the solstitial QBO-driven circulation is equatorially asymmetric (extending into the winter hemisphere).

An important new development in the quantitative study of stratospheric transport has been the use of data assimilation techniques to produce comprehensive global datasets of stratospheric temperatures and winds (Swinbank and O'Neill, 1994; Gelman *et al.*, 1994). These datasets have been the basis for a large number of papers on chemical transport over the last five years or so, including simulations of polar seasonal ozone depletion (see Sections 7.5.4 and 7.6.1). Manney *et al.* (1996) and Coy and Swinbank (1997) compare such datasets and note differences between them, as well as differences with radiosonde observations. Agreement is generally good, with the largest numerical disagreements tending to occur at the most dynamically active times, e.g., during sudden warmings. The global datasets tend to weaken vertical temperature gradients compared with individual high-resolution satellite instruments. There are also systematic differences in some cases between the global datasets and radiosonde ascents, especially over Antarctica (Manney *et al.*, 1996).

### 7.3.2 Global View of Transport and Mixing

*Long-lived tracers are observed to have similar global distributions, whose morphology is controlled by the competing effects of diabatic advection and isentropic mixing. Many tracers exhibit compact relationships in the lower stratosphere, where their lifetimes are long. These relationships are understood theoretically in terms of stratospheric mixing and may differ between tropics and extratropics, and between the wintertime polar vortex and midlatitudes. Isentropic mixing is most intense within the midlatitude "surf zone" and weakest at its edges. Below about 16 km altitude, the vortex edge barrier disappears, and mixing reaches high latitudes. In this region, known as the "lowermost stratosphere," isentropic surfaces are no longer confined to the stratosphere but intersect the midlatitude tropopause, and rapid isentropic mixing with the troposphere is possible.*

Since Jones and Pyle (1984) noted the similar meridional distributions of $N_2O$ and $CH_4$ in Limb Infrared Monitor of the Stratosphere (LIMS) observations of the

stratosphere, it has been recognized that long-lived stratospheric constituent mixing ratios display similar structures. The characteristic observed structure is illustrated in Figure 6-3 of Chapter 6 of this Assessment. For a tracer of tropospheric origin, high concentrations are found in the tropics, corresponding to "young" air (see Section 7.3.3.1 for a discussion of "age"); there are regions of strong gradients in the subtropics, weak gradients in midlatitudes and, in winter, strong gradients at the edge of the polar vortex, within which the oldest air, low in tropospheric source gases, is found.

Holton (1986) and Mahlman *et al.* (1986) explained the slopes of zonal-mean tracer contours as a balance between the slope-steepening effects of the diabatic circulation and the slope-flattening effects of mixing, resulting in a characteristic poleward-downward slope of such contours that is determined by transport alone, and so is the same for all sufficiently long-lived species. Plumb and Ko (1992) showed that these same arguments explained the observations of compact relationships between different long-lived species (e.g., Fahey *et al.*, 1990; Murphy *et al.*, 1993), provided mixing is sufficiently fast. (True compactness can be achieved only when mixing is infinitely fast, and so is never achieved in reality.) The characteristics of the tracer-tracer relationships have been used to determine net global fluxes (Murphy and Fahey, 1994), lifetimes (Volk *et al.*, 1997; see Section 7.3.3.1), and mixing rates (see Section 7.3.3.3).

The classical picture of the Brewer-Dobson circulation has been significantly refined in recent years. The phenomenology of stratospheric transport and mixing reveals a number of distinct regions, depicted in Figure 7-6. Evolution of wintertime stratospheric potential vorticity (PV) maps indicates a contrast between the "surf zone" of midlatitudes, stirred by breaking of the dominant quasi-stationary Rossby waves, and the relatively undisturbed polar vortex (McIntyre and Palmer, 1983). High-resolution modeling results show that the wave-breaking process is associated with erosion of the vortex through detrainment of air from the vortex edge, thus sharpening the edge (Juckes and McIntyre, 1987). This air is typically stretched out into filaments, as seen clearly in high-resolution transport calculations and inferred from aircraft observations (e.g., Waugh *et al.*, 1994; Newman *et al.*, 1996). Although there are occasional events in which small amounts of midlatitude air are injected into the vortex (Plumb *et al.*, 1994),

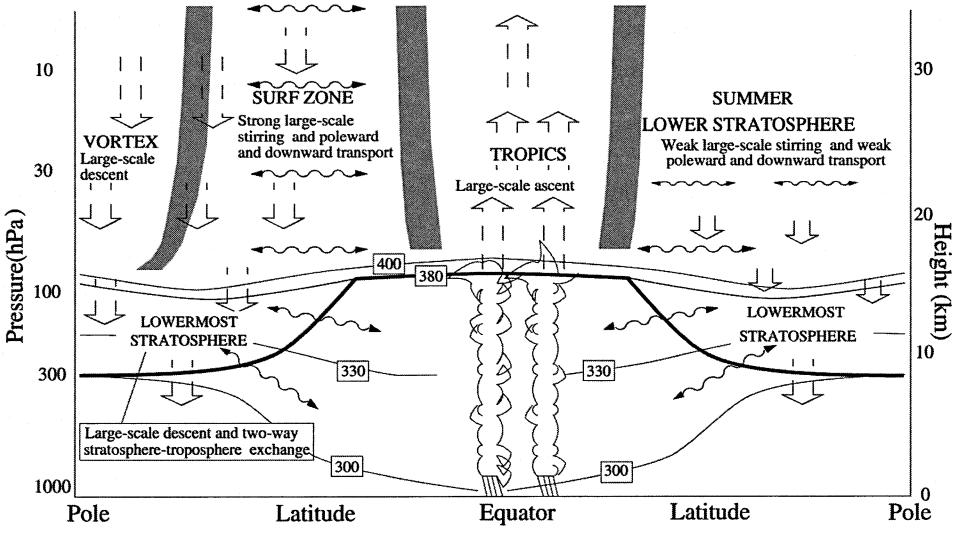


**Figure 7-6.** Schematic of the principal regions of the lower stratosphere with distinct transport characteristics. Broad arrows denote the diabatic circulation, wavy arrows denote stirring along isentropic surfaces. The thick solid line starting at about 7 km at the pole and ending at about 15 km at the equator is the tropopause, i.e., the notional boundary between troposphere below and stratosphere above. Isentropic surfaces (300K, 330K, 380K, and 400K) are drawn as thin solid lines in the troposphere and lower stratosphere. Isentropic surfaces in the remainder of the stratosphere may be assumed to be roughly horizontal. See text for further discussion.

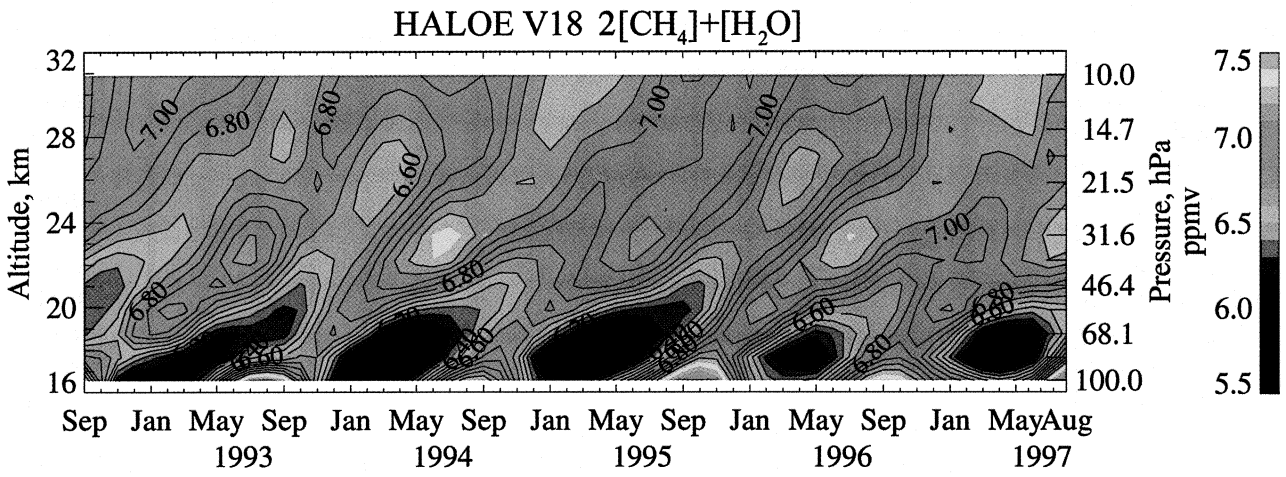


**Figure 7-7.** Height-time section of the quantity $2CH_4 + H_2O$ (the variable part of total hydrogen) between 12°S and 12°N, derived from HALOE data from Mote *et al.* (1998).

particularly in the NH, the vortex itself is less disturbed than the "surf zone," and the inner regions of the vortex are substantially isolated from midlatitudes (see Section 7.3.3.2). In situ data from ER-2 transects often show extremely sharp gradients of tracers close to the vortex edge (e.g., Schoeberl *et al.*, 1992).

McIntyre (1990) suggested on dynamical grounds that the surf zone also possesses a subtropical edge, isolating the tropics from surf zone stirring. Such a supposition is supported by observations of a "tropical stratospheric reservoir" of aerosols from tropical volcanic eruptions (Dyer and Hicks, 1968; Grant *et al.*, 1996) and of material from nuclear bomb tests (Feely and Spar, 1960); of strong subtropical tracer gradients (Randel *et al.*, 1993; Tuck *et al.*, 1997); of different tracer relationships between tropical and midlatitude air (Murphy *et al.*, 1993; Plumb, 1996; Volk *et al.*, 1996); and of the relatively undiluted ascent within the tropics of the "tape recorder" signal of the annual cycle of water vapor (Mote *et al.*, 1996) (see Figure 7-7). Erosion processes, similar to those seen at the vortex edge, are evident in high resolution transport calculations based on observed winds (Chen *et al.*, 1994; Waugh, 1996) and in dynamical models (Norton, 1994; Polvani *et al.*, 1995; O'Sullivan, 1997).

The location of the tropical reservoir and the gradients at its edge exhibit a seasonal variation, with the center in the summer hemisphere and steeper gradients during winter (Randel *et al.*, 1993; Grant *et al.*, 1996). This variation is consistent with the seasonal variation in upwelling discussed earlier, together with the seasonal variation in Rossby wave breaking: there is stronger wave breaking during winter and this produces a wider surf zone and increased transport away from the tropical edge, producing steeper gradients (Waugh, 1996). The seasonal variation in location of the tropical reservoir increases with altitude, and there is also a significant influence from the QBO (Randel *et al.*, 1998).

Because diabatic transport is so slow in the stratosphere, there is an important dynamical distinction between isentropic surfaces that lie entirely within the stratosphere, and those that intersect the midlatitude tropopause. Holton *et al.* (1995) refer to the region containing the latter, where there may be rapid isentropic exchange with the troposphere, as the "lowermost stratosphere" (see Section 7.3.4.1). Thus, in contrast to the region above, the lowermost stratosphere is bounded on its equatorward side by the tropopause, rather than by the tropical stratosphere. It seems that the distinct vortex/surf zone separation does not exist within the lowermost stratosphere (see Section 7.3.3.2), although why this should be the case is not well understood.

### 7.3.3 Quantification of Transport and Mixing

*The time lag between tropospheric and stratospheric concentrations of time-varying species is a probability distribution of transit times. The time lag of a conserved tracer with linear trend is equal to the mean of this probability distribution (the so-called "mean age"), but the time lag for tracers with nonlinear time dependence or loss processes differs from the mean age.*

*Mean age may not be appropriate for dealing with chlorofluorocarbons (CFCs) and short-lived CFC replacements whose temporal profiles are expected to be highly nonlinear over the next decade.*

*Observational, modeling, and theoretical studies all indicate that above 16 km, the inner vortex region in both hemispheres is substantially isolated from midlatitudes. However, there is greater exchange between the vortex edge region and midlatitudes, and below 16 km (the "sub-vortex" region). Analysis of tracer observations shows that the time scale for entrainment into the tropics is around 15 months in the lowest few kilometers of the stratosphere. This entrainment rate is much weaker than both the detrainment rate from the tropics and the mixing rates within the surf zone.*

*In the surf zone, air drawn out of the polar vortex or the tropics is stirred by the large-scale flow, leading to the formation of filaments and laminae in chemical tracer fields. Analysis of high-resolution aircraft tracer data suggests that, in some average sense, air is well mixed on vertical scales of about 50 m and horizontal scales of about 10 km. It follows that for typical surf-zone stretching rates, filaments of polar or tropical air will survive for about 20-25 days before they become mixed with their surroundings.*

#### 7.3.3.1 Transport Time Scales

Tropospheric concentrations of many long-lived trace gases vary with time, and there is a time lag between these concentrations and those in the stratosphere. Determining these time lags is crucial for calculating the concentrations of many species, and especially the available inorganic chlorine and hence the potentially active chlorine.

If the diabatic circulation alone was responsible for transport, then there would be a single pathway and "transit" time for transport from the tropopause to a given location in the stratosphere, and the time lag in concentration would be the same for all species. However, because of mixing within the stratosphere, air parcels comprise many components with different transport histories and there is not a single transit time; rather, there is a probability distribution of transit times, known as the "age spectrum" (Kida, 1983).

The mean of the probability distribution is the "mean age" (Hall and Plumb, 1994). The mean age is equivalent to the time lag in concentration only for a conserved tracer with linear trend; if the time dependence is nonlinear or if there are chemical loss processes in the stratosphere, the time lag will differ from the mean age (Hall and Plumb, 1994). The zonal-mean contours of mean age are very similar to those of long-lived tracers with upper stratospheric sinks, i.e., the contours bulge upward in the tropics and down at high latitudes, and the oldest values occur in the wintertime polar upper stratosphere (see Figure 7-8a, and compare with Figure 6-3 of Chapter 6 of this Assessment). Note that the spatial distribution of mean age is very different from what it would be if air were transported only by the diabatic circulation; in the latter case, the oldest air would be found in the polar lower stratosphere (Rosenlof, 1995).

The mean age has been estimated from measurements of several different tracers with approximately linear trends, e.g., sulfur hexafluoride ($SF_6$) (Harnisch *et al.*, 1996; Waugh *et al.*, 1997b; Volk *et al.*, 1997), $CO_2$ (Bischof *et al.*, 1985; Schmidt and Khedim, 1991; Boering *et al.*, 1996), CFC-115 ($CClF_2CF_3$) (Pollock *et al.*, 1992; Daniel *et al.*, 1996), and hydrogen fluoride (HF) (Russell *et al.*, 1996). Note that although $CO_2$ has an approximately linear trend, it also has a strong seasonal variation, which complicates calculations of the mean age (Hall and Prather, 1995). Also chemical loss processes in the upper stratosphere affect estimates of mean age from CFC-115. Results from the above studies show that the mean age (relative to the tropical tropopause) at 20 km varies from around 1 year in the tropics to 4 to 6 years at high latitudes (see examples given in Figure 7-8b), and at 30 km it varies from 4 to 5 years in the subtropics to 7 to 9 years at high latitudes. In general, both 2-D and 3-D model results vary widely and have difficulty reproducing these numbers.

The time scale for vertical propagation within the tropical stratosphere has been derived from measurements of both $H_2O$ (Hintsa *et al.*, 1994; Mote *et al.*, 1996; Weinstock *et al.*, 1995) and $CO_2$ (Boering *et al.*, 1996). These calculations yield similar time scales, which are broadly consistent with ascent rates derived from diabatic circulation calculations based on satellite measurements, with more rapid ascent during northern winter than northern summer (see Section 7.3.1). Note that although model calculations suggest that the rate of propagation of the annual signal will be close to the diabatic vertical velocity, it is not clear that there should be exact agreement (Waugh *et al.*, 1997b).

Modeling studies indicate that the age spectrum is generally broad and asymmetric (Kida, 1983; Hall and

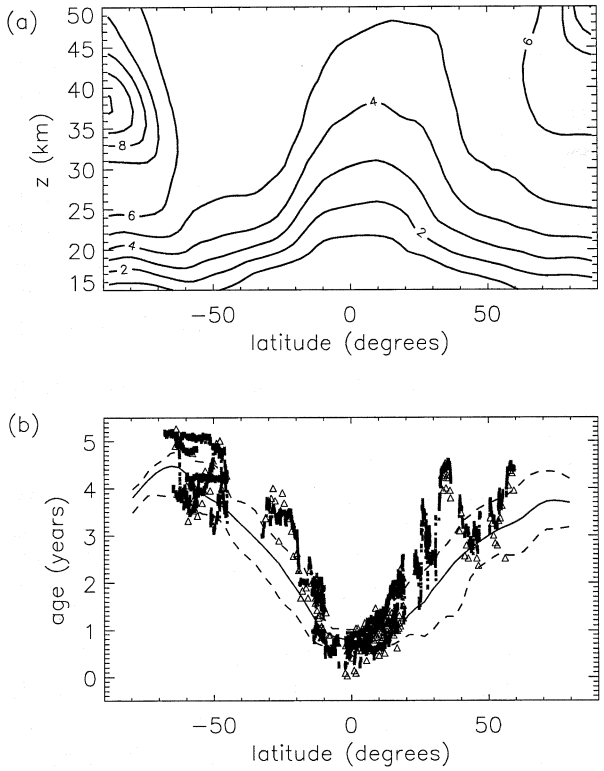


**Figure 7-8.** Mean age relative to the tropical tropopause as determined from a 3-D chemical transport model and from measurements. (a) Altitude-latitude contour plot of mean age for the zonal mean in October, as determined from a model calculation of a linearly increasing conserved tracer. Contours are for 1.0, 2.0, ..., 10.0 years. (b) Latitudinal variation of mean age at 20 km in October. The solid curve is the zonal-mean model value, while dashed curves are the minimum and maximum values around a latitude circle at this altitude. The symbols are mean age derived from aircraft measurements of $SF_6$ (triangles) and $CO_2$ (solid squares) from October and November 1994 (Boering *et al.*, 1996; Volk *et al.*, 1997). Note that the good agreement between the above model and data is not generally true; the modeled mean ages are younger than observed for most other models. Adapted from Waugh *et al.* (1997b).

Plumb, 1994; Hall and Waugh, 1997a) (see Figure 7-9) with the mean age much older than both the most likely transit time and the propagation time of an annually repeating tracer. It is only within the lower tropical stratosphere, where the age spectra are strongly peaked, that these various times are approximately equal.

The mean age has been used to account for the temporal variation in tropospheric concentrations when determining stratospheric halogen budgets from source gas measurements (see Section 7.5.1) and when using these tracers in tracer-tracer correlation studies (e.g., Vohralik *et al.*, 1998; Volk *et al.*, 1997). However the nonlinear growth and chemical losses of these species may affect these calculations. This effect may be significant over the next decade when the time trends in CFCs and short-lived CFC replacements are expected to be highly nonlinear (see Chapter 1).

A different class of transport time scale to the above is the time for transport out of the stratosphere from a given location. These time scales are important for understanding, for example, the impact of aircraft emissions and volcanic aerosols on stratospheric ozone. Several 2-D and 3-D modeling studies have calculated the mean lifetime (residence time) of aircraft emissions (e.g., Weaver *et al.*, 1996; Schoeberl *et al.*, 1998). The calculated lifetimes vary from one to three years, with 3-D models generally yielding shorter lifetimes than 2-D models. As with transport into the stratosphere, there will be a probability distribution of (residence) times for transport out of the stratosphere, but the characteristics of this probability distribution have not been examined.

### 7.3.3.2 Exchange Time Scales

As discussed in Section 7.3.2, there exist polar and tropical "reservoirs" in the lower and middle stratosphere, with weak exchange between these reservoirs and the midlatitude surf zone. Rates of exchange across the edges of these reservoirs play an important role in determining the global distribution of ozone and ozone-related species. This has long been recognized for the winter polar vortices. In the tropics, the impact is primarily on troposphere-stratosphere time lags and stratospheric residence times.

There is an extensive body of research into the rate of transport into and out of the polar vortices. A difficulty when comparing these studies is the different definitions of vortex edge that have been used (such as the wind

troposphere, with larger scale upwelling playing an increasingly important role as one moves upward through the tropical tropopause layer. In the lower stratosphere above 70 mb or so, the flux is almost certainly dominated by the large-scale upwelling, which may be thought of as taking upwards whatever water vapor mixing ratios are imposed in the dehydration regions. Because, as noted in Section 7.3.1, temperatures in the tropical lower stratosphere exhibit an annual cycle, the imposed water vapor mixing ratios are also expected to show an annual cycle, with minimum values in NH winter when the temperatures are lowest. This cycle is recorded on each layer of air moving upward through the tropical tropopause, just as a signal is recorded on a magnetic tape as it passes the head of a tape recorder (Holton *et al.*, 1995; Mote *et al.*, 1996). The upward moving signal is observed in water vapor mixing ratios (see Figure 7-7). This "tape recorder" hypothesis explains why observations of water vapor at Panama in NH summer show a minimum value considerably less than saturation values associated with NH summer temperatures and at a level about 3 km above the local tropopause (Holton *et al.*, 1995).

In the simplest form of the freeze-drying hypothesis, the water vapor mixing ratio is set by the ice saturation mixing ratio at the minimum temperature experienced by an air parcel. Even assuming that ice particles form immediately upon supersaturation, this neglects the possibility that ice particles may be carried along with the air parcel and simply re-evaporate (and hence re-moisten the air) when the temperature of the parcel increases. Cloud-scale processes, including microphysics, may therefore be important in allowing effective dehydration. Observations from the Stratosphere-Troposphere Exchange Project (STEP) campaign showed examples of a cumulus anvil where it appeared that excess ice had fallen out, leaving air that contained water vapor mixing ratios close to local ice saturation values (of 1.7 ppmv) (Holton *et al.*, 1995). However other observations showed that in anvil regions of high ice crystal content (200 ppmv or more of water vapor as ice), about 2% of the mass was in particles of size less than 10 microns (Knollenberg *et al.*, 1993), which would take over a day to fall 1 km. Re-evaporation, which would increase water vapor mixing ratios by 4 ppmv or more, is therefore a real possibility.

Various mechanisms have been suggested that might lead to larger particle sizes and therefore to decreased probability of re-evaporation. Because particles that form over several days rather than several hours tend to be somewhat larger (Jensen and Toon, 1994; see Section 7.2.2), variations in temperatures experienced by air parcels on longer time scales may lead to more effective dehydration. Such variations might arise through tropical Kelvin wave propagation (Tsuda *et al.*, 1994) or through large-scale advection. Another possibility is growth of ice crystals in turbulent mixing taking place in radiatively destabilized anvils (Danielsen, 1982). It is also the case that if an air parcel experiences many freezing events, then even if particle fall rates are small the net effect of many such events may be to reduce water vapor mixing ratios to stratospheric values. Potter and Holton (1995) noted this possibility in association with freezing events associated with small-scale gravity waves.

Notwithstanding the above questions, it should be noted that although minimum large-scale temperatures in NH winter seem to be consistent with the minimum water vapor mixing ratios, minimum large-scale temperatures in NH summer seem too high to account for the maximum water vapor mixing ratios observed in the lower stratosphere as part of the "tape recorder" signal (Mote *et al.*, 1996). There is evidence for lower temperatures on small scales in radiosonde observations (e.g., Atticks and Robinson, 1983), but whether this can account for the maximum mixing ratios is not yet clear.

## 7.4 COUPLED PROCESSES

### 7.4.1 Mesoscale Structure and Its Impact

*Mesoscale structure (i.e., horizontal scales between a few km and a few hundred km), which is well below the resolution of current global models, may have a systematic impact on chemical evolution. Gravity waves, particularly mountain waves, can cause mesoscale temperature fluctuations of up to 10 K about the mean. During the lower excursions of such temperature fluctuations, ice PSCs can form and are observed as mother-of-pearl clouds. Despite their short lifetimes, the large surface areas of these particles make them highly efficient processors of chlorine species. Also, there is evidence that acid hydrates might nucleate on these ice particles, which continue to exist downstream of the waves. Such phenomena have been shown to yield chemical processing rates substantially enhanced above the synoptic mean values that would be predicted in global models. A second potentially important source*

*of error in prediction of chemical evolution is inaccurate representation of the process of mixing. Studies of the ClO-dimer formation reaction in polar ozone destruction and the deactivation of PSC-processed air have confirmed sensitivity to mixing, or equivalently model resolution, in certain locations. However, the quantitative extent to which mesoscale temperature fluctuations and filamentary structures influence ozone loss cannot be answered now.*

Rates of chemical and microphysical processes often have nonlinear dependencies on temperature or concentration. Accurate predictions of the large-scale effects of these processes therefore require the effects of smaller-scale variations in temperature and concentration fields to be taken into account. At the present resolution of global chemical models (see Section 7.5.4), important unresolved structure, due to gravity waves and filaments (see Section 7.3.3.3), lies in the mesoscale.

### 7.4.1.1 Temperature Fluctuations

There is substantial observational evidence of mesoscale temperature fluctuations in the lower stratosphere caused by internal gravity waves (e.g., Bacmeister *et al.*, 1996). Peak-to-peak amplitudes of 2 K (corresponding to vertical displacements of about 200 m) are typical (Murphy and Gary, 1995). Given the strong temperature dependence of heterogeneous reactions like HCl + $ClONO_2$ (Ravishankara and Hanson, 1996), the reactive uptake coefficient is underestimated when synoptic-scale temperatures are used instead of the realistic mesoscale temperature field. Murphy and Ravishankara (1994) showed that the neglect of mesoscale fluctuations could underpredict the effective reactive uptake coefficient of the $ClONO_2$ + HCl reaction by a factor of 2.

Mountain-forced gravity waves, in particular, often have large amplitudes and, in extreme cases, can cause deviations from the synoptic average of more than 10 K (e.g., Gary, 1989), leading to PSCs and rapid chemical processing. Such topographically induced Type-2 PSCs are well known as mother-of-pearl clouds. An example is shown in Figure 7-11. The filamentary structure in the backscatter ratio of the cloud (panel a) is interpreted as particle streaks and used to construct air parcel trajectories. The observation can be interpreted as quasi-Lagrangian with air moving from left to right. The trajectory indicated by the white line reveals temperature fluctuations of up to 13 K peak-to-peak with cooling/

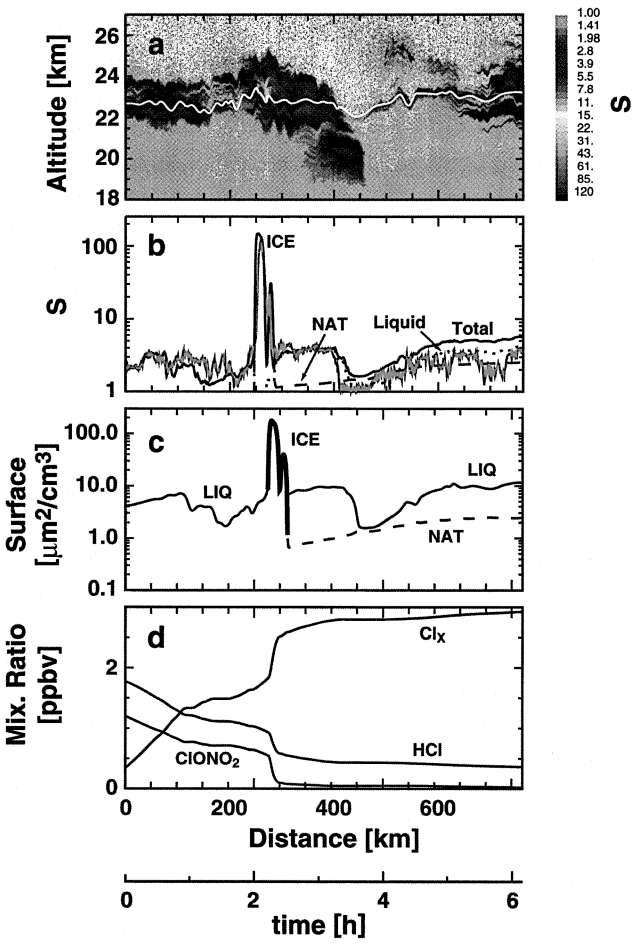


**Figure 7-11.** Lidar measurements of 15 January 1995 along a flight across the Scandinavian Alps by the German DLR Falcon. (a) Backscatter ratio at 532-nm laser wavelength, *S*. Lower panels refer to trajectory marked as white curve. (b) Black curves: backscatter calculated by a microphysical model coupled to a non-spherical particle backscatter code; red curve: measurement. (c) Calculated particle surface area. (d) Chemical box model results with $Cl_x = (2 \times Cl_2) + (2 \times Cl_2O_2) + ClO$ based on the surface areas given in (c). Adapted from Carslaw *et al.* (1998).

heating rates of more than 100 K/h. The spot at 250 km (~2h) with very high backscatter indicates the formation of ice particles, which means that the minimum temperature was more than 10 K below the synoptic temperature based on the European Centre for Medium-Range Weather Forecasts (ECMWF) analysis.

(and ternary solutions) can activate chlorine comparably to NAT PSCs simplifies our understanding (of chlorine activation) because the complex phase transformations of solid PSCs may not have to be understood (this may not be true for short-term events, see Section 7.2.2).

Recent modeling studies show that denitrification is not a prerequisite for extensive ozone loss (Portmann *et al.*, 1996; Brasseur *et al.*, 1997). This is due to heterogeneous/multiphase activation of chlorine on condensed matter during springtime, either on NAT PSCs, ternary solutions, or sulfate aerosols. In addition to reforming active chlorine, reactions such as $ClONO_2$+ HCl and $ClONO_2 + H_2O$ also reform nitric acid and thus chemically limit the release of $NO_x$. Furthermore, even in the absence of $NO_x$, active chlorine can be lost to HCl due to its gas phase reformation by $Cl + CH_4$. The presence of Cl is assured during springtime, even in the absence of NO, by the photolysis of chlorine-containing molecules. Figure 7-12 shows the sensitivity of the Garcia-Solomon two-dimensional model (Solomon *et al.*, 1996), assuming only liquid aerosols, to denitrification and dehydration. This shows that although somewhat larger loss is found with a 90% denitrification, the difference is relatively small. Also, relatively smaller changes in the amount of dehydration (less than 40% removal of water vapor) cause a comparable change in the ozone loss as the 90% denitrification. This is due to the strong dependence of the reaction rates on the water content of SSAs. Similar behavior is found in simulations assuming only NAT is present, although in this case the availability of NAT is also directly influenced by the amount of water and nitric acid.

Taken together, these studies suggest that solid PSC events are not essential for Antarctic ozone hole formation (i.e., heterogeneous activation of chlorine, followed by sustainment of active chlorine through springtime due to denitrification), but instead all that is needed are aerosols (whether liquid or solid) and cold temperatures. Portmann *et al.* (1996) show that even a 2 K change in mean temperature has as much effect as denitrification in the model simulation, while a 5 K increase in mean temperature can nearly eliminate the ozone hole. Carslaw and Peter (1997) have recently suggested that reactions such as $HCl + ClONO_2$ may be up to a factor of 100 times slower on NAT compared with liquid aerosols; in this case, it would be difficult to produce an ozone hole with NAT PSCs and the dominance of liquid aerosols will be indicated.

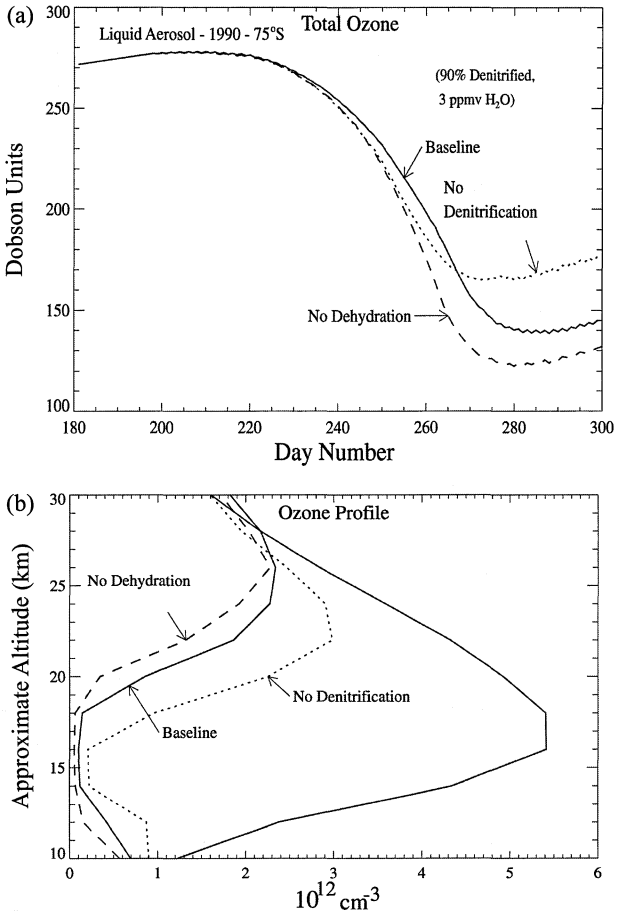


**Figure 7-12.** Sensitivity of the Garcia-Solomon two-dimensional model to denitrification and dehydration at 75°S during springtime (figure 12 of Portmann *et al.* (1996)). The total ozone time series and the profiles corresponding to the minimum total ozone are shown. The unmarked line in (b) is the ozone profile before depletion.

### Arctic

The Arctic vortex is considerably more dynamically active than the Antarctic vortex. This causes the Arctic vortex to break up much earlier than in the south and, even while the vortex is present, temperatures are much warmer than in the southern vortex. See WMO (1995) for an extensive discussion on the difference between the northern and southern vortices.

Chemical ozone loss is more difficult to detect in the Northern Hemisphere due to its smaller extent and the increased variability of ozone. However, the strong correlation between cold temperatures (i.e., those below

about 195 K) and large abundances of ClO has been extensively documented (e.g., Waters *et al.*, 1995; Santee *et al.*, 1995). In fact, ClO values inside the northern vortex during winter can sometimes be as large as those in the southern vortex. However, the amount of ozone depletion caused by the ClO depends also on the amount of sunlight experienced by the chlorinated radicals. Thus activation later in the winter and in spring causes more extensive ozone depletion than earlier activation. However, even activation that occurs during polar night can cause ozone depletion if the vortex is sufficiently asymmetric to allow parcels to intersect sunlight during part of their trajectories.

There is increasing evidence that liquid aerosols play a dominant role in chlorine activation in the Arctic. Bregman *et al.* (1997) show that reactions on liquid aerosol are necessary to explain aircraft observations during the Stratosphere-Troposphere Exchange Experiment by Aircraft Measurement (STREAM) mission in 1993 in the lowermost stratosphere at isentropic surfaces below about 375 K. Tie *et al.* (1997) show that the colder temperatures in spring 1993 compared with 1992 caused greater activation due to enhanced reactions on liquid aerosols.

The potential importance of dehydration and denitrification in the Arctic region has not been quantitatively addressed. Earlier studies suggested that denitrification would be necessary to cause large ozone losses in the Arctic region (Brune *et al.*, 1991; Salawitch *et al.*, 1993) but these studies did not include the recently measured reactions on liquid aerosols, and thus are potentially overly sensitive to denitrification as a means of maintaining active chlorine. Dehydration would likely reduce Arctic ozone loss due to the reduction in the liquid aerosol reaction rates, as in the Antarctic.

### 7.4.3 Lessons from Mt. Pinatubo

*The eruption of Mt. Pinatubo was an atmospheric dynamics and chemistry "experiment" on a global scale. Considerable evidence shows that the enhanced aerosol levels caused a reduction in total ozone during winter and spring in the extratropics. It is possible that volcanic influences since 1979 may be confused with solar cycle variations due to the roughly 10-year spacing of the El Chichón and Mt. Pinatubo eruptions, which both occurred near the transition from solar maximum to minimum. The Mt. Pinatubo eruption shows that future ozone recovery could be strongly affected by volcanic eruptions.*

The eruption of Mt. Pinatubo in June 1991 injected a very large amount of sulfur dioxide into the tropical lower stratosphere, which was quickly transformed into a sulfate aerosol. This is probably the largest natural stratospheric perturbation of the century. It was an episodic perturbation, however, and differs from the major anthropogenic stratospheric perturbations, which are long-lived. Thus, other stratospheric forcing agents, such as chlorine loading, were essentially constant during the volcanic perturbation, allowing the possible separation of the volcanic effects. Large changes in stratospheric dynamics, radiative transfer, and trace gases occurred and they provided a valuable test of our ability to quantify and model the changes. (See WMO (1995) for an extensive discussion on the detection, transport, and modeling of the changes, and Chapter 3 of this Assessment for a discussion of the aerosol properties and morphology.) The longer persistence of the aerosol allowed higher chlorine activation beyond the period of perturbed dynamics and provided evidence for chlorine-catalyzed ozone destruction during that period.

Record-low ozone abundances were observed after the Mt. Pinatubo eruption, and model calculations indicate that these depletions were related to multiphase chemistry in the sulfate aerosols (WMO, 1995). Most early studies only included reaction (7-1) (Section 7.2.3), which is efficient at nearly all temperatures, and reaction (7-2), which is only efficient at cold temperatures. At midlatitudes, the reduction of $NO_x$ due to reaction (7-1) causes an increase in ClO due to a shift in the partitioning of ClO and $ClONO_2$. $HO_x$ radicals are also generally increased by the reduction in $NO_2$. These effects both increased the chemical ozone loss rates in the lower stratosphere. Figure 7-13 shows two-dimensional model calculations of the ozone anomaly compared with those computed from the Total Ozone Mapping Spectrometer (TOMS) measurements (Tie *et al.*, 1994). Dynamical variations related to the QBO (which the model does not include) have been removed from the TOMS data using regression (Randel *et al.*, 1995). The model reproduces the general shape and magnitude of the anomalies quite well, suggesting that much of the anomaly is indeed chemical.

Due to improved understanding of processes in or on condensed matter (see Section 7.2.3) it is now recognized that reactions directly involving HCl are efficient in sulfate aerosol at cold temperatures, especially reactions (7-3) and (7-4). This implies that volcanically perturbed aerosol could have an enhanced role at

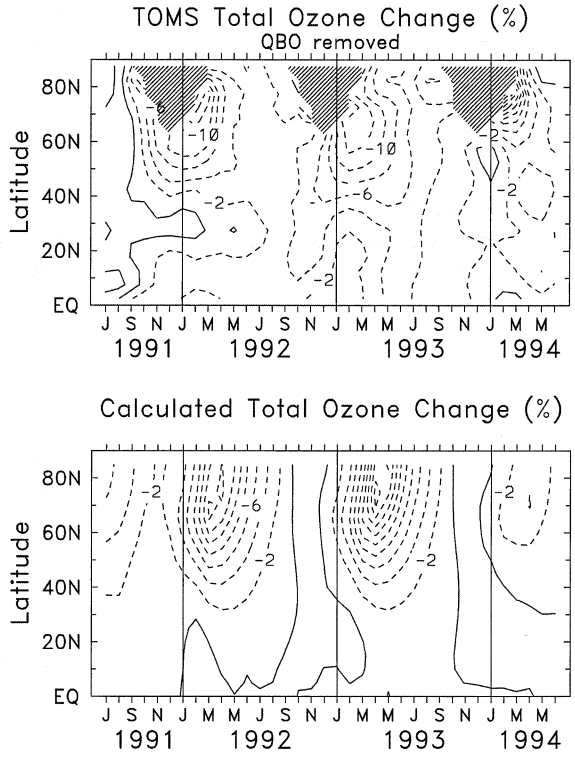


**Figure 7-13.** Total ozone anomalies from a two-dimensional model compared with those computed from TOMS V6 data. Note that the effect of the QBO has been removed from the TOMS data (the model has no QBO). The model includes both chemical and radiative effects due to sulfate aerosols. Adapted from Tie *et al.* (1994) and Randel *et al.* (1995). Contour interval is 2%.

midlatitudes (Solomon *et al.*, 1996; Solomon *et al.*, 1998) and high latitudes (Portmann *et al.*, 1996; Tie *et al.*, 1997), because these reactions greatly enhance the effectiveness of sulfate aerosol at activating chlorine when temperatures are cold. This could explain why the Northern Hemisphere ozone anomaly is larger in 1993 (when it was colder) than in 1992, even though the aerosol loading was higher in 1992 (Tie *et al.*, 1997). Bromine nitrate hydrolysis, reaction (7-5), also adds to the enhancement of free radicals due to the volcanic aerosols, causing increased potential for ozone loss.

Enhanced Antarctic ozone losses were well documented after the eruption of Mt. Pinatubo, especially in the lowermost stratosphere (Hofmann and Oltmans, 1993; Hofmann *et al.*, 1995). These enhanced losses were due to the high efficiency of reactions (7-3) and (7-4) at cold temperatures and the likely presence of sulfate aerosol (or ternary solutions) inside the vortex. Portmann *et al.* (1996) also have suggested that the eruption of El Chichón in 1982 accelerated the severity of the ozone hole in the early 1980s due to this mechanism.

Hofmann and Solomon (1989) suggested that the El Chichón eruption had caused ozone losses at midlatitudes in the early and mid-1980s, and predicted that an eruption occurring later with higher $Cl_y$ would lead to larger depletions. The Mt. Pinatubo eruption and recent laboratory measurements have strengthened this view. Model calculations now show that aerosol perturbations have influenced stratospheric ozone at midlatitudes since at least 1980 (Solomon *et al.*, 1996; Jackman *et al.*, 1996; Callis *et al.*, 1997). In addition, the reduction of model $NO_x$ in the lower stratosphere due to reactions on sulfate aerosols (even during background conditions) has been partially responsible for increasing model-based ozone trends around 20 km, bringing better agreement between models and measurements (although significant discrepancies remain below approximately 16 km; see Section 7.6.2). Solomon *et al.* (1996) have suggested that the roughly ten-year separation of the El Chichón and Mt. Pinatubo eruptions, which both occurred before solar minimum, could confuse efforts to remove the solar cycle from the long-term ozone record by statistical methods (see Figure 7-14), especially at mid and high latitudes.

## 7.5 QUANTIFICATION AND PREDICTION OF OZONE CHANGES

To understand the cause of ozone changes requires a quantitative accounting for those changes in terms of known processes. Ozone in the lower stratosphere is directly affected by both chemistry and transport. In general, the chemical ozone loss rates cannot be measured directly because they are slow compared to the transport and mixing time scales. (One exception is when the ozone loss rates are relatively large, as in the Arctic springtime vortex; depletion under these circumstances has been measured by the "Match" method; see Section 7.6.1). Therefore, one needs to calculate, rather than measure, the ozone changes. This requirement leads to a hierarchy of models, which are distinguished by the extent to which they are constrained. The more constrained models give more reliable results,

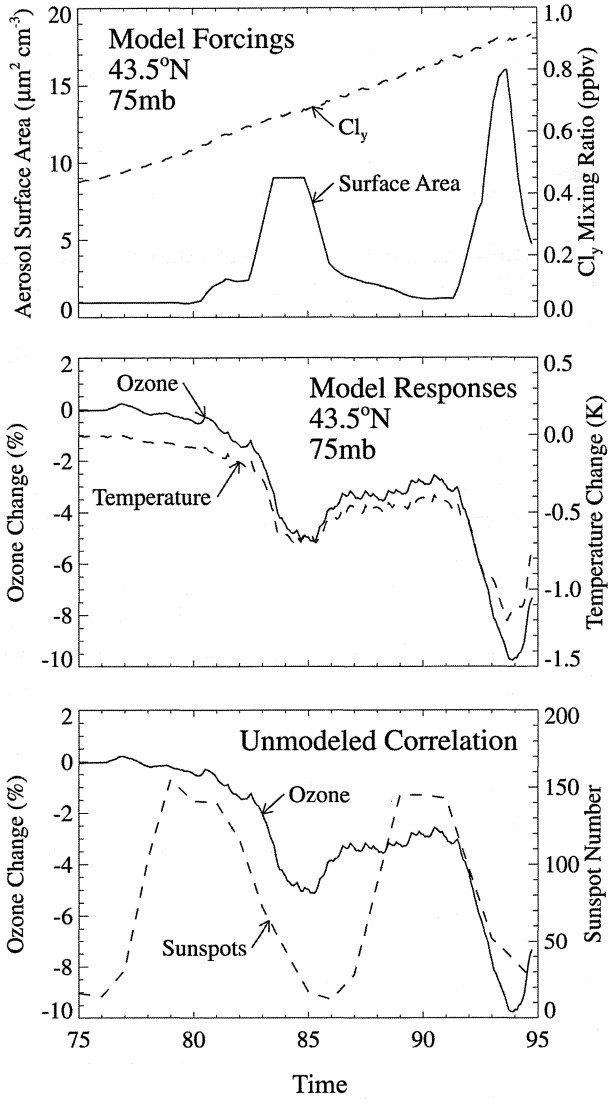


**Figure 7-14.** Two-dimensional model results suggesting that volcanic and solar cycle variations in ozone could be highly correlated since approximately 1980. The model is forced with chlorine ($Cl_y$) and volcanic (surface area) changes since 1975, resulting in the ozone and temperature variations shown in the middle panel. The similarity between the model ozone field (which includes no solar cycle effects) and a proxy for the solar cycle (sunspot number) is shown in the bottom panel. Adapted from Solomon *et al.* (1996).

but they address only a piece of the problem; hence, they are not useful for making predictions. In the most constrained case, local chemical ozone loss rates can be quantified at a fixed location or by following a moving air parcel, using observed temperature and measured chemical composition (especially of the involved free radicals). In the least constrained case, a general circulation model with fully interactive ozone chemistry can, in principle, predict future ozone changes under a specified anthropogenic forcing scenario. In this section, we briefly examine the status of these methods.

### 7.5.1 Local Chemical Ozone Loss

*Available field observations are generally consistent with our theoretical and laboratory-derived understanding of chemical ozone loss rates. Uncertainties in some processes that impact ozone are significant. Observations in the lowest part of the extratropical stratosphere within a few km above the tropopause remain very limited. Partitioning of reactive families at midlatitudes is fairly well understood qualitatively. The diurnal dependence of $HO_x$ species indicates a new source of $HO_x$, now thought to be photolysis of HOBr formed in $BrONO_2$ hydrolysis. Calculations that use the total and relative contributions to chemical loss rates of midlatitude ozone continue to support the view that $HO_x$ is the major catalyst that chemically controls the extrapolar lower stratospheric ozone abundance, although the $NO_x$, $Cl_x$, and $Br_x$ species compete effectively with $HO_x$.*

Comparisons with atmospheric observations form an important test of the accuracy of our theoretical and laboratory-derived understanding of chemical processes as implemented in models. Measurements also constrain the abundance of species for which our knowledge of controlling processes is inadequate. Observations of chemical constituents above 20 km have improved notably in coverage and accuracy since the last Assessment (WMO, 1995); but observations in the lowest few km of the extratropical stratosphere remain very limited. Constraints placed by some of the field observations on chemistry have been noted in Section 7.2. A few others are discussed below with the aim to use field measurements to constrain the ozone loss rates.

Measured distributions of total $NO_y$ from aircraft in the lower stratosphere extend from 70°S to 70°N in spring and fall seasons (see, e.g., Fahey *et al.*, 1996). Profiles of $NO_y$ measured from balloon (Kondo *et al.*,

1994, 1996) are very consistent with the aircraft results. $NO_y$ is also estimated from the sum of components measured by space-based spectrometers (e.g., Russell *et al.,* 1988). $NO_y$ distributions from UARS (Morris *et al.*, 1997) and ATMOS (Rinsland *et al.*, 1996b) satellite measurements are very similar to those from aircraft. The accuracy of $NO_y$ measurements in the lower stratosphere is estimated to be less than roughly 20%. Thus, the overall abundance of $NO_y$ is reasonably well defined in the lower stratosphere.

$Cl_y$ is not measured as a total, but deduced from other observations, as discussed in Chapter 1 of this Assessment. The deduced $Cl_y$ is accurate to within several hundred pptv, which becomes a large fraction of the mean $Cl_y$ at altitudes near the tropopause but is sufficiently good for higher altitudes. These deduced amounts may be in error because of the nonlinear changes in total chlorine with time (see Section 7.3.3.1).

The unexpectedly low values of HCl reported by Webster *et al.* (1994) and attributed by them to volcanically enhanced sulfate surface area were discussed in the previous Assessment; these low values have yet to be resolved theoretically or experimentally. $Cl_y$ partitioning from ATMOS (Michelsen *et al.*, 1996; Chang *et al.*, 1996) and balloon (Chance *et al.*, 1996) measurements is consistent with model results within noted uncertainties below about 25 km. HCl measurements from ATMOS exceed those from the ER-2 by 10 to 40% for nearly identical locations; the cause of the difference is not clear (Chang *et al.*, 1996). UARS measurements of HCl and $ClONO_2$ (Dessler *et al.*, 1995a) suggest that models do underpredict $ClONO_2$ relative to HCl near 20 km, but not as much as that inferred from Webster *et al.* (1994). The increase in HCl/$Cl_y$ with decreasing sulfate loading following Mt. Pinatubo as measured from UARS (Dessler *et al.*, 1997) is about 16% from July 1992 to June 1996.

Determination of inorganic bromine ($Br_y$) is discussed in Chapter 1. There are discrepancies in values of stratospheric BrO derived from different estimates and measurements. One estimate of $Br_y$ is obtained from summing the bromine content of organic bromine compounds measured in the lower stratosphere and the troposphere and adjusting for slight trends in their abundances (Schauffler *et al.*, 1993; Fabian *et al.*, 1994; Wamsley *et al.*, 1998). Uncertainty in $Br_y$ derived by this method is estimated to be ±2 pptv (Wamsley *et al.*, 1998). Alternatively, $Br_y$ has been estimated from the abundances of BrO measured, in situ, around 20 km and deriving the abundances of other bromine compounds ($BrONO_2$, HOBr, HBr, etc.). The value of $Br_y$ that is deduced by this method (~20 pptv) agrees, with an uncertainty of about ±50% at those altitudes, with the $Br_y$ abundances derived from organic bromine measurements. The large uncertainty of ~50% is mainly due to uncertainties in the in situ observations of BrO (Wamsley *et al.*, 1998). (It should be noted, however, that the larger reported values for BrO are inconsistent with the lower values of estimated $CBr_y$.) Values of $Br_y$ derived from ground-based measurements of BrO appear to be somewhat better defined (e.g., Fish *et al.,* 1997), yielding around 20 pptv of $Br_y$. The values of $Br_y$ estimated by the above two methods agree within the large uncertainties associated with them. However, there are a few possible inconsistencies. The $Br_y$ estimated from some in situ BrO observations may be 30 to 40% higher than that derived from organic bromine ($CBr_y$). If true, short-lived organics may be contributing to the stratospheric bromine budget, or there are inadequacies in our understanding of bromine chemistry. Also, some of the in situ observations of Avallone *et al.* (1995) yield BrO values lower than those used by Wamsley *et al.* (1998). If the lower values are correct, the calculated $Br_y$ would be in better agreement with the values shown in Figure 1-18b of this Assessment. Thus, given the uncertainty in the partitioning between BrO and other constituents within the bromine family and the uncertainties in measured abundances, there is still a significant range in the estimates of total inorganic bromine, varying between ~15 and 25 pptv.

Recent ground-based measurements (e.g., Arpag *et al.,* 1994; Richter *et al.,* 1998; Aliwell *et al.,* 1997) using zenith-viewing UV absorption spectroscopy provide a reasonably consistent picture of stratospheric BrO column amounts, with largest column amounts at high latitudes in winter, decreasing in spring and at lower latitudes. The slant column measurements imply BrO concentrations maximize near and below 20 km, with mixing ratios of 5-10 pptv. Height-resolved observations of BrO, both by in situ resonance fluorescence (Avallone *et al.*, 1995; McKinney *et al.*, 1997) and more recently by balloonborne solar occultation (Pundt *et al.*, 1998; Harder *et al.*, 1998), show BrO mixing ratios increasing from about 5 to 15 pptv in the height range 20-30 km; the observations are also consistent with ground-based observations noted above.

Inside the denoxified chemically activated vortex, where BrCl is thought to be the principal nighttime

reservoir, both remote sensing (ground-based and balloonborne) and in situ measurements show BrO abundances that are broadly consistent with photochemical simulations. The seasonal variation in midlatitude BrO total column abundances, measured by ground-based methods, suggests that BrO amounts are governed by seasonal variations in $NO_2$ abundances (Fish *et al.*, 1997; Richter *et al.*, 1998). However, balloonborne solar occultation measurements in less denoxified air (outside the polar vortex, or in late spring inside the vortex) indicate that in the presence of large amounts of $NO_2$, absolute concentrations of BrO in the 15-25 km range exceed those expected based on current chemistry understanding (Pundt *et al.*, 1998; Harder *et al.*, 1998). Therefore, the current understanding of the $BrONO_2$ reservoir may not be adequate. The implication of this possible inadequacy for the Ozone Depletion Potentials (ODPs) of bromine compounds is as yet unknown.

The measurements of BrO (see above), HBr (Nolt *et al.* (1997) and references therein), and upper limits for HOBr (Johnson *et al.*, 1995) are broadly consistent with $Br_y$ partitioning from models. The effectiveness of the $BrONO_2 + H_2O$ reaction on atmospheric sulfate aerosol is difficult to diagnose from atmospheric observations of bromine; however, there are indications based on observations of column BrO that it does occur (Slusser *et al.*, 1997) (see below about early morning OH production). Recently, large nighttime concentrations (~20 pptv) of a new bromine species, symmetric bromine dioxide (OBrO), have been inferred via remote sensing (Renard *et al.*, 1997). Accounting for OBrO in such a large abundance, if present, awaits further work.

The significant components of $HO_x$ in the lower stratosphere, OH and $HO_2$, are measured directly from the ER-2 (Figure 7-15) (Wennberg *et al.*, 1994; Wennberg *et al.*, 1995). OH mixing ratios at the same altitude and solar zenith angle do not vary much with latitude and, hence, temperature, ozone, or other constituent mixing ratios within the sampled conditions. Measurements of $HO_x$ generally seem to be slightly higher than those expected from models (Wennberg *et al.*, 1995; Salawitch *et al.*, 1994) and suggest possible missing processes. The $OH/HO_2$ ratio, however, is consistent with theory, reaction rate coefficients, and measured abundances of reactant species that control $HO_x$ partitioning (Cohen *et al.*, 1994). Diurnal measurements of $HO_x$ species (Salawitch *et al.*, 1994) have shown that a (photolytic) source of $HO_x$, in addition to the $O(^1D)$ source, is

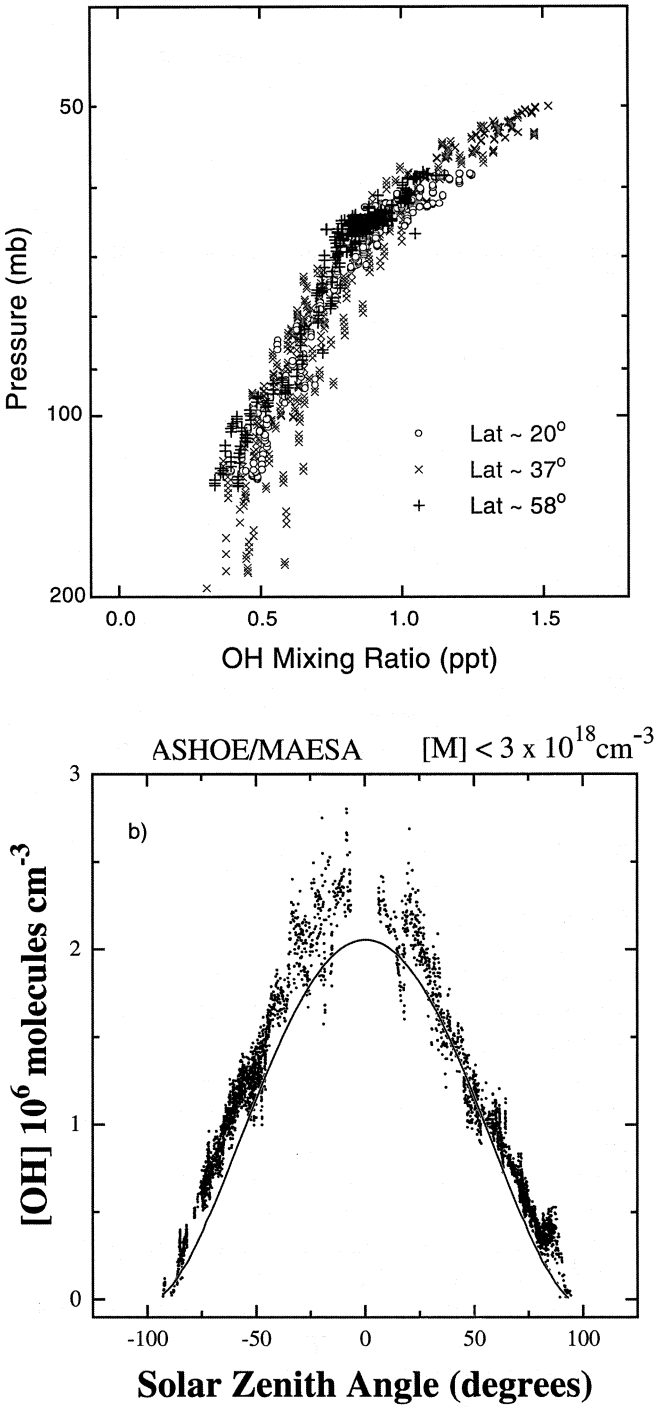


**Figure 7-15.** (a) OH mixing ratio versus altitude and (b) OH concentration as a function of solar zenith angle, adapted from Wennberg *et al.* (1994) with additional data from recent campaigns. The solid curve is a model prediction from Wennberg *et al.* (1994).

In recent years, "off-line" chemical transport models (CTMs) have become widely used (e.g., Rood *et al.*, 1991; Chipperfield *et al.*, 1993, 1994a, 1995; Lefèvre *et al.*, 1994). In these CTMs the wind and temperature fields (from global meteorological analyses or GCM output) are input to the model, which then advects the trace species and updates the chemistry. CTMs therefore do not treat the feedback between chemistry and dynamics. These models have a number of advantages over GCMs. CTMs are cheaper to run, as the dynamics and radiation are not calculated. Also, if the CTM is forced by meteorological analyses the model is then "constrained" and can be used for direct comparison with a range of observations, thereby testing our current understanding of atmospheric chemistry. Finally, for processes where a realistic temperature field is essential, such as PSC processing, the meteorological analyses are superior to current GCM simulations.

Because of the large computational cost, many 3-D model studies have concentrated on simulations of a few months for situations where the 3-D formulation has definite advantages over 2-D (latitude-height) models. Therefore a number of workers have studied the seasonal evolution of chlorine activation and ozone loss in the polar regions. Lefèvre *et al.* (1994) used an off-line CTM, forced by ECMWF analyses, to study the chemical evolution of the 1991/92 Arctic winter. The model gave good agreement with Microwave Limb Sounder (MLS) satellite observations of enhanced polar ClO, especially in terms of location. The Arctic winter of 1994/95 has been studied by Chipperfield (1998) using a model formulated with an isentropic vertical coordinate. As the quasi-horizontal motion in the stratosphere occurs on isentropic surfaces, this coordinate reduces the spurious vertical mixing associated with isobaric levels (Chipperfield *et al.*, 1996). Figure 7-18 (top panel) shows a comparison of column ozone observations at Sodankyla (68°N, 27°E) with calculations from a 3-D CTM forced by United Kingdom Meteorological Office (UKMO) analyses. Note that the CTM captures the large day-to-day variability in column ozone seen at this site. This variability is due to rapid, horizontal motion associated with the movement of the polar vortex. As the CTM is forced by meteorological analyses, it captures this motion well. Figure 7-18 (top panel) also shows results from a model simulation in which the initial ozone field is advected as a passive tracer. This quantifies the chemical ozone destruction that has occurred and is around 50 DU by late March in the model.

Despite the great success of CTMs in reproducing many features of the observed ozone distribution, there is evidence that the models underestimate the winter/spring depletion at high latitudes. Edouard *et al.* (1996) reported results from the "REPROBUS" chemical transport model of Météo-France for the Arctic winter 1994/95, which indicated that the model underestimated the chemical loss derived from ground-based observations by 40%. Hansen *et al.* (1997) compared observations from Ny Ålesund (78°N, 12°E) during the 1995/96 Arctic winter with 3-D CTM calculations using UKMO analyses. They found that the model gave good quantitative agreement with the observations in January, but by late March the model overestimated the observed ozone by around 50% near 18 km, suggesting that the model either underpredicted the chemical destruction or overpredicted the poleward transport of ozone.

There are several possible reasons why 3-D CTMs may underestimate the observed depletion. First the model transport (and/or initialization) needs to be realistic so that, for example, the model produces sufficient descent at high latitudes leading to large concentrations of inorganic chlorine and bromine in the polar lower stratosphere similar to observations.

Following this dynamical "priming," the model chemistry then needs to activate sufficient $ClO_x$ to destroy ozone mainly through the ClO/BrO and ClO/ClO cycles. The large-scale temperature analyses used to force CTMs tend to smooth out low temperatures. For example, Knudsen (1996) found that ECMWF temperatures were on average 1.4 K too warm compared with sondes near the NAT point at 50 hPa, while Pullen and Jones (1997) found a similar bias of 1.7 K with UKMO analyses. This implies that models forced by these analyses will underestimate chlorine activation, especially where the temperatures are close to the onset temperature of PSCs. The large-scale temperature fields will also miss the mesoscale activation effects described in Section 7.4.1.1.

Following the activation of chlorine, uncertainties in the laboratory data pertinent to the key catalytic cycles limit the accuracy of model predictions. Fish and Burton (1997) used a trajectory model to perform a Monte-Carlo-type study for Arctic (and midlatitude) ozone depletion. They found that these kinetic uncertainties alone place an uncertainty ($1\sigma$) of ±25% on model calculations of polar ozone loss. As expected, given the principal polar catalytic ozone loss cycles, this uncertainty was dominated by uncertainties in the rate

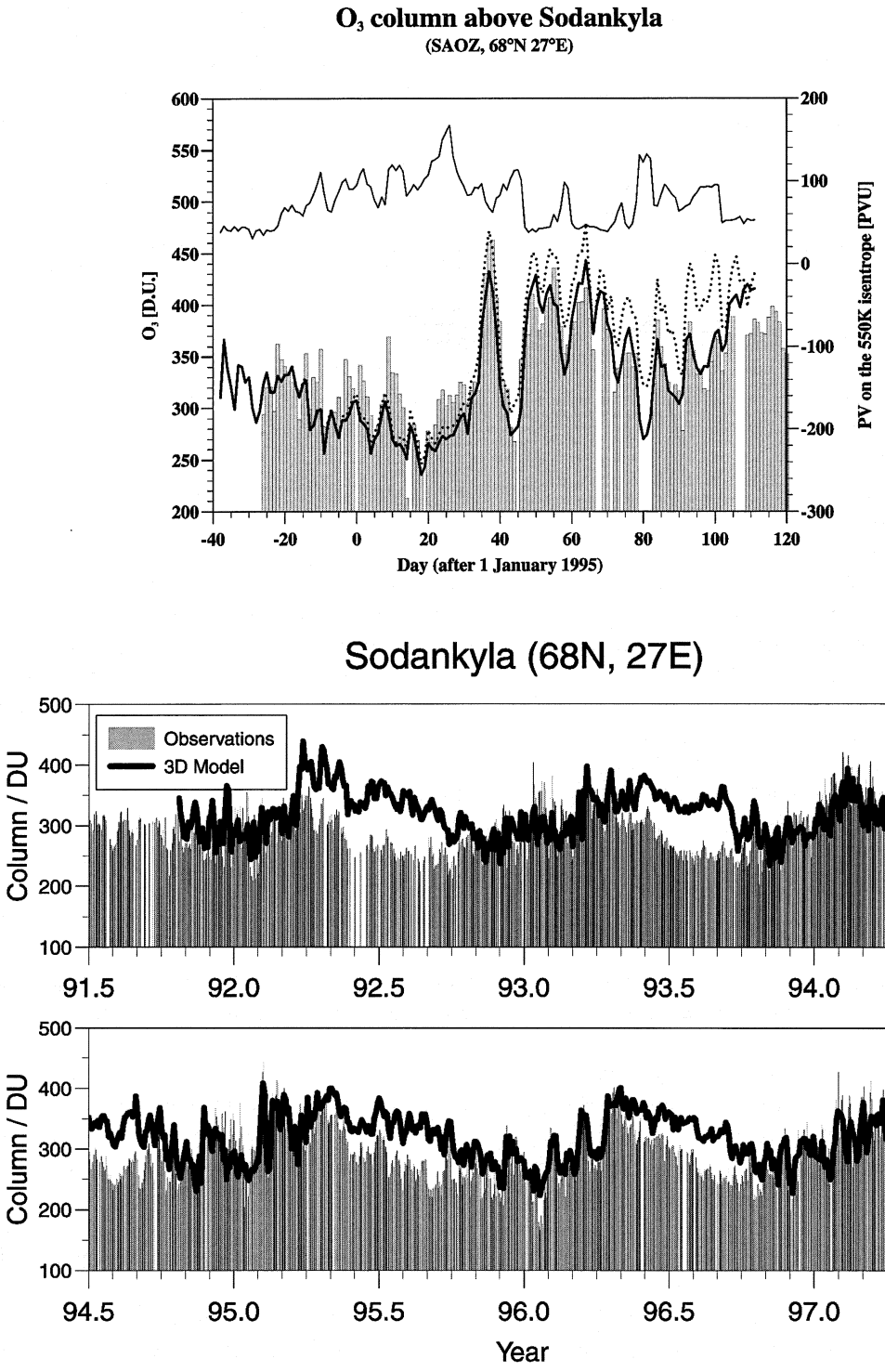


**Figure 7-18.** Observed ozone column at Sodankyla (68°N) with results from two simulations using the Cambridge University SLIMCAT chemical transport model. Top panel: horizontal resolution of 2.5° latitude × 5.6° longitude. The potential vorticity is shown in the top curve. The dotted line is obtained when $O_3$ is advected as a passive tracer. Bottom panels: with multi-year integration with horizontal resolution of 7.5° latitude × 7.5° longitude. Figures adapted from Chipperfield (1998).

coefficient for the ClO + BrO reaction and the photolysis rate of $Cl_2O_2$ (see Section 7.2.1).

The additional potential problem with coarse resolution in global models leading to excessive mixing and rapid deactivation of chlorine is discussed in Section 7.4.1.2. Yet another uncertainty in simulation of polar winter ozone loss is that treatment of heterogeneous or multiphase chemistry in 3-D models, like all other models, is limited by our incomplete understanding (Section 7.2.3). In addition, detailed microphysical treatments are generally too expensive to include in 3-D codes.

The coupling of polar regions and midlatitudes has also been studied with seasonal, and longer, 3-D CTM runs. When off-line CTMs use the same meteorological analyses as used in contour advection studies, they too will capture filamentary structure if run at sufficiently high resolution. For example, Pyle *et al.* (1995) showed that a CTM integrated for June and October 1994 with a horizontal resolution of about 1.5 × 1.5 degrees reproduced well midlatitude filaments of polar air observed in situ by the NASA ER-2 aircraft. Eckman *et al.* (1996) and Brasseur *et al.* (1997) used moderate resolution CTMs (7.5 × 7.5 and 2.8 × 5.6 degrees, respectively) to investigate the evolution of the Antarctic ozone hole and the export of ozone-poor air into midlatitudes. After the polar vortex breakdown in December, the transport and dilution of this air resulted in a column ozone decrease of about 2 to 4% at midlatitudes. Brasseur *et al.* (1997) also noted a 1% decrease in the tropics and a decrease in upper tropospheric ozone.

Because 3-D CTM simulations using analyzed winds are able to simulate horizontal transport well at time and spatial scales in the range of planetary to synoptic waves, they are able to simulate ozone in the lower stratosphere well over time scales up to several weeks, given an initialization from observations. Early simulations diverged from observations after several weeks because of systematic biases in the diabatic circulation (Rood *et al.*, 1991). Improvements in meteorological analysis methods have produced more consistent circulations (e.g., Weaver *et al.*, 1993), which allow longer successful integrations. CTMs using winds from GCMs also have difficulty getting a proper balance between wave-driven and diabatic transport (see Section 7.5.3). Ozone abundances in the lower stratosphere, where most of the overhead column resides, are the result of a balance between transport and chemistry on time scales of several weeks to months. This balance has a distinct annual cycle. Thus a test of the accuracy of the representation of these processes requires calculations over seasonal to annual time scales.

In general, 3-D seasonal to multi-year simulations of ozone show many similarities to observed variations. An off-line simulation using winds from the National Center for Atmospheric Research (NCAR) Community Climate Model-2 (CCM2) with "full" gas phase chemistry (Rasch *et al.*, 1995) showed good correspondence with observations for the mean and seasonal variations of tropical lower stratospheric ozone and tropical-midlatitude gradients of column ozone. The model did not simulate the vortex breakup well nor the springtime build-up of ozone at high latitudes, but the summertime decrease was similar to that observed.

A multi-year CTM run with winds from the NASA Langley GCM and gas phase chemistry (Eckman *et al.*, 1995) simulated the observed seasonal shift in the tropical minimum of column ozone; however, the calculated mean tropical ozone was significantly lower than that observed and the tropical midlatitude gradient too strong, suggesting excessively strong ascent in the tropics. The high-latitude maximum in the Northern Hemisphere was slightly overestimated and the summertime decline was too slow, while the Southern Hemisphere maximum was underestimated, leading to questions on the balance between mixing and the diabatic circulation. An auxiliary run including heterogeneous chemistry and PSCs improved the representation of total ozone in the southern winter vortex but had little effect elsewhere.

An annual simulation using winds from the Goddard data assimilation system (GEOS-DAS) and linearized ozone chemistry (Douglass *et al.*, 1996) produced a generally good seasonal cycle for total ozone compared with observations, although with some biases in the mean, especially in the tropics and high latitudes (Figure 7-17). The improvement in ability of their 3-D CTM versus a 2-D model to simulate the ozone annual cycle at midlatitudes was found to be largely the result of the explicit three-dimensional representation of seasonal variations in tropopause height. The source of the bias was diagnosed to be the result of an inaccurate balance between horizontal wave and vertical mean transport, which varies with altitude in the upper troposphere and lower stratosphere. A more recent simulation with GEOS-DAS winds and full chemistry (Douglass *et al.*, 1997) shows that ozone gradients may be reasonably well-simulated, even when transport of longer-lived tracers is poor, because of the influence of photochemistry on ozone. Over a longer (multi-year) simulation even this agreement could diverge as the tracer

fields controlling the production of reactive species become distorted.

Steil *et al.* (1998) have reported results of a 15-year integration of a troposphere/lower stratosphere GCM coupled with a detailed chemistry scheme. The model gave a generally good simulation of the ozone seasonal cycle, and interhemispheric asymmetry in chlorine activation. However, the dynamical fields from the GCM were a limiting factor, notably, the GCM did not produce realistic (downward) transport in the polar regions.

To date, 3-D chemistry and transport models have not been used to calculate interannual changes in ozone resulting from trends in CFCs. The potential model problems regarding diabatic circulations uncovered in shorter simulations remain to be solved. However, the apparent lack of climate drift found in annual and multi-year ozone simulations (Douglass *et al.*, 1996; Chipperfield, 1998) suggests that trend calculations may be possible soon with increasing computer power. Note that 3-D CTMs driven by analyzed winds will be able to simulate interannual ozone changes due to dynamical variations as well as ozone changes from trace gas trends. Figure 7-18 (bottom panel) shows results from a multi-year CTM integration (Chipperfield, 1998) compared with column observations at Sodankyla indicating that the CTM does indeed capture some of the observed interannual variability, e.g., the relatively low values during winter 1992/93.

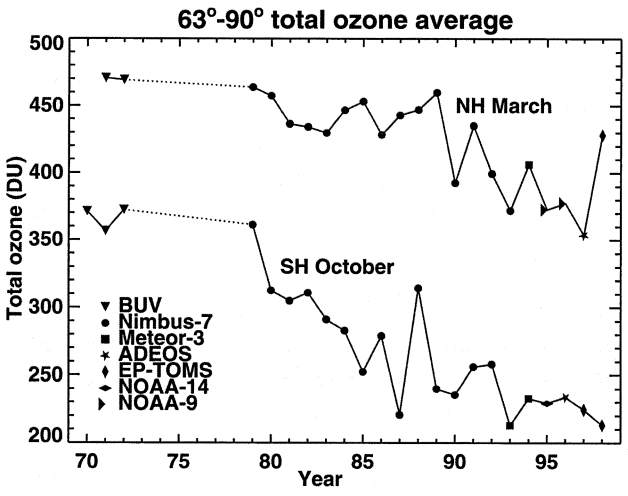


**Figure 7-19.** Spring average total ozone values in the latitude range 63 to 90 degrees in both hemispheres. Update of the figure presented by Newman *et al.* (1997).

## 7.6 CURRENT UNDERSTANDING OF OZONE DEPLETION IN THE LOWER STRATOSPHERE

### 7.6.1 Polar Seasonal Depletion

*Late-winter/springtime ozone levels in the Arctic have decreased substantially over the past decade. Within the Arctic vortex, local ozone destruction has been measured and, during the past few years, attributed to halogen-induced ozone destruction. Because of natural variability and difficulty in quantification, uncertainties remain in the partitioning of the observed column depletion between chemical and transport-related factors. Ozone destruction is highly dependent on temperature: the colder the temperature, the larger the ozone destruction (all else being equal). The expected levels of ozone for colder polar temperatures are also lower because of reduced transport of ozone into the polar vortex associated with a weaker diabatic circulation and a stronger vortex. Several of the past years in the Arctic have been particularly cold. It appears that local ozone destruction in the Arctic stratosphere contributes to the observed levels being lower than what would be expected for a pre-CFC atmosphere. This is consistent with our understanding of the mechanisms for ozone destruction based on studies of the Antarctic, where seasonal ozone loss continues unabated.*

Large springtime ozone depletion has continued in the Antarctic polar region throughout the 1990s (Figure 7-19). This seasonal column depletion first became visible in the late 1970s, grew through the 1980s, and has changed little during the 1990s. The depletions in the 1990s have been fairly constant because the polar seasonal ozone loss has been essentially complete (nearly 100%) over a deep layer of the Antarctic stratosphere (Figure 7-20). The further depletion seen in 1993 was probably due to increased aerosol from the Mt. Pinatubo eruption, which depleted ozone at altitudes lower than in previous years (Hofmann *et al.*, 1997).

Our observational knowledge and basic understanding of Antarctic depletion has not changed greatly since the last Assessment (WMO, 1995). However, there have been some important advances. The first-order picture that the Antarctic ozone depletion is due to stratospheric chlorine and bromine compounds, activated by heterogeneous or multiphase reactions at

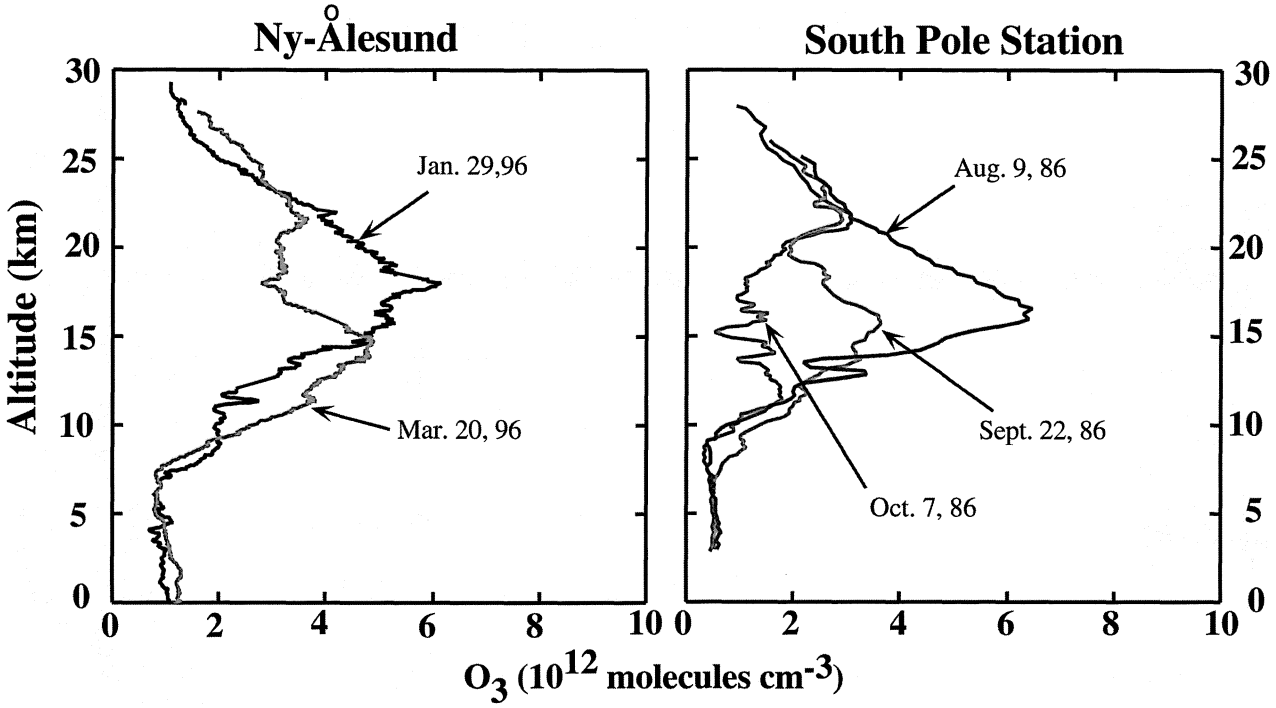


**Figure 7-20.** Ozone abundance as a function of altitude obtained from balloonborne ozonesondes at Ny-Ålesund in the Arctic region for 1995/96 winter (left panel) (Hartwig Gernandt, Alfred-Wegener Institute for Polar and Marine Research, Potsdam, Germany, personal communication, 1998) and at the South Pole station in the Antarctic for 1986 winter (right panel) (Hofmann *et al.*, 1997). The blue curves show ozone levels before its depletion is initiated. The red curves show the depletion of ozone. The depletion of ozone in the 15-20 km region observed in the mid-1990s in the Arctic is reminiscent of that observed in the Antarctic a decade earlier. Ozone depletion continues into late spring in the Antarctic (green curve), unlike the case in the Arctic. Single profiles may not really represent chemical ozone depletion because of dynamical factors. The shown profile is not due to dynamics and care has been taken to identify dynamical effects.

cold temperatures, is well established by direct observations and by recent model studies (see Section 7.4.2). The model studies have also shown that the details of denitrification, wintertime activation, or even the existence of solid PSCs are not essential (although they are observed) for estimating the overall $O_3$ loss. This is because chlorine activation is rapid at cold temperatures on all forms of stratospheric condensed matter, and cold temperatures together with vortex isolation persist into springtime, when sunlight can act to destroy ozone. In contrast, as discussed below, the rates of dynamical supply and chemical removal compete in the Arctic and they need to be well quantified to estimate the overall ozone loss.

Figure 7-19 shows a marked decrease in springtime total ozone in the Arctic since the late 1980s, reminiscent of that seen in the Antarctic ten years earlier. The development of the vertical structure of ozone mixing ratios within the recent Arctic vortex during winter and early spring is also somewhat reminiscent of the Antarctic (Figure 7-20). Yet, one cannot immediately conclude that the Arctic springtime ozone decrease seen in Figure 7-19 has occurred for exactly the same set of reasons as in the Antarctic. First, the Arctic decrease has occurred during a time when the stratospheric chlorine loading, though already high, was not changing rapidly. Second, the Arctic and Antarctic are quite different in certain respects.

One important difference is that the Arctic vortex is much smaller and more distorted than the Antarctic vortex. Thus, although 63-90°S coincides reasonably well with the Antarctic vortex, the changes in March

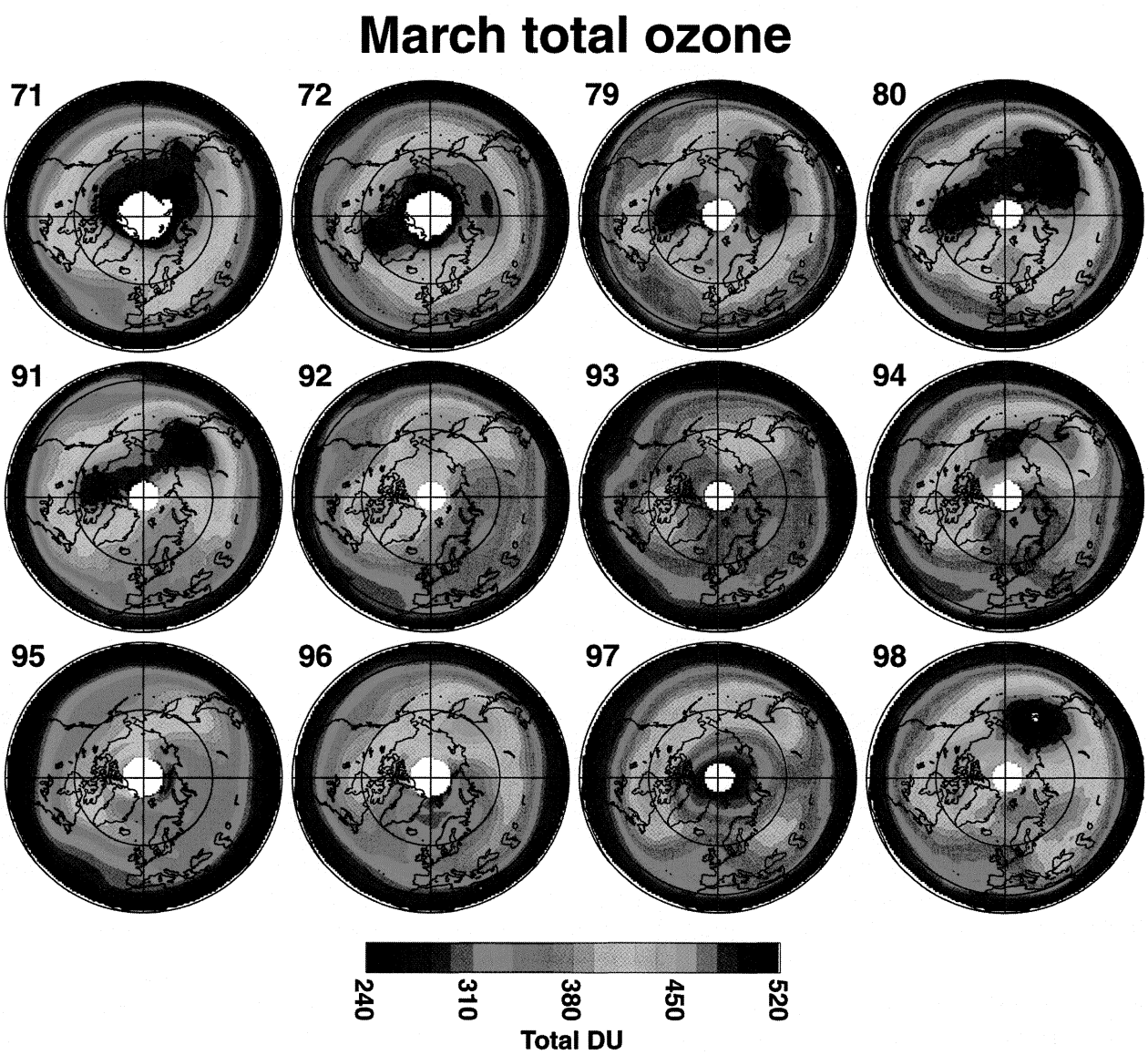


**Figure 7-21.** March monthly average total ozone polar stereographic images for the Arctic. The 1971 and 1972 data are from Nimbus 4 BUV, the 1979-1993 data are from Nimbus 7 TOMS, the 1994 data are from Meteor 3 TOMS, the 1995 and 1996 data are from NOAA-9 SBUV/2, and the 1997 and 1998 data are from Earth Probe TOMS.

average 63-90°N total ozone values seen in Figure 7-19 combine changes both within and outside the Arctic polar vortex. While total ozone amounts measured by satellite instruments since 1970 are very large over the entire polar cap during the early years of observations, a distinct minimum in the Arctic region is usually apparent during the 1990s (Figure 7-21). These satellite observations are supported by ground-based observations, which report extremely low ozone column amounts in recent years, significantly below long-term means (Chapter 4). There is also a significant reduction during the 1990s in the relatively large values that form a croissant structure just outside the vortex. Thus, one must be careful when interpreting Figure 7-19, because the geographical areas in the two hemispheres do not represent the same dynamical regions.

Another important difference between the Arctic and Antarctic is that there is significant interannual

variability in the spatial distribution of Arctic ozone (Figure 7-21). Generally speaking, the springtime Arctic ozone distribution during the 1990s has been more Antarctic in character, with a relative minimum inside the vortex. However, the Arctic vortex is generally centered further off the pole (associated with larger planetary-wave forcing), which means that air parcels can be exposed to sunlight earlier in the season than in the Antarctic, even if the vortex is smaller. Thus the conditions for Arctic depletion are considerably more complex than in the Antarctic, because the potential for ozone loss is not limited to springtime and not all of the Arctic region is conducive to ozone depletion.

Given our present understanding of Antarctic ozone depletion, to produce significant chemical loss in the Arctic requires cold enough temperatures for rapid chlorine activation, exposure to sunlight, and sufficient vortex isolation to allow time for these chemical processes to act. Indeed, meteorological conditions in the Arctic during the 1990s have, generally speaking, been more Antarctic in character, with the vortex being colder and more persistent than in the recent past, especially in 1996/97 (e.g., Coy *et al.,* 1997). But because these meteorological conditions necessarily involve a concomitant reduction in ozone transport into the polar region, it is clear that dynamical and chemical signals are strongly intertwined. Conversely, we would also expect any dynamical signal in ozone associated with a stronger vortex and less transport to involve a concomitant reduction of Arctic temperatures which, in the presence of the current high level of chlorine loading, would lead to enhanced chemical loss.

The decadal trend in the seasonal ozone depletion is difficult to quantify in the Arctic because of the great interannual variability of meteorological conditions, which produces variability in ozone transport as well as in chemical loss (via variability in temperatures and degree of vortex isolation). The recent years of low Arctic ozone are characterized by relatively low planetary wave activity, producing less diabatic descent; thus, as noted above, temperatures inside the Arctic vortex have been colder and more persistent in the recent past (Figure 7-22). This points to a decadal shift in Arctic meteorological conditions, which could well be due to decadal variability in the tropospheric circulation and hence in planetary wave forcing (e.g., Thompson and Wallace, 1998), or even to a long-term change in climate (see Chapter 12). However the reasons for this particular shift are not understood, nor are we able to predict its persistence. For example, the winter of 1997/98 did not exhibit a cold, persistent Arctic vortex. Note that the enhanced chemical ozone loss expected under these more Antarctic-like meteorological conditions would also produce a radiative feedback, leading to still colder temperatures (see Randel and Wu, 1998; also see Chapter 5).

Because of the above reasons, it is best to look on shorter time scales to quantify chemical loss. In the Arctic, even diagnosing seasonal chemical ozone loss requires a careful separation of changes due to chemistry from those due to dynamics. A number of methods have been developed in recent years for this purpose.

One method, known as Match (von der Gathen *et al.*, 1995; Rex *et al.*, 1998), makes use of pairs of ozonesonde profiles, around five days apart in time, which are matched through Lagrangian trajectory calculations so that they sample the same air mass. By sampling the same air mass, the observed ozone changes can be ascribed to chemistry. von der Gathen *et al.* (1995) calculated ozone loss rates of up to 0.25% per sunlit hour on the 475 K isentropic surface (~18 km altitude), which integrated to give a roughly 40% local loss inside the vortex during January and February of 1992. Confidence in the technique was obtained because the observed depletion only occurred during sunlit times, as would be expected from our understanding of chemical ozone depletion. Chemical ozone depletions have subsequently been evaluated with this method for other Arctic winters (e.g., Rex *et al.,* 1998), with much more extensive spatial and temporal coverage of the vortex. Figure 7-23 shows results from the colder winter of 1994/95. Ozone loss was calculated from about 370 K to 600 K during January through March. The maximum deduced loss rates were over $1.5 \times 10^{11}$ molecule $cm^{-3}$ $day^{-1}$ (~3.3% $day^{-1}$) at 425 K (about 18 km) in March, and the accumulated total chemical loss in this altitude range through January-March was calculated to be about 125 DU.

The Match technique has the advantage of providing direct quantification of local chemical ozone loss, because it considers ozone changes over short periods for which air masses retain their integrity. Its disadvantage is that it is difficult to quantify total ozone loss over the vortex using only the ozonesonde matches and it does not work when ozone losses are small. Two alternative techniques use satellite measurements to provide vortex-averaged estimates, but must consider changes over longer time periods for which the concept of an air mass is more questionable. Thus the strengths and weaknesses of the Match technique and these two

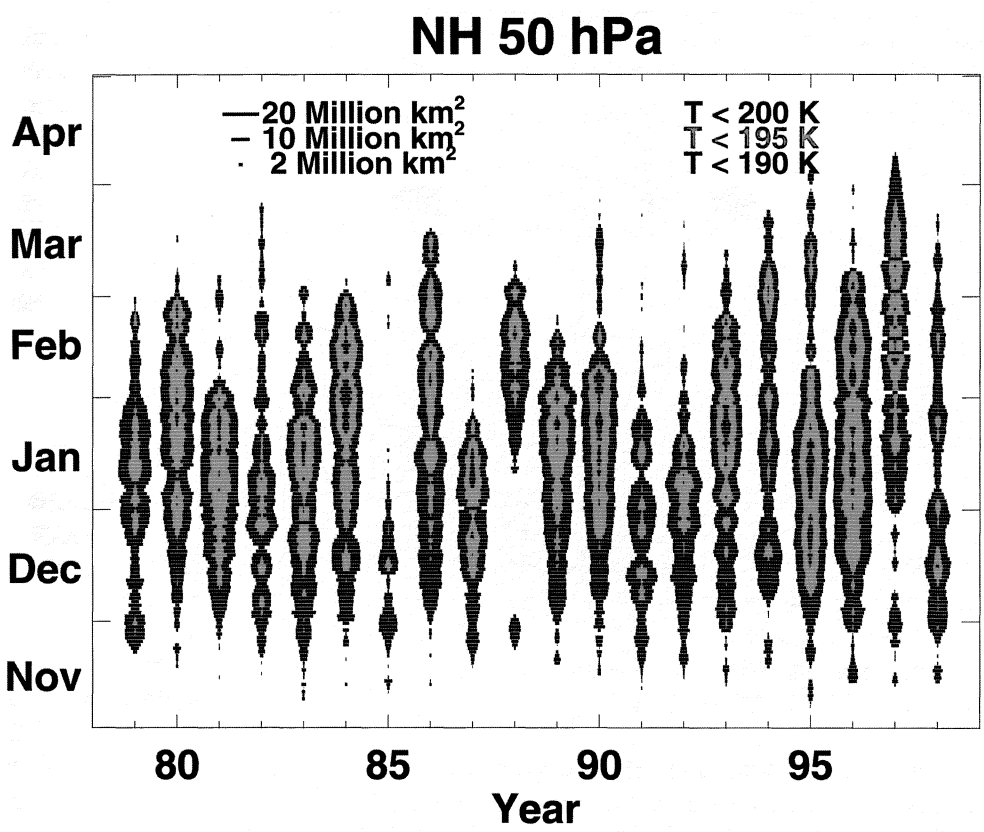


**Figure 7-22.** Time evolution of the areal coverage of cold 50 hPa temperatures in the Arctic polar region for each winter from 1979 to 1998. The width of each line is proportional to the temperature surface area coverage (see top left key), while the line color represents a particular temperature (see top right key). For example, in early November, there are no observed temperatures below 200 K in the polar region, while the 200 K areal coverage during January oftentimes exceeds 20 million km$^2$. Note also that 190 K temperatures (blue) are infrequent, and typically cover only a few million km$^2$. (Supplied by Paul Newman, NASA Goddard Space Flight Center, U.S.).

techniques, described below, are complementary.

The first alternative technique (e.g., Manney *et al.*, 1995b, 1997) uses MLS satellite observations of $O_3$ in the lower and middle stratosphere together with calculated three-dimensional trajectories to estimate the effect of transport in compensating for in situ chemical loss. Because this technique does not explicitly include mixing, a large number of closely associated trajectories are used. The results indicate that a considerable fraction of the chemical loss that occurs during late-winter/spring is masked by transport, to the extent that there is often little relation between local chemical loss and observed changes in column ozone. The calculated $O_3$ losses tend to follow periods of activated chlorine, provided there is sunlight. For example, in 1996/97 the greatest abundances of ClO at 465 K (~18 km) were observed in late February, and a vortex-averaged chemical depletion of 0.6 ppmv (20%) was estimated to occur at this altitude during March and early April (Manney *et al.*, 1997).

The second alternative technique (Müller *et al.*, 1996, 1997) uses simultaneous HALOE satellite observations of $O_3$ and $CH_4$ within the vortex to construct equivalent vertical profiles of $O_3$ that factor out the effects of diabatic descent by treating $CH_4$ as an air mass label. Changes in $O_3$ for each value of $CH_4$ are then summed to provide an estimate of total chemical ozone loss within the vortex. Such a calculation should give a reasonable estimate of the vortex-averaged chemical ozone loss if the air within the vortex is isolated during the period of analysis and subject only to unmixed descent. The effects

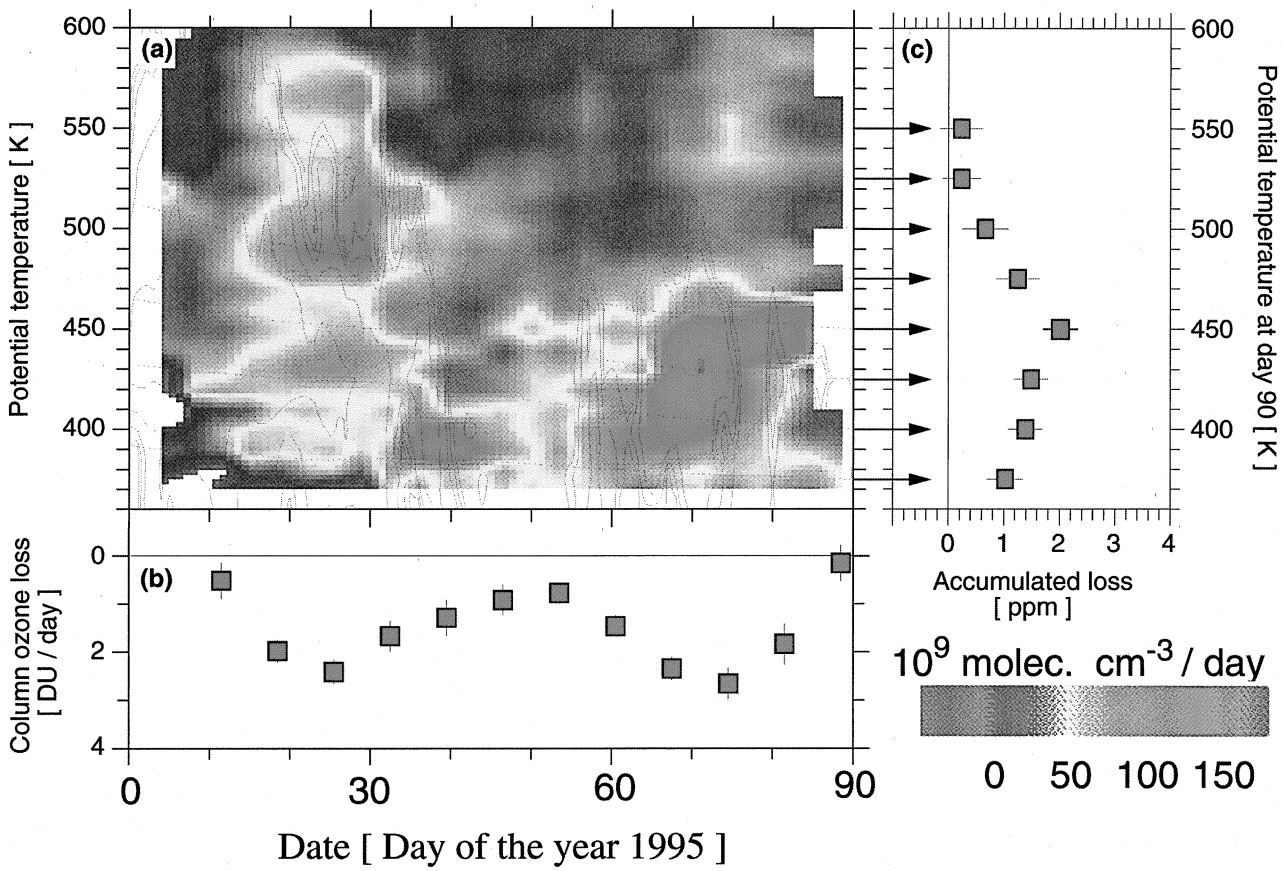


**Figure 7-23.** (a) Contour plot showing the ozone loss rate as a function of date and potential temperature. A total of 1470 matches contributed to this plot. There was significant ozone loss when the temperatures were cold enough for PSCs to form (see Rex *et al.*, 1998). (b) Ozone column loss rates obtained by integrating the local loss rates from 370 K to 600 K. The accumulated column loss over the winter is 127 ± 14 DU (corresponding to 36 ± 4%, with 350 DU as the vortex-averaged ozone column at day one). (c) The accumulated ozone loss integrated over time between day 1 and day 90 (day 20-90, day 40-90, day 50-90 for the upper most levels, respectively) in the air masses subsiding to indicated levels. All error bars show 1σ uncertainties. (Adapted from Rex *et al.*, 1998).

of mixing on the accuracy of the estimate are yet to be determined. This technique has been used to estimate chemical ozone losses between November/December and March/April during the Arctic winters of 1991/92 through 1996/97 (Müller *et al.*, 1997). The losses range from 50 DU (1996/97) to 120-160 DU (1995/96), with more than 50% local loss in the lower stratosphere in the latter.

The above studies, taken together, clearly show that significant chemical ozone depletion has occurred inside the polar vortex in recent Arctic winters, and is, therefore, an important component of the observed reduction in column $O_3$ seen in Figure 7-19. These studies also show that enhanced ozone depletion inside the Arctic vortex is due to a combination of cold temperatures, high active chlorine, and exposure to sunlight, consistent with our theoretical expectations. Significantly, although cold Arctic winters before the build-up of anthropogenic chlorine, such as that in 1967, were characterized (as we would expect) by low ozone, the ozone abundances were never as low as those seen recently (Fioletov *et al.*, 1997).

Chemical ozone depletion in the Arctic has been simulated by constraining models, to various degrees, with observations. Models that use measured ClO amounts and isentropic transport derived from analyzed winds have succeeded in broadly reproducing the observed ozone losses (Mackenzie *et al.*, 1996). Such studies provide strong evidence that the qualitative picture of chemical ozone loss is correct. However, they

are only valid for short time periods (less than seasonal) and thus cannot directly model the long-term ozone trend. Models that predict both the ozone and chlorine fields over longer time periods have been less successful (Chipperfield *et al.*, 1996; Hansen *et al.*, 1997). These models tend to underpredict the ClO fields, possibly due to unresolved mesoscale structure (see Section 7.4.1) or other model deficiencies (see Section 7.5.4). In addition, even these model simulations have not been run over long enough time periods to calculate the long-term trend, i.e., the possible contribution of a transport-induced change to the trend has not been directly estimated.

The croissant shaped region in the Arctic, referred to earlier, bridges the high-latitude vortex region with the midlatitudes. While less dramatic than the ozone depletions inside the vortex, the ozone losses in this region are still quite large and mostly seasonal, exhibiting a maximum during March (Figure 7-21 and Chapter 4). Unfortunately, the Lagrangian-based methods that have been successfully used inside the vortex to identify chemical ozone depletion cannot be used here because the time scales for ozone loss are too long. In this respect, the problem of attribution is similar to that encountered with midlatitude decadal trends (see Section 7.6.2 below). Based on our present understanding of ozone chemistry, we expect in situ chemical loss driven by direct chlorine activation on sulfate aerosol during cold temperature excursions. Two-dimensional model results including this effect can indeed reproduce the trend and some of the variability in ozone in this region (50-60°N) when constrained by observed zonal-mean temperatures together with the effects of temperature fluctuations driven by observed planetary-wave amplitudes (Solomon *et al.*, 1998). However, it has not been possible to quantify the possible role of transport changes in this region, or the influence of within-Arctic ozone loss (2-D models do not represent transport within the vortex edge region very well; see Section 7.5.2).

Thus, while a large body of evidence supports the conclusion that chemical ozone loss is occurring seasonally in the Arctic, uncertainties remain in the partitioning of the long-term trend between purely local chemical loss and other factors. Despite their differences, the physical and chemical environment in the Arctic has many similarities to the Antarctic. The conceptual picture that cold temperatures activate chlorine, and that the chlorine available for ozone depletion thus depends on total chlorine as well as on temperature, is valid in both hemispheres. The primary complications in quantifying and attributing the ozone depletion in the Arctic are the difficulties in estimating the transport and containment in the vortex, and difficulty in predicting the temperatures. Temperatures are especially important because they are in a regime where very small decreases cause very large increases in activation of chlorine. Yet, it is clear that the depletions in the Arctic during the 1990s are due to colder temperatures in the presence of chlorine loading that was already high. In contrast, the increased depletions observed in the Antarctic during the 1980s were the result of increased chlorine loading in the presence of temperatures that were already cold. The extent of late-winter/spring ozone depletion in the Arctic during the next few years will depend on meteorological conditions.

### 7.6.2 Midlatitude Trends

*There is a large body of evidence that shows that the increased chlorine and bromine loading has contributed to the observed midlatitude ozone depletion (with the chemical loss principally occurring via midlatitude chemical processes). However, quantification of the processes contributing to this depletion is not complete. In particular, the balance between changes due to chlorine-related chemical processes and the (likely smaller) decadal variations in the circulation is not known. Obtaining such a quantitative understanding will probably require models that accurately represent chemistry, aerosol loading, temperature, and transport (including interannual and decadal variations). Recent laboratory and field studies suggest that iodine compounds from the troposphere do not contribute more than about 10% of the local observed depletion of ozone in the lowest part of the stratosphere. The role of cirrus clouds is unclear and could be a significant contributor to the ozone depletion in the lowest part of the stratosphere.*

Ground-based and satellite observations both show decadal decreases in column ozone in the midlatitudes of both hemispheres (see Chapter 4). The major contributor to the column loss is the decrease in the lower stratosphere around 20 km, even though the fractional local depletion in the upper stratosphere is comparable to that in the lower stratosphere. In contrast to the polar seasonal depletion discussed in Section 7.6.1, the decadal trend in ozone at midlatitudes is markedly smaller than the seasonal cycle and is comparable in magnitude to the natural interannual variability. The decadal trend in

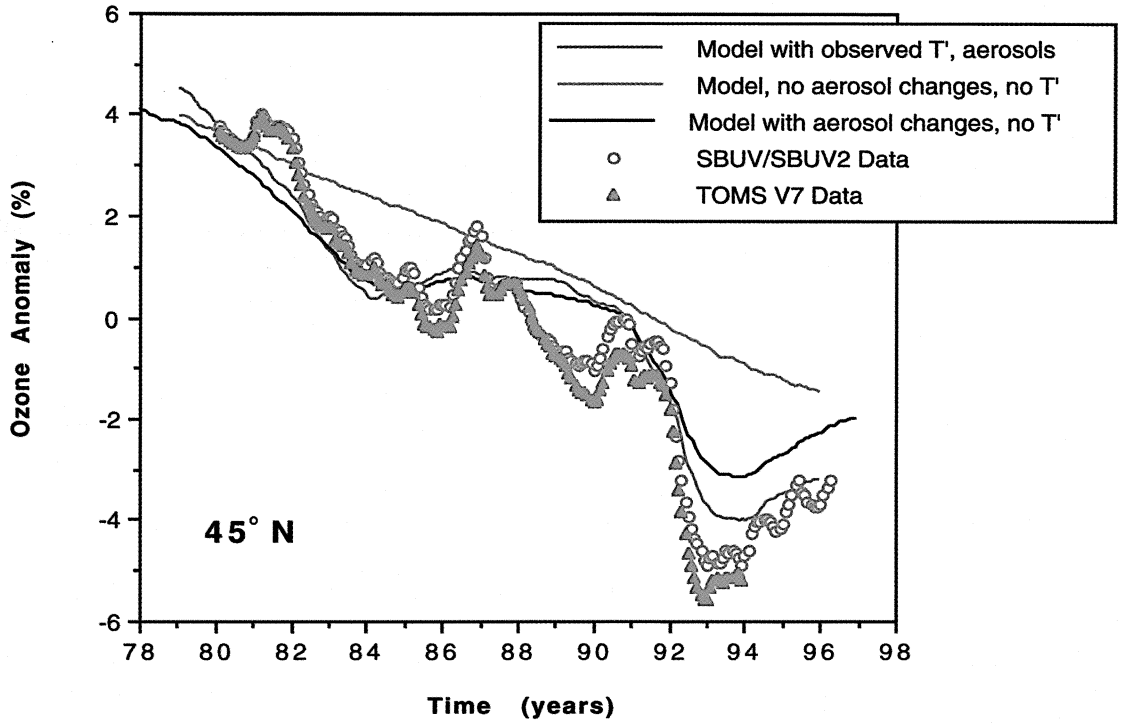


**Figure 7-24.** Observed and calculated total ozone anomalies from 1979 to 1997 at 45°N. All cases shown are smoothed by a 25-month running mean to average over both the annual cycle and the QBO. Red triangles show the zonally averaged TOMS V7 data and the blue circles show the combined SBUV/SBUV2 data. All model results shown include chlorine and bromine increases. In addition, the red line shows the model results including observed aerosol variations and zonal mean temperature and planetary wave temperature amplitudes (T') estimated from National Centers for Environmental Prediction (NCEP) observations. The black line is similar to the red line except the planetary wave temperature amplitudes are not used in the model. The green line shows model results with constant 1979 aerosol observation used throughout the calculation. (Adapted from Plate 1 of Solomon *et al.* (1996) using TOMS V7 data and model results from Solomon *et al.*, 1998).

the monthly mean values at high latitudes also shows a clear downward trend. The magnitude of the column ozone decadal trend and the vertical variation in the fractional depletion have been revised in this Assessment. This revision shows that significant uncertainty still remains in the quantification of the trend, especially in the last few years (see Chapter 4).

Because of the difficulty in obtaining the quantitative trend estimates from data, it is critical that we use the pattern of the ozone changes in time and space and attempt to attribute the patterns, rather than the precise magnitudes, of the changes to causes. Important signatures are provided by the latitudinal, vertical, and seasonal dependence of the trends, as well as by the effects of volcanic eruptions.

The Mt. Pinatubo eruption, in particular, had a major impact on midlatitude ozone (see Section 7.4.3). The direct radiative-dynamical effects due to the aerosol cloud were mostly confined to the first year after the eruption, but the ozone perturbation lasted for several years (see Figure 7-24), suggesting that chemical effects from the increased aerosol played a significant role. Based on laboratory studies of heterogeneous/multiphase processes and analysis of in situ measurements, increased volcanic aerosol is expected to enhance ozone depletion in midlatitudes in the presence of current chlorine loading because the amount of reactive chlorine species would be greatly enhanced in such situations. Note that without

chlorine, stratospheric ozone would, in contrast, be expected to increase with an increase in volcanic aerosol because enhanced volcanic aerosol will decrease the levels of nitrogen oxides and thereby reduce ozone loss by $NO_x$ catalytic cycles (Solomon *et al.*, 1998; Tie and Brasseur, 1995). Indeed, increases in ozone abundances in the middle stratosphere, where $NO_x$ is the dominant catalyst (see Section 7.5.1), are visible in HALOE data following the Mt. Pinatubo eruption (Mickley *et al.*, 1998). Figure 7-24 shows the smoothed anomalies from satellite measurements of ozone for the 1979-1995 period compared with a two-dimensional model simulation (Solomon *et al.*, 1996; Solomon *et al.*, 1998). The model ozone variation is dominated by the trend in chlorine (and a smaller trend in bromine) along with the volcanic perturbation of the aerosols. The dramatic decreases observed after the Mt. Pinatubo eruption are reproduced, together with the ozone decrease after the El Chichón eruption in 1982 and the relatively flat period during the late 1980s.

The Mt. Pinatubo eruption illustrates the strong nonlinear coupling that exists between natural (volcanic) and anthropogenic (halogen) effects. Statistical regression techniques, based on an assumption of linear superposition, cannot be expected to separate natural from anthropogenic parts of this signal.

While the pattern of the model-based ozone anomalies shown in Figure 7-24 and those derived by Jackman *et al.* (1996) is similar in many respects to that of the observations, the magnitude is not exactly the same. The differences in magnitude could be due to various shortcomings of the 2-D models (see Section 7.5.2) or due to uncertainties in the derived trend (see Chapter 4). Note also that existing 2-D model results have used a fixed dynamical forcing, and changes in dynamical forcing could well be an important contributor to the signal (see further discussion below). Yet regardless of the differences in magnitude, the agreement in the timing of changes in midlatitude ozone between model and observations provides strong evidence for the dominant role of chlorine (and bromine) in causing the observed ozone changes following the Mt. Pinatubo eruption.

The vertical profile of the trends provides a second important signature for the cause of the ozone depletion. Chemical effects of increasing chlorine and bromine, largely due to multiphase chemistry in aerosols, give an ozone depletion with a vertical dependence consistent with that observed, namely, with greater depletion in the lower stratosphere than in the middle stratosphere (Chapter 4). This vertical dependence arises because while chlorine is a major contributor to ozone loss in the lower stratosphere, its relative contribution decreases with altitude before increasing again in the upper stratosphere. However there are quantitative differences between observations and the results from 2-D models, which are likely related both to uncertainties in the trends and to deficiencies in the models. For example, 2-D models are not expected to accurately represent the transport in the lowermost stratosphere (below about 16 km) (see Section 7.5.2). Possible chlorine activation on cirrus clouds (see below) is also not explicitly included in some of the above models. Because of the above reasons, uncertainties in simulations of ozone depletion in 2-D models, especially at altitudes just above the tropopause, are not surprising.

Other signatures of the ozone change include the latitudinal variation and seasonal cycle of the trend in total ozone. These can be summarized as enhanced depletion at higher latitudes, larger depletion in northern midlatitudes than in southern midlatitudes, and with the largest effect (in both hemispheres) in winter and spring (Chapter 4). These features are qualitatively consistent with the impact and temperature dependence of heterogeneous/multiphase reactions. Possible factors that contribute to the NH/SH asymmetry are the colder temperature and lower water abundances in the SH, differences in the amplitude of longitudinal asymmetries, and differences in the rate of ozone transport. It does not appear that the asymmetry between North Pole and South Pole directly affects midlatitudes, at least not above 16 km (see further discussion below). While a detailed understanding of these patterns is not well characterized, the overall trends in time and space are consistent with the hypothesis that chlorine and bromine are the primary cause of the lower stratospheric ozone depletion in the midlatitudes.

Our understanding and modeling of midlatitude chemistry is based to some extent on analyses of photochemistry over the Antarctic and the Arctic, where temperatures are cold enough to extensively activate chlorine and subsequently deplete ozone. In the lower stratosphere, hydrolysis of $N_2O_5$ on sulfate aerosol indirectly enhances active chlorine and direct activation of $Cl_y$ at cold temperatures also impacts radical speciation. $HO_x$ and $NO_x$ catalytic cycles dominate midlatitude ozone loss, but the $ClO_x$ catalytic cycle is a significant ozone loss mechanism at altitudes below 25 km (see Section 7.5.1). Increasing chlorine then leads

to enhanced ozone loss in this region. Midlatitude ozone depletion in the lower stratosphere is thus more like that in the polar regions than that in the upper stratosphere: in the lower stratosphere temperatures are low enough for chlorine activation, and ozone production regions are far away; thus, significant ozone depletion can occur even for significantly slower ozone loss rates than those found in polar regions or in the upper stratosphere.

In view of the polar (high latitude) ozone depletion, an important question is how much of the midlatitude ozone trend might be due to polar effects. This is related to basic questions of how well we understand the stratospheric circulation. Observational and 3-D modeling studies indicate that above 16 km only a small amount of polar processed air is transported into midlatitudes before the vortex breaks up, and that this process will not have a large impact on midlatitude ozone (see Section 7.3.3.2). However, there are indications that there is greater transport of polar processed air below 16 km, and that this process may play a role in midlatitude low altitude ozone depletion. Also, 3-D modeling studies suggest that post-vortex ozone dilution has an impact on midlatitude ozone in both the Southern (e.g., Brasseur *et al.*, 1997; Eckman *et al.*, 1996) and Northern (Hadjinicolaou *et al.*, 1997) Hemispheres. There is also a clear springtime signature of Antarctic vortex dilution in $NO_y$ and $H_2O$ poleward of 50°S (Nevison *et al.*, 1997; Rosenlof *et al.*, 1997).

Although natural interannual variability cannot account for the large ozone depletion following the volcanic eruptions, it cannot be conclusively eliminated as a cause of the observed decadal midlatitude ozone decline. Simulations with both 2-D (e.g., Callis *et al.*, 1997; Jackman *et al.*, 1996; Schneider *et al.*, 1991) and 3-D (Hadjinicolaou *et al.*, 1997) models indicate that interannual variability in the stratospheric circulation may be a significant contributor to interannual changes in midlatitude ozone. For example, Hadjinicolaou *et al.* (1997) reproduce many of the changes in column ozone in northern midlatitudes during 1992 to 1994 (in particular, the recovery in 1993) in a model that includes interannual variability in the meteorology but no heterogeneous/multiphase chemistry. Furthermore, a statistical link has been found between the observed decadal changes in stratospheric ozone and the observed changes in lower stratospheric circulation (Hood *et al.*, 1997), as well as between ozone changes and changes in the wave forcing that drives the stratospheric circulation (Fusco and Salby, 1998). Fusco and Salby point to the striking observed anticorrelation between interannual variations of extratropical and tropical total ozone as providing further evidence for the role of variations in the Brewer-Dobson circulation. While this anti-correlation clearly holds on time scales of a few years, it does not necessarily apply on longer time scales; indeed, there is no statistically significant decadal trend in total ozone in the tropics (Chapter 4). Note also that a decadal trend in the strength of the Brewer-Dobson circulation should be reflected in compensating trends in tropical and extratropical temperatures (see Section 7.3.1), and such a trend is not seen in Figure 7-5.

Interpreting the statistical relationships referred to above is not, in any case, straightforward. Because of the synergy that exists between dynamics and chemistry, a trend in chemical ozone loss driven by a change in dynamical conditions, such as has occurred in the Arctic late-winter/spring over the last decade (see Section 7.6.1), would in the context of a statistical regression analysis be explained by the dynamical proxy. In fact, dynamical and chemical effects interact strongly and it is not simply a case of one effect or the other (see further discussion in Section 7.7).

Future trends in ozone at midlatitudes (i.e., ozone recovery as chlorine and bromine loading decreases in the future) are dependent on any trends in stratospheric circulation. Trends in lower stratospheric temperature will also be critical because activation of chlorine on condensed matter is highly temperature dependent. These effects make lower stratospheric ozone particularly sensitive to future climate change.

In addition to the chemical processes discussed above, other processes have been invoked to account for the observed ozone depletion in the lowermost stratosphere: (a) activation of chlorine via heterogeneous/multiphase reactions on condensed matter in the tropopause region and (b) iodine-catalyzed ozone destruction.

The same heterogeneous/multiphase reactions that occur in the polar regions can also take place in the tropopause region. It is well known that the altitude where the ozone starts to increase toward stratospheric values is generally about 1 km below the thermal tropopause. If the elevated ozone is due to stratospheric air, non-zero $Cl_y$ should also be present in this region. Additionally, the water vapor mixing ratios are much higher in this altitude region compared to higher altitudes (Oltmans and Hofmann, 1995; Holton *et al.*, 1995) and, thus, many key heterogeneous reactions (Hanson and

Ravishankara, 1994) must be rapid. Based on in situ ER-2 data for aerosol and chemical composition and 2-D model calculations for the concentrations of the chlorine-containing gas phase species, Borrmann *et al.* (1997) showed that heterogeneous chlorine activation could be close to or exceed that from the gas phase OH + HCl reaction. Solomon *et al.* (1997, 1998) showed that multiphase reactions on the aerosol of the tropopause region could enhance ClO sufficiently to make a significant contribution to the ozone depletion in northern midlatitudes.

Some field data suggest that ClO increases are due to chlorine activation in the tropopause region. Solomon *et al.* estimated an average ClO enhancement of about 50% at the tropical tropopause because of the nearly continuous presence of cirrus clouds there as indicated by the satellite observations. Borrmann *et al.* (1997) showed that up to 2.7 parts per trillion by volume (pptv) of ClO could be formed in a single cirrus cloud event, albeit with considerable uncertainties. Their model calculations also indicate that it will take several days for the enhanced ClO to return to "clear sky" levels. Thus the impact of the heterogeneous chemistry may last longer than a specific cloud event itself. Other evidence for this process comes from observations of unusually low ozone concentrations inside cirrus clouds (Reichardt *et al.*, 1996) and the reduced $NO/NO_y$ ratio and ClO abundances near 90 pptv observed by Keim *et al.* (1996) in a layer of volcanic aerosol 500 m above the midlatitude tropopause.

Ozone trends in the lowermost stratosphere may also be affected by iodine-chlorine chemistry. Based on the observed abundance of natural iodine compounds in the troposphere, Solomon *et al.* (1994) assumed that up to 1 pptv of iodine could be present in the lower stratosphere. If such an abundance of iodine was present in the lower stratosphere, they suggested that a large fraction of the decadal trend of ozone in the lowermost stratosphere could be due to the reaction between IO and ClO; the abundance of IO remained constant while that of ClO increased due to the increasing chlorine loading, i.e., the trend in ozone arises because of the trend in chlorine. They assumed a rate coefficient for the reaction of ClO with IO of $1 \times 10^{-10}$ $cm^3$ $molecule^{-1}$ $s^{-1}$, based on analogy with known reactions of IO with IO and of ClO with BrO. The rate coefficient for this reaction has now been measured to be 5 times slower at lower stratospheric temperatures (Turnipseed *et al.*, 1997). In addition, long-path atmospheric ultraviolet (UV) absorption measurements have placed limits of < 0.2 pptv for IO in the lower stratosphere (Pundt *et al.*, 1998; Wennberg *et al.*, 1997). Based on these two sets of findings, it appears that iodine may not contribute very significantly to the observed lower stratospheric ozone depletion (Gilles *et al.*, 1997). However, Solomon *et al.* (1997) show that cirrus enhancement of ClO could lead to an increased efficiency of iodine such that even 0.1 pptv of IO could lead to a 10% increase of the ozone loss rate. Thus, contributions of iodine to the lower stratospheric ozone depletion cannot be ruled out, but their contribution to the column ozone decreases should be small. Yet, it appears that injection of iodine to the stratosphere would be detrimental to the ozone in this region.

## 7.7 SYNTHESIS

Chemical, microphysical, and dynamical processes each play critical roles in determining the abundance of ozone in the lower stratosphere. (N.B. In this section, for brevity, "dynamics" is understood to include radiation as well as wave forcing and transport.) Often, these processes can reinforce each other with regard to changing ozone levels, while in other situations they tend to cancel or reduce the effect of one another. In situations where the dynamical processes are separable in time and space from the chemical processes, it is possible to detect, quantify, and, even, attribute the ozone changes to certain causes. However, it is never possible to truly separate microphysics from either chemistry or dynamics; dynamics forces temperature changes, while chemistry controls the concentration of the many constituents such as $HNO_3$ that make up the various types of condensed matter. Our understanding is not yet sufficient to quantitatively deal with a situation where the effects of all three kinds of processes are not separable.

Given this situation, can we answer the question: What is causing lower stratospheric ozone depletion? In other words, in what way is the lower stratosphere of today different from that of the 1970s? What agents that force alterations in ozone abundance have changed during this period? What caused their changes?

Over the last few decades there has been a definite increase in the abundance of stratospheric halogens, which chemically forces a change in the system. Our current understanding of stratospheric chemistry implies that, if all other things remained the same, the chlorine increase should lead to ozone depletion. However, this does not mean that we can therefore attribute the changes

Appenzeller, C., J.R. Holton, and K.H. Rosenlof, Seasonal variation of mass transport across the tropopause, *J. Geophys. Res.*, *101*, 15071-15078, 1996b.

Arnold, F., V. Burger, K. Gollinger, M. Roncossek, J. Schneider, and S. Spreng, Observations of nitric acid perturbations in the winter Arctic stratosphere: Evidence for PSC-sedimentation, *J. Atmos. Chem.*, *30*, 49-59, 1998.

Arpag, K.H., P.V. Johnston, H.L. Miller, R.W. Sanders, and S. Solomon, Observations of the stratospheric BrO column over Colorado, 40N, *J. Geophys. Res.*, *99*, 8175-8181, 1994.

Atkinson, R., D.L. Baulch, R.A. Cox, R.F. Hampson, J.A. Kerr, M.J. Rossi, and J. Troe, Evaluated kinetic and photochemical data for atmospheric chemistry: Supplement V, IUPAC subcommittee on gas kinetic data evaluation for atmospheric chemistry, *J. Phys. Chem. Ref. Data*, *26*, 521-1011, 1997.

Atticks, M.G., and G.D. Robinson, Some features of the structure of the tropical tropopause, *Quart. J. Roy Meteorol. Soc.*, *109*, 295-308, 1983.

Avallone, L.M., and M.J. Prather, Photochemical evolution of ozone in the lower tropical stratosphere, *J. Geophys. Res.*, *101*, 1457-1461, 1996.

Avallone, L.M., S.M. Schauffler, W.H. Pollock, L.E. Heidt, E.L. Atlas, and K.R. Chan, In situ measurements of BrO during AASE II, *Geophys. Res. Lett.*, *22*, 831-834, 1995.

Bacmeister, J.T., S.D. Eckermann, P.A. Newman, L. Lait, K.R. Chan, M. Loewenstein, M.H. Proffitt, and B.L. Gary, Stratospheric horizontal wavenumber spectra of winds, potential temperature, and atmospheric tracers observed by high-altitude aircraft, *J. Geophys. Res.*, *101*, 9441-9470, 1996.

Ball, S.M., G. Hancock, S.E. Martin, and J.C.P.D. Moira, A direct measurement of the $O(^1D)$ quantum yields from the photodissociation of ozone between 300 and 328 nm, *Chem. Phys. Lett.*, *264*, 531-538, 1997.

Balluch, M.G., and P.H. Haynes, Quantification of lower stratospheric mixing processes using aircraft data, *J. Geophys. Res.*, *102*, 23487-23504, 1997.

Banham, S.F., A.B. Horn, T.G. Koch, and J.R. Sodeau, Ionisation and solvation of stratospherically relevant molecules on ice films, *Faraday Discuss. Chem. Soc.*, *100*, 321-332, 1995.

Beagley, S.R., J. de Grandpré, J.N. Koshyk, N.A. McFarlane, and T.G. Shepherd, Radiative-dynamical climatology of the first generation Canadian middle atmosphere model, *Atmos.-Ocean*, *35*, 293-331, 1997.

Beekman, M., G. Ancellet, and G. Mégie, Climatology of tropospheric ozone in southern Europe and its relation to potential vorticity, *J. Geophys. Res.*, *99*, 12841-12854, 1994.

Bekki, S., On the possible role of aircraft-generated soot in the middle latitude ozone depletion, *J. Geophys. Res.*, *102*, 10751-10758, 1997.

Bischof, W., R. Borchers, P. Fabian, and B.C. Kruger, Increased concentration and vertical distribution of carbon dioxide in the stratosphere, *Nature*, *316*, 708-710, 1985.

Boer, G.J., and M. Lazare, Some results concerning the effect of horizontal resolution and gravity wave drag on simulated climate, *J. Climate*, *1*, 789-806, 1988.

Boering, K.A., B.C. Daube, S.C. Wofsy, M. Loewenstein, J.R. Podolske, and E.R. Keim, Tracer-tracer relationships and lower stratospheric dynamics: $CO_2$ and $N_2O$ correlations during SPADE, *Geophys. Res. Lett.*, *21*, 2567-2571, 1994.

Boering, K.A., S.C. Wofsy, B.C. Daube, H.R. Schneider, M. Loewenstein, J.R. Podolske, and T.J. Conway, Stratospheric mean ages and transport rates from observations of carbon dioxide and nitrous oxide, *Science*, *274*, 1340-1343, 1996.

Bojkov, R.D., and V.E. Fioletov, Estimating the global ozone characteristics during the last 30 years, *J. Geophys. Res.*, *100*, 16537-16551, 1995.

Borrmann, S., S. Solomon, L. Avallone, D. Toohey, and D. Baumgardner, On the occurrence of ClO in cirrus clouds and volcanic aerosol in the tropopause region, *Geophys. Res. Lett.*, *24*, 2011-2014, 1997.

Boville, B.A., Middle atmosphere version of CCM2 (MACCM2): Annual cycle and interannual variability, *J. Geophys. Res.*, *100*, 9017-9039, 1995.

Bowman, K.P., Global patterns of the quasi-biennial oscillation in total ozone, *J. Atmos. Sci.*, *46*, 3328-3343, 1989.

Bowman, K.P., Barotropic simulation of large-scale mixing in the Antarctic polar vortex, *J. Atmos. Sci.*, *50*, 2901-2914, 1993.

Bowman, K.P., and A.J. Kruger, A global climatology of total ozone from the Nimbus 7 total ozone mapping spectrometer, *J. Geophys. Res.*, *90*, 7967-7976, 1985.

Brasseur, G.P., X.X. Tie, P.J. Rasch, and F. Lefèvre, A three-dimensional simulation of the Antarctic ozone hole: Impact of anthropogenic chlorine on the lower stratosphere and upper troposphere, *J. Geophys. Res.*, *102*, 8909-8930, 1997.

Bregman, A., M. van den Broek, K.S. Carslaw, R. Müller, T. Peter, M.P. Scheele, and J. Lelieveld, Ozone depletion in the late winter lower Arctic stratosphere: Observations and model results, *J. Geophys. Res.*, *102*, 10815-10828, 1997.

Brewer, A.W., Evidence for a world circulation provided by the measurements of helium and water vapour distribution in the stratosphere, *Quart. J. Roy. Meteorol. Soc.*, *75*, 351-363, 1949.

Brune, W.H., J.G. Anderson, D.W. Toohey, D.W. Fahey, S.R. Kawa, R.L. Jones, D.S. McKenna, and L.R. Poole, The potential for ozone depletion in the Arctic polar stratosphere, *Science*, *252*, 1260-1266, 1991.

Burkholder, J.B., R.L. Mauldin III, R.J. Yokelson, and A.R. Ravishankara, Kinetic, thermochemical, and spectroscopic study of $Cl_2O_3$, *J. Phys. Chem.*, *97*, 7597-7605, 1993.

Burkholder, J.B., A.R. Ravishankara, and S. Solomon, UV/visible and IR absorption cross sections of $BrONO_2$, *J. Geophys. Res.*, *100*, 16793-16800, 1995.

Butchart, N., and J. Austin, Middle atmosphere climatologies from the troposphere-stratosphere configuration of the UKMO's unified model, *J. Atmos. Sci.*, *55*, 2782-2809, 1998.

Callis, L.B., M. Natarajan, J.D. Lambeth, and R.E. Boughner, On the origin of midlatitude ozone changes: Data analysis and simulations for 1979-1993, *J. Geophys. Res.*, *102*, 1215-1228, 1997.

Cariolle, D., M. Amodei, and P. Simon, Dynamics of the ozone distribution in the winter stratosphere: Modelling the interhemispheric differences, *J. Atmos. Terr. Phys.*, *54*, 627-640, 1992.

Carslaw, K.S., and T. Peter, Uncertainties in reactive uptake coefficients for solid stratospheric particles-1. Surface chemistry, *Geophys. Res. Lett.*, *24*, 1743-1746, 1997.

Carslaw, K.S., B.P. Luo, S.L. Clegg, T. Peter, P. Brimblecombe, and P.J. Crutzen, Stratospheric aerosol growth and $HNO_3$ gas phase depletion from coupled $HNO_3$ and water uptake by liquid particles, *Geophys. Res. Lett.*, *21*, 2479-2482, 1994.

Carslaw, K.S., S.L. Clegg, and P. Brimblecombe, A thermodynamic model of the system HCl-$HNO_3$-$H_2SO_4$-$H_2O$ including solubilities of HBr from < 200 to 328 K, *J. Phys. Chem.*, *99*, 11557-11574, 1995.

Carslaw, K.S., T. Peter, and S.L. Clegg, Modeling the composition of liquid stratospheric aerosols, *Rev. Geophys.*, *35*, 125-154, 1997.

Carslaw, K.S., M. Wirth, A. Tsias, B.P. Luo, A. Dörnbrack, M. Leutbecher, H. Volkert, W. Renger, J.T. Bacmeister, and T. Peter, Particle microphysics and chemistry in remotely observed mountain polar stratospheric clouds, *J. Geophys. Res.*, *103*, 5785-5796, 1998.

Chance, K., W.A. Traub, D.G. Johnson, K.W. Jucks, P. Ciarpallini, R.A. Stachnik, R.J. Salawitch, and H.A. Michelsen, Simultaneous measurements of stratospheric $HO_x$, $NO_x$, and $Cl_x$: Comparison with a photochemical model, *J. Geophys. Res.*, *101*, 9031-9043, 1996.

Chang, A.Y., R.J. Salawitch, H.A. Michelsen, M.R. Gunson, M.C. Abrams, R. Zander, C.P. Rinsland, J.W. Elkins, G.S. Dutton, C.M. Volk, C.R. Webster, R.D. May, D.W. Fahey, R.S. Gao, M. Loewenstein, J.R. Podolske, R.M. Stimpfle, D.W. Kohn, M.H. Proffitt, J.J. Margitan, K.R. Chan, M.M. Abbas, A. Goldman, F.W. Irion, G. Manney, M.J. Newchurch, and G.P. Stiller, A comparison of measurements from ATMOS and instruments aboard the ER-2 aircraft: Halogenated gases, *Geophys. Res. Lett.*, *23*, 2393-2396, 1996.

Chatfield, R.B., Anomalous $HNO_3/NO_x$ ratio of remote tropospheric air: Conversion of nitric acid to formic acid and $NO_x$? *Geophys. Res. Lett.*, *21*, 2705-2708, 1994.

Chen, P., The permeability of the Antarctic vortex edge, *J. Geophys. Res.*, *99*, 20563-20571, 1994.

Chen, P., Isentropic cross-tropopause mass exchange in the extratropics, *J. Geophys. Res.*, *100*, 16661-16673, 1995.

Chen, P., J.R. Holton, A. O'Neill, and R. Swinbank, Isentropic mass exchange between the tropics and extratropics in the stratosphere, *J. Atmos. Sci.*, *51*, 3006-3028, 1994.

Chipperfield, M.P., Multiannual simulations with a three-dimensional chemical transport model, *J. Geophys. Res.*, in press, 1998.

Chipperfield, M.P., D. Cariolle, P. Simon, R. Ramaroson, and D.J. Lary, A three-dimensional modeling study of trace species in the Arctic lower stratosphere during winter 1989-90, *J. Geophys. Res.*, *98*, 7199-7218, 1993.

Chipperfield, M.P., D. Cariolle, and P. Simon, A 3-D chemical transport model study of chlorine activation during EASOE, *Geophys. Res. Lett.*, *21*, 1467-1470, 1994a.

Flesch, R., B. Wassermann, B. Rothmund, and E. Ruhl, Photodissociation of A($^2A_2$)-Excited OClO and its aggregates, *J. Phys. Chem.*, *98*, 6263-6271, 1994.

Folkins, I., and C. Appenzeller, Ozone and potential vorticity at the subtropical tropopause break, *J. Geophys. Res.*, *101*, 18787-18792, 1996.

Fritts, D.C., and T.E. VanZandt, Spectral estimates of gravity wave energy and momentum fluxes: Part I, Energy dissipation, acceleration, and constraints, *J. Atmos. Sci.*, *50*, 3685-3694, 1993.

Fukao, S., M.D. Yamanaka, N. Ao, W. Hocking, T. Sato, M.Y. Tamamoto, T. Nakamura, T. Tsuda, and S. Kato, Seasonal variability of vertical eddy diffusivity in the middle atmosphere: 1, Three-year observations by the middle and upper atmosphere radar, *J. Geophys. Res.*, *99*, 18973-18987, 1994.

Fusco, A.C., and M.L. Salby, Interannual variations of total ozone and their relationship to variations of planetary wave activity, *J. Clim.*, in press, 1998.

Gao, R.S., D.W. Fahey, R.J. Salawitch, S.A. Lloyd, D.E. Anderson, R. DeMajistre, C.T. McElroy, E.L. Woodbridge, R.C. Wamsley, S.G. Donnelly, L.A. Del Negro, M.H. Proffitt, R.M. Stimpfle, D.W. Kohn, S.R. Kawa, L.R. Lait, M. Loewenstein, J.R. Podolske, E.R. Keim, J.E. Dye, J.C. Wilson, and K.R. Chan, Partitioning of the reactive nitrogen reservoir in the lower atmosphere of the Southern Hemisphere: Observations and modeling, *J. Geophys. Res.*, *102*, 3935-3949, 1997.

Garcia, R.R., and B.A. Boville, "Downward control" of the mean meridional circulation and temperature distribution of the polar winter stratosphere, *J. Atmos. Sci.*, *51*, 2238-2245, 1994.

Gary, B.L., Observational results using the microwave temperature profiler during the Airborne Antarctic Ozone Experiment, *J. Geophys. Res.*, *94*, 11223-11231, 1989.

Gelman, M.E., A.J. Miller, R.M. Nagatani, and C.S. Long, Use of UARS data in the NOAA stratospheric monitoring program, *Adv. Space Res.*, *14* (9), 21-31, 1994.

Gettelman, A., J.R. Holton, and K.H. Rosenlof, Mass fluxes of $O_3$, $CH_4$, $N_2O$, and $CF_2Cl_2$ in the lower stratosphere calculated from observational data, *J. Geophys. Res.*, *102*, 19149-19159, 1997.

Gilles, M.K., A.A. Turnipseed, J.B. Burkholder, A.R. Ravishankara, and S. Solomon, Kinetics of the IO radical: 2, Reaction of IO with BrO, *J. Phys. Chem. A.*, *101*, 5526-5534, 1997.

Goodman, J., S. Verma, R.F. Pueschel, P. Hamill, G.V. Ferry, and D. Webster, New evidence of size and composition of polar stratospheric cloud particles, *Geophys. Res. Lett.*, *24*, 615-618, 1997.

Grant, W.B., E.V. Browell, C.S. Long, L.L. Stowe, R.G. Grainger, and A. Lambert, Use of volcanic aerosols to study the tropical stratospheric reservoir, *J. Geophys. Res.*, *101*, 3973-3988, 1996.

Grose, W.L., J.E. Nealy, R.E. Turner, and W.T. Blackshear, Modeling the transport of chemically active constituents in the stratosphere, in *Transport Processes in the Middle Atmosphere*, pp. 229-250, Reidel, Dordrecht, Holland, 1987.

Hadjinicolaou, P., J.A. Pyle, M.P. Chipperfield, and J.A. Kettleborough, Effect of interannual meteorological variability on middle latitude ozone, *Geophys. Res. Lett.*, *24*, 2993-2996, 1997.

Hall, T.M., and R.A. Plumb, Age as a diagnostic of stratospheric transport, *J. Geophys. Res.*, *99*, 1059-1070, 1994.

Hall, T.M., and M.J. Prather, Seasonal evolutions of $N_2O$, $O_3$, and $CO_2$: Three-dimensional simulations of stratospheric correlations, *J. Geophys. Res.*, *100*, 16699-16720, 1995.

Hall, T.M., and D.W. Waugh, Timescales for the stratospheric circulation derived from tracers, *J. Geophys. Res.*, *102*, 8991-9001, 1997a.

Hall, T.M., and D.W. Waugh, Tracer transport in the tropical stratosphere due to vertical diffusion and horizontal mixing, *Geophys. Res. Lett.*, *24*, 1383-1387, 1997b.

Hamilton, K., Effects of an imposed quasi-biennial oscillation in a comprehensive troposphere-stratosphere-mesosphere general circulation model, *J. Atmos. Sci.*, *55*, 2393-2418, 1998.

Hamilton, K., R.J. Wilson, J.D. Mahlman, and L.J. Umscheid, Climatology of the SKYHI troposphere-stratosphere-mesosphere general circulation model, *J. Atmos. Sci.*, *52*, 5-43, 1995.

Hansen, G., T. Svenoe, M. Chipperfield, A. Dahlback, and U.P. Hoppe, Evidence of substantial ozone depletion in winter 1996/97 over northern Norway, *Geophys. Res. Lett.*, *24*, 799-802, 1997.

Hanson, D.R., The uptake of $HNO_3$ onto ice, NAT, and frozen sulfuric acid, *Geophys. Res. Lett.*, *19*, 2063-2066, 1992.

Hanson, D.R., Reaction of $N_2O_5$ with $H_2O$ on bulk liquids and on particles and the effect of dissolved $HNO_3$, *Geophys. Res. Lett.*, *24*, 1087-1090, 1997a.

Hanson, D.R., Surface-specific reactions on liquids, *J. Phys. Chem. B.*, *101*, 4998-5001, 1997b.

Hanson, D.R., and E.R. Lovejoy, The reaction of $ClONO_2$ with submicrometer sulfuric acid aerosol, *Science*, *267*, 1326-1328, 1995.

Hanson, D.R., and E.R. Lovejoy, Heterogeneous reaction in sulfuric acid: HOCl and HCl as a model system, *J. Phys. Chem.*, *100*, 6397-6405, 1996.

Hanson, D.R., and A.R. Ravishankara, Investigation of the reactive and nonreactive processes involving $ClONO_2$ and HCl on water and nitric acid doped ice, *J. Phys. Chem.*, *96*, 2682-2691, 1992.

Hanson, D.R., and A.R. Ravishankara, Uptake of HCl and HOCl onto sulfuric acid: Solubilities, diffusivities and reaction, *J. Phys. Chem.*, *97*, 12309-12319, 1993.

Hanson, D.R., and A.R. Ravishankara, Reactive uptake of $ClONO_2$ onto sulfuric acid due to reaction with HCl and $H_2O$, *J. Phys. Chem.*, *98*, 5728-5735, 1994.

Hanson, D.R., and A.R. Ravishankara, Heterogeneous chemistry of bromine species in sulfuric acid under stratospheric conditions, *Geophys. Res. Lett.*, *22*, 385-388, 1995.

Hanson, D.R., A.R. Ravishankara, and S. Solomon, Heterogeneous reactions in sulfuric acid aerosols: A framework for model calculations, *J.Geophys. Res.*, *99*, 3615-3629, 1994.

Hanson, D.R., A.R. Ravishankara, and E.R. Lovejoy, Reaction of $BrONO_2$ with $H_2O$ on submicron sulfuric acid aerosol and the implications for the lower stratosphere, *J. Geophys. Res.*, *101*, 9063-9069, 1996.

Harder, H., C. Camy-Peyret, F. Ferlemann, R. Fitzenberger, T. Hawat, H. Osterkamp, D. Perner, U. Platt, M. Schneider, P. Vradelis, and K. Pfeilsticker, Stratospheric BrO profiles measured at different latitudes and seasons: Atmospheric observations, *Geophys. Res. Lett.*, *25*, 3843-3846, 1998.

Harnisch, J., R. Borchers, P. Fabian, and M. Maiss, Tropospheric trends for $CF_4$ and $C_2F_6$ since 1982 derived from $SF_6$ dated stratospheric air, *Geophys. Res. Lett.*, *23*, 1009-1102, 1996.

Harwood, M.H., J.B. Burkholder, and A.R. Ravishankara, Photodissociation of $BrONO_2$ and $N_2O_5$: Quantum yields for $NO_3$ production at 248, 308, and 352.5 nm, *J. Phys. Chem. A.*, *102*, 1309-1317, 1998.

Hasebe, F., Quasi-biennial oscillations of ozone and diabatic circulation in the equatorial stratosphere, *J. Atmos. Sci.*, *51*, 729-745, 1994.

Haynes, P.H., and J. Anglade, The vertical-scale cascade of atmospheric tracers due to large-scale differential advection, *J. Atmos. Sci.*, *54*, 1121-1136, 1997.

Haynes, P.H., and W.E. Ward, The effect of realistic radiative transfer on potential vorticity structures, including influence of background shear and strain, *J. Atmos. Sci.*, *50*, 3431-3453, 1993.

Haynes, P.H., C.J. Marks, M.E. McIntyre, T.G. Shepherd, and K.P. Shine, On the "downward control" of extratropical diabatic circulations by eddy-induced mean zonal forces, *J. Atmos. Sci.*, *48*, 651-678, 1991.

Henson, B.F., K.R. Wilson, and J.M. Robinson, A physical absorption model of the dependence of $ClONO_2$ heterogeneous reactions on relative humidity, *Geophys. Res. Lett.*, *23*, 1021-1024, 1996.

Hess, P.G., and D. O'Sullivan, A three dimensional modeling study of the extra-tropical quasi-biennial oscillation in ozone, *J. Atmos. Sci.*, *52*, 1539-1554, 1995.

Highwood, E.J., and B.J. Hoskins, The tropical tropopause, *Quart. J. Roy. Meteorol. Soc.*, *124*, 1579-1604, 1998.

Hines, C.O., Doppler spread parameterization of gravity-wave momentum deposition in the middle atmosphere: Part I, Broad and quasi monochromatic spectra and implementation, *J. Atmos. Solar Terr. Phys.*, *59*, 387-400, 1997.

Hintsa, E.J., E.M. Weinstock, A.E. Dessler, J.G. Anderson, M. Loewenstein, and J.R. Podolske, SPADE $H_2O$ measurements and the seasonal cycle of stratospheric water vapor, *Geophys. Res. Lett.*, *21*, 2559-2562, 1994.

Hofmann, D.J., and S.J. Oltmans, Anomalous Antarctic ozone during 1992: Evidence for Pinatubo volcanic aerosol effects, *J. Geophys. Res.*, *98*, 18555-18561, 1993.

Hofmann, D.J., and S. Solomon, Ozone destruction through heterogeneous chemistry following the eruption of El Chichón, *J. Geophys. Res.*, *94*, 5029-5041, 1989.

Hofmann, D.J., S.J. Oltmans, B.J. Johnson, J.A. Lathrop, J.M. Harris, and H. Vomel, Recovery of ozone in the lower stratosphere at the South Pole during the spring of 1994, *Geophys. Res. Lett.*, *22*, 2493-2496, 1995.

Hofmann, D.J., S.J. Oltmans, J.M. Harris, B.J. Johnson, and J.A. Lathrop, Ten years of ozonesonde measurements at the South Pole: Implications for recovery of springtime Antarctic ozone, *J. Geophys. Res.*, *102*, 8931-8943, 1997.

Holton, J.R., A dynamically based transport parameterization for one-dimensional photochemical models of the stratosphere, *J. Geophys. Res.*, *91*, 2681-2686, 1986.

Holton, J.R., and H.-C. Tan, The influence of the equatorial quasi-biennial oscillation on the global circulation at 50 mb, *J. Atmos. Sci.*, *37*, 2200-2208, 1980.

Holton, J.R., P.H. Haynes, M.E. McIntyre, A.R. Douglass, R.B. Rood, and L. Pfister, Stratosphere-troposphere exchange, *Rev. Geophys.*, *33*, 403-439, 1995.

Hood, L.L., J.P. McCormack, and K. Labitzke, An investigation of dynamical contributions to mid-latitude ozone trends in winter, *J. Geophys. Res.*, *102*, 13079-13093, 1997.

Horinouchi, T., and S. Yoden, Wave-mean flow interaction associated with a QBO like oscillation in a simplified GCM, *J. Atmos. Sci.*, *55*, 502-526, 1998.

Hu, J.H., and J.P.D. Abbatt, Reaction probabilities for $N_2O_5$ hydrolysis on sulfuric acid and ammonium sulfate aerosols at room temperature, *J. Phys. Chem. A.*, *101*, 871-878, 1997.

Hübler, G., D.W. Fahey, K.K. Kelly, D.D. Montzka, M.A. Carroll, A.F. Tuck, L.E. Heidt, W.H. Pollock, G.L. Gregory, and J.F. Vedder, Redistribution of reactive odd nitrogen in the lower Arctic stratosphere, *Geophys. Res. Lett.*, *17*, 453-465, 1990.

Ingham, T., D. Bauer, J. Landgraf, and J.N. Crowley, The UV-visible absorption cross sections of gaseous HOBr, *J. Phys. Chem. A.*, *102*, 3293-3298, 1998.

Iraci, L.T., and M.A. Tolbert, Heterogeneous interaction of formaldehyde with cold sulfuric acid: Implications for the upper troposphere and lower stratosphere, *J. Geophys. Res.*, *102*, 16099-16107, 1997.

Iraci, L.T., T.J. Fortin, and M.A. Tolbert, Dissolution of sulfuric acid tetrahydrate at low temperatures and subsequent growth of nitric acid trihydrate, *J. Geophys. Res.*, *103*, 8491-8498, 1998.

Jackman, C.H., E.L. Fleming, S. Chandra, D.B. Considine, and J.E. Rosenfield, Past, present, and future modeled ozone trends with comparisons to observed trends, *J. Geophys. Res.*, *101*, 28753-28767, 1996.

Jaeglé, L., C.R. Webster, R.D. May, D.W. Fahey, E.L. Woodbridge, E.R. Keim, R.S. Gao, M.H. Proffitt, R.M. Stimpfle, R.J. Salawitch, S.C. Wofsy, and L. Pfister, In situ measurements of the $NO_2$/NO ratio for testing atmospheric photochemical models, *Geophys. Res. Lett.*, *21*, 2555-2558, 1994.

Jensen, E.J., and O.B. Toon, Ice nucleation in the upper troposphere: Sensitivity to aerosol number density, temperature and cooling rate, *Geophys. Res. Lett.*, *21*, 2019-2022, 1994.

Jensen, E.J., O.B. Toon, H.B. Selkirk, J.D. Spinhirne, and M.R. Schoeberl, On the formation and persistence of subvisible cirrus clouds near the tropical tropopause, *J. Geophys. Res.*, *101*, 21361-21375, 1996.

Johnson, D.G., W.A. Traub, K.V. Chance, and K.W. Jucks, Detection of HBr and upper limits for HOBr: Bromine partitioning in the stratosphere, *Geophys. Res. Lett.*, *22*, 1373-1376, 1995.

Jones, D.B.A., H.R. Schneider, and M.B. McElroy, Effects of the quasi-biennial oscillation on the zonally averaged transport of tracers, *J. Geophys. Res.*, *103*, 11235-11249, 1998.

Jones, P.W., K. Hamilton, and R.J. Wilson, A very high resolution general circulation model simulation of the global circulation in Austral winter, *J. Atmos. Sci.*, *54*, 1107-1116, 1997.

Jones, R.L., and J.L. Pyle, Observations of $CH_4$ and $N_2O$ by the Nimbus-7 SAMS: A comparison with in-situ data and two-dimensional numerical model calculations, *J. Geophys. Res.*, *89*, 5263-5279, 1984.

Juckes, M.N., and M.E. McIntyre, A high resolution, one-layer model of breaking planetary waves in the stratosphere, *Nature*, *328*, 590-596, 1987.

Jucks, K.W., D.G. Johnson, K.V. Chance, W.A. Traub, R.J. Salawitch, and R.A. Stachnik, Ozone production and loss rate measurements in the middle stratosphere, *J. Geophys. Res.*, *101*, 28785-28792, 1996.

Kawa, S.R., P.A. Newman, L.R. Lait, M.R. Schoeberl, R.M. Stimpfle, D.W. Kohn, C.R. Webster, R.D. May, D. Baumgardner, J.E. Dye, J.C. Wilson, K.R. Chan, and M. Loewenstein, Activation of chlorine in sulfate aerosol as inferred from aircraft observations, *J. Geophys. Res.*, *102*, 3921-3933, 1997.

Keim, E.R., D.W. Fahey, L.A. Del Negro, E.L. Woodbridge, R.S. Gao, P.O. Wennberg, R.C. Cohen, R.M. Stimpfle, K.K. Kelly, E.J. Hintsa, J.C. Wilson, H.H. Jonsson, J.E. Dye, D. Baumgardner, S.R. Kawa, R.J. Salawitch, M.H. Proffitt, M. Loewenstein, J.R. Podolske, and K.R. Chan, Observations of large reductions in the $NO/NO_y$ ratio near the mid-latitude tropopause and the role of heterogeneous chemistry, *Geophys. Res. Lett.*, *23*, 3223-3226, 1996.

Kelly, K.K., M.H. Proffitt, K.R. Chan, M. Loewenstein, J.R. Podolske, S.E. Strahan, J.C. Wilson, and D. Kley, Water vapor and cloud water measurements over Darwin during the STEP 1987 tropical mission, *J. Geophys. Res.*, *98*, 8713- 8723, 1993.

Kida, H., General circulation of air parcels and transport characteristics derived from a hemispheric GCM: Part 2, Very long-term motions of air parcels in the troposphere and stratosphere, *J. Meteorol. Soc. Japan*, *61*, 510-522, 1983.

Klassen, J., Z. Hu, and L.R. Williams, Diffusion coefficients for HCl and HBr in 30 wt % to 72 wt % sulfuric acid at temperatures between 220 and 300 K, *J. Geophys. Res.*, *103*, 16197-16202, 1998.

Knollenberg, R.G., K. Kelly, and J.C. Wilson, Measurements of high number densities of ice crystals in the tops of tropical cumulonimbus, *J. Geophys. Res.*, *98*, 8639-8664, 1993.

Knudsen, B.M., Accuracy of Arctic stratospheric temperature analyses and the implications for the prediction of polar stratospheric clouds, *Geophys. Res. Lett.*, *23*, 3747-3750, 1996.

Kolb, C.E., D.R. Worsnop, M.S. Zahniser, P. Davidovits, L.F. Keyser, M.-T. Leu, M.J. Molina, D.R. Hanson, A.R. Ravishankara, L.R. Williams, and M.A. Tolbert, Laboratory studies of atmospheric heterogeneous chemistry, Chapter 18 in *Progress and Problems in Atmospheric Chemistry*, edited by J.R. Barker, pp. 771-875, World Scientific Publishing, Singapore, 1995.

Kondo, Y., U. Schmidt, T. Sugita, P. Aimedieu, M. Koike, H. Ziereis, and Y. Iwasaka, Total reactive nitrogen, $N_2O$, and ozone in the winter Arctic stratosphere, *Geophys. Res. Lett.*, *21*, 1247-1250, 1994.

Kondo, Y., U. Schmidt, T. Sugita, A. Engel, M. Koike, P. Aimedieu, M.R. Gunson, and J. Rodriguez, $NO_2$ correlation with $N_2O$ and $CH_4$ in the midlatitude stratosphere, *Geophys. Res. Lett.*, *23*, 2369-2372, 1996.

Kondo, Y., T. Sugita, R.J. Salawitch, M. Koike, and T. Deshler, Effect of Pinatubo aerosols on stratospheric NO, *J. Geophys. Res.*, *102*, 1205-1213, 1997.

Koop, T., and K.S. Carslaw, Melting of $H_2SO_4{\cdot}4H_2O$ particles upon cooling: Implications for polar stratospheric clouds, *Science*, *272*, 1638-1641, 1996.

Koop, T., U.M. Biermann, W. Raber, B.P. Luo, P.J. Crutzen, and T. Peter, Do stratospheric aerosol droplets freeze above the ice frost point? *Geophys. Res. Lett.*, *22*, 917-920, 1995.

Koop, T., B.P. Luo, U.M. Biermann, P.J. Crutzen, and T. Peter, Freezing of $HNO_3/H_2SO_4/H_2O$ solutions at stratospheric temperatures: Nucleation statistics and experiments, *J. Phys. Chem. A.*, *101*, 1117-1133, 1997a.

Koop, T., K.S. Carslaw, and T. Peter, Thermodynamic stability of PSC particles, *Geophys. Res. Lett.*, *24*, 2199-2202, 1997b.

Kritz, M.A., S.W. Rosner, E.F. Danielsen, and H.B. Selkirk, Air mass origins and troposphere-to-stratosphere exchange associated with mid-latitude cyclogenesis and tropopause folding inferred from $Be^7$ measurements, *J. Geophys. Res.*, *96*, 17405-17414, 1991.

Kritz, M.A., S.W. Rosner, K.K. Kelly, M. Loewenstein, and K.R. Chan, Radon measurements in the lower tropical stratosphere: Evidence for rapid vertical transport and dehydration of tropospheric air, *J. Geophys. Res.*, *98*, 8725-8736, 1993.

Larichev, M., F. Maguin, G. LeBras, and G. Poulet, Kinetics and mechanism of the BrO + $HO_2$ reaction, *J. Phys. Chem.*, *99*, 15911-15918, 1995.

Larsen, N., B.M. Knudsen, J.M. Rosen, N.T. Kjome, R. Neuber, and E. Kyrö, Temperature histories in liquid and solid PSC formation, *J. Geophys. Res.*, *102*, 23505-23517, 1997.

Lary, D.J., M.P. Chipperfield, R. Toumi, and T. Lenton, Heterogeneous atmospheric bromine chemistry, *J. Geophys. Res.*, *101*, 1489-1504, 1996.

Lary, D.J., A.M. Lee, R. Toumi, M.J. Newchurch, M. Pirre, and J.B. Renard, Carbon aerosols and atmospheric photochemistry, *J. Geophys. Res.*, *102*, 3671-3682, 1997.

Lefèvre, F., G.P. Brasseur, I. Folkins, A.K. Smith, and P. Simon, Chemistry of the 1991-1992 stratospheric winter: Three-dimensional model simulations, *J. Geophys. Res.*, *99*, 8183-8195, 1994.

Li, Z., R.R. Friedl, and S.P. Sander, Kinetics of the $HO_2$ + BrO reaction over the temperature range 233-348 K, *J. Chem. Soc. Faraday Trans.*, *93*, 2683-2691, 1997.

Lindzen, R.S., Turbulence and stress due to gravity wave and tidal breakdown, *J. Geophys. Res.*, *86*, 9707-9714, 1981.

Lipson, J.B., M.J. Elrod, T.W. Beiderhase, L.T. Molina, and M.J. Molina, Temperature dependence of the rate constant and branching ratio for the OH + ClO reaction, *J. Chem. Soc. Faraday Trans.*, *93*, 2665-2673, 1997.

London, J., The observed distribution of atmospheric ozone and its variations, in *Ozone in the Free Atmosphere*, edited by R.C. Whitten and S.S. Prasad, pp. 11-80, Van Nostrand-Reinhold, Princeton, N. J., 1985.

Longfellow, C.A., T. Imamura, A.R. Ravishankara, and D.R. Hanson, HONO solubility and heterogeneous reactivity on sulfuric acid surfaces, *J. Phys. Chem. A.*, *102*, 3323-3332, 1998.

Lovejoy, E.R., and D.R. Hanson, Measurement of the kinetics of reactive uptake by submicron sulfuric acid particles, *J. Phys. Chem.*, *99*, 2080-2087, 1995.

Mackenzie, I.A., R.S. Harwood, L. Froidevaux, W.G. Read, and J.W. Waters, Chemical loss of polar vortex ozone inferred from UARS MLS measurements of ClO during the Arctic late winters of 1993, *J. Geophys. Res.*, *101*, 14505-14518, 1996.

Mahlman, J.D., H. Levy II, and W.J. Moxim, Three-dimensional simulations of stratospheric $N_2O$ predictions for other trace constituents, *J. Geophys. Res.*, *91*, 2687-2707, 1986.

Manney, G.L., L. Froidevaux, J.W. Waters, and R.W. Zurek, Evolution of Microwave Limb Sounder ozone and the polar vortex during winter, *J. Geophys. Res.*, *100*, 2953-2972, 1995a.

Manney, G.L., R.W. Zurek, L. Froidevaux, J.W. Waters, A. O'Neill, and R. Swinbank, Lagrangian transport calculations using UARS data: Part II, Ozone, *J. Atmos. Sci.*, *52*, 3069-3081, 1995b.

Manney, G.L., R. Swinbank, S.T. Massie, M.E. Gelman, A.J. Miller, R. Nagatani, A. O'Neill, and R.W. Zurek, Comparison of UK Meteorological Office and US National Meteorological Center stratospheric analyses during northern and southern winter, *J. Geophys. Res.*, *101*, 10311-10334, 1996.

Manney, G.L., L. Froidevaux, M.L. Santee, R.W. Zurek, and J.W. Waters, MLS observations of Arctic ozone loss in 1996-97, *Geophys. Res. Lett.*, *24*, 2697-2700, 1997.

Manzini, E., and L. Bengtsson, Stratospheric climate and variability from a general circulation model and observations, *Climate Dyn.*, *12*, 615-639, 1996.

Martin, S.C., D. Salcedo, L.T. Molina, and M.J. Molina, Deliquescence of sulfuric acid tetrahydrate following volcanic eruption or denitrification, *Geophys. Res. Lett.*, *25*, 31-34, 1998.

McIntyre, M.E., Middle atmosphere dynamics and transport: Some current challenges to our understanding, in *Dynamics, Transport and Photochemistry in the Middle Atmosphere of the Southern Hemisphere*, NATO Advanced Research Workshop, edited by A. O'Neill, pp. 1-18, Kluwer, Dordrecht, Holland, 1990.

McIntyre, M.E., The stratospheric polar vortex and subvortex: Fluid dynamics and midlatitude ozone loss, *Proc. R. Soc. London*, *A352*, 227-240, 1995.

McIntyre, M.E., and T.N. Palmer, Breaking planetary waves in the stratosphere, *Nature*, *305*, 593-600, 1983.

McKinney, K.A., J.M. Pierson, and D.W. Toohey, A wintertime in situ profile of BrO between 17 and 27 km in the Arctic vortex, *Geophys. Res. Lett.*, *24*, 853-856, 1997.

Medvedev, A.S., and G.P. Klaassen, Vertical evolution of gravity wave spectra and the parameterization of associated wave drag, *J. Geophys. Res.*, *100*, 25841-25853, 1995.

Meilinger, S.K., T. Koop, B.P. Luo, T. Huthwelker, K.S. Carslaw, P.J. Crutzen, and T. Peter, Size-dependent stratospheric droplet composition in lee wave temperature fluctuations and their potential role in PSC freezing, *Geophys. Res. Lett.*, *22*, 3031-3034, 1995.

Michelsen, H.A., R.J. Salawitch, M.R. Gunson, C. Aellig, N. Kampfer, M.M. Abbas, M.C. Abrams, T.L. Brown, A.Y. Chang, A. Goldman, F.W. Irion, M.J. Newchurch, C.P. Rinsland, G.P. Stiller, and R. Zander, Stratospheric chlorine partitioning: Constraints from shuttle-borne measurements of [HCl], [$ClNO_3$], and [ClO], *Geophys. Res. Lett.*, *23*, 2361-2364, 1996.

Mickley, L.J., J.P.D. Abbatt, J.E. Frederick, and J.M. Russell III, Response of summertime odd nitrogen and ozone at 17 mb to Mount Pinatubo aerosol over the southern mid-latitudes: Observations from HALOE, *J. Geophys. Res.*, *102*, 23573-23582, 1998.

Minschwaner, K., A.E. Dessler, J.W. Elkins, C.M. Volk, D.W. Fahey, M. Loewenstein, J.R. Podolske, A.E. Roche, and K.R. Chan, The bulk properties of isentropic mixing into the tropics in the lower stratosphere, *J. Geophys. Res.*, *101*, 9433-9439, 1996.

Moore, T.A., M. Okumura, M. Tagawa, and T.K. Minton, Dissociation dynamics of $ClONO_2$ and relative Cl and ClO product yields following photoexcitation at 308 nm, *Faraday Discuss. Chem. Soc.*, *100*, 295-307, 1995.

Morris, G.A., D.B. Considine, A.E. Dessler, S.R. Kawa, J. Kumer, J. Mergenthaler, A. Roche, and J.M. Russell III, Nitrogen partitioning in the middle stratosphere as observed by the Upper Atmosphere Research Satellite, *J. Geophys. Res.*, *102*, 8955-8965, 1997.

Mote, P.W., K.H. Rosenlof, M.E. McIntyre, E.S. Carr, J.C. Gille, J.R. Holton, J.S. Kinnersley, H.C. Pumphrey, J.M. Russell III, and J.W. Waters, An atmospheric tape recorder: The imprint of tropical tropopause temperatures on stratospheric water vapor, *J. Geophys. Res.*, *101*, 3989-4006, 1996.

Mote, P.W., T.J. Dunkerton, M.E. McIntyre, E.A. Ray, P.H. Haynes, and J.M. Russell III, Vertical velocity, vertical diffusion, and dilution by midlatitude air in the tropical lower stratosphere, *J. Geophys. Res.*, *103*, 8651-8666, 1998.

Müller, R., and T. Peter, The numerical modelling of the sedimentation of polar stratospheric cloud particles, *Ber. Bunsenges. Phys. Chem.*, *96*, 353-361, 1992.

Müller, R., P.J. Crutzen, J.-U. Grooß, C. Brühl, J.M. Russell, and A.F. Tuck, Chlorine activation and ozone depletion in the Arctic vortex: Observations by the Halogen Occultation Experiment on the Upper Atmosphere Research Satellite, *J. Geophys. Res.*, *101*, 12531-12554, 1996.

Müller, R., P.J. Crutzen, J.-U. Grooß, C. Brühl, J.M. Russell, H. Gernandt, D.S. McKenna, and A.F. Tuck, Severe chemical ozone loss in the Arctic during the winter 1995-96, *Nature*, *389*, 709-712, 1997.

Murphy, D.M., and D.W. Fahey, An estimate of the flux of stratospheric reactive nitrogen and ozone into the troposphere, *J. Geophys. Res.*, *99*, 5325-5332, 1994.

Murphy, D.M., and B.L. Gary, Mesoscale temperature fluctuations and polar stratospheric clouds, *J. Atmos. Sci.*, *52*, 1753-1760, 1995.

Murphy, D.M., and A.R. Ravishankara, Temperature averages and rates of stratospheric reactions, *Geophys. Res. Lett.*, *21*, 2471-2474, 1994.

Murphy, D.M., A.F. Tuck, K.K. Kelly, K.R. Chan, M. Loewenstein, J.R. Podolske, M.H. Proffitt, and S.E. Strahan, Indicators of transport and vertical motion from correlations between in-situ measurement in the airborne Antarctic ozone experiment, *J. Geophys. Res.*, *94*, 11669-11685, 1989.

Murphy, D.M., D.W. Fahey, M.H. Proffitt, S.C. Liu, K.R. Chan, C.S. Eubank, S.R. Kawa, and K.K. Kelly, Reactive nitrogen and its correlation with ozone in the lower stratosphere and upper troposphere, *J. Geophys. Res.*, *98*, 8751-8773, 1993.

Nevison, C.D., S. Solomon, R.R. Garcia, D.W. Fahey, E.R. Keim, M. Loewenstein, J.R. Podolske, R.S. Gao, R.C. Wamsley, S.G. Donnelly, and L.A. Del Negro, Influence of Antarctic denitrification on two-dimensional model $NO_y/N_2O$ correlations in the lower stratosphere, *J. Geophys. Res.*, *102*, 13183-13192, 1997.

Newchurch, M.J., M. Allen, M.R. Gunson, R.J. Salawitch, G.B. Collins, K.H. Huston, M.M. Abbas, M.C. Abrams, A.Y. Chang, D.W. Fahey, R.S. Gao, F.W. Irion, M. Loewenstein, G. Manney, H.A. Michelsen, J.R. Podolske, C.P. Rinsland, and R. Zander, Stratospheric NO and $NO_2$ abundances from ATMOS solar-occultation measurements, *Geophys. Res. Lett.*, *23*, 2373-2376, 1996.

Newell, R.E., and S. Gould-Stewart, A stratospheric fountain, *J. Atmos. Sci.*, *38*, 2789-2796, 1981.

Newman, P.A., L.R. Lait, M.R. Schoeberl, M. Seablom, L. Coy, R. Rood, R. Swinbank, M. Proffitt, M. Loewenstein, J.R. Podolske, J.W. Elkins, C.R. Webster, R.D. May, D.W. Fahey, G.S. Dutton, and K.R. Chan, Measurements of polar vortex air in the midlatitudes, *J. Geophys. Res.*, *101*, 12879-12891, 1996.

Newman, P.A., J.F. Gleason, R.D. McPeters, and R.S. Stolarski, Anomalously low ozone over the Arctic, *Geophys. Res. Lett.*, *24*, 2689-2692, 1997.

Ngan, K., and T.G. Shepherd, Comments on some recent measurements of anomalously steep $N_2O$ and $O_3$ tracer spectra in the stratospheric surf zone, *J. Geophys. Res.*, *102*, 24001-24004, 1997.

Nickolaisen, S.L., R.R. Friedl, and S.P. Sander, Kinetics and mechanism of the ClO + ClO reaction: Pressure and temperature dependences of the bimolecular and termolecular channels and thermal decomposition of chlorine peroxide, *J. Phys. Chem.*, *98*, 155-169, 1994.

Rinsland, C.P., M.R. Gunson, R.J. Salawitch, H.A. Michelsen, R. Zander, M.J. Newchurch, M.M. Abbas, M.C. Abrams, G.L. Manney, A.Y. Chang, F.W. Irion, A. Goldman, and E. Mahieu, ATMOS/ATLAS 3 measurements of stratospheric chlorine and reactive nitrogen partitioning inside and outside the November 1994 Antarctic vortex, *Geophys. Res. Lett.*, *23*, 2365-2368, 1996a.

Rinsland, C.P., M.R. Gunson, R.J. Salawitch, M.J. Newchurch, R. Zander, M.M. Abbas, M.C. Abrams, G.L. Manney, H.A. Michelsen, A.Y. Chang, and A. Goldman, ATMOS measurements of $H_2O + 2CH_4$ and total reactive nitrogen in the November 1994 Antarctic stratosphere: Dehydration and denitrification in the vortex, *Geophys. Res. Lett.*, *23*, 2397-2400, 1996b.

Robinson, G.D., The transport of minor atmospheric constituents between troposphere and stratosphere, *Quart. J. Roy. Meteorol. Soc.*, *106*, 227-254, 1980.

Robinson, G.N., D.R. Worsnop, J.T. Jayne, and C.E. Kolb, Heterogeneous uptake of $ClONO_2$ and $N_2O_5$ by sulfuric acid solutions, *J. Geophys. Res.*, *102*, 3583-3601, 1997.

Roche, A.E., J.B. Kumer, J.L. Mergenthaler, R.W. Nightingale, W.G. Uplinger, G.A. Ely, J.F. Potter, D.J. Wuebbles, P.S. Connell, and D.E. Kinnison, Observations of lower-stratospheric $ClONO_2$, $HNO_3$, and aerosol by the UARS CLAES experiment between January 1992 and April 1993, *J. Atmos. Sci.*, *51*, 2877-2902, 1994.

Rogaski, C.A., D.M. Golden, and L.R. Williams, Reactive uptake and hydration experiments on amorphous carbon treated with $NO_2$, $SO_2$, $O_3$, $HNO_3$, and $H_2SO_4$, *Geophys. Res. Lett.*, *24*, 381-384, 1997.

Rood, R.B., A.R. Douglass, J.A. Kaye, M.A. Geller, Y. Chi, D.J. Allen, E.M. Larson, E.R. Nash, and J.E. Nielsen, Three-dimensional simulations of wintertime ozone variability in the lower stratosphere, *J. Geophys. Res.*, *96*, 5055-5071, 1991.

Rosenfield, J.E., D.B. Considine, P.E. Meade, J.T. Bacmeister, C.H. Jackman, and M.R. Schoeberl, Stratospheric effects of Mount Pinatubo aerosol studied with a coupled two-dimensional model, *J. Geophys. Res.*, *102*, 3649-3670, 1997.

Rosenlof, K.H., Seasonal cycle of the residual mean meridional circulation in the stratosphere, *J. Geophys. Res.*, *100*, 5173-5191, 1995.

Rosenlof, K.H., A.F. Tuck, K.K. Kelly, J.M. Russell III, and M.P. McCormick, Hemispheric asymmetries in water vapor and inferences about transport in the lower stratosphere, *J. Geophys. Res.*, *102*, 13213-13234, 1997.

Rowley, D.M., M.H. Harwood, R.A. Freshwater, and R.L. Jones, A novel flash photolysis/UV absorption system employing charge-coupled device (CCD) detection: A study of the BrO + BrO reaction at 298 K, *J. Phys. Chem.*, *100*, 3020-3029, 1996.

Russell, J.M. III, C.B. Farmer, C.P. Rinsland, R. Zander, L. Froidevaux, G.C. Toon, B. Gao, J. Shaw, and M. Gunson, Measurements of odd nitrogen compounds in the stratosphere by the ATMOS experiment on Spacelab 3, *J. Geophys. Res.*, *93*, 1718-1736, 1988.

Russell, J.M. III, M. Luo, R.J. Cicerone, and L.E. Deaver, Satellite confirmation of the dominance of chlorofluorocarbons in the global stratospheric chlorine budget, *Nature*, *379*, 526-529, 1996.

Salawitch, R.J., S.C. Wofsy, E.W. Gottliev, L.R. Lait, P.A. Newman, M.R. Schoeberl, M. Loewenstein, J.R. Podolske, S.E. Strahan, M.H. Proffitt, C.R. Webster, R.D. May, D.W. Fahey, D. Baumgardner, J.E. Dye, J.C. Wilson, K.K. Kelly, J.W. Elkins, and J.G. Anderson, Chemical loss of ozone in the Arctic polar vortex in the winter of 1991-1992, *Science*, *261*, 1146-1149, 1993.

Salawitch, R.J., S.C. Wofsy, P.O. Wennberg, R.C. Cohen, J.G. Anderson, D.W. Fahey, R.S. Gao, E.R. Keim, E.L. Woodbridge, R.M. Stimpfle, J.P. Koplow, D.W. Kohn, C.R. Webster, R.D. May, L. Pfister, E.W. Gottlieb, H.A. Michelsen, G.K. Yue, M.J. Prather, J.C. Wilson, C.A. Brock, H.H. Jonsson, J.E. Dye, D. Baumgardner, M.H. Proffitt, M. Loewenstein, J.R. Podolske, J.W. Elkins, G.S. Dutton, E.J. Hintsa, A.E. Dessler, E.M. Weinstock, K.K. Kelly, K.A. Boering, B.C. Daube, K.R. Chan, and S.W. Bowen, The diurnal variation of hydrogen, nitrogen, and chlorine radicals: Implications for the heterogeneous production of $HNO_2$, *Geophys. Res. Lett.*, *21*, 2551-2554, 1994.

Sander, S.P., R.P. Friedl, and Y.L. Yung, Rate of formation of the ClO dimer in the polar stratosphere: Implications for ozone loss, *Science*, *245*, 1095-1098, 1989.

Santee, M.L., W.G. Read, J.W. Waters, L. Froidevaux, G.L. Manney, D.A. Flower, R.A. Jarnot, R.S. Harwood, and G.E. Peckham, Interhemispheric differences in polar stratospheric $HNO_3$, ClO, and $O_3$, *Science*, *267*, 849-852, 1995.

Schauffler, S.M., L.E. Heidt, W.H. Pollock, T.M. Gilpin, J.F. Vedder, S. Solomon, R.A. Lueb, and E.L. Atlas, Measurements of halogenated organic compounds near the tropical tropopause, *Geophys. Res. Lett.*, *20*, 2567-2570, 1993.

Schmidt, U., and A. Khedim, In situ measurements of carbon dioxide in the winter arctic vortex and at mid-latitudes: An indicator of the age of stratospheric air, *Geophys. Res. Lett.*, *18*, 763-766, 1991.

Schneider, H.R., M.K.W. Ko, and C.A. Peterson, Interannual variations of ozone: Interpretation of 4 years of satellite observations of total ozone, *J. Geophys. Res.*, *96*, 2889-2896, 1991.

Schoeberl, M.R., L.R. Lait, P.A. Newman, and J.E. Rosenfield, The structure of the polar vortex, *J. Geophys. Res.*, *97*, 7859-7882, 1992.

Schoeberl, M.R., A.E. Roche, J.M. Russell III, D. Ortland, P.B. Hays, and J.W. Waters, An estimation of the dynamical isolation of the tropical lower stratosphere using UARS wind and trace gas observations of the quasi-biennial oscillation, *Geophys. Res. Lett.*, *24*, 53-56, 1997.

Schoeberl, M.R., C.H. Jackman, and J.E. Rosenfield, A Lagrangian estimate of aircraft effluent lifetime, *J. Geophys. Res.*, *103*, 10817-10825, 1998.

Searle, K., M.P. Chipperfield, S. Bekki, and J.A. Pyle, The impact of spatial averaging on calculated polar ozone loss: 1. Model experiments, *J. Geophys. Res.*, *103*, 25397-25408, 1998a.

Searle, K., M.P. Chipperfield, S. Bekki, and J.A. Pyle, The impact of spatial averaging on calculated polar ozone loss: 2. Theoretical analysis, *J. Geophys. Res.*, *103*, 25409-25416, 1998b.

Seisel, S., and M.J. Rossi, The heterogeneous reaction of HONO and HBr on ice and on sulfuric acid, *Ber. Bunsenges. Phys. Chem.*, *101*, 943-955, 1997.

Selkirk, H.B., The tropopause cold trap in the Australian Monsoon during STEP/AMEX, *J. Geophys. Res.*, *98*, 8591-8610, 1993.

Sen, B., G.C. Toon, G.B. Osterman, J.F. Blavier, J.J. Margitan, R.J. Salawitch, and G.K. Yue, Measurements of reactive nitrogen in the stratosphere, *J. Geophys. Res.*, *103*, 3571-3585, 1998.

Shepherd, T.G., K. Semeniuk, and J.N. Koshyk, Sponge layer feedbacks in middle atmosphere models, *J. Geophys. Res.*, *101*, 23447- 23464, 1996.

Shindell, D.T., D. Rind, and P. Lonergan, Climate change and the middle atmosphere: Part IV, Ozone photochemical response to doubled $CO_2$, *J. Climate*, *11*, 895-918, 1998a.

Shindell, D.T., D. Rind, and P. Lonergan, Increased polar stratospheric ozone losses and delayed eventual recovery owing to increasing greenhouse-gas concentrations, *Nature*, *392*, 589-592, 1998b.

Silvente, E., R.C. Richter, M. Zheng, and A.J. Hynes, Relative quantum yields for $O(^1D)$ production in the photolysis of ozone between 301 and 336 nm: Evidence for the participation of a spin-forbidden channel, *Chem. Phys. Lett.*, *264*, 309-315, 1997.

Slusser, J.R., D.J. Fish, E.K. Strong, R.L. Jones, H.K. Roscoe, and A. Sarkissian, Five years of $NO_2$ vertical column measurements at Faraday (65°S): Evidence for the hydrolysis of $BrONO_2$ on Pinatubo aerosols, *J. Geophys. Res.*, *102*, 12987-12993, 1997.

Sobel, A., R.A. Plumb, and D.W. Waugh, On methods of calculating transport across the polar vortex edge, *J. Atmos. Sci.*, *25*, 2241-2260, 1997.

Solomon, S., R.R. Garcia, and A.R. Ravishankara, On the role of iodine in ozone depletion, *J. Geophys. Res.*, *99*, 20491-20499, 1994.

Solomon, S., R.W. Portmann, R.R. Garcia, L.W. Thomason, L.R. Poole, and M.P. McCormick, The role of aerosol trends and variability in anthropogenic ozone depletion at northern midlatitudes, *J. Geophys. Res.*, *101*, 6713-6727, 1996.

Solomon, S., S. Borrmann, R.R. Garcia, R. Portmann, L. Thomason, L.R. Poole, D. Winker, and M.P. McCormick, Heterogeneous chlorine chemistry in the tropopause region, *J. Geophys. Res.*, *102*, 21411-21429, 1997.

Solomon, S., R.W. Portmann, R.R. Garcia, W. Randel, R. Nagatani, J. Gleason, L. Thomason, L.R. Poole, and M.P. McCormick, Ozone depletion at mid-latitudes: Coupling of volcanic aerosols and temperature variability to anthropogenic chlorine, *Geophys. Res. Lett.*, *25*, 1871-1874, 1998.

Sparling, L.C., J.A. Kettleborough, P.H. Haynes, M.E. McIntyre, J.E. Rosenfield, M.R. Schoeberl, and P.A. Newman, Diabatic cross-isentropic dispersion in the lower stratosphere, *J. Geophys. Res.*, *102*, 25817-25829, 1997.

Sparling, L.C., A.R. Douglass, and M.R. Schoeberl, An estimate of the effect of unresolved structure on modeled ozone loss from aircraft observations of ClO, *Geophys. Res. Lett.*, *25*, 305-308, 1998.

Steil, B., M. Dameris, C. Brühl, P.J. Crutzen, V. Grewe, M. Ponater, and R. Sausen, Development of a chemistry module for GCMs: First results of a multiannual integration, *Ann. Geophys.*, *16*, 205-228, 1998.

Stimpfle, R.M., J.P. Koplow, R.C. Cohen, D.W. Kohn, P.O. Wennberg, D.M. Judah, D.W. Toohey, L.M. Avallone, J.G. Anderson, R.J. Salawitch, E.L. Woodbridge, C.R. Webster, R.D. May, M.H. Proffitt, K. Aiken, J.J. Margitan, M. Loewenstein, J.R. Podolske, L. Pfister, and K.R. Chan, The response of ClO radical concentrations to variations in $NO_2$ radical concentrations in the lower stratosphere, *Geophys. Res. Lett.*, *21*, 2543-2546, 1994.

Strahan, S.E., and J.D. Mahlman, Evaluation of the SKYHI general circulation model using aircraft $N_2O$ measurements: 2, Tracer variability and diabatic meridional circulation, *J. Geophys. Res.*, *99*, 10319-10332, 1994.

Swinbank, R., and A. O'Neill, A stratosphere-troposphere data assimilation system, *Mon. Weather Rev.*, *122*, 686-702, 1994.

Tabazadeh, A., and O.B. Toon, The presence of metastable $HNO_3/H_2O$ solid phases in the stratosphere inferred from ER-2 data, *J. Geophys. Res.*, *101*, 9071-9078, 1996.

Tabazadeh, A., R.P. Turco, K. Drdla, M.Z. Jacobson, and O.B. Toon, A study of type I polar stratospheric cloud formation, *Geophys. Res. Lett.*, *21*, 1619-1622, 1994.

Tabazadeh, A., O.B. Toon, and P. Hamill, Freezing behavior of stratospheric sulfate aerosols inferred from trajectory studies, *Geophys. Res. Lett.*, *22*, 1725-1728, 1995.

Takahashi, K., M. Kishigami, Y. Matsumi, M. Kawasaki, and A.J. Orr-Ewing, Observation of the spin-forbidden $O(^1D) + O_2(X^3\Sigma^-_g)$ channel in the 317-327 nm photolysis of ozone, *J. Chem. Phys.*, *105*, 5290-5293, 1996.

Takahashi, M., Simulation of the stratospheric quasi-biennial oscillation using a general circulation model, *Geophys. Res. Lett.*, *23*, 661-664, 1996.

Talukdar, R.K., C.A. Longfellow, M.K. Gilles, and A.R. Ravishankara, Quantum yield of $O(^1D)$ in the photolysis of ozone between 289 and 329 nm as a function of temperature, *Geophys. Res. Lett.*, *25*, 143-146, 1998.

Tan, D.G.H., P.H. Haynes, A.R. MacKenzie, and J.A. Pyle, The effects of fluid-dynamical stirring and mixing on the deactivation of stratospheric chlorine, *J. Geophys. Res.*, *103*, 1585-1605, 1998.

Teitelbaum, H., J. Moustaoui, J. Ovarlez, and H. Kelder, The role of atmospheric waves in the laminated structure of ozone profiles at high latitude, *Tellus*, *48A*, 442-455, 1996.

Thompson, D.W.J., and J.M. Wallace, Observed linkages between Eurasian surface air temperature, the North Atlantic Oscillation, Arctic sea level pressure, and the stratospheric polar vortex, *Geophys. Res. Lett.*, *25*, 1297-1300, 1998.

Thuburn, J., and D.G.H. Tan, A parameterization of mixdown time for atmospheric chemicals, *J. Geophys. Res.*, *102*, 13037-13049, 1997.

Tie, X.X., and G. Brasseur, The response of stratospheric ozone to volcanic eruptions: Sensitivity to atmospheric chlorine loading, *Geophys. Res. Lett.*, *22*, 3035-3038, 1995.

Tie, X., G.P. Brasseur, B. Briegleb, and C. Granier, Two-dimensional simulation of Pinatubo aerosol and its effect on stratospheric ozone, *J. Geophys. Res.*, *99*, 20545-20562, 1994.

Tie, X., C. Granier, W. Randel, and G.P. Brasseur, Effects of interannual variation of temperature on heterogeneous reactions and stratospheric ozone, *J. Geophys. Res.*, *102*, 23519-23527, 1997.

Toon, G.C., C.B. Farmer, L.L. Lowes, P.W. Schaper, J.F. Blavier, and R.H. Norton, Infrared aircraft measurements of stratospheric composition over Antarctica during September 1987, *J. Geophys. Res.*, *94*, 16571-16596, 1989a.

Toon, O.B., R.P. Turco, J. Jordan, J. Goodman, and G. Ferry, Physical processes in polar stratospheric ice clouds, *J. Geophys. Res.*, *94*, 11359-11380, 1989b.

Toon, O.B., E.V. Browell, S. Kinne, and J. Jordan, An analysis of Lidar observations of polar stratospheric clouds, *Geophys. Res. Lett.*, *17*, 393-396, 1990.

Tsias, A., A.J. Prenni, K.S. Carslaw, T.P. Onasch, B.P. Luo, A.A. Tolbert, and T. Peter, Freezing of polar stratospheric clouds in orographically induced strong warming events, *Geophys. Res. Lett.*, *24*, 2303-2306, 1997.

Tsuda, T., Y. Murayama, H. Wiryosumarto, S.W.B. Harijono, and S. Kato, Radiosonde observations of equatorial atmospheric dynamics over Indonesia: 1, Equatorial waves and diurnal tides, *J. Geophys. Res.*, *99*, 10491-10506, 1994.

Tuck, A.F., A comparison of one-, two-, and three-dimensional model representations of stratospheric gases, *Phil. Trans. R. Soc. London A*, *2909*, 477-494, 1979.

Tuck, A.F., Synoptic and chemical evolution of the Antarctic vortex in late winter and early spring, *J. Geophys. Res.*, *94*, 11687-11737, 1989.

Tuck, A.F., T. Davies, S.J. Hovde, M. Noguer-Alba, D.W. Fahey, S.R. Kawa, K.K. Kelly, D.M. Murphy, M.R. Proffitt, J.J. Margitan, M. Loewenstein, J.R. Podolske, S.E. Strahan, and K.R. Chan, Polar stratospheric cloud processed air and potential vorticity in the Northern Hemisphere lower stratosphere at mid-latitudes during winter, *J. Geophys. Res.*, *97*, 7883-7904, 1992.

Tuck, A.F., D. Baumgardner, K.R. Chan, J.E. Dye, J.W. Elkins, S.J. Hovde, K.K. Kelly, M. Loewenstein, J.J. Margitan, R.D. May, J.R. Podolske, M.H. Proffitt, K.H. Rosenlof, W.L. Smith, C.R. Webster, and J.C. Wilson, The Brewer-Dobson circulation in light of high altitude in situ aircraft observations, *Quart. J. Roy. Meteorol. Soc.*, *123*, 1-71, 1997.

Tung, K.K., and H. Yang, Global QBO in circulation and ozone: Part I, Reexamination of observational evidence, *J. Atmos. Sci.*, *51*, 2699-2707, 1994.

Turnipseed, A.A., M.K. Gilles, J.B. Burkholder, and A.R. Ravishankara, Kinetics of the IO radical: 1, Reaction of IO with ClO, *J. Phys. Chem. A.*, *101*, 5517-5525, 1997.

Tyndall, G.S., C.S. Kegley-Owen, J.J. Orlando, and J.G. Calvert, Quantum yield for $Cl(^2P)$, ClO, and $O(^3P)$ in the photolysis of chlorine nitrate at 308 nm, *Faraday Trans. Chem. Soc.*, *93*, 2675-2682, 1997.

Vaughan, G., and C. Timmis, Transport of tropospheric air into the lower midlatitude stratosphere, *Quart. J. Roy. Meteorol. Soc.*, *124*, 1559-1578, 1998.

Vohralik, P.F., L.K. Randeniya, I.C. Plumb, and K.R. Ryan, Use of correlations between long-lived atmospheric species in assessment studies, *J. Geophys. Res.*, *103*, 3611-3627, 1998.

Volk, C.M., J.W. Elkins, D.W. Fahey, R.J. Salawitch, G.S. Dutton, J.M. Gilligan, M.H. Proffitt, M. Loewenstein, J.R. Podolske, K. Minschwaner, J.J. Margitan, and K.R. Chan, Quantifying transport between the tropical and mid-latitude lower stratosphere, *Science*, *272*, 1763-1768, 1996.

Volk, C.M., J.W. Elkins, D.W. Fahey, G.S. Dutton, J.M. Gilligan, M. Loewenstein, J.R. Podolske, and K.R. Chan, On the evaluation of source gas lifetimes from stratospheric observations, *J. Geophys. Res.*, *102*, 25543-25564, 1997.

von Clarmann, T., G. Wetzel, H. Oelhaf, F. Friedl-Vallon, A. Linden, G. Maucher, M. Seefeldner, O. Trieschmann, and F. Lefèvre, $ClONO_2$ vertical profile and estimated mixing ratios of ClO and HOCl in winter Arctic stratosphere from Michelson interferometer for passive atmospheric sounding limb emission spectra, *J. Geophys. Res.*, *102*, 16157-16168, 1997.

von der Gathen, P., M. Rex, N.R.P. Harris, D. Lucic, B.M. Knudsen, G.O. Braathen, H. DeBacker, R. Fabian, H. Fast, M. Gil, E. Kyrö, R.M. Mikkelsen, J. Stahelin, and C. Varotsos, Observational evidence for chemical ozone depletion over the Arctic in winter 1991-92, *Nature*, *375*, 131-134, 1995.

Wamsley, P.R., J.W. Elkins, D.W. Fahey, and G.S. Dutton, Distribution of halon-1211 in the upper troposphere and lower stratosphere and the 1994 total bromine budget, *J. Geophys. Res.*, *103*, 1513-1526, 1998.

Wang, P.H., M.P. McCormick, L.R. Poole, W.P. Chu, G.K. Yue, G.S. Kent, and K.M. Skeens, Tropical high cloud characteristics derived from SAGE II extinction measurements, *Atmos. Res.*, *34*, 53-83, 1994.

Waters, J.W., G.L. Manney, W.G. Read, L. Froidevaux, D.A. Flower, and R.F. Jarnot, UARS MLS observations of lower stratospheric ClO in the 1992-93 and 1993-94 winter vortices, *Geophys. Res. Lett.*, *22*, 823-826, 1995.

Wauben, W.M.F., R. Bintanja, P.F.J. van Velthoven, and H. Kelder, On the magnitude of transport out of the Antarctic polar vortex, *J. Geophys. Res.*, *102*, 1229-1238, 1997.

Waugh, D.W., Seasonal variation of isentropic transport out of the tropical stratosphere, *J. Geophys. Res.*, *101*, 4007-4023, 1996.

Waugh, D.W., R.A. Plumb, R.J. Atkinson, M.R. Schoeberl, L.R. Lait, P.A. Newman, M. Loewenstein, D.W. Toohey, L.M. Avallone, C.R. Webster, and R.D. May, Transport of material out of the stratospheric Arctic vortex by Rossby wave breaking, *J. Geophys. Res.*, *99*, 1071-1078, 1994.

Waugh, D.W., R.A. Plumb, D.W. Fahey, K.A. Boering, G.S. Dutton, E. Keim, R.S. Gao, B.C. Daube, S.C. Wofsy, M. Loewenstein, J.R. Podolske, K.R. Chan, M.H. Proffitt, K.K. Kelly, P.A. Newman, and L.R. Lait, Mixing of polar air into middle latitudes as revealed by tracer-tracer scatter plots, *J. Geophys. Res.*, *102*, 13119-13134, 1997a.

Waugh, D.W., T.M. Hall, W.J. Randel, K.A. Boering, S.C. Wofsy, B.C. Daube, J.W. Elkins, D.W. Fahey, G.S. Dutton, C.M. Volk, and P. Vohralik, Three-dimensional simulations of long-lived tracers using winds from MACCM2, *J. Geophys. Res.*, *102*, 21493-21513, 1997b.

Weaver, C.J., A.R. Douglass, and R.B. Rood, Thermodynamic balance of three-dimensional stratospheric winds derived from a data assimilation procedure, *J. Atmos. Sci.*, *50*, 2987-2993, 1993.

Weaver, C.J., A.R. Douglass, and D.B. Considine, A 5 year simulation of supersonic aircraft emission transport using a three-dimensional model, *J. Geophys. Res.*, *101*, 20975-20984, 1996.

Webster, C.R., R.D. May, L. Jaeglé, H. Hu, S.P. Sander, M.R. Gunson, G.C. Toon, J.M. Russell III, R.M. Stimpfle, J.P. Koplow, R.J. Salawitch, and H.A. Michelsen, Hydrochloric acid and the chlorine budget of the lower stratosphere, *Geophys. Res. Lett.*, *21*, 2575-2578, 1994.

Weinstock, E.M., E.J. Hintsa, A.E. Dessler, and J.G. Anderson, Measurements of water vapor in the tropical lower stratosphere during the CEPEX campaign: Results and interpretation, *Geophys. Res. Lett.*, *22*, 3231-3234, 1995.

Wennberg, P.O., R.C. Cohen, R.M. Stimpfle, J.P. Koplow, J.G. Anderson, R.J. Salawitch, D.W. Fahey, E.L. Woodbridge, E.R. Keim, R.S. Gao, C.R. Webster, R.D. May, D.W. Toohey, L.M. Avallone, M.H. Proffitt, M. Loewenstein, J.R. Podolske, K.R. Chan, and S.C. Wofsy, Removal of stratospheric $O_3$ by radicals: In situ measurements of OH, $HO_2$, NO, $NO_2$, ClO, and BrO, *Science*, *266*, 398-404, 1994.

Wennberg, P.O., T.F. Hanisco, R.C. Cohen, R.M. Stimpfle, L.B. Lapson, and J.G. Anderson, In situ measurements of OH and $HO_2$ in the upper troposphere and stratosphere, *J. Atmos. Sci.*, *52*, 3413-3420, 1995.

Wennberg, P.O., J.W. Brault, T.F. Hanisco, R.J. Salawitch, and G.H. Mount, Atmospheric column abundance of IO: Implications for stratospheric ozone, *J. Geophys. Res.*, *102*, 8887-8898, 1997.

Williams, L.R., and F.S. Long, Viscosity of supercooled sulfuric acid solutions, *J. Phys. Chem*, *99*, 3748-3751, 1995.

WMO (World Meteorological Organization), *Scientific Assessment of Ozone Depletion: 1994*, Global Ozone Research and Monitoring Project—Report No. 37, Geneva, 1995.

Wofsy, S.C., R.J. Salawitch, J.H. Yatteau, M.B. McElroy, B.W. Gandrud, J.E. Dye, and D. Baumgardner, Condensation of $HNO_3$ on falling ice particles: Mechanism for denitrification of the polar stratosphere, *Geophys. Res. Lett.*, *17*, 449-452, 1990.

Woodman, R.F., and P.K. Rastogi, Evaluation of effective eddy diffusive coefficients using radar observations of turbulence in the stratosphere, *Geophys. Res. Lett.*, *11*, 243-246, 1984.

Wyslouzil, B.E., K.L. Carleton, D.M. Sonnenfroh, W.T. Rawlins, and S. Arnold, Observation of hydration of single, modified carbon aerosols, *Geophys. Res. Lett.*, *21*, 2107-2110, 1994.

Yokelson, R.J., J.B. Burkholder, and A.R. Ravishankara, Photodissociation of $ClONO_2$: 2, Time-resolved absorption studies of product quantum yields, *J. Phys. Chem. A.*, *101*, 6667-6678, 1997.

Yulaeva, E., J.R. Holton, and J.M. Wallace, On the cause of the annual cycle in tropical lower stratospheric temperatures, *J. Atmos. Sci.*, *51*, 169-174, 1994.

Zhang, R., M.T. Leu, and L.F. Keyser, Hydrolysis of $N_2O_5$ and $ClONO_2$ on the $H_2SO_4/HNO_3/H_2O$ ternary solutions under stratospheric conditions, *Geophys. Res. Lett.*, *22*, 1493-1496, 1995.

Zhang, R., M.T. Leu, and M.J. Molina, Formation of polar stratospheric clouds on preactivated background aerosols, *Geophys. Res. Lett.*, *23*, 1669-1672, 1996.

Zhang, R., M.T. Leu, and L.F. Keyser, Heterogeneous chemistry of $HO_2NO_2$ in liquid sulfuric acid, *J. Phys. Chem. A.*, *101*, 3324-3330, 1997.

Zondlo, M.A., S.B. Barone, and M.A. Tolbert, Uptake of $HNO_3$ on ice under upper tropospheric conditions, *Geophys. Res. Lett.*, *24*, 1391-1394, 1997.

# CHAPTER 8

# Tropospheric Ozone and Related Processes

**Lead Authors:**
J. Lelieveld
A.M. Thompson

**Coauthors:**
R.D. Diab
Ø. Hov
D. Kley
J.A. Logan
O.J. Nielsen
W.R. Stockwell
X. Zhou

**Contributors:**
R. Guicherit
D.J. Jacob
M. Kuhn
J.B. Milford
H. Sidebottom
J. Stähelin

## SCIENTIFIC SUMMARY

A concerted effort continues in the deduction of trends in tropospheric ozone from the sparse in situ record. Trends are reported regionally or at stations where monitoring is conducted. Surface ozone increases, typically observed in Northern Hemisphere midlatitudes, have slowed considerably in the past decade. At the South Pole, there continues to be a decrease in surface ozone associated with the Antarctic lower stratospheric ozone depletion.

- Since the 1994 Assessment (WMO, 1995), a thorough evaluation of tropospheric ozone profiles can be summarized as follows:

  - Midlatitude: Three stations over Europe, which have had the greatest increases in free tropospheric ozone since 1970, show a major change in trends since 1980. Only Payerne shows an increase during the period 1980-1996; Uccle shows no change and Hohenpeissenberg a statistically marginal decrease. The two U.S. stations with regular ozonesonde launches (Wallops Island and Boulder) also show no significant change or a slight decrease since 1980. Of three Japanese stations, two show increases of 5-15%/decade, though not all significant; one station shows no trend. Canadian stations show a small decrease in free tropospheric ozone since 1980.

  - Tropics and Southern Hemisphere: There is only one tropical site with sufficient data for trends: Natal, Brazil, shows a 10-20%/decade increase only in the middle troposphere and possibly not significant; the record becomes too sparse for trends after 1992. There is no trend in free tropospheric ozone at Lauder, New Zealand, where the record began in 1986.

- Observations of ozone and other photochemically reactive species during field campaigns have been made with greater focus on understanding the interaction of chemistry and dynamics on local scales. Processes affecting reactive nitrogen species have been elucidated on several intensive campaigns. The free tropospheric nitric oxide (NO) and total reactive nitrogen climatology has been extended in aircraft campaigns in both Northern and Southern Hemispheres. Systematic sampling has extended the NO database along commercial aviation routes. Continental outflow downwind of industrial activity in Northern Hemisphere midlatitudes strongly enhances ozone budgets over large regions of the North Atlantic and North Pacific. Measurement campaigns in the tropics and subtropics show continental influences from long-range transport of biomass-burning emissions, although NO from lightning may also play a significant role in the tropical ozone budget.

  - Reliable instrumentation for hydroxyl radicals (OH), hydroperoxyl radicals ($HO_2$), and organic peroxyl radicals ($RO_2$) has been a breakthrough development since the last Assessment. Intercomparisons on the ground, and model interpretation of ground-based and airborne OH and related measurements show that our theoretical understanding of OH is not complete. With the constraint of ancillary measurements, it can be shown that data-model discrepancies tend to be greatest under polluted conditions and that odd hydrogen ($HO_x$) sinks, rather than sources, are probably not accounted for. In the upper troposphere, under certain conditions, acetone and the recycling of peroxides following deep convective transport appear to be important $HO_x$ sources. On a global scale, inferences about the total OH budget range from no trend in the past decade to a slightly positive trend.

  - Model intercomparisons and uncertainty studies show that photolysis rates, representations of stratospheric-tropospheric exchange, and imprecise pathways in organic oxidation chains continue to limit the reliability of models used in interpretive ozone studies and predictions. Models continue to suggest intriguing possibilities for heterogeneous and multiphase reactions affecting ozone in a major way, but experimental confirmation is lacking for the most part.

**Table 8-1. Estimated emissions of ozone precursors.** Best estimates are listed, with ranges given in parentheses.

| Sources | $CH_4$ (Tg/yr) | CO (Tg/yr) | NMHC (Tg C/yr) | $NO_x$ (Tg N/yr) |
|---|---|---|---|---|
| Energy use | 110 (65-155) | 500 (300-900) | 70 (60-100) | 22 (20-24) |
| Aircraft | | | | 0.5 (0.2-1) |
| Biomass burning | 40 (10-70) | 500 (400-700) | 40 (30-90) | 8 (3-13) |
| Vegetation | | 100 (60-160) | 400 (230-1150) | |
| Soils | | | | 7 (5-12) |
| Lightning | | | | 5 (2-20) |
| Ruminants | 85 (60-105) | | | |
| Rice paddies | 80 (30-120) | | | |
| Animal wastes | 30 (15-45) | | | |
| Landfills | 40 (20-60) | | | |
| $NH_3$ oxidation | | | | 0.9 (0-1.6) |
| $N_2O$ breakdown* | | | | 0.6 (0.4-1) |
| Domestic sewage | 25 (20-30) | | | |
| Wetlands | 145 (115-175) | | | |
| Oceans | 10 (5-15) | 50 (20-200) | 50 (20-150) | |
| Freshwaters | 5 (1-10) | | | |
| $CH_4$ hydrates | 10 (5-15) | | | |
| Termites | 20 (1-40) | | | |
| **Total** | **600** (520-680) | **1150** (780-1960) | **560** (340-1490) | **44** (30-73) |

* $NO_y$ produced in the stratosphere and transported to the troposphere.

coarse resolution (typically >100 km); Mahlman (1997) suggests that higher resolution models are required.

## 8.2 OZONE TRENDS

This section is an update on tropospheric ozone trends since the previous Assessment (WMO, 1995, Chapters 5 and 7). It begins with an update on budgets of two ozone precursors, $NO_x$ and NMHC; trends in the other important $O_3$ precursors, methane and CO, are covered in Chapter 2 (Section 2.5). Because tropospheric ozone is not measured globally by satellite, except in limited regions, the amount of data available for trends analysis is limited to surface monitoring sites and a few stations where ozonesonde launches have been of consistent frequency and quality for deduction of trends.

### 8.2.1 Ozone Precursor Trends

#### 8.2.1.1 Nitrogen Oxides

Estimates of nitrogen oxide emissions have recently been assessed by Benkovitz *et al.* (1996) and Lee *et al.* (1997a). Yienger and Levy (1995) estimated soil nitric oxide (NO) emissions and concluded that anthropogenic land-use significantly enhances the natural emissions. It appears that in the tropics, soil emissions (5-12 Tg N/yr) account for more than 50% of the tropospheric $NO_x$ budget. The natural $NO_x$ source from lightning has been reevaluated and is almost certainly less than 20 Tg N/yr and probably less than 10 Tg N/yr (Lawrence *et al.*, 1995; Price *et al.*, 1997). In constructing a global monthly climatology of lightning $NO_x$, Price *et al.* (1997) found that the main uncertainties in quantifying the lightning $NO_x$ source are related to the energy densities in lightning strokes, the $NO_x$ production per unit energy, and the global extrapolation of these highly variable processes.

Biomass burning constitutes an important anthropogenic $NO_x$ source in the tropics and subtropics of the Americas, Africa, and southern Asia, contributing 3-13 Tg N/yr. The relatively large uncertainty range is mostly due to the limited information available about the amount of biomass burned in forest and savanna fires and the nitrogen content of the fuel. In comparison with

fossil fuel combustion, biomass burning occurs at much lower temperatures, so that $NO_x$ production from $N_2$ and $O_2$ conversion is much less efficient. Most biomass-burning $NO_x$ results from organic nitrogen transformation while a substantial part of the emissions occur as reduced nitrogen species (Lobert *et al.*, 1991).

The dominant contemporary source of $NO_x$ to the atmosphere is fossil fuel combustion (Table 8-1). However, some national emission inventories have uncertainties as large as 50%. Nevertheless, there is no doubt that in the U.S. (EPA, 1996) and Europe (Veldt, 1985) anthropogenic emissions of $NO_x$ and NMHC in both regions were very much lower in the beginning of this century than at present. Emissions in the U.S. increased from about 0.75 Tg N in 1900 to about 6 Tg N at present. In discussing recent trends in $NO_x$, it is useful to separate emissions from fossil fuel combustion in the boundary layer ("surface" sources) and from aircraft. Surface emissions of $NO_x$ increased by 20% from 1970 to 1980 in the United States and by 27% in Western Europe, and remained approximately constant up to 1990, as reviewed by Logan (1994). U.S. emissions stayed constant until 1994, then decreased by 9% in 1995 (EPA, 1996). Comparison of the CORINAIR (COre INventories AIR) inventories for 1990 and 1994 indicates that emissions in western Europe (16 countries including eastern Germany in 1990) decreased by 8% from 1990 to 1994. The countries with the largest emissions trends were: Germany, -25%; United Kingdom, -14%; France and Spain, +6%. It is likely that emissions in most of eastern Europe have declined since 1990, because of the decline in fossil fuel consumption, 28% from 1990 to 1994 (Marland and Boden, 1997). The only location with a substantial increase in $NO_x$ emissions in the Northern Hemisphere is Asia, about 4%/yr from 1985 to 1987 (Kato and Akimoto, 1992). The largest contribution to Asian emissions is that of China. Here emissions are unregulated and should parallel growth in fossil fuel combustion, ~7%/yr from 1990 to 1994. Emissions from China increased from 1.5 Tg N/yr in 1980 (Kato and Akimoto, 1992) to 3.1 Tg N/yr in 1994, based on fossil fuel growth statistics given by Marland and Boden (1997). During the same period, U.S. emissions remained constant at 6.3 Tg N/yr (EPA, 1996), and the U.S. contributed 30% to the global emissions of $NO_x$ from fossil fuel combustion in 1985, 21 Tg N, 90% of which are in the Northern Hemisphere (Benkovitz *et al.*, 1996).

Emissions of $NO_x$ from aircraft have increased significantly since 1970 and continue to increase. Emissions of $NO_x$ from aircraft were 0.30 Tg N in 1976, 0.39 Tg in 1984, and 0.51 Tg in 1992, and are projected to be 1.26 Tg in 2015 (S. Baughcum, Boeing Company, U.S., personal communication, 1998). Slightly over half of the aircraft emissions take place between 9 and 13 km in the Northern Hemisphere (Baughcum *et al.*, 1996). There were regional differences in the increase in jet fuel consumption in the 1970s, 17% in the U.S. and 55% in western Europe, while the use increased about 35% in both regions in the 1980s (Logan, 1994). A significant fraction of the emissions are injected into the stratosphere in winter and spring, but in summer almost all emissions take place in the troposphere.

The growth of civil aviation is expected to continue (BAe/Airbus, 1995; Boeing, 1997) as quoted in Brasseur *et al.* (1998), although the rates of growth are slowing with time (15% in the 1970s, 9% in the 1980s, to an estimated 5% from 2000-2015). Growth rates are predicted to vary significantly for the different regions of the world. The differences in the average growth rates between the two forecasts are small compared to actual growth during this period: 225% (Airbus) or 270% (Boeing). Aviation consumes 2.3% of the fossil fuels used worldwide, of which about 80% is consumed by civil aviation. As a consequence of the improvements in engine and aircraft fuel efficiencies, the fuel increase is 70-80% of the traffic increase. Military aircraft have traditionally used about 20% of the aviation fuel. With the reduction in military activity, less aviation fuel is used for this purpose, but it is difficult to predict future consumption levels due to a lack of fixed operational practices and flight patterns and because of national security.

Two comprehensive inventories, Abatement of Nuisance Caused by Air Traffic/European Commission (ANCAT/EC) and National Aeronautics and Space Administration (NASA), have been developed in recent years and are widely used by atmospheric modelers. Both incorporate an extensive air traffic movements database, assumptions about flight operations, and a methodology for prediction of emissions over the entire flight. Comparisons of the fuel and $NO_x$ data, from the initial inventories of the two groups (Gardner *et al.*, 1995; Wuebbles *et al.*, 1993), showed significant differences that have been reported elsewhere (WMO, 1995). Recent revisions result in considerably closer agreement (Gardner *et al.*, 1997; Baughcum *et al.*, 1996; Metwally, 1995).

### 8.2.3 Ozone Trends above the Surface

Measurements of the vertical distribution of ozone have been made with ozonesondes for about 30 years. The majority of sonde stations are located at middle and high latitudes of the Northern Hemisphere. Shorter time series are available for a few stations in the subtropics, tropics, and Southern Hemisphere. The primary source of results used here is analysis of ozone trends (WMO, 1998) sponsored by SPARC (Stratospheric Processes and Their Role in Climate) and the IOC (International Ozone Commission), discussed in Chapter 4. The latter report gives a detailed discussion of the quality of ozonesonde data. As part of the SPARC/IOC study, ozonesonde data were reevaluated and reprocessed by those responsible for the individual programs for the stations for which trends were analyzed, with the exception of the data for Wallops Island and Canada. The latter data were obtained from the World Ozone and Ultraviolet Data Centre (WOUDC), and the Canadian data are described by Tarasick *et al.* (1995).

Two groups carried out independent trend analyses of the sonde data, Logan and Megretskaia of Harvard University (LM), and Taio, Choi, and Zhang of the

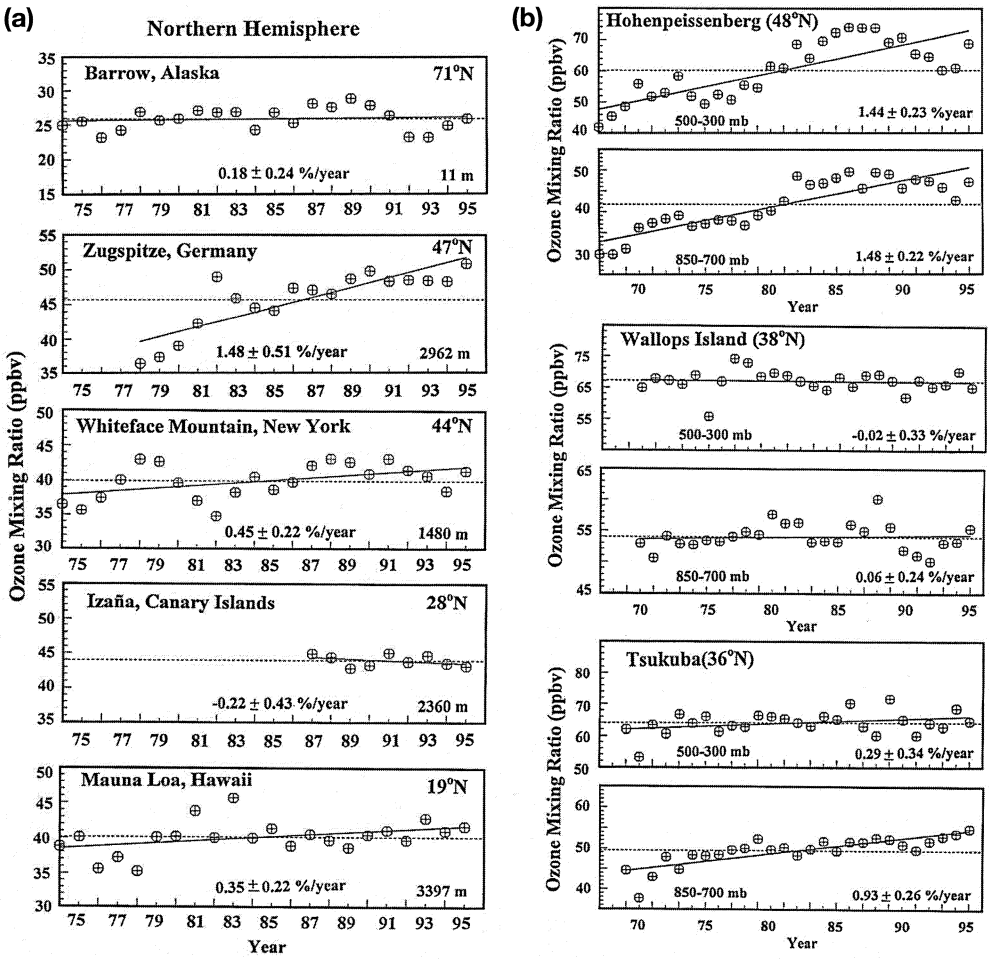


**Figure 8-1.** Panel (a): Annual average ozone mixing ratios (ppbv) for surface ozone measuring sites. The dashed line is the long-term average. The solid line is the linear least squares fit to the monthly anomalies. The linear trend and 95% confidence interval in percent per year is given with the plot for each location. (From Oltmans *et al.*, 1998.) Panel (b): Annual average ozone mixing ratios and trends from ozonesonde data for two layers in the troposphere (850-700 hPa and 500-300 hPa) at Hohenpeissenberg, Tsukuba (Tateno), and Wallops Island. (From Oltmans *et al.*, 1998.)

University of Chicago (TCZ). Trends were calculated by both groups for the period 1970-1996 and by one group (LM) also for 1980-1996. The two groups used different data selection criteria and different statistical models, as discussed in WMO (1998). They derive similar trends, however, and most of the differences are ascribed to the data selection criteria rather than to the statistical models. The trends are generally in reasonable agreement with results published earlier for somewhat shorter time periods by Logan (1994), Miller *et al.* (1995), Tarasick *et al.* (1995), Akimoto *et al.* (1994), Harris *et al.* (1997), Bojkov and Fioletov (1997), and Oltmans *et al.* (1998).

Trends in tropospheric ozone derived by the two groups are shown in Figure 4-36 of Chapter 4 of this Assessment. The most obvious feature of this figure is that there are significant spatial variations in the magnitude and sign of the tropospheric trends. The largest increases, 5-25%/decade for 1970-1996, are found over Europe (Hohenpeissenberg, Payerne, and Uccle) and extend from the surface to 300 mb. Bojkov and Fioletov (1997) analyzed trends relative to the tropopause location and found that the increase at Hohenpeissenberg is significant up to 1 km below the tropopause (which is located between 200 and 250 mb). Data from Japan show increases in ozone for 1970-1996 of 5-15%/decade, primarily below 500 mb; only Kagoshima shows an increase at 300 mb (Figure 8-2), which is well below the tropopause at this sub-tropical station. There is no evidence for such large increases over North America, as emphasized in WMO (1995). In the eastern U.S. (Wallops Island), the increase is less than 5%/decade. There has been no increase in ozone over Canada for 1970-1996, with some evidence for a decrease; however, the Canadian data prior to 1980 is of low quality (WMO, 1998). The trends shown in Figure 4-36 derived by TCZ are less negative for the Canadian stations, more positive for the European stations and Wallops Island, and about the same for the Japanese stations, compared to those derived by LM. Part of this difference is caused by TCZ referencing the trend to ozone in 1970, and LM referencing the trend to the mean of the time series. Results from both groups for the tropospheric column trends in Dobson units (DU)/decade are in close agreement (WMO, 1998). Oltmans *et al.* (1998) report an increase of 15%/decade for Hohenpeissenberg for 1968-1995. They also find no trend at Wallops Island and results very similar to those in Figure 4-36 for Tateno (called Tsukuba in Figure 8-1). They analyzed only these three stations, selected for the consistency of their record, and used the data at WOUDC.

There is a major change in trends for the period 1980-1996 compared to 1970-1996 in Europe, as shown in Figure 8-2. There is no significant trend for Uccle and a marginally significant decrease for Hohenpeissenberg in the middle troposphere for 1980-1996: only Payerne shows an increase, of about 10%/decade. There are concerns about the consistency of the tropospheric data for Payerne in the 1980s (WMO, 1998). The trends for the later period are smaller because the increases in ozone occurred primarily before 1985, and ozone values have not increased significantly since then, as shown in Figure 8-2. Two of the Japanese stations have increases of 5-15%/decade, not all of which are significant, while Tateno, with the best data record of the three stations, shows no trend in ozone. The Canadian stations show decreases of 2 to 8%/decade, and these are more reliable than the results for 1970-1996 because electrochemical concentration cell (ECC) sondes were used exclusively after 1980. Previous analyses of the Canadian ECC data also showed decreases (Logan, 1994; Tarasick *et al.*, 1995; Oltmans *et al.*, 1998). In the U.S., Wallops Island shows no significant trend, and Boulder shows a decrease of 5% /decade in the mid-troposphere since 1980. There is no significant trend in the middle troposphere at Hilo, Hawaii, since 1982, or in Lauder, New Zealand, since 1986. Oltmans *et al.* (1998) find no significant trend in ozone for Hohenpeissenberg, Boulder, Wallops Island, Tateno, and Hilo for 1979-1995 in the middle troposphere, in agreement with the results in Figure 8-2, while Bodeker *et al.* (1998) find no significant trend for Lauder.

Trend data for tropical ozone are sparse. Limited sonde data from Natal, Brazil, suggest an increase of 10-20%/decade in the middle and upper troposphere for 1978-1991, but the trends are significant only for 400-600 mb (Logan, 1994). Few sondes were flown in 1993-1996 (V.W.J.H. Kirchhoff, Instituto Nacional de Pesquisas Espaciais, Brazil, personal communication, 1997), so that reliable trends cannot be determined for recent years. TOMS data have been used to infer the column of ozone in the lower troposphere off the west coast of South America (Jiang and Yung, 1996; Kim and Newchurch, 1996). Jiang and Yung (1996) find an increase in ozone in a very small region at 25°S west of South America to be 5-15%/decade for 1979-1993. The same technique applied to the New Guinea area indicates a 1%/yr increase in lower tropospheric ozone (Kim and

**Table 8-4. Summary of major findings from campaigns in the Northern Hemisphere.**

| Campaign | Location | Key Findings | Authors |
|---|---|---|---|
| PEM-West A | East Asia/northern Pacific Ocean | Well-aged marine air maintains continental signature up to ~10 days.<br>Asian plumes with 60-80 ppbv $O_3$ in the low troposphere over the Pacific.<br>Sources of tropospheric $NO_x$ cannot yet be accurately defined.<br>Continental sources important for $O_3$ in western Pacific troposphere.<br>NMHC of minor importance for $O_3$ in N. Pacific troposphere. | Gregory *et al.* (1996); Browell *et al.* (1996a); Singh *et al.* (1996); Kondo *et al.* (1996); Davis *et al.* (1996) |
| MLOPEX 2 | Mauna Loa Observatory | Free tropospheric net $O_3$ formation ~1.5 ppbv/day (24 hr average). | Cantrell *et al.* (1996a,b) |
| NARE | North Atlantic Ocean | In low troposphere anthropogenic $O_3$ exceeds $O_3$ transported by STE.<br>Anthropogenic influence supported by alkyl nitrate measurements.<br>Summertime pollution transports from N. America mostly confined to boundary layer.<br>Pollutant plumes travel hundreds of km over N. Atlantic; strong $H_2O_2$ formation can occur (>4 ppbv). | Fehsenfeld *et al.* (1996); Roberts *et al.* (1996); Buhr *et al.* (1996); Daum *et al.* (1996) |
| POLINAT | North Atlantic flight corridor | Major aircraft exhaust signatures detected.<br>Small fraction of $NO_x$ is oxidized to $HNO_3$ in plumes. | Schlager *et al.* (1997) |
| NOXAR | Tropopause region at 10°-70°N | Background $NO_x$ ~20-200 pptv.<br>Extended areas with $NO_x$ >1 ppbv. | Brunner (1998) |
| STRAT | Sub-tropical upper troposphere | Photolysis of acetone and peroxides from convective transports major OH source. | Jaeglé *et al.* (1997) |
| SUCCESS | Upper troposphere central U.S. | $NO_x$ mostly from surface sources.<br>Rapid uptake of $HNO_3$ by ice clouds. | Jaeglé *et al.* (1998); Weinheimer *et al.* (1998) |
| TOHPE | Colorado | Measured $NO_x$/OH relation in agreement with theory.<br>Model calculations overpredict OH by ~50%, possibly due to heterogeneous chemistry. | Eisele *et al.* (1997); Mount and Williams (1997); McKeen *et al.* (1997) |
| PEM-West B | East Asia/northern Pacific Ocean | Troposphere throughout the Pacific Rim is influenced by Asian outflow.<br>Confirmation that convection over land *is* and marine convection *is not* accompanied by significant lightning $NO_x$ production.<br>Upper tropospheric $NO_y$ significantly influenced by lightning and aircraft exhausts.<br>Measured $NO_y$ partitioning can be reproduced by photochemical model. | Gregory *et al.* (1997); Kawakami *et al.* (1997); Koike *et al.* (1997); Thompson *et al.* (1997a) |

## 8.3 ANTHROPOGENIC PERTURBATIONS TO TROPOSPHERIC OZONE

Much effort has been devoted to field campaigns to determine anthropogenic effects of the North American and Asian continents on the Atlantic and Pacific Oceans, respectively. Major field campaigns are listed in Tables 8-4 and 8-5. Regional campaigns have also been conducted to assess urban influences on rural tropospheric ozone and reactive nitrogen, NMHC, OH, hydroperoxy radicals ($HO_2$), peroxy radicals ($RO_2$), and other photochemically active species.

### 8.3.1 Northern Hemisphere

Whereas ozone is a major focus of major field experiments, precursor species have been measured with improved accuracy and precision, thus increasing confidence in calculation of ozone-forming tendencies and regional budgets. This section summarizes advances and gaps related to assessing global ozone in two areas: (1) long-range transport and regional studies; (2) advances in the understanding of NMHC and reactive nitrogen chemistry and climatologies. Assessment of progress in measuring and interpreting OH, $HO_2$, and $RO_2$ is covered in Section 8.6.

#### 8.3.1.1 Tropospheric Ozone and Transport

In the 1993 North Atlantic Regional Experiment (NARE) summertime intensive (Table 8-4), much of the ozone northeast of the American continent is attributed to North American emissions (Fehsenfeld *et al.*, 1996). Although elevated CO is a tracer for the anthropogenic origin of the ozone, the sum of C1-C4 hydrocarbons may be an even stronger indicator of the human input to photochemical ozone formation (Roberts *et al.*, 1996). In some cases well-defined pollution plumes leave the North American continent at altitudes below about 2 km (Daum *et al.*, 1996; Kleinman *et al.*, 1996). Such plumes can travel hundreds of km over the North Atlantic, with up to 20 ppbv $NO_y$, 480 ppbv CO, and 150 ppbv ozone. Hydrogen peroxide ($H_2O_2$) levels of 4 ppbv were encountered during NARE, with excursions to over 11 ppbv (Weinstein-Lloyd *et al.*, 1996). In the relatively cleaner free troposphere, $H_2O_2$ appeared to correlate strongly with the product of ozone and water vapor, consistent with our understanding of gas-phase $H_2O_2$ formation under relatively $NO_x$-poor conditions. Note that from surface sampling of ozone at Mace Head (Ireland, 53°N, 9°W), it is deduced that surface destruction of ozone is effective. The seasonal ozone maximum occurs in spring, not during the summer North American maximum.

Similar conclusions about transport of ozone downwind from a major continental source can be drawn from the trace gas measurements that were part of the APARE (East Asian-North Pacific Regional Experiment) NASA DC-8 PEM-West A (Pacific Exploratory Mission, September-October 1991) and PEM-West B (February-March 1994) experiments. Typical profiles from the airborne lidar and in situ ozone instruments for the PEM-West A campaign appear in Figure 8-3. Westerly winds transported pollutant plumes with ozone mixing ratios of about 60-80 ppbv to the Pacific. These plumes were not always industrial in origin, but were sometimes of biomass-burning origin. Most Asian pollution was transported below 2 km altitude toward the North Pacific (Talbot *et al.*, 1996), but significant transport also occurred at 8-12 km (Gregory *et al.*, 1997). Hydrocarbon tracers confirm that most of the upper-level ozone originates from convectively transported pollution from Asia (Blake *et al.*, 1996). However, acetylene/CO ratios indicate some contributions from larger distances farther away (Smyth *et al.*, 1996).

Stratosphere-troposphere exchange (STE) played a role in enriching tropospheric ozone levels during PEM-West A; even at low latitudes ozone reached 40-60 ppbv as a result of this transport. However, at low latitudes and low altitudes in the western Pacific region during late summer and fall, easterly winds prevailed, carrying clean ozone-poor air (<10 ppbv) to the continent. This clean air is comparable to the low $O_3$ concentrations recorded by balloonborne ozonesondes over the equatorial central Pacific by Kley *et al.* (1996).

Mauna Loa, Hawaii (20°N, 156°W, at 3.4 km elevation), is a ground station in the free troposphere that gives the chemical composition in a northeasterly trade wind regime (Atlas and Ridley, 1996). A 20-year surface ozone record has been obtained for Mauna Loa (Oltmans *et al.*, 1996), showing that ozone is relatively abundant in the winter-spring half year, with a maximum reached in March through May. Trajectories show that this coincides with large-scale descending motion and, therefore, it is assumed that stratospheric intrusions have a large influence on the mean ozone concentration. Model calculations are in agreement with this assumption (Roelofs and Lelieveld, 1997). Polluted Asian air masses are indicated as contributors to the springtime maximum

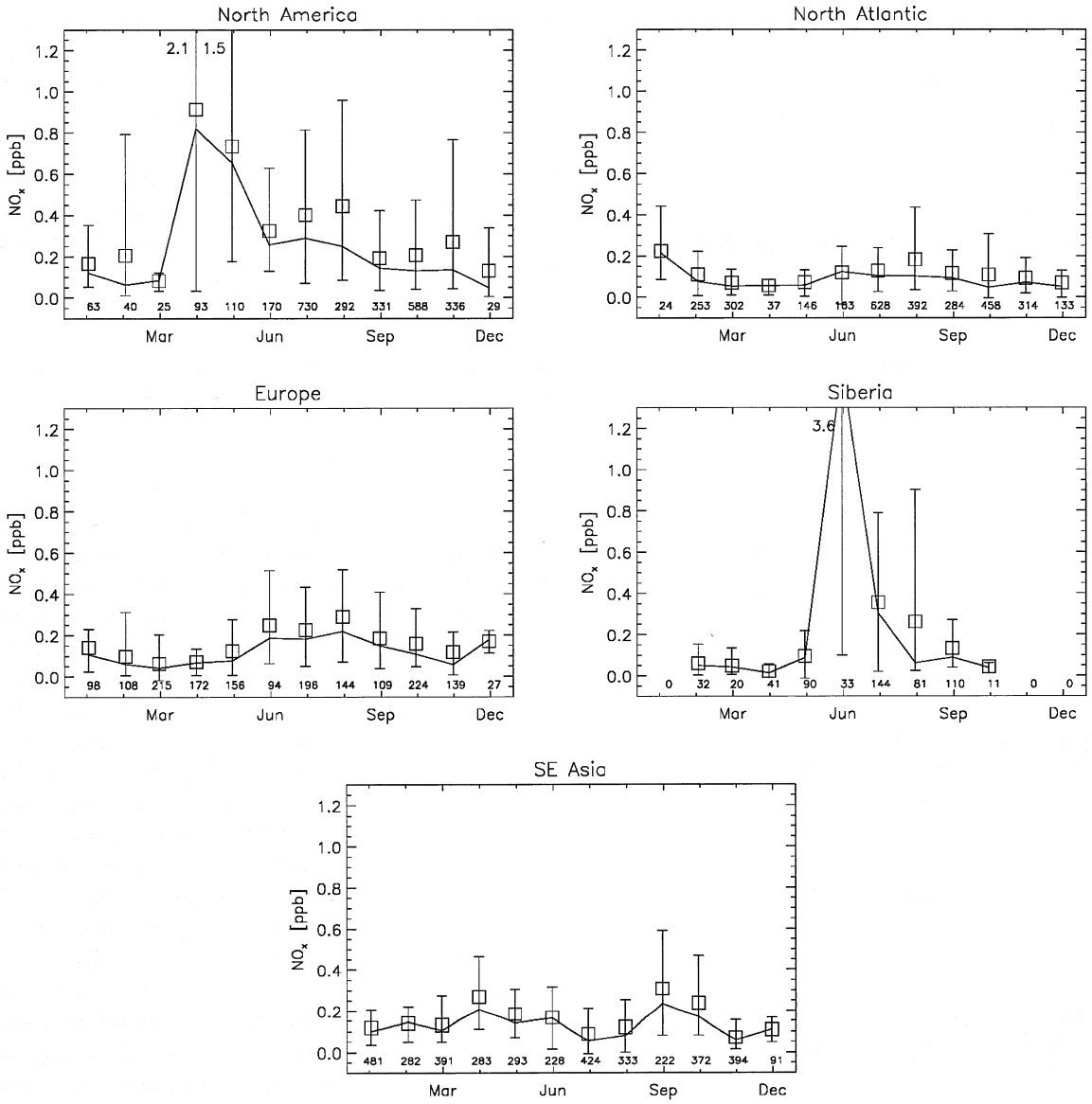


**Figure 8-5.** Seasonal variation of the monthly mean $NO_x$ concentrations of the upper troposphere from the NOXAR (Nitrogen OXide and ozone concentration measurements along Air Routes) programme. The tropopause altitude was calculated by using the 2-PVU (potential vorticity unit) surface from European Centre for Medium-Range Weather Forecasts (ECMWF) analyses. Median values are connected by solid lines. Squares denote monthly mean values and the vertical bars represent the range between the 10% and 90% quantiles of the monthly distributions. Numbers at the bottom denote the sample size (2-minute averages). Latitude and longitude range of the four selected regions: North America: 30-60˚N, 60-90˚W (90% quantiles for April and May: 2.1 and 1.5 ppbv); North Atlantic: 40-60˚N, 10-40˚W; Europe: 40-60˚N, 0-30˚E; Siberia: 50-70˚N, 60-90˚E; Southeast Asia, 10-30˚N, 70-120˚E (June: mean 1.7 ppbv, median: 1.5 ppbv) (Brunner, 1998).

for NO, nitrogen dioxide ($NO_2$), and $O_3$ measurements (Brunner, 1998) operated from Zürich to destinations in the U.S. and the Far East. Large $NO_x$ plumes with concentrations of several ppbv were frequently observed in the vicinity of aircraft. Further, $NO_x$ concentrations up to more than 1 ppbv were observed over extended areas (100-1500 km); these were ascribed to continental pollution. The results of upper tropospheric $NO_x$ measurements from more than 500 flights for regions sampled between spring 1995 and spring 1996 are depicted in Figure 8-5. It is difficult to generalize about $NO_x$ sources. Jaeglé *et al.* (1998) infer from the springtime SUCCESS experiment (SUbsonic aircraft: Contrail and Cloud Effects Special Study) that over the central U.S., convectively transported surface $NO_x$ was the predominant upper tropospheric $NO_x$ source.

The high latitude lower troposphere in the Northern Hemisphere has been studied for many years because pollutants accumulate in this region during winter. Measurements in Svalbard (79°N, 12°E) and Poker Flat, Alaska (65°N, 147°W), of $O_3$, PAN, and several important ozone precursors by Beine *et al.* (1997) and Herring *et al.* (1997) show that PAN decomposition at these locations in spring appears to be a significant $NO_x$ source. Whereas the $NO_x$ is probably mostly of anthropogenic origin, transported to the region as PAN, much of the NMHC may be natural.

### 8.3.2 Southern Hemisphere: Effects of Biomass Burning on Ozone

The striking feature of the Southern Hemisphere is the large-scale tropospheric ozone enhancement observed over the tropical Atlantic in the austral spring. High column ozone (50 Dobson units (DU) or more) extends from South America across the Atlantic, over Africa and at subtropical latitudes, to the Indian Ocean (Fishman *et al.*, 1990). Since the last Assessment (WMO, 1995), the contribution of biomass burning on the African and South American continents during the dry season to this maximum (Browell *et al.*, 1996a; Fishman *et al.*, 1996; Thompson *et al.*, 1996a,b) was confirmed by observations during the TRACE-A (Transport and Atmospheric Chemistry near the Equator-Atlantic) and SAFARI (Southern African Fire-Atmosphere Research Initiative) campaigns. Key findings of these campaigns and other Southern Hemisphere experiments appear in Table 8-5.

Several issues not yet resolved during the SAFARI/TRACE-A campaigns are: (1) fire emissions of trace gases over the southern African continent, based on remotely sensed fire counts and emissions factors (Scholes *et al.*, 1996b; Justice *et al.*, 1996), were much lower than previously thought; for example, they were too low to support CO calculated by global models; (2) African savanna soils appear to be a greater source of biogenic $NO_x$ than previously estimated; (3) lightning $NO_x$ played a significant role in upper tropospheric ozone formation, but this is not yet quantified (Thompson *et al.*, 1996a,b); (4) in southern Africa south of 20°S, an in situ, non-biomass-burning source may have dominated the local ozone budget (Tyson *et al.*, 1997).

During SAFARI/TRACE-A, the role of transport was clarified by a trajectory climatology (Garstang *et al.*, 1996) and a global circulation model study (Krishnamurti *et al.*, 1996). Surface emissions are trapped in the lower atmosphere in a large-scale anticyclonic recirculation extending over hundreds to thousands of kilometers, leading to the accumulation of ozone and ozone precursors (Tyson *et al.*, 1996; Thompson *et al.*, 1996a). Elevation to the upper levels can only occur during periodic synoptic-scale disturbances or at the beginning of the wet season, when convective activity commences. Exit from the African subcontinent occurs both to the west, where the dominant pathway is in the semi-permanent easterly wave and occurs below the 3 km stable layer, and to the east, as a rising plume below the 5-km stable layer. South of 20°S, transport to the Indian Ocean is dominant, accounting for over 90% of the trajectory pathways, which explains high ozone concentrations observed over the Indian Ocean. Ozone downwind from African burning was detected over the western subtropical Pacific during the PEM-Tropics A field mission in September 1996 (Schultz *et al.*, 1998).

In Brazil, the presence of enhanced tropospheric ozone at the ozonesonde station of Natal has long been ascribed to biomass burning in the dry season (August-October) (Logan and Kirchhoff, 1986). Observations (Kirchhoff *et al.*, 1996) have shown that the difference between sites close to the biomass burn source region and a control site is greater in the lower 2 km than in the upper troposphere. The role of convective transport in contributing to elevated ozone over South America and the Atlantic, which had been predicted in earlier modeling studies (Thompson *et al.*, 1997b), was confirmed from observations taken during the TRACE-A experiment. Following deep convection, downwind ozone production

water vapor pressure (Jaeglé *et al.*, 1997). Model calculations by Prather and Jacob (1997) suggest that photolysis of peroxides, notably $CH_3OOH$, that have been transported from the boundary layer by deep convection, contribute to OH formation as well.

### 8.4.2 Uncertainties in Gas-Phase Processes

Section 8.5.3 describes the propagation of kinetics inaccuracies in model calculations. Although uncertainties in many processes can be now be assessed, the chemistry of organic compounds remains a major source of uncertainty in chemical mechanisms affecting ozone and OH. Even the predictions of highly detailed explicit mechanisms derived completely from first principles are uncertain because, in spite of extensive recent research (DeMore *et al.*, 1997; Le Bras, 1997; Atkinson *et al.*, 1998), there continues to be a dearth of laboratory kinetics data. Although the rate constants for the primary reactions of OH, $O_3$, and $NO_3$ with many organic compounds have been measured, there have been relatively few product yield studies or studies aimed at understanding the chemistry of reaction products.

There is little available data on the chemistry of compounds with carbon numbers greater than 3 or 4 and most of the chemistry of these compounds is based upon extrapolating experimental studies of the reactions of lower molecular weight compounds. The chemistry of intermediate oxidation products, including aldehydes, ketones, alcohols, and ethers, is particularly significant for biogenics like isoprene and terpenes (Stockwell *et al.*, 1997). The most recent detailed mechanism for isoprene underpredicts PAN by about 40% for isoprene/$NO_x$ experiments even though PAN is predicted well for methylvinyl ketone/$NO_x$ and methacrolein/$NO_x$ experiments (Carter and Atkinson, 1997).

The reactions of peroxy radicals ($RO_2$) can be important under nighttime conditions when nitric oxide concentrations are low. The $RO_2$-$RO_2$ reactions and $NO_3$-$RO_2$ reactions lower PAN concentrations by about 40% and increase organic peroxide concentrations by about 25% through their impact on nighttime chemistry (Stockwell *et al.*, 1995; Kirchner and Stockwell, 1996, 1997).

### 8.4.3 Heterogeneous and Multiphase Processes

Heterogeneous reactions are defined as those reactions that occur on the surfaces of aerosol particles and droplets, whereas multiphase reactions are those that occur in a bulk liquid such as cloud water or deliquesced aerosol particles. It has been proposed, and in some cases, demonstrated through model sensitivity studies, that these processes have a significant effect on tropospheric constituents. An evaluation of some of these processes is given in Ravishankara (1997).

Particles may affect gas-phase tropospheric concentrations through both chemical and physical processes. Reactions occurring on aerosol particles or in cloud water droplets may have a significant effect on tropospheric constituents either directly, or indirectly through a perturbed radiation field (Baker, 1997; Andreae and Crutzen, 1997). Sedimentation of aerosol particles or rainout removes soluble species from the gas phase, leaving behind relatively insoluble species. The following is a summary of heterogeneous processes for which calculations or observations suggest some significance, but for which a complete assessment is still lacking:

(a) Formation of ozone is suppressed by the removal of $HO_2$ radicals and highly reactive stable species such as formaldehyde (HCHO) (Lelieveld and Crutzen, 1991). This process is thought to be most effective under clean conditions; Jonson and Isaksen (1993) calculated an ozone reduction between 10 and 30% globally for $NO_x$-poor conditions. (Section 8.6.2 describes observations of $HO_2$ loss in clouds.) A study by Liang and Jacob (1997), however, derives an effect of merely about 3% globally on tropospheric ozone through cloud removal of $HO_x$. Zhang *et al.* (1998) derive much larger effects, for example, in-cloud $O_3$-formation reductions up to 100%. Hence uncertainties remain large.

(b) Dissolved transition metals such as copper, iron, and manganese may counteract ozone reduction effects by clouds. Calculations show that the ozone destruction rate by clouds is decreased by 45 to 70% for clean conditions (Matthijsen *et al.*, 1995; Walcek *et al.*, 1997). In polluted areas with high $NO_x$ concentrations, the photochemical formation rate of ozone is also decreased (Lelieveld and Crutzen, 1991). Matthijsen *et al.* (1995) concluded that the reaction between Fe(II) and ozone increases the ozone destruction rate in polluted areas by a factor of 2 to 20 depending on the iron concentration. PAN may be converted to $NO_x$ through the scavenging of acetyl peroxy radicals by cloud water, even though PAN itself is not very soluble (Villalta *et al.*, 1996). This process tends to increase ozone concentrations.

(c) The most important multiphase reactant is often water, and many hydrolysis reactions have a somewhat heterogeneous character because the reactions are so fast that they are completed at or very near to the water surface (Hanson *et al.*, 1994). $N_2O_5$ rapidly hydrolyzes in the presence of liquid water, whereas its reaction with $H_2O$ is extremely slow in the gas phase (DeMore *et al.*, 1997).

(d) Organic-containing aerosols formed from emissions of organic compounds from biogenic and anthropogenic sources may be important (Mazurek *et al.*, 1991; Odum *et al.*, 1997). There is increasing evidence that the organic fraction of aerosols is considerable (Smyth *et al.*, 1996).

(e) The marine boundary layer contains sea-salt aerosols that contain high concentrations of halides. Halides and their reaction products may be released from the sea-salt aerosols through the scavenging and reactions of compounds such as $NO_3$, $N_2O_5$, and HOBr (Vogt *et al.*, 1996; Sander and Crutzen, 1996). The water content of the sea-salt aerosol may be an important variable for characterizing the chemistry of these aerosols (Rood *et al.*, 1987; Ravishankara, 1997).

(f) Heterogeneous reactions occurring on ice, windblown dust, fly ash, and soot may be important (Dentener *et al.*, 1996). Heterogeneous reactions on cirrus clouds involving ice, $N_2O_5$, and other species may be important in removing reactive nitrogen from the upper troposphere. Borrmann *et al.* (1997) detected reactive chlorine within upper tropospheric cirrus clouds, which may contribute to in situ ozone loss. Weinheimer *et al.* (1998) obtained observational evidence for $HNO_3$ removal on wave cloud particles and concluded that all the ambient nitric acid (25-75 pptv) was depleted within a couple of minutes after ice cloud formation. Soot may reduce $HNO_3$ to $NO_x$ (Hauglustaine *et al.*, 1996a; Rogaski *et al.*, 1997; Lary *et al.*, 1997).

Incorporation of nitric acid and other solubles in ice clouds may contribute to their vertical redistribution. Gravitational settling and evaporation of cloud droplets and ice particles can induce a significant downward flux of $HNO_3$ and $H_2O_2$, and affect related trace gases such as OH and $NO_x$ (Lawrence and Crutzen, 1998). This finding may help explain why many models tend to overestimate $HNO_3$ in the upper troposphere.

## 8.5 GLOBAL MODELING OF TROPOSPHERIC OZONE AND RELATED SPECIES

Since the previous Assessment (WMO, 1995), many studies have been published in which global 3-D models are used to represent the complex interactions among the ozone precursors, e.g., $NO_x$ and CO, loss processes, and physical and chemical variability determined by meteorological conditions in the troposphere. Table 8-6 lists results from several global CTMs (chemistry-transport models) now in use. Both dynamical (Section 8.5.1) and chemical mechanisms (Section 8.5.2) of these models have been intercompared. Models have been evaluated through comparisons with observations (Section 8.5.4), although comprehensive data are limited to intensive field campaigns, which are sparse in spatial and temporal coverage. This picture should change as more satellites with tropospheric sampling capabilities become available.

### 8.5.1 Intercomparison of Model Transport Schemes

Transport properties are evaluated through tracer tests. Radon-222 ($^{222}Rn$), which is emitted from soils and has a radioactive lifetime of 5.5 days, is used for evaluation of model simulation of small-scale meteorological processes, such as boundary layer venting by convection and frontal activity. Jacob *et al.* (1997) summarized a study of 20 global models for which comparison with $^{222}Rn$ was made to intercompare parameterizations of sub-grid convection. Although models tended to capture the location and timing of synoptic weather systems, $^{222}Rn$ concentrations in the upper troposphere were often ill-simulated, indicating that deep convection is not well represented. Upper tropospheric simulations are highly sensitive to the treatment of moist convection (Mahowald *et al.*, 1995) and to the spatial scale of deep convection (Lelieveld and Crutzen, 1994; Pickering *et al.*, 1995).

The limitations of present-day treatments of transport in global 3-D models are a major source of uncertainty in the global model assessment of tropospheric ozone. For example, Allen *et al.* (1996) used a model that simulates transport based on data assimilation for a multi-year simulation. They found that transport of the ozone precursor CO may explain up to 90% of the CO interannual variability at coastal

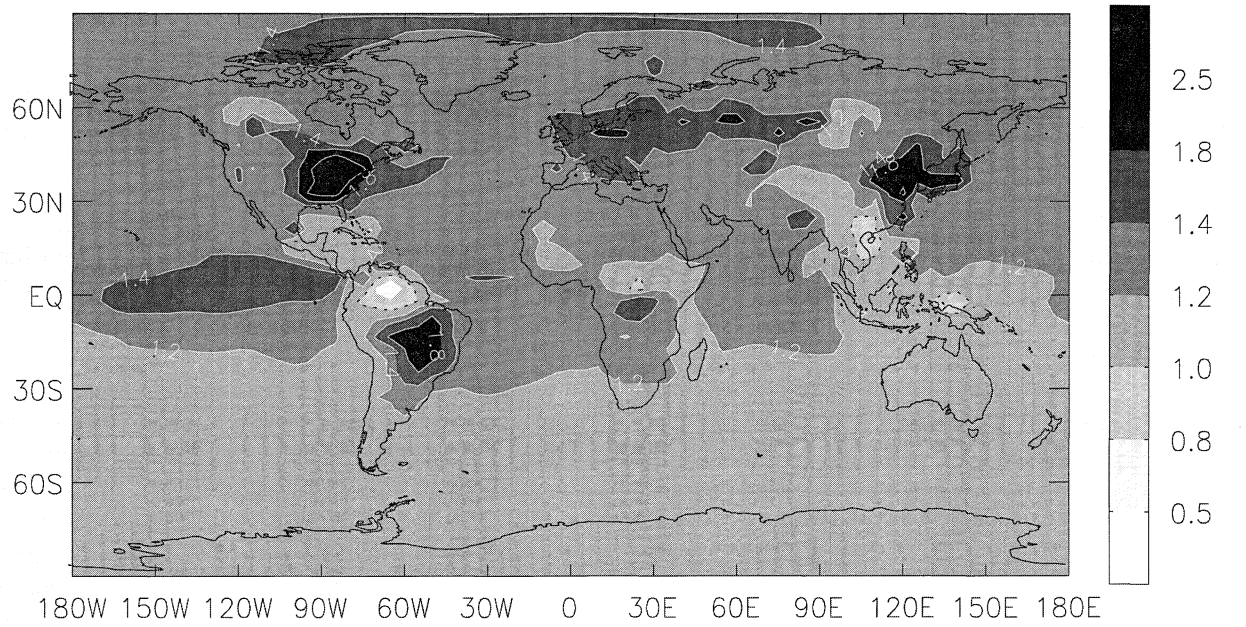


**Figure 8-7.** Model calculation of surface ozone for the year 1993, comparing a simulation that accounts for NMHC-$CH_4$-CO emissions and chemistry, and one that only accounts for $CH_4$-CO chemistry (Houweling *et al.*, 1998). These ratios are relatively high in areas of strong anthropogenic NMHC emissions (darkest), indicating that large-scale $O_3$ levels are enhanced by up to a factor of 2-3 by natural and anthropogenic NMHC emissions (e.g., in the eastern U.S.). The black dashed lines indicate the 1.0 contour. Note that, e.g., over the Amazon basin, natural NMHC cause an ozone reduction.

*et al.*, 1997; Roelofs and Lelieveld, 1997; Wang *et al.*, 1998a,b). Thus, net photochemical formation of ozone is the difference between two large numbers (Table 8-6). Net transport into and out of the troposphere, signified by the difference between stratospheric input and dry deposition, is also the difference between two numbers of comparable magnitude.

Individual models give insight into mechanistic complexities. For example, close balance between chemical production and chemical loss of ozone in the tropospheric column appears to be maintained at all latitudes except at high latitudes in winter (Wang *et al.*, 1998c). This balance implies in particular that ozone in the tropical troposphere, which plays a key role in the global oxidizing capacity of the atmosphere, is sustained largely by tropical sources of $NO_x$ (Jacob *et al.*, 1996). Nonmethane hydrocarbon chemistry increases the global tropospheric ozone inventory by 10-20% (Figure 8-7); this relatively small perturbation reflects compensating effects from increases and decreases in ozone production in different regions of the troposphere (Wang *et al.*, 1998c). The latter study shows that most of the NMHC effect on ozone takes place via perturbation to the $NO_x$ budget, involving the formation of PAN as a reservoir for long-range transport of $NO_x$.

Export of PAN from polluted boundary layers can provide a major reservoir of $NO_x$ for remote regions of the atmosphere (Moxim *et al.*, 1996). Most of the PAN production over the United States appears to be driven by interaction of anthropogenic $NO_x$ with biogenic isoprene (Horowitz *et al.*, 1998). In the boundary layer, strong horizontal PAN gradients occur between the continents and oceans, with maxima in polluted environments, whereas in the free troposphere PAN is distributed relatively zonally. In the Northern Hemisphere PAN reaches maximum levels in the cold high latitudes. In the Southern Hemisphere PAN maxima occur at latitudes north of 30°S, in association with biomass burning.

In summary, it appears that the influence of PAN on $NO_x$ in remote locations (and presumably on ozone) is mostly exerted in the lower troposphere. In the upper troposphere PAN releases of $NO_x$ at relatively low temperatures do not strongly affect ozone distributions.

This is confirmed by the Lamarque *et al.* (1996) $NO_x$ "labeling" study, which showed that photochemical ozone formation in the Southern Hemisphere free troposphere is mostly controlled by the natural lightning $NO_x$ source, except in the dry season, when biomass-burning emissions augment ozone formation (Thompson *et al.*, 1996a,b). In the Northern Hemisphere the calculated free tropospheric $NO_x$ is largely determined by fossil fuel combustion, aircraft emissions, and lightning (Lamarque *et al.*, 1996).

Both regional and global chemistry-transport models are being employed to estimate exports from the polluted boundary layer in industrialized regions to the global environment. Ozone is formed over these areas from NMHC chemistry in the presence of $NO_x$. With NMHC chemistry added to global models (Müller and Brasseur, 1995; Berntsen and Isaksen, 1997), it appears that NMHC deplete OH in the vicinity of sources, in particular near natural sources that do not co-emit $NO_x$ (Houweling *et al.*, 1998). On the other hand, NMHC breakdown leads to intermediate species, such as acetone, that can release OH at greater distance from the sources (Singh *et al.*, 1995). This affects the global distribution of OH, for example, by increasing the OH gradients between continental and marine environments (Houweling *et al.*, 1998). The global 3-D model study of Wang *et al.* (1998c) indicates that NMHC chemistry decreases the global abundance of tropospheric OH by 15%, whereas Houweling *et al.* (1998) conclude that the net effect on OH (and thus, e.g., on methyl chloroform and methane) is only small. Hence this issue remains associated with important uncertainty.

Although significant amounts of ozone are transported from North America toward the western North-Atlantic region, this ozone mixes with natural ozone from the stratosphere in synoptic weather systems (Moody *et al.*, 1996). Nevertheless, especially over the western Atlantic Ocean, ozone, CO, and $NO_y$ show strong positive correlations, a clear signature of pollutant outflow from the U.S. (Parrish *et al.*, 1993; Chin *et al.*, 1994; Atherton *et al.*, 1996). Model simulations by Kasibhatla *et al.* (1996) suggest that the summertime North Atlantic mid-troposphere contains at least 50% more ozone compared to natural levels, even though during summer net ozone destruction prevails in the marine boundary layer. Most net ozone production appears to take place during the period April-June in this area, with cross-Atlantic transport of pollutant ozone reaching a maximum during spring (Roelofs and Lelieveld, 1997).

An important region of emerging pollutant emissions is the rapidly developing southeastern part of Asia. Strong indications of significant photochemical pollution have, for example, been reported by Liu *et al.* (1990), Sunwoo *et al.* (1994), Chao *et al.* (1996), Akimoto *et al.* (1996), and Kok *et al.* (1997). Industrial growth in rapidly developing countries, such as China and India, will perturb the atmosphere regionally in the next few decades (Elliot *et al.*, 1997). The degree to which this has global consequences depends on dynamics as well as sources. For example, the monsoon circulation may enhance pollutant transports toward the free troposphere in (Northern Hemisphere) summer by convection and towards the Indian and Pacific Oceans during winter. If anthropogenic emissions from southern Asia are transported toward the Inter-Tropical Convergence Zone (ITCZ), direct injection of ozone into the tropical upper troposphere could take place, leading to significant radiative forcing of climate.

Berntsen and Isaksen (1997) have calculated the contributions of several regions to the global tropospheric ozone budget. Europe is the largest source of photochemically formed ozone with a net contribution of nearly 97 Tg/yr, followed by North America with 77 Tg/yr. Asia appears to be developing strongly with a current net ozone flux of almost 65 Tg/yr. Berntsen and Isaksen (1997) calculate that the troposphere in the Northern Hemisphere, over the Atlantic and Pacific Oceans, is a region of strong net photochemical ozone destruction, mostly in the mid-troposphere.

## 8.6 TROPOSPHERIC OH: MEASUREMENTS, MODELING, OXIDIZING CAPACITY

### 8.6.1 Surface OH Measurements

A breakthrough in the ability to evaluate the tropospheric oxidizing capacity and photochemical mechanisms has been the development of reliable instrumentation for in situ measurements of OH and other oxidizing free radicals. In situ OH measurements and associated detailed studies of chemical OH production and destruction processes have been conducted in several ground-based campaigns, including a major intercomparison effort. During the Tropospheric OH Photochemistry Experiment (TOHPE) campaign in Colorado, it was confirmed that, especially under relatively clean conditions, OH is mostly controlled by

organic acids). There now exists a large database of rate coefficients for the reactions of OH radicals with CFC alternatives that is continuously evaluated (DeMore *et al.*, 1997) and provides a means of calculating consistent tropospheric lifetimes for these compounds. Moreover, this database allows rate coefficients to be estimated within a factor of about 2 for compounds for which there are no experimental data available.

The reaction of halocarbons with OH radicals in air leads to rapid formation of haloalkyl peroxy radicals that react with three important tropospheric trace gases: $NO_2$, $HO_2$, and NO. The relative importance of these reactions is dictated by the rate coefficients for reactions with the peroxy ($CX_3CYZOO$) radicals and their ambient concentrations (X, Y, Z = H, Br, Cl, or F). Reaction of haloalkyl peroxy radicals with $NO_2$ and $HO_2$ leads to the formation of the corresponding peroxynitrates ($CX_3CYZOONO_2$) and hydroperoxides ($CX_3CYZOOH$). These species appear to be rather short-lived and undergo photolysis, thermal decomposition, or reaction with OH radicals, leading to the regeneration of peroxy ($CX_3CYZOO$) or the formation of alkoxy ($CX_3CYZO$) radicals (WMO, 1995).

The reactions of haloalkyl peroxy radicals with NO have generally been assumed to result in quantitative formation of $NO_2$ and the corresponding haloalkoxy radicals (WMO, 1995). However, studies on one of the most important CFC substitutes, $CF_3CH_2F$ (HFC-134a) have called into question this basic premise (Wallington *et al.*, 1996). This important question pertains to the fate of the alkoxy radical, $CF_3CFHO$. The alkoxy radical, assumed to be formed with a yield close to 100%, may either decompose via carbon-carbon bond cleavage to give CHFO or react with molecular oxygen. Reaction with $O_2$ forms $CF_3CFO$, which, following uptake in clouds or surface water, is hydrolyzed to $CF_3COOH$. The estimated atmospheric yield of $CF_3COOH$ due to emission of $CF_3CH_2F$ thus depends critically on laboratory measurements of the relative importance of the reaction with $O_2$ and the decomposition.

Experimental studies on the reactions of $CF_3CHFO$ radicals have generally employed the self-reaction of the corresponding peroxy radical as the alkoxy radical source. However, the study of the oxidation of HFC-134a by Wallington *et al.* (1996) also employed the reaction of $CF_3CHFO_2$ radicals with NO as the alkoxy radical source. The experimental results showed a reduced yield of $CF_3CFO$, thereby implying that the decomposition of $CF_3CHFO$ radicals is more favorable when they are generated from reaction of the peroxy radical with NO rather than from self-reaction of $CF_3CHFOO$ radicals.

From the above considerations, it is evident that calculations of the yield of $CF_3CFO$, and hence $CF_3COOH$, from the atmospheric oxidation of $CF_3CH_2F$, based on experiments in which $CF_3CHFO$ radicals were generated from the self-reaction of $CF_3CHFOO$, are likely to overestimate the yield of $CF_3COOH$. Previously, the yield of $CF_3COOH$ obtained from the atmospheric degradation of HFC-134a was calculated to be 29-36%. Incorporation of the results of Wallington *et al.* (1996) into the model revises the yield down to 7-20%.

There has been further support (Møgelberg *et al.* 1997; Manning and Sidebottom, 1997) for the conclusions drawn by Wallington *et al.* (1996). These findings appear to be particularly relevant for systems where haloalkoxy radicals may react by both C-C bond fission and reaction with $O_2$.

### 8.7.2 Reactions of Haloalkoxy Radicals

The reaction pathways for haloalkoxy radicals ultimately determine the primary degradation products and depend on the number and chemical identity of the halogen atoms in the parent molecule. A number of new studies on the reaction of haloalkoxy radicals, including C3 and C4 compounds, have been carried out since the last WMO report (1995) and have increased the understanding of haloalkoxy radical chemistry (Nielsen *et al.*, 1994; Møgelberg *et al.*, 1995a,b,c,d; Giessing *et al.*, 1996; Møgelberg *et al.*, 1996; Chen *et al.*, 1997; Barry *et al.*, 1997). A number of general conclusions concerning the relative importance of the possible reaction pathways for haloalkoxy radicals may be drawn from the experimental data:

(a) $CX_2ClO$ and $CX_2BrO$ radicals eliminate a Cl or Br atom to produce $CX_2O$, except for $CH_2ClO$ and $CH_2BrO$, where reaction with $O_2$ to give CHClO and CHBrO is the dominant reaction.

(b) $CH_2FO$ and $CHF_2O$ radicals react with $O_2$ to form CHFO and $CF_2O$. Loss of $CF_3O$ is largely determined by reaction with $CH_4$ or NO to generate $CF_2O$.

(c) $RCH_2O$ and RCHOR radicals (R = haloalkyl group) react with $O_2$ to form the corresponding aldehydes and ketones, respectively.

(d) $RCCl_2O$ and RCClFO radicals react predominantly by Cl atom elimination to give the corresponding acyl chlorides and fluorides rather than by C-C bond fission.

(e) $RCF_2O$ radicals undergo C-C bond cleavage to form $CF_2O$.

(f) RCHYO radicals (Y = Cl or F) have three important reaction channels: C-C bond fission (producing CHYO), HCl elimination (giving haloacyl radicals), and reaction with $O_2$ (to form acyl halides). The relative importance of these three reaction pathways is a function of temperature, $O_2$ pressure, and total pressure and will therefore vary considerably with altitude.

### 8.7.3 Halogenated Carbonyl Compounds

Halogenated carbonyl compounds are generated in the troposphere from the degradation of all CFC substitutes and undergo significant chemical or physical transformation in the troposphere.

The final tropospheric degradation products of the CFC substitutes are thus HCl, HF, oxides of carbon, and halogenated carboxylic acids. Although atmospheric chloride and fluoride production from CFC substitutes is insignificant compared to natural sources, some concern has been expressed about the environmental impact of halogenated carboxylic acids, particularly trifluoroacetic acid (TFA) (AFEAS, 1994a,b). Trifluoroacetic acid is chemically very stable and has no known abiotic sinks in the environment. It has been suggested that the acid could accumulate in seasonal wetlands (AFEAS, 1994a,b). However, at the levels predicted to arise from the use of CFC substitutes, trifluoroacetic acid is unlikely to have any impact on micro-organisms, plants, or animals.

### 8.7.4 Hydrofluoroethers (HFEs)

Kinetic studies on the reaction of OH radicals with a variety of HFEs have been reported in the literature (Zhang *et al.*, 1992; Garland *et al.*, 1993; Orkin *et al.*, 1994; Hsu and DeMore, 1995; O'Sullivan *et al.*, 1997; Wallington *et al.*, 1997, 1998). The experimental results indicate that hydrofluoroethers are significantly less reactive than the parent (fully hydrogenated) ethers and that, as for HFCs, their reactivity depends to a large extent on the number and positions of fluorine atoms in the molecule. This large variation in reactivity yields tropospheric lifetimes for removal by OH radicals that are as short as 45 days ($CF_3CH_2OCH_3$) and as long as 75 years ($CF_3OCHF_2$). Nevertheless, the activating effect of the oxygen atom in HFEs means that, in general, the tropospheric lifetimes for HFEs are considerably shorter than the structurally analogous HFCs.

There have also been several investigations on the oxidation of HFEs (O'Sullivan *et al.*, 1997; Wallington *et al.*, 1997, 1998). The experimental evidence to date suggests that the behavior of the alkoxy radicals formed in the oxidation of hydrofluoroethers is entirely analogous to the alkoxy radicals generated from the oxidation of non-fluorinated ethers. For example, the alkoxy radicals $CF_3CH_2OCHOCF_3$ and $C_4F_9OCH_2O$, generated from $CF_3CH_2OCH_2CF_3$ and $C_4F_9OCH_3$ respectively, react to produce the formates $CF_3CH_2OCHO$ and $C_4F_9OCHO$. Unfortunately, there is no data available concerning the reaction rates of these products with OH radicals or their photolysis rates. However, since formates are considerably less reactive towards OH radicals than their parent ethers, one can assume that these fluorinated formates are likely to be similarly unreactive. On this basis, it seems that reaction with OH radicals is not likely to be a significant loss process for fluorinated formates. Uptake by clouds and rainwater followed by hydrolysis to produce fluorinated organic acids is the most likely scenario.

## 8.8 AVIATION AND THE GLOBAL ATMOSPHERE

Air traffic in the upper troposphere and lower stratosphere has reached a volume where the emissions of gases and particles may be affecting the physical and chemical properties of the atmosphere in a major way (Schumann, 1997; Derwent *et al.*, 1998; Friedl, 1997; Brasseur *et al.*, 1998). An update of the atmospheric impact of subsonic aircraft since the last ozone Assessment (Chapter 11 in WMO, 1995) will appear in a dedicated IPCC-sponsored Assessment (IPCC, 1999), to which the reader is referred.

## 8.9 CONCLUSIONS

The reader is referred to the Scientific Summary in the beginning of this chapter for a recapitulation of the Chapter's major points. The following paragraphs discuss some uncertainties and areas for which the next Assessment may show advances.

Ozone trends continue to be difficult to establish

Cantrell, C.A., R.E. Shetter, T.M. Gilpin, and J.G. Calvert, Peroxy radicals measured during Mauna Loa Observatory Photochemistry Experiment 2: The data and first analysis, *J. Geophys. Res.*, *101*, 14643-14652, 1996b.

Cantrell, C.A., R.E. Shetter, J.G. Calvert, F.L. Eisele, E. Williams, K. Baumann, W.H. Brune, P.S. Stevens, and J.H. Mather, Peroxy radicals from photostationary state deviations and steady state calculations during the tropospheric OH experiment at Idaho Hill, Colorado, 1993, *J. Geophys. Res.*, *102*, 6396-6378, 1997.

Carslaw, N., L.J. Carpenter, J.M.C. Plane, B.J. Allan, R.A. Burgess, K.C. Clemitshaw, H. Coe, and S.A. Penkett, Simultaneous observations of nitrate and peroxy radicals in the marine boundary layer, *J. Geophys. Res.*, *102*, 18917-18933, 1997.

Carter, W.P.L., and R. Atkinson, Development and evaluation of a detailed mechanism for the atmospheric reactions of isoprene and $NO_x$, *Int. J. Chem. Kinet.*, *28*, 497-530, 1997.

Chao, L., T. Jie, and Z. Xiuji, Measurements and model simulations of surface ozone variations at different background concentrations of the precursors, *Acta Meteor. Sinica*, *10*, 215-221, 1996.

Chen, J., V. Young, H. Niki, and H. Magid, Kinetic and mechanistic studies for reactions of $CF_3CH_2CHF_2$ (HFC-245fa) initiated by H-atom abstraction using atomic chlorine, *J. Phys. Chem.*, *101*, 2648-2653, 1997.

Chin, M., D.J. Jacob, J.W. Munger, D.D. Parrish, and B.G. Doddridge, Relationship of ozone and carbon monoxide over North America, *J. Geophys. Res.*, *99*, 14565-14573, 1994.

Crutzen, P.J., and P.H. Zimmermann, The changing chemistry of the troposphere, *Tellus*, *43AB*, 136-151, 1991.

Daum, P.H., L.I. Kleinman, L. Newman, W.T. Luke, J. Weinstein-Lloyd, C.M. Berkowitz, and K.M. Busness, Chemical and physical properties of plumes of anthropogenic pollutants transported over the North Atlantic during the North Atlantic Regional Experiment, *J. Geophys. Res.*, *101*, 29029-29042, 1996.

Davis, D.D., J. Crawford, G. Chen, W. Chameides, S. Liu, J. Bradshaw, S. Sandholm, G. Sachse, G. Gregory, B. Anderson, J. Barrick, A. Bachmeier, J. Collins, E. Browell, D. Blacke, S. Rowland, Y. Kondo, H. Singh, R. Talbot, B. Heikes, J. Merrill, J. Rodriguez, and R.E. Newell, Assessment of ozone photochemistry in the western North-Pacific as inferred from PEM-West A observations during the fall 1991, *J. Geophys. Res.*, *101*, 2111-2134, 1996.

Davis, D.D., G. Chen, P. Kasibhatla, A. Jefferson, D. Tanner, F. Eisele, D. Lenschow, W. Neff, and H. Berresheim, DMS oxidation in the Antarctic marine boundary layer: Comparison of model simulations and field observations of DMS, DMSO, $DMSO_2$, $H_2SO_4$(g), MSA(g), and MSA(p), *J. Geophys. Res.*, *103*, 1657-1678, 1998.

DeMore, W.B., S.P. Sander, D.M. Golden, R.F. Hampson, M.J. Kurylo, C.J. Howard, A.R. Ravishankara, C.E. Kolb, and M.J. Molina, *Chemical Kinetics and Photochemical Data for Use in Stratospheric Modeling, Evaluation Number 12*, U.S. National Aeronautics and Space Administration, Jet Propulsion Laboratory, California Institute of Technology, Pasadena, Calif., 1997.

Dentener, F.J., G.R. Carmichael, Y. Zhang, J. Lelieveld, and P.J. Crutzen, The role of mineral aerosol as a reactive surface in the global troposphere, *J. Geophys. Res.*, *101*, 22869-22889, 1996.

Derwent, R.G., R.R. Friedl, I.L. Karol, H. Kelder, V.W.J.H. Kirchhoff, T. Ogawa, M.J. Rossi, and P. Wennberg, Impacts of aircraft emissions on atmospheric ozone, Provisional draft of Chapter 2, in *Aviation and the Global Atmosphere*, Intergovernmental Panel on Climate Change, in preparation, 1998.

Dessler, A.E., E.J. Hintsa, E.M. Weinstock, J.G. Anderson, and K.R. Chan, Mechanisms controlling water vapor in the lower stratosphere: "A tale of two stratospheres", *J. Geophys. Res.*, *100*, 23167-23172, 1995.

Diab, R.D., A.M. Thompson, M. Zunckel, G.J.R. Coetzee, J. Combrink, G.E. Bodeker, J. Fishman, F. Sokolic, D.P. McNamara, C.B. Archer, and D. Nganga, Vertical ozone distribution over southern Africa and adjacent oceans during SAFARI-92, *J. Geophys. Res.*, *101*, 23823-23834, 1996.

Donahue, N.M., M.K. Dubey, R. Mohrschladt, K.L. Demerjian, and J.G. Anderson, High-pressure flow study of the reactions $OH+NO_x \rightarrow HONO_x$: Errors in the falloff region, *J. Geophys. Res.*, *102*, 6159-6168, 1997.

Donahue, N.M., J.H. Kroll, J.G. Anderson, and K.L. Demerjian, Direct observation of OH production from the ozonolysis of olefins, *Geophys. Res. Lett.*, *25*, 59-62, 1998.

Dunker, A.M., The decoupled direct method for calculated sensitivity coefficients in chemical kinetics, *J. Chem. Phys.*, *81*, 2385-2393, 1984.

Eisele, F.L., D.J. Tanner, C.A. Cantrell, and J.G. Calvert, Measurements and steady state calculations of OH concentrations at Mauna Loa Observatory, *J. Geophys. Res.*, *101*, 14665-14679, 1996.

Eisele, F.L., G.H. Mount, D. Tanner, A. Jefferson, R. Shetter, J.W. Harder, and E.J. Williams, Understanding the production and interconversion of the hydroxyl radical during the Tropospheric OH Photochemistry Experiment, *J. Geophys. Res.*, *102*, 6457-6465, 1997.

Elbern, H., J. Kowol, R. Sladkovic, and A. Ebel, Deep stratospheric intrusions: A statistical assessment with model guided analysis, *Atmos. Environ.*, *31*, 3207-3226, 1997.

Elliot, S., M. Shen, D.R. Blake, R. Lu, A.G. Russell, C.Y.J. Kao, G.E. Streit, X.P. Zhao, E.I. McCreary, F.S. Rowland, M.J. Brown, and R.P. Turco, Atmospheric effects of the emerging mainland Chinese transportation system at and beyond the regional scale, *J. Atmos. Chem.*, *27*, 31-70, 1997.

Emmons, L.K., M.A. Carroll, D.A. Hauglustaine, G.P. Brasseur, C. Atherton, J. Penner, S. Sillman, H. Levy, F. Rohrer, W.M.F. Wauben, P.F.J. VanVelthoven, Y. Wang, D. Jacob, P. Bakwin, R. Dickerson, B. Doddridge, C. Gerbig, R. Honrath, G. Hübler, D. Jaffe, Y. Kondo, J.W. Munger, A. Torres, and A. Volz-Thomas, Climatologies of $NO_x$ and $NO_y$: A comparison of data and models, *Atmos. Environ.*, *31*, 1851-1904, 1997.

EPA (U.S. Environmental Protection Agency), *National Air Pollutant Emissions Trends, 1900-1995*, EPA-454/R-96-007, U.S. Environmental Protection Agency, Research Triangle Park, N.C., 1996.

Fehsenfeld, F.C., P. Daum, W.R. Leaitch, M. Trainer, D.D. Parrish, and G. Hübler, Transport and processing of $O_3$ and $O_3$ precursors over the North Atlantic: An overview of the 1993 North Atlantic Regional Experiment (NARE) summer intensive, *J. Geophys. Res.*, *101*, 28877-28891, 1996.

Fiore, A.M., D.J. Jacob, J.A. Logan, and J.H. Yin, Long-term trends in ground level ozone over the contiguous United States: 1980-1995, *J. Geophys. Res.*, *103*, 1471-1480, 1998.

Fishman, J., C.E. Watson, J.C. Larsen, and J.A. Logan, The distribution of tropospheric ozone determined from satellite data, *J. Geophys. Res.*, *95*, 3599-3617, 1990.

Fishman, J., J.M. Hoell Jr., R.D. Bendura, R.J. McNeal, and V.W.J.H. Kirchhoff, NASA GTE TRACE A Experiment (September-October 1992): Overview, *J. Geophys. Res.*, *101*, 23865-23879, 1996.

Folkins, I., P.O. Wennberg, T.F. Hanisco, J.G. Anderson, and R.J. Salawitch, OH, $HO_2$, and NO in two biomass burning plumes: Sources of $HO_x$ and implications for ozone production, *Geophys. Res. Lett.*, *24*, 3185-3188, 1997.

Fried, A., S. McKeen, S. Sewell, J. Harder, B. Henry, P. Goldan, W. Kuster, E. Williams, K. Baumann, R. Shetter, and C. Cantrell, Photochemistry of formaldehyde during the 1993 Tropospheric OH Photochemistry Experiment, *J. Geophys. Res.*, *102*, 6283-6296, 1997.

Friedl, R. (ed.), *Atmospheric Effects of Subsonic Aircraft: Interim Assessment Report of the Advanced Subsonic Technology Program*, U.S. National Aeronatics and Space Administration, Goddard Space Flight Center, Greenbelt, Md., 1997.

Gao, D., W.R. Stockwell, and J.B. Milford, Global uncertainty analysis of a regional scale gas-phase chemical mechanism, *J. Geophys. Res.*, *101*, 9107-9119, 1996.

Gardner, R.M., M. Williams, C. Shoreman, I. Piper, P. Newton, M. Leech, B. Stonehouse, R. Flak, D. Lee, C.J. Hume, T. Cook, M. Metcalfe, C. Walker, B. Massé, S. Korolitski, C. Baudoin, H. Wieting, D. Lenormand, A. Depitre, E. Herms, J. Pavaux, S. Dumont, M. O'Hanrahan, A. Schmitt, M. Lecht, M. Dameris, F. Deidewig, D. Wurzel, J. Peper, W. Fransen, S. Ernedal, W. Bula, E. Fleuti, B.O. Näs, K. Morris, H.P. Roth, W. Förtsch, A. Rowland, J.K. Adams, R. Dunker, H. Neuman, J.P. Desgranges, P. Wiederkehr, C. Vandenberghe, R. Harman, R. Stewart, D. Lister, N. Louisnard, R. Sausen, and C. Johnson, A global inventory of aircraft $NO_x$ emissions, in *AERONOX Impact of $NO_x$ Emissions from Aircraft upon the Atmosphere at Flight Altitudes 8-15 km*, edited by U. Schumann, pp. 129-194, European Commission, Directorate - General XII for Science and Development, Publication on Research Related to Aeronautics and Environment, Brussels, 1995.

Gardner, R.M., K. Adams, T. Cook, F. Deidewig, S. Ernedal, R. Falk, E. Fleuti, E. Herms, C.E. Johnson, M. Lecht, D.S. Lee, M. Leech, D. Lister, B. Massé, M. Metcalfe, P. Newton, A. Schmitt, C. Vandenbergh, R. VanDrimmelen, ANCAT/EC (The Abatement of Nuisances Caused by Air Transport/ European Commission) global inventory of NOx emissions from aircraft, *Atmos. Environ.*, *31*, 1751-1766, 1997.

Garland, N.L., L.J. Medhurst, and H.H. Nelson, Potential chlorofluorocarbon replacements: OH reaction rate constants between 250 and 315 K and infrared absorption spectra, *J. Geophys. Res.*, *98*, 23107-23111, 1993.

Garstang, M., P.D Tyson, R. Swap, M. Edwards, P. Kollberg, and J.A. Lindesay, Horizontal and vertical transport of air over southern Africa, *J. Geophys. Res.*, *101*, 23721-23736, 1996.

Gettelman, A., J.R. Holton, and K.H. Rosenlof, Mass fluxes of $O_3$, $CH_4$, $N_2O$ and $CF_2Cl_2$ in the lower stratosphere calculated from observational data, *J. Geophys. Res.*, *102*, 19149-19159, 1997.

Giessing, A.M.B., A. Freilberg, T. Møgelberg, J. Sehested, M. Bilde, T.J. Wallington, and O.J. Nielsen, Atmospheric chemistry of HFC-227ca: Spectrokinetic investigation of the $CF_3CF_2CF_2O_2$ radical, its reaction with NO and $NO_2$, and the atmospheric fate of the $CF_3CF_2CF_2O$ radical, *J. Phys. Chem.*, *100*, 6572-6576, 1996.

Gleason, J.F., N.C. Hsu, and O. Torres, Biomass burning smoke measured using backscattered ultraviolet radiation: SCAR-B and Brazilian smoke interannual variability, *J. Geophys. Res.*, in press, 1998.

Goldan, P.D., W.C. Kuster, and F.C. Fehsenfeld, Nonmethane hydrocarbon measurements during the Tropospheric OH Photochemistry Experiment, *J. Geophys. Res.*, *102*, 6315-6324, 1997.

Granier, C., J.F. Müller, S. Madronich, and G.P. Brasseur, Possible causes for the 1990-1993 decrease in the global tropospheric CO abundances: A three-dimensional sensitivity study, *Atmos. Environ.*, *30*, 1673-1682, 1996.

Greenberg, J.P., D. Helmig, and P.R. Zimmerman, Seasonal measurements of nonmethane hydrocarbons and carbon monoxide at the Mauna Loa Observatory during the Mauna Loa Observatory Photochemistry Experiment 2, *J. Geophys. Res.*, *101*, 14581-14598, 1996.

Gregory, G.L., B.E. Anderson, and E.V. Browell, Influence of lower tropospheric ozone on total column ozone as observed over the Pacific Ocean during the 1991 PEM-West A expedition, *J. Geophys. Res.*, *101*, 1919-1930, 1996.

Gregory, G.L., J.T. Merrill, M.C. Shipham, D.R. Blake, G.W. Sachse, and H.B. Singh, Chemical characteristics of tropospheric air over the Pacific Ocean as measured during PEM-West-B: Relationship to Asian outflow and trajectory history, *J. Geophys. Res.*, *102*, 28275-28285, 1997.

Guenther, A., C.N. Hewitt, D. Erickson, R. Fall, C. Geron, T. Graedel, P. Harley, L. Klinger, M. Lerdau, W.A. McKay, T. Pierce, B. Scholes, R. Steinbrecher, R. Tallamraju, J. Taylor, and P. Zimmerman, A global model of natural volatile organic compound emissions, *J. Geophys. Res.*, *100*, 8873-8892, 1995.

Guicherit, R., Ozone on an urban and regional scale-with special reference to the situation in the Netherlands, in *Tropospheric Ozone-Regional and Global Scale Interactions*, edited by I.S.A. Isaksen, *NATO series C, Vol. 227*, pp. 49-62, Reidel Publ., Dordrecht, The Netherlands, 1988.

Hanson, D.R., A.R. Ravishankara, and S. Solomon, Heterogeneous reactions in sulfuric acid aerosols: A framework for model calculations, *J. Geophys. Res.*, *99*, 3615-3629, 1994.

Harris, N.R.P., G. Ancellet, L. Bishop, D.J. Hofmann, J.B. Kerr, R.D. McPeters, M. Prendez, W.J. Randel, J. Staehelin, B.H. Subbaraya, A. Volz-Thomas, J. Zawodny, and C.S. Zerefos, Trends in stratospheric and free tropospheric ozone, *J. Geophys. Res.*, *102*, 1571-1590, 1997.

Hauglustaine, D.A., B.A. Ridley, S. Solomon, P.G. Hess, and S. Madronich, $HNO_3/NO_x$ ratio in the remote troposphere during MLOPEX2: Evidence for nitric acid reduction on carbonaceous aerosols? *Geophys. Res. Lett.*, *23*, 2609-2612, 1996a.

Hauglustaine, D.A., S. Madronich, B.A. Ridley, J.G. Walega, C.A. Cantrell, and R.E. Shetter, Observed and model calculated photostationary state at Mauna Loa Observatory during MLOPEX 2, *J. Geophys. Res.*, *101*, 14681-14696, 1996b.

Heikes, B.G., M. Lee, J. Bradshaw, S. Sandholm, D.D. Davis, J. Crawford, J. Rodriguez, S. Liu, S. McKeen, D. Thornton, A. Bandy, G. Gregory, R. Talbot, and D. Blake, Hydrogen peroxide and methylhydroperoxide distributions related to ozone and odd hydrogen over the North Pacific in the fall of 1991, *J. Geophys. Res.*, *101*, 1891-1905, 1996.

Heintz, F., U. Platt, H. Flentje, and R. Dubois, Long-term observation of nitrate radicals at the Tor station, Kap Arkona (Rügen), *J. Geophys. Res.*, *101*, 22891-22910, 1996.

Helmig, D., W. Pollock, J. Greenberg, and P. Zimmerman, Gas chromatography and mass spectrometry analysis of volatile organic trace gases at Mauna Loa Observatory, Hawaii, *J. Geophys. Res.*, *101*, 14697-14710, 1996.

Herman, J.R., P.K. Bhartia, O. Torres, C. Hsu, C. Seftor, and E. Celarier, Global distribution of UV-absorbing aerosols from Nimbus 7/TOMS data, *J. Geophys. Res.*, *102*, 16911-16922, 1997.

Herring, J.A., D.A. Jaffe, H.J. Beine, S. Madronich, and D.R. Blake, High-latitude springtime photochemistry: Part II, Sensitivity studies of ozone production, *J. Atmos. Chem.*, *27*, 155-178, 1997.

Hoffmann, T., J.R. Odum, F. Bowman, D. Collins, D. Klokow, R.C. Flagan, and J.H. Seinfeld, Formation of organic aerosols from the oxidation of biogenic hydrocarbons, *J. Atmos. Chem.*, *26*, 189-222, 1997.

Holland, F., U. Aschmutat, M. Hessling, A. Hofzumahaus, and D.H. Ehhalt, Highly time resolved measurements of OH during POPCORN using laser-induced fluorescence spectroscopy, *J. Atmos. Chem.*, in press, 1998.

Holton, J.R., P.H. Haynes, M.E. McIntyre, A.R. Douglass, R.B. Rood, and L. Pfister, Stratosphere-troposphere exchange, *Rev. Geophys.*, *33*, 403-439, 1995.

Horowitz, L.W., J. Liang, G.M. Gardner, and D.J. Jacob, Export of reactive nitrogen from North America during summertime, *J. Geophys. Res.*, *103*, 13451-13476, 1998.

Houweling, S., F. Dentener, and J. Lelieveld, The impact of non-methane hydrocarbon compounds on tropospheric photochemistry, *J. Geophys. Res.*, *103*, 10673-10696, 1998.

Hov, Ø. (ed.), *Tropospheric Ozone Research: Tropospheric Ozone in the Regional and Sub-Regional Context*, Springer-Verlag, Berlin, Germany, 1997.

Hsu, K.J., and W.B. DeMore, Temperature-dependent rate constants and substituent effects for the reactions of hydroxyl radicals with three partially fluorinated ethers, *J. Phys. Chem.*, *99*, 11141-11146, 1995.

Hudson, R.D., J.-H. Kim, and A.M. Thompson, On the derivation of tropospheric column ozone from radiances measured by the total ozone mapping spectrometer, *J. Geophys. Res.*, *100*, 11137-11145, 1995.

IPCC (Intergovernmental Panel on Climate Change), *Climate Change 1995: The Science of Climate Change*, edited by J.T. Houghton, L.G. Meira Filho, B.A. Callander, N. Harris, A. Kattenberg, and K. Maskell, Cambridge University Press, Cambridge, U.K., 1996.

IPCC (Intergovernmental Panel on Climate Change), *Aviation and the Global Atmosphere: A Special Report of IPCC Working Groups I and III*, edited by J.T. Houghton, D. Lister, J. Penner, M. McFarland, D. Griggs, and D. Dokken, Cambridge University Press, Cambridge, U.K., in preparation, 1999.

Jacob, D.J., J.A. Logan, G.M. Gardner, R.M. Yevich, C.M. Spivakovsky, and S.C. Wofsy, Factors regulating ozone over the United States and its export to the global atmosphere, *J. Geophys. Res.*, *98*, 14817-14826, 1993.

Jacob, D.J., B.G. Heikes, S.M. Fan, J.A. Logan, D.L. Mauzerall, J.D. Bradshaw, H.B. Singh, G.L. Gregory, R.W. Talbot, D.R. Blake, and G.W. Sachse, Origin of ozone and $NO_x$ in the tropical troposphere: A photochemical analysis of aircraft observations over the South Atlantic basin, *J. Geophys. Res.*, *101*, 24235-24250, 1996.

Jacob, D.J., M.J. Prather, P.J. Rasch, R.L. Shia, Y.J. Balkanski, S.R. Beagley, D.J. Bergmann, W.T. Blackshear, M. Brown, M. Chiba, M.P. Chipperfield, J. deGrandpre, J.E. Dignon, J. Feichter, C. Genthon, W.L. Grose, P.S. Kasibhatla, I. Kohler, M.A. Kritz, K. Law, J.E. Penner, M. Ramonet, C.E. Reeves, D.A. Rotman, D.Z. Stockwell, P.F.J. VanVelthoven, G. Verver, O. Wild, H. Yang, and P. Zimmerman, Evaluation and intercomparison of global atmospheric transport models using $^{222}Rn$ and other short-lived tracers, *J. Geophys. Res*, *101*, 5953-5970, 1997.

Jaeglé, L., D.J. Jacob, P.O. Wennberg, C.M. Spivakovsky, T.F. Hanisco, E.J. Lanzendorf, E.J. Hintsa, D.W. Fahey, E.R. Keim, M.H. Proffitt, E.L. Atlas, F. Flocke, S. Schauffler, C.T. McElroy, C. Midwinter, L. Pfister, and J.C. Wilson, Observed OH and $HO_2$ in the upper troposphere suggests a major source from convective injection of peroxides, *Geophys. Res. Lett.*, *24*, 3181-3184, 1997.

Jaeglé, L., D.J. Jacob, W.H. Brune, D. Tan, I.C. Faloona, A.J. Weinheimer, B.A. Ridley, T.L. Campos, and G.W. Sachse, Sources of $HO_x$ and production of ozone in the upper troposphere over the United States, *Geophys. Res. Lett.*, *25*, 1709-1712, 1998.

Jiang, Y., and Y.L. Yung, Concentrations of tropospheric ozone from 1979 to 1992 over tropical Pacific South America from TOMS data, *Science*, *272*, 714-716, 1996.

Jonson, J.E., and I.S.A. Isaksen, Tropospheric ozone chemistry: The impact of cloud chemistry, *J. Atmos. Chem.*, *16*, 99-122, 1993.

Justice, C.O., J.D. Kendall, P.R. Dowty, and R.J. Scholes, Satellite remote sensing of fires during the SAFARI campaign using NOAA Advanced Very High Resolution Radiometer data, *J. Geophys. Res.*, *101*, 23851-23863, 1996.

Kasibhatla, P., H. Levy II, A. Klonecki, and W.L. Chameides, Three-dimensional view of the large-scale tropospheric ozone distribution over the North-Atlantic Ocean during summer, *J. Geophys. Res.*, *101*, 29305-29316, 1996.

Kato, N., and H. Akimoto, Anthropogenic emissions of $SO_2$ and $NO_x$ in Asia: Emissions inventory, *Atmos. Environ.*, *26A*, 2997-3017, 1992.

Kaufman, Y.J. , R. Kleidman, M.D. King, and D.E. Ward, SCAR-B Fires in the tropics: Properties and their remote sensing from EOS-MODIS, *J. Geophys. Res.*, SCAR-B Special Issue, in press, 1998.

Kawakami, S., Y. Kondo, M. Koike, H. Nakajima, G.L. Gregory, G.W. Sachse, R.E. Newell, E.V. Browell, D.R. Blake, J.M. Rodriguez, and J.T. Merrill, Impact of lightning and convection on reactive nitrogen in the tropical free troposphere, *J. Geophys. Res.*, *102*, 28367-28384, 1997.

Kim, J.H., and M.J. Newchurch, Biomass-burning influence on tropospheric ozone over the eastern Pacific Ocean: The influences of biomass burning and tropospheric dynamics, *Geophys. Res. Lett.*, *23*, 3723-3726, 1996.

Kim, J.H., and M.J. Newchurch, Biomass-burning influence on tropospheric ozone over New Guinea and South America, *J. Geophys. Res.*, *103*, 1455-1462, 1998.

Kim, J.H., R.D. Hudson, and A.M. Thompson, A new method of deriving time-averaged tropospheric column ozone over the tropics using Total Ozone Mapping Spectrometer (TOMS) radiances: Intercomparison and analysis using TRACE A data, *J. Geophys. Res.*, *101*, 24317-24330, 1996.

Kirchhoff, V.W.J.H., J.R. Alves, F.R. da Silva, and J. Fishman, Observations of ozone concentrations in the Brazilian cerrado during the TRACE A field expedition, *J. Geophys. Res.*, *101*, 24029-24042, 1996.

Kirchner, F., and W.R. Stockwell, Effect of peroxy radical reactions on the predicted concentrations of ozone, nitrogenous compounds and radicals, *J. Geophys. Res.*, *101*, 21007-21022, 1996.

Kirchner, F., and W.R. Stockwell, Correction to "Effect of peroxy radical reactions on the predicted concentrations of ozone, nitrogenous compounds and radicals" by F. Kirchner and W.R. Stockwell, *J. Geophys. Res.*, *102*, 10871, 1997.

Kleinman, L.I., P.H. Daum, Y.-N. Lee, S.R. Springston, L. Newman, W.R. Leaitch, C.M. Banic, G.A. Isaac, and J.I. MacPherson, Measurement of $O_3$ and related compounds over southern Nova Scotia: 1, Vertical distributions, *J. Geophys. Res.*, *101*, 29043-29060, 1996.

Kley, D., H. Geiss, and V.A. Mohnen, Concentrations and trends of tropospheric ozone precursor emissions in the USA and Europe, in *The Chemistry of the Atmosphere: Its Impact on Global Change*, edited by J.G. Calvert, pp. 245-259, Blackwell Sci., Cambridge, Mass., 1994.

Kley, D., P.J. Crutzen, H.G.J. Smit, H. Vömel, S.J. Oltmans, H. Grassl, and V. Ramanathan, Observations of near-zero ozone concentrations over the convective Pacific: Effects on air chemistry, *Science*, *274*, 230-233, 1996.

Koike, M., Y. Kondo, S. Kawakami, H. Nakajima, G.L. Gregory, G.W. Sachse, H.B. Singh, E.V. Browell, J.T. Merrill, and R.E. Newell, Reactive nitrogen and its correlation with $O_3$ and CO over the Pacific in winter and early spring, *J. Geophys. Res.*, *102*, 28385-28404, 1997.

Kok, G.L., J.A. Lind, and M. Fang, An airborne study of the air quality around the Hong Kong territory, *J. Geophys. Res.*, *102*, 19043-19057, 1997.

Komala, N., S. Saraspriya, K. Kita, and T. Ogawa, Tropospheric ozone behaviour observed in Indonesia, *Atmos. Environ.*, *30*, 1851-1856, 1996.

Kondo, Y., H. Ziereis, M. Koike, S. Kawakami, G.L. Gregory, G.W. Sachse, H.B. Singh, D.D. Davis, and J.T. Merrill, Reactive nitrogen over the Pacific Ocean during PEM-West A, *J. Geophys. Res.*, *101*, 1809-1828, 1996.

Krishnamurti, T.N., M.C. Sinha, M. Kanamitsu, D. Oosterhof, H. Fuelberg, R. Chatfield, D.J. Jacob, and J. Logan, Passive tracer transport relevant to the TRACE A experiment, *J. Geophys. Res.*, *101*, 23889-23907, 1996.

Krol, M., P.J. van Leeuwen, and J. Lelieveld, Global OH trend inferred from methylchloroform measurements, *J. Geophys. Res.*, *103*, 10697-10711, 1998.

Kuhn, M., P.J.H. Builtjes, D. Poppe, D. Simpson, W.R. Stockwell, Y. Andersson-Sköld, A. Baart, M. Das, F. Fiedler, Ø. Hov, F. Kirchner, P.A. Makar, J.B. Milford, M.G.M. Roemer, R. Ruhnke, A. Strand, B. Vogel, and H. Vogel, Intercomparison of the gas-phase chemistry in several chemistry and transport models, *Atmos. Environ.*, *32*, 693-709, 1998.

Lamarque, J.-F., G.P. Brasseur, P.G. Hess, and J.-F. Müller, Three-dimensional study of the relative contributions of the different nitrogen sources in the troposphere, *J. Geophys. Res.*, *101*, 22955-22968, 1996.

Lary, D.J., A.M. Lee, R. Toumi, M.J. Newchurch, M. Pirre, and J.B. Renard, Carbon aerosols and atmospheric photochemistry, *J. Geophys. Res.*, *102*, 3671-3682, 1997.

Lawrence, M.G., and P.J. Crutzen, The impact of cloud particle gravitational settling on soluble trace gas distributions, *Tellus*, submitted, 1998.

Lawrence, M.G., W.L. Chameides, P.S. Kasibhatla, H. Levy, and W. Moxim, Lightning and atmospheric chemistry: The rate of atmospheric NO production, in *Handbook of Atmospheric Electrodynamics*, *Vol. 1*, edited by H. Volland, CRC Press, Boca Raton, Fla., 1995.

Lawrimore, J.H., M. Das, and V.P. Aneja, Vertical sampling and analysis of nonmethane hydrocarbons for ozone control in urban North Carolina, *J. Geophys. Res.*, *100*, 22785-22793, 1995.

Le Bras, G. (ed.), *Chemical Processes in Atmospheric Oxidation*, Springer-Verlag, Berlin, Germany, 1997.

Lee, D.S., I. Köhler, E. Grobler, F. Rohrer, R. Sausen, L. Gallardo-Klenner, J.G.J. Olivier, F.J. Dentener, and A.F. Bouwman, Estimations of global $NO_x$ emissions and their uncertainties, *Atmos. Environ.*, *31*, 1735-1749, 1997a.

Lee, M., B.G. Heikes, D.J. Jacob, G. Sachse, and B. Anderson, Hydrogen peroxide, organic hydroperoxide, and formaldehyde as primary pollutants from biomass burning, *J. Geophys. Res.*, *102*, 1301-1309, 1997b.

Lelieveld, J., and P.J. Crutzen, The role of clouds in tropospheric photochemistry, *J. Atmos. Chem.*, *12*, 229-267, 1991.

Lelieveld, J., and P.J. Crutzen, Role of deep cloud convection in the ozone budget of the troposphere, *Science*, *264*, 1759-1761, 1994.

Lelieveld, J., F. Arnold, B. Bregman, V. Bürger, P. Crutzen, H. Fischer, P. Siegmund, P. van Velthoven, and A. Waibel, Chemical perturbation of the lowermost stratosphere through exchange with the troposphere, *Geophys. Res. Lett.*, *24*, 603-606, 1997.

Levine, J.S., E.L. Winstead, D.A.B Parsons, M.C. Scholes, R.J. Scholes, W.R. Cofer III, D.R. Cahoon Jr., and D.I. Sebacher, Biogenic soil emissions of nitric oxide (NO) and nitrous oxide ($N_2O$) from savannas in South Africa: The impact of wetting and burning, *J. Geophys. Res.*, *101*, 23689-23697, 1996.

Levy, H. II, P.S. Kasibhatla, W.J. Moxim, A.A. Klonecki, A.I. Hirsch, S.J. Oltmans, and W.L. Chameides, The global impact of human activity on tropospheric ozone, *Geophys. Res. Lett.*, *24*, 791-794, 1997.

Liang, J., and D.J. Jacob, Effect of aqueous phase cloud chemistry on tropospheric ozone, *J. Geophys. Res.*, *102*, 5993-6001, 1997.

Liang, J., L.W. Horowitz, D.J. Jacob, Y. Wang, A.M. Fiore, J.A. Logan, G.M. Gardner, and J.W. Munger, Seasonal budgets of reactive nitrogen species and ozone over the United States, and export fluxes to the global atmosphere, *J. Geophys. Res.*, *103*, 13435-13450, 1998.

Liu, C.-M., S.C. Liu, and S.-H. Shen, A study of Taipei ozone problem, *Atmos. Environ.*, *24A*, 1461-1472, 1990.

Liu, S.C., S.A. McKeen, E.Y. Hsie, X. Lin, K.K. Kelly, J.D. Bradshaw, S.T. Sandholm, E.V. Browell, G.L. Gregory, G.W. Sachse, A.R. Bandy, D.C. Thornton, D.R. Blacke, F.S. Rowland, R. Newell, B.G. Heikes, H. Singh, and R.W. Talbot, Model study of tropospheric trace species distribution during PEM-West A, *J. Geophys. Res.*, *101*, 2073-2085, 1996.

Lobert, J.M., D.H. Scharffe, W.M. Hao, T.A. Kuhlbush, R. Sewen, P. Warneck, and P.J. Crutzen, Experimental evaluation of biomass burning emissions: Nitrogen and carbon containing compounds, in *Global Biomass Burning: Atmospheric Climatic and Biospheric Implications*, edited by J.S. Levine, pp. 289-304, MIT Press, Cambridge Mass., 1991.

Logan, J.A., Trends in the vertical distribution of ozone: An analysis of ozone sonde data, *J. Geophys. Res.*, *99*, 25553-25585, 1994.

Logan, J.A., and V.W.J.H Kirchhoff, Seasonal variations of tropospheric ozone at Natal, Brazil, *J. Geophys. Res.*, *91*, 7875-7881, 1986.

Mahlman, J.D., Dynamics of transport processes in the upper troposphere, *Science*, *276*, 1079-1983, 1997.

Mahowald, N.M., P.J. Rasch, and R.G. Prinn, Cumulus parameterizations in chemical transport models, *J. Geophys. Res.*, *100*, 26173-26189, 1995.

Manning, M., and H. Sidebottom, On the role of activated haloalkoxy radicals in the degradation of HCFC and HFC molecules, in *The Proceedings of the AFEAS Workshop*, Washington D.C., 1997.

Marenco, A., H. Gouget, P. Nedelec, J.P. Pages, and F. Karcher, Evidence of a long-term increase in tropospheric ozone from Pic du Midi data series, Consequences: Positive radiative forcing, *J. Geophys. Res.*, *99*, 16617-16632, 1994.

Marland, G., and T. Boden, Global, Regional, and National $CO_2$ Emissions, in *Trends: A Compendium of Data on Global Change*, Carbon Dioxide Information Analysis Center, Oak Ridge National Laboratory, Oak Ridge, Tenn., 1997.

Matthijsen, J., P.J.H. Builtjes, and D.L. Sedlak, Cloud model experiments of the effect of iron and copper on tropospheric ozone under marine and continental conditions, *Meteorol. Atmos. Phys.*, *57*, 43-60, 1995.

Mauldin, R.L. III, S. Madronich, S.J. Flocke, F.L. Eisele, G.J. Frost, and A.S.H. Prevot, New insights on OH: Measurements around and in clouds, *Geophys. Res. Lett.*, *24*, 3033-3036, 1997.

Mazurek, M.A., G.R. Cass, and B.R.T. Simoneit, Biological input to visibility-reducing aerosol particles in the remote arid southwestern United States, *Environ. Sci. Technol.*, *25*, 684-694, 1991.

McCroskey, P.S., and G.J. McRae, *Documentation for the Direct Decoupled Sensitivity Analysis Method—DDM, Report*, Department of Chemical Engineering, Carnegie Mellon University, Pittsburgh, Penn., 1987.

McKeen, S.A., E.-Y. Hsie, and S.C. Liu, A study of the dependence of rural ozone on ozone precursors in the eastern United States, *J. Geophys. Res.*, *96*, 15377-15394, 1991.

McKeen, S.A., G. Mount, F. Eisele, E. Williams, J. Harder, P. Goldan, W. Kuster, S.C. Liu, K. Baumann, D. Tanner, A. Fried, S. Sewell, C. Cantrell, and R. Shetter, Photochemical modeling of hydroxyl and its relationship to other species during the Tropospheric OH Photochemistry Experiment, *J. Geophys. Res.*, *102*, 6467-6493, 1997.

Metwally, M., *Jet Aircraft Engine Emissions Database Development, 1992 Military, Charter and Non-scheduled Traffic*, NASA Contractor Report 4686, National Aeronautics and Space Administration, Washington, D.C., 1995.

Miller, A.J., G.C. Tiao, G.C. Reinsel, D. Wuebbles, L. Bishop, J. Kerr, M. Nagatani, J.J. DeLuisi, and C.L Mateer, Comparisons of the observed ozone trends in the stratosphere through examination of Umkehr and balloon sonde data, *J. Geophys. Res.*, *100*, 11209-11217, 1995.

Møgelberg, T., O.J. Nielsen, J. Sehested, T.J. Wallington, and M.D. Hurley, Atmospheric chemistry of HFC-272ca: Spectrokinetic investigation of the $CF_3CF_2CH_2O_2$ radical, its reactions with NO and $NO_2$, and the fate of the $CF_3CF_2CH_2O$ radical, *J. Phys. Chem.*, *99*, 1995-2001, 1995a.

Møgelberg, T., J. Platz, O.J. Nielsen, J. Sehested, and T.J. Wallington, Atmospheric chemistry of HFC-236fa: Spectrokinetic investigation of the $CF_3CHO_2(\cdot)CF_3$ radical, its reaction with NO and the fate of the $CF_3CHO(\cdot)CF_3$ radical, *J. Phys. Chem.*, *99*, 5373-5378, 1995b.

Møgelberg, T., O.J. Nielsen, J. Sehested, and T.J. Wallington, Atmospheric chemistry of HCFC-133a: The UV absorption spectra of $CF_3CClH$ and $CF_3CClHO_2$ radicals, reactions of $CF_3CClHO_2$ with NO and $NO_2$, and fate of $CF_3CClHO$ radical, *J. Phys. Chem.*, *99*, 13437-13444, 1995c.

Møgelberg, T., A. Freilberg, A.M.B. Giessing, J. Sehested, M. Bilde, T.J. Wallington, and O.J. Nielsen, Atmospheric chemistry of HFC-236cb: Spectrokinetic investigation of the $CF_3CF_2CFHO_2$ radical, its reaction with NO and $NO_2$, and the fate of the $CF_3CF_2CFHO$ radical, *J. Phys. Chem.*, *99*, 17386-17393, 1995d.

Møgelberg, T., J. Sehested, M. Bilde, T.J. Wallington, and O.J. Nielsen, Atmospheric chemistry of $CF_3CFHCF_3$ (HFC-227ea): Spectrokinetic investigation of the $CF_3CFO_2(\cdot)CF_3$ radical, its reaction with NO and $NO_2$, and the fate of the $CF_3CFO(\cdot)CF_3$ radical, *J. Phys. Chem.*, *21*, 8882-8889, 1996.

Møgelberg, T., J. Sehested, G.S. Tyndall, J.J. Orlando, J.M. Fracheboud, and T.J. Wallington, Atmospheric chemistry of HFC-236cb: Fate of the alkoxy radical $CF_3CF_2CFHO$, *J. Phys. Chem.*, *101*, 2828-2832, 1997.

Moody, J.L., J.C. Davenport, J.T. Merrill, S.J. Oltmans, D.D. Parrish, J.S. Holloway, H. Levy II, G.L. Forbes, M. Trainer, and M. Buhr, Meteorological mechanisms for transporting $O_3$ over the western North Atlantic Ocean: A case study for August 24-29, 1993, *J. Geophys. Res.*, *101*, 29213-29227, 1996.

Mount, G.H., and E.J. Williams, An overview of the Tropospheric OH Photochemistry Experiment, Fritz Peak/Idaho Hill, Colorado, Fall 1993, *J. Geophys. Res.*, *102*, 6171-6186, 1997.

Moxim, W.J., H. Levy II, and P.S. Kasibhatla, Simulated global tropospheric PAN: Its transport and impact on $NO_x$, *J. Geophys. Res.*, *101*, 12621-12638, 1996.

Müller, J.-F., and G. Brasseur, IMAGES: A three-dimensional chemical transport model of the global troposphere, *J. Geophys. Res.*, *100*, 16445-16490, 1995.

Murphy, D.M., and D.W. Fahey, An estimate of the flux of stratospheric reactive nitrogen and ozone into the troposphere, *J. Geophys. Res.*, *99*, 5325-5332, 1994.

Nielsen, O.J., E. Gamborg, J. Sehested, T.J. Wallington, and M.D. Hurley, Atmospheric chemistry of HFC-143a: Spectrokinetic investigation of the $CF_3CH_2O_2$ radical, its reactions with NO and $NO_2$, and fate of $CF_3CH_2O$, *J. Phys. Chem.*, *98*, 9518-9525, 1994.

Novelli, P.C., K.A. Maserie, and P.M. Lang, Distribution and trends of carbon monoxide in the lower troposphere, *J. Geophys. Res.*, *103*, 19015-19033, 1998.

O'Brien, J.M., P.B. Shepson, K. Muthuramu, C. Hao, H. Niki, D.R. Hastie, R. Taylor, and P.B. Roussel, Measurements of alkyl and multifunctional organic nitrates at a rural site in Ontario, *J. Geophys. Res.*, *100*, 22795-22804, 1995.

Odum, J.R., T.P.W. Jungkamp, R.J. Griffin, R.C. Flagan, and J.H. Seinfeld, The atmospheric aerosol-forming potential of whole gasoline vapor, *Science*, *276*, 96-99, 1997.

Olson, J., M. Prather, T. Berntsen, G. Carmichael, R. Chatfield, P. Connell, R. Derwent, L. Horowitz, S.X. Jin, M. Kanakidou, P. Kasibhatla, R. Kotamarthi, M. Kuhn, K. Law, J. Penner, L. Perliski, S. Sillman, F. Stordal, A. Thompson, and O. Wild, Results from the Intergovernmental Panel on Climatic Change photochemical model intercomparison (Photocomp), *J. Geophys. Res.*, *102*, 5979-5991, 1997.

Oltmans, S.J., D.J. Hofmann, J.A. Lathrop, J.M. Harris, W.D. Komhyr, and D. Kuniyuki, Tropospheric ozone during Mauna Loa Observatory Photochemistry Experiment 2 compared to long-term measurements from surface and ozonesonde observations, *J. Geophys. Res.*, *101*, 14569-14580, 1996.

Oltmans, S.J., A.S. Lefohn, H.E. Scheel, J.M. Harris, H. Levy, I.E. Galbally, E.G. Brunke, C.P. Meyer, J.A. Lathrop, B.J. Johnson, D.S. Shadwick, E. Cuevas, F.J. Schmidlin, D.W. Tarasick, H. Claude, J.B. Kerr, O. Uchino, and V. Mohnen, Trends of ozone in the troposphere, *Geophys. Res. Lett.*, *25*, 139-142, 1998.

Orkin, V.L., V.G. Khamaganov, A.G. Guschin, B. Laszlo, R.E. Huie, and M.J. Kurylo, Rate constants for the reactions of OH with hydrofluorocarbons, *Abstracts of Papers of The American Chemical Society*, *208:* 240-ENVR, Part 1, 1994.

O'Sullivan, N., J. Wenger, and H. Sidebottom, Kinetics and mechanisms of the OH radical initiated degradation of fluorinated ethers, in *Proceedings of the 7th European Symposium on Physico-Chemical Behaviour of Atmospheric Pollutants: The Oxidizing Capacity of the Troposphere*, pp. 77-84, Office for Official Publications of the European Communities, Luxembourg (EUR 17482) ISBN 92-828-0158-6, 1997.

Parrish, D.D., J.S. Holloway, M. Trainer, P.C. Murphy, L.G. Forbes, and F.C. Fehsenfeld, Export of North-American ozone pollution to the North-Atlantic Ocean, *Science*, *259*, 1436-1439, 1993.

Parsons, D.A.B., M.C. Scholes, R.J. Scholes, and J.S. Levine, Biogenic NO emissions from savanna soils as a function of fire regime, soil type, soil nitrogen, and water status, *J. Geophys. Res.*, *101*, 23683-23688, 1996.

Penkett, S.A., P.S. Monks, L.J. Carpenter, K.C. Clemitshaw, G.P. Ayers, R.W. Gillett, I.E. Galbally, and C.P. Meyer, Relationships between ozone photolysis rates and peroxy radical concentrations in clean marine air over the Southern Ocean, *J. Geophys. Res.*, *101*, 12805-12817, 1997.

Pickering, K.E., A.M. Thompson, D.P. McNamara, W.-K. Tao, A.M. Molod, and R.B. Rood, Vertical transport by convective clouds: Comparisons between cloud-scale and global-scale models, *Geophys. Res. Lett.*, *22*, 1089-1092, 1995.

Pickering, K.E., A.M. Thompson, Y.S. Wang, W.K. Tao, D.P. McNamara, V.W.J.H. Kirchhoff, B.G. Heikes, G.W. Sachse, J.D. Bradshaw, G.L. Gregory, and D.R. Blake, Convective transport of biomass burning emissions over Brazil during TRACE A, *J. Geophys. Res.*, *101*, 23993-24012, 1996.

Poppe, D., J. Zimmermann, R. Bauer, T. Brauers, D. Bruning, J. Callies, H.P. Dorn, A. Hofzumahaus, F.J. Johnen, A. Khedim, H. Koch, R. Koppmann, H. London, K.P. Muller, R. Neuroth, C. Plassdulmer, U. Platt, F. Rohrer, E.P. Roth, J. Rudolph, U. Schmidt, M. Wallasch, and D.H. Ehhalt, Comparison of measured OH concentrations with model calculations, *J. Geophys. Res.*, *99*, 16633-16642, 1994.

Prather, M.J., and D.J. Jacob, A persistent inbalance between $HO_x$ and $NO_x$ photochemistry of the upper troposphere driven by deep tropical convection, *Geophys. Res. Lett.*, *24*, 3189-3192, 1997.

# CHAPTER 9

# Ultraviolet Radiation at the Earth's Surface

**Lead Authors:**
J.R. Herman
R.L. McKenzie

**Coauthors:**
S.B. Diaz
J.B. Kerr
S. Madronich
G. Seckmeyer

**Contributors:**
G. Bernhard
M. Blumthaler
B. Bodhaine
C.R. Booth
E. Celarier
P. Forster
N. Krotkov
J. Lenoble
K. Leszczynski
C.S. Long
B. Mayer
F. Mims
P. Neale
R. Piacentini
K. Ryan
H. Slaper
J. Slusser
R. Wooldridge
C.S. Zerefos

# CHAPTER 9

## ULTRAVIOLET RADIATION AT THE EARTH'S SURFACE

### Contents

## SCIENTIFIC SUMMARY

The advances and new findings that have occurred in the ultraviolet (UV) radiation field since the publication of the previous Assessment (WMO, 1995) include the following:

- The inverse relationship between decreasing ozone amount and increasing UV-B radiation has been reconfirmed and firmly established in both theory and measurements. The measured effects of ozone, albedo, altitude, clouds and aerosols, and geographic differences are much better understood.

- The number, distribution, and quality of UV-irradiance (energy per unit area per unit time) instruments have greatly improved throughout the world. However, there are still regions of sparse coverage.

- Well-calibrated UV-irradiance spectral time series are now available at some ground sites for periods of up to 9 years, where changes in UV-B irradiance have been detected (e.g., 1.5% per year at 300 nm, 0.8% per year at 305 nm) at midlatitudes (near 40°) that are consistent with expected changes from the decreasing amounts of ozone. However, the long-term stability needed for trend estimates has been demonstrated for only a few ground-based UV instruments. Either the records are not long enough or the instrument stability is insufficient to reliably determine decadal change at most midlatitude sites. Other factors limiting the detection of long-term trends are that clouds, albedo, aerosols, and short-term ozone changes produce local daily, monthly, and interannual changes that are larger than the long-term trend. It is important for long-term trend detection that both UV-A and UV-B be measured separately along with ancillary data (e.g., ozone and aerosols).

- The anomalous UV-trend estimates from the Robertson-Berger (RB) meter network located in the United States are now understood. Corrections have been applied to the data, which now show no significant trends for the latitude range of the instruments' locations. It was concluded that the data from the U.S. RB network alone are unsuitable for trend detection.

- Increases in UV-B irradiance in the Northern Hemisphere at high latitudes have been attributed to the low ozone amounts in the winter and spring of 1995, 1996, and 1997.

- New types of filter instruments have been developed, using narrower band pass at a few selected wavelengths and greater filter stability specifications than previous broadband instruments. These simpler instruments may yield results with accuracy comparable to that of grating spectroradiometers (5 to 10%) and should permit a wider geographical distribution of measuring sites for UV irradiance. This is especially important to address the lack of sufficient observing sites in some regions.

- New satellite estimates of global (latitude ±65°) UV irradiance, which now include cloud, surface albedo, and aerosol effects, are available using radiative transfer models and measured radiances from Total Ozone Mapping Spectrometer (TOMS) instruments. The satellite-estimated UV irradiances have been compared with ground-based measurements at a single site, Toronto. The weekly-average results agree to within 5% for snow-free conditions. Further comparisons at other sites are necessary to validate the accuracy and applicability of the techniques over a wide range of observing conditions. This may be especially important when accounting for local aerosol extinctions.

- TOMS satellite data have been used to estimate long-term decadal changes in zonally averaged global and seasonal patterns in UV irradiance from 1979 to 1992. The results showed that the UV-B irradiances increased (see table below), while UV-A irradiances remained unchanged. At individual sites, changes in UV-A irradiances have occurred because of changes in local cloudiness and aerosol amounts.

**Zonal Average UV-Erythemal Trends (Percent Increase per Decade) 1979 to 1992.**

| Latitude | January | April | July | October | Annual ± 2σ |
|---|---|---|---|---|---|
| 50° to 65°N | 6 | 4 | 2 | 4 | 3.7 ± 3 |
| 35° to 50°N | 3 | 3 | 2 | 2 | 3 ± 2.8 |
| 30°S to 30°N | 0 | 0 | 0 | 0 | 0 ± 2 |
| 35° to 50°S | 4 | 2 | 2 | 6 | 3.6 ± 2 |
| 50° to 65°S | 4 | 5 | 8 | 14 | 9 ± 6 |

- Zonally averaged UV-irradiance trend determinations from satellite data that include cloud effects yield numbers nearly identical to those from clear-sky estimates. However, the currently estimated UV trends are slightly lower than the clear-sky values in the 1994 Assessment because of the new TOMS ozone algorithm (see Chapter 4).

- Measurements at several ground sites have indicated differences between UV irradiances in the Northern and Southern Hemispheres that are larger than explained by the known differences in ozone amount and Sun-Earth separation. This may indicate that other factors such as aerosols could be involved. Satellite estimates show smaller irradiance differences between the hemispheres than do ground-based measurements.

- Several intercomparisons of UV-irradiance instruments of different types have been conducted in various countries. These have helped identify instrument capabilities and limitations. Currently, the best intercomparisons of different instruments at the same location are within ±5% absolute accuracy. However, this "best" accuracy estimate does not represent the general level of agreement between geographically distributed networks of similar and different instruments over extended periods of time. Significant improvements have been made to reduce errors in the cosine response, stray light rejection, and wavelength alignment.

- Expansion of the World Ozone and Ultraviolet Radiation Data Centre (WOUDC) in Canada and the European database, Scientific UV Data Management/UV Radiation in the Arctic; Past, Present, and Future (SUVDAMA/UVRAPPF), has significantly improved the availability and distribution of data to researchers studying the effects and behavior of UV-B radiation. Extensive sources of UV information have become available on the Internet.

- Significant improvements have been made in calibration of ground-based instruments. This has been achieved through instrument intercomparisons and the use of newly developed central calibration facilities, although additional calibration facilities would continue to meet needs. After validation, satellite estimations of UV irradiance may serve as a comparison standard between widely separated ground-based instruments in a manner similar to that used for the ground-based ozone network.

- Different classes of radiative transfer models have been intercompared and found to agree within 1% for irradiances. However, for some radiative transfer approximations (e.g., delta-Eddington) the gains in computational speed are offset by losses in accuracy. Two-stream models have accuracies on the order of 5% for moderate optical depths and can have errors exceeding 10% for large optical depths (small irradiances).

- Public interest related to UV exposure has been addressed by establishing a standardized UV index in many countries, based on estimates of ozone and, in some cases, cloud cover and surface albedo, to provide daily information about the intensity of UV radiation.

## 9.1 INTRODUCTION

The ultraviolet (UV) region (200-400 nm) of the solar radiation spectrum accounts for a small fraction of the total radiant energy that reaches the Earth's surface. Wavelengths shorter than 280 nm (UV-C) are important for atmospheric photochemistry, but they are completely absorbed in the atmosphere by ozone ($O_3$), molecular oxygen ($O_2$), and other minor atmospheric species, and do not reach the ground. The remaining UV spectral region is arbitrarily subdivided into two subregions: UV-B and UV-A. The UV-B component (280-315 nm) is of particular interest because it is strongly absorbed by ozone, and it increases when the atmospheric ozone amount decreases. This spectral region has significant impact on important biomolecules, such as deoxy-ribonucleic acid (DNA) and proteins, and therefore, on living organisms. The UV-A region (315-400 nm) is largely unaffected by ozone. Although the photons are somewhat less energetic than those in the UV-B range, they still have important biological effects (e.g., sunburn). Both UV-A and UV-B radiation have important impacts on various materials and chemical processes on the Earth's surface and in the atmosphere. Although the internationally agreed boundary between the UV-A and UV-B is at 315 nm, some authors whose work is cited in this document prefer to use a boundary at 320 nm, because there is still significant ozone absorption between 315 and 320 nm.

Since the last evaluation, there has been extensive publication of new results in the field of UV research. More emphasis has been put into ground-based spectral measurements, satellite-derived estimates (combining backscattered radiance data and a radiative transfer model) of UV-irradiance (energy per unit area per unit time) reaching the Earth's surface, and radiative transfer studies.

This chapter reviews progress made since the previous Assessment (WMO, 1995, Chapter 9) in our understanding of UV radiation that reaches the Earth's surface. In addition, this review identifies some of the most important outstanding problems in the quantitative determination of UV irradiances. The impacts of UV irradiance increases (e.g., effects on the biosphere, including human health and materials) are outside the scope of this report and are discussed in the United Nations Environment Programme (UNEP) "Effects Panel" reports (UNEP 1991, 1994, 1998). Impacts on tropospheric chemistry that may result from changes in UV radiation fields are discussed in Chapter 10 of this report and are also found in UNEP (1998); predicted effects of future changes in UV are discussed in Chapter 11 (UNEP, 1998).

## 9.2 GROUND-BASED OBSERVATIONS OF UV

The majority of UV-A and UV-B instruments fall into the following classes:

1. broadband radiometers (e.g., to match the erythemal, or "sunburning," action spectrum (McKinlay and Diffey, 1987)),
2. multi-channel medium-spectral-resolution (2-10 nm resolution) instruments, or
3. high-resolution spectrometers (0.5-1 nm resolution).

The multi-channel instruments sample irradiance at a number of fixed wavelength bands determined by the transmission of individual filters. The spectrometers usually sample at a uniform wavelength interval comparable with or smaller than their resolution (typically 0.5 nm or better). Most UV-A and UV-B instruments are designed to measure the amount of radiation falling on a horizontal surface (direct plus diffuse irradiance, known as global irradiance).

In recent years there have been developments in new types of instrumentation to measure actinic UV radiation (multi-directional radiances), rather than downwelling irradiance alone (e.g., McElroy, 1995; Shetter and Müller, 1998). Such measurements are useful in studies of atmospheric photochemical processes.

### 9.2.1 Broadband and Multi-Channel Filter Instruments

Broadband radiometers have provided an important source of UV-irradiance information over wide geographic areas and over long time periods. Compared with multi-channel spectroradiometers, their low cost and rapidity of measurement make them very attractive for monitoring UV irradiances. Considerable efforts in quality control and assurance are required to produce scientifically useful information. Changes in their spectral response or sensitivity can lead to errors that are difficult to detect. Multi-channel filter instruments have an advantage in making nearly simultaneous measurements at many wavelengths, compared with

grating spectroradiometers, which typically require several minutes to complete a wavelength scan. Simultaneous wavelength measurements are useful for separating cloud and aerosol effects from ozone effects.

There has been continuing strong interest in the historical record for broadband instruments, particularly in the much-discussed work of Scotto *et al.* (1988), which showed a decline in annually integrated UV irradiance measured by eight Robertson-Berger (RB) meters in the continental United States between 1974 and 1985. The average trend based on the eight stations was -0.7% per year, while the statistically significant values for individual stations varied from -0.5 to -1.0% per year. DeLuisi and Barnett (1992) uncovered a potential shift in calibration of the RB-meter network in 1980 that could remove the downward trend found by Scotto *et al.* (1988). A reanalysis of the RB-meter data (Weatherhead *et al.*, 1997), with an extension through 1991 but without including a term in the time series analysis to account for "mean level shifts," showed a UV-irradiance decrease of 0.6% per year, in agreement with the original work by Scotto *et al.* (1988). However, when corrections are made for mean level shifts, which may be due to calibration changes and other instrument-related problems, the resulting overall trend is found by Weatherhead *et al.* to be +0.2% per year (not statistically significant). In many cases Weatherhead *et al.* found that the adjustments to the instruments were not traceable to physical causes in the log records. This makes the use of the U.S. RB-meter network unsuitable for detecting long-term trends. The small rate of increase is also in agreement with recent analysis of UV-irradiance trends estimated from Total Ozone Mapping Spectrometer (TOMS) satellite data (J.R. Herman *et al.*, 1996) for the same geographical region.

### 9.2.2 Spectroradiometers

Spectroradiometers consist of medium- and high-spectral-resolution filter and grating instruments. These cover the entire UV-A and UV-B range of wavelengths with the purpose of both measuring the amount of UV irradiance and determining the atmospheric processes that contribute to UV-irradiance attenuation (e.g., ozone, sulfur dioxide ($SO_2$), aerosols) and variability (e.g., ozone, clouds). Their increased cost and maintenance are offset by the increase of spectral detail available, their ability to independently determine ozone and aerosol amounts, and their ability to estimate the extraterrestrial UV flux. Changes in ozone amount produce a clear spectral signature that is quite different from UV-irradiance changes produced by aerosols, clouds, and surface reflectivity. Unlike broadband instruments, spectroradiometers can separate ozone effects from the variability produced by clouds by using the longer UV-A wavelengths that are not absorbed by ozone.

The number and quality of spectroradiometers used for studies of UV radiation at the surface have improved significantly since the last Assessment. Generally, the time period of observations is still too short to determine UV-irradiance trends unambiguously with these instruments. However, they have been used to demonstrate the spectrally resolved effects of changes in ozone amount, cloud cover, surface albedo, and observing altitude.

### 9.2.3 Instrument Deployment and Data Archival

Although there has been a significant increase in the number of instruments deployed and in the effort to calibrate these instruments, many problems remain. The addition of several calibration facilities or regional instrumental quality assurance centers should help to reduce the problems in future years. Examples are the National Oceanic and Atmospheric Administration (NOAA) calibration facilities in Boulder, Colorado, to calibrate broadband and spectral instruments; the Atmospheric Environment Service, Toronto, of Environment Canada; the Radiation and Nuclear Safety Authority, Helsinki, Finland (STUK); and the German reference instrument center in Garmisch-Partenkirchen.

Assessing the impact of ultraviolet radiation on biological processes requires accurate and sustained monitoring of UV irradiances over the entire globe from both ground (e.g., Kerr and McElroy, 1993) and satellite instruments (J.R. Herman *et al.*, 1996), if short-term changes or coincidental biological phenomena are to be distinguished from those caused by long-term UV-irradiance changes. The ground-based instruments are necessary to understand the effects of clouds, aerosols, and local terrain on UV radiation reaching the ground, whereas only the satellite estimation of UV radiation can give the global and regional perspective necessary for understanding the overall effects of UV radiation at the Earth's surface.

Many parts of the world now maintain large networks of ground-based UV-irradiance instruments of

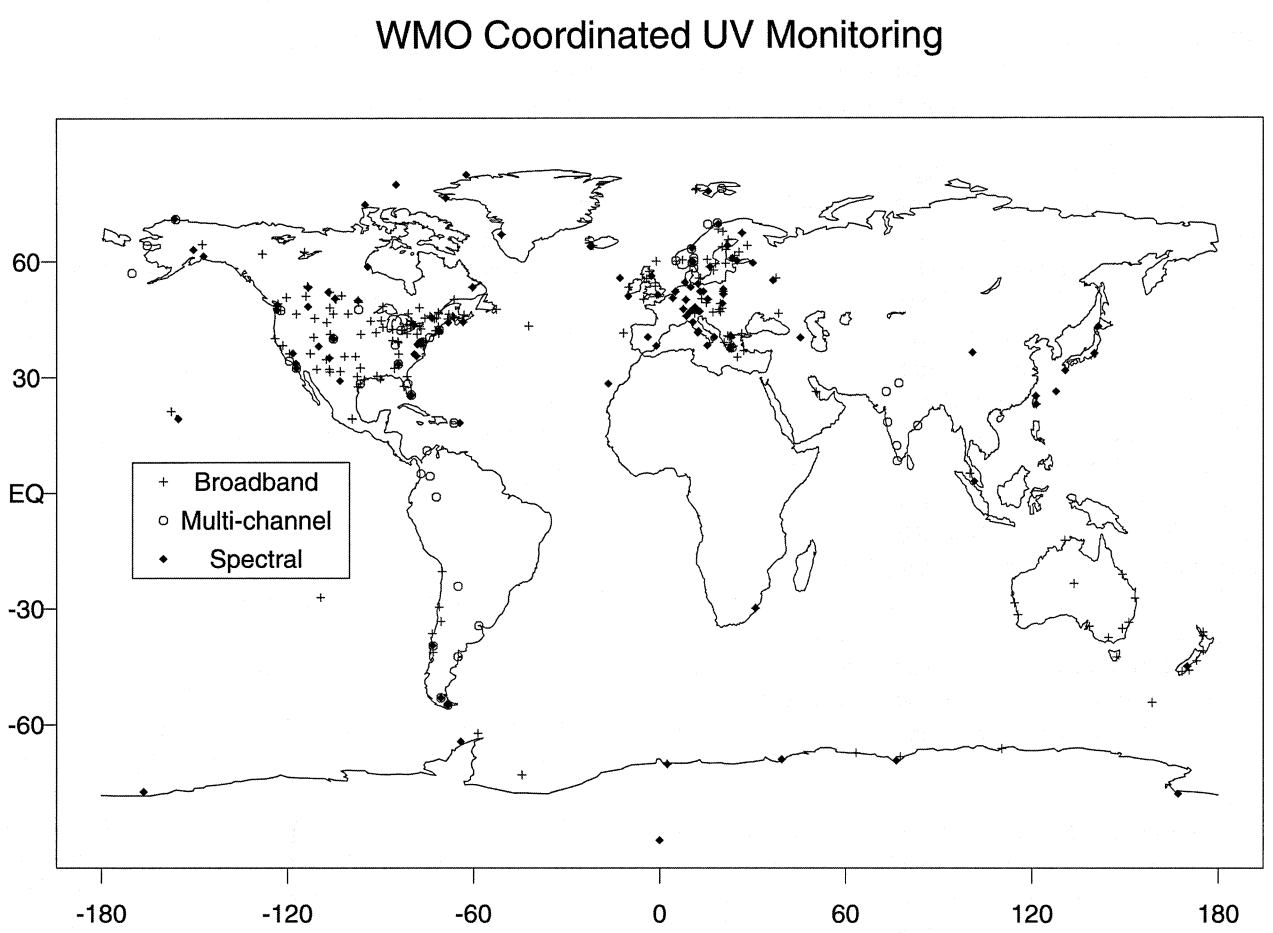


**Figure 9-1.** Map showing the global distribution of surface-based instruments monitoring UV radiation. (Updated from Weatherhead and Webb, 1997.)

various types. Most prominent among these are the networks operating in Canada, the United States, Japan, and Europe. For the Southern Hemisphere, one important installation is in Lauder, New Zealand. In South America and the Antarctic Peninsula, several new UV-irradiance instruments have been installed and are collecting data. In this network project, involving scientists from Chile, Argentina, and various other countries, the disparate networks are brought together within a centralized data processing and quality control facility in Ushuaia, Argentina. This South American network is based on a model of the U.S. network, where a collection of smaller UV-irradiance networks (e.g., the U.S. Department of Agriculture (USDA), U.S. National Science Foundation (NSF), U.S. Environmental Protection Agency (EPA), U.S. National Oceanic and Atmospheric Administration (NOAA), and universities), comprised of different instruments, is linked by standardized protocols, intercomparisons, and calibrations. A map of prominent ozone and UV monitoring sites is shown in Figure 9-1.

Progress has also been made in standardizing the archival of UV-irradiance data. The primary archive of spectral UV-irradiance data is at the World Ozone and Ultraviolet Radiation Data Centre (WOUDC) in Toronto (Wardle *et al.*, 1997). The WOUDC database consists of more than 600,000 spectra representing more than 120 station-years from 23 sites. There are plans to make the database available on compact disk-read only memory (CD-ROM) media. Other datasets are recently available from individual groups (e.g., Gardiner *et al.*, 1993; McKenzie *et al.*, 1993) and from the emerging European database, Scientific UV Data Management/UV Radiation in the Arctic: Past, Present, and Future (SUVDAMA/UVRAPPF). An additional repository of UV-irradiance

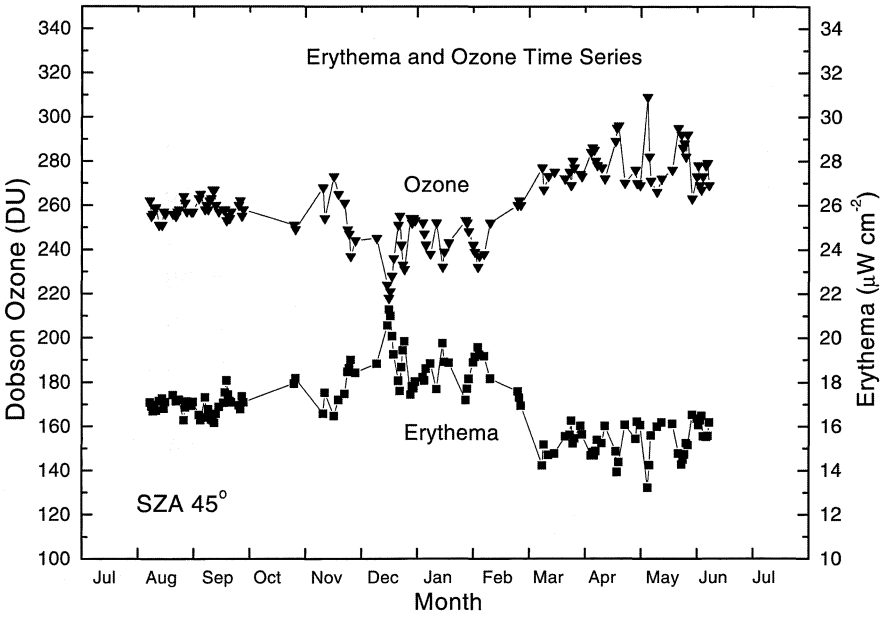


**Figure 9-2.** Measured erythemal irradiances (lower curve) from an ultraviolet spectroradiometer at SZA 45° compared with total ozone (upper curve) for 132 clear mornings during July 1995 to July 1996 at Mauna Loa Observatory (19.5°N, 155.6°W, 3.4 km), showing the inverse relationship between erythemal UV and ozone amount. (From Bodhaine *et al.*, 1997.)

data from 26 European stations has been established in the Finnish Meteorological Institute, Helsinki, Finland (Scientific Data Management, SUVDAMA/UVRAPPF), which is planned to have close links with WOUDC. Radiative transfer studies using the archived data have already provided experimental corroboration of the modeled relationship between ozone and UV irradiance (WMO, 1992, 1995).

Multi-year spectral and broadband data are also available from networks of instruments operated by the National Science Foundation on CD-ROM (Booth *et al.*, 1994), from the U.S. Department of Agriculture UV-B monitoring program operated by Colorado State University (Bigelow *et al.*, 1998), from the NOAA Integrated Surface Irradiance Study (Hicks *et al.*, 1996), and from several other groups (e.g., the Japan Meteorological Agency, the U.S. Environmental Protection Agency) (Gardiner *et al.*, 1993; McKenzie *et al.*, 1993; Kerr and McElroy, 1993; Ito *et al.*, 1994).

### 9.2.4 Relationship between Ozone and UV

There is excellent experimental evidence that UV-irradiance increases at the Earth's surface are directly correlated with ozone decreases in the atmosphere (Kerr and McElroy, 1993; Madronich *et al.*, 1995; Varotsos and Kondratyev, 1995; Bodhaine *et al.*, 1996, 1997). The model-predicted effect of decreasing atmospheric ozone content on surface-UV irradiance has been confirmed by process studies from ground-based instrumentation (WMO, 1992, 1995).

The anticorrelation is most clearly seen when measurements are filtered to remove the effects of the meteorological factors discussed in Section 9.4. For example, measurements from the high-altitude Mauna Loa Observatory (MLO, 3.4 km), which is relatively cloud free and pollution free, show strong anticorrelations (see Figure 9-2) between ozone and erythemally weighted UV irradiance over a full year of measurements at fixed solar zenith angle (SZA) (Bodhaine *et al.*, 1996, 1997).

The same spectra have been used to calculate the wavelength-dependent sensitivity of UV to ozone changes. Figure 9-3 shows that the measured sensitivity increases strongly toward shorter wavelengths and demonstrates that a 1% reduction in ozone causes a 7% increase in UV irradiance at 295 nm (SZA = 45°, ozone = 265 Dobson units (DU)). The increasing sensitivity of

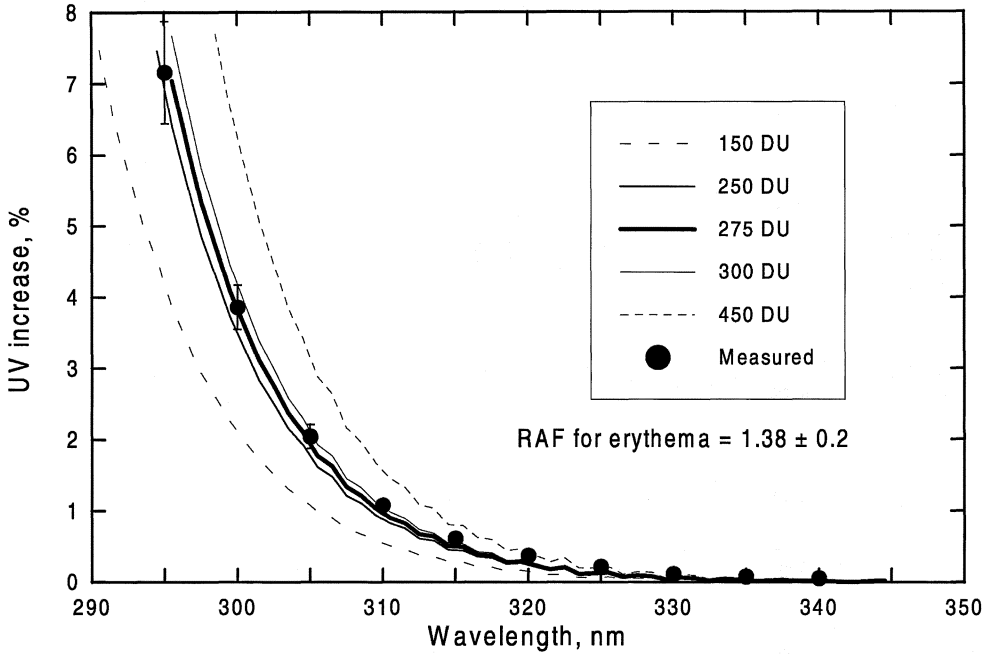


**Figure 9-3.** The measured wavelength-dependent sensitivity of UV to a 1% decrease in ozone at SZA 45° for 132 clear days during July 1995 to July 1996 at Mauna Loa Observatory. The curves show the calculated sensitivity for several assumed ozone amounts. (Based on Bodhaine *et al.*, 1997.)

UV irradiance for a given SZA to changes in ozone amount at shorter wavelengths is as predicted based on larger ozone absorption coefficients. The deduced radiation amplification factor (RAF) for erythema from this dataset is in agreement within the experimental uncertainty.

For most conditions, the RAF (see below) can be derived using Equations (9-1) and (9-2), without the need for a full radiative transfer calculation, from $\alpha\Omega\sec(\theta)$, where $\theta$ = SZA < 50° is the solar zenith angle:

$$\frac{dF}{F} \approx -\alpha\Omega\frac{d\Omega}{\Omega}\sec(\theta) \qquad (9\text{-}1)$$

where $\alpha$ is the ozone absorption coefficient; $\Omega$ is the ozone column amount; and $F$ is the irradiance.

The sensitivity of UV to small changes in ozone may be expressed as a radiation amplification factor, defined as

$$\mathrm{RAF} \equiv -\frac{dF/F}{d\Omega/\Omega} \cong \alpha\Omega\sec(\theta) \qquad (9\text{-}2a)$$

Equation (9-2b) is a modified form of Equation (9-2a) that was proposed by Madronich (1994) as more suitable for estimating the RAF when the changes $\Omega - \Omega^*$ and $F - F^*$ are large (Madronich and deGruijl, 1994):

$$\mathrm{RAF} = -\frac{\ln\frac{F^*}{F}}{\ln\frac{\Omega^*}{\Omega}} \qquad (9\text{-}2b)$$

For many biologically weighted action spectra, the RAF is approximately constant over a wide range of ozone and SZA (Madronich *et al.*, 1995).

For larger SZA (greater than 50°) and high ozone amounts, deviations from Equation (9-2a) can occur because of the Umkehr effect (Mateer, 1965), which occurs when most of the direct solar UV radiation at high SZA (near the horizon) is absorbed by ozone along the large slant path to the observer's site. In this case, the global radiation (scattered plus direct) consists of mainly diffuse radiation that scatters high in the atmosphere above the observer's site. These scattered photons have a shorter optical path through the ozone than do the

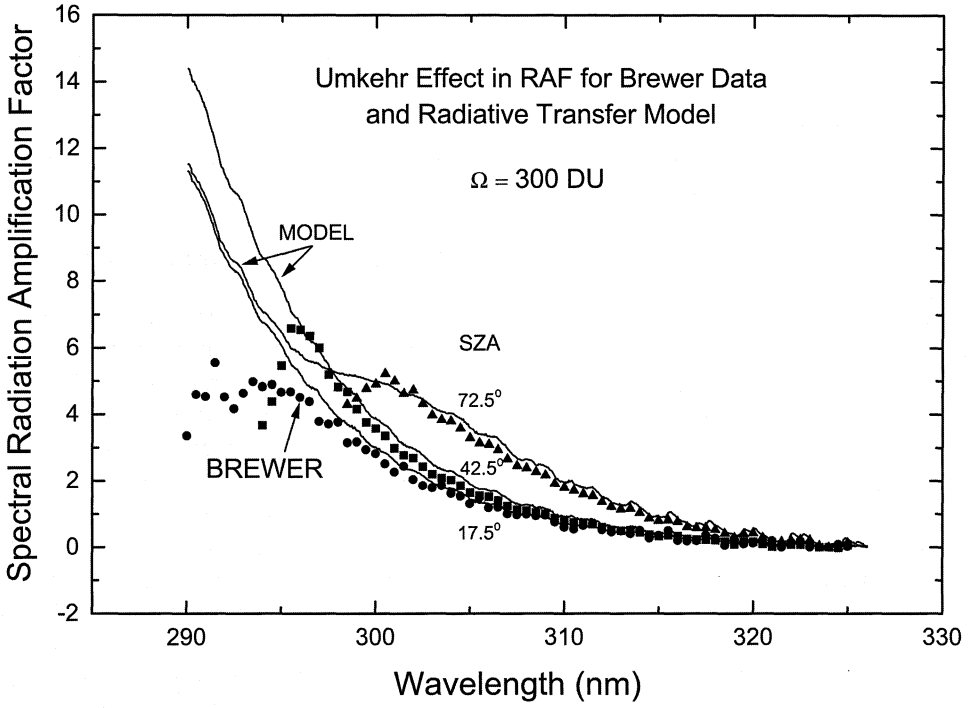


**Figure 9-4.** A comparison of the measured and calculated sensitivities to a 1% ozone reduction, for ozone amount = 300 DU. The model results (solid lines) show the onset of the Umkehr effect for solar zenith angle 72.5°. The measured values, obtained from a Brewer instrument (single monochromator), diverge from the model at shorter wavelengths. (From Fioletov *et al.*, 1997.)

photons in the direction of the direct beam, and therefore a reduced RAF compared with the prediction of Equation (9-2a) (Brühl and Crutzen, 1989). Under such conditions (see Figure 9-4), the sensitivity of UV to changes in ozone decreases toward shorter wavelengths, relative to predictions from Equation (9-2a) (Fioletov *et al.*, 1997). These conditions are usually unimportant from a biological point of view, because the irradiances are small compared to noon conditions (except in the polar spring and autumn).

An extensive analysis of UV-B irradiance and its dependence on total ozone is reported by Fioletov *et al.* (1997). About 300,000 spectra made by Brewer spectrophotometers at seven stations in Canada and Japan between 1989 and 1995 were used to establish a statistical relationship. Irradiance values at wavelengths between 300 and 325 nm were normalized to the value at 324 nm, where the effects of ozone absorption are nearly negligible. The dependence of these normalized spectra on SZA, and the nearly simultaneous measurements of total ozone, were determined for solar zenith angles between 27.5° and 87.5°. The analysis provides an empirical wavelength-by-wavelength measure of the increase of UV-B irradiance for a 1% decrease of total ozone. These values were found to be essentially the same for clear and cloudy conditions (except for very heavy clouds) and are in good agreement with model results for longer wavelengths and moderate SZA (see Figure 9-4).

### 9.2.5 Instrument Calibration and Measurement Uncertainties

All types of UV-radiation instruments share some common problems related to the accuracy of the data obtained. Many of these are related to the steep slope of the irradiance spectrum in the UV-B region caused by the increasing ozone-absorption coefficient with decreasing wavelength (320 to 250 nm).

Other problems are related to the instrumentation. These include errors resulting from (1) calibration-lamp accuracy (radiometric calibration), (2) stray-light

problems, (3) slit-function or spectral-response characterization, (4) diffuser cosine corrections for irradiance instruments, and (5) wavelength calibration for spectroradiometers and narrowband filter instruments. These error sources are discussed in detail in the following subsections. The combined effect of these and other error sources leads to overall accuracies of ±5% to ±15%.

The requirements to achieve the necessary long-term repeatability have been considered by the Network for the Detection of Stratospheric Change (NDSC) as well as by the World Meteorological Organization (WMO) (e.g., McKenzie *et al.*, 1997b).

#### 9.2.5.1 Radiometric Calibration

One source of uncertainty concerns tracing the absolute calibration to a common standard, such as maintained by the U.S. National Institute of Standards and Technology (NIST), the German Physikalisch Technische Bundesanstalt (PTB), and the British National Physical Laboratories (NPL). Standard lamps used by national standards laboratories can disagree by more than ±2% in the UV-B region (Walker *et al.*, 1991). Also, there is evidence indicating that individual lamps behave differently with regard to stability, both in the short term (calibration to calibration) and long term (drift over several years).

One investigation into the use of the Langley method as an alternative to lamp calibrations has been conducted at two sites (Table Mountain, Colorado, and Mauna Loa, Hawaii) of the 25-site network of UV Multi-Filter Rotating Shadowband Radiometers (UV-MFRSRs, 2-nm spectral resolution, full-width half-maximum (FWHM)) by the USDA UV-B Monitoring Program (Bigelow *et al.*, 1998). Preliminary results of the application of this method (Bigelow *et al.*, 1998) show good agreement between radiative transfer estimates of the irradiances and measurements from the UV-MFRSR instruments, but disagreement with measurements made at Table Mountain with a Brewer spectroradiometer.

An alternative calibration approach is a variation of the Langley method (a method of measured radiances at different sun angles extrapolated to zero-air mass (Schmid and Wehrli, 1995)), which uses the measured extraterrestrial solar irradiance as an absolute reference (Wilson and Forgan, 1995; Schmid *et al.*, 1998). This method has the potential to avoid problems of lamp variabilities, although it cannot be used for UV-B wavelengths at sites where diurnal variations of total ozone often occur (Kerr and McElroy, 1993; Kohler, 1986; Kerr, 1998) and at sites with changing aerosol conditions.

#### 9.2.5.2 Stray-Light Rejection

Another consideration for UV measurements is the effect of stray light. It is often the case that stray light from wavelengths with a relatively high radiation amount adds significantly to the signal being registered at nearby wavelengths that are several orders of magnitude less. This is particularly important for wavelengths less than 305 nm, because the radiation at the ground increases by several orders of magnitude from 290 nm to 325 nm. The direct method to overcome this problem is to use double monochromators that typically have out-of-band contributions of about 1 part in $10^6$ to $10^8$ compared to 1 part in $10^3$ to $10^4$ for a single monochromator. The recent deployment of double-monochromator Brewer instruments to reduce stray-light problems has improved accuracy at short wavelengths compared to widely deployed single-monochromator versions (Bais *et al.*, 1996). However, it is possible to partially correct data from single-monochromator instruments, provided the details of the stray-light spectrum are known. Some of the data from single monochromators currently archived in the WOUDC (see Section 9.2.3) have had a stray-light correction applied. The use of band-pass filters with sharp wavelength cutoffs can improve the performance of single monochromators.

#### 9.2.5.3 Spectral Response

An important part of the UV-irradiance calibration process is the accurate determination of the spectral response of an instrument. For a filter instrument (either broad or medium band), the combined spectral transmission of the filter and the spectral alignment of the sensor must be known. Accurate knowledge of the spectral response function is necessary for comparing with radiative transfer models and with other instruments. The filter transmission and sensor response can be measured either separately or together. The wavelength response of spectroradiometers is often determined by using spectral scans of lamps with emission lines at known wavelengths.

tion (McKinlay and Diffey, 1987) used to estimate the probability of skin reddening from UV exposure. There are also differences in the weighting functions produced by different manufacturers, as well as differences in corrections required for errors in the cosine response function. Field intercomparisons of broadband measurements with spectral data have revealed the importance of the SRFs.

One such comparison, the WMO/STUK Intercomparison of Erythemally Weighted Radiometers, was undertaken by the Radiation and Nuclear Safety Authority in Helsinki, Finland, in cooperation with the University of Innsbruck and with support from the WMO (Leszczynski *et al.*, 1997, 1998). During this intercomparison, the erythemally weighted (EW) radiometers were compared with two spectroradiometers in solar radiation, and the cosine and spectral responsivities of all participating instruments were measured in the laboratory. Most of the instruments (16 of 20) involved in the intercomparison were from a single manufacturer (Solar Light Company (SLC) meters).

Based on the laboratory measurements, the correction factors required to eliminate the errors due to non-ideal characteristics were calculated as functions of SZA and ozone. Figure 9-6a demonstrates that the calculated correction factor to eliminate the error due to the deviation of the SRF from the CIE weighting function (CIE = International Lighting Commission (France)) is a strong function of total ozone content and of solar elevation.

Examples of instruments manufactured by other companies (i.e.,Yankee Environmental Systems, Inc., Vital Technologies Co., and Scintec Atmosphären Messtechnik GMBH) were also included in the study. The spectral responsivity correction factor for one of these instruments is compared with the SLC meters in Figure 9-6b. The figure also shows that the conversion to the CIE-weighted UV irradiance has significant variability even between instruments from the same manufacturer, due to slight differences in SRFs. If instrument-to-instrument differences in cosine response are factored in, the correction factors show only slightly greater variability.

During the intercomparison in solar radiation in Helsinki (60.2°N, 25.0°E), the broadband instruments were calibrated using simultaneously measured CIE-weighted solar spectra as a reference. To intercompare the calibration results, the calibration factors were averaged over solar elevations higher than 35°. The wide range of the average values, from 0.87 to 1.75, indicates that the comparability of UV monitoring can be significantly improved by centralized calibration. The uncertainty of the spectroradiometric solar measurements was estimated as ±6% at its best, while the overall uncertainty of the spectroradiometric calibration of the EW radiometers under the prevailing atmospheric conditions was estimated as ±10%. The study represents a useful step in the international standardization of results from these instruments. It would be useful to repeat this procedure at regular intervals, preferably at a site that allows for a greater range of solar elevations for the measurements.

An intercomparison between broadband and spectroradiometric measurements was carried out to determine correction factors during different observing conditions including cloudy skies (Mayer and Seckmeyer, 1996). When the derived correction factors were used, good agreement was obtained after correcting for spectral mismatch and for cosine errors. Bodhaine *et al.* (1998) have recently studied the ozone dependence of broadband sensors and developed a calibration strategy using irradiance data obtained at Mauna Loa, Hawaii.

### 9.2.7 UV-Irradiance Trends from Ground-Based Measurements

Because of the cloud and aerosol variability that occurs over large regions from year to year, and over longer periods of several years, it is very difficult to detect UV-B increases caused by the few percent long-term decreases in ozone amounts for latitudes between 35° and 65° in both hemispheres. Consequently, there were only a few studies demonstrating the expected upward trend in UV as ozone has declined (Basher *et al.*, 1994; WMO, 1995, Chapter 9). More recent studies are discussed below. At higher latitudes, ozone trends are much larger. The large Antarctic springtime ozone decreases (70%) and large springtime decreases in the Arctic region during the last 3 years (30%) have caused large increases in UV-B irradiance that are easily detectable (Booth *et al.*, 1998).

The long-term stability of 1 to 2% per decade, needed to detect midlatitude UV-B trends, has yet to be demonstrated. Use of shorter wavelengths (290-300 nm) to take advantage of the larger percentage UV-irradiance increases caused by ozone decreases (see Figure 9-3) reduces the stability requirements, but increases calibration and stray-light problems.

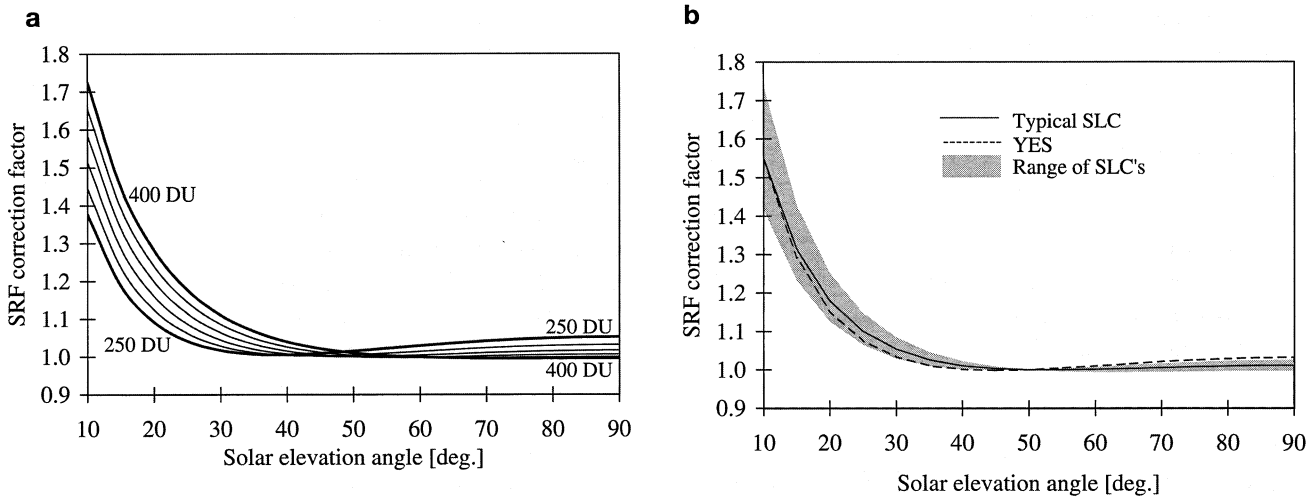


**Figure 9-6.** (a) Correction factors for eliminating errors due to non-ideal spectral response function (SRF) for a typical example of the model SL 501 V.3 radiometers, as a function of solar elevation angle, for total ozone content of 250 to 400 DU. The correction factors have been normalized to unity at an ozone content of 325 DU and solar elevation angle of 50°. (From Leszczynski *et al.*, 1997, 1998.) (b) The range of the correction factors for 16 similar instruments (model SL 501 V.3 radiometers). Correction factors for the YES UV-B-1 radiometer and the "typical" SLC radiometer have also been included for comparison. The correction factors were calculated for an ozone column of 325 DU and have been normalized to unity at a solar elevation angle of 50°. (From Leszczynski *et al.*, 1997, 1998.)

The effects of meteorological variability can be reduced by considering the ratio of irradiances at UV-B to UV-A wavelengths, as long as there are no significant wavelength-dependent instrument changes during the measurement period (Frederick *et al.*, 1993; Bais *et al.*, 1997). The use of ratios may also reduce the effect of absolute calibration errors (Vaughan *et al.*, 1997), but no conclusions can be drawn about changes in the absolute UV irradiance. Channels centered at 305 nm and 340 nm have the needed ozone sensitivity and suitability for observing cloud and haze effects, respectively.

If the absolute UV-A irradiances are monitored, the attenuation effects on UV-B and UV-A irradiance caused by clouds, aerosol haze, and ozone effects can be obtained. Using UV-A measurements and ozone amounts, the results of radiative transfer calculations, matched to a few well-calibrated measured irradiances, can be used to reconstruct the entire UV spectrum at the resolution of the most accurately measured extra-terrestrial solar irradiance (0.15 nm).

The observation period covered by well-calibrated multi-channel radiometers is still too short to reliably detect midlatitude (<55°) trends resulting from ozone changes. Even for clear-sky data, a minimum period of about 11 years is desirable from the viewpoint of removing solar cycle and QBO (quasi-biennial oscillation) effects (Stolarski *et al.*, 1991; Herman and Larko, 1994). The interannual variation in monthly-average UV-B irradiance from meteorological causes (clouds and haze) is generally comparable to or greater than that caused by monthly-average percentage variation in overhead column-ozone content. This results in trend-determination uncertainties that are larger than the expected trends.

The effects of clouds on detecting local trends of UV-B irradiance have been studied using cloud cover estimates from co-located Earth Radiation Budget Experiment (ERBE) data and ozone data obtained from the Total Ozone Mapping Spectrometer (TOMS) (Lubin and Jensen, 1995). The paper examined how the established ozone-amount trends compare with the cloud-induced variability in UV irradiances. Lubin and Jensen (1995) found that throughout many temperate regions (large parts of continental Europe, North and South America, New Zealand, Australia, and southern Africa) the interannual variability in cloud opacity is sufficiently small that by the end of the century, biologically

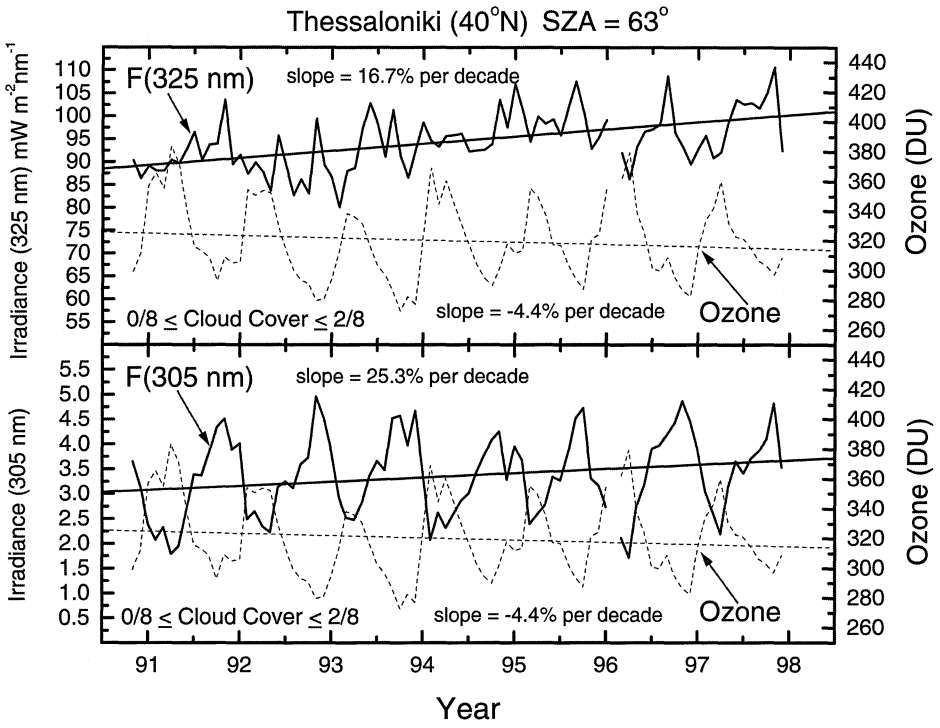


**Figure 9-9.** Time series of monthly mean values of solar UV irradiance (solid lines) at 325 nm (top panel) and at 305 nm (bottom panel) measured at 63° SZA under clear-sky conditions, and total ozone (dashed lines), at Thessaloniki, Greece (40°N), during the period from November 1990 to December 1997. Cloud fraction numbers can range from 0/8 (entirely clear skies) to 8/8 (entirely overcast). Straight lines represent linear regressions on the monthly mean data from November 1990 to November 1997. (Updated from Zerefos *et al.*, 1997.)

(Bruxelles-Uccle, Garmisch-Partenkirchen, and Reykjavik) show similar anticorrelations with ozone. The authors point out that the estimated slopes from the linear least-squares fits to the data vary strongly with the length of the irradiance time series and so should not be taken as an estimate of irradiance trends until much longer time series are available.

A study using RB meters (1976-1992) and a 501 Biometer (1993-1994) located at Belsk, Poland (52°N), found increases in UV irradiance of 1.9 ± 2.8% per decade for the April to October period and 3.2 ± 3.1% per decade for the November to March period (1-standard deviation error estimates). These UV-irradiance changes include local cloud-cover increases that partially offset UV-irradiance increases due to stratospheric ozone decreases (Krzyscin, 1996; Nemeth *et al.*, 1996). While the trends appear to indicate a seasonal difference, the variances in the data are sufficiently large that neither of the seasonal trends is statistically different from zero.

Large apparent increases in UV-B were reported by Gurney (1998) at Barrow, Alaska (71.2°N, 159°W), over a 5-year period (1991 to 1995). The data appear to show absolute irradiance decreases at both 305 and 340 nm, but the irradiance ratio $F(305)/F(340)$ showed an increase. The results implied an increase of 15-50% over the study period for all months except June, the month of maximum UV irradiance, which showed a decrease. However, the study period included the anomalous period of low ozone in 1992-1993. Furthermore, for most months the increases were not statistically significant. Available concurrent ozone measurements were not considered in the study.

The increasing frequency of extreme events (ozone amounts outside the envelope of values from the years 1979 to 1990) may be another indicator of long-term atmospheric change (Seckmeyer *et al.*, 1994b). Very low ozone has been reported over Canada (spring 1997) associated with extremely low stratospheric

temperatures, and with ice-crystal formation in the troposphere and lower stratosphere, within an unusually stable north-polar vortex region. Other enhancements in UV irradiance, caused by short-term ozone decreases, have been reported recently in Europe (Seckmeyer *et al.*, 1997) and Hawaii (Hofmann *et al.*, 1996).

Because of the difficulty of detecting small, systematic long-term changes hidden in the large dynamic range of daily and seasonal changes (see Figures 9-7 and 9-8), the long-term stability of UV-B instrumentation must be improved and maintained over decadal time scales. Unlike the satellite measurements that can remove much of the local variability by geographic averaging, the ground-based measurements must also deal with local meteorological effects (clouds and haze, and, in some regions, possible changes in surface albedo) that show systematic multi-year changes. Systematic differences and variable calibration drifts between different instruments in a network may partly negate the benefits of ground-based geographical averaging. The calculated UV irradiance results from satellite observations of ozone amounts, scene reflectivity (clouds), surface reflectivity, and aerosol amounts over the entire globe may prove useful in the future for checking consistency with the conclusions drawn from local ground-based studies.

Although measurements from polluted sites will be of interest to epidemiologists and for process studies, instruments designed to monitor trends due to ozone depletion should generally be located at remote sites where tropospheric changes from local pollution effects are minimized (Grant, 1988).

## 9.3 SATELLITE ESTIMATIONS OF UV IRRADIANCE

Satellite estimations of UV have recently become available from TOMS (Total Ozone Mapping Spectrometer, November 1978 to May 1993, August 1991 to December 1994, August 1996 to present) satellite instruments. The estimated UV irradiances form a global daily image of the spectral and geographic distribution of UV irradiance over the UV-A and UV-B range. The TOMS UV-irradiance estimates are calculated using derived values of ozone amounts, cloud reflectivities, aerosol amounts, and scene reflectivity, from measured backscattered radiances and extraterrestrial solar flux (Cebula *et al.*, 1994, 1996). Surface UV irradiances have also been estimated from the Earth Radiation Satellite-2 (ERS-2) Global Ozone Monitoring Experiment (GOME) and the National Oceanic and Atmospheric Administration (NOAA) Advanced Very High Resolution Radiometer (AVHRR) satellite instruments (Meerkoetter *et al.*, 1997).

Satellite estimates of UV irradiance at the Earth's surface can give regional and global views of its variation and long-term trends. Estimates are not sensitive to the stratospheric ozone profile shape except at very high SZA (>70°), but are slightly sensitive to variations in the tropospheric distribution of ozone because of multiple scattering effects. A 10% perturbation in the amount of tropospheric ozone would produce less than a 2% change in the diffuse component of the global irradiance (diffuse + direct) at 300 nm, and smaller changes at longer wavelengths. The direct component is not affected by profile shape. At 30° SZA the 300-nm diffuse component is less than half of the global irradiance, and the fraction decreases gradually with increasing wavelength. Therefore, a profile shape error in the troposphere would produce less than a 1% perturbation in the global irradiance for the same amount of total column ozone. This error estimate applies to both the Northern and Southern Hemispheres even though there may be less tropospheric ozone in the south than in the north at comparable latitudes.

The TOMS satellite instruments have obtained contiguous global coverage of ozone, aerosol, and scene-reflectivity (cloud) measurements since November 1978, which have been converted into estimates of the UV irradiance. On the basis of the 1979-1994 TOMS satellite data record, ozone changes are statistically significant at latitudes larger than 35°N or 35°S (McPeters *et al.*, 1996) and have been observed by the distributed network of ground-based UV-Dobson instruments with a sufficiently long record. Because TOMS data showed that there has been no trend in zonally averaged cloud reflectivity (J.R. Herman *et al.*, 1996), a zonally distributed network of UV-B sensitive instruments should also detect the UV-irradiance changes caused by the ozone trend. For example, at latitudes between 35° and 40° the zonal average ozone change is about 2 to 3% per decade and produces a corresponding 2.5 to 3.5% per decade change in UV irradiance at 310 ± 0.5 nm or in the spectrally weighted erythemal irradiance range between 290 and 400 nm. Larger percentage changes occur at shorter wavelengths (about 7 to 11% at 300 nm). From satellite data, the zonally averaged decadal trend in erythemal

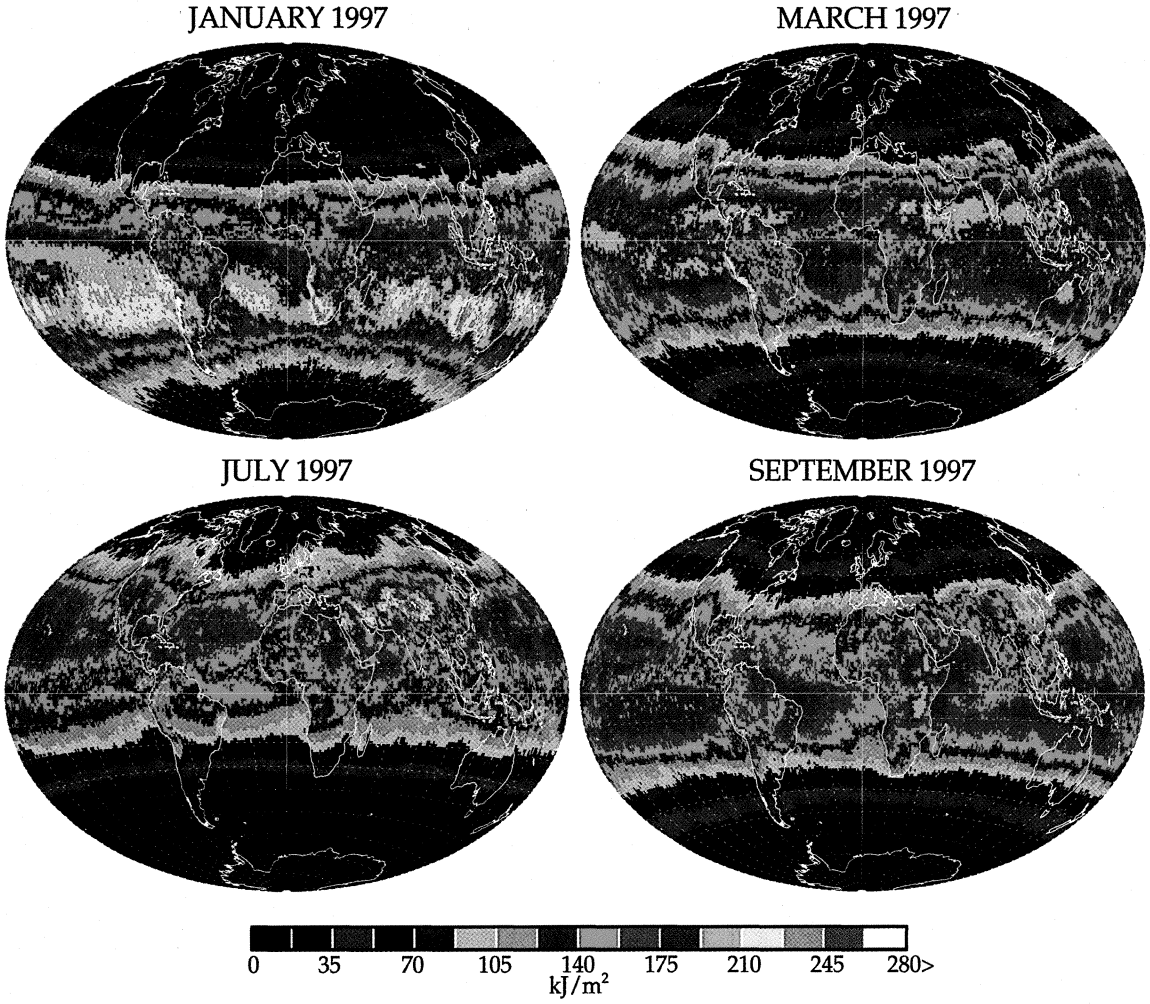


**Figure 9-11.** Global maps from TOMS-estimated irradiances of the monthly erythemal exposure for January, March, July, and September, including the effects of ozone, clouds, aerosols, and surface reflectivity. (Updated from J.R. Herman *et al.*, 1996, 1997; Krotkov *et al.*, 1998.)

cloud transmissivity, and surface albedo determined from TOMS data on a 1° by 1° grid (McPeters *et al.*, 1996; J.R. Herman *et al.*, 1996; Herman and Celarier, 1997; Krotkov *et al.*, 1998), and includes the decreases in UV irradiance caused by absorbing and nonabsorbing aerosols based on the attenuation calculations contained in Krotkov *et al.* (1998) and the global distributions of aerosols in Herman *et al.* (1997). Terrain height tables are used in addition to TOMS data. For most locations, only a single near-noon measurement is made each day for atmospheric and surface properties. Although the reductions in UV irradiance by absorbing aerosols are only estimates, because of the assumed height of the absorbing aerosol plumes at 3 km (see discussion below) (Torres *et al.*, 1998), the aerosol dataset used is the only one currently available over both land and oceans.

As expected, the highest values of exposure are near the seasonal sub-solar points (SZA ~ 0°) between ±23° latitude, in regions of elevated altitude (e.g., Andes Mountains), and in regions that are relatively free of clouds for the given month (e.g., South Africa and Australia in January and in large regions over the oceans). In July, during the Northern Hemisphere summer, very high exposures are estimated over the Sahara, Saudi Arabia, the southwestern United States, and the Himalayan mountain regions in northern India

and southern China. The equinox at March produces high exposure values throughout equatorial Africa, the southern part of the Arabian Peninsula, southern India, Malaysia, and Indonesia. Even though the SZAs in September are nearly the same as in March, the increased number of cloudy days produces lower exposures during September.

A measurement-modeling comparison between TOMS-measured ozone and reflectivity as inputs into a radiative transfer calculation (Dave, 1964; Eck *et al.*, 1995) and the Toronto Brewer instrument (Kerr and McElroy, 1993) showed very good agreement over a wide range of seasonal and cloud conditions. Recent studies using a larger sample of data show a seasonal difference, with the largest differences occurring in the winter months (G. Labow, Raytheon STX, United States, personal communication, 1998; V. Fioletov, Atmospheric Environment Service, Canada, personal communication, 1998). A new UV CD-ROM for erythemal exposure will be available from the National Aeronautics and Space Administration (NASA) Goddard Space Flight Center (GSFC), based on the TOMS ozone and 380-nm radiance data for Nimbus/TOMS (1979 to May 1993) and on 360-nm reflectivity for Earth Probe/TOMS (since August 1996). The 1996 version of the TOMS UV CD-ROM used an incorrect version of the erythemal action spectrum given in Booth *et al.* (1993).

It should be emphasized that satellite-borne sensors do not directly measure surface UV irradiances or any other atmospheric characteristic. All quantitative satellite measurements infer Earth surface or atmospheric properties using radiative transfer calculations. The major uncertainties in satellite UV-irradiance estimation are due to possible undetected variability in small-scale (sub-pixel) boundary layer extinctions from aerosols, tropospheric ozone, and clouds. The coarse spatial resolution can also be a useful feature, compared with the localized measurements of ground-based instruments, because the satellite-borne measurements estimate the average irradiance striking the geographic area covered by the instrument's field of view (26 to 100 km for Earth Probe/TOMS, 50 to 200 km for Nimbus-7/TOMS), including the average transmissivity of the cloud and aerosol fields from measurements of their backscattered radiances over the TOMS field of view. The transmissivity is essentially an energy balance estimate assuming a Lambertian equivalent reflectivity over the field of view.

The spatial resolution of the current satellite UV-radiance instruments does not resolve the effects of broken clouds or small-scale cloud structure. A simple example is when the direct sun is observed through broken clouds from the ground. Even for rather large fractional cloud cover, it has been shown that if the sun is not obscured, the UV irradiance measured at the surface remains close to the clear-sky value (e.g., Blumthaler *et al.*, 1994) or can exceed it for some cloud conditions. Conversely, for small fractional cloud cover in the TOMS field of view, the ground-based observation may have the sun obscured by clouds and measure a smaller radiance than estimated from the TOMS data. This means that daily comparisons of satellite data with ground-based measurements may disagree substantially even though weekly or monthly averages may agree quite well (Eck *et al.*, 1995). This will not be true if there is a systematic cloud amount bias at the ground site compared to adjacent areas.

Observations at higher spatial resolution, of about 1 km at near-UV wavelengths (412 nm), have been made by the SEAWIFS (Sea-viewing Wide Field-of-view Sensor) satellite instrument. These observations may be of use for estimating the effects of broken clouds on the larger pixels used by TOMS ($26 \times 26$ km$^2$ to $100 \times 150$ km$^2$). Finally, the frequency of satellite overpasses is such that the modeled diurnal variations arising from cloud or aerosol effects are not realistic (see discussion in Section 9.6.3). Well-maintained, strategically located ground-based instruments are needed to verify the applicability of satellite-derived estimations of surface UV radiation.

### 9.3.3 UV Extinction by Aerosols

Of the major factors affecting surface UV, only ozone has a known widespread long-term change (decrease), and only for latitudes between 35° and the poles. For major sources of UV-absorbing aerosols (dust and smoke), only the biomass-burning smoke over South America shows a systematic increase since 1979 (Herman *et al.*, 1997). An analysis of zonal-average reflectivity, based on the 1979-1993 TOMS backscattered radiance data, indicates that the global- and zonal-average UV transmission by clouds (of all types combined) plus nonabsorbing aerosol (all Mie-scattering aerosols of size 0.07 microns (μm) or greater) has not changed significantly (J.R. Herman *et al.*, 1996). Scattering from particulates smaller than about 0.07 μm is not easily distinguished from the Rayleigh scattering background

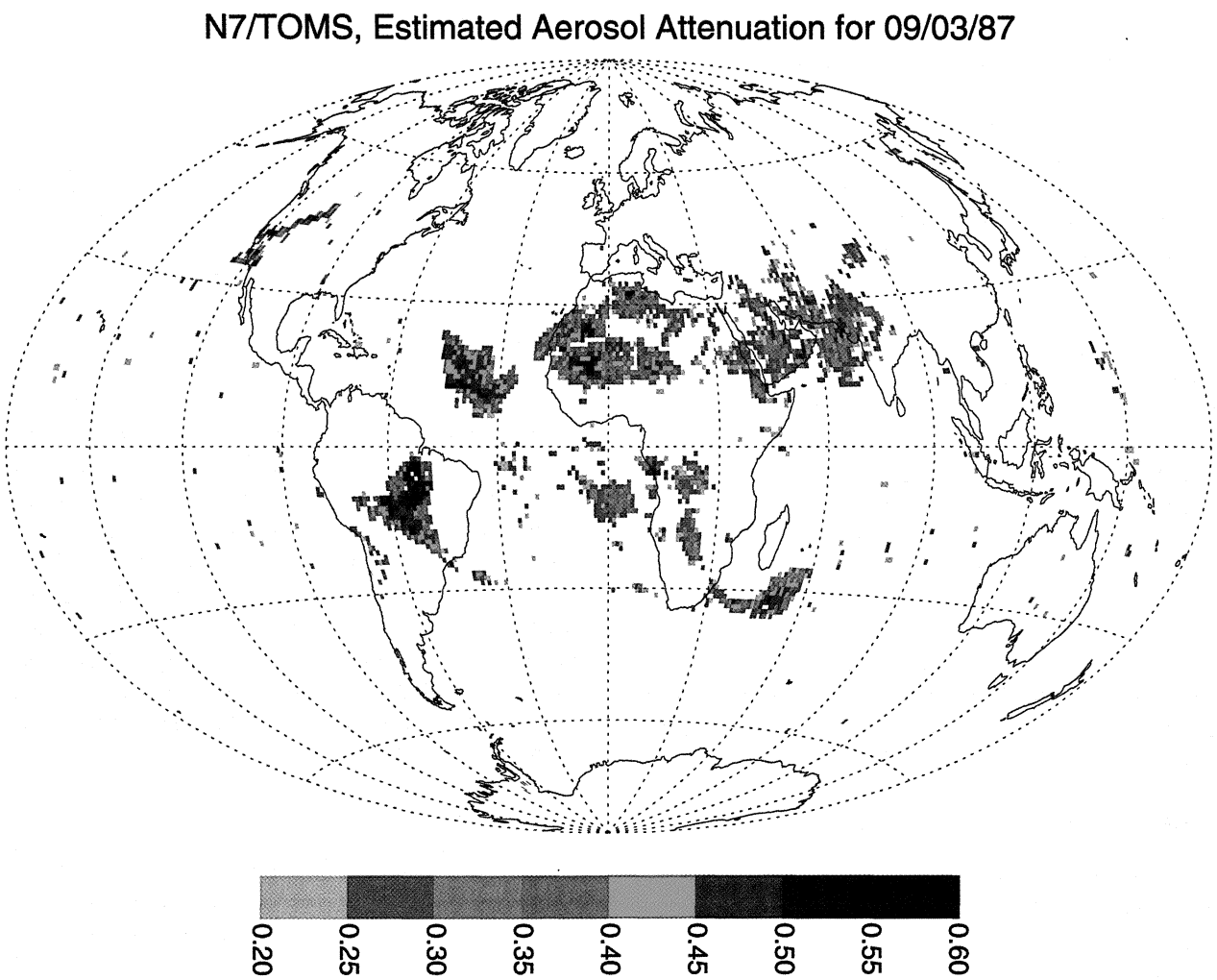


**Figure 9-12.** Map of the percentage of UV-irradiance reduction relative to clear-sky irradiance, on 3 September 1987, using an assumed aerosol plume height of 2.9 km, showing the effect of Saharan desert dust and biomass burning in South America, southern Africa, and California. The estimated errors are 7.5% for smoke and 11% for dust for a ±0.5-km error in assumed height. The irradiance reduction method is not sensitive to absorbing aerosols below about 1.5 km. (From Krotkov *et al.*, 1998.)

at the observing wavelengths of TOMS (360 or 380 nm). However, regional changes in cloud or aerosol cover may have changed UV doses at ground level (Liepert *et al.*, 1994; Seckmeyer *et al.*, 1994b).

TOMS estimations of aerosol amount (Herman *et al.*, 1997; Torres *et al.*, 1998; Krotkov *et al.*, 1998) can be used to calculate the aerosol attenuation of UV irradiance for the Earth's surface between ±65°. The sample UV-irradiance attenuation map shown in Figure 9-12 was derived assuming that the height of the aerosol layer was known. In this case, the altitude was assumed to be uniform at 2.9 km. Comparisons of derived optical depths with sunphotometer optical depths (Torres *et al.*, 1998) show that 2.9 km is a good average first-order approximation. Using a constant altitude neglects some seasonal changes such as the increase in height over the Sahara during the summer months. TOMS is unable to distinguish absorbing aerosols from sub-pixel clouds or nonabsorbing aerosols when their optical depths are less than 0.1 or if they are below about 1.5 km in altitude. This means that it is unlikely that TOMS, by itself, will be able to detect weakly absorbing aerosols near the surface, often found in urban atmospheres.

The map in Figure 9-12 shows that aerosol absorption can produce very large reductions in UV irradiance (~50 ± 12%) in certain parts of the world. One sees the effects of smoke from a west-coast Canadian forest fire that is moving in the southwesterly direction, biomass burning in South America and Africa, and desert dust blowing both east and west from the Saharan region of Africa. These estimates are consistent with ground-based sunphotometer observations (Torres *et al.*, 1998) showing agreement in optical depths that are equivalent to observing a 50% or more reduction in surface UV radiation due to smoke from widespread biomass burning in the Brazilian rain forest. The data shown in the map have been truncated so as not to show lower amounts of absorbing aerosol (optical depth less than 0.4) that appear to be more widely distributed away from the sources of biomass burning and dust. If validated, these plumes with lower optical depth would result in a 5 to 10% reduction in UV radiation. The recent Indonesian fires had dense smoke plumes that were observed by TOMS, AVHRR, GOME, and SEAWIFS satellite instruments. On the basis of the TOMS observations, optical depths greater than 5 occurred, which resulted in estimated reductions in UV irradiance of 90%.

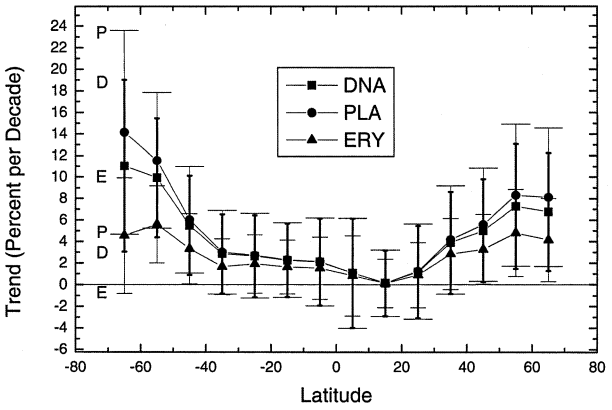


**Figure 9-13.** The percentage change per decade in action-spectra-weighted annual UV exposure as a function of latitude estimated from TOMS data (1979-1992) including cloud effects. The error bars indicate uncertainties of 2 standard deviations (from combined instrument error and variability in the UV-irradiance data). The symbols P and PLA stand for the plant damage action spectrum, D and DNA stand for the DNA damage action spectrum, and E and ERY stand for the erythemal action spectrum (J.R. Herman *et al.*, 1996).

### 9.3.4 Trends in UV Irradiance

The satellite determinations of changes in zonally averaged, decadal global UV exposure are summarized in Figure 9-13 as a function of latitude (J.R. Herman *et al.*, 1996). The exposure changes are computed for three different action spectra: (1) erythema (McKinlay and Diffey, 1987), (2) DNA damage (Setlow, 1974), and (3) plant damage (Caldwell *et al.*, 1986). The UV-irradiance changes are based on the TOMS reflectivity and ozone amounts from 1979 to 1992. The results include both ozone changes in the stratosphere and troposphere, and the effect of clouds and non-absorbing aerosols, but did not include the effect of absorbing aerosols (dust and smoke).

The results show that no statistically significant changes have occurred for latitudes equatorward of 35°, but that increases in UV-irradiances between 40° and 65° have been substantial for any of the standard action spectra (Madronich and de Gruijl, 1994; J.R. Herman *et al.*, 1996; Weatherhead *et al.*, 1997). In the Northern Hemisphere the UV-irradiance increases have occurred over the densely populated regions of Europe, Canada, and Russia, while in the Southern Hemisphere, the largest increases are over the southern portions of Argentina and Chile. The large statistical-uncertainty bars in the calculated linear fits to the UV-exposure changes are caused largely by the interannual variability in ozone amount at all latitudes, and to a smaller extent by the annual variability of zonally averaged cloudiness. As part of the study of UV-irradiance changes since 1979, it was determined that there has been no statistically significant change in zonal average reflectivity (a surrogate for effective cloudiness, or cloud fraction combined with optical depth) for latitudes between ±65°, even though there have been changes in regional reflectivities or cloud amounts.

TOMS-derived UV trends after 1992 cannot easily be estimated at present, because the continuous Nimbus-7/TOMS (November 1978 to May 1993) data record was broken in May 1993. The non-sun-synchronous (212-day orbital-precession period) Meteor-3/TOMS (August 1991 to December 1994) overlapped Nimbus-7/TOMS for over a year. After sufficient operating time, Earth Probe/TOMS (August 1996 to present) data may be used, in conjunction with other satellite and ground-based data, to fill in the data gap and to extend the trends.

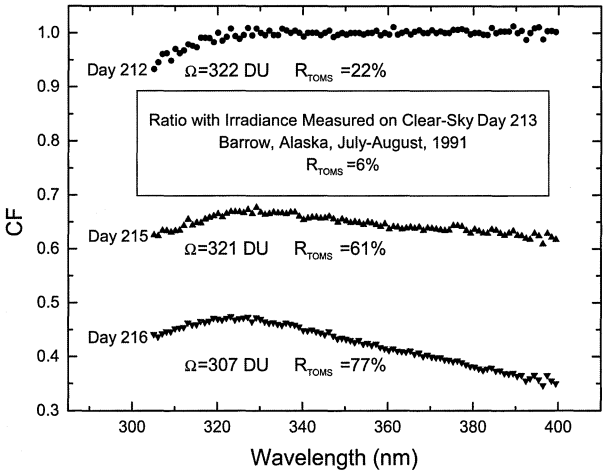


**Figure 9-15.** Wavelength dependence of cloud transmittance in a Rayleigh-scattering atmosphere for different ozone amounts (Ω) and cloud amounts (reflectivities, *R*). The cloud factor (CF) is from measurements made by spectroradiometer at Barrow, Alaska, July-August 1991; CF = ratio of cloudy-sky irradiance to clear-sky irradiance (day 213, $R_{TOMS}$ = 6%). (CD-ROM data from Booth *et al.*, 1993, 1998.)

show that the average UV irradiance for the period 1968-1992 has decreased at Moscow by 15-20% (with some seasonal dependence). At the same time, the average cloud fraction has increased significantly (for lower layer clouds by 27% and for all cloud layers by 14%).

Measurements at Raleigh, North Carolina (Estupinan *et al.*, 1996), show the UV-irradiance attenuation for unbroken clouds (up to 99%) and haze (5 to 23%). However, for broken convective-type cumulus clouds of large vertical extent, increases of up to 27% have been observed (see also Nack and Green, 1974; Seckmeyer *et al.*, 1996; Frederick and Steele, 1995). Additional measurements of UV-B under partially cloudy conditions using a Brewer spectrometer in North Carolina show increases over clear-sky values of as much as 11% (Schafer *et al.*, 1996). According to Estupinan *et al.* (1996), broken cloud fields of types with small vertical extent show no excess of UV irradiance over clear-sky values. Additional validation studies at different locations are needed to further quantify the enhancements found in these studies.

Analysis of data from the Canadian Brewer network indicates that the effects of thin clouds, which reduce irradiance by up to 50%, are nearly the same for wavelengths between 280 and 325 nm (Fioletov *et al.*, 1997; Wardle *et al.*, 1997). The effect of cloud cover on reducing global irradiance has little dependence on zenith angle. However, large convective clouds that reduce irradiance values to less than 10% of clear-sky values show enhanced ozone absorption effects that are likely caused by increased multiple scattering within the cloud and in the regions above and below the cloud. Recent measurements have been conducted of the angular distribution of diffuse radiation underneath overcast skies (Grant *et al.*, 1997). They show that the ratio of measured irradiance under overcast skies was not correlated with cloud-base height, opaque cloud fraction, or solar zenith angle. Grant and Heisler (1997) found that the rate of change $N_r$ (or relative distribution) of both UV-A and UV-B radiances with SZA (θ) for solar-obscured overcast skies can be modeled as

$$N_r = 0.426\frac{1+1.23\cos(\theta)}{1+1.23} \qquad (9\text{-}3)$$

### 9.4.3 Altitude

As has been shown from numerous radiative transfer studies, UV irradiances change with the observing altitude because of changes in scattering and absorption. The altitude dependence varies with both SZA and wavelength. Therefore, it is not possible to describe the change with altitude by a single number in percent per kilometer (Duguay, 1995; Seckmeyer *et al.*, 1997; Krotkov *et al.*; 1998). For example, Seckmeyer *et al.* (1997) found that the monthly erythemally weighted irradiation is between 25% and 90% higher on the Zugspitze (3-km altitude) than at the lower site in Garmisch-Partenkirchen (0.73 km) within a 5-month period. The variability in the differences indicates that they are caused by a combination of several factors, including Rayleigh scattering, cloud effects, air pollutants (e.g., tropospheric ozone), aerosols, and surface albedo. These results show that data from a single site are not sufficient to determine the altitude effect for UV irradiance at sites other than the measurement site.

Regional differences in the altitude dependence of UV irradiance have also been reported by Blumthaler *et al.* (1997) based on measurements made at Jungfraujoch, Switzerland (3.576-km altitude), and Innsbruck, Austria (0.577-km altitude), where daily clear-sky erythemal doses have been compared. The paper showed an increase of 8% per km for total irradiance, 9% per km

for UV-A, and 18% per km for erythemal effective irradiance during the summer. It also showed that the altitude dependence of the direct radiance is larger than that of the global radiance at all wavelengths.

A study of the altitude dependence of UV irradiance in clean, dry air in South America showed much smaller altitude gradients than in Europe and in more polluted regions of the continent than reported in the previous Assessment (WMO, 1995). The gradients that were determined for global irradiances, as well as the direct and diffuse components separately, depended on wavelength and on SZA (Piazena, 1996). As expected, global and direct irradiances increased with altitude, whereas the diffuse component decreased. In the UV-B range, global irradiances generally increased by 8-10% per km for SZA > 70°, which is still a somewhat larger increase than predicted for clear sky.

High-altitude results (3.4 km) from an ultraviolet spectroradiometer installed at Mauna Loa Observatory (MLO) in Hawaii have been reported by Bodhaine *et al.* (1996, 1997). For observations at SZA = 45°, the erythemally weighted UV irradiance at MLO can exceed 0.21 $Wm^{-2}$, which is approximately 15-20% greater than that seen at clean-air sites near sea level (e.g., Lauder, New Zealand) for similar ozone amounts. For overhead sun conditions at MLO, the largest value of erythemal UV irradiance was 0.51 $Wm^{-2}$. For now, this is probably the highest recorded value of erythemal irradiance anywhere on the Earth's surface, as would be expected for these conditions.

### 9.4.4 Aerosols

Changing aerosol (and cloud) conditions can lead to increases or decreases in UV irradiance (Justus and Murphey, 1994; Mims and Frederick, 1994; Forster and Shine, 1995; Dahlback, 1996; Zerefos *et al.*, 1994; Olmo and Alados-Arboledas, 1995). In general, the backscatter from volcanic aerosol decreases the erythemal UV irradiance by about 5% (Tsitas and Yung, 1996). At high SZA, when there is a thin aerosol layer at an altitude where the direct solar beam is still a significant component of the total irradiance, the amount of UV-B at the surface can be increased while at the same time the amount of UV-A is decreased (e.g., Forster and Shine, 1995). This is because of the reduced average optical path through the ozone layer for scattered radiation compared to the direct beam. The short-wavelength portions of UV-B (<300 nm) are absorbed sufficiently by ozone so that its surface irradiance is increased by the presence of additional high-altitude scattering, while UV-A is reduced by the additional amount scattered back to the top of the atmosphere (Tsitas and Yung, 1996). This effect is especially important at high latitudes where the proportion of scattered irradiance to direct-beam irradiance is larger due to higher SZA (Taalas *et al.*, 1997).

Atmospheric aerosols affect the amount of global irradiance received at the Earth's surface after scattering and absorption. The largest aerosol reductions in UV irradiance are associated with the major sources of dust and smoke in Africa and South America (Herman *et al.*, 1997). The reductions in these regions frequently exceed 50% of the clear-sky value. The amount of UV-irradiance reduction depends strongly on the absorption properties of the aerosols. Most of the aerosols in the Northern Hemisphere are sulfates or other industrial pollutants whose Mie scattering reduces the surface UV irradiance by about 10% (Krotkov *et al.*, 1998).

There are relatively small plumes of UV-absorbing aerosols that strongly reduce surface UV irradiance over urban areas such as Los Angeles, Mexico City, Beijing, or Berlin, or downwind from regions of seasonal forest fires (e.g., Canada, California, and Russia). Smaller UV-irradiance reductions of 10 to 20% also occur under the widespread nonabsorbing aerosols prevalent in the Northern Hemisphere (Seckmeyer *et al.*, 1994b; Krotkov *et al.*, 1998) and in small regions of the Southern Hemisphere (see also Ryan *et al.*, 1996).

In localized regions where there are increased atmospheric pollutants from anthropogenic activities, the reduction of pollutants for health reasons may have the effect of increasing UV radiation at the ground closer to preindustrial levels for the region. In addition to pollution, long-term increases of cloudiness may have significantly decreased UV irradiation in Central Europe since the 1950s, and may be partly masking an upward trend of UV irradiances caused by ozone depletion (Seckmeyer *et al.*, 1994b; Nezval, 1996; Varotsos *et al.*, 1995; Zerefos *et al.*, 1997). Observations by Feister and Grewe (1995) showed UV-irradiance enhancements arising from decreases in the ozone amount and changes in the average amount of cloudiness over middle Europe (52°N) for the years 1992 and 1993.

The effect of aerosols on UV-B irradiances was quantified using data from clear days over a 3-year period (1989-1991) at Toronto (Kerr, 1998). Results of this analysis show that for the aerosols present over this site,

reductions in global irradiance are about 20-30% of the reductions in direct irradiance. That is, if aerosols were to reduce the direct irradiance by 10%, the global irradiance would be reduced by 2-3%. The reduction has little wavelength dependence and is in reasonable agreement with radiative transfer models results for aerosols that are nearly nonabsorbing (single scattering albedo > 0.95; Krotkov *et al.*, 1998). The residual variability, after considering the effects of ozone absorption and aerosol scattering, was between 2 and 5% over the 3-year period.

### 9.4.5 Surface Albedo Variations (Snow)

For most conditions at non-polar latitudes, the surface reflectivity at UV wavelengths is less than 10% for ground without snow or for water (Herman and Celarier, 1997). The snow-free surface reflectivities (Lambert equivalent reflectivities) estimated from the TOMS radiance data range from a minimum of about 2% over vegetation-covered land to about 8% over some portions of the Sahara desert and over large areas of the ocean that are relatively free from UV-absorbing phytoplankton. There is a small seasonal dependence in the estimated surface reflectivity, but the reflectivity always stays below about 8% except in regions where there is snow or ice cover. All the TOMS estimates of surface irradiance use the estimated UV-reflectivity climatology generated from 14 years of Nimbus-7/TOMS data.

The occurrence of snow on the ground is the main factor that causes large surface albedo changes in the UV. Results of a study reported in Wardle *et al.* (1997) summarize the effects of snow on UV irradiance at seven sites in Canada. The irradiance at 324 nm was used as an indicator, because ozone has negligible absorption at this wavelength. The variation due to zenith angle was removed by normalizing the observed irradiance at 324 nm to that expected under a clear sky at the same zenith angle. A comparison of observations taken with snow on the ground and those taken without snow shows an enhancement in the normalized 324-nm irradiance ranging from 8% (Halifax) to 39% (Churchill). When there was no snow on the ground, the normalized 324-nm irradiance was nearly constant for all seven stations. Snow has significantly different enhancements at different stations, likely because of terrain or snow quality differences. For example, the enhancements in the Arctic (Resolute, 35%, and Churchill, 39%), with flat and "white" terrain, are larger than those seen at urban sites (Toronto, 12%, and Halifax, 8%).

Even if the snow/ice surface reflectivity does not depend on wavelength, the reflectivity-amplification of UV irradiance is not neutral, but has a strong maximum of about 0.5 near 320 nm for a surface reflectivity of 0.8 (Lenoble, 1998; Krotkov *et al.*, 1998; Chubarova, 1993, 1998) (see Figure 9-16). This maximum occurs for both clear-sky and cloudy-sky cases. However, for cloudy skies the slope from 320 nm to 400 nm is very small compared with the clear-sky case, because of the nearly wavelength-independent reflection from the clouds. Increased atmospheric Rayleigh scattering back to the surface at shorter wavelengths causes the increasing effect of changes in surface reflectivity with wavelength (from 400 nm to 320 nm). The small structure seen starting at about 330 nm is caused by ozone absorption. For wavelengths shorter than 320 nm the increasing ozone absorption dominates the increasing Rayleigh scattering, or cloud reflection, and results in a smaller UV-irradiance increase relative to 320 nm. The formal solution for the results presented in Figure 9-16 is given (in percent) as

$$\frac{dF}{F} = 100 \frac{S_b}{1 - R_s S_b} \frac{dR_s}{R_s} \qquad (9\text{-}4)$$

Here $S_b$ is the wavelength-dependent fraction of radiation backscattered from the atmosphere back to the surface. $S_b$(320 nm) is frequently greater than 0.6 for clouds and about 0.4 for clear sky. $R_S$ is the surface reflectivity; $R_S \approx 0.05$ for ground and $R_S > 0.8$ for fresh snow. $F$ is the irradiance at the Earth's surface.

Figure 9-16 also shows the effect on modeled UV irradiances of an uncertainty in knowledge of the surface reflectivity. For clear skies the errors in the irradiances are roughly 0.5% for each percent uncertainty in the surface reflectivity. The presence of significant cloud cover, and particularly cloud cover over snow, can lead to large errors in estimated UV irradiances from model calculations that assume a constant albedo. Errors in surface reflectivity affect the estimate of UV irradiances from satellite data and affect the derivation of atmospheric parameters (e.g., ozone and aerosol amounts) from ground-based measurements using global solar irradiance (direct + diffuse), but not those using the direct solar component alone. These results have not been validated against ground-based measurements.

Away from snow and ice, the reflection problems for satellite retrievals of UV are minimized because of

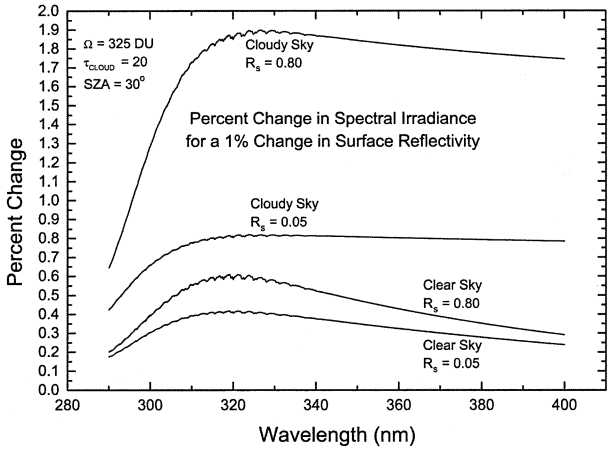


**Figure 9-16.** Reflectivity amplification of UV irradiances as a function of wavelengths for ground reflectivity ($R_S$ = 0.05) and fresh-snow/ice conditions ($R_S$ = 0.80) for clear and cloudy ($\tau_{cloud}$ = 20) skies with column ozone amount 325 DU, SZA = 30°, and $dR_S$ = 0.01. (Adapted from Lenoble, 1998.)

the low values of reflectivity in the UV of 4 to 8% (Eck *et al.*, 1987; Herman and Celarier, 1997) over both land and water. Even lower values of about 1% in the UV-B, 2% at 400 nm, and 4.5% at 450 nm have been measured over long grass in New Zealand (McKenzie *et al.*, 1996). There the albedos tend to increase at large SZAs, implying that the surface is not strictly Lambertian. Because of the low reflectivities and large amount of scattering in the boundary layer, moderate percentage errors in assumed surface reflectivity have little effect on the UV irradiance. There are also problems with realistically representing boundary layer scattering because of the difficulties in haze characterization for each particular case (Schwander *et al.*, 1997).

## 9.5 GEOGRAPHIC DIFFERENCES IN UV IRRADIANCES

The major causes of geographic differences in peak summer or annually integrated UV irradiances are differences in latitude (i.e., SZA); regional differences in cloud, ozone, and aerosol amounts; differences in terrain height; and a larger Sun-Earth separation during the summer in the Northern Hemisphere compared with the austral summer.

### 9.5.1 Mid and Low Latitude

While low-latitude regions (±20°) have not experienced any significant long-term declines in ozone amounts, these regions receive the highest amounts of daily UV irradiance except for a few locations at extremely high elevations. Because of the very dense populations in and near this latitude region, it is important to understand UV exposure and any possible increases. Measurements of surface UV irradiance in Penang, Malaysia (5.5°N, 100°E), have been made to establish the diurnal and seasonal dependence. It was shown that the surface irradiance routinely reaches the extreme zone (UV index > 9; see Section 9.7) for about 5 hours each day. Because ozone is nearly constant with the seasons, the modulation of UV irradiance is mainly by clouds. An extension to these data (M. Ilyas, University of Science-Malaysia, personal communication, 1998) shows that the amount of UV irradiance reaching the surface was reduced substantially during haze events from Indonesian biomass burning during 1997 and1998.

Investigations of geographic differences based on measurements from the same instrument (Seckmeyer and McKenzie, 1992; Bernhard and Seckmeyer, 1997) have shown that for clear-sky observing conditions and similar SZA, UV irradiances measured in New Zealand are much higher than in Central Europe. For example, the DNA and erythemal action-spectra-weighted irradiances are larger in New Zealand by factors of 1.81 and 1.44, respectively. The average difference in total column ozone between the two sites is 53 DU (New Zealand has less ozone). The ozone difference contributes to an increase in DNA action-spectra-weighted UV irradiance by a factor of 1.58 ± 0.1. The corresponding factor for erythemal action-spectra-weighted irradiance is 1.28 ± 0.1. Although stratospheric ozone is the dominant factor, a part of the differences arises from Sun-Earth separation differences, and changes in tropospheric pollution (ozone, aerosols), which has increased in Central Europe (Staehelin and Schmid, 1991; Seckmeyer and McKenzie, 1992) compared with the relatively clean Southern Hemisphere atmosphere.

In a study that also considered clouds, geographical differences in erythemally weighted UV irradiance were investigated on the basis of measurements of five spectroradiometers and several broadband UV-irradiance meters (Seckmeyer *et al.*, 1995) from four different groups (Garmisch-Partenkirchen, the National Institute of Water & Atmospheric Research (NIWA), the

Australian Radiation Laboratory (ARL), and the U.S. National Science Foundation (NSF)). Before the survey, the spectroradiometers were brought together for an intercomparison campaign. Based on the results of this examination, adjustments were made to correct for systematic calibration differences seen in the spectroradiometric data in order to achieve consistency between four different groups of instruments. The broadband UV-irradiance meters were calibrated in the field against the spectroradiometers.

Data from 12 locations, ranging from the South Pole to Barrow, Alaska, were analyzed to study geographic differences in UV. For each site, daily integrals of erythemal irradiance measured during summer months, maxima, and monthly means of the daily integrals were compared. Data from 1991 were used at Australian sites. At other sites, data were from 1993-1994. At low latitudes, these irradiances appear to be similar in both hemispheres. However, for mid and high latitudes, it was found that geographic differences in UV irradiance clearly exceed the measurement uncertainties (less than ±10%). The latitudinal variations seen in the summer months are shown in Figure 9-17a. Observed latitudinal gradients of UV irradiance in the Southern Hemisphere were much smaller than in the north, with mid-southern latitudes receiving approximately 40-50% more UV irradiance than corresponding sites in the Northern Hemisphere. An example is the difference observed between Lauder, New Zealand (45.05°S, 169.67°E), and Neuherberg, Germany (50°N, 6.95°E), for similar seasonal conditions, but very different ozone amounts (266 DU in Lauder and 352 DU in Neuherberg, ~30% difference) (Seckmeyer and McKenzie, 1992). In the Seckmeyer *et al.* (1995) study, hemispheric differences are most pronounced at high latitudes, consistent with the results of the previous study by Seckmeyer and McKenzie (1992), where only clear-sky conditions were investigated. In summer months the daily UV doses at high southern latitudes, and at the South Pole, are greater than at midlatitudes in the Northern Hemisphere. The largest maximum daily dose for all sites considered was for Palmer Station, Antarctica (Figure 9-17b). The measurements were considered as a first step to estimate geographic differences in UV. These latitudinal differences are much larger than those shown by the satellite retrievals from the summer of 1997 (Figure 9-11). Further studies are required to understand these discrepancies and to determine whether the differences are representative of zonal means.

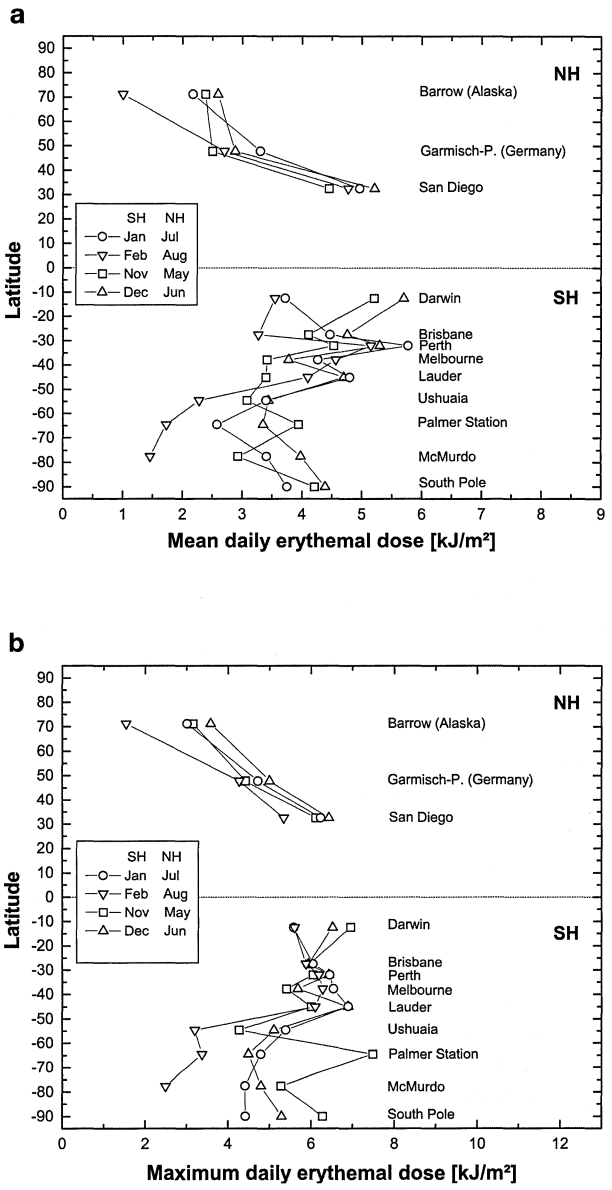


**Figure 9-17.** Measured monthly mean (a) and maximum (b) of the daily integrals of erythemal UV irradiance during the summer months in the Northern Hemisphere (NH) and Southern Hemisphere (SH) as a function of latitude, including effects of aerosols, cloud, altitude, and ground albedo (from Seckmeyer *et al.*, 1995).

Latitudinal variability of UV irradiance has also been investigated using a mobile spectroradiometer and comparisons with a radiative transfer model. Bernhard *et al.* (1997) measured the difference in solar UV irradiances between Southern Germany (47.5°N) and tropical Australia (19°S). The data from Australia are from a 1-month campaign during the austral summer of 1995-1996. The maximum values of erythemally weighted irradiance on clear-sky days were 372 mW $m^{-2}$ (Australia) and 234 mW $m^{-2}$ (Germany), which gives a difference of about 60%. For cloudless days there was good agreement with radiative transfer model calculations, with the differences explained by the smaller SZA and lower ozone amounts in Australia.

### 9.5.2 High Latitude (North and South)

The maximum variability of UV-B caused by ozone changes, on time scales of daily to yearly, occurs at high latitudes (above 50°) in both hemispheres. However, year-to-year differences in cloudiness are generally the largest source of interannual variability in monthly integrated UV irradiance measured at the ground (Frederick *et al.*, 1993; Diaz *et al.*, 1994; Frederick *et al.*, 1994). This can vary from one location to the next, depending on the timing and severity of ozone depletions. At the NSF site in Ushuaia, Argentina (54.6°S), the lowest ozone column amounts (1988-1997) were in the years 1995 to1997. The highest UV irradiances occurred whenever the ozone-hole region (220 DU contour) elongated into an elliptical shape that rotated over South America and the cloud cover was minimal. The highest 24-hour integrated irradiance (exposure) occurred during the coincidental occurrence of cloud-free days with small ozone depletion (less than 10%) during the longer days of mid-summer, rather than during the much more severe ozone depletions in early spring (Diaz *et al.*, 1994).

TOMS observations of ozone amounts over Ushuaia show a steady decline since 1980 on top of large day-to-day variability (Bojkov and Fioletov, 1995a; Bojkov *et al.*, 1995a; Diaz *et al.*, 1994, 1996). Using ground-based measurements from an NSF high-resolution spectroradiometer, the modeled increase in UV irradiance for 1989-1993 relative to the 1979-1983 period was estimated to be 80% at 300 nm and 35% at 305 nm for a 15% ozone decrease (about 345 DU to 300 DU). Bojkov *et al.* (1995a) state that the 300-nm irradiance observed during the spring (October) is as high as it is 4 months later during the summer. The characteristic spectral shape of the percentage change demonstrates that the increase in UV irradiance is caused by ozone decreases. Kirchhoff *et al.* (1997) found similar results, where measurements were made using a Brewer (single monochromater) spectroradiometer at Punta Arenas, Chile. The research shows significant enhancements in UV-B during the days when ozone-poor Antarctic air passes over portions of South America. Results from a cruise originating in Punta Arenas, Chile (53°S), near the tip of South America, and traveling to 71°S near Palmer station showed that the average UV-B radiation (280-330 nm) inside the Antarctic ozone hole was double the average measured outside the region. At the same time, UV-A irradiances were not affected (Wendler and Quackenbush, 1996).

Increased UV-B radiation has occurred over the Arctic and high-latitude regions surrounding the Arctic (e.g., northern Canada and Russia), corresponding to more frequent occurrences of low ozone amounts during the spring (Bojkov *et al.*, 1995b; Bojkov and Fioletov, 1997; Gurney, 1998). For example, with clear-sky conditions, the percentage increases in UV irradiance at 300 nm, 305 nm, and 310 nm are expected to be 65%, 33%, and 17%, respectively, from an average 10% springtime ozone decrease near 50°N. Data from Canada during 1996 and 1997 showed even lower ozone values than found by Bojkov *et al.* (1995b) and correspondingly high UV-B irradiances (Fioletov *et al.*, 1997). Some of the ozone decrease, and therefore UV irradiance increase, is associated with colder stratospheric temperatures in recent years (e.g., Ramaswamy *et al.*, 1996).

### 9.5.3 Antarctica

At the South Pole (~90°S) the only solar angle variation comes from the seasonal cycle, with the solar elevation angles ranging from 23° (summer) to angles below the horizon. The dominant features in the Antarctic are the high surface reflectivity for UV irradiance from ice and snow and the large SZA. Both of these features increase the amount of diffuse irradiance at the surface relative to the direct irradiance. Grenfell *et al.* (1994) measured variations in snow albedo at Amundsen-Scott South Pole Station and the Vostok Station, finding a nearly uniform high value (0.96-0.98) across the visible and UV spectrum (300-400 nm), nearly independent of snow grain size and SZA. Under clear skies Grenfell *et al.* (1994) found that significant errors in apparent albedo can result if the instrument's cosine

response collector plate is not made parallel to the local surface instead of the horizon. Perturbations by clouds are relatively small at this site, because of the high surface albedo and the extremely cold temperatures that keep clouds from becoming optically thick. As is normal for Antarctica, the highest instantaneous UV irradiances (erythema, or UV-B) do not occur at the time of the greatest ozone depletion, but at a time closer to the summer solstice, combining the effects of higher SZAs with relatively low ozone. Although the relative seasonal increases are large, the absolute monthly UV exposures at this site are less than summer values at mid or low latitudes, but exceed values in the Northern Hemisphere with comparable SZA.

## 9.6 COMPARISON OF CALCULATIONS WITH OBSERVATIONS

The problem of successfully comparing different measurements of UV irradiances at the Earth's surface is tied directly to accurate modeling using radiative transfer calculations and the availability of relevant input data. Most published radiative transfer calculations are essentially plane-parallel multiple-scattering methods, with some having spherical geometry included for the primary and first-order scattering (pseudo-spherical). Some methods of calculation are more suitable for certain situations related to large optical depths (variations of doubling methods) and some are more suitable for including complex aerosol-scattering phase functions (variations on Gauss-Seidel methods).

The Gauss-Seidel method (Herman and Browning, 1965) has been used for radiative transfer calculations ranging from the UV to the IR. This method can handle such conditions as a non-Lambertian reflecting surface (Ahmad and Fraser, 1982), polarization, all orders of multiple scattering, thick aerosol clouds (Herman *et al.*, 1980), a mixture of particle compositions with different vertical distributions (i.e., aerosols and water droplets), scattering by large particles, scattering by non-spherical particles, scattering in a spherical atmosphere (B.M. Herman *et al.*, 1996), and thermal emission.

### 9.6.1 Intercomparison of Radiative Transfer Models

One study of detailed comparisons of backscattered radiances has been made with the following codes: the TOMS Ozone Processing Team's version of the Gauss-Seidel code (the Herman-Flittner code); the pure Rayleigh scattering code of Dave (1964) (used to create the TOMS Version 7 look-up tables); the Dave Fourier expansion Mie and Rayleigh scattering code (Dave and Gazdag, 1970) (used to analyze atmospheric aerosols and their effects on UV irradiance (Torres *et al.*, 1998; Krotkov *et al.*, 1998)); and the unpolarized version of the discrete ordinates radiative transfer method (DISORT) method (Stamnes *et al.*, 1988) with the pseudo-spherical correction added. All the comparisons show agreement in the inferred surface irradiances to better than 1% when the atmospheric model is the same. However, the differences in inferred radiances between codes including polarization (Dave, 1964; Dave and Gazdag, 1970; Herman and Browning, 1965) and those not including polarization (Stamnes *et al.*, 1988) can be as large as 10% for a pure Rayleigh atmosphere.

Recently, full spherical geometry calculations (e.g., B.M. Herman *et al.*, 1996), which are required to model UV irradiance at large SZAs, have become possible on moderately fast computers. These have been compared with much faster plane-parallel computations. For irradiances, comparisons of pseudo-spherical calculations with full spherical geometry calculations show 1% agreement to approximately 84° SZA.

Irradiance calculations can neglect polarization as a reasonable approximation. However, for calculating radiances at the Earth's surface, the models should include polarization effects. For small to moderate optical depths ($\tau = 2$ to 5) of scattering within clouds, polarization effects are important for radiances at the Earth's surface. For larger Mie scattering optical depths ($\tau > 10$), the solutions including polarization and those neglecting polarization agree to within 1%. Radiative transfer calculations suitable for large optical depths neglecting polarization are much faster computationally than methods including polarization.

For irradiance calculations with SZA < 84°, different modeling methods agree well. However, to represent the real atmosphere, there remain a number of outstanding problems. From the viewpoint of local UV irradiance and radiance, the next important problem is that of modeling cloud effects for broken cloud fields, cloud fields containing different cloud types, and multi-layer broken clouds. An additional problem is dealing with reflections from the Earth's surface, particularly over snow and ice with and without clouds (Lenoble, 1998; see also Figure 9-16). There are also remaining problems with the angular distribution of reflections

(non-Lambertian reflections) and the interactions with clouds.

Various approximate methods have been used for computational efficiency. Use of these methods may compromise the accuracy needed to compare with measurements. Forster and Shine (1995) compared the accuracy of the delta-Eddington and discrete-ordinate approximations for calculating high-wavelength-resolution UV irradiances at the Earth's surface. For certain atmospheric conditions, differences were greater than 10% in integrated UV-B between the delta-Eddington and eight-stream discrete-ordinate model.

Two-stream modeling of clear-sky and all-sky spectral irradiances during a full annual cycle (1992) were compared for Ushuaia, Argentina (55°S) (Diaz *et al.*, 1996). Measured irradiances at 340 nm were used to characterize the attenuation provided by cloudy skies. When irradiances in the range of 302.5 to 320 nm were corrected for cloud attenuation, both sets of data showed agreement, with correlation coefficients ranging from 0.97 to 0.99. At high SZA the differences are consistent with the neglect of spherical geometry in the calculated irradiances.

Model comparisons have been carried out using data from Toronto, Canada (Eck *et al.*, 1995), tropical Australia (Bernhard *et al.*, 1997), Greece (Weihs and Webb, 1997b), and southern Germany (Mayer *et al.*, 1997). The results suggest that accurate UV-A (for cloud attenuation) and ozone measurements combined with multiple-scattering radiative transfer calculations can provide the UV irradiances over the 280-400 nm range. Surface UV irradiances in the presence of broken clouds have been modeled using Monte Carlo methods (Geogdzhaev *et al.*, 1996, 1997). It should also be possible to use the approximate, but computationally faster, independent-pixel methods (Marshak *et al.*, 1998). A recent study by Loeb and Davies (1996) based on analysis of 1 year of Earth Radiation Budget Satellite (ERBS) reflectivity data between ±30° latitude, matched on a pixel basis to plane-parallel model calculations, showed a systematic shift toward larger reflectivities with increasing SZA relative to the observations. At nadir, differences were found to be about 10% and increased to 30% at large SZA (near 90°), the differences being attributed to the three-dimensional characteristics of real clouds compared with a plane-parallel simulation.

It is desirable to perform wide-ranging parameter studies on various standard radiative transfer models to eliminate computational artifacts. One such study (Forster, 1995) examined the influence of surface albedo, ozone profile, cloud, and aerosol on the UV irradiances calculated by the discrete-ordinate model. This was done to understand the causes of the largest modeling uncertainties and to allow calculation of errors for subsequent model predictions. The study showed that at 50°N in midsummer, the effect on UV-B caused by a decrease in total column ozone could be partially offset by the addition of an urban-type aerosol. Weihs and Webb (1997a,b) added to the parameter space testing in Forster (1995); they give a useful discussion of how uncertainties in model input parameters translate into UV irradiance errors.

For the purposes of calculating UV-forecasting indices (see Section 9.7) it has been shown (e.g., Diaz *et al.*, 1996; Koepke *et al.*, 1998) that two-stream models are adequate.

### 9.6.2 Clear-Sky Comparisons with Observations

Blumthaler *et al.* (1996) have compared measurements taken in Europe at sites that are considered relatively clear of aerosols (Lerwick, Scotland, 60.15°N, 1.17°W, and Esrange, Sweden, 67.88°N, 21.12°E) with a site with heavy pollution (Ispra, Italy, 45.8°N, 8.6°E). The data were compared with aerosol-free modeling results. The comparison showed a strong dependence of UV-B sky radiance on the presence of aerosol particles and a possible dependence on tropospheric ozone because of increased scattering from aerosols. The absolute disagreement with model results is considerable, but the deviation from the predicted shapes shows the aerosol effect clearly. Zeng *et al.* (1994) have compared clear-sky measurements before and after the Mt. Pinatubo eruption, and with a snow-covered surface, with the results from a discrete-ordinates radiative transfer model. Their comparison suggests that reasonable clear-sky diffuse/direct ratios can be computed if the atmospheric density, ozone amounts, surface albedo, and aerosol optical properties are known.

Clear-sky surface UV-B measurements in Greece have been compared with a discrete-ordinates model that included nonabsorbing aerosols in the first few kilometers above the ground (Wang and Lenoble, 1994). Agreement to about 6% was observed over a wide wavelength (290-350 nm) and SZA range (44-75°) for both global and direct irradiances, and it was concluded that the model output might be used as a means of

validating instrument calibration and long-term maintenance. The authors also suggest that the models be used to extrapolate into the short-wavelength regions for which most instruments fail to provide correct values. The agreement found is consistent with the results of an uncertainty analysis of model input parameters by Schwander *et al.* (1997).

An extensive study comparing measured and calculated UV spectral irradiances has been carried out by Mayer *et al.* (1997). Approximately 1200 clear-sky spectra obtained over a 2-year period (1994 to 1996) were used, covering the wavelength range 290-410 nm, for SZAs ranging up to 80°. The spectra represent a dynamic range of approximately $10^6$ in irradiance. Ozone column amounts and wavelength-dependent aerosol optical depths were derived from near-simultaneous direct-sun spectra. When these were used as inputs to the radiative transfer model (pseudo-spherical version of DISORT), the modeled global irradiance showed excellent agreement with the measured irradiances over the full range of SZA and wavelengths tested. Although there were systematic differences of up to 11%, the variances were generally smaller than 2-3%, which is within the range of instrument noise. Since that paper (Mayer *et al.*, 1997) was published, the instrument data analysis procedures were improved by changing the lamp standard, correcting for small drifts in the working standard, correcting for amplifier and detector non-linearities, and improving the cosine correction. The resulting model-measurement differences were reduced significantly and are shown in Figure 9-18.

The close agreement between model and measurement over such a wide range gives confidence in both the ability of the measurements to sustain accuracy over long periods and the ability of the radiative transfer model to accurately predict the effects of future changes for clear-sky conditions. For all of these observations at Garmisch-Partenkirchen, a constant single-scattering albedo was assumed. However, a recent study (Kylling *et al.*, 1998) suggests that in more polluted conditions (e.g., Thessaloniki), variations in this parameter can also be important.

### 9.6.3 General Comparisons with Observations

Spectral measurements have been compared with discrete-ordinates radiative-transfer model results for both clear and cloudy conditions (Forster *et al.*, 1995; Weihs and Webb, 1997b). Measurements and model agreed to within 6-10% for clear-sky UV-B irradiances, with worse agreement at short wavelengths ($\lambda < 300$ nm). This result is consistent with earlier work of Wang and Lenoble (1994). For cloudy skies, Weihs and Webb found the agreement was worse, with deviations between measurements and calculations of ±10% at two locations. The uncertainty of model input parameters was also shown to be an important contributing factor, especially measurements of the aerosol optical depth.

The uncertainties in modeled UV irradiances are

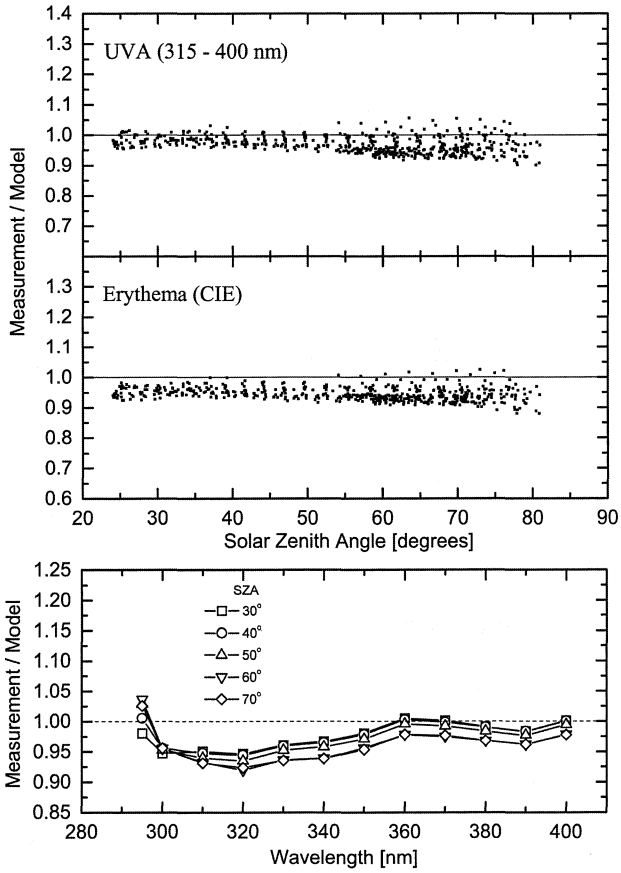


**Figure 9-18.** Comparison of measured (at Garmisch-Partenkirchen) and modeled spectral irradiances for clear skies. Top panels: Measurement/model ratios for UVA irradiance (315-400 nm) and erythemal UV irradiance as a function of SZA. Bottom panel: Measurement/model ratios of UV irradiance as a function of wavelength, for several values of SZA. (Updated from Mayer *et al.*, 1997.)

largely due to the limited accuracy and availability of input data characterizing the state of the atmosphere and the extraterrestrial irradiance. Neglecting extraterrestrial irradiance uncertainties, the best results that can be expected with model inputs of ozone, aerosol, and $SO_2$ are about 5% uncertain (Schwander *et al.*, 1997). The authors also conclude that these results cannot be improved significantly, even when measured values of vertical profiles of all atmospheric constituents are used. If only observed visibility is used instead of measured aerosol properties, then uncertainty is about 10-15%. In addition to atmospheric uncertainties, part of the difficulty in comparing model calculations of absolute irradiance is with the input solar irradiances (see Figure 9-10). In the UV-B region, satellite instruments differ at the 5% level (Cebula *et al.*, 1996), giving a fundamental uncertainty between model results and ground-based measurements.

Results from the Dave (1964) multiple-scattering code for a pure Rayleigh atmosphere containing a cloud correction term were compared (Eck *et al.*, 1995) with measurements from the Brewer #14 instrument in Toronto (Kerr and McElroy, 1993). The model was adjusted to the data by using independently measured cloud reflectivities ($R$) and ozone amounts from TOMS to determine the amount of UV-irradiance reduction in the 300- to 325-nm range. It was found that the simple cloud attenuation model (1 - ($R$ - 0.05)/0.95) gave an estimate of the observed irradiance as a function of wavelength and as a function of the day of the year to better than 10%. Daily values could differ by much more than 10% because of the difference between the field of view of the spectroradiometer and the TOMS satellite that might contain different amounts of cloud and aerosol cover.

A sample comparison between the Toronto Brewer data and UV irradiance calculated using TOMS data for a single day (8 August 1996) is shown in Figure 9-19. The clear-sky curve uses the TOMS-measured ozone amount of 290 DU and a surface reflectivity of 4%. The same calculation was made using the estimated cloud cover ($\tau_{CLOUD}$ = 40.4) from the TOMS-measured backscattered radiances at 360 nm. The results show an apparent good instantaneous agreement between the Toronto Brewer measurement at the time of the TOMS overpass. However, it also shows the large difference that can occur if the time of the TOMS overpass is shifted by a few minutes relative to the Brewer measurement time or if the local cloud cover changes. Figure 9-19 also shows the error that can occur if the TOMS data are used to estimate daily UV exposure unless the UV irradiance from enough days (at least 1 week) are combined to average out different daily cloud and aerosol amounts in the instruments' fields of view.

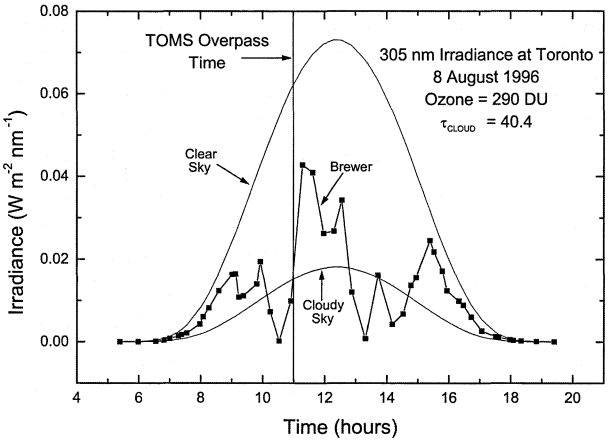


**Figure 9-19.** UV irradiances derived from radiative transfer results (smooth curves) for clear and cloudy skies compared with corresponding ground-based measurements (squares) for 8 August 1996 at Toronto Canada (43.5°N, 79.3°W). The vertical straight line marks the time of the Earth-Probe/TOMS overpass of Toronto (from WOUDC database).

## 9.7 LOCAL PREDICTABILITY AND FORECASTING

Since the 1994 Assessment report (WMO, 1995, Chapter 9), an international agreement has been reached on defining a UV-irradiance index for the dissemination of UV exposure information to the public (WMO, 1994). The UV index has been used in daily weather reports and in forecasts used by the media in several countries (see Appendix). In Canada, where the UV index was developed and first used, and in the United States, predictions of the UV index include advection effects of measured ozone fields and estimates of cloud attenuation (Long, 1996; Burrows, 1997). In Canada, the ozone measurements are from the network of Brewer instruments, whereas in the United States, satellite measurements of ozone and cloud-amount predictions are used.

Similar products involving the UV index are available in other countries (e.g., Australia; Rikus, 1997). The UV index gives a regional prediction of the amount of UV irradiance expected on a scale that is essentially a danger index for human exposure, but is intended to be applicable to other processes involving UV damage as well. It is based on incidence on a horizontal surface only and can underestimate the risk for surfaces in other orientations, such as surfaces that are oriented toward the sun (McKenzie *et al.*, 1997a). The NOAA method of ozone-amount estimation used in UV-irradiance forecasting (Long, 1996; Long *et al.*, 1996) has been compared with a statistical approach using the global ozone maps from TOMS instead of the nadir views of SBUV/2, which are widely separated in longitude (Ziemke *et al.*, 1998). The results show that a modest improvement in UV-irradiance predictability can be obtained. Although not essential for all UV forecasting purposes, the ability to accurately predict cloud fields and their effect on UV irradiance remains a challenging problem (Burrows, 1997).

## REFERENCES


Ahmad, Z., and R.S. Fraser, An iterative radiative transfer code for ocean-atmosphere systems, *J. Atmos. Sci.*, *39*, 656-665, 1982.

Bais, A.F., C.S. Zerefos, C. Meleti, I.C. Ziomas, and K. Tourpali, Spectral measurements of solar UVB radiation and its relations to total ozone, $SO_2$ and clouds, *J. Geophys. Res.*, *98*, 5199-5204, 1993.

Bais, A.F., C.S. Zerefos, and C.T. McElroy, Solar UVB measurements with the double- and single-monochromator Brewer ozone spectrophotometers, *Geophys. Res. Lett.*, *23*, 833-836, 1996.

Bais, A.F., M. Blumthaler, A.R. Webb, J. Groebner, P.J. Kirsch, B.G. Gardiner, C.S. Zerefos, T. Svenoe, and T.J. Martin, Spectral UV measurements over Europe within the SESAME activities, *J. Geophys. Res.*, *102*, 8731-8736, 1997.

Balachandran, N.K., and D. Rind, Modeling the effects of UV variability and the QBO on the troposphere-stratosphere system: Part I, The middle atmosphere, *J. Clim.*, *8*, 2058-2079, 1995.

Basher, R.E., X. Zheng, and S. Nichols, Ozone-related trends in solar UV-B series, *Geophys. Res. Lett.*, *21*, 2713-2716, 1994.

Bernhard, G., and G. Seckmeyer, New entrance optics for solar spectral UV measurements, *Photochem. Photobiol.*, *65*, 923-930, 1997.

Bernhard, G., B. Mayer, and G. Seckmeyer, All weather comparisons between spectral and broadband (Robertson-Berger) UV meters, *Photochem. Photobiol.*, *64*, 792-799, 1996.

Bernhard, G., B. Mayer, and G. Seckmeyer, Measurements of spectral solar UV irradiance in tropical Australia, *J. Geophys. Res.*, *102*, 8719-8730, 1997.

Bigelow, D.S., J.R. Slusser, A.F. Beaubien, and J.H. Gibson, The USDA Ultraviolet Radiation Monitoring Program, *Bull. Amer. Meteorol. Soc.*, *79*, 601-615, 1998.

Blumthaler, M., W. Ambach, and M. Salzgeber, Effects of cloudiness on global and diffuse UV irradiance in a high-mountain area, *Theor. Appl. Climatol.*, *50*, 23-30, 1994.

Blumthaler, M., J. Grobner, M. Huber, and W. Ambach, Measuring spectral and spatial variations of UVA and UVB sky radiance, *Geophys. Res. Lett.*, *23*, 547-550, 1996.

Blumthaler, M., W. Ambach, and R. Ellinger, Increases in solar UV radiation with altitude, *J. Photochem. Photobiol. B: Biol.*, *39*, 130-134, 1997.

Bodeker, G.E., and R.L. McKenzie, An algorithm for inferring surface UV irradiance including cloud effects, *J. Appl. Meteorol.*, *35*, 1860-1877, 1996.

Bodhaine, B.A., R.L. McKenzie, P.V. Johnston, D.J. Hofmann, E.G. Dutton, R.C. Schnell, J.E. Barnes, S.C. Ryan, and M. Kotkamp, New ultraviolet spectroradiometer measurements at Mauna Loa Observatory, *Geophys. Res. Lett.*, *23*, 2121-2124, 1996.

Bodhaine, B.A., E.G. Dutton, R.L. McKenzie, and P.V. Johnston, Spectral UV measurements at Mauna Loa: July 1995-July 1996, *J. Geophys. Res.*, *23*, 2121-2124, 1997.

Bodhaine, B.A., E.G. Dutton, R.L. McKenzie, and P.V. Johnston, Calibrating broadband UV instruments: Ozone and solar zenith angle dependence, *J. Atmos. Oceanic Technol.*, *15*, 916-926, 1998.

Bojkov, R.D., and V.E. Fioletov, Estimating the global ozone characteristics during the last 30 years, *J. Geophys. Res.*, *100*, 16537-16551, 1995a.

Bojkov, R.D., and V.E. Fioletov, Total ozone variations in the tropical belt: An application for quality of ground-based measurements, *Meteorol. Atmos. Phys.*, *58*, 223-240, 1995b.

Bojkov, R.D., and V.E. Fioletov, Changes in lower stratospheric ozone over Europe and Canada, *J. Geophys. Res.*, *102*, 1337-1347, 1997.

Bojkov, R.D., V.E. Fioletov, and S.B. Diaz, The relationship between solar UV irradiance and total ozone from observations over southern Argentina, *Geophys. Res. Lett.*, *22*, 1249-1252, 1995a.

Bojkov, R.D., V.E. Fioletov, D.S. Balis, C.S. Zerefos, T.V. Kadygrova, and A.M. Shalamjansky, Further ozone decline during the northern hemisphere winter-spring of 1994-1995 and the new record low over Siberia, *Geophys. Res. Lett.*, *22*, 2729-2732, 1995b.

Booth, C.R., T.B. Lucas, T. Mestechkina, J.R. Tusson IV, D.A. Neuschuler, and J.H. Morrow, *NSF Polar Programs UV Spectrometer Network 1991-1993 Operations Report*, Biospherical Instruments Inc., San Diego, Calif., 1993.

Booth, C.R., T. Mestechkina, and J.H. Morrow, Errors in the reporting of solar irradiance using moderate bandwidth radiometers: An experimental investigation, *Proc. Soc. Photo.-Opt. Instrum. Eng.*, *2258*, 654-663, 1994.

Booth, C.R., J.C. Ehramjian, T. Mestechkina, L.W. Cabasug, J.S. Robertson, and J.R. Tusson, *NSF Polar Programs UV Spectroradiometer Network 1995-1997 Operations Report*, 241 pp., Biospheric Instruments Inc., San Diego, Calif., 1998.

Bordewijk, J.A., H. Slaper, H.A.J.M. Reinen, and E. Schlamann, Total solar radiation and the influence of clouds and aerosols in the biologically effective UV, *Geophys. Res. Lett.*, *22*, 2151-2154, 1995.

Brüeckner, G.E., K.L. Edlow, L.E. Floyd IV, J.L. Leon, and M.E. VanHoosier, The Solar Ultraviolet Spectral Irradiance Monitor (SUSIM) experiment on board the Upper Atmospheric Research Sattelite (UARS), *J. Geophys. Res.*, *98*, 10695-10711, 1993.

Brühl, C., and P.J. Crutzen, On the disproportionate role of tropospheric ozone as a filter against solar UV-B radiation, *Geophys. Res. Lett.*, *16*, 703-706, 1989.

Burrows, W.R., CART regression models for predicting UV radiation at the ground in the presence of cloud and other environmental factors, *J. Appl. Meteorol.*, *36*, 531-544, 1997.

Caldwell, M.M., L.B. Camp, C.W. Warner, and S.D. Flint, Action spectra and their key role in assessing biological consequences of solar UV-B radiation change, in *Stratospheric Ozone Reduction, Solar Ultraviolet Radiation and Plant Life*, edited by R.C. Worrest and M.M. Caldwell, pp. 87-111, Springer-Verlag, Berlin, 1986.

Cebula, R.P., and M.T. Deland, Comparisons of the NOAA-11 SBUV/2, UARS SOLSTICE, and UARS SUSIM Mg II solar activity proxy indexes, *Sol. Phys.*, *177*, 117-132, 1998.

Cebula, R.P., E. Hilsenrath, and M.T. Deland, Middle ultraviolet solar spectral irradiance measurements, 1985-1992, from SBUV/2 and SSBUV instruments, in *The Sun as Variable Star: Solar and Stellar Variations*, edited by J.M. Pap, C. Frolich, H.S. Hudson, and S.K. Folanki, pp. 81-88, Cambridge University Press, Cambridge, U.K., 1994.

Cebula, R.P., G.O. Thuillier, M.E. VanHoosier, E. Hilsenrath, M. Herse, G.E. Brueckner, and P.C. Simon, Observations of the solar irradiance in the 200-350-nm interval during the ATLAS-1 mission: A comparison among three sets of measurements—SSBUV, SOLSPEC, and SUSIM, *Geophys. Res. Lett.*, *23*, 2289-2292, 1996.

Chubarova, N.E., Transmission of total UV radiation through clouds of different types, *Izv. Atmos. Oceanic Phys.*, *29*, 639-645, 1993.

Chubarova, N.E., Ultraviolet radiation under broken cloud conditions as inferred from many-year ground-based observations, *Izv. Atmos. Oceanic Phys.*, *34*, 131-134, 1998.

Dahlback, A., Measurements of biologically effective UV doses, total ozone abundance and cloud effects with multi-channel moderate bandwidth filter instruments, *Appl. Opt.*, *35*, 6514-6521, 1996.

Dave, J.V., Meaning of successive iteration of the auxiliary equation in the theory of radiative transfer, *Astrophys. J.*, *140*, 1292-1303, 1964.

Dave, J.V., and J. Gazdag, A modified Fourier transform method for multiple scattering calculations in a plane parallel Mie atmosphere, *Appl. Opt.*, *9*, 1457-1466, 1970.

DeLand, M.T., and R.P. Cebula, NOAA-11 SBUV/2 solar spectral irradiance measurements 1989-1994: II, Results, validation, and comparisons, *J. Geophys. Res.*, *103*, 16251-16273, 1998a.

Kirchhoff, V.W.J.H., F. Zamorano, and C. Casiccia, UV-B enhancements at Punta Arenas, Chile, *J. Photochem. Photobiol. B: Biol.*, *38*, 174-177, 1997.

Kjeldstad, B., B. Johnsen, and T. Koskela (eds.), *The Nordic Intercomparison of Ultraviolet and Total Ozone Instruments at Izaña, October 1996*, Meteorological Publication 36, Finnish Meteorological Insitute, Helsinki, 1997.

Koepke, P., A. Bais, D. Balis, M. Buchwitz, H. De Backer, X. de Cabo, P. Eckert, P. Eriksen, D. Gillotay, A. Heikkila, T. Koskela, B. Lapeta, Z. Litynska, J. Lorente, B. Mayer, A. Renaud, A. Ruggaber, G. Schauberger, G. Seckmeyer, P. Seifert, A. Schmalwieser, H. Schwander, K. Vanicek, and M. Weber, Comparison of models used for UV-index calculations, *J. Photochem. Photobiol. B: Biol.*, in press, 1998.

Kohler, U., Recalibration of the Hohenpeissenberg Dobson spectrophotometer 104 presuming effective absorption coefficients, *J. Atmos. Chem.*, *4*, 359-373, 1986.

Koskela, T. (ed.), *The Nordic Intercomparison of Ultraviolet and Total Ozone Instruments at Izaña from 24 October to 5 November 1993: Final Report*, Meteorological Publications, Finnish Meteorological Institute, Helsinki, 1994.

Krotkov, N.A., P.K. Bhartia, J.R. Herman, V. Fioletov, and J. Kerr, Satellite estimation of spectral surface UV irradiance in the presence of tropospheric aerosols: 1, Cloud-free case, *J. Geophys. Res.*, *103*, 8779-8793, 1998.

Krzyscin, J.W., UV controlling factors and trends derived from the ground-based measurements taken at Belsk, Poland, 1976-1994, *J. Geophys. Res.*, *101*, 16797-16805, 1996.

Kylling, A., A. Albold, and G. Seckmeyer, Transmittance of a cloud is wavelength-dependent in the UV-range: Physical interpretation, *Geophys. Res. Lett.*, *24*, 397-400, 1997.

Kylling, A., A.F. Bais, M. Blumthaler, J. Schreder, and C.S. Zerefos, The effect of aerosols on solar UV irradiances during the PAUR campaign, *J. Geophys. Res.*, *103*, 26051-26060, 1998.

Lean, J.L., G.J. Rottman, H.L. Kyle, T.N. Woods, J.R. Hickey, and L.C. Puga, Detection and parameterization of variations in solar mid- and near-ultraviolet radiation (200-400 nm), *J. Geophys. Res.*, *102*, 29939-29956, 1997.

Lenoble, J., Modeling of the influence of snow reflectance on UV irradiance for cloudless sky, *Appl. Opt.*, *37*, 2441-2447, 1998.

Leszczynski, K., K. Jokela, L. Ylianttila, R. Visuri, and M. Blumthaler, *Report of the WMO/STUK Intercomparison of Erythemally-Weighted Solar UV Radiometers (Spring/Summer 1995, Helsinki, Finland)*, Global Atmosphere Watch Report No. 112, 90 pp., World Meteorological Organization, Geneva, 1997.

Leszczynski, K., K. Jokela, L. Ylianttila, R. Visuri, and M. Blumthaler, Erythemally weighted radiometers in solar UV monitoring: Results from the WMO/STUK intercomparison, *Photochem. Photobiol.*, *67*, 212-221, 1998.

Liepert, B., P. Fabian, and H. Groassl, Solar radiation in Germany—observed trends and an assessment of their causes: Part 1, Regional approach, *Contrib. Atmos. Phys.*, *67*, 15-29, 1994.

Liley, J.B., and R.L. McKenzie, Time-dependent wavelength non-linearities in spectrometers for solar UV monitoring, in *IRS'96: Current Problems in Atmospheric Radiation*, edited by W.L. Smith and K. Stamnes, Deepak, Hampton, Va., 1997.

Loeb, N.G., and R. Davis, Observational evidence of plane parallel modeling biases: Apparent dependence of cloud optical depth on solar zenith angle, *J. Geophys. Res.*, *101*, 1621-1634, 1996.

Long, C.S., *Ultraviolet Index Verification Report: Indicators of Surface Ultraviolet Radiation Observation Characteristics*, NOAA, National Centers for Environmental Predication, Washington, D.C., 1996.

Long, C.S., A.J. Miller, H.T. Lee, J.D. Wild, R.C. Przywarty, and D. Hufford, Ultraviolet index forecasts issued by the National Weather Service, *Bull. Amer. Meteorol. Soc.*, *77*, 729-748, 1996.

Lubin, D., and E.H. Jensen, Effects of clouds and stratospheric ozone depletion on ultraviolet radiation trends, *Nature*, *377*, 710-713, 1995.

Lubin, D., E.H. Jensen, and H.P. Gies, Global surface ultraviolet climatology from TOMS and ERBE data, *J. Geophys. Res.*, *103*, 26061-26091, 1998.

Madronich, S., Increases in biologically damaging UV-B radiation due to stratospheric ozone depletion: A brief review, *Arch. Hydrobiol.*, *43*, 17-30, 1994.

Madronich, S., and F.R. de Gruijl, Stratospheric ozone depeletion between 1979 and 1992: Implication for biologically active ultraviolet-B radiation and non-melanoma skin cancer incidence, *Photochem. Photobiol.*, *59*, 541-546, 1994.

Madronich, S., R.L. McKenzie, M. Caldwell, and L.O. Björn, Changes in ultraviolet radiation reaching the Earth's surface, *Ambio.*, *24*, 143-152, 1995.

Marshak, A., A. Davis, R.F. Calahan, and W.J. Wiscomb, Nonlocal independent pixel approximation: Direct and inverse problems, *IEEE Trans. Geosci. Remote Sens.*, *36*, 192-205, 1998.

Mateer, C.L., On the information content of Umkehr observations, *J. Atmos. Sci.*, *22*, 370-381, 1965.

Mayer, B., and G. Seckmeyer, All-weather comparison between spectral and broadband (Robertson-Berger) UV measurements, *Photochem. Photobiol.*, *64*, 792-799, 1996.

Mayer, B., G. Seckmeyer, and A. Kylling, Systematic long-term comparison of spectral UV measurements and UVSPEC modeling results, *J. Geophys. Res.*, *102*, 8755-8767, 1997.

McElroy, C.T., A spectroradiometer for the measurement of direct and scattered solar irradiance from on-board the NASA ER-2 high-altitude research aircraft, *Geophys. Res. Lett.*, *22*, 1361-1364, 1995.

McKenzie, R.L., P.V. Johnston, M. Kotkamp, A. Bittar, and J.D. Hamlin, Solar ultraviolet spectroradiometry in New Zealand: Instrumentation and sample results from 1990, *Appl. Opt.*, *31*, 6501-6509, 1992.

McKenzie, R.L., M. Kotkamp, G. Seckmeyer, R. Erb, C.R. Roy, H.P. Gies, and S.J. Toomey, First southern hemisphere intercomparison of measured solar UV spectra, *Geophys. Res. Lett.*, *20*, 2223-2226, 1993.

McKenzie, R.L., M. Kotkamp, and W. Ireland, Upwelling UV spectral irradiances and surface albedo measurements at Lauder, New Zealand, *Geophys. Res. Lett.*, *23*, 1757-1760, 1996.

McKenzie, R.L., K. Paulin, and M. Kotkamp, Erythemal UV irradiances at Lauder, New Zealand: Relationship between horizontal and normal incidence, *Photochem. Photobiol.*, *65*, 683-689, 1997a.

McKenzie, R.L., P.V. Johnston, and G. Seckmeyer, UV spectro-radiometry in the Network for the Detection of Stratospheric Change (NDSC), in *Solar Ultraviolet Radiation: Modelling, Measurements and Effects*, NATO ASI Series I, Vol. 52, edited by C.S. Zerefos and A.F. Bais, pp. 279-287, Springer-Verlag, Berlin, 1997b.

McKinlay, A.F., and B.L. Diffey, A reference action spectra for ultraviolet induced erythema in human skin, in *Human Exposure to Ultraviolet Radiation: Risks and Regulations*, edited by W.R. Passchier and B.M.F. Bosnajakovich, pp. 83-87, Elsevier, Amsterdam, 1987.

McPeters, R.D., S.M. Hollandsworth, L.E. Flynn, J.R. Herman, and C.J. Seftor, Long-term ozone trends derived from the 16-year combined Nimbus 7/ Meteor 3 TOMS version 7 record, *Geophys. Res. Lett.*, *23*, 3699-3702, 1996.

Meerkoetter, R., B. Wissinger, and G. Seckmeyer, Surface UV from ERS 2/GOME and NOAA/AVHRR data: A case study, *J. Geophys. Res.*, *24*, 1939-1942, 1997.

Mims, F.M. III, and J.E. Frederick, Cumulus clouds and UV-B, *Nature*, *371*, 291, 1994.

Mims, F.M. III, J.W. Ladd, and R.A. Blaha, Increased solar ultraviolet-B associated with record low ozone over Texas, *Geophys. Res. Lett.*, *22*, 227-230, 1995.

Nack, M.L., and A.E.S. Green, Influence of clouds, haze, and smog on the middle ultraviolet reaching the ground, *Appl. Opt.*, *13*, 2405-2415, 1974.

Nemeth, P., Z. Toth, and Z. Nagy, Effect of weather conditions on UV-B radiation reaching the Earth's surface, *J. Photochem. Photobiol. B: Biol.*, *32*, 177-181, 1996.

Nezval, E.I., Statistical characteristics of the UV irradiance in Moscow, 1968-1992, *Meteorol. Hydrol.*, *8*, 64-71, 1996.

Olmo, F.J., and L. Alados-Arboledas, Pinatubo eruption effects on solar radiation at Almeira (36.83°N, 2.41°W), *Tellus*, *47B*, 602-606, 1995.

Piazena, H., The effect of altitude upon the solar UV-B and UV-A irradiance in the topical Chilean Andes, *Sol. Energy*, *57*, 133-140, 1996.

Ramaswamy, V., M.D. Schwarzkopf, and W.J. Randel, Fingerprint of ozone depletion in the spatial and temporal pattern of recent lower-stratospheric cooling, *Nature*, *382*, 616-618, 1996.

Rikus, L., Prediction of UV-B dosage at the surface, *Aust. Meteorol. Mag.*, *46*, 211-222, 1997.

Rossow, W.B., and L.C. Garder, Cloud detection using satellite measurements of infrared and visible radiances for ISCCP, *J. Climate*, *6*, 2370-2393, 1993.

Rottman, G.J., T.N. Woods, and T.P. Sporn, Solar Stellar Irradiance Comparison Experiment 1: 1, Instrument design and operation, *J. Geophys. Res.*, *98*, 10667-10677, 1993.

Ryan, K.G., G.J. Smith, D.A. Rhoades, and R.B. Coppell, Erythemal ultraviolet insolation in New Zealand at solar zenith angles of 30° and 45°, *Photochem. Photobiol.*, *63*, 628-632, 1996.

Zeng, J., R. McKenzie, K. Stamnes, M. Wineland, and J. Rosen, Measured UV spectra compared with discrete ordinate method simulations, *J. Geophys. Res.*, *99*, 23019-23030, 1994.

Zerefos, C.S., K. Tourpali, and A.G. Bais, Further studies on possible volcanic signal to the ozone layer, *J. Geophys. Res.*, *99*, 25741-25746, 1994.

Zerefos, C.S., A.F. Bais, C. Meleti, and I.C. Ziomas, A note on the recent increase of solar UV-B radiation over northern middle latitudes, *Geophys. Res. Lett.*, *22*, 1245-1248, 1995a.

Zerefos, C.S., C. Meleti, A.F. Bais, and A. Lambros, The recent UVB variability over southeastern Europe, *J. Photochem. Photobiol. B: Biol.*, *31*, 15-19, 1995b.

Zerefos, C.S., D.S. Balis, A.F. Bais, D. Gillotay, P.C. Simon, B. Mayer, and G. Seckmeyer, Variability of UV-B at four stations in Europe, *Geophys. Res. Lett.*, *24*, 1363-1366, 1997.

Ziemke, J.R., S. Chandra, R.D. McPeters, and P.A. Newman, Dynamical proxies of column ozone with applications to global trend models, *J. Geophys. Res.*, *102*, 6117-6129, 1997.

Ziemke, J.R., J.R. Herman, J.L. Stanford, and P.K. Bhartia, Total ozone/UV-B monitoring and forecasting: Impact of clouds and the horizontal resolution of satellite retrievals, *J. Geophys. Res.*, *103*, 3865-3871, 1998.

# Appendix

## Internet Addresses for UV Sites

### Internet Sites with General UV Information

| | |
|---|---|
| http://www.biospherical.com/nsf/index.html | NSF UV Sites |
| http://uvb.asrc.cestm.albany.edu/ | USDA |
| http://insider.nrel.colostate.edu:8080/UVB/UVB.html | Colorado State University |
| http://uvb.nrel.colostate.edu/uvb | USDA |
| http://www.niwa.cri.nz/lauder | NIWA, New Zealand |
| http://www.noaa.gov/uvb/fctsh.html | NOAA UV index |
| http://www.epa.gov/ozone/uvindex/uvcalc.html | NOAA UV index |
| http://www.atdd.noaa.gov/isis/isis_frame.htm | NOAA |
| http://www.epa.gov/ozone/othlinks.html#uvindex | U.S. EPA |
| http://sedac.ciesin.org/ozone | CIESIN UV and Ozone |
| http://wwwsolar.nrl.navy.mil/susim_atlas_data.html | Solar Radiation: SUSIM |
| http://maia.colorado.edu/solstice | Solar Radiation: SOLSTICE |
| http://www-uars.gsfc.nasa.gov/cdrom_main.html | Solar Radiation: SOLSTICE |
| http://wrdc-mgo.nrel.gov | World Radiation Centre |
| http://www.ozone.fmi.fi/SUVDAMA/kuvaus.html | SUVDAMA Project |
| http://www.itek.norut.no/~olae/fastrt | UV Exposure Calculations |
| http://www.tor.ec.gc.ca/woudc | WOUDC Canada |
| http://jwocky.gsfc.nasa.gov | TOMS Homepage |
| http://www.ozone.fmi.fi/ | Finnish Meteorological Institute |

### Internet Sites with UV Index Information

| | | |
|---|---|---|
| http://www.bom.gov.au/bmrc/medr/uvi.html | Australia | (UV index) |
| http://www.smhi.se/uvindex/en/uvprog.htm | Sweden | (UV index) |
| http://nic.fb4.noaa.gov/products/stratosphere/uv_index | United States | (UV index) |
| http://www.ec.gc.ca/ozone/tocuvyou.htm | Canada | (UV index) |
| http://www.ozone.fmi.fi/o3group/o3home.html | Finland | (UV index) |
| http://www.niwa.cri.nz/lauder | New Zealand | (UV index) |
| http://www-med-physik.vu-wien.ac.at/uv/uv_home.htm | Austria | (UV index) |
| http://www.chmi.cz/meteo/ozon/hk.html | Czech Republic | (UV index) |

# CHAPTER 10

## CLIMATE EFFECTS OF OZONE AND HALOCARBON CHANGES

### Contents

## SCIENTIFIC SUMMARY

- **Increased penetration of UV radiation to the troposphere as a result of stratospheric ozone depletion leads to changes in key photochemical processes in the troposphere.** Model simulations have been used to estimate that a 1% decrease in global total ozone leads to a global increase of about 1.5% in the photolytic production of the first excited state of atomic oxygen, $O(^1D)$, from ozone. This results in a 0.7 to 1% increase in globally averaged tropospheric hydroxyl radical (OH). Since OH is the main oxidant for climatically important gases, such as methane ($CH_4$), hydrochlorofluorocarbons (HCFCs), and hydrofluorocarbons (HFCs), this change would be expected to decrease their lifetimes. Stratospheric ozone depletion may have contributed 20 to 40% of the reduction in $CH_4$ growth rate, and 25 to 40% of the carbon monoxide (CO) surface concentration decrease during the two years following the Mt. Pinatubo volcanic eruption in 1991. The effect on those species whose lifetimes depend on OH has not yet been quantified.

- **The first systematic calculations of the effects of ozone changes on climate using a general circulation model (GCM) have been reported.** Previous assessments highlighted the climatic importance of ozone changes near the tropopause. When taking into account the impact of ozone changes on cloudiness, this GCM study suggests that changes in lower tropospheric ozone are of similar importance to changes near the tropopause. This study suggests that, because of the cloud interactions, the ozone change since the late 1970s may have resulted in a surface temperature change 20-30% smaller than that implied by radiative forcing. Given the known difficulties in modeling cloud processes in GCMs, the generality of conclusions drawn from a single model must be treated with caution.

- **The global-average radiative forcing due to changes in stratospheric ozone since the late 1970s is estimated to be $-0.2 \pm 0.15$ Wm$^{-2}$.** The central value of this forcing estimate is about double the Intergovernmental Panel on Climate Change (IPCC, 1996) estimate, partly because the calculations now include the increased ozone losses during the 1990s. There remain uncertainties due to difficulties in defining the vertical profile of ozone change and in calculating the stratospheric temperature response to this change. The stratospheric ozone forcing may have offset about 30% of the forcing due to the increases in the well-mixed greenhouse gases since the late 1970s.

- **Recovery of stratospheric ozone would reduce the offset to the radiative forcing of the other greenhouse gases.** The ozone recovery will therefore lead to a more rapid increase in radiative forcing than would have occurred due to increases in other greenhouse gases alone.

- **The global-average radiative forcing due to increases in tropospheric ozone since preindustrial times is estimated to be $+0.35 \pm 0.15$ Wm$^{-2}$.** This estimate is consistent with the IPCC (1996) estimate of $0.4 \pm 0.2$ Wm$^{-2}$, but is based on a much wider range of model studies; significant uncertainties remain because of inter-model differences and the lack of data for evaluating the model results. Since the forcing due to the increases in "well-mixed" greenhouse gases since preindustrial times is about 2.5 Wm$^{-2}$, the tropospheric ozone changes may have enhanced this forcing by 10-20%.

- **Coupled ocean-atmosphere GCMs have been used to calculate the impact of stratospheric ozone loss on the thermal structure of the atmosphere.** The observed stratospheric ozone depletion appears to explain much of the observed temperature decrease in the lower stratosphere. The calculated altitude of the transition from tropospheric warming to stratospheric cooling is in better agreement with observations when ozone depletion is taken into account. The global average surface temperature is estimated to be about 0.1°C cooler over the past two decades as a result of the stratospheric ozone loss; this can be compared with the calculated warming of about 0.3°C over the same period, due to well-mixed greenhouse gas increases.

**Table 10-3. Sensitivity of the ozone photodissociation rates and of tropospheric chemical species to stratospheric ozone changes for the period 1979-1994, as defined in Equation (10-2).** The values reported here correspond to the relative change in global tropospheric annual average levels in *X* (%) resulting from a 1% decrease in total column ozone; the assumed scenarios are discussed in the cited publications. The type of model used is indicated in parentheses. Note that the values of Granier *et al.* (1996) correspond to the 1990-1994 period. The calculations indicated as Granier-1997 correspond to the 1979-1994 period and have been obtained using an updated version of the model used by Granier *et al.* (1996).

| Reference | X=J($O_3$) | X=OH | X=$O_3$ trop | X=$CH_4$ |
|---|---|---|---|---|
| Bekki *et al.* (1994) (2-D) | N/A | 0.86 | N/A | N/A |
| Fuglestvedt *et al.* (1994) (2-D) | 1.38 | 0.99 | -0.29 | -0.79 |
| Van Dop and Krol (1996) (1-D) | N/A | 0.45*X(J($O_3$)) | N/A | N/A |
| Granier *et al.* (1996) (3-D) | 1.57 | 0.82 | -0.32 | N/A |
| Granier-1997 (3-D JPL94) | 1.39 | 0.70 | -0.27 | N/A |
| Granier-1997 (3-D JPL97) | 1.27 | 0.74 | -0.29 | N/A |

tropospheric ozone through reactions R5 and R6. In regions where low levels of nitrogen oxides are found, the loss of ozone through R1 and R2 will also contribute to the reduction of ozone concentrations. The 2-D and 3-D models calculate a global decrease in tropospheric ozone as a result of decreasing stratospheric ozone. However, whereas the 3-D intermediate model of the annual and global evolution of species (IMAGES; Granier *et al.*, 1996) calculates a decrease in ozone at all latitudes and times of year, the 2-D model of Fuglestvedt *et al.* (1994) calculates a global ozone decrease, except for spring at mid- and high latitudes of the Northern Hemisphere, where an ozone increase is calculated. In this model, ozone precursors accumulate during winter, and when the UV radiation increases in spring, the chemical activity increases strongly, thereby affecting the ozone chemistry, leading to ozone net production for a period. In the perturbed case, the chemical activity starts earlier in the spring than in the unperturbed case. The difference between these results obtained by a 2-D and a 3-D model could be due to different spatial resolution, different parameterization of the chemical scheme involving nonmethane hydrocarbons (NMHCs), or lower nitrogen oxides concentrations calculated by the IMAGES model, making the role of reaction R7 less important than in the Fuglestvedt *et al.* (1994) study.

Two sets of 3-D model calculations were performed using the values of the J($O_3 \rightarrow O(^1D)$) quantum yields from DeMore *et al.* (1994) and DeMore *et al.* (1997) with an updated version of the IMAGES model (Granier *et al.*, 1996); the calculated values for the $\alpha$ sensitivity factor are reported in Table 10-3. Though the sensitivity of J($O_3$) is larger for the lower quantum yields reported in DeMore *et al.* (1994), the sensitivity of OH and tropospheric $O_3$ to total column ozone are slightly lower and higher, respectively, for quantum yields reported in DeMore *et al.* (1997). This may be due to the fact that absolute J($O_3 \rightarrow O(^1D)$) values and OH concentrations are higher in the latter case, resulting in a marginal global decrease in nitrogen oxides. It should be mentioned however that such results could be model-dependent and need to be confirmed by other model evaluations.

### 10.2.3 Changes in Greenhouse Gases and Ozone Precursor Budgets and Lifetimes Since 1979

The removal of most tropospheric trace gases, including CO and greenhouse gases like methane, HCFCs, and HFCs, is dominated by the reaction with OH. Therefore, any changes in tropospheric OH resulting from stratospheric ozone changes should be accompanied by changes in the growth rates of these trace gases. Furthermore, the atmospheric levels of CO and $CH_4$ are closely linked to their interaction with OH, because

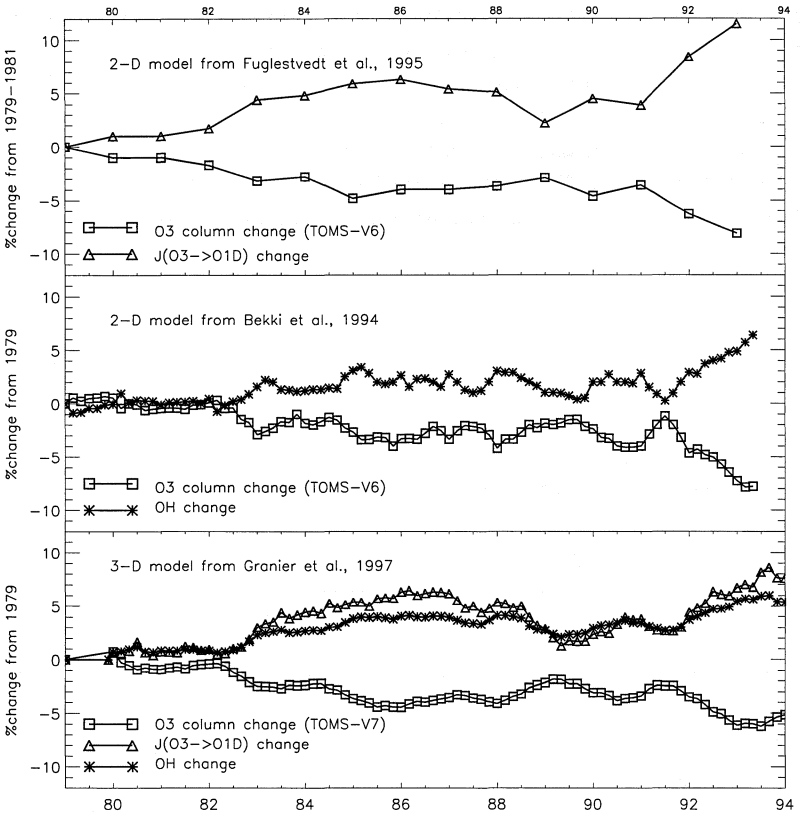


**Figure 10-1.** Relative change in total column ozone and calculated associated change in $J(O_3 \rightarrow O^1D)$ rate (top; from Fuglestvedt *et al.*, 1995), global tropospheric OH (middle; from Bekki *et al.*, 1994), and $J(O_3 \rightarrow O^1D)$ rate and global OH (bottom; from updated version of Granier *et al.*, 1996 (C. Granier, NOAA Aeronomy Laboratory, U.S., personal communication, 1997)).

changes in the emissions of CO may affect the levels and lifetime of $CH_4$, or vice versa, through induced changes in the global OH distribution. This section focuses on the impact of stratospheric ozone depletion on the evolution of tropospheric species; the impact of surface emissions changes is discussed in Chapter 8.

As discussed in Chapter 2, surface measurements from global networks have revealed a decline in the growth rate of $CH_4$ during the last decades, from 17-21 parts per billion by volume (ppbv) per year in the early 1980s to 12-14 ppbv/yr at the end of the 1980s. Measurements performed over the last few years indicate a growth rate of about 6 ppbv/yr in 1995-1996. Most of this reduction has been occurring in the Northern Hemisphere. The methane growth rate slowed down even more during the 1991-1993 period and showed a value between zero and 5 ppbv/yr at the end of 1992 (Dlugokencky *et al.*, 1994). Concentrations of CO, after showing a positive trend until the late 1980s, were characterized by a significant decrease from 1990 to 1993. A decrease of 7 ppbv/yr was observed in the Northern Hemisphere and 4 ppbv/yr in the Southern Hemisphere (Novelli *et al.*, 1994).

The 2-D models of Bekki *et al.* (1994) and Fuglestvedt *et al.* (1995) have calculated the change in the global tropospheric OH and $O_3$ distributions as well as the change in the $CH_4$ and CO trends resulting from stratospheric ozone decrease since the early 1980s. The 3-D IMAGES model (Granier *et al.*, 1996) has also been used to calculate changes in the global distributions of OH and $O_3$ over the 1979-1994 period. In these simulations, the total column ozone from Total Ozone Mapping Spectrometer (TOMS) measurements was used as an input for calculations of the photodissociation rates. Starting in June 1979 until the end of 1992, TOMS Nimbus-7 observations were used; an average of Nimbus-7 and Meteor-3 observations was used for the first four months of 1993; and Meteor-3 observations were used for the remainder of 1993 and the first months of 1994. Model studies performed before 1995 used Version 6 of TOMS measurements; the more recent simulations used Version 7 of the data.

Results from the different simulations are shown in Figure 10-1. Bekki *et al.* (1994) calculated an increase

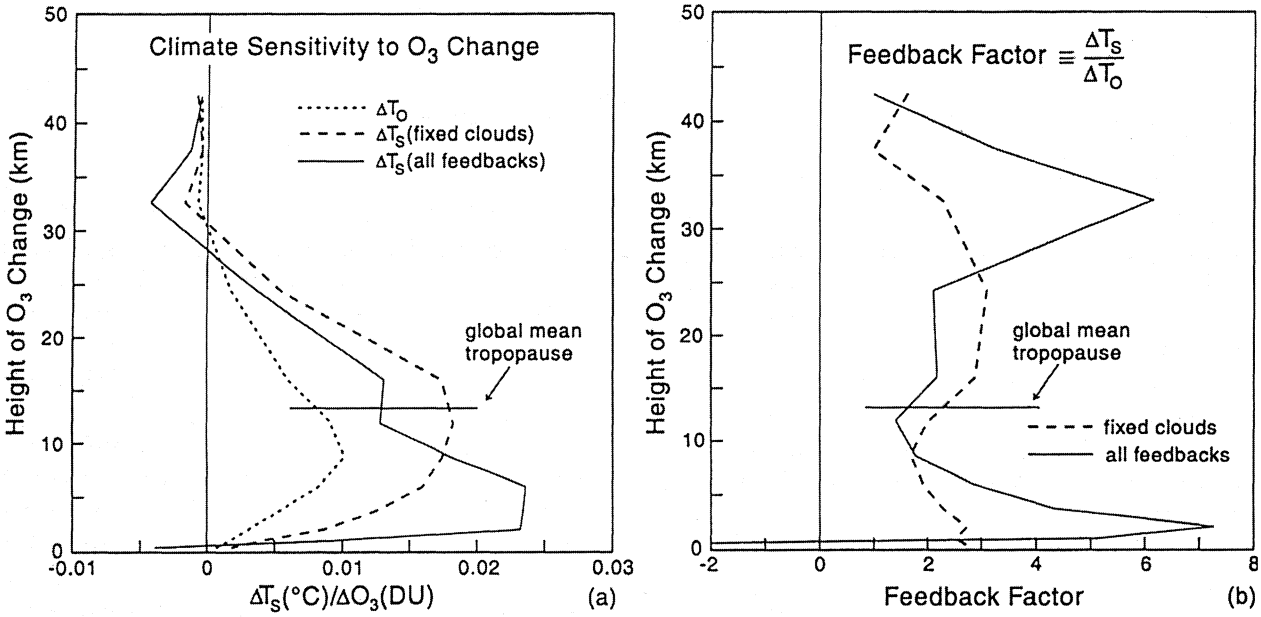


**Figure 10-2.** (a) Surface air temperature sensitivity of the GISS "Wonderland" GCM to a globally uniform change of 100 DU of atmospheric ozone as a function of the altitude at which the ozone is changed. $\Delta T_o$ is the surface temperature response without any climate feedbacks (i.e., clouds, sea ice, water vapor, and tropospheric lapse rate) allowed to operate; $\Delta T_S$ is the surface temperature response including feedbacks (either with or without cloud feedbacks). (b) Feedback factor, $\Delta T_S/\Delta T_o$, as a function of the altitude at which the ozone is changed. (From Hansen *et al.*, 1997a.)

Recent GCM experiments have also indicated that, on a global-mean basis, $\lambda$ is almost independent of forcing mechanism for more complex forcings such as, for example, spatially inhomogeneous sulfate aerosol radiative forcing (Cox *et al.*, 1995) and forcing due to changes in cloud properties (Ramaswamy and Chen, 1997). (There are indications (see below) that the degree to which $\lambda$ is independent of forcing mechanism depends on whether cloud feedbacks are incorporated in the model; whereas the study of Cox *et al.* (1995) incorporated cloud feedbacks, that of Ramaswamy and Chen (1997) did not.) Haywood *et al.* (1997) have also shown, in transient runs of a coupled ocean-atmosphere GCM, that the climate response to sulfate aerosol and greenhouse gas forcing is approximately equal to the sum of the response to each forcing individually; this additivity applied not only to global-mean changes but also to geographical patterns of surface temperature and precipitation changes.

It must be emphasised that expression (10-3) applies strictly to global-mean changes. Cox *et al.* (1995) and Ramaswamy and Chen (1997) have shown that the regional and even hemispheric-scale response to forcings with the same global-mean magnitude can be quite different. This shows, as noted in IPCC (1995), that even if the global-mean value of $\Delta F$ is small, due to a coincidental cancellation of different forcings of opposing signs but different geographical locations, significant sub-global-scale climate changes are still likely.

The most wide-ranging study to date of the relationship between radiative forcing and climate response, and the study of most relevance to the ozone issue, is that of Hansen *et al.* (1997a). They used a simplified version of the Goddard Institute for Space Studies (GISS) GCM that represents the planet as a 120°-longitude sector with nine levels in the vertical. An advantage of this model is that its computational efficiency permitted a larger range of systematic experiments than has hitherto been reported. The generality of the results from this study need to be tested using a range of GCMs, given the known difficulties in modeling cloud processes within GCMs and the relatively crude vertical resolution of this particular model.

Hansen *et al.* (1997a) performed experiments in which ozone was perturbed in each model layer sequentially when the model allowed no feedbacks and when the model included water vapor, sea ice, and tropospheric lapse rate feedbacks, both with cloud feedbacks ("all feedbacks") and without cloud feedbacks ("fixed clouds"). Figure 10-2a shows the surface warming as a function of the height of the ozone perturbation (applied as a constant 100-Dobson unit (DU) perturbation in each layer; the large perturbation was necessary to obtain a clear signal). Figure 10-2b shows the surface temperature response as a function of the height of the ozone perturbation, as a ratio of the "all feedbacks" and "fixed clouds" cases to the no-feedback case; if radiative forcing were an ideal concept, in the sense that $\lambda$ is independent of the nature of the forcing, then the ratios plotted in Figure 10-2b would be independent of height.

The no-feedback case (Figure 10-2a) shows a peak sensitivity in the upper troposphere/lower stratosphere; the fixed-cloud case generally amplifies the response by a factor of 2, with a reasonably similar shape. These results are qualitatively similar to those from 1DRCM studies of, for example, Wang *et al.* (1980) and Lacis *et al.* (1990), but in the GCM the averaging of latitudes with different tropopause heights and ozone profiles, as well as dynamical mixing, cause the effect of the ozone change to be less strongly peaked at the tropopause. Figure 10-2b shows that in the fixed-cloud case, the feedback factor is approximately independent of the height of the ozone perturbation. However, the inclusion of cloud feedbacks causes a dramatic change in the vertical pattern of the response; in particular, changes in lower tropospheric ozone have a much-heightened sensitivity relative to upper tropospheric changes.

Hansen *et al.* (1997a) also examined the forcing-response relationship using vertical and latitudinal profiles of ozone change based on observations (see also Sections 10.3.3, 10.3.4, and 10.3.5). One measure of the dependence of $\lambda$ on the forcing mechanism is the ratio of $\Delta T_s$ for a particular forcing to $\Delta T_s$ for an identical global-mean forcing due to a spectrally uniform change in solar output. With fixed clouds, the ozone forcing caused a 30% greater change in surface temperature than the same global-mean solar forcing, possibly because high-latitude forcings are found to be more effective than low-latitude forcings; with the inclusion of the GISS GCM's cloud feedbacks, however, the ozone forcing causes a 20-30% *smaller* change in surface temperature than the same global-mean solar forcing.

A number of other forcing-response studies have been reported using simpler models. These models lack the detailed interactions between thermodynamic and dynamic processes that are possible in GCMs and so are inherently less suitable for examining the relationship between radiative forcing and climate response; the results must be treated with much more caution. MacKay *et al.* (1997) used a 2-D (latitude-height) model to investigate the climate response to stratospheric ozone loss; their model did not include cloud feedbacks. They found that $\lambda$ for stratospheric ozone changes is about 3 times higher than it is for carbon dioxide. The difference in sensitivity is much larger than that found in the GCM study of Hansen *et al.* (1997a); for the equivalent experiments, the climate sensitivity was about 20% higher for the ozone loss than for the $CO_2$ change.

Bintanja *et al.* (1997) used a zonal-average energy balance climate model coupled to a simple zonal-mean ocean model. They explored forcing-response relationships for a range of idealized ozone perturbations in the absence of cloud feedbacks. They concluded that the strength of the ice-albedo feedback is dependent on the meridional distribution of radiative forcing. The feedback, and hence the overall climate response, was strongest when radiative forcings were largest over polar regions; this result is in at least qualitative agreement with the GCM study of Hansen *et al.* (1997a).

Forster *et al.* (1997) used a 1DRCM to investigate the dependence of the forcing-response relationship on the choice of tropopause height (see also Section 10.4.3). In such models, there is a natural choice of tropopause height, being the altitude at which the temperatures change from being in radiative-convective equilibrium to radiative equilibrium. They computed $\lambda$ using the forcing calculated at this tropopause and at two alternatives, the temperature minimum and the "WMO" tropopause (defined, with elaborations, as the pressure at which the lapse rate falls below 2 K km$^{-1}$). $\lambda$ was much less dependent on the nature of the forcing using the top-of-convection tropopause. This indicates that apparent variations in $\lambda$ in GCM studies may result from an inappropriate choice of tropopause. Unfortunately, in GCMs, as in the real world, it is less easy to define an appropriate tropopause than it is in a 1DRCM.

The overall conclusion of these studies is that radiative forcing remains a useful concept. In the future, if a sufficient consensus develops from similar

experiments with a range of models, it may be possible to develop an "effective" radiative forcing that accounts for the differences in $\lambda$ amongst different forcing mechanisms. This chapter continues to use radiative forcing, because it seems appropriate for comparing different studies of the same forcing mechanism, and there remains sufficient support from GCM studies to justify its continued use.

### 10.3.3 Direct Forcing due to Ozone Change

Ozone changes due to human activity are caused by substances that deplete ozone in the stratosphere and by precursors that generate ozone in the troposphere. In addition, to some extent, changes in ozone in the stratosphere can have an impact on ozone in the troposphere, and to a lesser extent vice versa, through stratosphere-troposphere exchange processes (see Chapters 7 and 8). As discussed in WMO (1995) and IPCC (1996), the radiative forcing due to ozone has a longwave as well as a shortwave component and there is a critical dependence on the vertical distribution of ozone changes.

The sensitivity of radiative forcing to the altitude of an ozone change has been discussed in relation to climate sensitivity (Section 10.3.2). Forster and Shine (1997) have used radiative transfer models and observed climatologies of temperatures and clouds to study the relative impact of ozone changes in separate altitude regions. They found, in agreement with the earlier work of Wang *et al.* (1980) and Lacis *et al.* (1990), that the region of largest influence is the tropopause region; but they also pointed to the fact that when relative rather than absolute changes in ozone are considered, the importance of ozone changes in the middle and upper troposphere, as well as the middle stratosphere, is strengthened relative to those near the tropopause. As discussed in Section 10.3.2, Hansen *et al.* (1997a) used a GCM, including all feedbacks (e.g., water vapor, clouds, and surface albedo). They found that, in their model at least, the impact of ozone changes in the mid-to-lower troposphere was much enhanced; they showed that this was mostly due to the impact of the ozone change on cloudiness.

In the stratosphere the temperatures will adjust to a new radiative balance when the ozone distribution is changed. This in turn alters the downwelling of longwave radiation through the tropopause, influencing the radiative forcing there. Radiative forcing taking this effect into account is called *adjusted* forcing, whereas the radiative forcing calculated neglecting the temperature change in the stratosphere is called the *instantaneous* forcing. When temperature changes are taken into account, they are usually calculated assuming that only the radiative balance is changed, and not the dynamical transport of heat in the stratosphere; this is called the fixed dynamical heating approximation. Thorough assessments of the impact of this approximation on the forcing are not yet available. Whereas the earlier work was a mixture of instantaneous and adjusted forcing, the newer work assessed here reports forcing including the temperature adjustment. In Sections 10.3.3.1 and 10.3.3.2, the "direct" radiative forcing (i.e., the forcing due to change in ozone alone) is reported. As discussed in Section 10.2, because ozone photolysis is a primary mechanism controlling the abundance of OH, and because ozone also controls the penetration of ultraviolet radiation, changes in ozone can also alter the concentrations of other radiatively active constituents; the "indirect" forcing due to such changes will be discussed in Section 10.3.4.

#### 10.3.3.1 Stratospheric Ozone

Stratospheric ozone influences the radiative balance by absorption and emission in the longwave as well as absorption in the shortwave region; the two wavelength regions have a different relative importance at different altitudes. A few studies were discussed in WMO (1995) and IPCC (1996): Ramaswamy *et al.* (1992), Hansen *et al.* (1993), Hauglustaine *et al.* (1994), and Molnar *et al.* (1994) all pointed to the strong dependence of the radiative forcing on the vertical distribution of ozone changes. The results were based on observed as well as modeled ozone changes. It was concluded that the radiative forcing due to human-made emissions of ozone-depleting substances was about -0.1 $Wm^{-2}$ with a factor of 2 uncertainty range.

Several new estimates have been made recently and are listed in Table 10-4. Some studies have adopted observed ozone changes, mostly satellite data, and typically report radiative forcing due to ozone changes during the last one or two decades. In Table 10-4 numbers are also given for the forcing per decade, under the assumption that the ozone trend has been linear. This is most likely not the case but is included to allow an easier comparison of the different studies.

Forster and Shine (1997) used an observed climatology of stratospheric temperatures and clouds.

**Table 10-4. Radiative forcing due to stratospheric ozone changes.** The radiative forcing per decade is also shown to facilitate comparison between calculations based on different time periods; this forcing is derived assuming the trend to be linear in time, which is unlikely to be the case.

| Reference | Radiative forcing ($Wm^{-2}$) | Forcing per decade ($Wm^{-2}$)/decade | Time period |
|---|---|---|---|
| Ramaswamy *et al.* (1992) | -0.08 | -0.07 | 1979-1990 |
| Hansen *et al.* (1993) | -0.2 | -0.1 | 1970-1990 |
| Hauglustaine *et al.* (1994) | +0.06 | +0.03 | 1970-1990 |
| Zhong *et al.* (1996) | -0.025 | -0.02 | 1979-1991 |
| Forster and Shine (1997) SAGE | -0.17 | -0.10 | 1979-1996 |
| Forster and Shine (1997) SBUV | -0.22 | -0.13 | 1979-1996 |
| Hansen *et al.* (1997a) SAGE/TOMS | -0.20 | -0.13 | 1979-1994 |
| Hansen *et al.* (1997a) SAGE/SBUV | -0.28 | -0.19 | 1979-1994 |
| Hansen *et al.* (1997b) | -0.3 | -0.2 | 1979-1994 |
| MacKay *et al.* (1997) | -0.06 | -0.05 | 1979-1990 |
| Shine *et al.* (1998) | -0.10 | -0.08 | 1979-1991 |
| Myhre *et al.* (1998a) | +0.05 | +0.02 | 1969-1996 |

They calculated radiative forcing to be -0.17 and -0.22 $Wm^{-2}$ based on ozone trends from the Stratospheric Aerosol and Gas Experiment (SAGE) and Solar Backscatter Ultraviolet (SBUV) spectrometer, respectively. In the SBUV case only the column data were used, and it was assumed that the ozone loss was limited to a 7-km region above the tropopause. The trends were extrapolated forward to 1996 on the assumption that trends would remain linear. As reported in Chapter 4, this assumption no longer looks justifiable, at least in midlatitudes. The combined effect of the reduced midlatitude trends and the enhanced loss in the Arctic on the radiative forcing has not yet been assessed.

Zhong *et al.* (1996) used observed total ozone change between 1979 and 1991 from TOMS. Like Ramaswamy *et al.* (1992), they distributed the ozone loss in a 7-km region above the tropopause. In contrast to calculating a temperature adjustment, they adopted satellite-observed temperature changes from the Microwave Sounding Unit (MSU). The resulting radiative forcing was -0.024 $Wm^{-2}$. Shine *et al.* (1998) used the same approach but used temperature changes based on radiosonde data. Unlike Zhong *et al.* (1996), they also included the 14-μm band. The resulting radiative forcing was -0.10 $Wm^{-2}$. The results of the two calculations must be seen in the perspective that the MSU data have a global coverage but only a limited vertical resolution, whereas the radiosonde temperatures have a better vertical resolution but only a sparse geographical coverage. It is further very important to note that the observed temperature changes can also have causes other than changes in ozone (see Chapter 5).

As discussed in Section 10.3.2, Hansen *et al.* (1997a) and Hansen *et al.* (1997b) used a GCM with a low vertical resolution to study climate effects of ozone changes. Changes in ozone concentration were taken from satellite observations. Their work, which is a pioneering GCM study using realistic ozone changes, also takes into account temperature changes and has the advantage that the temperature changes are dynamically consistent with the ozone changes. The resulting radiative forcing due to stratospheric ozone was -0.20 and -0.28 $Wm^{-2}$ for SAGE/TOMS and SAGE/SBUV, respectively. These results include a change in tropospheric ozone, which cannot easily be separated from the stratospheric component.

MacKay *et al.* (1997) calculated radiative forcing due to stratospheric ozone in a 2-D radiative-dynamical climate model, using observed satellite ozone changes. They calculated temperature changes in their model consistent with this ozone change and arrived at a radiative forcing of -0.06 $Wm^{-2}$. Their temperatures are

up to 20-30 K too low in certain regions of the lower stratosphere, a fact that may influence their results significantly.

As shown above, several calculations of the radiative forcing due to stratospheric ozone are based on satellite observations. It is worth noting that these results are uncertain (see discussion in Chapter 4 and in WMO (1995)), especially in the near-tropopause region, which is the most important region for the radiative forcing. Myhre *et al.* (1998a) on the other hand used ozone changes calculated in a 2-D chemical transport model (CTM). Their ozone loss was much weaker than in SAGE/SBUV in the lower stratosphere, consistent with ozone changes calculated in other CTMs, which are known to underestimate ozone loss there (see Chapter 7). The resulting change in radiative forcing was slightly positive, namely, +0.05 $Wm^{-2}$. A stronger ozone loss in the lower stratosphere would lead to a more negative radiative forcing.

On the basis of these newer studies, one can conclude that the radiative forcing due to changes in stratospheric ozone is still uncertain, due to large uncertainties in the vertical distribution of the ozone reductions as well as in temperature changes. Also the impact of recent changes in ozone trends (Chapter 4) has not been assessed. Our best estimate for the radiative forcing since the late 1970s is -0.2 $Wm^{-2}$ with an uncertainty range of ±0.15 $Wm^{-2}$; this uncertainty range is intended to approximately bracket the majority of published studies and is not a formal indication of uncertainty. In comparison, the best estimate of WMO (1995) and IPCC (1996) was -0.1 $Wm^{-2}$ with a factor of 2 uncertainty. These forcings will be placed in the perspective of other radiative forcings in Section 10.5. It is worth noticing that the future changes in forcing due to stratospheric ozone will depend on the timing and the rate of the recovery of stratospheric ozone (see Chapter 12). If it is assumed that stratospheric ozone loss is near its maximum, the radiative forcing due to stratospheric ozone will not grow much more negative before it starts to get less negative. Thus there will be a decrease in the extent to which stratospheric ozone changes offset the forcing due to the increases in other greenhouse gases (see, e.g., Solomon and Daniel, 1996).

### 10.3.3.2 Tropospheric Ozone

WMO (1995) and IPCC (1996) reported a large uncertainty in the forcing due to anthropogenically related increases in tropospheric ozone that originate from emissions of ozone precursors: $NO_x$, CO, $CH_4$, and nonmethane hydrocarbons. Again the uncertainty is connected to uncertainties in the changes in the ozone distribution; these changes are even less well documented than those of stratospheric ozone, for which at least changes in the total column can be inferred from ground-based and satellite observations. Chapter 8 reviews our understanding of tropospheric ozone and its changes, and associated observations. The calculations of radiative forcing presented here are mostly based on the use of chemical transport models; the ozone fields from these models are difficult to evaluate, particularly for the preindustrial period, because of the scarcity of appropriate observations.

Earlier work assessed in WMO (1995) was based on observations (Fishman, 1991; Marenco *et al.*, 1994) as well as model calculations (e.g., Hauglustaine *et al.*, 1994) of ozone change. Several recent studies, which are considered here, are based mostly on modeled ozone distributions (Table 10-5). When the numbers in Table 10-5 are compared, it should be kept in mind that they are based on a variety of assumptions. For example, not all results include temperature adjustment in the stratosphere and effects of clouds. Neglect of either of these effects has been estimated to lead to an overestimate of radiative forcing by approximately 10-25% (Berntsen *et al.*, 1997). This is because (i) clouds reduce the outgoing longwave radiation and hence also reduce the sensitivity to changes in greenhouse gas concentration and (ii) increases of tropospheric ozone reduce the absorption of radiation by ozone in the lower stratosphere, leading to a stratospheric cooling and reduced emission into the troposphere.

The work of Hansen *et al.* (1997b), already discussed for its stratospheric contribution, is based on GCM runs, but ozone distributions were taken from the model of the general universal tracer transport in the atmosphere (MOGUNTIA) 3-D CTM (Crutzen, 1994). The radiative forcing due to increases in tropospheric ozone since preindustrial time was estimated to be 0.3 $Wm^{-2}$. The MOGUNTIA model was also used by van Dorland *et al.* (1997), who calculated the radiative forcing to be 0.38 $Wm^{-2}$.

Chalita *et al.* (1996) used a similar approach to that of Hansen *et al.* (1997b), using ozone distributions from a 3-D CTM (IMAGES) to study climate impacts in a GCM. They reported a radiative forcing of 0.28 $Wm^{-2}$ due to an increase in tropospheric ozone. Temperature

**Table 10-5. Radiative forcing due to tropospheric ozone changes, all since preindustrial times.**

| Reference | Radiative forcing ($Wm^{-2}$) |
|---|---|
| Marenco *et al.* (1994) | 0.62 |
| Hauglustaine *et al.* (1994) | 0.55 |
| Lelieveld and van Dorland (1995) | 0.50 |
| Chalita *et al.* (1996) | 0.28 |
| Forster *et al.* (1996) Cambridge | 0.51 |
| Forster *et al.* (1996) UKMO | 0.30 |
| Hansen *et al.* (1997b) | 0.3 |
| Berntsen *et al.* (1997) Reading | 0.28 |
| Berntsen *et al.* (1997) OsloRad | 0.31 |
| Roelofs *et al.* (1997) | 0.42 |
| van Dorland *et al.* (1997) | 0.38 |

adjustment in the stratosphere was not taken into account. Berntsen *et al.* (1997) based their work on the Oslo 3-D CTM1 model. Two radiative forcing calculations, with two different radiative transfer models and with two different background levels for ozone, were performed. The resulting radiative forcing was estimated to be 0.28 and 0.31 $Wm^{-2}$ for the two radiation models. Roelofs *et al.* (1997) used ozone changes predicted using the European Centre Hamburg Model version 4 (ECHAM4) coupled to a tropospheric chemistry model to compute radiative forcing. They derived a value of 0.42 $Wm^{-2}$.

Forster *et al.* (1996) used two different 2-D CTM models to calculate the ozone increase since preindustrial time, namely, the Cambridge and the United Kingdom Meteorological Office (UKMO) models. The calculated radiative forcing was 0.51 and 0.30 $Wm^{-2}$, respectively, in the two cases.

Portmann *et al.* (1997) estimated tropical tropospheric ozone from ozonesonde profiles and ozone columns derived from satellite maps. They calculated the radiative forcing to give a global contribution of 0.1-0.4 $Wm^{-2}$ for changes in ozone since preindustrial time due to biomass burning. Clouds were not taken into account in their calculations. The largest forcing (0.4 $Wm^{-2}$) was calculated under the assumption that the preindustrial ozone concentration was 10 ppbv everywhere.

For radiative forcing due to tropospheric ozone changes, the uncertainties are slightly reduced since WMO (1995) and IPCC (1996). Large uncertainties remain, due to insufficient knowledge about the ozone distributions in the unperturbed as well as the present atmosphere. The ozone distribution is particularly uncertain in the tropics. Our best estimate of global-mean radiative forcing since the mid-1800s is 0.35 $Wm^{-2}$ with an uncertainty range ±0.15 $Wm^{-2}$. The uncertainty range is intended to approximately bracket results from a majority of studies and is not a formal indication of uncertainty. These forcings will be compared with other sources of radiative forcing in Section 10.5.

The total radiative forcing due to ozone changes in the troposphere and the stratosphere was estimated in IPCC (1996) to be 0.3 $Wm^{-2}$ (+0.4 $Wm^{-2}$ due to changes in tropospheric ozone and -0.1 $Wm^{-2}$ due to changes in stratospheric ozone). The new estimate is substantially smaller, with about 0.15 $Wm^{-2}$ as the best-estimate radiative forcing since preindustrial times (+0.35 $Wm^{-2}$ due to changes in tropospheric ozone and -0.20 $Wm^{-2}$ due to changes in stratospheric ozone).

### 10.3.4 Indirect Forcing due to Effects of Ozone Change on Other Constituents

Bekki *et al.* (1994) have calculated the radiative forcing associated with the reduction in the methane growth rate and also the forcing associated with increased tropospheric ozone concentrations resulting from stratospheric ozone changes observed from 1979 to 1994. Their results have shown an additional negative forcing for this period of -0.03 to -0.04 $Wm^{-2}$ (-0.02 $Wm^{-2}$ from the $CH_4$ change and -0.01 to -0.02 $Wm^{-2}$ due to tropospheric ozone changes).

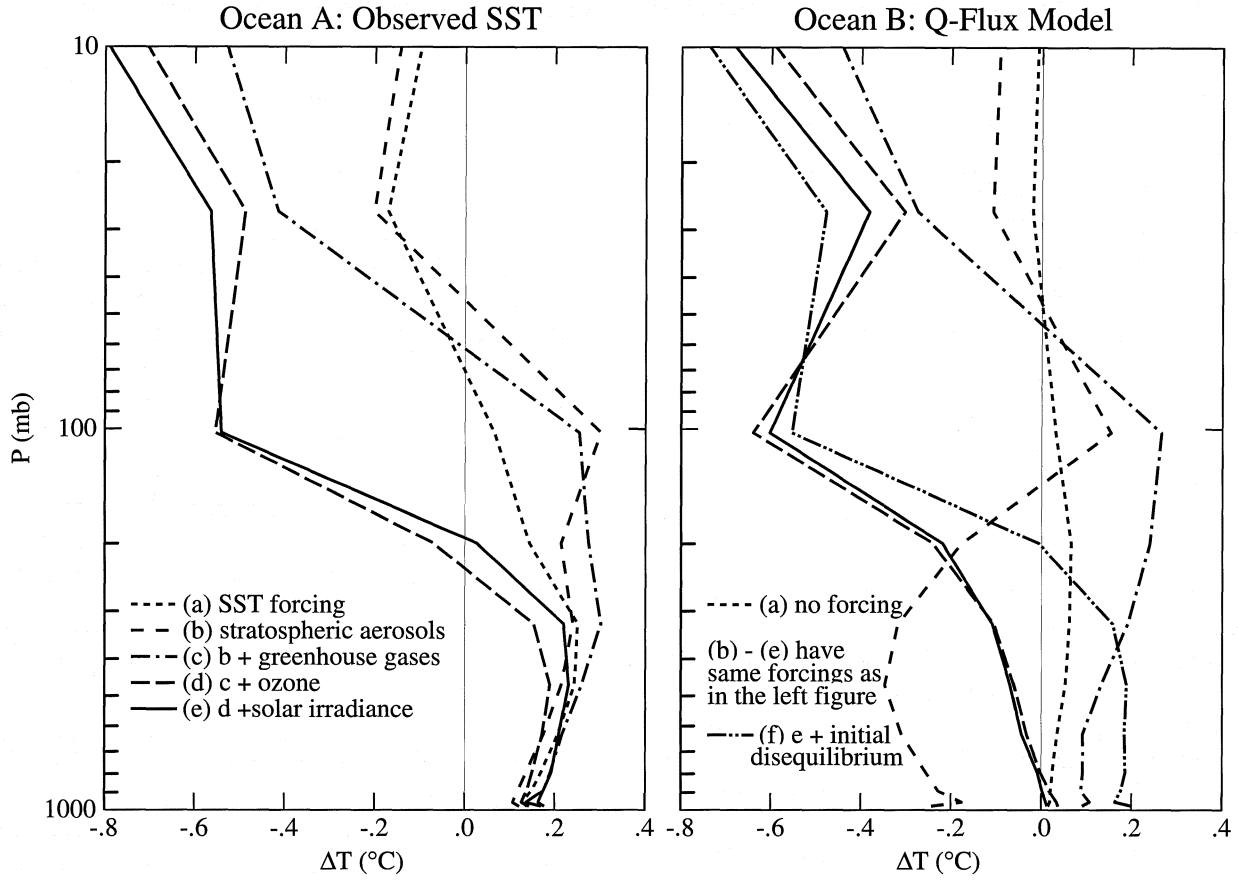


**Figure 10-3.** Change of the global-mean annual-mean temperature profile between 1979 and 1995 based on linear trends, calculated using the GISS GCM, as different climate forcing mechanisms are added one by one to the model. The figure on the left shows calculations using observed sea surface temperatures (SSTs). The figure on the right shows the calculation using a type of "mixed-layer" ocean model with prescribed horizontal transports of heat; on this figure the run labeled "initial disequilibrium" accounts for the fact that the climate was unlikely to be in global mean radiative balance at the top of the atmosphere at the beginning of the simulation in 1979, because of increases in greenhouse gas concentrations, and other radiative forcing mechanisms, prior to 1979. The results shown are an average of ensembles containing between five and ten members. (Figure adapted from Hansen *et al.*, 1997c.)

Another impact of stratospheric ozone depletion on climate forcing has been proposed by Toumi *et al.* (1994, 1995). OH oxidizes sulfur dioxide ($SO_2$) to gaseous sulfuric acid ($H_2SO_4$), which is a source of new $H_2SO_4$ particles via homogeneous nucleation; changes in the production of $H_2SO_4$ resulting from OH changes might affect not only the number of $H_2SO_4/H_2O$ particles but also the number of those particles that can act as condensation nuclei. Model results suggest that OH increases resulting from ozone depletion should have increased the mean gaseous sulfuric acid production by about 2% from 1980 to 1990. This, in turn, may have increased cloud condensation nuclei (CCN) and cloud droplet numbers. Estimations of the radiative forcing related to this process give a negative radiative forcing (via increased cloud reflectivity) that might be of a magnitude similar to the direct effect of ozone loss. However, Rodhe and Crutzen (1995) disputed whether this mechanism was of importance. No further studies on this topic have been reported, to our knowledge, since the last Assessment.

### 10.3.5 Climate Model Studies

The climate model studies discussed in Section 10.3.2 indicate that the forcings associated with ozone change cause a significant climatic effect (see also Section 10.5). However, in terms of detecting the influence of ozone change on climate, these studies are not sufficient to explore whether the history of forcing is consistent with the magnitude of observed changes (although they can be used to look for similarities between the modeled and observed patterns of climate change (see, e.g., Santer *et al.*, 1996)).

A more realistic approach is to model the transient response of the climate system to the time-evolving forcing, and to investigate the size of the ozone effect in the context of the effect of other forcing mechanisms (both natural and due to human activity) and unforced variability. Because of the inherently chaotic nature of climate variation, the robustness of any signal can be assessed by running the model several times with slightly different initial conditions. The number of members of such ensembles is generally limited by the available computer time.

WMO (1995) reported the results from the first transient GCM experiments to investigate the climatic impact of ozone loss. Since then Tett *et al.* (1996) and Hansen *et al.* (1997c) have reported further transient studies incorporating the effects of stratospheric ozone change. We are not aware of any studies that have examined, individually, the impact of tropospheric ozone changes. Tett *et al.* (1996) used a coupled ocean-atmosphere GCM and incorporated the effects of changes in well-mixed greenhouse gases, a representation of the direct effect of sulfate aerosols, and stratospheric ozone loss for the period 1961 to 1995. Ensemble experiments, with four members, were performed with a variety of combinations of forcings, and significance was assessed using a 700-year control run of the model in which forcing was kept constant.

Hansen *et al.* (1997c) used an atmospheric GCM with a variety of representations of the ocean, ranging from fixed (observed) sea surface temperatures to a sophisticated oceanic GCM. For the period 1979 to 1996, they incorporated the forcings due to well-mixed greenhouse gases, stratospheric ozone, volcanic aerosols, and solar irradiance; the forcings were added one by one, and ensembles included between five and ten members. Control integrations, with no imposed forcing, were also performed.

In both studies, the observed cooling of the lower stratosphere, derived from radiosonde analyses, was shown to be consistent with the model when ozone loss was included; this supports earlier evidence that the stratospheric cooling is due to human activity (see Chapter 5). Another important feature of these simulations is that the transition from tropospheric warming to stratospheric cooling (which is a feature of experiments in which changes of carbon dioxide concentration are the only forcing mechanism) occurs at a significantly lower altitude when the ozone loss is incorporated. The vertical profiles of the 1979-1995 temperature trend are shown in Figure 10-3 as different forcings are added to the Hansen *et al.* (1997c) model. Results are shown for both observed sea surface temperatures and a mixed-layer ocean. The effects of ozone changes on both the transition height and on lower-stratospheric temperatures are clearly seen. When model-simulated changes in sea surface temperature are included, the transition height is even lower. The height of the transition is in much better agreement with radiosonde analyses than calculations that just include the effects of increasing well-mixed greenhouse gas concentrations.

The effect of the ozone changes on surface temperature is less clear. Both Tett *et al.* (1996) and Hansen *et al.* (1997c) (see Figure 10-3 results for Ocean B) show that the ozone loss leads to a surface cooling, as expected from the radiative forcing. In the global mean, the cooling is about 0.1°C over a 15- to 20-year period; this can be compared to a warming, due to greenhouse gas increases, of about 0.2 to 0.3°C over the same period. However, unlike the ozone effects in the upper troposphere and lower stratosphere, this change is not significant compared to natural variability and does not lead to a significant improvement in the agreement between model and observations.

Bintanja *et al.* (1997) have used their energy balance climate model to compute the transient response to ozone perturbations. Because energy balance models do not simulate unforced variability in the climate system, the impact of forcings is easily diagnosed. They used somewhat idealized ozone changes based on recent observations and calculated the transient response over a 20-year period. Changes in lower stratospheric ozone led to a surface cooling of about 0.05°C; this cooling is reduced by a factor of 2 when increases in tropospheric ozone are included. Hence, there is a significantly smaller offset of the greenhouse-gas-induced warming

in this energy balance model study than in the GCM studies. The reasons for this are not obvious; they could relate to either the form of the imposed ozone depletions or the simple type of model used.

## 10.4 RADIATIVE FORCINGS AND GLOBAL WARMING POTENTIALS OF HALOCARBONS

### 10.4.1 Introduction

This section updates work reported in WMO (1995) and IPCC (1996) on the radiative forcing and Global Warming Potentials due to the CFCs, their replacements, or proposed replacements, and related molecules. Such information is important in assessing the desirability of using particular replacements. This area is of renewed importance following the 1997 Kyoto Protocol to the United Nations (UN) Framework Convention on Climate Change; if the Protocol is ratified, reductions of greenhouse gas emissions will be calculated using a "carbon dioxide equivalence," with the (100-year) Global Warming Potentials (GWPs) forming the basis for calculating this equivalence.

### 10.4.2 Recent Studies on the Spectroscopy of CFCs and their Substitutes

The accurate calculation of the radiative forcing of the CFCs and related species is reliant on good-quality data on the absorption cross sections at thermal infrared wavelengths. WMO (1995) briefly reviewed earlier data. For some gases, a spread exceeding 25% of the mean cross sections was found and there was little agreement on the sign, or indeed even the existence, of any temperature dependence.

Since WMO (1995) there have been a number of studies reporting new absorption cross sections. Imasu *et al.* (1995), Heathfield *et al.* (1998a, 1998c), and Cavalli *et al.* (1998) reported measurements for a number of halogenated ethers; Barry *et al.* (1997) measured the cross sections of $CF_3CH_2CF_2CH_3$ (HFC-365mfc); Gierczak *et al.* (1996) measured the cross sections of $CF_3CH_2CF_3$ (HFC-236fa) and $CF_3CHFCHF_2$ (HFC-236ea); Christidis *et al.* (1997) reported measurements for a number of HFCs, HCFCs, bromocarbons, iodocarbons, and some ethers. Newnham and Ballard (1995), Newnham *et al.* (1996), and Smith *et al.* (1996) measured $CH_2FCF_3$ (HFC-134a), $CH_3CClF_2$ (HCFC-142b), and $CH_2F_2$ (HFC-32), respectively, at high spectral resolution. Wallington *et al.* (1997) and Christensen *et al.* (1998) measured $C_4F_9OCH_3$ (HFE-7100) and $C_4F_9OC_2H_5$ (HFE-7200), respectively. Molina *et al.* (1995) measured nitrogen trifluoride ($NF_3$). Grossman *et al.* (1997), Pappasavva *et al.* (1997), and Good *et al.* (1998) reported cross sections derived from quantum mechanical modeling and showed that these can provide a reasonable alternative to direct measurements.

The integrated band-strengths for some molecules show significant spreads. In addition to the cases highlighted in WMO (1995), recent measurements of $CHClF_2$ (HCFC-22) at, or near, room temperature range (in units of $10^{-17}$ $cm^{-1}$ (molec $cm^{-2})^{-1}$) from 0.9 in McDaniel *et al.* (1991) to 0.97 in Anastasi *et al.* (1994) to 1.01 in Varanasi *et al.* (1994) and Pinnock *et al.* (1995) to 1.03 in Capellani and Restelli (1992) and Clerbaux *et al.* (1993). This gives a spread of about ±7% around the midpoint. Christidis *et al.* (1997) compiled a list of reported $CCl_3F$ (CFC-11) cross sections; correcting for the different spectral ranges used by different investigators, they found a standard deviation of about 6% for the strongest bands.

For gases for which measurements have only recently been reported, the degree of agreement between different studies is very variable. For example, the integrated cross sections of three fluorinated ethers listed by both Imasu *et al.* (1995) and Heathfield *et al.* (1998a) agree to within 3%. Heathfield *et al.*'s value for $CHF_2OCF_3$ (HFE-125) is 12% higher than that given by Christidis *et al.* (1997). Cavalli *et al.*'s (1998) value for $C_4F_9OCH_3$ is about 20% higher than that reported by Wallington *et al.* (1997). For HFC-32, Smith *et al.* (1996) found a surprisingly large pressure dependence (with the integrated cross section 10% lower for air-broadening at 1000 mb than for pure vapor); for similar conditions, their integrated cross section is 20% lower than that of Pinnock *et al.* (1995) (although Pinnock *et al.*'s value is now believed to be 8% too high (M.D. Hurley, Ford Motor Company, U.S., personal communication, 1998)).

There are a number of possible reasons for the spread in values. For some species, absorption on the cell walls can occur for certain types of cells; for example R.J. Knight and J. Ballard (Rutherford Appleton Laboratory, U.K., personal communication, 1998) report initial adsorption of pure HCFC-22 onto the walls of a stainless steel cell, which reduced gas concentrations by 5-10% in 30 minutes (see also Newnham and Ballard (1995) for a discussion concerning HCFC-142b). Other

problems can occur in using gas-air mixes if it is not ensured that the mixture is sufficiently homogeneous. If uncorrected, such problems could generate errors in the integrated cross section on the order of 10%.

In conclusion, for most (but not all) gases, currently available cross sections can probably be considered to be accurate to within about 10%, but no better than 5%. To improve confidence in the measurements, the causes of the differences amongst different measurement techniques would need to be identified and, if possible, corrected.

The radiative forcing due to the CFCs and their related molecules depends also on knowledge of the spectroscopy of overlapping species such as water vapor, carbon dioxide, and ozone. A new version of the high-resolution transmission (HITRAN) molecular absorption database (Rothman *et al.*, 1992) has been released. The new version, HITRAN 1996, updates the previous version, HITRAN 1992. HITRAN includes the positions, strengths, and half-widths of the major greenhouse gases throughout the infrared spectrum. Since 1986 the number of catalogued lines in the 0-3000 $cm^{-1}$ region has increased from about 260,000 to 870,000, but most of these are weak lines. Pinnock and Shine (1998) examined the effect of updates in the HITRAN database on calculations of radiative forcing for $CO_2$, $CH_4$, $O_3$, and nitrous oxide ($N_2O$). The effects of changes since HITRAN 1986 are less than 3%, and less than 1% since HITRAN 1992. Remaining spectroscopic uncertainties were estimated to cause errors of no more than 5% in the radiative forcing. Hence, errors from this source are likely to be smaller than current uncertainties in the absorption cross sections of the halocarbons.

### 10.4.3 Recent Radiative Forcing Studies

Many previous studies of the radiative forcing (which is defined in Section 10.3.2) due to CFCs and related molecules have been based on calculations with a single, normally global-mean, profile. Since the temperature, cloudiness, humidity, and ozone vary spatially, it is important to test how close the global mean of the radiative forcing is to the radiative forcing calculated with a global-mean profile.

Myhre and Stordal (1997) have considered in detail the sensitivity of the radiative forcing to both spatial and temporal averaging. For a range of well-mixed greenhouse gases, the error in the global-mean forcing was found to be about 1% or less if annual-mean rather than monthly-mean profiles were used. Similarly, the error using the daily-mean rather than the monthly-mean, or using diurnally varying rather than diurnal-mean profiles, was found to be less than 1%.

The errors due to spatial averaging were found to be more significant. Use of a single global-mean profile gave errors, for several CFCs, of around 5%. Myhre and Stordal (1997) showed that it is the latitudinal variation that must be represented to reduce this error; use of annual- and zonal-mean profiles at 10° resolution leads to an error of less than 0.5% compared to calculations at 2.5° × 2.5° resolution using monthly means. Freckleton *et al.* (1998) have shown that the error from using a global-mean profile can, for some well-mixed gases, be reduced by using just three profiles. Both Myhre and Stordal (1997) and Freckleton *et al.* (1998) have shown that alternative definitions of the position of the tropopause lead to differences in the radiative forcing of several percent.

Freckleton *et al.* (1998) examined the impact of inhomogeneities in the HFC and HCFC distributions. Distributions of five molecules, with lifetimes ranging from 2 to 26 years, were taken from a 2-D model (Wild *et al.*, 1996) assuming an idealized source distribution, predominantly in the Northern Hemisphere. The error in the global-mean forcing from assuming the gas to be well mixed at the global-mean surface concentration ranged from about 5% for gases with lifetimes exceeding 15 years, to almost 30% for gases with a two-year lifetime. Most of the error was due to vertical, rather than horizontal, inhomogeneity. The latitudinal distribution of the forcing was shown to also be affected by the averaging. The local forcing could be in error by a factor of 2 when short-lived gases were assumed to be well mixed; the sign of the error depends on the location relative to the emission sources.

IPCC (1996) reported a significant discrepancy between the radiative forcing for CFC-11 calculated using the IPCC (1990) formula (from Hansen *et al.*, 1988) and a more recent calculation (Pinnock *et al.*, 1995). Since then several other studies have investigated the CFC-11 forcing, and all conclude that the IPCC (1990) value of 0.22 $Wm^{-2}ppbv^{-1}$ is too low. Hansen *et al.* (1997a) use a GCM with an updated absorption cross section for CFC-11 (based on Christidis *et al.*, 1997) to derive their best estimate of 0.25 $Wm^{-2}ppbv^{-1}$; Myhre and Stordal (1997) also derive a value of 0.25 $Wm^{-2}ppbv^{-1}$ using their highest horizontal resolution and using a vertical profile from a chemical model. Christidis *et al.*

(1997), using their "best-guess" absorption cross section, a global-mean atmosphere, and Hansen *et al.*'s revised vertical profile, obtain 0.285 $Wm^{-2}ppbv^{-1}$. Good *et al.* (1998) obtain an instantaneous forcing of 0.25 $Wm^{-2}ppbv^{-1}$ using a global-mean atmosphere and vertical profiles from a chemical model.

On the basis of these calculations, we propose a revised value for CFC-11 of 0.25 $Wm^{-2}ppbv^{-1}$, but there remains some discrepancy amongst calculations that has not been fully resolved; sources of the discrepancy include the use of different cross sections, vertical profiles, averaging assumptions, and details of the radiation calculations.

Previous WMO and IPCC reports have reported the forcings due to CFC replacements relative to CFC-11. This procedure has clear difficulties when the CFC-11 forcing is revised, because it is unclear whether the absolute forcings for the other gases should use the original or revised CFC-11 forcing. Because of this, we present the absolute radiative forcings (in $Wm^{-2}ppbv^{-1}$), which are shown in Table 10-6. There is a need for a scaling of the literature values on the basis of whether clouds are included, whether stratospheric adjustment is performed, what atmosphere is used, and what vertical profile for the gas is assumed. The bases for these rescalings are given in the footnotes to the table, but given available information, these can only be regarded as approximate and are not always possible. It is believed that cloudy-sky, adjusted forcings are the most appropriate (see, e.g., IPCC, 1995; Hansen *et al.*, 1997a).

The number of gases for which radiative forcings are now reported has grown about threefold since previous assessments. Not all the gases in this table are likely to be used, because some will be excluded for toxicological or industrial reasons, and others are likely to be used in only small amounts in specialized applications. For completeness, however, all published values known to us are presented. Given the problems in accurate measurements of absorption cross sections and differences in methods in calculating the radiative forcing, these forcings can, at best, be regarded as accurate to 10%, and, for many, probably to no better than 20%.

Section 10.5 will present estimates of the present and possible future contributions of the replacement halocarbons to the radiative forcing.

## 10.4.4 Global Warming Potentials

Global Warming Potentials (GWPs) have been used in past ozone and climate assessments (WMO, 1995; IPCC, 1990, 1995, 1996) as a means of quantifying the potential integrated climate forcing of various greenhouse gases relative to carbon dioxide. GWPs have been used to motivate the choice of replacements for the CFCs and, as mentioned in Section 10.4.1, play a role in the Kyoto Protocol. In this section, after providing a brief summary of the GWP definition, we discuss and provide current estimates of both direct and indirect GWPs for numerous greenhouse gases. More details concerning the limitations of GWPs can be found in IPCC (1995, 1996).

### 10.4.4.1 Definitions

Knowledge of the radiative forcing of a gas (see Sections 10.3.2 and 10.4.3) is necessary in estimating the potential climate impact due to the release of some amount of that gas. However, radiative forcing does not differentiate between a gas that resides in the atmosphere for centuries and one that is destroyed in days.

#### *AGWPs*

An index that accounts for the importance of the residence time of a gas is the Absolute Global Warming Potential (AGWP) (see, e.g., IPCC, 1995). The AGWP of a species represents the integrated radiative forcing due to an instantaneous pulse of that gas over some time horizon. Mathematically, the AGWP is defined by

$$AGWP_x(t') = \int_0^{t'} F_x \exp(-t/\tau_x)dt \qquad (10\text{-}4)$$

where $F_x$ is the radiative forcing per unit mass of species $x$, $\tau_x$ is the atmospheric residence time constant of species $x$, and $t'$ is the time horizon of the particular AGWP calculation. Generally, $F_x$ is defined as the radiative forcing per kilogram of the gas added to the atmosphere, leading equation (10-4) to represent the total integrated forcing due to the addition of 1 kilogram of species $x$ at time 0 integrated to time $t'$. For most greenhouse gases, equation (10-4) is a simple expression with a constant radiative forcing per mass and a constant response time constant. In some cases, however, $F_x$ will depend on the background concentration of species $x$ or on the concentration of other gases that might absorb in similar spectral regions. In a few instances, the residence time,

$\tau_x$, can also depend on the atmospheric composition, while in even more complicated cases, the decay of an instantaneous pulse of certain gases (notably $CO_2$) cannot be represented by a single decay time constant even in an unchanging atmospheric composition scenario.

***GWPs***

A disadvantage of the AGWP quantity is that it is generally expressed in units of $Wm^{-2}kg^{-1}yr$ or $Wm^{-2}ppmv^{-1}yr$, which is often not the most intuitive way to convey the magnitude of a species' integrated forcing. A more typically used quantity involves the comparison of the integrated forcing (AGWP) of some species to the integrated forcing of another reference gas, often chosen to be $CO_2$; it is normal to compare equal mass emissions of the species and reference gas. Taking $CO_2$ to be the reference gas, the GWP of some species $x$ is given by

$$GWP_x(t') = \frac{\int_0^{t'} F_x \exp(-t/\tau_x)dt}{\int_0^{t'} F_{CO_2} R(t)dt} \qquad (10\text{-}5)$$

where the $CO_2$ forcing per unit mass, $F_{CO_2}$, depends on the background concentration of $CO_2$, and $R(t)$ represents the response function that describes the decay of an instantaneous pulse of $CO_2$. The GWP of a gas therefore expresses the integrated forcing of a pulse (of given small mass) of that gas relative to the integrated forcing of a pulse (of the same mass) of $CO_2$ over some time horizon. The GWPs of various greenhouse gases can then be easily compared to determine which will cause the greatest integrated radiative forcing over the time horizon of interest.

### 10.4.4.2 Direct GWPs

As discussed in IPCC (1995), atmospheric gases that absorb in infrared spectral regions generally tend to increase the net downward radiation at the tropopause because of their infrared absorptive and emissive properties. GWPs calculated considering only these forcings are referred to as *direct* GWPs because the emitted gas itself leads to additional radiative forcing. If a trace gas is present in sufficiently small quantities so that its absorption is optically thin, the radiative forcing will scale linearly with the additional atmospheric abundance of the gas. While most of the gases considered in Table 10-6 are in the optically thin limit, gases like $CO_2$, $N_2O$, and $CH_4$ are exceptions in which the linear scaling does not hold. The radiative forcing of each gas also depends on the concentration of species that absorb in the same spectral regions (in addition to the distribution of clouds). We assume here that the background concentrations of other gases remain constant.

The $CO_2$ response function used in this section is based on the "Bern" carbon cycle model (see IPCC, 1996) run for a constant mixing ratio of $CO_2$ over a period of 500 years; this is the same response function as used in IPCC (1996) and is a slight update on that used in WMO (1995). An analytical fit to this response function has been derived by L. Bishop (AlliedSignal Inc., U.S., personal comunication, 1998):

$$R(t) = \frac{279400 + 72240t + 730.4t^2}{279400 + 107000t + 3367t^2 + t^3} \qquad (10\text{-}6)$$

where $t$ is the time in years. This fits the model output with an absolute error of 0.002[1].

We have also assumed a different radiative forcing per kilogram of $CO_2$ compared to previous assessments. In previous work (WMO, 1995; IPCC, 1995, 1996) the formula used for the radiative forcing due to a pulse of $CO_2$ was given by

$$\Delta F = 6.3 \ln\left(1 + \frac{\varepsilon}{C_o}\right) \qquad (10\text{-}7)$$

where $C_0$ is the concentration of carbon dioxide before the addition of the pulse (in ppmv) and $\varepsilon$ is the magnitude of the $CO_2$ pulse in (ppmv). Because this formula was intended to reproduce the results of Hansen *et al.* (1988), but did so imperfectly, we will adopt the more complicated formula directly from Hansen *et al.* (1988)

[1] The integral of the response function, which can be used in the generation of GWPs, can be derived from the analytical fit using partial fractions such that

$$\int_0^t R(s)ds = 0.89025 \ln(0.34840t + 1) + 13.872 \ln(0.034259t + 1) + 715.64 \ln(0.00029986t + 1).$$

**Table 10-6. Absolute radiative forcing due to the CFCs, actual and proposed replacements, and related species.** See footnotes for details of the key and scalings. Molecular weights are included to facilitate the calculation of GWPs on a mass basis.

| Gas | | Molecular weight | Forcing ($Wm^{-2}$ $ppbv^{-1}$) | Notes |
|---|---|---|---|---|
| **Chlorofluorocarbons** | | | | |
| CFC-11 | $CCl_3F$ | 137.37 | 0.25 | $ |
| CFC-12 | $CCl_2F_2$ | 120.91 | 0.32 | m |
| CFC-13 | $CClF_3$ | 104.46 | 0.25 | m |
| CFC-113 | $CCl_2FCClF_2$ | 187.38 | 0.30 | m |
| CFC-114 | $CClF_2CClF_2$ | 170.92 | 0.31 | m |
| CFC-115 | $CF_3CClF_2$ | 154.47 | 0.26 | m |
| **Hydrochlorofluorocarbons** | | | | |
| HCFC-21 | $CHCl_2F$ | 102.92 | 0.17 | c |
| HCFC-22 | $CHClF_2$ | 86.47 | 0.22 | IPCC |
| HCFC-123 | $CF_3CHCl_2$ | 152.93 | 0.20 | IPCC |
| HCFC-124 | $CF_3CHClF$ | 136.48 | 0.22 | IPCC |
| HCFC-141b | $CH_3CCl_2F$ | 116.95 | 0.14 | IPCC |
| HCFC-142b | $CH_3CClF_2$ | 100.50 | 0.20 | IPCC |
| HCFC-225ca | $CF_3CF_2CHCl_2$ | 202.94 | 0.27 | IPCC |
| HCFC-225cb | $CClF_2CF_2CHClF$ | 202.94 | 0.32 | IPCC |
| **Hydrofluorocarbons** | | | | |
| HFC-23 | $CHF_3$ | 70.01 | 0.20 | IPCC |
| HFC-32 | $CH_2F_2$ | 52.02 | 0.13 | IPCC |
| HFC-41 | $CH_3F$ | 34.03 | 0.02 | pi |
| HFC-125 | $CHF_2CF_3$ | 120.02 | 0.23 | IPCC |
| HFC-134 | $CHF_2CHF_2$ | 102.03 | 0.18 | c |
| HFC-134a | $CH_2FCF_3$ | 102.03 | 0.19 | IPCC |
| HFC-143 | $CHF_2CH_2F$ | 84.04 | 0.13 | IPCC |
| HFC-143a | $CH_3CF_3$ | 84.04 | 0.16 | IPCC |
| HFC-152 | $CH_2FCH_2F$ | 66.05 | 0.09 | pa |
| HFC-152a | $CH_3CHF_2$ | 66.05 | 0.13 | IPCC |
| HFC-161 | $CH_3CH_2F$ | 48.06 | 0.03 | c |
| HFC-227ca | $CHF_2CF_2CF_3$ | 170.03 | 0.31 | c |
| HFC-227ea | $CF_3CHFCF_3$ | 170.03 | 0.30 | IPCC |
| HFC-236cb | $CH_2FCF_2CF_3$ | 152.04 | 0.23 | c |
| HFC-236ea | $CHF_2CHFCF_3$ | 152.04 | 0.30 | gi |
| HFC-236fa | $CF_3CH_2CF_3$ | 152.04 | 0.28 | mean of gi, pi |
| HFC-245ca | $CH_2FCF_2CHF_2$ | 134.05 | 0.23 | IPCC |
| HFC-245cb | $CH_3CF_2CF_3$ | 134.05 | 0.26 | c |
| HFC-272ca | $CH_3CF_2CH_3$ | 80.08 | 0.08 | IPCC |
| HFC-365mfc | $CF_3CH_2CF_2CH_3$ | 148.07 | 0.21 | b |
| HFC-43-10mee | $CF_3CHFCHFCF_2CF_3$ | 252.05 | 0.40 | IPCC |

**Table 10-6, continued**

| Gas | | Molecular weight | Forcing ($Wm^{-2}$ $ppbv^{-1}$) | Notes |
|---|---|---|---|---|
| **Chlorocarbons** | | | | |
| $CH_3CCl_3$ | | 133.41 | 0.06 | IPCC |
| $CCl_4$ | | 153.82 | 0.10 | IPCC |
| $CHCl_3$ | | 119.38 | 0.02 | IPCC |
| $CH_3Cl$ | | 50.49 | 0.01 | c, gr |
| $CH_2Cl_2$ | | 84.93 | 0.03 | IPCC |
| **Bromocarbons** | | | | |
| $CH_3Br$ | | 94.94 | 0.01 | c, gr |
| $CH_2Br_2$ | | 173.84 | 0.01 | c |
| $CHBrF_2$ | | 130.92 | 0.14 | c |
| Halon-1211 | $CBrClF_2$ | 165.36 | 0.30 | c |
| Halon-1301 | $CBrF_3$ | 148.91 | 0.32 | IPCC |
| **Iodocarbons** | | | | |
| $CF_3I$ | | 195.91 | 0.23 | c |
| $CF_3CF_2I$ | | 245.92 | 0.26 | c |
| **Fully fluorinated species** | | | | |
| $SF_6$ | | 146.05 | 0.52 | m |
| $CF_4$ | | 88.00 | 0.08 | m |
| $C_2F_6$ | | 138.01 | 0.25 | m |
| $C_3F_8$ | | 188.02 | 0.26 | r |
| c-$C_3F_6$ | | 150.02 | 0.42 | pa |
| $C_4F_{10}$ | | 238.02 | 0.33 | r |
| c-$C_4F_8$ | | 200.03 | 0.36 | IPCC |
| $C_5F_{12}$ | | 288.04 | 0.41 | r |
| $C_6F_{14}$ | | 338.04 | 0.49 | r |
| $NF_3$ | | 71.00 | 0.13 | mo |
| **Hydrofluoroethers and hydrochlorofluoroethers** | | | | |
| HFE-125 | $CF_3OCHF_2$ | 136.02 | 0.44 | mean of c, go, h |
| HFE-134 | $CHF_2OCHF_2$ | 118.03 | 0.45 | mean of go, h |
| HFE-143a | $CH_3OCF_3$ | 100.04 | 0.27 | go |
| HFE-227ea | $CF_3CHFOCF_3$ | 186.03 | 0.40 | i |
| HCFE-235da2 | $CF_3CHClOCHF_2$ | 184.49 | 0.38 | c |
| HFE-236ea2 | $CF_3CHFOCHF_2$ | 168.04 | 0.44 | i |
| HFE-236fa | $CF_3CH_2OCF_3$ | 168.04 | 0.34 | i |
| HFE-245cb2 | $CF_3CF_2OCH_3$ | 150.05 | 0.32 | i |
| HFE-245fa1 | $CHF_2CH_2OCF_3$ | 150.05 | 0.30 | i |
| HFE-245fa2 | $CF_3CH_2OCHF_2$ | 150.05 | 0.31 | c |
| HCFE-253cb2 | $CH_3OCF_2CHClF$ | 148.51 | 0.26 | h |

(using the conversion factor from temperature to radiative forcing reported in IPCC (1990)):

$$\Delta F = 3.35(f(C) - f(C_o)) \qquad (10\text{-}8)$$

where

$$f(C) = \ln(1 + 1.2C + 0.005C^2 + 1.4 \times 10^{-6} C^3) \qquad (10\text{-}9)$$

We assume a background $CO_2$ concentration of 364 ppmv, close to the present-day value (WMO (1995) used 354 ppmv). For this assumption, this expression agrees well with the adjusted cloudy-sky radiative forcing calculations of Myhre and Stordal (1997); see also Myhre *et al.* (1998b). The revised forcing is about 12% lower than that derived using the original IPCC expression. For a small perturbation in $CO_2$ from 364 ppmv, the forcing is 0.01548 $Wm^{-2}ppmv^{-1}$. This value is used in the GWP calculations presented here. Because of the changes in the $CO_2$ response function from WMO (1995) and the changes in the $CO_2$ forcing per mass, the $CO_2$ AGWPs differ from the values used in WMO (1995) by -12%, -9%, and -9% for the 20-, 100-, and 500-year time horizons, respectively. These decreases in the $CO_2$ AGWPs will lead to slightly larger GWPs for other gases, in the absence of other changes. The $CO_2$ AGWPs assumed for this chapter and those assumed in WMO (1995) are shown in Table 10-7. In order to allow traceability between different tabulations of GWPs, Table 10-7 also shows the AGWPs using the $CO_2$ decay function used in WMO (1995) and IPCC (1995) and the revised $CO_2$ forcing, and the new decay function and the original forcing.

In Tables 10-8 and 10-9, the direct GWPs (on a mass basis) for 88 gases are tabulated for time horizons of 20, 100, and 500 years in order to illustrate the radiative forcing impact over various integration times. The list consists of CFCs, HCFCs, HFCs, hydrochlorocarbons, bromocarbons, iodocarbons, fully fluorinated species, fluoroalcohols, and fluoroethers. The radiative forcings per kilogram were derived from the values given per ppbv in Table 10-6.

The lifetimes come from a variety of sources. Where revised recommendations have been made in Chapters 1 and 2, their values are adopted. For most of the other gases, the values given in Table 2.2 of IPCC (1996) are used; these values do not take into account the slight revision in methyl chloroform lifetime discussed in Chapter 2. Exceptions are $CH_3CF_3$ (HFC-143a) (+11%) and HFC-236fa (+8%); their increased lifetimes result from revised rate constants for reaction with OH (De More *et al.*, 1997) (and have been scaled to the revised OH lifetime for methyl chloroform given in Chapter 2). For species not previously listed, lifetimes have been taken from Imasu *et al.* (1995), Christensen *et al.* (1998), Christidis *et al.* (1997), Gierczak *et al.* (1996), Good *et al.* (1998), Heathfield *et al.* (1998b),

**Table 10-7. Absolute Global Warming Potentials for carbon dioxide for time horizons of 20, 100, and 500 years.** The value for the previous Assessment (WMO, 1995) is also shown, as well as the impact, individually, of the changes in the $CO_2$ forcing and the response function. Note that the WMO (1995) values are as used in IPCC (1995). The IPCC (1996) report used the revised response function but the old forcing; hence the absolute GWPs used in IPCC (1996) are those shown in the final row of this table.

| | Absolute Global Warming Potentials ($Wm^{-2}$ yr $ppmv^{-1}$) | | |
|---|---|---|---|
| | **20-Year** | **100-Year** | **500-Year** |
| This work | 0.207 | 0.696 | 2.241 |
| WMO (1995) | 0.235 | 0.768 | 2.459 |
| Using the revised forcing but the WMO (1995) response function | 0.209 | 0.684 | 2.188 |
| Using the WMO (1995) forcing but the revised response function | 0.238 | 0.800 | 2.576 |

**Table 10-8. Direct Global Warming Potentials (mass basis) relative to carbon dioxide** (for gases for which the lifetimes have been adequately characterized).

| Gas | | Lifetime (years) | Global Warming Potential (Time Horizon in years) | | |
|---|---|---|---|---|---|
| | | | 20 years | 100 years | 500 years |
| Carbon dioxide | $CO_2$ | See text | 1 | 1 | 1 |
| Methane[1] | $CH_4$ | 12.2* (a) | 64 | 24 | 7.5 |
| Nitrous oxide[2] | $N_2O$ | 120 (b) | 330 | 360 | 190 |
| **Chlorofluorocarbons** | | | | | |
| CFC-11 | $CCl_3F$ | 45 (b) | 6300 | 4600 | 1600 |
| CFC-12 | $CCl_2F_2$ | 100 (b) | 10200 | 10600 | 5200 |
| CFC-13 | $CClF_3$ | 640 (c) | 10000 | 14000 | 16300 |
| CFC-113 | $CCl_2FCClF_2$ | 85 (b) | 6100 | 6000 | 2700 |
| CFC-114 | $CClF_2CClF_2$ | 300 (a) | 7500 | 9800 | 8700 |
| CFC-115 | $CF_3CClF_2$ | 1700 (a) | 7100 | 10300 | 14300 |
| **Hydrochlorofluorocarbons** | | | | | |
| HCFC-21 | $CHCl_2F$ | 2.0 (d) | 700 | 210 | 65 |
| HCFC-22 | $CHClF_2$ | 11.8 (b) | 5200 | 1900 | 590 |
| HCFC-123 | $CF_3CHCl_2$ | 1.4 (a) | 390 | 120 | 36 |
| HCFC-124 | $CF_3CHClF$ | 6.1 (a) | 2000 | 620 | 190 |
| HCFC-141b | $CH_3CCl_2F$ | 9.2 (b) | 2100 | 700 | 220 |
| HCFC-142b | $CH_3CClF_2$ | 18.5 (b) | 5200 | 2300 | 720 |
| HCFC-225ca | $CF_3CF_2CHCl_2$ | 2.1 (a) | 590 | 180 | 55 |
| HCFC-225cb | $CClF_2CF_2CHClF$ | 6.2 (a) | 2000 | 620 | 190 |
| **Hydrofluorocarbons** | | | | | |
| HFC-23 | $CHF_3$ | 243 (b) | 11700 | 14800 | 11900 |
| HFC-32 | $CH_2F_2$ | 5.6 (a) | 2900 | 880 | 270 |
| HFC-41 | $CH_3F$ | 3.7 (a) | 460 | 140 | 43 |
| HFC-125 | $CHF_2CF_3$ | 32.6 (a) | 6100 | 3800 | 1200 |
| HFC-134 | $CHF_2CHF_2$ | 10.6 (a) | 3400 | 1200 | 370 |
| HFC-134a | $CH_2FCF_3$ | 13.6 (b) | 4100 | 1600 | 500 |
| HFC-143 | $CHF_2CH_2F$ | 3.8 (a) | 1200 | 370 | 120 |
| HFC-143a | $CF_3CH_3$ | 53.5 (d) | 6800 | 5400 | 2000 |
| HFC-152 | $CH_2FCH_2F$ | 0.5 (d) | 140 | 43 | 13 |
| HFC-152a | $CH_3CHF_2$ | 1.5 (a) | 630 | 190 | 58 |
| HFC-161 | $CH_3CH_2F$ | 0.25 (i) | 33 | 10 | 3 |
| HFC-227ea | $CF_3CHFCF_3$ | 36.5 (a) | 5800 | 3800 | 1300 |
| HFC-236cb | $CH_2FCF_2CF_3$ | 14.6 (i) | 3500 | 1400 | 430 |
| HFC-236ea | $CHF_2CHFCF_3$ | 8.1 (j) | 3100 | 1000 | 310 |
| HFC-236fa | $CF_3CH_2CF_3$ | 226 (d) | 7500 | 9400 | 7300 |
| HFC-245ca | $CH_2FCF_2CHF_2$ | 6.6 (a) | 2300 | 720 | 220 |
| HFC-365mfc | $CF_3CH_2CF_2CH_3$ | 10.2 (k) | 2600 | 910 | 280 |
| HFC-43-10mee | $CF_3CHFCHFCF_2CF_3$ | 17.1 (a) | 4000 | 1700 | 530 |

**Table 10-9. Direct Global Warming Potentials (mass basis) relative to carbon dioxide** (for gases for which the lifetime has been determined only via indirect means, rather than laboratory measurements, or for which there is uncertainty over the loss processes).

| Gas | | Lifetime (years) | Global Warming Potential (Time Horizon in years) | | |
|---|---|---|---|---|---|
| | | | 20 | 100 | 500 |
| $NF_3$ | | 740 (a) | 7700 | 10800 | 13100 |
| HFE-227ea | $CF_3CHFOCF_3$ | 11 (b) | 4200 | 1500 | 460 |
| HFE-236ea1 | $CF_3CHFOCHF_2$ | 5.8 (b) | 3100 | 960 | 300 |
| HFE-236fa | $CF_3CH_2OCF_3$ | 3.7 (b) | 1600 | 470 | 150 |
| HFE-245cb2 | $CF_3CF_2OCH_3$ | 1.2 (b) | 540 | 160 | 50 |
| HFE-245fa1 | $CHF_2CH_2OCF_3$ | 2.2 (b) | 940 | 280 | 86 |
| HFE-263fb2 | $CF_3CH_2OCH_3$ | 0.1 (b) | 37 | 11 | 3 |
| HFE-329mcc2 | $CF_3CF_2OCF_2CHF_2$ | 6.8 (b) | 2800 | 890 | 280 |
| HFE-338mcf2 | $CF_3CF_2OCH_2CF_3$ | 4.3 (b) | 1800 | 540 | 170 |
| HFE-347mcc3 | $CF_3CF_2CF_2OCH_3$ | 1.3 (b) | 470 | 140 | 43 |
| HFE-347mcf2 | $CF_3CF_2OCH_2CHF_2$ | 2.8 (b) | 1200 | 360 | 110 |
| HFE-356mec3 | $CF_3CHFCF_2OCH_3$ | 0.94 (b) | 330 | 98 | 30 |
| HFE-356pcc3 | $CHF_2CF_2CF_2OCH_3$ | 0.93 (b) | 360 | 110 | 33 |
| HFE-356pcf2 | $CHF_2CF_2OCH_2CHF_2$ | 2.0 (b) | 860 | 260 | 80 |
| HFE-356pcf3 | $CHF_2CF_2CH_2OCHF_2$ | 1.3 (b) | 590 | 180 | 55 |
| HFE-365mcf3 | $CF_3CF_2CH_2OCH_3$ | 0.11 (b) | 38 | 11 | 4 |
| HFE-374pc2 | $CHF_2CF_2OCH_2CH_3$ | 0.43 (b) | 160 | 47 | 14 |
| $(CF_3)_2CFOCH_3$ | | 3.5 (b) | 1100 | 340 | 110 |
| $(CF_3)_2CHOCHF_2$ | | 3.1 (b) | 1200 | 370 | 110 |
| $(CF_3)_2CHOCH_3$ | | 0.25 (b) | 88 | 26 | 8 |
| $CHF_2OCF_2OC_2F_4OCHF_2$ (H-Galden 1040x) | | 48 (c) | 12200 | 9300 | 3300 |
| $-(CF_2)_4CH(OH)-$ | | 0.85 (b) | 240 | 70 | 22 |
| $CF_3CH_2OH$ | | 0.46 (b) | 180 | 52 | 16 |
| $CF_3CF_2CH_2OH$ | | 0.43 (b) | 150 | 43 | 14 |
| $(CF_3)_2CHOH$ | | 1.4 (b) | 500 | 150 | 46 |

(a) Molina *et al.* (1995).
(b) Imasu *et al.* (1995).
(c) Christidis *et al.* (1997).

### 10.4.4.3 Indirect GWPs

Some trace species can exert a radiative forcing by their involvement in chemical reactions that alter the concentrations of other radiatively active gases. This forcing is referred to as an "indirect" forcing because the radiative change is caused by another species that is chemically perturbed by the presence of the trace gas, and not by absorption and emission of radiation by the trace gas itself. While direct GWPs are usually believed to be known reasonably accurately (±35%), indirect GWPs can be highly uncertain.

***Methane***

Four types of indirect effects due to the presence of atmospheric methane have been identified. The largest effect is potentially the production of ozone. This effect is difficult to quantify, however, because the magnitude of ozone production is highly dependent on the abundance and distribution of $NO_x$ (IPCC, 1996). Other indirect effects include the production of stratospheric water vapor, the production of carbon dioxide (from certain methane sources), and the increase in the methane adjustment time resulting from its coupling with OH (Brühl, 1993; Lelieveld and Crutzen, 1992; Prather, 1994, 1996; IPCC 1996). Because no additional calculations of the $CH_4$ GWPs have been presented since IPCC (1996), we adopt their values with a correction for our different $CO_2$ AGWPs. It should be noted that the climate forcing caused by $CO_2$ produced from the oxidation of $CH_4$ is not included in these GWP estimates. As discussed in IPCC (1996), it is often the case that this $CO_2$ is included in national carbon production inventories. Therefore, depending on how the inventories are combined, including the $CO_2$ production from $CH_4$ could result in "double counting" the radiative forcing of this $CO_2$.

***Carbon Monoxide***

Carbon monoxide leads to indirect radiative effects that are similar to those of methane. Unlike methane, however, the direct radiative forcing is likely to be significantly smaller than its indirect forcing (Evans and Puckrin, 1995; Sinha and Toumi, 1996; Daniel and Solomon, 1998). An atmospheric pulse of CO can lead to the production of ozone, with the magnitude of ozone formation dependent on the amount of $NO_x$ present. As with methane, this effect is quite difficult to quantify due to the highly variable and uncertain $NO_x$ distribution (Emmons *et al.*, 1997). The emission of CO also perturbs OH, which can then lead to an increase in the $CH_4$ concentration (Prather, 1996; Daniel and Solomon, 1998). Finally, the oxidation of the CO from fossil fuel emission by reaction with OH results in the formation of $CO_2$. Because of the difficulty in accurately calculating the amount of ozone produced by the addition of a pulse of CO, an accurate estimate of the entire indirect forcing of CO would most likely require a 3-D model. Because of the difficulties in calculating a CO GWP, we mention here only that Daniel and Solomon (1998), using a box model, have estimated an upper limit of 4 for the CO indirect GWP for the 100-year time horizon; it is likely that the actual value is closer to their lower limit of 1. As with $CH_4$, the production of $CO_2$ from oxidized CO can lead to double counting of this $CO_2$ and is therefore not considered in these estimates.

***Halocarbons***

In addition to their direct radiative forcing, chlorinated and brominated halocarbons can lead to a significant indirect forcing through their destruction of stratospheric ozone. By destroying stratospheric ozone, itself a greenhouse gas, halocarbons are likely to induce a negative indirect forcing that counteracts some or perhaps all, in certain cases, of their direct forcing. Quantifying the magnitude of the negative indirect forcing is quite difficult for several reasons. As discussed in Section 10.3, the negative forcing arising from the ozone destruction is highly dependent on the altitude profile of the ozone loss. Furthermore, the additional radiative effects due to enhanced tropospheric OH are potentially important and similarly difficult to quantify (Section 10.3.4). While recognizing these uncertainties, estimates have been made of the net radiative forcing due to particular halocarbons, which can then be used to determine net GWPs (including both direct and indirect effects). This was done by Daniel *et al.* (1995), where it was shown that if the enhanced tropospheric OH effect were ignored, and the negative forcing due to ozone loss during the 1980s was -0.08 $Wm^{-2}$, the net GWPs for the bromocarbons were significantly negative, illustrating the impact of the negative forcing arising from the bromocarbon-induced ozone depletion. While the effect on the chlorocarbon GWPs was less pronounced, it was significant as well. In Table 10-10 we have updated the indirect GWP results from Daniel *et al.* (constant-alpha case A) (but with the alpha increased from 40 to 60; see Chapter 2) to reflect the updated forcing and response of $CO_2$ and to account for an uncertainty in the 1980-1990

**Table 10-10. Net Global Warming Potentials (mass basis) of selected halocarbons.** (Updated from Daniel *et al.*, 1995.)

| Species | Time Horizon = 2010 (20 years) | | | Time Horizon = 2090 (100 years) | | |
|---|---|---|---|---|---|---|
| | Direct | Min | Max | Direct | Min | Max |
| CFC-11 | 6200 | -840 | 5090 | 4600 | -1680 | 3610 |
| CFC-12 | 10200 | 6720 | 9650 | 10600 | 6900 | 10020 |
| CFC-113 | 6100 | 1970 | 5450 | 6000 | 1740 | 5330 |
| $CH_3CCl_3$ | 450 | -2370 | 0 | 140 | -750 | 0 |
| $CCl_4$ | 2100 | -6530 | 740 | 1400 | -5850 | 260 |
| HCFC-22 | 5200 | 4330 | 5060 | 1900 | 1500 | 1840 |
| HCFC-123 | 390 | -90 | 310 | 120 | 0 | 100 |
| HCFC-124 | 2000 | 1510 | 1920 | 620 | 450 | 590 |
| HCFC-141b | 2100 | -70 | 1760 | 700 | -130 | 570 |
| HCFC-142b | 5200 | 4300 | 5060 | 2300 | 1740 | 2210 |
| Halon-1301 | 7900 | -99850 | -9110 | 6900 | -97030 | -9510 |

ozone radiative forcing of -0.03 to -0.19 $Wm^{-2}$. If the Daniel *et al.* analysis had considered the OH indirect effects, the GWPs in Table 10-10 would be further reduced.

## 10.5 PERSPECTIVE: THE NET EFFECT OF OZONE AND HALOCARBON CHANGES AND COMPARISONS WITH OTHER FORCINGS

As has been discussed in, for example, IPCC (1995, 1996) and Hansen *et al.* (1997c), there are a large number of ways in which human activity may affect radiative forcing. In addition to the effects of the well-mixed greenhouse gases and ozone, changes in aerosol concentrations resulting from fossil-fuel and biomass burning and changes in land use can all cause a radiative forcing both directly, by altering the scattering and absorbing properties of the atmosphere, and indirectly, via changes in cloud properties. Changes in solar irradiance and explosive volcanic eruptions also contribute.

The global-mean forcing due to well-mixed greenhouse gases is about 2.25 to 2.5 $Wm^{-2}$ since preindustrial times (e.g., IPCC, 1996; Myhre *et al.*, 1998b). Although this is several times the forcing due to ozone change, the ozone effects are significant. Changes in tropospheric ozone may enhance this forcing by 10 to 15% and, at the upper end of its uncertainty range, it may be of similar importance to methane, which is the second most important contributor to the well-mixed greenhouse gas forcing (with about 0.5 $Wm^{-2}$ since preindustrial times).

In addition, the tropospheric ozone forcing is of a similar size, but opposite sign, to many recent estimates of the direct forcing due to sulfate aerosols (see, e.g., IPCC 1996; van Dorland *et al.*, 1997; Feichter *et al.*, 1997; Chuang *et al.*, 1997). (The indirect forcing due to the impact of increased aerosols on cloud properties is highly uncertain but may be as negative as -1.5 $Wm^{-2}$ (e.g., IPCC, 1996; Feichter *et al.*, 1997; Chuang *et al.*, 1997).) The direct effect of sulfate aerosols has been included in several studies that have attempted to attribute climate changes to human activity (e.g., Santer *et al.*, 1996; Tett *et al.*, 1996; Mitchell *et al.*, 1995; Haywood *et al.*, 1997) whereas tropospheric ozone has not. Further, black carbon from fossil fuel and biomass burning may cause a significant positive forcing of a similar size (at least on a global-mean basis) but opposite sign to the sulfate aerosol effect (e.g., IPCC, 1996; Haywood and Ramaswamy, 1998; Hansen *et al.*, 1997c), and other components of the aerosol population may be significant (see, e.g., Tegen *et al.*, 1997). The direct effect of all aerosols may be much smaller than the effect of sulfate alone. Hence, the inclusion of changes in tropospheric ozone seems likely to be as important as the direct effect

of aerosols in studies attempting to detect and attribute the effect of human activity on climate.

The radiative forcing due to stratospheric ozone change is of a similar magnitude but opposite sign to the tropospheric ozone forcing. While it is important at the 10% level compared to the well-mixed greenhouse gas forcing since preindustrial times, as has been pointed out in earlier assessments, its importance over the shorter term may be considerably greater, given that most of its effect has occurred over the two most recent decades. The forcing since the late 1970s due to the well-mixed greenhouse gases is about 0.5 $Wm^{-2}$, so the ozone loss may have offset about 30% of this forcing. The ozone forcing constitutes an even higher proportion of the forcing due to the halocarbons that lead to the ozone loss. The total direct forcing from the halocarbons is about 0.25 $Wm^{-2}$ (see, e.g., IPCC, 1996), so our midrange estimate of the stratospheric ozone forcing offsets about 80% of this.

With the exception of HCFC-22, all the halogenated replacements are currently present in concentrations of only pptv, or less, so their contribution to radiative forcing is currently negligible. Using the global-mean concentrations from Chapter 2 and the forcings per ppbv from Table 10-6, the forcing due to HCFC-22 is about 0.025 $Wm^{-2}$ (IPCC, 1996), which is about an order of magnitude lower than the current contributions from all the CFCs. The total contribution using the 1996 concentrations of $CH_3CClF_2$ (HCFC-142b), $CH_3CCl_2F$ (HCFC-141b), and HFC-134a, from Chapter 2, gives a forcing of just a few thousandths of a Watt per square meter. Similarly the contributions from sulfur hexafluoride ($SF_6$) and the perfluorocarbons, using concentrations from Chapter 1, sum to less than 0.01 $Wm^{-2}$. The contribution from perfluoromethane ($CF_4$) is reduced from that given in IPCC (1996) because it was assumed there that the preindustrial concentration was zero whereas, as discussed in Chapter 1, there is evidence that the preindustrial concentration was 40 pptv (compared to a present-day concentration of about 70 pptv).

As reported in Chapters 1 and 2, the growth rate for many of the replacement species is high and their contribution to the rate of change of forcing is somewhat higher than their contribution to the cumulative forcing. For example, for $SF_6$, the forcing is about 0.1% of the forcing due to $CO_2$ since preindustrial times, but its current rate of change of forcing is 0.4% of the current rate of change of forcing due to $CO_2$. The values for $CHF_3$ (HFC-23) and $CF_4$ are similar.

Looking into the future, based on the estimates of the greenhouse gas concentrations in the 21st century from IPCC Scenario IS92a, as reported in IPCC (1996), the contribution of the HFCs would rise to 0.23 $Wm^{-2}$ by the year 2100, which can be compared to a total forcing from greenhouse gases, using the same scenario, of about 6 $Wm^{-2}$. These scenarios are, of course, highly uncertain given the nature of many of the underlying assumptions. The contributions due to the HCFCs after reaching a peak, at about double current levels, in around 2005, are expected to fall to zero by 2100, as a result of their phaseout under the terms of the Montreal Protocol and its Amendments. The contribution of CFCs is expected to fall to less than 0.1 $Wm^{-2}$ by 2100.

In conclusion, changes in ozone are an important contributor to the overall radiative forcing picture, and refinement of our understanding of these forcings will be important if our understanding of the wider impact of human activity on the climate is to be understood. Although stratospheric ozone depletion has partly offset the effects of any greenhouse-gas-induced forcing over the past decade, it may not continue to do so. If ozone recovers as is anticipated (see Chapter 12), the decadal increase in forcing due to the ozone recovery may, in the early part of the next century, enhance, by about 10%, the decadal increase in forcing due to the other greenhouse gases (Solomon and Daniel, 1996).

## REFERENCES

Anastasi, C., A.E. Heathfield, G.P. Knight, and F. Nicolaisen, Integrated absorption-coefficients of $CHClF_2$ (HCFC-22) and $CH_3Br$ in the atmospheric infrared window region, *Spectrochim. Acta, 50A*, 1791-1798, 1994.

Anklin, M., and R.C. Bales, Recent increase in $H_2O_2$ concentration at Summit, Greenland, *J. Geophys. Res., 102*, 19099-19104, 1997.

Barry, J., G. Locke, D. Scollard, H. Sidebottom, J. Treacy, C. Clerbaux, R. Colin, and J. Franklin, 1,1,1,3,3,-pentafluorobutane (HFC-365mfc): Atmospheric degradation and contribution to radiative forcing, *Int. J. Chem. Kinet., 29*, 607-617, 1997.

Bekki, S., K.S. Law, and J.A. Pyle, Effect of ozone depletion on atmospheric $CH_4$ and CO concentrations, *Nature, 371*, 595-597, 1994.

Berntsen, T., I.S.A. Isaksen, J.S. Fuglestvedt, G. Myhre, F. Stordal, R.S. Freckleton, and K.P. Shine, Effects of anthropogenic emissions on tropospheric ozone and radiative forcing, *J. Geophys. Res.*, *102*, 28101-28126, 1997.

Bintanja, R., J.P.F. Fortuin, and H. Kelder, Simulation of the meridionally and seasonally varying climate response caused by changes in ozone concentration, *J. Clim.*, *10*, 1288-1311, 1997.

Brühl, C., The impact of the future scenarios for methane and other chemically active gases on the GWP of methane, *Chemosphere*, *26*, 731-738, 1993.

Capellani, F., and G. Restelli, Infrared band strengths and their temperature dependence of the hydrohalocarbons HFC-134a, HFC-152a, HCFC-22, HCFC-123, and HCFC-142b, *Spectrochim. Acta*, *48A*, 1127-1131, 1992.

Cavalli, F., M. Glasius, J. Hjorth, B. Rindone, and N.R. Jensen, Atmospheric lifetimes, infrared spectra and degradation products of a series of hydrofluoroethers, *Atmos. Environ.*, *32*, 3767-3773, 1998.

Chalita, S., D.A. Hauglustaine, H. Le Treut, and J.-F. Müller, Radiative forcing due to increased tropospheric ozone concentrations, *Atmos. Environ.*, *30*, 1641-1646, 1996.

Christensen, L.K., J. Sehested, O.J. Nielsen, M. Bilde, T.J. Wallington, A. Guschin, L.T. Molina, and M.J. Molina, Atmospheric chemistry of HFE-7200 ($C_4F_9OC_2H_5$): Reaction with OH radicals, fate of $C_4F_9OCH_2CH_2O\cdot$ and $C_4F_9OCHO\cdot CH_3$ radicals, *J. Phys. Chem. A*, *102*, 4839-4845, 1998.

Christidis, N., M.D. Hurley, S. Pinnock, K.P. Shine, and T.J. Wallington, Radiative forcing of climate change by CFC-11 and possible CFC replacements, *J. Geophys. Res.*, *102*, 19597-19609, 1997.

Chuang, C.C., J.E. Penner, K.E. Taylor, A.S. Grossman, and J.J. Walton, An assessment of the radiative effects of anthropogenic sulfate, *J. Geophys. Res.*, *102*, 3761-3778, 1997.

Clerbaux, C., R. Colin, P.C. Simon, and C. Granier, Infrared cross sections and global warming potentials of 10 alternative hydrohalocarbons, *J. Geophys. Res.*, *98*, 10491-10497, 1993.

Cox, S.J., W.-C. Wang, and S.E. Schwartz, Climate response to radiative forcings by sulfate aerosols and greenhouse gases, *Geophys. Res. Lett*, *22*, 2509-2512, 1995.

Crutzen, P., Global tropospheric chemistry, in *Low Temperature Chemistry of the Atmosphere*, edited by G.K. Moortgat *et al.*, pp. 465-498, Springer-Verlag, Berlin, 1994.

Daniel, J.S., and S. Solomon, On the climate forcing of carbon monoxide, *J. Geophys. Res.*, *103*, 13249-13260, 1998.

Daniel, J.S., S. Solomon, and D. Albritton, On the evaluation of halocarbon radiative forcing and global warming potentials, *J. Geophys. Res.*, *100*, 1271-1285, 1995.

DeMore, W.B, S.P. Sander, D.M. Golden, R.F. Hampson, M.J. Kurylo, C.J. Howard, A.R. Ravishankara, C.E. Kolb, and M.J. Molina, *Chemical Kinetics and Photochemical Data for Use in Stratospheric Modeling, Evaluation Number 11*, JPL Publ. 94-26, Jet Propulsion Laboratory, Pasadena, Calif., 1994.

DeMore, W.B., S.P. Sander, D.M. Golden, R.F. Hampson, M.J. Kurylo, C.J. Howard, A.R. Ravishankara, C.E. Kolb, and M.J. Molina, *Chemical Kinetics and Photochemical Data for Use in Stratospheric Modeling, Evaluation Number 12*, JPL Publ. 97-4, Jet Propulsion Laboratory, Pasadena, Calif., 1997.

Dlugokencky, E.J., K.A. Masarie, P.M. Lang, P.P. Tans, L.P. Steele, and E.G. Nisbet, A dramatic decrease in the growth rate of atmospheric methane in the Northern Hemisphere during 1992, *Geophys. Res. Lett.*, *21*, 45-48, 1994.

Emmons, L.K., M.A. Carroll, D.A. Hauglustaine, G.P. Brasseur, C. Atherton, J. Penner, S. Sillman, H. Levy, F. Rohrer, W.M.F. Wauben, P.F.J. VanVelthoven, Y. Wang, D. Jacob, P. Bakwin, R. Dickerson, B. Doddridge, C. Gerbig, R. Honrath, G. Hübler, D. Jaffe, Y. Kondo, J.W. Munger, A. Torres, and A. Volz-Thomas, Climatologies of $NO_x$ and $NO_y$: A comparison of data and models, *Atmos. Environ.*, *31*, 1851-1904, 1997.

Evans, W.F.J., and E. Puckrin, An observation of the greenhouse radiation associated with carbon monoxide, *Geophys. Res. Lett.*, *22*, 925-928, 1995.

Feichter, J., U. Lohmann, and I. Schult, The atmospheric sulfur cycle in ECHAM-4 and its impact on the shortwave radiation, *Clim. Dyn.*, *13*, 235-246, 1997.

Fishman, J., The global consequences of increasing tropospheric ozone concentrations, *Chemosphere*, *22*, 685-695, 1991.

Forster, P.M. de F., and K.P. Shine, Radiative forcing and temperature trends from stratospheric ozone changes, *J. Geophys. Res.*, *102*, 10841-10857, 1997.

Forster, P.M. de F., C.E. Johnson, K.S. Law, J.A. Pyle, and K.P. Shine, Further estimates of radiative forcing due to tropospheric ozone changes, *Geophys. Res. Lett.*, *23*, 3321-3324, 1996.

Forster, P.M. de F., R.S. Freckleton, and K.P. Shine, On aspects of the concept of radiative forcing, *Clim. Dyn.*, *13*, 547-560, 1997.

Freckleton, R.S., E.J. Highwood, K.P. Shine, O. Wild, K.S. Law, and M.G. Sanderson, Greenhouse gas radiative forcing: Effects of averaging and inhomogeneities in trace gas distribution, *Quart. J. Roy. Meteorol. Soc.*, *124*, 2099-2127, 1998.

Fuglestvedt, J.S., J.E. Jonson, and I.S.A. Isaksen, Effects of reductions in stratospheric ozone on tropospheric chemistry through changes in photolysis rates, *Tellus*, *46B*, 172-192, 1994.

Fuglestvedt, J.S., J.E. Jonson, W.-C. Wang, and I.S.A. Isaksen, Response in tropospheric chemistry to changes in UV fluxes, temperatures and water vapor densities, in *Atmospheric Ozone as a Climate Gas*, edited by W.-C. Wang and I.S.A. Isaksen, NATO Series I 32, 143-162, Springer-Verlag, Berlin, 1995.

Gierczak, T., R.K. Talukdar, J.B. Burkholder, R.W. Portmann, J.S. Daniel, S. Solomon, and A.R. Ravishankara, Atmospheric fate and greenhouse warming potentials of HFC-236fa and HFC-236ea, *J. Geophys. Res.*, *101*, 12905-12911, 1996.

Good, D.A., J.S. Francisco, A.K. Jain, and D.J. Wuebbles, Lifetimes and global warming potentials for dimethyl ethers and for fluorinated ethers: $CH_3OCF_3$ (E143a), $CHF_2OCHF_2$ (E134), $CHF_2OCF_3$ (E125), *J. Geophys. Res.*, in press, 1998.

Granier, C., J.-F. Müller, S. Madronich, and G.P. Brasseur, Possible causes for the 1990-1993 decrease in the global tropospheric CO abundances: A three-dimensional sensitivity study, *Atmos. Environ.*, *30*, 1673-1682, 1996.

Grossman, A.S., Grant, K.E., W.E. Blass, and D.J. Wuebbles, Radiative forcing calculations for $CH_3Cl$ and $CH_3Br$, *J. Geophys. Res.*, *102*, 13651-13656, 1997.

Hansen, J., I. Fung, A. Lacis, D. Rind, S. Lebedeff, R. Ruedy, G. Russell, and P. Stone, Global climate changes as forecast by Goddard Institute for Space Studies 3-dimensional model, *J. Geophys. Res.*, *93*, 9341-9364, 1988.

Hansen, J., A. Lacis, R. Ruedy, M. Sato, and H. Wilson, How sensitive is the world's climate? *Res. Explor.*, *9*, 142-158, 1993.

Hansen, J., M. Sato, and R. Ruedy, Radiative forcing and climate response, *J. Geophys. Res.*, *102*, 6831-6864, 1997a.

Hansen, J., M. Sato, A. Lacis, and R. Ruedy, The missing climate forcing, *Philos. Trans. Roy. Soc. London B*, *352*, 231-240, 1997b.

Hansen, J., M. Sato, R. Ruedy, A. Lacis, K. Asamoah, K. Beckford, S. Borenstein, E. Brown, B. Cairns, B. Carlson, B. Curran, S. de Castro, L. Druyan, P. Etbarrow, T. Ferede, N. Fox, D. Gaffen, J. Glascoe, H. Gordon, S. Hollandsworth, X. Jiang, C. Johnson, N. Lawrence, J. Lean, J. Lerner, K. Lo, J. Logan, A. Luckett, M.P. McCormick, R. McPeters, R. Miller, P. Minnis, I. Ramberran, G. Russell, P. Russell, P. Stone, I. Tegen, S. Thomas, L. Thomason, A. Thompson, J. Wilder, R. Willson, and J. Zawodny, Forcing and chaos in interannual to decadal climate change, *J. Geophys. Res.*, *102*, 25679-25720, 1997c.

Hauglustaine, D.A., C. Granier, G.P. Brasseur, and G. Megie, The importance of atmospheric chemistry in the calculation of radiative forcing on the climate system, *J. Geophys. Res.*, *99*, 1173-1186, 1994.

Haywood, J.M., and V. Ramaswamy, Global sensitivity studies of the direct radiative forcing due to anthropogenic sulfate and black carbon aerosols, *J. Geophys. Res.*, *103*, 6043-6058, 1998.

Haywood, J.M., R.J. Stouffer, R.T. Wetherald, S. Manabe, and V. Ramaswamy, Transient response of a coupled model to estimated changes in greenhouse gas and sulfate concentrations, *Geophys. Res. Lett.*, *24*, 1335-1338, 1997.

Heathfield, A.E., C. Anastasi, J. Ballard, D.A. Newnham, and A. McCulloch, Integrated infrared absorption coefficients of $CF_3OCF_2H$ and $CH_3OCF_2CF_2H$ at 297, 253, and 213 K, *J. Quant. Spectrosc. Radiat. Transfer*, *59*, 91-97, 1998a.

Shine, K.P., R.S. Freckleton, and P.M. de F. Forster, Comment on "Climate forcing by stratospheric ozone depletion calculated from observed temperature trends," *Geophys. Res. Lett.*, *25*, 663-664, 1998.

Sigg, A., and A. Neftel, Evidence for a 50% increase in $H_2O_2$ over the past 200 years from a Greenland ice core, *Nature*, *351*, 557-559, 1991.

Sinha, A., and R. Toumi, A comparison of climate forcings due to chlorofluorocarbons and carbon monoxide, *Geophys. Res. Lett.*, *23*, 65-68, 1996.

Smith, K., D. Newnham, M. Page, J. Ballard, and G. Duxbury, Infrared band strengths and absorption cross-sections of HFC-32 vapour, *J. Quant. Spectrosc. Radiat. Transfer*, *56*, 73-82, 1996.

Solomon, S., and J.S. Daniel, Impact of the Montreal Protocol and its Amendments on the rate of change of global radiative forcing, *Clim. Change*, *32*, 7-17, 1996.

Takahashi, K., Y. Matsumi, and M. Kawasaki, Photodissociation processes of ozone in the Huggins band at 308-326 nm: Direct observation of $O(^1D_2)$ and $O(^3P_j)$ products, *J. Phys. Chem.*, *100*, 4084-4089, 1996.

Tegen, I., P. Hollrig, M. Chin, I. Fung, D. Jacob, and J. Penner, Contribution of different aerosol species to the global aerosol extinction optical thickness: Estimates from model results, *J. Geophys. Res.*, *102*, 23895-23915, 1997.

Tett, S.F.B., J.F.B. Mitchell, D.E. Parker, and M.R. Allen, Human influence on the atmospheric vertical temperature structure: Detection and observations, *Science*, *274*, 1170-1173, 1996.

Thompson, A.M., M.A. Huntley, and R.W. Stewart, Perturbations to tropospheric oxidants, 1985-2035, *J. Geophys. Res.*, *95*, 9829-9844, 1990.

Toumi, R., S. Bekki, and K.S. Law, Indirect influence of ozone depletion on climate forcing by clouds, *Nature*, *372*, 348-351, 1994.

Toumi, R., S. Bekki, and K.S. Law, Response to climate and CCN by Rodhe and Crutzen, *Nature*, *375*, 111, 1995.

Trolier, M., and J.R. Wiesenfeld, Relative quantum yield of $O(^1D_2)$ following photolysis between 275 and 325 nm, *J. Geophys. Res.*, *93*, 7119-7124, 1988.

Van Dop, H., and M. Krol, Changing trends in tropospheric methane and carbon monoxide: A sensitivity analysis of the OH-radical, *J. Atmos. Chem.*, *25*, 271-288, 1996.

van Dorland, R., F.J. Dentener, and J. Lelieveld, Radiative forcing due to tropospheric ozone and sulfate aerosols, *J. Geophys. Res.*, *102*, 28079-28100, 1997.

Varanasi, P., Z. Li, V. Nemtchinov, and A. Cherukuri, Spectral absorption coefficient data on HCFC-22 and $SF_6$ for remote sensing application, *J. Quant. Spectrosc. Radiat. Transfer*, *52*, 323-332, 1994.

Wallington, T.J., W.F. Schneider, J. Sehested, M. Bilde, J. Platz, O.J. Nielsen, L.K. Christensen, M.J. Molina, L.T. Molina, and P.W. Wooldridge, Atmospheric chemistry of HFE-7100 ($C_4F_9OCH_3$): Reaction with OH radicals, UV spectra, and kinetic data for $C_4F_9OCH_2\cdot$ and $C_4F_9OCH_2O_2\cdot$ radicals and the atmospheric fate of $C_4F_9OCH_2O\cdot$ radicals, *J. Phys. Chem. A.*, *101*, 8264-8274, 1997.

Wang, W.-C., J.P. Pinto, and Y.L. Yung, Climatic effects due to halogenated compounds in the Earth's atmosphere, *J. Atmos. Sci.*, *37*, 333-338, 1980.

Wild, O., O.V. Rattigan, R.L. Jones, J.A. Pyle, and R.A. Cox, 2-Dimensional modeling of some CFC replacement compounds, *J. Atmos. Chem.*, *25*, 167-199, 1996.

WMO (World Meteorological Organization), *Scientific Assessment of Ozone Depletion: 1991*, Global Ozone Research and Monitoring Project—Report No. 25, Geneva, 1992.

WMO (World Meteorological Organization), *Scientific Assessment of Ozone Depletion: 1994*, Global Ozone Research and Monitoring Project—Report No. 37, Geneva, 1995.

Zhong, W., R. Toumi, and J.D. Haigh, Climate forcing by stratospheric ozone depletion calculated from observed temperature trends, *Geophys. Res. Lett.*, *23*, 3183-3186, 1996.

# PART 4

## PREDICTIONS OF FUTURE CHANGES

### Chapter 11
HALOCARBON SCENARIOS FOR THE FUTURE OZONE LAYER AND RELATED CONSEQUENCES

### Chapter 12
PREDICTING FUTURE OZONE CHANGES AND DETECTION OF RECOVERY

# CHAPTER 11

## HALOCARBON SCENARIOS FOR THE FUTURE OZONE LAYER AND RELATED CONSEQUENCES

### Contents

## HALOCARBON SCENARIOS

- **Illegal production of ozone-depleting substances may delay the recovery of the ozone layer.** For example, illegal production of, in total, 20-40 ktonnes per year of CFC-12 and CFC-113 for the next 10-20 years would increase the equivalent effective chlorine loading above the 1980 level, integrated from now until the year the 1980 level is re-attained, by 1%-4% and delay the return to pre-1980 levels by about a year. Significant additional contributions may come from illegal production of halons.

- **Different scenarios of future effective chlorine loading lead to correspondingly different scenarios of future ozone amounts.** The exact ozone response is difficult to predict because of possible interactions with other global atmospheric changes. However, for the purpose of comparing the different scenarios, a simple scaling relationship between equivalent effective stratospheric chlorine loading and ozone depletion can be used if it is assumed that the ozone reductions observed during 1979-1991 were caused exclusively by the simultaneous increase in stratospheric effective chlorine. Within this approximation, the future evolution of ozone reductions follows closely the increases of effective chlorine above 1980 levels, with lowest ozone in about 1997, contemporaneous with maximum effective chlorine loading, and return to baseline (1980) values in 2052 (maximum production scenario) and 2033 (zero emissions scenario). At 45°N, the maximum reduction in the annually averaged ozone is expected to be about 15 Dobson units (DU), or about 4.3% lower than the 1980 value. At 45°S, the maximum reduction in the annually averaged ozone is expected to be about 20 DU, or about 6.2% lower than the 1980 value.

- **Decreases in the ozone column cause increases in surface UV radiation, if other factors (e.g., clouds, aerosols) remain unchanged.** For erythemally effective UV radiation ($UV_{ery}$, the integral of the product of the spectral irradiance and the spectral erythemal sensitivity), the temporal evolution of the scenario follows closely the increases of effective chlorine above 1980 levels, with highest UV irradiances in about 1997, contemporaneous with maximum effective chlorine loading, returning to baseline (1980) values in 2052 (maximum production scenario) and 2033 (zero emissions scenario). At 45°N, the maximum enhancement in the annually averaged $UV_{ery}$ is expected to be about 4.7%, while at 45°S it is estimated to be about 8.1%.

- **Many other biological effects of UV exposure are recognized in addition to erythema and skin cancer induction.** These have a broad range of sensitivity to ozone changes, primarily because of different sensitivities of the biological effects to various wavelengths of radiation. In the few cases for which the biological spectral sensitivity functions (action spectra) are known, scaling factors are derived that allow estimation of the effective biological radiation for each of these effects, relative to the changes in erythemal radiation expected from future changes in effective stratospheric chlorine loading. The potential impacts of higher UV irradiances at the Earth's surface are discussed in detail by the UNEP Panel on the Environmental Effects of Ozone Depletion (UNEP, 1998b).

- **The compilation of Ozone Depletion Potentials (ODPs) has been updated and expanded.** The ODPs of halogen-containing molecules have been updated, relative to the previous Assessment, based on new estimates of atmospheric lifetimes.

## 11.1 INTRODUCTION

Halocarbon compounds produced by human activities are believed to have been the primary agents of the stratospheric ozone reductions observed in the past two decades, as discussed in the previous chapters. International agreements (the Montreal Protocol and its Amendments and Adjustments) have achieved large reductions in the production and atmospheric release of these compounds, and a slowing or turnover of the growth rates has already been observed in the tropospheric concentrations of some specific ozone-destroying substances (see Chapters 1 and 2). Even so, the recovery of the ozone layer is expected to take a number of decades, primarily because of the already high atmospheric burden and long lifetimes of some of these ozone-depleting substances (ODSs). Any additional future emission of ODSs will further delay this recovery.

The purpose of this chapter is to compare a number of possible future ODS production/emission scenarios and to estimate, according to current scientific understanding, their relative impacts on the rate and timing of the recovery of the ozone layer. Of particular interest are the effects of possible additional regulatory measures that define the range of human control available within the context of the atmospheric halogen loading already present.

It must be emphasized that the main question in this chapter is not the exact prediction of future ozone amounts, but rather the sensitivity of the ozone layer to different ODS emissions scenarios, especially those within human control that could result from more stringent or less stringent regulatory measures. The actual future state of the ozone layer is uncertain, not solely from imperfect scientific understanding of the relevant atmospheric processes, but in large part from the present inability to predict natural events such as major volcanic eruptions (which enhance ozone depletion by chlorine; see Chapter 12), factors related to social, political, and economic developments into the next century, and interactions between stratospheric ozone concentrations and other possible global-scale atmospheric changes (e.g., the build-up of greenhouse gases; see again Chapter 12).

The sequence of events considered in this chapter is illustrated schematically in Figure 11-1. Numerous industrially produced halocarbons have been identified as potentially ozone destroying. Following their production, the ODSs may be converted to other compounds (with no emission to the atmosphere or effect on the ozone layer) or put into use where they can be effectively stored for considerable time before release to the atmosphere (e.g., halons in fire extinguishers). The delay times for release of these so-called banks of ODSs depend on their specific applications; in some cases, recovery and destruction of the banks is possible. Eventual emissions lead to the build-up of substantial reservoirs in the lower atmosphere (troposphere), where for many ODSs the destruction rates are slow due to their chemical inertness. However some other ODSs are destroyed mainly in the troposphere (e.g., hydrochlorofluorocarbons (HCFCs), methyl bromide), and for a few others, tropospheric destruction is also significant (e.g., Halon-1211). The surviving ODSs are gradually transported to the stratosphere. At sufficiently high altitudes in the stratosphere, enough short-wavelength ultraviolet (UV) radiation is available to photodissociate the ODSs and thus release ozone-destroying halogen

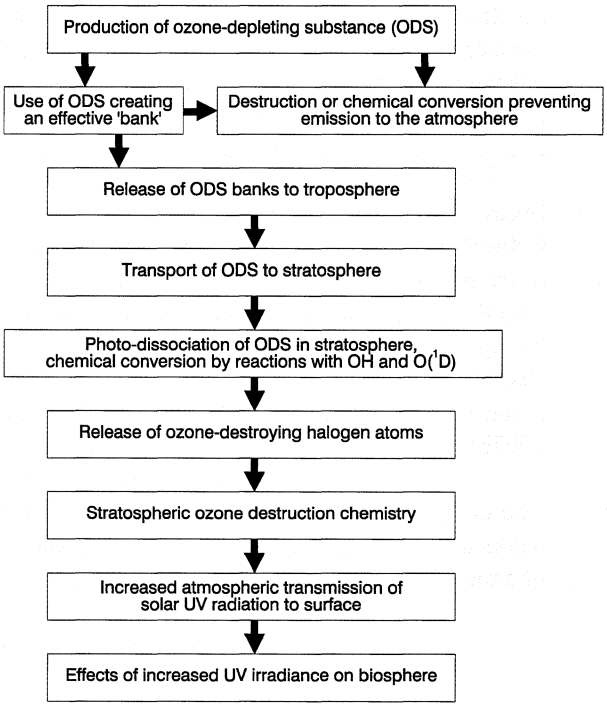


**Figure 11-1.** Chain of events connecting production of ozone-depleting substances (ODSs) to ultimate environmental effects of increased UV irradiance at the Earth's surface.

atoms. Reactions of ODSs with hydroxyl radicals (OH) and excited-state oxygen atoms ($O(^1D)$) also result in the release of ozone-destroying halogen atoms in the stratosphere. Before eventual removal from the stratosphere, these halogens can lead to substantial reductions of the ozone layer and therefore to an increase in the transmission of solar UV radiation to the Earth's surface (see Chapter 9), especially in the biologically important ultraviolet-B (UV-B) wavelength band (280-315 nm). Such increases in surface UV radiation can lead to increased stresses on the biosphere. A number of detrimental effects of UV exposure have been identified, most prominently the induction of skin cancer, ocular damage, immune system suppression, and other potential human and animal health effects; damage to terrestrial and aquatic plants; and probably complex and subtle effects on ecosystem vitality and composition. The environmental consequences of increased UV radiation are discussed in detail in the report of the UNEP Panel on the Environmental Effects of Ozone Depletion (UNEP, 1998b).

In this chapter, insofar as the purpose is primarily to evaluate the relative effects of different ODS production/emission scenarios, this sequence of events is represented by applying a series of scaling relationships: the relative ozone-destroying effectiveness of the many different ODS compounds is parameterized here by their respective Ozone Depletion Potentials (ODPs; see WMO, 1995); their cumulative contribution to the stratospheric halogen content is represented by the equivalent effective stratospheric chlorine (EESC, which includes contributions from both chlorine and bromine species; see Section 11.4.1 for its definition); the relation between EESC and stratospheric ozone is taken from the observed ozone reductions and contemporaneous EESC increases in recent years (here, 1980 to 1990); and the changes in biologically active surface UV irradiance, resulting from stratospheric ozone changes, are estimated using radiative transfer calculations assuming that all other factors affecting surface UV radiation (e.g., clouds, aerosols, local pollutants) are held constant. It should be recognized that none of these factors are expected to remain strictly constant, although at present even the sign of possible future changes is unknown. The ultimate impacts of surface UV radiation changes on the biosphere are not discussed in detail here (but see UNEP, 1998b).

## 11.2 CURRENT CONTROL MEASURES AND ODPs

In 1985 the first international agreement to protect the ozone layer was signed: the Vienna Convention. This was followed in 1987 by the first international control measures, i.e., the Montreal Protocol on Substances that Deplete the Ozone Layer. Since then the Montreal Protocol has been amended and adjusted several times, with major changes occurring in 1990 (London Amendments), in 1992 (Copenhagen Amendments), in 1995 (Vienna Adjustments), and the latest in 1997 (Montreal Amendments). The Vienna Convention has been ratified by 166 countries, the Montreal Protocol by 165, the London Amendments by 121 countries, and the Copenhagen Amendments by 79 (as of June 1998).

The control measures in the Protocol apply to the production and consumption of classes of ozone-depleting substances (Annexes), i.e., chlorofluorocarbons (CFCs), halons, hydrochlorofluorocarbons (HCFCs), hydrobromofluorocarbons (HBFCs), carbon tetrachloride ($CCl_4$), methyl chloroform ($CH_3CCl_3$), and methyl bromide ($CH_3Br$). This means that it is permissible to exchange a certain amount of production from one substance to another in the same class, provided the total production is within the limits set by the Protocol. Within a class, substances are weighted by their Ozone Depletion Potentials (ODPs), defined as the integrated change in total ozone per unit mass emission of a specific compound, relative to the integrated change in total ozone per unit mass emission of CFC-11. The calculation of ODPs by several methods was described in detail in WMO (1995), and updated values are shown in Table 11-1. Significant revision is noted for methyl bromide, because of changes in estimates of its lifetime, and to a lesser extent for several HCFCs, because of revised estimates of the lifetime of methyl chloroform (see Chapter 2), from which estimates of lifetimes of HCFCs are scaled (Wuebbles *et al.*, 1998).

In the Montreal Protocol and its Amendments and Adjustments, a distinction is made, with respect to the control measures, between developing and developed countries. Any country that is a developing country and whose annual calculated consumption of CFCs and halons is less than 0.3 kg per year per capita is entitled to a delay of 10 years or more (see Table 11-2) to comply with the control measures that hold for developed countries. Countries for which this applies are termed in the Protocol as Article 5 paragraph 1 countries. Other

**Table 11-1. Steady-State Ozone Depletion Potentials (ODPs).**

| | Trace Gas | Model-Derived ODP | Semiempirical ODP | ODP in Current Montreal Protocol[1] |
|---|---|---|---|---|
| Annex A-I | CFC-11 | 1.0 | 1.0 | 1.0 |
| | CFC-12 | 0.82 | 0.9 | 1.0 |
| | CFC-113 | 0.90 | 0.9 | 0.8 |
| | CFC-114 | 0.85 | | 1.0 |
| | CFC-115 | 0.40 | | 0.6 |
| Annex A-II | $CF_3Br$ (Halon-1301) | 12 | 13 | 10.0 |
| | $CF_2ClBr$ (Halon-1211) | 5.1 | 5 | 3.0 |
| | $C_2F_4Br_2$ (Halon-2402) | | | 6.0 |
| Annex B-II | $CCl_4$ | 1.20 | | 1.1 |
| Annex B-III | $CH_3CCl_3$ | 0.11 [2] | 0.12 | 0.1 |
| Annex C-I | HCFC-22 | 0.034 [2] | 0.05 | 0.055 |
| | HCFC-123 | 0.012 [2] | 0.02 | 0.02* |
| | HCFC-124 | 0.026 [2] | | 0.022* |
| | HCFC-141b | 0.086 [2] | 0.1 | 0.11* |
| | HCFC-142b | 0.043 [2] | 0.066 | 0.065* |
| | HCFC-225ca | 0.017 [2] | 0.025 | 0.025 |
| | HCFC-225cb | 0.017 [2] | 0.03 | 0.033 |
| Annex E | $CH_3Br$ | 0.37 [2] (0.2-0.5)[3] | 0.57 | 0.6 |
| Others | $CF_3I$ | <0.008 [2] | <0.008 | |
| | $CH_3Cl$ | 0.02 | | |
| | HFC-134a | $<1.5\times10^{-5}$ | $<5\times10^{-4}$ | |
| | HFC-23 | $<4\times10^{-4}$ | | |
| | HFC-125 | $<3\times10^{-5}$ | | |

* Corresponding isomer.
(1) Defined for regulatory purposes (UNEP, 1996).
(2) Update from WMO (1994) based on Wuebbles *et al.* (1998).
(3) See discussion in Chapter 2.

countries are termed Non-Article 5 paragraph 1 countries and comprise most of the developed countries.

Table 11-2 shows the current (since Montreal, September 1997) control measures for the different classes of substances and for both developed and developing countries. Currently the production and consumption of CFCs, halons, carbon tetrachloride, and methyl chloroform are phased out in the developed countries. The consumption (production+imports-exports) of HCFCs and the production of methyl bromide are frozen in developed countries and have to be phased out by 2030 and 2005, respectively. The currently phased-out substances are still allowed to be produced by developed countries for some essential uses, and for use by the developing countries to meet their basic domestics needs. Developing countries must phase out CFCs, halons, and carbon tetrachloride in 2010 and methyl chloroform in 2015; regulation of HCFCs begins

in 2016 with complete phase-out by 2040; and the production of methyl bromide has to be frozen in 2002 and phased out in 2015.

## 11.3 FUTURE EMISSIONS SCENARIOS

A set of future production and emission scenarios was constructed for ozone-depleting substances. The current control measures (Table 11-2) are used as the basis for the scenarios. Scenario A1 (see Tables 11-3 and 11-4) is the Baseline scenario, following the current regulations of the Montreal Protocol. Scenarios A2 and A4 describe the extreme cases with zero emissions and zero production, respectively, of ozone-depleting substances (ODSs). Scenario A3 describes the maximum production of ODSs allowed with the current control measures. Most other scenarios describe additional control measures on top of the Baseline scenario (A1). The additional control measures considered are a faster phase-out of CFCs, HCFCs, and methyl bromide, and the destruction of halons in existing equipment (halon banks). Also considered are the effects of illegal production of ODSs and essential-use exemptions. The potential effect of the different Amendments and Adjustments to the Montreal Protocol are also estimated. Table 11-3 gives the details of the scenarios.

The scenarios defined in this chapter are not designed to describe in the best possible way the future behavior of the chlorine and bromine species and of the depletion of the ozone layer, but rather to calculate the sensitivity of the EESC (indicator for the ozone layer; see Section 11.4.1) to possible additional future control measures, and to examine the effects of incomplete compliance with the Montreal Protocol. These scenarios are long-term scenarios, not intended to describe variations on time scales of a few years. Furthermore, with these scenarios we consider only their impact on the future ozone layer, not their role in other environmental issues such as, e.g., global warming. Most of the ODSs are greenhouse gases, and substances used as alternatives (e.g., HCFCs and hydrofluorocarbons (HFCs)) have smaller Ozone Depletion Potentials but are potent greenhouse gases (IPCC, 1996). Consideration of the effects of ODS reductions on different environmental issues could impose different constraints on future ODS scenarios (Wuebbles and Calm, 1997), which, however, are not considered here.

### 11.3.1 Baseline Scenario

The basis of the production and emission data of the Baseline scenario (A1) used here is given in Table 11-4. The emission data of all other scenarios are calculated by applying the conditions given in Table 11-3 to the production or emissions data of the Baseline (= reference) scenario. The scenarios with different control measures additional to the Montreal Amendments (1997) are assumed to start in 1996. The initial conditions for the scenarios (emissions and amount of substances present in the equipment as of 1995) are chosen to yield agreement with the atmospheric concentrations recently measured by the National Oceanic and Atmospheric Administration (NOAA) Climate Monitoring and Diagnostics Laboratory (CMDL) (Elkins *et al.*, 1998; Montzka *et al.*, 1996) and the Atmospheric Lifetime Experiment/Global Atmospheric Gases Experiment/Advanced Global Atmospheric Gases Experiment (ALE/GAGE/AGAGE) networks (Prinn *et al.*, 1998; see Chapters 1 and 2 of this Assessment). In Table 11-5 the ODS emissions for the Baseline scenario A1 are shown, while in Figure 11-2 the emissions are plotted by classes of substances (Annexes) weighted by their ODPs. Emissions of CFCs, carbon tetrachloride, and methyl chloroform have been decreasing since approximately the end of the 1980s (AFEAS, 1997). Before the phase-out of CFCs in the developed countries in 1996, the rate at which the emissions decreased depended on the amount produced and consumed and on the type of application and corresponding release time of the CFCs. The production of CFCs in developing countries was much smaller and is expected to be much smaller than the quantities produced in the developed countries in the 1980s; therefore, the emission from 1996 onward will be determined more by the quantities in the banks than by new production.

The production of CFCs reported by the developing countries to UNEP (1997b) is 107 ktonnes per year (ODP-weighted), while the maximum allowed production of CFCs for developing countries is 149 ktonnes per year from 1996 to 2004 (UNEP, 1994b). The production of CFCs in developing countries in 1995 in the Baseline scenario is 124 ktonnes per year (or 120 ktonnes-ODP weighted), increasing gradually to the maximum allowed production of 149 ktonnes per year in 2002.

The emissions are, for computational ease, calculated as a fraction of the bank for all scenarios. This

**Table 11-2. Current (Montreal Amendments, September 1997 (UNEP, 1997d)) reduction and phase-out schedules for ozone-depleting substance (ODS) production and consumption[1,2] for developed countries (Non-Article 5) and developing countries (Article 5).**

| | Developed countries (Non-Article 5) | Developing countries (Article 5) |
|---|---|---|
| CFC-11, -12, -113, -114, -115 (Annex A-I) | Base level[3] = 1986<br>1989: Freeze (July 1)[4]<br>1994: -75%<br>1996: Phase-out | Base level = Average of 1995-1997<br>1999: Freeze (July 1)<br>2005: -50%<br>2007: -85%<br>2010: Phase-out |
| Halons (Annex A-II) | Base level = 1986<br>1992: Freeze<br>1994: Phase-out | Base level = Average of 1995-1997<br>2002: Freeze<br>2005: -50%<br>2010: Phase-out |
| Other CFCs (Annex B-I) | Base level = 1989<br>1993: -20%<br>1994: -75%<br>1996: Phase-out | Base level = Average of 1998-2000<br>2003: -20%<br>2007: -85%<br>2010: Phase-out |
| Carbon tetrachloride (Annex B-II) | Base level = 1989<br>1995: -85%<br>1996: Phase-out | Base level = Average of 1998-2000<br>2005: -85%<br>2010: Phase-out |
| Methyl chloroform (Annex B-III) | Base level = 1989<br>1993: Freeze<br>1994: -50%<br>1996: Phase-out | Base level = Average of 1998-2000<br>2003: Freeze<br>2005: -30%<br>2010: -70%<br>2015: Phase-out |
| HCFCs consumption (Annex C-I) | Base level = 1989 + 2.8% of 1989 CFC<br>1996: Freeze<br>2004: -35%<br>2010: -65%<br>2015: -90%<br>2020: -99.5%<br>2030: Phase-out | Base level = 2015<br>2016: Freeze<br>2040: Phase-out |
| HBFCs (Annex C-II) | 1996: Phase-out | 1996: Phase-out |
| Methyl bromide (Annex E) | Base level = 1991<br>1995: Freeze<br>1999: -25%<br>2001: -50%<br>2003: -70%<br>2005: Phase-out + exemptions | Base level = Average of 1995-1998<br>2002: Freeze<br>2005: -20%<br>2015: Phase-out + exemptions |

[1] Exemptions to the production and consumption of ODS are allowed in developed countries for essential uses and to meet the basic domestic needs of developing countries. The latter may be maximally 10-15% of the base-level production (CFCs, carbon tetrachloride, methyl chloroform, halons, and methyl bromide).

[2] In the Montreal Protocol, consumption is defined as production plus imports minus exports.

[3] The reductions are always relative to the base level.

[4] The control measures take effect on January 1 of the year indicated, unless indicated otherwise.

**Table 11-3. Description of scenarios for ozone-depleting substances (ODSs)[1].** The Baseline scenario A1 (see Table 11-2) is used as the reference scenario for all other scenarios. When nothing is indicated for a substance, the values for the Baseline scenario are used.

| | Developed countries (Non-Article 5) | Developing countries (Article 5) |
|---|---|---|
| **Maximum/Minimum scenarios:** | | |
| **A1**: Baseline (Montreal Amendments 1997) = **Reference** | Baseline scenario according to the latest Amendments (1997) of the Montreal Protocol; see Table 11-4. | |
| **A2**: Zero emission | Emissions of all ODSs set to zero from 1999 onward; i.e., banks destroyed and production stopped. | |
| **A3**: Maximum production | Maximum production allowed for all ODSs with current (Montreal, 1997) control measures, including approved essential uses but no illegal production, i.e., A1 scenario plus 15% additional production (of the base level of CFC-11, CFC-12, CFC-113, carbon tetrachloride, and methyl chloroform) in developed countries for use in developing countries (data from UNEP (1994b)). | |
| **A4**: Zero production | Production of all ODSs set to zero from 1999 onward. | |
| **CFC and carbon tetrachloride scenario:** | | |
| **B3**: Phase-out of CFCs and $CCl_4$ by 2004 | Production of CFCs and $CCl_4$ set to zero from 2004 onward. | |
| **HCFC scenarios:** | | |
| **C1**: Reduce HCFC cap to 2% | Reducing the HCFC consumption[1] cap from 2.8% to 2.0% beginning in 2000 and phase-out in 2030. | |
| **C2**: Cap at 2% and phase-out of HCFCs by developed countries in 2015 | Reducing the HCFC consumption cap from 2.8% to 2.0% beginning in 2000 and advancing the phase-out to 2015, with interim cuts of 35% in 2004, 60% in 2007, 80% in 2010, and 95% in 2013. | |
| **C3**: Global phase-out of HCFCs by 2004 | Production of HCFCs set to zero from 2004 onward. | |
| | **Developed countries (Non-Article 5)** | **Developing countries (Article 5)** |
| **Methyl bromide scenario:** | | |
| **D3**: Phase out $CH_3Br$ by 2004 | Production of methyl bromide set to zero from 2004 onward. | |
| **Essential use scenarios:** | | |
| **E1**: No essential uses | All assigned essential uses (CFC-11, CFC-12, CFC-113, CFC-114, $CH_3CCl_3$, and Halon-2402) set to zero from 1996 onward (see Table 11-4) (UNEP, 1997a). | |
| **E2**: Essential uses for metered dose inhalers up to 2004 | Essential uses for metered dose inhalers (MDIs) extended for the years 2000-2004: 3 ktonnes of CFC-11, 6 ktonnes of CFC-12, and 1 ktonne of CFC-114. | |
| **Illegal production scenarios:** | | |
| **F1**: Illegal CFC production: low estimate | Noncompliance with the Protocol: low estimate for illegal CFC production: total of 20 ktonnes per year from 1996 through 2005 (CFC-12 and CFC-113 in a 2:1 ratio). | |

## Table 11-3, continued

| | Developed countries (Non-Article 5) | Developing countries (Article 5) |
|---|---|---|
| **F2**: Illegal CFC production: high estimate | Noncompliance with the Protocol: high estimate for illegal CFC production: total of 40 ktonnes per year from 1996 through 2015 (CFC-12 and CFC-113 in a 2:1 ratio). | |
| **F3**: Illegal halon production | Noncompliance with the Protocol: illegal production of Halon-1211: 2 ktonnes per year from 1996 through 2005. | |
| **Halon destruction scenarios:** | | |
| **G1**: Destruction of halon banks in 2000 | No emission of halons (including from existing equipment) after 1999. | |
| **G2**: Destruction of Halon-1211 bank in 2000 | No emission of Halon-1211 (including from existing equipment) after 1999. | |
| **G3**: Destruction of Halon-1301 bank in 2000 | No emission of Halon-1301 (including from existing equipment) after 1999. | |
| **G4**: Destruction of Halon-2402 bank in 2000 | No emission of Halon-2402 (including from existing equipment) after 1999. | |
| **Amendments to the Protocol:** | | |
| **H1**: No Protocol | No limitations on the production and consumption of ODSs: a 3% annual growth of CFCs, carbon tetrachloride, methyl chloroform, halons, HCFC-22, and anthropogenic methyl bromide from 1986 onward. A 3% annual growth was also used in WMO (1995). | |
| **H2**: Montreal Protocol (1987) | Freeze of CFCs in 1989, reduction of CFCs by 20% in 1994, 50% in 1999; freeze in halons in 1992. Other species as in scenario H1; additional HCFC-22 production to fully compensate the reduced CFC and carbon tetrachloride production. | Same growth as in No Protocol case. |
| **H3**: London Amendments (1990) | Phase-out of CFCs, carbon tetrachloride, and halons by 2000 and methyl chloroform by 2005 (plus interim reductions). Allowing an additional 15% production after phase-out for use in developing countries. Other species as in scenario H1; additional HCFC-22 production to fully compensate by mass the reduced CFC and carbon tetrachloride production. | Applying the London Amendments with a 10-year grace period. Additional HCFC-22 production to fully compensate by mass the reduced CFC and carbon tetrachloride production. |
| **H4**: Copenhagen Amendments (1992) | Phase-out of CFCs, carbon tetrachloride, and methyl chloroform by 1996, halons by 1994, and HCFCs by 2030. This equals scenario A1 except methyl bromide fixed at 1991 level and a 3.1% cap for HCFCs. | Applying the Copenhagen Amendments with a 10-year grace period. This equals scenario A1 except a 3% annual growth in methyl bromide and a 3% annual growth in HCFCs until phase-out in 2040. |
| **H5**: Vienna Adjustments (1995) | HCFC cap reduced to 2.8% and methyl bromide emissions reduced by 25% in 2001, 50% in 2003, and 100% in 2010. The rest as in the A1 scenario. | Freeze of HCFC consumption by 2016 and phase-out in 2040 and a freeze in methyl bromide emissions by 2002. This equals scenario A1 except methyl bromide emissions constant at 1991 level. |

[1] HCFC regulations apply to consumption. In these scenarios consumption and production are considered equal.

## Table 11-4. Basis of the production and emission estimates[1] for the Baseline scenario (A1).

| Class of substances | Production and emission description |
|---|---|
| CFCs | • Developed countries: production is zero.<br>• Developing countries: production increasing from the 1995 value to the maximum allowed value (UNEP, 1994b) in 2002. Reduction scheme according to the Protocol.<br>• Essential uses for developed countries for CFC-11, CFC-12, CFC-113, and CFC-114 as approved by UNEP (1997a). No essential uses after 1999.<br>• Bank in 1995: 1219 ktonnes for CFC-11, 791 ktonnes for CFC-12, 23.5 ktonnes for CFC-113, 22.6 ktonnes for CFC-114, and 31.2 ktonnes for CFC-115.<br>• Emissions[2] based on analysis of emission patterns during the period 1990-1995: 9% of the calculated bank of the previous year for CFC-11, 25% for CFC-12, 14% for CFC-114, and 30% for CFC-115. The emission of CFC-113 is 50% of the production of the previous year plus 50% of the production of the current year. |
| Halons | • Developed countries: production is zero.<br>• Developing countries: adapted from allowances under the Protocol (UNEP, 1994b) and reported data (UNEP, 1997b,c) (see McCulloch, 1992; Fraser *et al.*, 1998). Reduction schedule according to the Protocol.<br>• Essential uses for the developed countries for Halon-2402 as approved by UNEP (1997a). No essential uses after 1998.<br>• Bank in 1995: 67.6 ktonnes for Halon-1211, 75.2 ktonnes for Halon-1301, and 5.3 ktonnes for Halon-2402.<br>• Emissions: 11% of the calculated bank of the previous year for Halon-1211, 4% for Halon-1301, and 20% for Halon-2402 (SORG, 1996). |
| Carbon tetrachloride | • The emissions are linked to the production of CFC-11 and CFC-12 as well as other production processes. Based on historic production and emission data, the emission of carbon tetrachloride is assumed to be equal to 8% of the production of CFC-11 and CFC-12 (Simmonds *et al.*, 1998). Taking the different molecular masses into account, the emission of carbon tetrachloride is represented by 8% of [(154/137.5) × production CFC-11 + (154/121) × production CFC-12]. |
| Methyl chloroform | • Developed countries: production is zero (Midgley *et al.*, 1998).<br>• Developing countries: production based on Midgley and McCulloch (1995) and UNEP (1994b). Reduction schedule according to the Protocol.<br>• Essential uses approved for 1996-2001.<br>• The emission is in the same year as the production. |
| HCFCs | • Developed countries: production capped at the HCFC production in 1989 plus 2.8% of the CFC production in 1989 (=33011 ODP tonnes per year) with distribution among the products as in the revised IS92a scenario (IPCC, 1996). No additional production for developing countries.<br>• Developing countries: production is the difference between IS92a (IPCC, 1996) and the production in the developed countries. These numbers were interpolated from 5-year interval data (IPCC, 1996) to 1-year intervals. From 2016 to 2039 the production is fixed at the 2015 level.<br>• Bank in 1995: 768 ktonnes for HCFC-22, 148 ktonnes for HCFC-141b, 76.1 ktonnes for HCFC-142b, and zero for HCFC-123.<br>• Emissions: 28% of the calculated bank of the previous year for HCFC-22, 30% for HCFC-141b, 38% for HCFC-142b, and 5% for HCFC-123. |
| Methyl bromide | • Developed countries: in 1996 structural emissions of 4 ktonnes per year and agricultural emissions of 17 ktonnes per year (SORG, 1996 and Chapter 2), decreasing to zero in 2005 according to the Protocol.<br>• Emission in developing countries (agricultural) and critical use exemptions: 18 ktonnes per year for all years (1996-2100).<br>• Other emissions (e.g., natural) of methyl bromide, derived from the total loss of methyl bromide using a lifetime of 0.7 years (Chapter 2), amount to 167 ktonnes per year. |

1 The assumptions made in this scenario differ slightly from those made in the previous Assessment (WMO, 1995). See also Section 11.4.4.

2 The emissions are, for computational ease, calculated as a fixed percentage (release fraction) of the bank of the previous year. These release fractions are not necessarily the representation of the actual emission from a specific application.

**Table 11-5. Emissions of ozone-depleting substances (ktonnes per year) in the Baseline scenario (A1).**

| Year | CFC-11 | CFC-12 | CFC-113 | CFC-114 | CFC-115 | $CCl_4$ | $CH_3CCl_3$ | HCFC-22 | HCFC-141b | HCFC-142b | HCFC-123 | Halon-1211 | Halon-1301 | Halon-2402 | $CH_3Br$ |
|---|---|---|---|---|---|---|---|---|---|---|---|---|---|---|---|
| 1990 | 250 | 371 | 236 | 10.3 | 12.2 | 63 | 718 | 178 | 0 | 9 | 0 | 10.3 | 3.4 | 1.8 | 206 |
| 1991 | 210 | 352 | 184 | 6.3 | 12.6 | 49 | 635 | 193 | 0 | 13 | 0 | 10.4 | 3.9 | 1.8 | 206 |
| 1992 | 172 | 330 | 149 | 5.2 | 12.6 | 49 | 593 | 194 | 14 | 41 | 0 | 10.2 | 3.9 | 1.8 | 206 |
| 1993 | 138 | 279 | 99 | 4.6 | 12.6 | 44 | 380 | 190 | 14 | 26 | 0 | 9.6 | 3.4 | 1.8 | 206 |
| 1994 | 118 | 236 | 61 | 4.0 | 11.9 | 45 | 283 | 195 | 29 | 25 | 0 | 8.9 | 3.2 | 1.8 | 206 |
| 1995 | 105 | 173 | 48 | 3.1 | 10.9 | 40 | 234 | 183 | 46 | 29 | 0 | 7.8 | 3.1 | 1.8 | 206 |
| 1996 | 110 | 198 | 22 | 3.2 | 9.4 | 12 | 5 | 215 | 45 | 29 | 0 | 7.4 | 3.0 | 1.1 | 206 |
| 1997 | 103 | 169 | 22 | 2.9 | 6.6 | 12 | 5 | 242 | 62 | 35 | 2 | 7.8 | 2.9 | 0.9 | 206 |
| 1998 | 97 | 149 | 22 | 2.7 | 4.6 | 12 | 5 | 282 | 69 | 42 | 5 | 8.0 | 2.8 | 0.8 | 206 |
| 1999 | 91 | 133 | 23 | 2.5 | 3.2 | 12 | 5 | 318 | 69 | 46 | 9 | 8.1 | 2.8 | 0.7 | 201 |
| 2000 | 86 | 122 | 23 | 2.2 | 2.2 | 12 | 5 | 350 | 65 | 49 | 14 | 7.9 | 2.7 | 0.6 | 201 |
| 2001 | 81 | 113 | 24 | 1.9 | 1.6 | 12 | 5 | 392 | 64 | 54 | 20 | 7.6 | 2.6 | 0.4 | 196 |
| 2002 | 77 | 106 | 25 | 1.6 | 1.1 | 12 | 5 | 423 | 63 | 57 | 25 | 7.2 | 2.6 | 0.4 | 195 |
| 2003 | 73 | 102 | 25 | 1.4 | 0.8 | 12 | 5 | 445 | 63 | 59 | 30 | 6.7 | 2.5 | 0.3 | 190 |
| 2004 | 70 | 99 | 25 | 1.2 | 0.5 | 12 | 5 | 461 | 63 | 60 | 35 | 6.3 | 2.4 | 0.2 | 189 |
| 2005 | 67 | 96 | 19 | 1.0 | 0.4 | 6 | 3 | 432 | 57 | 54 | 38 | 5.9 | 2.3 | 0.2 | 181 |
| 2006 | 62 | 83 | 16 | 0.9 | 0.3 | 6 | 3 | 424 | 55 | 52 | 41 | 5.6 | 2.3 | 0.1 | 181 |
| 2007 | 58 | 74 | 11 | 0.8 | 0.2 | 3 | 3 | 418 | 53 | 50 | 43 | 5.0 | 2.2 | 0.1 | 181 |
| 2008 | 54 | 61 | 9 | 0.7 | 0.1 | 3 | 3 | 414 | 51 | 49 | 46 | 4.5 | 2.1 | 0.1 | 181 |
| 2009 | 50 | 51 | 7 | 0.6 | 0.1 | 3 | 3 | 412 | 50 | 48 | 48 | 4.1 | 2.1 | 0.1 | 181 |
| 2010 | 46 | 44 | 4 | 0.5 | 0.1 | 0 | 1 | 412 | 49 | 47 | 51 | 3.7 | 2.0 | 0.1 | 181 |
| 2011 | 42 | 33 | 2 | 0.4 | 0.0 | 0 | 1 | 368 | 43 | 40 | 51 | 3.3 | 1.9 | 0.0 | 181 |
| 2012 | 38 | 25 | 2 | 0.4 | 0.0 | 0 | 1 | 336 | 39 | 36 | 51 | 3.0 | 1.8 | 0.0 | 181 |
| 2013 | 35 | 19 | 0 | 0.3 | 0.0 | 0 | 1 | 313 | 36 | 33 | 52 | 2.6 | 1.8 | 0.0 | 181 |
| 2014 | 32 | 14 | 0 | 0.3 | 0.0 | 0 | 1 | 296 | 34 | 32 | 52 | 2.3 | 1.7 | 0.0 | 181 |
| 2015 | 29 | 10 | 0 | 0.2 | 0.0 | 0 | 0 | 283 | 33 | 31 | 53 | 2.1 | 1.6 | 0.0 | 167 |
| 2016 | 26 | 8 | 0 | 0.2 | 0.0 | 0 | 0 | 232 | 27 | 24 | 51 | 1.9 | 1.6 | 0.0 | 167 |
| 2017 | 24 | 6 | 0 | 0.2 | 0.0 | 0 | 0 | 196 | 23 | 20 | 50 | 1.7 | 1.5 | 0.0 | 167 |
| 2018 | 22 | 4 | 0 | 0.1 | 0.0 | 0 | 0 | 169 | 20 | 17 | 49 | 1.5 | 1.4 | 0.0 | 167 |
| 2019 | 20 | 3 | 0 | 0.1 | 0.0 | 0 | 0 | 150 | 18 | 16 | 48 | 1.3 | 1.4 | 0.0 | 167 |
| 2020 | 18 | 2 | 0 | 0.1 | 0.0 | 0 | 0 | 137 | 16 | 15 | 46 | 1.2 | 1.3 | 0.0 | 167 |
| 2025 | 11 | 1 | 0 | 0.1 | 0.0 | 0 | 0 | 77 | 10 | 9 | 40 | 0.7 | 1.1 | 0.0 | 167 |
| 2030 | 7 | 0 | 0 | 0.0 | 0.0 | 0 | 0 | 66 | 9 | 8 | 34 | 0.4 | 0.9 | 0.0 | 167 |
| 2035 | 4 | 0 | 0 | 0.0 | 0.0 | 0 | 0 | 63 | 8 | 8 | 30 | 0.2 | 0.7 | 0.0 | 167 |
| 2040 | 3 | 0 | 0 | 0.0 | 0.0 | 0 | 0 | 62 | 8 | 8 | 27 | 0.1 | 0.6 | 0.0 | 167 |
| 2060 | 0 | 0 | 0 | 0.0 | 0.0 | 0 | 0 | 0 | 0 | 0 | 10 | 0.0 | 0.3 | 0.0 | 167 |
| 2080 | 0 | 0 | 0 | 0.0 | 0.0 | 0 | 0 | 0 | 0 | 0 | 3 | 0.0 | 0.1 | 0.0 | 167 |
| 2100 | 0 | 0 | 0 | 0.0 | 0.0 | 0 | 0 | 0 | 0 | 0 | 1 | 0.0 | 0.1 | 0.0 | 167 |

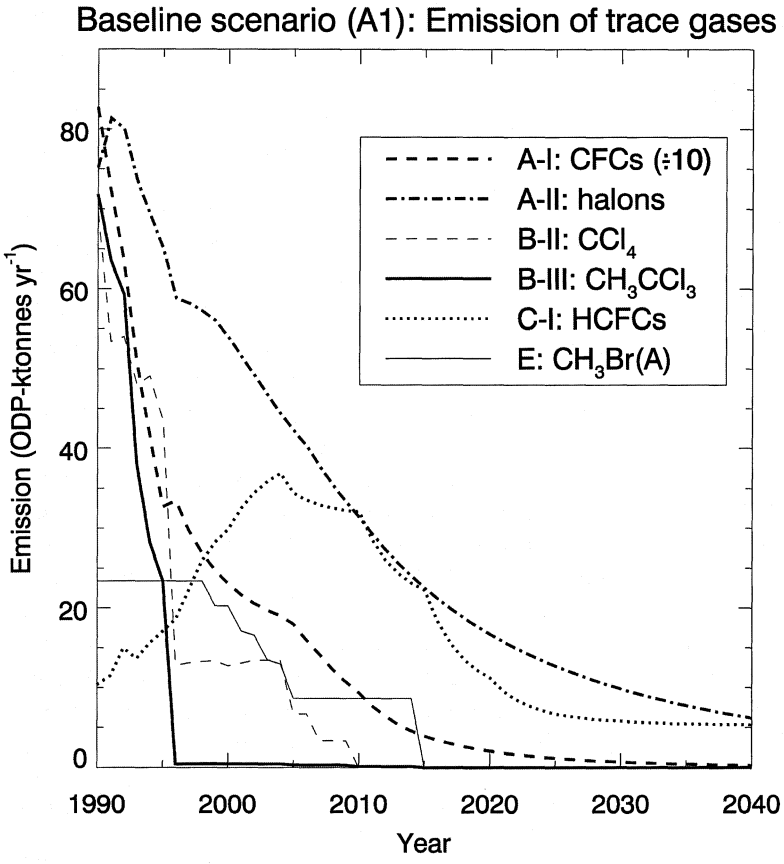


**Figure 11-2.** Emissions (ODP-weighted) of ozone-depleting substances of the Baseline scenario (A1). Note that CFC emissions were divided by a factor of 10 to be shown in this graph. For methyl bromide only the anthropogenic emissions are plotted. Substances are grouped by the Annexes (A-I, A-II,... E) defined in the Montreal Protocol.

fraction is based on an analysis of the quantities present in, and emitted from, the banks over the years 1990-1995. The banks and the emissions in this period are based on both emission inventories (e.g., AFEAS, 1997) and inverse modeling of the change in observed atmospheric concentrations. Each substance has its own release fraction, which is assumed to be constant from 1996 to 2100. Recycling and recovery of halocarbons are not considered explicitly in the scenarios.

### 11.3.2 Maximum and Minimum

After the phase-out date of CFCs, carbon tetrachloride, methyl chloroform, and halons in the developed countries, these substances are still allowed to be produced there for use in developing countries. The amount produced is maximally 15% of the base-level production. This additional production is accounted for in the Maximum production scenario (A3) for CFC-11, CFC-12, CFC-113, carbon tetrachloride, and methyl chloroform. The annual CFC production in developed countries for use in developing countries is almost equal to the maximum allowable production in developing countries, i.e., 149 ktonnes per year in developing countries (through 2004, with lower values from 2005 to 2009) versus 152 ktonnes per year in developed countries (through 2009) (UNEP, 1994b). Additional allowed production of halons in developed countries after 1994 is ignored in scenario A3, because the production of halons in developed countries already ceased in 1994.

It does not seem very likely that developed countries will produce ODSs up to maximum allowed values. For example, production in developed countries for 1990-1993 was approximately 40% below the allowed limits (AFEAS, 1997), and developing countries may also be below their allowed limits.

While scenario A3 describes the maximum production allowed within the current regulations, scenario A2 is a Zero emission case: all emissions are set to zero from 1999 onward, which would require an immediate stop in production and consumption of all ODSs, and destruction or prevention of emission of all ODSs from existing or new applications. This scenario,

although unrealistic from a practical point of view, describes, together with the Maximum production scenario A3, the maximum range that currently exists for additional control measures to protect the ozone layer by reducing the emissions of ODSs.

### 11.3.3 Carbon Tetrachloride and Methyl Chloroform

Historically, the emission of carbon tetrachloride was well represented by approximately 8% of the production of CFC-11 and CFC-12 (Simmonds *et al.*, 1998). This 8% is considered to contain both emissions from production losses of CFCs and fugitive emissions from carbon tetrachloride usage itself. In the future scenarios of Table 11-3, carbon tetrachloride emissions are therefore described by the same relationship. Considering the rapid decline in the atmospheric concentration of carbon tetrachloride (Chapter 1), the 8% might overestimate the emissions in the future scenarios. On the other hand, the maximum allowed carbon tetrachloride production (UNEP, 1994b) could result in an emission amount that is a factor of 3 larger. After complete phase-out of CFCs in 2010, the emission of carbon tetrachloride is expected to be essentially zero.

Methyl chloroform production in the developed world has ceased already (Midgley *et al.*, 1998), while the maximally allowed production of methyl chloroform in developing countries is 4.6 ktonnes per year through 2004, with lower levels thereafter. In the A3 scenario, developed countries are allowed to produce 98.4 ktonnes per year to satisfy the demands in developing countries (UNEP, 1994b).

### 11.3.4 Halons

In the Baseline scenario (Table 11-4), the production of halons is zero from 1995 onward in developed countries (UNEP, 1997b). In developing countries, the production of halons in 1995 is 41 ktonnes per year (ODP-weighted) (UNEP, 1997b). From 1996 onward this amount is extrapolated and reduced according to data from UNEP (1997c) and the limits of the Montreal Protocol, and distributed in the Baseline scenario between Halon-1211 and Halon-1301 (Fraser *et al.*, 1998). The production is larger than the maximum allowed production envisaged by UNEP (1994b).

The calculated bank of Halon-1211 in 1995 is 67.6 ktonnes, which is close to the 65.3 ktonnes (for Western Europe, Australia, North America, and Japan) reported by the Technology and Economic Assessment Panel (TEAP) of UNEP (1998a). The corresponding Halon-1211 emission we use for 1996 is 7.4 ktonnes per year (Table 11-5), which is more than twice the emission reported by TEAP of 3.4 ktonnes per year (UNEP, 1998a). The total emission of Halon-1211 in the 1980s and 1990s reported by TEAP is less than half of our emissions and cannot sustain the observed growth in atmospheric concentration (see Section 1.2.3 and Butler *et al.*, 1998).

The calculated bank of Halon-1301 in 1995 is 75.2 ktonnes compared with 38.0 ktonnes (for Western Europe, Australia, North America, and Japan) reported by TEAP (UNEP, 1998a). This difference is caused by the larger production of Halon-1301 for the whole period from 1975 to 1993 in the estimates we use (Fraser *et al.*, 1998) compared with those of TEAP. The bank estimated by TEAP does not include production from all developed countries and from the major developing countries, which according to UNEP (1997b) takes place. This might account for the different production and bank. The total emission we use for Halon-1301 from 1980 to 1995 of 58.2 ktonnes per year is only slightly larger than the 53.0 ktonnes per year reported by TEAP.

### 11.3.5 HCFCs

According to the Montreal Amendments of 1997 (Table 11-2), the consumption of HCFCs in developed countries is frozen in 1996. Reductions are mandatory from 2004 onward with a complete phase-out in 2030. Developing countries have to freeze their consumption of HCFCs in 2016 at the level of 2015, so there is no specified limit on their consumption (and production) until 2016. For HCFCs the Protocol deals with consumption; in this chapter the production of HCFCs is assumed to be equal to its consumption. A maximum allowable production level can therefore not be defined for HCFCs. The future HCFC production in developed and developing countries is estimated using the revised IS92a projections as reported in IPCC (1996). The production of HCFCs in developed countries is capped at the 1989 HCFC production plus 2.8% of the 1989 CFC production. Because the total production in developed countries was below the capped value in 1995, the maximum allowable production increases until 1999 and starts to decrease from 2004 onward following the reduction schedule of the Protocol. The HCFC production in developing countries is defined as the difference between the IS92a (IPCC, 1996) projections

and the production in developed countries. From 2015 to 2039 the production is held constant, and it is zero from 2040 onward in accordance with the Protocol. Because there are no limitations on HCFC use in developing countries until 2016, the estimated future HCFC production is not the maximally allowed production. The corresponding HCFC production is larger in developed countries than in developing countries until 2015, when a larger reduction applies to developed countries.

### 11.3.6 Methyl Bromide

The emissions of all substances discussed above are entirely of anthropogenic origin. Methyl bromide has both natural and anthropogenic sources and has considerable uncertainties in the source strengths (Chapter 2). The anthropogenic emissions in 1995 are estimated at 21 ktonnes per year in developed countries and 18 ktonnes per year in developing countries and for critical-use exemptions for developed countries. The natural emissions from the oceans and biomass burning are estimated to be 76 ktonnes per year (Yvon-Lewis and Butler, 1997; SORG, 1996).

The total emission of methyl bromide required to balance the total known sinks is estimated as 206 ktonnes per year. The discrepancy between this sink-based estimate and the known emissions, 91 ktonnes per year, is currently thought to be of natural origin and was added to the natural source of 76 ktonnes per year in the scenarios discussed in this chapter. If instead the sink of methyl bromide has been overestimated, or if a significant fraction of the unknown source is of anthropogenic origin and controllable under the Montreal Protocol, then the effect of control measures on the effective chlorine loading could be larger than estimated here.

### 11.3.7 Uncertainties in Baseline Scenario

Although scenario A1 is constructed in an attempt to represent reasonable emissions under the Protocol, it is possible that the emissions could be larger.

First, the reduction and phase-out dates of ODSs for developing countries start in 1999 for CFCs and a few years later for other substances. Therefore the base level to which the controls refer also lies at least partly in the future. This is especially significant for the consumption of HCFCs in developing countries, where no control measures apply until 2016 and the consumption is allowed to grow until then. This could increase the upper limit, although it is very unlikely to happen.

Second, the emission of carbon tetrachloride is taken to be proportional to the production of CFC-11 and CFC-12 and is therefore calculated as a fixed percentage of that production. The emission thus calculated is approximately one-third of the maximally allowed production (or emission) (UNEP, 1994b).

Third, there are uncertainties in the rates of release of ODSs to the atmosphere. In the scenarios the emissions are calculated as a fraction of the bank. This fraction is based on an analysis of the quantities present in, and emitted from, the banks over the years 1990-1995. The release fractions for the substances are held constant from 1996 to 2100. Destruction or changes in the use of ODSs could change the estimated release fraction and thereby the emissions and shape of the equivalent effective stratospheric chlorine (EESC) curve. The integrated EESC value discussed in Section 11.4.4 is not very sensitive to the release fractions chosen because the major part of the production and bank of the ODSs is released to the atmosphere before 2050. For the integrated EESC it is not important when the emissions occur; the ODSs that reach the stratosphere before the EESC value reaches the 1980 value (approximately 2050) contribute to the integrated value.

Fourth, the control measures apply to classes of substances (Annexes), several of which contain more than one substance. In these scenarios the distribution of the allowed production over the various substances of a class is based on the historic distribution and is assumed to stay the same in the future. A different distribution will only slightly affect the calculated EESC.

All these factors introduce uncertainties in the future emission scenarios and can affect the emissions possible within the current regulations.

### 11.3.8 Illegal Production

The emissions could also exceed the Baseline scenario if illegal production and illegal import/export occur. Illegal imports of CFCs are known to take place, for example, on the basis of custom interdiction reports. An estimated 10 ktonnes of CFCs are imported illegally into the European Union every year (C&I, 1997). The global amounts of ODSs may be significantly higher, with some estimates suggesting about 30 ktonnes per year. Future amounts and duration of such illegal production are uncertain. Illegal imports are equated to illegal production in scenarios F1 to F3 of Table 11-3.

These scenarios consider both low and high estimates for CFCs, i.e., 20 ktonnes per year for 10 years (scenario F1) or 40 ktonnes per year for 20 years (scenario F2), assigned to CFC-12 and CFC-113 in a 2:1 ratio. In the high-estimate scenario, the illegal production of CFC-12 amounts to 6% of the 1989 and 17% of the 1995 CFC-12 production. For CFC-113 these numbers are 5% of the 1989 and 30% of the 1995 production. Scenario F3 considers an illegal import of Halon-1211 of 2 ktonnes per year for 10 years. This 2 ktonnes corresponds to 12% of the 1989 production of Halon-1211 and 19% of the 1995 production.

### 11.3.9 Other Species

Emissions of methyl chloride are considered to be, for a large part, from biomass burning, with smaller emissions from industrial sources and the oceans (Section 2.2.4). Methyl chloride is not controlled by the Montreal Protocol. The atmospheric mixing ratio is approximately 550 parts per trillion (ppt) and there are no data suggesting a temporal trend in its atmospheric burden (see Chapter 2). No emissions of methyl chloride are therefore considered in the scenarios discussed in this chapter, but a fixed tropospheric mixing ratio of 550 ppt is used in the calculations. The contributions of other halocarbons, for example, methylene chloride ($CH_2Cl_2$), chloroform ($CHCl_3$), perchloroethene ($C_2Cl_4$), phosgene ($COCl_2$), dibromomethane ($CH_2Br_2$), bromoform ($CHBr_3$), and methyl iodide ($CH_3I$), to the stratospheric chlorine/bromine loading are ignored here because their contributions are expected to be small, and for several species no temporal trend is detected (see Chapter 2).

## 11.4 FUTURE CHLORINE AND BROMINE LOADING

### 11.4.1 Method of Calculating Equivalent Effective Stratospheric Chlorine (EESC)

The approach used here to relate emissions of various ozone-depleting substances to stratospheric ozone depletion is similar to that of Prather and Watson (1990) and previous assessment reports (WMO, 1992, 1995). The model adopted was used in WMO (1995) and described by Daniel *et al.* (1995), and it uses the equivalent effective stratospheric chlorine (EESC) concept. EESC is an index developed to represent the potential damage that a given mixture of ozone-depleting substances could cause to stratospheric ozone. Because of the impact of transport and other processes that depend on atmospheric attributes such as aerosol loading and temperature, equivalent effective stratospheric chlorine loading should not be regarded as a perfect gauge of the expected future ozone response. Instead, EESC can be thought of as a primary stratospheric forcing mechanism with the attribute that increasing chlorine/bromine loading will tend to lead to decreased ozone amounts.

In this model, abundances of the various ODSs are given by

$$\frac{d[x]}{dt} = S_x E_x - \frac{[x]}{\tau_x} \qquad (11\text{-}1)$$

where $[x]$ is the average tropospheric mixing ratio, $E_x$ is the emission rate of species $x$ obtained as described previously in Section 11.3, $\tau_x$ is the lifetime of $x$, and $S_x$ represents a factor used to convert a unit mass of species $x$ to an average tropospheric mixing ratio. The EESC is then calculated by

$$\mathrm{EESC}(t) = \sum_{\substack{Cl-containing \\ halocarbons}} n_x f_x [x]_{t-lag} + \alpha \sum_{\substack{Br-containing \\ halocarbons}} n_x f_x [x]_{t-lag} \qquad (11\text{-}2)$$

where $n_x$ represents the number of chlorine/bromine atoms in halocarbon $x$, $f_x$ represents the relative fractional chlorine/bromine release compared to CFC-11, *lag* is the average estimated transport time required for the halocarbon to travel from the troposphere to the stratosphere (taken here as 3 years), and $\alpha$ accounts for the relative impact of bromine compared to chlorine in destroying stratospheric ozone. The 3-year lag time for transport from the troposphere to the stratosphere agrees with midlatitude data of Figure 7-8 of Chapter 7. For the long-lived species (CFCs, halons, and carbon tetrachloride) the lifetimes of Table 13-1 of WMO (1995) were used. The lifetimes for HCFCs and methyl chloroform are given in Table 2-1 of Chapter 2. For methyl bromide a 0.7-year lifetime was used (see Chapter 2) and for HCFC-123 a 1.4-year lifetime (WMO, 1995).

There are two general categories of uncertainties concerning the use of Equation (11-2) as a method of comparing future halocarbon emission scenarios. The uncertainties in the first category relate to our ability to accurately calculate EESC from the quantities on the

right-hand side of Equation (11-2). Primary contributors to this category are uncertainties in the fractional halocarbon release and in alpha (for bromocarbons). Although the fractional halocarbon release has been estimated from measurements (Pollock *et al.*, 1992; Daniel *et al.*, 1995), its variation with altitude and latitude could make the choice of a "best guess" somewhat uncertain. Because of the importance of lower stratospheric ozone loss to column trends at middle and high latitudes, the values taken for this chapter are consistent with estimates of fractional halocarbon release in the lower stratosphere. The values adopted in this chapter are identical to those in WMO (1995), many of which were determined from observations (Daniel *et al.*, 1995). Determining the value of $\alpha$ is also complicated by variations with altitude, latitude, and season in some cases. It is widely accepted that $\alpha$ is roughly 40-60 for Antarctic ozone loss (see, e.g., WMO, 1995). In line with Chapter 2 of this Assessment (see Table 2-6), we adopt a value of 60 for $\alpha$ in representing globally averaged ozone loss. In Chapter 2 a bromine efficiency factor (combination of fractional release and $\alpha$) of 58 is used for methyl bromide, which corresponds to an $\alpha$ of 54. Such a difference in the value for $\alpha$ is well within the uncertainty range (see also Section 11.4.4.4). Furthermore, it should be noted that recent work (Danilin *et al.*, 1996) suggests that at high latitudes during winter the value of $\alpha$ may change in response to changing chlorine and bromine loading. Further work is necessary to determine if these results can be generalized to a globally applicable $\alpha$ value. In the previous Assessment (WMO, 1995) a value of 40 was used for $\alpha$. The larger $\alpha$ value used here has only a small effect on the EESC. Additional uncertainties in the calculation of EESC involve the appropriate choice of an effective lag time as well as the choice of which gases to consider as contributing to EESC. From Chapter 2, it is clear that a single lag time is not appropriate throughout the lower stratosphere. Our choice of 3 years therefore implies that the inorganic halogenated compounds in part of the stratosphere will respond more quickly (smaller lag time) to changes in tropospheric halocarbon emissions and more slowly (larger lag time) in other parts of the stratosphere. In this chapter, except for methyl bromide, we have not considered any halogenated source gases with global lifetimes less than 1 year. Although shorter-lived gases could certainly contribute to stratospheric chlorine and bromine, an estimate would have to be made concerning the amount transported to the stratosphere before they could be used in Equation (11-2).

The second category of uncertainty relates to the use of the equivalent effective stratospheric chlorine concept in analyzing future scenario options. As discussed in Section 11.1, a primary limitation of the EESC formalism is that it ignores all atmospheric changes (e.g., aerosol loading, stratospheric temperatures, etc.) that could affect stratospheric ozone other than the increase in chlorine and bromine loading. Another limitation relates to the use of a single globally averaged quantity (EESC) to represent a possible future evolution of stratospheric ozone depletion. Such an assumption ignores the fact that changes in chlorine and bromine will affect ozone differently depending on latitude, altitude, and season. Furthermore, Prather (1997) has pointed out that the stratospheric inorganic halogen loading arising from short-lived source gases like methyl bromide will not respond to changes in the tropospheric source gas concentrations according to the source gas lifetime, as would be suggested by the EESC formalism of Equation (11-2). While each of these criticisms illustrates imperfections in the application of EESC to describe future ozone depletion, EESC is a useful concept in comparing the differences between future halocarbon emission scenarios.

### 11.4.2 Future Development of Mixing Ratios

The temporal evolution of the average tropospheric mixing ratios calculated with Equation (11-1) is shown for the Baseline scenario in Figure 11-3. Several points should be noted in relation to this figure. First, the emissions of the Baseline scenario are defined for comparing the effects of different control measures, and therefore the mixing ratios shown in Figure 11-3 are not necessarily the most likely future values. Second, the scenario is based on classes of species, assuming that within each class the future partitioning of emissions among individual species will remain constant at the 1995 value. It is possible that future changes in the demand and use of the various compounds will affect the distribution of emissions within each class, so that different relations between the emissions and mixing ratios may result. Third, the scenarios are designed to compare the long-term effects of different additional control measures, not short-term changes in individual species. Fourth, the model used to calculate the mixing ratios from the emissions is a zero-dimensional (box) model, which by nature does not describe latitudinal,

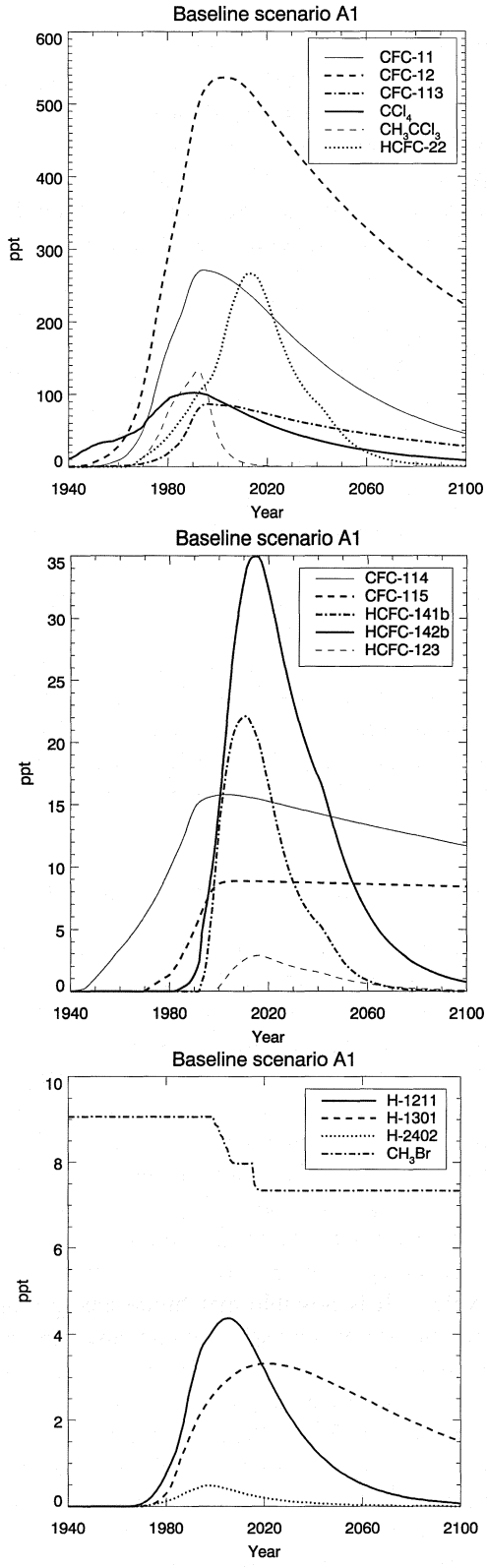


**Figure 11-3.** Temporal evolution of the average tropospheric mixing ratios of ODSs for the Baseline scenario (A1).

longitudinal, or vertical gradients in mixing ratios. The calculated values represent, therefore, a global average tropospheric mixing ratio and not a value at any specific location. Fifth, the time delay between production and release to the atmosphere is computed simply as a fixed fraction of the existing bank (the amount currently stored or being used in various applications). This fraction can change in the future, affecting the emissions and thus the concentrations of the species. From these considerations it is clear that the future evolution of the individual species as shown in Figure 11-3 should be viewed as representative but not necessarily an exact prediction. In particular, the precise year in which the mixing ratio of a species achieves its maximum value is quite sensitive to the above assumptions and should be viewed with some caution. The considerations discussed above hardly affect the time-integrated EESC that is used in Section 11.4.3 for comparing the different scenarios.

The evolution of concentrations, and hence EESC, of the ODSs is controlled by their lifetimes and emissions over time. For a few species the measured mixing ratios reached their maximum before or around 1996, e.g., CFC-11, CFC-113, carbon tetrachloride, and methyl chloroform (see Chapters 1 and 2). Partly because of their long lifetimes, CFC-12, CFC-114, and CFC-115 are expected to peak in the first decade of the 21$^{st}$ century. As discussed before, the future development of the HCFCs is more uncertain than of the CFCs. According to the Baseline scenario, the HCFCs are expected to reach their maximum value between 2005 and 2015. The evolution of Halon-1301 abundance is determined both by the atmospheric lifetime of 65 years and by the very slow release from the bank, i.e., the yearly emission is 4% of the amount in the bank (see also Butler *et al.*, 1998). According to the Baseline scenario, Halon-1211 and Halon-2402 will reach their maxima before 2010, whereas Halon-1301 will peak between 2015 and 2025. The short lifetime of methyl bromide causes its mixing ratio to respond rapidly to changes in the production and emission. The large natural emission determines the minimum value it can reach in the future.

### 11.4.3 Future Development of EESC

The equivalent effective stratospheric chlorine (EESC) is calculated using Equation (11-2) and the mixing ratios shown in Figure 11-3. The future evolution of the EESC (Baseline scenario) is shown in Figure 11-4. The maximum EESC is attained in the year 1997. Since the EESC is assumed to correspond directly and

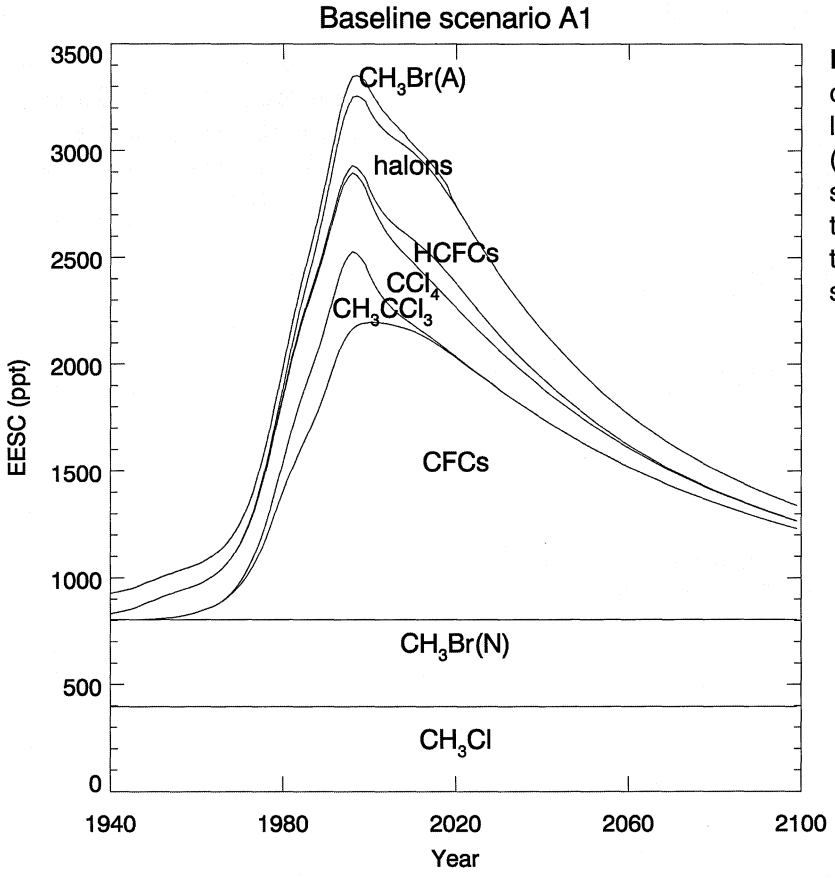


**Figure 11-4.** Contributions of the classes of substances to total equivalent effective stratospheric chlorine (EESC) according to the Baseline scenario (A1). Methyl bromide contributions from natural (N) and controlled anthropogenic (A) sources are shown separately.

linearly to the depletion of the ozone column, the maximum ozone depletion at midlatitudes is also expected to have occurred in 1997 (in the assumed absence of other natural and anthropogenic perturbations to ozone, and ignoring inter-annual and longer-term variability). After 1997, the ozone column amount is expected to begin gradual recovery. The expected rate of decrease of the EESC in the first half of the next century is 3 times slower than the increase in the 1970s and 1980s, i.e., -27 ppt/yr versus 81 ppt/yr.

In these calculations the ozone layer depletion is considered to be caused solely by active chlorine and bromine species. Other perturbations are ignored, such as changes in emissions of methane, nitrous oxide, and carbon dioxide; changes in stratospheric temperatures and aerosol loading; and aircraft emissions. The feedbacks stemming from ozone-related changes in tropospheric UV radiation and OH mixing ratios are also not taken into account in these analyses. Some of these effects are discussed in Chapters 10 and 12.

By far the largest contribution to the EESC comes from the CFCs. In 1995, CFCs made up 41% of the total EESC (natural and anthropogenic emissions). The next largest anthropogenic contributions come from carbon tetrachloride (11%) and methyl chloroform (11%). The other species contribute less, i.e., halons 9%, anthropogenic emissions of methyl bromide 2.9%, and the HCFCs 0.9% (in 1995). The natural emissions of methyl chloride and methyl bromide make relatively large contributions to the EESC, 12% each. According to this Baseline scenario, the contribution of HCFCs will increase from 0.9% in 1995 to a maximum of 4% of the total EESC between 2015 and 2020, because of an increase in HCFC emissions and a decrease in the total EESC. The contribution of the halons is expected to increase from 9% in 1995 to a maximum of 13% in about 2010.

### 11.4.4 Effects of Control Measures

The effects of changing EESC levels on ozone are nonlinear and generally complex. Ozone measurements at midlatitudes and in Antarctica show that ozone

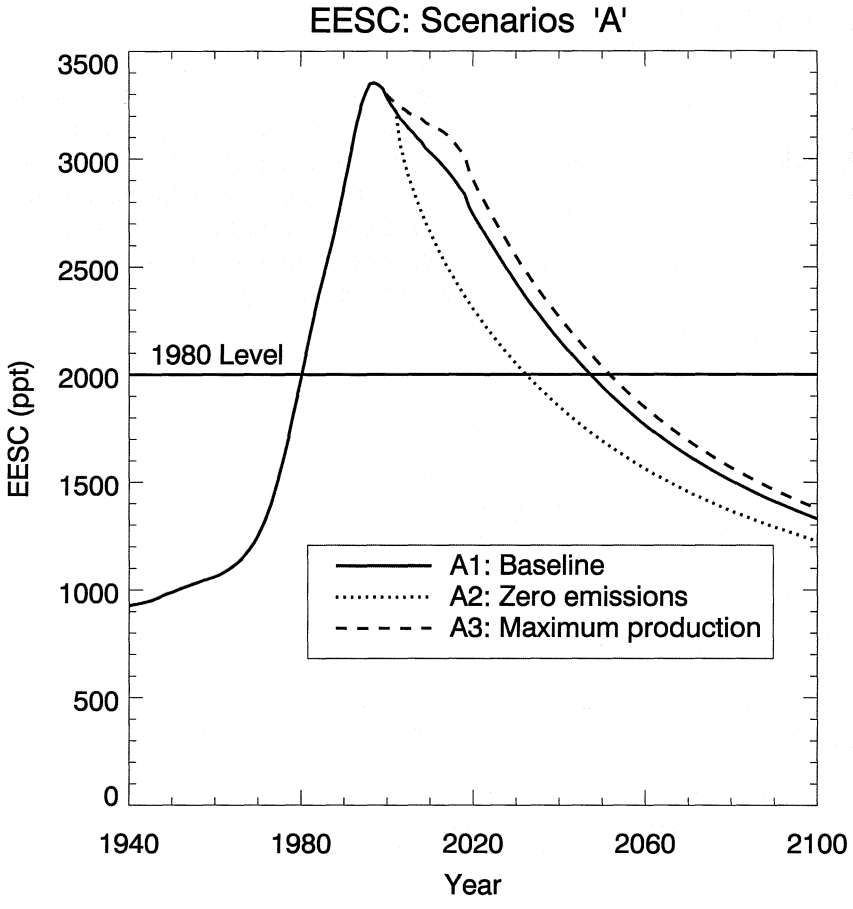


**Figure 11-5.** Equivalent effective stratospheric chlorine (EESC in ppt) for the Baseline (A1), Zero emissions (A2), and Maximum production (A3) scenarios.

depletion became observable in approximately 1980. For the purpose of comparing the impacts of different scenarios, 1980 is defined here as the reference year in which ozone depletion began, and the 1980 EESC value, 1.986 parts per billion (ppb) (see Figure 11-4), is considered as the threshold EESC level required for measurable ozone depletion. The same approach was used in WMO (1995). Any increments of EESC above the 1980 level are taken to result in ozone reductions, in proportion to the ozone/EESC trends observed between 1980 and 1990 (see Section 11-5 for details). If the EESC drops below the 1980 levels, ozone depletion is considered to cease, with the ozone layer returning to the natural background amount.

One useful measure of the impact of different future EESC reduction scenarios is the year (here termed year($x$)) in which the EESC is expected to drop below the 1980 threshold and therefore complete ozone recovery is assumed to result. Another useful measure is the time-integrated EESC (ppt-year) from 1998 through the year($x$) when the ozone depletion ceases. This quantity will be used to compare the effects of the different additional control measures. A third parameter is also defined as time-integrated EESC, but integrated from 1980 (rather than 1998) to year($x$), to help evaluate the impact that ozone depletion may have on ecological systems over the whole period of ozone depletion. Similar definitions were used in WMO (1995). The three parameters defined here are shown in Table 11-6 for comparison of the different scenarios. Positive values indicate that the integrated EESC levels exceed that of the Baseline scenario. Negative values indicate the effect additional control measures may have on the integrated EESC. Figure 11-5 shows the EESC from 1940 to 2100 for the Baseline (A1), Zero emission (A2), and Maximum production (A3) scenarios, while Figure 11-6 shows the potential effect on EESC of the different scenarios relative to the Baseline scenario.

The results presented here differ from those given in the previous Assessment (WMO, 1995) because

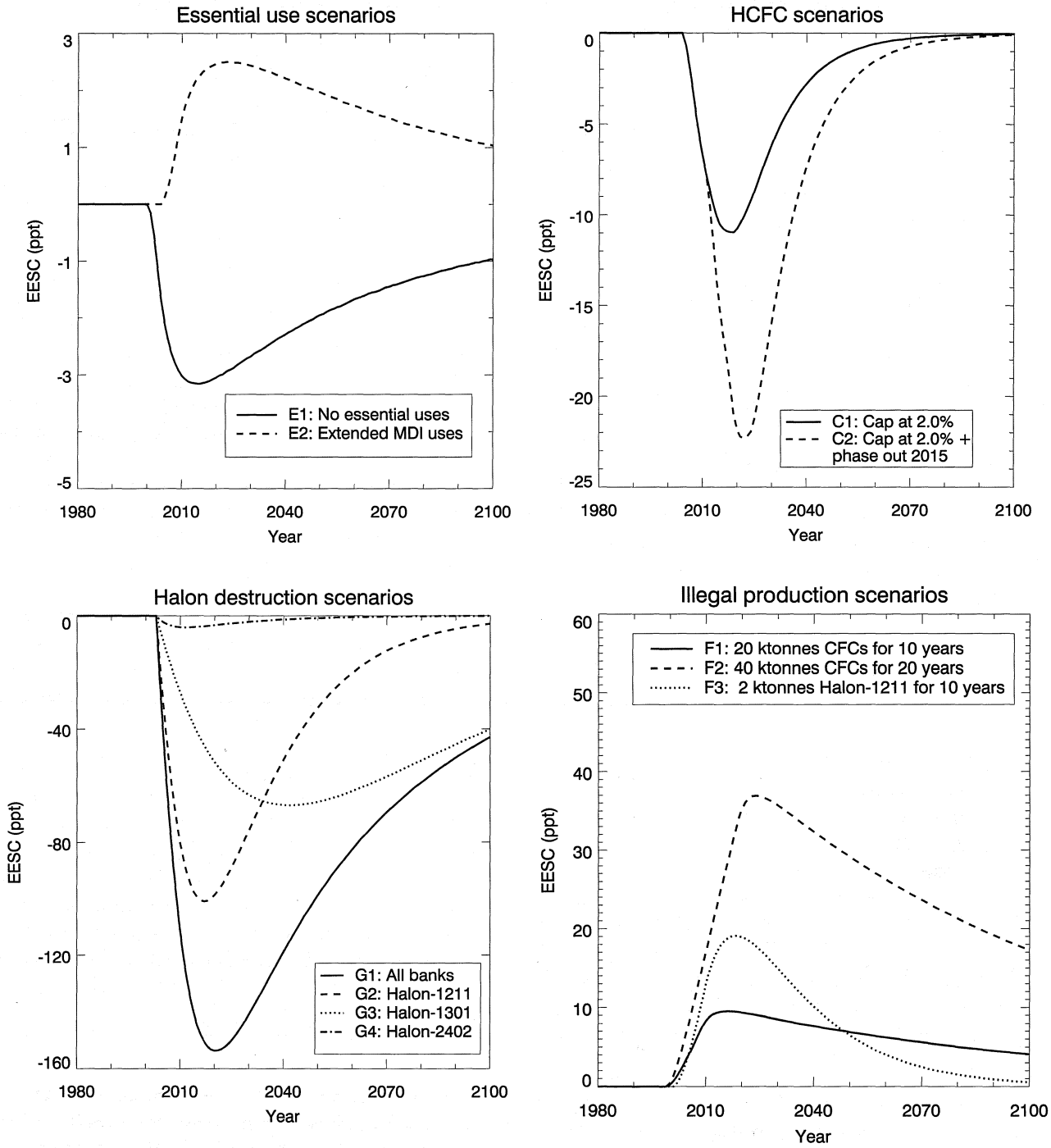


**Figure 11-6.** Change in EESC (ppt) relative to the Baseline scenario (A1) for the essential uses scenarios (E1 and E2), HCFC scenarios (C1 and C2), halon destruction scenarios (G1-G4), and illegal production scenarios (F1-F3). Negative values indicate that the scenario yields lower EESC values than the Baseline scenario (A1).

slightly different assumptions have been used for the Baseline scenario (A1). The most important difference is that in these scenarios we assume (in accordance with the Protocol) production of halons in developing countries, which was not considered in WMO (1995). The Baseline scenario therefore has a larger halon production than used in the previous Assessment. The production of CFCs in developing countries is also larger than in the previous Assessment. The assumption for this production in WMO (1995) was 10% of the total 1992 CFC production from 1996 to 2002 and decreasing to zero in 2006. In the current (1998) Assessment, this production is based on data from UNEP (1994b, 1997b); the amount is 20%-23% of the total 1992 CFC production from 1996 to 2004, decreasing to zero in 2010. The model used to calculate the mixing ratios and EESC values is the same as used before, but the parameterizations have been updated (i.e., new lifetimes for short-lived species and a factor of 60 for $\alpha$; see Section 11.4.1). A consequence of all the differences is that in the Baseline scenario A1, the EESC drops below the 1980 level in 2048, whereas this was 2045 in the previous Assessment (WMO, 1995). Because of uncertainties in the calculated values of alpha, we have examined the impact of a change in alpha from 60 to 80 on integrated EESC relative to the baseline scenario. This alpha change is larger than the expected uncertainty; it results in maximum decreases of a factor 1.1 for chlorine scenarios and maximum increases of a factor 1.2 for bromine scenarios.

Figure 11-7 shows the effect of completely halting production of CFCs, HCFCs, and methyl bromide ahead of the schedule specified by the current Protocol. Earlier termination of production yields larger reductions of integrated EESC, relative to the Baseline scenario. Among the three classes of compounds considered, the greatest benefit (i.e., largest EESC reduction) is achieved by an early stop in production of HCFCs and CFCs. For CFCs the avoidable production comes from developing countries, while for the HCFCs and methyl bromide it comes from both developed and developing countries. After a complete phase-out the change in integrated EESC is obviously zero. Figure 11-7 also shows the reduction in integrated EESC for each 1 Mtonne of avoided production, from which it is possible to estimate the benefits of partial reductions of allowed production.

#### 11.4.4.1 Maximum and Minimum Scenarios

Under the Baseline scenario (A1) (Figure 11-5 and Table 11-6) the EESC level is expected to fall below the threshold level for ozone depletion (i.e., the 1980 level) in about 2048. According to the Protocol, CFCs, carbon tetrachloride, and methyl chloroform are still allowed to be produced in developed countries for use in developing countries (see scenario A3). If this production were to take place it would have a large effect on the future integrated EESC (Table 11-6): the threshold level would be reached about 4 years later.

With the Zero emission (A2) scenario, the threshold level is expected to be reached in about 2033. The Zero emission scenario, which assumes zero production of ODSs and prevention of any release to the atmosphere for all ODSs contained in existing equipment by the end of 1998, shows the lower limit of stratospheric chlorine set by the chemical and physical processes in the atmosphere, i.e., the lifetimes of the species.

#### 11.4.4.2 CFCs and Carbon Tetrachloride Scenarios

Stopping the production of CFCs and carbon tetrachloride in all countries by 2004 (Figure 11-7 and scenario B3) may reduce the integrated EESC above the 1980 level by 2.5% over the next 50 years.

#### 11.4.4.3 HCFC Scenarios

Developed countries must, since 1996, freeze their consumption of HCFCs at a level that is capped at 2.8% of their 1989 CFC consumption plus the 1989 HCFC consumption. A full phase-out must be achieved in 2030. Reducing the cap to 2.0% is expected to yield an integrated EESC above the 1980 level of about 0.8% less over the next 50 years (scenario C1, Figure 11-6 and Table 11-6). A phase-out of HCFCs in 2015 in developed countries, with additional interim reductions as given by scenario C2, will yield an integrated EESC above the 1980 level that is about 1.6% less. The year of re-attaining the threshold for ozone depletion is hardly affected by these additional HCFC control measures.

Since the HCFCs were included in the Protocol in 1992, the estimated lifetimes of most of these compounds, and hence the estimated impacts on ozone, have decreased by 15%-25%. This, in effect, reduces the calculated impacts of allowed emissions under the Protocol by approximately the same amount compared

**Table 11-6. Comparison of the scenarios: the year when EESC drops below the 1980 level and integrated EESC differences (relative to Baseline scenario A1).**

| Scenario | Year ($x$) when EESC is expected to drop below 1980 value | Percent difference in $\int_{1980}^{x} EESC\,dt$ above the 1980 level relative to scenario A1 | Percent difference in $\int_{1998}^{x} EESC\,dt$ above the 1980 level relative to scenario A1 |
|---|---|---|---|
| **A1**: Baseline scenario = **Reference** | 2048 | 0 | 0 |
| **A2**: Zero emissions | 2033 | -30 | -42 |
| **A3**: Maximum production | 2052 | +12 | +18 |
| **A4**: Zero production | 2043 | -14 | -20 |
| **B3**: Phase-out of CFCs and carbon tetrachloride by 2004 | 2047 | -1.8 | -2.5 |
| **C1**: Reduce HCFC cap to 2% | 2048 | -0.6 | -0.8 |
| **C2**: Cap at 2% and phase-out HCFC in developed countries in 2015 | 2048 | -1.1 | -1.6 |
| **C3**: Global phase-out of HCFCs by 2004 | 2047 | -3.5 | -5.0 |
| **D3**: Phase-out of methyl bromide by 2004 | 2048 | -0.9 | -1.2 |
| **E1**: No essential uses | 2048 | -0.3 | -0.4 |
| **E2**: Additional MDI essential uses | 2048 | +0.2 | +0.3 |
| **F1**: Illegal CFC production: low estimate | 2048 | +0.8 | +1.1 |
| **F2**: Illegal CFC production: high estimate | 2049 | +2.8 | +4.0 |
| **F3**: Illegal Halon-1211 production | 2048 | +1.2 | +1.8 |
| **G1**: Destruction of all halon banks in 2000 | 2043 | -11 | -16 |
| **G2**: Destruction of Halon-1211 bank in 2000 | 2046 | -7 | -9 |
| **G3**: Destruction of Halon-1301 bank in 2000 | 2045 | -5 | -7 |
| **G4**: Destruction of Halon-2402 bank in 2000 | 2048 | -0.2 | -0.3 |
| **H1**: No Protocol | Not reached | +659* | +938* |
| **H2**: Montreal Protocol (1987) | Not reached | +365* | +519* |
| **H3**: London Amendments (1990) | Not reached | +152* | +216* |
| **H4**: Copenhagen Amendments (1992) | Not reached | +15* | +22* |
| **H5**: Vienna Adjustments (1995) | 2050 | +3.5 | +4.9 |

* Since the 1980 EESC level is not reached again, the integration is performed from the year 1980 (third column) or 1998 (fourth column), up to 2050.

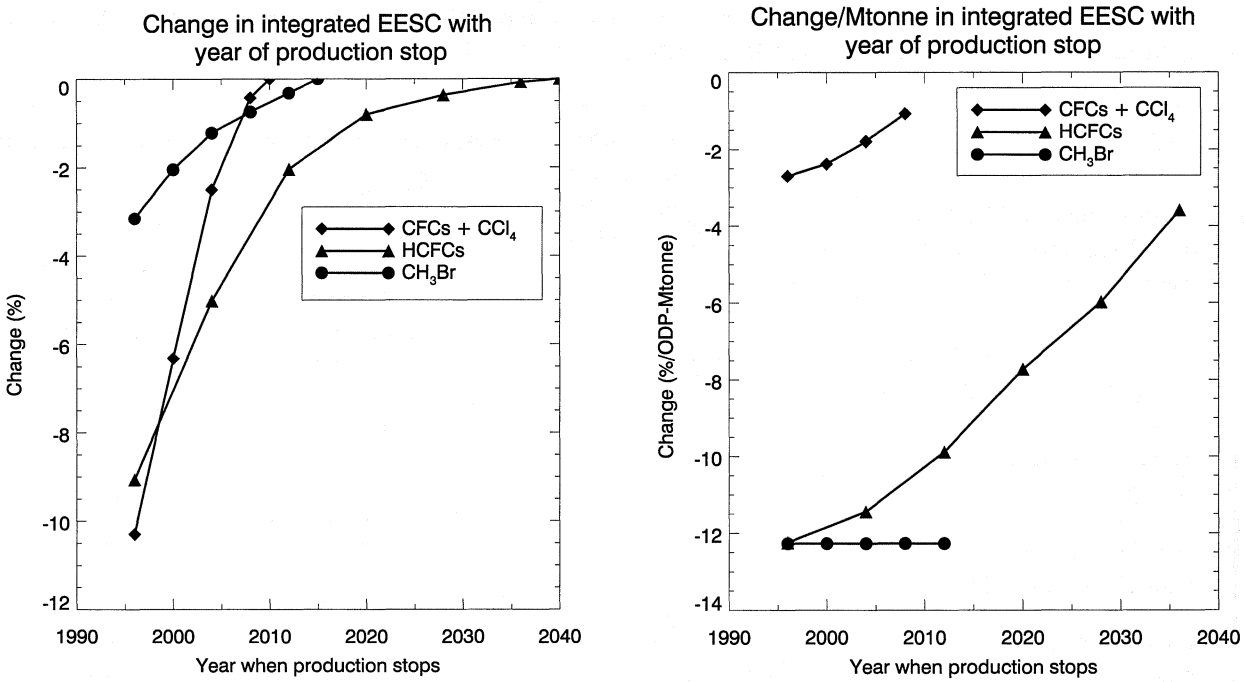


**Figure 11-7.** Percentage change (relative to the Baseline scenario) in integrated EESC above the 1980 level with a stop in production of CFCs, HCFCs, and methyl bromide in all countries in the year given by the horizontal axis. The integration is performed from 1998 to the year the EESC drops below the 1980 value. The right panel shows the percentage change in integrated EESC per avoided megatonne production (ODP-weighted).

with what was estimated when the limits were agreed on.

Stopping the production of HCFCs in all countries by 2004 (Figure 11-7 and scenario C3) may reduce the integrated EESC above the 1980 level by 5% over the next 50 years. The year of re-attaining the threshold for ozone depletion would hardly change. The effect of additional HCFC control measures for developing countries depends on the maximum amount they might produce in the future. The maximum allowed production is not defined; developing countries must freeze their HCFC consumption in 2016 at the level of 2015. If production is substantially more than assumed in the IS92a (IPCC, 1996) scenario, used as basis for the HCFC scenarios, the effects of additional HCFC control measures for developing countries would be larger.

#### 11.4.4.4 Methyl Bromide Scenarios

Because of the short lifetime of methyl bromide, its atmospheric mixing ratio responds rapidly to control measures. Moving forward the phase-out of methyl bromide from the current year of 2005 in developed countries and 2015 in developing countries to 2004 (Figure 11-7) may reduce the integrated EESC above the 1980 level by about 1% over the next 50 years (Table 11-6). The uncertainty about the budget of methyl bromide introduces uncertainties in the estimated effects of additional methyl bromide control measures. If a larger (smaller) fraction of the total sources than assumed in the scenarios used here were found to be of anthropogenic origin, and therefore potentially controllable under the Montreal Protocol, the effect of additional methyl bromide control measures would be greater (smaller).

#### 11.4.4.5 Essential Uses Scenarios

The contribution of the currently (Montreal 1997) allowed essential uses (see Table 11-4) (UNEP, 1997a) of CFC-11, CFC-12, CFC-113, CFC-114, methyl

**Table 11-7. Latitudinal dependence of annually averaged ozone, ozone trends, and ozone/EESC scaling factor, *s* (Equation 11-5).**

| Latitude, deg | $O_3$(1980), Dobson units | Trend, % per decade | Uncertainty in trend (2 sigma), % per decade | $O_3$/EESC scaling factor | Uncertainty (2 sigma) in $O_3$/EESC scaling factor |
|---|---|---|---|---|---|
| -55 | 346 | -5.7 | 3.2 | -0.126 | 0.070 |
| -45 | 325 | -4.0 | 2.6 | -0.089 | 0.056 |
| -35 | 297 | -2.6 | 2.0 | -0.058 | 0.044 |
| -25 | 274 | -1.1 | 1.9 | -0.024 | 0.043 |
| -15 | 263 | -0.4 | 1.8 | -0.009 | 0.039 |
| - 5 | 267 | -0.3 | 1.9 | -0.007 | 0.042 |
| 5 | 269 | -0.3 | 2.1 | -0.007 | 0.046 |
| 15 | 266 | -0.05 | 2.2 | -0.001 | 0.048 |
| 25 | 279 | -1.2 | 2.6 | -0.026 | 0.058 |
| 35 | 311 | -2.5 | 2.7 | -0.056 | 0.059 |
| 45 | 350 | -3.0 | 2.7 | -0.067 | 0.059 |
| 55 | 371 | -2.7 | 2.7 | -0.059 | 0.060 |

measurements obtained by the Total Ozone Mapping Spectrometer (TOMS) version 7, as given by McPeters *et al.* (1996). Some interpolation was carried out to put all ozone data onto a common spatial and temporal basis (10° latitude bands, monthly). The trends were determined from data collected from November 1978 (the operational start of TOMS) through June 1991, after which the data may be influenced for several years by the Mt. Pinatubo eruption.

In the linear regime between threshold and saturation, Equation (11-3) can be rewritten in the form,

$$\frac{O_3(t) - O_3(1980)}{O_3(1980)} = s\left(\frac{EESC(t) - EESC(1980)}{EESC(1980)}\right) \tag{11-4}$$

where the scaling factor $s$ is given by

$$s = \left(\frac{A}{O_3(1980)}\right)\left(\frac{EESC(1980)}{B}\right) \tag{11-5}$$

and expresses the percentage change in $O_3$ expected for a 1% increase in EESC. Table 11-7 summarizes the values used in the calculations, on the basis of annual averages. It should be noted that the ozone calculations were actually carried out at each latitude on a monthly basis in order to obtain the correct seasonal cycle of ozone for use in the UV calculations described below, then normalized to the yearly changes shown in this table.

## 11.5.2 Ozone/UV Scaling

There is strong theoretical expectation and ample observational evidence (see Chapter 9) that decreases in atmospheric ozone enhance the UV radiation reaching the Earth's surface, if all other factors affecting atmospheric transmission are constant (e.g., clouds). Here, we estimate the changes in biologically effective UV radiation corresponding to the different scenarios of future emissions of ozone-depleting substances. These estimates are based on ozone changes alone, that is, without consideration of any possible long-term changes in cloud cover, tropospheric pollutants, or other factors affecting atmospheric UV propagation.

### 11.5.2.1 Spectral Irradiance

The spectral irradiance at the surface, $F(\lambda)$ where $\lambda$ is the wavelength, is determined by the solar spectral irradiance incident at the top of the atmosphere and by the spectral transmission of the atmosphere. In particular, absorption by atmospheric ozone leads to strong attenuation of $F(\lambda)$ at wavelengths shorter than about

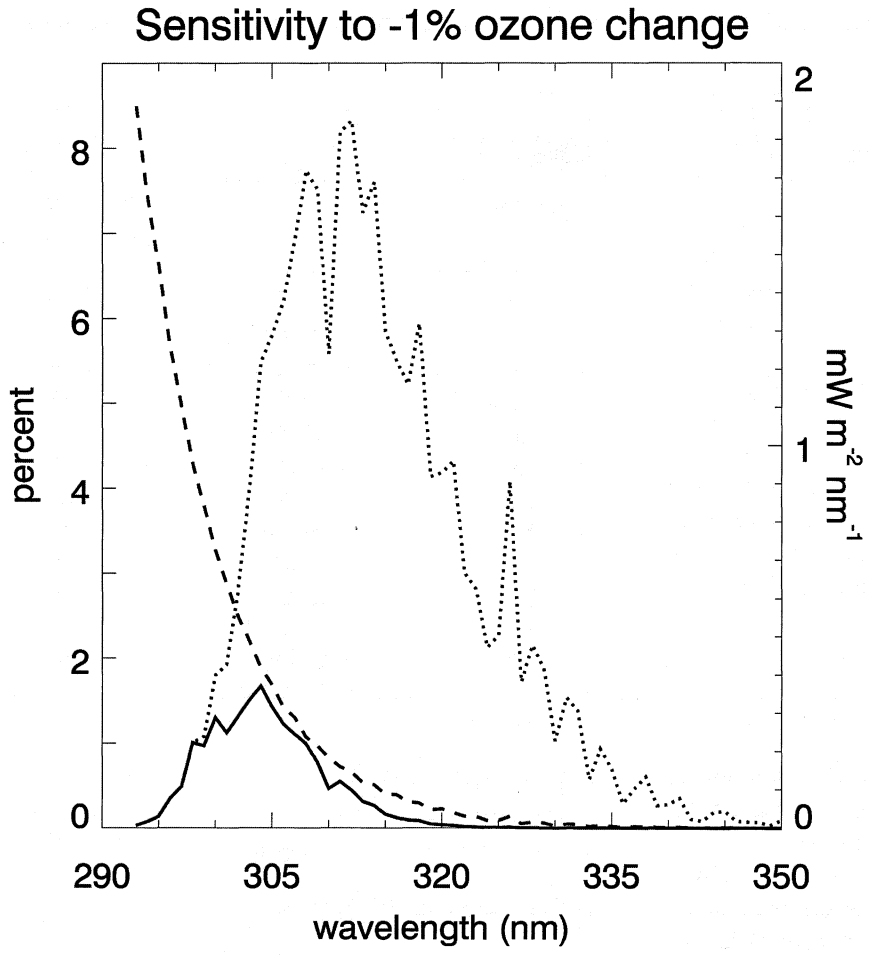


**Figure 11-9.** Spectral UV radiation changes for a 1% reduction in the total ozone column (from 300 to 297 Dobson units), for overhead sun. The dashed curve shows the percent increase in the spectral irradiance (left scale); the dotted curve shows the absolute change in spectral irradiance (right scale); and the solid curve shows the absolute change in spectral irradiance weighted by the erythemal action spectrum (right scale).

330 nm (see Chapter 9), with essentially negligible transmission near the short-wavelength side of the UV-B band (280-315 nm). Here, $F(\lambda)$ was calculated using a discrete ordinates radiative transfer model (Stamnes *et al.*, 1988) for cloud-free and aerosol-free conditions, 10% surface albedo, at 1-nm intervals over 280-400 nm (see Madronich *et al.* (1995) for additional details of the method). Although clouds and aerosols can attenuate UV radiation substantially, if assumed constant over the time of interest they have very little effect on the relative (percentage) changes in UV radiation stemming from stratospheric ozone depletion (WMO, 1990). Furthermore, zonally averaged UV trends estimated from TOMS satellite observations have been shown to be similar whether clouds are included or not in the derivation of the surface UV levels (Herman *et al.*, 1996).

The ozone-dependent UV increases are illustrated in Figure 11-9. A reduction in the column ozone leads to largest relative (percentage) increases in $F(\lambda)$ at the shortest wavelengths (dashed curve), as has also been confirmed by observations (e.g., McKenzie *et al.*, 1991; Kerr and McElroy, 1993; Fioletov and Evans, 1997). However, the absolute spectral irradiance decreases rapidly at these wavelengths (due to ozone absorption), so that its largest increments are seen to occur at somewhat longer wavelengths, in the 300-330 nm spectral region (dotted line). It is these additional photons that raise concerns about environmental consequences of ozone depletion.

The wavelength dependence of UV changes must be considered in detail when estimating biological impacts, because higher energy (shorter $\lambda$) photons are frequently much more damaging to target biological molecules than longer wavelength (lower energy) photons. The relative sensitivity to different wavelengths (the so-called action spectrum) has been determined for a number of biological effects (see also Section 11.5.4). Here, we use the action spectrum for skin erythema

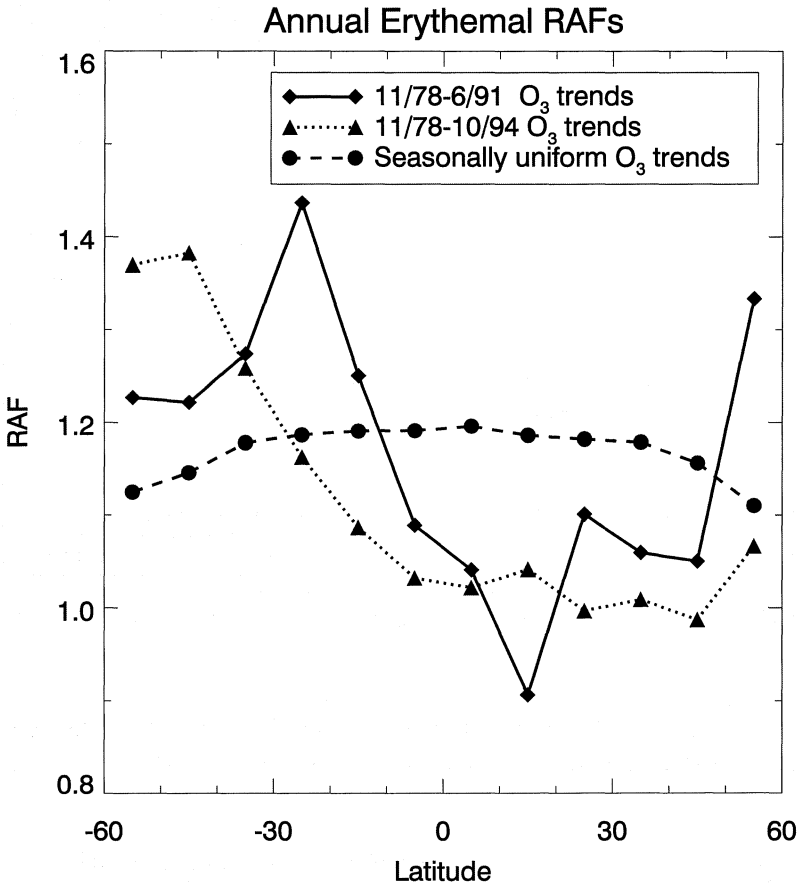


**Figure 11-12.** Latitudinal variation of the radiation amplification factor (RAF) for erythemal irradiance on an annual basis. At each latitude, values are computed from the detailed seasonal cycles of 1980 reference ozone, erythemal irradiance, and ozone trends (diamonds for trends for November 1978-June 1991; triangles for trends for November 1978-October 1994), or simply by assuming that ozone trends are uniform with season (circles).

variation expected if the ozone trend were applied uniformly (i.e., without seasonal dependence), with the residual latitude dependence arising solely from the prevailing solar zenith angles and average ozone levels characteristic of each latitude. For such seasonally uniform ozone changes, the annual RAFs are very similar to those obtained for instantaneous (monthly) erythemal doses shown in Figure 11-10.

### 11.5.3 Scenarios

Figure 11-13 shows the predicted changes in the annually averaged ozone column, and Figure 11-14 shows predicted changes in annually averaged $UV_{ery}$, at 45°S and 45°N for the Baseline, Zero emissions, and Maximum production EESC scenarios (A1, A2, and A3, respectively). The ozone changes are computed from the corresponding EESC scenarios using Equation (11-4) and the scaling factors given in Table 11-7 (e.g., at 45°N, a 0.067% ozone column reduction for each 1% increase in EESC above the 1980 level). The UV changes are similarly computed from the ozone changes, using Equation (11-8) and the scaling factors (RAFs) shown in Figure 11-12 (annual-based RAFs of ~1.05 at 45°N and ~1.22 at 45°S).

The time-evolution of ozone and UV radiation follows (by assumption) closely that of EESC, with minimum ozone (maximum $UV_{ery}$) in 1997 and return to 1980 levels in the years 2048 and 2033 for scenarios A1 and A2, respectively. At 45°N, the maximum reduction in the annually averaged ozone is expected to be about 15 DU, 4.3% lower than the 1980 value, leading to a maximum enhancement in the annually averaged $UV_{ery}$ of about 4.7%. At 45°S, the ozone reduction and $UV_{ery}$ increase are respectively 6.2% (about 20 DU) and 8.1%, in 1997 relative to the 1980 values. Seasonal patterns of these changes are expected (also by assumption) to follow those derived from TOMS ozone trends, e.g., with largest relative (percentage) increases in UV radiation occurring primarily during late winter and early spring in the Northern Hemisphere (see Figure 11-11) and more uniformly though the year in the Southern Hemisphere.

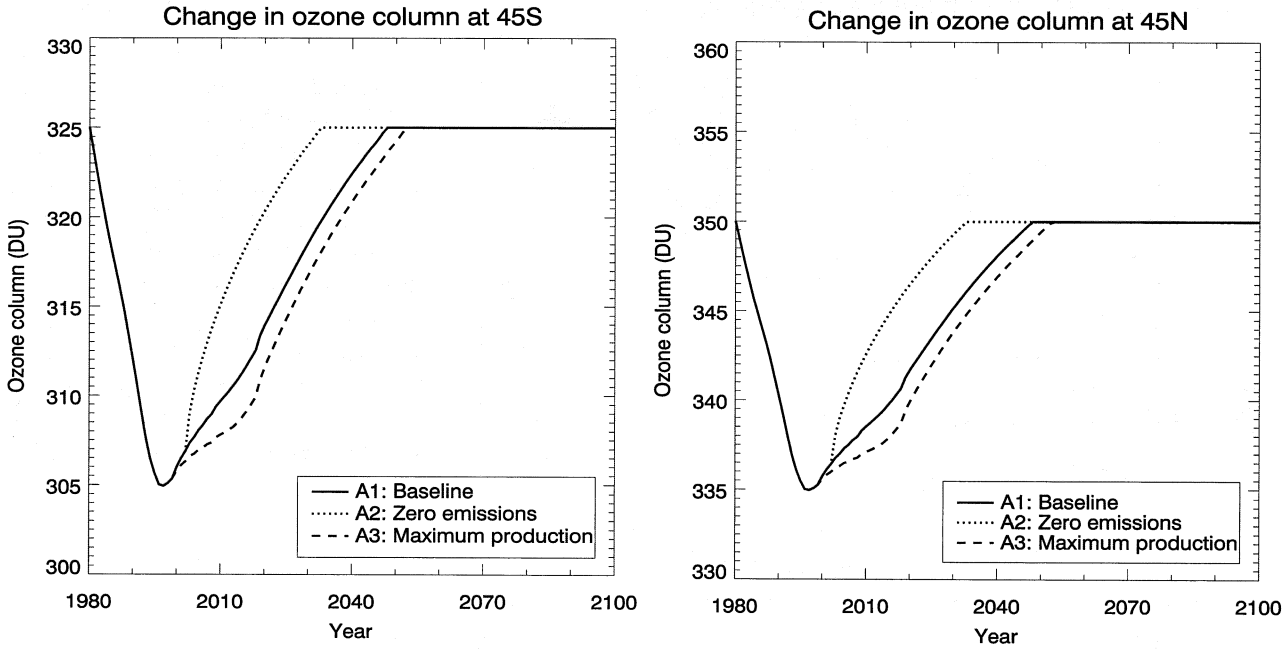


**Figure 11-13.** Changes in annually averaged ozone column amount at 45°S and 45°N, estimated from the EESC from the Baseline (A1), Zero emissions (A2), and Maximum production (A3) scenarios.

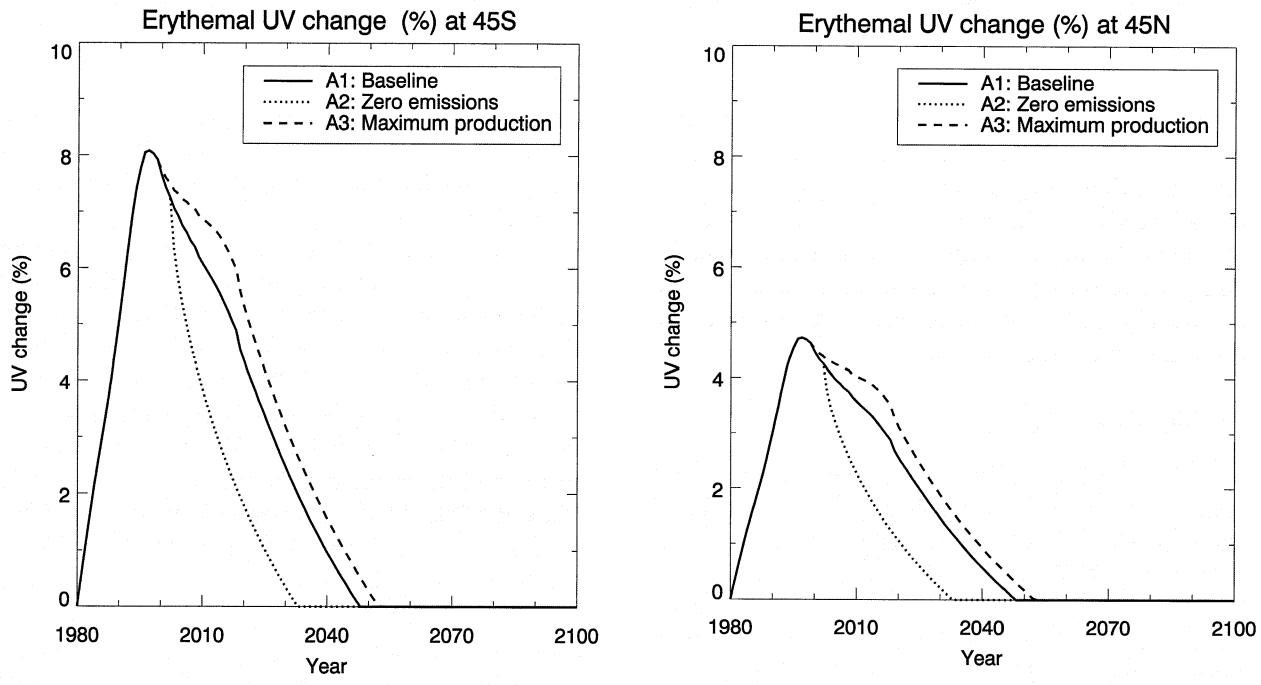


**Figure 11-14.** Changes (%) in annually averaged surface erythemal UV radiation at the Earth's surface at 45°S and 45°N, estimated from the EESC from the Baseline (A1), Zero emissions (A2), and Maximum production (A3) scenarios.

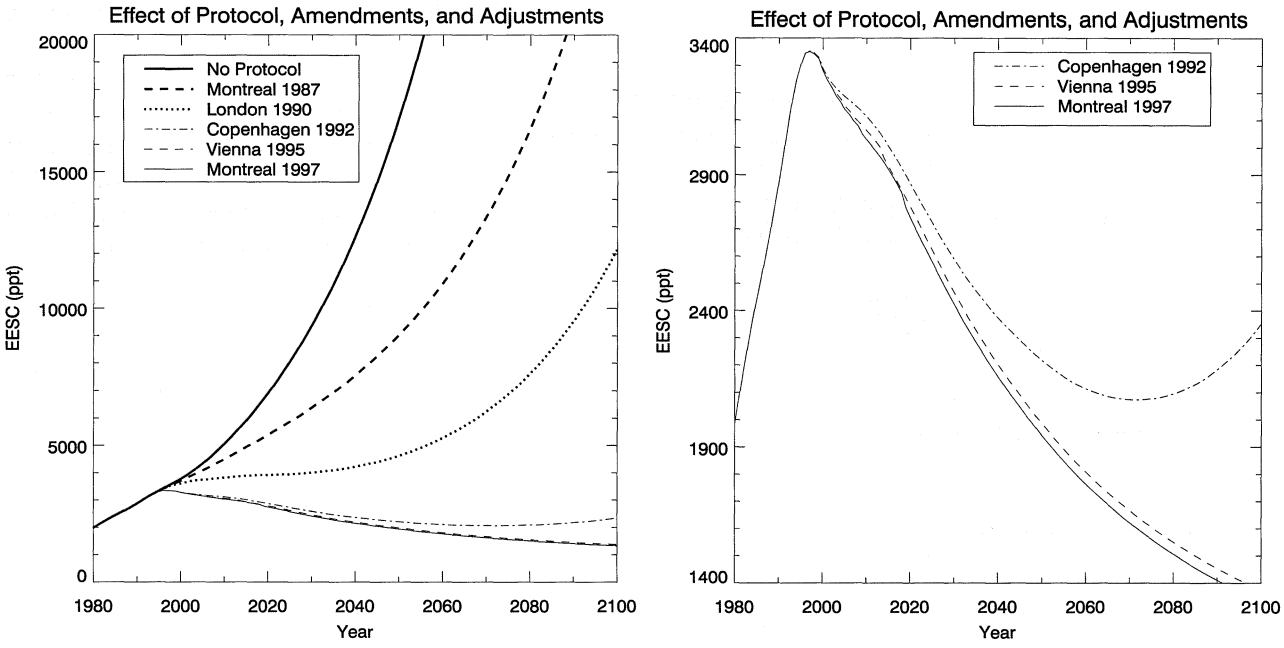


**Figure 11-15.** Estimated equivalent effective stratospheric chlorine represented by the various Amendments and Adjustments to the Montreal Protocol (scenarios H2-H5, A1), as well as a scenario with no international agreement on ozone-depleting substances (H1: No Protocol scenario: a 3%/year increase in production of CFCs, carbon tetrachloride, methyl chloroform, halons, HCFC-22, and methyl bromide). The more recent agreements are shown in greater detail for clarity.

The EESC increases for scenarios H1-H3 (No Protocol, Montreal 1987, and London 1990) are seen to be much larger than for the scenarios considered under the current regulations (compare Figures 11-8 and 11-16). The Adjustments of Vienna (1995), which limited the future production of methyl bromide, decrease the integrated EESC above the 1980 level by 17% (from +22% to +5%, relative to the current situation). An additional 5% reduction is achieved by the faster global phase-out of methyl bromide under the Amendments of Montreal (1997).

Figure 11-17 shows the increase in erythemal UV radiation at 45°N for the scenarios of No Protocol (H1) and scenarios of the Amendments and Adjustments to the Montreal Protocol. The method of calculation is similar to that described in Section 11-5, but was performed on a monthly (rather than yearly) basis to account for seasonally dependent saturation of ozone loss at the highest EESC levels (for details see Slaper *et al.*, 1996; Daniel *et al.*, 1995). The 3% per year growth assumed in the No Protocol scenario (H1) leads to more than doubling of the UV radiation by the middle of the next century, while the Montreal 1987 and London 1990 regulations delay this doubling by about 30 and 60 years, respectively. Only under the Vienna 1995 and Montreal 1997 regulations are UV radiation levels expected to decrease from current peak levels, returning to near-normal levels by the middle of the 21$^{st}$ century. The potential impacts that such UV radiation increases would have had on the biosphere are discussed in the Report of the Panel on the Environmental Effects of Ozone Depletion (UNEP, 1998b).

The full sequence of calculations, from ODS emissions to stratospheric chlorine loading, to ozone depletion and increases in surface UV radiation, and ultimately to environmental and economic impacts, has substantial uncertainties at each step, as has already been discussed. The impacts of these uncertainties are reduced somewhat here by considering only relative (percentage) changes, e.g., for UV radiation, and by using simple scaling relations based on observations, e.g., satellite-derived ozone changes and their correlation with measured stratospheric chlorine loading. A more critical issue is the assumption that future stratospheric ozone

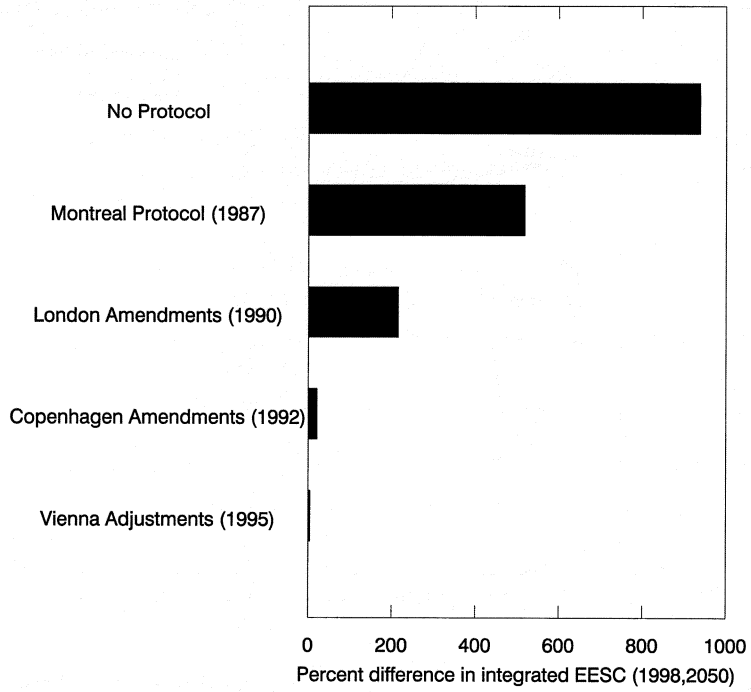


**Figure 11-16.** Percent difference in integrated equivalent effective stratospheric chlorine (EESC) above the 1980 level (relative to the Baseline scenario) of different Amendments to the Montreal Protocol (scenarios H1 to H5). The integration was performed from 1998 to 2050 (see Table 11-6).

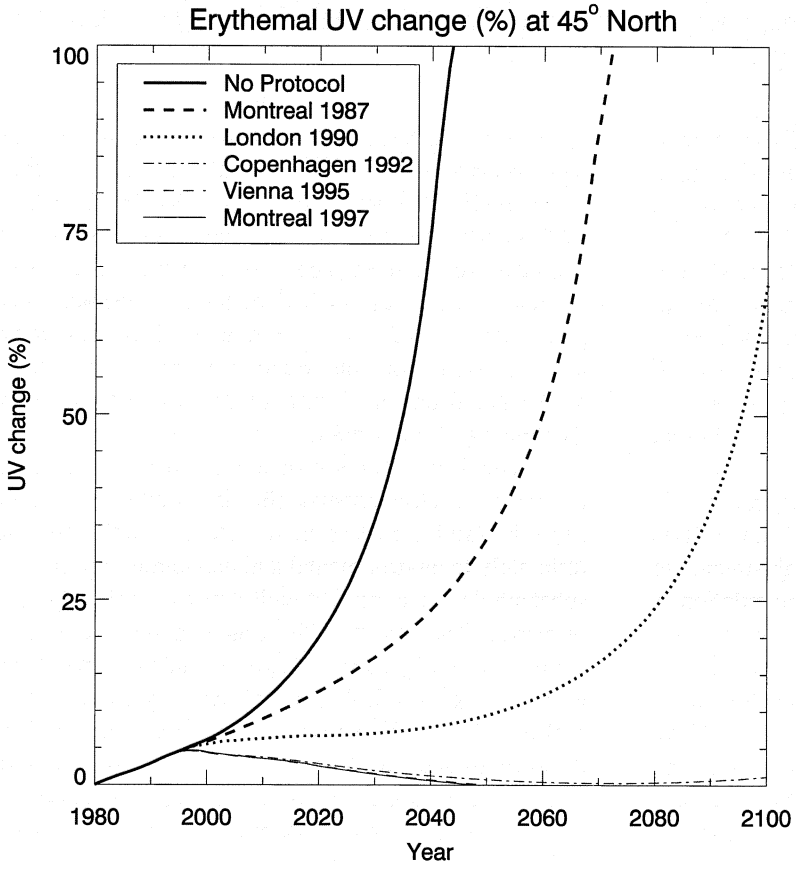


**Figure 11-17.** Estimated increase (%) in surface erythemal UV radiation at 45°N for the various Amendments and Adjustments of the Montreal Protocol (scenarios H2-H5, A1), as well as a scenario with no international agreement on ozone-depleting substances (H1: No Protocol scenario). Adapted from Slaper *et al.* (1996).

will respond to halogen loading in much the same way as observed in the 1980s, assuming in essence that the future atmosphere will be in all other regards similar to that of the recent few decades. Other long-term changes in the global atmosphere are known to be occurring, in large part associated with human activities. In particular, strong interactions between tropospheric climate change and stratospheric ozone chemistry and dynamics have been identified, but they have not yet been quantified with confidence and continue to be a topic of active research (see Chapter 12). Thus, it is emphasized again that the calculations presented here are not intended as accurate predictions of future levels of stratospheric ozone or surface UV radiation, but are limited to the purpose of comparing the relative impacts of different future scenarios of ODS production and emission.

## REFERENCES


AFEAS (Alternative Fluorocarbons Environmental Acceptability Study), *Production, Sales, and Atmospheric Release of Fluorocarbons through 1995*, Grant Thornton Company, Washington, D.C., 1997.

Bodhaine, B.A., R.L. McKenzie, P.V. Johnston, D.J. Hofmann, E.G. Dutton, R.C. Schnell, J.E. Barnes, S.C. Ryan, and M. Kotkamp, New ultraviolet spectroradiometer measurements at Mauna Loa Observatory, *Geophys. Res. Lett.*, *23*, 2121-2124, 1996.

Booth, R.C., and S. Madronich, Radiation amplification factors - improved formulation accounts for large increases in ultraviolet radiation associated with Antarctic ozone depletion, in *Ultraviolet Radiation and Biological Research in Antarctica*, pp. 39-42, American Geophysical Union Antarctic Research Series, Washington, D.C., 1994.

Butler, J.H., S.A. Montzka, A.D. Clarke, J.M. Lobert, and J.W. Elkins, Growth and distribution of halons in the atmosphere, *J. Geophys. Res.*, *103*, 1503-1511, 1998.

C&I, CFC smugglers caught in the act, *Chem. Ind.*, *15*, 578, 1997.

Daniel, J.S., S. Solomon, and D.L. Albritton, On the evaluation of halocarbon radiative forcing and global warming potentials, *J. Geophys. Res.*, *100*, 1271-1285, 1995.

Danilin, M.Y., N.D. Sze, M.K.W. Ko, J.M. Rodriguez, and M.J. Prather, Bromine-chlorine coupling in the Antarctic ozone hole, *Geophys. Res. Lett.*, *23*, 153-156, 1996.

Elkins, J.W., J.H. Butler, D.F. Hurst, S.A. Montzka, F.L. Moore, and T.M. Thompson, private communication of information located on the NOAA/CMDL Nitrous Oxide and Halocompounds (NOAH) World Wide Web site (http://www.cmdl.noaa.gov/noah), Boulder, Colo., 1998. [Updated data available on anonymous ftp site (file://ftp.cmdl.noaa.gov/noah), 1998.]

Fioletov, V.E., and W.F.J. Evans, The influence of ozone and other factors on surface radiation, in *Ozone Science: A Canadian Perspective on the Changing Ozone Layer*, edited by D.I. Wardle, J.B. Kerr, C.T. McElroy, and D.R. Francis, pp. 73-90, University of Toronto Press, 1997.

Fraser, P.J., D.E. Oram, C.E. Reeves, S.A. Penkett, and A. McCulloch, Southern hemispheric halon trends (1978-1998) and global halon emissions, *J. Geophys. Res.*, submitted, 1998.

Herman, J.R., P.K. Bhartia, J. Kiemke, Z. Ahmad, and D. Larko, UV-B increases (1979-1992) from decreases in total ozone, *Geophy. Res. Lett.*, *23*, 2117-2120, 1996.

IPCC (Intergovernmental Panel on Climate Change), *Climate Change 1995: The Science of Climate Change*, edited by J.T Houghton, L.G. Meira Filho, J. Bruce, H. Lee, B.A. Callander, E. Haites, N. Harris, and K. Maskell, Cambridge University Press, 572 pp., Cambridge, U.K., 1996.

Kerr, J.B., and C.T. McElroy, Evidence for large upward trends in ultraviolet-B radiation linked to ozone depletion, *Science*, *262*, 1032-1034, 1993.

Madronich, S., R.L. McKenzie, M.M. Caldwell, and L.O. Bjorn, Changes in ultraviolet radiation reaching the Earth's surface, *Ambio*, *24*, 143-152, 1995.

McCulloch, A., Global production and emissions of bromochlorodifluoromethane and bromotrifluoromethane (Halons 1211 and 1301), *Atmos. Environ.*, *26A*, 1325-1329, 1992.

McKenzie, R.L., W.A. Matthews, and P.V. Johnston, The relationship between erythemal UV and ozone, derived from spectral irradiance measurements, *Geophys. Res. Lett.*, *18*, 2269-2272, 1991.

McKinlay, A.F., and B.L. Diffey, A reference action spectrum for ultraviolet induced erythema in human skin, in *Human Exposure to Ultraviolet Radiation: Risks and Regulations*, edited by W.R. Passchler and B.F.M. Bosnjakovic, pp. 83-87, Elsevier, Amsterdam, 1987.

McPeters, R.D., S.M. Hollandsworth, L.E. Flynn, J.R. Herman, and C.J. Seftor, Long-term ozone trends derived from the 16-year combined Nimbus 7/ Meteor 3 TOMS version 7 record, *Geophys. Res. Lett.*, *23*, 3699-3702, 1996.

Midgley, P.M., and A. McCulloch, The production and global distribution of emissions to the atmosphere of 1,1,1-trichloroethane (methyl chloroform), *Atmos. Environ.*, *29*, 1601-1608, 1995.

Midgley, P.M., A. McCulloch, and P.G. Simmonds, The phase-out of methyl chloroform and the decline in tropospheric chlorine, in *Proceedings of Eurotrac Symposium*, Garmisch-Partenkirchen, Germany, April 1998, edited by P.M. Borrell and P. Borrell, WITpress, Southampton, in press, 1998.

Montzka, S.A., J.H. Butler, R.C. Myers, T.M. Thompson, T.H. Swanson, A.D. Clarke, L.T. Lock, and J.W. Elkins, Decline in the tropospheric abundance of halogen from halocarbons: Implications for stratospheric ozone depletion, *Science*, *272*, 1318-1322, 1996.

Pollock, W.H., L.E. Heidt, R.A. Lueb, J.F. Vedder, M.J. Mills, and S. Solomon, On the age of stratospheric air and ozone depletion potentials in polar regions, *J. Geophys. Res.*, *97*, 12993-12999, 1992.

Prather, M.J., Timescales in atmospheric chemistry: $CH_3Br$, the ocean, and ozone depletion potentials, *Global Biogeochem. Cycles*, *11*, 393-400, 1997.

Prather, M.J., and R.T. Watson, Stratospheric ozone depletion and future levels of atmospheric chlorine and bromine, *Nature*, *344*, 729-734, 1990.

Prather, M., P. Midgley, F.S. Rowland, and R. Stolarski, The ozone layer: The road not taken, *Nature*, *381*, 551-554, 1996.

Prinn, R.G., D.M. Cunnold, P.J. Fraser, R.F. Weiss, P.G. Simmonds, F.N. Alyea, L.P. Steele, and D. Hartley, The ALE/GAGE/AGAGE network, Dataset No. DB-1001, private communication of information located on World Wide Web site, (http://cdiac.esd.ornl.gov/ndps/alegage.html), DOE-CDIAC World Data Center (Email: cpd@ornl.gov), 1998.

Simmonds, P.G., D.M. Cunnold, R.F. Weiss, R.G. Prinn, P.J. Fraser, A. McCulloch, F.N. Alyea, and S. O'Doherty, Global trends and emission estimates of carbon tetrachloride ($CCl_4$) from *in-situ* background observations from July 1978 to June 1996, *J. Geophys. Res.*, *103*, 16017-16027, 1998.

Slaper, H., G.J.M. Velders, J.S. Daniel, F.R. de Gruijl, and J.C. van der Leun, Estimates of ozone depletion and skin cancer depletion and skin cancer incidence to examine the Vienna Convention achievements, *Nature*, *384*, 256-258, 1996.

SORG (Stratospheric Ozone Review Group), *Stratospheric Ozone 1996*, DoE Ref. No. 96DPL0021, edited by J.A. Pyle, J. Austin, M.P. Chipperfield, R.A. Cox, J.C. Farman, L.J. Gray, N.R.P. Harris, R.L. Jones, A. McCulloch, A. O'Neill, S.A. Penkett, C.E. Reeves, H.K. Roscoe, K.P. Shine, R. Toumi, and A.R. Webb, Department of the Environment, London, U.K., 1996.

Stamnes, K., S.C. Tsay, W. Wiscombe, and K. Jayaweera, Numerically stable algorithm for discrete-ordinate-method radiative transfer in multiple scattering and emitting layers, *Appl. Opt.*, *27*, 2502-2509, 1988.

UNEP (United Nations Environment Programme), *Environmental Effects of Stratospheric Ozone Depletion: 1991 Update*, edited by J.C. van der Leun, M. Tevini, and R.C. Worrest, Nairobi, Kenya, 1991.

UNEP (United Nations Environment Programme), *Environmental Effects of Ozone Depletion: 1994 Assessment*, edited by J.C. van der Leun, X. Tang, and M. Tevini, Nairobi, Kenya, 1994a.

UNEP (United Nations Environment Programme), *Meeting of the Needs of Article 5 Parties for Controlled Substances during the Grace and Phase-out Periods: An Update*, UNEP/OzL.Pro/ WG.1/11/5, Nairobi, Kenya, 1994b.

UNEP (United Nations Environment Programme), *Handbook for the International Treaties for the Protection of the Ozone Layer: The Vienna Convention (1985), The Montreal Protocol (1987)*, Fourth Edition, pp. 36-39, Nairobi, Kenya, 1996.

UNEP (United Nations Environment Programme), *Issues before the Open-Ended Working Group at its Fifteenth Meeting*, UNEP/OzL.Pro/WG.1/15/ 2/Add 7, Nairobi, Kenya, 1997a.

UNEP (United Nations Environment Programme), *Production and Consumption of Ozone Depleting Substances 1986-1995*, Nairobi, Kenya, 1997b.

UNEP (United Nations Environment Programme), *China's Halon Sector Strategy*, UNEP/OzL.Pro/ExCom/23/11, Nairobi, Kenya, 1997c.

UNEP (United Nations Environment Programme), *Report of Ninth Meeting of the Parties to the Montreal Protocol on Substances That Deplete the Ozone Layer*, UNEP/OzL.Pro.9/12, Nairobi, Kenya, 1997d.

UNEP (United Nations Environment Programme), *Technology and Economic Assessment Panel: April 1998 Report*, Nairobi, Kenya, 1998a.

UNEP (United Nations Environment Programme), *Environmental Effects of Ozone Depletion: 1998 Assessment*, edited by J.C. van der Leun, X. Tang, and M. Tevini, Nairobi, Kenya, in press, 1998b.

WMO (World Meteorological Organization), *Scientific Assessment of Ozone Depletion: 1989*, Global Ozone Research and Monitoring Project—Report No. 20, Geneva, 1990.

WMO (World Meteorological Organization), *Scientific Assessment of Ozone Depletion: 1991*, Global Ozone Research and Monitoring Project—Report No. 25, Geneva, 1992.

WMO (World Meteorological Organization), *Report of the WMO Meeting of Experts on UV-B Measurements, Data Quality and Standardization of UV Indices*, Global Atmosphere Watch—Report No. 95, Geneva, 1994.

WMO (World Meteorological Organization), *Scientific Assessment of Ozone Depletion: 1994*, Global Ozone Research and Monitoring Project—Report No. 37, Geneva, 1995.

Wuebbles, D.J., and J.M. Calm, An environmental rationale for retention of endangered chemicals, *Science*, *278*, 1090-1091, 1997.

Wuebbles, D.J., A. Jain, R. Kotamarthi, V. Naik, and K.O. Patten, Replacements for CFCs and halons and their effects on stratospheric ozone, in *Recent Advances in Stratospheric Processes*, edited by T.R. Nathan and E. Cordero, Research Signpost, India, in press, 1998.

Yvon-Lewis, S.A., and J.H. Butler, The potential effect of oceanic biological degradation on the lifetime of atmospheric $CH_3Br$, *Geophys. Res. Lett.*, *24*, 1227-1230, 1997.

# CHAPTER 12

# Predicting Future Ozone Changes and Detection of Recovery

**Lead Authors:**
D.J. Hofmann
J.A. Pyle

**Coauthors:**
J. Austin
N. Butchart
C.H. Jackman
D.E. Kinnison
F. Lefèvre
G. Pitari
D.T. Shindell
R. Toumi
P. von der Gathen

**Contributors:**
S. Bekki
C. Brühl
P.S. Connell
M. Dameris
E.L. Fleming
S.M. Hollandsworth
S.J. Oltmans
L.K. Randeniya
M. Rex
B. Rognerud
S. Smyshlyaev
H. Teyssèdre
G.J.M. Velders
D.K. Weisenstein
J.R. Ziemke

# CHAPTER 12

## PREDICTING FUTURE OZONE CHANGES AND DETECTION OF RECOVERY

### Contents

## SCIENTIFIC SUMMARY

A range of models has been used to investigate future changes in ozone in response to changing atmospheric emissions of source gases and greenhouse gases. A significant advance is the use of three-dimensional (3-D) models in these studies. The detection of the beginning of recovery of ozone (where recovery is defined as the response of ozone to reductions in chemical ozone loss due to the halogens) is considered for the first time in this Assessment.

**All other things being equal, stratospheric ozone levels should rise as the halogen loading falls in response to regulation. However, the future behavior of ozone will also be affected by the changing atmospheric abundances of methane ($CH_4$), nitrous oxide ($N_2O$), sulfate aerosol, and changing climate. Thus, for a given halogen loading in the future, the atmospheric ozone abundance will not be the same as found for that loading in the past. Because of these additional factors, observation of the beginning of ozone recovery is expected to be delayed beyond the time of maximum stratospheric halogen loading.**

### Model predictions of future ozone

- Ten two-dimensional (2-D) models were used to investigate the response of ozone to past and future changes in halogen loading as well as $CH_4$, $N_2O$, and sulfate aerosol. The models provide a reasonable representation of the general structure of recent observed local and column ozone trends, giving credence to their ability to represent future ozone change.

  - In integrations to 2050, excluding the possibility of major volcanic eruptions in the future, the lowest global ozone is predicted to have occurred in the years immediately following the eruption of Mt. Pinatubo in 1991.

  - After 2000, ozone levels are predicted to recover slowly toward their pre-1980 values. The modeled recovery depends sensitively on the emission scenarios for the halogens, and for $CH_4$, $N_2O$, and sulfate aerosol density.

  - Increases in future $CH_4$ will shorten the recovery period. Increases in $N_2O$ and sulfate aerosol surface area density will extend the recovery period. In one model that tested the effects of projected future $CO_2$ increases, the recovery period was shortened.

  - The methane scenario used here as a baseline had a lower growth rate than in previous Assessments and lengthened the modeled ozone recovery significantly. Understanding the methane trend is an important priority for understanding the future ozone recovery.

  - Model simulations show that future volcanic events at low inorganic chlorine ($Cl_y$) abundances will not significantly affect the rate of recovery.

- Polar ozone loss in recent Northern Hemisphere winters has demonstrated a large dependence on meteorological conditions, and especially temperature. Those winters with the lowest polar lower stratospheric temperatures have shown largest ozone losses. Recovery of ozone is evidently strongly dependent on meteorological conditions.

- Advances in computing power have allowed the first simulations of future ozone using coupled 3-D models.

  - Three-dimensional models highlight that future Arctic ozone loss is very sensitive to changes in the strength, frequency, and timing of sudden warnings.

atmospheric circulation. The amount of ozone in the atmosphere depends on the speed with which ozone is moved from its source to its sink (or from regions with short to long photochemical time constants (see, for example, Brewer and Wilson, 1968)). Thus changes in the circulation, from whatever cause, could lead to changes in ozone abundance, a further point that we discuss in Section 12.2.

Some other anthropogenic influences on ozone are considered very briefly in Section 12.3. These include the increasing emissions from sub- and supersonic aircraft and the possible role of various rocket launchers. We note that the Intergovernmental Panel on Climate Change (IPCC) is assembling a special report on aviation and the environment (IPCC, 1999). That report will provide a detailed assessment. Accordingly the discussion presented here has not attempted to duplicate that major effort.

## 12.2 CALCULATION OF FUTURE OZONE CHANGE

This section will first present calculations of ozone loss versus time, based on a scenario of future halogen loading. The basic scenario considered is essentially A3 of Chapter 11 of this Assessment, which describes the maximum halogen loading of the atmosphere, following maximum allowed production of ozone-depleting substances under the Montreal Protocol. We will then consider the question of the uncertainty in the calculated ozone layer response to possible feedbacks in the system, e.g., changing temperature or changing levels of source gases ($CH_4$, $H_2O$, $N_2O$, etc.). The calculations will be based on a range of models, from two-dimensional (2-D) models to fully coupled chemical-radiative-dynamical models that are now becoming available. The uncertainty issue will be considered again later in Section 12.4, where we consider the detection of the ozone layer recovery.

Two-dimensional models have been widely used for assessment studies for many years. Their formulation has continued to advance, and they represent ideal tools for a range of studies of stratospheric change over long time periods. In this Assessment, in Section 12.2.1, the 2-D model calculations of the global, decadal behavior of ozone are emphasized. Three-dimensional (3-D) chemical transport models (CTMs), with circulations forced by meteorological analyses, have been used increasingly in recent years. Here, in Section 12.2.2, they are used to study the sensitivity of Arctic ozone loss to meteorological conditions. Finally, long-term assessment of the coupled stratospheric system requires 3-D circulation models that include detailed descriptions of chemistry. Such models are now being developed. Generally, they have not yet been run for sufficiently long periods (nor have they been sufficiently validated) to assess the long-term trend in global ozone. However, they have been applied to studies of polar ozone loss, with boundary conditions appropriate to the next decade or so, and these polar studies are discussed in Section 12.2.3.

### 12.2.1 Ozone Change Calculated by 2-D Models

As reported in the *Scientific Assessment of Ozone Depletion: 1994* (WMO, 1995), nine 2-D models were used to derive the ozone trend from 1980 up to the year 2050. These models generally all predicted maximum ozone depletion between 1995 and 2000, consistent with the imposed surface chlorine source gas abundance. However, during this period, the differences in the magnitudes of the individual model-derived ozone depletions were substantial. This difference was amplified in Northern Hemisphere high latitudes, where ranges in ozone depletion varied by a factor of 2. In addition, one very striking result from that Assessment was the model-derived variations in the rate of ozone recovery. Some models did not recover to the 1980 ozone abundance until 2050, while others reached the 1980 ozone abundance as early as 2020. These 2-D calculations will be reassessed here in models including the latest developments in dynamical formulation and in gas- and heterogeneous-phase chemistry.

The stratosphere is a highly coupled system and, for example, the ozone distribution depends on the distribution of many other species and on the stratospheric temperature and circulation. The sensitivity of halogen-induced ozone perturbations to changes in these other parameters has been considered by many authors in the past (see, for example, WMO, 1986). Recently, Velders (1997) used the Netherlands National Institute of Public Health and the Environment (RIVM) 2-D model to investigate the sensitivity of ozone recovery to assumptions about concurrent changes in halocarbons, $CH_4$, $N_2O$, and temperature trends. The base scenario IS92a (IPCC, 1996), used within the context of the model, recovered to 1980 ozone abundances around the year 2065. This calculation did not include the change in stratospheric temperature caused mainly by increases in

**Table 12-1. The 2-D models participating in the Assessment.**

| Model Name | Institution | Investigators | References |
|---|---|---|---|
| **AER** | Atmospheric and Environmental Research Inc., *U.S.* | M. Ko, D. Weisenstein, and C. Scott | Weisenstein *et al.*, 1998 |
| **CAM** | University of Cambridge, *U.K.* | S. Bekki and J. Pyle | Bekki and Pyle, 1994 |
| **CSIRO** | Commonwealth Scientific and Industrial Research Organization, Telecommunications and Industrial Physics, *Australia* | K. Ryan, I. Plumb, P. Vohralik, and L. Randeniya | Randeniya *et al.*, 1997 |
| **GSFC** | Goddard Space Flight Center, *U.S.* | C. Jackman, E. Fleming, and D. Considine | Jackman *et al.*, 1996a |
| **LLNL** | Lawrence Livermore National Laboratory, *U.S.* | P. Connell and D. Kinnison | Kinnison *et al.*, 1994 |
| **MPIC** | Max-Planck-Institute for Chemistry, *Germany* | C. Brühl, J. Grooß, and P. Crutzen | Grooß *et al.*, 1998 |
| **OSLO** | University of Oslo, *Norway* | I. Isaksen and B. Rognerud | Zerefos *et al.*, 1997 |
| **RIVM** | National Institute of Public Health and the Environment, *Netherlands* | G.J.M. Velders | Velders 1995; Law and Pyle, 1993 |
| **SUNY_SPB** | State University of New York at Stony Brook, *U.S.*, and Russian State Hydrometeorological Institute, St. Petersburg, *Russia* | S. Smyshlyaev, V. Dvortsov, V. Yudin, and M. Geller | Smyshlyaev and Yudin, 1995 |
| **UNIVAQ** | University of L' Aquila, *Italy* | G. Pitari, B. Grassi, and G. Visconti | Pitari *et al.*, 1993 |

$CO_2$ emissions. When the chemical effect of this temperature change is considered, the recovery of ozone to 1980 levels occurs earlier, in the year 2040. In an extreme case where $CH_4$ and $N_2O$ abundances and temperature were held constant at 1990 conditions, while allowing CFCs to trend following IS92a, the model-derived ozone recovery occurred in 2080. Results of the model simulation described above highlight the importance of understanding, within the context of multi-dimensional models, the interactions that individual source gases, like $CH_4$ and $N_2O$, and temperature change have on the overall ozone recovery. In general, $CH_4$ increases tend to mitigate halogen influence on ozone by converting halogen odd-oxygen loss radicals to reservoir species, therefore reducing the ozone recovery time (WMO, 1995; Jackman *et al.*, 1996a; Velders, 1997). Increases in $N_2O$ have the opposite effect on ozone. Here, $N_2O$ increases will increase the abundance of nitrogen oxides ($NO_x$) in the stratosphere, increasing odd-oxygen loss from $NO_x$ catalytic processes. This increased odd-oxygen ($O_x$) loss process is more important than the mitigation of chlorine oxide ($ClO_x$) and bromine oxide

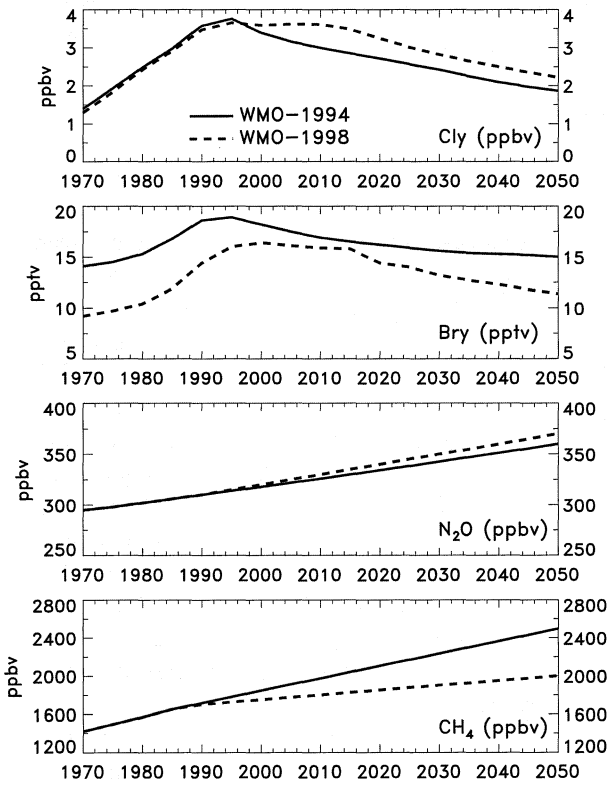


**Figure 12-1.** Comparison of surface boundary conditions (mixing ratios) between the 1994 WMO ozone Assessment (solid line) and this Assessment (dashed line) for $Cl_y$, $Br_y$, $N_2O$, and $CH_4$.

dependent trend in these constituents is obtained from several sources. For the CFCs, HCFCs, and halons, the past and future trend is obtained from Chapter 11, with a very small change in the boundary conditions for HCFC-123 that reflects slightly different assumptions about banking. Note that this difference makes a minuscule difference to integrated halogen loading. The production and consumption data of scenario A3 is based on the Amendments of the Montreal Protocol (Table 11-2). Scenario A3 does not necessarily describe the actual evolution of the future atmospheric concentrations. What it describes is the maximum chlorine and bromine loading of the atmosphere following the maximum allowed production of ozone-depleting substances. We chose to use scenario A3 here as a conservative representation (in terms of the removal from the atmosphere of ozone-depleting substances) of the Montreal Protocol. See Chapter 11 for a detailed discussion and Table 11-3 for a comparison of various scenarios.

The initial conditions for the scenarios up to 1995 (emissions and amount of substances present in the equipment) are made in agreement with the measured data from the National Oceanic and Atmospheric Administration/Climate Monitoring and Diagnostics Laboratory (NOAA/CMDL) and Atmospheric Lifetime Experiment/Global Atmospheric Gases Experiment/ Advanced GAGE (ALE/GAGE/AGAGE) networks. From 1996 onward the Montreal Protocol as amended is applied to the production and consumption for both developed and developing countries. After the phase-out date of CFCs, carbon tetrachloride, methyl chloroform, and halons in the developed countries, these substances are still allowed to be produced by the developed countries for use in developing countries. The amount produced is maximally 15% of the base-level production. This additional production is accounted for in scenario A3 for CFCs, carbon tetrachloride, and methyl chloroform. The emission of carbon tetrachloride is represented well by approximately 8% of the production of CFC-11 and -12. The consumption of HCFCs is based on the revised IS92a data as reported in IPCC (1996). The methyl bromide emissions are based on the data given in Chapter 2. The emissions of the CFCs, halons, and HCFCs are calculated as a fraction of the bank of the species. This fraction is based on an analysis of the quantities in the banks and emitted over the years 1990-1995, and held constant for all future years.

In Figure 12-1, a comparison of the surface total inorganic chlorine and total inorganic bromine ($Cl_y$ and $Br_y$) forcing for this Assessment and the 1994 Assessment (WMO, 1995) is shown. From 1970 through 1995, the surface $Cl_y$ mixing ratios for the two Assessments are consistent; however, after 1995 $Cl_y$ in this Assessment is significantly higher than that used in the 1994 Assessment. The reassessment of $CH_3Br$ has significantly lowered the $Br_y$ surface forcing relative to the 1994 Assessment (see Chapter 2). $CH_4$ and $N_2O$ surface values used are given in Figure 12-1 and in Table 12-2 and are consistent with the 1994 Assessment up to 1990. After 1990, $N_2O$ values are prescribed to increase at 1 ppbv/yr through 2050. This is essentially identical to scenario IS92a (IPCC, 1996). The $CH_4$ values are prescribed to increase at 5 parts per billion by volume per year (ppbv/yr), significantly less than that which the IS92a scenario would suggest or than that used in the

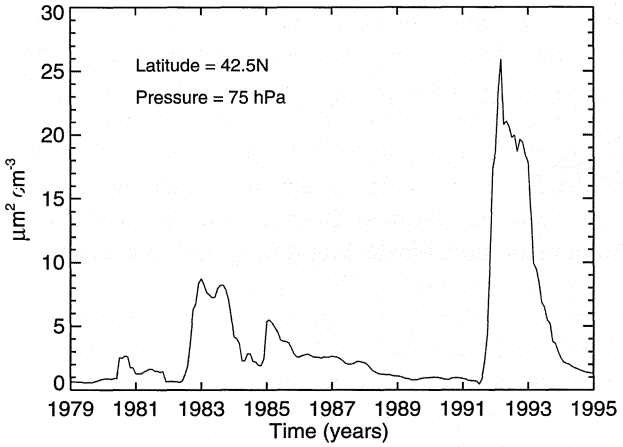


**Figure 12-2.** Time-dependent sulfate aerosol surface area density ($\mu m^2$ $cm^{-3}$) derived from SAGE I and II, SAM II, and SME data at 42.5°N and 75 hPa.

1994 WMO Assessment. This trend is believed to be more consistent with present changes in $CH_4$ (see Chapter 2). The sensitivity of the calculated ozone to these changes will be addressed in one set of model integrations and described in Section 12.2.1.3.

In all but one of the participating models listed in Table 12-1, the seasonally varying circulations were not modified between 1970 and 2050. However, the CAM 2-D model is a fully interactive model, meaning that the temperature and circulation are consistent with the model-derived heating rates. If $CO_2$ is varied in this model, the net heating rates will change and modify both the model-derived temperature and circulation in a consistent manner. For the scenarios examined here, $CO_2$ was fixed at its 1995 value. To examine the sensitivity to changing $CO_2$, a further calculation was performed using a time-dependent $CO_2$ surface boundary condition. Between 1970 and 1990 the time-dependent $CO_2$ was taken from the 1991 WMO Assessment (WMO, 1992). After 1990, and up to 2050, the IS92a scenario for $CO_2$ change was used (IPCC, 1996). This scenario increased surface $CO_2$ from 354 parts per million by volume (ppmv) in 1990 to 509 ppmv in 2050 (see Table 12-2). For this 2-D calculation, the emphasis is on the global behavior of ozone. Results from more sophisticated coupled 3-D models are presented in Section 12.2.3, with particular attention placed on the polar response.

The sulfate aerosol surface area density (SAD) climatology is derived using extinction measurements from Stratospheric Aerosol and Gas Experiment I (SAGE I), SAGE II, Stratospheric Aerosol Measurement (SAM II), and Solar Mesosphere Explorer (SME) data (see Rosenfield *et al.*, 1997). The SAM II data consist of monthly zonal-mean 1-μm extinction data taken between 1979 and 1995. The latitudinal coverage is limited to high latitudes for both hemispheres. The SAGE I and SAGE II data also consist of monthly-mean 1-μm aerosol extinction values. The temporal coverage is between 1979-1981 and 1985-1995 for SAGE I and SAGE II, respectively. The SME data are derived from weekly zonal-mean 6.8-μm aerosol extinction values between 1982 and 1984. This SAD was used by Jackman *et al.* (1996a) to study past, present, and future ozone trends. In Figure 12-2 the magnitude of lower stratospheric (75 hPa), middle latitude (42.5°N) SAD is shown. The impact of both the El Chichón (April 1982) and Mt. Pinatubo (June 1991) eruptions can easily be distinguished, as can the smaller eruption of Ruiz (November 1985). The use of the same derived SAD climatology in all the 2-D models is an advance on the last Assessment, in which the models used a range of surface area densities.

The ensemble of time-dependent scenarios is shown in Table 12-3. Scenario A/A3 is taken as the baseline scenario for the sensitivity studies. The modeling groups were asked first to generate a 1970 steady-state atmosphere with the source gas surface boundary conditions for 1970 given in Table 12-2. The 1979 seasonally varying SAD was used for the 1970 spin-up. After ozone steady state was reached, the models were integrated in a time-dependent manner again using the source gas surface boundary values in Table 12-2 (linearly interpolated between supplied temporal points). Between 1970 and 1979 the SAD was kept constant at the volcanically clean 1979 conditions. After 1979, the models were integrated up to 1995 using both the observed source gas boundary condition and the satellite-derived SAD. The 1979-1995 integration is labeled scenario A in Table 12-3. Scenario A3 is the future integration component of scenario A (years 1995 through 2050). Here, the time-dependent source gas boundary conditions are taken from Chapter 11 (see above discussion). The SAD is seasonally fixed using the 1995 data.

Scenarios B-D are an attempt to understand the sensitivity of each assessment model to varying $CH_4$ and $N_2O$ surface boundary conditions. This sensitivity analysis is built on the 1994 WMO Assessment (see

**Table 12-3. Definitions for the 2-D model scenarios.**

| Scenario | Period (years) | Aerosol Surface Area Density (SAD) | Halocarbon Boundary Conditions | $CH_4$ Boundary Conditions | $N_2O$ Boundary Conditions |
|---|---|---|---|---|---|
| A | 1979-1995 | 1979-1995 | Trend | Trend | Trend |
| A3 | 1996-2050 | 1995 | Trend | Trend | Trend |
| B | 1996-2050 | 1995 | Trend | Fixed at 1995 | Fixed at 1995 |
| C | 1996-2050 | 1995 | Trend | Fixed at 1995 | Trend |
| D | 1996-2050 | 1995 | Trend | Trend | Fixed at 1995 |
| E | 2000-2050 | Repeating 1980-1995 period, starting in 2000, 2016, and 2032 | Trend | Trend | Trend |
| F | 1996-2050 | 2% annual increase* | Trend | Trend | Trend |

* The percent increase in SAD is geometric, e.g., SAD (year $Y$) = SAD (1995) × $(1.02)^{(Y-1995)}$

Chapter 6 of WMO, 1995) and recent work of Velders (1997). In scenario B, the $CH_4$ and $N_2O$ surface mole fractions are held constant from 31 December 1995 through 31 December 2050. All other surface source gases are allowed to vary as in scenario A3. $CH_4$ and $N_2O$ are individually held fixed at 31 December 1995 conditions in cases C and D, respectively. For all cases, B-D, the SAD is set to the seasonally varying 1995 values.

To understand better the SAD sensitivity of the ozone recovery, the potential impact of future volcanic eruptions is addressed in scenario E. The 1980 through 1995 period (which includes two major eruptions) was repeated sequentially starting in the years 2000, 2016, and 2032. Under the conditions of this scenario, the future volcanic events will then occur under significantly different $Cl_y$, $Br_y$, $N_2O$, and $CH_4$ abundances.

In addition to trying to understand the potential impact of large volcanic events on the stratospheric SAD, this Assessment also examines the sensitivity of the ozone recovery to a potential annual, monotonic increase in background sulfate (for example, from dimethyl sulfide (DMS), carbonyl sulfide (OCS), or sulfur dioxide ($SO_2$) tropospheric sources or possible increased aircraft emissions). Here, in scenario F, the SAD was assumed to increase at a geometric rate of 2% per year starting from 1995.

#### 12.2.1.2 Modeling the Observed Trends in Ozone

Recently, two model studies have investigated the ozone trend between 1980 and 1995 (Solomon *et al.*, 1996; Jackman *et al.*, 1996a). These studies forced the 2-D models with observed sulfate aerosol SAD, solar-cycle-varying ultraviolet (UV) flux, and source gas boundary conditions. Both studies stressed the importance of using SAD derived from satellite measurements. Without inclusion of volcanically enhanced SAD from El Chichón and Mt. Pinatubo, it was impossible to match the temporal shape and magnitude of the observed ozone trend. In Jackman *et al.* (1996a), with inclusion of the above processes, the GSFC 2-D model derivation of global (65°S to 65°N) column ozone changes was in reasonable agreement with changes observed by the Total Ozone Mapping Spectrometer (TOMS). However, local ozone change was larger in the model at 45 km. This is consistent with the known excess abundance of model-derived ClO relative to Upper Atmosphere Research Satellite (UARS) Microwave Limb Sounder (MLS) data (Waters *et al.*, 1996). In this model integration, there was no allowance for the possible $ClO + OH \rightarrow HCl + O_2$ reaction. In the study of Solomon *et al.* (1996) the shape of the ozone trends is matched well but the model underestimates the observed middle-latitude temporal ozone variation by a factor of 1.5. Recent calculations (Solomon *et al.*, 1998) with an improved version of the model, including observed temperatures and their variability, now also

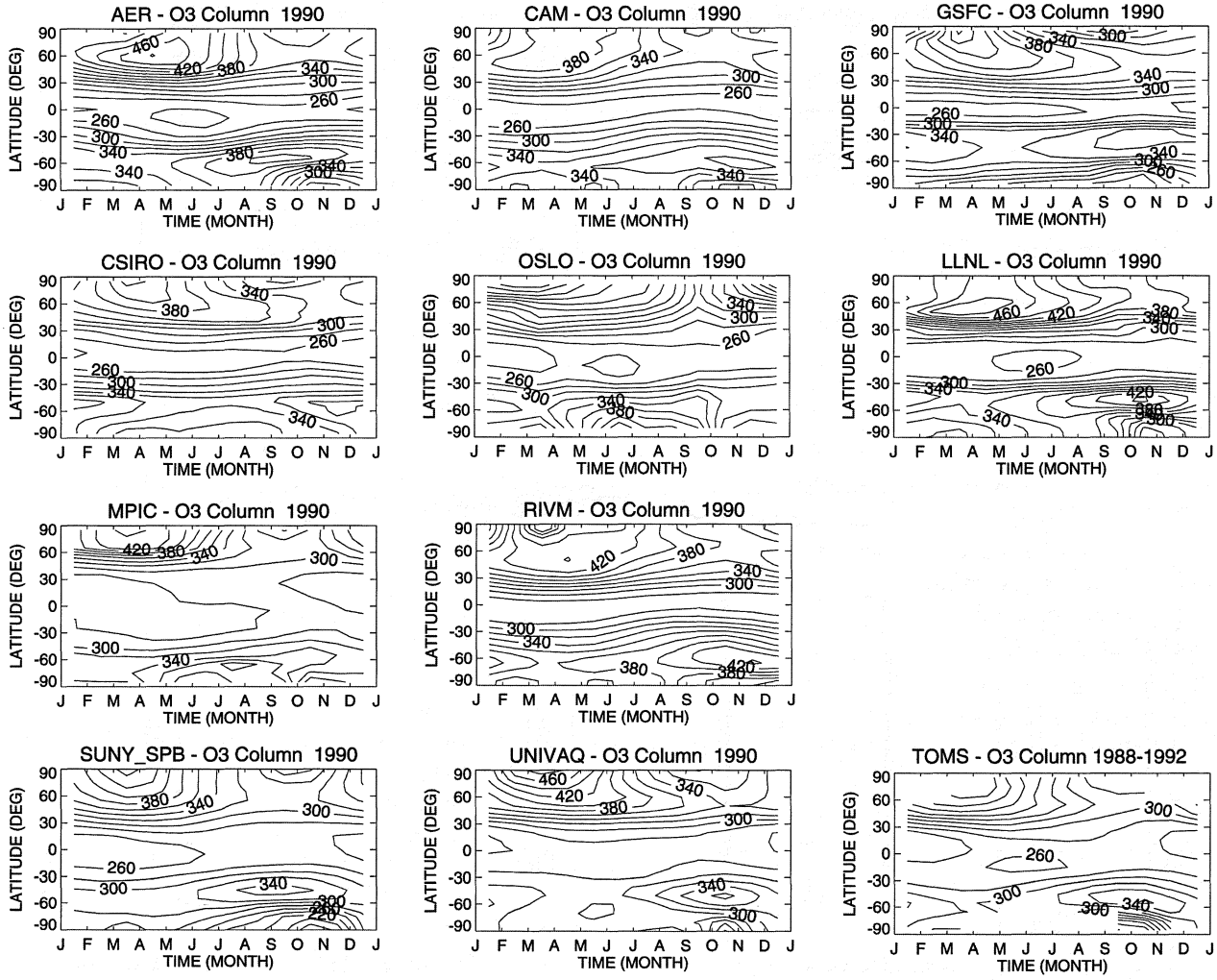


**Figure 12-3.** Model-derived total column ozone (DU) as a function of latitude and month of the year for 10 models for the year 1990. Observed data, given in last frame, are from TOMS Version 7, 1988-1992 average.

reproduce the magnitudes of the trend rather well (see Chapter 7).

In Figure 12-3, calculated column abundance of ozone for 1990 is shown along with the 1988-1992 column ozone derived from TOMS Version 7. In general the models represent the TOMS column ozone seasonality, with column ozone peaks occurring at high latitudes in the spring hemispheres and a minimum in the tropics. However, it is evident that stratospheric circulations within these 10 assessment models are strikingly different. The depth of the Southern Hemisphere "ozone hole" is also quite different among these 10 models, which suggests that the sensitivity to $Cl_y$, $Br_y$, and aerosol odd-oxygen loss processes may be quite different. All but two of the participating assessment models (CSIRO and RIVM) have detailed representation of spring high-latitude cold aerosol chemistry. However, both the CSIRO and RIVM models do have reactions that represent heterogeneous processes on liquid binary sulfate.

The trend in local ozone between 1979 and 1993 from scenario A is shown in Figure 12-4. Here the model results are compared with data from the Solar Backscatter Ultraviolet spectrometer (SBUV) and SBUV/2 measurements using a linear regression model to derive local ozone trends (see also SAGE I/II ozone trends in Chapter 4, Figure 4-32, which indicate slightly larger trends in the upper stratosphere). The linear regression

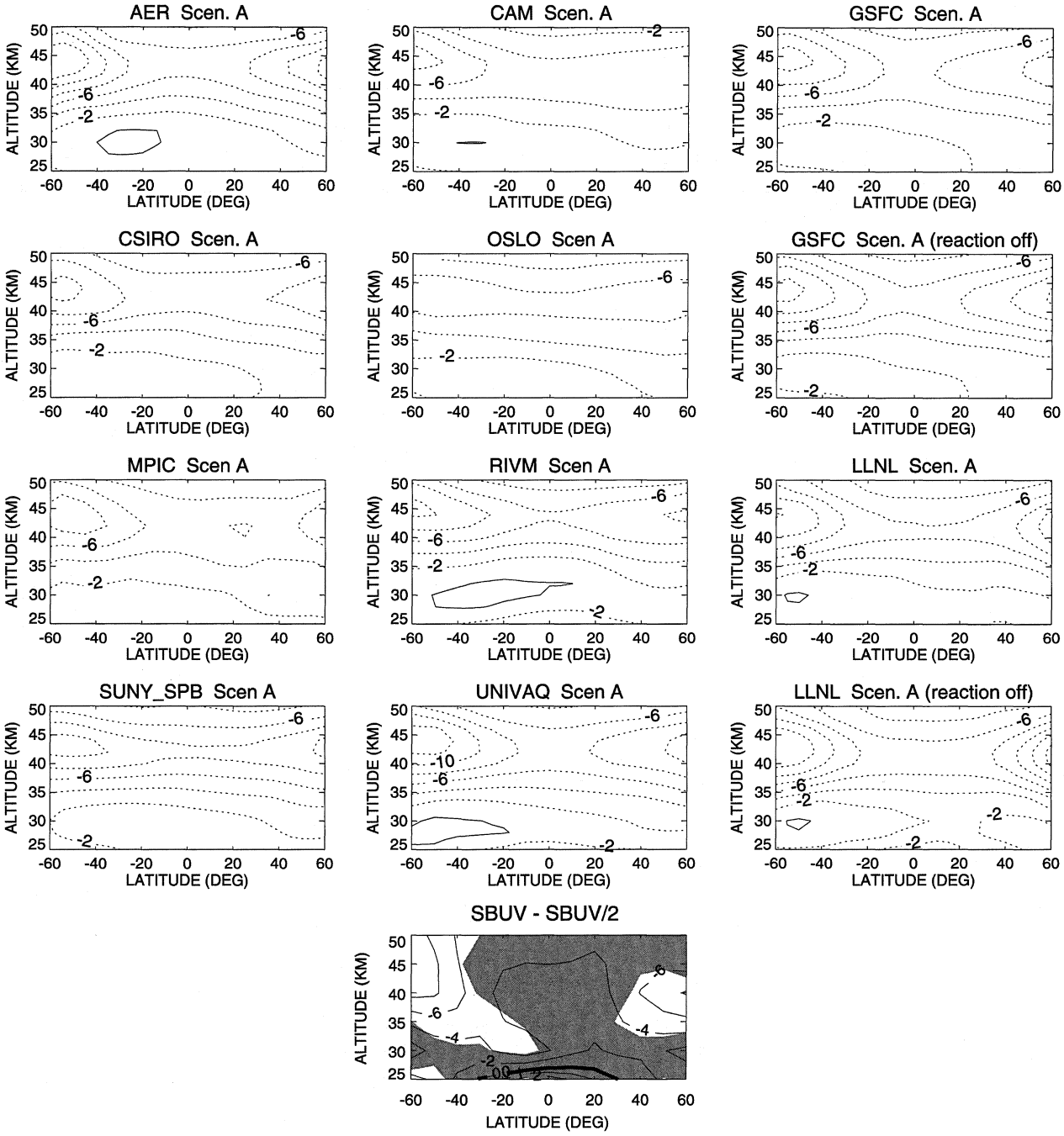


**Figure 12-4.** Model-derived local ozone trend (% per decade) for the period 1979 through 1993 as a function of altitude and latitude for scenario A using linear regression analyses for 10 models, and for the GSFC and LLNL models with the reaction ClO + OH → HCl + $O_2$ omitted. The observed trends (last frame) are from SBUV and SBUV/2 measurements. The shaded area in the observed trend indicates regions where there is no statistically significant trend.

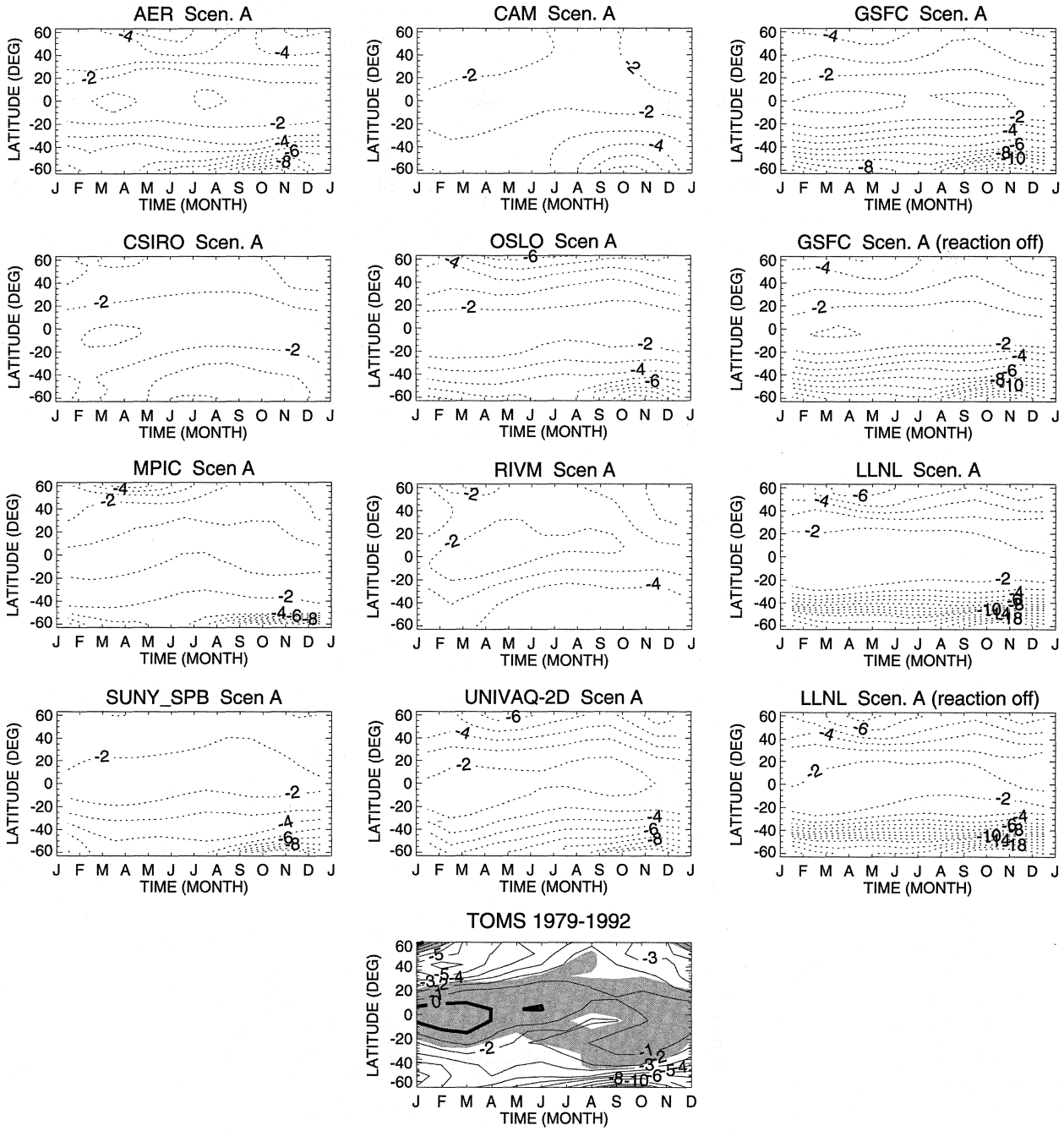


**Figure 12-5.** Model-derived column ozone trends (% per decade) for the period 1979-1992 as a function of latitude and month of the year for scenario A using linear regression analyses (see text) for 10 models, and for the GSFC and LLNL models with the reaction ClO + OH → HCl + $O_2$ omitted. The observed trends (last frame) are derived from TOMS Version 7 data. The shaded area in the observed trend indicates regions where there is no statistically significant trend.

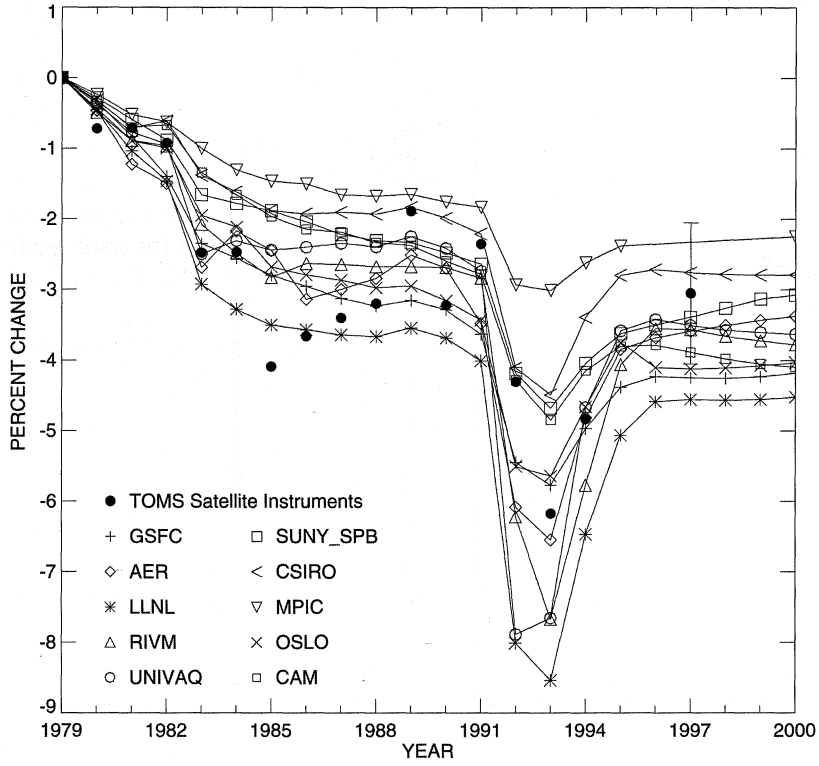


**Figure 12-6.** Percentage change in global (65°S-65°N) annual-average total column ozone, relative to year 1979, for 10 models for scenario A/A3 compared to observations using TOMS Version 7 data.

model consisted of a seasonal cycle, quasi-biennial oscillations, the 11-year solar cycle, and a linear trend (Hollandsworth *et al.*, 1995). The similarities between the model-derived local ozone trends and the data provide reassurance of satisfactory model performance. The shaded areas in the SBUV-SBUV/2 trends indicate regions where there is no statistically significant trend. All of the model-derived trends peak at about the correct altitude and most have magnitudes similar to the SBUV-SBUV/2 trends. In addition, the LLNL and GSFC 2-D models were used to test the sensitivity of the calculated trend to exclusion of the reaction channel $ClO + OH \rightarrow HCl + O_2$. For the past trends, both models' estimates exceed the observed trend when this reaction is omitted.

Figure 12-5 shows the TOMS Version 7 column ozone trend based on 14 years of data taken from January 1979 through December 1992 along with the derived trends from the 10 assessment models during the same period. Both the models and data were again analyzed using a linear regression model (Hollandsworth *et al.*, 1995). In general, the assessment models reproduce the gross characteristics of the TOMS ozone trend. They show the large decrease in the Southern Hemisphere spring, consistent with Antarctic "ozone hole" chemical processes. From this column trend analysis, it is evident that the RIVM and CSIRO models do not include a polar cold aerosol representation. For northern midlatitude (approximately 40-50 degrees) winter, in the Northern Hemisphere, most of the models underestimate the ozone trend, as described in Solomon *et al.* (1996).

The percentage change in global (65°S-65°N) annual average total column ozone, relative to 1979, is shown for the 10 models and compared with TOMS observations (primarily Nimbus-7 and Meteor-3 TOMS data, except for the 1997 data point taken from Earth Probe TOMS) in Figure 12-6. The shape of the ozone trend with time is similar for all the models but there is a significant spread of magnitudes (for example, by approximately 2% about a mean of 2.5% between 1984 and 1990 and by over 5% immediately after the Mt. Pinatubo eruption in 1991). This spread is not surprising. Figures 12-3 and 12-5 have already demonstrated the differences between the models, arising in part from differences in modeled circulation. Furthermore, there are model differences in the formulation of gas-phase and, especially, heterogeneous chemistry. Note also that none of the models include radiative feedback after the volcanic eruptions, which could have changed the circulation (see, for example, Kinne *et al.*, 1992; Michelangeli *et al.*, 1989; Pitari, 1993; Hadjinicolaou *et*

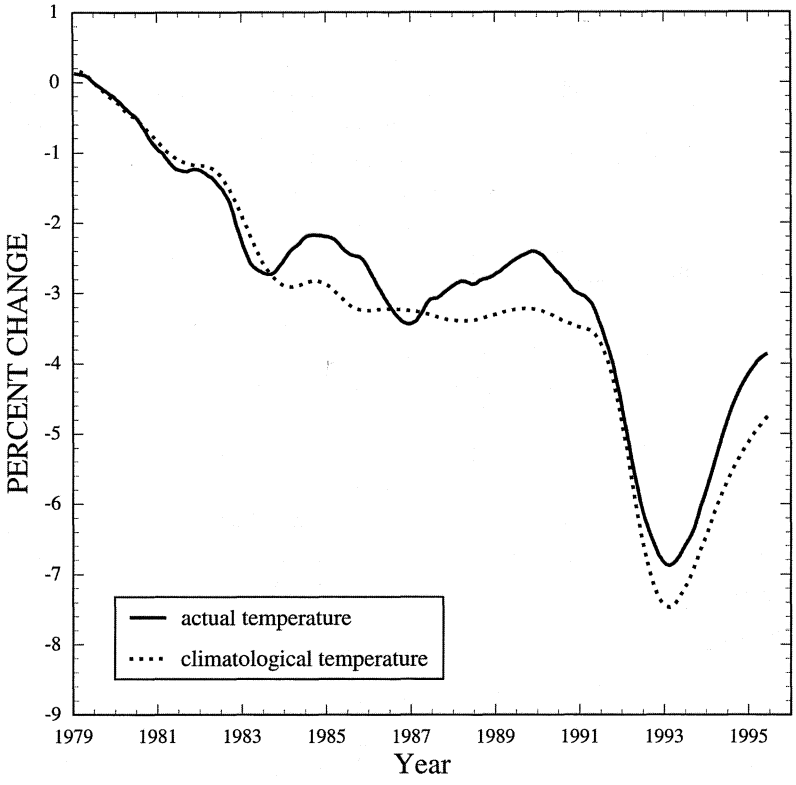


**Figure 12-7.** Percentage change in global (65°S-65°N) column ozone using a 24-month running mean for the AER model. The solid line represents an integration that includes the use of the mean temperature and temperature probability distribution about the zonal mean taken for each year between 1979 and 1995. The dashed line uses an 8-year average of both mean temperature and temperature probability distributions.

*al.*, 1997). For this reason, comparison between the models and the TOMS data must be treated with caution. With these caveats, several models tend to represent the trend in ozone during the 1980s reasonably well but overestimate the Mt. Pinatubo period. Other models underestimate the trend in the 1980s but seem to be in good agreement during and after the Mt. Pinatubo period.

The formulation of heterogeneous reactions is one reason why the models have different responses to aerosol-induced ozone depletion. For example, the AER 2-D model incorporates a method in which the kinetic rate constants are calculated using both zonal monthly-mean temperatures and temperature probability distributions to account for longitudinal deviations from the monthly zonal mean (see also Solomon *et al.*, 1998). To determine the sensitivity of the result, a second calculation was performed using a temperature climatology averaged over the years 1979-1995. Figure 12-7 shows the global-average ozone column changes calculated by the AER model with climatological temperatures and with year-by-year temperatures. The calculation with year-by-year temperatures shows more structure and year-to-year variability than the climatological case. The trends are similar until 1984; however, from 1984 to 1986, from 1988 to 1991, and from 1992 to 1995, the calculation with year-by-year temperatures shows less ozone depletion than the climatological calculation. Most of this difference relates to temperature variability at high latitudes in winter, which broadens the climatological distributions. The LLNL model shows a large sensitivity to Pinatubo-aerosol-induced ozone depletion because it used a single year (1996) to derive its temperature probability distribution. This year was colder than the climatological average, and therefore derived ozone trends in the LLNL model are overestimated for some years.

#### 12.2.1.3 Ozone Recovery—Model Sensitivity to Key Parameters

There are many factors that can affect the decadal time span of ozone recovery in model-derived trend studies and potentially within the present and future atmosphere. As mentioned in the introduction, the future abundances of $Cl_y$, $Br_y$, $CH_4$, $N_2O$, stratospheric sulfate aerosol, and climate conditions can significantly modify model-derived ozone recovery. Figure 12-8 shows the time variation of calculated $Cl_y$ and $Br_y$ for 50°N at 20 km for the 10 models. As previously discussed in the 1994 Assessment (WMO, 1995), there is a very large

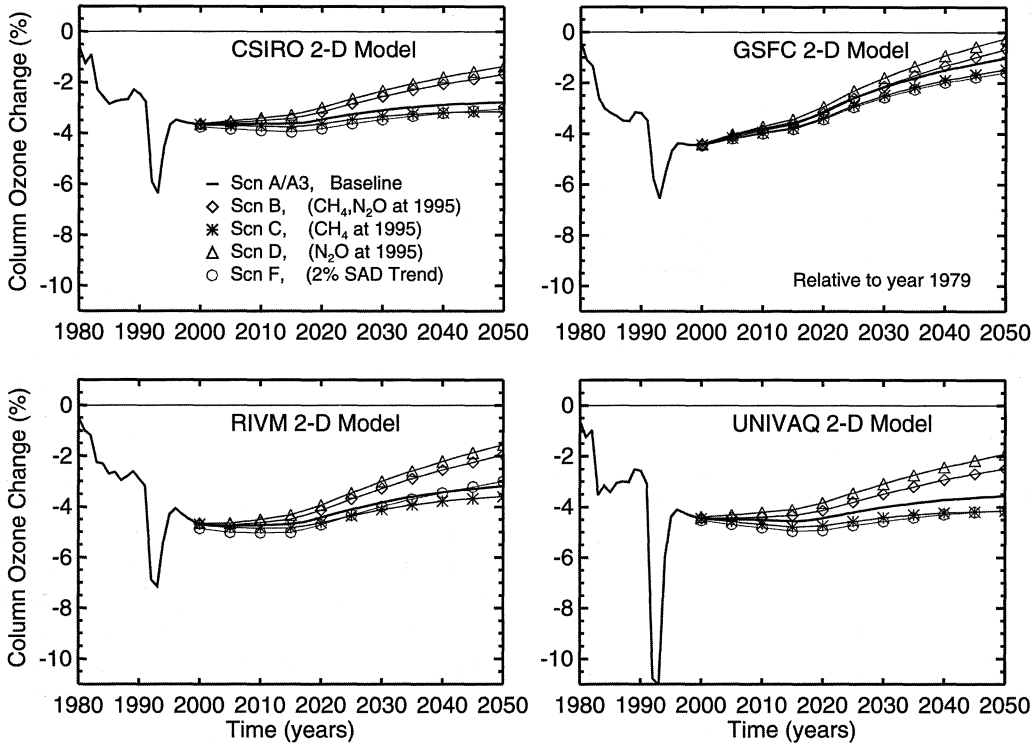


**Figure 12-13.** Percentage change in annual-average column ozone relative to year 1979 at 45°N latitude between 1980 and 2050 for several emission scenarios to test the model sensitivity to $CH_4$, $N_2O$, and SAD. Sensitivity tests for scenarios A through D, and F (see Table 12-3) are shown for the CSIRO, GSFC, RIVM, and UNIVAQ models.

Four modeling groups completed the entire set of sensitivity scenarios A-D and F. In Figure 12-13, the results of these models are shown at 45°N latitude. In all cases the sensitivity to $CH_4$, $N_2O$, and sulfate aerosol is consistent between models. When $CH_4$ is fixed at 1995 conditions (scenario C), the recovery is extended. When $N_2O$ is fixed at 1995 conditions (scenario D), the recovery is shortened. When both $N_2O$ and $CH_4$ are fixed at 1995 conditions (scenario B), the ozone recovery is shortened, but not to the extent of scenario D. When background stratospheric aerosol is allowed to increase annually by 2% per year (scenario F), the impact is to extend the recovery in three of the four models, with a magnitude similar to the impact of fixing $CH_4$ at 1995 conditions. The RIVM model initially extends the ozone recovery; however, around year 2040, the additional aerosol SAD hastens the ozone recovery relative to scenario A3.

Recently, laboratory measurements (Lipson *et al.*, 1997) have suggested that there may be a significant branching ratio for the $ClO + OH \rightarrow HCl + O_2$ reaction. As shown earlier, including this reaction improved the past trend comparisons for the LLNL and GSFC models relative to observations. The impact of the reaction on ozone recovery was also investigated in this study. For both models, the reaction changes the absolute magnitude of the ozone depletion by a small amount but does not impact the overall recovery rate. However, it is interesting that during the El Chichón and Mt. Pinatubo periods, including the $ClO + OH \rightarrow HCl + O_2$ branch mitigates ozone depletion; at later times there is a crossover where the absolute ozone reduction is greater when the reaction is included. Under lower $Cl_y$ abundance, the additional $ClO_x$ (when the reaction is omitted) is interfering with $NO_x$ odd-oxygen catalytic loss processes, mitigating ozone depletion.

In understanding the time frame over which ozone recovery will occur, one should also consider the impacts of future volcanic eruptions. As mentioned previously, between 1980 and 1995, there were two large volcanic events that significantly affected ozone trends (Solomon

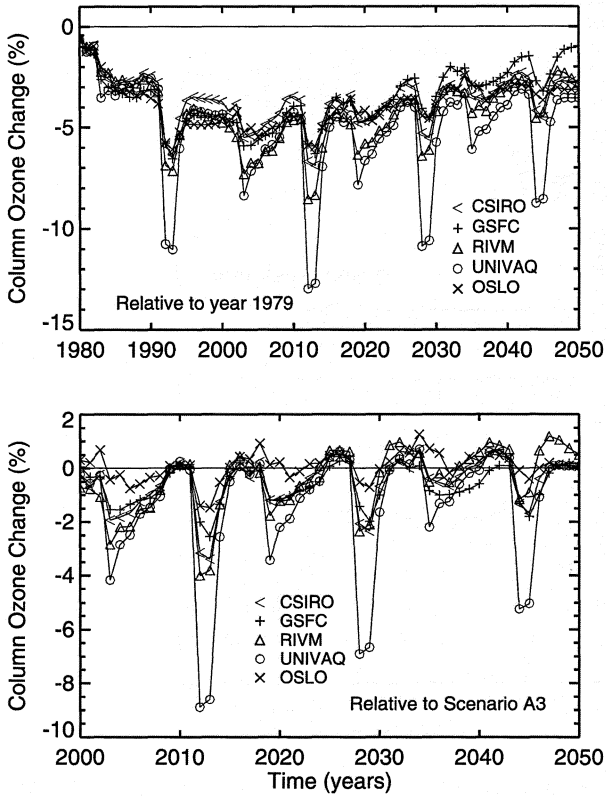


**Figure 12-14.** Top panel: Percentage change in annual average column ozone relative to year 1979 at 45°N latitude between 1980 and 2050 for five models, for volcanic eruption sensitivity scenario E (see Table 12-3). Bottom panel: The scenario A3 ozone trend has been subtracted to emphasize volcanic effects alone.

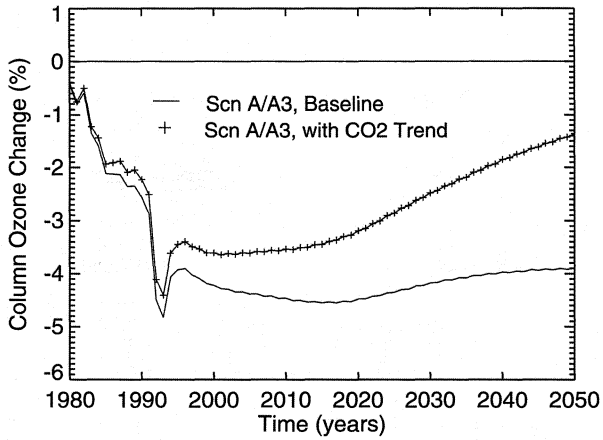


**Figure 12-15.** Percentage change in annual-average column ozone relative to year 1979 for the CAM 2-D model at 45°N latitude between 1980 and 2050. The solid line represents using $CO_2$ surface boundary conditions fixed at 1995 levels between 1979 and 2050. The line with crosses represents using a time-dependent trend of $CO_2$ (see Table 12-2).

*et al.*, 1996; Jackman *et al.*, 1996a). These events occurred during a period of high chlorine abundance. Tie *et al.* (1994) suggest that at lower chlorine abundance the impact of a major volcanic eruption will be less significant and could even increase ozone. In order to study the impact of high SAD in periods when chlorine abundance is much lower than present, scenario E was constructed. During the 1980 through 2050 period, four El Chichón- and Mt. Pinatubo-like eruptions were simulated (see Table 12-3). As indicated in Figure 12-14, the largest ozone reduction from this series of volcanic events occurred around 2010. This is a period of peak $Cl_y$ levels in the stratosphere, before significant reduction has set in (see Figure 12-8). In Figure 12-14, the underlying ozone trend component has also been subtracted from scenario E. This emphasizes the importance that $Cl_y$ and $Br_y$ abundances will have on the magnitude of the impact of a given volcanic event in the future. During the decade of the 2040s, the magnitude of the ozone reduction following a Mt. Pinatubo-sized eruption is reduced substantially. Thus, while Mt. Pinatubo-sized eruptions will have an effect on the magnitude of ozone depletion as long as halogens are present in the stratosphere, eruptions occurring at decadal intervals, as investigated here, are not expected to substantially alter the eventual ozone layer recovery over the long term.

An important sensitivity to be quantified is the role that future climatic conditions play in extending or mitigating the ozone recovery. In this study, the CAM 2-D model was allowed to respond to changes in $CO_2$ trends. Results from this sensitivity study are shown in Figure 12-15. For scenario A/A3, without $CO_2$ trends, the model recovery is very slow. The increases in $CO_2$ lead to reduced stratospheric temperatures, which then reduce the gas-phase destruction of ozone. In consequence the modeled ozone recovery is significantly accelerated. The model circulation will also change and will impact ozone levels. A more detailed discussion of the impact of changing greenhouse gas concentrations on polar ozone is given in Section 12.2.3.

**Table 12-4. Forcings and/or processes that affect model-derived ozone recovery.**

| Forcing or Process | Magnitude | Direction |
|---|---|---|
| Higher future $CO_2$ | Large | Shorten* |
| Higher future $Cl_y$ trends | Moderate | Lengthen |
| Higher future $CH_4$ trends | Moderate | Shorten |
| Higher future $N_2O$ trends | Moderate | Lengthen |
| Higher future sulfate aerosol loading | Moderate | Lengthen |
| A series of volcanic eruptions | Small | Lengthen |

* Midlatitude result based on one 2-D model. See also the discussion of 3-D models in Section 12.2.3, where increased greenhouse gases delay polar ozone recovery, particularly in the next 10 to 20 years.

#### 12.2.1.4 Summary

There are many factors that influence the ozone recovery as the atmosphere returns to pre-1980 halogen loading. In this section we have specifically considered 2-D model calculations of the global ozone behavior over many decades. We have discussed the model sensitivity to halogen loading, to $CH_4$ and $N_2O$ emission rates, to variations in aerosol SAD, and to the radiative impact of increasing $CO_2$. Depending on the model, the recovery of global ozone to pre-1980 conditions is reached at about 2050 on one extreme to potentially never on the other. Reducing the methane increase rate, in line with recent measurements, leads to a significant increase in the time for the ozone layer to recover.

Table 12-4 is a list of "forcings" and/or "processes" that affect the model-derived ozone recovery in the calculations discussed here, in approximate order of significance. "Large" magnitude denotes significant deviation from the baseline recovery—greater than ±30 years or a large (greater than ±2%) absolute difference in column ozone change between the baseline and perturbed forcing in 2050. "Moderate" denotes a significant change, modifying the recovery by less than ±30 years from the baseline, or the absolute difference in column ozone change between the baseline and perturbed forcing in 2050 is greater than ±1%. "Small" signifies that the change will affect the recovery period by less than ±5 years, or the absolute difference in column ozone between the baseline and perturbed forcing in 2050 is less than ±0.5%.

To put the list in context, it needs to be stressed that the magnitude of any effect will depend on the magnitude of the forcing. The classifications given in Table 12-4 relate directly to the different forcing scenarios considered earlier. These are necessarily uncertain. Thus, larger increases in future halogen loading (or any of the other forcings) than those considered here could lead to a "large" effect.

The sensitivities to forcing as presented in Table 12-4 are consistent between the various 2-D models. The magnitudes must be put into perspective by considering the large inter-model differences predicted for the A3 scenario in 2050 (see Figure 12-9).

### 12.2.2 Chemical Transport Models

Chemical transport models (CTMs), with circulations and temperatures forced by observations, have been used increasingly in recent years. They have been able to reproduce many observed features of the perturbed lower stratosphere, including the substantial Arctic ozone depletions that have been seen in recent years. These models can now be used for assessment purposes and, especially, for sensitivity studies.

#### 12.2.2.1 Sensitivity to Halogen Loading

The Cambridge CTM has been used to study the sensitivity of ozone depletion within the polar vortex to varying levels of $Cl_y$ and $Br_y$ (Chipperfield and Pyle, 1998). Results are shown in Figure 12-16. The figure shows that within the range of $Cl_y$ and $Br_y$ values tested, the chlorine loading has the strongest influence on ozone loss. For example, at 475 K with $Br_y$ fixed at 30 pptv, increasing $Cl_y$ from 2.0 ppbv to 3.3 ppbv to 4.0 ppbv increases the maximum average ozone depletion from 16% to 35% to 44%, respectively. In contrast, for a fixed $Cl_y$ of 3.3 ppbv, increasing $Br_y$ from 20 pptv to 30 pptv only increases the maximum ozone depletion from 30%

to 35%. This dependence of the ozone loss on $Cl_y$ and $Br_y$ is qualitatively consistent with the results of Danilin *et al.* (1996).

The greater sensitivity of the calculated ozone loss to chlorine reduction is one reason why recovery should be more visible in the Antarctic than the Arctic (since the ClO + ClO cycle is relatively more important there than ClO + BrO). Antarctic integrations with the Cambridge CTM (Chipperfield and Pyle, 1998) confirm that a change in chlorine loading from 3 ppbv to 2 ppbv produces a larger absolute reduction in ozone loss than in the Arctic.

#### 12.2.2.2 Sensitivity to Lower Stratospheric Temperatures

Although not run in coupled chemistry and climate mode, CTMs have demonstrated that the ozone loss in the Arctic is very sensitive to stratospheric temperatures. Figure 12-17 shows the minimum temperature north of 50°N at 50 hPa from the European Centre for Medium-Range Weather Forecasts (ECMWF) analysis for the Arctic winters of 1991/92 to 1996/97. The differing meteorology of the first four winters has been discussed by Chipperfield *et al.* (1996). Recent winters (1994/95, 1995/96, 1996/97) have all been cold, with periods of record low temperatures. In 1995/96, temperatures fell below the 195K NAT threshold in early December and dipped below the ice point in mid-January. Temperatures remained low until late February. In contrast, in 1994/95 temperatures rose earlier in February followed by a short low-temperature period in mid-March. The winter of 1996/97 started particularly warm, but temperatures dropped below the 195K threshold in mid-January and remained low throughout March, which saw many days with record minima.

Figure 12-18 shows the average ozone depletions calculated in the Arctic lower stratosphere (475K surface) for each year since 1993/94, assuming no change in stratospheric halogen loading. Earlier years were reported in Chipperfield *et al.* (1996). There is a large difference in the calculated ozone loss between the years. In the warm winter of 1993/94 the average depletion calculated is about 15%. Much larger ozone losses are calculated in those years (1994/95, 1995/96 and 1996/97) with lowest stratospheric temperatures. In 1996/97 the calculated depletion began much later but, with low temperatures coinciding with the return of sunlight, ultimately was approximately the same (nearly 25%) as

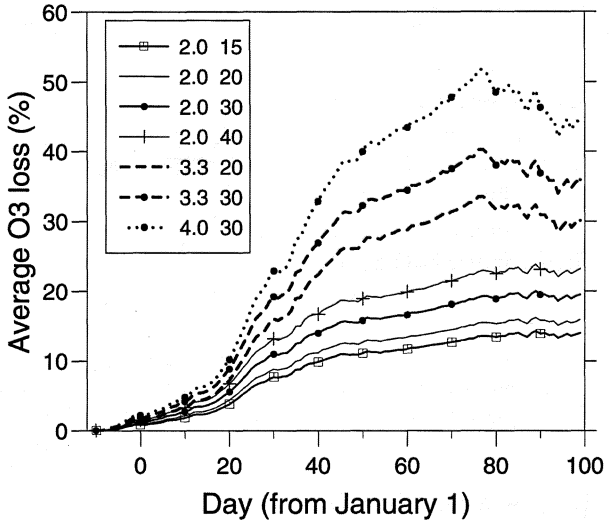


**Figure 12-16.** Variation of ozone loss (%) calculated within the Arctic polar vortex at 475 K for different values of $Cl_y$ (left in the legend, ppbv) and $Br_y$ (right in the legend, pptv) using the Cambridge CTM (Chipperfield and Pyle, 1998). The edge of the vortex was defined at 36 potential vorticity units (PVU) at 475 K.

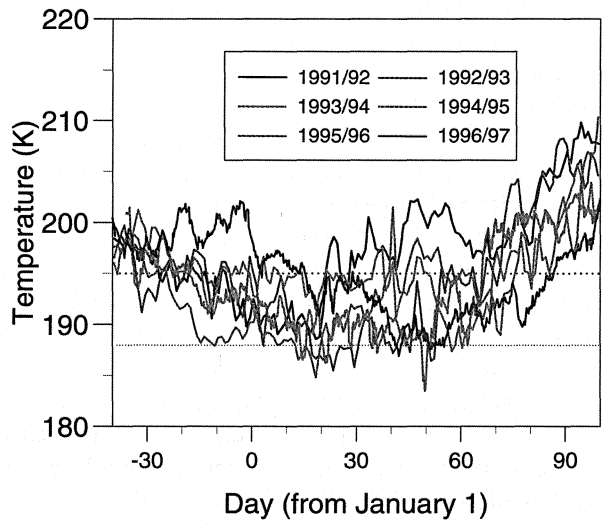


**Figure 12-17.** Minimum temperature in the ECMWF analysis at 50 hPa poleward of 50°N for the Arctic winters 1991/92 to 1996/97. Also indicated are the approximate formation temperatures of Type-1 (upper line) and Type-2 (lower line) PSCs. Figure updated from Chipperfield *et al.* (1996).

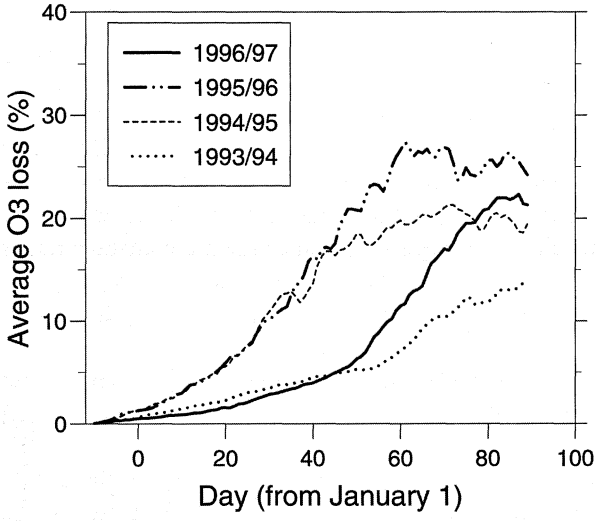


**Figure 12-18.** Area-weighted average chemical ozone loss (%) poleward of 60°N at 475 K for the Arctic winters 1993/94 to 1996/97, calculated in the Cambridge CTM (Chipperfield and Pyle, 1998).

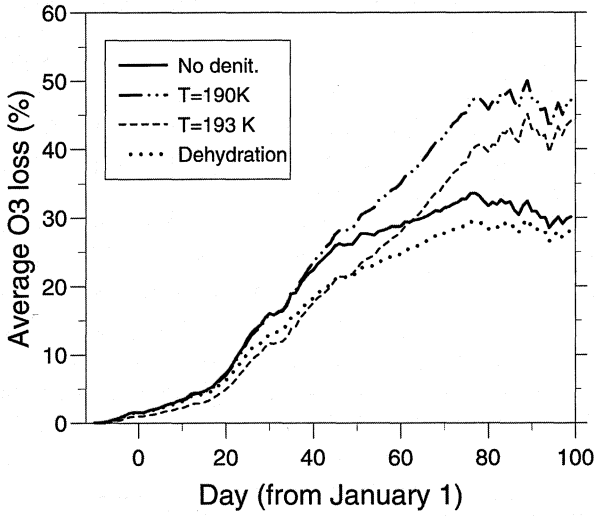


**Figure 12-19.** Sensitivity of Arctic ozone loss (%) within the polar vortex at 475 K, assuming different temperature thresholds for denitrification (and also dehydration) in the Cambridge CTM (Chipperfield and Pyle, 1998).

in 1995/96. The calculations demonstrate that Arctic ozone loss is very sensitive to lower stratospheric temperatures. Any systematic cooling of the stratosphere (so that, for example, the lower temperatures in recent years might become the norm) would have a very significant impact on stratospheric ozone recovery, a point we consider in more detail in Section 12.2.3 using coupled chemical-radiative-dynamical models.

A related experiment is that of Danilin *et al.* (1998), which used the AER photochemical box model including heterogeneous chemistry to investigate the influence of an imposed stratospheric cooling on Arctic ozone depletion. These results indicate that a 1-K cooling of the lower stratosphere was equivalent to increasing chlorine loading by 0.40-0.95 ppbv for current conditions. The results also imply that continued cooling of the stratosphere over the coming decades, similar to that observed over the past decades, could compensate for decreasing chlorine levels. In a long-term calculation for conditions at 70°N using heterogeneous reactions on NAT surfaces, the model predicts that a cooling trend of -0.05 K $yr^{-1}$ (a conservative estimate based on observations) leads to maximum ozone losses from about 2005 to 2020, with recovery to 1995 levels delayed past 2045. These results suggest the likelihood of a delay in the expected recovery of the ozone layer in the Arctic.

Should extensive denitrification occur in the Arctic polar vortex (similar to that in the Antarctic vortex) then the potential for ozone depletion could be enhanced. The sensitivity of the ozone depletion to the degree of denitrification is shown in Figure 12-19 in a calculation with the Cambridge CTM. One experiment assumed that $HNO_3$ was permanently removed from the gas phase at temperatures below 190 K. At 475 K this has the effect of delaying chlorine recovery and extending the period of rapid ozone depletion. The maximum average ozone depletion is increased from 30% in the control run ("No denit.," identical to the 3.3-ppbv $Cl_y$, 20-pptv $Br_y$ curve shown in Figure 12-16) to 40% when denitrification is included. A further experiment assumed the higher threshold for denitrification of 193 K. At 475 K this causes a reduction in ozone depletion. The removal of $NO_y$ prevents the formation of $ClONO_2$ as active chlorine decays. With sporadic PSC processing that occurs in the Arctic, the low $ClONO_2$ inhibits the further rapid activation of the chlorine contained in HCl (reaction (12-4), Section 12.2.1.1a).

### 12.2.3 Three-Dimensional Chemistry-Climate Models

The most important radiatively active gases in the atmosphere are water vapor, carbon dioxide, and ozone. An increase of these greenhouse gases is expected to produce a warming in the troposphere and a cooling in the stratosphere and a change in the dynamics. The predicted stratospheric cooling is generally expected to reduce homogeneous chemical destruction of ozone, while increasing heterogeneous destruction. Circulation changes will also alter ozone transport and hence its distribution.

In the stratosphere, where the chemical and dynamical transport time scales for ozone are roughly comparable, three-dimensional photochemical models, in which the simulated ozone is used to compute model radiative heating rates, are needed to provide a complete picture of stratospheric ozone and its future behavior. Additionally, the sensitivity to radiative and other perturbations will require simulations of the order of a decade or more to take into account the natural variability of the system. In practice the cost of running such models has, to date, resulted in other simplifications such as restricting the length of integrations to time scales of only a few years or less or simplifying the tropospheric simulation. At the time of the last Assessment (WMO, 1995), 3-D models in the literature included mechanistic models with full chemistry, low-resolution general circulation models (GCMs) with full chemistry, or more complete GCMs with a simplified chemistry. Computer power has only relatively recently reached the stage where comprehensive GCMs can be used with fairly complete stratospheric chemistry schemes. Coupled chemistry-climate models have not yet reached the level of maturity and confidence of climate models.

In mechanistic models, the dynamical situation in the stratosphere is controlled by the forcing at the model lower boundary. Granier and Brasseur (1991) were the first to use such a model to simulate an Antarctic ozone hole in a 3-D model, while Austin and Butchart (1992) demonstrated the importance of interhemispheric differences in polar ozone simulations. Knight *et al.* (1998) investigated the impact of the Mt. Pinatubo eruption on stratospheric ozone and found that the largest effect, a decrease of about 20 DU, occurred at the edge of the ozone hole, broadly in agreement with observations (Randel *et al.*, 1995). Butchart and Austin (1996) investigated the effect of the QBO on the Antarctic ozone hole to explore the hypothesis of Garcia and Solomon (1987) that deep ozone holes were experienced during westerly phases. The model results (Figure 12-20) suggest that the quasi-biennial oscillation (QBO) does indeed modulate the Antarctic ozone but that this occurs primarily through transport rather than heterogeneous chemistry. The above studies have shown that while mechanistic models reproduce the main characteristics of ozone behavior observed in the atmosphere, they also imply the need for more complete modeling treatments of the atmospheric system.

Short integrations of a low-resolution GCM with stratospheric chemistry have been performed by Pitari and Rizi (1993) in investigating the impact of aerosols from the Mt. Pinatubo eruption. Further short integrations using fairly comprehensive stratospheric chemistry in much more extensive GCMs have also been completed by Rasch *et al.* (1995) and Austin *et al.* (1997). The latter study demonstrated the need for a large number of vertical levels to simulate stratospheric dynamics sufficiently accurately, thereby increasing the computational cost further. Multi-year integrations with GCMs with comprehensive chemistry have been or currently are being run with the European Centre Hamburg model (ECHAM3/CHEM) (Steil *et al.*, 1998; Dameris *et al.*, 1998), the Météo-France Centre National de Recherches Météorologiques ARPROBUS model (Lefèvre *et al.*, 1994), and the UKMO chemistry-climate model (Austin *et al.*, 1997).

Experiments with fairly complete representation of climate processes but with limited chemistry have also been run for longer periods. Of those GCMs that include proper representations of the middle atmosphere (Table 1 of Hamilton (1996) lists many of these), there are comparatively few published predictions of possible changes of the stratospheric climate (Fels *et al.*, 1980; Boville, 1986; Rind *et al.*, 1990).

The Goddard Institute for Space Studies (GISS) climate model (Shindell *et al.*, 1997, 1998a,b; Rind *et al.*, 1998) and the EMÉRAUDE climate model used formerly at Météo-France (Cariolle and Deque, 1986; Cariolle *et al.*, 1990; Mahfouf *et al.*, 1993) have been run with a simple representation of stratospheric chemistry. However, because the chemical and dynamical transport time scales for ozone are roughly comparable in the stratosphere, using such simplified chemistry will have its limitations.

A brief description of the various 3-D models that have been used for ozone predictions is presented in

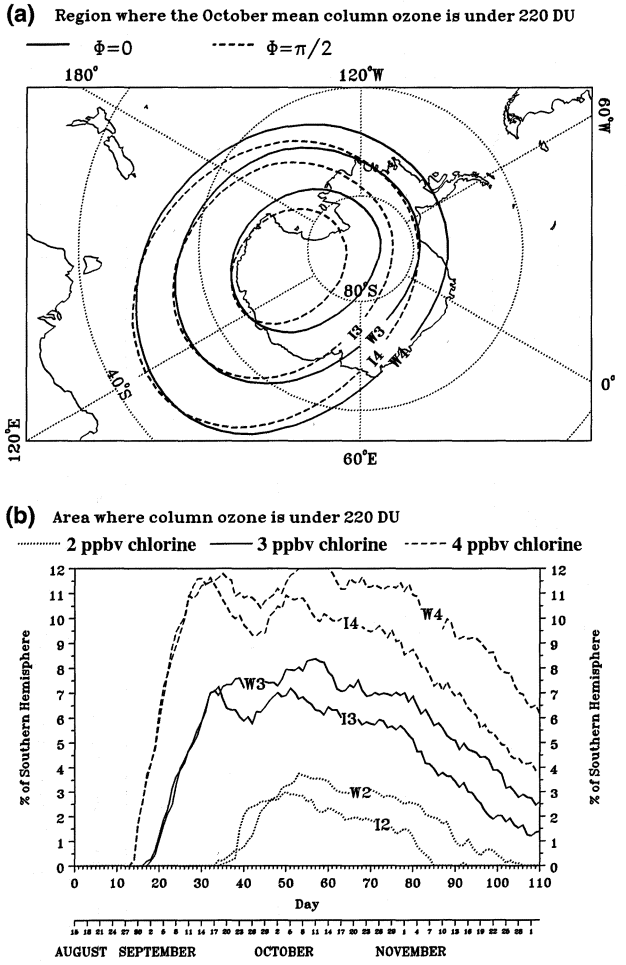


**Figure 12-20.** (a) Area enclosed by the 220-DU total ozone contour for the UKMO model investigating the impact of the QBO on the Antarctic ozone hole for varying levels of chlorine (from Butchart and Austin, 1996). The curves are labeled with the total chlorine amount in ppbv (2, 3 or 4) and the QBO phase (W denotes westerly; I denotes seven months later). Φ in the figure is the phase of the quasi-biennial oscillation at 24 km, where Φ = 0 corresponds to the westerly phase and Φ = π/2 is intermediate between the westerly and easterly phase (Φ = π). (b) Time history of the 220-DU contour area; labeling is the same as in (a).

Table 12-5. These models have a number of significant differences, including the region(s) of the atmosphere covered (i.e., troposphere, stratosphere, mesosphere), the resolution, the physics included, and the parameterization of ozone chemistry, both homogeneous and heterogeneous. These differences complicate a comparison of model results, but can be used to suggest which issues may be most important in influencing the future ozone distribution.

In the rest of this section we discuss in more detail the calculations of ozone change that have been performed with coupled chemistry-climate models. In Section 12.2.3.1, published results of doubled-$CO_2$ experiments are discussed, while results of new experiments to consider the transient ozone response to greenhouse gas forcing over the next two decades are presented in Section 12.2.3.2. For the transient experiments, emphasis is placed on the results in polar latitudes, where the largest response is expected. We recall the earlier caveat that these coupled models are relatively new and, for example, most have not yet been run for decadal time scales. By considering several models, our aim in this Assessment has been to emphasize those results that are most robust. The development of coupled models is an important advance; they will play an increasingly important role in future assessments of the state of the ozone layer.

### 12.2.3.1 Doubled-$CO_2$ Experiments

Doubled-$CO_2$ experiments can be grouped into two main types: transient and equilibrium. Since the coupled atmosphere-ocean system has considerable inertia, its response to increasing greenhouse gas concentrations can take considerable time. Similar to tropospheric models (IPCC, 1996), the result is that a transient experiment should show a muted atmospheric and oceanic response to doubled $CO_2$ as compared with an equilibrium experiment with the same model. In the GCM experiments that modeled the ozone response to doubled $CO_2$, two were equilibrium (UNIVAQ and GISS), while the EMÉRAUDE simulation was transient. A more recent experiment with the UNIVAQ model examined the ozone response to an increase of $CO_2$ up to 500 ppmv (Pitari and Visconti, 1994), as predicted for the year 2050 (see WMO, 1992). The GISS stratospheric model gives a response ratio (transient/equilibrium) of 63% at the surface, 60% in the upper troposphere at 150 hPa, 47% in the lower stratosphere at 68 hPa, and 67% in the upper

## Table 12-5. The 3-D (chemistry-climate) models.

| Model | References | Horizontal Resolution | Vertical Layers | Vertical Extent | Tropospheric/ Stratospheric Dynamics | Gas-Phase Chemistry | Hetero-geneous Chemistry | Greenhouse Gas Forcing | Temperature Response to Greenhouse Gases |
|---|---|---|---|---|---|---|---|---|---|
| UNIVAQ | Golombeck and Prinn, 1986; Pitari *et al.*, 1992 | Spectral, rhomboidal 6, ~10° × 20° | 25 | Surface to 71.6 km | Not properly represented due to spectral truncation | Detailed | Simplified | Equilibrium $2 \times CO_2$ | On-line, global balance approximation in troposphere |
| EMÉRAUDE | Mahfouf *et al.*, 1993 | T = 42, ~2.8° × 2.8° | 30 | Surface to 80 km | Full general circulation model | Linearized scheme | None | Transient $2 \times CO_2$ | On-line, based on SST changes from Hamburg GCM (Cubash *et al.*, 1992) |
| UKMO Mechanistic | Austin *et al.*, 1992; Austin and Butchart, 1994 | 5° × 5° | 32 | 316 to 0.0316 hPa (~8 to 72 km) | Planetary waves prescribed at lower boundary* | Detailed | Detailed | Equilibrium $2 \times CO_2$ | Calculated in separate experiment with similar model, then prescribed for chemistry runs |
| UKMO Chemistry-Climate | Austin *et al.*, 1997 | 2.5° × 3.75° | 49 | Surface to 65 km | Full general circulation model | Detailed | Detailed | Projected increases, 1990-2015 | On-line, based on SST changes from separate atmosphere/ ocean coupled simulation |
| ECHAM3/ CHEM | Roeckner *et al.*, 1992; Steil *et al.*, 1998 | Triangular 21, ~5.6° × 5.6° | 19 | Surface to 10 hPa | Model top location limits stratospheric dynamics | Detailed | Detailed | Projected increases, 1990-2015 | Calculated in separate experiment with related model, then prescribed for chemistry runs |
| Arpège/ REPROBUS (ARPROBUS) | Deque and Piedelievre, 1995; Lefèvre *et al.*, 1994 | T = 21, ~5.6° × 5.6° | 41 | Surface to 80 km | Full general circulation model | Detailed | Detailed | Projected increases, 1995-2015 | On-line, based on SST changes from separate atmosphere/ ocean coupled simulation |
| GISS | Rind *et al.*, 1998; Shindell *et al.*, 1998a | 8° × 10° | 23 | Surface to 85 km | Full general circulation model | Simplified† | Simplified | Projected increases, 1959-2070, and Equilibrium $2 \times CO_2$ | On-line, including SSTs |

The models described in the bottom four rows are used in Section 12.2.3.2 to assess future ozone changes.

* Various planetary wave amplitudes were prescribed at the model's lower boundary to simulate a variety of atmospheric conditions.

† Parameterized ozone chemical responses to temperature and radiative forcings only; ozone transport changes calculated offline (non-interactively) from the doubled-$CO_2$ experiments.

stratosphere at 1.5 hPa, all for equatorial areas. This is similar to the range 47-83% seen in tropospheric models (Table 6-3 of IPCC, 1996). This factor can then be used in the comparison of results from the stratospheric models run in transient doubled-$CO_2$ experiments with those run in equilibrium doubled-$CO_2$ experiments.

### *12.2.3.1a Temperature and Dynamics Changes*

There is significant model-to-model variation in temperature response. Figure 12-21 gives the annual-average temperature response to $CO_2$ doubling in the GISS model, including the feedback of ozone changing the absorption of radiation. Comparisons with the tropospheric models included in IPCC (1996) show a similar pattern of warming, notably including the temperature increase in the equatorial upper troposphere. The warming in the upper troposphere is found in various of the models considered here, but its magnitude varies significantly. For example, the UNIVAQ model gives a warming of 2 to 4 K, which is considerably smaller than the GISS model warming of up to 10 K. However, the UNIVAQ model uses a Newtonian cooling approximation in the troposphere and does not calculate heating rates explicitly. The EMÉRAUDE model also gave a smaller warming of about 2.5 K, although some of the discrepancy with the GISS model can be accounted for by the transient nature of the experiment. The EMÉRAUDE model found a transient doubled-$CO_2$ surface warming of 1.4 K, near the low end of the 1.3-3.8 K range for similar experiments (IPCC, 1996). The GISS model gave a surface warming of 4.2 K in a climate run with no stratosphere (as compared with 5.1 K in the GISS troposphere-stratosphere model (Rind *et al.*, 1998)), toward the high end of the 2.1-4.6 K range seen in similar experiments (IPCC, 1996). The temperature response in these two models may therefore represent the range of results based on the variability in current climate models.

The tropospheric warming in the GISS model is so large that it extends up into the lower stratosphere. This warming, and the associated circulation changes, affects the transport of heat in the stratosphere, as well as directly altering the radiative flux. Therefore, the degree of warming in the upper troposphere must be thought of as one of the largest sources of uncertainty in estimating the ozone response to increasing greenhouse gases.

In the midlatitude and equatorial upper stratosphere, the coupled models discussed here all show a large cooling of between 6 and 12 degrees, as expected

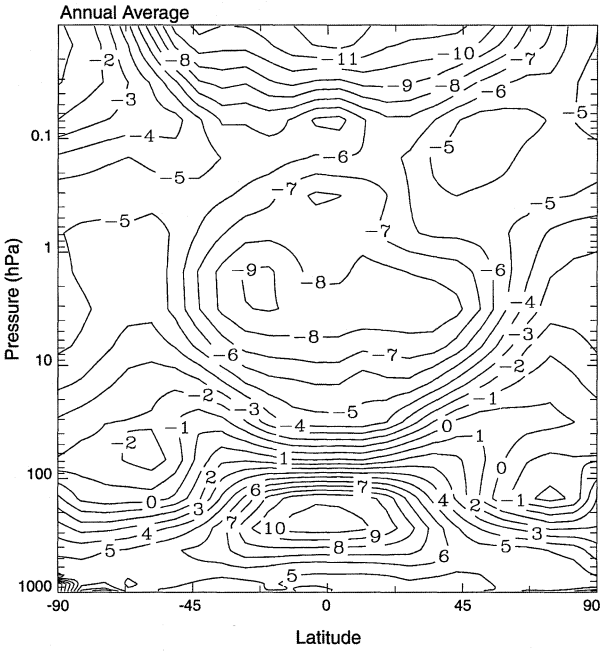


**Figure 12-21.** Zonal-mean annual-average temperature change (K) induced by doubling $CO_2$ in the GISS model. The values shown have been averaged over the last 20 years of a 50-year run, after the model had reached equilibrium with the doubled $CO_2$.

from greenhouse gas increases (Fels *et al.*, 1980; Boville, 1986; Rind *et al.*, 1990). The magnitude of the cooling is reduced by about 20% by the ozone chemical feedback (see, for example, Rind *et al.*, 1998; Shindell *et al.*, 1998a). In the midlatitude and equatorial lower stratosphere, however, the models disagree, with the GISS model finding a slight warming driven by its tropospheric warming while the other models have a cooling. At high latitudes throughout the stratosphere, there are considerable differences in the temperature response, which are associated with differences in modeled circulation changes.

All the models produce an enhanced residual circulation in response to increasing greenhouse gases, causing an increased transport of ozone to high latitudes, though the magnitude of the increase varies between models. The UNIVAQ experiment with 500 ppmv $CO_2$ found ozone increases of about 10% of the background values at high latitudes due to circulation changes. Changes in lower stratospheric temperature gradients and consequently zonal winds alter the propagation of planetary waves. This can affect the frequency of sudden

warmings in the models. Again, there is considerable variability between the models. The EMÉRAUDE model finds an increased frequency of Northern Hemisphere sudden stratospheric warmings. On the other hand, the GISS model gives a reduction in the frequency of sudden warmings, leading to a more stable, colder polar vortex, with significant effects on Arctic ozone loss.

#### *12.2.3.1b Ozone Changes*

Lower temperatures slow down the rates of the homogeneous chemical reactions that destroy ozone, so that the cooling found in the upper stratosphere in the models results in increased ozone. An increased overhead column reduces the amount of UV reaching the lower stratosphere, decreasing the photochemical production of ozone there, in addition to ozone changes induced by temperature and circulation changes.

Changes in total column ozone amounts are available for the UNIVAQ, EMÉRAUDE, and GISS models. All three models show increases, of up to 4%, in the equatorial region where the temperature responses are similar. However, the UNIVAQ model experiment with 500 ppmv $CO_2$ showed a decrease in the tropical ozone column, as the additional upwelling outweighs the chemical changes in the middle stratosphere.

At middle latitudes, there was cooling throughout the stratosphere in the UNIVAQ and EMÉRAUDE models, leading to column increases. In the GISS model, the lower stratosphere warmed, leading to a temperature-induced ozone decrease there, which combines with a decrease induced by the larger overhead ozone column. These generally outweigh the upper stratospheric ozone increase, giving a net column decrease.

At high latitudes, the results from the models generally differ more sharply. The EMÉRAUDE model did not include heterogeneous chemistry, while the UNIVAQ model did include a simplified heterogeneous chemistry scheme. The GISS model was run both with and without heterogeneous chemistry. The UNIVAQ model, and GISS model without heterogeneous chemistry, found ozone column changes of -1% to +7% and -2% to +5%, respectively. The seasonal variation also agrees quite well between these models. Both show a slight column loss at high southern latitudes during the austral fall/winter, and column increases before and after. The EMÉRAUDE model found column increases of +4% to +9% at high southern latitudes, however, and showed increases at all times of the year. The differences likely arise from the inclusion or lack of heterogeneous chemistry and from the varied predictions of the future frequency of sudden warmings.

In the polar spring lower stratosphere, heterogeneous chemistry on PSCs can lead to severe ozone loss, which is particularly sensitive to small changes in temperature. PSC formation is dependent upon local temperatures, therefore adding to the uncertainty of model predictions. Model experiments incorporating parameterized heterogeneous chemistry have been performed with the UNIVAQ and GISS models using constant chlorine abundances. The model response obviously depends critically on both the background temperatures calculated in the model, and the perturbations to those temperatures as greenhouse gases increase. For the Antarctic spring, when a large ozone hole forms with current $CO_2$ amounts, the doubling of $CO_2$ has a fairly small impact. In these models, the primary effects are an increase in the areal extent and the duration of the ozone hole.

In the Arctic, the UNIVAQ model finds that the total ozone column decreases by approximately 2% relative to $1 \times CO_2$. However, only a single fairly warm year was simulated in the experiment. The UKMO mechanistic model was used to simulate the seasonal evolution for several different years (Austin *et al.*, 1992; Austin and Butchart, 1994). During winters in which no stratospheric warmings occurred, total ozone decreased by about 35% (Figure 12-22), similar to, though slightly smaller than, the losses of up to 50% seen in years without warmings in the GISS model (Shindell *et al.*, 1998a). Note that the three models were run with chlorine loadings of 2.5-3.6 ppbv, which are now considered too large for the doubled-$CO_2$ atmosphere.

### 12.2.3.2 Transient Ozone Response

Three-dimensional experiments using coupled chemistry-climate models with realistic projections of chlorine loading and greenhouse gas emissions are essential for predictions of future ozone. Advances in computing power and our understanding of stratospheric processes have only recently allowed the first such simulations. Results from the GISS model (Shindell *et al.*, 1998b) and the ECHAM3/CHEM model (Dameris *et al.*, 1998) have been published. Two further experiments have recently been completed with the ARPROBUS and the UKMO chemistry-climate models. A preliminary analysis from these two models has also

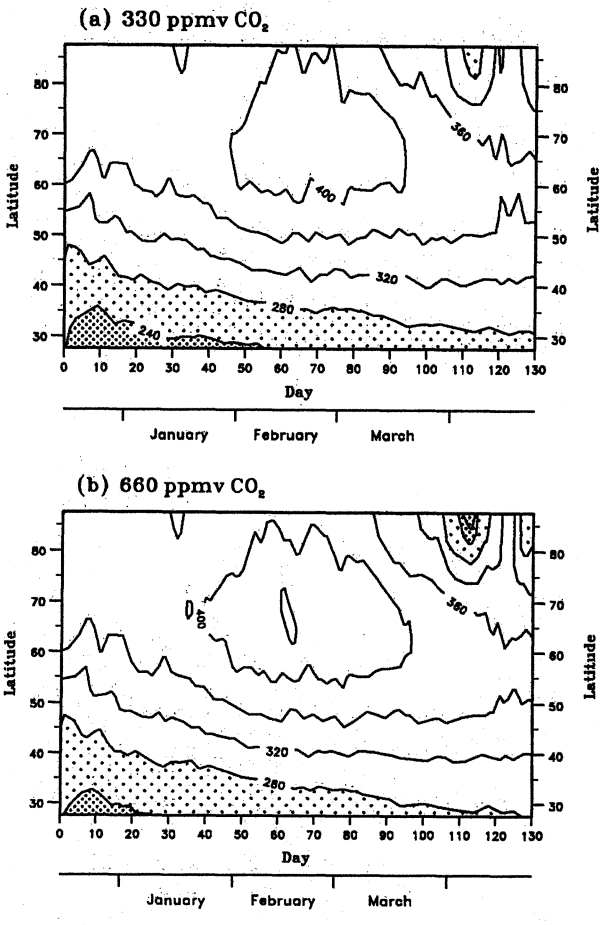


**Figure 12-22.** Model simulations of the time evolution of total ozone (DU) in mid and high latitudes of the Northern Hemisphere for the winter of 1990 using (a) current levels (330 ppmv) of carbon dioxide and (b) doubled levels (660 ppmv) of carbon dioxide (from Austin and Butchart, 1994). The contours are at 40-DU intervals. Light stippling indicates values between 240 and 280 DU; heavy stippling indicates values below 240 DU. Note in particular the lower values of ozone near 80°N after day 100 for the doubled-$CO_2$ case.

been performed for this Assessment, providing valuable indications of the robustness of the conclusions of the published work.

The GISS model is a full general circulation model that uses chemistry based upon parameterizations derived in a 2-D model. The chemistry is interactive with the model's radiation, but ozone transport is calculated in a non-interactive manner. Future chlorine and CFC amounts were based on current emission limits, while greenhouse gas emissions ($CO_2$, $CH_4$, and $N_2O$) were similar to the IS92a (IPCC, 1996) scenario (see Figure 1 of Shindell *et al.*, 1998b). The model simulated conditions from 1959 through 2070. Sea surface temperature (SST) changes were calculated on-line in this model.

The ECHAM3/CHEM general circulation model (Roeckner *et al.*, 1992; Steil *et al.*, 1998) was used in time slice simulations for 1991 and 2015 conditions (Dameris *et al.*, 1998). This model has a detailed treatment of homogeneous and heterogeneous chemistry. However, with a model top located in the middle stratosphere at 10 mb, this model cannot properly reproduce planetary wave propagation in the stratosphere (Austin *et al.*, 1997; Rind *et al.*, 1998). Nevertheless, the model is able to reproduce realistic Northern Hemisphere vortex variability in terms of shape and location (Grewe *et al.*, 1998). The model was run with non-interactive chemistry so that chemical changes did not feed back on the radiation or dynamics. Projected greenhouse gases were included and chlorine amounts went from 3.2 ppbv in 1991 to 2.7 ppbv in 2015 (a faster reduction in chlorine loading than discussed in Chapter 11 of this Assessment). The ECHAM3/CHEM simulations also included changes in tropospheric ozone. The model predicted an increasing trend in tropospheric ozone, driven by emissions of ozone precursors. Because this is the only model described here that included changes in tropospheric ozone, the calculated changes in column ozone should be offset from the models with stratospheric chemistry alone. The model was run for 14 years for each set of conditions (1991 and 2015). Results were averaged over the last 10 years to provide a picture of the average behavior for each set of trace gas loadings with the influence of the initial conditions removed by the 4-year start-up period. SST changes were taken from a transient simulation with a coupled atmosphere-ocean GCM.

The ARPROBUS model is a combination of the Arpège-climat GCM and the REPROBUS CTM. Arpège-climat is the climate version of the Arpège/Integrated Forecast System (IFS) weather prediction model developed jointly by Météo-France and ECMWF. Doubled-$CO_2$ experiments using Arpège-climat (Timbal *et al.*, 1997; Douville *et al.*, 1998) have shown climate responses close to the projections of previous similar studies performed elsewhere. The REPROBUS CTM

calculates the evolution of 55 species with a detailed treatment of the homogeneous and heterogeneous chemistry. This model has often been used for case studies of polar stratospheric winters, giving results in rather good agreement with experimental data in terms of $NO_y$, chlorine activation, and ozone loss (e.g., von Clarmann *et al.*, 1997; Lefèvre *et al.*, 1994; Lefèvre *et al.*, 1998; Payan *et al.*, 1998; Renard *et al.*, 1997; Wetzel *et al.*, 1997). For the simulations presented here the ARPROBUS coupled model was integrated at T21 (5.6°) horizontal resolution, on 41 levels from the ground up to 80 km. The ozone field was exchanged every 6 hours between the CTM and the radiative code of the GCM for a fully interactive coupling between chemistry, radiation, and dynamics. Like the ECHAM3/CHEM model, ARPROBUS was run for 6 years for both 1995 and 2015 conditions. IPCC projections of greenhouse gases were used in the model experiments, while chlorine amounts went from 3.7 ppbv in 1995 to 3.3 ppbv in 2015 (again a slightly faster reduction in chlorine loading than assumed in scenario A3 in Chapter 11). SST changes were calculated in a separate transient experiment with the Arpège-climat GCM coupled to an ocean model.

An upgraded version of the troposphere-stratosphere configuration of the UKMO Unified Model (Butchart and Austin, 1998) has been run from 1990 to 2050, assuming greenhouse gas changes specified under scenario IS92a (IPCC, 1996). Sea surface temperature was taken from a coupled ocean-atmosphere version of the Unified Model (Mitchell *et al.*, 1995; Johns *et al.*, 1997). This integration provided dynamical initial conditions for 16-month, fully coupled chemistry integrations at 5-year intervals beginning with 1 March 1994. Appropriate sea surface conditions were obtained from the coupled atmosphere-ocean version of the model. Only the last 12 months of the simulations were used in the analysis presented here, which allowed the model 4 months to come into approximate equilibrium with radiative forcing. Chlorine trends were taken from Chapter 11 of this Assessment, while bromine trends were assumed to increase through 2010. The treatment of chemistry is of similar complexity to the ARPROBUS model. While only 1-year snapshots were performed, the fact that the results are representative can be assessed qualitatively by noting that changes occur steadily throughout the period. The dynamical climatology of the model is in reasonable agreement with observations (Butchart and Austin, 1998), while the trends predicted in the troposphere agree with previous studies (see, for example, Mitchell *et al.*,1995). In the upper stratosphere the model response to increasing greenhouse gases is consistent with past temperature trends (Chapter 5). The chemical performance of the model was investigated in Austin *et al.* (1997) and found to be satisfactory for the current atmosphere. Further calculations with improved versions of the model support these conclusions.

#### *12.2.3.2a Temperature and Dynamics Changes*

For the behavior of polar ozone, temperatures in the winter/spring lower stratosphere are most important. Figure 12-23 shows the zonal-mean temperature difference between 2015 and 1995 for February and September for the four models. All the models show a tropospheric warming and a general stratospheric cooling, as expected. The magnitudes of the upper tropospheric warmings are fairly similar in the four models, though the ECHAM3/CHEM model shows a larger warming in September and the ARPROBUS model shows a smaller warming in February. A distinct maximum in the tropics appears in the GISS, ECHAM3/CHEM, and UKMO models. In the lower stratosphere, the ECHAM3/CHEM model shows a larger cooling than the other three models, except in the Arctic during February, when the GISS and UKMO models show a cooling of more than 4 K. The GISS and ARPROBUS models include ozone radiative feedback, while the ECHAM3/CHEM and UKMO model results do not, which may partially account for some of the differences.

Analysis of the GISS model results showed that the Arctic winter/spring cooling in that model results from both greenhouse-gas-induced radiative cooling and dynamical changes. The changes in the temperature structure of the atmosphere, especially the increase in the upper troposphere/lower stratosphere latitudinal temperature gradient, increase the lower stratospheric zonal winds, altering the propagation of planetary waves so as to reduce the frequency of Northern Hemisphere sudden stratospheric warmings in the model. The ECHAM3/CHEM model also predicts a colder Arctic vortex but, with a top at 10 hPa, is unable to simulate stratospheric dynamics completely, so that it may not have been able to predict the frequency of sudden warmings properly. The UKMO model also shows its strongest stratospheric cooling in the Arctic region. The ARPROBUS model simulated a colder vortex on average for 2015 conditions, although the magnitude of changes within the vortex can be distorted in the zonal-mean

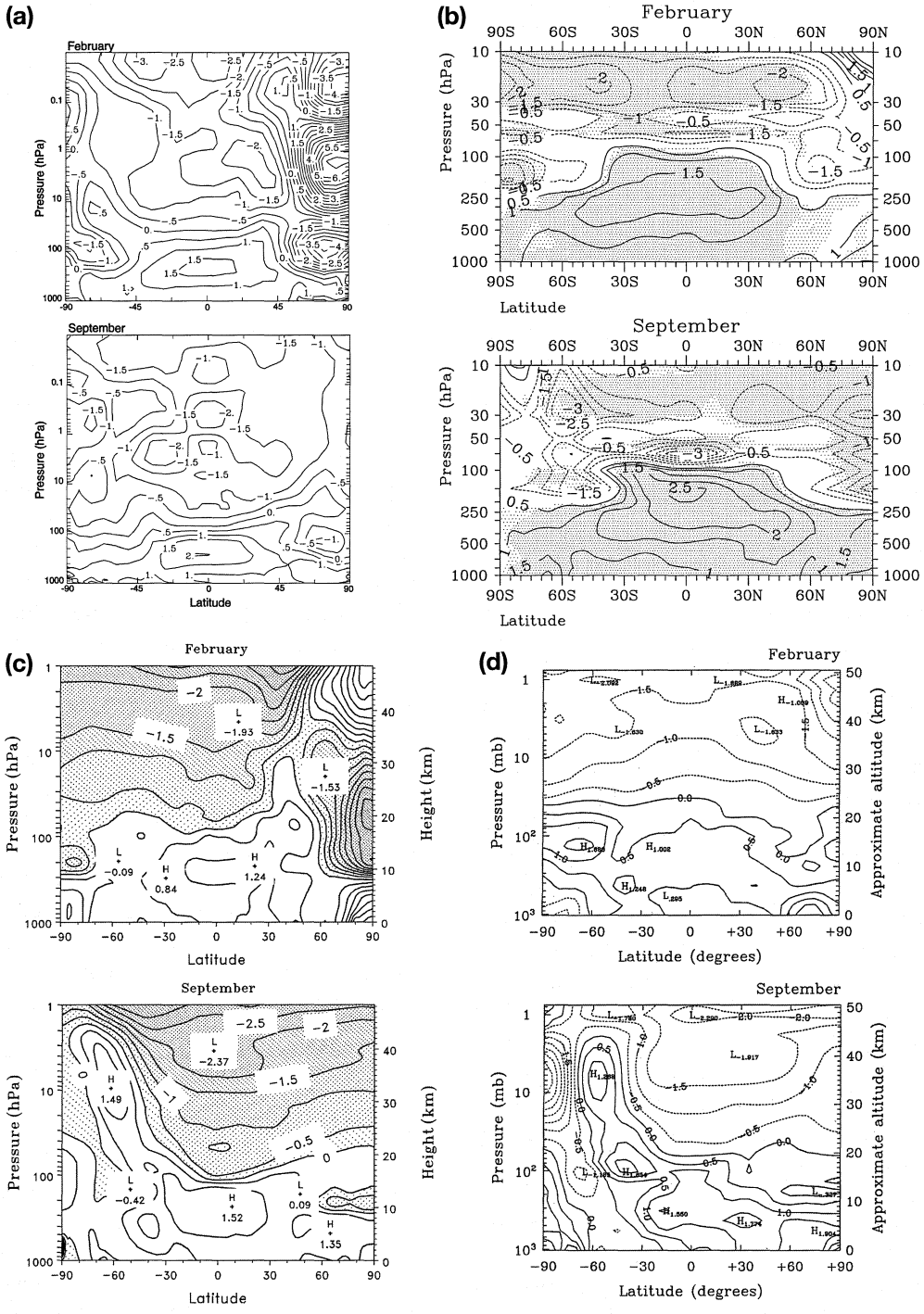


**Figure 12-23.** Zonal mean temperature changes forced by projected greenhouse gas and halogen emissions during February and September between 2015 and 1995 for four models. (a) GISS model. Note the large cooling in the Arctic lower stratosphere during February. (b) ECHAM3/CHEM model. Shaded areas indicate regions of significant changes. (c) UKMO model. Shaded areas indicate areas with a temperature decrease. (d) ARPROBUS model. Contours of reduced temperature are represented by dashed lines.

averaging of the highly asymmetric Arctic vortex. Given the large variability and that the results for this model are only a 5-year average, it is difficult to draw conclusions about the frequency of sudden warmings.

Another factor linked to the strength of the Arctic cooling is the positive feedback of increased ozone depletion included in the GISS and ARPROBUS simulations, but not in the UKMO dynamical and ECHAM3/CHEM simulations. The lower temperatures in the Arctic vortex found in all four models are consistent with the observed temperature trends. The wintertime Arctic vortex area with temperatures below 195 K has increased considerably over the past three decades (Pawson and Naujokat, 1997), in accordance with an overall stratospheric cooling trend (see Chapter 5 of this Assessment). Wintertime lower stratospheric zonal winds have increased over the last decades as well (Kodera and Koide, 1997), as takes place in the GISS model. Recent Arctic winters have also shown large ozone losses and an increasingly stable and persistent polar vortex (see, for example, Manney *et al.*, 1996; Zurek *et al.*, 1996; Müller *et al.*, 1997a,b; Rex *et al.*, 1997; Newman *et al.*, 1997). In the first 8 years of the 1990s, there has been only one Arctic major warming during December-February, as compared with five that occurred during the 1980s. Increasing greenhouse gases, coupled with the reduction in ozone in the lower stratosphere (see Chapter 5), may be responsible for this abrupt decrease in warmings, and hence for the very large Arctic ozone destruction measured in recent winters.

In the Antarctic lower stratosphere during September there is a noticeable difference between the results of the GISS and ECHAM3/CHEM models, and the more recent results of the ARPROBUS and UKMO models. The first two models show a significant cooling over the polar region, although the changes are typically much smaller than those predicted for the Arctic winter/spring. In contrast the other two models show a warming in the midlatitude stratosphere with the cooling over the pole only occurring above about 20 km. For the UKMO results, which include no ozone-radiative feedback, the most likely cause of the warming is an increase in planetary wave propagation; it is also possible that this occurred in the ARPROBUS model. Therefore the preliminary results from these two models appear to indicate the opposite response, in terms of planetary wave propagation, for the Southern Hemisphere winter to that found by all the models for the late northern winter. Note again that the ECHAM3/CHEM model, with a top at 10 hPa, may not have been able to accurately predict the changes in planetary waves.

In summary, all four GCMs that ran transient chemistry-climate experiments show a general cooling trend in the polar lower stratosphere in the Arctic in February and above 20 km in the Antarctic spring. The degree of cooling varies from model to model, with the largest uncertainties arising from varied dynamical responses and whether the radiative feedback of ozone changes was included in the calculations. In the Arctic, sudden stratospheric warmings are extremely important in determining the polar springtime lower stratospheric temperatures. Changes in the frequency of sudden stratospheric warmings can best be assessed in the models with long-term simulations and an upper boundary above the stratopause, such as employed in the UKMO (dynamical simulation) and GISS models. Both experiments produced a reduction in the frequency of stratospheric warmings over the next several decades, leading to a more stable, colder polar vortex in the Arctic, although for the UKMO results, the frequency of warmings increased again during subsequent decades.

#### *12.2.3.2b Ozone Changes*

Minimum column ozone predictions are shown in Figure 12-24 for the Arctic and the Antarctic along with observations. The GISS model predicts maximum Arctic ozone losses during the period 2005-2020, roughly a decade after the peak stratospheric chlorine loading, clearly showing the influence in the model of increasing greenhouse gases. Without this greenhouse gas forcing, maximum losses would of course occur when the maximum chlorine amount is present. Although a decrease in the abundance of lower tropospheric halogens has recently been observed (Elkins *et al.*, 1993; Montzka *et al.*, 1996), implying that stratospheric loading should begin to decrease in several years, the recovery of polar stratospheric ozone will, according to the GISS model, likely be delayed beyond the forthcoming stratospheric maximum halogen loading by climate forcing. In the ECHAM3/CHEM model, there is also a delay in the recovery of polar ozone relative to that seen without climate forcing (Dameris *et al.*, 1998). These results do not show a significant recovery of stratospheric ozone in the Arctic or Antarctic by 2015 relative to 1990, despite the 0.5-ppbv reduction in chlorine loading assumed over this period. Again, that model has a 10-hPa top, limiting its simulation of the dynamical response to greenhouse gas increases.

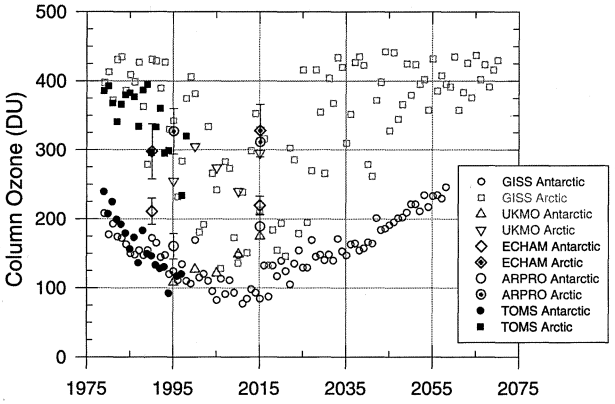


**Figure 12-24.** Minimum total column ozone south of 65 degrees averaged over the last 3 days of September, except for 1993 for which 23-25 September was used (Antarctic), and north of 65 degrees averaged over the last 3 days of March (Arctic), as seen in TOMS Version 7 data (filled circles and squares), and in the models (GISS–open circles and squares; UKMO–triangles; ARPROBUS–circles with error bars giving the range; ECHAM3/CHEM–diamonds with error bars giving the standard deviation). Note that the four models used somewhat different projections of chlorine loading (see text). Additionally, the ECHAM3/CHEM model included a tropospheric ozone increase with time, which has been subtracted.

The minimum Arctic ozone column amounts from the UKMO results shown in Figure 12-24 are higher than the GISS model results but also show continued low ozone until at least 2010. For the Antarctic, the ozone hole appears slightly later than observed; thus the UKMO results shown here are for the first week of October. Minimum ozone occurs in 1994 but an ozone increase does not become significant until 2009. The ARPROBUS results are similar to the UKMO values, showing an increase in ozone in the Antarctic but no significant change in the Arctic. It is important to note that the models used different assumptions regarding the change in chlorine loading between 2015 and 1995. The UKMO and GISS models used projections with a slow chlorine decrease during this period, 0.2 and 0.1 ppbv, respectively, similar to that used by the 2-D models (scenario A3 of Chapter 11). In contrast, the chlorine in the ARPROBUS and ECHAM3/CHEM models decreased by 0.4 and 0.5 ppbv, respectively (2015 relative to 1990 for the ECHAM3/CHEM model), a decline somewhere between the WMO 1994 Assessment (WMO, 1995) and the present Assessment baseline cases (see Figure 12-1). This may at least partially account for the differences between the model results.

Although the overall frequency of sudden warmings has decreased, variability in the Arctic is still large during the late 1990s and early 2000s in the GISS model, as shown in Figure 12-25. For example, the model year 1998 was fairly warm, leading to relatively weak ozone depletion in that year as compared with years just before and after. The GCM does not represent the particular meteorological conditions found in any given year, but rather gives representative conditions based on the input trends that drive the simulation. The onset of severe Arctic ozone depletion in the model during the 1990s is well represented, as seen in the comparison between modeled and observed ozone shown in Figure 12-24. Ozone depletion is significantly deeper in the model years 2001 and 2002, which show the most ozone loss during the 2000-2005 period. Note that these figures show model results including only climatological zonal mean ozone transport, illustrating how temperature variations with longitude lead to asymmetric chemical ozone destruction. As discussed in Shindell *et al.* (1998b), changes in transport in the GISS model have little effect on polar ozone through 2015 relative to chemical losses, though the inclusion of longitudinally varying transport would reduce the symmetry about the pole seen at middle and low latitudes.

A comparison between 1995 and 2015 total ozone during the spring in both hemispheres is shown in Figure 12-26 for the GISS model. These years are representative of typical conditions for the 1990s and 2010s, respectively, as values for these single years are quite similar to the 1990s and 2010s decadally averaged values. The impact of the increasing greenhouse gases on Antarctic losses is fairly small, as depletion is already so extreme. The ozone hole persists for a longer time as temperatures stay low progressively longer with greenhouse forcing. Variability is much less in the Antarctic than in the Arctic, indicating that the Antarctic will likely be a better location for observations of recovery, as discussed in Section 12.4. Arctic losses increase significantly by 2015, as was seen in Figure 12-24.

The ECHAM3/CHEM model predicts an Antarctic ozone hole in 2015 that is fairly similar to that predicted for 1990, as shown in Figure 12-27. In the Arctic, the model shows a small, non-significant recovery in column

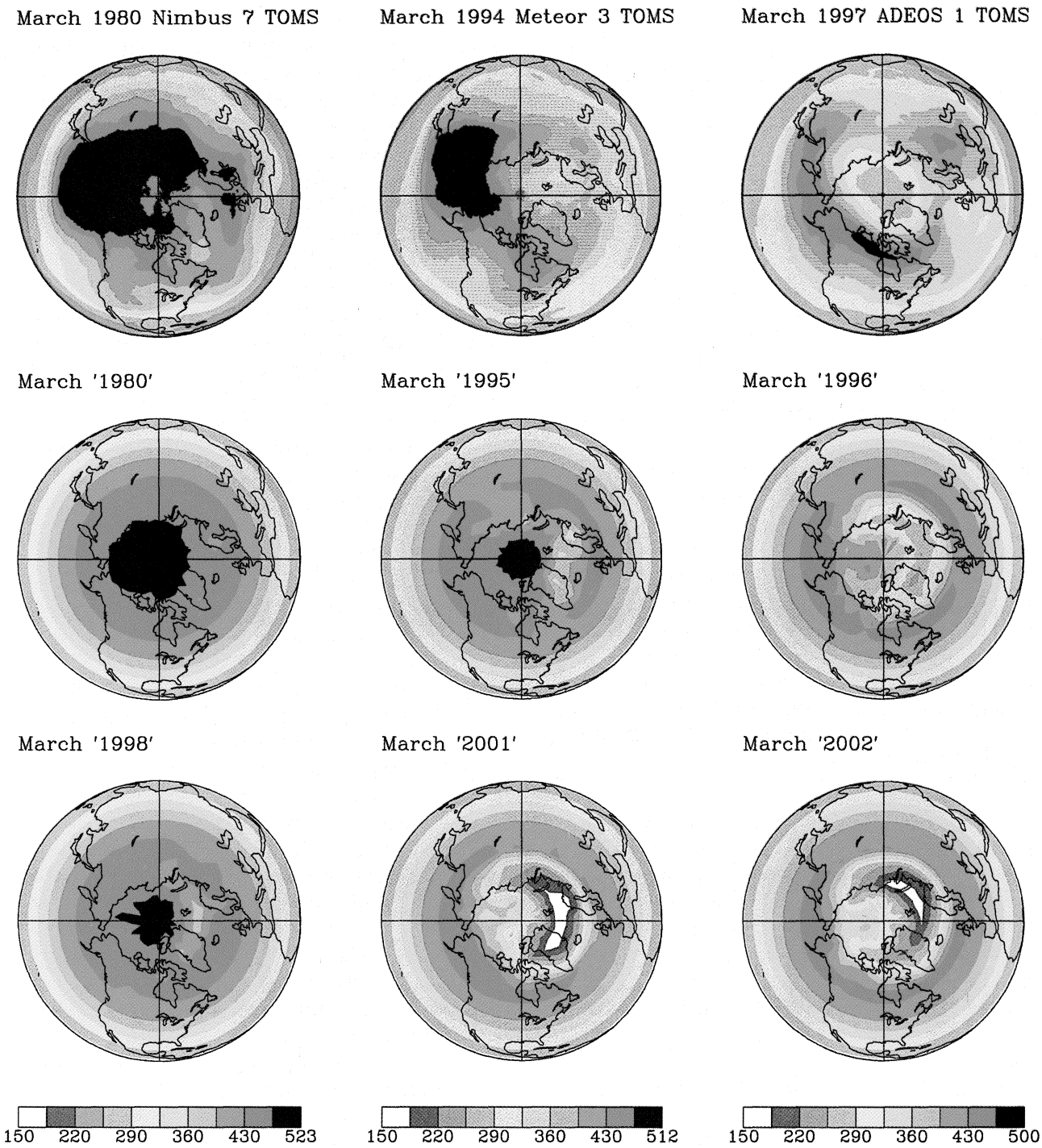


**Figure 12-25.** Observed and modeled ozone column (DU) averaged over the last week of March. The first three panels are TOMS observations, while the last six are GISS model output. Values are given for the indicated years, with model years in quotes to indicate that they do not represent actual years. The largest scale division represents all values over 465 DU.

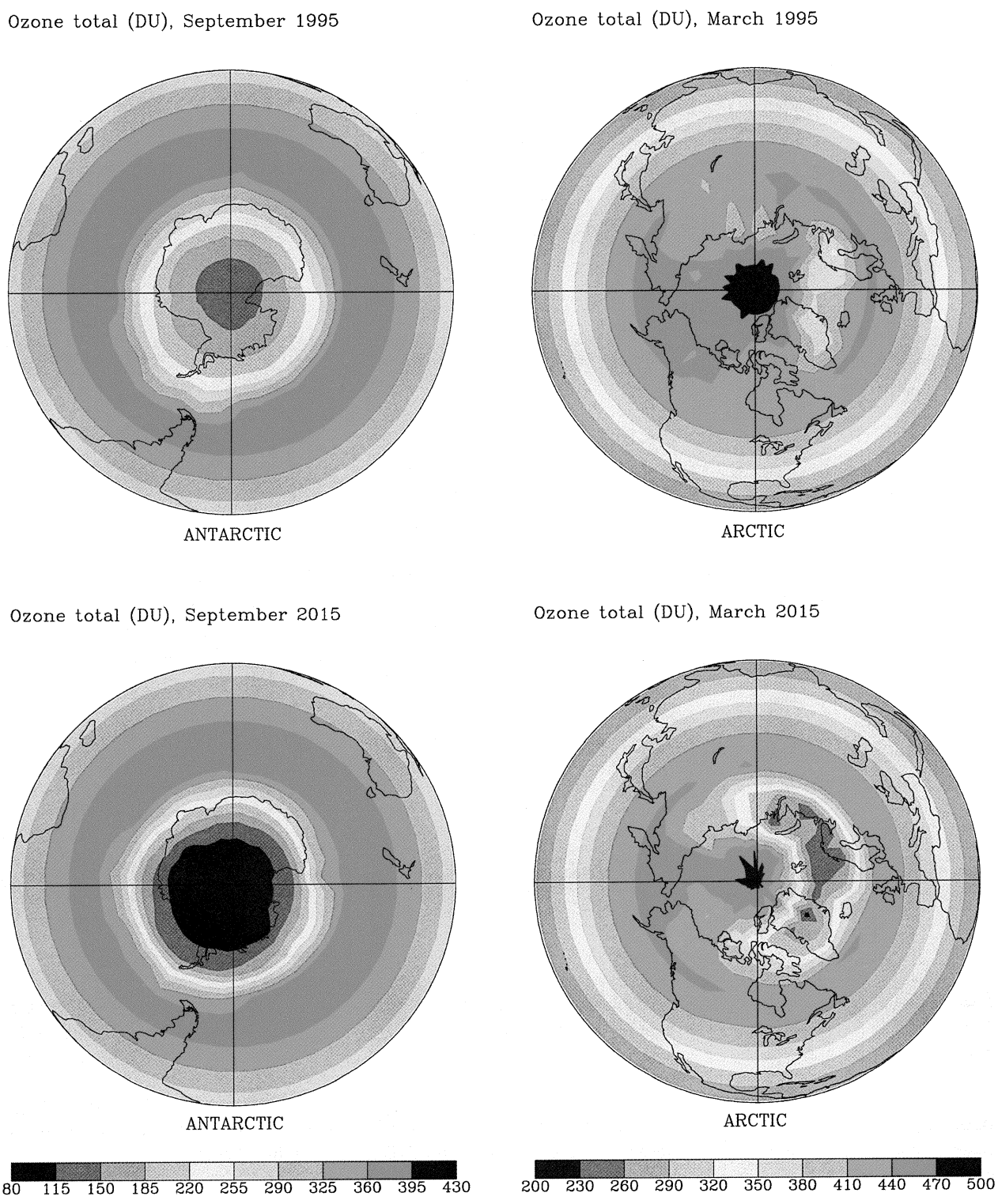


**Figure 12-26.** Total column ozone amounts (DU) in the GISS model for September and March 1995 and 2015. The results are each from a single year, though these values do not differ significantly from 10-year averages around each time period.

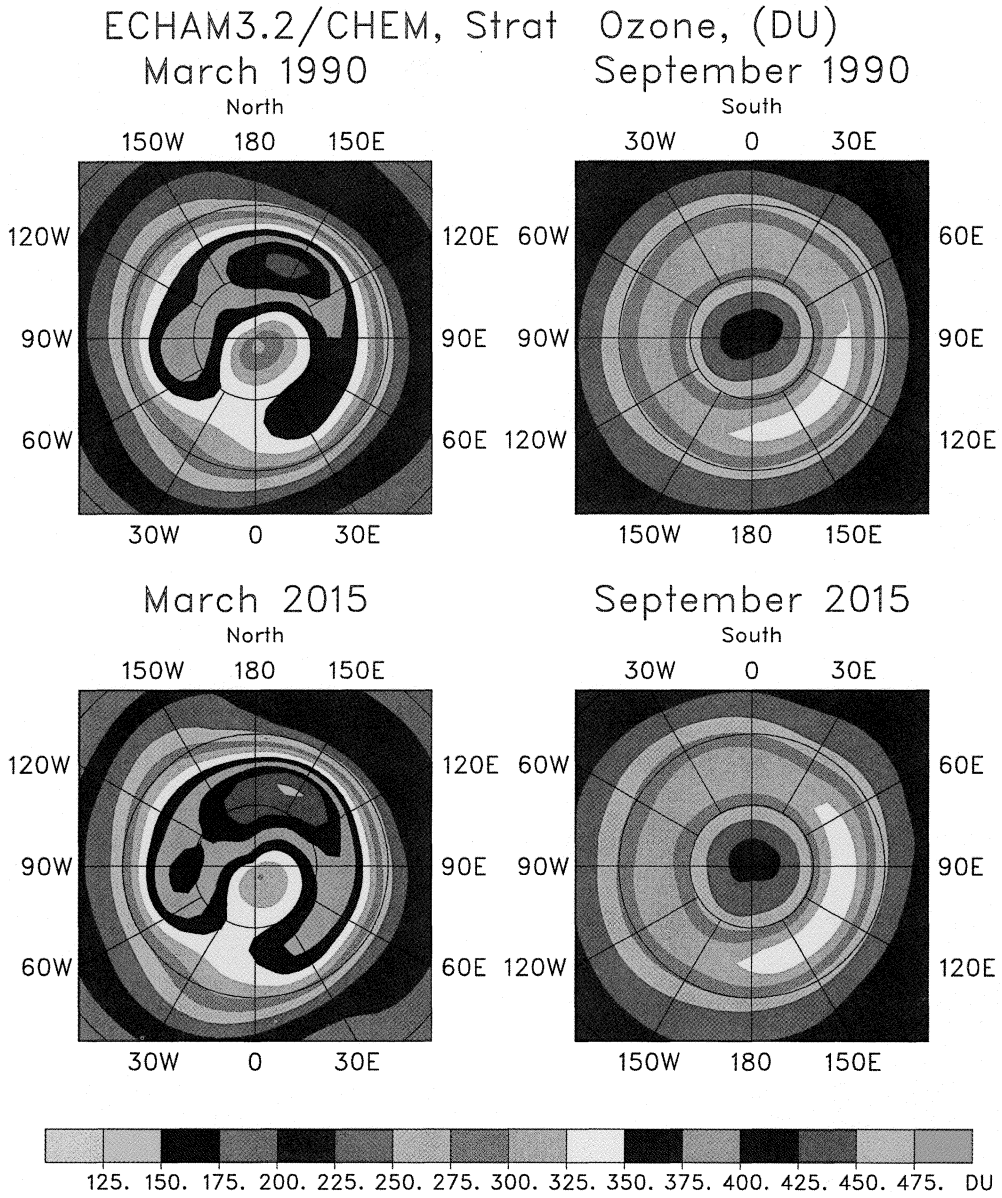


**Figure 12-27.** Total column ozone amounts (DU) in the ECHAM3/CHEM model for March and September 1990 and 2015. Tropospheric ozone has been removed for consistency with the other models, which did not include tropospheric ozone changes. All results have been averaged over 10 years of model simulations.

ozone by 2015. Stratospheric ozone loss remained roughly constant, indicating that the large decrease in chlorine loading was compensated for by the influence of reduced lower stratospheric temperatures in the model. We note again that the simulation assumed a decrease in chlorine loading of 0.5 ppbv (16%) by 2015 relative to 1990, which is much larger than the base case considered by the 2-D models in this chapter.

The UKMO model results (Figure 12-28) show a maximum in the depth of the Antarctic ozone hole in 1994, and as greenhouse gases increased, the depth of the hole did not initially change significantly. By 2009,

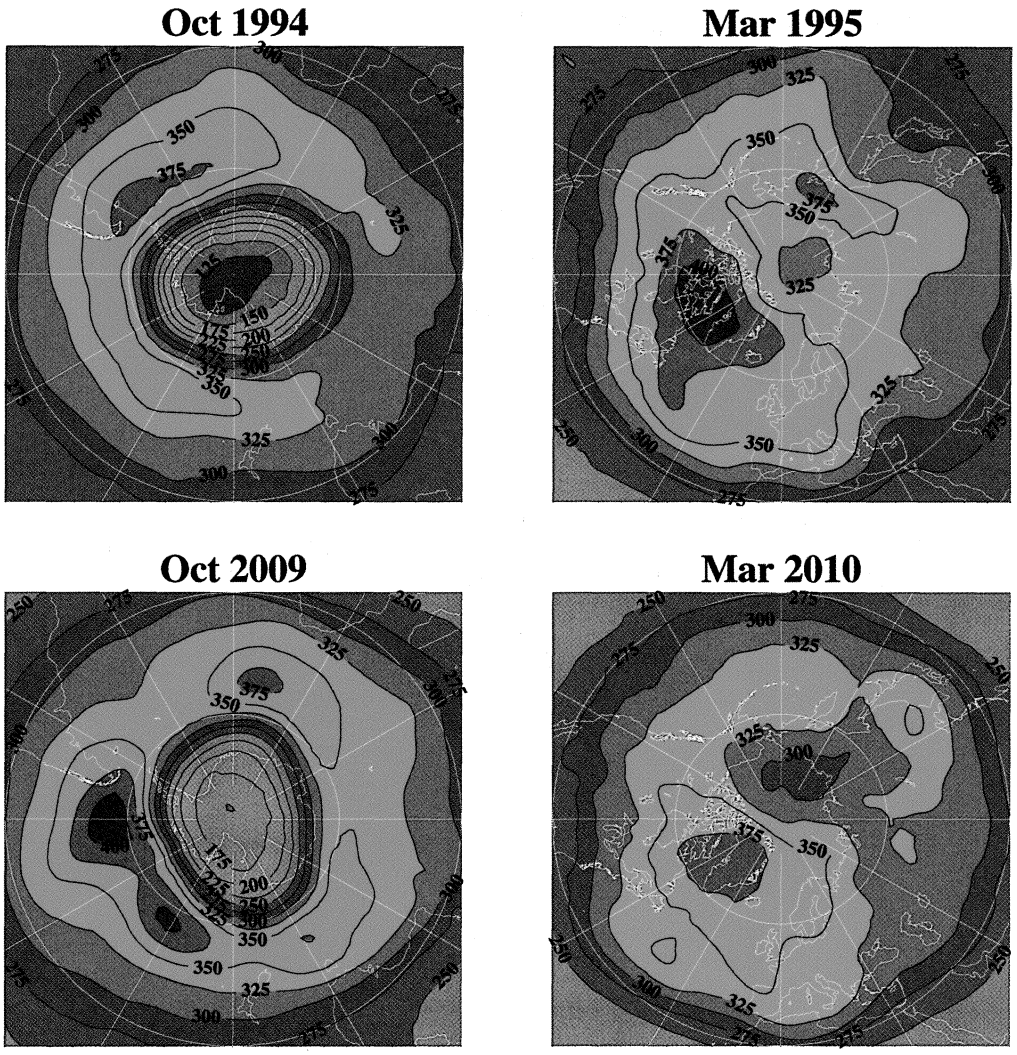


**Figure 12-28.** Total column ozone amounts (DU) in the UKMO model for October and March 1994/1995 and 2009/2010. The results are each from a single modeled year.

in the ozone hole, total ozone increased by some 40 DU due to a reduction in homogeneous ozone destruction and an increase in ozone transport. For the Arctic, the UKMO model results showed a generally decreasing ozone amount until 2010. Thereafter ozone recovered, indicating a delayed recovery of ozone in the Arctic relative to the Antarctic. Note that the results shown in Figure 12-28 are for 2009/2010, which is the time when the largest contrast with 1995 was simulated in the Northern Hemisphere (although it must be emphasized that the results are only available at 5-year intervals).

The ARPROBUS model shows a significant increase in column ozone over Antarctica during the spring of 2015 relative to 1995 (Figure 12-29). This is due to the decrease in the amount of chlorine projected in the 2015 atmosphere, which outweighs in the model the effect of the increase in greenhouse gas concentrations. Over the Arctic, the cooling predicted by the model led to a larger number of polar stratospheric clouds (PSCs). Compared to the 1995 simulation, this caused a March-average loss of about 30 DU in the vortex.

In summary, three of the models show increased ozone losses within the Arctic vortex, while the ECHAM3/CHEM model shows no significant changes. An additional effect of the Arctic springtime ozone losses

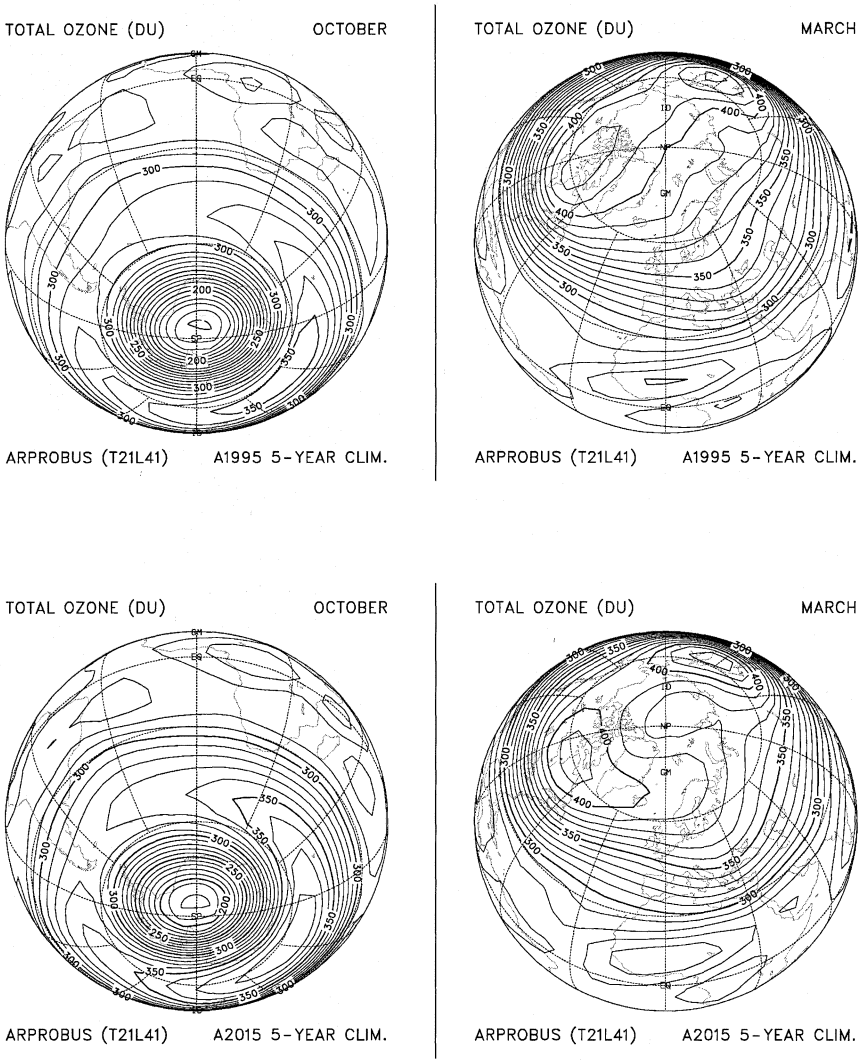


**Figure 12-29.** Total column ozone amounts (DU) in the ARPROBUS model for October and March 1995 (top) and 2015 (bottom). All results have been averaged over 5 years of model simulations.

has been to reduce the annual cycle in high-latitude total ozone in all four models. We note that in the simulations discussed here (doubled $CO_2$ and transient), the ECHAM3/CHEM and ARPROBUS models include chemical changes in species other than ozone that are expected to occur with increasing greenhouse gases. These include the production of additional water from the oxidation of increasing methane, additional odd nitrogen from the increasing emissions of nitrous oxide ($N_2O$), and indirect effects such as changes in stratospheric water vapor due to changes in tropospheric temperatures and dynamics. Also, the UKMO model includes additional odd nitrogen from $N_2O$ increases.

### 12.2.3.3 Conclusions

Advances in computing power have allowed the first simulations of future ozone using coupled 3-D models. Despite these improvements, there are considerable differences between the results of individual models. For example, at high latitudes throughout the stratosphere, the temperature response of models to increasing greenhouse gases, which is associated with differences in modeled circulation changes, varies significantly. Further development of stratospheric GCMs is necessary for them to reach a consensus regarding predictions of chemistry-climate interactions

in the stratosphere such as that now seen in predictions of surface parameters by climate models.

Models highlight that future Arctic ozone loss is very sensitive to changes in the frequency of sudden stratospheric warmings. As greenhouse gases increase, the transient simulations described here predict a strong cooling of the Arctic vortex, consistent with recent observed trends that show a cooling and a reduced frequency of sudden warmings. This cooling trend has a significant impact on Arctic ozone loss through the extremely temperature-sensitive chemistry in this region. All four coupled chemistry-climate models show the same or greater ozone depletion in the Arctic in 2015 as in 1995, despite assumed reductions in chlorine loading ranging from 3% to 16%. Two models give trends through the coming two decades (rather than snapshots at just two times). Both showed steadily increasing ozone loss through 2010, with recovery beginning roughly 1 to 10 years later. All the models indicate that the onset of Arctic ozone recovery is likely to be delayed past the maximum in stratospheric chlorine abundances.

The UKMO and ARPROBUS simulations show the onset of ozone recovery from halogen-induced depletion occurring earlier by 5 years or more in the Antarctic than in the Arctic, while the GISS and ECHAM models show similar timing in the two hemispheres. All the models show a larger degree of variability in the Arctic than in the Antarctic, however, suggesting that observations of Antarctic ozone will likely provide a better indicator of ozone recovery than Arctic observations.

## 12.3 OTHER PERTURBATIONS

Several factors, other than those discussed in Section 12.2, are important in regulating the levels of stratospheric ozone. Natural processes such as solar cycle ultraviolet flux variations and charged-particle precipitation can serve to either mitigate or enhance ozone changes. Anthropogenic activities such as rocket or shuttle launches, nuclear explosions, and aircraft can also have an influence.

### 12.3.1 Natural Processes

Solar cycle ultraviolet flux variations, charged-particle precipitation, and interannual and quasi-biennial dynamical changes can all have an influence on ozone. These processes are discussed in the following sections.

#### 12.3.1.1 Solar Cycle Variations

Solar cycle variations in ultraviolet (UV) flux have been observed and simulated to vary with the 11-year solar cycle and 27-day solar rotation periods (e.g., Brasseur and Simon, 1981; Garcia *et al.*, 1984; Callis *et al.*, 1985; Hood *et al.*, 1993; Huang and Brasseur, 1993; Chandra and McPeters, 1994; Fleming *et al.*, 1995). Brasseur (1993) showed a latitudinal dependence in the total ozone response, with 1% larger levels in the tropics and 1.5% in high latitudes at solar maximum compared to solar minimum. Jackman *et al.* (1996a) used solar UV flux variations measured by the Solar-Stellar Irradiance Comparison Experiment (SOLSTICE) instrument aboard UARS along with F10.7-cm flux variations as a transfer standard for non-UARS observing years (prior to September 1991) to derive solar UV changes beginning from 1947. These computations predicted variations in global total ozone of 1.2% from solar maximum to minimum. Both Brasseur (1993) and Jackman *et al.* (1996a) predictions are in reasonable agreement with the value of 1.2% derived by Reinsel *et al.* (1987), using a statistical analysis of the Dobson data on ozone and the F10.7-cm flux, and the 1-2% values cited in Chapter 7 of WMO (1992). The solar UV flux does have a significant effect on total ozone and will need to be considered when studying future ozone changes.

While the total ozone variation predicted in various models agrees fairly well with the observations, the vertical profile of the observed change greatly underestimates the ozone response to solar variations in the upper stratosphere (McCormack and Hood, 1996). Given that variations in heating rates in the upper stratosphere induced by solar irradiance variations can exert a considerable influence on dynamics (see, for example, Balachandran and Rind, 1995), this deficiency in the models will limit their ability to accurately reproduce the total atmospheric response to the solar cycle. Results from current models should therefore be interpreted with caution. Finally, the impact of the solar cycle on climate, which probably occurs through changing stratospheric ozone (Haigh, 1996), should be considered.

#### 12.3.1.2 Charged-Particle Precipitation

Charged particles in the form of galactic cosmic rays, solar flare particles, relativistic electron precipitations, and auroral electrons and photoelectrons have all been predicted to have an effect on ozone (see

references in Jackman (1993) and Chapter 2 of WMO (1992)). Charged-particle effects are largest at polar latitudes, although the magnitude of the effects on ozone is still open to a great deal of discussion and uncertainty. The largest predicted decreases in total ozone from charged particles are a few percent at polar northern latitudes as a result of very large and energetic solar flare particle events (see, for example, Crutzen *et al.*, 1975; Jackman *et al.*, 1995).

The effects of charged particles on ozone are much reduced at lower latitudes, with solar flare particle events and galactic cosmic rays predicted to cause small changes in annually integrated total ozone between 65°N and 65°S by a maximum of 0.22% and 0.02%, respectively (Jackman *et al.*, 1996a). Although the magnitude and frequency of relativistic electron precipitations are still quite uncertain, Callis *et al.* (1997) have computed changes in global total ozone of 0.5% from these events over the 1979 to 1990 time period. Auroral electrons and photoelectrons produce $NO_y$ in the thermosphere with subsequent transport to the stratosphere and may also have an impact on stratospheric ozone. Although Siskind *et al.* (1997) have recently shown evidence of significant transport of this thermospheric $NO_y$ to the upper stratosphere, the effects on total ozone are not well quantified.

### 12.3.2 Anthropogenic Activities

Other anthropogenic activities besides halogen production and release may have caused or will cause ozone change. These activities include rocket launches, aircraft emissions in the lower stratosphere from the current fleet of aircraft, and a possible future fleet of supersonic aircraft.

#### 12.3.2.1 Shuttle and Rocket Launches

Summaries of the effects of exhaust products from rockets are given in Chapter 10 of WMO (1992), the American Institute of Aeronautics and Astronautics report (AIAA, 1991), and by Jackman (1994). Since these publications there has been further substantial research activity regarding the impact of rockets on stratospheric ozone. Significant research on the chemistry in rocket plumes has been undertaken in the past several years. Ross (1996) has simulated total ozone loss of greater than 8% in areas of approximately 100 $km^2$ under a Space Shuttle plume about 1 hour after launch. Such small areas of significant total ozone loss would be difficult for the TOMS instrument to measure with its field of view of about 1600 $km^2$ (Syage and Ross, 1996). Instruments aboard a WB-57F aircraft have measured molecular chlorine ($Cl_2$), ozone ($O_3$), and particles in Titan IV, Space Shuttle, and Delta exhaust plumes (Ross *et al.*, 1997a,b), showing enhanced $Cl_2$ and reduced ozone.

Jones *et al.* (1995) have computed the atmospheric impact of the Ariane 5 rocket. Emissions of inorganic chlorine, water vapor, and aluminum oxide were all considered. The steady-state 2-D model calculation, assuming the chlorine and water vapor emissions for 10 Ariane 5 launches per year, shows small losses of ozone (<0.1%). These losses appear to be independent of the form in which chlorine was released. The aluminum oxide emissions are calculated to add modest increases (~1%) to the stratospheric aerosol mass with the same launch scenario. Jackman *et al.* (1996b) investigated the impact of the chlorine emission on the stratosphere using a launch scenario of nine Space Shuttles and three Titan IV rockets per year and found maximum decreases in ozone of 0.14% in the middle to upper stratosphere. Athough the calculated impact on profile and total ozone is computed to be quite small, inclusion of heterogeneous chemistry was found to increase the total ozone loss by a factor of 2.5.

Molina *et al.* (1997) have measured relatively high reaction probabilities (~0.02%) for the reaction $ClONO_2 + HCl \rightarrow HNO_3 + Cl_2$ on aluminum oxide (alumina) particles. These measurements have been considered in a recent global modeling study (Jackman *et al.*, 1998), which indicated that the alumina particles could be responsible for about one-third of the total ozone depletion from solid fuel rockets. Jackman *et al.* (1998) used historical U.S. launch rates of solid fuel rockets and computed annually averaged global total ozone losses of 0.025% by the year 1997.

It is expected that there will be a higher rate of launches in the future, given the upcoming construction of the International Space Station and proposed launches of the Ariane 5. The computed, relatively minuscule effects on stratospheric ozone are, therefore, expected to increase. Future studies of possible stratospheric ozone effects from rockets should focus on the global launch rates, including not only NASA and European Space Agency (ESA) launches but also launches by other space agencies around the world.

#### 12.3.2.2 Current Fleet of Subsonic Aircraft

The fleet of subsonic aircraft, operating primarily in the upper troposphere and lower stratosphere, has increased substantially over the past few decades and is expected to increase significantly in the next century. Airplane engines emit $CO_2$, $H_2O$, $NO_x$, CO, hydrocarbons, carbon soot, and sulfur oxides ($SO_x$), which can all have an influence on the background atmosphere. A number of studies have been completed in recent years on the effects of subsonic aircraft on the atmosphere. Recent assessments of the atmospheric effects of subsonic aircraft emissions were completed by NASA (Friedl *et al.*, 1997) and the European Commission (Brasseur *et al.*, 1998), and included new model computations as well as summaries of the past work on this subject. The Intergovernmental Panel on Climate Change (IPCC) is also examining the impact of aircraft on the atmosphere and is presently enabling the production of a special report on aviation and the global atmosphere (IPCC, 1999), in collaboration with the Ozone Scientific Assessment Panel of UNEP and in conjunction with the International Civil Aviation Organization (ICAO). Changes in lower stratospheric and upper tropospheric ozone caused by increases in subsonic traffic in the future could be a factor when considering future anthropogenic influences on ozone.

#### 12.3.2.3 High Speed Civil Transports

The aviation community is investigating the possibility of developing, marketing, and producing a fleet of High Speed Civil Transports (HSCTs) that would operate in the stratosphere. Another component of the IPCC aviation report is the influence of HSCTs on the background atmosphere. Of primary interest are the potential effects on ozone from a fleet of HSCTs. These aircraft could cruise at Mach 2.4 with a range of 5000 to 6500 nautical miles. The primary market for this new fleet of supersonic passenger aircraft will be the Atlantic and Pacific flight corridors, decreasing the average subsonic travel time by over a factor of 2. This HSCT fleet will cruise primarily in the lower stratosphere, within an ozone-rich region. Emissions from this proposed fleet will predominantly occur at Northern Hemisphere midlatitudes. Trace constituents from HSCT engines are produced from (1) direct combustion of the kerosene-based fuel components forming $H_2O$, $CO_2$, CO, $CH_4$, nonmethane hydrocarbons, and soot; (2) impurities in the fuel (e.g., sulfur, forming $SO_2$); and (3) high-temperature processes, breaking down atmospheric nitrogen to form $NO_x$ ($NO + NO_2$). The IPCC special report (IPCC, 1999) will include an assessment of the impacts of a possible HSCT fleet. This information will also be important to understanding future anthropogenic influences on atmospheric ozone.

#### 12.3.2.4 Other Effects

In addition to those processes responsible for changing stratospheric ozone, there are others that may affect the troposphere, including surface emissions of $NO_x$, $SO_x$, CO, and hydrocarbons. Some of these emissions may increase in the future, leading to ozone production in the troposphere and adding slightly to the ozone column. Convective lifting of these emissions could also affect the tropopause region. No modeling of these processes has been included in this chapter but their effects are discussed in more detail in Chapter 7.

## 12.4 DETECTION OF THE EXPECTED RECOVERY OF THE OZONE LAYER

One of the scientific highlights of the first decades of the 21st century will likely be the uncovering of evidence for the turnaround in stratospheric ozone depletion owing to the reduction in the emission of ozone-depleting chemicals. Observation of this recovery is important because it will show that the formulation and enforcement of regulations associated with the Montreal Protocol and its Amendments was an effective course to follow. However, as already indicated in this chapter, there are many uncertainties associated with ozone recovery, for example, the possibility of future volcanic eruptions, and they will all impact our ability to actually observe the recovery.

It is the purpose of this section to identify those indicators that might be used for the earliest possible evidence of the beginning of ozone layer recovery. For this purpose, we define the beginning of recovery as a measurable increase in ozone toward pre-1980 values. Clearly, another important observation will be a pre-recovery period, i.e., a cessation of a worsening of ozone depletion. It might be argued that the pre-recovery stage has already begun in Antarctica, where the springtime ozone hole has remained very severe but relatively unchanged since about 1992; however, this observation is mainly due to saturation in which nearly all the ozone

is lost in certain regions of the stratosphere each spring. Thus the cessation of the downward trend in total ozone in the Antarctic spring is not an indication of the pre-recovery stage. As indicated in Chapter 4, there has been a lessening of the downward trend in ozone at mid-latitudes when compared to a linear extrapolation of trends observed in the 1980s (see Figure 4-12). While the cause of this trend diminution is unknown, it should not yet be considered an observation of pre-recovery as the length of the period of reduced trends is inadequate at this time. Confirmation of the pre-recovery of global ozone, a cessation of a downward trend, will require additional observations into the next decade. Obviously, a volcanic event the size of Mt. Pinatubo would further delay this confirmation.

### 12.4.1 Antarctic Ozone Hole

The phenomenon of chemical ozone depletion was first unequivocally observed in Antarctica because of its magnitude there, with about two-thirds of the overlying ozone destroyed during the month of September at the present time (Hofmann *et al.*, 1994) (about one-third when it was uncovered from data at Halley Bay in 1983 (Farman *et al.*, 1985)). Although springtime Antarctic chemical ozone depletion in recent years appears to be saturated (total ozone destruction) in the 14-19 km altitude region (Hofmann *et al.*, 1997), at the boundaries of the ozone hole the chemical processes are not saturated. These regions, because they have relatively small interannual variability, may provide useful indicators of ozone recovery. It is likely that the earliest evidence for recovery of chemical ozone depletion will be obtained in Antarctica for several reasons:

- The signal-to-noise ratio of the depletion phenomenon is large.
- The natural variability of ozone in the polar vortex during the springtime depletion event is small relative to that observed at midlatitudes or in the Arctic.
- As indicated in Section 12.2, the effects of climate change on ozone depletion, for example, cooling of the stratosphere, will be less than at midlatitudes or the Arctic because any additional cooling in the winter Antarctic stratosphere will be relatively smaller.
- As indicated in Section 12.2, chlorine, as opposed to bromine, dominates the ozone loss process to a greater extent in the Antarctic; thus a lag in bromine reduction will have a smaller effect on recovery there.

It is the purpose of this section to explore observations of the springtime Antarctic ozone hole to identify characteristic features that may be useful in observing the beginning of ozone recovery early in the 21$^{st}$ century.

We consider both satellite and balloonborne measurements. The latter have the advantage that they can observe the vertical profile of ozone depletion during the September period when rapid ozone destruction occurs. Satellite measurements utilizing solar ultraviolet radiation are generally capable of observing only the total column in sunlit regions and thus cannot examine the September rate of ozone decline in the interior of the continent, where perturbations related to transport effects near the continental periphery are absent. Surface-based Dobson instruments have the same disadvantage. In addition, total-ozone measuring devices are subject to variations above and below the ozone hole region, which cause considerable variability not present in the vertical profile of ozone (Hofmann, 1996). However, a distinct advantage of satellite measurements is their ability to map out the horizontal size of the ozone depletion region.

#### 12.4.1.1 Area of the 220-Dobson Unit Contour

Although satellite instruments of the backscatter ultraviolet type cannot observe the entire Antarctic continental interior during September, they can map out a particular ozone contour in sunlight, and by late September to early October, when the depletion phenomenon reaches its maximum extent, can define the maximum geographical size of the ozone hole. The 220-DU contour has been used for this purpose in the past. At this ozone level, the depletion phenomenon is not saturated and thus is sensitive to halogen changes. For this exercise we use the TOMS series of instruments, which is able to define the contours accurately with its scanning mode of operation. The TOMS instruments have a continuous record from 1979 to the present, with 1995 missing. These include instruments on board Nimbus-7 from 1979 to 1993, Meteor-3 in 1994, and Earth Probe from mid-1996 to the present.

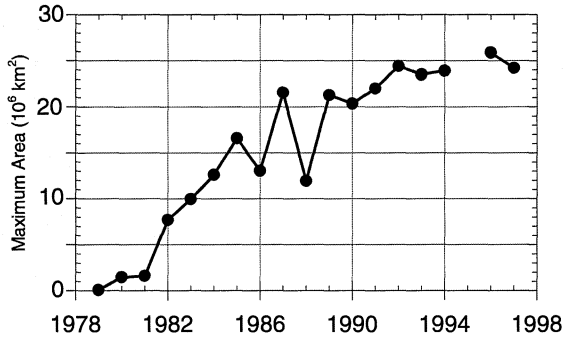


**Figure 12-30.** The maximum area interior to the 220-DU total ozone contour over Antarctica during springtime ozone depletion as measured by TOMS instruments since 1979.

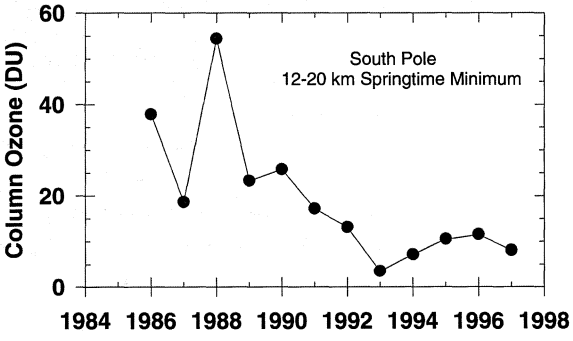


**Figure 12-31.** The minimum in the 12-20 km ozone column during Antarctic springtime ozone depletion since 1986 as determined from ozonesondes at the South Pole.

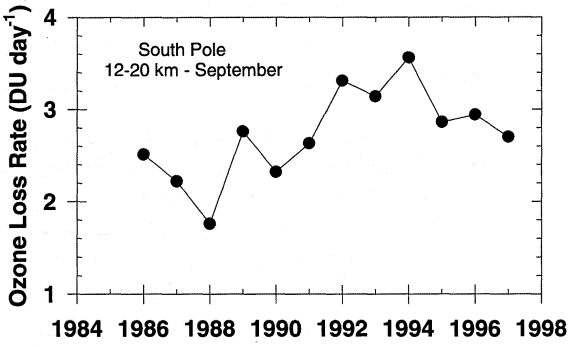


**Figure 12-32.** The 12-20 km ozone loss rate averaged over the month of September since 1986 as determined from ozonesondes at the South Pole.

Figure 12-30 shows the maximum area of the 220-DU contour since 1979, as determined from TOMS data. The time variation of the maximum area of the 220-DU contour has been relatively smooth, except for the year 1988, when the polar vortex broke up unusually early and the ozone hole never fully developed. The maximum area appears to have reached a peak value of about 25 million square kilometers in recent years. A gradual reduction below this asymptotic value in the future could be used as an indicator of the beginning of recovery.

### 12.4.1.2 September Ozone Reduction at 12-20 km from Ozonesonde Profiles

In order to avoid complications related to variability in total ozone associated with transport effects above the ozone hole, the vertical profile of ozone loss as determined by ozonesondes in Antarctica has been scrutinized for characteristic features that might be used in the early detection of recovery of the ozone hole (Hofmann *et al.*, 1997). By restricting observations to the 12-20 km region, where springtime Antarctic ozone is primarily affected by polar stratospheric cloud (PSC)-related, chemically induced depletion, one can substantially reduce the variability in observations of the ozone loss phenomenon. Figure 12-31 shows the springtime minimum in the 12-20 km integrated ozone amount since ozonesonde measurements began at the South Pole in 1986. The lowest value of this parameter occurred in 1993, mainly as a result of additional depletion in the 12-18 km region associated with aerosol particles from the Mt. Pinatubo eruption (Hofmann *et al.*, 1994). Since 1995, the minimum amount of ozone in the 12-20 km column has been about 10 DU. Increases to values of 20 DU or above (last seen before 1990) could be used as an indicator of the beginning of ozone recovery.

Because ozone is totally destroyed over a portion of the 12-20 km altitude range (about 14-19 km), the amount of ozone in this region may not be a sensitive indicator of halogen changes. However, the rate of ozone loss during the development of springtime Antarctic ozone depletion is not subject to saturation but is proportional to halogen amounts, other parameters such as temperature and sunlight remaining the same. The annual rate of ozone decline at the South Pole during September in the 12-20 km region is shown in Figure 12-32. These data were determined from the slope of the ozone versus time curves during September. This parameter is apparently affected by a quasi-biennial

component above 18 km, possibly related to varying transport processes (Hofmann *et al.*, 1997); however, it appears to have reached a pseudo-equilibrium value of about 3 DU per day in recent years. Values as low as 2.5 DU per day have not been seen since before 1990, and thus a return to this value could be used as another indicator of the beginning of recovery.

#### 12.4.1.3 Vertical Extension of the Ozone Hole

As indicated earlier, the ozone hole phenomenon is undersaturated at its horizontal boundary (for example the 220-DU contour); similarly saturation is absent at its upper boundary where temperatures are not low enough for substantial formation of polar stratospheric clouds. As halogen levels in the stratosphere have increased, the vertical extension of the Antarctic ozone hole has also increased. Where the top of the ozone depletion region was below 22 km in 1986 (Hofmann *et al.*, 1987), it now extends up to 24 km (Hofmann *et al.*, 1997). Figure 12-33 shows the 15 August to 15 October time development of the 22-24 km ozone column since 1986 as determined by ozonesondes at the South Pole. Considerably lower springtime values have been present at 22-24 km in the 1990s as compared to the 1980s. Figure 12-34 shows the 15 September to 1 October average amount of ozone between 22 and 24 km for each year since 1986. A departure from values near 20 DU began in about 1991, and values appear to be varying around the 15-DU value since 1992. The 1997 value was poorly defined, as a week of soundings was missed in late September owing to balloon problems. It is also likely that this parameter displays a sizable QBO component, possibly related to temperature. Because this region is not affected by volcanic aerosol (Hofmann *et al.*, 1994), a return to values consistently above 15 DU would be a sensitive indicator of ozone hole recovery as halogens decline. Future temperature trends related to greenhouse gas emissions may influence the recovery of the 22-24 km ozone column to some extent; this effect needs to be modeled for the upper reaches of the ozone hole.

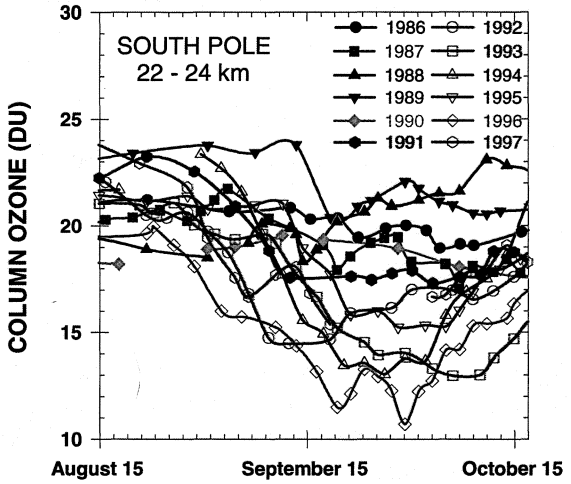


**Figure 12-33.** The 22-24 km ozone column versus time from 15 August to 15 October since 1986 as determined from ozonesondes at the South Pole.

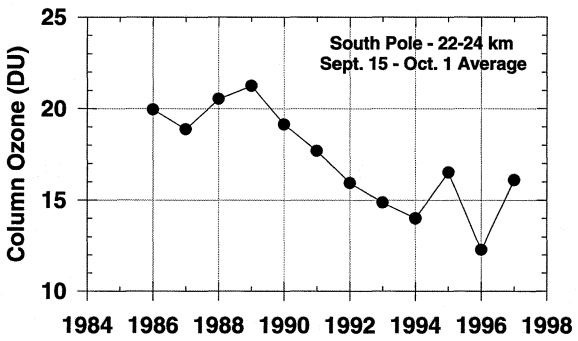


**Figure 12-34.** The 22-24 km average ozone column for the 15 September to 1 October period since 1986 as determined from ozonesondes at the South Pole.

### 12.4.2 Arctic Springtime Ozone Loss

Ozone loss during Arctic spring has been detected since the end of the last decade (Hofmann *et al.*, 1989; Schoeberl *et al.*, 1990; McKenna *et al.*, 1990; Hofmann and Deshler, 1991; Koike *et al.*, 1991; Kyrö *et al.*, 1992; Proffitt *et al.*, 1993; Braathen *et al.*, 1994; Larsen *et al.*, 1994; Manney *et al.*, 1994; Bojkov *et al.*, 1995; von der Gathen *et al.*, 1995; Manney *et al.*, 1995, 1996; Müller *et al.*, 1996; Donovan *et al.*, 1997; Hansen *et al.*, 1997; Manney *et al.*, 1997; Müller *et al.*, 1997a,b; Newman *et al.*, 1997; Rex *et al.*, 1997; Goutail *et al.*, 1998; Knudsen *et al.*, 1998; Rex *et al.*, 1998a,b), mainly during major international campaigns (the Airborne Arctic Stratosphere Expedition (AASE) I & II, the European Arctic Stratospheric Ozone Expedition (EASOE), and the Second European Stratospheric Arctic and Midlatitude Experiment (SESAME)). During the springtime of the years 1995, 1996, and 1997, chemically induced ozone loss in the Arctic reached an extent that

rivals the springtime loss in the Antarctic, one decade earlier (Müller *et al.*, 1997a,b). These enhanced ozone losses were related to increases in ozone-destroying chemicals and to unusually cold Arctic winters in the stratosphere. It is expected that ozone loss in the Arctic will continue; however, in contrast to the Antarctic this will occur in a largely unpredictable fashion.

It is expected that the detection of recovery in the Arctic springtime ozone loss will be more difficult compared to the Antarctic and the globe in general for two reasons. First of all, quantifying the ozone loss signal itself is more difficult because of the strong meteorological variability within a winter/spring period. An Eulerian view of the ozone loss by measurements at one station alone will in general not be able to cover all aspects due to this variability. Efforts have been undertaken to overcome this problem, and today several independent methods are available that reliably quantify ozone losses. These methods can be classified into satellite-borne measurements such as the Halogen Occultation Experiment (HALOE) and Microwave Limb Sounder (MLS) onboard the Upper Atmospheric Research Satellite (UARS), and measurements made by the Système d'Analyse par Observation Zénithale (SAOZ) and ozonesonde network. However, every method has its advantages and disadvantages and its own way to quantify ozone losses. The output quantities have to be compared with great care because of the intrinsic assumptions of the different methods. Such comparisons will be needed in any trend analysis if certain methods will be available for limited time periods only.

Second, the variability of the ozone loss signal from year to year is strongest in the Arctic. As described in more detail in Chapters 4, 5, and 7 of this Assessment, differences in ozone losses above both polar caps are due to the consequences of deviating meteorological conditions. The Arctic vortex in general is smaller, less stable, and shorter-lived than its Antarctic counterpart. The most important consequence is the temperature, which is roughly 10 K higher in the Arctic compared to the Antarctic stratosphere. The springtime polar ozone loss is directly related to heterogeneous reactions taking place on the surface of polar stratospheric cloud particles. Above Antarctica the temperature remains well below the formation temperature of all known PSC types in major parts of the lower stratosphere during most of the winter. Any meteorological variability from year to year will have only a minor influence on the magnitude of the ozone loss. Above the Arctic, temperatures usually reach the formation temperature of Type-1 PSCs (the PSC type with the highest formation temperature) in limited space regions and time periods. Therefore the strong meteorological variability above the Arctic from year to year, with temperature around the PSC threshold, leads to considerable variability in PSC existence and consequently in ozone loss.

It is thus clear that the springtime ozone loss above the Arctic is determined not only by the chlorine and bromine content but also by temperature effects. Furthermore, it is to be expected that during the early decades after the maximum in stratospheric chlorine loading, when the chlorine reduction is rather small, any trend in the springtime ozone loss will be mainly dominated by any temperature trend or even by any change in temperature variability, e.g., in the frequency of stratospheric warmings. It must be stated clearly that even if no significant ozone recovery is detectable in the coming decades, or even worse if an ongoing downward trend of Arctic ozone in the coming years continued, depletion of Arctic ozone would likely have been worse without the efforts that have been undertaken in the phase-out of CFCs.

Due to the uncertainties described above, any prediction of Arctic ozone will have a large year-to-year variability. As an example, Figure 12-24 showed the total ozone predictions of a coupled 3-D model (GISS) (Shindell *et al.*, 1998b) for the Arctic case in comparison to the Antarctic case. For these reasons, any indicator for future ozone recovery in the Arctic will not be as reliable as the indicators described earlier for the Antarctic, and should be interpreted with great care, taking into account the variability of the meteorology of the included winter/spring periods.

As stated in the beginning of this chapter, recovery is here defined as the effects expected due to a decrease in anthropogenic chlorine and bromine related to the Montreal Protocol. Therefore those indicators of recovery that are best suited are those that suffer least from meteorological/dynamical influences. An example is the Arctic chemical ozone depletion rate during the time period of total chlorine activation each winter. The depletion rate, given as a change of the ozone mixing ratio per sunlit hour, should be proportional to chlorine/bromine levels. However, even this basic approach is fraught with difficulties. First, the depletion rate is proportional to air pressure. This is due to the fact that the ClO dimer production reaction, which is the time-limiting reaction during the catalytic ozone loss cycle,

depends on a third-body concentration. Therefore the depletion rate is strongly height dependent. Second, the $Cl_y$ content itself is height dependent and the diabatic descent rate of the polar air masses can vary substantially from winter to winter. As a result, the $Cl_y$ content and thus the maximum depletion rates for different winters at a given altitude vary due to this dynamical effect. If used as an indicator for Arctic ozone recovery, these effects have to be taken into account. However, an advantage of this indicator is that it would be insensitive to any future temporal aerosol loading and to especially low temperature events that could lead to denitrification.

A method that is able to determine, as a primary analysis product, the chemical ozone depletion rate in the form of a change of the ozone mixing ratio per sunlit hour is the Match approach (von der Gathen *et al.*, 1995; Rex *et al.*, 1997, 1998a,b) already mentioned in Chapters 4 and 7. This approach provides the depletion rate as a function of time and altitude (see, for example, Figure 7-23) inside the polar vortex. Maximum depletion rates during the time periods and height ranges of total chlorine activation for three winters are shown in Figure 12-35. In future analyses covering additional winters, each altitude level should be compared to a pre-winter altitude level from which an air mass began its descent due to diabatic cooling. These values must be corrected for pressure relevant during the time of maximum ozone depletion.

It should be noted that this type of analysis is not limited to the Match approach. Any technique that is not affected by dynamical processes (e.g., diabatic movements, mixing processes) and that is able to provide ozone depletion rates resolved in time and altitude can be useful (see, for example, Manney *et al.* 1995; Knudsen *et al.*, 1998). If depletion rates are given in changes of ozone mixing ratio per day, they can be converted to changes of the mixing ratio per sunlit hour by including sunlight conditions inside the polar vortex.

Other quantities connected to Arctic ozone loss are less appropriate as indicators of Arctic ozone recovery. Quantities such as ozone loss integrated during the entire winter/spring seasons in total (column density) or at a given altitude (concentration) will be considerably variable from year to year (see, for example, Figure 12-24). It is expected that early ozone recovery will not be detected from such data. However, most of the currently available measurement techniques are able to contribute to this dataset, for example, those discussed in Manney *et al.* (1994), Müller *et al.* (1996), and Goutail *et al.* (1998).

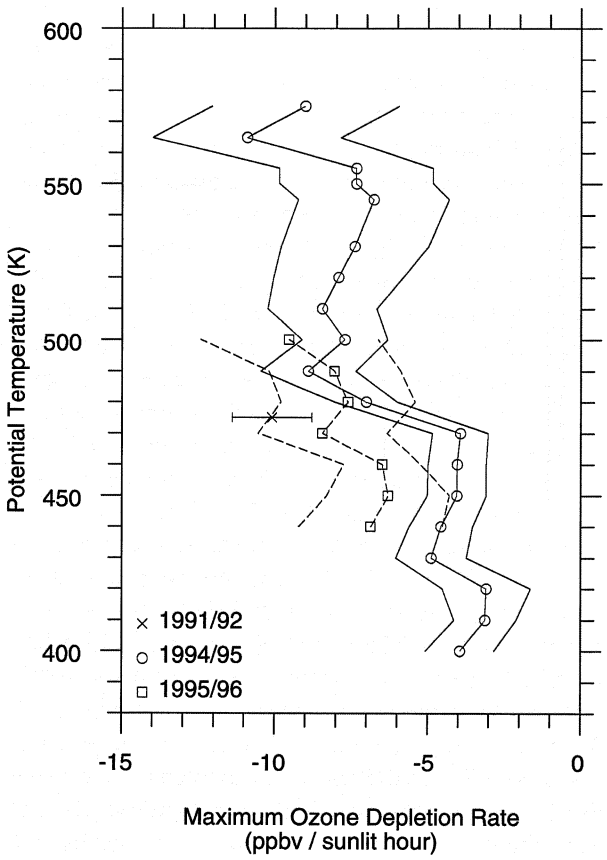


**Figure 12-35.** Maximum ozone depletion rates, together with the error ranges, during times of total chlorine activation in three Arctic winters as determined by Match campaigns. During the relatively warm winter of 1991/92, total chlorine activation may have occurred only at an altitude of 475 K potential temperature. In 1995/96, reliable rates during the time period of total activation have been determined for a short height interval only.

### 12.4.3 Midlatitude Ozone Decline

Ozone at midlatitudes is subject to many natural as well as anthropogenic forced variations. Sophisticated linear regression schemes including the seasonal cycle, linear trend, quasi-biennial oscillation, and 11-year solar cycle have been applied to deduce ozone trends (see Chapter 4 of this Assessment). These analyses indicate that the downward trend attributed to chlorine and bromine is about 4% for 65°S to 65°N from 1979 to 1995, or about 2.5% per decade. A relatively large variability, related to dynamic, solar cycle, and volcanic effects, of

about ±1%, exists. Detection of the recovery of a change this small with this large a variability will be a statistical challenge.

Analysis of future changes in middle- and low-latitude ozone (both NH and SH) will primarily require a long-term data record from satellites, with ground-based and balloon measurements for comparisons and cross calibration. At present the Earth Probe-TOMS is making total ozone measurements and NOAA-14 SBUV/2, SAGE II, MLS, and HALOE instruments are measuring profile ozone. Future instruments to measure total ozone include Meteor-3 TOMS (launch in 2000) and ENVISAT (launch in late 1999/early 2000). The Advanced Earth Observing Satellite 2-Improved Limb Atmospheric Sounder 2 (ADEOS 2-ILAS 2) and the Earth Observing System-Chemistry (EOS-CHEM) satellite (launch in 2003) are expected to measure profile ozone.

Because midlatitude ozone is subject to many chemically and dynamically driven variations, it will be difficult to verify its expected recovery. Solar maximum (predicted to occur around the turn of the century) or a particular period of stratospheric dynamics that forces ozone increases could easily be misinterpreted as the beginning of an ozone recovery from the halogen-caused ozone minimum.

Because of possible secondary effects on ozone such as stratospheric temperature reductions related to climate change, as discussed in Section 12.2, changes in total inorganic chlorine amount ($Cl_y$), while not a direct measure of ozone recovery itself, will be easier to measure than ozone. Combined with a model that deals with the temperature effects on heterogeneous chemistry, it will allow predictions of future trends in ozone to be made. But it must be kept clear that in the end there are no substitutes for the actual observation of recovery of the ozone layer.

As indicated in Chapter 1 of this Assessment, tropospheric chlorine levels peaked in early 1994 (Montzka *et al.*, 1996). Russell *et al.* (1996) have shown with HALOE-measured HCl and hydrogen fluoride (HF) that the time lag for transport of tropospheric gases to 55 km is about 6 ± 2 years. This means that $Cl_y$ should peak at 55 km between 1998 and 2002. Continued monitoring of HCl by HALOE and future monitoring of HCl by EOS-CHEM near 55 km should provide a clear signal of total chlorine reduction in the middle atmosphere, because HCl accounts for 93-95% of the inorganic chlorine family (Russell *et al.*, 1996; Jackman *et al.*, 1996a).

Stratospheric HF has no significant known natural sources; thus it would also be very useful to monitor its peak and subsequent reduction. Although the HF at 55 km should peak about the same time as HCl, a definitive decrease may not be measurable until several years later. The GSFC 2-D model (Jackman *et al.*, 1996a) predicts HCl at 55 km peaking in 1998 and decreasing shortly thereafter. The same model predicts HF at 55 km peaking around the year 2000, but not decreasing substantially until 2010. The reason for this predicted difference in the behavior of HCl and HF lies in the differences among the lifetimes of the CFC source gases. CFC source gas molecules containing more atoms of chlorine generally have shorter atmospheric lifetimes than those containing more atoms of fluorine (see Table 13-1 of WMO, 1995).

Monitoring of ozone in the upper stratosphere (near 40 km), where percentage ozone reductions are more accurately defined than in the lower stratosphere (see Chapter 4), would presumably provide for a more accurate analysis of recovery at midlatitudes. Outside the polar regions, the upper stratosphere is essentially in photochemical equilibrium and should respond rapidly to changes in chlorine (see Chapter 6). The upper stratosphere is also above the aerosol layer, so that temperature trends related to climate change that might affect heterogeneous chemical rates should not have as large an effect. Ozone in this region is affected by the change in seasons and 11-year solar cycle, as well as chlorine amounts, but both of these natural variations can be removed through fairly straightforward analysis techniques. Increases in $CO_2$ are also expected to reduce stratospheric temperatures and thereby slow gas-phase destruction of ozone. Figure 12-36 shows predicted ozone changes at 40 km, 45°N from the CAM 2-D model for integrations with and without the feedback on stratospheric temperature due to $CO_2$ trends. A slow recovery in ozone is seen beginning about the year 2000 when $CO_2$ feedback is included, which is not present in the model results without the $CO_2$-induced temperature decrease. Interpretation of a measured increase in ozone at 40 km during the first half of the next century will not be simple and will require the use of a model that accurately describes changing halogen loadings and chemistry-climate feedback. Furthermore, the 40-km ozone loss does not represent a very large portion of the total column and realistically would not tell one much about what is happening in the more important lower stratospheric region, where a much larger amount of ozone is lost. Thus, while some measure of ozone

recovery may be extracted from the upper stratospheric data in the future, it will not be conclusive for the total ozone column, which drives increases in surface ultraviolet radiation. However, for scientific purposes, early observation of ozone recovery at 40 km would be reassuring.

### 12.4.4 Ozone Recovery Scenarios and Expected Dates of Recovery

The goal of this section is to provide the best possible estimate of the expected date of observation of the beginning of ozone recovery through use of the indicators in the previous section and modeled results of expected future variations. Because of the considerable variability in all the indicators of recovery and because of the large uncertainties in model predictions of future ozone levels, this goal is difficult to achieve with much accuracy. However, because regulations were put in place to stop the downward trend in ozone, it is imperative to provide information that can be used to assess the effectiveness of these regulations.

#### 12.4.4.1 The Standard Scenario

For the standard scenario we use the equivalent effective stratospheric chlorine (EESC) scenario A/A3 (see Chapter 11 of this Assessment). Scenario A has been determined from the emissions that have occurred up to the present, and scenario A3 consists of the maximum emissions allowed in the future under the Montreal Protocol and reaches 1980 values of about 2 ppb in approximately the year 2052, thus providing a conservative estimate of recovery. As indicated in Table 11-6, except for scenarios A2 and A4 (zero emissions and zero production scenarios), the mean recovery year for the other 16 scenarios is 2047.6 with a standard deviation of 1.9 years. Thus the choice of the maximum emissions scenario does not introduce a large uncertainty in the estimated recovery year. The main difference between scenario A3 and that used in the 1994 Assessment (WMO, 1995) is the relatively flat EESC region between about 2000 and 2020, related to new estimates of the future trends in CFCs, halons, and HCFCs given in Chapter 11.

In Figure 12-37a we assume that ozone will respond directly to EESC, and any perturbations related to greenhouse gas and climate changes, etc., are ignored. The degree of variability in three indicators (the TOMS global total ozone anomaly (Figure 12-37b), the South Pole and Halley October Dobson total ozone values (Figure 12-37c), and the South Pole ozonesonde 12-20 km September ozone loss rates (Figure 12-37d)) is used to construct a recovery curve with bounds for each that include about 90% of the data points prior to 1998. The beginning of recovery is assumed to have been observed when the value of ozone (ozone loss rate) has increased (decreased) to within one unit of the variability above (below) the minimum (maximum) values. The South Pole recovery indicators have been described in detail by Hofmann *et al.* (1997), who investigated detection of ozone hole recovery for EESC levels given in WMO (1995). As indicated earlier, the earliest detection of the beginning of recovery will likely occur in Antarctica, mainly because of the large signal and the lower dynamic variability inside the polar vortex. For EESC recovery considerations alone (scenario A3), the ozonesonde-measured ozone loss rate would document the beginning of recovery as early as 2015 while the beginning of global ozone recovery would not be detectable for an additional 10 or so years. The global ozone pre-recovery period, a cessation of the downward ozone trend, would be apparent during the next decade, based on the predicted EESC trend alone and assuming the absence of major volcanic eruptions.

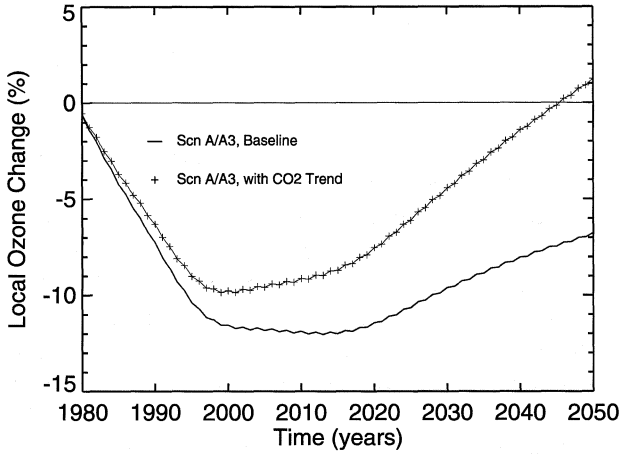


**Figure 12-36.** Percentage change in annual average ozone concentration at 40 km relative to year 1979 for the CAM model at 45°N latitude between 1980 and 2050. The solid line represents using $CO_2$ surface boundary conditions fixed at 1995 levels between 1979 and 2050. The line with crosses represents using a time-dependent trend of $CO_2$ (see Table 12-2).

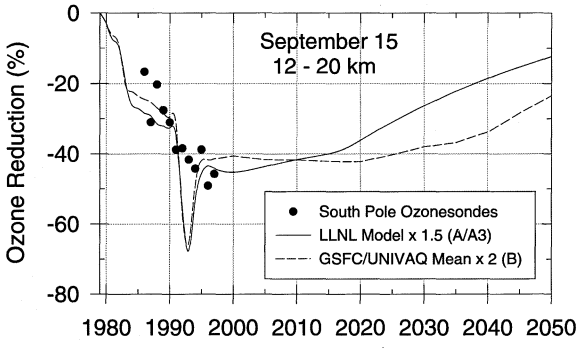


**Figure 12-40.** The percentage reduction relative to 1979 in the 12-20 km ozone column at the South Pole on 15 September for scenario A/A3 from the LLNL model compared to the ozonesonde measurements from 1986 to 1997. The ozonesonde reference value was obtained from a series of ozonesondes at South Pole in September 1971 (Hofmann *et al.*, 1997). Also shown is the average response for scenario B ($CH_4$ and $N_2O$ fixed at 1995 levels) for the GSFC and UNIVAQ models. All of the models had to be adjusted to bring them into the range of the measurements.

predicted cessation of the downward trend early in the next century.

In summary, while models indicate that the maximum ozone depletion will occur within the next two decades, uncertainties related to emission scenarios of greenhouse gases and climate change make estimates of the beginning of ozone layer recovery unreliable. Even in Antarctica, where it is believed that the earliest and least ambiguous observation of the beginning of ozone recovery will be possible, the estimated effects of greenhouse gases and climate change indicate that unambiguous detection of the beginning of the recovery of the ozone layer will not occur until well into the next century, beyond the maximum loading of ozone-depleting gases. Barring major volcanic eruptions during the next decade, a cessation of the downward trend in midlatitude ozone should be observed and would be a harbinger of the coming recovery.

## REFERENCES

AIAA (American Institute of Aeronautics and Astronautics), *Atmospheric Effects of Chemical Rocket Propulsion*, Report of an AIAA Workshop, June 28-29, 1991, Sacramento, Calif., 52 pp., Washington, D.C., 1991.

Austin, J., and N. Butchart, A three-dimensional modeling study of the influence of planetary wave dynamics on polar ozone photochemistry, *J. Geophys. Res.*, *97*, 10165-10186, 1992.

Austin, J., and N. Butchart, The influence of climate change and the timing of stratospheric warmings on Arctic ozone depletion, *J. Geophys. Res.*, *99*, 1127-1145, 1994.

Austin, J., N. Butchart, and K. Shine, Possibility of an Arctic ozone hole in a doubled-$CO_2$ climate, *Nature*, *360*, 221-225, 1992.

Austin, J., N. Butchart, and R.S. Swinbank, Sensitivity of ozone and temperature to vertical resolution in a GCM with coupled stratospheric chemistry, *Quart. J. Roy. Meteorol. Soc.*, *123*, 1405-1431, 1997.

Balachandran, N., and D. Rind, Modeling the effects of UV variability and the QBO on the troposphere-stratosphere system: Part I, The middle atmosphere, *J. Clim.*, *8*, 2058-2079, 1995.

Bekki, S., and J.A. Pyle, A two-dimensional modeling study of the volcanic eruption of Mount Pinatubo, *J. Geophys. Res.*, *99*, 18861-18869, 1994.

Bojkov, R.D., V.E. Fiolotov, D.S. Bais, C.S. Zerefos, T.V. Kadygrova, and A.M. Shalamjansky, Further ozone decline during the Northern Hemisphere winter-spring of 1994-1995 and the new record low ozone, *Geophys. Res. Lett.*, *22*, 2729-2732, 1995.

Boville, B., Detecting $CO_2$-induced temperature changes in the stratosphere, *Adv. Space Res.*, *6*, 45-48, 1986.

Braathen, G.O., M. Rummukainen, E. Kyrö, U. Schmidt, A. Dahlback, T.S. Jorgensen, R. Fabian, V.V. Rudakov, M. Gil, and R. Borchers, Temporal development of ozone within the Arctic vortex during the winter of 1991/92, *Geophys. Res. Lett.*, *21*, 1407-1410, 1994.

Brasseur, G., The response of the middle atmosphere to long-term and short-term solar variability: A two-dimensional model, *J. Geophys. Res.*, *98*, 23079-23090, 1993.

Brasseur, G., and P.C. Simon, Stratospheric chemical and thermal response to long-term variability in solar UV irradiance, *J. Geophys. Res.*, *86*, 7343-7362, 1981.

Brasseur, G.P., R.A. Cox, D. Hauglustaine, I. Isaksen, J. Lelieveld, D.H. Lister, R. Sausen, U. Schumann, A. Wahner, and P. Wiesen, European Scientific Assessment of the Atmospheric Effects of Aircraft Emissions, *Atmos. Environ.*, *32*, 2329-2422, 1998.

Brewer, A.W., and A.W. Wilson, The regions of formation of atmospheric ozone, *Quart. J. Roy. Meteorol. Soc.*, *94*, 249-265, 1968.

Butchart, N., and J. Austin, On the relationship between the quasi-biennial oscillation, total chlorine, and the Antarctic ozone hole, *Quart. J. Roy. Meteorol. Soc.*, *122*, 183-217, 1996.

Butchart, N., and J. Austin, Middle atmosphere climatologies from the troposphere-stratosphere configuration of the UKMO's unified model, *J. Atmos. Sci.*, *55*, 2782-2809, 1998.

Callis, L.B., J.C. Alpert, and M.A. Geller, An assessment of thermal, wind, and planetary wave changes in the middle and lower atmosphere due to 11-year UV flux variations, *J. Geophys. Res.*, *90*, 2273-2282, 1985.

Callis, L.B., M. Natarajan, J.D. Lambeth, and R.E. Boughner, On the origin of midlatitude ozone changes: Data analysis and simulations for 1979-1993, *J. Geophys. Res.*, *102*, 1215-1228, 1997.

Cariolle, D., and M. Deque, Southern Hemisphere medium-scale waves and total ozone disturbances in a spectral general circulation model, *J. Geophys. Res.*, *91*, 10825-10846, 1986.

Cariolle, D., A. Lassere-Bigory, and J.-F. Royerand, A general circulation model simulation of the springtime Antarctic ozone decrease and its impact on midlatitudes, *J. Geophys. Res.*, *95*, 1883-1898, 1990.

Chandra, S., and R.D. McPeters, The solar cycle variation of ozone in the stratosphere inferred from Nimbus 7 and NOAA 11 satellites, *J. Geophys. Res.*, *99*, 20665-20671, 1994.

Chipperfield, M.P., and J.A. Pyle, Model sensitivity studies of Arctic ozone depletion, *J. Geophys. Res.*, in press, 1998.

Chipperfield, M.P., A.M. Lee, and J.A. Pyle, Model calculations of ozone depletion in the Arctic polar vortex for 1991/92 to 1994/95, *Geophys. Res. Lett.*, *23*, 559-562, 1996.

Crutzen, P.J., I.S.A. Isaksen, and G.C. Reid, Solar proton events: Stratospheric sources of nitric oxide, *Science*, *189*, 457-458, 1975.

Cubasch, U., K. Hasselmann, H. Hock, E. Maier-Reimer, U. Mikalojewicz, B. Santer, and R. Sausen, Time-dependent greenhouse warming computations with a coupled ocean-atmosphere model, *Clim. Dyn.*, *8*, 55-69, 1992.

Dameris, M., V. Grewe, R. Hein, C. Schnadt, C. Brühl, and B. Steil, Assessment of the future development of the ozone layer, *Geophys. Res. Lett.*, *25*, 3579-3582, 1998.

Danilin, M.Y., N.-D. Sze, M.K.W. Ko, J.M. Rodriguez, and M.J. Prather, Bromine-chlorine coupling in the Antarctic ozone hole, *Geophys. Res. Lett.*, *23*, 153-156, 1996.

Danilin, M.Y., N.-D. Sze, M.K.W. Ko, J.M. Rodriguez, and A. Tabazadeh, Stratospheric cooling and Arctic ozone recovery, *Geophys. Res. Lett.*, *25*, 2141-2144, 1998.

DeMore, W.B., S.P. Sander, D.M. Golden, R.F. Hampson, M.J. Kurylo, C.J. Howard, A.R. Ravishankara, C.E. Kolb, and M.J. Molina, *Chemical Kinetics and Photochemical Data for Use in Stratospheric Modeling*, Evaluation No. 12, JPL Publ. 97-4, Jet Propulsion Laboratory, Pasadena, Calif., 1997.

Déqué, M., and J.P. Piedelievre, High resolution climate simulation over Europe, *Clim. Dyn.*, *11*, 321-339, 1995.

Donovan, D.P., H. Fast, Y. Makino, J.C. Bird, A.I. Carswell, J. Davies, T.J. Duck, J.W. Kaminski, C.T. McElroy, R.L. Mittermeier, S.R. Pal, V. Savastiouk, D. Velkov, and J.A. Whiteway, Ozone, column ClO, and PSC measurements made at the NDSC Eureka Observatory (80°N, 86°W) during the spring of 1997, *Geophys. Res. Lett.*, *24*, 2709-2712, 1997.

Douville, H., S. Planton, J.-F. Royer, and S. Tyteca, Climatic impact of $CO_2$ doubling: Part I, Radiative effects on global and regional climates, *J. Geophys. Res.*, submitted, 1998.

Elkins, J.W., T.M. Thompson, T.H. Swanson, J.H. Butler, B.D. Hall, S.O. Cummings, D.A. Fisher, and A.G. Raffo, Decrease in the growth rates of atmospheric chlorofluorocarbons 11 and 12, *Nature*, *364*, 780-783, 1993.

Farman, J.C., B.G. Gardiner, and J.D. Shanklin, Large losses of total ozone in Antarctica reveal seasonal $ClO_x/NO_x$ interaction, *Nature*, *315*, 207-210, 1985.

Knudsen, B.M., N. Larsen, I. St. Mikkelsen, J.-J. Morcrette, G.O. Braathen, E. Kyrö, H. Fast, H. Gernandt, H. Kanzawa, H. Nakane, V. Dorokhov, V. Yushkov, G. Hansen, M. Gil, and R.J. Shearman, Ozone depletion in and below the Arctic vortex for 1997, *Geophys. Res. Lett.*, *25*, 627-630, 1998.

Kodera, K., and H. Koide, Spatial and seasonal characteristics of recent decadal trends in the northern hemispheric troposphere and stratosphere, *J. Geophys. Res.*, *102*, 19433-19447, 1997.

Koike, M., Y. Kondo, M. Hayashi, Y. Iwasaka, P.A. Newman, M. Helten, and P. Aimedieu, Depletion of Arctic ozone in the winter 1990, *Geophys. Res. Lett.*, *18*, 791-794, 1991.

Kyrö, E., P. Taalas, T.S. Jorgensen, B. Knudsen, F. Stordal, G. Braathen, A. Dahlback, R. Neuber, B.C. Krüger, V. Dorokhov, V.A. Yushkov, V.V. Rudakov, and A. Torres, Analysis of the ozone soundings made during the first quarter of 1989 in the Arctic, *J. Geophys. Res.*, *97*, 8083-8091, 1992.

Lait, L.R., M.R. Schoeberl, and P.A. Newman, Quasi-biennial modulation of the Antarctic ozone depletion, *J. Geophys. Res.*, *94*, 11559-11571, 1989.

Larsen, N., B. Knudsen, I. St. Mikkelsen, T.S. Jorgensen, and P. Eriksen, Ozone depletion in the Arctic stratosphere in early 1993, *Geophys. Res. Lett.*, *21*, 1611-1614, 1994.

Law, K.S., and J.A. Pyle, Modeling trace gas budgets in the troposphere: 1, Ozone and odd nitrogen, *J. Geophys. Res.*, *98*, 18377-18400, 1993.

Lefèvre, F., G.P. Brasseur, I. Folkins, A.K. Smith, and P. Simon, Chemistry of the 1991-92 stratospheric winter: Three-dimensional model simulations, *J. Geophys. Res.*, *99*, 8183-8195, 1994.

Lefèvre, F., F. Figarol, K. Carslaw, and T. Peter, The 1997 Arctic ozone depletion quantified from three-dimensional model simulations, *Geophys. Res. Lett.*, *25*, 2425-2428, 1998.

Lipson, J.B., M.J. Elrod, T.W. Beiderhase, L.T. Molina, and M.J. Molina, Temperature dependence of the rate constant and branching ratio for the OH + ClO reaction, *J. Chem. Soc., Faraday Trans.*, *93*, 2665-2673, 1997.

Mahfouf, J.F., D. Cariolle, J.-F. Royer, J.-F. Geleyn, and B. Timbal, Response of the Météo-France climate model to changes in $CO_2$ and sea surface temperature, *Clim. Dyn.*, *9*, 345-362, 1993.

Manney, G.L., L. Froidevaux, J.W. Waters, R.W. Zurek, W.G. Read, L.S. Elson, J.B. Kumer, J.L. Mergenthaler, A.E. Roche, A.O'Neill, R.S. Harwood, I. MacKenzie, and R. Swinbank, Chemical ozone depletion of ozone in the Arctic lower stratosphere during winter 1992-93, *Nature*, *370*, 429-434, 1994.

Manney, G.L., R.W. Zurek, L. Froidevaux, and J.W. Waters, Evidence for Arctic ozone depletion in late February and early March 1994, *Geophys. Res. Lett.*, *22*, 2941-2944, 1995.

Manney, G.L., M.L. Santee, L. Froidevaux, J.W. Waters, and R.W. Zurek, Polar vortex conditions during the 1995-96 Arctic winter: Meteorology and MLS ozone, *Geophys. Res. Lett.*, *23*, 3203-3206, 1996.

Manney, G.L., L. Froidevaux, M.L. Santee, R.W. Zurek, and J.W. Waters, MLS observations of Arctic ozone loss in 1996-1997, *Geophys. Res. Lett.*, *24*, 2697-2700, 1997.

McCormack, J.P., and L.L. Hood, Apparent solar cycle variations of upper stratospheric ozone and temperature: Latitude and seasonal dependencies, *J. Geophys. Res.*, *101*, 20933-20944, 1996.

McKenna, D.S., R.L. Jones, L.R. Poole, S. Solomon, D.W. Fahey, K.K. Kelly, M.H. Proffitt, W.H. Brune, M. Loewenstein, and K.R. Chan, Calculations of ozone destruction during the 1988/89 Arctic winter, *Geophys. Res. Lett.*, *17*, 553-556, 1990.

McPeters, R.D., S.M. Hollandsworth, L.E. Flynn, J.R. Herman, and C.J. Seftor, Long-term ozone trends derived from the 16-year combined Nimbus 7/ Meteor 3 TOMS Version 7 record, *Geophys. Res. Lett.*, *23*, 3699-3702, 1996.

Michelangeli, D.V., M. Allen, and Y.L. Yung, Chichón volcanic aerosols: Impact of radiative, thermal, and chemical perturbations, *J. Geophys. Res.*, *94*, 18429-18443, 1989.

Mitchell, J.F.B., T.C. Johns, J.M. Gregory, and S.F.B. Tett, Climate response to increasing levels of greenhouse gases and sulphate aerosols, *Nature*, *376*, 501-504, 1995.

Molina, M.J., L.T. Molina, R. Zhang, R.F. Meads, and D.D. Spencer, The reaction of $ClONO_2$ with HCl on aluminum oxide, *Geophys. Res. Lett.*, *24*, 1619-1622, 1997.

Montzka, S.A., J.H. Butler, R.C. Myers, T.M. Thompson, T.H. Swanson, A.D. Clarke, L.T. Lock, and J.W. Elkins, Decline in the tropospheric abundance of halogen from halocarbons: Implications for stratospheric ozone depletion, *Science*, *272*, 1318-1322, 1996.

Müller, R., P.J. Crutzen, J.-U. Grooß, C. Brühl, J.M. Russell III, and A.F. Tuck, Chlorine activation and ozone depletion in the Arctic vortex: Observations by the Halogen Occultation Experiment on the Upper Atmosphere Research Satellite, *J. Geophys. Res.*, *101*, 12531-12554, 1996.

Müller, R., P.J. Crutzen, J.-U. Grooß, C. Brühl, J.M. Russell III, H. Gernandt, D.S. McKenna, and A.F. Tuck, Severe chemical ozone loss in the Arctic during the winter of 1995-96, *Nature*, *389*, 709-712, 1997a.

Müller, R., J.-U. Grooß, D.S. McKenna, P.J. Crutzen, C. Brühl, J.M. Russell III, and A.F. Tuck, HALOE observations of the vertical structure of chemical ozone depletion in the Arctic vortex during winter and early spring 1996-1997, *Geophys. Res. Lett.*, *24*, 2717-2720, 1997b.

Newman, P.A., J.F. Gleason, R.D. McPeters, and R.S. Stolarski, Anomalously low ozone over the Arctic, *Geophys. Res. Lett.*, *24*, 2689-2692, 1997.

Park, J.H., M.K.W. Ko, C.H. Jackman, and R.A. Plumb (eds.), *Report of the 1997 Models and Measurements Workshop*, November 3-5, 1997, Williamsburg, Virginia, NASA Ref. Publ., National Aeronautics and Space Administration, Washington, D.C., in press, 1998.

Pawson, S., and B. Naujokat, Trends in daily wintertime temperatures in the northern stratosphere, *Geophys. Res. Lett.*, *24*, 575-578, 1997.

Payan, S., C. Camy-Peyret, P. Jeseck, T. Hawat, G. Durry, and F. Lefèvre, First direct simultaneous HCl and $ClONO_2$ profiles in the Arctic vortex, *Geophys. Res. Lett.*, submitted, 1998.

Pitari, G., A numerical study of the possible perturbation of stratospheric dynamics due to Pinatubo aerosols: Implications for tracer transport, *J. Atmos. Sci.*, *50*, 2443-2461, 1993.

Pitari, G., and V. Rizi, An estimate of the chemical and radiative perturbation of stratospheric ozone following the eruption of Mt. Pinatubo, *J. Atmos. Sci.*, *50*, 3260-3276, 1993.

Pitari, G., and G. Visconti, Possible effects of $CO_2$ increase on the high-speed civil transport impact on ozone, *J. Geophys. Res.*, *99*, 16879-16896, 1994.

Pitari, G., S. Palermi, G. Visconti, and R.G. Prinn, Ozone response to a $CO_2$ doubling: Results from a stratospheric circulation model with heterogeneous chemistry, *J. Geophys. Res.*, *97*, 5953-5962, 1992.

Pitari, G., V. Rizi, L. Ricciardulli, and G. Visconti, High-speed civil transport impact: The role of sulfate, nitric acid trihydrate, and ice aerosols studied with a two-dimensional model including aerosol physics, *J. Geophys. Res.*, *98*, 23141-23164, 1993.

Proffitt, M.H., K. Aikin, J.J. Margitan, M. Loewenstein, J.R. Podolske, A. Weaver, K.R. Chan, H. Fast, and J.W. Elkins, Ozone loss inside the northern polar vortex during the 1991-1992 winter, *Science*, *261*, 1150-1154, 1993.

Randel, W.J., F. Wu, J.M. Russell III, J.W. Waters, and L. Froidevaux, Ozone and temperature changes in the stratosphere following the eruption of Mount Pinatubo, *J. Geophys. Res.*, *100*, 16753-16764, 1995.

Randeniya, L.K., P.F. Vohralik, I.C. Plumb, and K.R. Ryan, Heterogeneous $BrONO_2$ hydrolysis: Effect on $NO_2$ columns and ozone at high latitudes in summer, *J. Geophys. Res.*, *102*, 23543-23557, 1997.

Rasch, P.J., B.A. Boville, and G.P. Brasseur, A three-dimensional circulation model with coupled chemistry for the middle atmosphere, *J. Geophys. Res.*, *100*, 9041-9071, 1995.

Reinsel, G.C., G.C. Tiao, A.J. Miller, D.J. Wuebbles, P.S. Connell, C.L. Mateer, and J.J. DeLuisi, Statistical analysis of total ozone and stratospheric Umkehr data for trends and solar cycle relationship, *J. Geophys. Res.*, *92*, 2201-2209, 1987.

Renard, J.B., F. Lefèvre, M. Pirre, C. Robert, and D. Huguenin, Vertical profile of the nighttime stratospheric OClO, *J. Atmos. Chem.*, *26*, 65-76, 1997.

Rex, M., N.R.P. Harris, P. von der Gathen, R. Lehmann, G.O. Braathen, E. Reimer, A. Beck, M.P. Chipperfield, R. Alfier, M. Allaart, F. O'Connor, H. Dier, V. Dorokhov, H. Fast, M. Gil, E. Kyrö, Z. Litynska, I. St. Mikkelsen, M.G. Molyneux, H. Nakane, J. Notholt, M. Rummukainen, P. Viatte, and J. Wenger, Prolonged stratospheric ozone loss in the 1995-96 Arctic winter, *Nature*, *389*, 835-838, 1997.

Rex, M., P. von der Gathen, N.R.P. Harris, D. Lucic, B.M. Knudsen, G.O. Braathen, S.J. Reid, H. De Backer, H. Claude, R. Fabian, H. Fast, M. Gil, E. Kyrö, I. St. Mikkelsen, M. Rummukainen, H.G. Smit, J. Stähelin, C. Varotsos, and I. Zaitcev, In situ measurements of stratospheric ozone depletion rates in the Arctic winter 1991/92: A Lagrangian approach, *J. Geophys. Res.*, *103*, 5843-5853, 1998a.

Rex, M., P. von der Gathen, G.O. Braathen, S.J. Reid, N.R.P. Harris, M. Chipperfield, E. Reimer, A. Beck, R. Alfier, R. Krüger-Carstensen, H. De Backer, D. Balis, C. Zerefos, F. O'Connor, H. Dier, V. Dorokhov, H. Fast, A. Gamma, M. Gil, E. Kyrö, M. Rummukainen, Z. Litynska, I. St. Mikkelsen, M. Molyneux, and G. Murphy, Chemical ozone loss in the Arctic winter 1994/95 as determined by the Match technique, *J. Atmos. Chem.*, in press, 1998b.

Rind, D., R. Suozzo, N.K. Balachandran, and M.J. Prather, Climate change and the middle atmosphere: Part I, the doubled $CO_2$ climate, *J. Atmos. Sci.*, *47*, 475-494, 1990.

Rind, D., D. Shindell, P. Lonergran, and N.K. Balachandran, Climate change and the middle atmosphere: Part III, The doubled $CO_2$ climate revisited, *J. Clim.*, *11*, 876-894, 1998.

Roeckner, E., K. Arpe, L. Bengtsson, S. Brinkop, L. Dumenil, M. Esch, E. Kirk, F. Lunkheit, M. Ponater, B. Rockel, R. Sausen, U. Schlese, S. Schubert, and M. Windelband, *Simulation of the Present-Day Climate with the ECHAM Model: Impact of Model Physics and Resolution*, Max-Planck-Institut für Meteorologie Report 93, Max-Planck-Institut für Meteorologie, Hamburg, 1992.

Rosenfield, J.E., D.B. Considine, P.E. Meade, J.T. Bacmeister, C.H. Jackman, and M.R. Schoeberl, Stratospheric effects of Mount Pinatubo aerosol studied with a coupled two-dimensional model, *J. Geophys. Res.*, *102*, 3649-3670, 1997.

Ross, M., Local effects of solid rocket motor exhaust on stratospheric ozone, *J. Spacecr. Rockets*, *33*, 144-153, 1996.

Ross, M.N., J.O. Ballenthin, R.B. Gosselin, R.F. Meads, P.F. Zittel, J.R. Benbrook, and W.R. Sheldon, In-situ measurement of $Cl_2$ and $O_3$ in a stratospheric solid rocket motor exhaust plume, *Geophys. Res. Lett.*, *24*, 1755-1758, 1997a.

Ross, M.N., J.R. Benbrook, W.R. Sheldon, P.F. Zittel, and D.L. McKenzie, Observation of stratospheric ozone depletion in rocket exhaust plumes, *Nature*, *390*, 62-64, 1997b.

Russell, J.M. III, M. Luo, R.J. Cicerone, and L.E. Deaver, Satellite confirmation of the dominance of chlorofluorocarbons in the global stratospheric chlorine budget, *Nature*, *379*, 526-529, 1996.

Schoeberl, M.R., M.H. Proffitt, K.K. Kelly, L.R. Lait, P.A. Newman, J.E. Rosenfield, M. Loewenstein, J.R. Podolske, S.E. Strahan, and K.R. Chan, Stratospheric constituent trends from ER-2 profile data, *Geophys. Res. Lett.*, *17*, 469-427, 1990.

Shindell, D.T., S. Wong, and D. Rind, Interannual variability of the Antarctic ozone hole in a GCM: Part I, The influence of tropospheric wave variability, *J. Atmos. Sci.*, *54*, 2308-2319, 1997.

Shindell, D.T., D. Rind, and P. Lonergan, Climate change and the middle atmosphere: Part IV, Ozone photochemical response to doubled $CO_2$, *J. Clim.*, *11*, 895-918, 1998a.

Shindell, D.T., D. Rind, and P. Lonergan, Increased polar stratospheric ozone losses and delayed eventual recovery due to increasing greenhouse gas concentrations, *Nature*, *392*, 589-592, 1998b.

Siskind, D.E., J.T. Bacmeister, M.E. Summers, and J.M. Russell III, Two-dimensional model calculations of nitric oxide transport in the middle atmosphere and comparison with Halogen Occultation Experiment data, *J. Geophys. Res.*, *102*, 3527-3545, 1997.

Smyshlyaev, S.P., and V.A. Yudin, Numerical simulation of the aviation release impact on the ozone layer, *Izv. Atmos. Oceanic Phys.*, *31*, 116-125, 1995.

Solomon, S., R.W. Portmann, R.R. Garcia, L.W. Thomason, L.R. Poole, and M.P. McCormick, The role of aerosol variations in anthropogenic ozone depletion at northern midlatitudes, *J. Geophys. Res.*, *101*, 6713-6727, 1996.

Solomon, S., R.W. Portmann, R.R. Garcia, W. Randel, F. Wu, R. Nagatani, J. Gleason, L. Thomason, L.R. Poole, and M.P. McCormick, Ozone depletion at mid-latitudes: Coupling of volcanic aerosols and temperature variability to anthropogenic chlorine, *Geophys. Res. Lett.*, *25*, 1871-1874, 1998.

Steil, B., M. Dameris, C. Brühl, P.J. Crutzen, V. Grewe, M. Ponater, and R. Sauser, Development of a chemistry module for GCMs: First results of a multi-annual integration, *Ann. Geophys.*, *16*, 205-228, 1998.

Syage, J.A., and M.N. Ross, An assessment of the total ozone mapping spectrometer for measuring ozone levels in a solid rocket plume, *Geophys. Res. Lett.*, *23*, 3227-3230, 1996.

Tie, X.X., G.P. Brasseur, B. Briegleb, and C. Granier, Two-dimensional simulation of Pinatubo aerosol and its effects on stratospheric ozone, *J. Geophys. Res.*, *99*, 20545-20562, 1994.

Timbal, B., J.F. Mahfouf, J.-F. Royer, U. Cubasch, and J.M. Murphy, Comparison between doubled $CO_2$ time-slice and coupled experiments, *J. Clim.*, *10*, 1463-1469, 1997.

Velders, G.J.M., *Scenario Study of the Effects of CFC, HCFC, and HFC Emissions on Stratospheric Ozone*, Report No. 722201 006, National Institute of Public Health and the Environment, The Netherlands, 1995.

Velders, G.J.M., *Effect of Greenhouse Gas Emissions on Stratospheric Ozone Depletion*, Report No. 722201 011, National Institute of Public Health and the Environment, The Netherlands, 1997.

von Clarmann, T., G. Wetzel, H. Oelhaf, F. Fried-Vallon, A. Linden, G. Maucher, M. Seefeldner, O. Trieschmann, and F. Lefèvre, $ClONO_2$ vertical profile and estimated mixing ratios of ClO and HOCl in the winter Arctic stratosphere from MIPAS limb emission spectra, *J. Geophys. Res.*, *102*, 16157-16168, 1997.

von der Gathen, P., M. Rex, N.R.P. Harris, D. Lucic, B.M. Knudsen, G.O. Braathen, H. De Backer, R. Fabian, H. Fast, M. Gil, E. Kyrö, I. St. Mikkelsen, M. Rummukainen, J. Stähelin, and C. Varotsos, Observational evidence for chemical ozone depletion over the Arctic in winter 1991-92, *Nature*, *375*, 131-134, 1995.

Waters, J.W., W.G. Read, L. Froidevaux, T.A. Lungu, V.S. Perun, R.A. Stachnik, R.F. Jarnot, R.E. Cofield, E.F. Fishbein, D.A. Flower, J.R. Burke, J.C. Hardy, L.L. Nakamura, B.P. Ridenoure, Z. Shippany, R.P. Thurstans, L.M. Avallone, D.W. Toohey, R.L. DeZafra, and D.T. Shindell, Validation of UARS Microwave Limb Sounder ClO measurements, *J. Geophys.*, *101*, 10091-10127, 1996.

Weisenstein, D.K., M.K.W. Ko, I.G. Dyominov, G. Pitari, L. Ricciardulli, G. Visconti, and S. Bekki, The effects of sulfur emissions from HSCT aircraft: A 2-D model intercomparison, *J. Geophys. Res.*, *103*, 1527-1547, 1998.

Wetzel, G., T. von Clarmann, H. Oelhaf, F. Fried-Vallon, A. Linden, G. Maucher, M. Seefeldner, O. Trieschmann, and F. Lefèvre, $HNO_3$ and $N_2O_5$ vertical profiles in the winter arctic stratosphere from MIPAS limb emission spectra, *J. Geophys. Res.*, *102*, 19177-19186, 1997.

WMO (World Meteorological Organization), *Atmospheric Ozone 1985, Assessment of Our Understanding of the Processes Controlling Its Present Distribution and Change*, Global Ozone Research and Monitoring Project—Report No. 16, Geneva, 1986.

WMO (World Meteorological Organization), *Scientific Assessment of Ozone Depletion: 1991*, Global Ozone Research and Monitoring Project—Report No. 25, Geneva, 1992.

WMO (World Meteorological Organization), *Scientific Assessment of Ozone Depletion: 1994*, Global Ozone Research and Monitoring Project—Report No. 37, Geneva, 1995.

Zerefos,C.S., K. Tourpali, B.R. Bojkov, D.S. Balis, B. Rognerud, and I.S.A. Isaksen, Solar activity-total column ozone relationships, observations and model studies with heterogeneous chemistry, *J. Geophys. Res.*, *102*, 1561-1569, 1997.

Zurek, R.W., G.L. Manney, A.J. Miller, M.E. Gelman, and R.M. Nagatani, Interannual variability of the north polar vortex in the lower stratosphere during the UARS mission, *Geophys. Res. Lett.*, *23*, 289-292, 1996.

# APPENDICES

**A**
List of International Authors, Contributors, and Reviewers

**B**
Major Acronyms and Abbreviations

**C**
Chemical Formulae and Nomenclature

# APPENDIX A

# LIST OF INTERNATIONAL AUTHORS, CONTRIBUTORS, AND REVIEWERS

## COCHAIRS

| | | |
|---|---|---|
| Daniel L. Albritton | National Oceanic and Atmospheric Administration | US |
| Pieter J. Aucamp | Ptersa Environmental Consultants | South Africa |
| Gérard Mégie | Service d'Aéronomie du CNRS | France |
| Robert T. Watson | The World Bank | US |

## AUTHORS AND CONTRIBUTORS

### FREQUENTLY ASKED QUESTIONS ABOUT OZONE

**Coordinator**

| | | |
|---|---|---|
| Gérard Mégie | Service d'Aéronomie du CNRS | France |

### PART 1. HALOCARBON, OZONE, AND TEMPERATURE CHANGES

CHAPTER 1: LONG-LIVED OZONE-RELATED COMPOUNDS

**Chapter Lead Authors**

| | | |
|---|---|---|
| Ronald G. Prinn | Massachusetts Institute of Technology | US |
| R. Zander | Université de Liège | Belgium |

**Coauthors**

| | | |
|---|---|---|
| Derek M. Cunnold | Georgia Institute of Technology | US |
| James W. Elkins | NOAA Climate Monitoring and Diagnostics Laboratory | US |
| Andreas Engel | Universität Frankfurt | Germany |
| Paul J. Fraser | CSIRO Division of Atmospheric Research | Australia |
| Michael R. Gunson | California Institute of Technology/Jet Propulsion Laboratory | US |
| Malcolm K.W. Ko | Atmospheric and Environmental Research, Inc. | US |
| Emmanuel Mahieu | Université de Liège | Belgium |
| Pauline M. Midgley | M & D Consulting | Germany |
| James M. Russell III | Hampton University | US |
| C. Michael Volk | Universität Frankfurt | Germany |
| Ray F. Weiss | University of California at San Diego | US |

**Contributors**

| | | |
|---|---|---|
| Donald R. Blake | University of California at Irvine | US |

| | | |
|---|---|---|
| James H. Butler | NOAA Climate Monitoring and Diagnostics Laboratory | US |
| David W. Fahey | NOAA Aeronomy Laboratory | US |
| Jochen Harnisch | Max-Planck-Institut für Aeronomie | Germany |
| Dana E. Hartley | Georgia Institute of Technology | US |
| Dale F. Hurst | NOAA Climate Monitoring and Diagnostics Laboratory/CIRES | US |
| Nicholas B. Jones | National Institute of Water & Atmospheric Research Ltd. (NIWA) | New Zealand |
| Manfred Maiss | Max-Planck-Institut für Chemie | Germany |
| Archie McCulloch | ICI Chemicals & Polymers Ltd. | UK |
| Stephen A. Montzka | NOAA Climate Monitoring and Diagnostics Laboratory | US |
| David E. Oram | University of East Anglia | UK |
| Stuart A. Penkett | University of East Anglia | UK |
| Curtis P. Rinsland | NASA Langley Research Center | US |
| Ross J. Salawitch | California Institute of Technology/Jet Propulsion Laboratory | US |
| Sue M. Schauffler | National Center for Atmospheric Research | US |
| Ulrich Schmidt | Universität Frankfurt | Germany |
| Peter G. Simmonds | University of Bristol | UK |
| Thayne M. Thompson | NOAA Climate Monitoring and Diagnostics Laboratory | US |
| Geoffrey C. Toon | California Institute of Technology/Jet Propulsion Laboratory | US |

## CHAPTER 2: SHORT-LIVED OZONE-RELATED COMPOUNDS

### Chapter Lead Authors

| | | |
|---|---|---|
| Michael J. Kurylo | National Institute of Standards and Technology; NASA Headquarters | US |
| José M. Rodríguez | Atmospheric and Environmental Research, Inc. | US |

### Coauthors

| | | |
|---|---|---|
| Meinrat O. Andreae | Max-Planck-Institut für Chemie | Germany |
| Elliot L. Atlas | National Center for Atmospheric Research | US |
| Donald R. Blake | University of California at Irvine | US |
| James H. Butler | NOAA Climate Monitoring and Diagnostics Laboratory | US |
| Shyam Lal | Physical Research Laboratory | India |
| David J. Lary | Centre for Atmospheric Science, University of Cambridge | UK |
| Pauline M. Midgley | M & D Consulting | Germany |
| Stephen A. Montzka | NOAA Climate Monitoring and Diagnostics Laboratory | US |
| Paul C. Novelli | NOAA Climate Monitoring and Diagnostics Laboratory | US |
| Claire E. Reeves | University of East Anglia | UK |
| Peter G. Simmonds | University of Bristol | UK |
| L. Paul Steele | CSIRO Division of Atmospheric Research | Australia |
| William T. Sturges | University of East Anglia | UK |
| Ray F. Weiss | University of California at San Diego | US |
| Youko Yokouchi | National Institute for Environmental Studies | Japan |

### Contributors

| | | |
|---|---|---|
| Derek M. Cunnold | Georgia Institute of Technology | US |
| Ed Dlugokencky | NOAA Climate Monitoring and Diagnostics Laboratory | US |
| James W. Elkins | NOAA Climate Monitoring and Diagnostics Laboratory | US |
| David E. Etheridge | CSIRO Division of Atmospheric Research | Australia |

| | | |
|---|---|---|
| Paul J. Fraser | CSIRO Division of Atmospheric Research | Australia |
| Dana E. Hartley | Georgia Institute of Technology | US |
| Malcolm K.W. Ko | Atmospheric and Environmental Research, Inc. | US |
| Sasha Madronich | National Center for Atmospheric Research | US |
| Emmanuel Mahieu | Université de Liège | Belgium |
| Andrew Matthews | National Institute of Water & Atmospheric Research Ltd. (NIWA) | New Zealand |
| Archie McCulloch | ICI Chemicals & Polymers Ltd. | UK |
| David E. Oram | University of East Anglia | UK |
| John J. Orlando | National Center for Atmospheric Research | US |
| Stuart A. Penkett | University of East Anglia | UK |
| Sue M. Schauffler | National Center for Atmospheric Research | US |
| Shari A. Yvon-Lewis | NOAA Atlantic Oceanographic and Meteorological Laboratory | US |

## CHAPTER 3: GLOBAL DISTRIBUTIONS AND CHANGES IN STRATOSPHERIC PARTICLES

### Chapter Lead Authors

| | | |
|---|---|---|
| Sophie Godin | Service d'Aéronomie du CNRS | France |
| Lamont R. Poole | NASA Langley Research Center | US |

### Coauthors

| | | |
|---|---|---|
| Slimane Bekki | Service d'Aéronomie du CNRS | France |
| Terry Deshler | University of Wyoming | US |
| Niels Larsen | Danmarks Meteorologiske Institut | Denmark |
| Thomas Peter | Max-Planck-Institut für Chemie | Germany |

### Contributors

| | | |
|---|---|---|
| Alberto Adriani | Consiglio Nazionale della Richerche Istituto di Fisica dell'Atmosfera | Italy |
| John Barnes | NOAA Climate Monitoring and Diagnostics Laboratory | US |
| Richard Bevilacqua | Naval Research Laboratory | US |
| Christine David | Service d'Aéronomie du CNRS | France |
| Guido Di Donfrancesco | Consiglio Nazionale della Richerche Istituto di Fisica dell'Atmosfera | Italy |
| Michael Fromm | Computational Physics, Inc. | US |
| Mark Hervig | University of Wyoming | US |
| Horst Jäger | Fraunhofer-Institut für Atmosphärische Umweltforschung | Germany |
| Beiping Luo | Zhenjiang Rietschle Machinery Company, Ltd. | China |
| Roland Neuber | Alfred Wegener Institute | Germany |
| Mary Osborn | Science Applications International Corporation | US |
| Wolfgang Renger | Deutsche Forschungsanstalt für Luft- und Raumfahrt | Germany |
| Larry Thomason | NASA Langley Research Center | US |
| Osamu Uchino | Japan Meteorological Agency | Japan |
| Martin Wirth | Deutsche Forschungsanstalt für Luft- und Raumfahrt | Germany |

## CHAPTER 4: OZONE VARIABILITY AND TRENDS

### Chapter Lead Authors

| | | |
|---|---|---|
| Rumen D. Bojkov | World Meteorological Organization | Switzerland |
| Robert Hudson | University of Maryland | US |

### Coauthors

| | | |
|---|---|---|
| Lane Bishop | AlliedSignal Inc. | US |
| Vitali Fioletov | Atmospheric Environment Service | Canada |
| James M. Russell III | Hampton University | US |
| Richard Stolarski | NASA Goddard Space Flight Center | US |
| Osamu Uchino | Japan Meteorological Agency | Japan |
| Christos Zerefos | Aristotle University of Thessaloniki | Greece |

### Contributors

| | | |
|---|---|---|
| Roger Atkinson | Bureau of Meteorology | Australia |
| Dimitrios S. Balis | Aristotle University of Thessaloniki | Greece |
| P.K. Bhartia | NASA Goddard Space Flight Center | US |
| H. Claude | Meteorological Observatory Hohenpeißenberg | Germany |
| Lawrence E. Flynn | Software Corporation of America | US |
| Robert Guicherit | Netherlands Organization for Applied Scientific Research (TNO) | The Netherlands |
| Fumio Hasebe | Ibaraki University | Japan |
| G.J. Labow | Raytheon STX Inc. | US |
| Jennifer A. Logan | Harvard University | US |
| Richard D. McPeters | NASA Goddard Space Flight Center | US |
| Alvin J. Miller | NOAA NWS Climate Prediction Center | US |
| Rolf Müller | Forschungszentrum Jülich | Germany |
| Ruben Piacentini | Planetario y Observatorio de Rosario | Argentina |
| William J. Randel | National Center for Atmospheric Research | US |
| Herman Smit | Forschungszentrum Jülich | Germany |
| B.H. Subbaraya | Physical Research Laboratory | India |
| Kleareti Tourpali | Aristotle University of Thessaloniki | Greece |
| Peter von der Gathen | Alfred Wegener Institute | Germany |
| Ahmed Zand | Tehran University | Iran |

Members of the SPARC/IOC Profile Trends Panel

## CHAPTER 5: TRENDS IN STRATOSPHERIC TEMPERATURES

### Chapter Lead Authors

| | | |
|---|---|---|
| Marie-Lise Chanin | Service d'Aéronomie du CNRS | France |
| V. Ramaswamy | NOAA Geophysical Fluid Dynamics Laboratory | US |

### Coauthors

| | | |
|---|---|---|
| Dian J. Gaffen | NOAA Air Resources Laboratory | US |
| William J. Randel | National Center for Atmospheric Research | US |
| Richard B. Rood | NASA Goddard Space Flight Center | US |
| Masato Shiotani | Hokkaido University | Japan |

### Contributors

| | | |
|---|---|---|
| James K. Angell | NOAA Air Resources Laboratory | US |
| J. Barnett | Oxford University | UK |
| Piers M. de F. Forster | University of Reading | UK |
| Melvyn E. Gelman | NOAA NWS Climate Prediction Center | US |
| James Hansen | NASA Goddard Institute for Space Studies | US |

| | | |
|---|---|---|
| Philippe Keckhut | Service d'Aéronomie du CNRS | France |
| Yuri Koshelkov | Central Aerological Observatory | Russia |
| Karin Labitzke | Freie Universität Berlin | Germany |
| J.-J. Roger Lin | Research and Data Systems Corporation | US |
| E.V. Lysenko | Central Aerological Observatory | Russia |
| John Nash | U.K. Meteorological Office | UK |
| Alan O'Neill | University of Reading | UK |
| M. Daniel Schwarzkopf | NOAA Geophysical Fluid Dynamics Laboratory | US |
| Keith P. Shine | University of Reading | UK |
| Richard Swinbank | NASA Goddard Space Flight Center | US |
| Osamu Uchino | Japan Meteorological Agency | Japan |

## PART 2. ADVANCES IN UNDERSTANDING THE PROCESSES INVOLVED

### CHAPTER 6: UPPER STRATOSPHERIC PROCESSES

#### Chapter Lead Authors

| | | |
|---|---|---|
| Rolf Müller | Forschungszentrum Jülich | Germany |
| Ross J. Salawitch | California Institute of Technology/Jet Propulsion Laboratory | US |

#### Coauthors

| | | |
|---|---|---|
| Paul J. Crutzen | Max-Planck-Institut für Chemie | Germany |
| William A. Lahoz | University of Reading | UK |
| Gloria L. Manney | California Institute of Technology/Jet Propulsion Laboratory | US |
| Ralf Toumi | Imperial College | UK |

#### Contributors

| | | |
|---|---|---|
| David B. Considine | University of Maryland; NASA Goddard Space Flight Center | US |
| Simon J. Evans | Imperial College | UK |
| Jens-Uwe Grooß | Forschungszentrum Jülich | Germany |
| Charles H. Jackman | NASA Goddard Space Flight Center | US |
| Kenneth W. Jucks | Harvard-Smithsonian Center for Astrophysics | US |
| Douglas E. Kinnison | Lawrence Livermore National Laboratory | US |
| Alvin J. Miller | NOAA NWS Climate Prediction Center | US |
| Gary A. Morris | Valparaiso University | US |
| Gerald E. Nedoluha | Naval Research Laboratory | US |
| Cynthia D. Nevison | National Center for Atmospheric Research | US |
| William J. Randel | National Center for Atmospheric Research | US |
| A.R. Ravishankara | NOAA Aeronomy Laboratory | US |
| James M. Russell III | Hampton University | US |
| Karen H. Sage | NASA Langley Research Center | US |
| Michelle L. Santee | California Institute of Technology/Jet Propulsion Laboratory | US |
| David E. Siskind | Naval Research Laboratory | US |
| Michael E. Summers | Naval Research Laboratory | US |
| Jörg Trentmann | Max-Planck-Institut für Chemie | Germany |
| Ray H.J. Wang | Georgia Institute of Technology | US |
| Jerry Ziemke | Software Corporation of America | US |

## CHAPTER 7: LOWER STRATOSPHERIC PROCESSES

### Chapter Lead Authors

| | | |
|---|---|---|
| A.R. Ravishankara | NOAA Aeronomy Laboratory | US |
| Theodore G. Shepherd | University of Toronto | Canada |

### Coauthors

| | | |
|---|---|---|
| Martyn Chipperfield | Centre for Atmospheric Science, University of Cambridge | UK |
| Peter Haynes | Centre for Atmospheric Science, University of Cambridge | UK |
| Randy Kawa | NASA Goddard Space Flight Center | US |
| Thomas Peter | Max-Planck-Institut für Chemie | Germany |
| Alan Plumb | Massachusetts Institute of Technology | US |
| Bob Portmann | NOAA Aeronomy Laboratory | US |
| William J. Randel | National Center for Atmospheric Research | US |
| Darryn Waugh | Johns Hopkins University | US |
| Doug Worsnop | Aerodyne Research, Inc. | US |

### Contributors

| | | |
|---|---|---|
| Stephan Borrmann | Universität Mainz | Germany |
| Byron Boville | National Center for Atmospheric Research | US |
| Ken Carslaw | Max-Planck-Institut für Chemie | Germany |
| Rod Jones | Centre for Atmospheric Science, University of Cambridge | UK |
| Mike Mozurkewich | York University | Canada |
| Rolf Müller | Forschungszentrum Jülich | Germany |
| Donal O'Sullivan | NorthWest Research Associates, Inc. | US |
| Gilles Poulet | Laboratoire de Combustion et Systèmes Réactifs du CNRS | France |
| Michel Rossi | Ecole Polytechnique Fédérale de Lausanne | Switzerland |
| Stan Sander | California Institute of Technology/Jet Propulsion Laboratory | US |

## CHAPTER 8: TROPOSPHERIC OZONE AND RELATED PROCESSES

### Chapter Lead Authors

| | | |
|---|---|---|
| Jos Lelieveld | Institute for Marine and Atmospheric Research Utrecht (IMAU) | The Netherlands |
| Anne M. Thompson | NASA Goddard Space Flight Center | US |

### Coauthors

| | | |
|---|---|---|
| Roseanne D. Diab | University of Natal | South Africa |
| Øystein Hov | Norsk Institutt for Luftforskning (NILU) | Norway |
| Dieter Kley | Forschungszentrum Jülich | Germany |
| Jennifer A. Logan | Harvard University | US |
| Ole J. Nielsen | Risø National Laboratory | Denmark |
| William R. Stockwell | Fraunhofer-Institut für Atmosphärische Umweltforschung | Germany |
| Xiuji Zhou | Chinese Academy of Meteorological Sciences | China |

### Contributors

| | | |
|---|---|---|
| Robert Guicherit | Netherlands Organization for Applied Scientific Research (TNO) | The Netherlands |
| Daniel J. Jacob | Harvard University | US |
| Michael Kuhn | Fraunhofer-Institut für Atmosphärische Umweltforschung | Germany |

| | | |
|---|---|---|
| Jana B. Milford | University of Colorado | US |
| Howard W. Sidebottom | University College Dublin | Ireland |
| Johannes Stähelin | Eidgenössische Technische Hochschule Hönggerberg | Switzerland |

## PART 3. IMPACTS OF OZONE CHANGES

### CHAPTER 9: ULTRAVIOLET RADIATION AT THE EARTH'S SURFACE

#### Chapter Lead Authors

| | | |
|---|---|---|
| Jay R. Herman | NASA Goddard Space Flight Center | US |
| Richard L. McKenzie | National Institute of Water & Atmospheric Research Ltd. (NIWA) | New Zealand |

#### Coauthors

| | | |
|---|---|---|
| Susana Diaz | Centro Austral de Investigaciones Cientificas (CADIC) | Argentina |
| James B. Kerr | Atmospheric Environment Service | Canada |
| Sasha Madronich | National Center for Atmospheric Research | US |
| Gunther Seckmeyer | Fraunhofer-Institut für Atmosphärische Umweltforschung | Germany |

#### Contributors

| | | |
|---|---|---|
| Germar Bernhard | Fraunhofer-Institut für Atmosphärische Umweltforschung | Germany |
| Mario Blumthaler | Universität Innsbruck | Austria |
| Barry A. Bodhaine | NOAA Climate Monitoring and Diagnostics Laboratory | US |
| C. Rocky Booth | Biospherical Instruments, Inc. | US |
| Edward Celarier | Software Corporation of America | US |
| Piers M. de F. Forster | University of Reading | UK |
| Nickolay Krotkov | Raytheon STX Inc. | US |
| Jacqueline Lenoble | Université des Sciences et Technologies de Lille 1 | France |
| Kirsti Leszczynski | Radiation and Nuclear Safety Authority (STUK) | Finland |
| Craig S. Long | NOAA NWS Climate Prediction Center | US |
| Bernhard Mayer | Fraunhofer-Institut für Atmosphärische Umweltforschung | Germany |
| Forrest Mims | Sun Photometer Atmospheric Network | US |
| Patrick Neale | Smithsonian Environmental Research Center | US |
| Ruben Piacentini | Planetario y Observatorio de Rosario | Argentina |
| Ken G. Ryan | Industrial Research Limited | New Zealand |
| Harry Slaper | National Institute of Public Health and the Environment (RIVM) | The Netherlands |
| James R. Slusser | Colorado State University | US |
| Russell Wooldridge | IDEA Corporation | US |
| Christos Zerefos | Aristotle University of Thessaloniki | Greece |

### CHAPTER 10: CLIMATE EFFECTS OF OZONE AND HALOCARBON CHANGES

#### Chapter Lead Authors

| | | |
|---|---|---|
| Claire Granier | Service d'Aéronomie du CNRS; NOAA Aeronomy Laboratory | France/US |
| Keith P. Shine | University of Reading | UK |

#### Coauthors

| | | |
|---|---|---|
| John S. Daniel | NOAA Aeronomy Laboratory | US |

| | | |
|---|---|---|
| James Hansen | NASA Goddard Institute for Space Studies | US |
| Shyam Lal | Physical Research Laboratory | India |
| Frode Stordal | Norsk Institutt for Luftforskning (NILU) | Norway |

### Contributors

| | | |
|---|---|---|
| Slimane Bekki | Service d'Aéronomie du CNRS | France |
| Lane Bishop | AlliedSignal Inc. | US |
| Jan Fuglestvedt | Universitetet I Oslo Centre for International Climate and Environmental Research | Norway |
| Jan-Eiof Jonson | Universitetet I Oslo | Norway |
| Sasha Madronich | National Center for Atmospheric Research | US |
| Gunnar Myhre | Universitetet I Oslo | Norway |

## PART 4. PREDICTIONS OF FUTURE CHANGES

### CHAPTER 11: HALOCARBON SCENARIOS FOR THE FUTURE OZONE LAYER AND RELATED CONSEQUENCES

### Chapter Lead Authors

| | | |
|---|---|---|
| Sasha Madronich | National Center for Atmospheric Research | US |
| Guus J.M. Velders | National Institute of Public Health and the Environment (RIVM) | The Netherlands |

### Coauthors

| | | |
|---|---|---|
| John S. Daniel | NOAA Aeronomy Laboratory | US |
| Murari Lal | Indian Institute of Technology | India |
| Archie McCulloch | ICI Chemicals & Polymers Ltd. | UK |
| Harry Slaper | National Institute of Public Health and the Environment (RIVM) | The Netherlands |

### Contributors

| | | |
|---|---|---|
| Mack McFarland | DuPont Fluoroproducts | US |
| Pauline M. Midgley | M & D Consulting | Germany |
| Nelson A. Sabogal | United Nations Environment Programme | Kenya |
| Susan Solomon | NOAA Aeronomy Laboratory | US |
| Donald J. Wuebbles | University of Illinois | US |

### CHAPTER 12: PREDICTING FUTURE OZONE CHANGES AND DETECTION OF RECOVERY

### Chapter Lead Authors

| | | |
|---|---|---|
| David J. Hofmann | NOAA Climate Monitoring and Diagnostics Laboratory | US |
| John A. Pyle | Centre for Atmospheric Science, University of Cambridge | UK |

### Coauthors

| | | |
|---|---|---|
| John Austin | U.K. Meteorological Office | UK |
| Neal Butchart | U.K. Meteorological Office | UK |
| Charles H. Jackman | NASA Goddard Space Flight Center | US |
| Douglas E. Kinnison | Lawrence Livermore National Laboratory | US |
| Franck Lefèvre | Météo-France, Centre National de Recherches Météorologiques | France |

| | | |
|---|---|---|
| Giovanni Pitari | Università degli Studi dell'Aquila | Italy |
| Drew Shindell | NASA Goddard Institute for Space Studies | US |
| Ralf Toumi | University of Cambridge | UK |
| Peter von der Gathen | Alfred Wegener Institute | Germany |

### Contributors

| | | |
|---|---|---|
| Slimane Bekki | Service d'Aéronomie du CNRS; University of Cambridge | France/UK |
| Christoph Brühl | Max-Planck-Institut für Chemie | Germany |
| Peter S. Connell | Lawrence Livermore National Laboratory | US |
| Martin Dameris | Deutsche Forschungsanstalt für Luft- and Raumfahrt | Germany |
| Eric L. Fleming | Space Applications Corporation | US |
| Stacey M. Hollandsworth | Space Applications Corporation | US |
| Samuel J. Oltmans | NOAA Climate Monitoring and Diagnostics Laboratory | US |
| Lakshman Randeniya | CSIRO Telecommunications and Industrial Physics | Australia |
| Markus Rex | Alfred Wegener Institute | Germany |
| Bjoerg Rognerud | Universitetet I Oslo | Norway |
| Sergei P. Smyshlyaev | Russian State Hydrometeorological Institute | Russia |
| Hubert Teyssèdre | Météo-France, Centre National de Recherches Météorologiques | France |
| Guus J.M. Velders | National Institute of Public Health and the Environment (RIVM) | The Netherlands |
| Debra K. Weisenstein | Atmospheric and Environmental Research, Inc. | US |
| Jerry Ziemke | Software Corporation of America | US |

## Chapter Editorial Contributors

### CHAPTER 1: LONG-LIVED OZONE-RELATED COMPOUNDS

| | | |
|---|---|---|
| Nada Derek | CSIRO Division of Atmospheric Research | Australia |
| L. Kubrick | Massachusetts Institute of Technology | US |
| Kathy A. Wolfe | Computer Sciences Corporation | US |
| Diane Zander | Université de Liège | Belgium |

### CHAPTER 2: SHORT-LIVED OZONE-RELATED COMPOUNDS

| | | |
|---|---|---|
| Kathy A. Wolfe | Computer Sciences Corporation | US |

### CHAPTER 5: TRENDS IN STRATOSPHERIC TEMPERATURES

| | | |
|---|---|---|
| Gail Haller | NOAA Geophysical Fluid Dynamics Laboratory | US |
| Cathy Raphael | NOAA Geophysical Fluid Dynamics Laboratory | US |
| Jeff Varanyak | NOAA Geophysical Fluid Dynamics Laboratory | US |

### CHAPTER 6: UPPER STRATOSPHERIC PROCESSES

| | | |
|---|---|---|
| Stephan Böttcher | Tel Aviv University | Israel |

## CHAPTER 7: LOWER STRATOSPHERIC PROCESSES

| | | |
|---|---|---|
| LeAnn Droppleman | NOAA Aeronomy Laboratory | US |

## CHAPTER 8: TROPOSPHERIC OZONE

| | | |
|---|---|---|
| Matthew G. Seybold | Steven Myers and Associates Corporation/NASA Goddard Space Flight Center | US |

## CHAPTER 11: SCENARIOS FOR THE FUTURE OZONE LAYER AND RELATED CONSEQUENCES

| | | |
|---|---|---|
| Chris Fischer | National Center for Atmospheric Research | US |

## CHAPTER 12: PREDICTING FUTURE OZONE CHANGES AND DETECTION OF RECOVERY

| | | |
|---|---|---|
| Ann Thorne | NOAA Climate Monitoring and Diagnostics Laboratory | US |

## REVIEWERS

| | | |
|---|---|---|
| Daniel L. Albritton | National Oceanic and Atmospheric Administration | US |
| Georgios T. Amanatidis | European Commission | Belgium |
| James K. Angell | NOAA Air Resources Laboratory | US |
| Pieter J. Aucamp | Ptersa Environmental Consultants | South Africa |
| Linnea Avallone | University of Colorado | US |
| Darrel Baumgardner | National Center for Atmospheric Research | US |
| Lane Bishop | AlliedSignal Inc. | US |
| Mario Blumthaler | Universität Innsbruck | Austria |
| Greg Bodeker | National Institute of Water & Atmospheric Research Ltd. (NIWA) | New Zealand |
| Barry A. Bodhaine | NOAA Climate Monitoring and Diagnostics Laboratory | US |
| Rumen D. Bojkov | World Meteorological Organization | Switzerland |
| Guy Brasseur | National Center for Atmospheric Research | US |
| Christoph Brühl | Max-Planck-Institut für Chemie | Germany |
| William H. Brune | Pennsylvania State University | US |
| Neal Butchart | U.K. Meteorological Office | UK |
| Pablo O. Canziani | Universidad de Buenos Aires | Argentina |
| Daniel Cariolle | Météo-France, Centre National de Recherches Météorologiques | France |
| Marie-Lise Chanin | Service d'Aéronomie du CNRS | France |
| Cathy Clerbaux | Service d'Aéronomie du CNRS | France |
| Michael Coffey | National Center for Atmospheric Research | US |
| R.A. Cox | Centre for Atmospheric Science, University of Cambridge | UK |
| Paul J. Crutzen | Max-Planck-Institut für Chemie | Germany |
| John S. Daniel | NOAA Aeronomy Laboratory | US |
| Richard Derwent | U.K. Meteorological Office | UK |
| Susana Diaz | Centro Austral de Investigaciones Cientificas (CADIC) | Argentina |
| Ed Dlugokencky | NOAA Climate Monitoring and Diagnostics Laboratory | US |
| Thomas Duafala | Tri-Cal Research Division | US |
| Dieter H. Ehhalt | Institut für Chemie und Dynamik der Geosphäre | Germany |
| James W. Elkins | NOAA Climate Monitoring and Diagnostics Laboratory | US |

| | | |
|---|---|---|
| Christine A. Ennis | NOAA Aeronomy Laboratory/CIRES | US |
| David W. Fahey | NOAA Aeronomy Laboratory | US |
| Jack Fishman | NASA Langley Research Center | US |
| Piers M. de F. Forster | University of Reading | UK |
| J. Paul F. Fortuin | Koninklijk Nederlands Meteorologisch Instituut (KNMI) | The Netherlands |
| Paul J. Fraser | CSIRO Division of Atmospheric Research | Australia |
| Lucien Froidevaux | California Institute of Technology/Jet Propulsion Laboratory | US |
| Marvin A. Geller | State University of New York at Stony Brook | US |
| Sophie Godin | Service d'Aéronomie du CNRS | France |
| Allen Goldstein | College of Natural Resources | UK |
| George S. Golitsyn | Russian Academy of Sciences | Russia |
| Claire Granier | Service d'Aéronomie du CNRS; NOAA Aeronomy Laboratory | France/US |
| William B. Grant | NASA Langley Research Center | US |
| Robert Guicherit | Netherlands Organization for Applied Scientific Research (TNO) | The Netherlands |
| Neil R.P. Harris | European Ozone Research Coordinating Unit | UK |
| Alain Hauchecorne | Service d'Aéronomie du CNRS | France |
| Didier Hauglustaine | National Center for Atmospheric Research | US |
| Jay R. Herman | NASA Goddard Space Flight Center | US |
| David J. Hofmann | NOAA Climate Monitoring and Diagnostics Laboratory | US |
| James R. Holton | University of Washington | US |
| Robert Hudson | University of Maryland | US |
| Drusilla Hufford | U.S. Environmental Protection Agency | US |
| Abdel Moneim Ibrahim | Egyptian Meteorological Authority | Egypt |
| Mohammad I. Ilyas | Universiti Sains Malaysia | Malaysia |
| Ivar S.A. Isaksen | Universitetet I Oslo | Norway |
| Tomoyuki Ito | Japan Meteorological Agency | Japan |
| Evgeny A. Jadin | Central Aerological Observatory | Russia |
| Rod Jones | Centre for Atmospheric Science, University of Cambridge | UK |
| Torben S. Jørgensen | Danmarks Meteorologiske Institut | Denmark |
| David Karoly | Monash University | Australia |
| Jack A. Kaye | NASA Headquarters | US |
| Hennie Kelder | Koninklijk Nederlands Meteorologisch Instituut (KNMI) | The Netherlands |
| James B. Kerr | Atmospheric Environment Service | Canada |
| Jhoon Kim | Korea Aerospace Research Institute | Republic of Korea |
| Volker Kirchhoff | Instituto Nacional de Pesquisas Espaciais (INPE) | Brazil |
| Malcolm K.W. Ko | Atmospheric and Environmental Research, Inc. | US |
| Kunihiko Kodera | Meteorological Research Institute | Japan |
| Yutaka Kondo | Nagoya University | Japan |
| Janusz Krzyścin | Polish Academy of Sciences | Poland |
| Michael J. Kurylo | National Institute of Standards and Technology; NASA Headquarters | US |
| Murari Lal | Indian Institute of Technology | India |
| Yuan-Pern Lee | National Tsing Hua University | Taiwan |
| Jos Lelieveld | Institute for Marine and Atmospheric Research Utrecht (IMAU) | The Netherlands |
| Joel M. Levy | NOAA Office of Global Programs | US |
| Jennifer A. Logan | Harvard University | US |
| Craig S. Long | NOAA NWS Climate Prediction Center | US |
| Sasha Madronich | National Center for Atmospheric Research | US |
| Jerry D. Mahlman | NOAA Geophysical Fluid Dynamics Laboratory | US |
| Andrew Matthews | National Institute of Water & Atmospheric Research Ltd. (NIWA) | New Zealand |
| M. Patrick McCormick | Hampton University | US |

| | | |
|---|---|---|
| Archie McCulloch | ICI Chemicals & Polymers Ltd. | UK |
| Mack McFarland | DuPont Fluoroproducts | US |
| Danny McKenna | Forschungszentrum Jülich | Germany |
| Richard L. McKenzie | National Institute of Water & Atmospheric Research Ltd. (NIWA) | New Zealand |
| Gérard Mégie | Service d'Aéronomie du CNRS | France |
| Pauline M. Midgley | M & D Consulting | Germany |
| Alvin J. Miller | NOAA NWS Climate Prediction Center | US |
| Philippe Mirabel | Université Louis Pasteur | France |
| Masa Miyauchi | Japan Meteorological Agency | Japan |
| Mario J. Molina | Massachusetts Institute of Technology | US |
| Rolf Müller | Forschungszentrum Jülich | Germany |
| Hideaki Nakane | National Institute for Environmental Studies | Japan |
| Paul A. Newman | NASA Goddard Space Flight Center | US |
| Samuel J. Oltmans | NOAA Climate Monitoring and Diagnostics Laboratory | US |
| Michael Oppenheimer | Environmental Defense Fund | US |
| Stuart A. Penkett | University of East Anglia | UK |
| Joyce Penner | University of Michigan | US |
| Thomas Peter | Max-Planck-Institut für Chemie | Germany |
| Michel Pirre | Service d'Aéronomie du CNRS | France |
| Jean-Pierre Pommereau | Service d'Aéronomie du CNRS | France |
| Lamont R. Poole | NASA Langley Research Center | US |
| Michael Prather | University of California at Irvine | US |
| M. Margarita Préndez | Universidad de Chile | Chile |
| Ronald G. Prinn | Massachusetts Institute of Technology | US |
| John A. Pyle | Centre for Atmospheric Science, University of Cambridge | UK |
| V. Ramaswamy | NOAA Geophysical Fluid Dynamics Laboratory | US |
| William J. Randel | National Center for Atmospheric Research | US |
| A.R. Ravishankara | NOAA Aeronomy Laboratory | US |
| George C. Reid | NOAA Aeronomy Laboratory | US |
| Henning Rodhe | Stockholms Universitet | Sweden |
| José M. Rodríguez | Atmospheric and Environmental Research, Inc. | US |
| James M. Rosen | University of Wyoming | US |
| James M. Russell III | Hampton Univesity | US |
| Keith R. Ryan | CSIRO Telecommunications and Industrial Physics | Australia |
| Nelson A. Sabogal | United Nations Environment Programme | Kenya |
| Ross J. Salawitch | California Institute of Technology/Jet Propulsion Laboratory | US |
| Eugenio Sanhueza | Instituto Venezolano de Investigaciones Cientificas (IVIC) | Venezuela |
| Ulrich Schmidt | Universität Frankfurt | Germany |
| Ulrich Schumann | Deutsche Forschungsanstalt für Luft- und Raumfahrt | Germany |
| Theodore G. Shepherd | University of Toronto | Canada |
| Keith P. Shine | University of Reading | UK |
| Susan Solomon | NOAA Aeronomy Laboratory | US |
| Johannes Stähelin | Eidgenössische Technische Hochschule Hönggerberg | Switzerland |
| Leopoldo Stefanutti | Istituto di Riccrea sulle Onde Elettromagnetiche del Consiglio Nazionale della Richerche | Italy |
| William R. Stockwell | Fraunhofer-Institut für Atmosphärische Umweltforschung | Germany |
| B.H. Subbaraya | Physical Research Laboratory | India |
| Petteri Taalas | Finnish Meteorological Institute | Finland |
| Xiao-Yan Tang | Peking University | China |
| Anne M. Thompson | NASA Goddard Space Flight Center | US |

| | | |
|---|---|---|
| Brian Toon | University of Colorado | US |
| Michael Trainer | NOAA Aeronomy Laboratory | US |
| Osamu Uchino | Japan Meteorological Agency | Japan |
| Jan C. van der Leun | University Hospital | The Netherlands |
| Karel Vanicek | Czech Hydrometeorological Institute | Czech Republic |
| Guus J.M. Velders | National Institute of Public Health and the Environment (RIVM) | The Netherlands |
| Guido Visconti | Università degli Studi dell'Aquila | Italy |
| Andreas Volz-Thomas | Forschungszentrum Jülich | Germany |
| Wei-Chyung Wang | State University of New York at Albany | US |
| Joe Waters | California Institute of Technology/Jet Propulsion Laboratory | US |
| Robert T. Watson | The World Bank | US |
| Ray F. Weiss | University of California at San Diego | US |
| Paul O. Wennberg | California Institute of Technology | US |
| James C. Wilson | University of Denver | US |
| Donald J. Wuebbles | University of Illinois | US |
| Vladimir Yushkov | Central Aerological Observatory | Russia |
| Ahmed Zand | Tehran Unversity | Iran |
| R. Zander | Université de Liège | Belgium |
| Christos Zerefos | Aristotle University of Thessaloniki | Greece |

## Ozone Peer-Review Meeting

*Les Diablerets, Switzerland*
*June 1-5, 1998*

| | | |
|---|---|---|
| Daniel L. Albritton | National Oceanic and Atmospheric Administration | US |
| Georgios T. Amanatidis | European Commission | Belgium |
| Pieter J. Aucamp | Ptersa Environmental Consultants | South Africa |
| Lane Bishop | AlliedSignal Inc. | US |
| Rumen D. Bojkov | World Meteorological Organization | Switzerland |
| Marie-Lise Chanin | Service d'Aéronomie du CNRS | France |
| R.A. Cox | Centre for Atmospheric Science, University of Cambridge | UK |
| Paul J. Crutzen | Max-Planck-Institut für Chemie | Germany |
| John S. Daniel | NOAA Aeronomy Laboratory | US |
| Susana Diaz | Centro Austral de Investigaciones Cientificas (CADIC) | Argentina |
| Thomas Duafala | Tri-Cal Research Division | US |
| Dieter H. Ehhalt | Institut für Chemie und Dynamik der Geosphäre | Germany |
| James W. Elkins | NOAA Climate Monitoring and Diagnostics Laboratory | US |
| Christine A. Ennis | NOAA Aeronomy Laboratory/CIRES | US |
| David W. Fahey | NOAA Aeronomy Laboratory | US |
| Paul J. Fraser | CSIRO Division of Atmospheric Research | Australia |
| Lucien Froidevaux | California Institute of Technology/Jet Propulsion Laboratory | US |
| Marvin A. Geller | State University of New York at Stony Brook | US |
| Sophie Godin | Service d'Aéronomie du CNRS | France |
| Claire Granier | Service d'Aéronomie du CNRS; NOAA Aeronomy Laboratory | France/US |
| Neil R.P. Harris | European Ozone Research Coordinating Unit | UK |
| Jay R. Herman | NASA Goddard Space Flight Center | US |
| David J. Hofmann | NOAA Climate Monitoring and Diagnostics Laboratory | US |

| | | |
|---|---|---|
| James R. Holton | University of Washington | US |
| Robert Hudson | University of Maryland | US |
| Abdel Moneim Ibrahim | Egyptian Meteorological Authority | Egypt |
| Mohammad I. Ilyas | Universiti Sains Malaysia | Malaysia |
| Ivar S.A. Isaksen | Universitetet I Oslo | Norway |
| Rod Jones | Centre for Atmospheric Science, University of Cambridge | UK |
| James B. Kerr | Atmospheric Environment Service | Canada |
| Michael J. Kurylo | National Institute of Standards and Technology; NASA Headquarters | US |
| Murari Lal | Indian Institute of Technology | India |
| Jos Lelieveld | Institute for Marine and Atmospheric Research Utrecht (IMAU) | The Netherlands |
| Jennifer A. Logan | Harvard University | US |
| Sasha Madronich | National Center for Atmospheric Research | US |
| M. Patrick McCormick | Hampton University | US |
| Mack McFarland | DuPont Fluoroproducts | US |
| Danny McKenna | Forschungszentrum Jülich | Germany |
| Richard L. McKenzie | National Institute of Water & Atmospheric Research Ltd. (NIWA) | New Zealand |
| Gérard Mégie | Service d'Aéronomie du CNRS | France |
| Rolf Müller | Forschungszentrum Jülich | Germany |
| Hideaki Nakane | National Institute for Environmental Studies | Japan |
| Paul A. Newman | NASA Goddard Space Flight Center | US |
| Samuel J. Oltmans | NOAA Climate Monitoring and Diagnostics Laboratory | US |
| Stuart A. Penkett | University of East Anglia | UK |
| Thomas Peter | Max-Planck-Institut für Chemie | Germany |
| Lamont R. Poole | NASA Langley Research Center | US |
| M. Margarita Préndez | Universidad de Chile | Chile |
| John A. Pyle | Centre for Atmospheric Science, University of Cambridge | UK |
| V. Ramaswamy | NOAA Geophysical Fluid Dynamics Laboratory | US |
| William J. Randel | National Center for Atmospheric Research | US |
| A.R. Ravishankara | NOAA Aeronomy Laboratory | US |
| José M. Rodríguez | Atmospheric and Environmental Research, Inc. | US |
| James M. Russell III | Hampton University | US |
| Nelson A. Sabogal | United Nations Environment Programme | Kenya |
| Ross J. Salawitch | California Institute of Technology/Jet Propulsion Laboratory | US |
| Eugenio Sanhueza | Instituto Venezolano de Investigaciones Cientificas (IVIC) | Venezuela |
| Theodore G. Shepherd | University of Toronto | Canada |
| Keith P. Shine | University of Reading | UK |
| Susan Solomon | NOAA Aeronomy Laboratory | US |
| William R. Stockwell | Fraunhofer-Institut für Atmosphärische Umweltforschung | Germany |
| B.H. Subbaraya | Physical Research Laboratory | India |
| Petteri Taalas | Finnish Meteorological Institute | Finland |
| Osamu Uchino | Japan Meteorological Agency | Japan |
| Jan C. van der Leun | University Hospital | The Netherlands |
| Karel Vanicek | Czech Hydrometeorological Institute | Czech Republic |
| Guus J.M. Velders | National Institute of Public Health and the Environment (RIVM) | The Netherlands |
| Robert T. Watson | The World Bank | US |
| Ray F. Weiss | University of California at San Diego | US |
| Donald J. Wuebbles | University of Illinois | US |
| Ahmed Zand | Tehran University | Iran |
| R. Zander | Université de Liège | Belgium |
| Christos Zerefos | Aristotle University of Thessaloniki | Greece |

### Sponsoring Organizations Liaisons

Rumen D. Bojkov World Meteorological Organization Switzerland
K.M. Sarma United Nations Environment Programme Kenya
Daniel L. Albritton National Oceanic and Atmospheric Administration US
Michael J. Kurylo National Institute of Standards and Technology; NASA Headquarters US
Georgios T. Amanatidis European Commission Belgium

### Coordinating Editor

Christine A. Ennis NOAA Aeronomy Laboratory/CIRES US

### Editorial Staff

Debra Dailey-Fisher NOAA Aeronomy Laboratory US
Christine C. Sweet NOAA Environmental Research Laboratories US
Jeanne S. Waters NOAA Aeronomy Laboratory US

### Publication Design and Layout

VISUAL SCIENCE INC.
David Gallant
Elizabeth J. Graves
Scott Lininger
Julianne Snider

### Conference Coordination and Documentation

Rumen D. Bojkov World Meteorological Organization Switzerland
Marie-Christine Charriére World Meteorological Organization Switzerland
Christine A. Ennis NOAA Aeronomy Laboratory/CIRES US
Jeanne S. Waters NOAA Aeronomy Laboratory US

### Conference Support

Catherine A. Burgdorf NOAA Aeronomy Laboratory/CIRES US
Marie-Christine Charriére World Meteorological Organization Switzerland
Rose M. Kendall Computer Sciences Corporation US
Jeanne S. Waters NOAA Aeronomy Laboratory US
Kathy A. Wolfe Computer Sciences Corporation US

### Computing and Networking Support

Catherine A. Burgdorf NOAA Aeronomy Laboratory/CIRES US
Walter J. Harrop NOAA Aeronomy Laboratory US
Ken Jamieson NOAA Aeronomy Laboratory/CIRES US
Sarah Thompson NOAA Aeronomy Laboratory/CIRES US

# APPENDIX B

# MAJOR ACRONYMS AND ABBREVIATIONS

| | |
|---|---|
| AASE | Airborne Arctic Stratospheric Expedition |
| ACATS-IV | Airborne Chromatograph for Atmospheric Trace Species-IV |
| ACE | Aerosol Characterization Experiment |
| ADEOS | Advanced Earth Observing Satellite |
| AER | Atmospheric and Environmental Research, Inc. (United States) |
| AFEAS | Alternative Fluorocarbons Environmental Acceptability Study |
| AGAGE | Advanced Global Atmospheric Gases Experiment |
| AGWP | Absolute Global Warming Potential |
| ALE | Atmospheric Lifetime Experiment |
| ALIAS | Aircraft Laser Infrared Absorption Spectrometer |
| ANCAT/EC | Abatement of Nuisance Caused by Air Traffic/European Commission |
| APARE | East Asian-North Pacific Regional Experiment |
| ARL | Air Resources Laboratory (NOAA) |
| ARL | Australian Radiation Laboratory (Australia) |
| ASHOE/MAESA | Airborne Southern Hemisphere Ozone Experiment/Measurements for Assessing the Effects of Stratospheric Aircraft |
| asl | above sea level |
| ASTEX/MAGE | Atlantic Stratocumulus Transition Experiment/Marine Aerosol and Gas Exchange |
| ATLAS | Atmospheric Laboratory for Applications and Science |
| ATMOS | Atmospheric Trace Molecule Spectroscopy |
| AVHRR | Advanced Very High Resolution Radiometer |
| AWI | Alfred Wegener Institute (Germany) |
| | |
| BEF | Bromine Efficiency Factor |
| BLP | Bromine Loading Potential |
| BM | Brewer-Mast (ozonesonde) |
| BUV | Backscatter-Ultraviolet (spectrometer) |
| | |
| CAC | Climate Analysis Center (now CPC) |
| CCM | community climate model-2 |
| CCN | cloud condensation nuclei |
| CD-ROM | compact disk–read only memory |
| CF | cloud factor |
| CFC | chlorofluorocarbon |
| CGAA | Cape Grim Air Archive (Tasmania) |
| CICERO | Centre for International Climate and Environmental Research, Universitetet I Oslo (Norway) |
| CIE | International Lighting Commission (France) |
| CIESIN | Consortium for International Earth Science Information Network |
| CIRES | Cooperative Institute for Research in Environmental Sciences (United States) |
| CITE | Chemical Instrument Test and Evaluation |
| CLAES | Cryogenic Limb Array Etalon Spectrometer |
| CMDL | Climate Monitoring and Diagnostics Laboratory (NOAA) |

**ACRONYMS**

| | |
|---|---|
| mbar | millibar |
| MBGC | Methyl Bromide Global Coalition |
| MBL | marine boundary layer |
| MDI | metered dose inhaler |
| MIT | Massachusetts Institute of Technology (United States) |
| MLO | Mauna Loa Observatory (NOAA) |
| MLOPEX | Mauna Loa Observatory Photochemistry Experiment |
| MLS | Microwave Limb Sounder |
| MOGUNTIA | model of the general universal tracer transport in the atmosphere |
| MOPITT | Measurement Of Pollution In The Troposphere |
| μm | micrometers, micron ($10^{-6}$ meters) |
| MPAE | Max-Planck-Institute for Aeronomy (Germany) |
| MPIC | Max-Planck-Institute for Chemistry (Germany) |
| MSU | Microwave Sounding Unit |
| | |
| NAD | nitric acid dihydrate |
| NAP | nitric acid pentahydrate |
| NASA | National Aeronautics and Space Administration (United States) |
| NAT | nitric acid trihydrate |
| NBS | National Bureau of Standards (now NIST) |
| NCAR | National Center for Atmospheric Research (United States) |
| NCEP | National Centers for Environmental Prediction |
| NDSC | Network for the Detection of Stratospheric Change |
| NH | Northern Hemisphere |
| NIST | National Institute of Standards and Technology (formerly NBS, United States) |
| NIWA | National Institute of Water & Atmospheric Research Ltd. (New Zealand) |
| nm | nanometer ($10^{-9}$ meters) |
| NMHC | nonmethane hydrocarbon |
| NOAA | National Oceanic and Atmospheric Administration (United States) |
| NOHALICE | Nitrous Oxide and Halocarbons Intercomparison Experiment |
| NPL | National Physical Laboratory (United Kingdom) |
| NSF | National Science Foundation (United States) |
| NWS | National Weather Service (United States) |
| | |
| ODF | opacity distribution functions |
| ODP | Ozone Depletion Potential |
| ODS | ozone-depleting substance |
| OGI | Oregon Graduate Institute |
| OHP | Observatoire de Haute Provence (Haute Provence Observatory, France) |
| O3MD | ozone mass deficiency |
| OPC | optical particle counter |
| | |
| PAN | peroxyacetyl nitrate |
| PEM | Pacific Exploratory Mission |
| PFC | perfluorocarbon |
| POAM | Polar Ozone and Aerosol Measurement |
| POLARIS | Photochemistry of Ozone Loss in the Arctic Region in Summer |
| POLINAT | Pollution from Aircraft Emissions in the North Atlantic Flight Corridor |

| | |
|---|---|
| ppb | parts per billion |
| ppbv | parts per billion by volume |
| ppm | parts per million |
| ppmv | parts per million by volume |
| ppt | parts per trillion |
| pptv | parts per trillion by volume |
| PSC | polar stratospheric cloud |
| PTB | Physikalisch Technische Bundesanstalt (Germany) |
| PV | potential vorticity |
| PVU | potential vorticity unit |
| QBO | quasi-biennial oscillation |
| RAF | Radiation Amplification Factor |
| RB | Robertson-Berger Network |
| RCM | radiative-convective model |
| RIVM | National Institute of Public Health and the Environment (The Netherlands) |
| R/V | research vessel |
| SAD | surface area density |
| SAFARI | Southern African Fire-Atmosphere Research Initiative |
| SAGE | Stratospheric Aerosol and Gas Experiment |
| SAH | sulfuric acid hemihexahydrate |
| SAM | Stratospheric Aerosol Measurement |
| SAMS | Stratospheric and Mesospheric Sounder |
| SAO | semi-annual oscillation |
| SAOZ | Système d'Analyse par Observation Zénithale |
| SAT | sulfuric acid tetrahydrate |
| SBUV/SBUV2 | Solar Backscatter Ultraviolet Spectrometer |
| SCAR-B | Smoke, Clouds, and Radiation-Brazil |
| SCATE | Sulfur Chemistry in the Antarctic Troposphere Experiment |
| SEAWIFS | Sea-Viewing Wide Field-of-View Sensor |
| SEFDH | Seasonally Evolving Fixed Dynamical Heating |
| SESAME | Second European Stratospheric Arctic and Midlatitude Experiment |
| SH | Southern Hemisphere |
| SIO | Scripps Institution of Oceanography (United States) |
| SLS | Submillimeter Limb Sounder |
| SME | Solar Mesosphere Explorer |
| SOAPEX | Southern Ocean Atmospheric Photochemistry Experiment |
| SORG | Stratospheric Ozone Review Group (U.K. Department of the Environment) |
| SOLSPEC | Solar Spectrum (instrument) |
| SOLSTICE | Solar Stellar Irradiance Comparison Experiment |
| SPARC | Stratospheric Processes and their Role in Climate (WCRP) |
| SPOT | Satellite Pour l'Observation de la Terre |
| SSA | stratospheric sulfate aerosol |
| SSBUV | Shuttle Solar Backscatter Ultraviolet Spectrometer |
| SST | sea surface temperature |
| SSU | Stratospheric Sounding Unit |

**ACRONYMS**

| | |
|---|---|
| STE | stratosphere-troposphere exchange |
| STS | supercooled ternary solution |
| STRAT | Stratospheric Tracers of Atmospheric Transport |
| STREAM | Stratosphere-Troposphere Exchange Experiment by Aircraft Measurement |
| STTA | Stratospheric Temperature Trends Assessment (SPARC) |
| STUK | Finnish Center for Radiation and Nuclear Safety (Finland) |
| SUNY | State University of New York (United States) |
| SUCCESS | SUbsonic Aircraft Contrail and Cloud Effects Special Study |
| SUSIM | Solar Ultraviolet Spectral Irradiance Monitor |
| SUSPEN | Standardization of Ultraviolet Spectroradiometry in Preparation of a European Network |
| SUVDAMA | Scientific UV Data Management |
| SZA | solar zenith angle |
| | |
| TEAP | Technology and Economic Assessment Panel |
| TFA | trifluoroacetic acid |
| Tg | teragram ($10^{12}$ grams) |
| TIROS | Television and InfraRed Observational Satellite |
| TOHPE | Tropospheric OH Photochemistry Experiment |
| TOMS | Total Ozone Mapping Spectrometer |
| TOVS | TIROS Operational Vertical Sounder |
| TRACE-A | Transport and Atmospheric Chemistry near the Equator-Atlantic |
| | |
| UARS | Upper Atmosphere Research Satellite |
| UCI | University of California at Irvine (United States) |
| UEA | University of East Anglia (United Kingdom) |
| UH | University of Heidelberg (Germany) |
| UKMO | United Kingdom Meteorological Office |
| UK | United Kingdom |
| UN | United Nations |
| UNEP | United Nations Environment Programme |
| US | United States |
| USDA | U.S. Department of Agriculture |
| USGS | United States Geological Survey |
| UT | University of Tokyo (Japan) |
| UV | ultraviolet |
| UVRAPPF | UV Radiation in the Arctic: Past, Present, and Future |
| UV-MFRSR | UV Multi-Filter Rotating Shadowband Radiometer |
| | |
| WAS | whole-air samplers |
| WCRP | World Climate Research Programme |
| WMO | World Meteorological Organization |
| WOUDC | World Ozone and Ultraviolet Radiation Data Centre (Canada) |
| WVMS | Water Vapor Millimeter-wave Spectrometer |

# APPENDIX C
# CHEMICAL FORMULAE AND NOMENCLATURE

## HALOGEN-CONTAINING SPECIES

| | | | |
|---|---|---|---|
| Cl | atomic chlorine | Br | atomic bromine |
| $Cl_2$ | molecular chlorine | $Br_2$ | molecular bromine |
| ClO | chlorine monoxide | BrO | bromine monoxide |
| OClO | chlorine dioxide | | |
| $Cl_2O_2$ | dichlorine peroxide (ClO dimer) | | |
| ClONO | chlorine nitrite, nitryl chloride | | |
| $ClONO_2$ | chlorine nitrate | $BrONO_2$ | bromine nitrate |
| HCl | hydrogen chloride (hydrochloric acid) | HBr | hydrogen bromide |
| HOCl | hypochlorous acid | HOBr | hypobromous acid |
| BrCl | bromine chloride | | |
| $Cl_y$ | inorganic chlorine | $Br_y$ | inorganic bromine |
| $CCl_y$ | organic chlorine | $CBr_y$ | organic bromine |
| $ClO_x$ | chlorine radicals | $BrO_x$ | bromine radicals |
| | | | |
| F | atomic fluorine | I | atomic iodine |
| HF | hydrogen fluoride (hydrofluoric acid) | HI | hydrogen iodide |
| $SF_6$ | sulfur hexafluoride | IO | iodine monoxide |
| $NF_3$ | nitrogen trifluoride | | |
| $F_y$ | inorganic fluorine | | |
| $CF_y$ | organic fluorine | | |

### HALOCARBONS

#### Chlorofluorocarbons (CFCs)

| | |
|---|---|
| CFC-10 | $CCl_4$ |
| CFC-11 | $CCl_3F$ |
| CFC-12 | $CCl_2F_2$ |
| CFC-13 | $CClF_3$ |
| CFC-14 | $CF_4$ |
| CFC-113 | $CCl_2FCClF_2$ |
| CFC-114 | $CClF_2CClF_2$ |
| CFC-115 | $CClF_2CF_3$ |
| CFC-116 | $CF_3CF_3$ |

#### Hydrochlorofluorocarbons (HCFCs)

| | |
|---|---|
| HCFC-21 | $CHCl_2F$ |
| HCFC-22 | $CHClF_2$ |
| HCFC-123 | $CF_3CHCl_2$ |
| HCFC-124 | $CF_3CHClF$ |
| HCFC-141b | $CCl_2FCH_3$ |
| HCFC-142b | $CClF_2CH_3$ |
| HCFC-225ca | $CF_3CF_2CHCl_2$ |
| HCFC-225cb | $CClF_2CF_2CHClF$ |

#### Hydrofluorocarbons (HFCs)

| | | | |
|---|---|---|---|
| HFC-23 | $CHF_3$ | HFC-227ca | $CF_3CF_2CHF_2$ |
| HFC-32 | $CH_2F_2$ | HFC-227ea | $CF_3CHFCF_3$ |
| HFC-41 | $CH_3F$ | HFC-236cb | $CF_3CF_2CH_2F$ |
| HFC-125 | $CF_3CHF_2$ | HFC-236ea | $CF_3CHFCHF_2$ |

## CHEMICAL FORMULAE

| | |
|---|---|
| HFC-134 | $CHF_2CHF_2$ |
| HFC-134a | $CF_3CH_2F$ |
| HFC-143 | $CHF_2CH_2F$ |
| HFC-143a | $CH_3CF_3$ |
| HFC-152 | $CH_2FCH_2F$ |
| HFC-152a | $CH_3CHF_2$ |
| HFC-161 | $CH_3CH_2F$ |
| HFC-236fa | $CF_3CH_2CF_3$ |
| HFC-245ca | $CHF_2CF_2CFH_2$ |
| HFC-245cb | $CF_3CF_2CH_3$ |
| HFC-272ca | $CH_3CF_2CH_3$ |
| HFC-365mfc | $CF_3CH_2CF_2CH_3$ |
| HFC-43-10mee | $CF_3CHFCHFCF_2CF_3$ |

### Halons

| | |
|---|---|
| Halon-1202 | $CBr_2F_2$ |
| Halon-1211 | $CBrClF_2$ |
| Halon-1301 | $CBrF_3$ |
| Halon-2402 | $CBrF_2CBrF_2$ |

### Hydrofluoroethers (HFEs)

| | |
|---|---|
| HFE-125 | $CF_3OCHF_2$ |
| HFE-134 | $CHF_2OCHF_2$ |
| HFE-143a | $CH_3OCF_3$ |
| HFE-245fa2 | $CF_3CH_2OCHF_2$ |
| HFE-245cb2 | $CHF_2CF_2OCH_3$ |

### Chlorocarbons

| | |
|---|---|
| $CH_3Cl$ | methyl chloride |
| $CH_2Cl_2$ | methylene chloride, dichloromethane |
| $CHCl_3$ | chloroform, trichloromethane |
| $CCl_4$ | carbon tetrachloride |
| $CH_3CCl_3$ | methyl chloroform |
| $C_2HCl_3$ | trichloroethene, trichloroethylene |
| $C_2Cl_4$ | tetrachloroethene, perchloroethene |
| $C_2H_4Cl_2$ | dichloroethane |
| $C_2H_2Cl_4$ | tetrachloroethane |
| $C_2H_2Cl_2$ | vinyledene chloride |
| $C_4Cl_6$ | hexachlorobutadiene |
| $COCl_2$ | phosgene, carbonyl chloride |

### Bromocarbons

| | |
|---|---|
| $CH_3Br$ | methyl bromide |
| $CH_2Br_2$ | methylene bromide, dibromomethane |
| $CHBr_3$ | bromoform, tribromomethane |
| $CH_2BrCH_2Br$ | ethylene dibromide, 1,2 dibromoethane |
| $CH_2BrCH_2CH_3$ | 1-bromopropane, n-propyl bromide |

### Iodocarbons

| | |
|---|---|
| $CH_3I$ | methyl iodide |
| $CH_2I_2$ | diiodomethane |
| $CH_3CH_2I$ | ethyl iodide |
| $CH_3CHICH_3$ | isopropyl iodide |
| $CH_2ICH_2CH_3$ | 1-iodopropane, n-propyl iodide |

### Fluorocarbons

| | |
|---|---|
| $CF_4$ | perfluoromethane, carbon tetrafluoride |
| $C_2F_6$ | perfluoroethane |
| $C_3F_8$ | perfluoropropane |
| c-$C_3F_6$ | perfluorocyclopropane |
| $C_4F_{10}$ | perfluorobutane |
| c-$C_4F_8$ | perfluorocyclobutane |
| $C_5F_{12}$ | perfluoropentane |
| $C_6F_{14}$ | perfluorohexane |
| $COF_2$ | carbonyl fluoride |
| $CF_3COF$ | trifluoroacetyl fluoride |
| TFA | trifluoroacetic acid ($CF_3COOH$) |

### Others

| | |
|---|---|
| $CHBr_2Cl$ | dibromochloromethane |
| $CH_2BrCl$ | bromochloromethane |
| $CHBrCl_2$ | bromodichloromethane |
| $CH_2ClI$ | chloroiodomethane |
| $CF_3I$ | iodotrifluoromethane |
| $CHBrF_2$ | difluorobromomethane |
| $CF_3CHBrCl$ | halothane |
| $CF_3CF_2I$ | iodopentafluoroethane |
| COClF | chlorofluorocarbonyl |
| $CF_3COCl$ | trifluoroacetyl chloride |

## OTHER CHEMICAL SPECIES

| | | | |
|---|---|---|---|
| O | atomic oxygen | H | atomic hydrogen |
| $O(^3P)$ | atomic oxygen (ground state) | $H_2$ | molecular hydrogen |
| $O(^1D)$ | atomic oxygen (first excited state) | OH | hydroxyl radical |
| $O_2$ | molecular oxygen | $HO_2$ | hydroperoxyl radical |
| $O_3$ | ozone | $H_2O$ | water |
| $O_x$ | odd oxygen (O, $O(^1D)$, $O_3$) or oxidant ($O_3 + NO_2$) | $H_2O_2$ | hydrogen peroxide |
| | | $HO_x$ | odd hydrogen (H, OH, $HO_2$, $H_2O_2$) |
| N | atomic nitrogen | $HO_2NO_2$ | peroxynitric acid, pernitric acid |
| $N_2$ | molecular nitrogen | $CH_3OONO_2$ | methylperoxynitrate |
| $N_2O$ | nitrous oxide | PAN | peroxyacetylnitrate ($CH_3C(O)OONO_2$) |
| NO | nitric oxide | $RONO_2$ | alkyl nitrates |
| $NO_2$ | nitrogen dioxide | | |
| $NO_3$ | nitrogen trioxide, nitrate radical | NAD | nitric acid dihydrate ($HNO_3 \cdot 2H_2O$) |
| $N_2O_5$ | dinitrogen pentoxide | NAT | nitric acid trihydrate ($HNO_3 \cdot 3H_2O$) |
| $ClONO_2$ | chlorine nitrate | NAP | nitric acid pentahydrate ($HNO_3 \cdot 5H_2O$) |
| $HNO_2$, HONO | nitrous acid | | |
| $HNO_3$ | nitric acid | $NH_3$ | ammonia |
| $NO_x$ | nitrogen oxides ($NO + NO_2$) | | |
| $NO_y$ | odd nitrogen (usually includes NO, $NO_2$, $NO_3$, $N_2O_5$, $ClONO_2$, $HNO_4$, $HNO_3$) | | |
| S | atomic sulfur | $SF_6$ | sulfur hexafluoride |
| $SO_2$ | sulfur dioxide | $CS_2$ | carbon disulfide |
| $SO_x$ | sulfur oxides | COS, OCS | carbonyl sulfide |
| $H_2SO_4$ | sulfuric acid | $H_2S$ | hydrogen sulfide |
| SAM | sulfuric acid monohydrate ($H_2SO_4 \cdot H_2O$) | | |
| SAT | sulfuric acid tetrahydrate ($H_2SO_4 \cdot 4H_2O$) | | |
| SAH | sulfuric acid hemihexahydrate ($H_2SO_4 \cdot 6.5H_2O$) | | |
| C | carbon atom | | |
| CO | carbon monoxide | | |
| $CO_2$ | carbon dioxide | | |
| NMHC | nonmethane hydrocarbon | $CH_2O$ | formaldehyde |
| $CH_4$ | methane | $CH_3COCH_3$ | acetone |
| $C_2H_6$ | ethane | $CH_3OOH$ | methyl hydroperoxide |
| $C_3H_8$ | propane | $CH_3COO$ | methyl peroxy radical |
| $C_2H_4$ | ethylene, ethene | $CH_3C(O)OO$ | acetyl peroxy radical |
| $C_2H_2$ | acetylene, ethyne | RO | alkoxy radicals |
| | | $RO_2$ | organic peroxy radical |